Spin Models with Dissipation: Part I

Yury Holubeu *

November 29, 2025

This draft is not aimed for distribution.

Contents

*https://yuriholubeu.github.io/, yuri.holubev@gmail.com

Preface to Part I

Amazing facts

(I'll reveal it later)

Puzzles for motivation

(I'll reveal it later)

Part I
Spin Models with Dissipation in a Nutshell

1 Main Formulas and Ideas

1.1 Quench dynamics and relaxation in isolated integrable quantum spin chains by Essler, Fagotti

1.2 Main Useful articles

1.2.1 Generalized Gibbs ensembles in weakly interacting dissipative systems and digital quantum computers

Main ideas

(???)

Setup

$$H_0 = \sum_q \varepsilon_q n_q + E_0 \tag{1.1}$$

$$\frac{d\rho}{dt} = -i[H_0, \rho] + \hat{\mathcal{D}}[\rho], \qquad \hat{\mathcal{D}}[\rho] := \epsilon \left(\sum_i L_i \rho L_i^\dagger - \frac{1}{2}\{L_i^\dagger L_i, \rho\} \right). \tag{1.2}$$

$$\rho_{\boldsymbol{\mu}}(t) = \frac{e^{-\sum_q \mu_q(t) n_q}}{\mathrm{Tr}[e^{-\sum_q \mu_q(t) n_q}]}. \tag{1.3}$$

$$\langle \dot{n}_q \rangle(t) \approx \mathrm{Tr}\left[n_q \hat{\mathcal{D}}[\rho_{\boldsymbol{\mu}}(t)] \right], \tag{1.4}$$

$$\dot{\mu}_q(t) = -\sum_{q'} (\chi^{-1})_{q,q'}(t) \, \langle \dot{n}_{q'} \rangle(t). \qquad \chi_{q,q'}(t) := \langle n_q n_{q'} \rangle_{\rho_{\boldsymbol{\mu}(t)}} - \langle n_q \rangle_{\rho_{\boldsymbol{\mu}(t)}} \langle n_{q'} \rangle_{\rho_{\boldsymbol{\mu}(t)}}. \tag{1.5}$$

$$\langle O \rangle_{\rho_{\boldsymbol{\mu}}} := \mathrm{Tr}[O \rho_{\boldsymbol{\mu}}].$$

For free Fermi gas $\chi_{q,q'}(t) = \delta_{q,q'} \, e^{-\mu_q(t)}/(1 + e^{-\mu_q(t)})^2$.

Continuous Model

$$H_0 = \sum_i J \sigma_i^x \sigma_{i+1}^x + h \sigma_i^z, \tag{1.6}$$

$$\sigma_j^z = 2 c_j^\dagger c_j - 1, \qquad \sigma_j^+ = e^{i\pi \sum_{l<j} n_j} c_j^\dagger, \tag{1.7}$$

$$c_j = \frac{e^{-i\pi/4}}{\sqrt{N}} \sum_q e^{iqj} c_q. \qquad c_q = u_q d_q - v_q d_{-q}^\dagger, \tag{1.8}$$

$$u_q = \frac{(\varepsilon_q + a_q)}{\sqrt{2\varepsilon_q(\varepsilon_q + a_q)}}, \qquad a_q = 2(J\cos q + h),$$
$$v_q = \frac{b_q}{\sqrt{2\varepsilon_q(\varepsilon_q + a_q)}}, \qquad b_q = 2J\sin q,$$

$$H = \sum_q \varepsilon_q \left(n_q - \frac{1}{2}\right), \qquad n_q = d_q^\dagger d_q. \qquad \epsilon_q = 2\sqrt{J^2 + 2hJ\cos q + h^2},$$

$$L_j := S_j^+ S_{j+1}^- + S_j^z + \frac{1}{2}\mathbb{1}_j. \tag{1.9}$$

$$L_j = \sum_{q,q'} \frac{e^{-ij(q-q')}}{N}(1 + e^{iq'})(u_q d_q^\dagger - v_q d_{-q})(u_{q'} d_{q'} - v_{q'} d_{-q'}^\dagger). \tag{1.10}$$

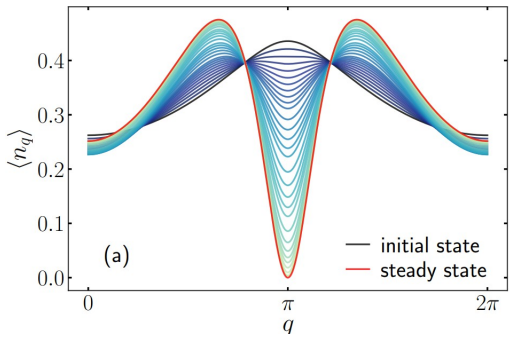

Figure 1.1: (a) Time evolution from an initial thermal mode occupation with $\beta = 0.323$ to a highly non-thermal steady state distribution, stabilized by $L_j = \sum_{q,q'} \frac{e^{-ij(q-q')}}{N}(1 + e^{iq'})(u_q d_q^\dagger - v_q d_{-q})(u_{q'} d_{q'} - v_{q'} d_{-q'}^\dagger)$. Parameters: $J = 1, h = 0.6, L = 10^5$.

$$\langle \dot{n}_q \rangle = \epsilon \sum_j \langle L_j^\dagger n_q L_j \rangle - \langle n_q L_j^\dagger L_j \rangle \tag{1.11}$$

$$\langle \dot{n}_q \rangle = \frac{2\epsilon}{N} \sum_{q'} f_{q',q}\langle n_{q'}\rangle\langle 1 - n_q\rangle - f_{q,q'}\langle n_q\rangle\langle 1 - n_{q'}\rangle + \tilde{f}_{q',q}\langle 1 - n_{q'}\rangle\langle 1 - n_q\rangle - \tilde{f}_{q,q'}\langle n_q\rangle\langle n_{q'}\rangle. \tag{1.12}$$

$$f_{q',q} = u_q^2 u_{q'}^2(1 + \cos q') + v_q^2 v_{q'}^2(1 + \cos q) - u_q v_q u_{q'} v_{q'}(1 + \cos q' + \cos q + \cos(q + q')),$$
$$\tilde{f}_{q',q} = v_q^2 u_{q'}^2(1 + \cos q) + u_q^2 v_{q'}^2(1 + \cos q') - u_q v_q u_{q'} v_{q'}(1 + \cos q' + \cos q + \cos(q - q')).$$

Digital quantum computer protocol

$$U_S = e^{-i\frac{\pi J}{2}\sum_j \sigma_j^x \sigma_{j+1}^x} e^{-i\frac{\pi h}{2}\sum_j \sigma_j^z} \equiv e^{-iH_{\text{FTFI}}}, \tag{1.13}$$

$$U_A = e^{-i\frac{\pi h_A}{2}\sum_j \tilde{\sigma}_j^z}, \tag{1.14}$$

$$U_{SA,\tau} = \prod_j e^{-i\lambda_\tau Q_j \otimes A_j}. \tag{1.15}$$

$$Q_j = S_j^+ S_{j+1}^- + S_j^- S_{j+1}^+, \quad A_j = \tilde{\sigma}_j^x, \tag{1.16}$$

$$U_T = U_{SA,T} U_A U_S \cdots U_{SA,1} U_A U_S, \tag{1.17}$$

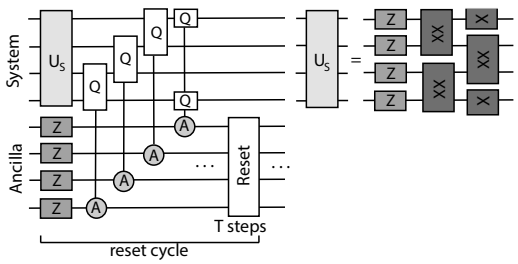

Figure 1.2: Scheme of realization of dissipative transverse field Ising, similar to Refs. [45, 8] and realistic to implement with a digital quantum computer.

$$U_S = \prod_{q\geq 0} e^{-i\Phi_q^\dagger X_q \Phi_q} e^{-i\Phi_q^\dagger Z_q \Phi_q}, \tag{1.18}$$

$\Phi_q = \{c_q, c_{-q}^\dagger\}^T$

$$\cos(\tilde{\epsilon}_q) = \cos(\pi J)\cos(\pi h) - \sin(\pi J)\sin(\pi h)\cos(q). \tag{1.19}$$

$c_q = \tilde{u}_q d_q - \tilde{v}_q^* d_{-q}^\dagger,$

$$\begin{aligned}
\tilde{u}_q &= \frac{(\xi_q + \tilde{a}_q)}{\sqrt{2\xi_q(\xi_q+\tilde{a}_q)}}, \qquad \tilde{v}_q = \frac{\tilde{b}_q}{\sqrt{2\xi_q(\xi_q+\tilde{a}_q)}}, \\
\tilde{a}_q &= \sin(\pi J)\cos(\pi h)\cos(q) + \cos(\pi J)\sin(\pi h), \\
\tilde{b}_q &= -e^{-i\pi h}\sin(\pi J)\sin(q), \\
\xi_q &= \sqrt{\tilde{a}_q^2 + |\tilde{b}_q|^2},
\end{aligned} \tag{1.20}$$

$$H_{\text{FTFI}} = \sum_q \tilde{\epsilon}_q \left(n_q - \frac{1}{2}\right), \; n_q = d_q^\dagger d_q. \tag{1.21}$$

$\rho_{\boldsymbol{\mu}}(N_c) = (1/Z)e^{-\sum_q \mu_q(N_c) n_q},$

$$\begin{aligned}
\rho_{\boldsymbol{\mu}}(N_c+1) - \rho_{\boldsymbol{\mu}}(N_c) \approx \sum_{j,\omega,\omega'} &-i\,\mathrm{Im}(\mathcal{A}_{\omega,\omega'})[\mathrm{Q}_{\mathrm{j},\omega'}^\dagger \mathrm{Q}_{\mathrm{j},\omega}, \rho_{\boldsymbol{\mu}}(\mathrm{N_c})] + \\
&+ \mathfrak{a}_{\omega,\omega'}\Big(Q_{j,\omega}\rho_{\boldsymbol{\mu}}(N_c)Q_{j,\omega'}^\dagger - \frac{1}{2}\{Q_{j,\omega'}^\dagger Q_{j,\omega}, \rho_{\boldsymbol{\mu}}(N_c)\}\Big).
\end{aligned} \tag{1.22}$$

$$\begin{aligned}
\mathfrak{a}_{\omega,\omega'} &= \sum_{\tau=1}^{T} \lambda_\tau e^{i\tau(\omega'-\pi h_A)} \sum_{\tau'=1}^{T} \lambda_{\tau'} e^{-i\tau'(\omega-\pi h_A)}, \\
\mathcal{A}_{\omega,\omega'} &= \sum_{\tau=1}^{T}\sum_{\tau'=1}^{\tau} \lambda_\tau \lambda_{\tau'} e^{i(\omega'\tau - \omega\tau' + \pi h_A(-\tau+\tau'))},
\end{aligned} \tag{1.23}$$

$Q_{j,\omega} = \sum_{\alpha,\beta,\tilde{E}_\beta - \tilde{E}_\alpha = \omega} |\alpha\rangle\langle\alpha|Q_j|\beta\rangle\langle\beta|.$

$$\begin{aligned}
\langle n_q(N_c+1)\rangle - \langle n_q(N_c)\rangle = \frac{2}{N}\sum_{q'} &g_{q',q}\big(\langle n_{q'}\rangle\langle 1-n_q\rangle \mathfrak{a}_{\epsilon_{q'}-\epsilon_q} - \langle n_q\rangle\langle 1-n_{q'}\rangle \mathfrak{a}_{\epsilon_q-\epsilon_{q'}}\big) \\
&+ \tilde{g}_{q',q}\big(\langle 1-n_{q'}\rangle\langle 1-n_q\rangle \mathfrak{a}_{-\epsilon_{q'}-\epsilon_q} - \langle n_q\rangle\langle n_{q'}\rangle \mathfrak{a}_{\epsilon_{q'}+\epsilon_q}\big).
\end{aligned} \tag{1.24}$$

$g_{q',q} = (1+\cos(q+q'))|\tilde{u}_{q'}\tilde{u}_q - \tilde{v}_{q'}^*\tilde{v}_q|^2,$
$\tilde{g}_{q',q} = (1+\cos(q'-q))|\tilde{u}_{q'}\tilde{v}_q - \tilde{v}_{q'}^*\tilde{u}_q|^2,$

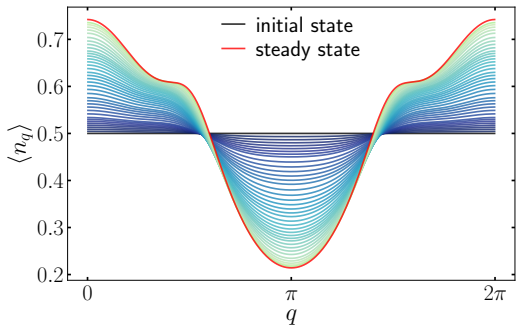

Figure 1.3: Time evolution of the mode occupation from an initial infinite temperature state. A highly non-thermal steady-state distribution is reached, which could be stabilized by the system-ancilla coupling in a digital quantum computer. Parameters: $J = 0.8, h = 0.45, h_A = 0.8, T = 6,\ L = 500, \lambda_\tau = \sqrt{\epsilon} = 0.1$.

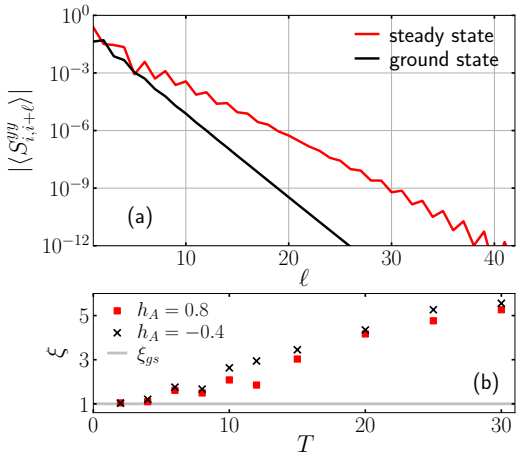

Figure 1.4: (a) Decay of correlations $|\langle S^{yy}_{i,i+\ell}\rangle|$, Eq. (8.32), as a function of ℓ in the steady-state GGE and the ground state for $h_A = 0.8, T = 6$. As a signature of the stabilized non-thermal GGE, operators that overlap with local conserved quantities of transverse field Ising models show a slower decay of spatial correlations compared to the ground state. (b) Different choices of system-ancilla coupling parameters (field h_A and cycle duration T) yield different correlation lengths ξ. Quite generically, longer cycles lead to slower decay of spatial correlations and thus more non-thermal states. Parameters: $J = 0.8, h = 0.45, L = 500$.

$$
\begin{aligned}
C_0 &= H_0 \\
C_2 &= \sum_j J S^{xx}_{j,j+2} - h S^{yy}_{j,j+1} - h S^{xx}_{j,j+1} - J\sigma^z_j \\
C_{2\ell>2} &= \sum_j J S^{xx}_{j,j+\ell+1} - h_x S^{yy}_{j,j+\ell} - h_x S^{xx}_{j,j+\ell} + J S^{yy}_{j,j+\ell-1} \\
C_{2\ell-1} &= J \sum_j S^{yx}_{j,j+\ell} - S^{xy}_{j,j+\ell}.
\end{aligned}
\tag{1.25}
$$

$S^{\alpha\beta}_{i,j} = \sigma^\alpha_i \sigma^z_{i+1} \ldots \sigma^z_{j-1} \sigma^\beta_j$.

Comparison of approaches for steady-state calculation

(2) Iterative steady state calculation:

$\rho^{(0)}_{\tilde{\boldsymbol{\lambda}}} \propto e^{-\tilde{\lambda}^{(0)}_0 H_0}$,

$$\tilde{C}_k = \sum_q w_q^{(k)} n_q, \;\; w_q^{(k)} \propto \mathrm{Tr}[n_q \hat{\mathcal{D}} \rho_{\tilde{\boldsymbol{\lambda}}}^{(k-1)}], \tag{1.26}$$

$\{\tilde{\lambda}_{k'}^{(k)}\}$
$\rho_{\tilde{\boldsymbol{\lambda}}}^{(k)} \propto e^{-\sum_{k'=0}^{k} \tilde{\lambda}_{k'}^{(k)} \tilde{C}_{k'}}$
$\langle \tilde{C}_{k'} \rangle = 0,$
(3) Truncated GGE (most local conserved quantities):
$C_{2\ell} = \sum_q \cos(q\ell)\epsilon_q n_q$ for even ones ($C_0 = H_0$) and as $C_{2\ell-1} = 2J \sum_q \sin(q\ell) n_q$ for odd ones [37]. If one includes only N_i most local ones, $2\ell < N_i$, then the complexity of finding the truncated steady state GGE scales as $\mathcal{O}(LN_i^2)$.
(4) Time propagation:
$\langle \psi_0 | n_q | \psi_0 \rangle = \mathrm{Tr}\left[n_q \frac{e^{-\sum_{q'} \mu_{q'}(0) n_{q'}}}{\mathrm{Tr}[e^{-\sum_{q'} \mu_{q'}(0) n_{q'}}]} \right].$

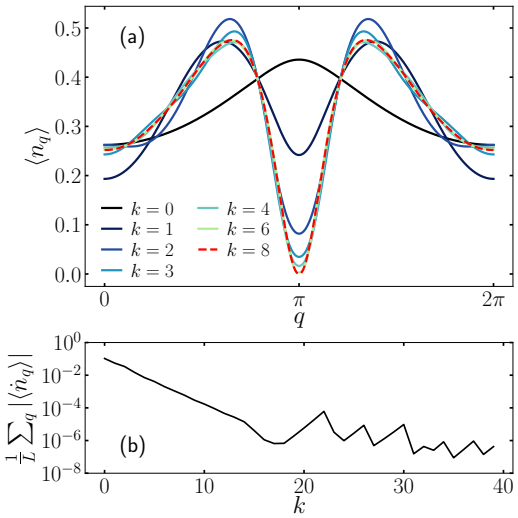

Figure 1.5: (a) Convergence to the steady state mode occupation at different iterative steps k. In the $k = 0$ step, the steady state is approximated by a thermal state. In the following iterative steps, additional leading conserved operators are added to a truncated GGE. A decent convergence is obtained in finite number of steps. (b) After the initial improvement of results with increasing number of iterative steps, for chosen parameters, $k > 18$ iterative steps fail to improve the results further. However, this happens in the regime where results are converged for all practical purposes. Parameters: $J = 1, h = 0.6, L = 10^5$.

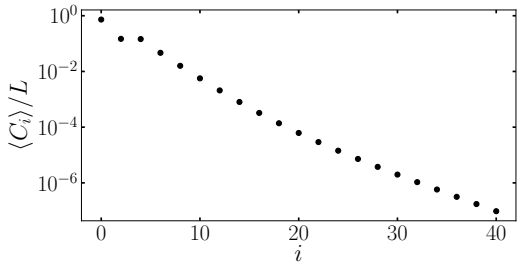

Figure 1.6: Steady state expectation values of local conserved quantities (8.32). With increasing support, the importance of even conserved quantities decays exponentially. Expectation values of odd observables are zero due to symmetry. Parameters: $J = 1$, $h = 0.6$, $L = 10^5$.

1.2.2 Perturbative approach to weakly driven many-particle systems in the presence of approximate conservation laws by Lenarčič, Lange, Rosch

Main ideas

Model

$$\hat{\mathcal{L}}_0\rho = -i[H_0,\rho], \quad \hat{\mathcal{L}}_1\rho = \begin{cases} -i[\epsilon H_1,\rho], \\ \epsilon\hat{\mathcal{D}}\rho. \end{cases} \tag{1.27}$$

$$\hat{\mathcal{D}}\rho = \sum_\alpha \left(L_\alpha \rho L_\alpha^\dagger - \frac{1}{2}\{L_\alpha^\dagger L_\alpha,\rho\}\right) \tag{1.28}$$

$$\lim_{t\to\infty}\rho(t) = \rho_\infty = \rho_0 + \delta\rho. \tag{1.29}$$

$\rho_0 = \lim_{\epsilon\to 0}\lim_{t\to\infty}\rho(t)$.

$$\delta\rho = -\hat{\mathcal{L}}^{-1}\hat{\mathcal{L}}_1\rho_0, \quad \hat{\mathcal{L}}^{-1} \to \lim_{\eta\to 0}(\hat{\mathcal{L}} - \eta\hat{1})^{-1}. \tag{1.30}$$

$\hat{\mathcal{L}}\rho_\infty = \hat{\mathcal{L}}_1\rho_0 + \hat{\mathcal{L}}\delta\rho = 0$
$\hat{\mathcal{L}}_0\rho_0 = 0$.

Zeroth order: generalized Gibbs ensemble

$$\rho_0 = \frac{e^{-\sum_i \lambda_i C_i}}{\mathrm{Tr}[e^{-\sum_i \lambda_i C_i}]}, \tag{1.31}$$

Determination of λ_i

$$\begin{aligned} \langle \dot{C}_i\rangle &= \mathrm{Tr}[C_i\hat{\mathcal{L}}\rho_\infty] \\ &= \mathrm{Tr}[C_i\hat{\mathcal{L}}_1\rho_0] + \mathrm{Tr}[C_i\hat{\mathcal{L}}_1\delta\rho] \approx \mathrm{Tr}[C_i\hat{\mathcal{L}}_1\rho_0] \end{aligned} \tag{1.32}$$

$i = 1, ..., N_c$.
$\mathrm{Tr}[C_i\hat{\mathcal{L}}_0\delta\rho] = 0, \qquad \hat{\mathcal{L}}_0^\dagger C_i = i[H_0, C_i] = 0$

$$\mathrm{Tr}[C_i\hat{\mathcal{L}}_1\rho_0] \stackrel{!}{=} 0 \tag{1.33}$$

For the case $\mathrm{Tr}[C_i\hat{\mathcal{L}}_1\rho_0] = 0$
$(X+Y)^{-1} = X^{-1} - (X+Y)^{-1}YX^{-1}$,
$\delta\rho = -\hat{\mathcal{L}}_0^{-1}\hat{\mathcal{L}}_1\rho_0 + \hat{\mathcal{L}}^{-1}\hat{\mathcal{L}}_1\hat{\mathcal{L}}_0^{-1}\hat{\mathcal{L}}_1\rho_0$.
$\mathrm{Tr}[C_i\hat{\mathcal{L}}_1\delta\rho] = 0$

$$\mathrm{Tr}[C_i\hat{\mathcal{L}}_1\hat{\mathcal{L}}_0^{-1}\hat{\mathcal{L}}_1\rho_0] \stackrel{!}{=} 0. \tag{1.34}$$

$\Lambda \equiv \min(|Re\ \lambda|; Re\ \lambda < 0),\ \hat{\mathcal{L}}\rho = \lambda\rho,$

Periodic driving

$$\rho(t) = \sum_n e^{-in\omega t}\rho^{(n)},\ n \in \mathbb{Z}, \tag{1.35}$$

$\rho^{(-n)} = \rho^{(n)\dagger}$, $\omega = 2\pi/T$.
$\boldsymbol{\rho} = \{\dots \rho^{(-1)}, \rho^{(0)}, \rho^{(1)}, \dots\}$

$$\hat{\boldsymbol{\mathcal{L}}} = \hat{\boldsymbol{\mathcal{L}}}_0 + \hat{\boldsymbol{\mathcal{L}}}_1 \tag{1.36}$$

$$\hat{\boldsymbol{\mathcal{L}}}_1^{nm} = \hat{\mathcal{L}}_1^{n-m} = \frac{1}{T}\int_0^T \hat{\mathcal{L}}_1(t)e^{i\omega(n-m)t}dt \tag{1.37}$$

$$\hat{\boldsymbol{\mathcal{L}}}_0^{nm} = (in\omega + \hat{\mathcal{L}}_0)\delta_{nm} \tag{1.38}$$

$\dot{\rho} = \sum_n e^{-in\omega t}(-in\omega\rho^{(n)} + \dot{\rho}^{(n)})$.

Projection operators and effective forces

$\hat{P} = \hat{P}_{\rho_0}$
$\delta\rho_\parallel = \sum_i \delta\lambda_i\, \partial\rho_0/\partial\lambda_i$

$$\hat{P}X \equiv -\sum_{i,j} \frac{\partial\rho_0}{\partial\lambda_i}\ (\chi^{-1})_{ij}\mathrm{Tr}[C_j X] \tag{1.39}$$

$$\hat{Q}X \equiv (\hat{1} - \hat{P})X = X - \hat{P}X \tag{1.40}$$

$\chi_{ij} = -\mathrm{Tr}[C_i\, \partial\rho_0/\partial\lambda_j] = \langle C_i C_j\rangle_{0,c}$
$\mathrm{Tr}[A\rho] = \langle A\rangle$ and $\mathrm{Tr}[A\rho_0] = \langle A\rangle_0$
$\langle AB\rangle_{0,c} = \langle AB\rangle_0 - \langle A\rangle_0\langle B\rangle_0$
$\hat{Q}^2 = \hat{Q}$ and $\hat{P}^2 = \hat{P}$ with $\hat{P}\delta\rho_\parallel = \delta\rho_\parallel$
$\mathrm{Tr}[(\hat{P}^\dagger A)\delta\rho] = \mathrm{Tr}[A(\hat{P}\delta\rho)]$.

$$\hat{P}^\dagger A = -\sum_{ij} C_i\ (\chi^{-1})_{ji}\ \mathrm{Tr}\left[A\frac{\partial\rho_0}{\partial\lambda_j}\right]. \tag{1.41}$$

$\mathrm{Re}[\sigma(\omega)] = \pi D(T)\delta(\omega) + \sigma_{\mathrm{reg}}(\omega)$.
$D(T) = \frac{\beta}{L}\langle(\hat{P}^\dagger J)J\rangle_c$

$$\hat{P}\dot{\rho} \approx \sum_i \frac{\partial\rho_0}{\partial\lambda_i}\frac{\partial\lambda_i}{\partial t} = \sum_i \frac{\partial\rho_0}{\partial\lambda_i}F_i. \tag{1.42}$$

$$\dot{\lambda}_i = F_i \approx -\sum_j (\chi^{-1})_{ij}\mathrm{Tr}[C_j\dot{\rho}] = -\sum_j (\chi^{-1})_{ij}\langle\dot{C}_j\rangle$$

$F_i = -\sum_j (\chi^{-1})_{ij}\mathrm{Tr}[C_j\hat{\mathcal{L}}_1\rho_0]$.

$$\hat{P}(\hat{\mathcal{L}}_1\rho_0) = 0. \tag{1.43}$$

$$\hat{P}(\hat{\mathcal{L}}_1\hat{\mathcal{L}}_0^{-1}\hat{\mathcal{L}}_1\rho_0) = 0. \tag{1.44}$$

Numerical construction of ρ_0

$$\mathcal{Q} = \{|n\rangle\langle m| \text{ with } E_n^0 = E_m^0\}. \tag{1.45}$$

$$\hat{\mathcal{L}}_{nm}^{\mathcal{Q}} = \mathrm{Tr}\,[\mathcal{Q}_n^\dagger \hat{\mathcal{L}}_1 \mathcal{Q}_m]. \tag{1.46}$$

$$\hat{\mathcal{L}}_{nm}^{\mathcal{Q}} = -\mathrm{Tr}\,[\mathcal{Q}_n^\dagger \hat{\mathcal{L}}_1 \hat{\mathcal{L}}_0^{-1} \hat{\mathcal{L}}_1\ \mathcal{Q}_m]. \tag{1.47}$$

$$\tilde{P}X = \sum_{n,m} \langle n|X|m\rangle \delta_{E_n^0, E_m^0}\ |n\rangle\langle m| \tag{1.48}$$

Perturbation theory

$$\langle C_i\rangle = \mathrm{Tr}\big(C_i(\rho_0 + \delta\rho)\big) = \mathrm{Tr}\big(C_i(\rho_0 + \delta\rho_\parallel)\big) \tag{1.49}$$

Markovian perturbation

$$\delta\rho = -\hat{\mathcal{L}}^{-1}\hat{Q}\hat{\mathcal{L}}_1\rho_0. \tag{1.50}$$

$\hat{\mathcal{L}}_1 = (\hat{P}+\hat{Q})\hat{\mathcal{L}}_1(\hat{P}+\hat{Q})$

$$\hat{\mathcal{L}}^{-1}\hat{Q} = (\hat{\mathcal{L}}_0 + \hat{\mathcal{L}}_1)^{-1}\hat{Q} = (\hat{\mathcal{L}}_0 + \hat{P}\hat{\mathcal{L}}_1\hat{P})^{-1} \tag{1.51}$$
$$\times\sum_{n=0}^{\infty}\big[-(\hat{P}\hat{\mathcal{L}}_1\hat{Q} + \hat{Q}\hat{\mathcal{L}}_1\hat{P} + \hat{Q}\hat{\mathcal{L}}_1\hat{Q})(\hat{\mathcal{L}}_0 + \hat{P}\hat{\mathcal{L}}_1\hat{P})^{-1}\big]^n\hat{Q}.$$

$$(\hat{\mathcal{L}}_0 + \hat{P}\hat{\mathcal{L}}_1\hat{P})^{-1}\hat{P} = (\hat{P}\hat{\mathcal{L}}_1\hat{P})^{-1}\hat{P} \sim \mathcal{O}(1/\epsilon) \tag{1.52}$$
$$(\hat{\mathcal{L}}_0 + \hat{P}\hat{\mathcal{L}}_1\hat{P})^{-1}\hat{Q} = (\hat{Q}\hat{\mathcal{L}}_0\hat{Q})^{-1}\hat{Q} \sim \mathcal{O}(1)$$

$\hat{P}\hat{\mathcal{L}}_0 = \hat{\mathcal{L}}_0\hat{P} = 0.$
$(\hat{P}\hat{\mathcal{L}}_1\hat{P})^{-1}$ and $(\hat{Q}\hat{\mathcal{L}}_0\hat{Q})^{-1}$ in

$$\delta\rho \approx \delta\rho_{1,\parallel} + \delta\rho_{1,\perp} + \mathcal{O}(\epsilon^2),$$
$$\delta\rho_{1,\parallel} = (\hat{P}\hat{\mathcal{L}}_1\hat{P})^{-1}\ \hat{P}\hat{\mathcal{L}}_1\hat{Q}\ \hat{\mathcal{L}}_0^{-1}\ \hat{Q}\hat{\mathcal{L}}_1\rho_0, \tag{1.53}$$
$$\delta\rho_{1,\perp} = -\hat{\mathcal{L}}_0^{-1}\ \hat{Q}\hat{\mathcal{L}}_1\rho_0. \tag{1.54}$$

$\hat{Q}(\hat{Q}\hat{\mathcal{L}}_0\hat{Q})^{-1}\hat{Q} = \hat{Q}\hat{\mathcal{L}}_0^{-1}\hat{Q},$

$$(\hat{P}\hat{\mathcal{L}}_1\hat{P})^{-1}\hat{P}X = -\sum_{pr}\frac{\partial\rho_0}{\partial\lambda_p}(M^{-1})_{pr}\ \mathrm{Tr}[C_r X], \tag{1.55}$$

$M_{pr} = -\mathrm{Tr}[C_p\,\hat{\mathcal{L}}_1(\partial\rho_0/\partial\lambda_r)],$

$$\langle C_i\rangle_1 = \mathrm{Tr}\left[C_i(\hat{P}\hat{\mathcal{L}}_1\hat{P})^{-1}\hat{P}\hat{\mathcal{L}}_1\hat{Q}\hat{\mathcal{L}}_0^{-1}\hat{Q}\hat{\mathcal{L}}_1\rho_0\right] \tag{1.56}$$
$$= \sum_{jk}\chi_{ij}\,(M^{-1})_{jk}\,\mathrm{Tr}\big[C_k\hat{\mathcal{L}}_1\hat{Q}\hat{\mathcal{L}}_0^{-1}\hat{Q}\hat{\mathcal{L}}_1\rho_0\big] \tag{1.57}$$

$(\hat{P}\hat{\mathcal{L}}_1\hat{P})^{-1} \sim 1/\epsilon.$

Missing conservation laws

$$\rho_0^{[t]} = \frac{\exp\left[-\sum_i \lambda_i^{[t]} C_i^{[t]}\right]}{\mathrm{Tr}[e^{-\sum_i \lambda_i^{[t]} C_i^{[t]}}]} \tag{1.58}$$

$\chi_{ij}^{[mm]} = \langle C_i^{[m]} C_j^{[m]} \rangle_{0,\mathrm{c}}$
$\chi_{ij}^{[mt]} = \langle C_i^{[m]} C_j^{[t]} \rangle_{0,\mathrm{c}}$,

$$\hat{P}_m\, X = -\sum_{i,j} \frac{\partial \rho_0}{\partial \lambda_i^{[m]}}\Big|_{\rho_0^{[t]}} ((\chi^{[mm]})^{-1})_{ij}\ \mathrm{Tr}[C_j^{[m]} X] \tag{1.59}$$

$(\partial\rho_0/\partial\lambda_i^{[m]})\big|_{\rho_0^{[t]}} = -(C_i^{[m]} - \langle C_i^{[m]}\rangle_0)\rho_0$.
$\hat{P} = \hat{P}_t + \hat{P}_m$
$\delta\lambda_k = \lambda_k - \lambda_k^{[t]}$

$$\begin{aligned} \rho_0 &= \rho_0^{[t]} + \delta\rho_0, \\ \delta\rho_0 &= -\rho_0^{[t]} \sum_k \delta\lambda_k \bar{C}_k,\ \bar{C}_k = C_k - \langle C_k\rangle_0 \end{aligned} \tag{1.60}$$

$\boldsymbol{\delta\lambda} = A^{-1}\boldsymbol{a}$

$$\begin{pmatrix} \boldsymbol{\delta\lambda}^{[t]} \\ \boldsymbol{\delta\lambda}^{[m]} \end{pmatrix} = \begin{pmatrix} A^{[tt]} & A^{[tm]} \\ A^{[mt]} & A^{[mm]} \end{pmatrix}^{-1} \begin{pmatrix} 0 \\ \boldsymbol{a}^{[m]} \end{pmatrix} \tag{1.61}$$

$$\begin{aligned} (\boldsymbol{a}^{[m]})_i &= \mathrm{Tr}[C_i^{[m]} \hat{\mathcal{L}}_1 \rho_0^{[t]}] = \langle \dot{C}_i^{[m]} \rangle_0 \\ A_{ij}^{[IJ]} &= \mathrm{Tr}[C_i^{[I]} \hat{\mathcal{L}}_1 (\bar{C}_j^{[J]} \rho_0^{[t]})] = \langle \dot{C}_i^{[I]} \bar{C}_j^{[J]} \rangle_{0,\mathrm{c}} \end{aligned}$$

$$\begin{aligned} \langle \delta C_i^{[t]} \rangle_0 &= -\left(\chi^{[tt]} \big(A^{-1}\big)^{[tm]}\ \boldsymbol{a}^{[m]}\right)_i \\ &\approx \left(\chi^{[tt]} \big(A^{[tt]}\big)^{-1} A^{[tm]} \big(A^{[mm]}\big)^{-1}\ \boldsymbol{a}^{[m]}\right)_i \end{aligned} \tag{1.62}$$

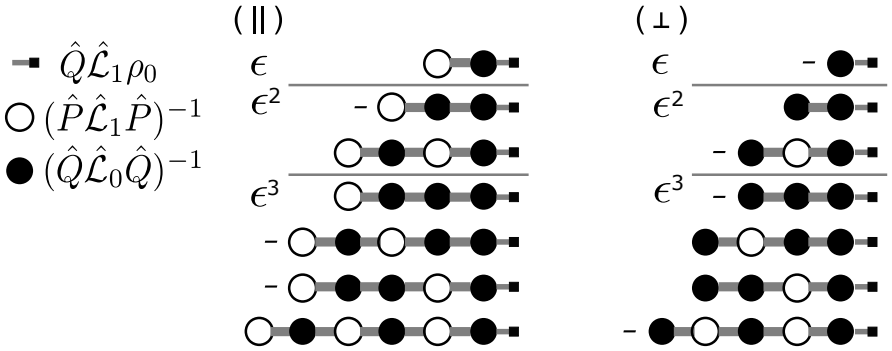

Figure 1.7: Diagrammatic depiction of the structure of corrections to the zeroth order density matrix ρ_0. One draws all possible combinations of open and filled circles starting to the right with a filled circle connected to a small square representing ρ_0. Then one eliminates all diagrams with a direct connection of two open circles. The order of the diagram is given by the number of filled circles, the sign by the total number of lines. The number of terms to order ϵ^n is given by 2^n. Note that the corrections to order n in the perpendicular and parallel sector are simply related by the relation $\delta\rho_{n,\|} = -(\hat{P}\hat{\mathcal{L}}_1\hat{P})^{-1}(\hat{P}\hat{\mathcal{L}}_1\hat{Q})\,\delta\rho_{n,\perp}$.

$$\langle \delta C_i^{[t]} \rangle_0 = -\mathrm{Tr}\left[C_i^{[t]} \hat{P}_t \left(\hat{P}\hat{\mathcal{L}}_1\hat{P}\right)^{-1} \hat{P}_m \hat{\mathcal{L}}_1 \rho_0^{[t]} \right] \tag{1.63}$$
$$\approx \mathrm{Tr}\left[C_i^{[t]} (\hat{P}_t\hat{\mathcal{L}}_1\hat{P}_t)^{-1} (\hat{P}_t\hat{\mathcal{L}}_1\hat{P}_m)(\hat{P}_m\hat{\mathcal{L}}_1\hat{P}_m)^{-1} \hat{P}_m\hat{\mathcal{L}}_1\rho_0^{[t]} \right]$$

$$\hat{Q}_t(\hat{Q}_t\hat{\mathcal{L}}_0\hat{Q}_t)^{-1}\hat{Q}_t = -\frac{\hat{P}_m}{\eta} + O(\eta^0) \tag{1.64}$$

$$\langle \delta C_i^{[t]} \rangle \approx \tag{1.65}$$
$$-\mathrm{Tr}\left[C_i^{[t]} (\hat{P}_t\hat{\mathcal{L}}_1\hat{P}_t)^{-1} (\hat{P}_t\hat{\mathcal{L}}_1\hat{P}_m) \frac{1}{\eta} \hat{P}_m\hat{\mathcal{L}}_1\rho_0 \right] + O(\eta^0)$$

Unitary driving, $\hat{P}\hat{\mathcal{L}}_1\hat{P} = 0$

For $\hat{P}\hat{\mathcal{L}}_1\hat{P} = 0$ the exact inverse of the Liouvillian in the $\hat{P}$ sector is given by $\hat{P}\hat{\mathcal{L}}^{-1}\hat{P} = -\hat{P}(\hat{P}\hat{\mathcal{L}}_1\hat{Q}(\hat{Q}\hat{\mathcal{L}}\hat{Q})^{-1}\hat{Q}\hat{\mathcal{L}}_1\hat{P})^{-1}\hat{P}$,

$$\hat{P}\hat{\mathcal{L}}^{-1}\hat{P} = \hat{P}(\hat{P}\hat{\mathcal{L}}_2\hat{P})^{-1}\hat{P} + \mathcal{O}(\epsilon^{-1}) \tag{1.66}$$

$$\hat{\mathcal{L}}_2 = -\hat{\mathcal{L}}_1\hat{Q}\left(\hat{Q}\hat{\mathcal{L}}_0\hat{Q}\right)^{-1}\hat{Q}\hat{\mathcal{L}}_1. \tag{1.67}$$

$\hat{P}\hat{\mathcal{L}}_2\hat{P} \propto \epsilon^2$

$\mathrm{Tr}[C_i\hat{\mathcal{L}}_2\rho_0] = 0$,

$$\hat{P}\hat{\mathcal{L}}_2\rho_0 = 0. \tag{1.68}$$

$$(\hat{\mathcal{L}}_0 + \hat{\mathcal{L}}_1)^{-1} = \left((\hat{\mathcal{L}}_0 + \hat{P}\hat{\mathcal{L}}_2\hat{P}) + (\hat{\mathcal{L}}_1 - \hat{P}\hat{\mathcal{L}}_2\hat{P})\right)^{-1} \tag{1.69}$$

Example: Interacting Fermions with particle-gain and loss

Lindblad dynamics in a small system

$$H_0 = \sum_{n=1}^{L} e_n c_n^\dagger c_n + U \sum_{n_1>n_2, n_3<n_4} c_{n_1}^\dagger c_{n_2}^\dagger c_{n_3} c_{n_4} \tag{1.70}$$

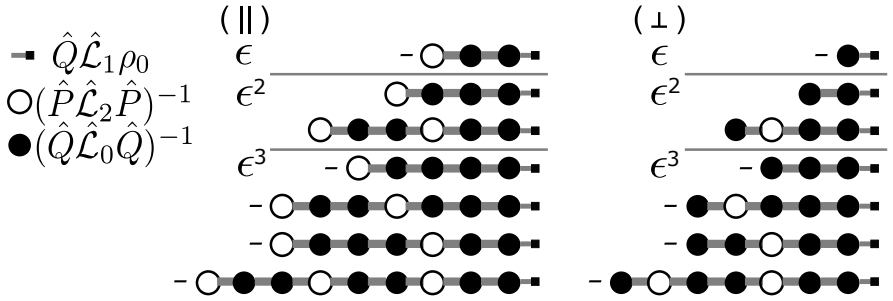

Figure 1.8: Diagrammatic depiction of the corrections $\delta\rho$ to the zeroth order density matrix ρ_0 for cases where $\hat{P}\hat{\mathcal{L}}_1\hat{P} = 0$ (unitary driving). One first draws all possible combinations of open and filled circles starting to the right with a filled circle connected to ρ_0 (small square). Then one eliminates all diagrams with neighboring open circles, all with the combination open-filled-open, and finally also the combination open-filled-ρ_0 (small square). The order is given by the number of filled minus the number of open circles, the sign by the total number of circles. The number of terms to order ϵ^n is 2^n. Some diagrams do, however, vanish for monochromatic perturbations, see appendix **??**.

$e_n = n/L$.
$L_n^g = c_n^\dagger$ and $L_n^l = c_n$

$$\hat{\mathcal{L}}_1 = \epsilon(\hat{D}_g + D_l) \tag{1.71}$$
$$\hat{D}_g = \sum g_n \left(L_n^g \rho L_n^{g\,\dagger} - \frac{1}{2}\{L_n^{g\,\dagger} L_n^g, \rho\} \right)$$
$$\hat{D}_l = \sum l_n \left(L_n^l \rho L_n^{l\,\dagger} - \frac{1}{2}\{L_n^{l\,\dagger} L_n^l, \rho\} \right)$$

$$g_n = \frac{1}{4}, \quad l_n = e_n \tag{1.72}$$

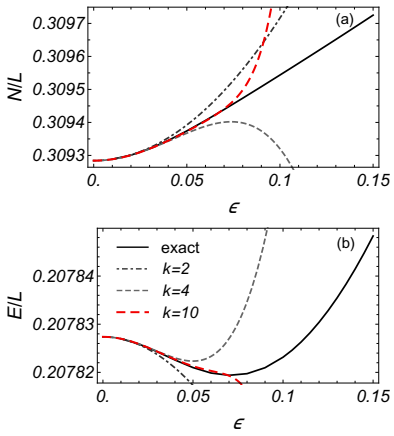

Figure 1.9: (Color online) Expectation values of (a) particle and (b) energy density as a function of perturbation strength ϵ, calculated from the exact steady state density matrix (solid line) or using our perturbation theory up to k-th order in ϵ on systems size $L = 4$, and interaction strength $U = 0.3$.

Boltzmann dynamics

$$\frac{df_e}{dt} = M[f]_e + \epsilon\, D[f]_e \tag{1.73}$$
$$M[f]_e = \int_0^1 de_1 de_2 de_3\, \delta(e + e_1 - e_2 - e_3) \times (\bar{f}_e \bar{f}_{e_1} f_{e_2} f_{e_3} - f_e f_{e_1} \bar{f}_{e_2} \bar{f}_{e_3})$$
$$= \frac{1}{L^2} \sum_{i,j,l} (\bar{f}_e \bar{f}_{e_i} f_{e_j} f_{e_l} - f_e f_{e_i} \bar{f}_{e_j} \bar{f}_{e_l})\ \delta_{e+e_i, e_j+e_l}$$
$$D[f]_e = -l_e f_e + g_e \bar{f}_e \tag{1.74}$$

$\bar{f}_e = (1 - f_e)$.

$$f_e(t \to \infty) = \sum_m \epsilon^m f_e^m. \tag{1.75}$$

$$f_e^0(\beta, \mu) = \frac{1}{1 + e^{\beta(e-\mu)}} \quad \leftrightarrow \quad \rho_0,$$
$$M[f^0(\beta, \mu)]_e = 0 \quad \leftrightarrow \quad \hat{\mathcal{L}}_0 \rho_0 = 0 \tag{1.76}$$

Table 1: Comparison of semi-classical open Boltzmann dynamics for level occupation function and quantum Liovillian formulation for density matrix

Boltzmann	Liouvillian
occupation function f_e	density matrix ρ
$\frac{df_e}{dt} = M[f]_e + \epsilon\, D[f]_e$	$\frac{d\rho}{dt} = \hat{\mathcal{L}}_0\rho + \hat{\mathcal{L}}_1\rho$
$f_e(t\to\infty) = f_e^0 + \delta f_e$	$\rho(t\to\infty) = \rho_0 + \delta\rho$
Fermi function: $f_e^0 = \frac{1}{1+e^{\beta(e-\mu)}}$	GGE: $\rho_0 = \frac{e^{-\lambda_i C_i}}{\mathrm{Tr}[e^{-\lambda_i C_i}]}$
conservation laws and scalar product	
$c_i(e)$ and $q_i^{\beta,\mu}$	C_i and $\partial\rho_0/\partial\lambda_i$
$\int de\, c_i(e) f_e$	$\mathrm{Tr}[C_i\rho] = \langle C_i\rangle$
$\chi_{ij}(\beta,\mu) = -\int de\, c_i(e)\, q_j^{\beta,\mu}(e)$	$\chi_{ij} = -\mathrm{Tr}[C_i \partial\rho_0/\partial\lambda_j]$
zeroth order perturbation theory	
$\int de\, c_i(e)\epsilon D[f^0]_e = 0$	$\mathrm{Tr}[C_i\hat{\mathcal{L}}_1\rho_0] = 0$
$\hat{P}\big[D[f^0]\big] = 0$	$\hat{P}(\hat{\mathcal{L}}_1\rho_0) = 0$
first order corrections	
$\boldsymbol{f}_\perp^1 = -(QM^{(0)}Q)^{-1}Q\boldsymbol{D}[\boldsymbol{f}^0]$	$\delta\rho_{1,\perp} = -(\hat{Q}\hat{\mathcal{L}}_0\hat{Q})^{-1}\ \hat{Q}\hat{\mathcal{L}}_1\rho_0$
$\boldsymbol{f}_\parallel^1 = (PD^{(1)}P)^{-1}PD^{(1)}Q\times$ $\times(QM^{(0)}Q)^{-1}Q\boldsymbol{D}[\boldsymbol{f}^0]$	$\delta\rho_{1,\parallel} = (\hat{P}\hat{\mathcal{L}}_1\hat{P})^{-1}\hat{P}\hat{\mathcal{L}}_1\hat{Q}\ \times$ $\times\hat{\mathcal{L}}_0^{-1}\hat{Q}\hat{\mathcal{L}}_1\rho_0$

Zeroth order—

$$\frac{1}{L}\frac{dE}{dt} \approx \epsilon \int de\; e\big(-l_e f_e^0 + g_e(1-f_e^0)\big) \stackrel{!}{=} 0$$
$$\frac{1}{L}\frac{dN}{dt} \approx \epsilon \int de\; \big(-l_e f_e^0 + g_e(1-f_e^0)\big) \stackrel{!}{=} 0 \tag{1.77}$$

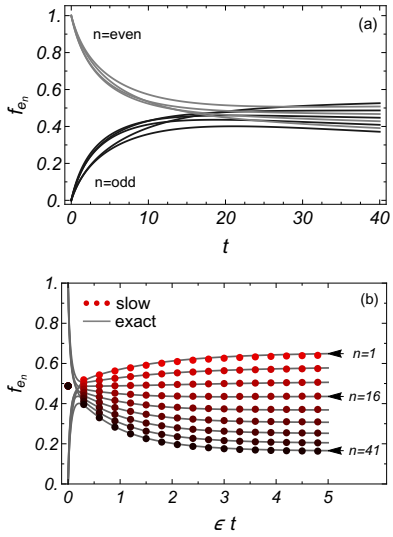

Figure 1.10: (Color online) Time evolution of the occupation function f_{e_n} shown for $n = 1, 6, 11, \ldots, 41$ ($L = 41$) and $\epsilon = 0.01$ starting from an initial state with $f_{e_n} = 1$ ($f_{e_n} = 0$) for states with even (odd) n, respectively. (a) On short time scales the system relaxes towards a state with $\beta \approx 0$ and equal occupation of all levels. (b) The time evolution toward the steady state occurs on a time scale set by $1/\epsilon$ and therefore the time axis has been rescaled by a factor ϵ. The points are obtained by solving the time evolution of the Lagrange parameters using Eq. (1.82) which then determine a Fermi distribution function. The comparison with the exact solution of the Boltzmann equation (lines) shows that this allows for a quantitative description of the slow dynamics for small ϵ.

Projection operator —

$$q_1^{\beta,\mu}(e) = \frac{\partial f_e^0}{\partial \beta}, \quad q_2^{\beta,\mu}(e) = \frac{\partial f_e^0}{\partial(-\beta\mu)} \tag{1.78}$$

$$c_1(e) = e,\; c_2(e) = 1 \tag{1.79}$$

$$\hat{P}[X] = -\sum_{i,j=1}^{2} q_i^{\beta,\mu}(e)\; (\chi^{-1})_{ij} \int de\, (c_j(e)X(e)) \tag{1.80}$$
$$\chi_{ij}(\beta,\mu) = -\int de\, c_i(e)\, q_j^{\beta,\mu}(e).$$

$$\int de\, c_i(e) D[f^0]_e = 0 \quad \leftrightarrow \quad \mathrm{Tr}[C_i \hat{\mathcal{L}}_1 \rho_0] = 0$$

$$\hat{P}\big[D[f^0]\big] = 0 \quad \leftrightarrow \quad \hat{P}(\hat{\mathcal{L}}_1 \rho_0) = 0.$$

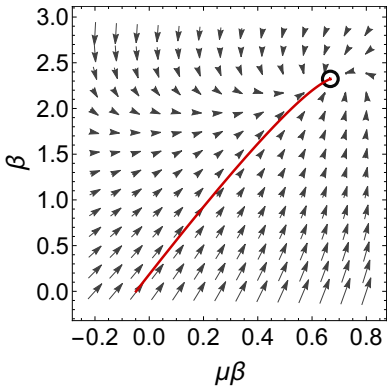

Figure 1.11: (Color online) Force fields calculated using Eq. (1.81) shown for $L = 41$. The force fields determine the time evolution of the Lagrange parameters according to Eq. (1.82). The red solid line shows the trajectory for the initial conditions used in Fig. 1.10, where a comparision to the exact solution of the Boltzmann equation is shown. The unique stationary state is indicated by a black circle.

Relaxation towards the steady state —

$$F_i(\beta,\mu) = -\left(\chi^{-1}\right)_{ij} \int de\, c_j(e)\, \epsilon D[f^0]_e \tag{1.81}$$

$$\frac{d\beta}{dt}(t) = F_1(t), \quad \frac{d(-\beta\mu)}{dt}(t) = F_2(t), \tag{1.82}$$

Perturbation theory for the steady state —
$f_e = f_e^0 + \epsilon f_e^1$

$$\begin{aligned} 0 &= \epsilon(M^{(0)} + \epsilon D^{(1)})[f^1] + \epsilon D[f^0] \\ \Leftrightarrow f^1 &= -(M^{(0)} + \epsilon D^{(1)})^{-1} D[f^0] \end{aligned} \tag{1.83}$$

$$\begin{aligned} M[f]_{e_n} &\approx \epsilon \sum_{n'} M^{(0)}_{n,n'} f^1_{e_{n'}} \\ (-l_{e_n} f_{e_n} + g_{e_n} \bar{f}_{e_n}) &\approx D[f^0]_{e_n} + \epsilon \sum_{n'} D^{(1)}_{n,n'} f^1_{e'_n}. \end{aligned} \tag{1.84}$$

$$\begin{aligned} \boldsymbol{f}^1 &= \boldsymbol{f}^1_{\parallel} + \boldsymbol{f}^1_{\perp}, \\ \boldsymbol{f}^1_{\perp} &= -(QM^{(0)}Q)^{-1}\ \boldsymbol{D}[\boldsymbol{f}^0] \\ \boldsymbol{f}^1_{\parallel} &= (PD^{(1)}P)^{-1}\ PD^{(1)}Q\ (QM^{(0)}Q)^{-1}\ \boldsymbol{D}[\boldsymbol{f}^0], \end{aligned} \tag{1.85}$$

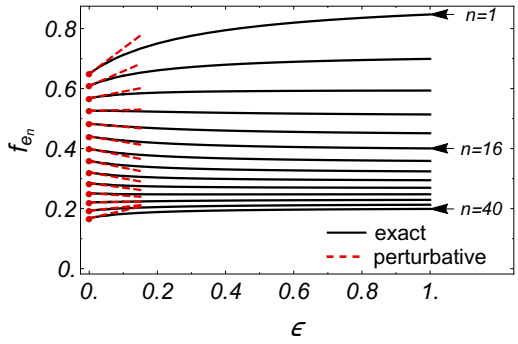

Figure 1.12: (Color online) Level occupation f_{e_n} as a function of perturbation strength ϵ. Solid lines are obtained from the exact calculation using Boltzmann equation, Eq. (1.73), while dashed lines are obtained from our perturbative approach, including zeroth and first order in ϵ. Only every third n is shown for system with $L = 41$ single-particle states.

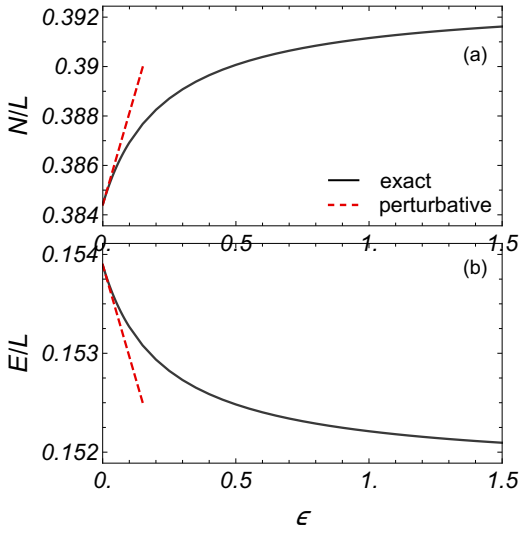

Figure 1.13: (Color online) (a) Particle and (b) energy density as a function of perturbation strength ϵ. The dashed line shows the result of perturbation theory, including zeroth and first order in ϵ.

1.3 Well-known applications, experiments

1.3.1 Stable Quantum-Correlated Many Body States through Engineered Dissipation by Google Collaboration

Theory

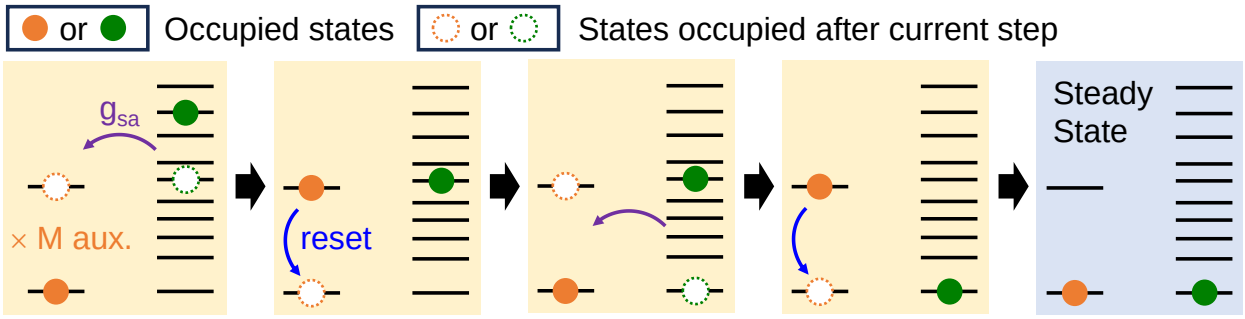

Figure 1.14: Dissipative cooling of a many-body system (green dot) to its ground state via a reservoir comprising M auxiliary two-level systems (orange dot), schematically illustrated as a sequence of steps.

$$\hat{H}_{\mathrm{TFIM}} = -g\sum_{j=1}^{L}\hat{Z}_j + J\sum_{j=1}^{L-1}\hat{X}_j\hat{X}_{j+1} \tag{1.86}$$

$$\hat{U} = e^{-\frac{i\pi J}{2}\sum_{j=1}^{L-1}\hat{X}_j\hat{X}_{j+1}}e^{\frac{i\pi g}{2}\sum_{j=1}^{L}\hat{Z}_j}. \tag{1.87}$$

$$\langle\hat{C}_{jk}\rangle = \langle\hat{Y}_j\hat{P}_{j+1,k-1}\hat{Y}_k\rangle, \tag{1.88}$$

$\hat{P}_{j+1,k-1} = \prod_{n=j+1}^{k-1}\hat{Z}_n.$

$$\mathrm{MI} = S_{\mathrm{A}}^{(2)} + S_{\mathrm{B}}^{(2)} - S_{\mathrm{AB}}^{(2)}, \tag{1.89}$$

$S^{(2)} = -\log_2 \mathrm{Tr}\rho^2$

Supplementary Materials for "Stable Quantum-Correlated Many Body States through Engineered Dissipation"

Experimental details and additional data

CPHASE and fSim gates

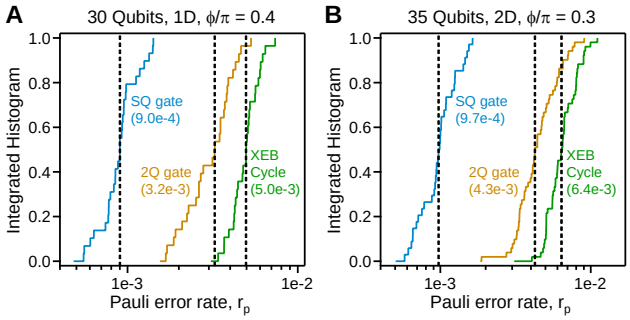

Figure 1.19: Single-qubit and CPHASE gate fidelities. (A) Integrated histograms of Pauli error rates r_{p} associated with single-qubit $\sqrt{X}$ and $\sqrt{Y}$ rotations (blue), two-qubit CPHASE gate with $\phi/\pi = 0.4$ (brown) and an XEB cycle (green). Median value of each histogram is listed within the figure and also indicated with a vertical dashed line. The results are obtained with a 1D chain of 30 qubits and gates executed in parallel. (B) Same as panel **a** but with $\phi/\pi = 0.3$ and 35 qubits in 2D. Gates are also executed in parallel.

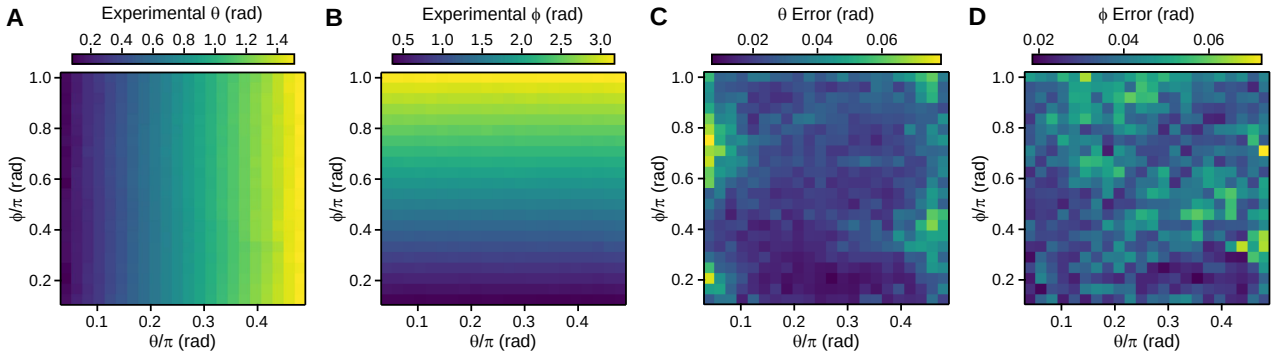

Figure 1.20: Continuously tunable fSim gates. (A) The experimentally measured values of θ as a function of target θ and ϕ, averaged over 25 qubit pairs in a chain of 26 qubits. (B) Same as panel A but with experimentally measured values of ϕ plotted. (C) Root-mean-squared differences between target and measured values of θ, averaged over all 25 qubit pairs. (D) Same as panel C but with the error in ϕ shown.

Stabilization of single-qubit states

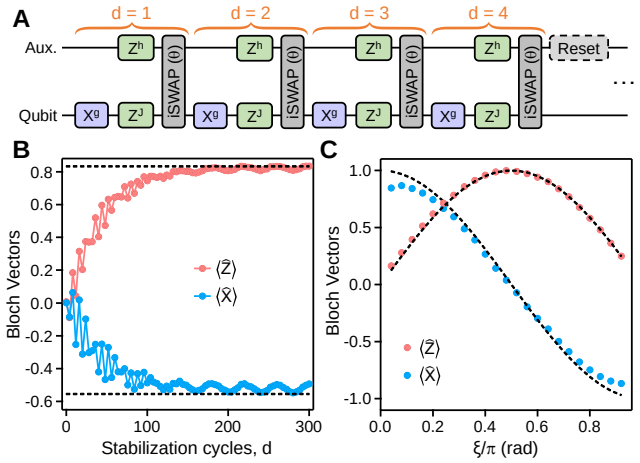

Figure 1.21: Stabilization of single-qubit states. (A) Circuit schematic for stabilizing states of a single qubit using a single auxiliary. (B) Bloch vectors of the single qubit, $\langle \hat{Z} \rangle$ and $\langle \hat{X} \rangle$, as a function of number of stabilization cycles d. Here $J = 0.18$, $g = -0.12$, $\theta = 0.09$ rad and $h = \sqrt{g^2 + J^2}$. Dashed lines indicate the Bloch vectors corresponding to an eigenstate of the single-qubit Hamiltonian $\hat{H}_{1q} = g\hat{X} + J\hat{Z}$. Readout errors have been corrected in the data via experimentally obtained readout errors. (C) Bloch vectors (averaged between $d = 280$ and $d = 300$) as a function of ξ, where $J = A \sin \xi$, $g = A \cos \xi$ and $A = \frac{0.3}{|\sin \xi| + |\cos \xi|}$. $\theta = 0.09$ rad in this plot. Dashed lines indicate the Bloch vectors corresponding to an eigenstate of the single-qubit Hamiltonian at each ξ.

Circuit optimization and comparison with quantum trajectory simulations

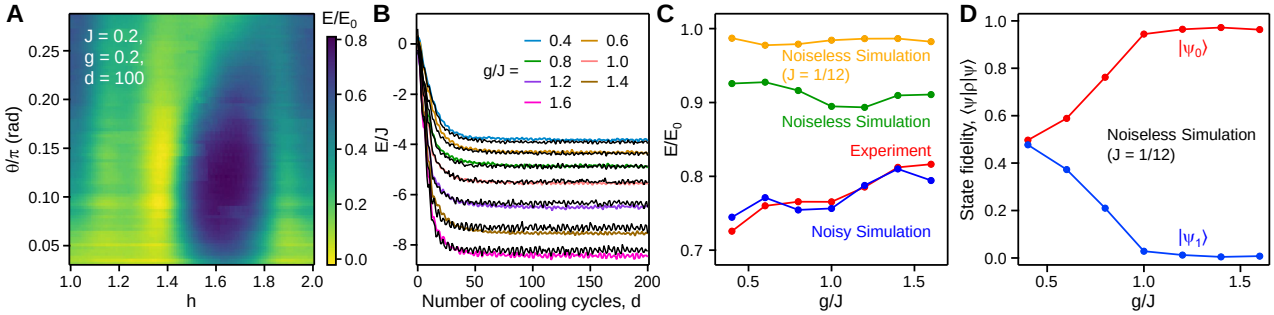

Figure 1.22: Circuit parameter optimization and comparison with quantum trajectory simulations. (A) Experimentally measured ratio between the energy E at $d = 100$ and the ground state energy E_0, as a function of gate parameters θ and h (see Fig. 2 of the main text). $L = 6$ in this plot. (B) Experimentally obtained (colored lines) and numerically simulated (black dashed lines) energies E of the 6-site TFIM as a function of d and for different values of g/J. (C) Steady state energy ratio E/E_0 as a function of g/J, obtained through experiment (red), noisy simulation (blue) and noiseless simulation (green). Noiseless simulation results using a smaller Trotter angle $J = 1/12$ are also shown, where the auxiliary reset is applied every 12 cycles. (D) Steady state fidelities with respect to the ground ($|\psi_0\rangle$) and excited ($|\psi_1\rangle$) states of the 6-site TFIM, computed from noiseless simulation and $J = 1/12$.

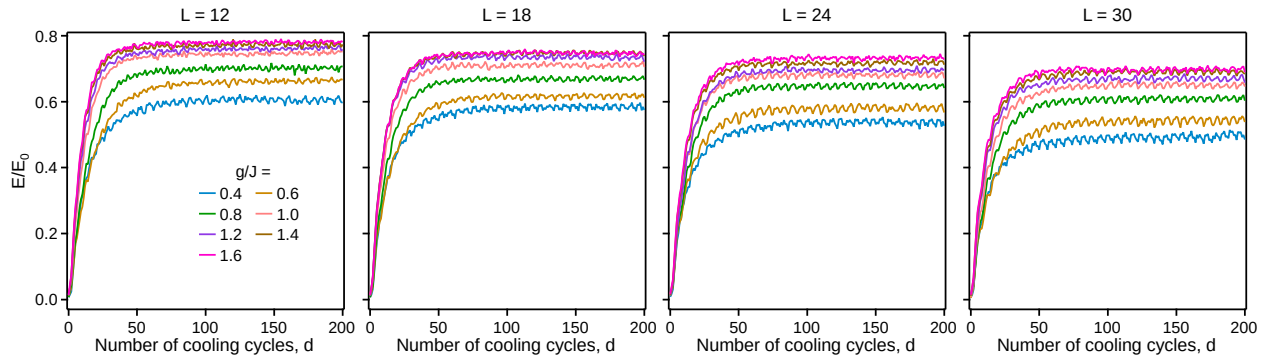

Figure 1.23: **Time-dependence of energy for large 1D TFIM chains.** Ratio between the measured energy $E = \langle \hat{H}_{\mathrm{TFIM}} \rangle$ and the ground state energy E_0 as a function of the number of cooling cycles d. Data are shown for chain lengths of $L = 12$, 18, 24 and 30.

Time-dependent energy for large 1D TFIM

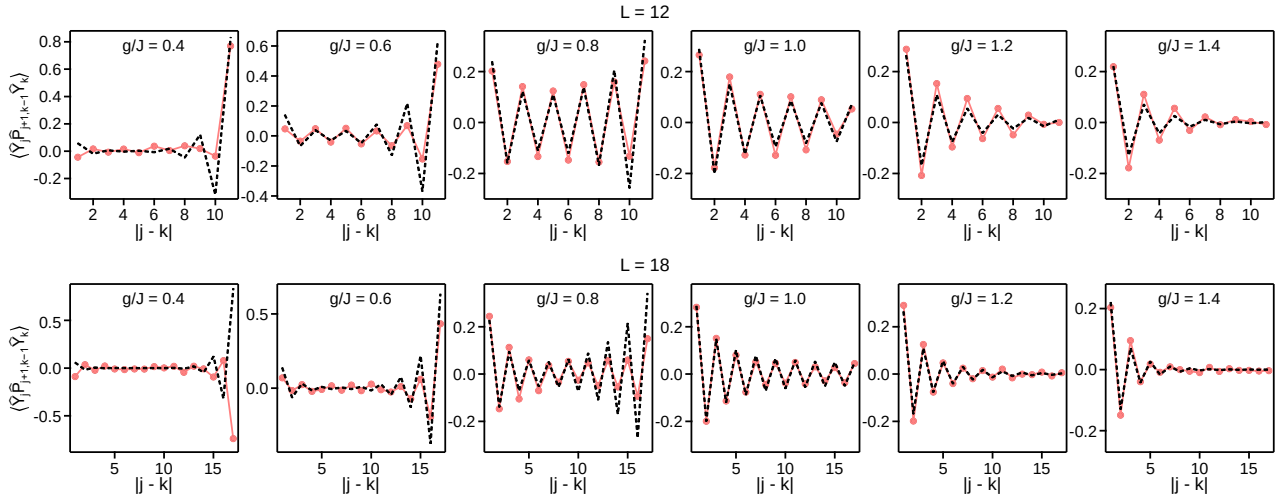

Figure 1.24: Detailed experimental data of quantum correlations $\langle \hat{Y}_j \hat{P}_{j+1,k-1} \hat{Y}_k \rangle$ for $L = 12$ and $L = 18$, across the quantum phase transition. Solid symbols are experimental results constructed from purified 1RDMs and dashed lines are exact ground state calculations.

Additional quantum correlation data

Rényi entropy and entanglement structure of the steady state

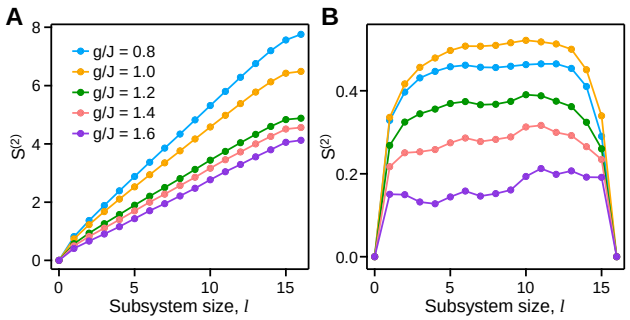

Figure 1.25: Rényi entropy and entanglement structure of the steady state. (A) Second-order Rényi entropy $S^{(2)}$ for different subsystem sizes l, measured on a 16-qubit chain after it has been dissipatively cooled with $d = 100$ cycles. For each subsystem size, the data are averaged over all possible chains of length l. To scramble the steady state, we use 30 sets of randomly chosen single-qubit Clifford gates and perform 3 million measurement shots on each set. (B) Error-mitigated values of $S^{(2)}$ as a function of l.

Mechanism of dissipative cooling

Eigenmodes of the Floquet transverse-field Ising model

$$\hat{U} = e^{-\frac{i\pi J}{2}\sum_{j=1}^{L-1}\hat{X}_j\hat{X}_{j+1}} e^{\frac{i\pi g}{2}\sum_{j=1}^{L}\hat{Z}_j}. \tag{1.90}$$

$$\hat{a}_{2j-1} = \left[\prod_{k=1}^{j-1}\hat{Z}_k\right]\hat{X}_j, \quad \hat{a}_{2j} = \left[\prod_{k=1}^{j-1}\hat{Z}_k\right]\hat{Y}_j. \tag{1.91}$$

$$\hat{a}_{2j-1} = \hat{c}_j^\dagger + \hat{c}_j, \quad \hat{a}_{2j} = i\left(\hat{c}_j^\dagger - \hat{c}_j\right).$$

$$\hat{Z}_j = -i\hat{a}_{2j-1}\hat{a}_{2j}, \quad \hat{X}_j\hat{X}_{j+1} = -i\hat{a}_{2j}\hat{a}_{2j+1}. \tag{1.92}$$

$$\hat{U}^\dagger\hat{a}_k\hat{U} = \sum_{l=1}^{2L} K_{kl}\hat{a}_l. \tag{1.93}$$

$$\hat{\eta} = \sum_{j=1}^{L}\psi_{2j-1}\hat{a}_{2j-1} + \psi_{2j}\hat{a}_{2j}. \tag{1.94}$$

$$\cos\phi_q = \cos(\pi J)\cos(\pi g) - \sin(\pi J)\sin(\pi g)\cos q. \tag{1.95}$$

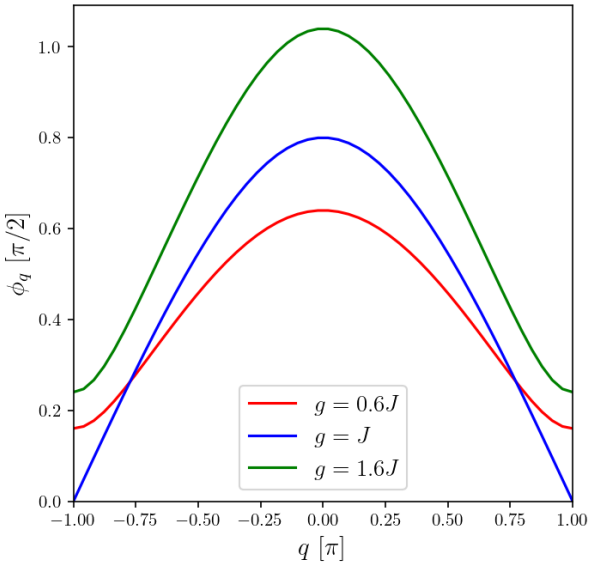

Figure 1.26: The quasienergy band spectrum ϕ_q defined in (20.10) as a function of the quasimomentum q, for $J = 0.2$, g within antiferromagnetic phase ($g = 0.6J$), at critical point ($g = J$) and within paramagnetic phase ($g = 1.6J$). At the critical point the band gap closes.

$$\begin{aligned} v'_{2j-1} &= -\sin(\pi J)\sin(\pi g)v_{2j-3} + \sin(\pi J)\cos(\pi g)v_{2j-2} + \cos(\pi J)\cos(\pi g)v_{2j-1} + \cos(\pi J)\sin(\pi g)v_{2j}, \\ v'_{2j} &= -\cos(\pi J)\sin(\pi g)v_{2j-1} + \cos(\pi J)\cos(\pi g)v_{2j} - \sin(\pi J)\cos(\pi g)v_{2j+1} - \sin(\pi J)\sin(\pi g)v_{2j+2}, \end{aligned} \tag{1.96}$$

$$v'_1 = \cos(\pi g)v_1 + \sin(\pi g)v_2, \tag{1.97}$$

$$v'_{2L} = -\sin(\pi g)v_{2L-1} + \cos(\pi g)v_{2L}. \tag{1.98}$$

$\underline{\psi}'^q = e^{-i\phi_q}\underline{\psi}^q$

$$\begin{pmatrix} v^q_{2j-1} \\ v^q_{2j} \end{pmatrix} = \frac{e^{iq(j-1)}}{\sqrt{L}} \begin{pmatrix} \chi^q_1 \\ \chi^q_2 \end{pmatrix}, \tag{1.99}$$

$$\begin{pmatrix} \cos(\pi J)\cos(\pi g) - \sin(\pi J)\sin(\pi g)e^{-iq} & \cos(\pi J)\sin(\pi g) + \sin(\pi J)\cos(\pi g)e^{-iq} \\ -\cos(\pi J)\sin(\pi g) - \sin(\pi J)\cos(\pi g)e^{iq} & \cos(\pi J)\cos(\pi g) - \sin(\pi J)\sin(\pi g)e^{iq} \end{pmatrix} \begin{pmatrix} \chi^q_1 \\ \chi^q_2 \end{pmatrix} = e^{-i\phi_q} \begin{pmatrix} \chi^q_1 \\ \chi^q_2 \end{pmatrix}. \tag{1.100}$$

$$\underline{n}(q) = \begin{pmatrix} \sin(2\mu_q)\cos\xi_q \\ \sin(2\mu_q)\sin\xi_q \\ \cos(2\mu_q) \end{pmatrix} \equiv \frac{1}{\sin(\phi_q)} \begin{pmatrix} \sin(\pi J)\cos(\pi g)\sin q \\ -\cos(\pi J)\sin(\pi g) - \sin(\pi J)\cos(\pi g)\cos q \\ -\sin(\pi J)\sin(\pi g)\sin q \end{pmatrix}, \tag{1.101}$$

$$\begin{pmatrix} \chi^q_1 \\ \chi^q_2 \end{pmatrix} = \begin{pmatrix} \cos\mu_q \\ e^{i\xi_q}\sin\mu_q \end{pmatrix}. \tag{1.102}$$

$$\begin{pmatrix} \psi^q_{2j-1} \\ \psi^q_{2j} \end{pmatrix} = \frac{1}{\sqrt{L}} \begin{pmatrix} e^{i\delta_q}\chi_1^{-q} & \chi^q_1 \\ e^{i\delta_q}\chi_2^{-q} & \chi^q_2 \end{pmatrix} \begin{pmatrix} e^{-iq(j-1)} \\ e^{iq(j-1)} \end{pmatrix}, \tag{1.103}$$

$$e^{i\delta_q} = \frac{-(e^{-i\phi_q} - \cos(\pi J)) + e^{i\xi_q}\sin(\pi g)\tan\mu_q}{(e^{-i\phi_q} - \cos(\pi J))\tan\mu_q + \sin(\pi g)e^{-i\xi_q}}. \tag{1.104}$$

$$e^{2iq(L-1)} = -\left[\frac{(e^{-i\phi_q} - \cos(\pi J)) - e^{i\xi_q}\tan\mu_q\sin(\pi g)}{(e^{i\phi_q} - \cos(\pi J))e^{i\xi_q}\tan\mu_q + \sin(\pi g)}\right]^2. \tag{1.105}$$

$$q_\alpha \sim \frac{\pi(\alpha - 1)}{L}, \quad \alpha \in (1, L). \tag{1.106}$$

Perturbation theory for Floquet evolution

$$\hat{\mathcal{U}} = \hat{U}_{\rm SA}\hat{U}_{\rm A}\hat{U}_{\rm S}, \tag{1.107}$$

$$\hat{U}_{\rm SA} = e^{i\theta\hat{K}}, \tag{1.108}$$

$$\hat{A}_I(s) = \hat{U}_0^{-s}\hat{A}\hat{U}_0^{s}, \tag{1.109}$$

$$\hat{\mathcal{U}}^M = \hat{U}_0\mathcal{T}\prod_{s=1}^{M} e^{i\theta\hat{K}_I(s)}, \tag{1.110}$$

$$\hat{U}_{\rm S}^{-M}\rho^{(n+1)}\hat{U}_{\rm S}^{M} = \rho^{(n)} - \theta^2\sum_{\substack{s_2=1\\ s_1<s_2}}^{M}{\rm Tr}_A[\hat{K}_I(s_2),[\hat{K}_I(s_1),\rho^{(n)}\otimes\rho^0_{\rm A}]] - \frac{\theta^2}{2}\sum_{s=1}^{M}{\rm Tr}_A[\hat{K}_I(s),[\hat{K}_I(s),\rho^{(n)}\otimes\rho^0_{\rm A}]]. \tag{1.111}$$

$$\rho^{(n)}_{\rm int} \equiv \hat{U}_{\rm S}^{-Mn}\rho^{(n)}\hat{U}_{\rm S}^{Mn}. \tag{1.112}$$

Application to the Floquet TFIM: secular approximation

$$\hat{U}_{\rm A} = e^{i\frac{\pi h}{2}\hat{Z}_a}, \quad \hat{K} = \frac{1}{2}\left(\hat{X}_a\hat{X}_1 + \hat{Y}_a\hat{Y}_1\right). \tag{1.113}$$

$$\hat{U}_{\rm S} = e^{-i\sum_k \phi_k\hat{\eta}_k^\dagger\hat{\eta}_k}, \quad \hat{U}_{\rm A} = e^{-i\pi h\hat{d}^\dagger\hat{d}}, \quad \hat{K} = \hat{d}^\dagger\hat{c}_1 + \hat{c}_1^\dagger\hat{d}, \tag{1.114}$$

$$\hat{c}_1 = \sum_k \alpha_k\hat{\eta}_k + \beta_k\hat{\eta}_k^\dagger, \quad \hat{c}_1^\dagger = \sum_k \alpha_k^*\hat{\eta}_k^\dagger + \beta_k^*\hat{\eta}_k. \tag{1.115}$$

$${\rm Tr}_A(\hat{d}^\dagger\hat{d}\rho_{\rm A}(0)) = 1, \quad {\rm Tr}_A(\hat{d}\hat{d}^\dagger\rho_{\rm A}(0)) = 0. \tag{1.116}$$

$$\hat{K}_I(s) = \sum_k \alpha_k e^{i(\pi h-\phi_k)s}\hat{d}^\dagger\hat{\eta}_k + \beta_k e^{i(\pi h+\phi_k)s}\hat{d}^\dagger\hat{\eta}_k^\dagger + {\rm h.c.}, \tag{1.117}$$

$$\frac{d\rho^{(n)}_{\rm int}}{dn} - i\left[\rho^{(n)}_{\rm int}, \Delta H_{\rm S}\right] =$$

$$+\sum_{k=1}^{L} W^+(q_k)\left(\eta_k^\dagger\rho_{\rm int}\eta_k - \frac{1}{2}\left\{\eta_k\eta_k^\dagger,\rho_{\rm int}\right\}\right) + W^-(q_k)\left(\eta_k\rho_{\rm int}\eta_k^\dagger - \frac{1}{2}\left\{\eta_k^\dagger\eta_k,\rho_{\rm int}\right\}\right), \tag{1.118}$$

$$W^\pm(q) \equiv 2\pi M\theta^2\ |\psi_1^q \pm i\psi_2^q|^{\,2}\delta_M(\phi_q \pm \pi h), \tag{1.119}$$

$$|\psi_1^q \pm i\psi_2^q|^2 = \frac{1}{L}f_q^\pm, \qquad f_q^\pm = 4\left|\cos(\mu_q)\cos\left(\frac{\delta_q}{2}\right) \mp \sin(\mu_q)\sin\left(\xi_q - \frac{\delta_q}{2}\right)\right|^2. \tag{1.120}$$

$$\Delta H_{\rm S} = \frac{M\theta^2}{L}\sum_{k=1}^{L}\Delta(q_k)\,\eta_k^\dagger\eta_k - \Delta_0$$

$$\Delta(q) = \sum_{\sigma=\pm} f_q^\sigma\mathcal{P}_M\left(\frac{1}{\phi_q + \sigma\pi h}\right), \qquad \Delta_0 = \frac{M\theta^2}{L}\sum_{\mu=1}^{L} f_q^+\mathcal{P}_M\left(\frac{1}{\mathcal{E}_\mu + \pi h}\right)$$

$$\delta_M(x) = \frac{1}{2\pi M}\frac{\sin\left(\frac{Mx}{2}\right)^2}{\sin\left(\frac{x}{2}\right)^2}, \qquad \mathcal{P}_M\left(\frac{1}{x}\right) = \frac{1}{M}\sum_{m=1}^{M}\sum_{l=1}^{m-1}\sin(xl)$$

$$n_k = \left\langle\eta_k^\dagger\eta_k\right\rangle = \left(1 + \frac{f_q^-}{f_q^+}\frac{\delta_M(\pi h-\phi_q)}{\delta_M(\pi h+\phi_q)}\right)^{-1} \tag{1.121}$$

1RDM of the Ising chain and purification

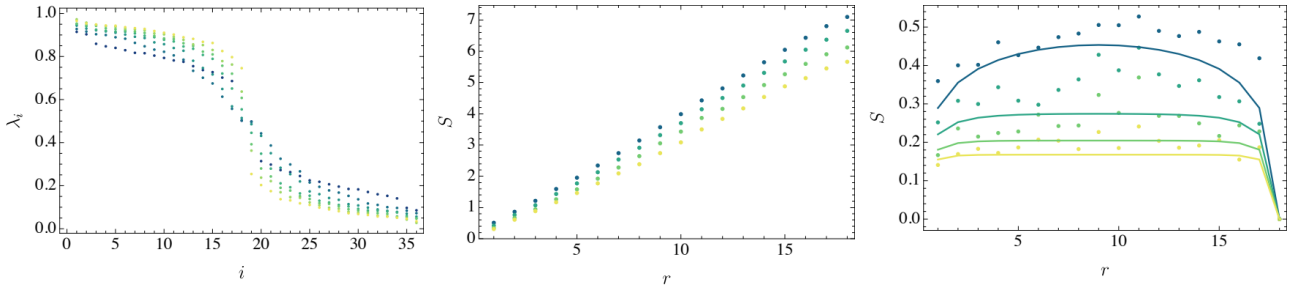

Figure 1.29: Left panel: Eigevalues of the 1RDM, D, in the NESS of the Kicked Ising model for $L = 18$ qubits. The parameters are $(g, J) = (0.08, 0.2)$ and $g = (0.6, 0.8, \ldots 1.6)J$ for $J = 0.25$. Lighter colours denote increasing g. Middle panel: The dependence of entanglement entropy for a quadratic fermionic system described by the experimental 1RDM, D. We only plot the parameters $g/J \geq 1$. Right panel: Same as before for the purified 1RDM, D_{pure}. Full lines correspond to the values for the exact vacuum of the Kicked Ising model, Eq. (20.5).

$$D = \frac{1}{2}\begin{pmatrix} D^{oo} & D^{oe} \\ D^{eo} & D^{ee}, \end{pmatrix}, \quad D^{oo}_{i,j} = \langle a_{2i-1}a_{2j-1}\rangle, \quad D^{oe}_{i,j} = \langle a_{2i-1}a_{2j}\rangle, \quad D^{eo}_{i,j} = \langle a_{2i}a_{2j-1}\rangle, \quad D^{ee}_{i,j} = \langle a_{2i}a_{2j}\rangle, \quad i \tag{1.122}$$

$$F_{ij} = \begin{pmatrix} F^{+-} & F^{--} \\ F^{++} & F^{-+}, \end{pmatrix}, \quad F^{+-}_{i,j} = \langle \eta_i^\dagger \eta_j\rangle, \quad F^{++}_{i,j} = \langle \eta_i^\dagger \eta_j^\dagger\rangle, \quad F^{-+}_{i,j} = \langle \eta_i \eta_j^\dagger\rangle, \quad F^{--}_{i,j} = \langle \eta_i \eta_j\rangle, \tag{1.123}$$

$$F^{+-}_{i,i} = \langle \eta_i^\dagger \eta_i\rangle.$$

$$\min |D - D_{pure}|_F, \quad \mathrm{tr} D_{pure} = L, D^2_{pure} = D_{pure}, \tag{1.124}$$

$$\mathrm{spec}(D) = \lambda_i, \quad i \in \{1, 2L\}, \quad \lambda_i \geq \lambda_{i+1}. \tag{1.125}$$

Comparison between dissipative and unitary state preparation protocols

$$G_n(\theta_n, \phi_n) = e^{i\frac{\phi_n}{2}\hat{Z}_{i_n}} e^{-i\frac{\theta_n}{2}\left(\hat{X}_{i_n}\hat{Y}_{i_{n+1}} - \hat{Y}_{i_n}\hat{X}_{i_{n+1}}\right)}, \qquad B = \hat{X}_L, \tag{1.126}$$

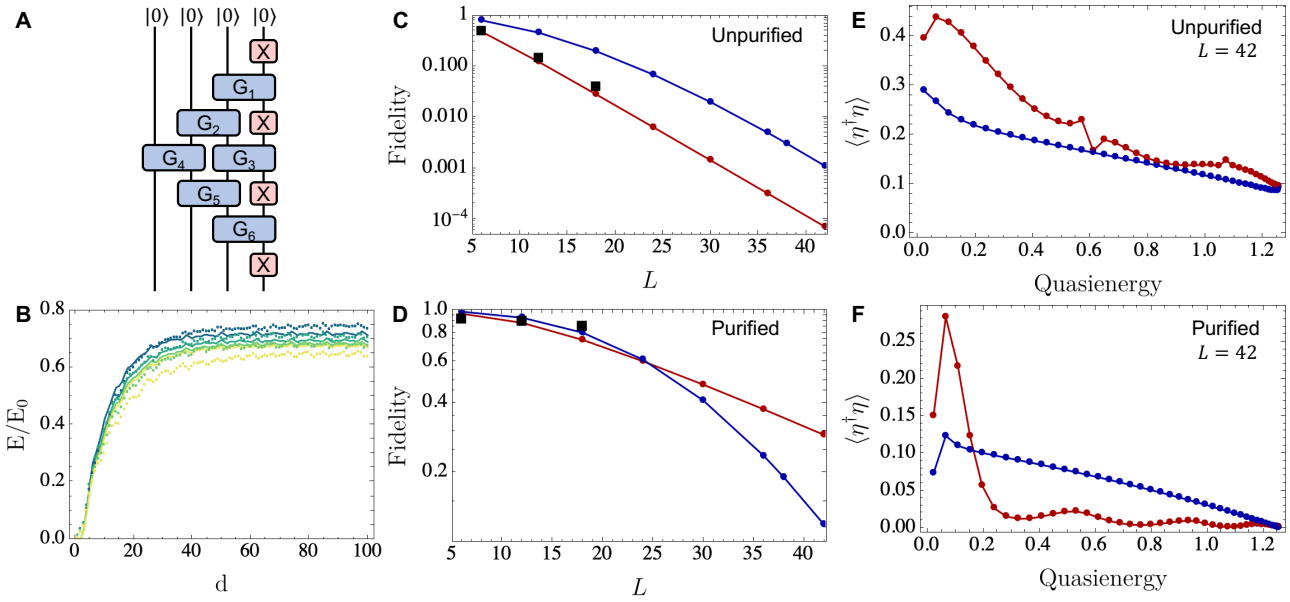

Figure 1.30: (A) Illustration of the state preparation protocol [62], for a system of $L = 4$ qubits. Every qubit is initialized in its ground state. (B) Comparison of energy convergence between experimental data (points) and simulations (lines) at the critical point ($g = J = 0.2$) of the Floquet TFIM (Eq. (20.5)). System sizes $L = \{12, 18, 24, 30\}$ are represented by blue to yellow colors. (C) Fidelity between the exact vacuum state of Floquet TFIM unitary $\hat{U}$ at the aforementioned critical point, and the states prepared by simulating the dissipative (red) and unitary (blue) protocols. Black squares denote the experimental values for $\{6, 12, 18\}$ qubits. (D) Same as (C), for the purified states according to the method described in Section 20.5. (E,F) Unpurified and purified quasiparticle occupations for the simulated protocols. We observe that the purified states generated by the dissipative protocol have considerably lower high-energy quasiparticle occupations.

Transport in Floquet XXZ under maximal pumping

Model and setup

$$H_{XXZ} = \sum_{i=1}^{L-1} h_i, \quad h_i = \theta \left(\sigma_i^+ \sigma_{i+1}^- + \text{h.c.}\right) + \phi n_i n_{i+1}, \tag{1.127}$$

$$U_{XXZ} = U_{even} U_{odd}, \qquad U_{even} = \prod_{i=1}^{N/2} \text{FSim}_{2i,2i+1}, \qquad U_{odd} = \prod_{i=1}^{N/2-2} \text{FSim}_{2i+1,2i+2}, \qquad . \tag{1.128}$$

$$\text{FSim}_{i,i+1}(\theta, \phi) = \exp\left(i h_i(\theta, \phi)\right). \tag{1.129}$$

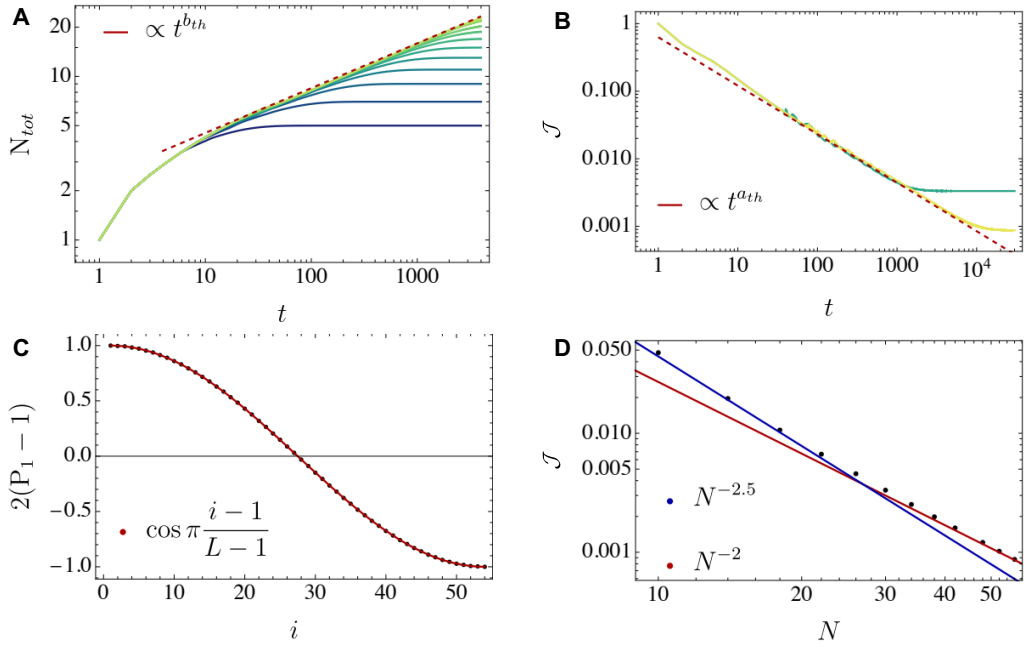

Figure 1.31: Numerical simulations of quantum transport in the boundary-driven Floquet XXZ chain at the isotropic point $\phi = 2\theta = \pi/2$, in the absence of external decoherence. The bond dimension of the MPDO is truncated to $\chi = 128$. (A) Time dependence of the total number of particles into the system $N_{tot} = \sum_{i=2}^{N-1} n_i$ for system sizes of $N = 10 - 56$ qubits (blue to yellow colors), as a function of the number of driving cycles. We find a power-law scaling law with an exponent $b_{th} \sim 0.2746$ which develops after an initial transient. (B) Pumping current as a function of time for $N = 30, 56$ qubits exhibits an exponent $a_{th} = -0.7178 \approx b_{th} - 1$. (C) A normalized local particle number in the NESS as a function of qubit position for $N = 56$. The cosine function is the strong driving limit prediction for the case of solvable boundaries, at the isotropic point of the XXZ Hamiltonian [45]. (D) NESS current scaling with the system size. We observe that for larger system sizes $\mathcal{J} \propto N^{-2}$ while for smaller sizes the exponent is slightly larger.

$$K^1_{1,i} = \frac{n_i + \sigma_i^+}{\sqrt{2}} \quad K^1_{2,i} = \frac{n_i - \sigma_i^+}{\sqrt{2}} \qquad K^0_{1,i} = \frac{1 - n_i + \sigma_i^-}{\sqrt{2}} \quad K^0_{2,i} = \frac{1 - n_i - \sigma_i^-}{\sqrt{2}}, \tag{1.130}$$

$$\sum_{l=1}^{2} K^1_{l,i}\rho(K^1_{l,i})^\dagger = |1_i\rangle\langle 1_i|\mathrm{tr}_i\rho \equiv \mathcal{K}^1_i(\rho), \qquad \sum_{l=1}^{2} K^0_{l,i}\rho(K^0_{l,i})^\dagger = |0_i\rangle\langle 0_i|\mathrm{tr}_i\rho \equiv \mathcal{K}^0_i(\rho), \tag{1.131}$$

$\sum_{l=1}^{2}(K^m_{l,i})^\dagger K^m_{l,i} = 1_{2\times 2}$.
$\mathcal{K}^{m_1 m_2} = \mathcal{K}^{m_1}_1 \otimes \mathcal{K}^{m_2}_2$.

$$U_B = \mathrm{iSWAP}_{(a,1),1}\mathrm{iSWAP}_{(a,2),L}, \qquad \mathrm{iSWAP}_{(a,i),j} = \mathrm{FSim}_{(a,i),j}\left(\frac{\pi}{2}, 0\right). \tag{1.132}$$

$$\rho(d+1) = U_{XXZ}U_B\mathcal{K}^{m_1 m_2}\left(\rho(d)\right)U_B^\dagger U_{XXZ}^\dagger. \tag{1.133}$$

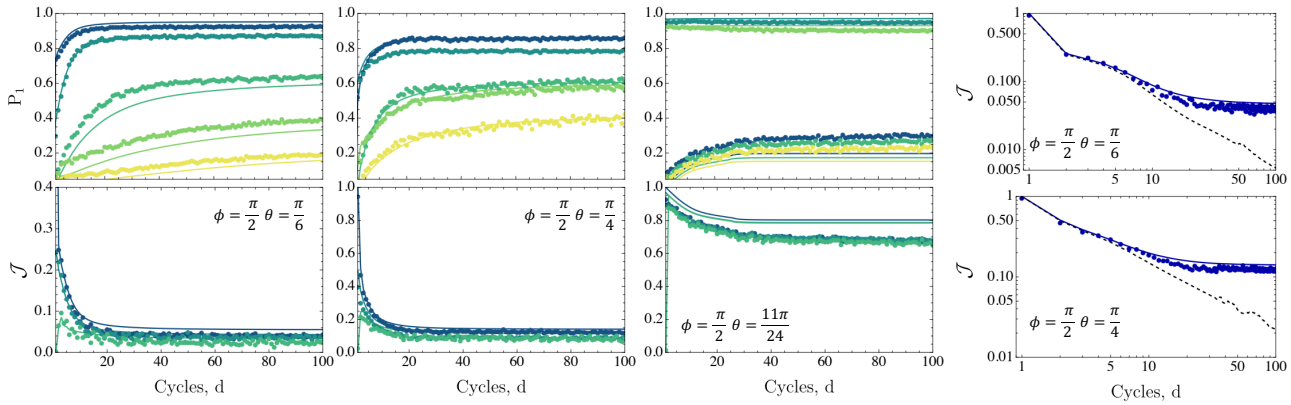

Figure 1.32: Left three columns: A comparison between the experimental data and tensor-network simulations in the presence of weak decoherence. For the numerical simulations we used MPDO parametrization of the density matrix with bond dimension $\chi = 500$. The top 3 plots show the particle numbers of the five system qubits closest to the left auxiliary, where color varies according to position, $1 \to 5$ corresponding to blue $\to$ yellow. The bottom plots illustrate the three local currents closest to the auxiliary site. The values of decoherence are $(\gamma_\theta, \gamma_\phi) = (0.01, 0.03), (0.016, 0.038), (0.016, 0.038)$ for the three values of parameters $\theta = \pi/6, \pi/4, 11\pi/24$, respectively. Right column: The decay of the pumping current $\mathcal{J} = \mathcal{J}_{in}$ as a function of time for different parameters. The points denote experimental data and the solid lines are the result of the simulation in the presence of the weak decoherence specified above. The dashed line shows the decoherence-free simulation.

$$\mathcal{D} = \bigotimes_{i=1}^{N} \mathcal{D}_i, \qquad \mathcal{D}_i \begin{pmatrix} \rho_{1,1} & \rho_{1,0} \\ \rho_{0,1} & \rho_{0,0} \end{pmatrix} = \begin{pmatrix} e^{-\gamma_\theta}\rho_{1,1} & e^{-\gamma_\phi-\gamma_\theta/2}\rho_{1,0} \\ e^{-\gamma_\phi-\gamma_\theta/2}\rho_{0,1} & (1-e^{-\gamma_\theta})\rho_{1,1} + \rho_{0,0} \end{pmatrix}, \tag{1.134}$$

Dynamics and steady state in the absence of decoherence at the isotropic point

$N_{tot} = \int_t dt\,(\mathcal{J}_{in}(t) - \mathcal{J}_{out}(t))$.

Effects of decoherence on the dynamics and the steady state

(??)

1.3.2 An Open-System Quantum Simulator with Trapped Ions by Barreiro et al.

1.4 Articles for potential applications

1.4.1 Collective Excitations and Nonequilibrium Phase Transition in Dissipative Fermionic Superfluids

Main ideas

Dissipative BCS theory.

$$H = \sum_{\boldsymbol{k}\sigma} \epsilon_{\boldsymbol{k}} c^\dagger_{\boldsymbol{k}\sigma} c_{\boldsymbol{k}\sigma} - U_{\mathrm{R}} \sum_i c^\dagger_{i\uparrow} c^\dagger_{i\downarrow} c_{i\downarrow} c_{i\uparrow}, \tag{1.135}$$

$$\frac{d\rho}{dt} = \mathcal{L}\rho = -i[H,\rho] - \frac{\gamma}{2}\sum_i (\{L_i^\dagger L_i, \rho\} - 2L_i \rho L_i^\dagger), \tag{1.136}$$

$L_i = c_{i\downarrow}c_{i\uparrow}$

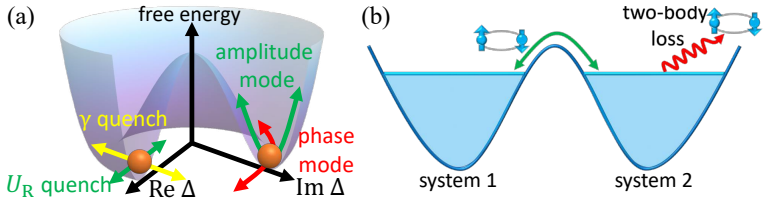

Figure 1.33: (a) Schematic illustration of the amplitude and phase modes in a Mexican-hat free-energy potential as a function of the complex order parameter Δ, when either the interaction $U_{\rm R}$ or the dissipation γ is suddenly switched on. A sudden quench of the interaction $U_{\rm R}$ and that of the dissipation γ kick Δ in a direction parallel and perpendicular to the radial direction, respectively. Note that a finite change of γ excites both the phase and amplitude modes. (b) Two superfluids coupled via a Josephson junction, where one superfluid (system 2) is subject to two-body loss.

$$Z = {\rm tr}\rho = \int \mathcal{D}[c_-, \bar{c}_-, c_+, \bar{c}_+]e^{iS} = 1, \tag{1.137}$$

with an action

$$S = \int_{-\infty}^{\infty} dt \Big[\sum_{\boldsymbol{k}\sigma} (\bar{c}_{\boldsymbol{k}\sigma+} i\partial_t c_{\boldsymbol{k}\sigma+} - \bar{c}_{\boldsymbol{k}\sigma-} i\partial_t c_{\boldsymbol{k}\sigma-}) - H_+ + H_- + \frac{i\gamma}{2} \sum_i (\bar{L}_{i+}L_{i+} + \bar{L}_{i-}L_{i-} - 2L_{i+}\bar{L}_{i-}) \Big], \tag{1.138}$$

$H_\alpha = \sum_{\boldsymbol{k}\sigma} \epsilon_{\boldsymbol{k}} \bar{c}_{\boldsymbol{k}\sigma\alpha} c_{\boldsymbol{k}\sigma\alpha} - U_{\rm R} \sum_i \bar{c}_{i\uparrow\alpha}\bar{c}_{i\downarrow\alpha}c_{i\downarrow\alpha}c_{i\uparrow\alpha}$, $L_{i\alpha} = c_{i\downarrow\alpha}c_{i\uparrow\alpha}$, and $\bar{L}_{i\alpha} = \bar{c}_{i\uparrow\alpha}\bar{c}_{i\downarrow\alpha}$ $(\alpha = +, -)$.

$$S = \int dt \Big\{ \sum_{\boldsymbol{k}} \Big[\bar{\psi}^t_{\boldsymbol{k}+} \begin{pmatrix} i\partial_t - \epsilon_{\boldsymbol{k}} & -\Delta \\ -\Delta^* & -i\partial_t + \epsilon_{\boldsymbol{k}} \end{pmatrix} \psi_{\boldsymbol{k}+} - \bar{\psi}^t_{\boldsymbol{k}-} \begin{pmatrix} i\partial_t - \epsilon_{\boldsymbol{k}} & -\Delta \\ -\Delta^* & -i\partial_t + \epsilon_{\boldsymbol{k}} \end{pmatrix} \psi_{\boldsymbol{k}-} \Big] \Big\}, \tag{1.139}$$

$\bar{\psi}_{\boldsymbol{k}\alpha} = (\bar{c}_{\boldsymbol{k}\uparrow\alpha}, \quad c_{-\boldsymbol{k}\downarrow\alpha})^t$ and $\psi_{\boldsymbol{k}\alpha} = (c_{\boldsymbol{k}\uparrow\alpha}, \quad \bar{c}_{-\boldsymbol{k}\downarrow\alpha})^t$ $(\alpha = +, -)$.

$$\Delta = -\frac{U}{N_0} \sum_{\boldsymbol{k}} {\rm tr}(c_{-\boldsymbol{k}\downarrow}c_{\boldsymbol{k}\uparrow}\rho) \equiv -\frac{U}{N_0} \sum_{\boldsymbol{k}} \langle c_{-\boldsymbol{k}\downarrow}c_{\boldsymbol{k}\uparrow}\rangle, \tag{1.140}$$

$U = U_R + i\gamma/2$

$$\frac{d\rho}{dt} = -i[H_{\rm eff}, \rho], \tag{1.141}$$

$$H_{\rm eff} = \sum_{\boldsymbol{k}} \Psi^\dagger_{\boldsymbol{k}} \begin{pmatrix} \epsilon_{\boldsymbol{k}} & \Delta \\ \Delta^* & -\epsilon_{\boldsymbol{k}} \end{pmatrix} \Psi_{\boldsymbol{k}}, \tag{1.142}$$

where $\Psi_{\boldsymbol{k}} = (c_{\boldsymbol{k}\uparrow}, \quad c^\dagger_{-\boldsymbol{k}\downarrow})^t$

by $\boldsymbol{\sigma}_{\boldsymbol{k}} = \frac{1}{2}\Psi^\dagger_{\boldsymbol{k}} \cdot \boldsymbol{\tau} \cdot \Psi_{\boldsymbol{k}}$ and $H_{\rm eff} = 2\sum_{\boldsymbol{k}} \boldsymbol{b}_{\boldsymbol{k}} \cdot \boldsymbol{\sigma}_{\boldsymbol{k}}$, where $\boldsymbol{\tau} = (\tau_x, \quad \tau_y, \quad \tau_z)$

$[\sigma^j_{\boldsymbol{k}}, \sigma^k_{\boldsymbol{k}}] = i\epsilon_{jkl}\sigma^l_{\boldsymbol{k}}$.

$$\frac{d\boldsymbol{\sigma}_{\boldsymbol{k}}}{dt} = 2\boldsymbol{b}_{\boldsymbol{k}} \times \boldsymbol{\sigma}_{\boldsymbol{k}}, \tag{1.143}$$

$$\boldsymbol{b}_{\boldsymbol{k}} = ({\rm Re}\Delta, \quad -{\rm Im}\Delta, \quad \epsilon_{\boldsymbol{k}}). \tag{1.144}$$

$$\Delta = |\Delta| e^{i\theta} = -\frac{U}{N_0} \sum_{\boldsymbol{k}} (\sigma^x_{\boldsymbol{k}} - i\sigma^y_{\boldsymbol{k}}). \tag{1.145}$$

$$\frac{1}{N_0}\frac{dN}{dt} = -\frac{2\gamma|\Delta|^2}{|U|^2}, \tag{1.146}$$

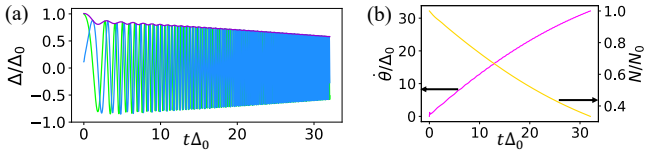

Figure 1.34: Dynamics of a superfluid after the atom loss with $\gamma = 2.81\Delta_0$ is switched on for the initial state with $U_{\rm R} = 12.2\Delta_0$ and bandwidth $W = 46.8\Delta_0$, where Δ_0 is the superfluid order parameter in the absence of the atom loss. (a) Real parts (light green), imaginary parts (blue), and the amplitude (violet) of the order parameter. (b) Angular velocity (pink) and particle number (yellow) plotted against time. The figures indicate a chirped phase rotation and an amplitude oscillation of Δ.

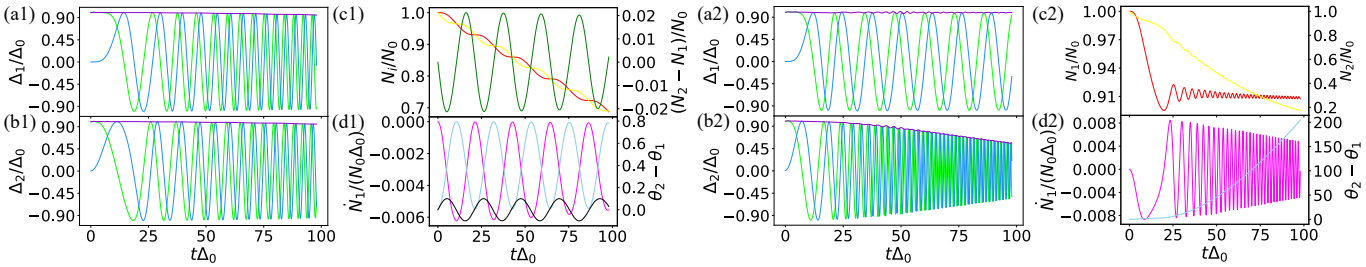

Figure 1.35: Dynamics of two fermionic superfluids after the switch-on of the atom loss γ and the tunnel coupling $V = 0.02\Delta_0$ with $U_{\rm R} = 3.06\Delta_0$ and bandwidth $W = 5.11\Delta_0$, where $\gamma = 0.03\Delta_0$ for (a1)-(d1) and $\gamma = 0.06\Delta_0$ for (a2)-(d2). (a), (b) Real parts (light green), imaginary parts (blue), and amplitudes (violet) of the order parameter for systems 1 and 2. (c) Particle numbers of system 1 (red) and system 2 (yellow), and their difference [green, in (c1)]. (d) Josephson current (pink) and phase difference (light blue) between the two systems. The black curve in (d1) shows an oscillation at frequency $\omega_{\rm L}$ for comparison.

Collective excitations: Leggett mode.

$$H_{\rm tun} = -\frac{V}{N_0} \sum_{\boldsymbol{k}\boldsymbol{k}'} (c^\dagger_{1\boldsymbol{k}\uparrow} c^\dagger_{1-\boldsymbol{k}\downarrow} c_{2-\boldsymbol{k}'\downarrow} c_{2\boldsymbol{k}'\uparrow} + \text{H.c.}), \tag{1.147}$$

$H_{\rm sys} = H_1 + H_2 + H_{\rm tun} = H'_1 + H'_2$, where $H_i \equiv \sum_{\boldsymbol{k}\sigma} \epsilon_{\boldsymbol{k}} c^\dagger_{i\boldsymbol{k}\sigma} c_{i\boldsymbol{k}\sigma} + \sum_{\boldsymbol{k}} (\Delta_i c^\dagger_{i\boldsymbol{k}\uparrow} c^\dagger_{i-\boldsymbol{k}\downarrow} + \text{H.c.})$ $(i = 1, 2)$

$H'_i \equiv H_i - V/N_0 \sum_{\boldsymbol{k}\boldsymbol{k}'} (\langle c_{j-\boldsymbol{k}'\downarrow} c_{j\boldsymbol{k}'\uparrow} \rangle c^\dagger_{i\boldsymbol{k}\uparrow} c^\dagger_{i-\boldsymbol{k}\downarrow} + \text{H.c.})$ $[(i,j) = (1,2)$ or $(2,1)]$.

$\boldsymbol{b}_{i\boldsymbol{k}} = (\text{Re}\Delta'_i, \quad -\text{Im}\Delta'_i, \quad \epsilon_{i\boldsymbol{k}})$,

$d\boldsymbol{\sigma}_{i\boldsymbol{k}}/dt = 2\boldsymbol{b}_{i\boldsymbol{k}} \times \boldsymbol{\sigma}_{i\boldsymbol{k}}$.

$\Delta_1 = |\Delta_1| e^{i\theta_1} = -\frac{U_{\rm R}}{N_0} \sum_{\boldsymbol{k}} (\sigma^x_{1\boldsymbol{k}} - i\sigma^y_{1\boldsymbol{k}})$

$\Delta_2 = |\Delta_2| e^{i\theta_2} = -\frac{U}{N_0} \sum_{\boldsymbol{k}} (\sigma^x_{2\boldsymbol{k}} - i\sigma^y_{2\boldsymbol{k}})$,

$\Delta'_i = \Delta_i - V/N_0 \sum_{\boldsymbol{k}} (\sigma^x_{j\boldsymbol{k}} - i\sigma^y_{j\boldsymbol{k}})$

$$\frac{1}{N_0}\frac{dN_1}{dt} = -\frac{4V|\Delta_1||\Delta_2|}{U_{\rm R}|U|} \sin(\theta_2 - \theta_1 + \delta), \tag{1.148}$$

$\delta = \tan^{-1}(-\gamma/2U_{\rm R})$

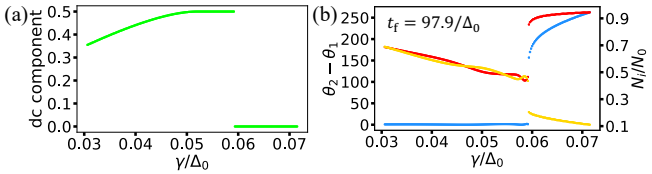

Figure 1.36: (a) DC component of the Josephson oscillation defined by $(\max_{0\le t\le t_{\rm f}}\{\sin(\theta_2(t)-\theta_1(t)+\delta)\}+\min_{0\le t\le t_{\rm f}}\{\sin(\theta_2(t)-\theta_1(t)+\delta)\})/2$ with $t_{\rm f}=97.9/\Delta_0$. (b) Phase difference between the two systems (blue) and particle numbers of system 1 (red) and system 2 (yellow) after a sufficiently long time ($t_{\rm f}=97.9/\Delta_0$). The parameters used are $U_{\rm R}=3.06\Delta_0$, $V=0.02\Delta_0$, and $W=5.11\Delta_0$.

$(\max_{0\le t\le t_{\rm f}}\{\sin(\theta_2(t)-\theta_1(t)+\delta)\}+\min_{0\le t\le t_{\rm f}}\{\sin(\theta_2(t)-\theta_1(t)+\delta)\})/2$

Conclusions.—We have investigated the loss-quench dynamics of fermionic superfluids, and have demonstrated that the dynamics exhibits amplitude and phase modes with chirped oscillations, the latter of which is a salient feature of a dissipative superfluid. To observe the chirped phase rotation, we have proposed a Josephson junction comprised of dissipative and nondissipative superfluids. We have shown that the relative-phase Leggett mode can be detected from the Josephson current for weak dissipation. Remarkably, when dissipation becomes strong, the superfluids exhibit the unique nonequilibrium phase transition triggered by particle loss. Our prediction can be tested with ultracold atomic systems of ^{6}Li [83, 84], for example, by introducing dissipation using photoassociation processes [50, 59]. It is of interest to explore how the dimensionality or confinement by a trap potential affects the dynamics and associated collective modes [15, 16, 17, 18].

1.5 Other Useful articles

1.5.1 Time-dependent GGEs in open quantum systems by Lange, Lenarčič, Rosch

Introduction

Model

$$H_0 = J\sum_j \boldsymbol{S}_j\cdot\boldsymbol{S}_{j+1} \tag{1.149}$$

$$\partial_t\rho = (\hat{\mathcal{L}}_0+\hat{\mathcal{L}}_1)\,\rho \tag{1.150}$$
$$\hat{\mathcal{L}}_0\rho = -i[H_0,\rho],\qquad \hat{\mathcal{L}}_1\rho = \epsilon\left(\gamma\hat{\mathcal{D}}^{(1)}+(1-\gamma)\hat{\mathcal{D}}^{(2)}\right)\rho$$

$$\hat{\mathcal{D}}^{(i)} = J\sum_k\left(L_k^{(i)}\rho L_k^{(i)\dagger}-\frac{1}{2}\{L_k^{(i)\dagger}L_k^{(i)},\rho\}\right) \tag{1.151}$$

$$L_k^{(1)} = S_k^z;\qquad L_k^{(2)} = \frac{1}{2}(S_k^+S_{k+1}^- + iS_{k+1}^-S_{k+2}^+) \tag{1.152}$$

Time-dependent generalized Gibbs ensembles

$$\lim_{\epsilon\to 0}\rho(t) \overset{\text{loc}}{=} \rho_{GGE}(t) \quad \text{for } t=\frac{1}{\epsilon J}\tau \tag{1.153}$$

$$\rho_{GGE}(t) = \frac{e^{-\sum_i \lambda_i(t)C_i}}{\mathrm{Tr}[e^{-\sum_i \lambda_i(t)C_i}]} \tag{1.154}$$

$\lim_{\epsilon\to 0}\mathrm{Tr}[A\,\rho(t)] = \mathrm{Tr}[A\,\rho_{GGE}(t)]$.

$$\mathrm{Tr}[C_i\,\dot\rho(t)] \overset{!}{=} \mathrm{Tr}[C_i\,\dot\rho_{GGE}(t)] \tag{1.155}$$

$\dot\rho = (\hat{\mathcal{L}}_0+\hat{\mathcal{L}}_1)\rho \approx (\hat{\mathcal{L}}_0+\hat{\mathcal{L}}_1)\rho_{GGE} = \hat{\mathcal{L}}_1\rho_{GGE}$
$\dot\rho_{GGE}(t) = -\sum \dot\lambda_j \rho_{GGE}(t)\,(C_j - \langle C_j\rangle_{GGE})$
$\langle A\rangle_{GGE} = \mathrm{Tr}[A\,\rho_{GGE}(t)]$

$$\dot\lambda_i = F_i(t) \tag{1.156}$$

$$\begin{aligned} F_i(t) &\approx -\sum_j (\chi(t)^{-1})_{ij}\mathrm{Tr}[C_j\hat{\mathcal{L}}_1\rho_{GGE}(t)] \\ &= -\sum_j (\chi^{-1})_{ij}\langle \dot C_j\rangle_{GGE} \end{aligned} \tag{1.157}$$

$$\chi_{ij}(t) = \langle C_iC_j\rangle_{GGE} - \langle C_i\rangle_{GGE}\langle C_j\rangle_{GGE}$$

$$\hat P(t)X := -\sum_{i,j}\frac{\partial\rho_{GGE}(t)}{\partial\lambda_i}(\chi(t)^{-1})_{ij}\mathrm{Tr}[C_jX] \tag{1.158}$$

$\hat P(t)\dot\rho_{GGE}(t) = \dot\rho_{GGE}(t)$,
$\hat{\mathcal{L}}_0\rho_{GGE} = 0$,
$\hat P(t)\hat{\mathcal{L}}_0\delta\rho = 0$,
$\hat{\mathcal{L}}_1\delta\rho \sim \epsilon^2$.

$$\hat P(t)\delta\dot\rho + \dot\rho_{GGE} = \hat P(t)\hat{\mathcal{L}}_1\rho_{GGE} + \mathcal{O}(\epsilon^2) \tag{1.159}$$

$\dot\rho_{GGE} = \hat P(t)\hat{\mathcal{L}}_1\rho_{GGE}$

Time-dependent block-diagonal density matrices

$$\rho_{BD}(t) = \sum_{E_n=E_m}\lambda_{nm}(t)\,|n\rangle\langle m| \tag{1.160}$$

$$\dot\lambda_{nm}(t) = \sum_{E_{n'}=E_{m'}} M_{nm,n'm'}\,\lambda_{n'm'}(t) \tag{1.161}$$

$$M_{nm,n'm'} = \mathrm{Tr}[\,|m\rangle\langle n|\,\hat{\mathcal{L}}_1\,|n'\rangle\langle m'|\,] \tag{1.162}$$

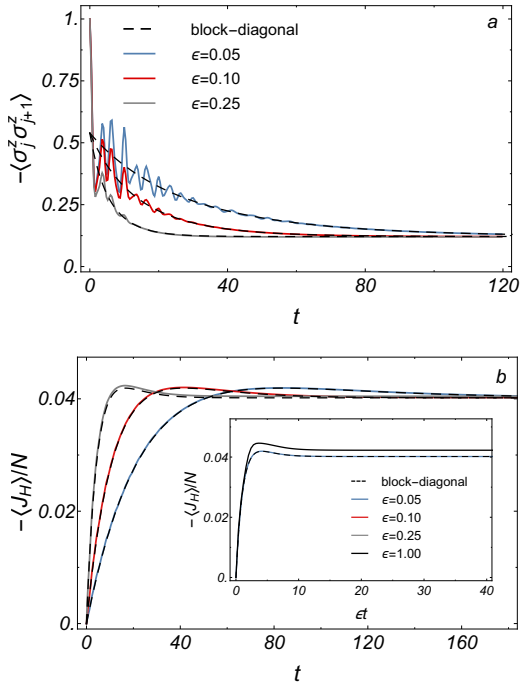

Figure 1.37: Exact time evolution of a weakly perturbed Heisenberg model ($N = 8$, $\gamma = 0.8$, $J = 1$) for three small values of ϵ. The dashed lines show the result for the time evolution of the block-diagonal density matrix using Eqs. (9.12,9.13). (a) Decay of the nearest-neighbor spin-correlation. (b) For the heat current rapid oscillations on a time scale of order $1/J = 1$ are absent as J_H is a conservation law of H_0. For the values of ϵ shown in the plot the dashed lines follow the solid lines: the block-diagonal density matrices correctly describe the time evolution with high precision. Inset: At large $\epsilon = 1.0$ discrepancies are visible.

Numerical Results

Time evolution for small systems

$$J_H = J^2 \sum_j (\boldsymbol{S}_j \times \boldsymbol{S}_{j+1}) \cdot \boldsymbol{S}_{j+2} \tag{1.163}$$

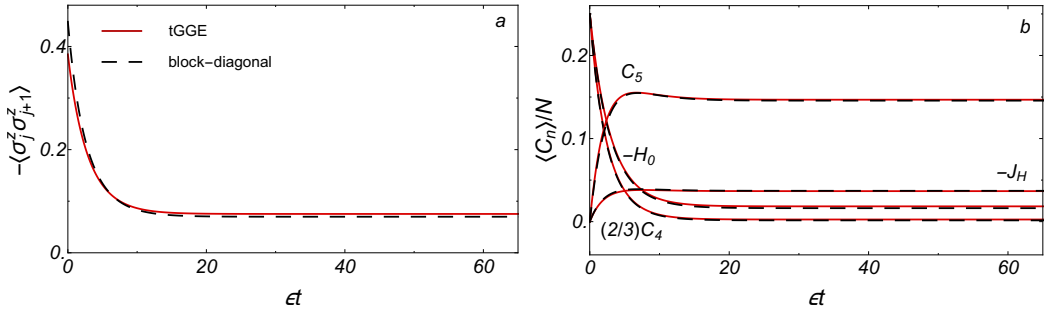

Figure 1.38: Comparision of the results obtained from the truncated GGE (solid line) and the block-diagonal density matrix (dashed). (a) Antiferromagnetic nearest neighbor spin correlations, (b) Approximate conservation laws, C_5, $-J_H$, $-H_0$, and $(2/3)C_4$. All quantities change on a time scale of order $1/\epsilon$. Parameters: $\gamma = 0.8$, $J = 1$, $N = 14$.

Time evolution of truncated GGE

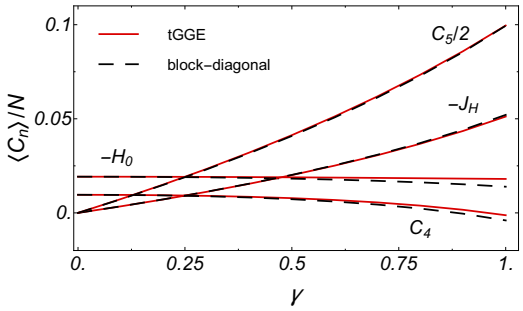

Figure 1.39: Expectation values of conservation laws in the stationary state ($t \to \infty$) as a function of γ, which controls the nature of the dissipative terms ($N = 14$, $J = 1$). As in Fig. 9.2, a comparison of the truncated GGE (solid lines) the block-diagonal density matrix (dashed) is shown. For $\gamma = 0$ the system heats up to infinite temperatue and all conservation laws vanish in the thermodynamic limit. Due to finite size effects small finite values are obtained form H and C_4.

Finite-size, finite-ϵ, and truncation effects

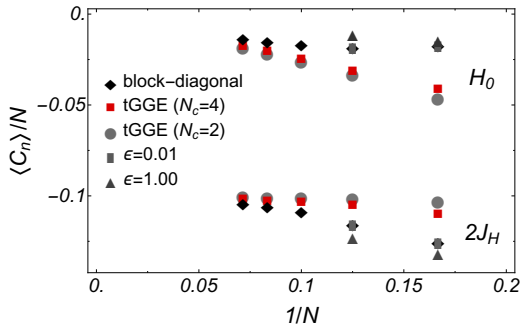

Figure 1.40: Steady-state expectation value of the energy, $\langle H_0\rangle$, and the heat current, $\langle J_H\rangle$, as function of the inverse system size, $1/N$ ($N = 6, 8, 10, 12, 14$), for the truncated GGE with 2 and 4 conservation laws and the block-diagonal ensemble. For the smallest system size, $N = 6, 8$, we also show the exact results for $\epsilon = 0.01$, which practially coincides with the the block-diagonal ensemble, and for $\epsilon = 1.0$ ($\gamma = 1$).

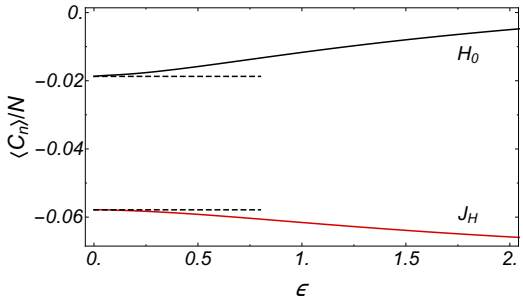

Figure 1.41: Steady-state expectation value of the energy, $\langle H_0\rangle$, and the heat current, $\langle J_H\rangle$ as function of the strength ϵ of the integrability-breaking Lindblad terms ($N = 8$, $J = 1$, $\gamma = 1$). For $\epsilon \to 0$ the result of the block-diagonal ensemble (dashed line) is recovered.

Perturbation theory for steady state

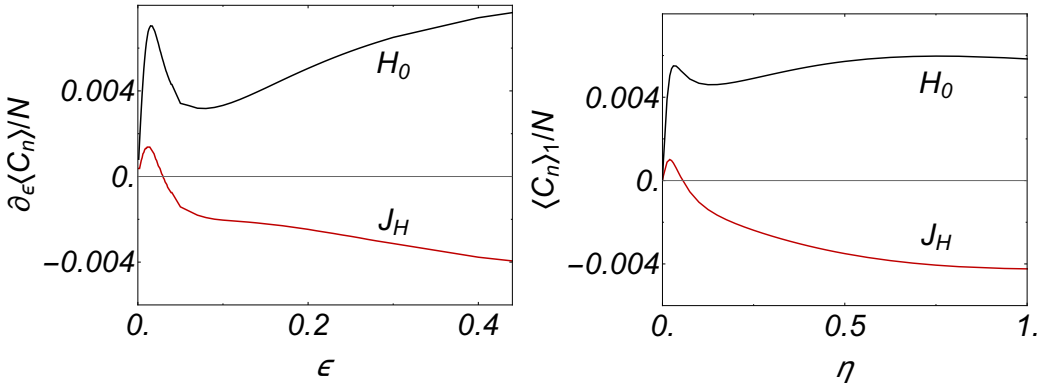

Figure 1.42: Left panel: Derivative of energy and heat current, $\frac{d\langle H\rangle}{d\epsilon}$ and $\frac{d\langle J_H\rangle}{d\epsilon}$, as function of the strength of perturbation ϵ calculated for $\gamma = 1$, $J = 1$ and $N = 8$. Right panel: Calculation of the coefficient linear in ϵ from perturbation theory [18] as function of the broadening η for the same parameters.

Effective forces and γ dependence of steady-state expectation values

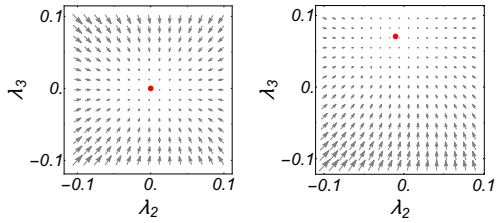

Figure 1.43: Effective force field (F_2, F_3) in the vicinity of the steady state (red point) in the plane spanned by the Lagrange parameters $\lambda_2 = \beta$ and λ_3 using $e^{-\beta H - \lambda_3 J_H}$ as an ansatz for ρ_{GGE} $(N = 8)$. Left: For $\gamma = 0$ the system approaches an infinite temperature state since the Lindblad operator $L^{(1)}$ is constantly heating the system up. Right: At $\gamma = 1$ the system is attracted towards a non-equilibrium state with finite stationary values of both λ_2 and λ_3.

1.5.2 Pumping approximately integrable systems

$$\rho_0 \sim \exp\left(-\sum_i \lambda_i C_i\right) \tag{1.164}$$

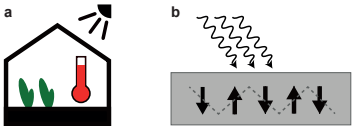

Figure 1.45: (a) A well-insulated greenhouse exposed to sunshine can heat up significantly since energy within it is approximately conserved. (b) As the heat current in spin chain materials is approximately conserved even weak terahertz radiation can induce large heat current. Material candidates must have appropriate crystal structure, schematically denoted by dashed lines indicating alternating chemical bonds.

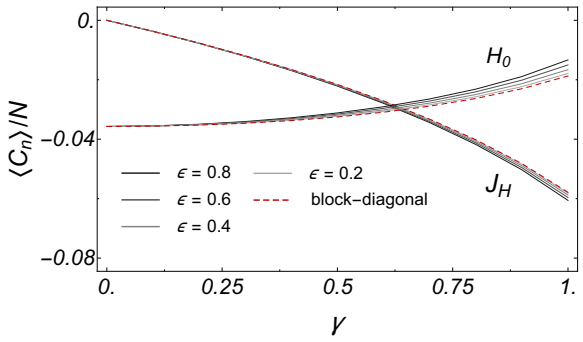

Figure 1.44: Steady state expectation values of the energy and the heat current J_H as a function of γ parametrizing the type of Markovian coupling. For a system of $N = 8$ sites the steady state is shown at $J = 1$ for several values of ϵ and also for the limit $\epsilon \to 0$ where the block-diagonal ensemble becomes exact.

Results

Weakly driven system.

$$\dot{\rho} = \hat{\mathcal{L}}\rho, \quad \hat{\mathcal{L}} = \hat{\mathcal{L}}_0 + \epsilon\hat{\mathcal{L}}_1, \tag{1.165}$$

$\hat{\mathcal{L}}_0\rho = -i[H_0, \rho]$

Markovian perturbation.

$$\langle \dot{C}_i \rangle = \mathrm{Tr}\,(C_i\hat{\mathcal{L}}\rho_0) = \mathrm{Tr}\,(C_i\epsilon\hat{\mathcal{L}}_1\rho_0) \stackrel{!}{=} 0, \tag{1.166}$$

$\hat{\mathcal{L}}_0\rho_0 = -i[H_0, \rho_0] = 0.$

$$\hat{P}X \equiv -\sum_{i,i'} \frac{\partial\rho_0}{\partial\lambda_i}\,(\chi^{-1})_{ii'}\mathrm{Tr}\,(C_{i'}X), \tag{1.167}$$

$\chi_{ii'} = -\mathrm{Tr}\,(C_i\partial\rho_0/\partial\lambda_{i'}).$

$$\hat{\mathcal{L}}_0\rho_0 = 0, \quad \hat{P}(\hat{\mathcal{L}}_1\rho_0) = 0. \tag{1.168}$$

Hamiltonian perturbation.

$$\hat{\mathcal{L}}_0\rho_0 = 0, \quad \hat{P}(\hat{\mathcal{L}}_1\hat{\mathcal{L}}_0^{-1}\hat{\mathcal{L}}_1\rho_0) = 0. \tag{1.169}$$

Model.

$$H_0 = \sum_j \frac{J}{2}(S_j^+ S_{j+1}^- + S_j^- S_{j+1}^+) + \Delta S_j^z S_{j+1}^z - BS_j^z. \tag{1.170}$$

$$H_\mathrm{d} = \epsilon_\mathrm{d} J \sum_j \Big((-1)^{j+1}\mathbf{S}_j \cdot \mathbf{S}_{j+1}\sin(\omega t) + (-1)^j S_j^z \cos(\omega t)\Big), \tag{1.171}$$

$$H_\mathrm{ph} = \epsilon_\mathrm{ph} J \sum_j \Big(\mathbf{S}_j \cdot \mathbf{S}_{j+1}(a_j + a_j^\dagger) + \gamma_\mathrm{m}(S_j^x S_{j+1}^z + S_j^z S_{j+1}^x)(a_j + a_j^\dagger)\Big).$$

Steady state.

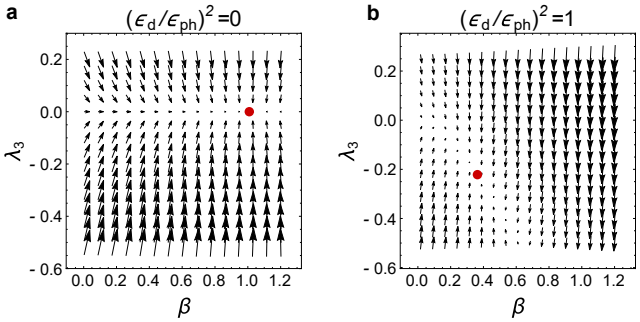

Figure 1.46: Effective force $\boldsymbol{F}$ in the space of Lagrange parameters (β, λ_3) using $e^{-\beta H_0 - \lambda_3 C_3}$ as an ansatz for the generalized Gibbs ensemble. Parameters: $J = \Delta = -B = \omega = \omega_{\rm ph} = T_{\rm ph}$. Lagrange parameters (β, λ_3) are plotted in units $1/J$ and $1/J^2$, respectively. (a) In the absence of an external driving, $\epsilon_{\rm d} = 0$, the stable fixed point (red dot) is given by the thermal ensemble, $\beta = 1/T_{\rm ph}$, $\lambda_3 = 0$. (b) When the system is driven by $H_{\rm d}$ ($\epsilon_{\rm d} = \epsilon_{\rm ph}$), it heats up and λ_3 becomes finite.

$\hat{P}\dot{\rho} = \sum_i \frac{\partial \rho_0}{\partial \lambda_i} F_i$
$\dot{\lambda}_i \approx F_i,$

$$F_i = \sum_{i'} (\chi^{-1})_{ii'} \mathrm{Tr}\,(C_{i'}\ \epsilon\hat{\mathcal{L}}_1 \hat{\mathcal{L}}_0^{-1} \epsilon \hat{\mathcal{L}}_1 \rho_0) \tag{1.172}$$

$\mathcal{Q} = \{|n\rangle\langle m|$ with $E_m^0 = E_n^0\}$, where $H_0|n\rangle = E_n^0|n\rangle$.

$$\mathcal{L}^{\mathcal{Q}}_{mn} = -\mathrm{Tr}\,(Q_m^\dagger\ \epsilon\hat{\mathcal{L}}_1 \hat{\mathcal{L}}_0^{-1} \epsilon \hat{\mathcal{L}}_1 Q_n), \tag{1.173}$$

$\chi \boldsymbol{F} = 0$ or $\mathcal{L}^{\mathcal{Q}} \rho_0 = 0$ by $\epsilon_{\rm ph}^2$.

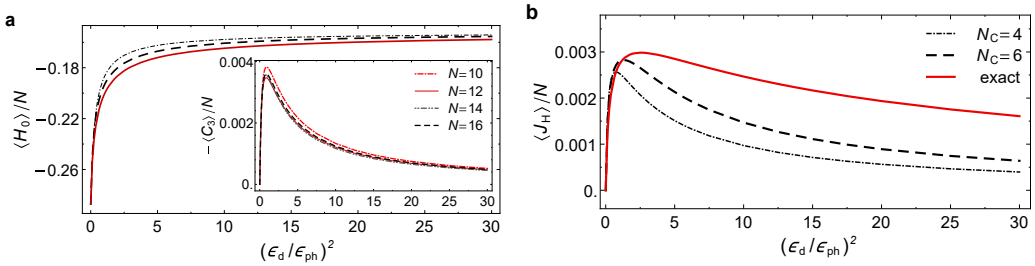

Figure 1.47: Expectation values of (a) energy and (b) heat current densities for a weakly driven spin chain, $\epsilon_{\rm d}, \epsilon_{\rm ph} \to 0$, as functions of the ratio of driving strength $\epsilon_{\rm d}$ and phonon coupling $\epsilon_{\rm ph}$. Red solid lines: exact result taking into account all 7969 conservation laws of a system of $N = 12$ sites. (a) For the energy accurate results are already obtained with a GGE ensemble based on $N_{\rm C} = 4$ (dot-dashed lines) or $N_{\rm C} = 6$ (dashed lines) conserved quantities. (b) Also the heat current $J_{\rm H} = C_3 - BJ_{\rm S}$ is qualitatively well described by the GGE ensemble but quantitative deviations are larger. Inset: Finite size analysis for (local) C_3 based on GGE ensemble with $N_{\rm C} = 6$ conserved quantities. Parameters: $J = 1, \Delta = 0.8, B = -1.0, \omega = 1.6\ \omega_{\rm ph}, \omega_{\rm ph} = T_{\rm ph} = 1$.

Methods

Perturbing around ρ_0.

$$\hat{\mathcal{L}}^{-1}\hat{P} \sim \mathcal{O}(\epsilon^{-1}), \tag{1.174}$$

$$(\hat{X}+\hat{Y})^{-1} - \hat{X}^{-1} = -(\hat{X}+\hat{Y})^{-1}\hat{Y}\hat{X}^{-1}$$

$$\begin{aligned} \hat{X} &= \hat{P}\epsilon\hat{\mathcal{L}}_1\hat{P}, \\ \hat{Y} &= \hat{\mathcal{L}}_0 + \hat{Q}\epsilon\hat{\mathcal{L}}_1\hat{Q} + \hat{P}\epsilon\hat{\mathcal{L}}_1\hat{Q} + \hat{Q}\epsilon\hat{\mathcal{L}}_1\hat{P}, \end{aligned} \tag{1.175}$$

$\hat{Q} := \hat{1} - \hat{P}; \qquad \hat{X} + \hat{Y} = \hat{\mathcal{L}}.$

$$\begin{aligned} \hat{\mathcal{L}}^{-1}\hat{P} &= (\hat{X}+\hat{Y})^{-1}\hat{P} \\ &= \hat{X}^{-1}\hat{P} - (\hat{X}+\hat{Y})^{-1}\ \hat{Q}\ \hat{Y}\ \hat{P}\ \hat{X}^{-1}\hat{P} \\ &\sim \mathcal{O}(\epsilon^{-1}) + \mathcal{O}(1) \end{aligned} \tag{1.176}$$

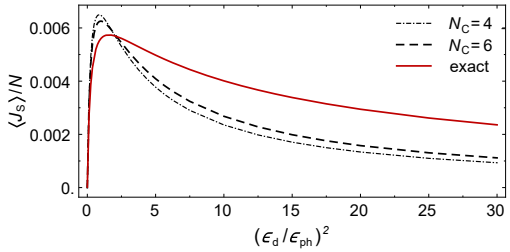

Figure 1.48: For vanishing magnetic field a spin current (but no heat current) is generated within our model for finite ratios of $\epsilon_{\rm d}/\epsilon_{\rm ph}$. The expectation value of spin current density is again maximal for $\epsilon_{\rm d}/\epsilon_{\rm ph} \approx 1$. Parameters: $J = 1, \Delta = 0.8, \omega = 1.6\,\omega_{\rm ph}, \omega_{\rm ph} = T_{\rm ph} = 1, N = 12$.

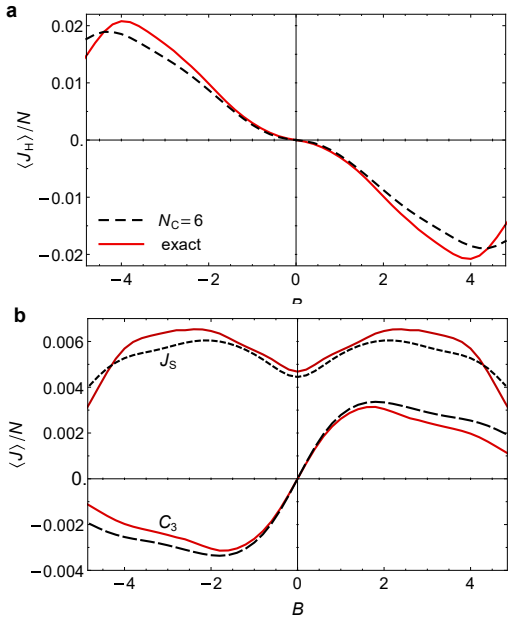

Figure 1.49: (a) Heat current $J_{\rm H}$, (b) spin current $J_{\rm S}$, and C_3 densities as a function of external magnetic field B obtained from a GGE ensemble with $N_{\rm C} = 6$ conserved quantities (dashed) or from an exact calculation (solid) including all conservations. Parameters: $(\epsilon_{\rm d}/\epsilon_{\rm ph})^2 = 2.5$, $J = 1, \Delta = 0.8, \omega = 1.6\,\omega_{\rm ph}, \omega_{\rm ph} = T_{\rm ph} = 1, N = 12$.

Conservation laws of the XXZ Heisenberg model.

$$J_{\rm H}(B=0) = C_3 = J^2 \sum_j (\boldsymbol{S}'_j \times \boldsymbol{S}''_{j+1}) \cdot \boldsymbol{S}'_{j+2} \tag{1.177}$$

$S'^a_j = \sqrt{\lambda_a} S^a_j, S''^a_j = \sqrt{\lambda_z/\lambda_a} S^a_j$
$\lambda_z = \Delta/J$, $\lambda_x = \lambda_y = 1$.

$$J_{\rm H} = J^2 \sum_j (\boldsymbol{S}'_j \times \boldsymbol{S}''_{j+1}) \cdot \boldsymbol{S}'_{j+2} - B J_{\rm S}. \tag{1.178}$$

$$J_{\rm S} = i\frac{J}{2} \sum_j (S^+_j S^-_{j+1} - S^-_j S^+_{j+1}) \tag{1.179}$$

$$J^c_{\rm S} = \sum_{\tilde{n}} |\tilde{n}\rangle\langle\tilde{n}|J_S|\tilde{n}\rangle\langle\tilde{n}|$$

Floquet formulation.

$$\rho = \sum_n e^{-in\omega t}\rho^{(n)}, n \in \mathbb{Z} \tag{1.180}$$

$$\begin{aligned} F^{(\rm d)}_i = \frac{2\pi}{N}\epsilon^2_{\rm d} \sum_{i'} (\chi^{-1})_{ii'} \sum_{m,k} \rho_m (C_{i',m} - C_{i',k}) \times \\ \times \Big\{ |\langle k|H^{(+)}_{\rm d}|m\rangle|^2 \delta(E^0_k - E^0_m - \omega) \\ + |\langle k|H^{(-)}_{\rm d}|m\rangle|^2 \delta(E^0_k - E^0_m + \omega) \Big\} \end{aligned} \tag{1.181}$$

Phonon coupling.

$$\begin{aligned} F^{(\rm ph)}_i = 2\pi\epsilon^2_{\rm ph} \sum_{i'} (\chi^{-1})_{ii'} \sum_{m,k} \rho_m (C_{i',m} - C_{i',k}) \\ \times J^2 \left(|\langle k|\mathbf{S}_j \cdot \mathbf{S}_{j+1}|m\rangle|^2 + \gamma^2_{\rm m} |\langle k|S^x_j S^z_{j+1} + S^z_j S^x_{j+1}|m\rangle|^2 \right) \\ \times \Big((n_{\rm B}(E^0_m - E^0_k) + 1)\ A^{(\rm ph)}(E^0_m - E^0_k) \\ + n_{\rm B}(E^0_k - E^0_m)\ A^{(\rm ph)}(E^0_k - E^0_m) \Big) \end{aligned} \tag{1.182}$$

$n_{\rm B}(E) = 1/(e^{E/T_{\rm ph}} - 1)$

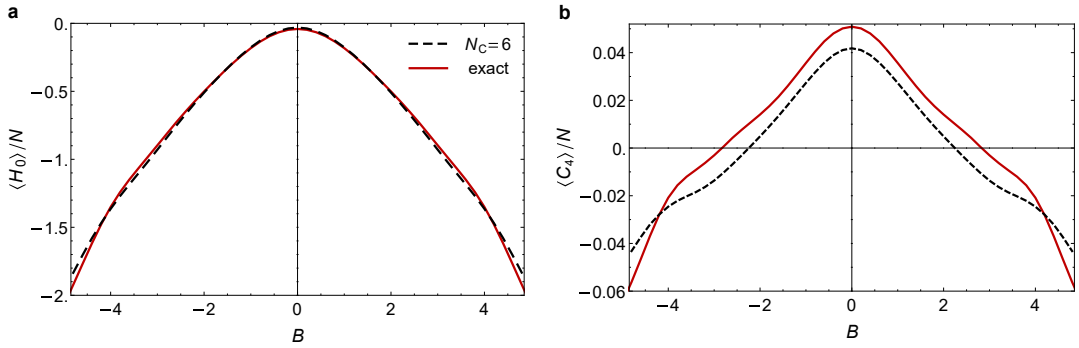

Figure 1.50: (a) The energy density and (b) the expectation value of another conserved quantity C_4 (4-spin operator) as a function of magnetic field B, obtained from calculation using all conserved quantities (solid) and a GGE with $N_C = 6$ (quasi-) local conserved quantities (dashed).

Part II
My Theory of Spin Models with Dissipation

2 Main Theory

2.1 How To Describe Open Spin Systems?

2.1.1 General idea

(???)

2.1.2 Which systems can we describe by it?

(write some of them explicitly, and write, which and why we can't describe by it?)

2.1.3 Features of GGE

How GGE ansatz is connected with entanglement?

(????????????? have no idea now)

3 Examples of addition of openness

(I'll do them after I understand main concepts)

3.1 BCS with openness

Part III
Examples and Solved Problems

Part IV
Famous Reviews and Important Articles

4 Equilibration, thermalisation, and the emergence of statistical mechanics in closed quantum systems by Gogolin, Eisert

Abstract

We review selected advances in the theoretical understanding of complex quantum many-body systems with regard to emergent notions of quantum statistical mechanics.

We cover topics such as equilibration and thermalisation in pure state statistical mechanics,

the eigenstate thermalisation hypothesis,

the equivalence of ensembles,

non-equilibration dynamics following global and local quenches as well as ramps.

(so what are conclusions about them?)

We also address initial state independence, absence of thermalisation, and many-body localisation.

We elucidate the role played by key concepts for these phenomena, such as

Lieb-Robinson bounds,

entanglement growth,

typicality arguments,

quantum maximum entropy principles and the generalised Gibbs ensembles,

and quantum (non-)integrability.

We put emphasis on rigorous approaches and present the most important results in a unified language.

4.1 Introduction

(here, there is just a litr review)

At the time when quantum theory was developed in a creative rush in the last years of the twenties of the previous century, classical statistical physics was already a mature field of research. The landmark book "Elementary principles in statistical mechanics" [1] authored by Gibbs had already been published in 1902, which is seen by many as the the birth of modern statistical mechanics [2].

So, as soon as the mathematical framework of the "neue Mechanik", the new mechanics, as von Neumann called it in 1929, was established, significant efforts were made by him to prove ergodicity and a tendency to evolve into states that maximise entropy, which became known as the H-theorem, in this setting [3]. The field of quantum statistical mechanics soon emerged and can by now be considered an important pillar of theoretical physics [4].

(todo: study history of statistical mechanics at least for some days)

Still, some foundational yet fundamental questions remain open, much related to the questions raised by von Neumann.

While maximum entropy principles provide a starting point for the understanding of the ensembles of quantum statistical mechanics, it seems much less clear how quantum states taking extremal values for the entropy are being achieved via microscopic dynamics.

After all, at the fundamental level, quantum many-body systems follow the Schrödinger equation, giving rise to unitary dynamics. It is far from obvious, therefore, in what precise way interacting quantum many-body systems can equilibrate.

The microscopic description of quantum mechanical systems following the dynamical equations of motion is still in some tension with the picture arising from the ensemble description of quantum statistical mechanics. That is to say, the questions of equilibration and thermalisation in what we will call pure-state quantum statistical mechanics remained largely unresolved until very recently.

These foundational questions came back with a vengeance not too long ago. Old puzzles and new questions of quantum many-body systems out of equilibrium re-entered the centre of attention and are again much in the focus of present-day research in quantum many-body theory. This remarkable renaissance is primarily due to three concomitant factors in physics research.

The first and arguably most important source of inspiration has been an experimental revolution.

Fueled by enormous improvements in experimental techniques it became feasible to control quantum systems with many degrees of freedom.

An entirely new arena for the study of physics of interacting quantum many-body systems emerged.

This is particularly true for the development of techniques to cool and trap ultra-cold atoms and to subject them to optical lattices [5, 6, 7, 8, 9, 10] or suitable confinements, giving rise to low-dimensional continuous systems [11, 12, 13, 14, 15, 16].

(I have no idea now what is in these articles?)

Similarly, systems of trapped ions [17, 18], as well as hybrid systems [19], allow to precisely study the physics of interacting systems in the laboratory [20, 21, 22, 23, 3, 25].

(a lot of articles...)

In such highly controlled settings, equilibration and thermalisation dynamics has been studied [26, 27, 28, 29, 30].

Especially setups with optical lattices allow for the realisation of condensed-matter-like interacting many-body systems in the laboratory, but with fine grained control over the model parameters and geometries.

Questions concerning the out of equilibrium dynamics of such systems were suddenly not only important out of academic curiosity, but became pragmatically motivated questions important to understand experimentally realisable physical situations.

The second major development is the broad availability of new machines: supercomputers.

With the vastly increased computing power and massive parallelisation as well as novel numerical techniques such as tensor network methods [31] and the density-matrix renormalisation group method [32], it has become possible to simulate the dynamics of large quantum systems for relatively long times.

Methods for exact diagonalisation have been brought to new levels [33, 34, 35], complemented by quantum Monte Carlo techniques [36, 37], and applications of dynamical mean field theory [38] and density functional theory [39, 40].

(big topics)

There is an enormous body of numerical works on questions of equilibration and thermalisation in closed quantum systems and the dynamics of quantum phase transitions [41, 42,

43, 44, 45, 46, 47, 48, 49], often with a focus on so-called quenches, i.e., rapid changes of the Hamiltonian [50, 51, 33, 34, 52, 53, 54, 55, 56].

(a lot of articles)

This body of numerical work is complemented by partly or entirely analytical studies that capture these and related phenomena in concrete systems or classes of models (often integrable ones) [57, 58, 59, 60, 61, 62, 63, 64, 65, 66]. We will discuss these works in more detail later.

Last but not least, our understanding of quantum mechanics has improved significantly since the time of von Neumann.

(how???)

The availability of new mathematical methods — in part motivated by research in quantum information theory — is the third driving force. These techniques have made some of the old questions become more tractable than before, while at the same time new paradigms of approaching the key questions have emerged. This lead to works inspired by notions of typicality and random states [67, 68, 69, 70, 71].

Also, notions of quantum information propagation, such as Lieb-Robinson bounds [72, 73, 74, 75], and research on entanglement in many-body systems [76, 77, 78, 79, 80, 21] can be classified as contributing to this development.

(what is it???? have no idea now)

All in all, this is already too large a topic to cover in full depth in a single review of reasonable length. Hence, in this article we address and cover only a subset of these developments and questions. We will mostly concentrate on the theoretical and analytical insights, however always making an effort to put them into the context of evidence collected through numerical simulations and important experimental developments.

In physics, one can often say a "lot about little", or "little about a lot". In this review, we take the latter approach, by sticking to general and conceptual statements on interacting many-body systems in a quantum-information inspired rigorous language, so where only relatively "little" can be said. These statements, however, apply to "a lot", that is, to an immense variety of models.

At the heart of the approach advocated here lies the attempt to use only standard quantum mechanics and no additional postulates to explain the emergence of thermodynamic behaviour, and to do this in a mathematically rigorous and general way. It is an invitation to elaborate how much of statistical mechanics and thermodynamics can be derived from quantum mechanics. The term "derived" here means to justify the well established methods and postulates of equilibrium and non-equilibrium statistical mechanics by means of the microscopic picture provided by quantum mechanics. Following Refs. [67, 81], we shall call this approach pure state quantum statistical mechanics.

The level of detail and rigour that we are aiming at in this work necessarily also mean that an awkwardly large number of interesting questions and research results will have to be left unmentioned. In this sense, this article is not meant to be a comprehensive review.

1. We have authored together with Mathis Friesdorf a complementing accompanying review [82] in Nature Physics that takes a much more physical perspective, where local interacting many-body systems out of equilibrium are in the focus of attention and experimental developments are more comprehensively discussed.

A lot what is left out here is covered there. In this article, in contrast, we advocate a more mathematical mindset and language, and at the same time have a more limited scope, but the

covered topics are discussed in more depth. To complete the picture of the subject, and in addition to Ref. [82], we recommend a number of further review articles and books that cover what we do not have the space to cover here:

2. The book by Gemmer, Michel, and Mahler [69] entitled "Quantum thermodynamics" advertises an approach towards the foundations of thermodynamics that is in spirit close to the approach of this work.

   (look at it at least ones!!!)

   The focus is, however, more on notions of typicality, which we will discuss in Section 4.6, but which is not a central topic of the present review. Moreover, the first edition of the book is from 2004, and even though it has been extended in the second edition from 2009, much of the newer material that takes the centre stage in this work is not covered.

3. The editorial of a New Journal of Physics focus issue on the "Dynamics and thermalisation in isolated quantum many-body systems" by Cazalilla and Rigol [83] not only explains the significance of the individual articles published in the focus issue to the more general endeavour of developing a better understanding of the coherent dynamics of quantum many-body systems.

   (look at it at least ones!!!)

   On top of that it gives an overview of many of the currently pursued research directions and many additional references. This renders this editorial a good entry point into the more recent literature on the subject and makes it an excellent read. At the same time, it provides only very little background information, almost no historical context, and assumes that the reader is already familiar with the jargon of the field.

4. A colloquium in Reviews in Modern Physics by Polkovnikov, Sengupta, Silva, and Vengalattore [84] is entitled "Non-equilibrium dynamics of closed interacting quantum systems".

   (look at it at least ones!!! I have added it to this note)

   This work gives an excellent overview of recent theoretical and experimental insights concerning such systems, but focuses mainly on the dynamics following so-called quenches, i.e., rapid changes in the Hamiltonian of a system and the eigenstate thermalisation hypothesis (ETH). We will discuss the ETH in Section 4.7.2, but the scope of the present work is considerably broader and we will also take a slightly different, quantum information theory inspired, point of view and put the focus more on analytical results.

5. A review entitled "Equilibration and thermalisation in finite quantum systems" by Yukalov [46] contains a review of the history of both the experimental realisation of coherently evolving, well controlled quantum systems and the observation and numerical investigation of equilibration and thermalisation in such systems. In addition it contains results on equilibration in closed systems with a continuous density of states and in systems undergoing so-called non-destructive measurements.

   (looks interesting)

6. The review Ref. [85] on the thermodynamics of stochastic processes. It covers important topics such as fluctuation(-dissipation) theorems, entropy production, and (autonomous) thermal machines, which have been extensively studied in recent years and which are related to but not elaborated on in this work.

7. Finally, the review "The role of quantum information in thermodynamics" [86] overviews recent developments in the interplay between the fields of quantum information and thermodynamics. It focuses on foundations of statistical mechanics and on resource-theoretic aspects of thermodynamics. More explicitly, it covers equilibration and thermalisation, state transformation under different constraints and resources, work extraction, the work cost of information-processing tasks, inconvertibility of energy and correlations, and fluctuation relations.

These articles and books together, in conjunction with the present review, rather accurately cover the state of affairs. It is the purpose of this article to fill the gap left by the above mentioned works.

4.2 Preliminaries and notation

(here, there is a revision of relevant basics of QM.Good idea to revise it)
(todo: add paragraphs here, it is a big section!)
In order to facilitate the discussion in later chapters, we carefully introduce the notation and introduce a number of fundamental concepts in this section. The presentation is limited to the minimum necessary to make the following statements well-defined. An effort has been made to make this introduction self-contained. However, a basic knowledge of quantum theory, analysis, linear algebra, group theory and related subjects is assumed.

To begin with, we fix some general notation. Given a positive integer $n \in \mathbf{Z}^+$ we use the short hand notation $[n] \coloneqq (1, \dots, n)$ for the (ordered) range of numbers from 1 to n and set $[\infty] \coloneqq \mathbf{Z}^+$. Given a set X we denote its cardinality by $|X|$. If X has a universal superset $\mathcal{V} \supset X$, we write $X^c \coloneqq \mathcal{V} \setminus X$ for its complement. Given two sets X, Y we write $X \cup Y$ and $X \cap Y$ for their union and intersection. To stress that a set $\mathcal{V}$ is the union of two disjoint sets X, Y, i.e., $X \cap Y = \emptyset$ we write $\mathcal{V} = X \dot\cup Y$. Given a set X of sets we write $\cup X \coloneqq \bigcup_{x \in X} x$ for the union of the sets in X. For sequences S, $|S|$ denotes the length of the sequence. When we define sets or sequences in terms of their elements we use curly $\{\,\cdot\,\}$ or round $(\,\cdot\,)$ brackets respectively.

We use the (Bachmann-)Landau symbols O, Ω and Θ to denote asymptotic growth rates of real functions $f, g \colon \mathbf{R} \to \mathbf{R}$. In particular

$$f(x) \in O(g(x)) \iff \limsup_{x \to \infty} |f(x)/g(x)| < \infty, \tag{4.1}$$

and for Ω we adopt the convention from complexity theory that

$$f(x) \in \Omega(g(x)) \iff g(x) \in O(f(x)) \tag{4.2}$$

and write $f(x) \in \Theta(g(x))$ if both $f(x) \in O(g(x))$ and $f(x) \in \Omega(g(x))$. To simplify the notation we work with natural, or Planck units such that in particular the Planck constant $\hbar$ and the Boltzmann constant k_B are equal to 1.

Let $\mathcal{H}$ be a separable Hilbert space over $\mathbf{C}$ with inner product $\langle\varphi\rangle\psi$ for $|\varphi\rangle, |\psi\rangle \in \mathcal{H}$. We denote by $\mathcal{B}(\mathcal{H})$ be the space of bounded operators and by $\mathcal{T}(\mathcal{H})$ the space of trace class operators on the Hilbert space $\mathcal{H}$, i.e., those $A \in \mathcal{B}(\mathcal{H})$ whose trace TrA is finite. The trace class operators $\rho \in \mathcal{T}(\mathcal{H})$, whose associated linear functional $Tr(\rho\,\cdot\,)$ is non-negative, i.e., $\forall A \geq 0 \colon Tr(\rho\, A) \geq 0$ and which have unit trace $Tr\rho = 1$, form the convex set $\mathcal{S}(\mathcal{H})$ of (quantum) states or density operators. An operator $A \in \mathcal{B}(\mathcal{H})$ is self-adjoint if $A = A^\dagger$.

An operator $\Pi \in \mathcal{B}(\mathcal{H})$ is a projector if $\Pi\,\Pi = \Pi$. The rank of an operator $A \in \mathcal{B}(\mathcal{H})$, denoted by $rank(A)$, is the dimension of its image. An operator $U \in \mathcal{B}(\mathcal{H})$ is called unitary if $U^\dagger U = U\,U^\dagger = \mathbb{1}$. It turns out that in the finite dimensional setting considered here $\mathcal{S}(\mathcal{H}) \subset \mathcal{O}(\mathcal{H})$ is the convex set of self-adjoint, non-negative operators with unit trace. The extreme point of that set are rank one projectors and are called pure states. The elements of the subspace $\mathcal{O}(\mathcal{H}) \subset \mathcal{B}(\mathcal{H})$ of self-adjoint operators are called observables.

Given a bounded operator $A \in \mathcal{B}(\mathcal{H})$ and a state $\rho \in \mathcal{S}(\mathcal{H})$, we will write the expectation value of A in state ρ is as

$$\langle A \rangle_\rho \coloneqq Tr(A\,\rho). \tag{4.3}$$

The most general measurements possible in quantum mechanics are so-called positive operator valued measurements (POVMs) [87]. A POVM with K measurement outcomes is a sequence $M = (M_k)_{k=1}^K$ of operators $M_k \in \mathcal{B}(\mathcal{H})$, called POVM elements, with the property that

$$\sum_{k=1}^{K} M_k = \mathbb{1}. \tag{4.4}$$

Upon measuring a system in state $\rho \in \mathcal{S}(\mathcal{H})$ with the POVM M, outcome number k is obtained with probability $Tr(M_k\,\rho)$. When we say that an observable $A \in \mathcal{O}(\mathcal{H})$, with spectral decomposition $A = \sum_{k=1}^{d_A} a_k\,\Pi_k$, is measured, we mean that the POVM $M = (\Pi_k)_{k=1}^{d_A}$ is measured and the measurement device outputs the value a_k when outcome k is obtained. The average value output by the device in measurements of identically prepared systems is then indeed given by Eq. (4.3). A measurement of a POVM where all the POVM elements are projectors is called a projective measurement. The measurement statistic of a POVM in a state ρ is the vector of probabilities $Tr(M_k\,\rho)$.

The most general (quantum) operations in quantum mechanics are captured by so-called completely positive trace preserving maps, also-called quantum channels [87]. We call maps $\mathcal{B}(\mathcal{H}) \to \mathcal{B}(\mathcal{H})$ superoperators. We denote the identity superoperator by $\mathrm{id}\colon \mathcal{B}(\mathcal{H}) \to \mathcal{B}(\mathcal{H})$. A linear map $C\colon \mathcal{O}(\mathcal{H}) \to \mathcal{O}(\mathcal{H})$ is then called completely positive trace preserving if for all separable Hilbert spaces $\mathcal{H}'$ it holds that

$$\forall \rho \in \mathcal{S}(\mathcal{H} \otimes \mathcal{H}')\colon \quad (C \otimes \mathrm{id})\,\rho \in \mathcal{S}(\mathcal{H} \otimes \mathcal{H}'). \tag{4.5}$$

In the finite dimensional setting considered here, it turns out that fixing $\mathcal{H}' = \mathcal{H}$ in Eq. (4.5) already gives a necessary and sufficient condition for a map $C\colon \mathcal{O}(\mathcal{H}) \to \mathcal{O}(\mathcal{H})$ to be completely positive trace preserving [87]. We denote the set of all completely positive trace preserving maps on $\mathcal{S}(\mathcal{H})$ by $\mathcal{T}^+(\mathcal{H})$.

Throughout most of this review we will work in the framework of finite dimensional quantum mechanics. That is, if not explicitly stated otherwise, we consider systems that are described by a Hilbert space $\mathcal{H}$ over $\mathbf{C}$ whose dimension $d \coloneqq \dim(\mathcal{H})$ is finite, bosonic systems constituting an important exception.

For every $1 \leq p < \infty$ the Schatten p-norm of an operator $A \in \mathcal{B}(\mathcal{H})$ is defined as [88]

$$\|A\|_p \coloneqq \left[\sum_{j=1}^{d} (s_j(A))^p\right]^{1/p}, \tag{4.6}$$

where $(s_j(A))_{j=1}^d$ is the ordered, i.e., $s_1(A) \geq \cdots \geq s_d(A)$, sequence of non-negative, real singular values of A. We refer to the Schatten ∞-norm as the operator norm and call the Schatten 1-norm trace norm The Schatten p-norms are ordered in the sense that [88]

$$\forall A \in \mathcal{B}(\mathcal{H})\colon \|A\|_p \leq \|A\|_{p'} \iff p \geq p' \tag{4.7}$$

and in the converse direction the following inequalities hold [88]

$$\|\cdot\|_1 \leq \sqrt{d}\|\cdot\|_2 \leq d\|\cdot\|_\infty. \tag{4.8}$$

For quantum states a natural and frequently used distance measure is the trace distance [87]

$$\forall \rho,\sigma \in \mathcal{S}(\mathcal{H}): \quad \mathcal{D}(\rho,\sigma) \coloneqq \frac{1}{2}\|\rho-\sigma\|_1. \tag{4.9}$$

It is, up to the factor of $1/2$, the metric induced by the trace norm $\|\cdot\|_1$. Its relevance stems from the fact that it is equal to the maximal difference between the expectation values of all normalised observables in the states ρ and σ, i.e., [87]

$$\mathcal{D}(\rho,\sigma) = \max_{A\in\mathcal{O}(\mathcal{H}):\, 0\leq A\leq \mathbb{1}} Tr(A\,\rho) - Tr(A\,\sigma). \tag{4.10}$$

The trace distance is non-increasing under completely positive trace preserving maps $C \in \mathcal{T}^+(\mathcal{H})$, i.e., $\mathcal{D}(C(\rho),C(\sigma)) \leq \mathcal{D}(\rho,\sigma)$ and invariant under unitary operations, i.e., $\mathcal{D}\left(U\,\rho\,U^\dagger),U\,\sigma\,U^\dagger\right) = \mathcal{D}(\rho,\sigma)$. Moreover, if one is given an unknown quantum system and is promised that with probability $1/2$ it is either in state ρ or state σ, then the maximal achievable probability $p_{\max}$ for correctly identifying the state after a single measurement of the optimal observable from Eq. (4.10) is given by [89, 90]

$$p_{\max} = \frac{1+\mathcal{D}(\rho,\sigma)}{2}. \tag{4.11}$$

Inspired by this, one can define the distinguishability of two quantum states under a restricted set $\mathcal{M}$ of POVMs. The optimal success probability for single shot state discrimination is then again given by an expression of the form (4.11), but with $\mathcal{D}(\rho,\sigma)$ replaced by [91]

$$\mathcal{D}([,\mathcal{M})]\rho\sigma \coloneqq \sup_{M\in\mathcal{M}} \frac{1}{2}\sum_{k=1}^{|M|} |Tr(M_k\,\rho) - Tr(M_k\,\sigma)|, \tag{4.12}$$

and it holds that

$$\mathcal{D}([,\mathcal{M})]\rho\sigma \leq \mathcal{D}(\rho,\sigma)\,. \tag{4.13}$$

with equality for all $\rho,\sigma\in\mathcal{S}(\mathcal{H})$ if and only if $\mathcal{M}$ is a dense subset of the set of all POVMs [91]. It is worth noting that $\mathcal{D}([,\mathcal{M})]\cdot\,\cdot$ is a pseudometric on $\mathcal{S}(\mathcal{H})$, i.e., it is a symmetric, positive semidefinite bilinear form, but $\mathcal{D}([,\mathcal{M})]\rho\sigma = 0 \in \Longrightarrow\ \rho=\sigma$. For further properties of the distinguishability $\mathcal{D}([,\mathcal{M})]$ see for example Ref. [90].

Another frequently employed distance measure is the fidelity, defined for any two quantum states $\rho,\sigma\in\mathcal{S}(\mathcal{H})$ as[1]

$$\mathcal{F}(\rho,\sigma) \coloneqq Tr\left(\left(\rho^{1/2}\,\sigma\,\rho^{1/2}\right)^{1/2}\right)^2. \tag{4.14}$$

Similar to the trace distance, the fidelity is symmetric, i.e., $\mathcal{F}(\rho,\sigma)=\mathcal{F}(\sigma,\rho)$, non-decreasing under completely positive maps, and invariant under unitary operations. The fidelity is not a metric, but it is related to the trace distance via $1-\mathcal{F}(\rho,\sigma)^{1/2} \leq \mathcal{D}(\rho,\sigma) \leq (1-\mathcal{F}(\rho,\sigma))^{1/2}$. For pure states $\psi=|\psi\rangle\langle\psi|$ and $\varphi=|\varphi\rangle\langle\varphi|$ it reduces to the square of their overlap $\mathcal{F}(\psi,\varphi) = |\langle\psi\rangle\varphi|^2$.

The (time independent) Hamiltonian $H\in\mathcal{O}(\mathcal{H})$ of a finite dimensional quantum system has the spectral decomposition

$$H = \sum_{k=1}^{d'} E_k\,\Pi_k \tag{4.15}$$

[1] Some authors define the fidelity as the square root of the $\mathcal{F}$ used here.

where the $\Pi_k \in \mathcal{O}(\mathcal{H})$ are its orthogonal (and mutually orthogonal) spectral projectors and $d' \coloneqq |spec(H)| \leq d = \dim(\mathcal{H})$ is the number of distinct, ordered (energy) eigenvalues $E_k \in \mathbf{R}$ of H, i.e., $k < l \implies E_k < E_l$. The subspaces on which the Π_k project are called (energy) eigenspaces or energy levels. If H is non-degenerate it holds that $\Pi_k = |E_k\rangle\langle E_k|$ with $(|E_k\rangle)_{k=1}^d$ a sequence of orthonormal energy eigenstates of H and $d \coloneqq \dim(\mathcal{H})$ the dimension of $\mathcal{H}$.

The Hamiltonian H governs the time evolution $\rho\colon \mathbf{R} \to \mathcal{S}(\mathcal{H})$ of the state of a quantum system via the (Schrödinger-)von-Neumann-equation, which in the Schrödinger picture reads

$$\frac{\partial}{\partial t}\rho(t) = -\mathrm{i}[H, \rho(t)]. \tag{4.16}$$

Its formal solution can be given in terms of the time evolution operator, which in the case of time independent Hamiltonian dynamics is given by the operator exponential

$$\forall t \in \mathbf{R}\colon \quad U(t) \coloneqq \mathrm{e}^{-\mathrm{i}\,H\,t} \in \mathcal{B}(\mathcal{H}). \tag{4.17}$$

The time evolved quantum state at time t is then

$$\rho(t) \coloneqq U^\dagger(t)\,\rho(0)\,U(t), \tag{4.18}$$

with $\rho(0)$ the initial state at time $t = 0$.

The temporal evolution of the expectation value of an observable $A \in \mathcal{O}(\mathcal{H})$ then solves

$$\langle A\rangle_{\rho(t)} = Tr\big(A\,U^\dagger(t)\,\rho(0)\,U(t)\big) = Tr\big(U(t)\,A\,U^\dagger(t)\,\rho(0)\big). \tag{4.19}$$

One can thus equally well-define the time evolution of an observable $A\colon \mathbf{R} \to \mathcal{O}(\mathcal{H})$, with the initial value $A(0)$ given by the operator A from Eq. (4.19), by setting $A(t) \coloneqq U(t)\,A(0)\,U^\dagger(t)$, and consider a fixed quantum state $\rho \in \mathcal{S}(\mathcal{H})$, equal to the initial state $\rho(0)$ in Eq. (4.19). Then $\langle A(t)\rangle_\rho$ is equal to $\langle A\rangle_{\rho(t)}$ from Eq. (4.19) for all $t \in \mathbf{R}$. The time evolution $A\colon \mathbf{R} \to \mathcal{O}(\mathcal{H})$ of an observable in the Heisenberg picture solves the differential equation

$$\frac{\partial}{\partial t}A(t) = \mathrm{i}[H, A(t)]. \tag{4.20}$$

We call all observables $A \in \mathcal{O}(\mathcal{H})$ that commute with the Hamiltonian, i.e., for which $[H, A] \coloneqq A\,B - B\,A = 0$, conserved quantities. It follows directly from Eq. (4.20) that the expectation value of all conserved quantities is independent of time, irrespective of the initial state, which justifies the name. If the Hamiltonian H is non-degenerate, then exactly the observables that are diagonal in the same basis as H are conserved quantities. In the presence of degeneracies exactly the observables $A \in \mathcal{O}(\mathcal{H})$ for which some basis exists in which both A and H are diagonal are conserved quantities.

Given a function f depending on time, we define its finite time average

$$\overline{f}^T \coloneqq \frac{1}{T}\int_0^T f(t), \tag{4.21}$$

and its (infinite) time average

$$\overline{f} \coloneqq \lim_{T\to\infty} \overline{f}^T, \tag{4.22}$$

whenever the limit exists. In all cases we will be interested in, the existence of the limit in Eq. (4.22) is guaranteed by the theory of (Besicovitch) almost-periodic functions [92].

In particular we will encounter the time averaged state $\omega \coloneqq \overline{\rho}$, which is, in the finite dimensional case considered here, equal to the initial state $\rho(0)$ dephased with respect to the Hamiltonian H, i.e., $\omega = \$_H(\rho(0))$, with the de-phasing map acting as

$$\rho \mapsto \$_H(\rho) \coloneqq \sum_{k=1}^{d'} \Pi_k\,\rho\,\Pi_k \tag{4.23}$$

and $(\Pi_k)_{k=1}^{q'}$ the sequence of orthogonal spectral projectors of H.

We will encounter systems consisting of smaller subsystems. Often their Hamiltonian can be written as a sum of Hamiltonians that each act non-trivially only on certain subsets of the whole system. We will refer to such systems as composite (quantum) systems or as locally interacting (quantum) systems, depending on whether we want to stress that they consist of multiple parts or that the interaction between the parts has a special structure. The notion of locally interacting quantum systems can be formalised by means of an interaction (hyper)graph $\mathcal{G} \coloneqq (\mathcal{V}, \mathcal{E})$, which is a pair of a vertex set $\mathcal{V}$ and an edge set $\mathcal{E}$.

The vertex set $\mathcal{V}$ is the set of indices labeling the sites of the system and we will work under the assumption that $|\mathcal{V}| < \infty$. The Hilbert space $\mathcal{H}$ of such a system is either, in the case of spin systems, the tensor product $\bigotimes_{x\in\mathcal{V}} \mathcal{H}_{\{x\}}$ of the Hilbert spaces $\mathcal{H}_{\{x\}}$ of the individual sites $x \in \mathcal{V}$, or, in the case of fermionic or bosonic systems, the Fock space, or a subspace of the latter.

We will encounter bosons, which usually need to be described using infinite dimensional Hilbert spaces, only in Section 4.3.3, hence we want to avoid the technicalities of a proper treatment of infinite dimensional Hilbert spaces and unbounded operators in the framework of functional analysis. We will thus only introduce the minimal notation necessary to formulate the statements we will discuss in Section 4.3.3.

The sites $x \in \mathcal{V}$ of fermionic and bosonic composite systems are often called modes. In the case of fermions each mode is equipped with the Hilbert space $\mathcal{H}^f_{\{x\}} = \mathbf{C}^2$ with orthonormal basis $((|n\rangle_f)_{n=0}^1$, and in the case of bosons with the Hilbert space $\mathcal{H}^b_{\{x\}} = \ell^2$ of square summable sequences with orthonormal basis $(|n\rangle_b)_{n=0}^\infty$. For composite systems with exactly N fermions or bosons in M modes, i.e., $\mathcal{V} = [M]$, the Hilbert space is given by a so-called Fock layer. The Fock layer to particle number N is the complex span of the orthonormal Fock (basis) states $|n_1, \ldots, n_M\rangle_f$ or $|n_1, \ldots, n_M\rangle_b$ respectively, where for each $x \in \mathcal{V}$, n_x is the number of particles in mode x and thus $\sum_{x\in\mathcal{V}} n_x = N$ with $n_x \in \{0, 1\}$ in the case of fermions, and $n_x \in [N]$ in the case of bosons.

The full Fock space of a system of fermions or bosons is the Hilbert space completion of the direct sum of the Fock layers for each possible total particle number. For fermions it holds that $N \leq M$ due to the Pauli exclusion principle, and the resulting Hilbert space is hence finite dimensional. In the case of bosons N is independent of M and the Fock space is thus infinite dimensional already for a finite number of modes.

We define the fermionic and bosonic annihilation operators f_x and b_x on site x and the corresponding creation operators $f_x^\dagger$ and $b_x^\dagger$ (collectively often referred to as simply the fermionic/bosonic operators) via their action on the Fock basis states given by

$$f_x|n_1, \ldots, n_M\rangle_f = n_x(-1)^{\sum_{y=1}^{x-1} n_y}|\ldots, n_{x_1}, n_x - 1, n_{x+1}, \ldots\rangle_f, \tag{4.24}$$

$$f_x^\dagger|n_1, \ldots, n_M\rangle_f = (1 - n_x)(-1)^{\sum_{y=1}^{x-1} n_y}|\ldots, n_{x_1}, n_x + 1, n_{x+1}, \ldots\rangle_f \tag{4.25}$$

and

$$b_x|n_1, \ldots, n_M\rangle_b = \sqrt{n_x}|n_1, \ldots, n_{x_1}, n_x - 1, n_{x+1}, \ldots, n_M\rangle_b, \tag{4.26}$$

$$b_x^\dagger|n_1, \ldots, n_M\rangle_b = \sqrt{n_x + 1}|n_1, \ldots, n_{x_1}, n_x + 1, n_{x+1}, \ldots, n_M\rangle_b. \tag{4.27}$$

They satisfy the (anti) commutation relations

$$\{f_x, f_y\} = \{f_x^\dagger, f_y^\dagger\} = 0, \qquad \{f_x, f_y^\dagger\} = \delta_{x,y}, \tag{4.28}$$

$$[b_x, b_y] = [b_x^\dagger, b_y^\dagger] = 0, \qquad [b_x, b_y^\dagger] = \delta_{x,y}, \tag{4.29}$$

where for any two operators $A, B \in \mathcal{B}(\mathcal{H})$ $[A, B] \coloneqq AB - BA$ is the commutator and $\{A, B\} \coloneqq AB + BA$ the anti-commutator. We say that A, B commute or anti-commute if $[A, B] = 0$ or $\{A, B\} = 0$ respectively.

Any operator that commutes with the total particle number operator $\sum_{x\in\mathcal{V}} f_x^\dagger f_x$ or $\sum_{x\in\mathcal{V}} b_x^\dagger b_x$ respectively is called particle number preserving. In systems with particle number preserving Hamiltonians a constraint on the particle number can be used to make the description of bosonic systems with finite dimensional Hilbert spaces possible. The Hilbert space is then a finite direct sum of Fock layers. We say that a state has a finite particle number if it is completely contained in such a finite direct sum of Fock layers.

In systems of fermions, all operators can be written as polynomials of the fermionic operators. A polynomial of fermionic operators is called even/odd if it can be written as a linear combination of monomials that are each a product of an even/odd number of creation and annihilation operators. According to the fermion number parity superselection rule [93], only observables that are even polynomials in the fermionic operators can occur in nature. The same holds for the Hamiltonians and density matrices of such systems. Consequently, whenever we make statements about systems of fermions we assume that all observables, states and the Hamiltonian are even.

We refer to subsets of the vertex set $\mathcal{V}$ as subsystems. Generalising the notation introduced for the Hilbert spaces of the individual sites we denote the Hilbert spaces associated with a subsystem $X \subseteq \mathcal{V}$ by $\mathcal{H}_X$ and its dimension by $d_X \coloneqq \dim(\mathcal{H}_X)$. In the case of composite systems of fermions or bosons it is understood that if an upper bound on the total number of particles has been imposed, then $\mathcal{H}_X$ is taken to be the direct sum of Fock layers corresponding to the sites in X up to the total number of particles. The size of a (sub)system $X \subseteq \mathcal{V}$ is given by the number of sites or modes $|X|$, not the dimension of the corresponding Hilbert space.

For spin systems we define the support $supp(A)$ of an operator $A \in \mathcal{B}(\mathcal{H})$ as the smallest subset of $\mathcal{V}$ such that A acts like the identity outside of X. For systems of fermions or bosons we define the support of an operator via its representation as a polynomial in the respective creation and annihilation operators. The support is then the set of all site indices $x \in \mathcal{V}$ for which the polynomial contains a fermionic or bosonic operator acting on site x, e.g., $b_x^\dagger$ or f_x. The support of a POVMs is simply the union of the supports of its POVM elements. Similarly, we define the support $supp(C)$ of a superoperator $C\colon \mathcal{B}(\mathcal{H}) \to \mathcal{B}(\mathcal{H})$ as the smallest subset of $\mathcal{V}$ such that

$$\forall A \in \mathcal{B}(\mathcal{H})\colon \quad supp(A) \subseteq supp(C)^c \implies C(A) = A. \tag{4.30}$$

We say that an observable, POVM, or superoperator is local if the size of its support is small compared to and/or independent of the system size.

In order to fully exploit the notion of a subsystem we need to understand how the description of a joint system fits together with the description of a subsystem as an isolated system, i.e., how systems can be combined and decomposed. For every subsystem $X \subseteq \mathcal{V}$ there is a canonical embedding of $\mathcal{B}(\mathcal{H}_X)$ into $\mathcal{B}(\mathcal{H})$ that bijectively maps $\mathcal{B}(\mathcal{H}_X)$ onto the subalgebra of bounded linear operators $A \in \mathcal{B}(\mathcal{H})$ with $supp(A) \subseteq X$, and similarly for all operators that are polynomials of bosonic operators. In the case of spin systems the embedding is simply the natural embedding $A \in \mathcal{B}(\mathcal{H}_X) \mapsto A \otimes \mathbb{1}_{X^c} \in \mathcal{B}(\mathcal{H})$, where $\mathbb{1}_{X^c}$ denotes the identity operator on $\mathcal{H}_{X^c}$. In systems of fermions or bosons we associate to each operator on $\mathcal{H}_X$ the operator on $\mathcal{H}$ that has the same representation as a polynomial in the fermionic/bosonic operators, but, of course, in terms of the fermionic/bosonic operators of the full system with Fock space $\mathcal{H}$ rather than the fermionic/bosonic operators that act on $\mathcal{H}_X$. For systems of fermions, because of the phase in Eq. (4.24) that depends non-locally on the state, this embedding depends on the exact position the sites in X have in the vertex set $\mathcal{V}$. The vertex set should hence rather be called vertex sequence, but for even operators the phases cancel out, which is why we ignore this subtlety.

Conversely, for any $A \in \mathcal{B}(\mathcal{H})$ and any subsystem $X \subseteq \mathcal{V}\colon X \supseteq supp(A)$ that contains $supp(A)$ we define the truncation $A_{\restriction X} \in \mathcal{B}(\mathcal{H}_X)$ of A as the operator that acts on the sites/-modes in the subsystem X "in the same way" as A, in the sense that a truncation followed

by a canonical embedding gives back the original operator. In particular, for spin systems any $A \in \mathcal{B}(\mathcal{H})$ is of the form $A = A_{\restriction supp(A)} \otimes \mathbb{1}_{supp(A)^c}$. For general systems, the identity operator $\mathbb{1}$ of course satisfies $\mathbb{1}_X = \mathbb{1}_{\restriction X}$ for any $X \subset \mathcal{V}$.

We now turn to the edge set. The edge set $\mathcal{E}$ is the set of all subsystems $X \subset \mathcal{V}$ for which a non-trivial Hamiltonian term H_X with $supp(H_X) = X$ exists that couples the sites in X. The Hamiltonian of a locally interacting quantum system with edge set $\mathcal{E}$ — often just called a local Hamiltonian — is of the form

$$H = \sum_{X \in \mathcal{E}} H_X, \tag{4.31}$$

with $supp(H_X) = X$ for all $X \in \mathcal{E}$. Most Hamiltonians in the condensed-matter context or of cold atoms in optical lattices can be very well approximated by such locally interacting Hamiltonians. Generalising this notation to subsystems $X \subset \mathcal{V}$ that are not in $\mathcal{E}$ we define for any subsystem $X \subset \mathcal{V}$ the restricted Hamiltonian

$$H_X \coloneqq \sum_{Y \in \mathcal{E} \colon Y \subseteq X} H_Y \in \mathcal{O}(\mathcal{H}), \tag{4.32}$$

which obviously fulfils $supp(H_X) \subseteq X$. Note that we adopt the convention that H_X is an element of $\mathcal{O}(\mathcal{H})$ and not of $\mathcal{O}(\mathcal{H}_X)$.

We will also need the graph distance. In order to define it, we first need to give a precise meaning to a couple of intuitive terms: We say that two subsystems $X, Y \subset \mathcal{V}$ overlap if $X \cap Y \neq \emptyset$, a set $X \subset \mathcal{V}$ and a set $F \subset \mathcal{E}$ overlap if F contains an edge that overlaps with X, and two sets $F, F' \subset \mathcal{E}$ overlap if F overlaps with any of the edges in F'. A subset $F \subset \mathcal{E}$ of the edge set connects X and Y if F contains all elements of some sequence of pairwise overlapping edges such that the first overlaps with X and the last overlaps with Y and similarly for sites $x, y \in \mathcal{V}$.

The (graph) distance $d(X, Y)$ of two subsets $X, Y \subset \mathcal{V}$ with respect to the (hyper)graph $(\mathcal{V}, \mathcal{E})$ is zero if X and Y overlap and otherwise equal to the size of the smallest subset of $\mathcal{E}$ that connects X and Y. The diameter of a set $F \subset \mathcal{E}$ is the largest graph distance between any two sets $X, Y \in F$. We extend the definition of the graph distance to operators $A, B \in \mathcal{B}(\mathcal{H})$ and set $d(A, B) \coloneqq d(supp(A), supp(B))$.

We will also make use of the notion of reduced states, or marginals. Given a quantum state $\rho \in \mathcal{S}(\mathcal{H})$ of a composite system with subsystem $X \subset \mathcal{V}$ we write ρ^X for the reduced state on X, which is defined as the unique quantum state $\rho^X \in \mathcal{S}(\mathcal{H}_X)$ with the property that for any observable $A \in \mathcal{O}(\mathcal{H})$ with $supp(A) \subseteq X$

$$Tr(A_{\restriction X}\, \rho^X) = Tr(A\, \rho). \tag{4.33}$$

Defining the reduced state in systems of fermions in this way is important to avoid ambiguities [94]. We will denote the linear map $\rho \mapsto \rho^X$ by Tr_{X^c}. As Tr_{X^c} is linear we can naturally extend its domain to all of $\mathcal{B}(\mathcal{H})$ so that

$$Tr_{X^c} \colon \mathcal{B}(\mathcal{H}) \to \mathcal{B}(\mathcal{H}_X). \tag{4.34}$$

In the case of spin systems Tr_{X^c} is indeed the partial trace over $X^c = \mathcal{V} \setminus X$ as defined for example in Ref. [87]. For time evolutions $\rho \colon \mathbf{R} \to \mathcal{S}(\mathcal{H})$ we use the natural generalisation of the superscript notation, i.e., $\rho^X = Tr_{X^c} \circ \rho \colon \mathbf{R} \to \mathcal{S}(\mathcal{H}_X)$.

Correlations play a central role in the description of composite systems and hence in condensed matter physics and statistical mechanics. It is beyond the scope of this work to give a comprehensive overview of the different types and measures of correlations (see for example

Refs. [7, 96, 87, 97]). One important measure of correlation is the covariance, which for a quantum state $\rho \in \mathcal{S}(\mathcal{H})$ and two operators $A, B \in \mathcal{B}(\mathcal{H})$ is defined to be

$$cov_\rho(A,B) \coloneqq Tr(\rho\, A\, B) - Tr(\rho\, A) Tr(\rho\, B). \tag{4.35}$$

It satisfies

$$|cov_\rho(A,B)| \leq \left(\langle A^2\rangle_\rho \langle B^2\rangle_\rho\right)^{1/2} \tag{4.36}$$

and hence one often defines the correlation coefficient as $cov_\rho(A,B)/(\langle A^2\rangle_\rho \langle B^2\rangle_\rho)^{1/2}$. We will encounter a slightly generalised version of the covariance in Section 4.10.

The covariance is most interesting as a correlation measure if A and B act on disjoint subsystems, i.e., $supp(A) \cap supp(B) = \emptyset$. If for a given state $\rho \in \mathcal{S}(\mathcal{H})$ of a bipartite system with $\mathcal{V} = X \dot\cup Y$ and any two observables $A, B \in \mathcal{O}(\mathcal{H})$ with $supp(A) \subseteq X$ and $supp(B) \subseteq Y$ it holds that $cov_\rho(A,B) = 0$, then we say that ρ is uncorrelated with respect to the bipartition $\mathcal{V} = X \dot\cup Y$.

Uncorrelated states of spin systems are product states. Consider a bipartite spin system with Hilbert space H and vertex set $\mathcal{V} = X \dot\cup Y$. A quantum state $\rho \in \mathcal{S}(\mathcal{H})$ is said to be product with respect to this bipartition if $\rho = \rho^X \otimes \rho^Y$. We call a basis that consists entirely of product states a product basis.

Still in the setting of a bipartite spin system with Hilbert space H and vertex set $\mathcal{V} = X \dot\cup Y$, all quantum states of the form

$$\rho = \sum_j p_j\, \rho_j^X \otimes \rho_j^Y \tag{4.37}$$

with $(p_j)_j$ a probability vector, i.e., $\sum_j p_j = 1$ and $p_j \geq 0$ for all j, and $\rho_j^X \in \mathcal{S}(\mathcal{H}_X)$ and $\rho_j^Y \in \mathcal{S}(\mathcal{H}_Y)$ for all j, are called separable with respect to the bipartition $\mathcal{V} = X \dot\cup Y$. All states that can be prepared with local operations and classical communication (LOCC) are called separable, a notion that also holds true for bosonic or fermionic systems. Such states are correlated in general, but a classical mechanism can be held responsible for the correlations present. All states that are not separable are called entangled.

The Gibbs state or thermal state of a system with Hilbert space $\mathcal{H}$ and Hamiltonian $H \in \mathcal{O}(\mathcal{H})$ at inverse temperature $\beta \in \mathbf{R}$ is defined as

$$g[H](\beta) \coloneqq \frac{\mathrm{e}^{-\beta H}}{Z[H](\beta)} \in \mathcal{S}(\mathcal{H}), \tag{4.38}$$

where $Z[H]$ is the (canonical) partition function defined as

$$Z[H](\beta) \coloneqq Tr(\mathrm{e}^{-\beta H}). \tag{4.39}$$

The Gibbs state has the important property that it is the unique quantum state that maximises the von Neumann entropy

$$S(\rho) \coloneqq -Tr(\rho \log_2 \rho). \tag{4.40}$$

given the expectation value of the Hamiltonian [98]. This is a direct consequence of Schur's lemma [88] and the fact that the same statement holds in classical statistical mechanics, as can be seen from a straight forward application of the Lagrange multiplier technique. In fact, the inverse temperature β is nothing but the Lagrange parameter associated with the energy expectation value.

For locally interacting quantum systems with a Hamiltonian $H \in \mathcal{O}(\mathcal{H})$ of the form given in (4.31) we adopt the convention that for any subsystem $X \subset \mathcal{V}$

$$g^X[H](\beta) = Tr_{X^c}(g[H](\beta)) \in \mathcal{S}(\mathcal{H}_X) \tag{4.41}$$

denotes the reduction of the Gibbs state of the full system to the subsystem X (compare Eq. (4.33)).

The micro-canonical ensemble in quantum statistical mechanics takes the form of the micro-canonical state. Usually one defines the micro-canonical ensemble and state with respect to an energy interval $[E, E + \Delta]$. Here we make the slightly more general definition that will be useful later: The micro-canonical state to any subset $R \subseteq \mathbf{R}$ of the real numbers of a system with Hilbert space $\mathcal{H}$ and Hamiltonian $H \in \mathcal{O}(\mathcal{H})$ with spectral decomposition $H = \sum_{k=1}^{d'} E_k \Pi_k$ is defined as

$$\sqcap[H](R) := \frac{\sum_{k:E_k \in R} \Pi_k}{Z_{mc}[H](R)} \in \mathcal{S}(\mathcal{H}), \tag{4.42}$$

where $Z_{mc}[H]$ is the micro-canonical partition function defined as

$$Z_{mc}[H](R) := Tr(\sum_{k:E_k \in R} \Pi_k). \tag{4.43}$$

4.3 Equilibration

The dynamics of finite dimensional quantum system, as described in the previous section, is recurrent [99, 100, 101, 102, 103] and time reversal invariant. Hence, genuine equilibration in the sense of Boltzmann's H-Theorem [104] that implies that entropy can only grow over time (see also Section 4.12.1) is impossible. This apparent contradiction between the microscopic theory of quantum mechanics and the thermodynamic behaviour observed in nature is one of the main issues that any derivation of statistical mechanics and thermodynamics from quantum theory needs to solve.

We will see in this section that the unitary time evolution of pure states of such systems does imply in a surprisingly general and natural way that certain time dependent properties of quantum systems do dynamically equilibrate and that hence this apparent contradiction can be resolved to a large extend.

We will concentrate on two notions of equilibration: equilibration on average and equilibration during intervals. After an introduction of these two notions in Section 4.3.1 we will discuss them in detail in Sections 4.3.2 and 4.3.3. In particular we will give conditions under which equilibration in the respective sense can be ensured. In Section 4.3.4 we touch upon other notions of equilibration that have been investigated in the literature. Then we discuss Lieb-Robinson bounds, which limit the signal propagation in locally interacting quantum lattice systems, in Section 4.3.5 before we go on to survey results on the times scale on which equilibration happens in Section 4.3.6. We end this section with a brief description of fidelity decay in Section 4.3.7. In the next section, Section 4.4, we then put the discussed rigorous results into the perspective of the picture emerging from numerical simulations and the insights gained from analytic investigations of more specific models.

4.3.1 Notions of equilibration

In this section we define and compare two notions of equilibration compatible with the recurrent and time reversal invariant nature of unitary quantum dynamics in finite dimensional systems. These notions will capture the intuition that equilibration means that a quantity, after having been initialised at a non-equilibrium value, evolves towards some value and then stays close to it for an extended amount of time. At the same time, what we will call equilibration is less than what one usually associates with the evolution towards thermal equilibrium. We

will define a quantum version of the latter, call it thermalisation, and discuss it in detail in Section 4.7.

To keep the definition of equilibration as general as possible we will refer abstractly to time dependent properties of quantum systems, by which we mean functions $f\colon \mathbf{R} \to M$ that map time to some metric space M, for example $\mathbf{R}$ or $\mathcal{S}(\mathcal{H})$. The metric will allow us to quantify how close the value of such functions is for different times and in particular how close it is to the time average and "equilibrium values" of the function.

Properties that we will be interested in include for example the time evolution of expectation values of individual observables. We will also encounter subsystem equilibration. In this case the property is the time evolution of the state of the subsystem and the metric the trace distance. It will also be convenient to speak more generally of the apparent equilibration of the whole system with the metric then being the distinguishability under a restricted set of POVMs.

We will discuss the following two notions of equilibration in more detail:

Equilibration on average: We say that a time dependent property equilibrates on average if its value is for most times during the evolution close to some equilibrium value.

Equilibration during intervals: We say that a time dependent property equilibrates during a (time) interval if its value is close to some equilibrium value for all times in that interval.

The use of the notion of equilibration on average in the quantum setting goes back to at least the work of von Neumann [3] and has recently been developed further, in particular in Refs. [105, 106, 107, 91, 89, 108, 109, 110]. We will see that equilibration on average, especially for expectation values of observables as well as for reduced states of small subsystems of large quantum systems, is provably a very generic feature. In contrast, equilibration during intervals is a property that is expected to be generically the case for locally interacting many-body systems, and there is compelling numerical evidence for such a behaviour. To date, however, it has rigorously been proven only for specific models [111, 112].

Equilibration on average implies that the equilibrating property spends most of the time during the evolution close to its time average. This allows for a reasonable definition of an equilibrium state, which is then the time averaged or de-phased state. As we will see later in Section 4.7, this makes it possible to tackle the question of thermalisation in unitarily evolving quantum systems.

On the down side, a proof of equilibration on average alone does not immediately imply much about the time scale on which the equilibrium value is reached after a system is started in an out of equilibrium situation. We will see that even though it is possible to bound these time scales, the bounds obtainable in the general settings considered here are only of very limited physical relevance (see Section 4.3.6).

As we will see in the following, the statements on equilibration during intervals are much more powerful in this respect. They imply bounds on the time it takes to equilibrate that scale reasonably with the size of the system and hence prove equilibration on experimentally relevant time scales. On the other hand, in the few settings in which equilibration during intervals of reduced states of subsystems has been proven, it is known that the equilibrium states are not close to thermal states of suitably restricted Hamiltonians. In particulate, no proof of thermalisation (in the sense of the word we will defined later in Section 4.7.1) based on a result on equilibration during intervals is known to date. We discuss both notions of equilibration in detail in the following two sections.

4.3.2 Equilibration on average

In this section we discuss equilibration on average (see figure 4.2 for a graphical illustration). The outline is as follows: After giving some historic perspective we will go through the main ingredients that feature in the known results on equilibration on average and discuss their role in the arguments and to what extent they are physically reasonable and mathematically necessary. After this preparation we will state, prove and interpret the arguably strongest result on equilibration on average known to date.

Already the founding fathers of quantum mechanics realised that the unitary evolution of large, closed quantum systems, together with the immensely high dimension of their Hilbert space and quantum mechanical uncertainty, could possibly explain the phenomenon of equilibration. Most notable is an article of von Neumann [3] from 1929, which already contains a lot of the ideas and even variants of some of the results that can be found in the modern literature on the subject. The renewed interest in the topic of equilibration was to a large extent a consequence of the two independent theoretical works Refs. [106, 107]. The approach outlined there was then more recently refined and the results gradually strengthened. Important contributions are in particular Refs. [109, 91, 89]. Also very noteworthy is the often overlooked earlier work Ref. [105].

The first fact that plays a prominent role in the proofs of equilibration on average is the immensely high dimension of the Hilbert space of most many-body systems. The dimension of the Hilbert space of composite systems grows exponentially with the number of constituents. What actually matters, of course, is the number of significantly occupied energy levels, rather than the number of levels that are in principle available but not populated. For each $k \in [d']$ we define the occupation $p_k := Tr(\Pi_k\, \rho(0))$ of the k-th energy level, where $d' := |spec(H)| \leq d = \dim(\mathcal{H})$ is the number of distinct such levels. Refs. [105, 106] use $\max_k p_k$, the occupation of the most occupied level, to quantify the number of significantly occupied energy levels. Ref. [107] uses a quantity called effective dimension, denoted by $d^{\text{eff}}(\omega)$, which in our notation can be defined as

$$d^{\text{eff}}(\omega) := \frac{1}{\sum_{k=1}^{d'} p_k^2} \geq \frac{1}{\max_k p_k}. \tag{4.44}$$

If the initial state is taken to be an energy eigenstate, the resulting effective dimension is one, while that resulting from a uniform coherent superposition of $\tilde{d}$ energy eigenstates to different energies is $\tilde{d}$. This justifies the interpretation of $d^{\text{eff}}(\omega)$ as a measure of the number of significantly occupied states. It is also reciprocal to a quantity that is known mostly in the condensed matter literature as inverse participation ratio [113] and related to the time average of the Loschmidt echo [114, 66]. While using the effective dimension instead of the occupation of the most occupied level can lead to tighter bounds it has the disadvantage that it cannot be efficiently computed given a state and the Hamiltonian.

There are a number of different ways to argue why it is acceptable to restrict oneself to initial states that populate a large number of energy levels when trying to prove the emergence of thermodynamic behaviour from the unitary dynamics of closed systems. First, one can argue that initial states that only occupy a small subspace of the Hilbert space of a large system behave essentially like small quantum systems and such systems are anyway not expected to behave thermodynamically, but rather show genuine quantum behaviour. Second, one can invoke the inevitable limits to the resolution and precision of experimental equipment to conclude that preparing states that overlap only with a handful of the roughly $2^{10^{23}}$ energy levels of a macroscopic system is impossible, even if we had apparatuses that were many orders of magnitude more precise than the equipment available today [106, 109]. Finally, one can also take a more mathematical point of view and use results based on a phenomenon called measure concentration [115, 116] that guarantees that uniformly random pure states drawn from sufficiently large subspaces of a Hilbert space have, with extremely high probability, an

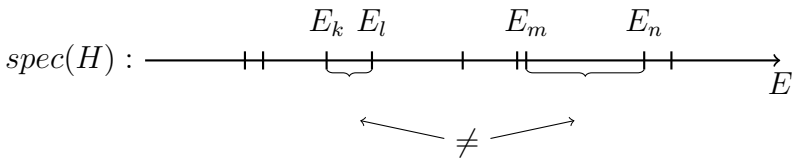

Figure 4.1: (Reproduction from Ref. [120]) Illustration of the non-degenerate energy gaps condition. No gap between two energy levels may occur more than once in the spectrum, but the individual levels may well be degenerate.

effective dimension with respect to any fixed, sufficiently non-degenerate Hamiltonian that is comparable to the dimension of that subspace [107, 117, 68, 118] (more on such typicality arguments in Section 4.6). If one is willing to assume that such states are physically natural initial states, this can justify the assumption of a large effective dimension. We will come back to this in Section 4.6 where we discuss typicality. For an earlier work that directly mingles typicality arguments and de-phasing to derive an equilibration result see also Ref. [119].

As we will see below, it is actually sufficient for equilibration that $\max'_k p_k$, the second largest of the energy level occupations, is small. Note that in the physically relevant situation of a system that is cooled close to its ground state $\max'_k p_k$ can be orders of magnitude smaller than $\max_k p_k$ or $1/d^{\text{eff}}(\omega)$. Although the proof of this extension of previous results is not trivial [109], the physical intuition behind it is clear: The expectation values of all observables of a system that is initialised in an energy eigenstate are already in equilibrium. What can prevent equilibration on average are not macroscopic populations of one energy level, but rather initial states that are coherent superpositions of a small number of energy eigenstates. Such states can show a behaviour reminiscent of Rabi-Oscillations and not exhibit equilibration.

The second main ingredient to the proofs of Refs. [3, 105, 106, 107] is the condition of non-degenerate energy gaps originally called the non-resonance condition. We say that a Hamiltonian H has non-degenerate energy gaps, if for every $k, l, m, n \in [d']$

$$E_k - E_l = E_m - E_n \implies (k = l \wedge m = n) \vee (k = m \wedge l = n), \tag{4.45}$$

i.e., if every energy gap $E_k - E_l$ appears exactly once in the spectrum of H (see figure 4.1). The original condition used in Refs. [3, 105, 106, 107] is stronger and excludes in addition all Hamiltonians with degeneracies, i.e., requires that $d' = d$. Although the non-degenerate energy gaps condition appears to be pretty technical at first sight, the motivation for imposing it can be made apparent by the following consideration: The main concern of Ref. [107] is the equilibration on average of the reduced state $\rho^S(t)$ of a small subsystem S of a bipartite system with $\mathcal{V} = S \dot\cup B$. If the Hamiltonian of the composite system is of the form

$$H = H_S + H_B, \tag{4.46}$$

i.e., S and B are not coupled (remember the definition of the restricted Hamiltonian in Eq. (4.32)), then $\rho^S(t)$ will simply evolve unitarily and equilibration of $\rho^S(t)$ is clearly impossible. Hence, one needs a condition that excludes such non-interacting Hamiltonians. Imposing the condition of non-degenerate energy gaps is a mathematically elegant, simple, and natural way to do this. It is easy to see that Hamiltonians of the form given in Eq. (4.46) have many degenerate gaps, as their eigenvalues are simply sums of the eigenvalues of H_S and H_B.

In the more recent literature, the condition of non-degenerate energy gaps has been gradually weakened. Ref. [91] defines the maximal number of energy gaps in any energy interval of width ϵ,

$$N(\epsilon) \coloneqq \sup_{E \in \mathbf{R}} |\{(k,l) \in [d']^2 \colon k \neq l \wedge E_k - E_l \in [E, E+\epsilon]\}|. \tag{4.47}$$

Note that $N(0)$ is the number of degenerate energy gaps and a Hamiltonian H satisfies the non-degenerate energy gaps condition if and only if $N(0) = 1$. The above definition allows to prove an equilibration theorem that still works if a system has a small number of degenerate energy gaps. Moreover, it has the advantage that it allows to make statements about the equilibration time. As we will see in the next theorem, equilibration on average can be guaranteed to happen on a time scale T that is large enough such that $T\,\epsilon \gg 1$ where ϵ must be chosen small enough such that $N(\epsilon)$ is small compared to the number of significantly populated energy levels.

The arguably strongest and most general result concerning equilibration on average in quantum systems can be obtained by combining the two recent works Refs. [91, 109]. In fact, we will see that it even goes slightly beyond a mere proof of equilibration on average, as it does have non-trivial implications for the time scales on which equilibration happens.

Theorem 1 (Equilibration on average)**.** *Given a system with Hilbert space $\mathcal{H}$ and Hamiltonian $H \in \mathcal{O}(\mathcal{H})$ with spectral decomposition $H = \sum_{k=1}^{d'} E_k\,\Pi_k$. For $\rho(0) \in \mathcal{S}(\mathcal{H})$ the initial state of the system, let $\omega = \$_H(\rho(0))$ be the de-phased state and define the energy level occupations $p_k \coloneqq Tr(\Pi_k\,\rho(0))$. Then, for every $\epsilon, T > 0$ it holds that (i) for any operator $A \in \mathcal{B}(\mathcal{H})$*

$$\overline{(\langle A\rangle_{\rho(t)} - \langle A\rangle_\omega)^2}^T \leq \|A\|_\infty^{\,2}\, N(\epsilon)\, f(\epsilon\,T)\, g((p_k)_{k=1}^{d'}), \tag{4.48}$$

and (ii) for every set $\mathcal{M}$ of POVMs

$$\overline{\mathcal{D}\left([,\mathcal{M})\right]\rho(t)\omega}^T \leq h(\mathcal{M})\,\left(N(\epsilon)\, f(\epsilon\,T)\, g((p_k)_{k=1}^{d'})\right)^{1/2}, \tag{4.49}$$

where $N(\epsilon)$ is defined in Eq. (4.47), $f(\epsilon\,T) \coloneqq 1 + 8\log_2(d')/(\epsilon\,T)$,

$$g((p_k)_{k=1}^{d'}) \coloneqq \min(\sum_{k=1}^{d'} p_k^2, 3\max{}'_k p_k), \tag{4.50}$$

and

$$h(\mathcal{M}) \coloneqq \min(|\cup\mathcal{M}|/4, \dim(\mathcal{H}_{supp(\mathcal{M})})/2), \tag{4.51}$$

with $\max'_k p_k$ the second largest element in $(p_k)_{k=1}^{d'}$, $\cup\mathcal{M}$ the set of all distinct POVM elements in $\mathcal{M}$, and $supp(\mathcal{M}) \coloneqq \bigcup_{M\in\cup\mathcal{M}} supp(M)$.

Proof. Eq. (4.48) for $g((p_k)_{k=1}^{d'})$ equal to the first argument of the min in Eq. (4.50) is Theorem 1 in Ref. [91]. The same statement, but with $g((p_k)_{k=1}^{d'})$ equal to the second argument in the min, follows from Eqs. (44), (50), (61), and (63) in Ref. [109]. With $|\cup U|$ in Eq. (4.51) replaced by the total number of all measurement outcomes, i.e., $\sum_{M\in\mathcal{M}} |M|$, Eq. (4.49), for $g((p_k)_{k=1}^{d'})$ equal to the first argument of the min in Eq. (4.50), is implied by Theorems 2 and 3 from Ref. [91]. A careful inspection of Eq. (B.1) in Ref. [91], however, reveals that the slightly stronger result holds. In particular, one can first use the bound

$$\max{}_{M(t)\in\mathcal{M}} D_{M(t)}(\rho(t),\omega) \leq \sum_{M_a\in\cup\mathcal{M}} |\,tr(M_a\,\rho(t)) - tr(M_a\,\omega)| \tag{4.52}$$

for the argument of the time average in the right hand side of the first line of Eq. (B.1) and then use the triangle inequality to pull the time average into the sum. For $g((p_k)_{k=1}^{d'})$ equal to the second argument the result follows using Eq. (4.48) instead of Theorem 1 from Ref. [91] in the proofs of Theorems 2 and 3 from Ref. [91]. □

What is the physical meaning of the theorem? The quantity $g((p_k)_{k=1}^{d'})$ is small, except if the initial state assigns large populations to few (but more than one) energy levels. For initial

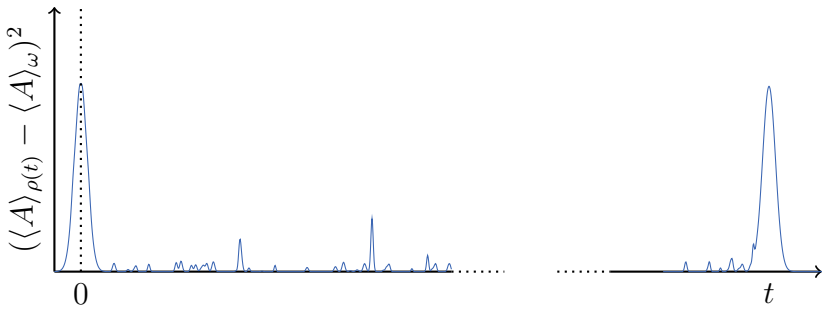

Figure 4.2: (Reproduced from Ref. [120]) Equilibration on average is compatible with the time reversal invariant and recurrent nature of the time evolution of finite dimensional quantum systems. The figure shows a prototypical example of equilibration on average. Started in a non-equilibrium initial condition at time 0 the expectation value of some observable A quickly relaxes towards the equilibrium value $\langle A\rangle_\omega$ and then fluctuates around it, with far excursions from equilibrium being rare. After very long times the system returns (close to) its initial state and so does the expectation value of the observable. A similar behaviour is observed when the initial state is evolved backwards in time.

states with a reasonable energy uncertainty and large enough systems it can be expected to be of the order of $O(1/d')$, i.e., reciprocal to the total number of distinct energy levels. The quantity $h(\mathcal{M})$ on the other hand can be thought of as a measure of the experimental capabilities in distinguishing quantum states and can reasonably be assumed to be much smaller than d'. In particular, when all measurements in $\mathcal{M}$ have a support contained inside of a small subsystem $S \subset \mathcal{V}$ it is bounded by $d_S/2$. Because of the conditions for equality in Eq. (4.13), the theorem then also implies an upper bound on $\overline{\mathcal{D}\left(\rho^S(t), \omega^S\right)}^T$ and hence proves subsystem equilibration on average.

For fixed H and $\epsilon > 0$ we have $\lim_{T\to\infty} f(\epsilon\, T) = 1$, hence the theorem proves, for a wide class of reasonable initial states, equilibration on average of all sufficiently small subsystems and apparent equilibration on average of the state of the full system under realistic restrictions on the number of different measurements that can be performed. In this sense it improves and generalises the results of Refs. [106, 107].

On what time scales is equilibrium reached? The product $N(\epsilon)\, f(\epsilon\, T)$, which is lower bounded by one, will typically be close to one only if T is comparable to d'^2, i.e., to the total number of energy gaps, and will otherwise be roughly of the order of $\Omega(d'^2/T)$ for smaller T. So, even under the favorable assumption that $g((p_k)_{k=1}^{d'})$ is of the order of $O(1/d')$, equilibration of a subsystem S can only be guaranteed after a time T that is roughly of the order of $\Omega(d_S^2\, d')$. Both d' and d_S typically grow exponentially with the size of the composite system and the subsystem S, respectively. Hence, times of the order of $\Omega(d_S^2\, d')$ are unphysical already for systems of moderate size. This weakness of theorems such as Theorem 1 has been criticised in Ref. [121] (see Section 4.3.6 for more details on equilibration times).

There are at least two possible replies to this criticism: First, it is known that there are systems in which equilibration does indeed take extremely long (see Section 4.3.6) and thus, being a very general statement, Theorem 1 is probably close to optimal. Proofs of shorter equilibration times will need further assumptions, such as locality or translation invariance of the Hamiltonian, and restrictions on the allowed measurements [91, 107]. Second, almost all systems in which equilibration has been studied and in which equilibration of some property on reasonable time scales could be demonstrated were found to exhibit equilibration towards the time average (see for example Refs. [69, 66, 60, 55, 122, 42, 123, 124]), so in these cases the upper bound on the equilibration time implied by Theorem 1 is not tight, but the theorem still captures the relevant physics. Transient equilibration to metastable states that precedes

equilibration to the time average seems to require special structure in the Hamiltonian. That the physics of such special systems is not captured by a result as general as Theorem 1 is not too surprising.

An interesting variant of the subsystem equilibration setting is investigated in Ref. [125], in which the subsystem S can initially be correlated (either classically or even quantum mechanically) with a reference system R. The "knowledge" about the initial state of S stored in the reference R can in principle help to distinguish the state $\rho^S(t)$ from ω^S. Still, by using decoupling theorems [126, 127, 128] and properties of smooth min and max entropies [129, 130] it is possible to show subsystem equilibration on average under conditions similar to those of Theorem 1, in the sense that the combined state of S and R is on average almost indistinguishable from $\omega^{SR} = \overline{\rho^{SR}}$.

In the above disquisition on equilibration we have put a focus on the more recent literature, however, many of the ideas behind the results mentioned above can already be found in the work of von Neumann [3]. We encourage the interested reader to consider the English translation [131] of this article and the discussion of von Neumann's results in Ref. [132] and the brief summary of parts of this article in Section 4.6 of this work.

Further statements concerning equilibration towards the de-phased state, which are related to those discussed above, can also be found in Refs. [133, 134, 135, 136]. We will discuss these works in more detail in Section 4.3.6.

4.3.3 Equilibration during intervals

In this section we investigate under which conditions equilibration during intervals can be guaranteed. After a brief overview of the literature on the topic we will concentrate on the results presented in Ref. [111]. Instead of reproducing the full proof we will only give the intuition behind it and describe the general structure. One reason for this is that Ref. [111] is concerned with a special class of bosonic Hamiltonians, so-called quadratic bosonic Hamiltonians, i.e., Hamiltonians that are quadratic polynomials in the bosonic creation and annihilation operators. For these Hamiltonians there exists a special formalism based on so-called covariance matrices that allows, for example, to calculate for a special class of initial states, namely Gaussian states, the time evolution of the expectation values of certain observables in a computationally efficient way. A full introduction of this formalism is beyond the scope of this review. More details can be found for example in Refs. [137, 138, 139, 140].

Equilibration during intervals of non-Gaussian initial states under certain quadratic Hamiltonians has been proven in Ref. [112] and the results have later been generalised and improved in Ref. [111]. The techniques are inspired by earlier works [141] on classical harmonic crystals, i.e., systems of coupled classical harmonic oscillators, and can be seen as bounds on the pre-asymptotic behaviour and an extension to finite system sizes of the results on equilibration of Ref. [142]. See also Refs. [142, 143, 144] for related results on equilibration starting from Gaussian initial states.

More precisely, the results on equilibration during intervals of Ref. [111] concern systems evolving under certain quadratic Hamiltonians of the form

$$H = \frac{1}{2} \sum_{x,y \in \mathcal{V}} \left(b_x^\dagger \, K_{x,y} \, b_y + b_x \, K_{x,y} \, b_y^\dagger \right) , \tag{4.53}$$

where $b_x, b_x^\dagger$ are the bosonic annihilation/creation operators on site $x \in \mathcal{V}$ and $K \in \mathbf{R}^{|\mathcal{V}| \times |\mathcal{V}|}$. The operator H, as defined in Eq. (4.53), is unbounded and hence, in principle, a careful treatment of the system with the methods of functional analysis [145, 146] would be necessary. The Hamiltonian in Eq. (4.53) is, however, particle number preserving. Thus, when we restrict to initial states with finite particle number the whole evolution happens in a finite dimensional

subspace of the Fock space. The Hamiltonian H and all relevant observables can then be represented by bounded operators on this subspace. We are hence back in the framework of finite dimensional quantum mechanics as introduced in Section 4.2 and the following statement is well-defined:

Theorem 2 (Equilibration during intervals)**.** *Consider the class of systems with a finite number of bosons in M modes on a ring with nearest neighbour interactions, i.e., $\mathcal{V} = [M]$ and $\mathcal{E} = \{(1,2),(2,3),\ldots,(M,1)\}$, evolving under a Hamiltonian of the form given in (4.53) with $K_{x,y} = -\delta_{|x-y| \bmod M,1}$. Let $\mathcal{H}$ be the direct sum of Fock layers up to the maximal particle number. If the initial state $\rho(0) \in \mathcal{S}(\mathcal{H})$ satisfies a form of decay of correlations (Assumptions 1–3 in Ref. [111]) and has time independent second moments (see Ref. [111]), then for every $S \subset \mathcal{V}$ and every $\epsilon > 0$ there exists a system size M^*, such that for all $M \geq M^*$ there exists a time t_{relax} independent of M and a time $t_{\text{rec}} \in \Omega(M^{6/7})$ such that there exists a Gaussian state $\tilde{\omega} \in \mathcal{S}(\mathcal{H})$ such that*

$$\forall t \in [t_{\text{relax}}, t_{\text{rec}}]: \quad \mathcal{D}\left(\rho^S(t), \tilde{\omega}^S\right) \leq \epsilon. \tag{4.54}$$

Proof. The theorem is essentially implied by Theorem 2 and Corollary 1 from Ref. [111], as well as the discussion between them. The scaling of the times t_{relax} and t_{rec} follows from Eq. (61) and Lemma 4 in Ref. [111]. □

The theorem proves equilibration during the interval $[t_{\text{relax}}, t_{\text{rec}}]$ of all small subsystems of a sufficiently large system. It is key to this type of equilibration that the state $\tilde{\omega}$ is a Gaussian state, even if the system was initially prepared in a non-Gaussian state. In fact, a similar convergence to a Gaussian state can be proven even in instances where the second moments are not constant in time. Then it is still true that non-Gaussian states become locally Gaussian over time, but local expectation values will then not become stationary. Again, it is important to note that the class of Hamiltonians considered here is special — the Hamiltonians are quadratic in the bosonic operators — but this does not apply to the initial states. The technical requirements on the initial state allow, for example, for ground states of gapped interacting local Hamiltonians. These conditions, precisely laid out in Ref. [111], ask for an algebraic decay of two- and four-point-functions, as well as an algebraic decay of correlations between Weyl operators belonging to distant regions.

The time t_{relax} depends on the size of the subsystem S under consideration, but is independent of the size of the composite system. It depends on the speed at which the Hamiltonian is able to transport correlations through the system and the length scale on which the correlations in the initial state decay. The time t_{rec} is a lower bound on the recurrence time and is slightly smaller than the time it takes for a signal to travel around the ring of bosonic modes.

4.3.4 Other notions of equilibration

In this section we briefly cover two other notions of equilibration for closed quantum systems. The first alternative notion of equilibration we want to discuss was proposed in Ref. [132] and further investigated in Ref. [147]. This work is closely related to an article of von Neumann [3]. There, von Neumann postulates that on large systems only a set of so-called macroscopic observables is accessible. The macroscopic observables are required to commute, thus they divide the Hilbert space in subspaces, so-called phase cells, each containing states that belong to the same sequence of eigenvalues for all the macroscopic observables (see also the more detailed discussion of Ref. [3] in Section 4.6). If one of the phase cells is particularly large, Ref. [132] associates it with thermal equilibrium and says that a system is in thermal equilibrium if and only if its state is almost entirely contained in that cell. Variants of the results from Ref. [3] can then be used to prove equilibration in this sense.

Reminding oneself that measurements of quantum systems are ultimately sampling experiments opens up an entirely new vista on the problem of equilibration, which leads us the second alternative notion of equilibration. Performing a measurement of an observable does neither provide the experimentalist with the measurement statistic nor does it yield the expectation value of the observable. Both can only be approximately determined by repeatedly performing the same experiment many times. How many repetitions are needed to distinguish whether the measurement statistic of a given observable is close or far from that predicted by equilibrium statistical mechanics? Such questions have been posed and partially answered in the fields of sample complexity [148, 149, 150] and state discrimination [151, 152]. Using the complexity of the task of collecting information about a quantum system as a justification for a statistical description was recently proposed in Ref. [153], which defines the concept of information theoretic equilibration. Essentially the authors of Ref. [153] are able to show that with the use of very fine grained observables pure quantum states are practically indistinguishable from states corresponding to statistical ensembles.

4.3.5 Lieb-Robinson bounds

An important tool for the study of equilibration phenomena is provided by Lieb-Robinson bounds [154, 155, 72]. They limit the speed at which excitations can travel through a quantum lattice system equipped with a locally interacting Hamiltonian. They can be viewed as an upper bound on group velocity of any excitation. In systems satisfying a Lieb-Robinson bound, information propagation is essentially contained within a causal cone, reminiscent of a "light cone" or "sound cone" (see Figure 4.3). Any excitations spreading faster than a maximum velocity are exponentially suppressed in the distance. Such bounds make rigorous the expectation that no instantaneous information propagation should be possible in quantum lattice models, and thereby immediately provide lower bounds to equilibration times for such models. The implications of Lieb-Robinson bounds to entanglement dynamics will be discussed in Section 4.4.3.

Concretely, Lieb-Robinson bounds are statements of the following type:

Theorem 3 (Lieb-Robinson bound (corollary of Theorem 1 from [75]))**.** *Consider a locally interacting fermionic or spin system with Hilbert space $\mathcal{H}$ and Hamiltonian $H \in \mathcal{O}(\mathcal{H})$. Let $A, B \in \mathcal{O}(\mathcal{H})$ be observables and denote $B(t) \coloneqq \mathrm{e}^{-\mathrm{i}Ht} B \mathrm{e}^{\mathrm{i}Ht}$. Then*

$$\|[A, B(t)]\|_\infty \leq C\|A\|_\infty \|B\|_\infty \mathrm{e}^{v|t|-d(A,B)} \tag{4.55}$$

where the Lieb-Robinson speed v depends only on the operator norm of the local terms of H and the coordination number $\max_{X\in\mathcal{E}} |\{Y \in \mathcal{E} : X \cap Y \neq \emptyset\}|$ of the interaction graph, and C is a constant that depends only on $\min(|supp(A)|, |supp(B)|)$.

The theorem says that the commutator $[A, B(t)]$ is exponentially suppressed with the distance between the support of A and a "light-cone" that grows with the time the observable B is evolved under the Hamiltonian H. As A could be one of the local terms of H this in particular implies that the distant terms of the Hamiltonian do not significantly influence the time evolution of B and that for any time t the operator $B(t)$ can be approximated by an observable with support only slightly larger than the base of the "light-cone" at that time.

Such "light-cone"-like dynamics has been systematically explored and put into the context of equilibration analytically and numerically [156, 77, 157, 112, 111, 78, 79, 158, 159, 160] as well as experimentally [27, 21, 28, 161, 30]. Similar bounds also exist for more general settings, like local Liouvillian dynamics [162, 163, 75], exponentially decaying but no longer strictly local interactions [72], as well as for certain long-ranged, i.e., power law like decaying, interactions

[72, 164, 159] as long as the exponent is sufficiently large. Such long-ranged interactions have been experimentally investigated in systems of trapped ions [21, 161].

Lieb-Robinson bounds can also be proven for certain systems with Hamiltonians with local terms with unbounded operator norm [165, 166, 167]. For example, for quadratic bosonic systems with Hamiltonians of the form

$$H = \frac{1}{2} \sum_{x,y \in \mathcal{V}} \left(b_x^\dagger \, K_{x,y} \, b_y + b_x \, K_{x,y} \, b_y^\dagger + b_x \, L_{x,y} \, b_y + b_x^\dagger \, L_{x,y} \, b_y^\dagger \right), \qquad K, L \in \mathbf{R}^{|\mathcal{V}| \times |\mathcal{V}|} \tag{4.56}$$

where $b_x, b_x^\dagger$ are again the bosonic annihilation/creation operators on site $x \in \mathcal{V}$ a Lieb-Robinson bound holds. Writing

$$K_{x,y} = \frac{Q_{x,y} + P_{x,y}}{2} \qquad\qquad L_{x,y} = \frac{Q_{x,y} - P_{x,y}}{2}, \tag{4.57}$$

such Hamiltonians can be cast into a form reflecting couplings between canonical positions $q_x := (b_x + b_x^\dagger)/\sqrt{2}$ and momenta $p_x := \mathrm{i}(b_x^\dagger - b_x)/\sqrt{2}$

$$H = \frac{1}{2} \sum_{x,y \in \mathcal{V}} \left(q_x \, Q_{x,y} \, q_y + p_x \, P_{x,y} \, p_y \right), \qquad Q, P \in \mathbf{R}^{|\mathcal{V}| \times |\mathcal{V}|}. \tag{4.58}$$

In this setting, local means that $K_{x,y} = L_{x,y} = Q_{x,y} = P_{x,y} = 0$ for $d(x,y) > R$ for some $R \in \mathbf{N}$. We write $d_{x,y} := d(x,y)/R$ and define $\tau := \max\{\|P\,Q\|_\infty^{1/2}, \|Q\,P\|_\infty^{1/2}\}\,|t|$, then the following Lieb-Robinson bound is valid:

Theorem 4 (Lieb-Robinson bounds for quadratic bosonic systems [167])**.** *Consider a Hamiltonian of the form given in Eq. (4.58) then*

$$\left. \begin{array}{l} \frac{\sqrt{\|PQ\|_\infty}}{\|P\|_\infty} \|[q_x(t), q_y]\|_\infty \\ \frac{\sqrt{\|PQ\|_\infty}}{\|Q\|_\infty} \|[p_x(t), p_y]\|_\infty \end{array} \right\} \leq \frac{\tau^{d_{x,y}+2} \cosh(\tau)}{d_{x,y}!}, \tag{4.59}$$

and

$$\left. \begin{array}{l} \|[q_x(t), p_y]\|_\infty \\ \|[p_x(t), q_y]\|_\infty \end{array} \right\} \leq \frac{\tau^{d_{x,y}} \cosh(\tau)}{d_{x,y}!}. \tag{4.60}$$

That is, for sufficiently large $d(x,y)$, one finds a faster-than-exponential decay of commutators between the canonical position and momentum operators. This gives rise to a "light cone" with the Lieb-Robinson velocity

$$v = \mathrm{e}\, R \max\{\|Q\,P\|_\infty^{1/2}, \|P\,Q\|_\infty^{1/2}\}. \tag{4.61}$$

Despite the results of Refs. [165, 166, 167], a full proof of a Lieb-Robinson bounds for a natural, interacting, infinite dimensional model, such as the Bose-Hubbard model with finite filling, is to date still missing.

A problem that has recently started to attract an increasing amount of attention is transport in disordered systems. For an XY spin chain with disordered interactions and disordered external magnetic field a Lieb-Robinson type bound of the form

$$\|[A, B(t)]\|_\infty \leq C\, n^2\, |t|\, \|A\|_\infty \|B\|_\infty \mathrm{e}^{-\eta\, d(A,B)} \tag{4.62}$$

with n the length of the chain and $C, \eta > 0$ constants was derived in Ref. [168] (see also Ref. [169] for a similar result). Notice that the bound is significantly more stringent than the

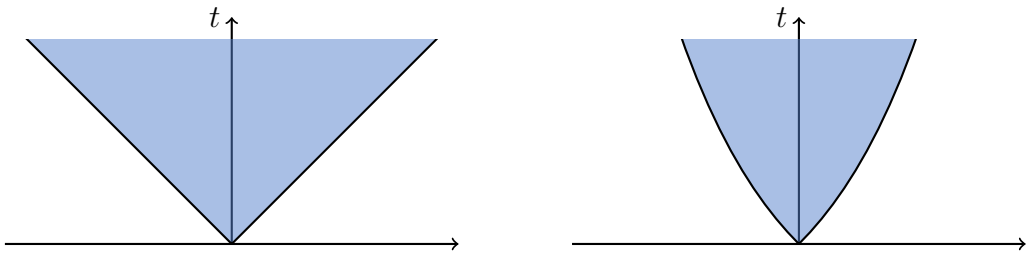

Figure 4.3: Schematic depiction of the Lieb-Robinson "light" cones in clean systems (a) and the more stringent bounds that can be derived in disordered systems (b). Outside the shaded area causal influences are exponentially suppressed.

ones we discussed before. In order for the right hand side to be significantly larger than zero, a time t that scales exponentially with the distance $d(A, B)$ is necessary (see Figure 4.3). Hence, in the considered disordered system information propagation is constrained to a region that is not even a cone — its radius only grows logarithmic with time. There is even evidence that for a given realisation of a disordered XY chain, one obtains a certain type of zero velocity Lieb-Robinson bound with high probability [170, 171]. We will return to the problem of transport and (many-body) localisation in disordered systems in Section 4.8.3.

4.3.6 Time scales for equilibration on average

In this section we summarise what is known about the time scales on which subsystem equilibration to the reduction of the de-phased state happens, i.e., on which time scales small subsystems equilibrate towards their time averaged state. We will see that it is possible to go beyond what Theorem 1 implies, but that all analytical results known to date that do so have the disadvantage of not being applicable to concrete Hamiltonians, but are only statements about all but few Hamiltonians from certain probability measures.

To discuss such results we will need to refer to and use methods of typicality and measure concentration. In particular, we will encounter the uniform or Haar measure $\mu_{\text{Haar}}[U(d)]$ on the unitary group $U(d)$ of dimension d and the probability $\mathbb{P}_{U\sim\mu_{\text{Haar}}[U(d)]}(A)$ that a given statement A holds for unitary operators $U \sim \mu_{\text{Haar}}[U(d)]$ drawn from the Haar measure. Readers unfamiliar with these constructions might want to refer to Section 4.6, where we discuss them in more detail.

We argued in the paragraphs following Theorem 1 that the bounds in Eq. (4.48) and Eq. (4.49) can be expected to become meaningful only if T is of the order of $\Omega(d_S^2\, d')$. As d' usually grows exponentially with the system size the equilibration times implied by Theorem 1 become physically meaningless already for medium sized systems.

There are good reasons to believe that without further assumptions on the Hamiltonian no significantly better general bounds on the subsystem equilibration time can hold. An example of a system that indeed can take exponentially long to equilibrate is a bipartite system in which the subsystem is only coupled to a low dimensional subspace of the Hilbert space of the bath. It can then take exponentially long before the Hamiltonian on the bath has rotated the state of the bath into this subspace, thereby effectively leaving the subsystem uncoupled for extremely long times (see Ref. [172] for a related construction). Such a coupling to a low dimensional subspace is necessarily non-local and hence unphysical. In Ref. [173], however, it is demonstrated that density inhomogeneities can persist also for exponentially long times even in translation invariant interacting lattice models. Very slow dynamics is also characteristic for

disordered and glassy systems.

Numerical evidence suggests that most natural, locally interacting systems without disorder started in reasonable initial states do not exhibit such extremely long equilibration times, see for example Refs. [33, 53, 54, 174, 60, 65, 69, 66, 55, 122, 42, 123, 64, 56, 175, 176], even though surprisingly slowly relaxing local observables can be constructed in some cases [177] and also power law approaches to equilibrium can occur [178].

As it is still unclear how the features of natural many-body models, such as locality of interactions, can be exploited to derive tighter bounds on equilibration time scales, Refs. [133, 134, 135, 136, 179] instead consider random Hamiltonians and Ref. [172] certain types of random observables, as well as a class of non-random low rank observables. We first cover the results of the type derived in Refs. [133, 134, 135, 136, 179] but concentrate on Ref. [134], as it goes beyond the rather unrealistic scenario of Hamiltonians with Haar random eigenstates.

As a warm-up, we shall, however, consider exactly the situation of Hamiltonians with Haar random eigenvectors. First, we define what a Haar random Hamiltonian is: Consider a system with Hilbert space $\mathcal{H}$ of dimension d and fix an observable $G \in \mathcal{O}(\mathcal{H})$. Then for $U \sim \mu_{\text{Haar}}[U(d)]$ the operator

$$H_G(U) \coloneqq U\, G\, U^\dagger \tag{4.63}$$

is a Haar random Hamiltonian. Of course, G and $H_G(U)$ share the same spectrum and eigenvalue multiplicities for any unitary U, but the energy eigenstates / spectral projectors of $H_G(U)$ are Haar random. Fixing G is thus equivalent to fixing the eigenvalues and degeneracies of the ensemble $H_G(U),\ U \sim \mu_{\text{Haar}}[U(d)]$ of Haar random Hamiltonians.

A quantity that will play an important role in the theorems to come is

$$f_G(t) \coloneqq \frac{1}{d} \sum_{k=1}^{d} \mathrm{e}^{-\mathrm{i}\, \tilde{E}_k\, t}, \tag{4.64}$$

where $(\tilde{E}_k)_{k=1}^d$ is the sequence of eigenvalues with respective multiplicity of G (and hence also of $H_G(U)$ for any unitary U). The function f_G can be interpreted as the Fourier transform of the sequence $(\tilde{E}_k)_{k=1}^d$ [134].

We can now state the first result of Ref. [134], which concerns quantum systems composed of spin-1/2 systems, so-called qubits, i.e., quantum systems whose Hilbert space is $\mathbf{C}^2$:

Theorem 5 (Equilibration under Haar random Hamiltonians [134, Result 1])**.** *Consider a bipartite system consisting of $|\mathcal{V}|$ many qubits, i.e., $\mathcal{V} = S \dot\cup B$ and $\mathcal{H} = \bigotimes_{x\in\mathcal{V}} \mathcal{H}_{\{x\}}$ with $\mathcal{H}_{\{x\}} = \mathbf{C}^2$ for all $x \in \mathcal{V}$, starting in a fixed initial state $\rho(0) \in \mathcal{S}(\mathcal{H})$. Then, for every $G \in \mathcal{O}(\mathcal{H})$, every $t \in \mathbf{R}$, and every $\epsilon > 0$ it holds that*

$$\mathbb{P}_{U\sim\mu_{\text{Haar}}[U(d)]}\left(\mathcal{D}\left(\rho^S(t), \omega^S_{H_G(U)}\right) > \frac{\sqrt{d_S}}{2\,\epsilon}\left(|f_G(t)|^4 + \frac{g_G^2}{d^2} + \frac{7}{d_B}\right)^{1/2}\right) < \epsilon, \tag{4.65}$$

where $\omega^S_{H_G(U)} \coloneqq Tr_B(\$_{H_G(U)}(\rho(0)))$ and $g_G \coloneqq \max_{k\in[d]} |\{l\colon \tilde{E}_l = \tilde{E}_k\}|$ with $(\tilde{E}_k)_{k=1}^d$ the sequence of eigenvalues with respective multiplicity of G.

A very similar result is also contained in Ref. [133]. Essentially, Theorem 5 connects the temporal evolution of the trace distance of $\rho^S(t)$ from the equilibrium state ω^S_G with the temporal evolution of $|f_G(t)|$. If the bath is large and the Hamiltonian has only few degeneracies, then for most Haar random Hamiltonians the distance $\mathcal{D}\left(\rho^S(t), \omega^S_{H_G(U)}\right)$ is small whenever $|f_G(t)|$ is small. This will make it possible to give bounds on equilibration time scales.

The above result can be extended to a more general ensemble of random Hamiltonians. More specifically, consider again the setting of a composite system of N qubits and the ensemble

$H_G(U)$, but now with $G \in \mathcal{O}(\mathcal{H})$ diagonal in some product basis and U given by a random circuit of circuit depth $C \in \mathbf{Z}^+$. Here, a circuit is a sequence of so-called quantum gates, i.e., unitary quantum channels that each act on only one or two qubits. The gates can be members of a so called universal gate set, i.e., a set of quantum gates such that any unitary can be approximated arbitrarily well by a circuit of gates from this set. The circuit depth of a circuit is the number of gates in the circuit. Finally, a random circuit is a circuit in which the gates have been drawn randomly according to some measure from a universal gate set. We write μ_C for the measure on unitaries induced by random circuits of circuit depth C with gates drawn uniformly at random from some fixed, finite universal gate set. It is known that $\lim_{C\to\infty} \mu_C = \mu_{\text{Haar}}[U(d)]$ and that for large enough C the measure μ_C approximates $\mu_{\text{Haar}}[U(d)]$ in the sense of being an approximate unitary design [180]. This holds regardless of which finite universal gate set is used.

For the random circuit ensemble of random Hamiltonians the following statement holds, which generalises Theorem 5:

Theorem 6 (Equilibration under random circuit Hamiltonians [134, Result 3])**.** *Consider a bipartite system consisting of $N := |\mathcal{V}|$ many qubits, i.e., $\mathcal{V} = S \dot\cup B$ and $\mathcal{H} = \bigotimes_{x\in\mathcal{V}} \mathcal{H}_{\{x\}}$ with $\mathcal{H}_{\{x\}} = \mathbf{C}^2$ for all $x \in \mathcal{V}$, starting in a fixed initial state $\rho(0)$. There exists a constant $\alpha \in \mathbf{R}$ that depends only on the universal gate set such that for every $G \in \mathcal{O}(\mathcal{H})$ diagonal in a product basis, every $t \in \mathbf{R}$, every circuit depth $C \in \mathbf{Z}^+$, and every $\epsilon > 0$*

$$\mathbb{P}_{U\sim\mu_C}\left(\mathcal{D}\left(\rho^S(t), \omega^S_{H_G(U)}\right) > \frac{\sqrt{d_S}}{2\,\epsilon}\left(|f_G(t)|^4 + \frac{g_G^2}{d^2} + \frac{7}{d_B} + d^3\, 2^{-\alpha\, C/N}\right)^{1/2}\right) < \epsilon, \tag{4.66}$$

where $\omega^S_{H_G(U)} := Tr_B(\$_{H_G(U)}(\rho(0)))$ and $g_G := \max_{k\in[d]} |\{l\colon \tilde E_l = \tilde E_K\}|$ with $(\tilde E_k)_{k=1}^d$ the sequence of eigenvalues with respective multiplicity of G.

As can be seen from Eq. (4.66), a slightly super-linear circuit complexity, i.e., $C = C(N) \notin O(N)$, is sufficient to make the additional term in Eq. (4.66) (compared to Eq. (4.65)) go to zero for large N.

If this is the case, and in addition N is large enough, the bath is much larger than the subsystem, i.e., $d_B \gg d_S$, and G has only few degeneracies, i.e., $g_G \ll d$, then the right hand side of both Eq. (4.65) and (4.66) is approximately equal to $|f_G(t)|^2\sqrt{d_S}/(2\,\epsilon)$. Hence, the bounds are non-trivial for reasonably small ϵ for all t for which $\sqrt{d_s}\,|f(t)|^2 \ll 1$. For which times t this is the case of course crucially depends on the spectrum that was fixed by fixing G.

The spectrum of the Ising model with transverse field, for example, leads to an approximately Gaussian decay of $|f(t)|^2$, implying an estimated equilibration time of the order of $O(N^{-1/2})$ [134]. For more general locally interacting Hamiltonians on D-dimensional lattices one can show equilibration times of the order of $O(N^{1/(5\,D)-1/2})$ [135].

This means that given an initial state $\rho(0)$, if G is chosen to be the Hamiltonian of the transverse field Ising model and $U \sim \mu_{\text{Haar}}[U(d)]$, then the dynamics under the Haar random Hamiltonian $H_G(U)$, which has the same spectrum as G, is, with high probability, such that the time evolution $\rho\colon \mathbf{R} \to \mathcal{S}(\mathcal{H})$ is such that the state of any small subsystem S equilibrates to the reduced state of the de-phased state on that subsystem, during a time of the order of $O(N^{-1/2})$. This, however, is in contradiction with the intuition that larger systems should take longer to equilibrate, simply because excitations in locally interacting spin systems travel with a finite speed (see also Section 4.3.5). One would expect that for locally interacting systems of N spins on a D dimensional regular lattice with nearest neighbour or short range interactions, subsystem equilibration should happen on a time scale of the order of $\Theta(N^{1/D})$, where $N^{1/D}$ is the linear size of the system, for many reasonable initial states.

Another point of criticism is that one can show that for Haar random Hamiltonians the subsystem equilibrium state is the maximally mixed state [135, Corollary 1] and a similar

statement can be shown for the random circuit ensemble of random Hamiltonians. Systems to which the above results apply can thus never exhibit subsystem equilibration to an interesting, e.g., finite temperature, state.

The reason for both of these problems is that neither the model of Haar random Hamiltonians nor that of Hamiltonians whose diagonalizing unitary is given by a random circuit with high circuit complexity are good models for realistic, locally interacting quantum systems. Simply put, even though random Hamiltonian ensembles have been successfully used to model certain features of realistic Hamiltonians in the context of random matrix theory [181, 182, 183, 184, 69, 185, 186, 187, 188], the eigenstates of reasonable locally interacting quantum systems are far from Haar random.

We hence turn to the results of Ref. [172] for concrete Hamiltonians and measurements. The main result of that work is a bound on the equilibration time of low rank measurements, i.e., POVMs with two outcomes, one of which is a low rank projector. Such measurements do not correspond to local observables, but rigorous bounds on their equilibration behaviour can be given even for concrete situations:

Theorem 7 (Fast equilibration of low rank observables [172])**.** *Given a system with Hilbert space* $\mathcal{H}$ *and non-degenerate Hamiltonian* $H \in \mathcal{O}(\mathcal{H})$ *with spectral decomposition* $H = \sum_{k=1}^{d} E_k \, |E_k\rangle\langle E_k|$*. For* $\rho(0) \in \mathcal{S}(\mathcal{H})$ *the initial state of the system, let* $\omega = \$_H(\rho(0))$ *be the de-phased state and define the energy level occupations* $p_k := \langle E_k|\rho(0)|E_k\rangle$*. Let* $\mathcal{M} = \{(\Pi, \mathbb{1} - \Pi)\}$ *with* Π *a rank* K *projector, then*

$$\overline{\mathcal{D}\left([\,, \mathcal{M})\right]\rho(t)\omega}^{T} \leq C \left(\eta(1/T)\, K\right)^{1/2} \tag{4.67}$$

with $C = 5\,\pi/(4\,\sqrt{1 - 1/\mathrm{e}}) + 1$ *and for any* $\Delta \geq 0$

$$\eta(\Delta) := \sup_{E \in \mathbf{R}} \sum_{k\colon\, E_k \in [E, E+\Delta]} p_k. \tag{4.68}$$

One can now show that η is lower bounded by $1/d^{\mathrm{eff}}(\omega)$ but also argue that, up to reasonably large T, it holds that $\eta(1/T) \leq C'/T$ with C' a constant that depends on the shape of the energy distribution of the initial state. In particular, the above theorem predicts an at least power-law like approach to equilibrium of low rank measurements on a time scale proportional to K/σ_E with σ_E the energy uncertainty in the initial state (for details see Ref. [172]).

In addition to the above results some lower bounds on equilibration time scales exist: For example, if a state has overlap only with energy eigenstates of the Hamiltonians in an energy interval of width ΔE, then the equilibration time is at least of the order of $\Omega(1/\Delta E)$ [118] (see also Ref. [189]). Similarly, if the Hamiltonian H of a bipartite system with $\mathcal{V} = S \,\dot\cup\, B$ is uncoupled, except for a small coupling Hamiltonian $H_I := H - H_S - H_B$, then the equilibration time is at least of the order of $\Omega(1/\|H_I\|_\infty)$ [118, Section 2.6.3]. Similarly, lower bounds on the equilibration and thermalisation time — as will be discussed in Section 4.7 — follow from bounds on the rate of change of certain entropies [125, 190]. In Ref. [191], lower bounds on the equilibration time of the type $\Omega(N^{1/2})$ have been obtained for a class of spin systems with long range interactions. For spin systems with short range interactions, Lieb-Robinson bounds (see Section 4.3.5) immediately imply lower bounds on the equilibration time for certain initial states that are of the order of the linear size of the system. Finally, in systems whose density of states can be approximated by a continuous function the Riemann-Lebesgue Lemma [192] can be used to give upper bounds on equilibration time scales [46]. Despite the large number of results the full problem still awaits a solution.

4.3.7 Fidelity decay

A scenario in which the equilibration behaviour has been studied in detail and is now particularly well understood is that of fidelity decay. Rather than looking at the expectation value of say a local observable the quantity, whose equilibration is of interest here is the fidelity between the initial state and the time evolved state at time t. For pure initial states $\psi(0) = |\psi\rangle\langle\psi| \in \mathcal{S}(\mathcal{H})$ and unitary time evolution under a Hamiltonian $H \in \mathcal{O}(\mathcal{H})$ the fidelity takes the simple form

$$\mathcal{F}\left(\psi(0), \psi(t)\right) = Tr(\psi(0)\,\psi(t)) = \left|\langle\psi|\mathrm{e}^{-\mathrm{i}\,H\,t}|\psi\rangle\right|^2 = \left|\sum_k |\langle\psi\rangle E_k|^2 \mathrm{e}^{-\mathrm{i}\,E_k\,t}\right|^2, \tag{4.69}$$

which makes apparent that it can be seen as the square of the Fourier transform of the weighted energy distribution of the initial state.

As $\psi(0)$ can be seen as a low rank (in fact rank one) observable, the result on the equilibration times of low rank observables (Theorem 7) can be used to bound the time scales on which fidelity decays. Below this, typically power-law bound a rich variety of different decay behaviours can be observed [193, 194, 195].

4.4 Investigations of equilibration for specific models

There is a large body of literature studying equilibration dynamics of quantum many-body systems partly with analytical, but mostly with numerical methods. These works typically focus on a specific model or a subclass of models. In this section we cover a selection of works in this direction. We will discuss many more works with a similar scope later in Section 4.7.6 once we have introduced the concept of thermalisation.

4.4.1 Global quenches

Often the behaviour of quantum systems after a suddenly altered Hamiltonian, a so called quench is considered. In this much discussed setting, the initial state $\rho(0)$ is, e.g., the ground state of a locally interacting Hamiltonian H_0, and following the sudden quench to a different locally interacting Hamiltonian H, properties of

$$\rho(t) = \mathrm{e}^{-\mathrm{i}\,t\,H}\,\rho(0)\,\mathrm{e}^{\mathrm{i}\,t\,H} \tag{4.70}$$

are explored. The seminal early study [196] introduces quenches to the literature and finds a "non-approach to equilibrium" in the XY model that is mapped to a quadratic fermionic system. Refs. [156, 61] use field theoretical methods to gain insight into the dynamics of correlation functions after quenches. If the final Hamiltonian is close to being critical, notions of universality are being identified at long times. The early work [51] investigates an out of equilibrium phase diagram of the Bose-Hubbard model, arising from quenches from the superfluid to Mott phase. Ref. [58] also considers out of equilibrium dynamics in the Bose-Hubbard model and discusses signatures of equilibration that can be probed using optical super-lattices. A similar setting is numerically analysed in Ref. [26], which is then taken as a benchmark for an experiment performing a dynamical quantum simulation. Ref. [197] numerically investigates quenches inside the Mott phase with a method most suitable for lattices with high coordination number. Ref. [198] studies the relaxation dynamics in XXZ chains following a quench, Here, a rich phenomenology emerges and both oscillatory and exponential relaxation are being observed. Counter-intuitively, the relaxation speed increases at a critical point for the anisotropy parameter. The seminal experimental work [5] also studies the on-equilibrium evolution of coherent states, being superpositions of different particle number states in a three dimensional optical

lattice, observing collapses and revivals. A very powerful tool in numerical studies is provided by time-dependent variants of the density-matrix renormalisation group (DMRG) approach and related tensor network approaches [32, 199, 200, 201]. An early example being Ref. [77], which studies the spreading of entanglement after quenches in Heisenberg spin chains. Noteworthy are Refs. [202, 58], which investigate equilibration with such methods in a setting described by the Bose-Hubbard model which can be realised with ultra cold atoms [26]. Ref. [203] uses time dependent DMRG methods to study the relaxation dynamics after quenches in the Tomonaga-Luttinger model and in systems of spin-less fermions and finds universal long time behaviour. Ref. [204] discusses the equilibration in the Bose-Hubbard and Fermi-Hubbard models following a global quench, employing an expansion in large coordination numbers. Ref. [54] uses quantum Monte Carlo techniques to investigates the equilibration dynamics after switching off the coupling of the Hubbard-model starting form a thermal state. Ref. [205] focuses on quenches in 1D spin-less fermions. Ballistic transport is observed, except if the quench is from a metallic state deep into the insulating phase, in which case local domains form reminiscent of the picture provided by the Kibble-Zurek mechanism [206, 207].

4.4.2 Local and geometric quenches

By no means are the sudden global quenches the only type of non-equilibrium situation considered in the literature. Local quenches are also frequently investigated [76, 208, 209, 21, 210], as well as geometric quenches [211, 212, 33], in which the system's response to a sudden alteration of its geometry is being studied. Ref. [211] considers general geometric quenches between systems integrable by means of the Algebraic Bethe ansatz and how it allows to compute overlaps between eigenstates of the old and new Hamiltonian. Ref. [212] investigates the dynamics of entanglement and equilibration after a geometric quench in the anisotropic spin-1/2 Heisenberg chain. Ref. [33] studies the relaxation after a "valve" between to previously isolated systems of hard-core bosons is opened. Refs. [76, 208] develop a quantum field theory approach to describe the growth of entanglement and the dynamics of correlation functions after a quench during which two uncoupled halves, initially in their ground state, of a translation invariant system are joined together. Refs. [210, 213] consider a related scenario in which two systems initially at different temperature are joined together and the authors also find equilibration. Also related is the series of works Refs. [214, 215, 216, 217, 27] in which properties of the non-equilibrium steady state are studied that can emerge in such a situation if the two systems are infinitely large. In particular, the steady state energy current and its fluctuations, as well as the time dependence of local observables are calculated. Refs. [219, 220] consider the non-equilibrium dynamics emerging from bringing two systems together in a language of conformal and relativistic quantum field theory. Ref. [209] presents a detailed numerical study of the time evolution under various, integrable and non-integrable, translation invariant spin Hamiltonians for several types of initial states, including domain wall states with all spin in the left half up and all in the right half down. This situation can be thought of as a local quench. A similar setting is analysed in Ref. [221] for XXZ chains, where equilibration is also found, albeit to a state that retains memory on its initial state. Local quenches and the subsequent (quasi-particle) dynamics can now also be probed experimentally with impressive precision [21].

4.4.3 Entanglement dynamics

Early on, it has been realised that the light-cone like propagation of excitations following global quenches is accompanied by a growth of entanglement if the initial state has low entanglement or even is a product state [157, 77, 76, 222, 78, 74]. Entanglement is always defined with respect to a separation of the system into distinct, spatially separate subsystems. Bipartite

entanglement of pure states with respect to a decomposition $\mathcal{V} = X \cup X^c$ for some subsystem $X \subset \mathcal{V}$ can be measured in terms of the entanglement entropy defined for any state ρ as

$$E_X(\rho) = S(\rho^X), \tag{4.71}$$

where S denotes the von Neumann entropy. In a precise sense, this is the "unique measure of entanglement" in this pure bipartite setting [97] and we call a pure state ρ uncorrelated (with respect to a decomposition $\mathcal{V} = X \cup X^c$) if $E_X(\rho) = 0$. Other Renyi entropies

$$E_X^p(\rho) = \frac{1}{1-p} \log_2(\mathrm{tr}((\rho^X)^p) \tag{4.72}$$

for $p > 0$, however, also play a role when it comes to questions of approximations of states with tensor network methods [223, 224]. Lieb-Robinson bounds imply an affine upper bound for the entanglement entropy following global quenches:

Observation 1 (Entanglement growth)**.** *For any locally interacting system with Hamiltonian H and any $X \subseteq \mathcal{V}$ it holds that*

$$E_X(\rho(t)) - E_X(\rho(0)) \in O(t). \tag{4.73}$$

Conversely, there exist pairs of (translation invariant) locally interacting Hamiltonians H and pure uncorrelated initial states $\rho(0)$ such that

$$E_X(\rho(t)) \in \Omega(t). \tag{4.74}$$

Moreover, if $\rho(0)$ is uncorrelated, then for t fixed and any family of subsystems $X \subset \mathcal{V}$ of increasing size the entanglement entropy scales only like the boundary of these subsets in the sense that

$$E_X(\rho(t)) \in O(|X_\partial|), \tag{4.75}$$

where X_∂ is the set of elements of the edge set $\mathcal{E}$ of the Hamiltonian that overlap with both X and X^c.

The first and last statements have been proven in Refs. [78, 74] and improved in Ref. [80]. The second statement follows from Refs. [222, 225]. The intuition behind these statements is clear: Following the ballistic propagation of quasi-particles, at most a linear growth of entanglement over any finite cut can be observed. This indeed follows from suitable Lieb-Robinson bounds. Similarly, such a bound can be saturated for quadratic models, so it is tight in this sense. At the same time, for each fixed time $t > 0$, the entanglement entropy follows what is called an area law [226] for the entanglement entropy, in that the entanglement scales at most like the boundary area $|X_\partial|$ of the subset X.

There is a large body of literature that corroborates the intuition behind this theorem [76, 77, 78, 80, 21, 79]. The early Ref. [77], for example, studies the spreading of entanglement after quenches in Heisenberg spin chains, Ref. [222] studies quadratic models, Ref. [76, 157] specifically develops the quasi-particle picture.

The above notion of entanglement is not the only one that can and has been meaningfully considered. The correlations present in states arising from out of equilibrium dynamics can also be captured in terms of bipartite entanglement of separated subsystems which jointly still form a small subset of the entire lattice. Since the state under consideration is then no longer pure, other measures of entanglement [227, 97] have to be employed, such as the entanglement of formation [228, 229] or the negativity [230, 231, 232]. Such entanglement measures have defining features of being monotone under local operations and classical communication (LOCC) and vanish on separable states as discussed in Eq. (4.37)).

While it is known from the monogamy of entanglement [233] that at any time most sites of a lattice are not entangled, in the course of entanglement dynamics, remote sites generically get entangled at suitable times [234, 235, 236]. The intuition is that "wave fronts" of entanglement propagate ballistically through the lattice. Such bipartite entanglement has already been experimentally observed in systems of trapped ions [21].

4.4.4 Ramps, slow quenches and the dynamics of quantum phase transitions

Many works discuss also non-instantaneous ramps and other instances of so-called slow quenches. In this context, the dynamics under a family of locally interacting Hamiltonians

$$H(t) = H_0 + f(t)\, V \tag{4.76}$$

is usually studied, with $f\colon [0,\infty[\to \mathbf{R}$ being a suitably slowly varying function and $\rho(0)$ the ground state of $H(0) = H_0$. Such a situation is specifically interesting when at an instance in time t_0 the Hamiltonian $H(t_0)$ undergoes a second order quantum phase transition. If the change of the Hamiltonian in time is sufficiently slow, far away from the phase transition the adiabatic theorem will be applicable and the state $\rho(t)$ is then well approximated by the instantaneous ground state of the Hamiltonian at that given time t. However, in the vicinity of the critical point, the Hamiltonian gap will close down, and no slow change of the Hamiltonian will be sufficiently slow such that the adiabatic theorem could still capture the situation at hand. This setting hence allows to explore the dynamics of quantum phase transitions. This review cannot give justice to this topic, which can be considered a research field in its own right. We still attempt to give a short sketch of important ideas.

The Kibble-Zurek mechanism provides an intuitive understanding of the phenomenology of such slow quenches across critical points [206, 207]. It is specifically well understood for thermal phase transitions, a setting in which it has also been experimentally tested [237, 238, 239]. For quantum phase transitions similar scaling laws can be derived in the limit of infinitely slow ramps, invoking adiabatic perturbation theory and universality arguments but the situation is more involved [240, 241, 242, 243]. Ref. [244], considers an exponential ramp from the superfluid phase into the insulating one and calculates the time dependence of various experimentally relevant quantities for this case, and Ref. [245] treats further analytically solvable ramps.

Ref. [246] experimentally probes the Mott-insulator to superfluid transition in the Bose-Hubbard model by slowly decreasing the ratio of the interaction energy to the hopping strength. Ref. [41] studies the Mott insulator to superfluid quantum phase transition experimentally with ultra cold atoms and compares the findings to extensive numerics for the Bose-Hubbard model, using exact diagonalisation and tensor network techniques. Also in the Bose-Hubbard model Refs. [247, 248] study the formation and melting of Mott-insulating domains during ramps with tDMRG methods. Ref. [249] analytically investigates finite time ramps of the inter-mode interaction strength in a Luttinger liquid model. The series of works Refs. [250, 251, 252] investigates the formation of topological defects after quenches that involve the breaking of a continuous rotational symmetry. For reviews on this field — to the extent it is understood to date — see Refs. [206, 240, 253].

4.5 Quantum maximum entropy principles

In this section we connect the pure state statistical mechanics framework with the canonical approach to justify the ensembles of statistical physics by means of a maximum entropy principle. We first show that the apparent equilibrium state in systems that equilibrate on average can always be defined in terms of an entropy maximisation under the constraint that

the expectation values of all conserved quantities are held fix. Then we will discuss the possibly surprising fact that in many cases, in particular following quenches of sufficiently complex quantum systems, equilibrium expectation values of many relevant observables are very well approximated by those in a state that is the entropy maximiser given a much smaller set of constants of motion — a so-called generalised Gibbs ensemble (GGE).

4.5.1 A maximum entropy principle based on all constants of motion

We have seen in Section 4.3.2 that if the expectation value of an observable or the reduced state of a subsystem equilibrates on average, then they necessarily equilibrate to their expectation value in, or the reduced state of, the time averaged/de-phased state $\omega = \overline{\rho} = \$_H(\rho(0))$. The state ω hence encodes the information necessary to describe the equilibrium properties of such a system. It turns out that it is also the maximum entropy state given all constants of motion:

Theorem 8 (Maximum entropy principle [254])**.** *Consider the time evolution $\rho\colon \mathbf{R} \to \mathcal{S}(\mathcal{H})$ of a quantum system with Hilbert space $\mathcal{H}$ and Hamiltonian $H \in \mathcal{O}(\mathcal{H})$. If the expectation value of an operator $A \in \mathcal{B}(\mathcal{H})$ equilibrates on average, then it equilibrates towards its time average, given by*

$$\overline{Tr(A\,\rho)} = Tr(A\,\omega), \tag{4.77}$$

where $\omega = \overline{\rho}$ is the unique quantum state that maximises the von Neumann entropy S, given all conserved quantities.

Proof. That the equilibrium value of the expectation value of A is given by $Tr(A\,\omega)$ follows directly from the definition of equilibration on average. The time averaged state ω is equal to the de-phased initial state

$$\$_H(\rho(0)) = \sum_{k=1}^{d'} \Pi_k\,\rho(0)\,\Pi_k. \tag{4.78}$$

The de-phasing map $\$_H$ is a so-called pinching and the von Neumann entropy is non-decreasing under pinchings [88, Problem II.5.5] (this is a generalisation of Schur's theorem). Furthermore, two states $\sigma_1, \sigma_2 \in \mathcal{S}(\mathcal{H})$ yield the same expectation values for all conserved quantities, i.e., all $A \in \mathcal{O}(\mathcal{H})$ that commute with the Hamiltonian $[A, H] = 0$, if and only if $\$_H(\sigma_1) = \$_H(\sigma_2)$. This already shows that ω has the maximal achievable von Neumann entropy given all conserved quantities (see also figure 4.4). It remains to show uniqueness. Let $\mathcal{B}$ be a basis of the linear span of all $A \in \mathcal{O}(\mathcal{H})$ with $[A, H] = 0$. The objective function of the maximisation problem, namely the von Neumann entropy, is a strictly concave function $S\colon \mathcal{S}(\mathcal{H}) \to \mathbf{R}$ and it is optimised over all $\sigma \in \mathcal{S}(\mathcal{H})$ under the finite number of affine equality constrains $\forall B \in \mathcal{B}\colon Tr(B\,\sigma) = Tr(B\,\rho(0))$. Under these conditions uniqueness follows from a standard result from convex optimisation [255]. □

Theorem 8 is very reminiscent of Jaynes' maximum entropy principle. It is in any case remarkable that it is not, as in Jaynes' approach, a postulate motivated by a subjective interpretation of probability that is taken as a starting point of a statistical theory, but a consequence of purely quantum mechanical considerations. The unitary quantum dynamics of closed systems alone gives rise to a maximum entropy principle.

Theorem 8 is at the same time not the end of the story. It says that the equilibrium expectation values of all observables that equilibrate on average can be calculated from the state that maximises the von Neumann entropy given all conserved quantities (compare also Ref. [256]). The number of all linearly independent conserved quantities of a composite quantum

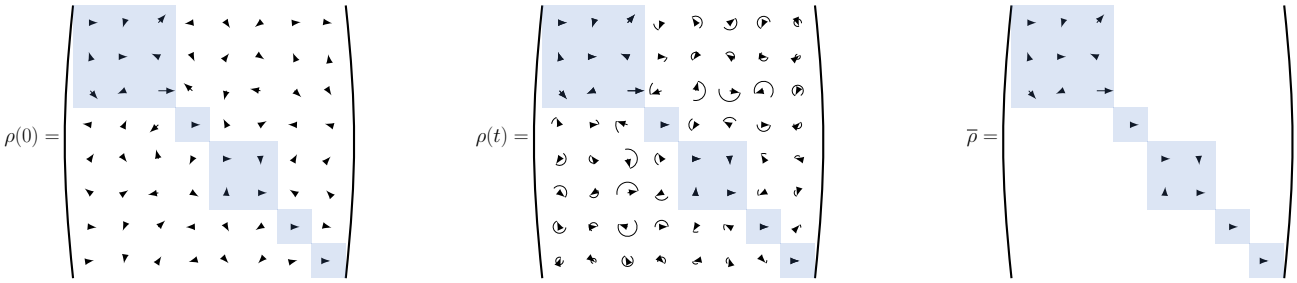

(a) (b) (c)

Figure 4.4: (Reproduction from Ref. [120]) Dephasing implies a maximum entropy principle. A quantum system started in an initial state $\rho(0)$ represented in panel (a) in an eigenbasis of its Hamiltonian H with degenerate subspaces corresponding to the squares, evolves (b) in a way such that time averaging its evolution (c) has the same effect as de-phasing the initial state with respect to H. The time averaged state $\overline{\rho}$ is the state that maximises the von Neumann entropy under the constraint that all conserved quantities give the same expectation value as in the initial state $\rho(0)$.

system, however, increases exponentially with the number of constituents, and finding each of them individually usually again requires resources that scale exponentially with the system size. The predictive power of Theorem 8 is hence rather limited.

4.5.2 Generalised Gibbs ensembles

In light of the insight discussed in the last section an interesting question to ask is [174]: "How many and which conserved quantities are actually relevant? Can one reasonably describe the equilibrium state by maximising entropy holding the expectation values of a much smaller number of possibly even efficiently obtainable conserved quantities fixed?"

For many practically relevant locally interacting Hamiltonians, a number of conserved quantities can be identified that are local in some sense. In fact, one of the possible definitions of quantum integrability (see also Section 4.9.2) is that there exists a number of conserved quantities scaling linearly in the system size. When such systems seemingly equilibrate to the time average state ω under unitary dynamics, this time average can not be expected to be described by a Gibbs ensemble. The system may, however, still be reasonably expected to equilibrate to the maximum entropy state given these suitably local constants of motion (see Refs. [84, 257, 258] and the references therein). Such a maximum entropy state is usually referred to as a generalised Gibbs ensemble (GGE) [42, 33, 112, 259, 260, 261, 64, 262].

More precisely, a conserved quantity is an observable $A \in \mathcal{O}(\mathcal{H})$ for which $[H, A] = 0$. Moreover, an operator $A \in \mathcal{O}(\mathcal{H})$ is called local if it is only supported on some $X \subset \mathcal{V}$, with $|X| = K$, for some constant $K \in \mathbf{N}$ independent of the system size.

Often, one considers conserved quantities that are approximately local. This notion can be made precise as follows. For simplicity, we restrict the attention to finite dimensional spin systems. For a region $X \subset \mathcal{V}$ and $l \in \mathbf{Z}^+$ denote by X_l the sets

$$X_l := \{x \in \mathcal{V} \colon d(x, X) < l\}, \tag{4.79}$$

of sites of the lattice that contain X as well as all sites within distance at most l from some site in X. For regions $X \subset \mathcal{V}$ define the map $\Gamma_X \colon \mathcal{B}(\mathcal{H}) \to \mathcal{B}(\mathcal{H})$ which acts on operators $A \in \mathcal{B}(\mathcal{H})$ as

$$\Gamma_X(A) := Tr_{X^c}(A) \otimes \mathbb{1}_{X^c} / d^{|X^c|}\,. \tag{4.80}$$

If $supp(A) \subseteq X$, then $\Gamma_X(A) = A$, otherwise it die-cuts away everything of A that acts non-trivially outside of X, i.e., for any $A \in \mathcal{B}(\mathcal{H})$ and $X \subseteq \mathcal{V}$ it holds that $supp(\Gamma_X(A)) \subseteq X$.

We call an operator (g, K)-local for some function $g\colon \mathbf{Z}^+ \to \mathbf{R}$ if there is some $X \subset \mathcal{V}$ of cardinality K such that

$$\|A - \Gamma_{X_l}(A)\|_\infty \leq \|A\|_\infty \, g(l). \tag{4.81}$$

Often, the function g is taken to be exponentially decaying

$$g(x) = c_1 \, \mathrm{e}^{-c_2 x} \tag{4.82}$$

for some suitable constants $c_1, c_2 > 0$. We call operators $A \in \mathcal{B}(\mathcal{H})$ that are (g, K)-local in this sense approximately local (with exponential tails). Taking g to be a step function gives the special case of (exactly) K-local operators.

Finally we define the notion of a quasi-local operator. Consider a translation invariant spin system, i.e., a system whose vertex set $\mathcal{V}$ corresponds to the sites of a regular lattice in a way such that its Hamiltonian $H \coloneqq \sum_{X \in \mathcal{E}} H_X$ is invariant under a set of translations $T_x\colon \mathcal{V} \to \mathcal{V}$ of the lattice, indexed by the element $x \in \mathcal{V}$ that is mapped to the first element of $\mathcal{V}$, in the sense that for all $x \in \mathcal{V}$ it holds that $T_x(H) \coloneqq \sum_{X \in \mathcal{E}} H_{T_x(X)} = H$. Thereby, and slightly abusing notation, we have implicitly defined the action of a translation T_x on operators $\mathcal{B}(\mathcal{H})$ in an obvious way. An operator $A \in \mathcal{B}(\mathcal{H})$ is then called quasi-local [21] if it can be written in the form

$$A = \frac{1}{|\mathcal{V}|} \sum_{x \in \mathcal{V}} T_x(B), \tag{4.83}$$

for some operator $B \in \mathcal{B}(\mathcal{H})$ that is approximately local with exponential tails.

We now give a precise definition of the generalised Gibbs ensemble in a way that seems useful in its own right:

Definition 1 (Generalised Gibbs ensemble)**.** *Let $K \in \mathbf{Z}^+$ and $g\colon \mathbf{Z}^+ \to \mathbf{R}$ be a suitably decaying function. Consider a system with locally interacting Hamiltonian $H \in \mathcal{O}(\mathcal{H})$ and a set $\mathcal{C}$ of constants of motion that are either local, approximately local, or quasi-local (as defined above), or the eigenmode occupations if the Hamiltonian is quadratic. The generalised Gibbs ensemble (GGE) of the system for a given initial state $\rho(0) \in \mathcal{S}(\mathcal{H})$ is then defined as*

$$\sigma_{\mathrm{GGE}} \coloneqq \arg\max_{\sigma \in \mathcal{S}(\mathcal{H})} \left\{ S(\sigma)\colon \forall A \in \mathcal{C}\colon Tr(A\,\sigma) = Tr(A\,\rho(0)) \right\}. \tag{4.84}$$

Note that the resulting state is always of the form

$$\sigma_{\mathrm{GGE}} \propto \mathrm{e}^{-\sum_{A \in \mathcal{C}} \beta_A A} \tag{4.85}$$

with generalised inverse temperatures (Lagrange multipliers) $\beta_A \in \mathbf{R}$, one for each conserved quantity $A \in \mathcal{C}_{|\mathcal{V}|}$. It is often clear what suitable sets of constants of motion are, for example in quenches to integrable systems. In situations in which these constants of motion are ambiguous, the GGE inherits the same ambiguity [264, 265, 266, 267]. As pointed out in the previous subsection, if all constants of motion are taken into account, then all finite dimensional systems equilibrate on average to the respective GGE if they equilibrate on average at all [254].

There is a large body of evidence that integrable quantum models indeed equilibrate to a suitable generalised Gibbs ensemble in this sense. The works Refs. [42, 33, 112] noticed the significance of the GGE early on. Refs. [268, 269, 64] discuss the behaviour of the one- and two-point correlation functions after a quench in various models, and it is found that the relaxation dynamics and equilibrium values can be well understood by means of a GGE. The validity of the generalised Gibbs ensemble is also studied in Ref. [261], where in particular, a quench of one-dimensional hard-core bosons in an optical lattice is considered, and in Ref. [270]

for a spin-1/2 Heisenberg XXZ chain with an anisotropy for various initial states, followed up by Ref. [260]. Ref. [271] develops a general method based on Wick's theorem that allows to show that the GGE correctly captures the equilibrium properties in certain quenches in solvable systems starting in thermal states, such as certain Ising chains, the Luttinger model, 1D hard-core bosons, and XX spin chains, and explains how quasi-particle occupations suffice to construct the GGE in these systems. Ref. [272] follows up on this by considering situations with interacting pre-quench Hamiltonians. In contrast, Ref. [273] considers a quench from quadratic to infinitely strongly interacting (hard core) bosons and obtains exact results on the time evolution and shows that the equilibrium state is described by a GGE; Ref. [274] follows up on this by analytical investigating how a trapping potential influences the equilibration dynamics and equilibrium properties. Ref. [275] analyses the GGE in the Lieb-Liniger model, finds potentially observable differences between the GGE and the grand canonical ensemble, and highlights that the GGE can turn out to be ill-defined if the initial expectation values of conserved quantities diverge. Ref. [276] discusses an interaction quench in the Lieb-Liniger model where the GGE implementation is not well defined and where also the idea of the representative state has been tested for the first time in a truly interacting model where no use of the conserved charges was made. Ref. [259] is generally concerned with integrable models. In this work, the concept of a "representative Hamiltonian eigenstate" is introduced and it is shown how to construct it efficiently by means of a generalised thermodynamic Bethe ansatz. For long times, the equilibrium values of local observables after a quench are given by this "representative Hamiltonian eigenstate". A framework for geometric quenches in integrable models based on the algebraic Bethe ansatz is developed in Ref. [211]. Refs. [266, 264, 277] study the crucial question of which constants of motion need to be included in the GGE to make it correctly reproduce the post quench equilibrium state. For certain quenches in an XXZ model and attractive Lieb-Liniger model they find that even if all known local conserved quantities are included the GGE it still fails to reproduce the equilibrium expectation values of even some local observables. It is conceivable that this is an indication that the model might have more (quasi-)local conserved quantities. Finding them all is a non-trivial task [9]. Trying to identify the physically most relevant observables, Ref. [267] proposes to rather try to find the best possible approximation to the dephased state ω with an ansatz of GGE form (4.85) with as few observables as possible and exemplifies that this allows for example to capture the dephased state of a locally interacting fermionic system much better than with the standard GGE containing only mode occupations.

In Ref. [279] the ability of the GGE to capture scenarios with repeated quenches is explored. Ref. [63] collects evidence that the GGE can correctly capture the long time limit of the expectation values of local operators in certain integrable models. Ref. [60] investigates differences between the infinite time time averaged equilibrium state of a translation invariant finite system and the infinite time limit of the state of the corresponding infinite system and whether their properties are captured by the GGE and which role is played by local conserved quantities common to both the initial and final Hamiltonian of a quench. Ref. [280] proposes generalised form factors for the analysis of correlation functions in generalised Gibbs ensembles.

4.6 Typicality

We have up to now managed to avoid the introduction of ensembles, or as one could say not put any probabilities by hand. However, ensembles and averages with respect to certain postulated probability distribution do play important roles in statistical mechanics. In this section we review some arguments that can be used in the framework of pure state statistical mechanics to justify their use. These approaches to explain the applicability of statistical mechanics are based on the insight that under certain assumptions most individual instances

of a situation lead to a behaviour that is very similarly to the average or typical behaviour.

4.6.1 Typicality for uniformly random state vectors

We begin by reviewing the most influential articles on the subject in historic order, starting with the works of Schrödinger [281] and von Neumann [3]. We will then state, prove, and discuss a general typicality theorem for uniformly random quantum state vectors. We finish this section with a discussion of typicality in other ensembles and the most common objections against typicality arguments.

The strategy behind justifications for the use of ensembles is to argue that most states drawn according to some reasonable measure from a set of physically reasonable states have approximately the same properties, so that for computations it is practical to work with an average state. This average state can, for example, turn out to be the state corresponding to a micro-canonical or canonical ensemble.

The use of such typicality arguments in the foundations of quantum statistical mechanics has a long history. First considerations along these lines already appear in a work by Schrödinger [281] from 1927. After an introduction into (first order) perturbation theory and a discussion of resonance phenomena in quantum mechanics with a focus on energy exchange in weakly interacting systems he goes on discussing what he calls a "statistical hypothesis"[2]. He aims at describing the long time behaviour of weakly interacting systems hoping to find thermodynamic behaviour. More specifically, he considers two systems that each have a pair of energy levels with the same gap. The coupling between them that mixes the levels is assumed to be weak. As his previous calculation had shown that the time averaged state depends on the initial state, he proposes to make an assumption about the initial energy level populations. His assumption is that the populations of the levels are proportional to the products of the degrees of degeneracy of the non-interacting levels. By introducing an entropy like quantity, he argues that if one of the systems is sufficiently large, this implies that when populations of energy levels whose reduced states on the small system are almost identical are combined, then the combined populations satisfy a canonical distribution. By this, he effectively argues that initial states fulfiling his "statistical hypothesis" have reduced states on the small system that are well described by thermal states.

The concept of typicality is even more prominent in an article by von Neumann [3] from 1929. His work has been translated by Tumulka [131] and reviewed and refined by Goldstein, Lebowitz, Mastrodonato, Tumulka, and Zanghi [132]. Von Neumann sets out to clarify "how it can be that the known thermodynamic methods of statistical mechanics enable one to make statements about imperfectly (e.g., only macroscopically) known systems that in most cases are correct."[3] He goes on to describe that this means to clarify "first, how the strange, seemingly irreversible behaviour of entropy emerges, and second, why the statistical properties of the (fictitious) micro-canonical ensemble can be assumed for the imperfectly known (real) systems, and that these questions will be tackled with the methods of quantum mechanics."[4] He further argues that the phase space of classical systems [282], a central object in Gibbs' formulation of classical statistical mechanics [1], should, in the context of quantum mechanics, be replaced by a system of mutually commuting macroscopic observables that approximate the

[2] German original [281]: "Statistische Hypothese".

[3] German original [3]: "[...] wie es kommt, dass die bekannten thermodynamischen Methoden der statistischen Mechanik es ermöglichen, über mangelhaft (d.h. nur makroskopisch) bekannte Systeme meistens richtige Aussagen zu machen."

[4] German original [3]: "Insbesondere, wie erstens das eigentümliche, irreversibel scheinende Verhalten der Entropy zustande kommt, und warum zweitens die statistischen Eigenschaften der (fiktiven) mikrokanonischen Gesamtheit für das mangelhaft bekannte (wirkliche) System unterstellt werden dürfen. Und zwar sollen diese Fragen mit den Mitteln der Quantenmechanik angegriffen werden."

true non-commuting quantum observables. Each sequence of eigenvalues of all macroscopic observables is associated with a phase cell, i.e., the subspace spanned by the state vectors that all give precisely these measurement outcomes for the macroscopic measurements, but which are macroscopically indistinguishable from each other. Following Ref. [132], we denote the projector onto the phase cell characterised by the sequence ν of macroscopic measurement outcomes by P_ν. The approximation of the microscopic observables is to be taken coarse enough, such that, for example, the commuting macroscopic position and momentum observables do not get in conflict with Heisenberg's uncertainty relation for the true microscopic position and momentum operators. One of von Neumann's main results is his "quantum ergodic theorem"[5]. Essentially, he is able to show the following (for details see the original article and Theorem 1 in Ref. [132]): Fix the dimensions $rank(P_\nu)$ of the phase cells, if they are all neither too small not too large, then for any fixed Hamiltonian without degeneracies and non-degenerate energy gaps (see also Section 4.3.2), most decompositions of the Hilbert space into phase cells with these dimensions have the property that, for all initial states and most times during the evolution, the evolving state of the system and a suitable micro-canonical state are approximately macroscopically indistinguishable. This property is called "normal typicality" by the authors of Ref. [132]. The result can actually be slightly generalised (Theorems 2 and 3 in Ref. [132]) and von Neumann's theorem can be reformulated into a statement about all initial states, all decompositions into phase cells, and most Hamiltonians [132].

It is worth noting that the notion of typicality in Refs. [3, 132] concerns not the quantum state (vector) but the set of macroscopic observables. The statement holds for most decompositions of the Hilbert space in phase cells (with certain properties), or most Hamiltonians, but for all initial states. In the following, typicality will mostly concern the quantum state (vector), i.e., we will encounter statements that hold for most (initial) state vectors.

Typicality arguments feature prominently in the PhD thesis of Lloyd [67] (see also Ref. [81]). Essentially he shows that for any fixed observable, if quantum state vectors are drawn uniformly at random from a subspace of a Hilbert space (we will soon make this more precise), then the mean square deviation of the expectation value of the observable in such a random state from that in the corresponding micro-canonical state is inverse proportional to the dimension of the subspace.

In a similar spirit, the concept of typicality is a cornerstone of the arguments in the book by Gemmer [69]. As a measure of typicality the authors propose the Hilbert space variance and derive bounds for the Hilbert space variance of various physically interesting quantities, ranging from expectation values of observables and distances of reduced states to entropies and purities. As in Ref. [67] and the present work, the aim is to use typicality to justify the methods of statistical mechanics and thermodynamics.

Many of the ideas of the works summarised above have later reappeared in Ref. [283] in which the term canonical typicality was coined. Ref. [283] is intended to be a clarification and extension of the work of Schrödinger [281], which we discussed earlier, and remarks in his book [284] on statistical thermodynamics. After a translation of the classical proof of the canonical ensemble from the micro-canonical one to the quantum setting, the authors argue that the law of large numbers implies that if a state vector is drawn uniformly at random from a high dimensional subspace, its reduced state on a small subsystem will look similar to the reduced state of the micro-canonical state corresponding to that subspace.

Before we go on, we must say more precisely what we mean by drawing a state vector uniformly at random from a subspace. Intuitively it should mean that any state from the subspace is as probable as any other. Mathematically this is made precise in the notion of left/right invariant measures [285]. Haar's theorem [286] implies that for any finite d there is a unique left and right invariant, countably additive, normalised measure on the unitary group

[5] German original [3]: "Ergodensatz [...] in der neuen Mechanik".

$U(d)$ [285]. We refer to this measure as the Haar measure on $U(d)$ and denote it by $\mu_{\text{Haar}}[U(d)]$. Left and right invariant means that for any unitary $U \in U(d)$ and any Borel set $\mathscr{B} \subseteq U(d)$

$$\mu_{\text{Haar}}[U(d)](\mathscr{B}) = \mu_{\text{Haar}}[U(d)](U\,\mathscr{B}) = \mu_{\text{Haar}}[U(d)](\mathscr{B}\,U), \tag{4.86}$$

where $U\,\mathscr{B}$ and $\mathscr{B}\,U$ are the left and right translates of $\mathscr{B}$. In this sense, the Haar measure $\mu_{\text{Haar}}[U(d)]$ is the uniform measure on $U(d)$.

The Haar measure on the group of unitaries that map a (restricted) subspace $\mathcal{H}_R \subseteq \mathcal{H}$ of dimension d_R into itself induces in a natural way a uniform measure $\mu_{\text{Haar}}[\mathcal{H}_R]$ on state vectors $|\psi\rangle \in \mathcal{H}_R$. We call state vectors drawn according to this measure, and also pure quantum states $|\psi\rangle\langle\psi|$ drawn according to the natural induced measure, Haar random and write $|\psi\rangle \sim \mu_{\text{Haar}}[\mathcal{H}_R]$.

A practical way to obtain state vectors distributed according to this measure is to fix a basis $(|j\rangle)_{j=1}^{d_R}$ for the subspace $\mathcal{H}_R$ and then draw the real and imaginary part of d_R complex numbers $(c_j)_{j=1}^{d_R}$ from normal distributions of mean zero and variance one. The state vector

$$|\psi\rangle = \frac{\sum_{j=1}^{d_R} c_j |j\rangle}{(\sum_{j=1}^{d_R} |c_j|^2)^{1/2}} \tag{4.87}$$

is then distributed according to $\mu_{\text{Haar}}[\mathcal{H}_R]$, i.e., $|\psi\rangle \sim \mu_{\text{Haar}}[H_R]$ [287]. We denote the probability that an assertion $\mathbb{A}(|\psi\rangle)$ about a state vector $|\psi\rangle$ is true if $|\psi\rangle \sim \mu_{\text{Haar}}[\mathcal{H}_R]$ by $\mathbb{P}_{|\psi\rangle\sim\mu_{\text{Haar}}[\mathcal{H}_R]}(\mathbb{A}(|\psi\rangle))$.

In the framework of measure theory [285], typicality can be seen as a consequence of the phenomenon of measure concentration [115, 116]. In particular a result known as Levy's lemma, has been used in Refs. [117, 68] to obtain theorems in the spirit of Refs. [67, 283], but with stronger bounds on the probabilities to observe large deviations from the (micro)canonical ensemble. Refs. [117, 68] focused mainly on reduced states of small subsystems of states drawn at random from high dimensional subspaces. Based on the same techniques, in Ref. [118], similar results have been obtained for the expectation values of individual observables on the full system as well as their variances, and for sets of commuting observables, developing further ideas of Ref. [3] concerning macroscopic measurements.

Furthermore, an extension to the distinguishability under a restricted set of POVMs is possible. We summarise these results in a single theorem, which, however, is not optimal in terms of constants and scaling (compare Refs. [68, 118] for details).

Theorem 9 (Measure concentration for quantum state vectors)**.** *Let $R \subset \mathbf{R}$ and let $\mathcal{H}_R \subseteq \mathcal{H}$ be the subspace of the Hilbert space $\mathcal{H}$ of a system with Hamiltonian $H \in \mathcal{O}(\mathcal{H})$ that is spanned by the eigenstates of H to energies in R and let $d_R := \dim(\mathcal{H}_R)$. Then for every $\epsilon > 0$ it holds that (i) for any operator $A \in \mathcal{B}(\mathcal{H})$*

$$\mathbb{P}_{|\psi\rangle\sim\mu_{\text{Haar}}[\mathcal{H}_R]}\left(|\langle A\rangle_{|\psi\rangle\langle\psi|} - \langle A\rangle_{\sqcap[H](R)}| \geq \epsilon\right) \leq 2\,\mathrm{e}^{-C\,d_R\,\epsilon^2/\|A\|_\infty^2}, \tag{4.88}$$

and (ii) for any set $\mathcal{M}$ of POVMs

$$\mathbb{P}_{|\psi\rangle\sim\mu_{\text{Haar}}[\mathcal{H}_R]}\left(\mathcal{D}\left([,\mathcal{M})\right]|\psi\rangle\langle\psi|\sqcap[H](R) \geq \epsilon\right) \leq 2\,h(\mathcal{M})^2\,\mathrm{e}^{-C\,d_R\,\epsilon^2/h(\mathcal{M})^2}, \tag{4.89}$$

where $C = 1/(36\,\pi^3)$ and

$$h(\mathcal{M}) := \min(|\cup\mathcal{M}|, \dim(\mathcal{H}_{supp(\mathcal{M})})). \tag{4.90}$$

Proof. Eq. (4.88) is Theorem 2.2.2 from Ref. [118]. We now prove Eq. (4.89) for $h(\mathcal{M})$ equal to the second argument of the min in Eq. (4.90). Let $S := \bigcup_{M\in\cup\mathcal{M}} supp(M)$ and remember that then for all $\rho, \sigma \in \mathcal{S}(\mathcal{H})$

$$\mathcal{D}\left([,\mathcal{M})\right]\rho\sigma \leq \mathcal{D}\left(\rho^S, \sigma^S\right). \tag{4.91}$$

Then Eq. (75) in Section VI.C of Ref. [68] yields the result. To finish the proof, note that Eq. (4.12) implies that for any $\rho, \sigma \in \mathcal{S}(\mathcal{H})$

$$\mathcal{D}\left([,\mathcal{M})\right]\rho\sigma \coloneqq \sup_{M\in\mathcal{M}} \frac{1}{2}\sum_{k=1}^{|M|} |Tr(M_k\,\rho) - Tr(M_k\,\sigma)| \tag{4.92}$$

$$\leq \frac{1}{2}\sum_{M\in\cup\mathcal{M}} |Tr(M\,\rho) - Tr(M\,\sigma)| \tag{4.93}$$

$$\leq \frac{1}{2}\,|\cup\mathcal{M}| \sup_{M\in\cup\mathcal{M}} |\langle M\rangle_\rho - \langle M\rangle_\sigma|. \tag{4.94}$$

Together with Boole's inequality this yields that for every $\sigma \in \mathcal{S}(\mathcal{H})$

$$\mathbb{P}_{|\psi\rangle\sim\mu_{\mathrm{Haar}}[\mathcal{H}_R]}\left(\mathcal{D}\left([,\mathcal{M})\right]|\psi\rangle\langle\psi|\sigma \geq \epsilon\right)$$

$$\leq 1 - \mathbb{P}_{|\psi\rangle\sim\mu_{\mathrm{Haar}}[\mathcal{H}_R]}\left(\bigcap_{M\in\cup\mathcal{M}} |\langle M\rangle_{|\psi\rangle\langle\psi|} - \langle M\rangle_\sigma| < \frac{2\,\epsilon}{|\cup\mathcal{M}|}\right) \tag{4.95}$$

$$= \mathbb{P}_{|\psi\rangle\sim\mu_{\mathrm{Haar}}[\mathcal{H}_R]}\left(\bigcup_{M\in\cup\mathcal{M}} |\langle M\rangle_{|\psi\rangle\langle\psi|} - \langle M\rangle_\sigma| \geq \frac{2\,\epsilon}{|\cup\mathcal{M}|}\right) \tag{4.96}$$

$$\leq \sum_{M\in\cup\mathcal{M}} \mathbb{P}_{|\psi\rangle\sim\mu_{\mathrm{Haar}}[\mathcal{H}_R]}\left(|\langle M\rangle_{|\psi\rangle\langle\psi|} - \langle M\rangle_\sigma| \geq \frac{2\,\epsilon}{|\cup\mathcal{M}|}\right). \tag{4.97}$$

The proof of the result for $h(\mathcal{M})$ equal to the first argument of the min in Eq. (4.90) can then be finished by choosing $\sigma = \sqcap[H](R)$, using Eq. (4.88), and the fact that for all $M \in \cup\mathcal{M}$ it holds that $\|M\|_\infty \leq 1$. Disregarding a favorable factor of 2 and using the (highly non-optimal) bound $|\cup\mathcal{M}| < |\cup\mathcal{M}|^2$ yields the unified result as stated in the theorem. □

A physically particularly relevant case is when $supp(\mathcal{M})$ is contained in some small subsystem $S \supseteq supp(\mathcal{M})$ and $R = [E, E+\Delta]$ is some energy interval. Then the theorem yields a probabilistic bound on the distance $\mathcal{D}\left(|\psi\rangle\langle\psi|^S, \sqcap^S[H]([E, E+\Delta])\right)$. If $|\psi\rangle \sim \mu_{\mathrm{Haar}}[\mathcal{H}_R]$ and the dimension d_R of the micro-canonical subspace $\mathcal{H}_R$ to the energies in the interval $[E, E+\Delta]$ fulfils $d_R \gg d_S$, then $\mathcal{D}\left(|\psi\rangle\langle\psi|^S, \sqcap^S[H]([E, E+\Delta])\right)$ is small with very high probability. That is, the reduced state on S of a random state from the subspace corresponding to the energy interval R is indistinguishable from the reduction of the corresponding micro-canonical state, with high probability.

The same holds in the more general setting that one has access only to a sufficiently small number of measurements, which in total have a sufficiently small number of different outcomes. If the total number of different outcomes $|\cup\mathcal{M}|$ is much smaller than the dimension of the subspace corresponding to the energy interval $[E, E+\Delta]$, a random state from this subspace is with high probability indistinguishable from the micro-canonical state.

For a family of Hamiltonians of locally interacting quantum systems with increasing system size, if Δ is kept fix and E is chosen such that $R = [E, E+\Delta]$ is not too close to the boundaries of the spectrum of the Hamiltonian, then d_R typically grows exponentially with the system size $|\mathcal{V}|$. For a locally interacting system with a macroscopic number of constituents one would thus need to be able to distinguish an astronomically large number of different measurement outcomes to have a realistic chance of distinguishing a random state from a micro-canonical state.

Similar methods as those used above were employed in Ref. [107] to prove that for Haar random pure states from high dimensional subspaces the effective dimension (which we encountered in Section 4.3.2) with respect to a fixed Hamiltonian is of the order of the dimension of the subspace, with probability exponentially close to one. The result can be generalised to certain measures over states that are product with respect to a bipartition $\mathcal{V} = S \dot\cup B$ [118].

4.6.2 Typicality for other measures over quantum state vectors

In addition to the Haar measure, other measures over quantum state vectors have been considered in the literature: This has been done in order to incorporate meaningful physical constraints into notions of typicality. Refs. [288, 289, 290, 291, 292, 293] introduce the mean energy ensemble. Instead of the uniform measure on a subspace corresponding to some energy interval, the mean energy ensemble consists of random state vectors which have a fixed energy expectation value with respect to some given Hamiltonian H. Under certain conditions on the spectrum of H it can be shown that the mean energy ensemble exhibits measure concentration [291]. In addition to that, it is possible to identify the typical reduced state of states drawn from the mean energy ensemble [291], and it can be shown that under certain conditions states from the mean energy ensemble typically have a high effective dimension [118].

Ref. [294] considers an ensemble of quantum state vectors of the form given in Eq. (4.87), in which the expansion coefficients $c_j = \langle j|\psi$ have fixed modulus but random phases. Concentration results, similar in spirit to Theorem 9, can be shown for this ensemble that yield typicality whenever sufficiently many energy levels are populated.

Ref. [295] extends the notion of typicality to the dynamics of systems. Similarly as in the mean energy ensemble, the authors define an ensemble of initial states that share the same expectation value with respect to some given observable and then investigate the time evolution of this expectation value under a Hamiltonian. The authors find dynamical typicality, i.e., that states that initially give similar expectation values also typically lead to a similar dynamical evolution of these expectation values.

Typicality can also be used to speed up numerical calculations. Instead of sampling over exponentially large sets of states, often drawing just a few representatives can already be sufficient to estimate expectation values [296]. Ref. [297] for example introduces the concept of minimally entangled typical quantum states, which, given a Hamiltonian H and inverse temperature β, constitute an ensemble of pure states whose average corresponds to the thermal state of H at inverse temperature β. The ensemble can be used to more efficiently calculate for example thermal expectation values of observables. A related approach, which has recently been put forward in Refs. [298, 299, 71, 70], is to investigate and exploit typicality in the context of so-called matrix product states. The effects of typicality allow for the numerical approximation of thermal expectation values of observables in situations where naive approaches are infeasible [70]. In Ref. [300] a method for numerically checking the validity of the eigenstate thermalisation hypothesis (see Section 4.7.2) is proposed that exploits techniques to apply exponentials of operators to random pure states. Typicality ensures that only few such random states are needed to obtain conclusive results, thereby vastly reducing the computational cost.

Typicality arguments are sometimes dismissed for being "unphysical" [301, 302]. Ref. [132], for example, contains a very interesting review of the mostly negative reception of von Neumann's quantum ergodic theorem (see also Section 4.6). Whether the concept of typicality is really superior to other approaches towards the foundations of statistical mechanics and thermodynamics, such as ergodicity, the principle of maximum entropy, or postulating ensembles, is to some extent a matter of personal taste. However, especially with respect to the latter, typicality has at last one important advantage: Instead of simply postulating that a certain ensemble yields a reasonable description of a certain physical situation, typicality shows, in a mathematically very well-defined way, when and why details do not matter. If most states anyway exhibit the same or very similar properties, then this does provide a heuristic, but pretty convincing, argument in favour of the applicability of ensembles. It is hence an argument supporting a description of large systems with ensembles.

4.7 Thermalisation

Given the findings presented in the last sections a natural question to ask is: When do closed quantum systems in pure states that evolve unitarily not only equilibrate, but actually thermalise in the sense that under reasonable restrictions on the experimental capabilities they appear to be thermalised or in thermodynamic equilibrium?

To make this question meaningful we will define the term thermalisation in this section. Then, in Section 4.7.2 and 4.7.3, we will discuss two general complementary approaches to explain and understand thermalisation in the framework of pure state quantum statistical mechanics in detail. The first approach is the so-called eigenstate thermalisation hypothesis (ETH), the second is based on a quantum version of the classical derivation of the canonical ensemble from the micro-canonical one, augmented with rigorous perturbation theory. The first approach is based mostly on assumptions on the eigenspaces/eigenstates of the Hamiltonian, while the second one instead requires stronger assumptions on the initial state. We then turn to a discussion of thermalisation in locally interacting translation invariant systems and a result concerning the equivalence of the canonical- and micro-canonical ensemble in Section 4.7.4. It is possible to interpolate between ETH approach and that based on assumptions on the initial state to some extent. We say more on that and on alternative notions of thermalisation in Section 4.7.5. We finish by surveying numerical investigations of thermalisation and analytical results concerning concrete model Hamiltonians or specific classes of systems in Section 4.7.6.

Throughout this section a focus will be put on subsystem thermalisation, i.e., the thermalisation of a small part (subsystem) of a large composite quantum system via the interaction with the rest of the system (bath). The whole composite system (subsystem and bath together) is thereby assumed to be in a pure state evolving according to the standard (Schrödinger-)von-Neumann-equation under some Hamiltonian H. Let $S \subset \mathcal{V}$ be the vertex set of the subsystem and $B = S^c$ that of the bath, then we will call the sum $H_S + H_B =: H_0$ of the two restricted Hamiltonians H_S and H_B the non-interacting Hamiltonian and $H_I := H - H_0$ the interaction Hamiltonian. We will say that a Hamiltonian H is non-interacting if $H = H_S + H_B$.

Whenever the term bath is used in the following it refers to this model of thermalisation. In particular we do not mean quantum systems that are already initially in a thermal state or other models of heat baths. It is crucial to note that approaches that explain thermalisation in quantum systems by investigating the behaviour of systems coupled to such thermal baths cannot solve the fundamental problem of thermalisation, as they leave open the question how the thermal bath became thermal in the first place.

4.7.1 What is thermalisation?

Whenever a term from one theory is used in a different context, a proper definition is mandatory. This is particularly true for terms as involved as thermalisation and thermodynamic equilibrium which, already in classical statistical mechanics, have several different meanings depending on the context. To take account of the complex nature of the term thermalisation we will not jump directly to a definition. Instead, we will consider a number of conditions that each capture certain aspects of thermalisation and whose fulfilment, depending on the context, one might or might not find necessary to say that a system has thermalised.

The catalog of properties that we will consider has been chosen with the setting of subsystem thermalisation in mind. Based on this discussion we will then carefully define what we consider sufficient to call a (sub)system thermalised, leaving open the possibility of defining other, possibly less strict, notions of thermalisation. In addition to that, we will also define the term subsystem initial state independence, a property that we regard as a necessary prerequisite for the thermalisation of subsystems, and which we will discuss in more detail in Section 4.8.

The aspects of thermalisation that we will use as a guideline for our definition of thermalisation are:

1. Equilibration: Equilibration is generally considered to be a necessary condition for thermalisation. In the following we will mostly be concerned with subsystem equilibration on average and apparent equilibration on average of the whole system under restricted sets of POVMs (see also Section 4.3.1).

2. Subsystem initial state independence: The equilibrium state of a small subsystem should be independent of the initial state of that subsystem. If a system exhibits some local exactly conserved quantities then one might still call it thermal and describe its equilibrium state by, for example, a so-called generalised Gibbs ensemble [303, 304, 42]. However, even such a behaviour is often already considered to be non-thermal. We will take the more cautious point of view that a system should not be considered thermalising if its equilibrium state depends on details of its own initial state, despite the absence of local exactly conserved quantities.

3. Bath state independence: It is generally expected that the equilibrium expectation values of local observables on a small subsystem are almost independent of the details of the initial state of the rest of the system, but should rather only depend on its "macroscopic properties", such as the energy density, which one would expect to have an influence on the temperature of the thermalising subsystem.

4. Diagonal form of the subsystem equilibrium state: The equilibrium state of a small subsystem should be approximately diagonal in the energy eigenbasis of a suitably defined "self-Hamiltonian". If the interaction with the bath makes the state of the subsystem approximately diagonal in some basis one could call this decoherence.

5. Gibbs state: Ultimately, one would like to recover the standard assumption of (classical) statistical physics that the equilibrium state is in some sense close to a Gibbs/thermal state.

In the light of Condition (1) it seems to be a sensible approach to define thermalisation on average or during an interval depending on the type of equilibration that goes along with thermalisation. Conditions (2) and (3) make clear that thermalisation should be defined with respect to sets of initial states. This leads us to the following definition of thermalisation:

Definition 2 (Thermalisation on average)**.** *We say that a system with Hilbert space $\mathcal{H}$ and Hamiltonian $H \in \mathcal{O}(\mathcal{H})$ thermalises on average with respect to a set $\mathcal{M}$ of POVMs and for a given set of initial states $\mathcal{S}_0 \subseteq \mathcal{S}(\mathcal{H})$ if for each state $\rho(0) \in \mathcal{S}_0$, the system apparently equilibrates on average to an equilibrium state $\omega = \$_H(\rho(0))$ that is close to a thermal state $g[\tilde{H}]\big(\beta(Tr(H\,\rho(0)))\big)$ for some Hamiltonian $\tilde{H}$ in the sense that for some suitable function $\beta\colon \mathbf{R} \to \mathbf{R}$ the distinguishability $\mathcal{D}\left([, \mathcal{M}]\omega g[\tilde{H}]\big(\beta(Tr(H\,\rho(0)))\big)\right)$ is sufficiently small.*

Definition 2 implicitly also defines thermalisation on average of subsystems. Just choose $\mathcal{M}$ to be the set of all POVMs with support on a subsystem $S \subset \mathcal{V}$ and $\tilde{H} = H_S$. If on the contrary $\mathcal{M}$ contains POVMs whose support covers the whole system, then $\tilde{H} = H$ is a natural choice. Moreover, in practice one would probably want that the function β has some physically nice properties, like being smooth and or monotonically decreasing. Thermalisation during intervals can be defined equivalently, but as we will not discuss it here, we keep the definition as simple as possible.

It seems worth emphasising again that the above definition does not say that a system thermalises if and only if the given conditions are met, but only says we call it thermalising

if at least the given conditions are met. It gives a set of conditions that are sufficient for thermalisation. In addition it shall be noted that for the case of subsystem thermalisation with a small subsystem our definition of thermalisation implies that the equilibrium state of the subsystem must be nearly independent of the subsystems initial state. We discuss subsystem initial state independence in more detail in Section 4.8.1.

An obvious question to ask now is: What are reasonable sets $\mathcal{S}_0$ of initial states? Particularly important is the energy distribution of the initial states, i.e., the sequence $(p_k)_{k=1}^{d'}$ of the energy level populations $p_k := Tr(\Pi_k \rho(0))$, as it is conserved under time evolution. Taking the classical derivation of the canonical ensemble from the micro-canonical one as a guideline, thermalisation can only be expected to happen for initial states whose energy distribution is not too wide, i.e., the energies of the significantly populated levels must be in an interval small compared to $\|H\|_\infty$. We will see in Sections 4.7.2 and 4.7.3 that such a condition will play an important role in proofs of thermalisation.

In the above definition of thermalisation on average we deliberately left open the question of what "sufficiently small" means. This is ultimately to be decided in the specific situation at hand. One would probably want that $\mathcal{D}([,\mathcal{M})]\omega g[\tilde{H}](\beta)$ somehow suitably decreases with the size of the system. However, we want to have a definition of thermalisation that is applicable to finite systems. Moreover, we want to avoid the technicalities of defining thermalisation for sequences of quantum systems of increasing size.

4.7.2 Thermalisation under assumptions on the eigenstates

At the center of the first approach to show thermalisation in quantum systems is the eigenstate thermalisation hypothesis (ETH). There exist various version of the ETH in the literature and we will give a more precise definition below, but a minimal version of the ETH can informally be phrased as follows: "A Hamiltonian fulfils the ETH if the expectation values of physically relevant observables in its energy eigenstates are approximately smooth functions of their energy." As we will see in this section, observables for which a system fulfils the ETH thermalise on average under reasonable conditions. The ETH is usually said to date back to the two works [305, 189]. As the role of these works is, however, often misunderstood it is worth starting this section with a short historical review:

Already in 1985 Ref. [49] investigated numerically how relatively small quantum systems equilibrate to a state that can be well described by statistical mechanics. The computational power available at that time made it possible to study a spin-1/2 Ising chain with up to seven sites in a transverse field by means of exact diagonalisation. Ref. [49] investigates the equilibration behaviour of both global and local observables and compares time averages with micro-canonical and canonical averages. The authors conclude that "both integrable and non-integrable quantum systems with as few as seven degrees of freedom can exhibit statistical behaviour for finite times." They also describe the reason for the statistical behaviour they observe, which is essentially the mechanism that is today known as the ETH: "If the expectation values [of an observable in the energy eigenstates] are smooth functions of the energy [...], then the short-time average of the observable will be very close to the ensemble average." In fact, it seems fair to say that the authors did anticipate large parts of the recent debate on equilibration and thermalisation in closed quantum systems. The last sentence of the abstract for example reads "This work clarifies the impact of integrability and conservation laws on statistical behaviour. The relation to quantum chaos is also discussed." It is remarkable that Ref. [49] is nevertheless essentially completely ignored by almost the whole recent literature centred around such questions (Refs. [46, 306] being notable exceptions).

In Ref. [305] a mechanism that can lead to the thermalisation of quantum systems is identified, which the author calls eigenstate thermalisation. A quantum and a classical version of a

hard sphere gas serve as prototypical examples to illustrate this mechanism. A central role is played by Berry's conjecture. It states that in certain quantum systems, whose classical counterparts exhibit classical chaos, the energy eigenstates to energies in the bulk of the spectrum are superpositions of plain waves with random phases and random Gaussian amplitudes [307]. It is argued that in the hard sphere gas, whose classical version is indeed chaotic, all energy eigenstates that satisfy Berry's conjecture have a single particle momentum distribution that is thermal. Finally, thermalisation is explained by the accumulation of relative phases between energy eigenstates due to time evolution. This de-phasing destroys any fine tuned setting of the phases that might have been present in the coherent superposition of energy eigenstates that made up the initial state. Such a fine tuning is necessary to get an initial state that is out of equilibrium.

Ref. [189] aims at providing a quantum mechanical justification for the applicability of statistical ensembles. The main idea is to model interacting composite quantum systems by starting with a non-interacting Hamiltonian that can be well understood, and then modelling generic effects of the interactions by adding a small random Hamiltonian — very much in the spirit of random matrix theory [186, 187, 188]. Due to the fact that composite quantum systems generically have exponentially dense spectra, i.e., either exponentially small gaps between neighbouring eigenvalues and/or exponentially large degenerate eigenspaces, any extremely small perturbation will typically mix an exponentially large number of energy eigenstates of the non-interacting Hamiltonian. This smears out their individual properties and should make the expectation values of physical observables in individual energy eigenstates of the perturbed Hamiltonian similar to those in a micro-canonical state with a similar mean energy.

A much more rigorous formulation of the idea behind eigenstate thermalisation can be found in Ref. [105] (see also Ref. [308]). This article considers bipartite systems with $\mathcal{V} = S \dot\cup B$, whose non-interacting part $H_0 = H_S + H_B$ of the Hamiltonian $H = H_0 + H_I$ is non-degenerate. The interaction Hamiltonian H_I is assumed to couple only neighbouring energy levels, i.e., it is of the form

$$\forall k \in [d]: \quad \langle E^0_k | H_I | E^0_{k'} \rangle = \lambda/2\, \delta_{|k-k'|,1} \tag{4.98}$$

for some $\lambda \in \mathbf{R}$ such that $\epsilon_B^{\max} \ll \lambda \ll \epsilon_S^{\min}$ with $\epsilon_B^{\max}$ the maximal spacing between the energy eigenvalues of H_B and $\epsilon_S^{\min}$ the minimal level spacing of H_S. It is first argued heuristically and then proved, under some additional technical assumptions, that such Hamiltonians indeed exhibit eigenstate thermalisation in the sense that for most k and all observables A_S with $supp(A_S) \subseteq S$ it holds that $\langle E_k | A_S | E_k \rangle \approx Tr(A_S\, g[H_S](\beta(E_k)))$ (see Eq. (5) and (6) in Ref. [308]).

The eigenstate thermalisation hypothesis (ETH) gained wide popularity after the very influential article Ref. [33], which states the ETH as follows:

Conjecture 1 (Eigenstate thermalisation hypothesis as stated in Ref. [33])**.** *The expectation value $\langle E_k|A|E_k\rangle$ of a few-body observable A in an eigenvector $|E\rangle_k$ of the Hamiltonian, with energy E_k, of a large interacting many-body system equals the thermal [...] average of A at the mean energy E_k.*

It is emphasised that thermal average in this context can also mean the micro-canonical average. Ref. [33] studies a system of hard core bosons on a lattice. It is demonstrated that the observed thermalisation can be explained by the fact that certain physically relevant observables have expectation values in most energy eigenstates that indeed resemble those in a micro-canonical state. The validity of numerous variants of the ETH has been studied extensively and in great detail at hand of many physically relevant models. This will be detailed in Section 4.7.6.

A slightly generalised and sharpened version of the ETH that captures the spirit of eigenstate thermalisation and applies to degenerate Hamiltonians is the following:

Definition 3 (Eigenstate thermalisation hypothesis (ETH))**.** *A Hamiltonian H fulfils the eigenstate thermalisation hypothesis in a set $R \subset \mathbf{R}$ of energies with respect to a set $\mathcal{M}$ of POVMs if and only if all its spectral projectors Π_k to energies $E_k \in R$ have the property that there is a sufficiently smooth function $\beta\colon R \to \mathbf{R}^+$ such that for each k with $E_k \in R$ it holds that for all normalised pure states $\psi \in \mathcal{S}(\mathcal{H})$ with the property $\psi \leq \Pi_K$ the distinguishability $\mathcal{D}\left([, \mathcal{M})\right]\psi g[H](\beta(E_k))$ is sufficiently small.*

Again, we have deliberately left open what is meant by "sufficiently smooth" and "sufficiently small".

It is still open under which precise conditions the ETH holds in this or a similar form. The rigorous derivations of Ref. [105] have so far not been generalised to more reasonable physical interactions. Methods to analytically check the ETH in "non-integrable models" that are interesting in the context of condensed matter theory currently seem to be out of reach. Very recently in Ref. [309] a statement reminiscent of the ETH was proved under fairly general conditions. More precisely, Ref. [309] shows weak local diagonality (Theorems 4 and 38) of the energy eigenstates of a certain type of Hamiltonian. In the language used here a slightly simplified version of this statement can be formulated as follows:

Theorem 10 (Weak local diagonality [309])**.** *Consider a locally interacting spin system with Hilbert space $\mathcal{H}$ and Hamiltonian $H \in \mathcal{O}(\mathcal{H})$ whose interaction graph $(\mathcal{V}, \mathcal{E})$ is a hypercubic lattice of spatial dimension D and let $S \subset B \subset \mathcal{V}$ be subsystems. Then there exist constants $C, c, v > 0$, which depend only on D and the local interaction strength $J := \max_{X \in \mathcal{E}} \|H_X\|_\infty$ of the Hamiltonian such that for any energy eigenstate $|E\rangle$ of H to energy E there exists a state $\rho_E^B \in \mathcal{S}(\mathcal{H}_B)$ that satisfies for any two energy eigenstates $|E_l^B\rangle, |E_m^B\rangle$ of $H_{B\restriction B}$ with energies E_l^B and E_m^B*

$$|\langle E_l^B | \rho_E^B | E_m^B \rangle| \leq \mathrm{e}^{-d(S,B^c)\,(E_l^B - E_m^B)^2/(8\,c\,v^2)} \tag{4.99}$$

and at the same time

$$\left\| Tr_{B\setminus S}(\rho_E^B) - Tr_{\mathcal{V}\setminus S}(|E\rangle\langle E|) \right\|_1 \leq C\, A^2\, J \left(\frac{d(S, B^c)}{4\,c\,v^2} \right)^{1/2} \mathrm{e}^{-c\,d(S,B^c)/2}. \tag{4.100}$$

Essentially the theorem tells us that if S is sufficiently far from the boundary of B, then for each energy eigenvector $|E\rangle$ of H there exists a state in $\mathcal{S}(\mathcal{H}_B)$ that is both approximately diagonal in the eigenbasis of $H_{B\restriction B}$ and locally on S hard to distinguish from $|E\rangle\langle E|$. If one could improve the result to the effect that it would show local indistinguishability not only from an approximately diagonal state but from a thermal state then it would constitute a proof of an ETH like statement. However, such a generalisation can almost surely hold only under additional assumptions [309].

The ETH, as defined in Definition 3, is sufficient for thermalisation in the following sense:

Observation 2 (Thermalisation in systems that fulfil the ETH)**.** *Systems whose Hamiltonian $H \in \mathcal{O}(\mathcal{H})$ fulfils the ETH, as stated in Definition 3, for a set $R \subset \mathbf{R}$ of energies with respect to a set $\mathcal{M}$ of POVMs, thermalise on average with respect to the set $\mathcal{M}$, in the sense of Definition 2, for all initial states for which the system apparently equilibrates on average with respect the restricted set $\mathcal{M}$ of POVMs (see also Section 4.3.1) and whose energy distribution is sufficiently narrow and contained in R, i.e., $E_k \notin R \implies Tr(\Pi_k\, \rho(0)) = 0$.*

The fact that the ETH is sufficient for thermalisation in this or a similar sense is widely known (see, for example, Refs. [105, 174]). It is worth noting that the strong requirement in Definition 3 that the distinguishability $\mathcal{D}\left([, \mathcal{M})\right]\psi g[H](\beta(E_k))$ must be small for all normalised pure states $\psi \leq \Pi_K$ is crucial for the above observation to hold. At the same time, this requirement obviously becomes harder to satisfy the more degenerate the Hamiltonian is.

If one takes the point of view that one should say that a system thermalises only if it thermalises in the sense of Definition 2 for all equilibrating initial states with a sufficiently narrow energy distribution, then fulfilment of the ETH is at the same time essentially also necessary for thermalisation. We will not make this statement fully rigorous, but the intuition behind it is as follows: If the ETH is not fulfilled, there should always exist initial states with a narrow energy distribution that only have overlap with energy levels that, for certain observables or POVMs, produce a measurement statistic that is sufficiently far from that of the closest thermal state. This distinguishability from the thermal state will then still be visible in the de-phased state and hence survive de-phasing and equilibration.

Such arguments, and the above mentioned apparent connection between the ETH and (non-)integrability, has lead some authors to proclaim [51, 202, 58, 33, 34, 310] that non-integrable systems thermalise and integrable systems do not. While there is evidence that in many models this is indeed the case, we will see in Section 4.8 and 4.9 that the situation is in fact more involved. We will given an overview of the numerical and analytical literature on thermalisation in the context of the ETH in Section 4.7.6.

We have seen that the ETH as defined in Definition 3 is by construction essentially sufficient and, in a certain sense, necessary for thermalisation. The necessary part, however, only holds if one is willing to call a system thermalising only if it thermalises for a given set of POVMs for all initial states with a sufficiently narrow energy distribution for which it also apparently equilibrates. Hence, there is the possibility to show thermalisation in systems that do not fulfil the ETH, if one is willing to restrict the class of allowed initial states. As we will see in the following this can indeed be done.

4.7.3 Subsystem thermalisation under assumptions on the initial state

In this section we discuss a second approach towards the problem of thermalisation that is independent of the eigenstate thermalisation hypothesis (ETH). Instead of making strong assumptions concerning the properties of the energy eigenstates of the Hamiltonian we will show thermalisation under stronger assumptions concerning the energy distribution of the initial state. This alternative and complementing approach is inspired by an argument from classical statistical mechanics, which we will lift to the quantum setting. The details of this approach were first worked out in Ref. [311].

The first motivation for this work comes from the fact that explaining thermalisation by using the eigenstate thermalisation hypothesis has one important drawback — that the ETH is indeed a hypothesis. One could make the provocative claim that this leads to the ironic situation that attempts to explain thermalisation by the ETH have the following problem: They essentially try to explain one phenomenon that is not well understood by another one that is almost as little understood [312].

The second motivation comes from the consideration that demanding thermalisation of all initial states with an energy distribution that is only required to be narrow but otherwise allowed to have arbitrary complex structure is asking for too much.

In the light of typicality arguments (Section 4.6) it seems plausible to restrict the class of initial states for which one tries to show thermalisation, or even to be content with an argument that shows thermalisation for most states from some measure. In addition, certain restrictions on the initial states are anyway already necessary to prove equilibration on average in the first place (Section 4.3.2), and practical limits on the experimental capabilities can be used to argue that many initial states of macroscopic objects are essentially impossible to prepare [109, 108, 106].

The third motivation comes from the known fact that in some systems the ETH is not

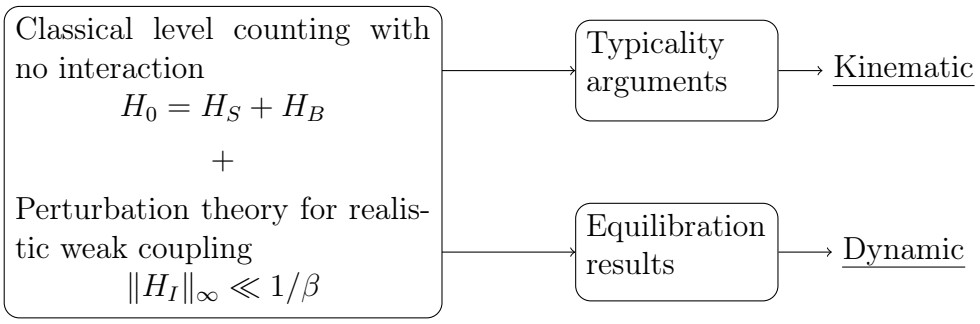

Figure 4.5: (Reproduction from Ref. [120]) Structure of the proof of thermalisation from Ref. [311].

fulfilled and this has been linked to the integrability of these models, while non-integrability is often associated with a fulfilment of the ETH and thermalisation (see for example Refs. [42, 33, 55, 313, 84, 261, 221, 63, 184, 271, 178]). What (non-)integrability even means in the context of quantum mechanics is, however, far from being settled [314, 315] (see also Section 4.9). It is thus of interest to approach the problem of thermalisation in a way that is independent of the concept of integrability.

As we will see in the following, restricting the class of initial states makes it possible to rigorously prove subsystem thermalisation on average without any reference to the ETH for both spin and fermionic systems. The overall structure of the argument is depicted in Figure 4.5. The result that we will derive and discuss in this section can be combined with either the typicality theorems from Section 4.6 or the dynamical equilibration theorems from Section 4.3. The former yields a kinematic thermalisation statement (Observation 4) that holds for most Haar random states from a certain subspace. The latter yields a dynamic thermalisation result (Observation 5) that proves thermalisation on average in the sense of Definition 2 for all initial states from a certain class of states. It is hence closer to the thermalisation statement obtained under the ETH (Observation 2), which we discussed in the last section.

In essence, the proofs of the statements presented in this section are translations of the classical derivation of the canonical ensemble for small subsystems of large weakly interacting systems that are described by a micro-canonical ensemble to the quantum setting. The main difficulty is that in quantum mechanics the interaction between the small subsystem and the bath not only shifts the eigenenergies of the non-interacting Hamiltonian, but, in addition, significantly perturbs the energy eigenstates. In many previous accounts of the thermalisation problem this issue has been partially overlooked or at least not been addressed rigorously. Compare for example Refs. [68, 117, 283].

How does the interaction influence the Hamiltonian? The eigenvalues of the interacting Hamiltonian are shifted at most by the operator norm of the interaction Hamiltonian with respect to those of the non-interacting Hamiltonian [88, Theorem III.2.1]. As long as the interaction is weak, in the sense that its operator norm is small compared to an energy uncertainty or measurement resolution, the change in the eigenvalues will thus be insignificant.

The energy eigenstates, or in the case of a degenerate Hamiltonian the spectral projectors, are much more fragile. Naive perturbation theory breaks down [316] as soon as the strength of the perturbation is larger than the gaps of the non-interacting Hamiltonian. The gaps of a locally interacting quantum system are, however, usually exponentially small in the system size. Indeed, if the non-interacting Hamiltonian H_0 and the interaction Hamiltonian H_I are not diagonal in the same basis, the energy eigenstates of $H = H_0 + H_I$ will usually be markedly different from those of H_0.

Before we tackle this problem, let us consider the non-interacting case, i.e., a Hamiltonian of the form $H_0 \coloneqq H_S + H_B$. Let H_0 and $H_{S\restriction S}$ have spectral decompositions $H_0 = \sum_k^{d_0'} E_k^0 \Pi_k^0$ and

$H_{S\restriction S} = \sum_l^{d'_S} E_l^S \, \Pi_l^S$, respectively. Moreover, let $(|\tilde{E}_l^S\rangle)_{l=1}^{d_S}$ and $(|\tilde{E}_m^B\rangle)_{m=1}^{d_B}$ be some orthonormal eigenbases with corresponding eigenvalues $(\tilde{E}_l^S)_{l=1}^{d_S}$ and $(\tilde{E}_m^B)_{m=1}^{d_B}$ of $H_{S\restriction S}$ and $H_{B\restriction B}$, respectively. The Hamiltonians $H_{S\restriction S}$, $H_{B\restriction B}$, and H_0 are allowed to have degeneracies, i.e., $l \neq l' \implies \tilde{E}_l^S \neq \tilde{E}_{l'}^S$ and $m \neq m' \implies \tilde{E}_m^B \neq \tilde{E}_{m'}^B$ and the bases are not unique. Remember that, on the other hand, by definition, the elements of the sequences $(E_k^0)_{k=1}^{d'_0}$ and $(E_l^S)_{l=1}^{d'}$ are distinct.

We first look at the case of spin systems. In such systems each of the spectral projectors Π_k^0 of H_0 is of the form

$$\Pi_k^0 = \sum_{l,m\colon \tilde{E}_l^S + \tilde{E}_m^B = E_k^0} |\tilde{E}_l^S\rangle\langle\tilde{E}_l^S| \otimes |\tilde{E}_m^B\rangle\langle\tilde{E}_m^B|. \tag{4.101}$$

The micro-canonical state $\sqcap[H_0]([E, E+\Delta])$ to an energy interval $[E, E+\Delta]$ is hence proportional to

$$\sqcap[H_0]([E, E+\Delta]) \propto \sum_{k\colon E_k^0 \in [E,E+\Delta]} \sum_{l,m\colon \tilde{E}_l^S + \tilde{E}_m^B = E_k^0} |\tilde{E}_l^S\rangle\langle\tilde{E}_l^S| \otimes |\tilde{E}_m^B\rangle\langle\tilde{E}_m^B|. \tag{4.102}$$

Its reduced state $\sqcap^S[H_0]([E, E+\Delta]) = Tr_B \sqcap[H_0]([E, E+\Delta])$ on S therefore satisfies

$$\begin{aligned}
\sqcap^S[H_0]([E, E+\Delta]) &\propto \sum_{k\colon E_k^0 \in [E,E+\Delta]} \sum_{l,m\colon \tilde{E}_l^S + \tilde{E}_m^B = E_k^0} |\tilde{E}_l^S\rangle\langle\tilde{E}_l^S| && (4.103)\\
&= \sum_{k\colon E_k^0 \in [E,E+\Delta]} \sum_{l=1}^{d_S} |\tilde{E}_l^S\rangle\langle\tilde{E}_l^S| \, |\{m\colon \tilde{E}_l^S + \tilde{E}_m^B = E_k^0\}| && (4.104)\\
&= \sum_{k\colon E_k^0 \in [E,E+\Delta]} \sum_{l=1}^{d'_S} \Pi_l^S \, |\{m\colon E_l^S + \tilde{E}_m^B = E_k^0\}| && (4.105)\\
&= \sum_{l=1}^{d'_S} \Pi_l^S \, |\{m\colon E_l^S + \tilde{E}_m^B \in [E, E+\Delta]\}| && (4.106)\\
&= \sum_{l=1}^{d'_S} \Pi_l^S \, \#_\Delta[H_{B\restriction B}](E - E_l^S), && (4.107)
\end{aligned}$$

where

$$\#_\Delta[H_{B\restriction B}](E) \coloneqq |\{m\colon \tilde{E}_m^B \in [E, E+\Delta]\}| = rank(\sqcap[H_{B\restriction B}]([E, E+\Delta])) \tag{4.108}$$

is the number of orthonormal energy eigenstates of the bath Hamiltonian H_B to energies in the interval $[E, E+\Delta]$.

For systems of fermions Eq. (4.101) does not hold, because the Hilbert space of the joint system is not the tensor product of the Hilbert spaces of the subsystems. However, the following quite lengthy calculation shows an equivalent result also for fermionic systems. Readers not interested in the details can safely jump directly to Observation 3.

Denote by $f_x, f_x^\dagger$ the fermionic annihilation and creation operators on $\mathcal{H}$ and by $\tilde{f}_x, \tilde{f}_x^\dagger$ with $x \in S$ those acting on $\mathcal{H}_S$ and for $x \in B$ those acting on $\mathcal{H}_B$. Furthermore, denote the vacuum state vector in $\mathcal{H}$ by $|0\rangle$ and the projectors in $\mathcal{B}(\mathcal{H})$ onto the subspace with no particle in system S or B by $|0\rangle\langle 0|_S$, and $|0\rangle\langle 0|_B$, respectively. The projectors $|0\rangle\langle 0|_S$, $|0\rangle\langle 0|_B$, and $|0\rangle\langle 0|$ are all even operators and $|0\rangle\langle 0| = |0\rangle\langle 0|_S \, |0\rangle\langle 0|_B$. For each $l \in [d_S]$ let $p_l^{H_S}$ be the representation of the eigenstate $|\tilde{E}_l^S\rangle$ as a polynomial in the fermionic operators on $\mathcal{H}_S$, i.e.,

$|\tilde{E}_l^S\rangle = p_l^{H_S}((\tilde{f}_s, \tilde{f}_s^\dagger)_{s\in S})\,|0\rangle_S$, and likewise for $p_m^{H_B}$. Note that the $p_l^{H_S}$ and the $p_m^{H_B}$ are either even or odd polynomials as otherwise the projectors $|\tilde{E}_l^S\rangle\langle\tilde{E}_l^S|$ and $|\tilde{E}_m^B\rangle\langle\tilde{E}_m^B|$ would not be even. Furthermore, note that commuting two polynomials that are both either even or odd gives a global minus sign only if both polynomials are odd. As H_S and H_B are even operators it is straight forward to verify that the states $|\tilde{E}_l^S + \tilde{E}_m^B\rangle := p_l^{H_S}((f_s, f_s^\dagger)_{s\in S})\,p_m^{H_B}((f_b, f_b^\dagger)_{b\in B})\,|0\rangle$ are eigenstates of H^0 to energy $\tilde{E}_l^S + \tilde{E}_m^B$. In fact, they form an orthonormal basis of $\mathcal{H}$ in which H^0, H_S, and H_B are jointly diagonal. For the sake of brevity we omit the subscripts $_{s\in S}$ and $_{b\in B}$ in the following calculation. It is again straight forward to verify that for any even operator $A \in \mathcal{B}(\mathcal{H})$ with $supp(A) \subseteq S$ it holds that

$$\begin{aligned}
&Tr\big(A\,|\tilde{E}_l^S + \tilde{E}_m^B\rangle\langle\tilde{E}_l^S + \tilde{E}_m^B|\big)\\
=&Tr\big(A\,p_l^{H_S}((f_s, f_s^\dagger))\,p_m^{H_B}((f_b, f_b^\dagger))\,|0\rangle\langle 0|_S\,|0\rangle\langle 0|_B\,p_m^{H_B}((f_b, f_b^\dagger))^\dagger\,p_l^{H_S}((f_s, f_s))^\dagger\big) &(4.109)\\
=&Tr\big(A\,p_l^{H_S}((f_s, f_s^\dagger))\,|0\rangle\langle 0|_S\,p_l^{H_S}((f_s, f_s^\dagger))^\dagger\,p_m^{H_B}((f_b, f_b^\dagger))\,|0\rangle\langle 0|_B\,p_m^{H_B}((f_b, f_b^\dagger))^\dagger\big) &(4.110)\\
=&Tr\big(A\,|\tilde{E}_l^S\rangle\langle\tilde{E}_l^S|\big). &(4.111)
\end{aligned}$$

The last step can be shown by explicitly writing out the trace in the Fock basis and inserting an identity between the operators that are supported on S and those supported on B.

Now, note that any operator $A \in \mathcal{B}(\mathcal{H})$ with $supp(A) \subseteq S$ can be written as a sum of an even and odd part and that only the even part can contribute to an expectation value of the form $Tr(A\,|\tilde{E}_l^S + \tilde{E}_m^B\rangle\langle\tilde{E}_l^S + \tilde{E}_m^B|)$. The above calculation is hence sufficient to show that (remember the definition of the partial trace in Eq. (4.34))

$$\forall l \in [d_S], m \in [d_B]\colon \quad Tr_B(|\tilde{E}_l^S + \tilde{E}_m^B\rangle\langle\tilde{E}_l^S + \tilde{E}_m^B|) = |\tilde{E}_l^S\rangle\langle\tilde{E}_l^S|. \tag{4.112}$$

Finally, realizing that

$$\begin{aligned}
&\sqcap[H_0]([E, E+\Delta])\\
&\quad= \sum_{k\colon E_k^0\in[E,E+\Delta]}\ \sum_{l,m\colon \tilde{E}_l^S+\tilde{E}_m^B=E_k^0} Tr_B(|\tilde{E}_l^S + \tilde{E}_m^B\rangle\langle\tilde{E}_l^S + \tilde{E}_m^B|)
\end{aligned} \tag{4.113}$$

yields an expression equivalent to Eq. (4.102) and the proof then proceeds analogously. We summarise the result of the above calculation in the following observation:

Observation 3 (Gibbs states as reductions of micro-canonical states of the non-interacting Hamiltonians)**.** *Let $[E, E+\Delta]$ be an energy interval and $H_0 = H_S + H_B$ a non-interacting Hamiltonian of a bipartite quantum system of spins or fermions with $\mathcal{V} = S \dot\cup B$. If for some $\beta \in \mathbf{R}$ it holds that*

$$\#_\Delta[H_{B\restriction B}](E) \propto \mathrm{e}^{-\beta E}, \tag{4.114}$$

then $\sqcap^S[H_0]([E, E+\Delta])$ takes the well known form of a thermal state, i.e.,

$$\sqcap^S[H_0]([E, E+\Delta]) \propto \sum_{l=1}^{d'_S} \Pi_l^S\,\mathrm{e}^{-\beta E_l^S} \propto g[H_{S\restriction S}](\beta) = g^S[H_0](\beta). \tag{4.115}$$

Note how β, which was introduced in Eq. (4.114) simply as a parameter describing the shape of the number of states, ends up being the inverse temperature of the thermal state $g[H_{S\restriction S}](\beta)$ of the subsystem S. Similar calculations (at least for spin systems) can be found for example in Refs. [283, 105, 294, 69] and in many textbooks on statistical mechanics.

For finite dimensional baths the proportionality $\#_\Delta[H_{B\restriction B}](E) \propto \mathrm{e}^{-\beta E}$ can never be exactly fulfilled simply because $\#_\Delta[H_{B\restriction B}](E)$ is not continuous. A detailed analysis [311, Appendix A] shows that if the logarithm of the number of states $\ln(\#_\Delta[H_{B\restriction B}](E))$ can be sufficiently well

approximated by a twice differentiable function whose second derivative is small compared to the width of the relevant energy range $[E - \|H_S\|_\infty, E + \|H_S\|_\infty]$, then Eq. (4.115) is fulfilled approximately. The first derivative of this approximation ends up being the inverse temperature of the thermal state, the second derivative enters the error bound.

It is widely known that natural locally interacting Hamiltonians H with bounded local terms "generically" have an approximately Gaussian number of states $\#_\Delta[H](E)$ if the system size is sufficiently large [69, Section 12.2] (see also Ref. [317, 318] for some rigorous results). It is more common to refer to the density of states in this case, which is essentially the limit of $\#_\Delta[H](E)/\Delta$ for Δ small and increasing system size. If the bath Hamiltonian H_B is taken to be such a model with a nearly Gaussian density and number of states, the approximation by a twice differentiable function is possible and the distance $\mathcal{D}\left(\sqcap^S[H_0]([E, E+\Delta]), g[H_{S\restriction S}](\beta)\right)$ can be bounded [311, Appendix B] and is usually exponentially small in the size of the bath. In the following we will call locally interacting systems that have this property "generic".

The value of β for which $\mathcal{D}\left(\sqcap^S[H_0]([E, E+\Delta]), g[H_{S\restriction S}](\beta)\right)$ is small depends on E. If $\#_\Delta[H_{B\restriction B}]$ is indeed close to a Gaussian, then $\ln(\#_\Delta[H_{B\restriction B}])$ can be well approximated by an inverted parabola. Its first derivative, which is essentially the optimal β, is large for low values of E, thus associating them with low temperatures. For values of E in the center of the spectrum it goes to zero, corresponding to infinite temperature, and becomes negative for even higher values of E.

In conclusion, we can say that the reduction on S of a micro-canonical state to an energy interval $[E, E+\Delta]$ of a system that is a composite system with $\mathcal{V} = S \dot\cup B$ and without any interaction between S and B, whose Hamiltonian H_B on B is a "generic" many-body Hamiltonian, will typically be exponentially close to a Gibbs state of H_S with an inverse temperature β that depends in a reasonable way on E. This works for all values of E that are neither too low nor too high. At the edges of the spectrum the number of states of the bath will be too low to allow for a good approximation of the number of states by a twice differentiable function. In addition, Δ must be both small compared to $\|H\|_\infty$ and large compared to the largest gaps in the spectrum of H in the relevant energy range.

Now we consider the influence of an interaction between S and B. The challenge posed by the fact that such an interaction will typically markedly perturb the energy eigenstates can be overcome by a perturbation theorem based on a result of Ref. [88] (see also Refs. [319, 320]) for projectors that are sums of spectral projectors.

Theorem 11 (Stability of sums of spectral projectors (implied by Theorem 1 of Ref. [311]))**.** *Given an energy interval $[E, E+\Delta]$ and two Hamiltonians $H, H' \in \mathcal{O}(\mathcal{H})$ with spectral decompositions $H = \sum_k E_k \Pi_k$ and $H' = \sum_k E'_k \Pi'_k$. Let P and P' be projectors that are sums of the spectral projectors Π_k and Π'_k to energies in $[E, E+\Delta]$ of H and H', respectively, i.e.,*

$$P := \sum_{k\colon E_k \in [E, E+\Delta]} \Pi_k \qquad \text{and} \qquad P' := \sum_{k\colon E'_k \in [E, E+\Delta]} \Pi'_k. \tag{4.116}$$

Then for every $\epsilon > 0$

$$\|P - P'\|_1 \leq \left(rank(P) + rank(P')\right) \frac{\|H - H'\|_\infty}{\epsilon} + rank(P_\epsilon) + rank(P'_\epsilon) \tag{4.117}$$

where

$$P_\epsilon := \sum_{k\colon E_k \in [E, E+\epsilon] \cup [E+\Delta-\epsilon, E+\Delta]} \Pi_k \tag{4.118}$$

and

$$P'_\epsilon := \sum_{k\colon E'_k \in [E, E+\epsilon] \cup [E+\Delta-\epsilon, E+\Delta]} \Pi'_k. \tag{4.119}$$

The rather technical theorem stated above has immediate consequences for the stability of micro-canonical states:

Corollary 1 (Stability of micro-canonical states [311]). *Given an energy interval* $[E, E+\Delta]$ *and two Hamiltonians* $H, H' \in \mathcal{O}(\mathcal{H})$ *with spectral decompositions* $H = \sum_k E_k \Pi_k$ *and* $H' = \sum_k E'_k \Pi'_k$ *it holds that for every* $\epsilon > 0$

$$\mathcal{D}\left(\sqcap[H]([E, E+\Delta]), \sqcap[H']([E, E+\Delta])\right) \leq \frac{\|H - H'\|_\infty}{\epsilon} + \frac{\Delta\Omega + \Omega_\epsilon}{2\,\Omega_{\max}}, \tag{4.120}$$

where $\Omega_{\min/\max} := \min / \max\left(rank(\sqcap[H]([E, E+\Delta])), rank(\sqcap[H']([E, E+\Delta]))\right)$, $\Omega := \Omega_{\max} - \Omega_{\min}$, *and*

$$\begin{aligned}\Omega_\epsilon :=& rank(\sqcap[H]([E, E+\epsilon] \cup [E+\Delta-\epsilon, E+\Delta])) \\ &+ rank(\sqcap[H']([E, E+\epsilon] \cup [E+\Delta-\epsilon, E+\Delta])).\end{aligned} \tag{4.121}$$

Proof. By the triangle inequality

$$\mathcal{D}\left(\sqcap[H]([E, E+\Delta]), \sqcap[H']([E, E+\Delta])\right) \leq \frac{\|P - P'\|_1 + \Delta\Omega}{2\,\Omega_{\max}} \tag{4.122}$$

with P, P' defined as in Eq. (4.116). Theorem 11 finishes the proof. □

What is the meaning of the corollary? The statement is non-trivial if $\|H - H'\|_\infty \ll \Delta$. Then one can expect that there exists an ϵ with the property that $\|H - H'\|_\infty \ll \epsilon \ll \Delta$, such that both $\|H - H'\|_\infty / \epsilon \ll 1$ and $(\Delta\Omega + \Omega_\epsilon)/(2\,\Omega_{\max}) \ll 1$. Under the assumption of an approximately uniform density of states one finds that $\Omega_\epsilon/(2\,\Omega_{\max}) \approx 2\,\epsilon/\Delta$ and $\Delta\Omega/(2\,\Omega_{\max}) \lessapprox \|H - H'\|_\infty/\Delta$ such that the optimal choice for ϵ is approximately $\epsilon \approx \sqrt{\|H - H'\|_\infty \Delta/2}$, which yields

$$\mathcal{D}\left(\sqcap[H](I), \sqcap[H'](I)\right) \lessapprox 4\left(\frac{\|H - H'\|_\infty}{\Delta}\right)^{1/2}. \tag{4.123}$$

While the above example provides some intuition for how powerful Theorem 11 and Corollary 1 are, the case of a uniform density of states is not the relevant situation if one is interested in showing thermalisation. As we have seen in the beginning of this section, for $\sqcap^S[H_0]([E, E+\Delta])$ to become approximately thermal it is necessary that the number of states of the bath grows exponentially with E. What happens in this case?

First, notice that the two terms in the right hand side of Eq. (4.120) are non-negative and hence must both be small individually for the inequality to become non-trivial. For the interesting case $H = H_0 + H_I$ and $H' = H_0$ this implies that it is necessary that $\|H_I\|_\infty \ll \epsilon$, so that the first term can become small. For the second term we restrict our attention to $\Omega_\epsilon/(2\,\Omega_{\max})$ as $\Delta\Omega$ can reasonably be assumed to be smaller than Ω_ϵ.

If to good approximation

$$\#_\Delta[H_0](E) \approx \#_\Delta[H](E) \propto \mathrm{e}^{-\beta E}, \tag{4.124}$$

then [311, Appendix H]

$$\frac{\Omega_\epsilon}{2\,\Omega_{\max}} \gtrapprox \frac{1 - \mathrm{e}^{-\beta\,\epsilon}}{2\,(1 - \mathrm{e}^{-\beta\,\Delta})}. \tag{4.125}$$

That is, for Corollary 1 to be non-trivial it must be possible to chose an ϵ such that

$$\beta\,\|H_I\|_\infty \ll \beta\,\epsilon \ll 1. \tag{4.126}$$

At the same time, if Eq. (4.124) is fulfilled, then also [311, Appendix H]

$$\frac{\Omega_\epsilon}{2\,\Omega_{\max}} \lessapprox \frac{\beta\,\epsilon}{1-\mathrm{e}^{-\beta\,\Delta}}. \tag{4.127}$$

Under the reasonable assumption that $\Delta\Omega/(2\,\Omega_{\max}) \ll 1$ the choice $\epsilon = \sqrt{\|H_I\|_\infty/\beta}$ yields

$$\mathcal{D}\left(\sqcap[H](I), \sqcap[H_0](I)\right) \lessapprox 2\frac{\sqrt{\beta\,\|H_I\|_\infty}}{1-\mathrm{e}^{-\beta\,\Delta}}, \tag{4.128}$$

which gives a non-trivial upper bound as long as

$$\|H_I\|_\infty \ll 1/\beta \ll \Delta. \tag{4.129}$$

Concluding, we can say that for reasonable bath Hamiltonians H_B, and if the coupling is weak enough and Δ large enough such that Eq. (4.129) is fulfilled, then one can expect that

$$\mathcal{D}\left(\sqcap^S[H]([E,E+\Delta]), g[H_{S\restriction S}](\beta)\right) \in O\left(\left(\beta\,\|H_I\|_\infty\right)^{1/2}\right), \tag{4.130}$$

i.e., that the reduced state on subsystem S of the micro-canonical state is close to a Gibbs state of the restricted Hamiltonian truncated to S. Corollary 1 and the above discussion quantify the errors in the approximate equalities Eq. (7) in Ref. [68] and Eq. (18) in Ref. [283].

For the rest of this section we consider a bipartite quantum system with $\mathcal{V} = S \dot\cup B$ of spins of fermions with Hamiltonian H. Let $H_0 \coloneqq H_S + H_B$ and $H_I \coloneqq H - H_0$. We are now in a position to state the kinematic version of the thermalisation result, which follows from the above discussion of Corollary 1 and Theorem 9.

Observation 4 (Most Haar random states are locally thermal [311])**.** *Let $R \coloneqq [E, E+\Delta]$ be an energy interval and $\mathcal{H}_R \subseteq \mathcal{H}$ the subspace spanned by all eigenstates of H to energies in R with dimension $d_R \coloneqq \dim(\mathcal{H}_R)$. If the bath has a "generic" locally interacting Hamiltonian with the property that for energies in $[E, E+\Delta]$ the logarithm of the number of states $\ln \#_\Delta[H_{B\restriction B}]$ can be well approximated by an affine function with slope β and if moreover Δ is sufficiently large and the interaction sufficiently weak such that*

$$\|H_I\|_\infty \ll 1/\beta \ll \Delta, \tag{4.131}$$

and the interval R is sufficiently far from the edges of the spectrum, then for every $\epsilon > 0$

$$\begin{aligned}\mathbb{P}_{|\psi\rangle\sim\mu_{\mathrm{Haar}}[\mathcal{H}_R]}\left(\mathcal{D}\left(|\psi\rangle\langle\psi|^S, g[H_{S\restriction S}](\beta)\right) \geq \epsilon + \delta(H_B) + O\left(\left(\beta\,\|H_I\|_\infty\right)^{1/2}\right)\right) \\ \leq 2\,d_S^2\,\mathrm{e}^{-C\,d_R\,\epsilon^2/d_S^2},\end{aligned} \tag{4.132}$$

where $C = 1/(36\,\pi^3)$ and $\delta(H_B)$ decreases fast with the size of the bath.

To state the dynamic result we introduce the notion of rectangular states [311]. We call a state $\rho \in \mathcal{S}(\mathcal{H})$ of a quantum system with Hilbert space $\mathcal{H}$ and Hamiltonian $H \in \mathcal{O}(\mathcal{H})$ rectangular with respect to an energy interval $[E, E+\Delta] \subset \mathbf{R}$ if de-phasing with respect to H yields the micro-canonical state corresponding to $[E, E+\Delta]$. For example, if H has no degeneracies, then a state is a rectangular state if, when expressed in the eigenbasis of H, it has non-zero matrix elements only in some diagonal block and the same value for each entry on the diagonal in this block. The class of rectangular states is not a very large class of states, but generally comprises a lot of pure states and usually also states that are out of equilibrium, in the sense that their reductions on a small subsystem are well distinguishable from a thermal state and at the same time have a sufficiently widespread energy distribution such that Theorem 1 can be used to guarantee equilibration on average. Nevertheless, all these states have a tendency to thermalise dynamically:

Observation 5 (Thermalisation on average [311]). *Let $R \coloneqq [E, E+\Delta]$ be an energy interval. Let the bath have a "generic" locally interacting Hamiltonian with the property that in an energy interval $[E, E+\Delta]$ the logarithm of the number of states $\ln(\#_\Delta[H_{B\restriction B}])$ can be well approximated by an affine function with slope β. If Δ is sufficiently large and the interaction sufficiently weak such that*

$$\|H_I\|_\infty \ll 1/\beta \ll \Delta, \tag{4.133}$$

and the interval R is sufficiently far from the edges of the spectrum, then the time evolution is such that the subsystem S thermalises on average, in the sense of Definition 2, for any initial state $\rho(0) \in \mathcal{S}(\mathcal{H})$ that is rectangular with respect to R in the sense that

$$\overline{\mathcal{D}\left(\rho^S(t), g[H_{S\restriction S}](\beta)\right)}^T \leq \frac{1}{2}\left(N(\epsilon)\, d_S^2\, g((p_k)_{k=1}^{d'})\right)^{1/2} + \delta(H_B) + O\left((\beta\,\|H_I\|_\infty)^{1/2}\right), \tag{4.134}$$

where $\delta(H_B)$ decreases fast with the size of the bath, and, as in Theorem 1,

$$N(\epsilon) \coloneqq \sup_{E\in\mathbf{R}} |\{(k,l) \in [d']^2 \colon k \neq l \wedge E_k - E_l \in [E, E+\epsilon]\}| \tag{4.135}$$

$$g((p_k)_{k=1}^{d'}) \coloneqq \min(\sum_{k=1}^{d'} p_k^2, 3\max\nolimits'_k p_k), \tag{4.136}$$

with $(p_k)_{k=1}^{d'}$ the energy populations, i.e., $p_k \coloneqq Tr(\Pi_k\,\rho(0))$, and $\max'_k p_k$ the second largest element in $(p_k)_{k=1}^{d'}$.

The class of rectangular states seems fairly unnatural on first sight, however, condition of being rectangular can be slightly weakened. For small deviations from a rectangular state Observation 5 still essentially holds, just an additional error must be taken into account. If the deviation from rectangular is in a sense uncorrelated with the relevant properties of the energy eigenstates, then even relatively large deviations should be tolerable as the errors will not accumulate but rather cancel each other out. In the worst case, however, the deviation from rectangular could be highly correlated with the expectation value of, say, a local observable. Then, even small deviations from rectangular can lead to noticeable deviations of the equilibrium state from a thermal state. that this can indeed happen in natural models for natural initial states [254]. In this sense the condition of being rectangular is necessary for thermalisation if no conditions on the energy eigenstates are to be imposed.

A comment on the notion of weak coupling used here is in order: The condition that is needed for the above results to be non-trivial is (compare Eq. (4.130))

$$\beta\,\|H_I\|_\infty \ll 1. \tag{4.137}$$

This is a significant improvement over the condition that would be necessary to guarantee that naive perturbation theory on the level of individual energy eigenstates is applicable (namely that $\|H_I\|_\infty$ is much smaller than the gaps of H_0). While the gaps of H_0 become exponentially small with the system size β can be expected to be an intensive quantity, i.e., to be independent of the system size. It may be worth noting that conditions similar to this have been considered in very practical contexts, say, when studying the thermalisation of two weakly coupled finite metallic grains [321].

In the case of a 1D system with short range interactions and if S is a set of consecutive sites $\|H_I\|_\infty$ is also intensive. In this case, Eq. (4.137) is a physically natural condition to call the coupling weak. In the analogous situation in higher dimensional lattices, for example a system with nearest neighbour interactions on a 2D square lattice and S the sites inside a ball around the origin, $\|H_I\|_\infty$, however, scales with the surface of the region S, making the above bounds useless already for medium sized $|S|$. Thus, the above results are not entirely satisfactory.

The reason for this is essentially that the trace distance is a very sensitive metric. If $\sqcap^S[H]([E, E+\Delta])$ and $g[H_{S\restriction S}](\beta)$ for the optimal β only differ slightly on each of the sites along the boundary of S, then their trace distance (at least as long as it is sufficiently far from one) will be approximately proportional to the surface of S. In consequence, the unfavourable scaling of the given error bounds is expected.

4.7.4 Thermalisation in translation invariant systems and equivalence of ensembles

Thermalisation and the related question of the equivalence of ensembles have recently also been investigated in the more concrete setting of (translation invariant) locally interacting systems on cubic lattices [309]. The additional structure can be used to go beyond the results discussed in Sections 4.7.3. In this section we discuss the main results of Ref. [309] and the generalisations achieved in Ref. [322].

More concretely, Refs. [309, 322] consider systems with k-local Hamiltonians on cubic lattices. A Hamiltonian H is k-local if for some spatial dimension $D \in \mathbf{Z}^+$ and linear size $n \in \mathbf{Z}^+$ the vertex set of the system is $\mathcal{V} = [n]^D$, the edge set $\mathcal{E}$ contains only subsystems X of diameter at most k measured in the graph distance of the lattice, and the corresponding local terms H have norm bounded by one, i.e., $\|H_X\|_\infty = 1$. Furthermore, a Hamiltonians H is called translation invariant if for any two subsystems $X, X' \subset \mathcal{V}$ that differ only by a translation on the lattice it holds that $H_X = H_{X'}$.

In Ref. [309] a family of translation invariant systems of increasing size is considered thermalising if they equilibrates on average to a state that, in the limit of infinite system size, becomes indistinguishable from thermal states of that stem. This is a very natural notion of thermalisation in the translation invariant setting. Ref. [309] contains theorems very reminiscent to both the kinematic thermalisation result (Observation 4) and the dynamical result (with a similar conditions on the initial state) on thermalisation on average (Observation 5) for this notions of thermalisation. The results of Ref. [309] are applicable in situations with strong coupling between subsystem and bath, i.e., $\|H_I\|_\infty > 1/\beta$ but are only asymptotic statements and work only for temperatures around which the translation invariant system has a "unique phase" (see Ref. [145, 309] for more details) in the limit of infinite system size. To understand what a "unique phase" is note that in the limit of infinite system size a translation invariant state ρ is given by a series of subsystems states ρ_X which for all $X \subseteq X' \subset \mathcal{V}$ fulfil the consistency conditions $\rho_X = Tr_{X^c}\rho_{X'}$. It is then instructive to define a translation invariant state ρ of the infinite system to be thermal if it minimises the free energy density

$$f(\rho) := \lim_{|X|\to\infty} \frac{Tr(H_X \rho_X) - S(\rho_X)/\beta}{|X|}. \tag{4.138}$$

Whenever $|\mathcal{V}|$ is finite, this definition is consistent with our definition of a thermal state from Eq. (4.38) and moreover the thermal state is unique. In infinite systems, however this is not the case any more and one hence says that a system has a "unique phase" around some inverse temperature β if for all inverse temperatures close to β the system has a unique thermal state in the above sense. At low temperatures this condition is often violated (for example in the 2D Ising model below the Curie temperature). In contrast, at high temperatures the existence of a unique phase is always ensured (see Section 4.10).

The kinematic and dynamics thermalisation results of Ref. [309] rest on a equivalence of ensembles theorem. Two ensembles, for example the canonical and micro-canonical ensemble, are said to be equivalent here if their corresponding states become indistinguishable on small subsystems when the total system size is increased. More concretely: given a locally interacting spin system with Hamiltonian $H \in \mathcal{O}(\mathcal{H})$ and an inverse temperature β, under which conditions

does there exist a suitable energy interval $[E, E+\Delta]$ such that for all sufficiently small subsystems $S \subset \mathcal{V}$ the distinguishability $\mathcal{D}\left(g^S[H](\beta), \sqcap^S[H]([E, E+\Delta])\right)$ is small. Unfortunately Ref. [309] does not give concrete finite size bounds on the distinguishability but only makes statements about the asymptotic behaviour.

This however was recently achieved in Ref. [322], together with a generalisation to systems without translation invariance. Before we can explain this result in more detail we need to introduce the notion of (ξ, z)-exponentially decaying correlations that is closely connected to the notion of a "unique state" encountered before. Remember the definition of the covariance from Eq. (4.35). A state ρ of a system on a lattice is said to have (ξ, z)-exponentially decaying correlations if for some constants $\xi, z \in \mathbf{R}^+$ and any two observables $A, B \in \mathcal{O}(\mathcal{H})$

$$cov_\rho(A, B) \leq \|A\|_\infty \|B\|_\infty N^z \, \mathrm{e}^{-d(A,B)/\xi}, \tag{4.139}$$

where d is again the graph distance of the lattice.

A simplified version of the main result of Ref. [322] can then be phrased as follows:

Theorem 12 (Equivalence of ensembles [322, Theorem 1])**.** *Fix a spatial dimension $D \in \mathbf{Z}^+$, a locality parameter $k \in \mathbf{Z}^+$, a linear region size $l \in \mathbf{Z}^+$, an inverse temperature β, and $\xi, z \in \mathbf{R}^+$. For $n \in \mathbf{Z}^+$ consider an infinite family of spin systems with vertex sets $\mathcal{V} = [n]^D$, Hilbert spaces $\mathcal{H}_\mathcal{V}$, and k-local Hamiltonians $H_\mathcal{V} \mathcal{O}(\mathcal{H})$. If the family of thermal states $g[H_\mathcal{V}](\beta)$ has (ξ, z)-exponentially decaying correlations, then for the family $\sqcap[H_\mathcal{V}]([E_\mathcal{V} - \Delta_\mathcal{V}/2, E_\mathcal{V} + \Delta_\mathcal{V}/2])$ of micro-canonical states with*

$$E_\mathcal{V} \coloneqq Tr(H_\mathcal{V}\, g[H_\mathcal{V}](\beta)) \tag{4.140}$$

and

$$\Delta_\mathcal{V} \coloneqq \left(\frac{1}{N} Tr\left(H_\mathcal{V}^2\, g[H_\mathcal{V}](\beta)\right) - Tr\left(H_\mathcal{V}\, g[H_\mathcal{V}](\beta)\right)^2 \right)^{1/2} \tag{4.141}$$

it holds that

$$\lim_{n\to\infty} \mathcal{D}\left(\sqcap^{X_\mathcal{V}}[H_\mathcal{V}]([E_\mathcal{V}, E_\mathcal{V} + \Delta_\mathcal{V}]), g^{X_\mathcal{V}}[H_\mathcal{V}](\beta)\right) = 0 \tag{4.142}$$

for any family $X_\mathcal{V} \subset \mathcal{V}$ of subsystems whose diameter grows at most as fast as $n^{1/(d+1)}$.

The main virtue of Ref. [322] is that it actually gives a concrete finite size bound on the average distance between the canonical and the micro-canonical state on hyper-cubic subsystems. In short, Ref. [322] shows that and how the canonical and micro-canonical states become indistinguishable on any sufficiently small subsystem when the total system size increases given that β is such that the thermal state of the total system has exponentially decaying correlations. We see later in Section 4.10 that at sufficiently high temperatures the necessary correlation decay can always be ensured.

4.7.5 Hybrid approaches and other notions of thermalisation

We have seen in the last sections that both approaches to explain thermalisation, the eigenstate thermalisation hypothesis and thermalisation under assumptions on the initial state, have their advantages and drawbacks. They can be understood as extreme scenarios. In most cases where thermalisation of closed quantum systems happens it is probably due to a mixture of the two effects. An interpolation between the two previously discussed approaches is provided by the eigenstate randomisation hypothesis (ERH) [323]. The ERH is a weaker condition than the ETH. Instead of demanding that for certain observables the expectation values of all individual energy eigenstates with nearby energies give approximately the same expectation value

(compare Conjecture 1 and Definition 3), the ERH requires only that the variance of certain coarse-grainings of the sequence of expectation values of an observable in the energy eigenstates becomes sufficiently small. This, together with a condition on the smoothness of the energy distribution of the initial state that is milder than what we required when we introduced the class of rectangular states, is sufficient to prove a thermalisation result that is similar in spirit to Observation 5 [323]. Again, numerical evidence for the validity of the ERH in certain models has been collected [323].

It seems worth repeating that the notion of thermalisation used here is surely not the only reasonable one. For example Ref. [132] works in the setting of macroscopic commuting observables of von Neumann, which we discussed briefly in Section 4.6. A system is declared to be in thermal equilibrium if there is a phase cell that is much larger than all others and the state of the system is almost completely contained in the subspace corresponding to this cell.

Many other definitions of thermalisation or thermal equilibrium in quantum many-body systems are possible. For example, in the context of the ETH it is sometimes said that a system is thermal if the expectation values of a given observable in the energy eigenstates of a system are, up to small fluctuations, smooth functions of the energy (compare for example Ref. [45]). The validity of fluctuation-dissipation theorems has also been considered as a condition for thermalisation [324, 325].

The notion of relative thermalisation [326] focuses on yet another aspect of thermalisation. Rather than being concerned with the closeness of an equilibrium state to a thermal state of some kind it stresses that a system can be considered truly thermal only if it is not correlated with any other relevant system, as otherwise phenomena such as anomalous heat flow, which go against the predictions of thermodynamic, can occur. In Ref. [326] a subsystem S is called approximately thermal relative to a reference system R, if the joint state ρ_{SR} is close in trace norm to a state of the form $\pi_S \otimes \rho_R$ with π_S being a suitable micro-canonical state. Decoupling techniques can be used to show that whenever certain entropic inequalities are fulfilled then most joint evolutions of S, R, and an environment lead to approximate relative thermalisation [326].

4.7.6 Investigations of thermalisation in concrete models

A large body of literature is concerned with investigations of thermalisation in specific quantum many-body models. Many of those studies are directly concerned with testing a variant of the eigenstate thermalisation hypothesis (ETH) at the level of individual eigenstates. The various eigenstate thermalisation hypotheses differ in whether they conjecture closeness to a micro-canonical or a canonical average and concerning the type of observables they supposedly apply to. Few body and (approximately) local observables are the two most frequently encountered choices.

The ETH gained wide popularity after the series of influential works [33, 34, 327]. They identify the ETH as the mechanism for thermalisation and study its breakdown close to integrability in systems of hardcore bosons by means of exact diagonalisation. Similar conclusions are reached in Ref. [181] for fermionic systems and the ETH is compared with other signatures of quantum chaos. Ref. [45] represents a sound and detailed study of the validity of the ETH in systems with a tunable integrability breaking term by means of finite size scaling and varying the strength of the integrability breaking term. Ref. [300] discusses the validity of the ETH in a simple model making use of a numerical technique that does not rely on exact diagonalisation. Ref. [328] presents a detailed study of the fluctuations of diagonal and off-diagonal matrix elements in the energy eigenbasis of certain physical observables in Heisenberg spin chains that confirms that in the non-integrable case the ETH is fulfilled. Ref. [178] finds a breakdown of thermalisation and the ETH in a non-integrable model of spin-less fermions with a power law

like random hopping term if the decay exponent is sufficiently large. In Ref. [329] the ETH is connected with von Neumann's quantum ergodic theorem and it is confirmed that after a quench from a model that fulfils the ETH to one that does not (for the system being integrable), a system can still behave thermal. Ref. [47] performs a finite size scaling analysis of the validity of the ETH in the (integrable) Lieb-Liniger model and demonstrates that a weaker version of the ETH still holds that is sufficient to guarantee apparent thermalisation for initial states that occupy sufficiently many energy eigenstates.

On top of that, a large body of literature exists that investigates all sorts of aspects of thermalisation and how various properties of the Hamiltonian and initial state influence it — in fact, this has a long history [330, 49]: Refs. [51, 58, 202, 30, 176] numerically and experimentally study transport and thermalisation in the (non-integrable) Bose-Hubbard model. Ref. [50] focuses on the (fermionic) Hubbard model at small interaction strength. Using flow techniques the temporal evolution investigated and is found to go trough three distinct regimes. After an initial build-up of correlations the system exhibits an intermediate, non-equilibrium, pre-thermalised, quasi-steady state and then eventually becomes indistinguishable from being thermalised. Similar pre-thermalisation effects – building upon the theoretical understanding discussed in Ref. [331] – have been observed in Ref. [204] in Bose- and Fermi-Hubbard models, in Ref. [332] in systems of spin-less fermions, and in Ref. [333] in instances of non-integrable quantum spin chains. Similar pre-thermalisation effects were also found in systems evolving under stochastically changing Hamiltonians [96, 335]. Ref. [336] studies the energy relaxation and thermalisation of hot electrons in quantum wires. Ref. [310] investigates the influence of the initial state on the time scales on which thermalisation happens in a non-integrable model. Ref. [174] looks at local and non-local conservation laws and how they influence the non-equilibrium dynamics and thermalisation. The equilibration and thermalisation after a quench to a coupled Hamiltonian of two identical uncoupled systems initially in thermal states at different temperatures is studied in [213] and thermalisation to a state close to a joint thermal state is found. Ref. [337] investigates conditions for equilibration and thermalisation (albeit in the sense of convergence in the limit $t \to \infty$) in the well studied model of a central harmonic oscillator linearly coupled to an infinite number of other oscillators starting from a non-thermal product initial state.

The bottom line of this large amount of investigations is as follows: The energy eigenstates in the bulk of the spectrum, i.e., those to energies that are neither too low nor too high, of sufficiently large and sufficiently complicated composite quantum systems seem to generically fulfil some variant of the ETH for certain physically meaningful local or few body observables. Equilibration of local and few body observables is a very common phenomenon shared by almost all reasonable locally interacting many-body models for wide classes of initial states. This in turn implies that those systems which fulfil a suitable variant of the ETH also almost always dynamically thermalise after being started in a non-equilibrium initial state, like for example after a quench.

Many studies moreover conclude that the fulfilment of the ETH is related to non-integrability or chaos [178, 181, 84, 329, 113, 313, 338, 45, 44, 45, 312]. Moreover, it is often suggested that systems fulfil the ETH and thermalise if and only if they are non-integrable [33, 34, 55, 339, 340], disordered systems being an important exception [254] (see also Section 4.8.3). What precisely the term non-integrable means in the context of many-body quantum mechanics and especially in systems without a well-defined classical limit and the relation between (non-)integrability and (exact) solvability are, however, still the subject of a lively debate [341, 314, 342, 48]. We will come back to this issue in Section 4.9.

4.8 Absence of thermalisation and many-body localisation

In the past section we have identified and discussed conditions under which locally interacting many-body systems exhibit thermodynamic behaviour like equilibration and thermalisation. Complementing these considerations, in this section we will identify and discuss scenarios in which thermalisation is prevented. In particular we will be concerned with situations in which a system fails to thermalise locally because small subsystems retain memory of their initial conditions. Quite intuitively the presence or absence of thermalisation is intimately linked to the transport properties of a system. After all, for thermalisation to happen stating from a non-equilibrium initial condition, some equalisation of initial imbalances in, for example, the spatial distribution of energy or particles must happen. We will see that the concept of entanglement, to what extend it is present in the eigenstates of a Hamiltonian and how it spreads through the system during time evolution, will be of great use to gain insights into such transport processes.

We start by formulating what we mean by absence of thermalisation and in particular define violation of subsystem initial state independence. The main part of this section will be dedicated to the discussion of physical situations in which one naturally expects such an absence of thermalisation to happen: systems with static disorder in the Hamiltonian. This will lead us to the intriguing phenomenon of (many-body) localisation, a type of localisation in which disorder and interactions interplay in a subtle fashion. In fact, one of the currently discussed definitions for many-body localisation in quantum systems takes the absence of thermalisation as its defining feature [343, 9, 345]. We make an attempt to survey the newly emerging debate concerning this phenomenon. After a brief introduction to Anderson localisation we discuss properties that can be expected from a many-body localised phase and collect different notions of many-body localisation.

4.8.1 Violation of subsystem initial state independence

We start with defining subsystem initial state independence. Roughly speaking, a system fulfils subsystem initial state independence for a certain set of initial states if changing only the subsystem part of an initial state from that set does not noticeably influence the equilibrium state of the subsystem. This can be put as follows:

Definition 4 (Subsystem initial state independence)**.** *We say that a composite system with Hilbert space $\mathcal{H}$ and Hamiltonian $H \in \mathcal{O}(\mathcal{H})$ satisfies subsystem initial state independence for subsystem S on average with respect to a given set of initial states $\mathcal{S}_0 \subseteq \mathcal{S}(\mathcal{H})$ if for all $\rho(0) \in \mathcal{S}_0$ the equilibrium state on S is sufficiently independent of its initial state in the sense that for every quantum channel $C \in \mathcal{T}^+(\mathcal{H})$ with support $supp(C) \subseteq S$ the states $\rho(0)$ and $C(\rho(0))$ have the property that $\mathcal{D}\left(Tr_{S^c}[\$_H(\rho(0))], Tr_{S^c}[\$_H(C(\rho(0)))]\right)$ is sufficiently small.*

If a system does not exhibit any local exactly conserved quantities, subsystem initial state independence, as defined in Definition 4, with respect to a sufficiently large set of initial states $\mathcal{S}_0 \subset \mathcal{S}$, can rightfully be considered a necessary condition for thermalisation of small subsystems, regardless of which precise definition of thermalisation is adopted.

As was shown in Ref. [254] subsystem initial state independence after a quench can be provably violated if the Hamiltonian exhibits a lack of entanglement in the eigenbasis. The central quantity in the argument is the effective entanglement in the eigenbasis. Given a bipartite spin system with $\mathcal{V} = S \dot\cup B$, Hilbert space $\mathcal{H}$, and Hamiltonian $H \in \mathcal{O}(\mathcal{H})$ with spectral decomposition $H = \sum_{k=1}^{d'} E_k \Pi_k$ we define for any pure state $\psi = |\psi\rangle\langle\psi| \in \mathcal{S}$ the effective entanglement in the eigenbasis as

$$R_{S|B}(\psi) \coloneqq \sum_{k=1}^{d'} p_k \, \mathcal{D}\left(Tr_B(\Pi_k \, \psi \, \Pi_k)/p_k, \psi^S\right), \tag{4.143}$$

with $p_k := Tr(\Pi_k \psi)$ the energy level populations. If the Hamiltonian is non-degenerate it takes the simpler form

$$R_{S|B}(\psi) = \sum_{k=1}^{d} p_k \mathcal{D}\left(Tr_B(|E_k\rangle\langle E_k|), \psi^S\right). \tag{4.144}$$

The name effective entanglement in the eigenbasis is justified by a result of Ref. [254], which bounds $R_{S|B}$ by a quantity that is closely related to the geometric measure of entanglement [346, 347, 348]. If the eigenstates of H are little entangled, and ψ is a suitably chosen product state, then $R_{S|B}(\psi)$ is small. In fact one can show [254, 120] that there exist many initial states that are perfectly distinguishable on the subsystem but that have both the properties needed to ensure equilibration on average of small subsystems according to Theorem 1 and a small $R_{S|B}$ if H is non-degenerate and its eigenbasis is only little entangled. The type of system that are naturally expected to show such a behaviour, as will be discussed in the subsequent subsection, are many-body localising systems. The effective entanglement in the eigenbasis can be used to bound how much closer the reduced states on S of two different initial states can move during equilibration on average in the following sense:

Theorem 13 (Distinguishability of de-phased states [254, Theorem 1])**.** *Consider a bipartite spin system with $\mathcal{V} = S \dot\cup B$, Hilbert space $\mathcal{H}$ and Hamiltonian $H \in \mathcal{O}(\mathcal{H})$. For $j \in \{1, 2\}$ let $\psi_j(0) = \psi_j^S(0) \otimes \psi_j^B(0) \in \mathcal{S}(\mathcal{H})$ be two initial product states and set $\omega^{S(j)} := Tr_B(\$_H(\psi_j(0)))$ then*

$$\mathcal{D}\left(\omega^{S(1)}, \omega^{S(2)}\right) \geq \mathcal{D}\left(\psi_1^S(0), \psi_2^S(0)\right) - R_{S|B}(\psi_1(0)) - R_{S|B}(\psi_2(0)). \tag{4.145}$$

If the state of the subsystem S equilibrates on average during the evolution under H for the two initial states, then the de-phased states $\omega^{S(j)} = Tr_B(\$_H(\psi_j(0)))$ are the respective equilibrium states. The theorem shows that if $R(\psi_1(0))$ and $R(\psi_2(0))$ are both small, then the subsystem equilibrium states $\omega^{S(1)}$ and $\omega^{S(2)}$ cannot be much less distinguishable than the initial states $\psi_1^S(0)$ and $\psi_2^S(0)$. We summarise this in the following observation:

Observation 6 (Absence of initial state independence)**.** *Consider a bipartite spin system with $\mathcal{V} = S \dot\cup B$ and Hilbert space $\mathcal{H}$. Let $\mathcal{H}_R \subseteq \mathcal{H}$ be a subspace of dimension $d_R := \dim(\mathcal{H}_R)$. If d_R is large and the Hamiltonian $H \in \mathcal{O}(\mathcal{H})$ has not too many degenerate energy gaps (see Theorem 1 for details) and an orthonormal basis $(|j\rangle)_{j=1}^{d_S}$ for $\mathcal{H}_S$ exists for which $\delta := \max_{k\in[d]} \delta_k$, with*

$$\delta_k := \min_{j\in[d_S]} \mathcal{D}\left(Tr_B|E_k\rangle\langle E_K|, |j\rangle\langle j|\right), \tag{4.146}$$

is small, then for every $j, j' \in [d_S]$ there exist many initial states of the bath $\psi^B(0) \in \mathcal{S}(\mathcal{H}_B)$ such that according to Theorem 1 both $|j\rangle\langle j| \otimes \psi^B(0)$ and $|j'\rangle\langle j'| \otimes \psi^B(0)$ lead to subsystem equilibration on average, but despite them having exactly the same initial state on the bath, the corresponding subsystem equilibrium states $\omega^{S(j)}$ and $\omega^{S(j')}$ remain well distinguishable for most times during the evolution, in the sense that their trace distance $\mathcal{D}\left(\omega^{S(j)}, \omega^{S(j')}\right)$ is significantly larger than zero whenever $j \neq j'$, because of Theorem 13.

A statement complementing Observation 6 can be found in Ref. [107, Section B] (see also Ref. [125] for a generalisation to mixed initial states and situations with initial correlations to reference system). There, it is shown that if the energy eigenstates of a non-degenerate Hamiltonian does contain a lot of entanglement, then subsystem initial state independence can be guaranteed.

In a very similar spirit as above, absence of initial state independence has also been studied later in Ref. [349], which gives a condition that is necessary for subsystem initial state independence. The article mostly studies a simplified version of this condition, which essentially demands that the reductions of most eigenvectors of the Hamiltonian must be sufficiently close to the maximally mixed state.

More recently, initial state independence was studied in Ref. [190, 125]). By using the decoupling method [126, 127, 128] and the formalism of so-called smooth min and max entropies [129, 130]. The authors show that it can be decided from just looking at one particular initial state whether a system satisfies initial state independence for most initial states. Moreover, they give sufficient and necessary entropic conditions for initial state independence of most initial states. The authors consider both subsystem initial state independence and bath initial state independence, i.e., the independence of the equilibrium state of the subsystem from the initial state of the bath. The results concerning the absence of subsystem initial state independence of Ref. [190], when compared to those of Ref. [254] discussed above, have the advantage that they apply to specific points in time instead of time averaged states and that the subsystem does not need to be small. On the other hand they only hold for most/typical initial states.

There exist several articles, including Refs. [52, 271, 339, 340], that numerically and analytically study related effects. Ref. [339] finds that the existence of few energy eigenstates that violate the eigenstate thermalisation hypothesis (see also Section 4.7.2 and in particular Definition 3) can lead to absence of thermalisation. Ref. [340] goes beyond the closed system setting and considers thermalisation and its absence in systems that are coupled to thermal baths and finds that certain integrable models do not thermalise. Ref. [52] studies quenches in a homogeneous XY quantum spin chain with transverse field starting in ground, excited, and thermal states. The authors find that after certain quenches local observables fail to thermalise and relate this behaviour to criticality. Ref. [271] investigates equilibration and thermalisation in exactly solvable models and finds that in such models correlation functions can retain memory of the initial conditions.

4.8.2 Anderson localisation

With the aim to develop a better understanding of particle and spin transport in materials with impurities, Anderson in his 1958 article [350] proposed a simple model for quantum mechanical particles in a lattice with a random potential and showed that the randomness can lead to a complete suppression of diffusion or transport. This phenomenon became known as Anderson localisation. More concretely, the model studied by Anderson is a tight-binding model on a cubic lattice of dimension D with a single particle hopping on the lattice sites. The Hilbert space is $\mathcal{H} = l^2(\mathbf{Z}^D)$ spanned by vectors $|x\rangle$ interpreted as the state with the particle at position $x \in \mathbf{Z}^D$. The random Hamiltonian of the Anderson model reads

$$H(V) = \sum_{x,y\in\mathbf{Z}^D\,:\,|x-y|=1} |x\rangle\langle y| + \lambda \sum_{x\in\mathbf{Z}^D} V_x\,|x\rangle\langle x|, \tag{4.147}$$

where $\lambda > 0$ and V a family of random numbers V_x drawn i.i.d. from a suitable distribution μ. The first term describes hopping between nearest neighbours in the lattice (Ref. [350] actually also considers more general longer range hopping), while the second represents a random on-site potential. For reviews on the Anderson model from the perspective of mathematical physics, see Refs. [351, 352, 353]. For a general overview written on the occasion of the 50th anniversary of the phenomenon see Ref. [354]. For a good book also providing significant historical context, see Ref. [352]. To simplify the discussion we concentrate on one spatial dimension $D = 1$, and assume that the distribution μ is absolutely continuous with a bounded density of compact support. Because of the existence of the rigorous mathematical literature, we moreover take the liberty to brush over some subtleties.

The Anderson model exhibits "localisation". This is true in at least two different senses of the term [351]: First, the random Hamiltonian (4.147) almost surely exhibits spectral localisation, meaning that it has a pure point spectrum (that densely fills all non-trivial open intervals contained in its almost sure spectrum) and that the associated eigenfunctions are exponentially

decaying. The latter means that $H(V)$ has a complete countable set of eigenvectors $\{|E_k\rangle\}_k$ obeying

$$\exists C > 0, \xi > 0 \colon \forall |E_k\rangle \; \exists x_0 \colon \forall x \colon \quad |\langle x | E_k| \leq C \, \mathrm{e}^{-|x-x_0|/\xi}. \tag{4.148}$$

Here $\xi > 0$ is called the localisation length scale. That is to say: Almost all Hamiltonian eigenvectors are exponentially clustering. For systems in in more than one dimension a similar statement holds either at sufficiently high disorder, or for energies sufficiently close to band edges. Note also that these results can be extended to finite systems, localisation then holding with high probability instead of almost surely.

Second, the model exhibits almost surely dynamical localisation. This can be captured as follows: The random Hamiltonian $H(V)$ is said to exhibits dynamical localisation in an open interval I if

$$\exists C > 0, \xi > 0 \colon \forall x, y \in \mathbf{Z}^D \colon \quad \mathbb{E}\big(\sup_{t \in \mathbf{R}} \langle x | \, e^{-\mathrm{i} \, H(V) \, t} \, \Pi_I \, |y\rangle \big) < C \, \mathrm{e}^{-|x-y|/\xi} \tag{4.149}$$

where Π_I is the spectral projector corresponding to the interval I. Dynamical localisation implies a complete absence of transport. In particular it implies that all moments of the "distance from the origin" operator $|X|$, which acts like $|X| \, |x\rangle = |x| \, |x\rangle$, are bounded uniformly in time, i.e., that

$$\forall p > 0, \;\; x, y \in \mathbf{Z}^D \colon \quad \sup_{t \in \mathbf{R}} \big\| |X|^q \, e^{-\mathrm{i} \, H(V) \, t} \, \Pi_I \, |\psi\rangle \big\| < \infty \tag{4.150}$$

for $|\psi\rangle$ any state vector with compact support almost surely. Despite the hopping term in the Hamiltonian, which in the absence of the disordered potential allows the particle to move through the lattice, in the Anderson model the particle "gets stuck". The probability of finding it on a site different from its starting point decays exponentially with the distance uniformly for all times. Dynamical localisation implies spectral localisation by the RAGE theorem, but the converse is not necessarily true.

The above discussion immediately carries over to, for instance, disordered quadratic fermionic systems in which the quasi-particles do not interact. In one spatial dimension, the corresponding Hamiltonian reads

$$H(V) = \sum_{x \in \mathbf{Z}} \Big(f_x^\dagger f_{x+1} + f_{x+1}^\dagger f_x \Big) + \sum_{x \in \mathbf{Z}} V_x \, f_x^\dagger f_x, \tag{4.151}$$

As the fermions do not interact in such quadratic models, each of them behaves as in Anderson's model and conductivity is completely lost. The Hamiltonian can also be readily related to local spin models by virtue of the Jordan Wigner transformation and Anderson's conclusion can be argued to still holds for interacting particles when the density is very low [350].

4.8.3 Many-body localisation

An intriguing, and in large parts still unsettled, question is whether and in what precise sense localisation survives in systems with interactions and significant particle densities. This issue has already been raised by Anderson [350, 355]. One expects that in models with sufficiently strong disorder some characteristics of Anderson localisation should survive in the presence of interactions. This new phase of matter is commonly referred to as the many-body localised (MBL) phase. In which sense and under which conditions this is in fact true is the subject of ongoing investigations. In fact, there is no complete consensus yet as to what precisely constitutes many-body localisation in the first place. In the following we collect and compare different points of view (see also Ref. [356]):

1. Suppression of transport and localisation in Fock space: The influential Ref. [357] gives significant evidence that indeed, localisation in the dynamical sense [170] is maintained in the presence of interactions, by invoking a combinatoric argument and perturbation theory: For sufficiently high disorder and sufficiently low temperature (and absence of a coupling to an external heat bath) it is demonstrated that the conductivity in a disordered fermionic lattice system is exactly zero. The argument makes use of the concept of localisation in Fock space introduced in Ref. [358] (see also Ref. [359]): Consider a fermionic system whose Hamiltonian is a sum of a quadratic Hamiltonian H_0 and an interaction term H_1. A many-body state is called localised if it is a superposition of only few of the (quasi-particle) eigenstates of H_0. If the relevant eigenstates of $H_0 + H_1$ are localised, i.e., all below a certain critical energy (called a mobility edge), in this sense then below a critical temperature the system exhibits zero conductivity.

2. Absence of thermalisation: Closely related to the characteristic suppression of transport in localised systems is the absence of thermalisation due to a violation of initial state independence (see also Section 4.8.1). This is a natural expectation, since one does not expect the eigenstate thermalisation hypothesis (ETH) to be valid within the MBL phase. Ref. [343] for example studies a disordered Heisenberg chain and finds a violation of the ETH and interprets this as one of the defining features of MBL. As was shown in Ref. [254] violation of initial state independence in disordered systems can be understood as a consequence of a lack of entanglement in the eigenbasis.

3. Clustering of correlations: Another definition puts the clustering of correlations of eigenvectors into the centre of attention. For quadratic models, it is expected that all Hamiltonian eigenvectors satisfy an area law [226] for the entanglement entropy. This means that in one dimension the von Neumann entropy of the reduced state of any energy eigenstate on any subsystem is upper bounded by a constant independent of the size of the subsystem. A similar feature has also been suggested as a possible definition for MBL [360]: One then calls a system many-body localising if, not necessarily all but at least many (in a suitable sense), eigenstates satisfy an area law. A proof of a uniform area law (in expectation) was recently given for the case of the XY chain with disordered transverse magnetic field in Ref. [361]. Numerically, there is strong evidence that this is indeed the case in disordered interacting models, at least below a mobility edge [35], so an energy scale that separates the MBL from the "ergodic" regime. A connection with the dynamical aspect of localisation [170] was recently established in Ref. [171], where it was shown that invoking different readings of dynamical localisation, it follows that either all or many energy eigenvectors follow an area law.

4. Logarithmic growth of entanglement: A yet different feature of MBL that has been suggested as a defining property is the logarithmic growth of entanglement in time. While the entanglement of generic local Hamiltonian models is expected to grow linearly in time (see also Section 4.3.5), quadratic models show a saturation of entanglement entropies. This is provably so, as a consequence of the complete suppression of transport. In interacting disordered models a slow — logarithmic in time — but unbounded growth of entanglement has been numerically observed [362, 363]. This feature is perfectly compatible with individual eigenstates exhibiting little entanglement. In fact, maybe counter-intuitively, an unbounded growth of entanglement already follows from localised Hamiltonian eigenstates together with a generic spectrum [364].

5. Approximately local constants of motion: Another discussed possibly defining feature of MBL is the presence of an extensive number of exactly or approximately local constants

of motion [365], with the feature that the Hamiltonian can be expressed entirely as a sum of polynomials in these quantities [364, 169, 366].

If indeed such local constants $\{A_j\}$ of motion can be found, (g, K)-local in the above sense for a suitable function g, violation of subsystem initial state independence and absence of thermalisation follow immediately: Since

$$Tr(A_j\rho(t)) = Tr(A_j\rho(0)) \tag{4.152}$$

is true for all times t, the system can possibly only equilibrate to a state that has the same values for these conserved quantities (see Section 4.5.2).

Other, quite sophisticated features also follow from the presence of such approximately local constants of motion. For example, one can derive a Lieb-Robinson type bound with a causal "cone" that grows only logarithmically in time [169] (see also Section 4.3.5). From such a bound one can derive that the entanglement entropy can grow at most logarithmic in time [169, 78, 74]. An similar bound has been also obtained in Ref. [168] for a disordered XY spin chain and Ref. [170] improves upon this by giving a zero velocity Lieb-Robinson bound in disorder average for this model.

A disadvantage of that definition is that it is far from clear how to construct or identify such approximately local constants of motion in the first place. In the disordered Ising model [367] and the XXZ spin chain [365] this is indeed possible, but no general strategy has yet been found [366]. Several of these defining features have also been connected and made plausible using real space renormalisation group approaches [368].

6. Poissonian level statistics: Properties of the energy level statistics of Hamiltonians have proved to be useful indicators for quantum chaos and integrability. It is hence natural to investigate the influence of disorder on the level statistics. A key quantity in this context is the distribution of gaps between consecutive energy eigenvalues. For quadratic models, this distribution typically is a Poissonian one. For interacting models, it is generally expected to follow a Wigner-Dyson type distribution [9, 35, 369, 370, 371].

   For typical many-body localised models, there is strong numerical evidence that the distribution is again close to Poissonian [35, 369, 358, 343, 9]. This can be quantified by the ratio of consecutive level spacings

$$r_j = \frac{\min(\delta_j, \delta_{j+1})}{\max(\delta_j, \delta_{j+1})}, \tag{4.153}$$

   with $\delta_j = E_j - E_{j-1}$ being the gap between consecutive energy levels. In the non-localised phase one can expect from Wigner's surmise leading to the Gaussian orthogonal (GOE) or unitary (GUE) ensemble that a disorder average of r_j yields a value close to $r_{\text{GOE}} \approx 0.5307$ or $r_{\text{GUE}} \approx 0.5996$, while for a Poisson distribution, that one expect in the MBL phase, one obtains on average $r_{\text{Poisson}} = 2\log 2 - 1 \approx 0.3863$.

   An extensive numerical analysis of this ratio of consecutive level spacings has been performed in Ref. [35] for the random field Heisenberg model on a ring. Also finds excellent agreement of the position of the cross over in the consecutive level spacings statistics with that of an area law / volume law crossover of the entanglement entropy and a crossover in the scaling of the participation entropies (a quantity closely related to the inverse participation ratio and the effective dimension discussed in Section 4.3.2). This work also calculates these quantities in an energy resolved fashion and finds that it can happen that for low energies a system shows strong signatures of a Poissonian distribution, while for higher energies, it resembles a Gaussian orthogonal ensemble consistent with the existence of a mobility edge in interacting systems.

7. Power-law approach to equilibrium: Ref. [372] identified a power law (as opposed to exponential) approach to equilibrium of local observables as a characteristic feature of the MBL phase. In addition the MBL phase has also been found to exhibit a slow power law like decay of the disorder average of the survival probability, i.e., the fidelity with the initial state, at long times [373] (see also Section 4.3.7).

Each of the definitions above only capture part of the intricate phenomenon of many-body localisation. In particular it is far from clear whether disorder is really necessary to realise all of the above qualifying features of many-body localisation. In fact, drawing intuition from classical glassy systems it is possible to design clean spin systems that show many of the features one would expect from a system with a MBL transition [374]. In fact many of the static properties discussed above may also occur in certain (nearly) integrable models without any disorder. Concerning the dynamical features of MBL, Ref. [375] for example demonstrates that the slow growth of entanglement entropies (4) can also exist in clean systems. The same holds for long lived metastable states that break a symmetry of the system [375, 376, 173, 374] (see also the effect of pre-thermalisation discussed in Section 4.7.6). It would be specifically intriguing to see rigorously whether fully translation invariant models can exhibit dynamical localisation in the sense of property (2) even for infinite time, similarly as this is possible for interacting disordered models [254].

In several physical architectures, Anderson and many-body localisation has already been experimentally observed. Ref. [377] discusses an experimental observation of exponential localisation of a Bose-Einstein condensate in a random potential generated with a laser speckle pattern. The recent Ref. [378] experimentally probes the many-body localisation transition in a system of ultra cold fermions in a disordered optical lattice by measuring the imbalance between the occupation of even and odd sites starting from a situation where only even sites are occupied, resembling the experimental situation of Ref. [26]. For sufficiently strong disorder the imbalance is found to no longer decay to zero even for long times, reflecting the absence of thermalisation and the violation of a subsystem initial state independence very much in the spirit of Ref. [254].

4.9 Integrability

In this section we discuss a concept that has recently started playing an important role in the debate on equilibration and thermalisation in closed quantum systems — the concept of integrability. It is often suggested or claimed that non-integrable systems thermalise, while integrable ones do not. This wisdom has become folklore knowledge that is often invoked in discussions and talks on the topic (compare also Refs. [33, 34, 55, 339, 340, 178, 181, 84, 329, 113, 313, 338, 45, 44]). In the following, we will briefly review the current state of affairs concerning the usage of the term (quantum) integrability in the context of equilibration and thermalisation in closed quantum systems, comment on the concept of integrability and investigate to which extend the circumstantial evidence concerning the connection between (non-)integrability and thermalisation can be substantiated.

To that end we will first recapitulate the definition of integrability in classical mechanics and then discuss obstacles for a generalisation of the concept of integrability to the quantum setting. This assessment is largely based on the previous works Refs. [379, 314, 254]. We finish with some speculations on the connection of quantum (non-)integrability and computational complexity.

4.9.1 In classical mechanics

In classical mechanics [380] (Liouville) integrability is a very well-defined concept. Consider a classical system with $n \in \mathbf{Z}^+$ degrees of freedom, each associated with a coordinate q_k and a corresponding momentum p_k. Then, in the Hamiltonian formalism, the $2\,n$ canonical coordinates $(q_k)_{k=1}^n$ and $(p_k)_{k=1}^n$ span the phase space $\mathscr{S}$ of the system [282]. We assume that the Hamiltonian function $\mathscr{H}\colon \mathscr{S} \to \mathbf{R}$, i.e., the energy functional, of the system is time independent. It then governs the time evolution of the system via Hamilton's equations [380]:

$$\forall k \in [n]\colon \qquad \dot{p}_k = -\frac{\partial \mathscr{H}}{\partial q_k} \qquad \dot{q}_k = \frac{\partial \mathscr{H}}{\partial p_k} \tag{4.154}$$

The dot indicates the derivative with respect to time of the corresponding quantity, i.e., $\dot{q}_k$ is the temporal change of q_k. Integrating these differential equations yields the phase flow $g^t_{\mathscr{H}}\colon \mathscr{S} \to \mathscr{S}$, which maps the initial phase space vector of a system at time 0 to that at time $t \in R$. Define for any two functions $F, G\colon \mathscr{S} \to \mathbf{R}$ their Poisson bracket $(F, G)\colon \mathscr{S} \to \mathbf{R}$ as

$$(F, G) \coloneqq \lim_{t \to 0} \frac{d}{dt}\, F \circ g^t_G, \tag{4.155}$$

where $\circ$ denotes function composition. It turns out that $(\,\cdot\,,\,\cdot\,)$ is bilinear and skew-symmetric [380]. A function $F\colon \mathscr{S} \to \mathbf{R}$ is called a first integral of motion under the evolution induced by $\mathscr{H}$ if $(F, \mathscr{H}) = 0$. More generally, if for $F, G\colon \mathscr{S} \to \mathbf{R}$ it holds that $(F, G) = 0$, then F and G are said to be in involution. We can now define Liouville integrability:

Definition 5 (Liouville integrability [380])**.** *A classical system with n degrees of freedom is called (Liouville) integrable if it entails a sequence $(F_k)_{k=1}^n$ of n independent first integrals of motion that are pairwise in involution.*

Liouville's theorem for integrable systems shows that Liouville integrable systems can be solved, i.e., the time evolution can be explicitly calculated, in a systematic way by quadratures, i.e., by direct integration of differential equations:

Theorem 14 (Corollary of Liouville's theorem for integrable systems [380])**.** *If a system is Liouville integrable, its time evolution can be solved by quadratures.*

In more detail: Liouville's theorem for integrable systems essentially ensures that, given the initial values of all canonical coordinates, the time evolution of an integrable system is confined to a smooth submanifold of the phase space that is diffeomorphic to an n-dimensional torus. The time evolution is quasi-periodic and can be described in terms of the so-called action angle coordinates $(\varphi_k)_{k=1}^n$ that parametrise the torus.

The action angle coordinates can be explicitly constructed from the sequence $(F_k)_{k=1}^n$ of n independent first integrals of motion and the values fixed for them. Fixing different values for the n first integrals of motion results in different tori. In the coordinate system of the action angle variables the equations of motion are given by $2\,n$ simple ordinary differential equations of the form $\dot{F}_k = 0$ and $\dot{\varphi}_k = w_k$, with $w_k \in \mathbf{R}$ being constants that depend on the values that were fixed for the n first integrals of motion.

If a Liouville integrable system is perturbed, then the time evolution is generally not confined to a torus anymore and cannot be derived in a systematic way. For small perturbations the Kolmogorov-Arnold-Moser (KAM) theorem ensures, under a so-called non-resonance condition, that most tori are only deformed and the time evolution on them is then still quasi-periodic [381, 185, 382].

In summary we have: Integrability in classical systems implies systematic solvability and thereby yields a qualitative classification of classical systems. Liouville integrable systems

are not ergodic (see Section 4.12.1) in the sense that their phase space trajectory does not explore the whole phase space, but is confined to a portion of it. Whether or not this implies that integrable systems cannot thermalise depends on the definition of thermalisation, but the motion of the system is quasi-periodic and hence no convergence of the state of the system in the limit $t \to \infty$ is possible. Non-integrability in classical systems is not sufficient for ergodicity or chaos and hence also not sufficient for notions of mixing or thermalisation based on these concepts. Still, the concept of Liouville integrability yields a classification of systems with strong implications for their physical behaviour.

4.9.2 In quantum mechanics

Ideally, a notion of quantum integrability should yield a classification that divides quantum systems into two classes, integrable ones and non-integrable ones, with markedly different physical properties. In addition it should, in some sense, be a generalisation of Liouville integrability. However, if one tries to generalize the concept of Liouville integrability to quantum systems in a straight forward manner, one immediately encounters problems (see also Ref. [341]):

Consider a quantum system with d dimensional Hilbert space $\mathcal{H}$ and Hamiltonian $H \in \mathcal{O}(\mathcal{H})$. An orthonormal eigenbasis $(|\tilde{E}_k\rangle)_{k=1}^d$ of H, with corresponding eigenvalues $(\tilde{E}_k)_{k=1}^d$, can always be constructed in a systematic way by diagonalising the Hamiltonian. The time evolution of an arbitrary initial state vector $|\psi\rangle \in \mathcal{H}$ is then given by

$$t \mapsto |\psi(t)\rangle := \sum_{k=1}^{d} |\langle \tilde{E}_k \rangle \psi| \, \mathrm{e}^{\mathrm{i}\,\tilde{\varphi}_k(t)} \, |\tilde{E}_k\rangle, \tag{4.156}$$

with $\tilde{\varphi}_k(t) := \arg(\langle \tilde{E}_k \rangle \psi) - \tilde{E}_k\, t$, where arg is the argument function, i.e., for every $c \in \mathbf{C}, c = |c|\, \mathrm{e}^{\mathrm{i}\,\arg(c)}$. The overlaps $\langle \tilde{E}_k \rangle \psi$ can also be calculated systematically, so the time evolution of a (finite dimensional) quantum system can always be obtained in a systematic way for any Hamiltonian and any initial state.

The analogy to the situation of Liouville integrable systems is striking: The dimension d plays the role of the number n of degrees of freedom of the system in the classical case. The linear functionals $|\langle \tilde{E}_k| \cdot |\colon \mathcal{H} \to \mathbf{R}$, induced by the eigenvectors of H, are analogous to the first integrals of motion in Liouville's theorem on integrable systems, and the time independent moduli of the overlaps $|\langle \tilde{E}_k \rangle \psi| = |\langle \tilde{E}_k \rangle \psi(t)|$ play the role of the values fixed for these constants of motion. Finally, the functions $\tilde{\varphi}_k$ in the right hand side of Eq. (4.156) satisfy differential equations analogous to those of the action angle variables, namely $\dot{\tilde{\varphi}}_k = \tilde{E}_k$, and the time evolution indeed happens on a d-torus. As in the classical case, the specific torus to which the evolution is confined depends on the values fixed for the conserved quantities. It seems that the dynamics of quantum systems is far less rich than that of classical systems. This constitutes a major obstacle for a good definition of quantum (non-)integrability.

Before going on, it is reasonable to give a set of conditions that a good notion of (non-)integrability for quantum systems should satisfy. It seems reasonable to demand [314] that a definition of quantum integrability should:

1. have implications for the physical behaviour,
2. be applicable to a large class of quantum systems,
3. be unambiguous,
4. be decidable for concrete models.

Unfortunately almost none of the existing frequently used notions of quantum integrability seems to fulfil all these criteria. The following is a list of some of the definitions of quantum integrability that have been introduced, together with exemplary references in which the corresponding definition appears or is used (see also Refs. [314, 254, 383, 379]). A system is quantum integrable:

1. If it exhibits n physically meaningful mutually commuting conserved quantities that are in some sense independent [42, 342, 279, 144, 384, 49] (see also Ref. [379] and the references therein) or depend linearly on some parameter of the Hamiltonian [341].
2. If it is integrable by the Bethe ansatz [383, 47, 45].
3. If it exhibits nondiffractive scattering [383].
4. If it has a classical limit that is integrable [385].
5. If its level statistics follows a Poisson law and is non-integrable if it is of Wigner-Dyson type [386, 178, 343, 387, 388, 185, 186, 48, 49].
6. If it does not exhibit level repulsion [389, 390].
7. If (many of) its eigenfunctions can be labeled in a certain way with quantum numbers [342, 390].
8. If it is exactly solvable in any way [45, 391, 342, 49].

In the first definition both physically meaningful and n can have very different meanings. It can, for example, in the case of composite systems, refer to local operators. The number n is usually taken to be equal to the number of degrees of freedom of the model or the number of constituents in the case of composite systems. In Ref. [341] n can be any number between zero and $d-1$, and models are then classified according to this number n. Similarly, independent can have several meanings, linearly independent and algebraically independent being popular choices. Usually all quadratic systems and systems such as the Hydrogen atom fall in this category. Models that are integrable according to this definition are often also integrable according to one of the other definitions given above (especially Definitions (2), (7), and (8)). Many of the definitions of integrability of this type suffer from the severe problem that if the definition is taken seriously, all quantum systems classify as integrable and hence it violates Condition (1) (see the discussion above and Refs. [379, 341] for a critic of such notions of integrability).

Definitions (2), (3), and (4) are only applicable to restricted classes of models and hence violate Condition (2) in the above list. The same holds, although arguably in a weaker sense, for Definition (6) and the version of Definition (1) of from Ref. [341], which are only applicable to systems which have a natural tuning parameter.

Definitions (5) and (6) suffer from the problem that also certain models that are usually regarded as integrable can have spectra that would classify them as non-integrable [315, 390]. In fact, it is trivial to construct such examples. In a composite systems of, say, spin-1/2 systems, one can simply take a Hamiltonian that is diagonal in the usual Pauli-Z product basis and which hence should clearly be classified as integrable and set its spectrum to be that of some non-integrable model. Moreover, natural tunable models are known that exhibit thermodynamic behaviour in both the regime that would be classified as integrable and the one that would be classified as non-integrable according to this definition [49]. Hence, these definitions violate Condition (3) and (1).

Especially Definitions (1) and (8) suffer from the problem that it might simply be a lack of imagination that prevents one from finding a relevant conserved quantity or from solving

a given model and thus violate Condition (4). This is well illustrated by the recent (partial) solution of the Rabi model, which was long thought to be non-integrable (see Ref. [342] and the references therein).

In conclusion, it seems fair to say that the question of how to define integrability in quantum mechanics is still to some extent open and even more so for quantum non-integrability. At the same time a number of very useful and promising indicators of and proposals for a definition of integrability exist (see also Refs. [341, 314] for more background information and recent proposals). Still, general claims that "non-integrable quantum systems thermalise" seem unjustified at present.

4.10 Decay of correlations and stability of thermal states

In this section we will somewhat depart from the pure state quantum statistical mechanics approach, as we will take the canonical ensemble for thermal states for granted and turn to a study of structural properties of such thermal states. This will bring us to the seemingly innocent question: What is the meaning of temperature on very small scales and in which sense is temperature really intensive, as is paradigmatically claimed in thermodynamics? The problem with assigning locally a temperature to a small subsystem of a global system in a thermal state is the following: Interactions between the subsystem and its environment generate correlations that can lead to noticeable deviations of the state of the subsystem from a thermal state. Given only a subsystem state, there is no canonical way to assign a temperature to the subsystem. We shall call this the locality of temperature problem.

This problem has been addressed in Refs. [392, 393, 394, 395], and more recently extensively studied in Ref. [396]. There, three theorems are proven: A truncation formula, which allows to express the influence of sets of locally interacting Hamiltonian terms on the expectation value of an observable in the thermal state of a locally interacting quantum system in terms of a correlation measure. A clustering of correlations result, which shows that above a universal critical temperature this correlation measure exhibits an exponential decay. And finally, a result that ensures local stability of thermal states above a universal critical temperature and thereby partially solves the locality of temperature problem.

4.10.1 Locality of temperature

These results build upon and significantly go beyond previous results on clustering of correlations in classical systems [397, 398], for quantum gases [399], i.e., translational invariant Hamiltonians in the continuum, and cubic lattices [400, 401, 402]. For the latter systems the existence and uniqueness of thermal states in the thermodynamic limit at high temperatures is proven and analyticity of correlations can be derived. Moreover, in the regime of high temperatures, n-point correlation functions have been shown to cluster for spin gases [398, 399] and translational invariant bosonic lattices [402].

To begin the more detailed discussion, we introduce a quantity that measures correlations. We define for any $\tau \in [0,1]$, any two operators $A, B \in \mathcal{B}(\mathcal{H})$, and any quantum state $\rho \in \mathcal{S}(\mathcal{H})$ the generalised covariance

$$cov_\rho^\tau(A,B) := Tr(\rho^\tau A \rho^{1-\tau} B) - Tr(\rho A)Tr(\rho B)\,. \tag{4.157}$$

The choice $\tau = 1$ gives the usual covariance[6]. As a side remark, the quantity $cov_\rho^\tau(A,B)$ also appears in studies of one dimensional models [403], where it can be written as a different times correlation function in terms of the transfer matrix of the system.

[6] For the fine print see [396].

The reason for introducing the general definition here is that it naturally appears in the truncation formula. Before we can state it we need one last piece of notation. For any subsystem $X \subset \mathcal{V}$ let $X_\partial \subset \mathcal{E}$ the set of edges that overlap with both X and its complement, i.e.,

$$X_\partial \coloneqq \{Y \in \mathcal{E} \colon Y \cap X \neq \emptyset \wedge Y \cap X^c \neq \emptyset\}. \tag{4.158}$$

We extend this notation to operators $A \in \mathcal{B}(\mathcal{H})$ and define

$$A_\partial \coloneqq \{Y \in \mathcal{E} \colon Y \cap supp(A) \neq \emptyset \wedge Y \cap supp^c(A)\}. \tag{4.159}$$

Theorem 15 (Truncation formula [396, Corollary 1 and 4])**.** *Consider a spin or fermionic system with Hilbert space $\mathcal{H}$ and let $H \in \mathcal{O}(\mathcal{H})$ be a locally interacting Hamiltonian with edge set $\mathcal{E}$. Let $B \subset \mathcal{E}$ and define for $s \in [0,1]$ the interpolating Hamiltonian $H(s) \coloneqq H - (1-s)\sum_{X \in B_\partial} H_X$. Then, for any operator $A \in \mathcal{B}(\mathcal{H})$ with $supp(A) \subset B$ it holds that*

$$Tr\big(A\, g[H_B](\beta)\big) - Tr\big(A\, g[H](\beta)\big) = \beta \int_0^1 \int_0^1 cov^\tau_{g[H(s)](\beta)}(A, \sum_{X \in B_\partial} H_X)\, \mathrm{d}\tau\, \mathrm{d}s\,. \tag{4.160}$$

The left hand side of Eq. (4.160) is the difference between the expectation value of A in the thermal states of the Hamiltonian H_B with only the terms contained in the region B and the full Hamiltonian H. The truncation formula quantifies how the expectation value of A changes when the terms that couple B to the rest of the system are added or removed, hence the name, and tells us that this change can be expressed exactly in terms of the generalised covariance.

It is important to note that Eq. (4.160) is an equality. The generalised covariance exactly captures the response of expectation values in the thermal state to truncations of the Hamiltonian. The truncation formula tells us that the response of the expectation value is small if and only if the right hand side of Eq. (4.160), which is an average over the generalised covariance times β, is small. In other words:

Observation 7 (Locality of temperature [396])**.** *Temperature can be defined locally on a given length scale if and only if the averaged generalised covariance is small compared to $1/\beta$ on that length scale.*

We will see shortly that if locally interacting spin or fermionic lattice systems are at a sufficiently high temperature, then the generalised covariance $cov^\tau_{g(\beta)}(A,B)$ between any to operators $A, B \in \mathcal{B}(\mathcal{H})$ decays exponentially with the graph distance $d(A,B)$ between their supports.

4.10.2 Clustering of correlations in high temperature thermal states

The following theorem applies to all Hamiltonians whose interaction (hyper)graph has a finite growth constant. To explain what this means we need some additional notation. A subset $F \subset \mathcal{E}$ of the edge set connects X and Y if F contains all elements of some sequence of pairwise overlapping edges such that the first overlaps with X and the last overlaps with Y and similarly for sites $x, y \in V$. A subset $F \subset \mathcal{E}$ of the edge set $\mathcal{E}$ that connects all pairs of its elements is called connected and connected subsets F are also called animals [404, 405]. The size $|F|$ of an animal F is the number of edges it contains. It turns out that for many interesting (hyper)graphs the number of animals of a given size that contain a given edge grows exponentially with the size, but not faster. That is, they have a finite growth constant. More precisely, the growth constant of a (hyper)graph $\mathcal{G} = (\mathcal{V}, \mathcal{E})$ is the smallest constant α satisfying

$$\forall k \in \mathbf{Z}^+ \colon \quad \sup_{X \in \mathcal{E}} |\{F \subset \mathcal{E} \text{ connected} \colon X \in F \wedge |F| = k\}| \leq \alpha^k. \tag{4.161}$$

For example, the growth constant α of the interaction graph of nearest neighbour Hamiltonians on D dimensional cubic lattices can be bounded by $2\,D\,\mathrm{e}$ (see Lemma 2 in Ref. [404]). Moreover, there is a finite growth constant α for any regular lattice [405], and there exist upper bounds on the growth constants of so-called spread-out graphs [404] that make it possible to bound the growth constant of the interaction hypergraphs of all l-local k-body Hamiltonians on regular lattices [396]. Where l-local k-body on a regular lattice means that $\mathcal{V}$ can be mapped onto the sites of a regular lattice such that $\mathcal{E}$ contains only subsystems which consist of at most k sites that are all contained in a ball (measured in the graph distance of the regular lattice) of diameter l. Apart from all l-local k-body Hamiltonians on regular lattices this also makes the following results indirectly applicable to systems with exponentially decaying interactions (such Hamiltonians can be exponentially well approximated by l-local k-body Hamiltonians) but not to Hamiltonians with algebraically decaying interactions, such as for example Coulomb or dipole interactions. We can now state the clustering of correlations result:

Theorem 16 (Clustering of correlations at high temperature [396, Theorem 2 and 4])**.** *Consider a locally interacting system of spins or fermions with Hilbert space $\mathcal{H}$ and Hamiltonian $H \in \mathcal{O}(\mathcal{H})$ with local interaction strength $J \coloneqq \max_{X\in\mathcal{E}} \|H_X\|_\infty$ and interaction (hyper)graph $\mathcal{G} = (\mathcal{V}, \mathcal{E})$ with growth constant α. Define the critical temperature*

$$\beta^* \coloneqq \ln\left((1+\sqrt{1+4/\alpha})/2\right)/(2\,J) \tag{4.162}$$

and the thermal correlation length

$$\xi(\beta) \coloneqq \left|1/\ln\left(\alpha\,\mathrm{e}^{2\,|\beta|\,J}(\mathrm{e}^{2\,|\beta|\,J}-1)\right)\right| . \tag{4.163}$$

Then, for every $|\beta| < \beta^*$, parameter $\tau \in [0,1]$, and every two operators $A, B \in \mathcal{B}(\mathcal{H})$ with $d(A,B) \geq \xi(\beta)\,\left|\ln\left(\ln(3)\,(1-\mathrm{e}^{-1/\xi(\beta)})/\min(|A_\partial|,|B_\partial|)\right)\right|$,

$$|cov^\tau_{g(\beta)}(A,B)| \leq \frac{4\,\min(|A_\partial|,|B_\partial|)\|A\|_\infty\,\|B\|_\infty}{\ln(3)\,(1-\mathrm{e}^{-1/\xi(\beta)})}\,\mathrm{e}^{-d(A,B)/\xi(\beta)}. \tag{4.164}$$

The above theorem implies that in thermal states above the critical temperature the correlations between any two $A, B \in \mathcal{B}(\mathcal{H})$ decay exponentially with their distance $d(A,B)$. Importantly, the critical temperature (4.162) is independent of global properties of H but only depends on the local interaction strength J and the growth constant α of its interaction (hyper)graph.

In the context of this work, the most important implication of Theorem 16 is the following result, which proves stability of thermal states above the critical temperature against local perturbations. More precisely, it shows that changing the Hamiltonian of a locally interacting quantum system only outside of a subsystem B has only limited influence on how thermal states to temperatures above the critical temperature look like in the interior $S \subset B$ of B if the distance between S and B_∂ is large enough:

Theorem 17 (Universal locality at high temperatures [396, Corollary 2 and 5])**.** *Let H be a Hamiltonian satisfying the conditions of Theorem 16, let β^* and $\xi(\beta)$ be defined as in Eq. (4.162) and Eq. (4.163), let $|\beta| < \beta^*$, and let $S \subset B \subseteq \mathcal{V}$ be subsystems with $d(S, B_\partial) \geq \xi(\beta)\,\left|\ln\left(\ln(3)\,(1-\mathrm{e}^{-1/\xi(\beta)})/|S_\partial|\right)\right|$. Then*

$$\mathcal{D}\left(g^S[H](\beta), g^S[H_B](\beta)\right) \leq \frac{v\,|\beta|\,J}{1-\mathrm{e}^{-1/\xi(\beta)}}\,\mathrm{e}^{-d(S,B_\partial)/\xi(\beta)}, \tag{4.165}$$

where $v \coloneqq 4\,|S_\partial|\,|B_\partial|/\ln(3)$.

If the conditions of the above theorem are met and the interior subsystem S is sufficiently far from the boundary B_∂ of B such that $d(S, B_\partial)$ is large and hence the right hand side of Eq. (4.165) small, then the reduced state $g^S[H](\beta)$ on S of the thermal state of H is almost independent of the terms of the Hamiltonian H that are not in the restricted Hamiltonian H_B.

Theorem 17 is not unexpected, but it is nevertheless remarkable that it can be shown in this generality for systems of both locally interacting spins and fermions. Even more so, because, as we have seen in the discussion of equilibration (Section 4.3) and especially in the section on equilibration time scales, a major obstacle for improving the statements we were able to make is that it seems to be hard to use the structure of natural many-body Hamiltonians, namely that interactions are usually few body and often short range. Theorem 17 is an instance of a result whose proof heavily relies on the locality structure of locally interacting Hamiltonians and is able to exploit their structure.

It is interesting to plug in the numbers of a specific model to see how physical the derived critical temperature is. As a concrete example consider the ferromagnetic two dimensional isotropic Ising Model without external field. The critical temperature of Theorem 16 and 17 is $1/(\beta^* J) = 2/\ln((1+\sqrt{1+1/\mathrm{e}})/2) \approx 24.58$, whereas the Curie temperature, i.e., the temperature at which the phase transition between the paramagnetic and the ferromagnetic phase happens is known to be $1/(\beta_c J) = 2/\ln(1+\sqrt{2}) \approx 2.27$ [406]. To put this into perspective however, it is worth noting that the above theorem still improves upon previously known bounds like for example that implied by Ref. [401], which yields $1/(\beta_c^* J) = 124$ and that it is a universal upper bound independent of details of the particular model. Given how difficult it is to calculate or even bound critical temperatures in lattice models (both classical and quantum) and that good bounds are known only for very few models the existence of such a non-trivial and universal upper bound is quite remarkable.

Besides being of fundamental interest, Theorem 17 has some obvious computational implications: It implies that for all $|\beta| < \beta^*$ reduced states of thermal states can be approximated with a computational cost independent of the system size and sub-exponential in the reciprocal approximation error (polynomially for systems in one dimension) [396]. The proof of Theorem 16 is based on a cluster expansion (see Lemma 6 in Ref. [396]) previously used in Ref. [407] to show that thermal states above a critical temperature can be approximated by so-called matrix product operators (MPOs). The subtleties of this approximation are often misunderstood. For details see the appendix of Ref. [396].

4.11 Conclusions

In this review, we have elaborated on a question that is at the heart of the foundations of quantum statistical mechanics: This is the question of how pure states evolving unitarily according to the Schrödinger equation can give rise to a wealth of phenomena that can rightfully be called thermodynamic. Individual observables and entire subsystems have a tendency to evolve towards equilibrium values/states and then stay close to them for most times during the evolution or extended time intervals. It turns out that the equilibrium properties can be captured by suitable maximum entropy principles implied by quantum mechanical dynamics alone. If a part of the system can be naturally identified as a bath and its complement as a distinguished subsystem, a weak interaction naturally leads to decoherence in the energy eigenbasis, and under additional conditions even equilibration to a thermal state can be guaranteed. We have also discussed properties of thermal states in lattice systems and in particular elaborated on precise conditions under which correlations decay exponentially. We have also reviewed systems where an absence of thermalisation is anticipated and the role played by many-body localisation played in this context.

Notions of information propagation as well as entanglement and correlation dynamics play

key roles in processes of equilibration and thermalisation. Complementing these dynamical approaches, the immensely large dimension of the Hilbert space of composite quantum systems can also justify the applicability of statistical ensembles via typicality arguments.

It goes without saying that we have only touched the tip of the iceberg: Many key questions had to be left unmentioned, despite the considerable length of the article. This is particularly regrettable with respect to the exciting experimental developments that have taken place over the recent years and now allow us to probe the questions at hand under remarkably precise conditions. The high degree of control offered by such experiments makes it possible to use them as quantum simulators assessing features quantitatively that are outside the scope of present analytical or numerical approaches.

At the same time, one reason for why many questions can not be satisfactory discussed here is that many key problems actually remain wide open, despite the enormous progress surveyed here. The question of what time scales are to be expected in equilibration is just as open as is a full understanding of thermalisation. And here the present review reveals its most important purpose: To serve as an invitation to this exciting field of research.

4.12 Remarks on the foundations of statistical mechanics

In this appendix we briefly sketch the most influential canonical approaches towards the foundations of thermodynamics and statistical mechanics. We will roughly follow the historical development, but emphasise more the problems and shortcomings of the respective approaches rather then their undeniable success and ingenuity.

Contrary to the rest of this work, this appendix is rather superficial. The main justification for the brevity is the existence of several comprehensive works on the topic, in particular the review by Uffink [2] and the book by Sklar [408], but also Refs. [104, 409, 410] and Chapter 4 in Ref. [69]. Adding yet another work to this list simply seems superfluous and a detailed review of the history of statistical mechanics is beyond the scope of this work. Also, we will brush over many of the more subtle issues of the classical approaches, such as the interpretation of probability and the problem of comparing discrete and continuous measures.

The intention of this appendix is to partially answer the legitimate question of a person already familiar with thermodynamics and statistical physics: "Why should I care about pure state quantum statistical mechanics? Weren't all the foundational questions already solved in the works from the 19th and early 20th century?" As we will see, despite the numerous attempts and the great amount of work that has been put into establishing a convincing justification for the methods of statistical mechanics it has "not yet developed a set of generally accepted formal axioms" [2], or, as E. T. Jaynes [303] puts it: "There is no line of argument proceding from the laws of microscopic mechanics to macroscopic phenomena that is generally regarded by physicists as convincing in all respects."

4.12.1 Canonical approaches

Thermodynamics was originally developed as a purely phenomenological theory. Prototypical for this era are the laws of Boyle–Mariotte and Gay–Lussac that state empirically observed relations between the volume, pressure, and temperature of gases.

The more widespread acceptance of the atomistic hypothesis in the 18th century opened up the way for a microscopic understanding of such empirical facts. The works of Clausius [411], Maxwell [412, 413], Boltzmann [414], and Gibbs [1] in the second half of the 19th and the beginning of the 20th century are often perceived as the inception of statistical mechanics (see also Refs. [415, 2, 408]). In this section we review some of these early attempts to develop a deeper understanding of thermodynamics based on microscopic considerations.

(a) Time reversal objection (Loschmidt)

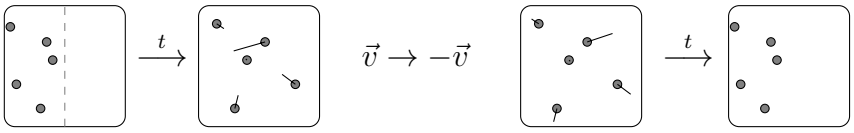

(b) Recurrence objection (Poincaré, Zermelo)

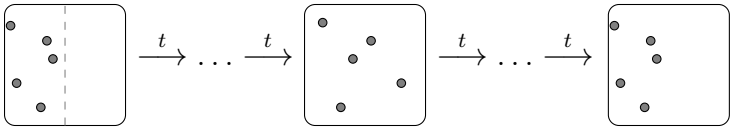

Figure 4.6: (Reproduction from Ref. [120]) The time reversal objection, also known as Loschmidt's paradox [416], but actually first published by William Thomson [417], states that it should not be possible to deduce time reversal asymmetric statements like the H-theorem, implied by the Boltzmann equation, from an underlying time reversal invariant theory. More explicitly, it argues that for any process that brings a system into an equilibrium state starting from a non-equilibrium situation, there exists an equally physically allowed reverse process that takes the system out of equilibrium. The initial state for that process is obtained from the equilibrium state by reversing all velocities (see Panel (a)). The recurrence objection, which is based on the Poincaré recurrence theorem but was made explicit by Zermelo [418], states that Boltzmann's H-theorem is in conflict with Hamiltonian dynamics, because it can be proven on very general grounds that all finite systems are recurrent, i.e., return arbitrarily close to their initial state after possibly very long times (see Panel (b)).

Boltzmann and the H-Theorem

One of Boltzmann's arguably most important contributions to the development of statistical mechanics is his derivation of what is known today as the Boltzmann equation and his H-theorem [414] (see also the first chapter of Boltzmann's book "Vorlesungen über Gastheorie. Bd. 1." [415] as well as Ref. [69, Chapter 4] and Ref. [408]).

In his 1872 article [414] Boltzmann aims at showing that the Maxwell-Boltzmann distribution is the equilibrium distribution of the speed of gas particles and that a gas with an initially different distribution must inevitably approach it. He tries to do this on the grounds of microscopic considerations and starts off from the prototypical model of the hard sphere gas. He takes for granted that in equilibrium the distribution of the particles should be "uniform" and that their speed distribution should be independent of the direction of movement. He assumes that the number of particles is large and introduces a continuously differentiable function he calls "distribution of state"[7], which is meant to approximate the (discrete) distribution of the speed of the particles. He then derives a differential equation for the temporal evolution of this function, known today as the Boltzmann equation. He also defines an entropy for the "distribution of state" and shows that it increases monotonically in time under the dynamics given by the Boltzmann equation, a statement he calls H-Theorem, after the letter H used for denoting the entropy.

During the derivation he makes several approximations. Essential is his "Stoßzahl Ansatz", later dubbed the "hypothesis of molecular disorder" in Ref. [415], which explicitly breaks the

[7] German original [414]: "Zustandsverteilung".

time reversal invariance of classical mechanics. This breaking of the time reversal symmetry is responsible for the temporal increase of entropy. Naturally this assumption has been much criticised. Famous are the time reversal objection of William Thomson and Loschmidt and the recurrence objection due to Poincaré and Zermelo [408] (see Figure 4.6). The bottom line of this debate, also later acknowledged by Boltzmann [419], is that any statement that implies the convergence of a finite system to a fixed equilibrium state/distribution in the limit of time going to infinity is incompatible with a time reversal invariant or recurrent microscopic theory. This is important for the notions of equilibration we discuss in Section 4.3.

Gibbs' ensemble approach

For many, Gibbs' book "Elementary principles in statistical mechanics" [1] from 1902 marks the birth of modern statistical mechanics [2]. Central in Gibbs' approach is the concept of an ensemble, which he describes as follows: "We may imagine a great number of systems of the same nature, but differing in the configurations and velocities which they have at a given instant [...] we may set the problem, not to follow a particular system through its succession of configurations, but to determine how the whole number of systems will be distributed among the various conceivable configurations and velocities at any required time [...]"

In fact, the book then is not so much concerned with (non-equilibrium) dynamics, but rather with the calculation of statistical equilibrium averages. Gibbs considers systems whose phase space is, as in Hamiltonian mechanics, spanned by canonical coordinates and introduces the micro-canonical, canonical, and grand canonical ensemble for such systems. He assumes that the number of states is high enough such that a description with a, as he calls it, "structure function", a kind of density of states, is possible. He shows how various thermodynamic relations for quantities such as temperature and entropy can be reproduced from his ensembles, if these quantities are properly defined in terms of the structure function.

Gibbs is mostly concerned with defining recipes for the description of systems in equilibrium. He gives little insight into why the ensembles he proposes capture the physics of thermodynamic equilibrium or how and why systems equilibrate in the first place [2]. Instead of addressing such foundational questions he is "contented with the more modest aim of deducing some of the more obvious propositions relating to the statistical branch of mechanics" [1].

(Quasi-)ergodicity

The ergodicity hypothesis was essentially born out of the incoherent use of different interpretations of probability by Boltzmann in his early work [420] and was formulated by him in Ref. [421] as follows: "The great irregularity of the thermal motion and the multitude of forces that act on a body make it probable that its atoms, due to the motion we call heat, traverse all positions and velocities which are compatible with the principle of [conservation of] energy."[8] The concept of ergodicity was made prominent by P. and T. Ehrenfest in Ref. [409], who proposed the ergodic foundations of statistical mechanics [2].

Roughly speaking, a system is called (quasi-)ergodic if it explores its phase space uniformly in the course of time for most initial states. Making precise what "uniformly", "most", and "in the course of time" mean in this context already constitutes a major challenge [2]. However, if one is willing to believe that a system at hand is ergodic in an appropriate sense then it readily follows that (infinite time) temporal averages of physical quantities in that system are (approximately and/or with "high probability") equal to certain phase space averages, such as for example that given by the micro-canonical ensemble.

The ergodic foundations of statistical mechanics are then roughly based on arguments along the following lines: Any physical measurement must be carried out during a finite time interval.

[8] The English translation is taken from Ref. [2].

What one actually observes is not an instantaneous value, but an average over this time span. The relevant time spans might seem short on a human time scale, but can at the same time be "close to infinite" compared to the microscopic time scales. Think for example of the process of measuring the pressure in a gas container with a membrane. The moment of inertia of the membrane is much too large to observe the spikes in the force due to hits by individual particles. It is thus reasonable to assume that observations are well described by (infinite time) averages of the corresponding quantities, which, if the system is quasi-ergodic, can be calculated by averaging in an appropriate way over phase space.

The arguably most striking objection against such reasoning is the following [408]: If it were in fact true that all realistic measurements could legitimately be described as infinite time averages, then the observation of any non-equilibrium dynamics, including the approach to equilibrium, would simply be impossible. The latter is manifestly not the case.

Besides this issue of the "infinite time" averages and the other problems mentioned above it is extraordinarily difficult to show that a given system is (quasi-)ergodic. Despite the ground breaking works of Birkhoff and von Neumann on the concept of metric transitivity, Sinai's work on dynamical billiards, and more recent approaches such as Khinchin's ergodic theorem, the full problem still awaits solution [2].

Jaynes' maximum entropy approach

Conceptually very different from the three previously discussed approaches is the work of Jaynes [303]. He fully embraces a subjective interpretation of probability and proposes to regard statistical physics as a "form of statistical inference rather than a physical theory". He then introduces a maximum entropy principle. In short, the maximum entropy principle states that in situations where the existing knowledge is insufficient to make definite predictions the best possible predictions can be reached by finding the distribution of the state space of the system that maximises the (Shannon) entropy and is compatible with the available knowledge. The principle is inspired by the work of Shannon [422] who, as Jaynes claims, had shown that the maximum entropy distribution is the one with the least bias towards the missing information [303]: "[The] maximum entropy distribution may be asserted for the positive reason that it is uniquely determined as the one which is maximally noncommittal with respect to missing information."

Moreover, in Ref. [303], Jaynes shows in quite some generality that the "usual computational rules [as presented in Gibbs' book [1]] are an immediate consequence of the maximum entropy principle". In addition, he points out various other advantages of his subjective approach. For example that it makes predictions "only if the available information is sufficient to justify fairly strong opinions", and that it can account for new information in a natural way.

While Jaynes' principle can be used to justify the methods of statistical mechanics it gives little insight into why and under which conditions these methods yield results that agree with experiments. In other words: The maximum entropy principle ensures that making predictions based on statistical mechanics is "best practice", but does not explain why this "best practice" is often good enough. The question "Why does statistical mechanics work?" hence remains partially unanswered.

A last point of criticism is that Ref. [303] works in a classical setting. While an extension to quantum mechanics is possible [304] the subjective interpretation of probability advertised by Jaynes is arguably less convincing or at least debatable in this setting, although this is of course to some extend a matter of taste [423, 424]. Problems arise because mixed quantum states can be written as convex combinations of pure states in more than one way so that more complicated arguments are needed to identify the von Neumann entropy as the right entropy measure to be maximised.

4.12.2 Closing remarks

Except for Jaynes subjective maximum entropy principle, all approaches we have discussed in this chapter differ in one important point from that advertised in the main part of this review: They are based on classical mechanics. The applicability of classical models to systems that behave thermodynamically is, however, questionable.

Consider for example two of the most prominently used models in statistical mechanics: The hard sphere model for gases and the Ising model for ferromagnetism. The atoms and molecules of a gas, as well as the interactions between them, in principle require a quantum mechanical description. Yet, it is often claimed that in the so-called Ehrenfest limit, i.e., if the spread of the quantum mechanical wave packets of the individual particles is small compared to the "radius" of the particles, the classical hard sphere approximation is eligible. It can, however, be shown that under reasonable conditions systems typically leave the Ehrenfest limit on timescales much shorter than those of usual thermodynamic processes [69, Chapter 4]. Moreover, whether the Ehrenfest limit constitutes a sufficient condition for the applicability of (semi-)classical approximations in the first place is debatable [425]. Similarly, the relevant elementary magnetic moments of a piece of iron, namely the electronic spins, are intrinsically quantum. In fact, it is known that classical physics alone cannot explain the phenomenon of ferromagnetism in a satisfactory way — a statement known as Bohr–van Leeuwen theorem [426, 427, 428]. The extremely simplified description employed in the Ising model can thus, despite its pedagogical value, arguably not capture all the relevant physics.

In addition to this, there are many situations where thermodynamic behaviour cannot be understood in a purely classical framework [429]: For example, black-body radiation cannot be understood without postulating a quantisation of energy to avoid the ultraviolet catastrophe. Further prime example for this are gases of indistinguishable particles. An application of classical physics leads to Gibbs' paradox for the mixing entropy and the statistics of Bose and Fermi gases at low temperatures cannot be explained classically. Last but not least, the "freezing out" of certain internal degrees of freedom of molecular gases, which impacts their heat capacities, cannot be understood in a convincing way from classical physics alone.

5 Generalized Gibbs ensemble in integrable lattice models by Vidmar, Rigol

(does this article tell us something more important than the results for two models? I don't think so now)

Abstract

The generalized Gibbs ensemble (GGE) was introduced ten years ago to describe observables in isolated integrable quantum systems after equilibration.

(why 10 years ago???)

Since then, the GGE has been demonstrated to be a powerful tool to predict the outcome of the relaxation dynamics of few-body observables in a variety of integrable models, a process we call generalized thermalization.

(not equilibration??)

This review discusses several fundamental aspects of the GGE and generalized thermalization in integrable systems. In particular, we focus on questions such as: which observables equilibrate to the GGE predictions and

(local???)

who should play the role of the bath;

(just all photons and particles around our system???)

what conserved quantities can be used to construct the GGE;
(all???)
what are the differences between generalized thermalization in noninteracting systems and in interacting systems mappable to noninteracting ones;
(which???)
why is it that the GGE works when traditional ensembles of statistical mechanics fail.

Despite a lot of interest in these questions in recent years, no definite answers have been given.
We review results for the XX model and for the transverse field Ising model.
(why these models are interesting???)
For the latter model, we also report original results and show that the GGE describes spin-spin correlations over the entire system. This makes apparent that there is no need to trace out a part of the system in real space for equilibration to occur and for the GGE to apply.

In the past, a spectral decomposition of the weights of various statistical ensembles revealed that generalized eigenstate thermalization occurs in the XX model (hard-core bosons).
Namely, eigenstates of the Hamiltonian with similar distributions of conserved quantities have similar expectation values of few-spin observables.
Here we show that generalized eigenstate thermalization also occurs in the transverse field Ising model.
(sounds expected...)

5.1 Summary and discussion

In summary, we have reviewed evidence that the GGE is the appropriate statistical ensemble to describe few-body observables after quantum quenches in different families of integrable models. We focused on two models and in finite systems, for which it can be shown that the GGE describes stationary values of few-particle (spin) correlations in the entire system: the XX model and the transverse field Ising model. For the XX model, we discussed several instances in which efficient numerical calculations allow one to demonstrate that generalized thermalization occurs in quenches in the absence of translational symmetry. For the transverse field Ising model, we focused on the comparison between the expectation values in the diagonal ensemble and the GGE after quenching the transverse field in translationally invariant systems. For several observables, we proved analytically that the difference between the two ensembles vanishes in the thermodynamic limit.

Even though these models can be mapped onto noninteracting spinless fermions, we argued that there is a fundamental difference between noninteracting fermions and the aforementioned models with respect to generalized thermalization. For noninteracting fermions, the time-averaged values of all one-body observables after a quench is given by the GGE, but some extensive sets of those observables may not equilibrate. In the interacting models, the average values of all one-body observables is also given by the GGE, and we argued that there are no extensive sets of one-body observables that do not equilibrate (in the absence of real space localization due to disorder or quasi-periodic potentials [51]).

The conserved quantities we utilized to construct the GGE were the occupations of single-particle eigenstates in the noninteracting fermionic models to which spins (hard-core bosons) can be mapped. As mentioned before, the onset of generalized thermalization did not depend on whether initial state or the final Hamiltonian exhibited translational invariance. This observation applies to systems in the presence of quasi-periodic potentials, but provided the potential strength is below the critical value needed for localization [51]. In contrast, as shown

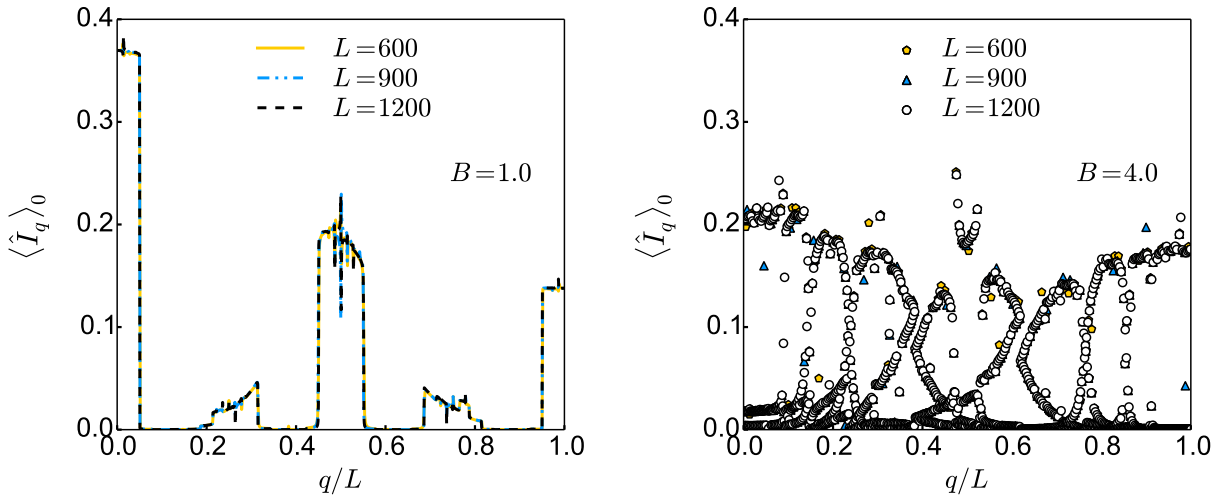

Figure 5.1: *Distribution of conserved quantities in the XX model after a quantum quench that introduces a quasi-periodic potential.* The conserved quantities $\langle \hat{I}_q \rangle_0$ in the XX model are the occupations of the single-particle eigenstates of the fermionic Hamiltonian, where $q = 1, 2, \ldots, L$. The curves display $\langle \hat{I}_q \rangle_0$ after a quench from the ground state of $H_{\rm XX}$ (5.3) in the presence of a (superlattice) potential $V_j = A\tilde{J}\cos(\frac{2\pi j}{T})$ with period $T = 4$ and amplitude $A = 8$. The quench consists of turning off the superlattice potential and turning on a quasi-periodic potential $V_j = B\tilde{J}\cos(2\pi\sigma j)$, with $B = 1$ (left panel) and $B = 4$ (right panel). Quasi-periodicity (sometimes referred to as quasi-disorder) is achieved by taking $\sigma = (\sqrt{5}-1)/2$. The transition between the delocalized and the localized phase occurs for $B_c = 2$. The average site occupancy is $N/L = 1/20$. The q-values are ordered with increasing eigenenergies of the single-particle eigenstates.

in Ref. [51], the GGE fails to predict the expectation values of observables after relaxation in the localized phase.

The failure of the GGE in the presence of localization can be attributed to the breakdown of statistical independence of macroscopic subsystems in the GGE, which results in the breakdown of the GGE description. This is due to the fact that conserved quantities in the localized phase are local but nonextensive, and cannot be thought of as extensive in a coarse grained way. In Fig. 5.1, we show conserved quantities in the XX model (ordered according to increasing eigenenergies), for the same initial state as in the left panel of Fig. 5.2, but now the quench consists of turning off the initial superlattice potential and turning on a quasi-periodic one. Results are shown for two strengths of the quasi-periodic potential after the quench. In the left panel in Fig. 5.1, the system is delocalized after the quench, while in the right panel in Fig. 5.1 the system is localized. Note that in the former case the results are qualitatively similar to those in the left panel of Fig. 5.2, while in the latter case they are starkly different. Coarse graining in the presence of localization leads to loss of information and cannot be carried out to generate effectively extensive quantities that are meaningful. Similarly, the GGE description is not expected to apply to many-body localized systems, in which the conserved quantities are also local and nonextensive [119, 120].

Another topic that we discussed in this review is the microscopic origin of generalized thermalization in integrable systems. Our results for the transverse field Ising model, and previous studies on the XX model, show that the GGE and the diagonal ensemble predict identical expectation values of observables in the thermodynamic limit despite the fact that they

are constructed using vastly different numbers of constraints. A spectral decomposition reveals that most of the weight in the diagonal ensemble and the GGE is carried by states that have similar expectation values of few-body (spin) observables. Since those states also have similar distributions of conserved quantities, these results support the hypothesis that generalized eigenstate thermalization is a generic feature in integrable systems, and calls for equivalent studies in integrable models that cannot be mapped onto noninteracting ones. Generalized eigenstate thermalization provides a microscopic understanding for the success of the GGE when traditional ensembles of statistical mechanics fail.

5.2 Introduction

Since the birth of statistical mechanics in the late 19th century, physicists have been fascinated by classical and quantum systems that cannot be understood using the traditional tools provided by this mighty framework. Of those extraordinary systems, our main focus in this review is on those that fall within the quantum realm. It is generally very difficult, usually impossible, to study the dynamics of macroscopic quantum systems far from equilibrium and to find their properties after they relax (if they do). The exact solution of two models of one-dimensional (1D) quantum magnets presented by Lieb, Schulz and Mattis in 1961 [1] (one of the models being the spin-1/2 XY spin model that we discuss later) provided the statistical physics community with powerful tools not only to study such systems in equilibrium, but also to explore their far-from-equilibrium dynamics. These models are prototypes of what we now know as integrable quantum systems [2]. After early studies of dynamics by Niemeijer [3], Mazur studied magnetization in the XY model and pointed out its nonergodic character [83]. This was followed by a series of works by Barouch and coworkers [5, 6, 7], which, using the modern terminology (to be introduced later), studied dynamics after quantum quenches. In those studies, it was apparent that traditional statistical mechanics did not describe observables after relaxation. It was later realized that conserved quantities in quantum spin chains play an important role in their transport properties, and that they may need to be taken into account for the interpretation of experiments in quasi-1D materials [5, 7]. In particular, the possibility of ballistic heat (and eventually spin [8]) transport at finite temperatures triggered many efforts to understand transport properties in 1D systems (for reviews see, e.g., Refs. [11, 12], and also the review by Vasseur and Moore in this volume [13]).

A new burst of activity in 1D systems and their nonequilibrium dynamics has come with recent advances in cooling, trapping, and manipulating gases of atoms and molecules to reach the quantum degeneracy regime [14, 15]. To constrain the dynamics to be effectively one dimensional, experimentalists use deep two-dimensional optical lattices [16, 17, 18] and atom chips [19]. Due to the high degree of isolation in those experiments (the gases are trapped by conservative potentials in ultrahigh vacuum), quantum coherence far from equilibrium can be preserved for long times, as demonstrated with the observation of collapse and revival phenomena in experiments with bosons [20, 35] and fermions [22]. It is interesting to note that, despite the fact that ultracold quantum gases are not in contact with thermal reservoirs, it was for a long time taken for granted that their steady state could be described using traditional ensembles of statistical mechanics. A pioneering experiment by Kinoshita, Wenger, and Weiss [17] demonstrated that this is not the case in 1D geometries. After taking an array of strongly interacting 1D Bose gases far from equilibrium, Kinoshita *et al* showed that the steady state of the observables measured in the experiment was not the one expected in thermal equilibrium. Such steady states, now called prethermalized states, have also been obtained and thoroughly studied in a remarkable set of experiments with weakly interacting Bose gases in atom chips [24, 29, 19] (see also the review by Langen, Gasenzer, and Schmiedmayer in this volume [27]). A

feature that these experimental setups have in common is their closeness to integrability. Other recent experiments that have studied near-integrable dynamics have dealt with strongly interacting bosons on 1D lattices [14, 29], as well as with Ising [30, 31] and Heisenberg [32, 33, 23] spin chains.

Shortly after the Kinoshita *et al* experiments, it was shown that, in a system of hard-core bosons far from equilibrium, observables exhibit relaxation to time-independent values that can be predicted by means of a generalized Gibbs ensemble (GGE) [1, 36]. The GGE was obtained by maximizing the entropy, à la Jaynes [37, 38], taking into account an extensive set of conserved quantities that made that particular hard-core boson model integrable. Since then, the validity of the GGE to describe observables in integrable systems after equilibration has been demonstrated in a wide range of 1D models including: Luttinger liquids [39, 239, 41], the $1/r$ fermionic Hubbard model [42], the sine-Gordon model [240], the transverse field Ising model [241, 41, 45, 242, 246, 48, 25, 27], hard-core bosons in quasiperiodic lattices [51], hard-core anyons [52], bosons with contact interactions [53, 54, 55, 56, 277, 58, 59], quantum field theories [60, 61, 250, 63], and spin-1/2 XXZ chains [64, 253, 274, 272, 273, 69].

The works mentioned above have addressed several important questions related to the GGE. Among those, some that we touch upon in this review are: Why and which observables relax to the GGE predictions? Is the locality of an observable essential for it to be described by the GGE? Are there fundamental differences between noninteracting models and interacting models mappable to noninteracting ones? Which conserved quantities should one use to construct the GGE? Under which circumstances does the GGE description break down? No definite answers have been given to those questions.

Here, we review numerical results and report original ones that provide answers to some of those questions in cases for which no analytic results are known. More specifically, we focus on two paradigmatic integrable models that can be mapped onto noninteracting ones: hard-core bosons (XX model) and the transverse field Ising model (see also the review by Essler and Fagotti in this volume [4]). For the latter model, we compute the spin-spin correlations in the entire system both in the so-called diagonal ensemble and in the GGE, and show that the trace distance of such correlations in both ensembles vanishes in the thermodynamic limit. This is the second instance known to us in which correlation functions in an entire system are shown to be described by the GGE prediction (see Ref. [52] for the first one). This demonstrates that the prevailing view that relaxation to the GGE prediction occurs only in real-space subsystems of isolated quantum systems is not justified. Moreover, our study of the statistical weights of the eigenstates of the Hamiltonian reveals that, for every observable studied, nonvanishing weights are only present in a region around the system's mean energy in which eigenstates have similar expectation values of observables. These results support the generalized eigenstate thermalization scenario discussed in Ref. [71], which can be thought of as a generalization of the eigenstate thermalization hypothesis [72, 73, 6] to integrable systems. It provides a microscopic understanding for the general success of the GGE.

The presentation is organized as follows. In Sec. 5.3, we introduce the models, the statistical ensembles, and specify the conserved quantities considered. Our exposition focuses on models that are mappable to noninteracting ones, which, as we argue in Sec. 5.4, should not be confused with noninteracting models. In Sec. 5.4, we present a theoretical discussion of the relaxation dynamics of experimentally relevant observables in a hard-core boson system. We show that values of the observables after relaxation are, up to finite size effects, those predicted by the GGE. In that section, we also introduce measures to quantify the differences between

results after relaxation and the GGE predictions, and discuss their scaling with system size. Furthermore, we review the case of noninteracting fermions for which some observables fail to equilibrate but their time averages are still predicted by the GGE. Section 5.5 is devoted to the analysis of various ensembles after quenches in the transverse field Ising model. We report results for the diagonal ensemble, the GGE, and the grand canonical ensemble, and show how the results for observables in the GGE converge to those in the diagonal ensemble with increasing system size. Section 5.6 is mainly devoted to a discussion of generalized eigenstate thermalization in the transverse field Ising model. We conclude with a summary and outlook in Sec. 5.1.

5.3 Models, Ensembles, and Conserved Quantities

This section is devoted to the introduction of the models and statistical ensembles that are the focus of this review. We also show results for the distributions of conserved quantities after various quenches. Those quantities, and their expectation values in the initial state, are the core objects for the construction of the GGE.

5.3.1 The XY model in the presence of a transverse magnetic field

The XY model in the presence of a transverse magnetic field [1], and, specially, some of its limits to be discussed below, are among the most studied models of quantum magnetism in 1D chains. The Hamiltonian can be written as:

$$\hat{H}_{\mathrm{XY}} = -J \sum_j \left[(1+\gamma) \hat{S}^x_j \hat{S}^x_{j+1} + (1-\gamma) \hat{S}^y_j \hat{S}^y_{j+1} \right] - h \sum_j \hat{S}^z_j \tag{5.1}$$

where $\hat{S}^x$, $\hat{S}^y$ and $\hat{S}^z$ are standard spin-1/2 operators, J is the exchange constant, h is the transverse magnetic field, and γ is the anisotropy parameter.

The Hamiltonian (5.1) is defined on a one-dimensional lattice with L sites, with either open (in the first sum, $j = 1, 2, \ldots, L-1$) or periodic (in the first sum, $j = 1, 2, \ldots, L$, with $\hat{S}^\alpha_{L+1} \equiv \hat{S}^\alpha_1$) boundary conditions.

We express the spin operators in terms of ladder operators $\hat{S}^\pm_j = \hat{S}^x_j \pm i \hat{S}^y_j$, which, in turn, can be expressed in terms of hard-core bosons as [15, 261]: $\hat{S}^+_j = \hat{b}^\dagger_j \sqrt{1-\hat{n}_j}$, $\hat{S}^-_j = \sqrt{1-\hat{n}_j}\, \hat{b}_j$, and $\hat{S}^z_j = \hat{n}_j - 1/2$, where $\hat{n}_j = \hat{b}^\dagger_j \hat{b}_j$.

(do this transformation, looks like an easy exercise)

In the hard-core boson language, the Hamiltonian (5.1) can be written as

$$\hat{H}_{\mathrm{XY}} = -\frac{J}{2} \sum_j \left(\hat{b}^\dagger_j \hat{b}_{j+1} + \mathrm{H.c.} \right) - \frac{\gamma J}{2} \sum_j \left(\hat{b}^\dagger_j \hat{b}^\dagger_{j+1} + \mathrm{H.c.} \right) - h \sum_j \hat{b}^\dagger_j \hat{b}_j + \frac{hL}{2}, \tag{5.2}$$

where the hard-core boson operators satisfy a local constraint $(\hat{b}_j)^2 = (\hat{b}^\dagger_j)^2 = 0$. One can see that, in the hard-core boson language, $\gamma = 0$ is special. In that limit, the Hamiltonian commutes with the total number of bosons ($\hat{N} = \sum_j \hat{b}^\dagger_j \hat{b}_j$), i.e., it is particle number conserving. This is known as the XX model in the spin language. In what follows, we treat the cases $\gamma = 0$ and $\gamma = 1$ separately.

Before focusing on the different limits of the Hamiltonian (5.2), let us comment on whether we should consider this model as interacting or not.

Hard-core bosons in Eq. (5.2) are interacting because of the local constraint that precludes multiple occupancy of lattice sites.

However, as we show in the next subsections, this model can be mapped onto a noninteracting one. Because of this mapping, the model in Eq. (5.2) is sometimes referred to as a noninteracting model.

An important point we want to stress in this review is that there are fundamental differences when it comes to equilibration and generalized thermalization between hard-core bosons (or spins) and the noninteracting fermions to which they can be mapped (as we know there are fundamental differences between their momentum distribution functions in equilibrium [76]).

(which difference???)

For noninteracting fermions there can exist extensive sets of one-body observables that do not equilibrate, while this is not the case for hard-core bosons (in the absence of localization due to disorder) [52]. How can such a fundamental difference be understood considering that there is a mapping between them? Mathematically, this follows from the fact that the mapping [see Eq. (5.4)] is a nonlocal one. Physically, we can understand that such differences emerge because the one-body sector of a many-body system of noninteracting fermions evolves unitarily, while, because of interactions, this is not the case for the one-body sector of a many-body system of hard-core bosons. We will discuss this further in the context of one example in Sec. 5.4.

The XX model: Hard-core bosons and noninteracting fermions.

When $\gamma = 0$, particle number conservation implies that the last two terms in Eq. (5.2) are constants that can be considered as an overall chemical potential. They are ignored in the discussion that follows for the XX model. One can generalize the hard-core boson Hamiltonian to account for a position dependent magnetic field in Eq. (5.1), by adding a site-dependent potential V_j (we define $\tilde{J} \equiv J/2$)

$$\hat{H}_{\rm XX} = -\tilde{J}\sum_j \left(\hat{b}_j^\dagger \hat{b}_{j+1} + \text{H.c.}\right) + \sum_j V_j\, \hat{b}_j^\dagger \hat{b}_j. \tag{5.3}$$

This is a model that can be realized by experimental groups using ultracold bosonic atoms in optical lattices in the limit of very strong onsite repulsive interactions between the bosons [14, 15]. It can be straightforwardly solved using the Jordan-Wigner transformation [15, 262], which maps spin-1/2 operators (and therefore hard-core bosons) onto spinless fermions:

$$\hat{S}_j^+ = \hat{f}_j^\dagger e^{-i\pi\sum_{l<j}\hat{f}_l^\dagger \hat{f}_l}, \quad \hat{S}_j^- = e^{i\pi\sum_{l<j}\hat{f}_l^\dagger \hat{f}_l}\hat{f}_j, \quad \text{and} \quad \hat{S}_j^z = \hat{f}_j^\dagger \hat{f}_j - 1/2, \tag{5.4}$$

where $\hat{f}_j$ and $\hat{f}_j^\dagger$ obey standard fermionic algebra. In the spinless fermion language, the Hamiltonian (5.3) reads:

$$\hat{H}_{\rm XX} = -\tilde{J}\sum_j \left(\hat{f}_j^\dagger \hat{f}_{j+1} + \text{H.c.}\right) + \sum_j V_j\, \hat{f}_j^\dagger \hat{f}_j. \tag{5.5}$$

In the presence of translational invariance, $V_j = 0$ (or constant) and periodic boundary conditions, a Fourier transform $\hat{f}_j = 1/\sqrt{L}\sum_k e^{ikj}\hat{f}_k$ diagonalizes the Hamiltonian (5.5): $\hat{H}_{\rm XX} = -2\tilde{J}\sum_k \cos(k)\hat{f}_k^\dagger \hat{f}_k$. The many-body eigenstates are hence products of single-particle states, $\prod_k \hat{f}_k^\dagger|\emptyset\rangle$, and the occupation of those single-particle states, $\hat{m}_k^f = \hat{f}_k^\dagger \hat{f}_k$, are constants of motion. This can be straightforwardly extended to systems that are not translationally invariant by, instead of performing a Fourier transform, numerically diagonalizing the Hamiltonian (5.5).

Due to its experimental relevance, the main observable that we consider in the context of $\hat{H}_{\rm XX}$ is the hard-core boson quasi-momentum distribution function

$$\hat{m}_k = \frac{1}{L}\sum_{j,l} e^{-i(l-j)k}\hat{b}_j^\dagger \hat{b}_l. \tag{5.6}$$

Its expectation value can be measured in experiments with ultracold quantum gases by means of the time-of-flight protocol [14]. Since we only deal with lattice systems, in the reminder of this review we will refer to the quasi-momentum as the momentum. Because of the nonlocal character of the mapping between hard-core bosons and spinless fermions, and as mentioned before, $\langle \hat{m}_k \rangle$ is fundamentally different in those two systems [76]. Once the fermionic problem has been solved, it is still challenging to obtain the momentum distribution of the hard-core bosons. Numerically, this can be achieved efficiently using properties of Slater determinants, as demonstrated for the ground state [78, 79], finite temperature [76], and for the quantum dynamics [80]. In contrast to the momentum distribution, the site occupations are identical for hard-core bosons and spinless fermions, $\langle \hat{n}_j \rangle = \langle \hat{b}_j^\dagger \hat{b}_j \rangle = \langle \hat{f}_j^\dagger \hat{f}_j \rangle$, and can therefore be calculated much more easily.

The transverse field Ising model.

The transverse field Ising model is obtained by substituting $\gamma = 1$ in Eqs. (5.1) and (5.2). For this model, which is not particle number conserving in the hard-core boson language, we restrict our analysis to the translationally invariant case. Using the Jordan-Wigner and a Fourier transformation on the resulting fermionic Hamiltonian leads to:

$$\begin{aligned} \hat{H}_{\mathrm{TFI}}^{(+)} &= \sum_{k \in \mathcal{K}^{(+)}} \left[a_k \left(\hat{f}_k^\dagger \hat{f}_k + \hat{f}_{-k}^\dagger \hat{f}_{-k} - 1 \right) - b_k \left(i \hat{f}_k^\dagger \hat{f}_{-k}^\dagger + \mathrm{H.c.} \right) \right], \\ H_{\mathrm{TFI}}^{(-)} &= \sum_{k \in \mathcal{K}^{(-)} > 0} \left[a_k \left(\hat{f}_k^\dagger \hat{f}_k + \hat{f}_{-k}^\dagger \hat{f}_{-k} - 1 \right) - b_k \left(i \hat{f}_k^\dagger \hat{f}_{-k}^\dagger + \mathrm{H.c.} \right) \right] \\ &\quad -(J+h) \hat{f}_0^\dagger \hat{f}_0 + (J-h) \hat{f}_\pi^\dagger \hat{f}_\pi + h, \end{aligned} \tag{5.7}$$

where $a_k = -J\cos(k) - h$ and $b_k = J\sin(k)$ [for $\gamma \neq 1$, $b_k = \gamma J \sin(k)$]. The sectors with even (+) and odd (-) number of fermions (from now on referred to as the even and odd sectors, respectively) are uncoupled and are treated separately.

(understand these sectors???? I think, I need to read a paper about it)

We note that, in the even sector, antiperiodic boundary conditions need to be used when mapping spins (hard-core bosons) onto spinless fermions [1]. As a result, the even and odd sectors are diagonalized in terms of different sets of wave vectors $\mathcal{K}^{(+)} = \{\pi/L + n2\pi/L \mid n = 0, 1, ..., L/2 - 1\}$ and $\mathcal{K}^{(-)} = \{n2\pi/L \mid n = 0, ..., L/2 - 1\}$, respectively. In Eqs. (5.7), the wave vectors are coupled in pairs $\{k, -k\}$. The only exception is found in the odd sector, in which a pair is formed by $k = 0$ and $k = \pi$. As seen in Eqs. (5.7), this pair is treated separately. Formally, the Hamiltonian can be expressed as $\hat{H}_{\mathrm{TFI}} = \hat{H}_{\mathrm{TFI}}^{(+)} \hat{\mathcal{P}}^{(+)} + \hat{H}_{\mathrm{TFI}}^{(-)} \hat{\mathcal{P}}^{(-)}$, where the operators $\hat{\mathcal{P}}^{(\pm)}$ act as projectors onto a given sector [81].

The Hamiltonians (5.7) are diagonalized by a Bogoliubov transformation $\hat{f}_k = u_k \hat{\eta}_k - v_k^* \hat{\eta}_{-k}^\dagger$, where $u_k = (\varepsilon_k + a_k)/\sqrt{2\varepsilon_k(\varepsilon_k + a_k)}$ and $v_k = ib_k/\sqrt{2\varepsilon_k(\varepsilon_k + a_k)}$. For $k = 0$ and $k = \pi$, the original Hamiltonian is already diagonal, we take $\hat{f}_k = \hat{\eta}_{-k}^\dagger$.

(check this, it should be easy)

This results in:

$$\hat{H}_{\mathrm{TFI}}^{(+)} = \sum_{k \in \mathcal{K}^{(+)}} \left[\varepsilon_k (\hat{\eta}_k^\dagger \hat{\eta}_k + \hat{\eta}_{-k}^\dagger \hat{\eta}_{-k}) - \varepsilon_k \right], \tag{5.8}$$

$$\hat{H}_{\mathrm{TFI}}^{(-)} = \sum_{k \in \mathcal{K}^{(-)} > 0} \left[\varepsilon_k (\hat{\eta}_k^\dagger \hat{\eta}_k + \hat{\eta}_{-k}^\dagger \hat{\eta}_{-k}) - \varepsilon_k \right] + (h+J) \hat{\eta}_0^\dagger \hat{\eta}_0 + (h-J) \hat{\eta}_\pi^\dagger \hat{\eta}_\pi - h,$$

with the energies of the noninteracting Bogoliubov quasiparticles being

$$\varepsilon_k = \sqrt{h^2 + 2hJ\cos k + J^2}. \tag{5.9}$$

[For $\gamma \neq 1$, one has an extra term in the sum inside the square root in Eq. (5.9), which reads $(\gamma^2 - 1)J^2 \sin^2(k)$].

The transverse field Ising model has a quantum phase transition at $h = 1$ between a ferromagnetic ground state ($h < 1$) and a paramagnetic one ($h > 1$) [200].

(what is meant by this???)

The ferromagnetic ground state is doubly degenerate in the thermodynamic limit (each sector contributes one state).

(why????)

In finite systems, the ferromagnetic ground state is nondegenerate and belongs to the even sector. The paramagnetic ground state is nondegenerate (both, in finite systems and in the thermodynamic limit) and also belongs to the even sector. Whenever nondegenerate, the ground state $|0\rangle$ is the vacuum for Bogoliubov quasiparticles:

$$|0\rangle = \prod_{k \in \mathcal{K}^{(+)}} \frac{1}{|v_k|} \hat{\eta}_k \hat{\eta}_{-k} |\emptyset\rangle \equiv |0,0\rangle \otimes \ldots \otimes |0,0\rangle \otimes \ldots \,. \tag{5.10}$$

All the eigenstates of the Hamiltonian (5.8) can be obtained by acting with products (with the proper set of wave vectors) of $\hat{\eta}_k^\dagger$ on the state $|0\rangle$. As a result, one can express any eigenstate of the Hamiltonian as

$$|n\rangle = |p_{k_1}^{[n]}, p_{-k_1}^{[n]}\rangle \otimes \ldots \otimes |p_{k_j}^{[n]}, p_{-k_j}^{[n]}\rangle \otimes \ldots \,. \tag{5.11}$$

In the expressions above, $|p_k^{[n]}, p_{-k}^{[n]}\rangle$ denotes the occupation of Bogoliubov quasiparticles with k and $-k$ in the n-th eigenstate of the Hamiltonian in a given sector. Each $\{k, -k\}$ subspace is spanned by the four vectors $\{|0,0\rangle, |1,1\rangle, |1,0\rangle, |0,1\rangle\}$. The occupation of the Bogoliubov quasiparticles are constants of motion in the transverse field Ising model.

5.3.2 The XXZ model

For completeness, we also present the Hamiltonian of the XXZ model:

$$\hat{H}_{\mathrm{XXZ}} = -J \sum_j \left(\hat{S}_j^x \hat{S}_{j+1}^x + \hat{S}_j^y \hat{S}_{j+1}^y + \Delta \hat{S}_j^z \hat{S}_{j+1}^z \right), \tag{5.12}$$

in which Δ sets the strength of the nearest-neighbor $\hat{S}^z \hat{S}^z$ interaction ($\Delta = 1$ corresponds to the Heisenberg point). In contrast to XY model in a transverse field, the XXZ Hamiltonian (5.12) cannot be mapped onto a noninteracting model.

Recent studies have shed light on new families of conserved quantities in this model [8, 69, 22, 2] (see also the review by Ilievski, Medenjak, Prosen and Zadnik in this volume [48]).

(is it a useful model??? seems no)

5.3.3 Quantum quenches and ensembles

In the reminder of this review we will be interested in what happens to the systems introduced previously after they are taken far from equilibrium. A standard protocol used for the latter purpose is that of a quantum quench. Namely, the system is prepared in an eigenstate of a given time-independent Hamiltonian (usually, as done here, in the ground state), and the dynamics is studied under a new time-independent Hamiltonian (called $\hat{H}$ in what follows). This can be thought of as an instantaneous change in the parameters describing a system and, hence, the term quantum quench.

Given the initial state $|\psi_0\rangle$, the time-evolving one can then be written as

$$|\psi(t)\rangle = e^{-i\hat{H}t}|\psi_0\rangle = \sum_n e^{-iE_n t}|n\rangle\langle n|\psi_0\rangle = \sum_n e^{-iE_n t}c_n|n\rangle, \tag{5.13}$$

where $\{|n\rangle\}$ is the complete set of eigenstates of $\hat{H}$ and $c_n = \langle n|\psi_0\rangle$ is the projection of the initial state onto eigenstate $|n\rangle$ (we set $\hbar \equiv 1$). Rather than in the evolution of the wave-functions, here we are interested on how observables $\hat{\mathcal{O}}$ evolve under quantum dynamics

$$\mathcal{O}(t) \equiv \langle\psi(t)|\hat{\mathcal{O}}|\psi(t)\rangle = \sum_{n,m}^{E_n\neq E_m} e^{-i(E_n-E_m)t}c_m^* c_n\langle m|\hat{\mathcal{O}}|n\rangle + \sum_{n,m}^{E_n=E_m} c_m^* c_n\langle m|\hat{\mathcal{O}}|n\rangle. \tag{5.14}$$

If an observable relaxes to a nearly time independent value (fluctuations about that value vanish with increasing system size and quantum revivals occur in time intervals that diverge with system size), i.e., if it equilibrates, then the equilibrated result for the observable is given (up to finite size effects) by the second term in the sum in Eq. (5.14). We note that this term includes both diagonal and off-diagonal matrix elements of degenerate eigenstates.

For generic quantum systems one expects no degeneracies in the absence of special symmetries, so only diagonal matrix elements are expected to contribute to the results after relaxation, i.e., we expect $\mathcal{O}(t)$ to relax to $\langle\hat{\mathcal{O}}\rangle_{\rm DE} \equiv {\rm Tr}[\hat{\rho}_{\rm DE}\hat{\mathcal{O}}]$, where

$$\hat{\rho}_{\rm DE} = \sum_n \rho_{\rm DE}^{[n]}\,|n\rangle\langle n| \tag{5.15}$$

is known as the diagonal ensemble density matrix [6], and $\rho_{\rm DE}^{[n]} = |c_n|^2$. This has been shown to occur in numerical studies of nonintegrable systems [6, 157, 158, 88]. Degeneracies are expected to arise in integrable systems. However, in the thermodynamic limit, they usually do not lead to differences between the equilibrated results and the predictions of the diagonal ensemble [71]. This, of course, unless the many-body spectrum of the integrable Hamiltonian has extensive degeneracies [42]. The latter is actually the case in the translationally invariant transverse field Ising model. In Sec. 5.3.4, we will nevertheless show that, for the quenches studied, degenerate states play no role in the dynamics and the diagonal ensemble correctly predicts the equilibrated results for observables.

One of the central questions that has been studied in the last ten years is whether, after relaxation following a quantum quench, observables can be described using traditional ensembles of statistical mechanics. Since the results from the latter ensembles agree in the thermodynamic limit (at least for the observables that we are interested in), and since there is no particle-number conservation in the transverse field Ising model, the only traditional ensemble of statistical mechanics that we consider here (for both the XX and the transverse field Ising model) is the grand canonical ensemble.

For the particle-number-conserving XX Hamiltonian (5.3), we write

$$\hat{\rho}_{\rm GE}^{\rm (XX)} = \frac{1}{Z_{\rm GE}^{\rm (XX)}} e^{-\beta(\hat{H}_{\rm XX}-\mu\hat{N})}, \tag{5.16}$$

where $\hat{N}$ is the total particle number operator and $Z_{\rm GE}^{\rm (XX)} = {\rm Tr}[e^{-\beta(\hat{H}_{\rm XX}-\mu\hat{N})}]$. The values of β and μ used to compare with the results from the quantum dynamics are set by constraining the mean energy and number of particles in the grand canonical ensemble to be the same as in the time-evolving state, i.e., $\langle\psi_0|\hat{H}|\psi_0\rangle = {\rm Tr}[\hat{\rho}_{\rm GE}^{\rm (XX)}\hat{H}]$ and $N = {\rm Tr}[\hat{\rho}_{\rm GE}^{\rm (XX)}\hat{N}]$.

For the (non-particle-number-conserving) transverse field Ising Hamiltonian (5.8), we have

$$\hat{\rho}_{\rm GE}^{\rm (TFI)} = \frac{1}{Z_{\rm GE}^{\rm (TFI)}} e^{-\beta\hat{H}_{\rm TFI}}, \tag{5.17}$$

where $Z_{\mathrm{GE}}^{(\mathrm{TFI})} = \mathrm{Tr}[e^{-\beta \hat{H}_{\mathrm{TFI}}}]$ and β is obtained by matching $\langle\psi_0|\hat{H}|\psi_0\rangle = \mathrm{Tr}[\hat{\rho}_{\mathrm{GE}}^{(\mathrm{TFI})}\hat{H}]$. In what follows, expectation values of observables in the grand canonical ensemble are denoted as $\langle\hat{\mathcal{O}}\rangle_{\mathrm{GE}} \equiv \mathrm{Tr}[\hat{\rho}_{\mathrm{GE}}\hat{\mathcal{O}}]$.

As already mentioned before, observables in integrable systems are not expected to relax to the predictions of the grand canonical ensemble.

(why???)

Instead, one expects them to relax to the predictions of the GGE, which is defined as

$$\hat{\rho}_{\mathrm{GGE}} = \frac{1}{Z_{\mathrm{GGE}}} e^{-\sum_k \lambda_k \hat{I}_k}, \tag{5.18}$$

where $\{\hat{I}_k\}$ is a set of nontrivial conserved quantities that exists because the system is integrable. The corresponding partition function is $Z_{\mathrm{GGE}} = \mathrm{Tr}[e^{-\sum_k \lambda_k \hat{I}_k}]$. The Lagrange multipliers $\{\lambda_k\}$ are fixed so that the GGE expectation value of each conserved quantity matches that in the initial state $\langle\psi_0|\hat{I}_k|\psi_0\rangle = \mathrm{Tr}[\hat{\rho}_{\mathrm{GGE}}\hat{I}_k]$. We denote the expectation values of observables in the GGE as $\langle\hat{\mathcal{O}}\rangle_{\mathrm{GGE}} \equiv \mathrm{Tr}[\hat{\rho}_{\mathrm{GGE}}\hat{\mathcal{O}}]$.

5.3.4 Conserved quantities

The XX model.

In the XX model, the set of conserved quantities $\hat{I}_q$ that we use to construct the GGE are the occupations of the single-particle eigenstates of the fermionic Hamiltonian (momentum modes occupations in a translationally invariant system). They can only take values zero or one, so the partition function of the GGE can be written as

$$Z_{\mathrm{GGE}} = \mathrm{Tr}[e^{-\sum_q \lambda_q \hat{I}_q}] = \prod_q (1 + e^{-\lambda_q}), \tag{5.19}$$

where $q = 1, 2, \ldots, L$. The expectation values of conserved quantities in the GGE can be written as

$$\langle\hat{I}_q\rangle_{\mathrm{GGE}} = Z_{\mathrm{GGE}}^{-1}\mathrm{Tr}[e^{-\sum_q \lambda_q \hat{I}_q}\hat{I}_q] = \frac{e^{-\lambda_q}}{1 + e^{-\lambda_q}}. \tag{5.20}$$

Since the GGE is constructed requiring that those expectation values are the same as in the initial state $\langle\hat{I}_q\rangle_0 = \langle\psi_0|\hat{I}_q|\psi_0\rangle$, one obtains the following expression for the Lagrange multipliers [1]

$$\lambda_q = \ln\left(\frac{1 - \langle\hat{I}_q\rangle_0}{\langle\hat{I}_q\rangle_0}\right), \tag{5.21}$$

and the partition function can then be written as

$$Z_{\mathrm{GGE}}^{-1} = \prod_q (1 - \langle\hat{I}_q\rangle_0). \tag{5.22}$$

The left panel of Fig. 5.2 displays the distribution of conserved quantities $\langle\hat{I}_q\rangle_0$ after turning off a superlattice potential in the XX model (with open boundary conditions) [1]. The system was initially in the ground state in the presence of the superlattice potential. The dynamics and generalized thermalization after this quench will be discussed in Sec. 5.4. The number of values of q is given by the number of lattice sites. They are ordered with increasing eigenenergies of the single-particle eigenstates, which are nondegenerate for open boundary conditions. As shown in the left panel in Fig. 5.2, a proper rescaling $q \to q/L$ makes the data for different system sizes collapse onto the same curve.

(how this was obtained???)

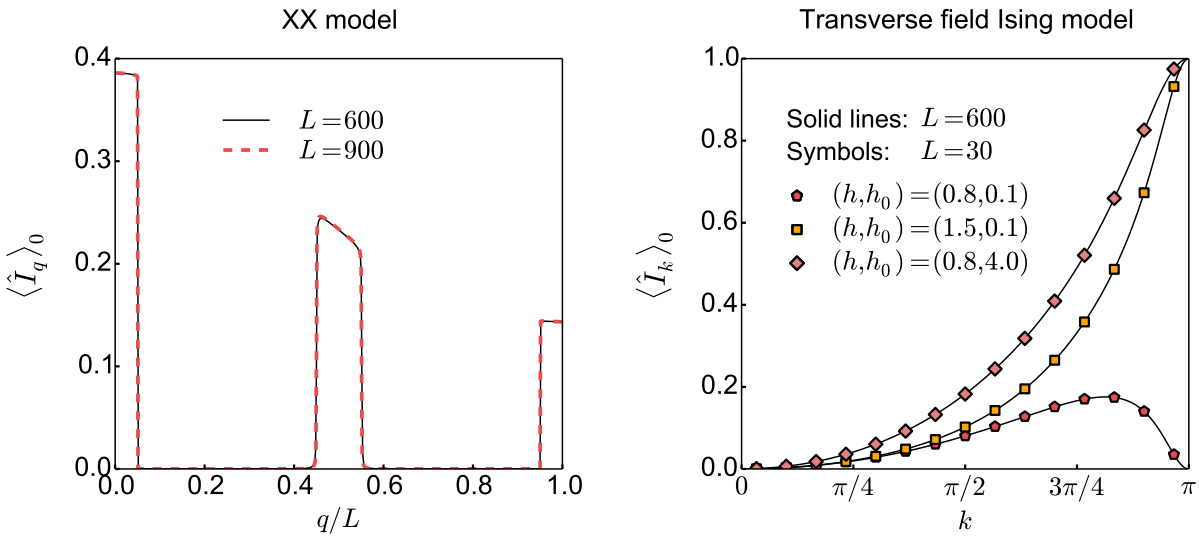

Figure 5.2: *Distribution of conserved quantities in the XX model and in the transverse field Ising model after a quantum quench.* The conserved quantities $\langle \hat{I}_q \rangle_0$ in the XX model (left panel) are the occupations of the single-particle eigenstates of the fermionic Hamiltonian, where $q = 1, 2, \ldots, L$. The curves display $\langle \hat{I}_q \rangle_0$ after a quench from the ground state of $H_{\rm XX}$ (5.3) in the presence of a (superlattice) potential $V_j = A\cos(\frac{2\pi j}{T})$ with period $T = 4$ and amplitude $A = 8\tilde{J}$. The quench consists of turning off the superlattice potential. The average site occupancy is $N/L = 1/20$ [1]. The q-values are ordered with increasing eigenenergies of the single-particle eigenstates. We discuss further results for this quantum quench in Sec. 5.4. In the transverse field Ising model (right panel), the conserved quantities $\langle \hat{I}_k \rangle_0$ are the occupations of the Bogoliubov quasiparticles. The plots display $\langle \hat{I}_k \rangle_0$ after quenches from the ground state of a system with transverse field h_0 to a final field h. Results are not shown for $k < 0$ since $\langle \hat{I}_{-k} \rangle_0 = \langle \hat{I}_k \rangle_0$. Further results for these quenches are discussed in Sec. 5.5.

The transverse field Ising model. Initial eigenstate.

In contrast to the XX model, for which the initial state in the expressions above can be any state (not necessarily an eigenstate of the Hamiltonian), for the transverse field Ising model we will restrict our analysis to initial states that are eigenstates of the Hamiltonian (5.8). In addition, we will focus on initial eigenstates that are in the even sector.

We are interested in the overlaps $c_n = \langle n|\psi_0\rangle$ of the initial state $|\psi_0\rangle$ with the eigenstates $\{|n\rangle\}$ of the final Hamiltonian. We write the latter using the notation in Eq. (5.11), and write the former as:

$$|\psi_0\rangle = |r_{k_1}, r_{-k_1}\rangle \otimes \ldots \otimes |r_{k_j}, r_{-k_j}\rangle \otimes \ldots \,. \tag{5.23}$$

As a result, c_n can be calculated as the product of the overlaps in each subspace $\{k, -k\}$, i.e., it can be written as a product of $L/2$ terms

$$c_n = \prod_{k \in \mathcal{K}^{(+)}} c_k^{[n]}. \tag{5.24}$$

For each k, $c_k^{[n]}$ can take four possible values. This results from the fact that $|r_k, r_{-k}\rangle$ and $|p_k^{[n]}, p_{-k}^{[n]}\rangle$ are each one of $|0,0\rangle, |1,1\rangle, |1,0\rangle$, and $|0,1\rangle$, which, in terms of spinless fermions, can

be written as

$$\begin{array}{rcrcl} |0,0\rangle & \equiv & \frac{1}{|v_k|}\hat{\eta}_k\hat{\eta}_{-k}|\emptyset\rangle & = & (-i)(u_k + v_k\hat{c}_k^\dagger\hat{c}_{-k}^\dagger)|\emptyset\rangle \\ |1,0\rangle & \equiv & \hat{\eta}_k^\dagger\left(\frac{1}{|v_k|}\hat{\eta}_k\hat{\eta}_{-k}\right)|\emptyset\rangle & = & (-i)\hat{c}_k^\dagger|\emptyset\rangle \\ |0,1\rangle & \equiv & \hat{\eta}_{-k}^\dagger\left(\frac{1}{|v_k|}\hat{\eta}_k\hat{\eta}_{-k}\right)|\emptyset\rangle & = & (-i)\hat{c}_{-k}^\dagger|\emptyset\rangle \\ |1,1\rangle & \equiv & \hat{\eta}_k^\dagger\hat{\eta}_{-k}^\dagger\left(\frac{1}{|v_k|}\hat{\eta}_k\hat{\eta}_{-k}\right)|\emptyset\rangle & = & i(v_k + u_k\hat{c}_k^\dagger\hat{c}_{-k}^\dagger)|\emptyset\rangle \end{array} . \tag{5.25}$$

The dependence on the Hamiltonian parameters before and after the quench enters through the parameters $u_k = u_k(J,h)$ and $v_k = v_k(J,h)$, which were introduced with the Bogoliubov transformation [see Eq. (5.8)].

Equation (5.25) shows explicitly why an initial eigenstate that belongs to either the even or odd sector has a nonzero overlap only with eigenstates in the same sector. On the level of $\{k,-k\}$ subspaces, states $|0,0\rangle$ and $|1,1\rangle$ do not couple to the states $|1,0\rangle$ and $|0,1\rangle$, and vice versa.

For the overlaps between the initial state and the eigenstates of the Hamiltonian we have that:
(i) If $r_k = 0$ and $r_{-k} = 0$, or $r_k = 1$ and $r_{-k} = 1$, then

$$c_k^{[n]} = \begin{cases} \pm\sqrt{\alpha_k} & \equiv \quad c_k^{(0)} \quad \text{if} \;\; p_k^{[n]} = r_k, \;\; p_{-k}^{[n]} = r_{-k} \\ 0 & \equiv \quad c_k^{(1)} \quad \text{if} \;\; p_k^{[n]} = 1, \;\; p_k^{[n]} = 0 \\ 0 & \equiv \quad c_k^{(2)} \quad \text{if} \;\; p_k^{[n]} = 0, \;\; p_{-k}^{[n]} = 1 \\ \pm i\sqrt{1-\alpha_k} & \equiv \quad c_k^{(3)} \quad \text{if} \;\; p_k^{[n]} \neq r_k, \;\; p_{-k}^{[n]} \neq r_{-k} \end{cases} . \tag{5.26}$$

(ii) If $r_k = 1$ and $r_{-k} = 0$, or $r_k = 0$ and $r_{-k} = 1$, then

$$c_k^{[n]} = \begin{cases} 0 \equiv c_k^{(0)} & \text{if} \;\; p_k^{[n]} = 0, \;\; p_{-k}^{[n]} = 0 \\ 1 \equiv c_k^{(1)} & \text{if} \;\; p_k^{[n]} = r_k, \;\; p_{-k}^{[n]} = r_{-k} \\ 0 \equiv c_k^{(2)} & \text{if} \;\; p_k^{[n]} \neq r_k, \;\; p_{-k}^{[n]} \neq r_{-k} \\ 0 \equiv c_k^{(3)} & \text{if} \;\; p_k^{[n]} = 1, \;\; p_{-k}^{[n]} = 1 \end{cases} . \tag{5.27}$$

Note that, in the expressions above, the superindex $[n]$ refers to the eigenstate number, while the superindex (ξ), with $\xi = 0,1,2,3$, labels one of the four possible values of $c_k^{[n]}$ for any given values of r_k and r_{-k} in the initial state.

In Eq. (5.26), we introduced the coefficient

$$\alpha_k = \frac{1}{2}\left(1 + \frac{a_k a_k^0 + b_k b_k^0}{\varepsilon_k \varepsilon_k^0}\right), \tag{5.28}$$

which is a central quantity in the calculations that follow. The coefficients a_k and b_k were introduced in Eq. (5.7), and ε_k is the single-particle energy defined in Eq. (5.9). We denote the parameters before the quench as J_0 and h_0 (they enter in a_k^0, b_k^0, and ε_k^0), and the parameters after the quench as J and h (they enter in a_k, b_k, and ε_k). If not stated otherwise, we set $J = J_0 = 1$.

An important fact apparent from Eqs. (5.26) and (5.27) is the normalization of the weights $\sum_{\xi=0}^{3}\left|c_k^{(\xi)}\right|^2 = 1$, no matter the values of r_k and r_{-k} in the initial state. That this must be the case follows from the normalization of the initial state

$$\langle\psi_0|\psi_0\rangle = \sum_n |c_n|^2 = \sum_n \prod_{k\in\mathcal{K}^{(+)}} \left|c_k^{[n]}\right|^2 = \prod_{k\in\mathcal{K}^{(+)}} \left(\sum_{\xi=0}^{3}\left|c_k^{(\xi)}\right|^2\right) = 1. \tag{5.29}$$

The conserved quantities we use to construct the GGE are the occupations of the Bogoliubov quasiparticles $\{\hat{I}_k \equiv \hat{\eta}_k^\dagger \hat{\eta}_k\}$. In the eigenstates of the Hamiltonian, $p_k^{[n]} = \langle n|\hat{I}_k|n\rangle$ can only take values 0 or 1. Using Eq. (5.21), this implies that

$$\langle n|e^{-\lambda_k \hat{I}_k}|n\rangle = \begin{cases} 1 & \text{if } p_k^{[n]} = 0 \\ \frac{\langle \hat{I}_k\rangle_0}{1-\langle \hat{I}_k\rangle_0} & \text{if } p_k^{[n]} = 1 \end{cases} . \tag{5.30}$$

As for traditional ensembles of statistical mechanics, one can write the density matrix of the GGE as a sum over the contribution from all the eigenstates of the Hamiltonian, $\hat{\rho}_{\rm GGE} = \sum_n \rho_{\rm GGE}^{[n]} |n\rangle\langle n|$. Using Eqs. (5.22) and (5.30), the weights $\rho_{\rm GGE}^{[n]}$ can be expressed solely through the expectation values of the conserved quantities in the initial state

$$\rho_{\rm GGE}^{[n]} = \prod_{k\in\{\mathcal{K}^{(+)},-\mathcal{K}^{(+)}\}}^{p_k^{[n]}=0} \left(1 - \langle \hat{I}_k\rangle_0\right) \prod_{k\in\{\mathcal{K}^{(+)},-\mathcal{K}^{(+)}\}}^{p_k^{[n]}=1} \langle \hat{I}_k\rangle_0. \tag{5.31}$$

Here, the index k of the momentum runs through all the possibles values (positive and negative) in the lattice, which we denote as $k \in \{\mathcal{K}^{(+)}, -\mathcal{K}^{(+)}\}$.

Hence, in order to determine $\rho_{\rm GGE}^{[n]}$, we only need to compute the expectation values $\langle \hat{I}_k\rangle_0$. This can be achieved using the overlaps

$$\langle \hat{I}_k\rangle_0 = \sum_{n,m} \langle\psi_0|m\rangle\langle m|\hat{I}_k|n\rangle\langle n|\psi_0\rangle = \sum_n^{p_k^{[n]}=1} |c_n|^2, \tag{5.32}$$

which means that the initial and final Hamiltonian parameters enter the GGE only through one parameter, namely, α_k. Equation (5.32) can be further simplified using the normalization of single-particle weights [Eq. (5.29)]. One gets that $\langle \hat{I}_k\rangle_0$ is nothing but $\left|c_k^{(\xi)}\right|^2$, where ξ is determined by $\{r_k, r_{-k}\}$. This leads to the general expression for the expectation values of conserved quantities:

$$\langle \hat{I}_k\rangle_0 = \begin{cases} 1-\alpha_k & \text{if} \quad r_k = 0 \quad \text{and} \quad r_{-k} = 0 \\ \alpha_k & \text{if} \quad r_k = 1 \quad \text{and} \quad r_{-k} = 1 \\ 1 & \text{if} \quad r_k = 1 \quad \text{and} \quad r_{-k} = 0 \\ 0 & \text{if} \quad r_k = 0 \quad \text{and} \quad r_{-k} = 1 \end{cases} . \tag{5.33}$$

An important clarification is in order at this point on the use of the GGE for finite XX and transverse field Ising systems. All expressions obtained so far for the GGE follow after a grand canonical trace. Such a trace is problematic in systems with periodic boundary conditions because the mapping between spins (hard-core bosons) and fermions requires that sectors with even number of fermions be treated with antiperiodic boundary conditions [1]. Instead, our expressions are obtained assuming that the boundary conditions are the same for sectors with even and odd particle numbers. To circumvent this problem, in all our calculations for the XX model we report results for systems with open boundary conditions, for which no such problem exists [76]. For the transverse field Ising model, for which periodic boundary conditions are chosen, the assumption that boundary conditions are the same for even and odd number of fermions (we use the one for even number of fermions) introduces an error. The effect of that error on the observables studied here decreases with increasing system size and vanishes in the thermodynamic limit, in which the boundary conditions become irrelevant, i.e., the error we have introduced in our calculations can be thought of as an additional finite-size effect.

The transverse field Ising model. Initial ground state.

In what follows we focus on quenches in finite systems from the ground state [$r_k = r_{-k} = 0$ in Eq. (5.23)] for a field h_0 to a final field h. Hence, the initial state in all our quenches belongs to the even sector. For these quenches, only $\sqrt{\mathcal{D}}$ of the weights in the diagonal ensemble are nonzero, where $\mathcal{D} = 2^L$ is the total size of the Hilbert space. This is because any eigenstate of the final Hamiltonian with $... \otimes |1,0\rangle \otimes ...$ or $... \otimes |0,1\rangle \otimes ...$ will have a vanishing overlap with the initial state. The nonzero weights are given by the expression

$$\rho_{\rm DE}^{[n]} = \prod_{k\in\mathcal{K}^+}^{p_k^{[n]}=0} \alpha_k \prod_{k\in\mathcal{K}^+}^{p_k^{[n]}=1} (1-\alpha_k), \tag{5.34}$$

which is a product of $L/2$ terms. The eigenstate spectrum of the transverse field Ising model has extensive degeneracies, which predominantly occur due to single occupancies of the $\{k,-k\}$ subspaces (the two singly occupied states are degenerate). After the quench from an initial ground state, none of the $\{k,-k\}$ subspaces is singly occupied. As a result, the eigenstates with nonzero weights in the diagonal ensemble are nondegenerate, except for some accidental (nonextensive) degeneracies.

The occupation of the conserved quantities (5.33) for an initial ground state simplifies to

$$\langle \hat{I}_k \rangle_0 = (1-\alpha_k). \tag{5.35}$$

The distribution of $\langle \hat{I}_k \rangle_0$ is shown in the right panel of Fig. 5.2 following three quenches of the transverse field $h_0 \to h$. When quenching from the paramagnetic ($h_0 > J$) to the ferromagnetic ($h < J$) side of the transverse field Ising model (or vice versa), the distribution increases monotonically with increasing k. In contrast, for quenches within the same phase, the distribution is peaked at some finite k and then decreases towards zero for $k \to \pi$. The behavior as $k \to \pi$ can be understood from Eq. (5.35), which gives $\langle \hat{I}_{k\to\pi} \rangle_0 = [1 - {\rm sgn}(h-J){\rm sgn}(h_0-J)]/2$.

Equation (5.35) also simplifies the expression for the weights in the GGE

$$\rho_{\rm GGE}^{[n]} = \prod_{k\in\mathcal{K}^{(+)}}^{p_k^{[n]}=p_{-k}^{[n]}=0} \alpha_k^2 \prod_{k\in\mathcal{K}^{(+)}}^{p_k^{[n]}\neq p_{-k}^{[n]}} \alpha_k(1-\alpha_k) \prod_{k\in\mathcal{K}^{(+)}}^{p_k^{[n]}=p_{-k}^{[n]}=1} (1-\alpha_k)^2. \tag{5.36}$$

It is important to realize that, when quenching from the ground state, all eigenstates of the final Hamiltonian ($\mathcal{D}$ states) can potentially have nonzero weights in the GGE. In contrast, as mentioned before, only $\sqrt{\mathcal{D}}$ eigenstates of the Hamiltonian have nonzero weights in the diagonal ensemble. It is therefore not at all obvious that the GGE should describe observables after equilibration. An interesting observation can be made for eigenstates that have nonzero weights in both ensembles. While their weight in the DE is $|c_n|^2$, their weight in the GGE is $|c_n|^4$.

Statistical independence of macroscopic subsystems in the GGE.

We note at this point that, in $\hat{\rho}_{\rm GGE}$, the conserved quantities appear in the form $e^{-\lambda_k \hat{I}_k}$, as in traditional ensembles of statistical mechanics. However, the conserved quantities selected by us (occupations of single-particle states) are not extensive as in traditional ensembles of statistical mechanics. Extensivity is required for the factorizability of the density matrix, which is needed to ensure statistical independence of macroscopic subsystems. Instead, in the exponential in $\hat{\rho}_{\rm GGE}$, we have an extensive number of intensive conserved quantities. This might lead one to conclude that our GGE is not a legitimate statistical ensemble.

There are two ways to see that our GGE leads to statistical independence of macroscopic subsystems. As shown in Fig. 5.2, the expectation values of the conserved quantities after the quenches are smooth functions (independent of the system size) of q/L for the XX model and k for the transverse field Ising model. Because of Eq. (5.21), the Lagrange multipliers are also smooth functions of q/L and k, respectively. One can then define extensive (coarse grained) integrals of motion $\hat{\mathcal{I}}_\alpha \equiv \sum_{\alpha' \in [\alpha-\delta_\alpha/2, \alpha+\delta_\alpha/2]} \hat{I}_{\alpha'}$, where $\alpha \equiv q/L$ ($\delta_\alpha \ll 1$) for the XX model and $\alpha \equiv k$ ($\delta_\alpha \ll \pi$) for the transverse field Ising model, such that $\hat{\rho}_{\rm GGE} \propto e^{-\sum_\alpha \lambda_\alpha \hat{\mathcal{I}}_\alpha}$ [71, 136]. Alternatively, extensive conserved quantities can be constructed by a linear transformation of $\{\hat{I}_k\}$, which enables ordering them according to their support on the lattice [25]. This latter construction is particularly appealing because it allows one to show that the larger the support of an extensive conserved quantity is the least it affects expectation values of local observables in the GGE. If one wants to compute a local observable with a given finite accuracy, one can then truncate the GGE to have a finite number of local extensive conserved quantities [25].

5.3.5 Expectation values of observables in the transverse field Ising model

Let us discuss how to compute expectation values of observables in the transverse field Ising model in the various ensembles of interest. For that, we write the expectation value of an observable $\hat{\mathcal{O}}$ in an ensemble μ (μ =DE, GE, or GGE), with weights $\{\rho_\mu^{[n]}\}$, as

$$\langle \hat{\mathcal{O}} \rangle_\mu = \sum_n \rho_\mu^{[n]} \langle n|\hat{\mathcal{O}}|n\rangle, \tag{5.37}$$

This expression can be further simplified if two conditions are met: (i) the weights $\rho_\mu^{[n]}$ factorize (as they do in the ensembles considered in this review), $\rho_\mu^{[n]} = \prod_{k\in\mathcal{K}^{(+)}} \rho_{k,\mu}^{[n]}$, and (ii) the eigenstate expectation values can be written as sums of single-particle contributions, $\langle n|\hat{\mathcal{O}}|n\rangle = \sum_{k\in\mathcal{K}^{(+)}} \langle n|\hat{\mathcal{O}}_k|n\rangle$. A single set of wave vectors needs to be chosen for the even and odd sectors. This, as we mentioned before, introduces an error whose effect in our observables of interest vanishes in the thermodynamic limit.

If the conditions above are met, we write

$$\langle n|\hat{\mathcal{O}}_k|n\rangle \equiv \begin{cases} \mathcal{O}_k^{(0)} & \text{if} \quad p_k^{[n]}=0 \quad \text{and} \quad p_{-k}^{[n]}=0 \\ \mathcal{O}_k^{(1)} & \text{if} \quad p_k^{[n]}=1 \quad \text{and} \quad p_{-k}^{[n]}=0 \\ \mathcal{O}_k^{(2)} & \text{if} \quad p_k^{[n]}=0 \quad \text{and} \quad p_{-k}^{[n]}=1 \\ \mathcal{O}_k^{(3)} & \text{if} \quad p_k^{[n]}=1 \quad \text{and} \quad p_{-k}^{[n]}=1 \end{cases} . \tag{5.38}$$

and

$$\rho_{k,\mu}^{[n]} \equiv \begin{cases} \rho_{k,\mu}^{(0)} & \text{if} \quad p_k^{[n]}=0 \quad \text{and} \quad p_{-k}^{[n]}=0 \\ \rho_{k,\mu}^{(1)} & \text{if} \quad p_k^{[n]}=1 \quad \text{and} \quad p_{-k}^{[n]}=0 \\ \rho_{k,\mu}^{(2)} & \text{if} \quad p_k^{[n]}=0 \quad \text{and} \quad p_{-k}^{[n]}=1 \\ \rho_{k,\mu}^{(3)} & \text{if} \quad p_k^{[n]}=1 \quad \text{and} \quad p_{-k}^{[n]}=1 \end{cases} . \tag{5.39}$$

Note that the ordering of $\mathcal{O}_k^{(\xi)}$ and $\rho_{k,\mu}^{(\xi)}$ according to ξ in the above equations follows the ordering in Eq. (5.26) for the case of the initial ground state, $r_k = r_{-k} = 0$. Equations (5.38) and (5.39), and the fact that the weights $\rho_{k,\mu}^{(\xi)}$ are normalized in the $\{k,-k\}$ subspaces, allows us to rewrite Eq. (5.37) as

$$\langle \hat{\mathcal{O}} \rangle_\mu = \sum_{k\in\mathcal{K}^{(+)}} \left(\sum_{\xi=0}^{3} \rho_{k,\mu}^{(\xi)} \mathcal{O}_k^{(\xi)} \right) . \tag{5.40}$$

We have already shown that the weights $\rho^{(\xi)}_{k,\mathrm{DE}}$ are normalized in the $\{k,-k\}$ subspaces. It is straightforward to show it for the GGE and the grand canonical ensemble. For example, for the GGE one can see from Eq. (5.36) that

$$\sum_{\xi=0}^{3}\rho^{(\xi)}_{k,\mathrm{GGE}}=\alpha_k^2+2\alpha_k(1-\alpha_k)+(1-\alpha_k)^2=1. \tag{5.41}$$

There is another important class of observables in the transverse field Ising model that can be straightforwardly evaluated in terms of single-particle contributions, but not as in Eq. (5.40). These observables, we call them $\hat{\mathcal{A}}$, can be written as

$$\langle\hat{\mathcal{A}}\rangle_\mu=\sum_n\rho_\mu^{[n]}\langle n|\hat{\mathcal{A}}_1|n\rangle\langle n|\hat{\mathcal{A}}_2|n\rangle, \tag{5.42}$$

where the expectation values $\langle\hat{\mathcal{A}}_1\rangle_\mu$ and $\langle\hat{\mathcal{A}}_2\rangle_\mu$ can be computed using Eq. (5.40). As a result, $\langle\hat{\mathcal{A}}\rangle_\mu$ reads:

$$\langle\hat{\mathcal{A}}\rangle_\mu=\langle\hat{\mathcal{A}}_1\rangle_\mu\langle\hat{\mathcal{A}}_2\rangle_\mu-\sum_{k\in\mathcal{K}^{(+)}}\left(\sum_{\xi=0}^{3}\rho^{(\xi)}_{k,\mu}\mathcal{A}^{(\xi)}_{1,k}\right)\left(\sum_{\xi'=0}^{3}\rho^{(\xi')}_{k,\mu}\mathcal{A}^{(\xi')}_{2,k}\right)+\sum_{k\in\mathcal{K}^{(+)}}\left(\sum_{\xi=0}^{3}\rho^{(\xi)}_{k,\mu}\mathcal{A}^{(\xi)}_{1,k}\mathcal{A}^{(\xi)}_{2,k}\right), \tag{5.43}$$

where $\mathcal{A}^{(\xi)}_{1,k}$ and $\mathcal{A}^{(\xi)}_{2,k}$ are defined as $\mathcal{O}^{(\xi)}_k$ is in Eq. (5.38).

Equations (5.40) and (5.43) allow us to calculate numerically, in polynomial time, various observables of interest for the transverse field Ising model, see Sec. 5.5.

5.4 Dynamics and the GGE in the XX model

In this section, we discuss the dynamics in the XX model after a quantum quench. We focus mostly on hard-core bosons and compare the results after relaxation to the predictions of the grand canonical ensemble and the GGE. As mentioned in the introduction, it was on hard-core boson systems for which it was first established the relevance of the GGE to describe equilibrated values of observables in isolated integrable systems [1, 36]. Here, we also discuss the behavior of noninteracting spinless fermions. We point out a fundamental difference between them and hard-core bosons in terms of equilibration and generalized thermalization.

5.4.1 Dynamics and generalized thermalization of hard-core boson systems

Some results for the first quench considered here have been already reported in Ref. [1].
(look at it ones!)
This quench was motivated by the experimental protocol followed by Kinoshita *et al* [17].
(???)
They pulsed a 1D lattice along an array of 1D Bose gases to take them far from equilibrium. The pulses generated peaks in the momentum distribution function of the bosons at multiples of the lattice wave-number. The oscillatory dynamics of those peaks was then studied by means of a special kind of time-of-flight measurements (the expansion was carried out in one dimension). Because of the observed oscillatory behavior of the peaks, this experiment is known as the quantum Newton's cradle.

The specific quench protocol we consider can be thought of as a simplified version of the experimental protocol. Our initial state is taken to be the ground state of hard-core bosons in the presence of a (superlattice) potential $V_j=A\cos(\frac{2\pi j}{T})$ [see Eq. (5.3)].

The period T is taken to be $T = 4$, and gives rise to four sharp peaks in the momentum distribution $m_k(t) = \langle\psi(t)|\hat{m}_k|\psi(t)\rangle$ at $t = 0$, as shown in Fig. 5.3(b). After the sudden turn off of the superlattice potential, $m_k(t)$ undergoes dynamics and relaxes to a new steady state distribution. We consider systems with 30 and 45 hard-core bosons in lattices with $L = 600$ and 900 sites, respectively, i.e., the average site occupation is very low (0.05). Because of this (the average interparticle distance is much larger than the lattice spacing), one can think of these systems as being in the continuum, which was the case studied in the experiments. The conserved quantities $\langle\hat{I}_q\rangle_0$ we use to construct the GGE [see Eq. (5.18)] are the occupations of the single-particle eigenstates of the final fermionic Hamiltonian (with open boundary conditions). Their distribution is shown in the left panel of Fig. 5.2.

In Fig. 5.3(a), we show the time evolution of $m_{k=0}(t)$ for the two system sizes considered. Remarkably, both can be seen to relax to the same steady-state result despite the fact that, because of quasi-long range order [80], the initial value of $m_{k=0}$ is different in both systems. By plotting $\tilde{m}_0(t) = [m_{k=0}(t) - m_{k=0}(t=0)]/m_{k=0}(t=0)$ vs t, one can see [inset in Fig. 5.3(a)] that the short time dynamics is essentially the same in both systems. Figure 5.3(a) also shows that the result after relaxation can be predicted by the GGE, and that it is clearly different from the grand canonical ensemble prediction. As mentioned before, whenever observables relax to the GGE predictions [as in Fig. 5.3(a)] we say that they exhibit generalized thermalization. We use the word "generalized" to differentiate this process from thermalization, namely, the relaxation to the predictions of traditional ensembles of statistical mechanics.

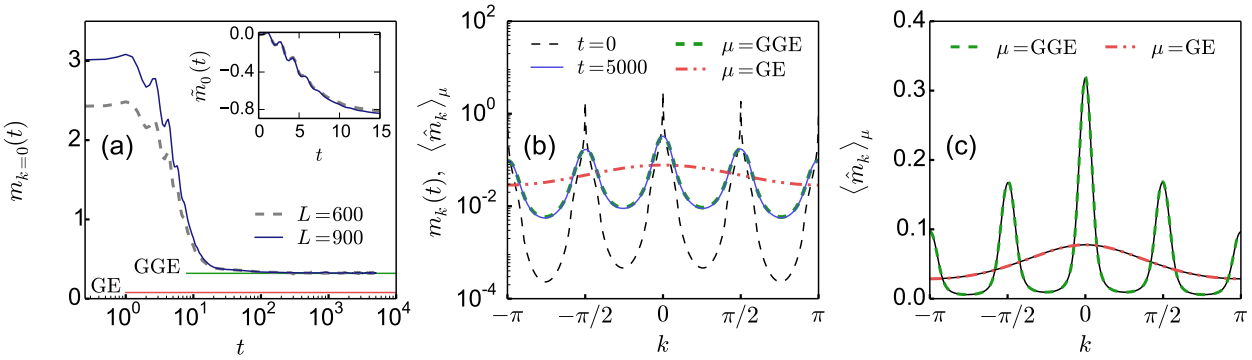

Figure 5.3: *Dynamics of the momentum distribution of hard-core bosons after a quantum quench and its description after relaxation.* The initial state is the ground state of $\hat{H}_{\rm XX}$, see Eq. (5.3), with a superlattice potential $V_j = 8\tilde{J}\cos(\pi j/2)$ and open boundary conditions. We consider systems with $N = 30$ and 45 hard-core bosons in $L = 600$ and 900 lattice sites, respectively, for which the average site occupancy is $n = N/L = 1/20$. At $t = 0$, the superlattice potential is turned off and the system is let evolve unitarily under $\hat{H}_{\rm XX}$. (a) Time evolution of $m_{k=0}(t)$ for $L = 600$ and 900. Horizontal lines denote the corresponding $\langle\hat{m}_{k=0}\rangle_{\rm GGE}$ and $\langle\hat{m}_{k=0}\rangle_{\rm GE}$ for $L = 900$. The inset displays the rescaled short-time evolution of $\tilde{m}_0(t)$ (see text) as a function of t. (b) The entire momentum distribution in the initial state ($t = 0$), at a long time after the quench ($t = 5000$ in units of $\hbar/\tilde{J}$), as well as $\langle\hat{m}_k\rangle_{\rm GGE}$ and $\langle\hat{m}_k\rangle_{\rm GE}$, for $L = 900$. (c) Results for $\langle\hat{m}_k\rangle_{\rm GGE}$ and $\langle\hat{m}_k\rangle_{\rm GE}$ in the system with $L = 600$ (thin solid lines) and $L = 900$ (thick dashed lines). The results for $L = 600$ were taken from Ref. [1].

(how to obtain this plot?????)

That generalized thermalization occurs in these systems is better seen in Fig. 5.3(b), in which we plot the entire momentum distribution functions in the initial state, at $t = 5000$ (in units of $\hbar/\tilde{J}$), as well as in the GGE and in the grand canonical ensemble. It is most remarkable that, after relaxation, the momentum distribution function of the hard-core bosons

retains information about the initial state by exhibiting four clearly resolved peaks at the same positions as in the initial state. The GGE accurately describes the entire momentum distribution after relaxation. This is in stark contrast to the prediction from the grand canonical ensemble [see Eq. (5.16)], which only exhibits a single broad peak (as expected in a system with no additional lattice). By comparing the results for systems with $L = 600$ and 900 lattices sites in Fig. 5.3(c), one can see that finite-size effects are negligible for the system sizes considered, i.e., one could think of these results as being in the thermodynamic limit.

An important question that needs to be addressed at this point is how the time fluctuations of observables, about the steady state result, behave with increasing system size. For hard-core bosons, this was studied in Refs. [51, 52, 71], while for noninteracting spinless fermions this was studied in Refs. [90, 266, 260, 93]. In the absence of localization due to disorder or quasi-periodic potentials, a remarkable finding has been that all one-body observables studied for hard-core bosons exhibit time fluctuations that decrease with increasing system size (as $1/L^{\kappa}$, with $\kappa = 1/2$ or 1). In contrast, some one-body observables for noninteracting spinless fermions do not equilibrate, while others exhibit time fluctuations that decrease with increasing system size (as $1/\sqrt{L}$). A decay of the time fluctuations as $1/\sqrt{L}$ is the characteristic scaling of the Gaussian equilibration scenario proposed in Ref. [90] for noninteracting spinless fermions.

To exemplify the starkly different behavior of some one-body observables for hard-core bosons and noninteracting spinless fermions, we review results from Ref. [52]. There, Wright *et al* studied the dynamics of systems initially prepared in the ground state of a box with twice as many sites as particles, which was then opened in a larger box with four times as many sites as particles (this kind of protocol is sometimes referred to as a geometric quench [94, 95]). A central quantity in that study was the distance between the instantaneous and the GGE momentum distribution, defined as

$$\Delta\mathcal{M}(t) = \frac{\sum_k |m_k(t) - \langle \hat{m}_k \rangle_{\rm GGE}|}{\sum_k \langle \hat{m}_k \rangle_{\rm GGE}}. \tag{5.44}$$

Figure 5.4(b) shows that, at long times, $\Delta\mathcal{M}(t)$ for hard-core bosons decreases with increasing system size. A finite-size scaling analysis of its average $\overline{\Delta\mathcal{M}(t)}$ reveals a power-law decrease $\propto 1/L$ [see Fig. 5.4(c)]. In contrast, one can clearly see in Figs. 5.4(a) and 5.4(c) that for noninteracting spinless fermions the average at long times does not decrease with increasing system size. One might think that this is the result of the fermionic momentum distribution function relaxing to something different from the GGE prediction. However, this is not the case, one can actually prove that the time average of all one-body observables in a noninteracting fermionic system is exactly equal to the GGE prediction, without any finite-size correction [260, 93].

The proof is straightforward if one uses the fact that the eigenstates of the many-body Hamiltonian are products of single-particle eigenstates [93]. Projecting $\hat{\rho}(t) = |\psi(t)\rangle\langle\psi(t)|$ onto the one-body sector, the time-evolving one-body density matrix takes the form

$$\hat{\rho}_{\rm ob}(t) = \sum_{q,q'} c_{qq'} e^{-i(\varepsilon_q - \varepsilon_{q'})t} |q\rangle\langle q'|. \tag{5.45}$$

In the absence of degeneracies in the single-particle spectrum (which is the case for the systems studied in this subsection), the infinite-time average of $\hat{\rho}_{\rm ob}(t)$ can be written as

$$\overline{\hat{\rho}_{\rm ob}(t)} = \lim_{t'\to\infty} \frac{1}{t'} \int_0^{t'} dt\, \hat{\rho}_{\rm ob}(t) = \sum_q \langle \hat{I}_q \rangle_0 |q\rangle\langle q|, \tag{5.46}$$

which is, by construction, the one-body density matrix in the GGE.

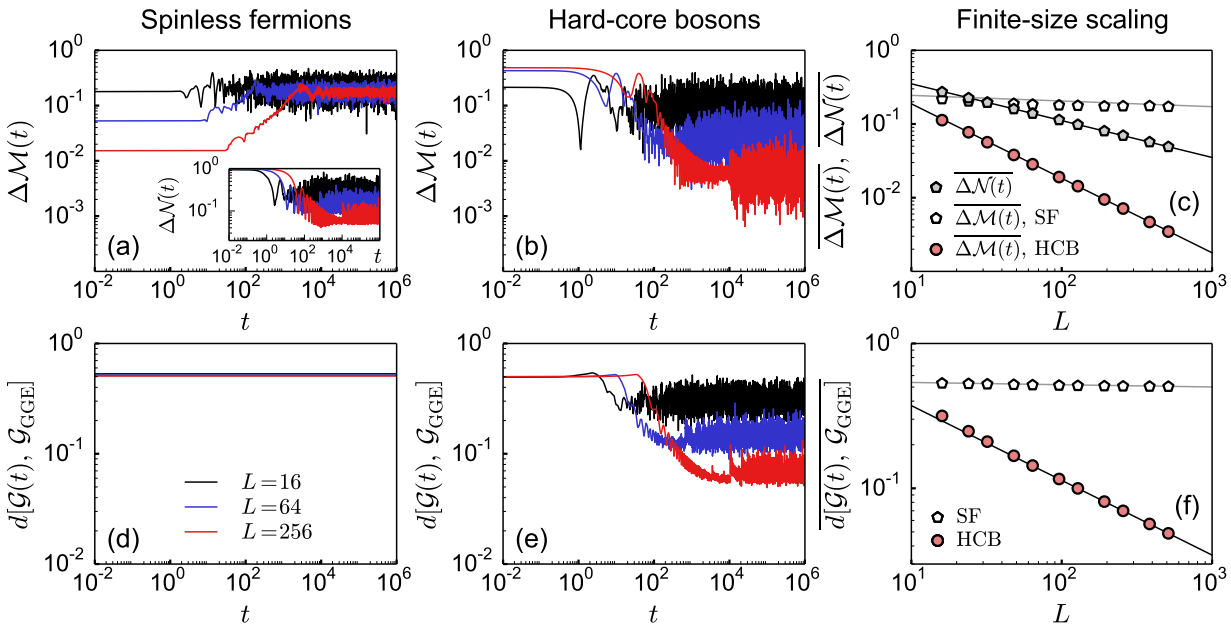

Figure 5.4: *Dynamics of the momentum distribution, site occupations and the trace distance after a quantum quench.* The initial state is the ground state of $\hat{H}_{\rm XX}$, see Eq. (5.3), in a box potential for a system with twice as many sites as particles N. The box is then opened in a larger box of size $L = 4N$. (a),(b) Distance between the instantaneous and the GGE momentum distribution $\Delta\mathcal{M}(t)$, Eq. (5.44), for spinless fermions (SF) and hard-core bosons (HCB), respectively. The inset in (a) shows the distance between the instantaneous and the GGE site occupations $\Delta\mathcal{N}(t)$, Eq. (5.47). (c) The average values of $\Delta\mathcal{M}(t)$ and $\Delta\mathcal{N}(t)$, in the time interval $t \in [10^5, 10^6]$, are plotted as a function of the system size L. Black solid lines are power-law fits $aL^{-\kappa}$ for $L \geq 96$, yielding $a = 1.93$, $\kappa = 1.01$ for $\overline{\Delta\mathcal{M}(t)}$ of hard-core bosons, and $a = 1.11$, $\kappa = 0.50$ for $\overline{\Delta\mathcal{N}(t)}$. (d),(e) The trace distance $d[\mathcal{G}(t), \mathcal{G}_{\rm GGE}]$, Eq. (5.48), is shown for the same systems as in (a),(b), respectively. (f) The average value of $d[\mathcal{G}(t), \mathcal{G}_{\rm GGE}]$, in the time interval $t \in [10^5, 10^6]$, is plotted as a function of the system size L. The black solid line is a power-law fit for hard-core bosons for the same lattice sizes as in (c), yielding $a = 1.22$ and $\kappa = 0.52$. Data taken from Ref. [52].

In contrast to the momentum distribution function, results for the distance between the instantaneous and the GGE site occupations

$$\Delta\mathcal{N}(t) = \frac{\sum_i |n_i(t) - \langle \hat{n}_i \rangle_{\rm GGE}|}{\sum_i \langle \hat{n}_i \rangle_{\rm GGE}}, \tag{5.47}$$

which is the same for hard-core bosons and spinless fermions, show that this quantity does decrease with increasing system size [see the inset of Fig. 5.4(a)]. A finite-size scaling in Fig. 5.4(c) reveals that, at long times, the average $\overline{\Delta\mathcal{N}(t)}$ decreases as $1/\sqrt{L}$.

5.4.2 Noninteracting vs interacting systems mappable to noninteracting ones

The results for one-body observables in the previous section, in which two observables exhibited equilibration for hard-core bosons, while only one exhibited it for noninteracting fermions, open the question of whether there will be non-equilibrating one-body observables for hard-core bosons of which we are not aware of. After all, hard-core bosons can be mapped onto noninteracting fermions, for which we already found a non-equilibrating one-body observable.

In order to answer this question, Wright *et al* studied the dynamics of the trace distance between the instantaneous and the GGE one-body density matrices [52]

$$d[\mathcal{G}(t),\mathcal{G}_{\rm GGE}]=\frac{1}{2N}{\rm Tr}\left[\sqrt{[\mathcal{G}(t)-\mathcal{G}_{\rm GGE}]^2}\right], \tag{5.48}$$

where $\mathcal{G}(t)$ is the instantaneous one-body density matrix, with elements $\mathcal{G}_{j,l}(t)=\langle\psi(t)|\hat{b}_j^\dagger\hat{b}_l|\psi(t)\rangle$ and $\langle\psi(t)|\hat{f}_j^\dagger\hat{f}_l|\psi(t)\rangle$ for hard-core bosons and noninteracting fermions, respectively, and $\mathcal{G}_{\rm GGE}$ is the one-body density matrix in the GGE, with matrix elements $\langle\hat{\mathcal{G}}_{j,l}\rangle_{\rm GGE}=\langle\hat{b}_j^\dagger\hat{b}_l\rangle_{\rm GGE}$ and $\langle\hat{f}_j^\dagger\hat{f}_l\rangle_{\rm GGE}$.

In Figs. 5.4(d) and 5.4(e), we plot the time evolution of the trace distance for the same systems as in Figs. 5.4(a) and 5.4(b). The plots show that while the trace distance for hard-core bosons decreases with increasing system size, the trace distance for fermions is constant. The latter is the result of the unitary dynamics of the fermionic one-body sector (the fermions are noninteracting) [52]. The finite-size scaling analysis in Fig. 5.4(f) reveals that the time average of $d[\mathcal{G}(t),\mathcal{G}_{\rm GGE}]$ for hard-core bosons at long times decreases as $1/\sqrt{L}$. Such a power-law decay provides an upper bound for the decay of the time fluctuations in all one-body bases (not only the site and momentum occupations). It shows that no extensive set of one-body observables exists in the hard-core boson system that will fail to exhibit generalized thermalization. This provides an alternative view to generalized thermalization in a closed system where the bath is usually thought of as the physical region of the system that is traced out. Here, the bath is provided by the $N-1$ particles that have been traced out.

Wright *et al* also studied hard-core anyons, which interpolate smoothly between hard-core bosons and noninteracting spinless fermions, while still being mappable onto the latter. Remarkably, they showed that hard-core anyons exhibit generalized thermalization in the same manner as hard-core bosons do, namely, the average of $d[\mathcal{G}(t),\mathcal{G}_{\rm GGE}]$ at long times vanishes with increasing system size as $1/\sqrt{L}$. This makes apparent that noninteracting fermions are a singular limit in this family of models. They are fundamentally different from the interacting models (hard-core bosons and anyons) that were mapped onto them. This is because, in noninteracting fermionic systems, extensive sets of one-body observables can fail to equilibrate, and, hence, can fail to exhibit generalize thermalization, while no such failure can occur for hard-core bosons and anyons. This is made explicit by the fact that the trace distance $d[\mathcal{G}(t),\mathcal{G}_{\rm GGE}]$ for spinless fermions is nonzero and constant in time, while the average of $d[\mathcal{G}(t),\mathcal{G}_{\rm GGE}]$ for hard-core bosons (anyons) at long times vanishes with increasing system size.

We should stress that in the quenches discussed in this section neither the initial state nor the final Hamiltonian exhibit translational invariance. Lack of translational invariance is a feature common to the quenches studied in Refs. [1, 36, 51, 52, 71], in which the GGE was also shown to predict the equilibrated values of observables in isolated integrable systems. Hence, the success of the GGE is in no way tied to translational invariance. We note that, because of open boundary conditions, the single-particle spectrum of the final Hamiltonian in the quenches discussed here (and in Refs. [1, 36, 51, 52, 71]) is nondegenerate. Extensive degeneracies in the single-particle spectrum after a quench, which occur when a system is translationally invariant, can be the source of subtleties in the GGE that is needed to describe observables after relaxation following a quench [42], specially from initial states that are not translationally invariant [96].

5.5 Ensembles in the transverse field Ising model

This section is devoted to the study of the paradigmatic transverse field Ising model. We consider different statistical ensembles in finite systems and study generalized thermalization of few-body observables.

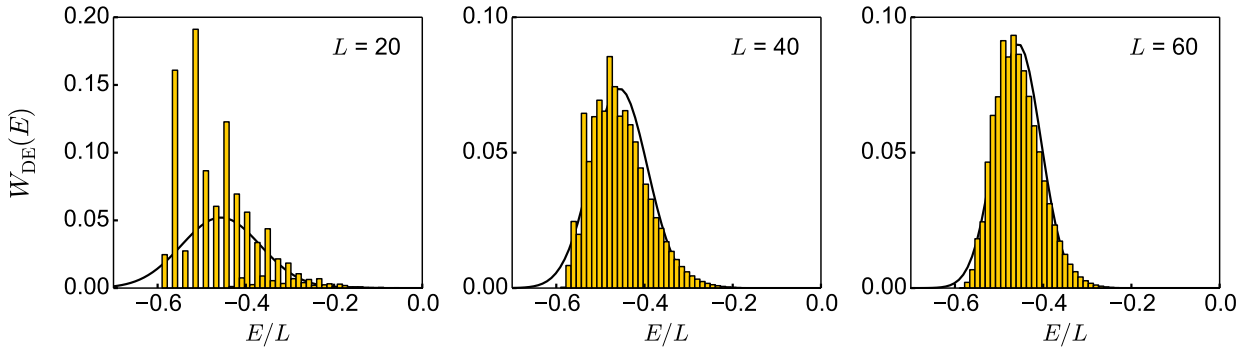

Figure 5.5: *Histogram of the energy distribution in the diagonal ensemble* $W_{\rm DE}(E)$ *for the transverse field Ising model.* We quench the transverse field from $h_0 = 4.0$ to $h = 0.8$. Solid lines are Gaussian functions $g(E) = \varepsilon_E/(\sqrt{2\pi}\sigma)e^{-(E-\bar{E})^2/(2\sigma^2)}$ with the mean energy $\bar{E} = \langle \hat{H} \rangle_{\rm DE}/L = -0.457$ (the ground-state energy for $h = 0.8$ is $E_{\rm gs}/L = -0.584$). We set the bin width $\varepsilon_E = 2|E_{\rm gs}|/100$. The width of $g(E)$ is $\sigma = \sigma_{\hat{H},{\rm DE}}/L$, where $\sigma_{\hat{H},{\rm DE}} = 0.4\sqrt{L}$ according to Eq. (5.54).

Many works in the last twenty years have studied the dynamics of the transverse field Ising model in finite chains [97, 98, 99, 100, 101, 102, 103]. However, we are not aware of studies that compare results obtained within the diagonal ensemble and the GGE. Here, we are particularly interested on how the differences between the predictions of those ensembles scale with the system size. We also report results for the predictions of the grand canonical ensemble (5.17).

We study quenches from the ground state at the transverse field h_0, to the final field h. Most of the ingredients needed to calculate the quantities discussed in this section were presented in Sec. 5.3. In some cases, the comparison between the diagonal ensemble and the GGE can be done at the level of analytic expressions. These are possible due to the noninteracting nature of the Hamiltonian (5.8).

5.5.1 Energy distributions

We start by analyzing the decomposition of statistical weights in the energy eigenbasis, i.e., the so-called energy distribution. In the diagonal ensemble, the energy distribution is defined as

$$W_{\rm DE}(E) = \sum_n |c_n|^2 \delta(E - E_n), \tag{5.49}$$

where E_n are the eigenenergies of the final Hamiltonian and $|c_n|^2$ are the weights of the initial state in the eigenstates of the final Hamiltonian [see Eq. (5.13)]. Coarse grained results for $W_{\rm DE}(E)$ are shown in Fig. 5.5, for quenches from the paramagnetic ground state to the ferromagnetic regime, and in Fig. 5.6, for quenches from the ferromagnetic ground state to the paramagnetic regime. In both cases, we consider chains with three different sizes. Our results show that, with increasing system size, $W_{\rm DE}(E)$ can be well approximated by a Gaussian function with the mean energy and the energy width of the diagonal ensemble.

The mean energy is calculated using Eq. (5.40) and the overlaps from Eq. (5.34)

$$\langle \hat{H} \rangle_{\rm DE} = \sum_{k \in \mathcal{K}^{(+)}} [\alpha_k(-\varepsilon_k) + (1-\alpha_k)\varepsilon_k] = -\sum_{k \in \mathcal{K}^{(+)}} (2\alpha_k - 1)\varepsilon_k, \tag{5.50}$$

where ε_k is the single-particle energy (5.9) and α_k has been defined in Eq. (5.28). The width is computed from

$$\sigma^2_{\hat{H},{\rm DE}} = \langle \hat{H}^2 \rangle_{\rm DE} - \langle \hat{H} \rangle^2_{\rm DE}. \tag{5.51}$$

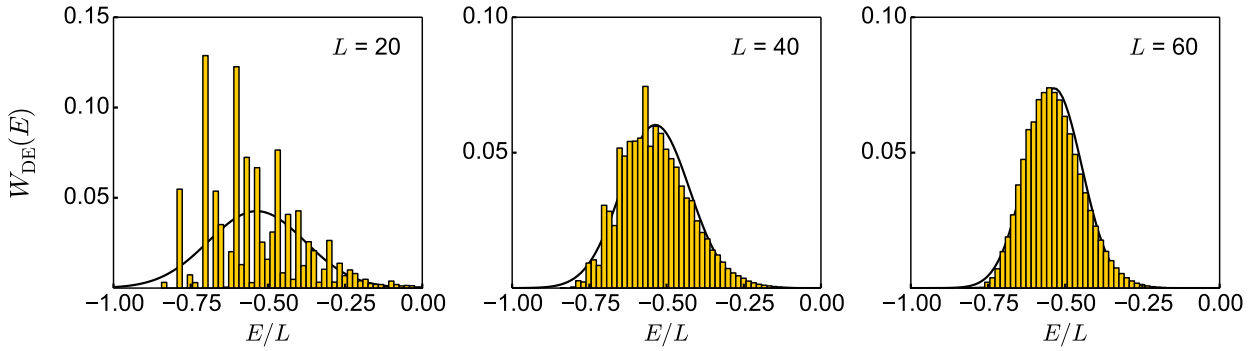

Figure 5.6: *Histogram of the energy distribution in the diagonal ensemble* $W_{\mathrm{DE}}(E)$ *for the transverse field Ising model.* We quench the transverse field from $h_0 = 0.1$ to $h = 1.5$. Solid lines are Gaussian functions $g(E) = \varepsilon_E/(\sqrt{2\pi}\sigma)e^{-(E-\bar{E})^2/(2\sigma^2)}$ with the mean energy $\bar{E} = \langle\hat{H}\rangle_{\mathrm{DE}}/L = -0.536$ (the ground-state energy for $h = 1.5$ is $E_{\mathrm{gs}}/L = -0.836$). We set the bin width $\varepsilon_E = 2|E_{\mathrm{gs}}|/100$. The width of $g(E)$ is $\sigma = \sigma_{\hat{H},\mathrm{DE}}/L$, where $\sigma_{\hat{H},\mathrm{DE}} = 0.7\sqrt{L}$ according to Eq. (5.54).

Since $\langle n|\hat{H}^2|n\rangle = \langle n|\hat{H}|n\rangle\langle n|\hat{H}|n\rangle$ in the energy eigenbasis, using Eq. (5.43), it follows that

$$\langle\hat{H}^2\rangle_{\mathrm{DE}} = \langle\hat{H}\rangle^2_{\mathrm{DE}} - \sum_{k\in\mathcal{K}^{(+)}}\left[\alpha_k(-\varepsilon_k) + (1-\alpha_k)\varepsilon_k\right]^2 + \sum_{k\in\mathcal{K}^{(+)}}\left[\alpha_k(-\varepsilon_k)^2 + (1-\alpha_k)\varepsilon_k^2\right], \tag{5.52}$$

which results in

$$\sigma^2_{\hat{H},\mathrm{DE}} = \sum_{k\in\mathcal{K}^{(+)}} 4\alpha_k(1-\alpha_k)\varepsilon_k^2. \tag{5.53}$$

Furthermore, by inserting the expressions for ε_k and α_k in Eq. (5.53) and taking the continuum limit, one obtains that the width of the energy distribution after the quench is

$$\frac{\sigma_{\hat{H},\mathrm{DE}}}{\sqrt{L}} = \begin{cases} \frac{1}{2}\left|1-\frac{h}{h_0}\right| & \text{if } h_0 > 1 \\ \frac{1}{2}h_0\left|1-\frac{h}{h_0}\right| & \text{if } h_0 < 1 \end{cases}. \tag{5.54}$$

We then see that the width is maximal for quenches $(h_0 = 0) \to (h \to \infty)$, and vice versa. Such quenches result in $\langle\hat{H}\rangle_{\mathrm{DE}} = 0$, which, in turn, corresponds to the energy in the grand canonical ensemble at infinite temperature. In the latter ensemble, one can calculate the width $\sigma_{\hat{H},\infty} \equiv \sigma_{\hat{H},\mathrm{GE}}(T\to\infty)$ analytically to get

$$\frac{\sigma_{\hat{H},\infty}}{\sqrt{L}} = \frac{\sqrt{1+h^2}}{2}. \tag{5.55}$$

This width agrees with the one in the limiting cases in the diagonal ensemble in which the field is quenched from zero to infinity or vice versa. A similar agreement between the widths in the diagonal ensemble and in the canonical ensemble was discussed in the Bose-Hubbard model for quenches of the onsite repulsion from infinite to zero [88].

By performing an analysis for the GGE similar to the one carried out for the diagonal ensemble, one finds that

$$\langle\hat{H}^2\rangle_{\mathrm{GGE}} = \langle\hat{H}\rangle^2_{\mathrm{GGE}} - \sum_{k\in\mathcal{K}^{(+)}}\left[\alpha_k^2(-\varepsilon_k) + (1-\alpha_k)^2\varepsilon_k\right]^2 + \sum_{k\in\mathcal{K}^{(+)}}\left[\alpha_k^2(-\varepsilon_k)^2 + (1-\alpha_k)^2\varepsilon_k^2\right], \tag{5.56}$$

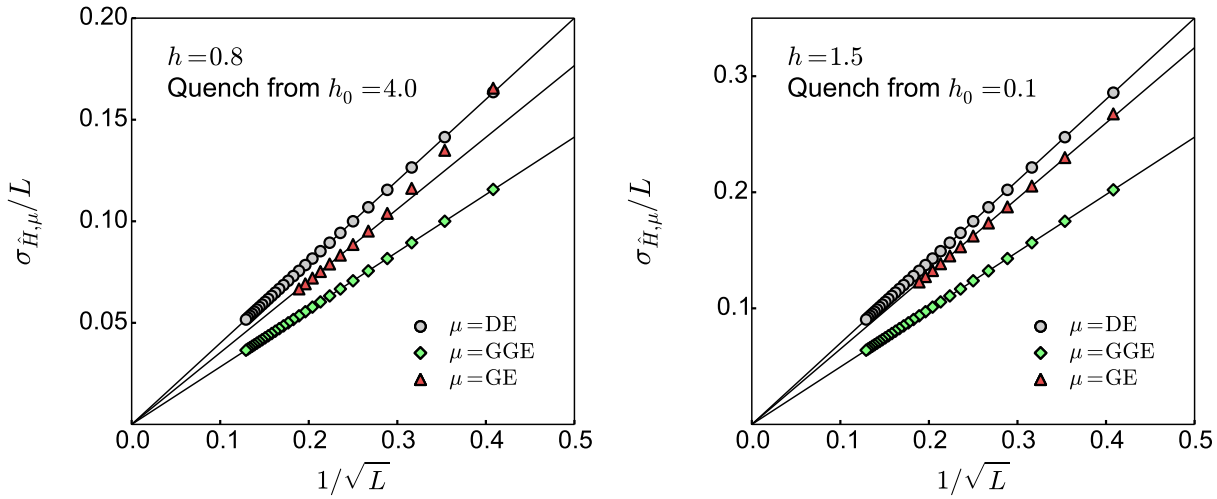

Figure 5.7: *Width of the energy distribution in the GGE, the grand canonical ensemble, and the diagonal ensemble.* Numerical results (symbols) are presented for quenches from $h_0 = 4.0$ to $h = 0.8$ (left panel) and $h_0 = 0.1$ to $h = 1.5$ (right panel), and are plotted as a function of $1/\sqrt{L}$. The lines following the results for the diagonal ensemble are $\sigma_{\hat{H},\mathrm{DE}} = 0.4\sqrt{L}$ (left panel) and $\sigma_{\hat{H},\mathrm{DE}} = 0.7\sqrt{L}$ (right panel), see Eq. (5.54). The lines following the results for the grand canonical ensemble are linear fits for $L \geq 16$, $\sigma_{\hat{H},\mathrm{GE}} = c_{\mathrm{GE}}\sqrt{L}$ with $c_{\mathrm{GE}} = 0.353$ (left panel) and $c_{\mathrm{GE}} = 0.649$ (right panel). For the GGE, $\sigma_{\hat{H},\mathrm{DE}}/\sigma_{\hat{H},\mathrm{GGE}} = \sqrt{2}$ is an exact result (see the derivation of Eq. (5.57)).

so that $\sigma^2_{\hat{H},\mathrm{GGE}} = \sum_{k\in\mathcal{K}^{(+)}} 2\alpha_k(1-\alpha_k)\varepsilon_k^2$. Therefore, the ratio of the widths of the energy distribution in the diagonal ensemble and the GGE is

$$\frac{\sigma_{\hat{H},\mathrm{DE}}}{\sigma_{\hat{H},\mathrm{GGE}}} = \sqrt{2}, \tag{5.57}$$

irrespective of the system size. This result can be intuitively understood already at the level of occupancies within a single $\{k,-k\}$ subspace. The diagonal ensemble only contains states with either both k-states empty or occupied (these states have energies $-\varepsilon_k$ and ε_k), while in the GGE all four states, including the ones with zero energy, have nonzero weight. By taking into account the appropriate weights [see Eqs. (5.34) and (5.36)] in both ensembles, one already recovers the factor $\sqrt{2}$ in Eq. (5.57).

In Fig. 5.7, we compare the scaling of the width of the energy distribution in the diagonal ensemble, the GGE, and in the corresponding grand canonical ensemble. In the latter, we calculated the temperature by computing the trace in Eq. (5.17) exactly, i.e., by taking the appropriate the sets of wave vectors $\mathcal{K}^{(+)}$ and $\mathcal{K}^{(-)}$ in the even and odd sectors, respectively. We report results for two quenches, one from the paramagnetic ground state to the ferromagnetic regime (left panel) and one from the ferromagnetic ground state to the paramagnetic regime (right panel). In all cases under consideration, $\sigma_{\hat{H},\mathrm{GE}}$ is smaller than $\sigma_{\hat{H},\mathrm{DE}}$, but larger than $\sigma_{\hat{H},\mathrm{GGE}}$. Figure 5.7 also shows that, as predicted for the diagonal ensemble and as expected for the grand canonical one, the energy widths vanish as $1/\sqrt{L}$ with increasing system size. That scaling of the widths is generic in quantum quenches within local Hamiltonians [6], no matter whether they are integrable or not.

In Fig. 5.8(a)–5.8(d), we plot $\sigma_{\hat{H},\mathrm{DE}}$, $\sigma_{\hat{H},\mathrm{GGE}}$ and $\sigma_{\hat{H},\mathrm{GE}}$ (rescaled by the infinite temperature result) for four different values of the final field h, and for an extended range of initial fields

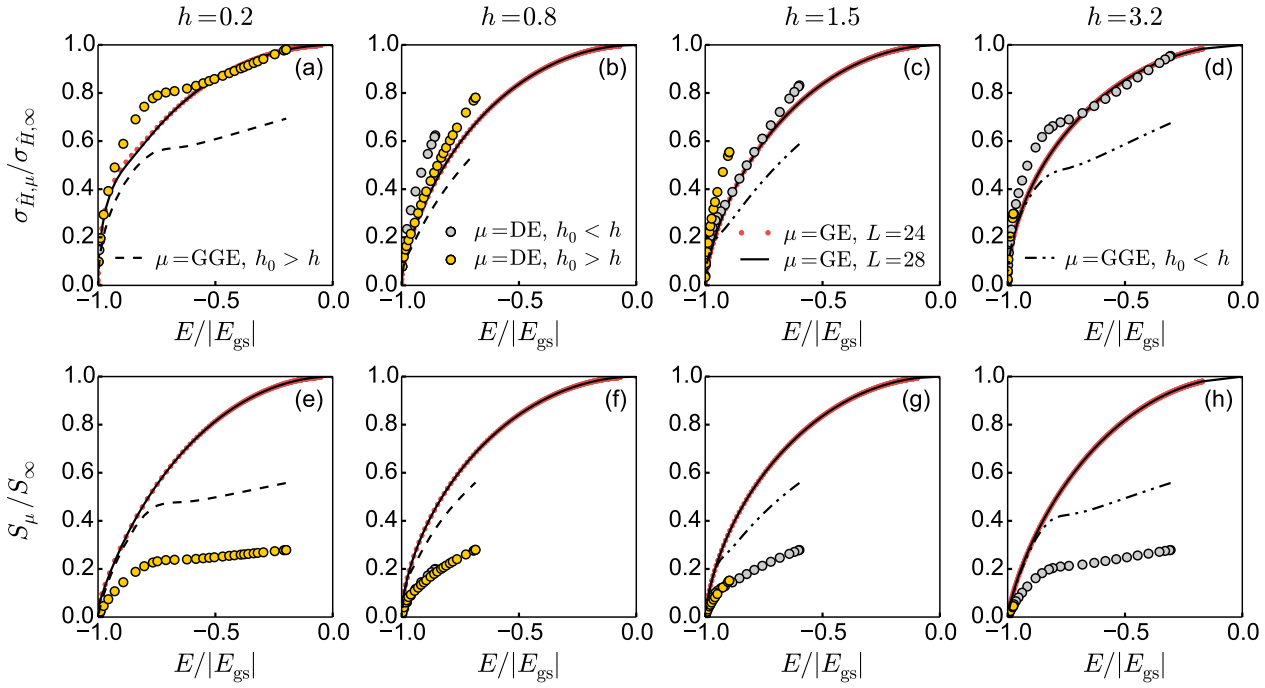

Figure 5.8: *Width of the energy distribution and entropy in the GGE, the grand canonical ensemble, and the diagonal ensemble.* (a)-(d) $\sigma_{\hat{H},\rm DE}$, $\sigma_{\hat{H},\rm GGE}$ and $\sigma_{\hat{H},\rm GE}$, (e)-(h) $S_{\rm DE}$, $S_{\rm GGE}$ and $S_{\rm GE}$, vs the mean energy (relative to the ground state) after quenches for many different values of h_0. Results are reported for four values of the field h after the quench (each column). For the diagonal ensemble, the values of the field h_0 ranged from 0.001 to 5000. For the GGE, $\sigma_{\hat{H},\rm DE}/\sigma_{\hat{H},\rm GGE} = \sqrt{2}$ and $S_{\rm GGE}/S_{\rm DE} = 2$. Black dashed lines correspond to quenches from $h_0 > h$ [panels (a)-(b) and (e)-(f), $h = 0.2$ and $h = 0.8$], and black dotted-dashed lines to quenches from $h_0 < h$ [panels (c)-(d) and (g)-(h), $h = 1.5$ and $h = 3.2$]. For the grand canonical ensemble, the solid lines are the exact results for $L = 28$. Red dotted lines, which in almost all cases overlap with solid lines, are shown for comparison and depict results for $L = 24$. All results are normalized to the $T = \infty$ values $\sigma_{\hat{H},\infty} = \sqrt{1+h^2}/2$, see Eq. (5.55), and $S_\infty = k_{\rm B} \log \mathcal{D}$.

h_0. These results provide an overview for when the widths of the diagonal and grand canonical ensembles are close to each other and when they are significantly different. In addition, Figs. 5.8(b) and 5.8(c) demonstrate how quenches that lead to the same mean energy can result in markedly different widths of the underlying diagonal ensemble (and, hence, of the GGE). The energy distributions $W_{\rm DE}(E)$ in Figs. 5.5 and 5.6, which are well fitted by a Gaussian function, may lead one to incorrectly conclude that the initial states considered sample "ergodically" the eigenstates of the final Hamiltonian and may result in true thermalization. The fact that this does not happen is what we discuss in the next sections.

5.5.2 Entropies

The results in the previous subsection make apparent that, by looking at coarse grained energy distributions, it might not be possible to differentiate an integrable from a nonintegrable system after a quench. This is where entropy calculations, in particular the calculation of the entropy in the diagonal ensemble [134, 125], make a difference. The entropies in the GGE,

diagonal, and grand canonical ensembles are computed as

$$S_\mu = -k_\mathrm{B}\mathrm{Tr}[\hat{\rho}_\mu \log \hat{\rho}_\mu], \tag{5.58}$$

where $\mu =$ GGE, DE, and GE, respectively.

Since the weights in all the ensembles factorize, Eq. (5.58) has the same structure as the expectation value of observables $\langle \hat{\mathcal{O}} \rangle_\mu$ in Eq. (5.37). Using Eq. (5.40) one can therefore express S_μ as the sum of single-particle contributions

$$S_\mu = -k_\mathrm{B} \sum_{k \in \mathcal{K}^{(+)}} \left(\sum_{\xi=0}^{3} \rho_{k,\mu}^{(\xi)} \log \rho_{k,\mu}^{(\xi)} \right). \tag{5.59}$$

The entropies in the diagonal ensemble and the GGE can be evaluated straightforwardly by inserting the weights in Eqs. (5.34) and (5.36), respectively, into Eq. (5.59). This yields

$$S_\mathrm{DE} = -k_\mathrm{B} \sum_{k \in \mathcal{K}^{(+)}} \left[\alpha_k \log(\alpha_k) + (1-\alpha_k) \log(1-\alpha_k) \right], \tag{5.60}$$

while in the GGE, one gets

$$\begin{aligned} &= -k_\mathrm{B} \sum_{k \in \mathcal{K}^{(+)}} \left[\alpha_k^2 \log(\alpha_k^2) + 2\alpha_k(1-\alpha_k) \log(\alpha_k(1-\alpha_k)) + (1-\alpha_k)^2 \log(1-\alpha_k)^2 \right] \\ &= -2k_\mathrm{B} \sum_{k \in \mathcal{K}^{(+)}} \left[\alpha_k \log(\alpha_k) + (1-\alpha_k) \log(1-\alpha_k) \right]. \end{aligned} \tag{5.61}$$

Closely related to what we found for the energy widths, the ratio

$$\frac{S_\mathrm{GGE}}{S_\mathrm{DE}} = 2 \tag{5.62}$$

is independent of the system size and also independent of the choice of the initial eigenstate. For an initial eigenstate that is not the ground state, the weights will in general differ from the ones in the expressions above. This occurs when, for a given $\{k, -k\}$ subspace, the overlap is nonzero only for one state (the case when $r_k \neq r_{-k}$). If that is the case, $\rho_{k,\mu}^{(\xi)}$ can only take values 1 or 0 and hence this subspace does not appear neither in S_DE nor in S_GGE, keeping their ratio unchanged. The factor 2 in Eq. (5.62) reflects the fact that the number of states that can have nonzero weight in the GGE is the square of the number of states that can have nonzero weight in the diagonal ensemble. Of course, the latter condition alone does not guarantee the result in Eq. (5.62). One also needs a special structure in the weights in the GGE and the diagonal ensemble. This doubling of the entropy in the GGE when compared to the diagonal ensemble has been discussed before in the context of the transverse field Ising model [138, 139] and for impenetrable bosons with contact interactions in one dimension [140].

In Figs. 5.8(e)-5.8(h), we show results for the diagonal, grand canonical, and the GGE entropies for the same quenches for which results were shown for the width of the energy distribution in Figs. 5.8(a)-5.8(d). The grand canonical entropy was calculated exactly on a finite system taking into account the proper sets of wave-numbers. The results reported were checked to have negligible finite-size effects. Two things to be remarked here is that the entropy in the diagonal ensemble is extensive, and that it exhibits extensive differences with the entropy of the grand canonical ensemble. Hence, the number of states involved in both ensembles increases exponentially with L, but their ratio vanishes with increasing L, i.e., the diagonal ensemble contains a vanishingly (exponentially) small fraction of the states in the grand canonical one. Recently, evidence has been reported that, for (generic) experimentally relevant initial states, the same happens in the thermodynamic limit in quenches to integrable models that cannot be mapped onto noninteracting ones [109, 130].

5.5.3 Generalized thermalization of spin correlations

Local observables.

The simplest local observable is the on-site magnetization $\hat{S}^z_j$. It was already pointed out in Ref. [100] that its expectation value in the GGE equals its long-time expectation value. Here we compare it to the expectation value computed in the diagonal ensemble.

The eigenstate expectation values for this observable equal

$$\langle n|\hat{S}^z_j|n\rangle = \frac{1}{L}\sum_k \left[|v_k|^2\left(1-p_k^{[n]}\right)+|u_k|^2 p_k^{[n]}\right]-\frac{1}{2}, \tag{5.63}$$

where the sum runs over all wave vectors[9]. The coefficients v_k and u_k have been introduced in the context of Eq. (5.8) and equal $|v_k|^2=(1-a_k/\varepsilon_k)/2$ and $|u_k|^2=(1+a_k/\varepsilon_k)/2$. Since the system under consideration is translationally invariant, the site index j does not appear on the r.h.s. of Eq. (5.63). An important insight we get from Eq. (5.63) is how to express $\langle n|\hat{S}^z_j|n\rangle$ as a sum of single-particle contributions. This allows us to calculate the expectation value of $\hat{S}^z_j$ in both the diagonal ensemble and the GGE using Eq. (5.40).

In the diagonal ensemble, we get

$$\langle \hat{S}^z_j\rangle_{\mathrm{DE}} = \frac{1}{L}\sum_{k\in\mathcal{K}^{(+)}} 2\left[\alpha_k|v_k|^2+(1-\alpha_k)|u_k|^2\right]-\frac{1}{2} = -\frac{1}{L}\sum_{k\in\mathcal{K}^{(+)}}(2\alpha_k-1)\,\frac{a_k}{\varepsilon_k}, \tag{5.64}$$

and in the GGE, we get

$$\langle \hat{S}^z_j\rangle_{\mathrm{GGE}} = \frac{1}{L}\sum_{k\in\mathcal{K}^{(+)}}\left[2\alpha_k^2|v_k|^2+2\alpha_k(1-\alpha_k)(|v_k|^2+|u_k|^2)+2(1-\alpha_k)^2|u_k|^2\right]-\frac{1}{2}. \tag{5.65}$$

Simplifying the latter expression results in

$$\langle \hat{S}^z_j\rangle_{\mathrm{GGE}} = \langle \hat{S}^z_j\rangle_{\mathrm{DE}}, \tag{5.66}$$

independently of the system size. This is an interesting result given that, in finite systems, our results for the GGE are approximate. The grand canonical trace we used did not account for the difference in boundary conditions between the even and odd sectors.

The standard procedure to calculate expectation values of off-diagonal operators $\hat{S}^a_j\hat{S}^a_{j+r}$ (with $a=\{x,y,z\}$ and $r\geq 1$) in many-body eigenstates $\{|n\rangle\}$ is to use the fermionic representation and express the Jordan-Wigner transformation (5.4) in terms of Majorana fermions using $e^{i\pi\hat{f}_l^\dagger\hat{f}_l}=\hat{F}^x_l\hat{F}^y_l$, where $\hat{F}^x_l=\hat{f}^\dagger_l+\hat{f}_l$ and $\hat{F}^y_l=\hat{f}^\dagger_l-\hat{f}_l$ [1]. This allows one to express the operators $\hat{S}^a_j\hat{S}^a_{j+r}$ in terms of a string of local fermionic operators acting from site j to site $j+r$. Since the model is quadratic, the application of Wick's theorem further decomposes the expectation values of a string of local operators in products of expectation values of two operators. The central object in the later decomposition is the operator

$$\langle n|\hat{G}(R)|n\rangle \equiv \langle n|\hat{F}^y_m\hat{F}^x_{m+R}|n\rangle = \frac{2}{L}\left(\sum_{k\in\mathcal{K}^{(+)}}\mathcal{C}_k^{\left(p_k^{[n]},p_{-k}^{[n]}\right)}(R)\right), \tag{5.67}$$

where

$$\mathcal{C}_k^{\left(p_k^{[n]},p_{-k}^{[n]}\right)}(R) = \begin{cases} \mathcal{C}_k^{(0)}(R) = \mathcal{C}_k(R) & \text{if } p_k^{[n]}=0,\ p_{-k}^{[n]}=0 \\ \mathcal{C}_k^{(1)}(R) = 0 & \text{if } p_k^{[n]}=1,\ p_{-k}^{[n]}=0 \\ \mathcal{C}_k^{(2)}(R) = 0 & \text{if } p_k^{[n]}=0,\ p_{-k}^{[n]}=1 \\ \mathcal{C}_k^{(3)}(R) = -\mathcal{C}_k(R) & \text{if } p_k^{[n]}=1,\ p_{-k}^{[n]}=1 \end{cases}, \tag{5.68}$$

[9] In the odd sector, however, the sum should not include $k=0$ and $k=\pi$, but should be extended to $\langle n|\hat{S}^z_j|n\rangle \to \langle n|\hat{S}^z_j|n\rangle(k\neq 0,k\neq\pi)+(2-p_{k=0}-p_{k=\pi})/L$. This is not needed for our calculations.

and

$$\mathcal{C}_k(R) = -\frac{a_k}{\varepsilon_k}\cos(kR) + \frac{b_k}{\varepsilon_k}\sin(kR). \tag{5.69}$$

Using Eq. (5.40), one can then calculate $\hat{G}(R)$ in the different ensembles to obtain

$$\langle \hat{G}(R)\rangle_{\mathrm{DE}} = \langle \hat{G}(R)\rangle_{\mathrm{GGE}} = \frac{2}{L}\sum_{k\in\mathcal{K}^{(+)}} (2\alpha_k - 1)\,\mathcal{C}_k(R). \tag{5.70}$$

The fact that the expectation value of $\hat{G}(R)$ is the same in the diagonal ensemble and in the GGE has its root in symmetric structure of this quantity in the $\{k,-k\}$ subspaces [see Eq. (5.68)], which shares similarities with the energy expectation values. It is also interesting to note that

$$\langle \hat{S}^z_j\rangle_{\mathrm{DE/GGE}} = \frac{1}{2}\langle \hat{G}(0)\rangle_{\mathrm{DE/GGE}}. \tag{5.71}$$

The structure of the nearest neighbor correlations of the x and y spin components is particularly simple because $\hat{S}^x_j\hat{S}^x_{j+1} = \hat{G}(1)/4$ and $\hat{S}^y_j\hat{S}^y_{j+1} = \hat{G}(-1)/4$. According to Eq. (5.70), this implies that

$$\langle \hat{S}^x_j\hat{S}^x_{j+1}\rangle_{\mathrm{DE}} = \langle \hat{S}^x_j\hat{S}^x_{j+1}\rangle_{\mathrm{GGE}}, \tag{5.72}$$

$$\langle \hat{S}^y_j\hat{S}^y_{j+1}\rangle_{\mathrm{DE}} = \langle \hat{S}^y_j\hat{S}^y_{j+1}\rangle_{\mathrm{GGE}}, \tag{5.73}$$

for any system size. As a result of Eqs. (5.66) and (5.72), not only does the average energy in the diagonal ensemble equal the one in the GGE, but also the expectation values of the individual terms in the transverse field Ising Hamiltonian are the same in both ensembles.

The next-nearest neighbor correlations of the x and y spin components are more involved since the eigenstate expectation values now contain products of two operators, $\langle n|\hat{S}^x_j\hat{S}^x_{j+2}|n\rangle = \frac{1}{4}\Big(\langle n|\hat{G}(1)|n\rangle^2 - \langle n|\hat{G}(0)|n\rangle\langle n|\hat{G}(2)|n\rangle\Big)$ and $\langle n|\hat{S}^y_j\hat{S}^y_{j+2}|n\rangle = \frac{1}{4}\Big(\langle n|\hat{G}(-1)|n\rangle^2 - \langle n|\hat{G}(0)|n\rangle\langle n|\hat{G}(-2)|n\rangle\Big)$. Nevertheless, using Eq. (5.43), the expectation values of these operators can still be calculated in polynomial time

$$\langle \hat{S}^x_j\hat{S}^x_{j+2}\rangle_\mu = \frac{1}{4}\Big(\langle \hat{G}(1)\rangle^2_\mu - \langle \hat{G}(0)\rangle_\mu\langle \hat{G}(2)\rangle_\mu\Big) + \tag{5.74}$$

$$+\left(\frac{1}{L}\right)^2\sum_{k\in\mathcal{K}^{(+)}}\left[\mathcal{C}_k(1)^2 - \mathcal{C}_k(0)\mathcal{C}_k(2)\right]\left[\rho^{(0)}_{k,\mu} + \rho^{(3)}_{k,\mu} - \left(\rho^{(0)}_{k,\mu} - \rho^{(3)}_{k,\mu}\right)^2\right] \tag{5.75}$$

$$\langle \hat{S}^y_j\hat{S}^y_{j+2}\rangle_\mu = \frac{1}{4}\Big(\langle \hat{G}(-1)\rangle^2_\mu - \langle \hat{G}(0)\rangle_\mu\langle \hat{G}(-2)\rangle_\mu\Big) + \tag{5.76}$$

$$+\left(\frac{1}{L}\right)^2\sum_{k\in\mathcal{K}^{(+)}}\left[\mathcal{C}_k(-1)^2 - \mathcal{C}_k(0)\mathcal{C}_k(-2)\right]\left[\rho^{(0)}_{k,\mu} + \rho^{(3)}_{k,\mu} - \left(\rho^{(0)}_{k,\mu} - \rho^{(3)}_{k,\mu}\right)^2\right]. \tag{5.77}$$

The second term in both equations is in fact very similar. First, using Eq. (5.69), we find $\mathcal{C}_k(1)^2 - \mathcal{C}_k(0)\mathcal{C}_k(2) = \mathcal{C}_k(-1)^2 - \mathcal{C}_k(0)\mathcal{C}_k(-2) = \sin^2 k$. Second, the weights in the diagonal ensemble equal $\rho^{(0)}_{k,\mathrm{DE}} + \rho^{(3)}_{k,\mathrm{DE}} - \left(\rho^{(0)}_{k,\mathrm{DE}} - \rho^{(3)}_{k,\mathrm{DE}}\right)^2 = 4\alpha_k(1-\alpha_k)$, which are twice the values in the GGE, where $\rho^{(0)}_{k,\mathrm{GGE}} + \rho^{(3)}_{k,\mathrm{GGE}} - \left(\rho^{(0)}_{k,\mathrm{GGE}} - \rho^{(3)}_{k,\mathrm{GGE}}\right)^2 = 2\alpha_k(1-\alpha_k)$. In addition, the expectation values of $\hat{G}(R)$ are the same in both ensembles.

We can then simplify Eqs. (5.74) and (5.76) to

$$\langle \hat{S}^x_j\hat{S}^x_{j+2}\rangle_{\mathrm{DE}} = \frac{1}{4}\Big(\langle \hat{G}(1)\rangle^2_{\mathrm{DE}} - \langle \hat{G}(0)\rangle_{\mathrm{DE}}\langle \hat{G}(2)\rangle_{\mathrm{DE}}\Big) + \frac{1}{L}\mathcal{Z}(1) \tag{5.78}$$

$$\langle \hat{S}^x_j\hat{S}^x_{j+2}\rangle_{\mathrm{GGE}} = \frac{1}{4}\Big(\langle \hat{G}(1)\rangle^2_{\mathrm{DE}} - \langle \hat{G}(0)\rangle_{\mathrm{DE}}\langle \hat{G}(2)\rangle_{\mathrm{DE}}\Big) + \frac{1}{2}\frac{1}{L}\mathcal{Z}(1) \tag{5.79}$$

for the x spin component, and in the same manner for the y spin component as

$$\langle \hat{S}^y_j \hat{S}^y_{j+2} \rangle_{\rm DE} = \frac{1}{4}\left(\langle \hat{G}(-1)\rangle^2_{\rm DE} - \langle \hat{G}(0)\rangle_{\rm DE}\langle \hat{G}(-2)\rangle_{\rm DE} \right) + \frac{1}{L}\mathcal{Z}(1) \tag{5.80}$$

$$\langle \hat{S}^y_j \hat{S}^y_{j+2} \rangle_{\rm GGE} = \frac{1}{4}\left(\langle \hat{G}(-1)\rangle^2_{\rm DE} - \langle \hat{G}(0)\rangle_{\rm DE}\langle \hat{G}(-2)\rangle_{\rm DE} \right) + \frac{1}{2}\frac{1}{L}\mathcal{Z}(1). \tag{5.81}$$

The term $\mathcal{Z}(1)$ denotes a sum that, more generally, we define as

$$\mathcal{Z}(r) = \frac{1}{L}\sum_{k\in\mathcal{K}^{(+)}} 4\alpha_k(1-\alpha_k)\sin^2(kr). \tag{5.82}$$

Equations (5.78)-(5.79) and (5.80)-(5.81) reveal that the expectation values of $\hat{S}^x_j\hat{S}^x_{j+2}$ and $\hat{S}^y_j\hat{S}^y_{j+2}$ in the diagonal ensemble and in the GGE are identical in the thermodynamic limit. Their difference for finite systems vanishes as:

$$\langle \hat{S}^x_j \hat{S}^x_{j+2} \rangle_{\rm DE} - \langle \hat{S}^x_j \hat{S}^x_{j+2} \rangle_{\rm GGE} = \langle \hat{S}^y_j \hat{S}^y_{j+2} \rangle_{\rm DE} - \langle \hat{S}^y_j \hat{S}^y_{j+2} \rangle_{\rm GGE} = \frac{1}{2L}\mathcal{Z}(1). \tag{5.83}$$

In the continuum limit, $\mathcal{Z}(1)$ can be expressed in terms of the transverse fields before and after the quench. For the quenches across the quantum critical point that we consider here, $(h-1)(h_0-1)<0$, it takes the form

$$\mathcal{Z}(1) = \frac{|h-h_0|}{16\,(\mathrm{Max}[h,h_0])^3}\left(3\,(\mathrm{Max}[h,h_0])^2 - [1+h_0h+(h_0h)^2]\right). \tag{5.84}$$

In Figs. 5.9(a)-5.9(b) and Figs. 5.10(a)-5.10(b), we present the numerical results for observables $\hat{\mathcal{O}} = \hat{S}^x_j\hat{S}^x_{j+2}$ and $\hat{\mathcal{O}} = \hat{S}^y_j\hat{S}^y_{j+2}$. We plot the relative difference between the predictions of different ensembles as

$$\Delta\langle\hat{\mathcal{O}}\rangle_\mu = \left| \frac{\langle\hat{\mathcal{O}}\rangle_\mu - \langle\hat{\mathcal{O}}\rangle_{\rm DE}}{\langle\hat{\mathcal{O}}\rangle_{\rm DE}} \right|, \tag{5.85}$$

where μ = GGE and GE. Results are presented for quenches starting in the paramagnetic ground state to the ferromagnetic regime (Fig. 5.9), and for quenches starting in the ferromagnetic ground state to the paramagnetic regime (Fig. 5.10). The agreement between the GGE and the diagonal ensemble, described by Eqs. (5.78)-(5.79) and Eqs. (5.80)-(5.81) and depicted in Figs. 5.9 and 5.10, shows that the observables considered exhibit generalized thermalization in the thermodynamic limit.

In contrast, results for the grand canonical ensemble in the insets in both figures make clear that these systems do not exhibit thermalization, namely, the grand canonical ensemble does not consistently predict expectation values of observables in the diagonal ensemble. We stress that no approximations have been made in the calculation of both the diagonal and the grand canonical ensemble predictions. In the latter case, this means that the eigenstates contain the proper set of wave vectors depending on whether they belong to the even or odd sector. Even though this limits our numerical calculations of $\langle\hat{\mathcal{O}}\rangle_{\rm GE}$ to at most $L\sim 30$ sites, the trend of the data in Figs. 5.9 and 5.10 is already robust. It makes apparent the failure of traditional statistical mechanics for this system.

Next, we compute the spin correlations in the z direction. An appealing property of these correlations is that their eigenstate expectation values can be expressed as a sum of products of two terms for arbitrary r, namely $\langle n|\hat{S}^z_j\hat{S}^z_{j+r}|n\rangle = \frac{1}{4}\left(\langle n|\hat{G}(0)|n\rangle^2 - \langle n|\hat{G}(r)|n\rangle\langle n|\hat{G}(-r)|n\rangle\right)$. This can be simplified using Eq. (5.43) to obtain

$$\begin{aligned}\langle \hat{S}^z_j \hat{S}^z_{j+r} \rangle_\mu = &\frac{1}{4}\left(\langle \hat{G}(0)\rangle^2_\mu - \langle \hat{G}(r)\rangle_\mu\langle \hat{G}(-r)\rangle_\mu \right) + \\ &+ \left(\frac{1}{L}\right)^2 \sum_{k\in\mathcal{K}^{(+)}} \left[\mathcal{C}_k(0)^2 - \mathcal{C}_k(r)\mathcal{C}_k(-r)\right]\left[\rho^{(0)}_{k,\mu} + \rho^{(3)}_{k,\mu} - \left(\rho^{(0)}_{k,\mu} - \rho^{(3)}_{k,\mu}\right)^2\right].\end{aligned} \tag{5.86}$$

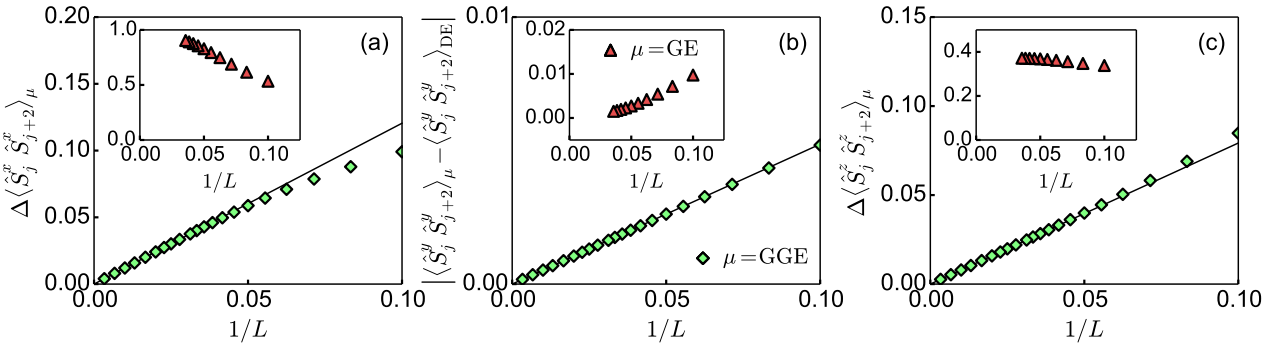

Figure 5.9: *Relative difference between observables in the GGE (main panels), the grand canonical ensemble (insets), and the diagonal ensemble.* Results are presented for the relative difference $\Delta\langle\hat{S}^a_j\hat{S}^a_{j+2}\rangle_\mu$, defined in Eq. (5.85), for $a = x$ in (a) and $a = z$ in (c). In (b), we plot $|\langle\hat{S}^y_j\hat{S}^y_{j+2}\rangle_\mu - \langle\hat{S}^y_j\hat{S}^y_{j+2}\rangle_{\rm DE}|$ since the diagonal ensemble result for this observable in the thermodynamic limit is very small, $\langle\hat{S}^y_j\hat{S}^y_{j+2}\rangle_{\rm DE} \approx -5.7\times10^{-4}$. Solid lines are functions c/L for the GGE results, where the coefficient c was obtained from Eqs. (5.78) and (5.79) for $\hat{S}^x_j\hat{S}^x_{j+2}$, Eqs. (5.80) and (5.81) for $\hat{S}^y_j\hat{S}^y_{j+2}$, and Eqs. (5.87) and (5.88) for $\hat{S}^z_j\hat{S}^z_{j+2}$, replacing sums by integrals. In all quenches the initial state is the ground state in the transverse field $h_0 = 4.0$ and the final field is $h = 0.8$.

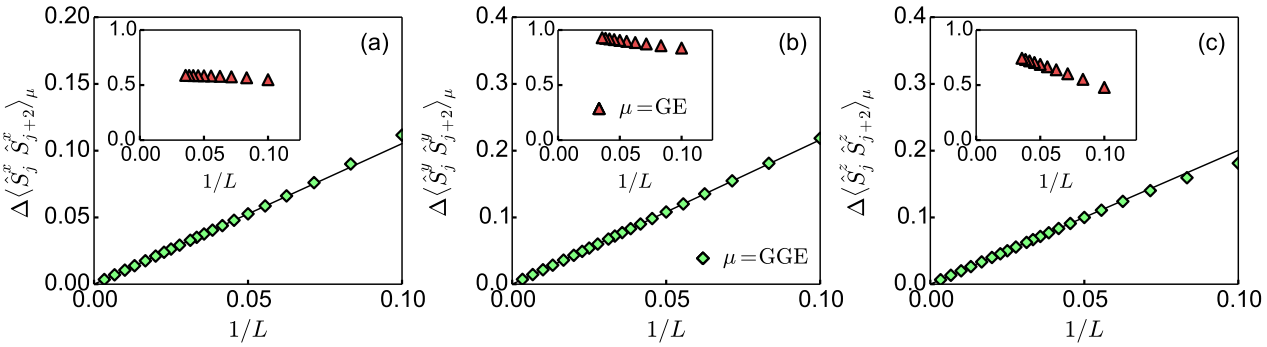

Figure 5.10: *Relative difference between observables in the GGE (main panels), the grand canonical ensemble (insets), and the diagonal ensemble.* Results are presented for the relative difference $\Delta\langle\hat{S}^a_j\hat{S}^a_{j+2}\rangle_\mu$, defined in Eq. (5.85), for $a = x$ in (a), $a = y$ in (b), and $a = z$ in (c). Solid lines are functions c/L for the GGE results, where the coefficient c was obtained from Eqs. (5.78) and (5.79) for $\hat{S}^x_j\hat{S}^x_{j+2}$, Eqs. (5.80) and (5.81) for $\hat{S}^y_j\hat{S}^y_{j+2}$ and Eqs. (5.87) and (5.88) for $\hat{S}^z_j\hat{S}^z_{j+2}$, replacing sums by integrals. In all quenches the initial state is the ground state in the transverse field $h_0 = 0.1$ and the final field is $h = 1.5$.

In addition, Eq. (5.69) implies that $\mathcal{C}_k(0)^2 - \mathcal{C}_k(r)\mathcal{C}_k(-r) = \sin^2(kr)$ and Eq. (5.71) gives $\langle\hat{S}^z_j\rangle_{\rm DE} = \frac{1}{2}\langle\hat{G}(0)\rangle_{\rm DE}$. One can therefore rewrite Eq. (5.86) as

$$\langle\hat{S}^z_j\hat{S}^z_{j+r}\rangle_{\rm DE} = \langle\hat{S}^z_j\rangle^2_{\rm DE} - \frac{1}{4}\langle\hat{G}(r)\rangle_{\rm DE}\langle\hat{G}(-r)\rangle_{\rm DE} + \frac{1}{L}\mathcal{Z}(r) \tag{5.87}$$

$$\langle\hat{S}^z_j\hat{S}^z_{j+r}\rangle_{\rm GGE} = \langle\hat{S}^z_j\rangle^2_{\rm DE} - \frac{1}{4}\langle\hat{G}(r)\rangle_{\rm DE}\langle\hat{G}(-r)\rangle_{\rm DE} + \frac{1}{2}\frac{1}{L}\mathcal{Z}(r). \tag{5.88}$$

This means that the expectation values of spin correlations in the z direction in the GGE and in the diagonal ensemble, for an arbitrary distance r, are identical in the thermodynamic limit. Their differences in finite chains vanish as $1/L$, as for $\hat{S}^x_j\hat{S}^x_{j+2}$ and $\hat{S}^y_j\hat{S}^y_{j+2}$.

In Figs. 5.9(c) and 5.10(c), we plot the relative distance $\Delta\langle\hat{S}^z_j\hat{S}^z_{j+2}\rangle_\mu$, defined in Eq. (5.85) (where μ = GGE, GE), for two sets of quenches. The scaling of $\Delta\langle\hat{S}^z_j\hat{S}^z_{j+2}\rangle_{\rm GGE}$ follows the prediction from Eqs. (5.87) and (5.88). The results for the grand canonical ensemble (inset) show clear differences with respect to the diagonal ensemble and, hence, the inadequacy of the grand canonical ensemble to describe observables after relaxation.

Trace distances.

We now turn our focus to spin correlations in the entire system, and ask the question of whether they can be described by the GGE in arbitrary bases (e.g., real space, momentum space, etc). As discussed in Sec. 5.4, the answer to this question has been affirmative for hard-core bosons (and, more generally, for hard-core anyons) in the XX Hamiltonian in the absence of translational invariance [52]. Here we address this question in the context of the translationally invariant transverse field Ising model.

The central object in this calculation is the density matrix $\mathcal{G}^a_\mu$, with matrix elements $\langle\hat{S}^a_j\hat{S}^a_l\rangle_\mu$ (for $a=\{x,y,z\}$). We use Eqs. (5.87) and (5.88) to calculate the spin correlations in the z direction $\langle\hat{S}^z_j\hat{S}^z_l\rangle_\mu$. For the spin correlations in the x direction, we calculate the eigenstate expectation values from the Toeplitz matrix [1]

$$\langle n|\hat{S}^x_j\hat{S}^x_{j+r}|n\rangle=\frac{1}{4}\begin{vmatrix}\langle n|\hat{G}(1)|n\rangle & \langle n|\hat{G}(2)|n\rangle & \dots & \langle n|\hat{G}(r)|n\rangle\\ \vdots & & & \vdots\\ \langle n|\hat{G}(-r+2)|n\rangle & \dots & \dots & \langle n|\hat{G}(1)|n\rangle\end{vmatrix}, \tag{5.89}$$

where the matrix elements $\langle n|\hat{G}(r)|n\rangle$ have been introduced in Eq. (5.67). Similarly, the eigenstate expectation values of spin correlations in the y direction are obtained as

$$\langle n|\hat{S}^y_j\hat{S}^y_{j+r}|n\rangle=\frac{1}{4}\begin{vmatrix}\langle n|\hat{G}(-1)|n\rangle & \langle n|\hat{G}(0)|n\rangle & \dots & \langle n|\hat{G}(r-2)|n\rangle\\ \vdots & & & \vdots\\ \langle n|\hat{G}(-r)|n\rangle & \dots & \dots & \langle n|\hat{G}(-1)|n\rangle\end{vmatrix}. \tag{5.90}$$

The eigenstate expectation values from Eqs. (5.89) and (5.90) are used to calculate expectation values of $\mathcal{G}^a_\mu$ in statistical ensembles.

We define the trace distance between the GGE, or the grand canonical ensemble, and the diagonal ensemble as

$$d[\mathcal{G}^a_{\rm DE},\mathcal{G}^a_\mu]=\frac{1}{2\mathcal{N}}{\rm Tr}\left\{\sqrt{(\mathcal{G}^a_{\rm DE}-\mathcal{G}^a_\mu)^2}\right\}, \tag{5.91}$$

where $\mu=$ GGE or GE. In all these cases, the normalization constant ($\mathcal{N}={\rm Tr}\,\mathcal{G}^a_\mu$) is $\mathcal{N}=L/4$. In contrast to Eq. (5.48), in which we compared instantaneous values to GGE predictions, here we compare predictions of ensembles. Taking into account that our system is translationally invariant, we define $\hat{\mathcal{S}}^a_r\equiv\hat{S}^a_j\hat{S}^a_{j+r}$, whose Fourier transform $\langle\hat{S}^a_k\rangle_\mu=(1/L)\sum_{j,l}e^{-i(l-j)k}\langle\hat{S}^a_j\hat{S}^a_l\rangle_\mu$ simplifies to

$$\langle\hat{S}^a_k\rangle_\mu=\frac{1}{4}+2\sum_{r=1}^{L/2-1}\cos(kr)\langle\hat{\mathcal{S}}^a_r\rangle_\mu+e^{-ikL/2}\langle\hat{\mathcal{S}}^a_{L/2}\rangle_\mu \tag{5.92}$$

and the trace distance can be calculated as

$$d[\mathcal{G}^a_{\rm DE},\mathcal{G}^a_\mu]=\frac{1}{2\mathcal{N}}\sum_k\left|\langle\hat{S}^a_k\rangle_{\rm DE}-\langle\hat{S}^a_k\rangle_\mu\right|. \tag{5.93}$$

A particularly simple expression can be obtained for the trace distance of spin correlations in the z direction. In this case, Eqs. (5.87) and (5.88) imply that

$$\langle\hat{S}^z_k\rangle_{\rm DE}-\langle\hat{S}^z_k\rangle_{\rm GGE}=\frac{1}{2L}\left[2\sum_{r=1}^{L/2-1}\cos(kr)\mathcal{Z}(r)+e^{-ikL/2}\mathcal{Z}(L/2)\right]. \tag{5.94}$$

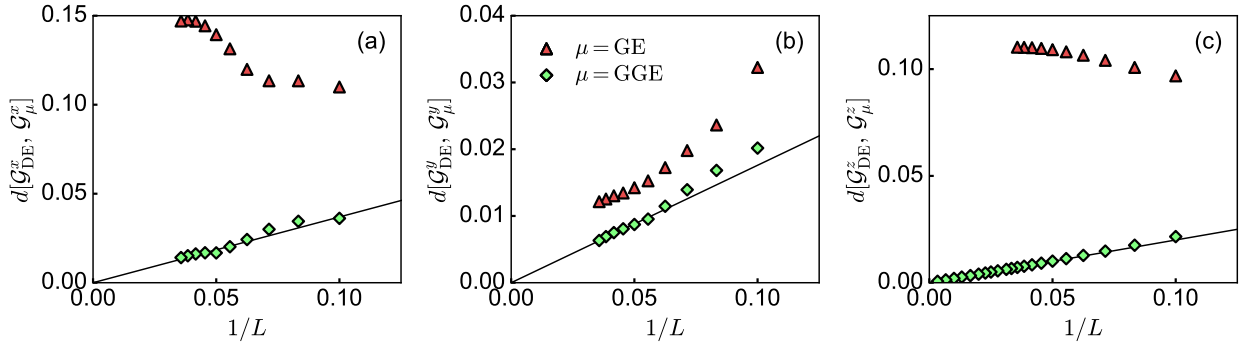

Figure 5.11: *Trace distance between spin correlations in the GGE, or the grand canonical ensemble, and the diagonal ensemble.* Results are presented for $d[\mathcal{G}^a_{\mathrm{DE}}, \mathcal{G}^a_\mu]$, defined in Eq. (5.91), for $a = x$ in (a), $a = y$ in (b), and $a = z$ in (c). Solid lines are fits to power laws c/L for the GGE results. The corresponding parameters $c = 0.37$ in (a) and $c = 0.18$ in (b) are obtained by fitting the data for $L \geq 18$. In panel (c), fitting the data for $L \geq 50$ yields $c = 0.20$. In all quenches the initial state is the ground state for the transverse field $h_0 = 4.0$ and the final field is $h = 0.8$.

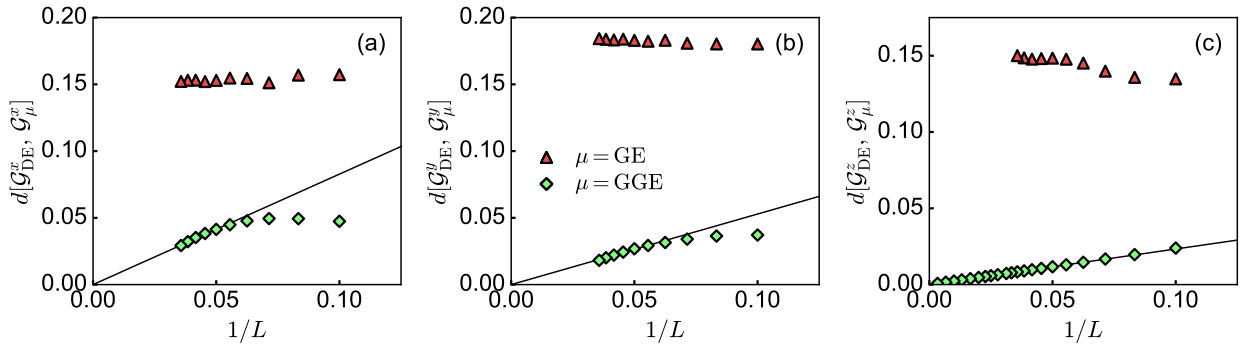

Figure 5.12: *Trace distance between spin correlations in the GGE, or the grand canonical ensemble, and the diagonal ensemble.* Results are presented for $d[\mathcal{G}^a_{\mathrm{DE}}, \mathcal{G}^a_\mu]$, defined in Eq. (5.91), for $a = x$ in (a), $a = y$ in (b), and $a = z$ in (c). Solid lines are fits to power laws c/L for the GGE results. The corresponding parameters $c = 0.83$ in (a) and $c = 0.53$ in (b) are obtained by fitting the data for $L \geq 18$. In panel (c), fitting the data for $L \geq 50$ yields $c = 0.23$. In all quenches the initial state is the ground state for the transverse field $h_0 = 0.1$ and the final field is $h = 1.5$.

Hence, we need to evaluate $\mathcal{Z}(r)$, introduced in Eq. (5.82). In the continuum limit, one can obtain a closed expression for $\mathcal{Z}(r)$. For quenches across the critical point, $(h-1)(h_0-1) < 0$, it reads

$$\mathcal{Z}(r) = \frac{|h-h_0|}{16\,(1-h_0 h)}\Bigg((\mathrm{Max}[h,h_0])^{-(2r+1)}[(\mathrm{Max}[h,h_0])^2 - 1] \\ +(\mathrm{Min}[h,h_0])^{2r-1}[(\mathrm{Min}[h,h_0])^2 - 1] + 2\left[(\mathrm{Max}[h,h_0])^{-1} - \mathrm{Min}[h,h_0]\right]\Bigg). \tag{5.95}$$

For large r, $\mathcal{Z}(r)$ approaches a constant. We plot the trace distance $d[\mathcal{G}^z_{\mathrm{DE}}, \mathcal{G}^z_\mu]$ in Figs. 5.11(c) and 5.12(c) for two different quenches. The trace distance between the diagonal ensemble and the GGE decays as a power law $\sim 1/L$, in contrast to the results in the grand canonical ensemble where no decay is observed.

In Figs. 5.11 and 5.12, we also show $d[\mathcal{G}^a_{\rm DE}, \mathcal{G}^a_{\rm GGE}]$ and $d[\mathcal{G}^a_{\rm DE}, \mathcal{G}^a_{\rm GE}]$ for two different quenches and the spin components $a = \{x, y\}$. As for nearest neighbor correlations, one can see that $d[\mathcal{G}^a_{\rm DE}, \mathcal{G}^a_{\rm GGE}]$ decreases with increasing system size, suggesting generalized thermalization of spin correlations on the entire lattice, while in most cases $d[\mathcal{G}^a_{\rm DE}, \mathcal{G}^a_{\rm GE}]$ increases or saturates. Granted, for trace distances finite size effects are stronger than for nearest neighbor correlations and power law behavior ($\sim 1/L$) in the decrease of the trace distance is only seen for the largest system sizes. Similar scaling of the differences between the diagonal ensemble predictions (or the time-average predictions) and the GGE for momentum distribution functions were found for the XX model in Refs. [51, 71].

It is important to stress that, after equilibration following a quench in the 1D systems discussed here, the spin correlations (and the one-body correlations for hard-core bosons) generally decay exponentially with the distance. Hence, despite the fact that trace distances for spin correlations (and the momentum distribution functions for hard-core bosons) are nonlocal by definition, they effectively behave as local quantities because of the exponential decay of correlations. These results make apparent that the relation between the locality of observables and the applicability of the GGE is a blurry one, because the operators may be by definition nonlocal, but effectively behave as local.

5.6 Generalized Eigenstate Thermalization

Looking back to the definition of the diagonal ensemble [Eq. (5.15)], and comparing it to the definition of the GGE [Eq. (5.18)], one cannot help but wonder why the GGE can describe observables after relaxation. The diagonal ensemble is constructed with an exponentially large (in the system size) number of parameters. They are the projection of the initial state onto the eigenstates of the final Hamiltonian. The GGE, on the other hand, is constructed with a polynomially large (in the system size) number of parameters. Those are the Lagrange multipliers, which are determined in terms of the occupations of the single-particle states used to diagonalize the integrable model after the quench. This means that the diagonal ensemble contains exponentially many more parameters than the GGE. The fact that the diagonal ensemble is more constrained than the GGE is apparent in our results for the entropies in both ensembles within the translationally invariant transverse field Ising model. We have shown that the entropy of the former is one half that of the latter. Numerical results in systems with no translational invariance have found that while the entropy of the GGE is always greater than that of the diagonal ensemble, the ratio between the two need not be 2 [136, 125, 137].

A way to understand how it is possible, in general, that two ensembles sampling vastly different number of states (the ratio between the number of states sampled by the diagonal ensemble and by the GGE vanishes exponentially fast with increasing system size) lead to the same results for observables (up to finite size effects) was put forward in Ref. [71]. There it was shown that, in a system of hard-core bosons, eigenstates of the Hamiltonian that have similar distributions of conserved quantities also have similar expectation values of observables (such as the occupation of momentum modes). This phenomenon was named *generalized eigenstate thermalization* after a related phenomenon in nonintegrable systems, namely, eigenstate thermalization [72, 73, 6]. A system is said to exhibit eigenstate thermalization if eigenstates with close energies have similar expectation values of observables (with deviations that decrease exponentially with increasing system size [112]). How generalized eigenstate thermalization can explain the success of the GGE, as well as the fact that it occurs in the transverse field Ising model, is something that we explain and exemplify in what follows. We note that related ideas have been discussed in the context of the so-called quench-action method [272, 273, 69, 113, 114] (see also the review by Caux in this volume [5]).

5.6.1 The XX model. Hard-core bosons

Before discussing generalized eigenstate thermalization in the transverse field Ising model, we summarize the main points and results reported in Ref. [71] and in a later study [93] of this phenomenon for hard-core bosons (XX model) with the Hamiltonian (5.3).

The fact that the total number of particles is conserved in such a model motivated the introduction of a microcanonical version of the GGE in Ref. [71], the generalized microcanonical ensemble[10] (GME). A key object in the construction of the GME is the target distribution of conserved quantities, which was chosen to be a coarse gained version of the distribution of conserved quantities in the initial state. An eigenstate of the Hamiltonian belongs to the GME if it has a distribution of the conserved quantities whose distance (see Ref. [71] for the definition of distance) to the target distribution is below some threshold, similarly to what one does to construct the microcanonical ensemble. The GME constructed this way was shown to accurately reproduce the expectation values of observables in the diagonal ensemble, in contrast to the traditional microcanonical ensemble, which was shown to fail. Having all the states that participated in the diagonal ensemble and in the GME, it was possible to show that the expectation value of observables in those states had a narrow distribution centered about the mean value predicted by the diagonal ensemble and a standard deviation that vanished with increasing system size, i.e., the exact weights and number of states used in each ensemble was not important [71]. Results obtained in Ref. [93] for hard-core bosons in the presence of a quasi-periodic potential were consistent with these findings, but only in the regime in which single-particle eigenstates were extended in real space, i.e., in the absence of localization.

These results are to be contrasted with what happens if one studies the expectation values of observables in all eigenstates of an integrable Hamiltonian that are within a narrow energy window [71, 171, 172]. In this case one finds that they exhibit a narrow distribution centered about the mean value predicted by traditional statistical mechanics, with a standard deviation that vanishes with increasing system size (as $1/\sqrt{L}$ [172]). This means that the only way in which observables in integrable systems can fail to thermalize after a quench is if the initial state samples a vanishingly small fraction of the states in the microcanonical window. This has been recently argued to be generic in quenches that are experimentally relevant [130].

5.6.2 The transverse field Ising model

In the hard-core boson language, the transverse field Ising model does not exhibit particle number conservation. This means that only the grand canonical ensemble and the GGE are meaningful for this model. Hence, we carry out a study parallel to the one in Refs. [71, 93] but considering grand canonical ensembles instead of microcanonical ones. We compute the eigenstate expectation values of all states in the diagonal ensemble and in the GGE. Since the former involves only the square root of all the eigenstates in the Hilbert space, we can carry out this calculation for twice as many sites as for the latter. We also calculate the weights of all states in both ensembles.

In Figs. 6.31 and 5.14, we show results for two observables and two different quenches. The plots provide a coarse grained view of the exact calculations described above. The top panels in the figures show the results obtained in the diagonal ensemble and the bottom panels show the results obtained in the GGE, for three different system sizes in each case (notice the difference in system sizes between the top and the bottom panels). The black regions mark the existence of eigenstates with those eigenenergies and expectation values of observables, but which have negligible weight in the ensembles. The fact that those black regions are wide and do not

[10] In has been proved in a recent study that the GME is the ensemble that correctly predicts the time average of observables in isolated classical systems [116].

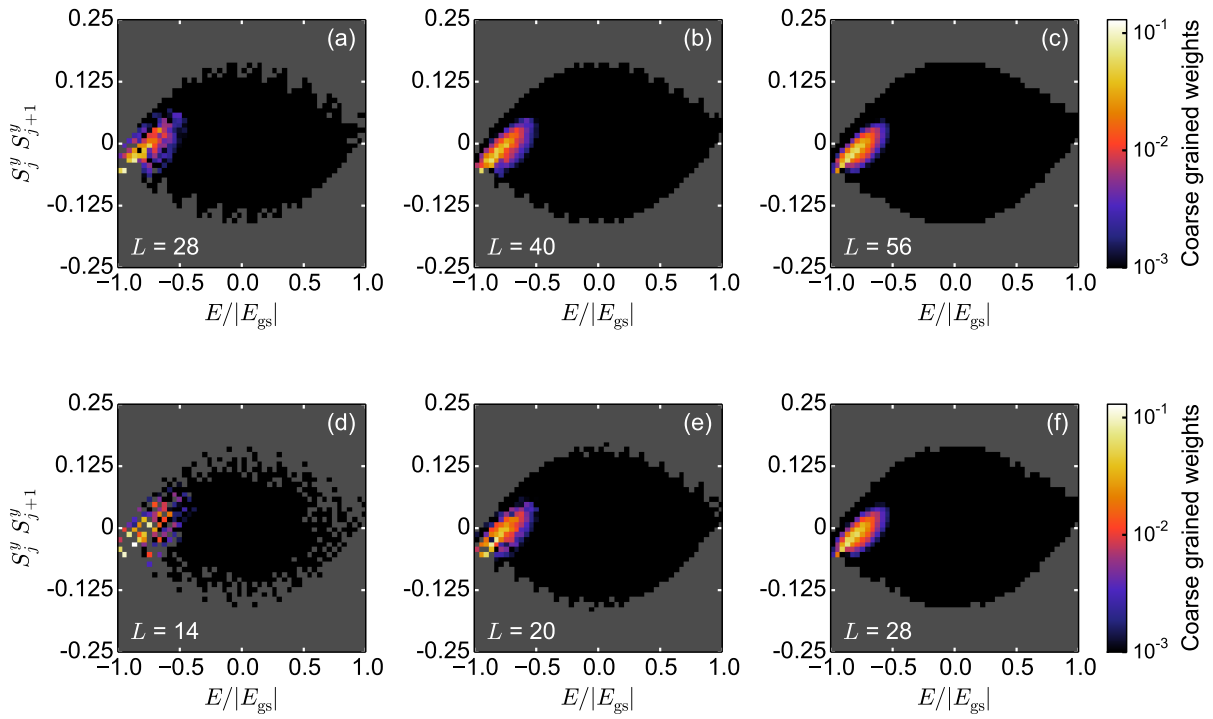

Figure 5.13: *Density plot of the weights of the Hamiltonian eigenstates in terms of their energies and eigenstate expectation values.* Results are presented for the nearest neighbor $S^y_j S^y_{j+1}$ correlations in the diagonal ensemble [panels (a)-(c)] and in the GGE [panels (d)-(f)]. We quench from the ground state for $h_0 = 4.0$ to $h = 0.8$. Black pixels mark the presence of eigenstates (with vanishing weight), while gray pixels denote their absence. Colored pixels show the nonvanishing weights $\rho^{[n]}_{\rm DE}$ and $\rho^{[n]}_{\rm GGE}$ in the diagonal ensemble and the GGE, respectively. We set the horizontal pixel width to be $\varepsilon_E = 2|E_{\rm gs}|/50$ and the vertical pixel width to be $\varepsilon_{\mathcal{O}} = (1/4) \times 2/50$. The ground-state energy for $h = 0.8$ is $E_{\rm gs}/L = -0.584$.

narrow with increasing system size make apparent that the transverse field Ising model does not exhibit eigenstate thermalization.

A remarkable feature seen in Figs. 6.31 and 5.14 is that the eigenstates of the Hamiltonian that contribute significantly to the diagonal ensemble and the GGE are narrowly distributed in the same region about a line (notice the log scale used for the coarse grained weights). If one forgets about the other eigenstates (the ones with negligible weights) the behavior seen in Figs. 6.31 and 5.14 is very similar to the one seen for various observables in nonintegrable one-dimensional systems, which exhibit eigenstate thermalization [157, 158].

We note that, in Figs. 6.31 and 5.14, the region with nonvanishing coarse grained weights shrinks in both directions as the system size increases. In the horizontal direction (energy axis), the width decreases as $\sim 1/\sqrt{L}$, as demonstrated in Fig. 5.7. Hence, here we focus on the variance for the vertical direction

$$\Sigma^2_{\hat{\mathcal{O}},\mu} = \sum_n \rho^{[n]}_\mu \langle n|\hat{\mathcal{O}}|n\rangle^2 - \left(\sum_n \rho^{[n]}_\mu \langle n|\hat{\mathcal{O}}|n\rangle\right)^2 , \tag{5.96}$$

where $\mu = \text{DE}, \text{GGE}$. Using Eqs. (5.40) and (5.43), Eq. (5.96) can be computed straightforwardly for the transverse magnetization $\hat{S}^z_j$, and the nearest neighbor spin-spin correlations $\hat{S}^x_j \hat{S}^x_{j+1}$ and $\hat{S}^y_j \hat{S}^y_{j+1}$.

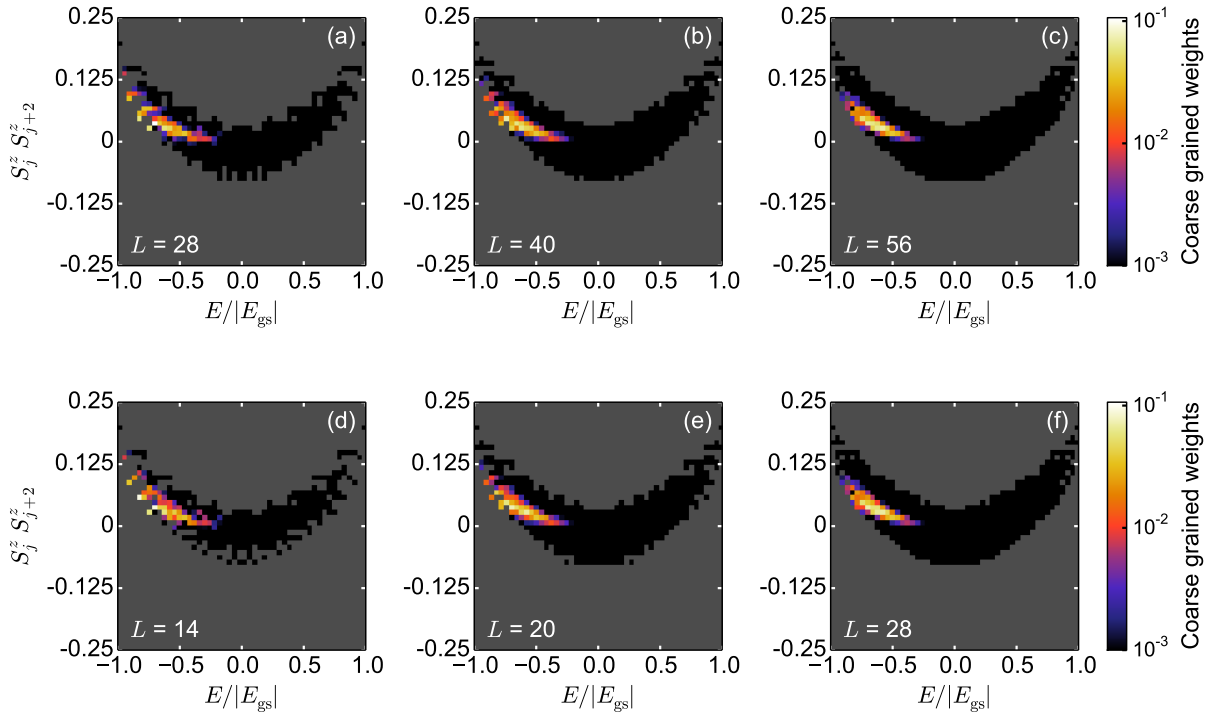

Figure 5.14: *Density plot of the weights of the Hamiltonian eigenstates in terms of their energies and eigenstate expectation values.* Results are presented for the nearest neighbor $S_j^z S_{j+2}^z$ correlations in the diagonal ensemble [panels (a)-(c)] and in the GGE [panels (d)-(f)]. We quench from the ground state for $h_0 = 0.1$ to $h = 1.5$. Black pixels mark the presence of eigenstates (with vanishing weight), while gray pixels denote their absence. Colored pixels show the nonvanishing weights $\rho_{\rm DE}^{[n]}$ and $\rho_{\rm GGE}^{[n]}$ in the diagonal ensemble and the GGE, respectively. We set the horizontal pixel width to be $\varepsilon_E = 2|E_{\rm gs}|/50$ and the vertical pixel width to be $\varepsilon_{\mathcal{O}} = (1/4) \times 2/50$. The ground-state energy for $h = 1.5$ is $E_{\rm gs}/L = -0.836$.

For the transverse magnetization, one can express $\Sigma^2_{\hat{S}^z_j,\mu}$ as

$$\Sigma^2_{\hat{S}^z_j,\mu} = \frac{1}{4}\left[\langle\hat{G}(0)\rangle_\mu\langle\hat{G}(0)\rangle_\mu - \left(\frac{2}{L}\right)^2 \sum_{k\in\mathcal{K}^{(+)}} \left(\sum_{\xi=0}^{3} \rho^{(\xi)}_{k,\mu}\mathcal{C}^{(\xi)}_k(0)\right)\left(\sum_{\xi'=0}^{3} \rho^{(\xi')}_{k,\mu}\mathcal{C}^{(\xi')}_k(0)\right)\right.$$
$$\left. + \left(\frac{2}{L}\right)^2 \sum_{k\in\mathcal{K}^{(+)}} \left(\sum_{\xi=0}^{3} \rho^{(\xi)}_{k,\mu}[\mathcal{C}^{(\xi)}_k(0)]^2\right) - \langle\hat{G}(0)\rangle^2_\mu\right], \tag{5.97}$$

where we have used that $\langle\hat{S}^z_j\rangle_{\rm DE} = \frac{1}{2}\langle\hat{G}(0)\rangle_{\rm DE}$, see Eq. (5.71). A further simplification of Eq. (5.97) can be achieved by replacing $\mathcal{C}^{(\xi)}_k(0)$ according to Eq. (5.68), which gives

$$\Sigma^2_{\hat{S}^z_j,\mu} = \frac{1}{L^2}\sum_{k\in\mathcal{K}^{(+)}} [\mathcal{C}_k(0)]^2\left[\rho^{(0)}_{k,\mu} + \rho^{(3)}_{k,\mu} - \left(\rho^{(0)}_{k,\mu} - \rho^{(3)}_{k,\mu}\right)^2\right]. \tag{5.98}$$

An expression for the sum of the weights above was obtained in the context of Eqs. (5.75) and (5.77), and, from Eq. (5.69), we get that $[\mathcal{C}_k(0)]^2 = (a_k/\varepsilon_k)^2$. Hence, in the diagonal ensemble, the variance of the distribution of $\hat{S}^z_j$ equals

$$\Sigma^2_{\hat{S}^z_j,{\rm DE}} = \frac{1}{L^2}\sum_{k\in\mathcal{K}^{(+)}} 4\alpha_k(1-\alpha_k)\left(\frac{a_k}{\varepsilon_k}\right)^2. \tag{5.99}$$

Equation (5.99) advances that the width of the distribution vanishes as $\Sigma_{\hat{S}^z_j,\mathrm{DE}} \sim 1/\sqrt{L}$ with increasing system size. This scaling is the same as for the width of the energy density distribution derived in Eq. (5.53). In addition, by inserting the weights of the GGE in Eq. (5.98), one gets

$$\frac{\Sigma_{\hat{S}^z_j,\mathrm{DE}}}{\Sigma_{\hat{S}^z_j,\mathrm{GGE}}} = \sqrt{2}. \tag{5.100}$$

The ratio above is the same as for the energy distribution (5.57). Furthermore, Eq. (5.99) can be evaluated analytically in the continuum limit. For the quenches across the critical point that we consider in this review, one gets

$$\Sigma^2_{\hat{S}^z_j,\mathrm{DE}} = \begin{cases} \frac{1}{4L}\left[1+\frac{h_0(2+h_0h)-h(3+4h_0h)}{4h^3}\right] & \text{if} \quad h>1 \quad \text{and} \quad h_0<1 \\ \frac{1}{16L}\left[1+\frac{1-2h_0h}{h_0^2}\right] & \text{if} \quad h<1 \quad \text{and} \quad h_0>1 \end{cases}. \tag{5.101}$$

This equation allows one to predict the prefactor c in $\Sigma_{\hat{S}^z_j,\mathrm{DE}} = c/\sqrt{L}$ and its functional dependence on the transverse magnetic fields. It turns out that the largest value of c (hence, the slowest decay of $\Sigma_{\hat{S}^z_j,\mathrm{DE}}$) is $c = 1/2$, which is realized for quenches in which $h \to \infty$.

It is straightforward now to carry out a similar calculation to determine the widths of $\hat{S}^x_j\hat{S}^x_{j+1}$ and $\hat{S}^y_j\hat{S}^y_{j+1}$. In analogy to Eq. (5.98), we get

$$\Sigma^2_{\hat{S}^x_j\hat{S}^x_{j+1},\mu} = \frac{1}{4L^2}\sum_{k\in\mathcal{K}^{(+)}} [\mathcal{C}_k(1)]^2 \left[\rho^{(0)}_{k,\mu}+\rho^{(3)}_{k,\mu}-\left(\rho^{(0)}_{k,\mu}-\rho^{(3)}_{k,\mu}\right)^2\right] \tag{5.102}$$

$$\Sigma^2_{\hat{S}^y_j\hat{S}^y_{j+1},\mu} = \frac{1}{4L^2}\sum_{k\in\mathcal{K}^{(+)}} [\mathcal{C}_k(-1)]^2 \left[\rho^{(0)}_{k,\mu}+\rho^{(3)}_{k,\mu}-\left(\rho^{(0)}_{k,\mu}-\rho^{(3)}_{k,\mu}\right)^2\right], \tag{5.103}$$

where the weights are identical as in Eq. (5.98). The only difference between the expressions for the different observables is the kernel function $\mathcal{C}_k(r)$ involved. The latter is given by Eq. (5.69), and can be simplified for $r = \pm 1$ to: $[\mathcal{C}_k(1)]^2 = 1 - h^2\sin^2(k)/\varepsilon_k^2$ and $[\mathcal{C}_k(-1)]^2 = \mathcal{C}_k(1)^2 + 2\sin(2k)a_kb_k/\varepsilon_k^2$. This leads to the following expressions for the widths in the diagonal ensemble

$$\Sigma^2_{\hat{S}^x_j\hat{S}^x_{j+1},\mathrm{DE}} = \frac{1}{4L^2}\sum_{k\in\mathcal{K}^{(+)}} 4\alpha_k(1-\alpha_k)\left(1-\frac{h^2\sin^2(k)}{\varepsilon_k^2}\right) \tag{5.104}$$

$$\Sigma^2_{\hat{S}^y_j\hat{S}^y_{j+1},\mathrm{DE}} = \Sigma^2_{\hat{S}^x_j\hat{S}^x_{j+1},\mathrm{DE}} + \frac{1}{4L^2}\sum_{k\in\mathcal{K}^{(+)}} 4\alpha_k(1-\alpha_k)\frac{2\sin(2k)a_kb_k}{\varepsilon_k^2}. \tag{5.105}$$

As for the transverse magnetization, the ratio between the widths in the diagonal ensemble and in the GGE equal

$$\frac{\Sigma_{\hat{\mathcal{O}},\mathrm{DE}}}{\Sigma_{\hat{\mathcal{O}},\mathrm{GGE}}} = \sqrt{2}, \tag{5.106}$$

for $\hat{\mathcal{O}} = \hat{S}^x_j\hat{S}^x_{j+1}$ and $\hat{\mathcal{O}} = \hat{S}^y_j\hat{S}^y_{j+1}$. This result is independent of the system size. Equations (5.104) and (5.105) can also be evaluated analytically in the continuum limit

$$\Sigma^2_{\hat{S}^x_j\hat{S}^x_{j+1},\mathrm{DE}} = \begin{cases} \frac{1}{64L}\left[1+h_0^2-\frac{2h_0}{h}\right] & \text{if} \quad h>1,\ h_0<1 \\ \frac{1}{64L}\left[4-3h^2-\left(\frac{h}{h_0}\right)(4-2h^2)+\left(\frac{h}{h_0}\right)^2\right] & \text{if} \quad h<1,\ h_0>1 \end{cases}, \tag{5.107}$$

and

$$\Delta\Sigma^2_{\hat{S}^y_j\hat{S}^y_{j+1},\mathrm{DE}} = \begin{cases} \frac{1}{64L}\left[\frac{2h_0(2-h_0^2)}{h}+\frac{6-5h_0^2+h_0^4}{h^2}-\frac{2h_0(4-h_0^2)}{h^3}-\frac{5-3h_0^2}{h^4}+\frac{4h_0}{h^5}\right] & \text{if} \quad h>1,\ h_0<1 \\ \frac{1}{64L}\left[3h^2-2+\frac{2h(1-h^2)}{h_0}-\frac{1+h^2}{h_0^2}+\frac{1}{h_0^4}\right] & \text{if} \quad h<1,\ h_0>1 \end{cases}, \tag{5.108}$$

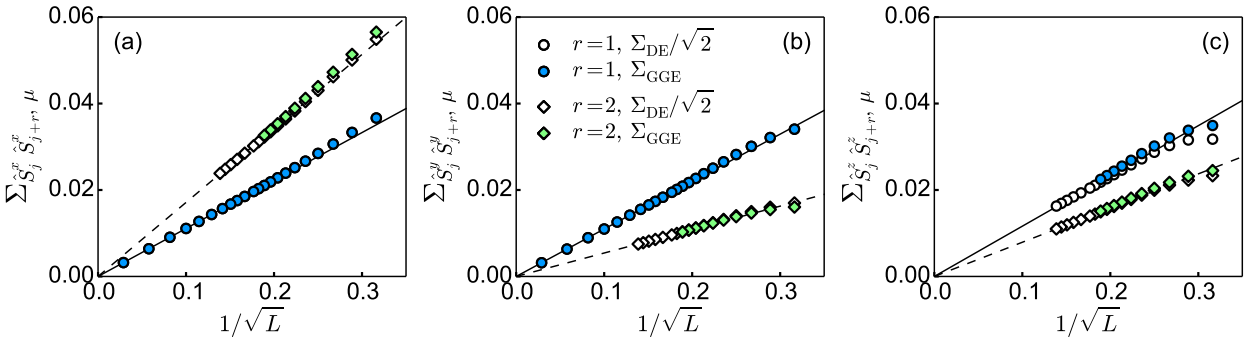

Figure 5.15: *Width $\Sigma_{\hat{\mathcal{O}},\mu}$ in the diagonal ensemble and in the GGE vs $1/\sqrt{L}$.* We quench from the ground state for $h_0 = 4.0$ to $h = 0.8$. For the diagonal ensemble, we plot $\Sigma_{\hat{\mathcal{O}},\rm DE}/\sqrt{2}$. The straight lines are functions $\gamma_{a,r}/\sqrt{L}$ $(a = x, y, z)$. For $a = x, y$ and $r = 1$ (solid lines), the parameter $\gamma_{a,r}$ is given by expressions in Eqs. (5.107) and (5.108), yielding $\gamma_{x,1} = 0.111$ and $\gamma_{y,1} = 0.110$. For all the other curves, $\gamma_{a,r}$ is obtained by fitting $\Sigma_{\hat{\mathcal{O}},\rm DE}/\sqrt{2}$ for $L \geq 30$. For $r = 1$ (solid line), we get $\gamma_{z,1} = 0.116$ in panel (c). For $r = 2$ (dashed lines), we get $\gamma_{x,2} = 0.171$ in panel (a), $\gamma_{y,2} = 0.054$ in panel (b), and $\gamma_{z,2} = 0.079$ in panel (c).

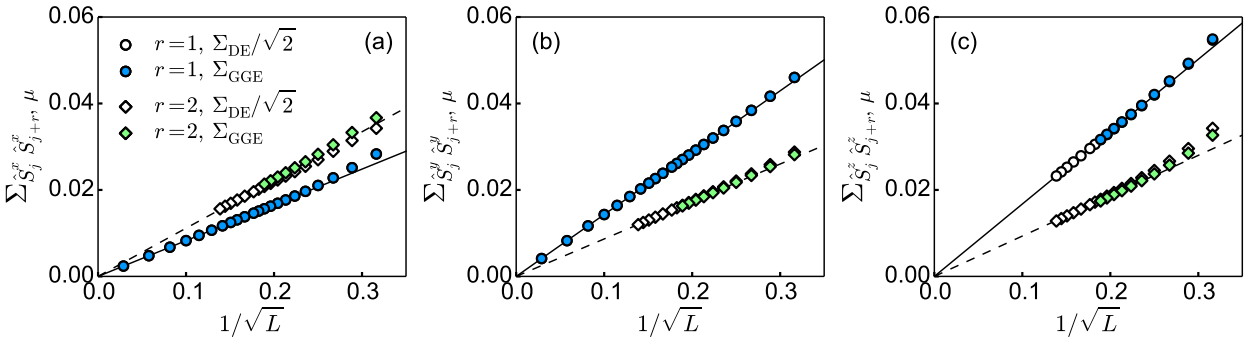

Figure 5.16: *Width $\Sigma_{\hat{\mathcal{O}},\mu}$ in the diagonal ensemble and in the GGE vs $1/\sqrt{L}$.* We quench from the ground state for $h_0 = 0.1$ to $h = 1.5$. For the diagonal ensemble, we plot $\Sigma_{\hat{\mathcal{O}},\rm DE}/\sqrt{2}$. The straight lines are functions $\gamma_{a,r}/\sqrt{L}$ $(a = x, y, z)$. For $a = x, y$ and $r = 1$ (solid lines), the parameter $\gamma_{a,r}$ is given by expressions in Eqs. (5.107) and (5.108), yielding $\gamma_{x,1} = 0.083$ and $\gamma_{y,1} = 0.143$. For all the other curves, $\gamma_{a,r}$ is obtained by fitting $\Sigma_{\hat{\mathcal{O}},\rm DE}/\sqrt{2}$ for $L \geq 30$. For $r = 1$ (solid line), we get $\gamma_{z,1} = 0.167$ in panel (c). For $r = 2$ (dashed lines), we get $\gamma_{x,2} = 0.112$ in panel (a), $\gamma_{y,2} = 0.087$ in panel (b), and $\gamma_{z,2} = 0.093$ in panel (c).

where $\Delta\Sigma^2_{\hat{S}^y_j \hat{S}^y_{j+1},\rm DE} = \Sigma^2_{\hat{S}^y_j \hat{S}^y_{j+1},\rm DE} - \Sigma^2_{\hat{S}^x_j \hat{S}^x_{j+1},\rm DE}$. In all cases, the widths vanish with increasing system size as $\Sigma_{\hat{\mathcal{O}},\rm DE} = c/\sqrt{L}$. For the spin correlations in the x direction, the largest prefactor is $c = 1/4$, obtained when quenching from the initial $h_0 > 1$ to the final field $h \to 0$. For the spin correlations in the y direction, the largest prefactor is $c = (1/8)\sqrt{14/5} \sim 0.209$, obtained when quenching from $h_0 \sim 0$ to $h = \sqrt{5/3}$.

In Figs. 5.15 and 5.16, we report results for six different observables $\hat{S}^a_j \hat{S}^a_{j+r}$, $a = \{x, y, z\}$ and $r = \{1, 2\}$, and two different quenches. The results for $\hat{S}^x_j \hat{S}^x_{j+1}$ and $\hat{S}^y_j \hat{S}^y_{j+1}$ were obtained using Eqs. (5.104) and (5.105), while the results for the other correlations were obtained through a brute force numerically evaluation of the diagonal ensemble and the GGE. We rescaled the data for the diagonal ensemble as $\Sigma_{\hat{\mathcal{O}},\rm DE}/\sqrt{2}$ to show the data collapse (when present). Interestingly, the expectation values obtained for $\hat{S}^z_j \hat{S}^z_{j+1}$, and all the next-nearest-neighbor spin-spin

correlations, reveal that Eq. (5.106) is not exactly fulfilled for all correlations in finite systems. Nevertheless, we find that $\Sigma_{\hat{\mathcal{O}},\mathrm{DE}}/\Sigma_{\hat{\mathcal{O}},\mathrm{GGE}} \to \sqrt{2}$ with increasing system size.

In all cases studied in Figs. 5.15 and 5.16, the width of the distribution of the observables vanishes with increasing system size a $1/\sqrt{L}$. Since the width of the energy distribution also vanishes as $1/\sqrt{L}$, this implies that the states that determine the outcome of the predictions of the diagonal ensemble and the GGE in the thermodynamic limit are located in the same point in the plane defined by the eigenstate expectation values of the observable and the energies. The exact distribution of weights in each ensemble plays no role. This is the reason why, in general, the GGE can predict the expectation values of observables after relaxation despite the fact that the number of parameters one specifies for the GGE is exponentially smaller than the number of parameters one specifies for the diagonal ensemble.

6 From Quantum Chaos and Eigenstate Thermalization to Statistical Mechanics and Thermodynamics by D'Alessio, Yariv Kafri, Polkovnikov, Rigol

(a big review of chaos and thermalization)

This review gives a pedagogical introduction to the eigenstate thermalization hypothesis (ETH), its basis, and its implications to statistical mechanics and thermodynamics.

In the first part, ETH is introduced as a natural extension of ideas from quantum chaos and random matrix theory.

To this end, we present a brief overview of classical and quantum chaos, as well as random matrix theory and some of its most important predictions.

The latter include the statistics of energy levels, eigenstate components, and matrix elements of observables.

Building on these, we introduce the ETH and show that it allows one to describe thermalization in isolated chaotic systems without invoking the notion of an external bath.

We examine numerical evidence of eigenstate thermalization from studies of many-body lattice systems. We also introduce the concept of a quench as a means of taking isolated systems out of equilibrium, and discuss results of numerical experiments on quantum quenches. The second part of the review explores the implications of quantum chaos and ETH to thermodynamics. Basic thermodynamic relations are derived, including the second law of thermodynamics, the fundamental thermodynamic relation, fluctuation theorems, the fluctuation-dissipation relation, and the Einstein and Onsager relations. In particular, it is shown that quantum chaos allows one to prove these relations for individual Hamiltonian eigenstates and thus extend them to arbitrary stationary statistical ensembles. In some cases, it is possible to extend their regimes of applicability beyond the standard thermal equilibrium domain. We then show how one can use these relations to obtain nontrivial universal energy distributions in continuously driven systems. At the end of the review, we briefly discuss the relaxation dynamics and description after relaxation of integrable quantum systems, for which ETH is violated. We present results from numerical experiments and analytical studies of quantum quenches at integrability. We introduce the concept of the generalized Gibbs ensemble, and discuss its connection with ideas of prethermalization in weakly interacting systems.

6.1 Introduction

Despite the huge success of statistical mechanics in describing the macroscopic behavior of physical systems [1, 2], its relation to the underlying microscopic dynamics has remained a

subject of debate since the foundations were laid [3, 4]. One of the most controversial topics has been the reconciliation of the time reversibility of most microscopic laws of nature and the apparent irreversibility of the laws of thermodynamics.

Let us first consider an isolated *classical* system subject to some macroscopic constraints (such as conservation of the total energy and confinement to a container). To derive its equilibrium properties, within statistical mechanics, one takes a fictitious ensemble of systems evolving under the same Hamiltonian and subject to the same macroscopic constraints. Then, a probability is assigned to each member of the ensemble, and the macroscopic behavior of the system is computed by averaging over the fictitious ensemble [5]. For an isolated system, the ensemble is typically chosen to be the microcanonical one. To ensure that the probability of each configuration in phase space does not change in time under the Hamiltonian dynamics, as required by equilibrium, the ensemble includes, with equal probability, all configurations compatible with the macroscopic constraints. The correctness of the procedure used in statistical mechanics to describe real systems is, however, far from obvious. In actual experiments, there is generally no ensemble of systems – there is one system – and the relation between the calculation just outlined and the measurable outcome of the underlying microscopic dynamics is often unclear. To address this issue, two major lines of thought have been offered.

In the first line of thought, which is found in most textbooks, one invokes the ergodic hypothesis [6] (refinements such as mixing are also invoked [7]). This hypothesis states that during its time evolution an ergodic system visits every region in phase space (subjected to the macroscopic constraints) and that, in the long-time limit, the time spent in each region is proportional to its volume. Time averages can then be said to be equal to ensemble averages, and the latter are the ones that are ultimately computed [6]. The ergodic hypothesis essentially implies that the “equal probability" assumption used to build the microcanonical ensemble is the necessary ingredient to capture the long-time average of observables. This hypothesis has been proved for a few systems, such as the Sinai billiard [8, 9], the Bunimovich stadium [10], and systems with more than two hard spheres on a d-dimensional torus ($d \geq 2$) [11].

Proving that there are systems that are ergodic is an important step towards having a mathematical foundation of statistical mechanics. However, a few words of caution are necessary. First, the time scales needed for a system to explore phase space are exponentially large in the number of degrees of freedom, that is, they are irrelevant to what one observes in macroscopic systems. Second, the ergodic hypothesis implies thermalization only in a *weak sense*. Weak refers to the fact that the ergodic hypothesis deals with *long-time averages of observables* and not with the *values of the observables at long times*. These two can be very different. Ideally, one would like to prove thermalization in a *strong sense*, namely, that instantaneous values of observables approach the equilibrium value predicted by the microcanonical ensemble and remain close to it at almost all subsequent times. This is what is seen in most experiments involving macroscopic systems. Within the strong thermalization scenario, the instantaneous values of observables are nevertheless expected to deviate, at some rare times, from their typical value. For a system that starts its dynamics with a non-typical value of an observable, this is, in fact, guaranteed by the Poincaré recurrence theorem [12]. This theorem states that during its time evolution any finite system eventually returns arbitrarily close to the initial state. However, the Poincaré recurrence time is exponentially long in the number of degrees of freedom and is not relevant to observations in macroscopic systems. Moreover, such recurrences are not at odds with statistical mechanics, which allows for atypical configurations to occur with exponentially small probabilities. We should stress that, while the ergodic hypothesis is expected to hold for most interacting systems, there are notable exceptions, particularly in low dimensions. For example, in one dimension, there are many known examples of (integrable or near integrable[11]) systems that do not thermalize, not even in the weak sense [13]. A famous

[11] We briefly discuss classical integrability and chaos in Sec. 6.2 and quantum integrability in Sec. 6.8

example is the Fermi-Pasta-Ulam numerical experiment in a chain of anharmonic oscillators, for which the most recent results show no (or extremely slow) thermalization [14, 15]. This problem had a major impact in the field of nonlinear physics and classical chaos (see, e.g., Ref. [16]). Relaxation towards equilibrium can also be extremely slow in turbulent systems [17] and in glassy systems [18].

In the second, perhaps more appealing, line of thought one notes that macroscopic observables essentially exhibit the same values in almost all configurations in phase space that are compatible with a given set of macroscopic constraints. In other words, almost all the configurations are equivalent from the point of view of macroscopic observables. For example, the number of configurations in which the particles are divided equally (up to non-extensive corrections) between two halves of a container is exponentially larger than configurations in which this is not the case. Noting that "typical" configurations vastly outnumber "atypical" ones and that, under chaotic dynamics each configuration is reached with equal probability, it follows that "atypical" configurations quickly evolve into "typical" ones, which almost never evolve back into "atypical" configurations. Within this line of thought, thermalization boils down to reaching a "typical" configuration. This happens much faster than any relevant exploration of phase space required by ergodicity. Note that this approach only applies when the measured quantity is macroscopic (such as the particle number mentioned in the example considered above). If one asks for the probability of being in a specific microscopic configuration, there is no meaning in separating "typical" from "atypical" configurations and the predictive power of this line of reasoning is lost. As appealing as this line of reasoning is, it lacks rigorous support.

Taking the second point of view, it is worth noting that while most configurations in phase space are "typical", such configurations are difficult to create using external perturbations. For example, imagine a piston is moved to compress air in a container. If the piston is not moved slowly enough, the gas inside the container will not have time to equilibrate and, as a result, during the piston's motion (and right after the piston stops) its density will not be uniform, that is, the system is not in a "typical" state. In a similar fashion, by applying a radiation pulse to a system, one will typically excite some degrees of freedom resonantly, for example, phonons directly coupled to the radiation. As a result, right after the pulse ends, the system is in an atypical state. Considering a wide range of experimental protocols, one can actually convince oneself that it is generally difficult to create "typical" configurations if one does not follow a very slow protocol or without letting the system evolve by itself.

At this point, a comment about time-reversal symmetry is in order. While the microscopic laws of physics usually exhibit time-reversal symmetry, notable exceptions include systems with external magnetic fields, the resulting macroscopic equations used to describe thermodynamic systems do not exhibit such a symmetry. This can be justified using the second line of reasoning – it is exponentially rare for a system to evolve into an "atypical" state by itself. Numerical experiments have been done (using integer arithmetic) in which a system was started in an atypical configuration, was left to evolve, and, after some time, the velocities of all particles were reversed. In those experiments, the system was seen to return to the initial (atypical) configuration [19]. Two essential points to be highlighted from these numerical simulations are: (i) after reaching the initial configuration, the system continued its evolution towards typical configurations (as expected, in a time-symmetric fashion) and (ii) the time-reversal transformation needed to be carried out with exquisite accuracy to observe a return to the initial (atypical) configuration (hence, the need of integer arithmetic). The difficulty in achieving the return increases dramatically with increasing system size and with the time one waits before applying the time-reversal transformation. It is now well understood, in the context of fluctuation theorems [20, 21], that violations of the second law (i.e., evolution from typical to atypical configurations) can occur with a probability that decreases exponentially with the number of degrees of freedom in the system. These have been confirmed experimentally (see,

e.g., Ref. [22]). As part of this review, we derive fluctuation theorems in the context of quantum mechanics [23, 24, 25].

Remarkably, a recent breakthrough [26, 27, 28] has put the understanding of thermalization in quantum systems on more solid foundations than the one discussed so far for classical systems. This breakthrough falls under the title of the eigenstate thermalization hypothesis (ETH). This hypothesis can be formulated as a mathematical ansatz with strong predictive powers [29]. ETH and its implications for statistical mechanics and thermodynamics are the subject of the review. As we discuss, ETH combines ideas of chaos and typical configurations in a clear mathematical form that is unparalleled in classical systems. This is remarkable considering that, in some sense, the relation between microscopic dynamics and statistical mechanics is more subtle in quantum mechanics than in classical mechanics. In fact, in quantum mechanics one usually does not use the notion of phase space as one cannot measure the positions and momenta of particles simultaneously. The equation dictating the dynamics (Schrödinger's equation) is linear which implies that the key ingredient leading to chaos in classical systems, that is, nonlinear equations of motion, is absent in quantum systems.

As already noted by von Neumann in 1929, when discussing thermalization in isolated quantum systems one should focus on physical observables as opposed to wave functions or density matrices describing the entire system [30]. This approach is similar to the one described above for classical systems, in which the focus is put on macroscopic observables and "typical" configurations. In this spirit, ETH states that the eigenstates of generic quantum Hamiltonians are "typical" in the sense that the statistical properties of physical observables[12] are the same as those predicted by the microcanonical ensemble. As we will discuss, ETH implies that the expectation values of such observables as well as their fluctuations in isolated quantum systems far from equilibrium relax to (nearly) time-independent results that can be described using traditional statistical mechanics ensembles [26, 27, 28]. This has been verified in several quantum lattice systems and, according to ETH, should occur in generic many-body quantum systems. We also discuss how ETH is related to quantum chaos in many-body systems, a subject pioneered by Wigner in the context of Nuclear Physics [31]. Furthermore, we argue that one can build on ETH not only to understand the emergence of a statistical mechanics description in isolated quantum systems, but also to derive basic thermodynamic relations, linear response relations, and fluctuation theorems.

When thinking about the topics discussed in this review some may complain about the fact that, unless the entire universe is considered, there is no such thing as an isolated system, i.e., that any description of a system of interest should involve a bath of some sort. While this observation is, strictly speaking, correct, it is sometimes experimentally irrelevant. The time scales dictating internal equilibration in "well-isolated" systems can be much faster than the time scales introduced by the coupling to the "outside world". It then makes sense to question whether, in experiments with well-isolated systems, observables can be described using statistical mechanics on time scales much shorter than those introduced by the coupling to the outside world. This question is of relevance to current experiments with a wide variety of systems. For example, in ultracold quantum gases that are trapped in ultrahigh vacuum by means of (up to a good approximation) conservative potentials [32, 33]. The near unitary dynamics of such systems has been observed in beautiful experiments on collapse and revival phenomena of bosonic [34, 35, 36] and fermionic [37] fields, lack of relaxation to the predictions of traditional ensembles of statistical mechanics [38, 39, 40], and dynamics in optical lattices that were found to be in very good agreement with numerical predictions for unitary dynamics [41]. In optical lattice experiments, the energy conservation constraint, imposed by the fact that the system are "isolated", has also allowed the observation of counterintuitive phenomena such as the formation of stable repulsive bound atom pairs [42] and quantum distillation [43] in

[12] We will explain what we mean by physical observables when discussing the ETH ansatz.

ultracold bosonic systems. Other examples of nearly isolated systems include nuclear spins in diamond [44], pump-probe experiments in correlated materials in which dynamics of electrons and holes are probed on time scales much faster than the relaxation time associated with electron-phonon interactions [45, 46], and ensembles of ultra-relativistic particles generated in high-energy collisions [47].

This review can naturally be separated in two parts, and an addendum. In the first part, Secs. 6.2–6.4, we briefly introduce the concept of quantum chaos, discuss its relation to random matrix theory (RMT), and calculate its implications to observables. We then introduce ETH, which is a natural extension of RMT, and discuss its implications to thermalization in isolated systems, that is, relaxation of observables to the thermal equilibrium predictions. We illustrate these ideas with multiple numerical examples. In the second part, Secs. 6.5–6.7, we extend our discussion of the implications of quantum chaos and ETH to dynamical processes. We show how one can use quantum chaos and ETH to derive various thermodynamic relations (such as fluctuation theorems, fluctuation-dissipation relations, Onsager relations, and Einstein relations), determine leading finite-size corrections to those relations, and, in some cases, generalize them (e.g., the Onsager relation) beyond equilibrium. Finally, in the addendum (Sec. 6.8), we discuss the relaxation dynamics and description after relaxation of integrable systems after a quench. We introduce the generalized Gibbs ensemble (GGE), and, using time-dependent perturbation theory, show how it can be used to derive kinetic equations. We note that some of these topics have been discussed in other recent reviews [48, 49, 50, 51, 52, 53] and special journal issues [54, 55].

6.2 Chaos and Random Matrix Theory (RMT)

6.2.1 Classical Chaos

In this section, we very briefly discuss chaotic dynamics in classical systems. We refer the readers to Refs. [56, 57], and the literature therein, for further information about this topic. As the focus of this review is on quantum chaos and the eigenstate thermalization hypothesis, we will not attempt to bridge classical chaos and thermalization. This has been a subject of continuous controversies.

While there is no universally accepted rigorous definition of chaos, a system is usually considered chaotic if it exhibits a strong (exponential) sensitivity of phase-space trajectories to small perturbations. Although chaotic dynamics are generic, there is a class of systems for which dynamics are not chaotic. They are known as integrable systems [58]. Specifically, a classical system whose Hamiltonian is $H(\mathbf{p},\mathbf{q})$, with canonical coordinates $\mathbf{q}=(q_1,\cdots,q_N)$ and momenta $\mathbf{p}=(p_1,\cdots,p_N)$, is said to be integrable if it has as many functionally independent conserved quantities $\mathbf{I}=(I_1,\cdots,I_N)$ in involution as degrees of freedom N:

$$\{I_j,H\}=0,\quad \{I_j,I_k\}=0,\quad \text{where}\quad \{f,g\}=\sum_{j=1,N}\frac{\partial f}{\partial q_j}\frac{\partial g}{\partial p_j}-\frac{\partial f}{\partial p_j}\frac{\partial g}{\partial q_j}. \tag{6.1}$$

From Liouville's integrability theorem [59], it follows that there is a canonical transformation $(p,q)\to(I,\Theta)$ (where I,Θ are called action-angle variables) such that $H(p,q)=H(I)$ [58]. As a result, the solutions of the equations of motion for the action-angle variables are trivial: $I_j(t)=I_j^0=$ constant, and $\Theta_j(t)=\Omega_j t+\Theta_j(0)$. For obvious reasons, the motion is referred to as taking place on an N-dimensional torus, and it is not chaotic.

To get a feeling for the differences between integrable and chaotic systems, in Fig. 6.1, we illustrate the motion of a particle in both an integrable and a chaotic two-dimensional cavity [60]. Figure 6.1(a) illustrates the trajectory of a particle in an integrable circular cavity. It is visually apparent that the trajectory is a superposition of two periodic motions along the

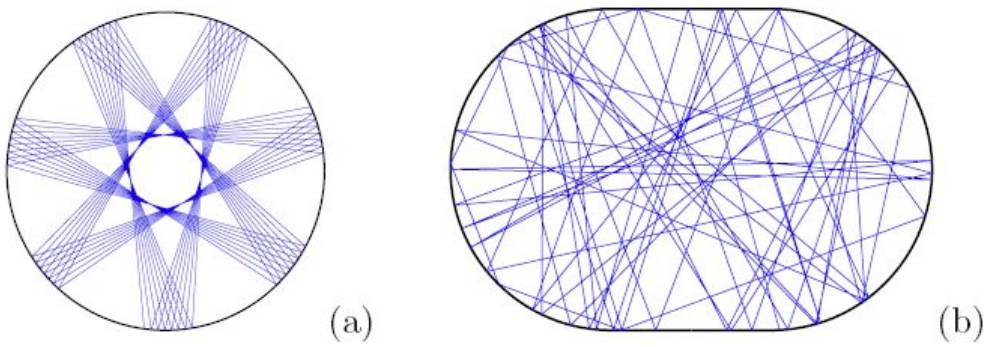

Figure 6.1: Examples of trajectories of a particle bouncing in a cavity: (a) non-chaotic circular and (b) chaotic Bunimovich stadium. The images were taken from scholarpedia [60].

radial and angular directions. This is a result of the system having two conserved quantities, energy and angular momentum [61]. Clearly, the long-time average of the particle density does not correspond to a uniform probability which covers phase space. Figure 6.1(b), on the other hand, shows a trajectory of a particle in a chaotic Bunimovich stadium [10], which looks completely random. If one compares two trajectories that are initially very close to each other in phase space one finds that, after a few bounces against the walls, they become uncorrelated both in terms of positions and directions of motion. This is a consequence of chaotic dynamics.

There are many examples of dynamical systems that exhibit chaotic behavior. A necessary, and often sufficient, condition for chaotic motion to occur is that the number of functionally independent conserved quantities (integrals of motion), which are in involution, is smaller than the number of degrees of freedom. Otherwise, as mentioned before, the system is integrable and the dynamics is “simple". This criterion immediately tells us that the motion of one particle, without internal degrees of freedom, in a one-dimensional system, described by a static Hamiltonian, is integrable. The energy provides a unique (up to a sign) relation between the coordinate and the momentum of the particle. In two dimensions, energy conservation is not sufficient to constrain the two components of the momentum at a given position in space, and chaos is possible. However, if an additional conservation law is present, e.g., angular momentum in the example of Fig. 6.1(a), then the motion is regular. As a generalization of the above, a many-particle system is usually considered chaotic if it does not have an extensive number of conserved quantities. For example, an ensemble of noninteracting particles in high-dimensional systems is not chaotic in this sense, even if each particle exhibits chaotic motion in the part of phase space associated with its own degrees of freedom. This due to the fact that the energy of each particle is separately conserved. However, one expects that interactions between the particles will lead to chaotic motion.

It is natural to ask what happens to an integrable system in the presence of a small integrability breaking perturbation. The KAM theorem (after Kolmogorov, Arnold, and Moser [62, 63, 64]) states that, under quite general conditions and for systems with a finite number of degrees of freedom, most of the tori that foliate phase space in the integrable limit persist under small perturbations [59]. This means that, in finite systems, there is a crossover between regular and chaotic dynamics.

It is instructive to see how chaos emerges in simple system. The easiest way to do this is to study one particle in one dimension and remove the energy conservation by applying a time-dependent protocol.

Very well-studied examples of such driven systems (usually exhibiting a coexistence of

chaotic and regular motion in different parts of phase space) include the Fermi-Ulam model [65], the Kapitza pendulum [66], and the kicked rotor [67, 68].

(I'll look later at them)

The latter example provides, perhaps, the simplest realization of a chaotic system. As an illustration, we discuss it in detail in Appendix 6.9.

6.2.2 Random Matrix Theory

(what is it????)

A focus of this review is on eigenstate thermalization which, as we argue in the following, is closely related to quantum chaos (see, e.g., Refs.[69, 70], for numerical studies that discuss it). In this section, we review results from quantum chaos that will be needed later. We refer the readers to more complete reviews on quantum chaos and RMT for further details [71, 72, 73, 74].

From the early days of quantum mechanics, it was clear that the classical notion of chaos does not directly apply to quantum-mechanical systems. The main reason is that Schrödinger's equation is linear and therefore cannot have exponentially departing trajectories for the wave functions. As a matter of fact, the overlap between two different quantum states, evolved with the same Hamiltonian, is constant in time. Also, while quantum mechanics can be formulated in a phase-space language, for example, using the Wigner-Weyl quantization [75, 76], one still does not have the notion of a trajectory (and thus its sensitivity to small perturbations) since coordinates and momenta of particles cannot be defined simultaneously due to the uncertainty principle. It is then natural to ask what is the analogue of chaotic motion in quantum systems.

To better understand this question, let us first consider the single-particle classical limit. For integrable systems, the physics was understood in the early days of quantum mechanics, based on Bohr's initial insight. Along allowed trajectories, the classical reduced action satisfies the quantization condition:

$$\oint pdq \approx 2\pi\hbar n\,. \tag{6.2}$$

Namely, the classical action is quantized in units of $\hbar$. In 1926, this conjecture was formalized by what is now known as the WKB (after Wentzel, Kramers, and Brillouin) approximation [77]. Essentially, the WKB quantization implies that, in the semi-classical limit, one has to discretize (quantize) classical trajectories. In chaotic systems, the situation remained unclear for a very long time. In particular, it was not clear how to quantize classical chaotic trajectories, which are not closed (in phase space). Initial attempts to resolve these issues go back to Einstein who wrote a paper about them already in 1917 (see Ref. [78] for details). However, the question was largely ignored until the 1970s when, after a pioneering work by Gutzwiller [79], it became the focus of much research broadly falling under the title of quantum chaos. To this day many questions remain unresolved, including the precise definition of quantum chaos [80].

A set of crucial results on which quantum chaos builds came from works of Wigner [31, 81, 82] who, followed by Dyson [83] and others, developed a theory for understanding the spectra of complex atomic nuclei. This theory is now known as RMT [73]. RMT became one of the cornerstones of modern physics and, as we explain later, underlies our understanding of eigenstate thermalization. Wigner's original idea was that it is hopeless to try to predict the exact energy levels and corresponding eigenstates of complex quantum-mechanical systems such as large nuclei. Instead, one should focus on their statistical properties. His second insight was that, if one looks into a small energy window where the density of states is constant, then the Hamiltonian, in a non *fine-tuned* basis, will look essentially like a random matrix. Therefore, by studying statistical properties of random matrices (subject to the symmetries

of the Hamiltonian of interest, such as time-reversal symmetry), one can gain insights on the statistical properties of energy levels and eigenstates of complex systems. This latter insight was very revolutionary and counterintuitive. It should be noted that whenever we attempt to diagonalize many-body physical Hamiltonians, we usually write them in special bases in which the resulting matrices are very sparse and the nonzero matrix elements are anything but random. This, however, does not contradict Wigner's idea which deals with "generic" bases.

The main ideas of RMT and the statistics of the energy levels (known as Wigner-Dyson statistics) can be understood using 2×2 Hamiltonians whose entries are random numbers taken from a Gaussian distribution [71, 72, 73, 74]:

$$\hat{H} \doteq \begin{bmatrix} \varepsilon_1 & \frac{V}{\sqrt{2}} \\ \frac{V^*}{\sqrt{2}} & \varepsilon_2 \end{bmatrix}. \tag{6.3}$$

Here the factor $1/\sqrt{2}$ in the off-diagonal matrix elements is introduced since, as it will become clear soon, this choice leaves the form of the Hamiltonian invariant under basis rotations. The Hamiltonian in Eq. (6.3) can be easily diagonalized and the eigenvalues are

$$E_{1,2} = \frac{\varepsilon_1+\varepsilon_2}{2} \pm \frac{1}{2}\sqrt{(\varepsilon_1-\varepsilon_2)^2+2|V|^2}. \tag{6.4}$$

If the system is invariant under time reversal (e.g., there is no external magnetic field) then the Hamiltonian can be written as a real matrix, so $V = V^*$. For simplicity, we draw ε_1, ε_2, and V from a Gaussian distribution with zero mean and variance σ. Using Eq. (6.4) one can compute the statistics of the level separations $P(E_1 - E_2 = \omega) \equiv P(\omega)$ (here and in what follows, unless otherwise specified, we set $\hbar$ to unity):

$$P(\omega) = \frac{1}{(2\pi)^{3/2}\sigma^3}\int d\varepsilon_1 \int d\varepsilon_2 \int dV\, \delta\left(\sqrt{(\varepsilon_1-\varepsilon_2)^2+2V^2}-\omega\right)\exp\left(-\frac{\varepsilon_1^2+\varepsilon_2^2+V^2}{2\sigma^2}\right). \tag{6.5}$$

Before evaluating the integral over ε_1, we make a change of variables $\varepsilon_2 = \varepsilon_1 + \sqrt{2}\xi$. Then, integrating over ε_1, which is a Gaussian integral, we are left with

$$P(\omega) = \frac{1}{2\pi\sigma^2}\int\int d\xi dV\, \delta\left(\sqrt{2\xi^2+2V^2}-\omega\right)\exp\left(-\frac{\xi^2+V^2}{2\sigma^2}\right). \tag{6.6}$$

The latter integrals can be evaluated using cylindrical coordinates, $V = r\cos(x)$, $\xi = r\sin(x)$, and one finds:

$$P(\omega) = \frac{\omega}{2\sigma^2}\exp\left[-\frac{\omega^2}{4\sigma^2}\right]. \tag{6.7}$$

In the absence of time-reversal symmetry, $\Re[V]$ and $\Im[V]$ can be treated as independent random variables and, carrying out a similar calculation using spherical coordinates, leads to:

$$P(\omega) = \frac{\omega^2}{2\sqrt{\pi}\,(\sigma^2)^{3/2}}\exp\left[-\frac{\omega^2}{4\sigma^2}\right]. \tag{6.8}$$

These distributions exhibit some remarkable (generic) properties: (i) there is level repulsion since the probability $P(\omega)$ of having energy separation ω vanishes as $\omega \to 0$ and (ii) the probability decays as a Gaussian at large energy separation. The two distributions (6.7) and (6.8) can be written as

$$P(\omega) = A_\beta\, \omega^\beta\, \exp[-B_\beta \omega^2], \tag{6.9}$$

where $\beta = 1$ in systems with time-reversal symmetry and $\beta = 2$ in systems that do not have time-reversal symmetry. The coefficients A_β and B_β are found by normalizing $P(\omega)$ and fixing

the mean level spacing. The normalized distributions, with an average level spacing set to one, are given by

$$P_1(\omega) = \frac{\pi}{2}\omega \exp\left[-\frac{\pi}{4}\omega^2\right], \qquad P_2(\omega) = \frac{32}{\pi^2}\omega^2 \exp\left[-\frac{4}{\pi}\omega^2\right]. \tag{6.10}$$

It turns out that the features described above are not unique to the 2×2 Hamiltonian (6.3). In fact, this simple example can be generalized to larger matrices. In particular, one can define an ensemble of matrices drawn from a random Gaussian distribution [72]:

$$P(\hat{H}) \propto \exp\left[-\frac{\beta}{2a^2}\mathrm{Tr}(\hat{H}^2)\right] \equiv \exp\left[-\frac{\beta}{2a^2}\sum_{ij} H_{ij}H_{ji}\right], \tag{6.11}$$

where a sets the overall energy scale and, as before, $\beta = 1$ refers to systems with time-reversal symmetry where all entries in the Hamiltonian are real and satisfy $H_{ij} = H_{ji}$, that is, the so-called Gaussian orthogonal ensemble (GOE), and $\beta = 2$ refers to systems without time-reversal symmetry, where the entities are complex and satisfy $H_{ij} = H^*_{ji}$, that is, the so-called Gaussian unitary ensemble (GUE).[13] Note that the factor of $\sqrt{2}$ in Eq. (6.3) ensures that the Hamiltonian is described by the distribution (6.11).

The choice of the ensemble in Eq. (6.11) is a natural one. The ensemble must be invariant under any orthogonal (GOE) or unitary (GUE) transformation, so the probability distribution can only depend on the invariant $\mathrm{Tr}(\hat{H}^2)$. It is Gaussian because $\mathrm{Tr}(\hat{H}^2)$ is a sum of many independent contributions and should therefore satisfy the central limit theorem. We will not discuss the details of the derivations of the level statistics for such random ensembles, which can be found in Refs. [74, 71, 73, 72, 84]. We only point out that the exact level spacing distributions (known as Wigner-Dyson distributions) do not have a closed analytic form. However, they are qualitatively (and quantitatively) close to the Wigner Surmise (6.9).

Following Wigner's ideas, it was possible to explain the statistical properties of the spectra of complex nuclei. However, for a long time it was not clear which are the "complex systems" for which RMT is generally applicable. In 1984, Bohigas, Giannoni, and Schmit, studying a single particle placed in an infinite potential well with the shape of a Sinai billiard, found that at high energies (i.e., in the semi-classical limit), and provided that one looks at a sufficiently narrow energy window, the level statistics is described by the Wigner-Dyson distribution [85]. Based on this discovery, they conjecture that the level statistics of quantum systems that have a classically chaotic counterpart are described by RMT (this is known as the BGS conjecture). This conjecture has been tested and confirmed in many different setups (we will show some of them in the next section). To date, only non-generic counterexamples, such as arithmetic billiards, are known to violate this conjecture [86]. Therefore, the emergence of Wigner-Dyson statistics for the level spacings is often considered as a defining property of quantum chaotic systems, whether such systems have a classical counterpart or not.

Chaotic Eigenfunctions

RMT allows one to make an important statement about the eigenvectors of random matrices. The joint probability distribution of components of eigenvectors can be written as [87, 72]

$$P_{\mathrm{GOE}}(\psi_1, \psi_2, \ldots, \psi_N) \propto \delta\left(\sum_j \psi_j^2 - 1\right), \quad P_{\mathrm{GUE}}(\psi_1, \psi_2, \ldots, \psi_N) \propto \delta\left(\sum_j |\psi_j|^2 - 1\right), \tag{6.12}$$

[13] There is a third ensemble, corresponding to $\beta = 4$, known as the Gaussian simplectic ensemble (GSE). We will not discuss here.

where ψ_j are the components of the wave functions in some fixed basis. This form follows from the fact that, because of the orthogonal (unitary) invariance of the random matrix ensemble, the distribution can depend only on the norm $\sqrt{\sum_j \psi_j^2}$ $\left(\sqrt{\sum_j |\psi_j^2|}\right)$ of the eigenvector, and must be proportional to the δ-functions in Eq. (6.12) because of the normalization [87]. Essentially, Eq. (6.12) states that the eigenvectors of random matrices are random unit vectors, which are either real (in the GOE) or complex (in the GUE). Of course, different eigenvectors are not completely independent since they need to be orthogonal to each other. However, because two uncorrelated random vectors in a large-dimensional space are, in any case, nearly orthogonal, in many instances the correlations due to this orthogonality condition can be ignored.

One may wonder about the classical limit of quantum eigenvectors. The latter are stationary states of the system and should therefore correspond to stationary (time-averaged) trajectories in the classical limit. In integrable systems with a classical limit, the quantum eigenstates factorize into a product of WKB-like states describing the stationary phase-space probability distribution of a particle corresponding to one of the trajectories [77]. However, if the system is chaotic, the classical limit of the quantum eigenstates is ill-defined. In particular, in the classical limit, there is no smooth (differentiable) analytic function that can describe the eigenstates of chaotic systems. This conclusion follows from the BGS conjecture, which implies that the eigenstates of a chaotic Hamiltonian in non-fine-tuned bases, including the real space basis, are essentially random vectors with no structure.

Let us address a point that often generates confusion. Any given (Hermitian) Hamiltonian, whether it is drawn from a random matrix ensemble or not, can be diagonalized and its eigenvectors form a basis. In this basis, the Hamiltonian is diagonal and RMT specifies the statistics of the eigenvalues. The statistical properties of the eigenstates are specified for an ensemble of random Hamiltonians *in a fixed basis*. If we fix the basis to be that of the eigenkets of the first random Hamiltonian we diagonalize, that basis will not be special for other randomly drawn Hamiltonians. Therefore, all statements made will hold for the ensemble even if they fail for one of the Hamiltonians. The issue of the basis becomes more subtle when one deals with physical Hamiltonians. Here, one can ask what happens if we diagonalize a physical Hamiltonian and use the eigenvectors obtained as a basis to write a slightly modified version of the same Hamiltonian (which is obtained, say, by slightly changing the strength of the interactions between particles). As we discuss below (see also Ref. [72]), especially in the context of many-body systems, the eigenstates of chaotic quantum Hamiltonians [which are away from the edge(s) of the spectrum][14] are very sensitive to small perturbations. Hence, one expects that the perturbed Hamiltonian will look like a random matrix when written in the unperturbed basis. In that sense, writing a Hamiltonian in its own basis can be considered to be a fine-tuning of the basis. It is in this spirit that one should take Wigner's insight. The sensitivity just mentioned in chaotic quantum systems is very similar to the sensitivity of classical chaotic trajectories to either initial conditions or the details of the Hamiltonian.

The Structure of the Matrix Elements of Operators

Let us now analyze the structure of matrix elements of Hermitian operators

$$\hat{O} = \sum_i O_i |i\rangle\langle i|, \quad \text{where} \quad \hat{O}|i\rangle = O_i|i\rangle, \tag{6.13}$$

[14] That one needs to be away from the edges of the spectrum can already be inferred from the fact that BGS found that the Wigner-Dyson distribution occurs only at sufficiently high energies [85]. We will discuss this point in detail when presenting results for many-body quantum systems.

within RMT. For any given random Hamiltonian, for which the eigenkets are denoted by $|m\rangle$ and $|n\rangle$,

$$O_{mn} \equiv \langle m|\hat{O}|n\rangle = \sum_i O_i \langle m|i\rangle\langle i|n\rangle = \sum_i O_i (\psi_i^m)^* \psi_i^n. \tag{6.14}$$

Here, $\psi_i^m \equiv \langle i|m\rangle$ and similarly for ψ_i^n. Recall that the eigenstates of random matrices in any basis are essentially random orthogonal unit vectors. Therefore, to leading order in $1/\mathcal{D}$, where $\mathcal{D}$ is the dimension of the Hilbert space, we have

$$\overline{(\psi_i^m)^*(\psi_j^n)} = \frac{1}{\mathcal{D}}\delta_{mn}\delta_{ij}\,, \tag{6.15}$$

where the average $\overline{(\psi_i^m)^*(\psi_j^n)}$ is over random eigenkets $|m\rangle$ and $|n\rangle$. This implies that one has very different expectation values for the diagonal and off-diagonal matrix elements of $\hat{O}$. Indeed, using Eqs. (6.14) and (6.15), we find

$$\overline{O_{mm}} = \frac{1}{\mathcal{D}}\sum_i O_i \equiv \bar{O}, \tag{6.16}$$

and

$$\overline{O_{mn}} = 0, \quad \text{for} \quad m \neq n. \tag{6.17}$$

Moreover, the fluctuations of the diagonal and off-diagonal matrix elements are suppressed by the size of the Hilbert space. For the diagonal matrix elements

$$\begin{aligned}\overline{O_{mm}^2} - \overline{O_{mm}}^2 &= \sum_{i,j} O_i O_j \overline{(\psi_i^m)^*\psi_i^m\,(\psi_j^m)^*\psi_j^m} - \sum_{i,j} O_i O_j \overline{(\psi_i^m)^*\psi_i^m}\;\overline{(\psi_j^m)^*\psi_j^m} \\ &= \sum_i O_i^2 \left(\overline{|\psi_i^m|^4} - (\overline{|\psi_i^m|^2})^2\right) = \frac{3-\beta}{\mathcal{D}^2}\sum_i O_i^2 \equiv \frac{3-\beta}{\mathcal{D}}\,\overline{O^2},\end{aligned} \tag{6.18}$$

where, as before, $\beta = 1$ for the GOE and $\beta = 2$ for the GUE. For the GOE (ψ_i^m are real numbers), we used the relation $\overline{(\psi_i^m)^4} = 3[\overline{(\psi_i^m)^2}]^2$, while for the GUE ($\psi_i^m$ are complex numbers), we used the relation $\overline{|\psi_i^m|^4} = 2(\overline{|\psi_i^m|^2})^2$. These results are a direct consequence of the Gaussian distribution of the components of the random vector ψ_i^m. Assuming that none of the eigenvalues O_i scales with the size of the Hilbert space, as is the case for physical observables, we see that the fluctuations of the diagonal matrix elements of $\hat{O}$ are inversely proportional to the square root of the size of the Hilbert space.

Likewise, for the absolute value of the off-diagonal matrix elements, we have

$$\overline{|O_{mn}|^2} - \left|\overline{O_{mn}}\right|^2 = \sum_i O_i^2 \overline{|\psi_i^m|^2|\psi_i^n|^2} = \frac{1}{\mathcal{D}}\overline{O^2}. \tag{6.19}$$

Combining these expressions, we see that, to leading order in $1/D$, the matrix elements of any operator can be written as

$$O_{mn} \approx \bar{O}\delta_{mn} + \sqrt{\frac{\overline{O^2}}{\mathcal{D}}}R_{mn}, \tag{6.20}$$

where R_{mn} is a random variable (which is real for the GOE and complex for the GUE) with zero mean and unit variance (for the GOE, the variance of the diagonal components R_{mm} is 2). It is straightforward to check that the ansatz (6.20) indeed correctly reproduces the mean and the variance of the matrix elements of $\hat{O}$ given by Eqs. (6.16)–(6.19).

In deriving Eqs. (6.16)–(6.19), we averaged over a fictitious ensemble of random Hamiltonians. However, from Eq. (6.20), it is clear that for large $\mathcal{D}$ the fluctuations of operators are small and thus one can use the ansatz (6.20) for a given fixed Hamiltonian.

6.2.3 Berry-Tabor Conjecture

In classical systems, an indicator of whether they are integrable or chaotic is the temporal behavior of nearby trajectories. In quantum systems, the role of such an indicator is played by the energy level statistics. In particular, for chaotic systems, as we discussed before, the energy levels follow the Wigner-Dyson distribution. For quantum integrable systems, the question of level statistics was first addressed by Berry and Tabor in 1977 [88]. For a particle in one dimension, which we already said exhibits non-chaotic classical dynamics if the Hamiltonian is time independent, we know that if we place it in a harmonic potential all levels are equidistant, while if we place it in an infinite well the spacing between levels increases as the energy of the levels increases. Hence, the statistics of the level spacings strongly depends on the details of the potential considered. This is unique to one particle in one dimension. It changes if one considers systems whose classical counterparts have more than one degree of freedom, for example, one particle in higher dimensional potentials, or many particles in one dimension. A very simple example of a non-ergodic system, with many degrees of freedom, would be an array of independent harmonic oscillators with incommensurate frequencies. These can be, for example, the normal modes in a harmonic chain. Because these oscillators can be diagonalized independently, the many-body energy levels of such a system can be computed as

$$E = \sum_j n_j \omega_j, \tag{6.21}$$

where n_j are the occupation numbers and ω_j are the mode frequencies. If we look into high energies, E, when the occupation numbers are large, nearby energy levels (which are very closely spaced) can come from very different sets of $\{n_j\}$. This means that the energy levels E are effectively uncorrelated with each other and can be treated as random numbers. Their distribution then should be described by Poisson statistics, that is, the probability of having n energy levels in a particular interval $[E, E + \delta E]$ will be

$$P_n = \frac{\lambda^n}{n!} \exp[-\lambda], \tag{6.22}$$

where λ is the average number of levels in that interval. Poisson and Wigner-Dyson statistics are very different in that, in the former there is no level repulsion. For systems with Poisson statistics, the distribution of energy level separations ω (with mean separation set to one) is

$$P_0(\omega) = \exp[-\omega], \tag{6.23}$$

which is very different from the Wigner Surmise (6.10). The statement that, for quantum systems whose corresponding classical counterpart is integrable, the energy eigenvalues generically behave like a sequence of independent random variables, that is, exhibit Poisson statistics, is now known as the Berry-Tabor conjecture [88]. While this conjecture describes what is seen in many quantum systems whose classical counterpart is integrable, and integrable quantum systems without a classical counterpart, there are examples for which it fails (such as the single particle in the harmonic potential described above and other harmonic systems [89]). Deviations from Poisson statistics are usually the result of having symmetries in the Hamiltonian that lead to extra degeneracies resulting in commensurability of the spectra.

The ideas discussed above are now regularly used when dealing with many-particle systems. The statistics of the energy levels of many-body Hamiltonians serves as one of the main indicators of quantum chaos or, conversely, of quantum integrability. As the energy levels become denser, the level statistics asymptotically approaches either the Wigner-Dyson or the Poisson distribution. It is interesting to note that in few-particle systems, like a particle in a billiard, the spectra become denser by going to the semi-classical limit by either increasing the energy

or decreasing Planck's constant, while in many-particle systems one can achieve this by going to the thermodynamic limit. This means that the level statistics indicators can be used to characterize whether a quantum system is chaotic or not even when it does not have a classical limit. This is the case, for example, for lattice systems consisting of spins 1/2 or interacting fermions described within the one-band approximation.

Finally, as we discuss later, the applicability of RMT requires that the energy levels analyzed are far from the edges of the spectrum and that the density of states as a function of energy is accounted for. The first implies that one needs to exclude, say, the ground state and low-lying excited states and the states with the highest energies (if the spectrum is bounded from above). It is plausible that in generic systems only states within subextensive energy windows near the edges of the spectrum are not described by RMT.

6.2.4 The Semi-Classical Limit and Berry's Conjecture

One of the most remarkable connections between the structure of the eigenstates of chaotic systems in the semi-classical limit and classical chaos was formulated by Berry [90], and is currently known as Berry's conjecture. (In this section, we return $\hbar$ to our equations since it will be important for taking the classical limit $\hbar \to 0$.)

In order to discuss Berry's conjecture, we need to introduce the Wigner function $W(\mathbf{x}, \mathbf{p})$, which is defined as the Wigner-Weyl transform of the density matrix $\hat{\rho}$ [75, 76]. For a pure state, $\hat{\rho} \equiv |\psi\rangle\langle\psi|$, one has

$$W(\mathbf{x}, \mathbf{p}) = \frac{1}{(2\pi\hbar)^{3N}} \int d^{3N}\xi \, \psi^* \left(\mathbf{x} + \frac{\boldsymbol{\xi}}{2}\right) \psi \left(\mathbf{x} - \frac{\boldsymbol{\xi}}{2}\right) \exp\left[-i\frac{\mathbf{p}\boldsymbol{\xi}}{\hbar}\right], \tag{6.24}$$

where $\mathbf{x}$, $\mathbf{p}$ are the coordinates and momenta of N-particles spanning a $6N$-dimensional phase space.

(why is it used and where????)

For a mixed state one replaces the product

$$\psi^* \left(\mathbf{x} + \frac{\boldsymbol{\xi}}{2}\right) \psi \left(\mathbf{x} - \frac{\boldsymbol{\xi}}{2}\right) \to \left\langle \mathbf{x} - \frac{\boldsymbol{\xi}}{2} \middle| \hat{\rho} \middle| \mathbf{x} + \frac{\boldsymbol{\xi}}{2} \right\rangle \equiv \rho \left(\mathbf{x} - \frac{\boldsymbol{\xi}}{2}, \mathbf{x} + \frac{\boldsymbol{\xi}}{2}\right), \tag{6.25}$$

where $\hat{\rho}$ is the density matrix. One can check that, similarly, the Wigner function can be defined by integrating over momentum

$$W(\mathbf{x}, \mathbf{p}) = \frac{1}{(2\pi\hbar)^{3N}} \int d^{3N}\eta \, \phi^* \left(\mathbf{p} + \frac{\boldsymbol{\eta}}{2}\right) \phi \left(\mathbf{p} - \frac{\boldsymbol{\eta}}{2}\right) \exp\left[i\frac{\mathbf{x}\boldsymbol{\eta}}{\hbar}\right], \tag{6.26}$$

where $\phi(\mathbf{p})$ is the Fourier transform of $\psi(\mathbf{x})$. From either of the two representations it immediately follows that

$$\int d^{3N}p \, W(\mathbf{x}, \mathbf{p}) = |\psi(\mathbf{x})|^2 \quad \text{and} \quad \int d^{3N}x \, W(\mathbf{x}, \mathbf{p}) = |\phi(\mathbf{p})|^2 \, . \tag{6.27}$$

The Wigner function is uniquely defined for any wave function (or density matrix) and plays the role of a quasi-probability distribution in phase space. In particular, it allows one to compute an expectation value of any observable $\hat{O}$ as a standard average [75, 76]:

$$\langle \hat{O} \rangle = \int d^{3N}x \, d^{3N}p \, O_W(\mathbf{x}, \mathbf{p}) W(\mathbf{x}, \mathbf{p}), \tag{6.28}$$

where $O_W(\mathbf{x}, \mathbf{p})$ is the Weyl symbol of the operator $\hat{O}$

$$O_W(\mathbf{x}, \mathbf{p}) = \frac{1}{(2\pi\hbar)^{3N}} \int d^{3N}\xi \left\langle \mathbf{x} - \frac{\boldsymbol{\xi}}{2} \middle| \hat{O} \middle| \mathbf{x} + \frac{\boldsymbol{\xi}}{2} \right\rangle \exp\left[-i\frac{\mathbf{p}\boldsymbol{\xi}}{\hbar}\right]. \tag{6.29}$$

We note that instead of the coordinate and momentum phase-space variables one can, for example, use coherent state variables to represent electromagnetic or matter waves, angular momentum variables to represent spin systems, or any other set of canonically conjugate variables [76].

Berry's conjecture postulates that, in the semi-classical limit of a quantum system whose classical counterpart is chaotic, the Wigner function of energy eigenstates (averaged over a vanishingly small phase space) reduces to the microcanonical distribution. More precisely, define

$$\overline{W(\mathbf{X},\mathbf{P})} = \int_{\Delta\Omega_1} \frac{dx_1 dp_1}{(2\pi\hbar)} \dots \int_{\Delta\Omega_N} \frac{dx_N dp_N}{(2\pi\hbar)} W(\mathbf{x},\mathbf{p}), \tag{6.30}$$

where $\Delta\Omega_j$ is a small phase-space volume centered around the point X_j, P_j. This volume is chosen such that, as $\hbar \to 0$, $\Delta\Omega_j \to 0$ and at the same time $\hbar/\Delta\Omega_j \to 0$. Berry's conjecture then states that, as $\hbar \to 0$,

$$\overline{W(\mathbf{X},\mathbf{P})} = \frac{1}{\int d^{3N}X d^{3N}P\, \delta[E - H(\mathbf{X},\mathbf{P})]} \delta[E - H(\mathbf{X},\mathbf{P})], \tag{6.31}$$

where $H(\mathbf{X},\mathbf{P})$ is the classical Hamiltonian describing the system, and $\delta[\dots]$ is a one-dimensional Dirac delta function. In Berry's words, "$\psi(\mathbf{x})$ is a Gaussian random function of $\mathbf{x}$ whose spectrum at $\mathbf{x}$ is simply the local average of the Wigner function $\overline{W(\mathbf{x},\mathbf{p})}$". Berry also considered quantum systems whose classical counterpart is integrable. He conjectured that the structure of the energy eigenstates of such systems is very different [90].

It follows from Berry's conjecture, see Eqs. (6.28) and (6.31), that the energy eigenstate expectation value of any observable in the semi-classical limit (of a quantum system whose classical counterpart is chaotic) is the same as a microcanonical average.

For a dilute gas of hard spheres, this was studied by Srednicki in 1994 [27]. Let us analyze the latter example in detail. Srednicki argued that the eigenstate corresponding to a high-energy eigenvalue E_n can chosen to be real and written as

$$\psi_n(\mathbf{x}) = \mathcal{N}_n \int d^{3N}p\, A_n(\mathbf{p}) \delta(\mathbf{p}^2 - 2mE_n) \exp[i\mathbf{p}\mathbf{x}/\hbar], \tag{6.32}$$

where $\mathcal{N}_n$ is a normalization constant, and $A_n^*(\mathbf{p}) = A_n(-\mathbf{p})$. In other words the energy eigenstates with energy E_n are given by a superposition of plane-waves with momentum $\mathbf{p}$ such that $E_n = \mathbf{p}^2/(2m)$. Assuming Berry's conjecture applies, $A_n(\mathbf{p})$ was taken to be a Gaussian random variable satisfying

$$\langle A_m(\mathbf{p}) A_n(\mathbf{p}')\rangle_{EE} = \delta_{mn} \frac{\delta^{3N}(\mathbf{p} + \mathbf{p}')}{\delta(|\mathbf{p}|^2 - |\mathbf{p}'|^2)}. \tag{6.33}$$

Here the average should be understood as over a fictitious "eigenstate ensemble" of energy eigenstates of the system indicated by "EE". This replaces the average over a small phase-space volume used by Berry. The denominator in this expression is needed for proper normalization.

From these assumptions, it follows that

$$\langle \phi_m^*(\mathbf{p}) \phi_n(\mathbf{p}')\rangle_{EE} = \delta_{mn}\, N_n^2\, (2\pi\hbar)^{3N} \delta(\mathbf{p}^2 - 2mE_n) \delta_V^{3N}(\mathbf{p} - \mathbf{p}'), \tag{6.34}$$

where $\phi_n(\mathbf{p})$ is the $3N$-dimensional Fourier transform of $\psi_n(\mathbf{x})$, and $\delta_V(\mathbf{p}) \equiv (2\pi\hbar)^{-3N} \int_V d^{3N}x \exp[i\mathbf{p}\mathbf{x}/\hbar]$ and $V = L^3$ is the volume of the system. It is straightforward to check, using Eqs. (6.34) and (6.26), that the Wigner function averaged over the eigenstate ensemble is indeed equivalent to the microcanonical distribution [Eq. (6.31)].

Using Eqs. (6.32)–(6.34) one can compute observables of interest in the eigenstates of the Hamiltonian. For example, substituting $\delta_V(\mathbf{0}) \to [L/(2\pi\hbar)]^{3N}$, one can calculate the momentum distribution function of particles in the eigenstate ensemble

$$\langle \phi_{nn}(\mathbf{p}_1)\rangle_{EE} \equiv \int d^3p_2 \dots d^3p_N \langle \phi_n^*(\mathbf{p})\phi_n(\mathbf{p})\rangle_{EE} = N_n^2 L^{3N} \int d^3p_2 \dots d^3p_N \delta(\mathbf{p}^2 - 2mE_n). \tag{6.35}$$

Finally, using the fact that $I_N(A) \equiv \int d^Np\delta(\mathbf{p}^2 - A) = (\pi A)^{N/2}/[\Gamma(N/2)A]$, which through the normalization of $\phi_n(\mathbf{p})$ allows one to determine $N_n^{-2} = L^{3N} I_{3N}(2mE_n)$, one obtains

$$\langle \phi_{nn}(\mathbf{p}_1)\rangle_{EE} = \frac{I_{3N-3}(2mE_n - \mathbf{p}_1^2)}{I_{3N}(2mE_n)} = \frac{\Gamma(3N/2)}{\Gamma[3(N-1)/2]} \left(\frac{1}{2\pi m E_n}\right)^{\frac{3}{2}} \left(1 - \frac{\mathbf{p}_1^2}{2mE_n}\right)^{\frac{(3N-5)}{2}}. \tag{6.36}$$

Defining a microcanonical temperature using $E_n = 3Nk_BT_n/2$, where k_B is the Boltzmann constant, and taking the limit $N \to \infty$ one gets

$$\langle \phi_{nn}(\mathbf{p}_1)\rangle_{EE} = \left(\frac{1}{2\pi m k_B T_n}\right)^{\frac{3}{2}} \exp\left(-\frac{\mathbf{p}_1^2}{2mk_BT_n}\right), \tag{6.37}$$

where we used that $\lim_{N\to\infty} \Gamma(N+B)/[\Gamma(N)N^B] = 1$, which is valid for $B \in \mathbf{R}$. We immediately see that the result obtained for $\langle \phi_{nn}(\mathbf{p}_1)\rangle_{EE}$ is the Maxwell-Boltzmann distribution of momenta in a thermal gas.

One can go a step further and show that the fluctuations of $\phi_{nn}(\mathbf{p}_1)$ about $\langle \phi_{nn}(\mathbf{p}_1)\rangle_{EE}$ are exponentially small in the number of particles [27]. Furthermore, it can be shown that if one requires the wave function $\psi_n(\mathbf{x})$ to be completely symmetric or completely antisymmetric one obtains, instead of the Maxwell-Boltzmann distribution in Eq. (6.37), the (canonical) Bose-Einstein or Fermi-Dirac distributions, respectively [27]. An approach rooted in RMT was also used by Flambaum and Izrailev to obtain, starting from statistical properties of the structure of chaotic eigenstates, the Fermi-Dirac distribution function in interacting fermionic systems [91, 92]. These ideas underlie the eigenstate thermalization hypothesis, which is the focus of this review.

In closing this section, let us note that formulating a slightly modified conjecture one can also recover the classical limit from the eigenstates. Namely, one can define a different coarse-graining procedure for the Wigner function:

$$\langle W(\mathbf{x},\mathbf{p})\rangle = \frac{1}{N_{\delta E}} \sum_{m \in E_m \pm \delta E} W_m(\mathbf{x},\mathbf{p}), \tag{6.38}$$

where the sum is taken over all, $N_{\delta E}$, eigenstates in a window δE, which vanishes in the limit $\hbar \to 0$ but contains an exponential (in the number of degrees of freedom) number of levels. We anticipate that in the limit $\hbar \to 0$ the function $\langle W(\mathbf{x},\mathbf{p})\rangle$ also reduces to the right-hand-side (RHS) of Eq. (6.30), that is,

$$\langle W(\mathbf{x},\mathbf{p})\rangle = \frac{1}{\int d^{3N}X d^{3N}P\, \delta[E - H(\mathbf{X},\mathbf{P})]} \delta[E - H(\mathbf{X},\mathbf{P})]. \tag{6.39}$$

However, this result does not require the system to be ergodic. While this conjecture has little to do with chaos and ergodicity, it suggests a rigorous way of defining classical microcanonical ensembles from quantum eigenstates. This is opposed to individual quantum states, which as we discussed do not have a well-defined classical counterpart.

6.3 Quantum Chaos in Physical Systems

6.3.1 Examples of Wigner-Dyson and Poisson Statistics

Random matrix statistics has found many applications since its introduction by Wigner. They extend far beyond the framework of the original motivation, and have been intensively explored in many fields (for a recent comprehensive review, see Ref. [93]). Examples of quantum systems whose spectra exhibit Wigner-Dyson statistics are: (i) heavy nuclei [94], (ii) Sinai billiards (square or rectangular cavities with circular potential barriers in the center) [85], which are classically chaotic as the Bunimovich stadium in Fig. 6.1, (iii) highly excited levels[15] of the hydrogen atom in a strong magnetic field [95], (iv) Spin-1/2 systems and spin-polarized fermions in one-dimensional lattices [69, 70]. Interestingly, the Wigner-Dyson statistics is also the distribution of spacings between zeros of the Riemann zeta function, which is directly related to prime numbers. In turn, these zeros can be interpreted as Fisher zeros of the partition function of a particular system of free bosons (see Appendix 6.10). In this section, we discuss in more detail some examples originating from over 30 years of research.

Heavy nuclei - Perhaps the most famous example demonstrating the Wigner-Dyson statistics is shown in Fig. 6.2. That figure depicts the cumulative data of the level spacing distribution obtained from slow neutron resonance data and proton resonance data of around 30 different heavy nuclei [96, 71]. All spacings are normalized by the mean level spacing. The data are shown as a histogram and the two solid lines depict the (GOE) Wigner-Dyson distribution and the Poisson distribution. One can see that the Wigner-Dyson distribution works very well, confirming Wigner's original idea.

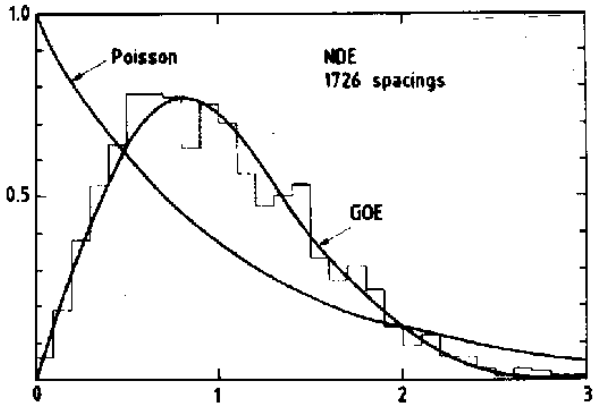

Figure 6.2: Nearest neighbor spacing distribution for the "Nuclear Data Ensemble" comprising 1726 spacings (histogram) versus normalized (to the mean) level spacing. The two lines represent predictions of the random matrix GOE ensemble and the Poisson distribution. Taken from Ref. [96]. See also Ref. [71].

Single particle in a cavity - Next, let us consider a much simpler setup, namely, the energy spectrum of a single particle in a cavity. Here, we can contrast the Berry-Tabor and BGS conjectures. To this end, in Fig. 6.3, we show the distribution of level spacings for two cavities: (left panel) an integrable rectangular cavity with sides a and b such that $a/b = \sqrt[4]{5}$ and $ab = 4\pi$ and (right panel) a chaotic cavity constructed from two circular arcs and two line segments (see inset) [80]. These two plots beautifully confirm the two conjectures. The distribution on the left panel, as expected from the Berry-Tabor conjecture, is very well described by the Poisson

[15] The low-energy spectra of this system exhibits Poissonian level statistics. This is understandable as, at low energies, the motion of the equivalent classical system is regular [95]. See also Fig. 6.4.

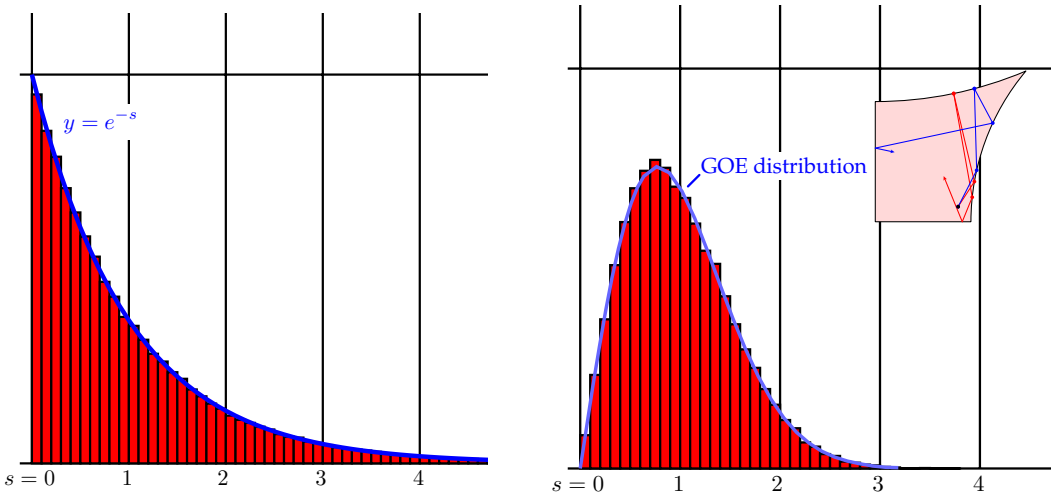

Figure 6.3: (Left panel) Distribution of 250,000 single-particle energy level spacings in a rectangular two-dimensional box with sides a and b such that $a/b = \sqrt[4]{5}$ and $ab = 4\pi$. (Right panel) Distribution of 50,000 single-particle energy level spacings in a chaotic cavity consisting of two arcs and two line segments (see inset). The solid lines show the Poisson (left panel) and the GOE (right panel) distributions. From Ref. [80].

distribution. This occurs despite the fact that the corresponding classical system has only two degrees of freedoms [recall that in the argument used to justify the Berry-Tabor conjecture, Eqs. (6.21)–(6.23), we relied on having many degrees of freedom]. The right panel depicts a level distribution that is in perfect agreement with the GOE, in accordance with the BGS conjecture.

Hydrogen atom in a magnetic field - A demonstration of a crossover between Poisson statistics and Wigner-Dyson statistics can be seen in another single-particle system – a hydrogen atom in a magnetic field. The latter breaks the rotational symmetry of the Coulomb potential

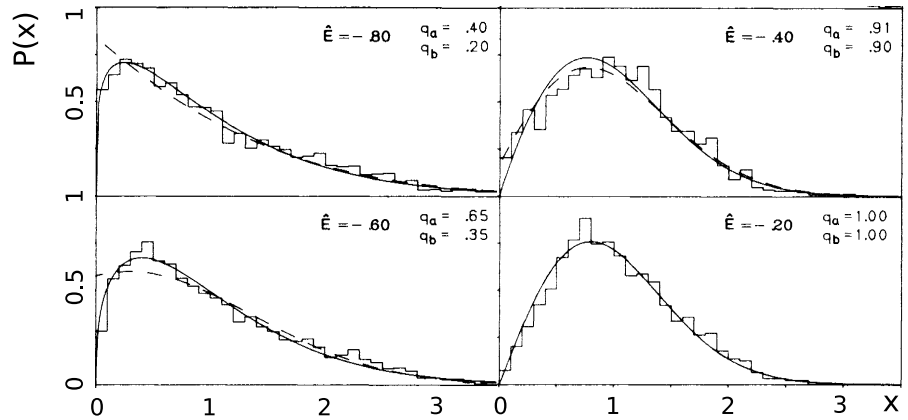

Figure 6.4: The level spacing distribution of a hydrogen atom in a magnetic field. Different plots correspond to different mean dimensionless energies $\hat{E}$, measured in natural energy units proportional to $B^{2/3}$, where B is the magnetic field. As the energy increases one observes a crossover between Poisson and Wigner-Dyson statistics. The numerical results are fitted to a Brody distribution (solid lines) [87], and to a semi-classical formula due to Berry and Robnik (dashed lines) [97]. From Ref. [95].

and hence there is no conservation of the total angular momentum. As a result, the classical system has coexistence of regions with both regular (occurring at lower energies) and chaotic (occurring at higher energies) motion [98]. Results of numerical simulations (see Fig. 6.4) show a clear interpolation between Poisson and Wigner-Dyson level statistics as the dimensionless energy (denoted by $\hat{E}$) increases [95]. Note that at intermediate energies the statistics is neither Poissonian nor Wigner-Dyson, suggesting that the structure of the energy levels in this range is richer. In the plots shown, the numerical results are fitted to a Brody distribution (solid lines) [87], which interpolates between the Poisson distribution and the GOE Wigner surmise, and to a semi-classical formula due to Berry and Robnik (dashed lines) [97]. We are not aware of a universal description of Hamiltonian ensembles corresponding to the intermediate distribution.

Lattice models - As we briefly mentioned earlier, RMT theory and the Berry-Tabor conjecture also apply to interacting many-particle systems that do not have a classical counterpart. There are several models in one-dimensional lattices that fall in this category. They allow one to study the crossover between integrable and nonintegrable regimes by tuning parameters of the Hamiltonian [33]. A few of these models have been studied in great detail in recent years [69, 99, 70, 100, 101, 102, 103, 104]. Here, we show results for a prototypical lattice model of spinless (spin-polarized) fermions with nearest and next-nearest neighbor hoppings (with matrix elements J and J', respectively) and nearest and next-nearest neighbor interactions (with strengths V and V', respectively) [69]. The Hamiltonian can be written as

$$\hat{H} = \sum_{j=1}^{L} \Big[-J \left(\hat{f}_j^\dagger \hat{f}_{j+1} + \text{H.c.} \right) + V \left(\hat{n}_j - \frac{1}{2} \right) \left(\hat{n}_{j+1} - \frac{1}{2} \right) \\ -J' \left(\hat{f}_j^\dagger \hat{f}_{j+2} + \text{H.c.} \right) + V' \left(\hat{n}_j - \frac{1}{2} \right) \left(\hat{n}_{j+2} - \frac{1}{2} \right) \Big] , \tag{6.40}$$

where $\hat{f}_j$ and $\hat{f}_j^\dagger$ are fermionic annihilation and creation operators at site j, $\hat{n}_j = \hat{f}_j^\dagger \hat{f}_j$ is the occupation operator at site j, and L is the number of lattice sites. Periodic boundary conditions are applied, which means that $\hat{f}_{L+1} \equiv \hat{f}_1$ and $\hat{f}_{L+2} \equiv \hat{f}_2$. A classical limit for this model can be obtained at very low fillings and sufficiently high energies. In the simulations presented below, the filling (N/L) has been fixed to 1/3. Therefore, quantum effects are important at any value of the energy. In this example, we approach a dense energy spectrum, and quantum chaos, by increasing the system size L. The Hamiltonian (6.40) is integrable when $J' = V' = 0$, and can be mapped (up to a possible boundary term) onto the well-known spin-1/2 XXZ chain [33].

It is important to stress that Hamiltonian (6.40) is translationally invariant. This means that when diagonalized in quasi-momentum space, different total quasi-momentum sectors (labeled by k in what follows) are decoupled. In addition, some of those sectors can have extra space symmetries, for example, $k = 0$ has reflection symmetry. Finally, if $J' = 0$, this model exhibits particle-hole symmetry at half-filling. Whenever carrying out an analysis of the level spacing distribution, all those discrete symmetries need to be accounted for, that is, one needs to look at sectors of the Hamiltonian that are free of them. If one fails to do so, a quantum chaotic system may appear to be integrable as there is no level repulsion between levels in different symmetry sectors. All results reported in this review for models with discrete symmetries are obtained after properly taking them into account.

In Fig. 6.5(a)–6.5(g), we show the level spacing distribution $P(\omega)$ of a system described by the Hamiltonian (6.40), with $L = 24$ (see Ref. [69] for further details), as the strength of the integrability breaking terms is increased. Two features are immediately apparent in the plots: (i) for $J' = V' = 0$, i.e., at the integrable point, $P(\omega)$ is almost indistinguishable from the Poisson distribution and (ii) for large values of the integrability breaking perturbation, $P(\omega)$ is almost indistinguishable from a Wigner-Dyson distribution [GOE in this case, as Eq. (6.40) is time-reversal invariant]. In between, as in Fig. 6.4, there is a crossover regime in which the

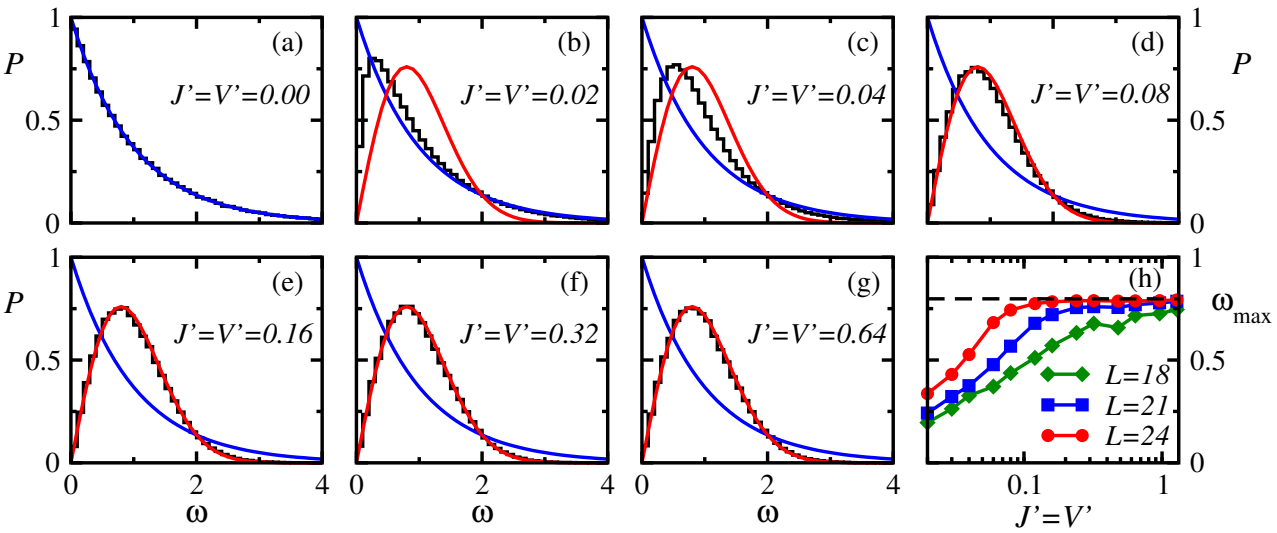

Figure 6.5: (a)–(g) Level spacing distribution of spinless fermions in a one-dimensional lattice with Hamiltonian (6.40). They are the average over the level spacing distributions of all k-sectors (see text) with no additional symmetries (see Ref. [69] for details). Results are reported for $L = 24$, $N = L/3$, $J = V = 1$ (unit of energy), and $J' = V'$ (shown in the panels) vs the normalized level spacing ω. The smooth continuous lines are the Poisson and Wigner-Dyson (GOE) distributions. (h) Position of the maximum of $P(\omega)$, denoted as $\omega_{\max}$, vs $J' = V'$, for three lattice sizes. The horizontal dashed line is the GOE prediction. Adapted from Ref. [69].

distribution is neither Poisson nor Wigner-Dyson. However, as made apparent by the results in panel (h), as the system size increases the level spacing statistics becomes indistinguishable of the RMT prediction at smaller values of the integrability breaking parameters. This suggests that, at least for this class of models, an infinitesimal integrability breaking perturbation is sufficient to generate quantum chaos in the thermodynamic limit. Recent numerical studies have attempted to quantify how the strength of the integrability breaking terms should scale with the system size for the GOE predictions to hold in one dimension [105, 106]. These works suggest that the strength needs to be $\propto L^{-3}$ for this to happen, but the origin of such a scaling is not understood. Moreover, it is unclear how generic these results are. In particular, in disordered systems that exhibit many-body localization, it has been argued that the transition from the Poisson to the Wigner-Dyson statistics occurs at a finite value of the interaction strength. This corresponds to a finite threshold of the integrability breaking perturbation even in the thermodynamic limit (see Ref. [51] and references therein).

6.3.2 The Structure of Many-Body Eigenstates

As we discussed in Sec. 6.2, RMT makes important predictions about the random nature of eigenstates in chaotic systems. According to Eq. (6.12), any eigenvector of a matrix belonging to random matrix ensembles is a random unit vector, meaning that each eigenvectors is evenly distributed over all basis states. However, as we show here, in real systems the eigenstates have more structure. As a measure of delocalization of the eigenstates over a given fixed basis one can use the information entropy:

$$\mathrm{S}_m \equiv -\sum_i |c_m^i|^2 \ln |c_m^i|^2, \tag{6.41}$$

where

$$|m\rangle = \sum_i c_m^i |i\rangle \tag{6.42}$$

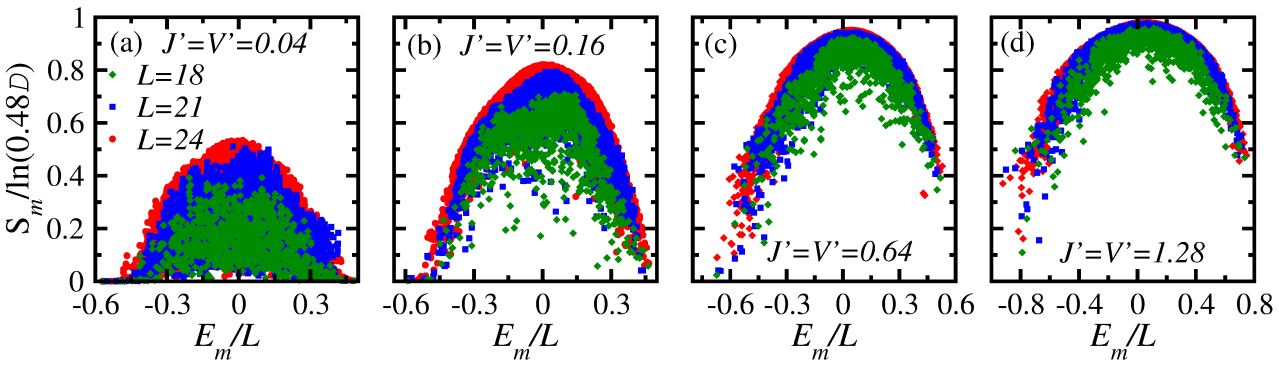

Figure 6.6: Information entropy (normalized using the GOE prediction) of the eigenstates of spinless fermions in a one-dimensional lattice with Hamiltonian (6.40). Results are reported for $L = 18$, 21, and 24, $N = L/3$, $J = V = 1$ (unit of energy), and $J' = V'$ (reported in the panels) vs the energy of the eigenstates. The information entropy is calculated in the basis of the eigenstates of the integrable Hamiltonian ($J = V = 1$ and $J' = V' = 0$), and in the $k = 2$ quasi-momentum sector ($\mathcal{D}$ is the number of states in that sector). See also Ref. [69].

is the expansion of the eigenstate $|m\rangle$ over some fixed basis $|i\rangle$. For the GOE, this entropy, irrespective of the choice of basis, should be $\mathrm{S}_{\mathrm{GOE}} = \ln(0.48\mathcal{D}) + \mathcal{O}(1/\mathcal{D})$ [93], where $\mathcal{D}$ is the dimensionality of the Hilbert space. However, numerical analyses of various physical systems indicate that S_m is only generically bounded from above by the RMT prediction [107, 69, 102]. This situation is characteristic of both few-particle and many-particle systems. For concreteness, we will illustrate this using the eigenstates of the Hamiltonian (6.40) (see Ref. [69] for details). For the fixed basis $|i\rangle$, we use the eigenstates of the integrable limit of this Hamiltonian, corresponding to $J' = V' = 0$. The results of the numerical simulations for the normalized Shannon entropy S_m/S_{GOE} are shown in Fig. 6.6 [we note that S_m and S_{GOE} were computed within a single quasi-momentum sector of the translationally invariant Hamiltonian (6.40)]. It is clear from the figure that the entropy of the states in the middle of the spectrum approaches the RMT prediction as the strength of the integrability breaking perturbation and the system size increase, while the states near the edges of the spectrum remain "localized". The latter, namely, that the lowest and highest (if the spectrum is bounded) energy states are usually non-chaotic, is a generic feature of physical systems with few-body interactions and no randomness.

Another implication of RMT is that the eigenstates of different Hamiltonians are essentially uncorrelated random vectors. This, of course, cannot be literary true in physical systems. Indeed, let us consider a family of Hamiltonians characterized by some continuous parameters like $\hat{H}(J', V')$ in Eq. (6.40). If we change $J' \to J' + \delta J'$ and $V' \to V' + \delta V'$, then, obviously, for sufficiently small changes, $\delta J'$ and $\delta V'$, the eigenstates of the Hamiltonians $\hat{H}(J', V')$ and $\hat{H}(J' + \delta J', V' + \delta V')$ will be almost the same. However, one can anticipate that a very small parameter change, likely vanishing exponentially with the system size, is sufficient to mix different eigenstates of the original Hamiltonian with nearby energies such that new eigenstates look essentially random in the old basis. This is indeed what is seen in the numerical simulations. In Fig. 6.7(a), we show the scaled information entropy S/S_{GOE} of the eigenstates of $\hat{H}(J' + \delta J', V + \delta V')$ in the basis of $\hat{H}(J', V')$ as a function of $\delta J' = \delta V'$. These results show that at fixed values of $\delta J'$ and $\delta V'$, the information entropy rapidly increases with the system size. In Fig. 6.7(b), we show the same entropy plot vs the integrability breaking perturbation, but now scaled by a power of the mean level spacing $\delta J'/(\delta\varepsilon)^{\alpha} = \delta V'/(\delta\varepsilon)^{\alpha}$. We found numerically that there is good data collapse for $\alpha \approx 0.43$. While it is necessary to study much larger system sizes to determine the exponent α accurately, for the system sizes available to us it is already apparent that the relevant strength of the integrability breaking perturbation needed

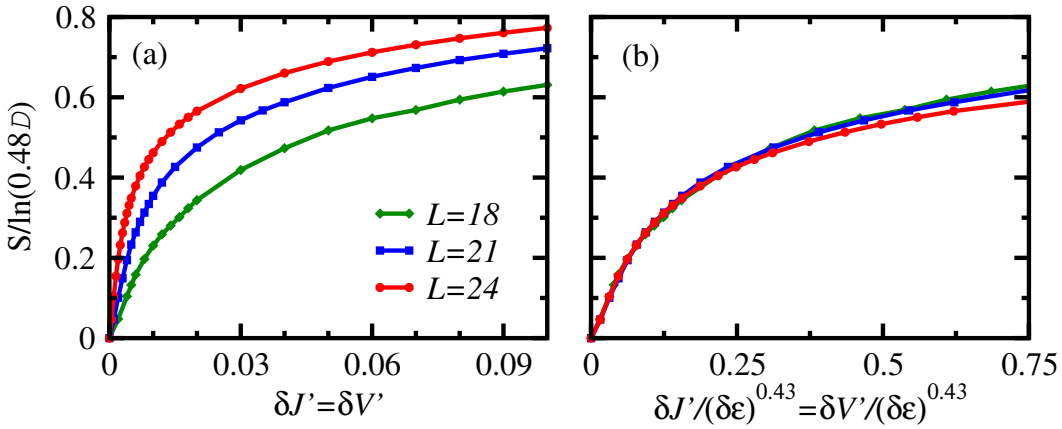

Figure 6.7: Average information entropy (normalized using the GOE prediction) of the eigenstates of spinless fermions in a one-dimensional lattice with Hamiltonian (6.41). The average is computed over the central 10% of the energy spectrum. Results are reported for $L = 18$, 21, and 24, $N = L/3$, $J = V = 1$ (unit of energy), and $J' = V'$ as one departs from $J' = V' = 0.5$. The information entropy is calculated in the basis of the eigenstates of the nonintegrable Hamiltonian with $J = V = 1$ and $J' = V' = 0.5$, and in the $k = 2$ quasi-momentum sector ($\mathcal{D}$ is the number of states in that sector). (a) The average information entropy is reported as a function of $\delta J' \equiv J' - 0.5 = \delta V' \equiv V' - 0.5$. (b) The average information entropy is reported as a function of $\delta J'/(\delta\varepsilon)^{0.43} = \delta V'/(\delta\varepsilon)^{0.43}$, where $\delta\varepsilon$ is the average level spacing between the eigenstates used to compute the average entropy.

for a complete randomization of the energy levels is exponentially small in the system size. Indeed $\delta\varepsilon \propto \exp[-S(E)]$, where $S(E)$ is the thermodynamic entropy of the system, which scales linearly in the system size, and E is the average energy of the eigenstates for which the information entropy is computed.

6.3.3 Quantum Chaos and Entanglement

So far, we have discussed manifestations of quantum chaos in the statistics of level spacings and in the properties of many-body Hamiltonian eigenstates. At the same time, as we discussed in Sec. 6.2, classical chaotic systems do not have a well-defined analogue of stationary eigenstates because they do not have closed stationary orbits. Chaos in classical systems is usually defined as the exponential divergence in time of nearby trajectories. But this language does not apply to quantum systems, which do not have a well-defined notion of a trajectory. So, it seems that there is a fundamental discrepancy between the quantum and classical ways of defining chaos. Nevertheless, this discrepancy is somewhat superficial and one can treat quantum and classical chaos on the same footing by analyzing delocalization of the system either in phase space or in energy space, and using appropriate entropy measures to characterize this delocalization. Using such measures, it is possible to smoothly interpolate between quantum and classical regimes in chaotic systems and analyze various quantum to classical crossovers. However, some care is needed in defining such measures. To this end, here we first discuss the problem for classical systems and then extend the ideas to quantum systems.

Let us consider a setup in which the system is prepared in some initial state and is allowed to evolve according to some time-independent Hamiltonian $\hat{H}$. If the initial state is a stationary state (namely, a stationary probability distribution) of some initial Hamiltonian $\hat{H}_0 \neq \hat{H}$ then this is what is usually called a quench. For example, one can consider a gas of particles in thermal equilibrium in a recipient with a given volume, and then one suddenly doubles the volume of the recipient, for example, by moving a piston. Alternatively, one can consider an

equilibrium system of spins (classical or quantum) in which one suddenly changes a magnetic field or the coupling between the spins. A strong physical manifestation of chaos in classical systems is delocalization in the available phase space after the quench. A standard measure of this delocalization is the entropy, which is defined in phase space as

$$S = -\int\int \frac{d\mathbf{x}d\mathbf{p}}{(2\pi\hbar)^D}\,\rho(\mathbf{x},\mathbf{p})\ln[\rho(\mathbf{x},\mathbf{p})], \tag{6.43}$$

where $\rho(\mathbf{x},\mathbf{p})$ is the classical probability distribution, D is the dimensionality of the phase space, and the usual factor of $(2\pi\hbar)^D$ is introduced to make the integration measure dimensionless. This entropy is maximized when $\rho(\mathbf{x},\mathbf{p})$ is uniform in the available phase space. If the system is isolated, then according to Liouville's theorem the entropy (6.43) is conserved in time [108]. This is a consequence of the incompressibility of classical trajectories, which implies that the phase-space volume occupied by any closed system does not change in time. Liouville's theorem and the lack of the entropy increase was a topic of controversy for a long time, since Boltzmann introduced his H-theorem.

To circumvent this problem and use entropy as a measure of delocalization in the available phase space, one can analyze the reduced probability distribution of N_A particles obtained by averaging over the positions and momenta of the remaining $N - N_A$ particles,

$$\begin{aligned}&\rho_A(\mathbf{x}_1,\ldots,\mathbf{x}_{N_A},\mathbf{p}_1,\ldots,\mathbf{p}_{N_A},t)\\ &\quad=\int\int d\mathbf{x}_{N_A+1}d\mathbf{p}_{N_A+1}\ldots d\mathbf{x}_N d\mathbf{p}_N\,\rho(\mathbf{x}_1,\ldots,\mathbf{x}_N,\mathbf{p}_1,\ldots,\mathbf{p}_N,t)\;,\end{aligned} \tag{6.44}$$

and compute the entropy of this reduced probability distribution. This entropy is not restricted by Liouville's theorem and after a quench, for sufficiently large subsystems of an ergodic system (and for $N_A \ll N$), it is expected to increase in time to the maximum value given by the Gibbs distribution.

In quantum systems, the situation is remarkably similar. Instead of a probability distribution one deals with a density matrix $\hat{\rho}$. A direct analogue of the classical (Liouville) entropy (6.43) is the von Neumann entropy:

$$S_{\text{vn}} = -\text{Tr}[\hat{\rho}\ln\hat{\rho}]. \tag{6.45}$$

Similar to classical systems, the von Neumann entropy is conserved in time for isolated systems, which is a simple consequence of unitary evolution. Hence, extending the analogy to classical systems, we can define the reduced density matrix of a quantum system using a partial trace (typically, one traces over a region in real space):

$$\hat{\rho}_A = \text{Tr}_B[\hat{\rho}] = \sum_{n_A,n'_A} |n_A\rangle\langle n'_A| \sum_{n_B}\langle n_A,n_B|\hat{\rho}|n'_A,n_B\rangle, \tag{6.46}$$

where $|n_A\rangle$ and $|n_B\rangle$ are the complete basis states of the subsystems A and B, respectively. One can then define the von Neumann entropy of the reduced density matrix

$$S^A_{\text{vn}} = -\text{Tr}_A[\hat{\rho}_A\ln\hat{\rho}_A]. \tag{6.47}$$

If the full density matrix is that of a pure state, that is, $\hat{\rho} = |\psi\rangle\langle\psi|$, then this entropy S^A_{vn} is also called the entanglement entropy. The entanglement entropy has been studied in the context of quenches and thermalization in clean interacting systems [109, 110, 111, 112, 113], as well as in disordered systems in the context of many-body localization following quantum quenches and in the presence of a periodic drive [114, 115, 116, 117, 118].

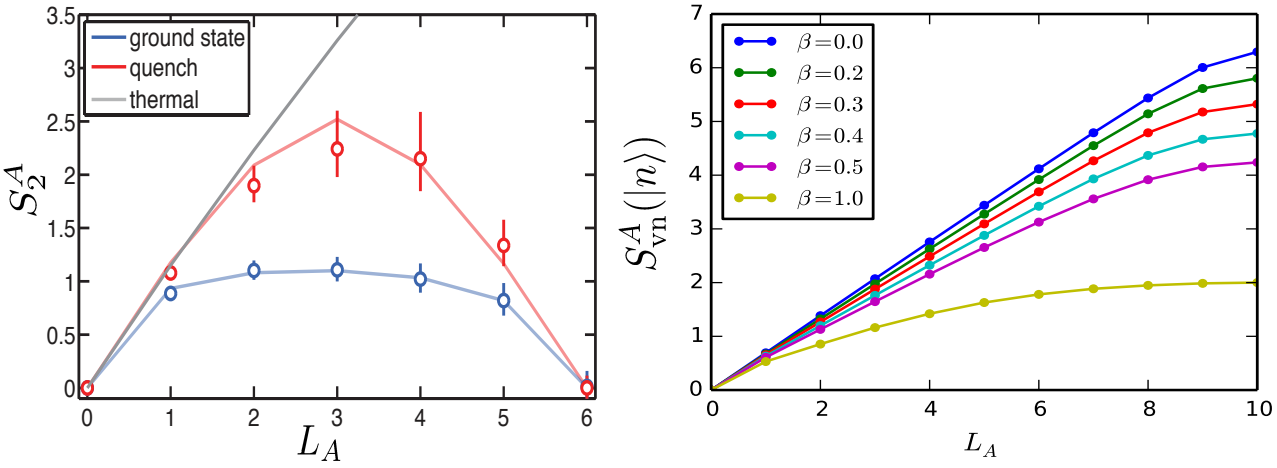

Figure 6.8: (Left panel) Second Renyi entanglement entropy vs subsystem size L_A for a six-site Bose-Hubbard chain measured at long times after a quench (red symbols) and in the ground state (blue symbols). Red and blue lines following the data points depict the theoretical predictions, while the gray (straight) line depicts the theoretical prediction for the Renyi entropy of the system in thermal equilibrium. From Ref. [120]. (Right panel) Entanglement entropy as a function of a subsystem size for different representative eigenstates of the spin-1/2 Hamiltonian (6.50) for $L = 20$. The inverse temperature β in both panels is obtained by matching the energies to those of systems in thermal equilibrium. The entanglement entropy grows linearly with L_A, when L_A and β are small, and coincides with the equilibrium entropy of the Gibbs ensemble. From Ref. [123].

These ideas were recently tested in experiments with small systems involving superconducting qubits [119] and ultracold atoms [120]. We will discuss the superconducting qubit experiment in the next section. Here, we review the results of the ultracold atom experiment. There, the authors prepared two identical chains each with six sites. The Hamiltonian describing the system is

$$\hat{H} = \frac{U}{2}\sum_{ij}\hat{n}_{i,j}(\hat{n}_{i,j}-1) - J_x\sum_{i,j}(\hat{a}^\dagger_{i,j}\hat{a}_{i+1,j} + \text{H.c.}) - J_y\sum_{i}(\hat{a}^\dagger_{i,1}\hat{a}_{i,2} + \text{H.c.}), \tag{6.48}$$

where $i = 1, \ldots, 6$ is the site coordinate along the x-direction and $j = 1, 2$ is the site coordinate along the y-direction. As usual, $\hat{a}^\dagger_{i,j}$ and $\hat{a}_{i,j}$ are the boson creation and annihilation operators, respectively, and $\hat{n}_{i,j} = \hat{a}^\dagger_{i,j}\hat{a}_{i,j}$ is the site occupation number.

The system was initialized in a Fock state with exactly one particle per site and both J_x and J_y being essentially equal to zero. At time $t = 0$, the tunneling along the x-direction (J_x) was quenched to $J_x/U \approx 0.64$, with J_y remaining negligible. The system was then allowed to evolve. This way, two identical copies of a many-body state were created. Implementing a swap operation [121, 122], it was possible to measure the second Renyi entanglement entropy for each chain:

$$S_2^A = -\ln\left[\text{Tr}\hat{\rho}_A^2\right]. \tag{6.49}$$

The latter is very similar to the von Neumann entanglement entropy. If the system is quantum chaotic, S_2^A is expected to coincide with the corresponding entropy in the thermal ensemble for $L_A/L < 1/2$ (up to finite-size corrections). We note that, in general, $S_{\rm vn}^A$ bounds S_2^A from above. The two entropies are equal for (maximally entangled) infinite temperature states and (non-entangled) product states.

In the left panel in Figure 6.8, we show the measured long-time result of the second Renyi entanglement entropy after the quench as a function of the subsystem size. It is remarkable

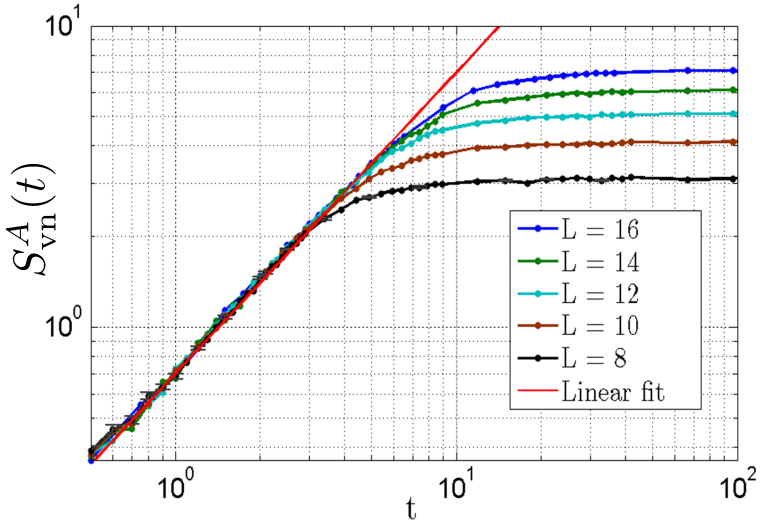

Figure 6.9: von Neumann's entropy of the reduced density matrix obtained after tracing one half of a spin-1/2 chain as a function of time (see text for details). The initial state corresponds to a product state of randomly polarized spins. The entropy grows linearly in time and saturates at a value which is very close to the maximum, corresponding to the infinite temperature state: $S_{\rm max} = L \ln 2/2 - 1/2$. From Ref. [112].

that, even for such a small system, S_2^A is very close to the entropy of a Gibbs ensemble with the same mean energy for the smallest subsystem sizes. This experiment shows that, even in small quantum systems, one can see clear signatures of quantum chaotic behavior.

Next, it is important to discuss theoretical predictions that closely follow the experimental findings. We focus on results for the spin-1/2 transverse field Ising chain, with Hamiltonian:

$$\hat{H} = \sum_{j=1}^{L} g\hat{\sigma}_j^x + \sum_{j=2}^{L-1} h\hat{\sigma}_j^z + (h-J)(\hat{\sigma}_1^z + \hat{\sigma}_L^z) + J\sum_{j=1}^{L-1} \hat{\sigma}_j^z\hat{\sigma}_{j+1}^z. \tag{6.50}$$

This model exhibits quantum chaos in the parameter range studied in Figs. 6.8 (right panel) and 6.9: $h = (\sqrt{5}+1)/4$, $g = (\sqrt{5}+5)/8$, and $J = 1$.

In the right panel in Fig. 6.8, we show the entanglement entropy for representative eigenstates of the Hamiltonian (6.50) as a function of the subsystem size [123]. Different curves are labeled according to the temperature of the Gibbs ensemble that has the same mean energy as the eigenstate. For small subsystem sizes, the entanglement entropy is clearly a linear function of the subsystem size (as in the experimental results for the second Renyi entanglement entropy shown in the left panel). Moreover, the slope is identical to the slope of the equilibrium entropy. As the subsystem size increases, the entanglement entropy deviates from the equilibrium result and the deviation increases as the effective temperature decreases. In Ref. [123], those deviations were argued to be subextensive in L for any fixed ratio $L_A/L < 1/2$. This means that, in the thermodynamic limit and for any nonvanishing effective temperature, the entanglement entropy of eigenstates in quantum chaotic systems is expected to have a triangular shape as a function of L_A/L, with a cusp at $L_A/L = 1/2$. This is a result of the eigenstate thermalization phenomenon that we discuss in Sec. 6.4.

More directly related to the experiments in Ref. [120], in Fig. 6.9 we show the temporal evolution of the entanglement entropy obtained numerically after tracing out one half of the lattice in the transverse field Ising model (6.50). The initial state corresponds to a product of spins with random orientations. Such a state has zero initial entropy. As seen in Fig. 6.9, the entropy $S_{\rm vn}^A$ grows linearly in time and then saturates (as expected) close to that of a random

pure state [124]: $S^* = L \ln 2/2 - 1/2$. This is exactly the result obtained in the right panel in Fig. 6.8 for $\beta = 0$. Following the findings in Fig. 6.9, one can anticipate that if one studies a classical ergodic spin chain, instead of a quantum spin chain, and begins the dynamics from a factorized probability distribution one would get a similar increase of the Liouville entropy of one half of the system.

6.3.4 Quantum Chaos and Delocalization in Energy Space

Another way to reveal delocalization of classical systems in available phase space is to study the time-averaged probability distribution over a time interval t_0

$$\rho_{t_0}(\mathbf{x}, \mathbf{p}) = \frac{1}{t_0} \int_0^{t_0} \rho(\mathbf{x}, \mathbf{p}, t) \tag{6.51}$$

and compute the entropy of this distribution. Because the negative logarithm is a convex function, using Jensen's inequality, it is straightforward to see that such an entropy can only increase as a function of t_0. For ergodic systems, it is expected that this entropy will increase to its maximally allowed value, that is, to the microcanonical entropy, because the system on average visits all points in phase space with equal probability. For non-ergodic systems, conversely, the system is expected to remain more localized in phase space even after time averaging, so that the entropy never reaches the microcanonical value.

Continuing the analogy with classical systems, a second possibility to use entropy to quantify quantum delocalization is to study the entropy of the time-averaged density matrix. Assuming that there are no degeneracies, the off-diagonal matrix elements of the density matrix in the basis of the Hamiltonian oscillate in time according to [77]:

$$\rho_{mn}(t) = \rho_{mn}(t_0) \exp[-i(E_m - E_n)(t - t_0)] \tag{6.52}$$

Therefore, in the quantum language, time averaging is equivalent to projecting the initial density matrix onto the diagonal subspace of the Hamiltonian, leading to what is known as the diagonal ensemble[16] density matrix [28]:

$$\hat{\rho}_{\mathrm{DE}} \equiv \bar{\hat{\rho}} \equiv \lim_{t_0 \to \infty} \frac{1}{t_0} \int_0^{t_0} \hat{\rho}(t) dt = \sum_m \rho_{mm} |m\rangle\langle m|. \tag{6.53}$$

Thus studying delocalization of the classical probability distribution in phase space at long times is equivalent, in the quantum language, to studying the spreading of the initial density matrix in the basis of the eigenstates of the Hamiltonian, or, simply, in energy space. From the discussion in Sec. 6.3.2, one can expect that the diagonal density matrix will generically be delocalized for quantum chaotic systems. For integrable systems, on the other hand, the diagonal density matrix can be more (or less) localized depending on the initial state.

The analogy between delocalization in energy space and classical chaos was recently explored experimentally in a system of three coupled superconducting qubits [119], which effectively represent three 1/2 spins. The experiment was carried out in the sector where the effective total spin is $S = 3/2$, and focused on periodic kicks with:

$$\hat{H}(t) = \frac{\pi}{2} \hat{S}_y + \frac{\kappa}{2S} \hat{S}_z^2 \sum_n \delta(t - n), \tag{6.54}$$

where $\hat{S}_y$ and $\hat{S}_z$ are spin operators. Like the kicked rotor model, this system in the $S \to \infty$ classical limit has a mixed phase space with both chaotic and regular trajectories. In the

[16] The diagonal ensemble will play a crucial role throughout this review.

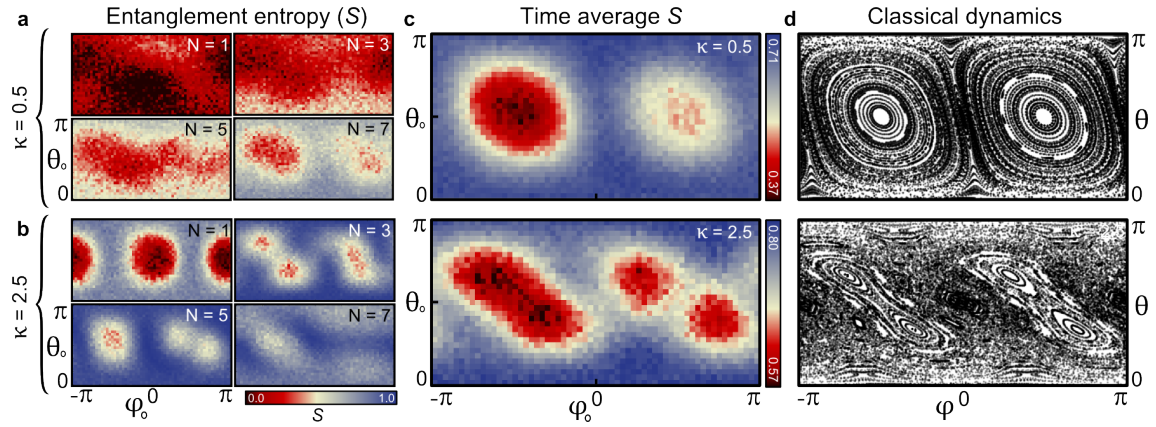

Figure 6.10: Left panels: entanglement entropy averaged over three different qubits after a different number of kicks N. In the color scale used, red signals a small entropy and blue signals the maximum entropy [ln(2)]. Different points on each panel correspond to different initial conditions, which are coherent states centered around the phase-space point (θ_0, ϕ_0). Middle panels: Floquet diagonal entropy, which was computed as the entropy of the full density matrix averaged over 20 kicks (top) and 10 kicks (bottom). Right panels: phase-space portrait of the classical system. The top and bottom panels depict results for different kick strengths: $\kappa = 0.5$ and $\kappa = 2.5$, respectively. From Ref. [119].

experiment, the quantum system was initialized in a coherent state centered around some point in the two-dimensional phase space. The system was then allowed to evolve under kicks and, after long times, both the entanglement entropy (of one qubit) and the diagonal entropy (the entropy of the time-averaged density matrix) were measured through quantum tomography. The results were contrasted with the phase-space dynamics of the $S \to \infty$ classical limit.

In Fig. 6.10, we show the dynamics of the entanglement entropy (left panels) and the entropy of the density matrix averaged over several periods, which is equivalent to the Floquet diagonal entropy (middle panels). The entropies are reported (in a color scale) for different initial coherent states centered around spherical angles (θ_0, ϕ_0). The right panels show the phase space portraits of the corresponding classical systems. Both the entanglement entropy and the Floquet diagonal entropy show strong correlations with classical regions of chaotic and non-chaotic motion, with higher entropy corresponding to more chaotic behavior. Interestingly, these correlations persist deep in the quantum regime ($S = 3/2$ is not particularly large). This experiment illustrates the ideas discussed in this and the previous section, namely, that quantum chaos results in delocalization of either the reduced density matrix of subsystems or the time-averaged density matrix of the full system.

To illustrate delocalization of an initial wave function among energy eigenstates in a larger quantum chaotic system, we follow Ref. [125], which reported results for quantum quenches in one-dimensional periodic chains of interacting spinless fermions with Hamiltonian (6.40), and hard-core bosons with Hamiltonian

$$\hat{H} = \sum_{j=1}^{L} \Big[-J \left(\hat{b}_j^\dagger \hat{b}_{j+1} + \text{H.c.} \right) + V \left(\hat{n}_j - \frac{1}{2} \right) \left(\hat{n}_{j+1} - \frac{1}{2} \right) - J' \left(\hat{b}_j^\dagger \hat{b}_{j+2} + \text{H.c.} \right) + V' \left(\hat{n}_j - \frac{1}{2} \right) \left(\hat{n}_{j+2} - \frac{1}{2} \right) \Big], \tag{6.55}$$

where $\hat{b}_j$ and $\hat{b}_j^\dagger$ are hard-core bosons annihilation and creation operators at site j, $\hat{n}_j = \hat{b}_j^\dagger \hat{b}_j$ is the occupation operator at site j, and L is the number of lattice sites. Hard-core bosons satisfy the same commutation relations as bosons but have the constraints $\hat{b}_j^2 = (\hat{b}_j^\dagger)^2 = 0$,

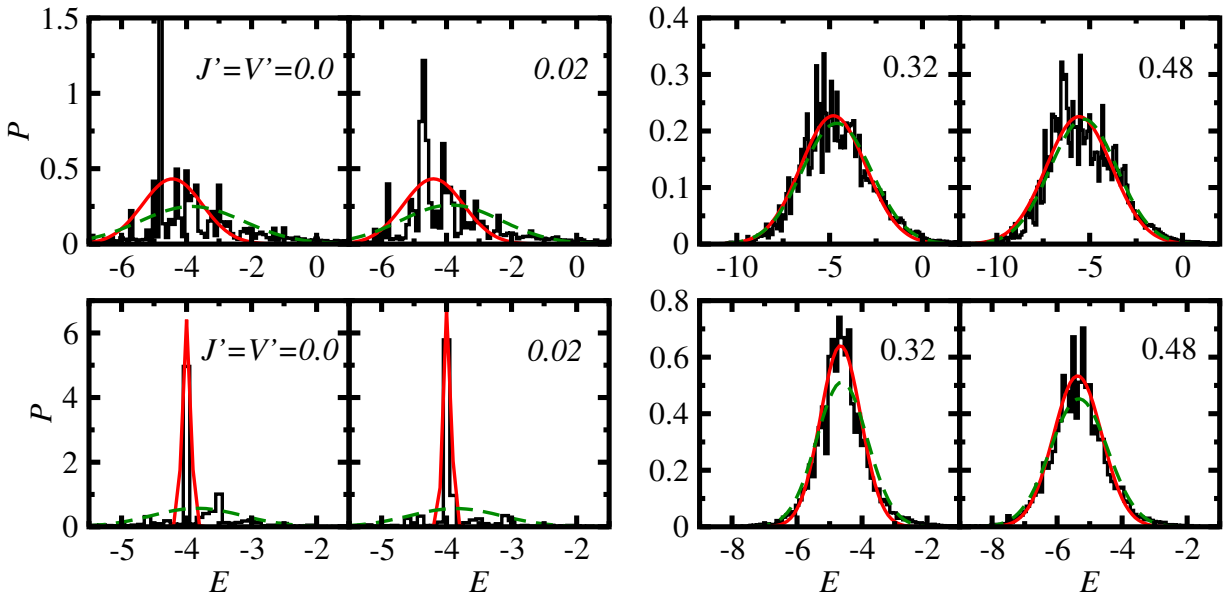

Figure 6.11: Normalized energy distribution function $P(E)$, see Eq. (6.56), after quenches in hard-core boson chains. Results are presented for two different initial states $|\psi_I\rangle$ corresponding to eigenstates of Hamiltonian (6.55) with $J_I = 0.5$, $V_I = 2$ (top panels) and $J_I = 2$, $V_I = 0.5$ (bottom panels). The final parameters of the Hamiltonian are $J = V = 1$. $J' = V'$ remain unchanged during the quench. Their values are indicated in the figure. Smooth solid lines: best Gaussian fit to $(\sqrt{2\pi}a)^{-1}\exp[-(E-b)^2/(2a^2)]$ for the parameters a and b; dashed lines: $(\sqrt{2\pi}\delta E)^{-1}\exp[-(E-\overline{E})^2/(2\delta E^2)]$, where $\overline{E} = \langle\psi_I|\hat{H}|\psi_I\rangle$ and $\delta E^2 = \langle\psi_I|\hat{H}^2|\psi_I\rangle - \langle\psi_I|\hat{H}|\psi_I\rangle^2$ is the energy variance after the quench. From Ref. [125].

which preclude multiple occupancy of the lattice sites [33]. For $J' = 0$, the hard-core boson Hamiltonian (6.55) can be mapped onto the spinless fermion Hamiltonian (6.40), up to a possible boundary term [33]. Like the spinless fermion Hamiltonian (6.40), the hard-core boson one (6.55) is integrable for $J' = V' = 0$ and nonintegrable otherwise.

In Fig. 6.11, we show the normalized energy distribution

$$P(E) = \sum_m p_m \delta(E - E_m), \tag{6.56}$$

where

$$p_m = |\langle m|\psi_I\rangle|^2, \tag{6.57}$$

and $\langle m|\psi_I\rangle$ is the projection of the initial state $|\psi_I\rangle$ on eigenstate $|m\rangle$. The results presented are for quenches in the hard-core boson chain. The top and bottom panels correspond to different initial states. The parameters of the final Hamiltonian are $J = V = 1$, and $J' = V'$ with the values indicated in the figure (increasing from left to right). Those plots make apparent that as the system becomes more quantum chaotic (larger $J' = V'$), the energy distribution becomes less sparse, which means that the initial state becomes more delocalized among the eigenstates of the final Hamiltonian. Another visible feature of the energy distribution is that in chaotic systems it rapidly approaches a Gaussian centered around the mean energy $\overline{E} = \langle\psi_I|\hat{H}|\psi_I\rangle$ and the width given by the variance of the energy in the initial state $\delta E^2 = \langle\psi_I|\hat{H}^2|\psi_I\rangle - \langle\psi_I|\hat{H}|\psi_I\rangle^2$. Similar results were obtained for quenches in the spinless fermion chain [125] and in other many-body Hamiltonians [126, 101, 102].

For states that are eigenstates of some Hamiltonian $\hat{H}_I$ and are decomposed in the eigenstates of a new Hamiltonian $\hat{H}_F$ (as we did above), the normalized energy distribution is also known as the strength function [127, 128, 129, 101, 102]. If $\hat{H}_F$ is taken to be $\hat{H}_I$ plus a perturbation, it has been shown that the normalized energy distribution (the strength function)

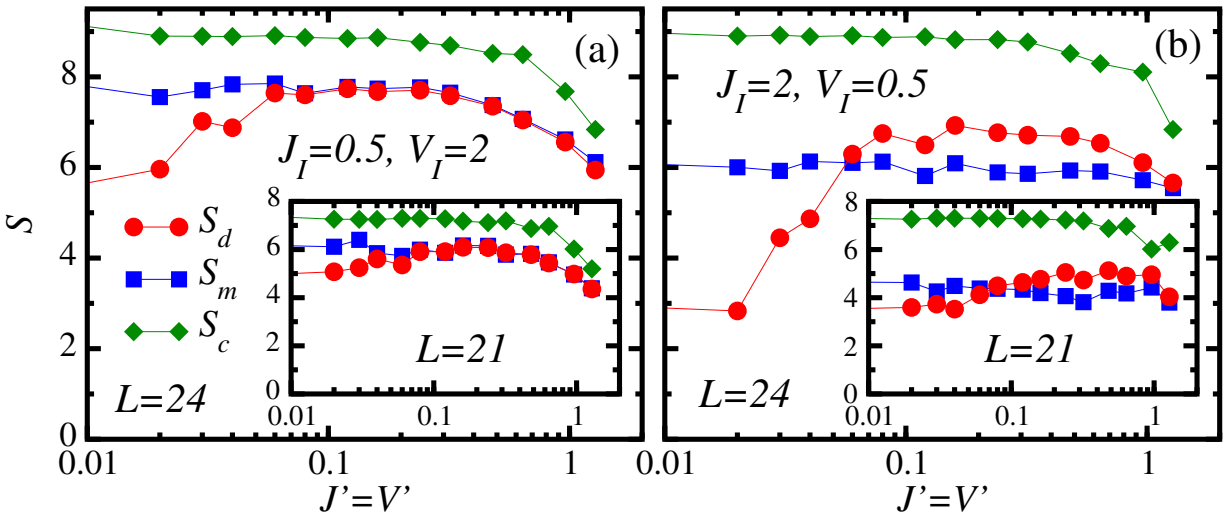

Figure 6.12: Entropies in hard-core boson chains with $L = 24$ (main panels) and $L = 21$ (insets). Results are reported for the diagonal entropy (S_d), the microcanonical entropy (S_m), and the canonical entropy (S_c), after quenches as those described in Fig. 6.11, for initial states corresponding to eigenstates of Hamiltonian (6.55) with $J_I = 0.5$, $V_I = 2$ (a) and $J_I = 2$, $V_I = 0.5$ (b). The final parameters of the Hamiltonian are $J = V = 1$. $J' = V'$ remain unchanged in the quench and their values are depicted in the x-axis. Thin lines joining the points are drawn to guide the eye. See also Ref. [125].

evolves from a Breit-Wigner form to a Gaussian form as the strength of the perturbation is increased [129, 101, 102]. The transition between those distributions, say, for a given state $|i\rangle$ (an eigenstate of $\hat{H}_I$), has been argued to occur as the average value of the nonzero off-diagonal matrix elements $|\langle i|\hat{H}_F|j\rangle|$ becomes of the same order of (or larger than) the average level spacing of the states $|j\rangle$ (also eigenstates of $\hat{H}_I$) for which $|\langle i|\hat{H}_F|j\rangle| \neq 0$ [101]. Hence, if $\hat{H}_F$ is quantum chaotic one expects that, provided that the system is large enough (the density of states increases exponentially fast with increasing system size), the normalized energy distribution will have a smooth Gaussian form after a quench independent of the nature of $\hat{H}_I$. It has been recently shown that this is not the case in generic (experimentally relevant) quenches to integrability. Namely, if $\hat{H}_F$ is integrable, the distribution of p_m [see Eq. (6.57)] ends up being sparse even in quenches whose initial states are thermal states of nonintegrable Hamiltonians [130] (see Sec. 6.8.3). The sparseness of p_m at integrability is apparent in Fig. 6.11 and, for much larger system sizes, has also been explicitly shown in Refs. [131, 132, 133].

To quantify the level of delocalization one can use the von Neumann entropy of the diagonal ensemble,[17] which is known as the diagonal entropy [134, 125]:

$$S_d = -\sum_m p_m \ln p_m. \tag{6.58}$$

This entropy is the same as the information entropy of the initial state in the basis of the Hamiltonian governing the evolution, which we analyzed in Fig. 6.7. In particular, the entropy plotted in that figure is the diagonal entropy of the eigenstates of the Hamiltonian $H(J' + \delta J', V' + \delta V')$ in the basis of the Hamiltonian $H(J', V')$, averaged over eigenstates.

In Fig. 6.12, we plot the diagonal entropy vs $J' = V'$ for quenches as those in Fig. 6.11, and systems with $L = 21$ and $L = 24$. We also plot the microcanonical entropy $S_m = \ln[\Omega(\bar{E})\delta E]$,

[17] One could also use the inverse participation ratio: IPR $= (\sum_m p_m^2)^{-1}$, with p_m defined as in Eq. (6.57). IPR $= 1$ if only one state is occupied and it is maximized when all states are occupied with equal probability: IPR $= \mathcal{D}$, where $\mathcal{D}$ is the dimension of the available Hilbert space.

and the canonical entropy $S_c = -\mathrm{Tr}[\hat{\rho}_{\mathrm{CE}} \ln \hat{\rho}_{\mathrm{CE}}]$, where $\hat{\rho}_{\mathrm{CE}} = \exp(-\beta \hat{H})/\mathrm{Tr}[\exp(-\beta \hat{H})]$ and the inverse temperature β is fixed such that $\mathrm{Tr}(\hat{H}\hat{\rho}_{\mathrm{CE}}) = \overline{E}$. In all the quenches in Figs. 6.11 and 6.12, the initial state was selected such that $\beta^{-1} \approx 3J$. Figure 6.12 shows that, as one departs from the integrable point ($J' = V' = 0$), the diagonal entropy becomes almost the same as the microcanonical entropy. This is up to finite-size effects, whose relevance to the results presented is made apparent by the differences between S_m and S_c. As the system size increases, S_m/L and S_c/L must approach each other as they are equal up to subextensive corrections. Numerical evidence that the diagonal entropy after a quench and the thermal equilibrium entropy are identical in nonintegrable systems in the thermodynamic limit has been obtained in numerical linked cluster expansion studies [135, 130]. We will explain why S_d/L agrees with the entropy in thermal equilibrium in Sec. 6.5.3, when we discuss the fundamental thermodynamic relation. On the other hand, in many numerical and analytical works it has been established that, in integrable systems, extensive differences generally occur between the diagonal entropy and the thermal entropy [125, 136, 137, 138, 139, 140, 135, 130] (see Sec. 6.8.3). In the spirit of our current discussion, this implies that integrable systems generally remain more localized in energy space.

6.4 Eigenstate Thermalization

6.4.1 Thermalization in Quantum Systems

In 1929, von Neumann wrote a remarkable paper in which he discussed how statistical mechanics behavior could emerge in quantum-mechanical systems evolving under unitary dynamics [30]. As mentioned in the Introduction, one of von Neumann's crucial insights was to focus on macroscopic observables, as opposed to focusing on the wave function or the density matrix of the entire system. He proved what he named the quantum ergodic theorem, which has been recently discussed in detail by Goldstein et al. in Ref. [141]. In the words of the latter authors, the quantum ergodic theorem (or "normal typicality")[18] states that "*for a typical finite family of commuting macroscopic observables, every initial wave function from a microcanonical energy shell evolves so that for most times in the long run, the joint probability distribution of these observables obtained from the unitarily time-evolved wave function is close to their microcanonical distribution*". This theorem was a very important first step in the study of thermalization in quantum systems. However, some shortcomings are immediately apparent given our discussion so far. For example, the theorem makes no distinction between integrable and nonintegrable systems, as such, it leaves one wondering about the role of integrability. Also, typical observables in von Neumann's sense need not be relevant to experiments. As we discuss in Sec. 6.4.2, von Neumann's theorem is related to RMT. Hidden in it is the seed for eigenstate thermalization [145], which is the topic of this section.

In the spirit of von Neumann's theorem, in this review thermalization refers to observables and is defined in a strong sense. Suppose that one prepares an isolated system in a nonstationary state with a well-defined mean energy, and subextensive energy fluctuations. An observable is said to thermalize if, during the time evolution of the system, it relaxes to the microcanonical prediction and remains close to it at most later times. Whether the isolated system is in a pure or mixed state is immaterial to the question of thermalization.

To understand the essential ingredients needed for thermalization to occur, let us consider a simple setup in which an isolated system is initially prepared in a pure state $|\psi_I\rangle$[19] and evolves

[18] Not to be confused with canonical typicality [142, 143, 144], which makes statements about the reduced density matrix of typical states in the microcanonical energy shell. As discussed in the introduction, experimental out-of-equilibrium states are atypical as a result of the way they are created. Canonical typicality does not tell how typical states can be reached.

[19] Everything we discuss in what follows can be straightforwardly generalized to mixed states.

under a time-independent Hamiltonian $\hat{H}$. We assume that the Hamiltonian has eigenvectors $|m\rangle$ and eigenvalues E_m, that is, $\hat{H}|m\rangle = E_m|m\rangle$. The time-evolving wave function can be written as

$$|\psi(t)\rangle = \sum_m C_m \mathrm{e}^{-iE_m t}|m\rangle, \tag{6.59}$$

where $C_m = \langle m|\psi_I\rangle$ (notice that we set $\hbar \to 1$); and we are interested in $t \geq 0$. Obviously, the density matrix of the system will remain that of a pure state at all times $[\rho(t)^2 = \rho(t)]$, that is, it can never become a mixed (thermal) density matrix. Now, let us look at the time evolution of some observable $\hat{O}$, which in the basis of the eigenstates of the Hamiltonian can be written as

$$\begin{aligned} O(t) \equiv \langle\psi(t)|\hat{O}|\psi(t)\rangle &= \sum_{m,\,n} C_m^* C_n e^{i(E_m - E_n)t} O_{mn} \\ &= \sum_m |C_m|^2 O_{mm} + \sum_{m,\,n\neq m} C_m^* C_n e^{i(E_m - E_n)t} O_{mn} \end{aligned} \tag{6.60}$$

where $O_{mn} = \langle m|\hat{O}|n\rangle$. As stated before, we say that the observable $\hat{O}$ thermalizes if: (i) after some relaxation time, the average expectation value of this observable agrees with the microcanonical expectation value and (ii) temporal fluctuations of the expectation value about the microcanonical prediction are small at most later times. This implies that the long-time average accurately describes the expectation value of $\hat{O}$ at almost all times and agrees with the microcanonical prediction.

The initial difficulties in reconciling these requirements with Eq. (6.60) are obvious. In the long-time average, the second sum in Eq. (6.60) averages to zero (provided there are no degeneracies, or that there is a nonextensive number of them) and we are left with the sum of the diagonal elements of $\hat{O}$ weighted by $|C_m|^2$. Some of the natural questions one can ask are: (i) Since the probabilities $|C_m|^2$ are conserved in time, how is it possible for $\sum_m |C_m|^2 O_{mm}$ to agree with the microcanonical average? (ii) Moreover, in many-body systems, the eigenenergies are exponentially close to each other and therefore, to make sure that the second sum in Eq. (6.60) averages to zero, one could potentially need to wait an exponentially (in system size) long time. Such a time, even for moderately small systems, could exceed the age of our universe, and therefore cannot be reconciled with the experimental observation that even large systems thermalize over much shorter time scales than the age of the universe (we observe them thermalize).

Remarkably, if the Hamiltonian $\hat{H}$ was a true random matrix, then using the RMT prediction for observables [namely that O_{mm} is independent of m and that O_{mn} for $m \neq n$ is exponentially small in the system size, see Eq. (6.20)] one finds that the observables thermalize in the sense specified above. This is because the first sum in Eq. (6.60) becomes independent of the initial state

$$\sum_m |C_m|^2 O_{mm} \approx \bar{O} \sum_m |C_m|^2 = \bar{O}, \tag{6.61}$$

that is, it agrees with the microcanonical result. Note that within RMT, the microcanonical ensemble has no energy dependence and is thus formally equivalent to the infinite temperature ensemble. It also becomes clear that exponentially long times may not be needed for relaxation. The off-diagonal matrix elements of $\hat{O}$ are exponentially small so, by destroying phase coherence between a finite fraction of the eigenstates with a significant contribution to the expectation value, it is possible to approach the infinite-time prediction with high accuracy in a time much shorter than the inverse (many-body) level spacing, which is required to destroy coherence between *all* eigenstates. We will come back to this later. The relevance of RMT for understanding thermalization in many-body quantum systems was discussed by Deutsch in a

seminal paper in the early 1990s [26]. There, he essentially extended Berry's conjecture to arbitrary quantum systems assuming that the eigenstates of ergodic Hamiltonians are essentially uncorrelated random vectors.

In order to describe observables in experiments, however, one needs to go beyond the RMT prediction. This because, in contrast to random matrices, in real systems: (i) thermal expectation values of observables depend on the energy density (temperature) of the system[20] and (ii) relaxation times are observable dependent. Hence, there is information in the diagonal and off-diagonal matrix elements of observables in real systems that cannot be found in RMT. In groundbreaking works throughout the 1990s, Srednicki provided the generalization of the RMT prediction that is needed to describe observables in physical systems [27, 146, 29]. Srednicki's ansatz is known as the ETH. It was first shown to apply to realistic quantum systems, where thermalization was observed for a strikingly small number of particles (5 bosons in 21 lattice sites), by Rigol et al. [28]. We should mention that, in a remarkable discussion of numerical experiments with 7 spins, Jensen and Shankar [147] advanced part of ETH [the first term on the RHS of Eq. (6.62)]. The smallness of the system they studied precluded them from observing a qualitatively different behavior between nonintegrable and integrable systems.

6.4.2 The Eigenstate Thermalization Hypothesis (ETH)

ETH can be formulated as an ansatz for the matrix elements of observables in the basis of the eigenstates of a Hamiltonian [29]:

$$O_{mn} = O\left(\bar{E}\right)\delta_{mn} + e^{-S\left(\bar{E}\right)/2} f_O\left(\bar{E},\omega\right) R_{mn}, \tag{6.62}$$

where $\bar{E} \equiv (E_m + E_n)/2$, $\omega \equiv E_n - E_m$, and $S(E)$ is the thermodynamic entropy at energy E. Crucially, $O\left(\bar{E}\right)$ and $f_O\left(\bar{E},\omega\right)$ are smooth functions of their arguments, the value $O\left(\bar{E}\right)$ is identical to the expectation value of the microcanonical ensemble at energy $\bar{E}$ and R_{mn} is a random real or complex variable with zero mean and unit variance ($\overline{R_{mn}^2} = 1$ or $\overline{|R_{mn}|^2} = 1$, respectively). While there is no rigorous understanding of which observables satisfy ETH and which do not, it is generally expected that Eq. (6.62) holds for all physical observables, namely, observables for which statistical mechanics applies (see, e.g., discussion in Ref. [108]). Specifically, ETH has been numerically verified for few-body observables in a variety of lattice models, no matter whether they are local or not (see Sec. 6.4.3). By few-body observables we mean n-body observables with $n \ll N$, where N is the number of particles, spins, etc, in the system. This is the class of observables that can be experimentally studied in macroscopic systems. Projection operators to the eigenstates of the many-body Hamiltonian, $\hat{P}_m = |m\rangle\langle m|$, are operators for which Eq. (6.62), as well as the predictions of statistical mechanics, do not hold. In a recent study of lattice systems, Garrison and Grover argued that ETH can hold for observables with support in up to $1/2$ of the system size [123].

The matrix elements of observables can be real or complex depending on the symmetries of the Hamiltonian and the basis used to diagonalize it. If the system obeys time-reversal symmetry, the eigenstates of the Hamiltonian can be chosen to be real and so will be the matrix elements of observables (Hermitian operators). This is not possible if the system does not obey time-reversal symmetry. By taking the Hermitian conjugate of Eq. (6.62), we see that the function $f_O(\bar{E},\omega)$ and the random numbers R_{mn} must satisfy the following relations

$$\begin{array}{llc} R_{nm} = R_{mn}, & f_O(\bar{E},-\omega) = f_O(\bar{E},\omega) & \text{(real matrix elements)} \\ R_{nm}^* = R_{mn}, & f_O^*(\bar{E},-\omega) = f_O(\bar{E},\omega) & \text{(complex matrix elements)}. \end{array} \tag{6.63}$$

[20] For simplicity, we assume that the energy is the only conserved quantity in the system. If there are other conserved quantities, they have to be treated in a similar fashion.

Srednicki's ansatz (6.62) is similar to the RMT result in Eq. (6.20). The differences are: (i) The diagonal matrix elements of observables $O(\bar{E})$ are not the same in all eigenstates. Rather, they are smooth functions of the energy of the eigenstates. (ii) For the off-diagonal matrix elements, on top of the small Gaussian fluctuations, there is an envelope function $f_O(\bar{E},\omega)$ that depends on the mean energy and the energy difference between the eigenstates involved. This ansatz is consistent with results obtained in the semi-classical limit of quantum systems whose classical counterpart is chaotic [148, 149, 26, 27, 150, 151, 152].

The ETH ansatz reduces to the RMT prediction if one focuses on a very narrow energy window where the function $f_O(\bar{E},\omega)$ is constant. In single-particle diffusive systems, this scale is given by the Thouless energy (see, e.g., Ref. [93]), which is essentially equal to Planck's constant divided by the diffusion time [153]:

$$E_T = \frac{\hbar D}{L^2}, \tag{6.64}$$

where D is the diffusion constant and L is the linear size of the system. As we discuss in Sec. 6.4.3, the same appears to be true in generic diffusive many-body quantum systems. Namely, that if one focuses on an energy shell of width $\omega < E_T$ then $f_O(E,\omega) \approx$ const, so that the ETH ansatz is identical to RMT. In other words, there is no structure in the eigenstates of ergodic Hamiltonians in an energy window narrower than the Thouless energy. As this window vanishes in the thermodynamic limit, RMT has a very limited range of applicability. Note, however, that the level spacing vanishes much faster with the system size. Therefore, there is still an exponentially large number of energy levels in the region where RMT applies. The situation can be more subtle in systems with subdiffusive, for example, glassy dynamics. One can anticipate that $f(\omega)$ will saturate at $\omega < \hbar/\tau^*$, where τ^* is the slowest physical time scale in the system. As long as the corresponding energy window contains exponentially many energy levels, one expects that RMT will apply in this window.[21] Conversely, the ETH ansatz does not have these RMT limitations and is believed to apply to arbitrary energies with the exception of the edges of the spectrum. As we will see later, in Sec. 6.6.8, the dependence of $f_O(E,\omega)$ on ω determines the decay of nonequal-time correlation functions. It also determines the relaxation time following a small perturbation about equilibrium (in the linear response regime) [29, 154]. In ergodic systems, it is expected that the diffusive time gives the slowest time scale in the system [155]. Within ETH, this follows from the fact that the function $f_O(E,\omega)$ becomes structureless (constant) for $\omega < E_T$.

ETH and Thermalization

The ETH ansatz (6.62) has immediate implications for understanding thermalization in many-body quantum systems. First, let us focus on the long-time average of observables. If there are no degeneracies in the energy spectrum, which is a reasonable assumption for generic quantum systems after removing all trivial symmetries, we obtain [using Eq. (6.60)]

$$\overline{O} \equiv \lim_{t_0\to\infty} \frac{1}{t_0}\int_0^{t_0} dt\, O(t) = \sum_m |C_m|^2 O_{mm} = \mathrm{Tr}\left[\hat{\rho}_{\mathrm{DE}}\hat{O}\right], \tag{6.65}$$

where ρ_{DE} is the density matrix of the diagonal ensemble, defined in Eq. (6.53). On the other hand, statistical mechanics predicts

$$O_{\mathrm{ME}} = \mathrm{Tr}\left[\hat{\rho}_{\mathrm{ME}}\hat{O}\right], \tag{6.66}$$

[21] In a very recent work by Luitz and Bar Lev [arXiv:1607.01012], the Gaussian ansatz for the off-diagonal matrix elements was found to hold for diffusive spin chains. At the same time it was found that, in sub-diffusive disordered chains, the distribution of off-diagonal matrix elements becomes non-Gaussian (it acquires long tails).

where $\hat{\rho}_{\rm ME}$ is the density matrix of the microcanonical ensemble (due to ensemble equivalence one can, of course, use a canonical, or any other equilibrium, density matrix instead). We then see that, independent of the actual values of C_m, so long as energy fluctuations in the diagonal ensemble

$$\delta E \equiv \sqrt{\langle\psi_I|\hat{H}^2|\psi_I\rangle - \langle\psi_I|\hat{H}|\psi_I\rangle^2} \tag{6.67}$$

are sufficiently small (e.g., behaving like in traditional statistical mechanics ensembles), $\overline{O}$ will agree (to leading order) with the statistical mechanics prediction $O_{\rm ME}$, provided that $\mathrm{Tr}\left[\hat{\rho}_{\rm ME}\hat{H}\right] = \langle\psi_I|\hat{H}|\psi_I\rangle \equiv \langle E\rangle$. This is because, using the ETH ansatz (6.62), one can rewrite Eqs. (6.65) and (6.66) as

$$\overline{O} \simeq O(\langle E\rangle) \simeq O_{\rm ME}. \tag{6.68}$$

Furthermore, given Eq. (6.62), one can quantify the difference between the two ensembles due to the fact that δE is finite. Indeed, expanding the smooth function $O(E)$ into a Taylor series around the mean energy $\langle E\rangle$

$$O_{mm} \approx O(\langle E\rangle) + (E_m - \langle E\rangle)\left.\frac{dO}{dE}\right|_{\langle E\rangle} + \frac{1}{2}(E_m - \langle E\rangle)^2\left.\frac{d^2O}{dE^2}\right|_{\langle E\rangle}, \tag{6.69}$$

and substituting this expansion into Eq. (6.65), we find

$$\overline{O} \approx O(\langle E\rangle) + \frac{1}{2}(\delta E)^2 O''(\langle E\rangle) \approx O_{\rm ME} + \frac{1}{2}\left[(\delta E)^2 - (\delta E_{\rm ME})^2\right] O''(\langle E\rangle), \tag{6.70}$$

where $\delta E_{\rm ME}$ are the energy fluctuations of the microcanonical ensemble, which are subextensive. If the energy fluctuations δE in the time-evolving system are subextensive, which is generically the case in systems described by local Hamiltonians (see, e.g., the discussion in Sec. 6.4.3), then the second term is a small subextensive correction to $O_{\rm ME}$, which is negligible for large system sizes. Moreover, the same Eq. (6.70) describes the difference between the equilibrium canonical and microcanonical expectation values of $\hat{O}$ if instead of δE^2 one uses energy fluctuations of the canonical ensemble. It is remarkable that, using ETH, one can show that $\overline{O} \simeq O_{\rm ME}$ without the need of making any assumption about the distribution of C_m, beyond the fact that it is narrow. This is to be contrasted with the standard statistical mechanics statement about equivalence of ensembles, for which it is essential that the energy distributions are smooth functions of the energy.[22]

Using the ETH ansatz, one can also calculate the long-time average of the temporal fluctuations of the expectation value of the observable $\hat{O}$

$$\sigma_O^2 \equiv \lim_{t_0\to\infty}\frac{1}{t_0}\int_0^{t_0} dt\,[O(t)]^2 - (\overline{O})^2 \tag{6.71}$$

$$= \lim_{t_0\to\infty}\frac{1}{t_0}\int_0^{t_0} dt \sum_{m,n,p,q} O_{mn}O_{pq}C_m^*C_nC_p^*C_q e^{i(E_m-E_n+E_p-E_q)t} - (\overline{O})^2 \tag{6.72}$$

$$= \sum_{m,n\neq m} |C_m|^2|C_n|^2|O_{mn}|^2 \leq \max|O_{mn}|^2 \sum_{m,n}|C_m|^2|C_n|^2 = \max|O_{mn}|^2 \propto \exp[-S(\bar{E})].$$

Thus, the time fluctuations of the expectation value of the observable are exponentially small in the system size. These fluctuations should not be confused with the fluctuations of the observable that are actually measured in experiments, which are never exponentially small

[22] The energy distributions after quenches to nonintegrable Hamiltonians are expected to be smooth, see Sec. 6.3.4. However, because of ETH, thermalization in nonintegrable systems occurs independently of whether the energy distributions are smooth or not.

[29, 28]. Instead, Eq. (6.72) tells us that at almost any point in time the expectation value of an observable $\hat{O}$ is the same as its diagonal ensemble expectation value. Thus the ETH ansatz implies ergodicity in the strong sense, that is, no time averaging is needed. In Sec. 6.6.8, we show that ETH implies that temporal fluctuations of extensive observables satisfy standard fluctuation-dissipation relations. Let us point in passing that the results discussed so far are not restricted to pure states. They all straightforwardly generalize to mixed states by using the following substitutions in Eqs. (6.60), (6.65), and (6.53): $C_m^* C_n \to \rho_{mn}$ and $|C_m|^2 \to \rho_{mm}$, where ρ_{mn} are the matrix elements of the initial density matrix in the basis of the eigenstates of the Hamiltonian.

To contrast Eq. (6.71) with the fluctuations of $\hat{O}$ seen in experiments, let us also show the expression for the latter:

$$\overline{\delta O^2} = \lim_{t_0\to\infty} \frac{1}{t_0}\int_0^{t_0} dt\, \langle\psi(t)|(\hat{O}-\overline{O})^2|\psi(t)\rangle = \sum_m |C_m|^2 (O^2)_{mm} - \overline{O}^2. \tag{6.73}$$

This quantity is nonzero even if the initial state is an eigenstate of the Hamiltonian ($|\psi_I\rangle = |m\rangle$), while σ_O is zero in that case. Assuming that δE is sufficiently small, and using the ETH ansatz for $\hat{O}^2$, we find

$$\overline{\delta O^2} \approx \delta O^2_{\rm ME} + \frac{1}{2}\left[O^{2\prime\prime}(\langle E\rangle) - 2O(\langle E\rangle)O''(\langle E\rangle)\right]\left[\delta E^2 - (\delta E_{\rm ME})^2\right]. \tag{6.74}$$

And we see that the fluctuations of $\hat{O}$ scale as the equilibrium statistical fluctuations of $\hat{O}$. However, in this case, there is a second term which can be of the same order. We note that Eq. (6.74) describes the difference between the canonical and microcanonical fluctuations of $\hat{O}$ if instead of δE^2 one uses energy fluctuations of the canonical ensemble, that is, same order corrections to fluctuations also occur in equilibrium statistical mechanics. In generic cases, for example, for extensive observables in systems away from critical points, $\sqrt{\overline{\delta O^2}}/\overline{O} \simeq \sqrt{\delta O^2_{\rm ME}}/O_{\rm ME} \simeq 1/\sqrt{V}$, where V is the volume of the system.

An important question that we leave unaddressed here is that of relaxation times. Namely, how long it takes for an observable to reach the diagonal ensemble result. The answer to this question depends on the observable, the initial state selected, and the specifics of the Hamiltonian driving the dynamics. As we will show when discussing results from numerical experiments, the relaxation times of observables of interest in lattice systems are not exponentially large. They actually need not even increase with increasing system size.

Summarizing our discussion so far, we see that the language used to describe thermalization in isolated quantum systems is quite different from that in classical systems. Chaos, ergodicity, and thermalization are hidden in the nature of the Hamiltonian eigenstates. Relaxation of observables to their equilibrium values is nothing but the result of dephasing, as follows from the second term (in the last line) in Eq. (6.60). Thus, the information about the eventual thermal state is encoded in the system from the very beginning, the time evolution simply reveals it. In classical systems, one usually thinks of thermalization in very different terms using the language of particle collisions and energy redistribution between different degrees of freedom. It is important to realize that both approaches describe exactly the same processes. In Sec. 6.8.4, we will briefly discuss how one can understand relaxation in weakly nonintegrable quantum systems through the language of quantum kinetic equations. Kinetic equations, when justified, provide a unified framework to describe relaxation in both quantum and classical systems.

ETH and the Quantum Ergodic Theorem

Now that we have formulated ETH and seen its consequences for the dynamics of isolated quantum systems, let us come back to von Neumann's ergodic theorem and discuss how it relates

to ETH (or, more precisely, to RMT) [145]. As said before, von Neumann was interested in understanding what happens to observables during the unitary time evolution of *all* possible states drawn from the microcanonical shell. His theorem was then about the behavior of typical observables at most times. To state it, we follow the discussion by Goldstein *et al.* in Ref. [141]. For a recent generalization of this theorem, see Ref. [156].

von Neumann considered a Hamiltonian $\hat{H}$ with eigenstates $|m\rangle$ and eigenvalues E_m, that is, $\hat{H}|m\rangle = E_m|m\rangle$, and focused on a microcanonical energy window of width δE around an energy E. This microcanonical energy window defines a Hilbert space $\mathscr{H}$ of dimension $\mathcal{D}$, which is spanned by $\mathcal{D}$ energy eigenstates $|m\rangle$ with energies $E_m \in (E - \delta E/2, E + \delta E/2)$. For example, every state in the microcanonical energy window can be decomposed as $|\psi\rangle = \sum_{m\in\mathscr{H}} C_m|m\rangle$, where $C_m = \langle m|\psi\rangle$. The Hilbert space $\mathscr{H}$ is then decomposed into mutually orthogonal subspaces $\mathscr{H}_\nu$ of dimensions d_ν, such that $\mathscr{H} = \bigoplus_\nu \mathscr{H}_\nu$ and $\mathcal{D} = \sum_\nu d_\nu$. Finally, the observables in $\mathscr{H}$ are written as $\hat{O} = \sum_\nu O_\nu \hat{P}_\nu$, where $\hat{P}_\nu$ is the projector onto $\mathscr{H}_\nu$. Here, both $\mathcal{D}$ and d_ν are assumed to be large. By definition, the expectation value of the observable at time t is $O(t) = \langle\psi|\exp[i\hat{H}t]\hat{O}\exp[-i\hat{H}t]|\psi\rangle$ while its microcanonical average is $\langle\hat{O}\rangle_{\rm ME} = \sum_{m\in\mathscr{H}}\langle m|\hat{O}|m\rangle/\mathcal{D}$. von Neumann's *quantum ergodic theorem* states that: In the absence of resonances in $\hat{H}$, namely, if $E_m - E_n \neq E'_m - E'_n$ unless $m = m'$ and $n = n'$, or $m = n$ and $m' = n'$, and provided that, for any ν,

$$\max_m \left(\langle m|\hat{P}_\nu|m\rangle - \frac{d_\nu}{\mathcal{D}}\right)^2 + \max_{m\neq n} |\langle m|\hat{P}_\nu|n\rangle|^2 \text{ is exponentially small,} \tag{6.75}$$

then

$$|O(t) - \langle\hat{O}\rangle_{\rm ME}|^2 < \epsilon\langle\hat{O}^2\rangle_{\rm ME} \tag{6.76}$$

for all but a fraction δ of times t, where ϵ and δ are small numbers. It is easy to see that condition (6.75) guarantees that the eigenstate expectation value of $\hat{O}$ is identical to the microcanonical prediction [145]. In fact:

$$\begin{aligned}\langle m|\hat{O}|m\rangle &= \sum_\nu O_\nu\langle m|\hat{P}_\nu|m\rangle \approx \sum_\nu O_\nu\frac{d_\nu}{\mathcal{D}}\\ &= \sum_{m\in\mathscr{H},\nu} O_\nu\frac{\langle m|\hat{P}_\nu|m\rangle}{\mathcal{D}} = \sum_{m\in\mathscr{H}}\frac{\langle m|\hat{O}|m\rangle}{\mathcal{D}} \equiv \langle\hat{O}\rangle_{\rm ME}\end{aligned} \tag{6.77}$$

where the second equality holds up to exponentially small corrections, see Eq. (6.75), and we have used that $\sum_{m\in\mathscr{H}}\langle m|\hat{P}_\nu|m\rangle = d_\nu$. Next, we have that

$$\langle m|\hat{O}|n\rangle = \sum_\nu O_\nu\langle m|\hat{P}_\nu|n\rangle, \tag{6.78}$$

which is exponentially small if $\langle m|\hat{P}_\nu|n\rangle$ is exponentially small [as required in Eq. (6.75)] and if O_ν is not exponential in system size (as expected for physical observables).

We then see that Eqs. (6.77) and (6.78) are nothing but the RMT predictions summarized in Eq. (6.20), or, equivalently, the ETH ansatz restricted to the Thouless energy window $\delta E \sim E_T = \hbar D/L^2$, where the function $f(\bar{E}, \omega)$ is approximately constant. Without this condition, Eq. (6.75) cannot be satisfied. Ultimately, Eqs. (6.20), (6.62) and (6.75) rely on the fact that the overlap between the energy eigenstates and eigenstates of the observables is exponentially small [145]. It is important to note that RMT provides a wealth of information about the statistics of the level spacings and of the eigenstate components, which we have connected to quantum chaotic Hamiltonians, that was absent in von Neumann's (much earlier) theorem. ETH goes beyond RMT (and the quantum ergodic theorem), as we mentioned before, because it addresses what happens outside the featureless Thouless energy shell.

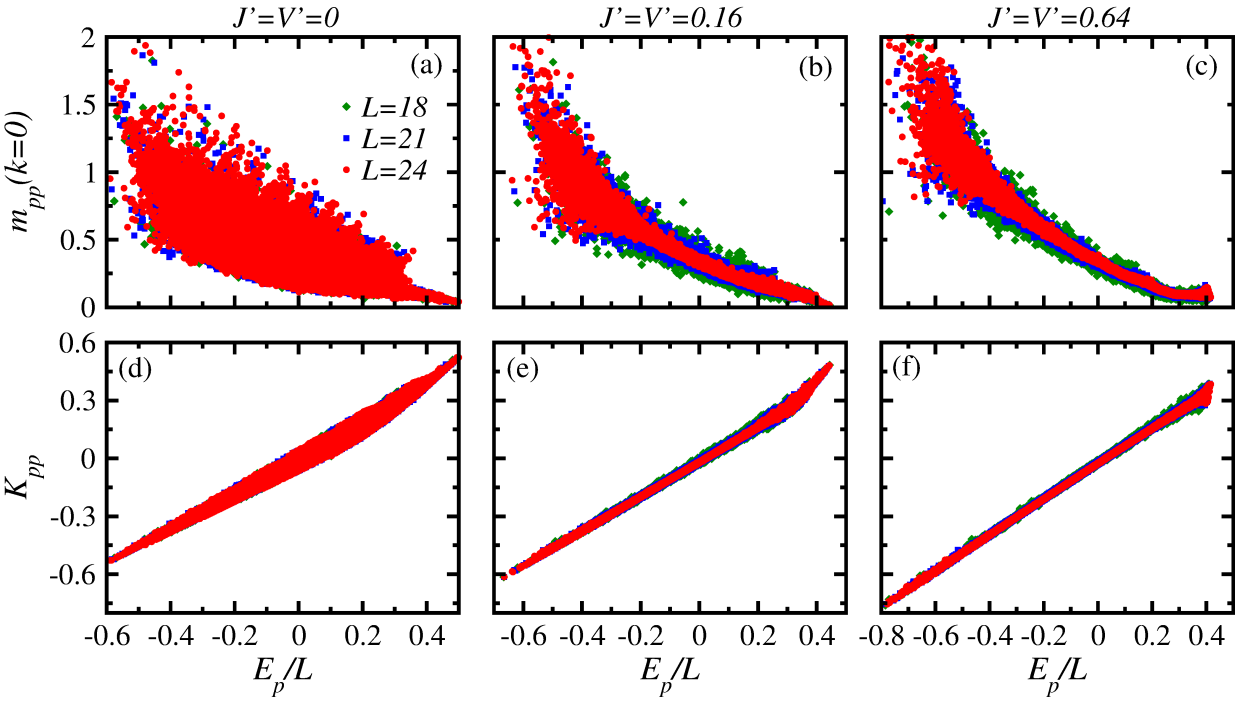

Figure 6.13: Eigenstate expectation values of the occupation of the zero momentum mode [(a)–(c)] and the kinetic energy per site [(d)–(f)] of hard-core bosons as a function of the energy per site of each eigenstate in the entire spectrum, that is, the results for all k-sectors are included. We report results for three system sizes ($L = 18$, 21, and 24), a total number of particles $N = L/3$, and for two values of $J' = V'$ [$J' = V' = 0.16$ in panels (b) and (e) and $J' = V' = 0.64$ in panels (c) and (f)] as one departs from the integrable point [$J' = V' = 0$ in panels (a) and (d)]. In all cases $J = V = 1$ (unit of energy). See also Ref. [157].

6.4.3 Numerical Experiments in Lattice Systems

Eigenstate Thermalization

Numerical evidence of the occurrence of eigenstate thermalization has been found in a number of strongly correlated nonintegrable lattice models in fields ranging from condensed matter to ultracold quantum gases. Such an evidence was first reported for a two-dimensional system of hard-core bosons [28], and, since then, among others, it has been reported for a variety of models of hard-core bosons and interacting spin chains [157, 158, 99, 70, 154, 159, 160, 161, 162, 163, 164], spinless and spinful fermions [158, 126, 165, 166], soft-core bosons [167, 168, 160, 169, 164], and the transverse field Ising model in two dimensions [170]. Below, we discuss the evidence for ETH separately for the diagonal and the off-diagonal matrix elements.

Diagonal matrix elements

We begin by illustrating the behavior of the diagonal matrix elements of observables in the lattice hard-core boson model in Eq. (6.55), which transitions between the integrable limit and the chaotic regime as $J' = V'$ departs from zero (see Sec. 6.3.4) [69].

In Fig. (6.13), we show in panels (a)–(c) the energy eigenstate expectation values of the zero momentum mode occupation

$$\hat{m}(k) = \frac{1}{L}\sum_{i,j} e^{ik(i-j)}\hat{b}_i^\dagger \hat{b}_j \ . \tag{6.79}$$

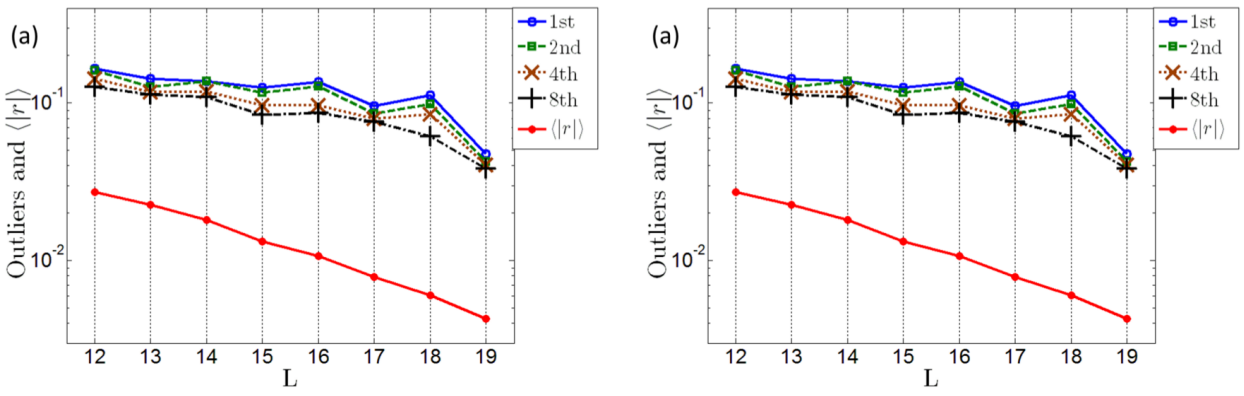

Figure 6.14: The first, second, fourth, and eighth largest values of r_p in the central half of the spectrum, as well as its mean value, are shown from top to bottom in both panels. (a) Results for the x-component of the magnetization in a nonintegrable transverse Ising Hamiltonian. (b) Results for the nearest neighbor density-density correlations in a nonintegrable hard-core boson Hamiltonian. From Ref. [161].

In panels (d)–(f), we show the kinetic energy per site

$$\hat{K} = \frac{1}{L}\sum_{j=1}^{L}\left[-J\left(\hat{b}_j^\dagger \hat{b}_{j+1} + \text{H.c.}\right) - J'\left(\hat{b}_j^\dagger \hat{b}_{j+2} + \text{H.c.}\right)\right]. \tag{6.80}$$

Eigenstate expectation values are plotted as a function of the eigenenergies per site (E_p/L), for three different system sizes as one increases $J' = V'$. The qualitative behavior of $m_{pp}(k=0)$ and K_{pp} vs E_p/L, depicted in Fig. (6.13), has been observed in other few-body observables and models studied in the literature, and, as such, is expected to be generic. The main features to be highlighted are: (i) At integrability, $m_{pp}(k=0)$ and K_{pp} can have quite different expectation values [see, particularly, $m_{pp}(k=0)$] in eigenstates of the Hamiltonian with very close energies. Moreover, the spread does not change with increasing system size and the variance (not shown) decreases as a *power law* of the system size. Similar results have been obtained in other integrable models for larger system sizes than those available from direct full exact diagonalization of the Hamiltonian [131, 132, 171, 172, 133]. (ii) As one departs from $J' = V'$, or as one increases the system size for any given value of $J' = V' \neq 0$, the spread (or maximal differences) between the eigenstate expectation values in eigenstates with very close energies decrease. This is true provided that the eigenstates are not too close to the edges of the spectrum.

Recently, Kim et al. [161] studied the eigenstate-to-eigenstate fluctuations $r_p = O_{p+1p+1} - O_{pp}$ of both the x-component of the magnetization in a nonintegrable transverse Ising chain with a longitudinal field and of the nearest neighbor density-density correlations in the nonintegrable hard-core boson model (6.55). The results for the average value of $|r_p|$, and for some of the largest values of r_p (in the central half of the spectrum), are shown in Fig. 6.14 as a function of the system size. They support the ETH expectation that eigenstate-to-eigenstate fluctuations decrease exponentially fast with increasing system size (similar results were obtained in Ref. [170] for the transverse field Ising model in two dimensions). Evidence that the variance of the eigenstate-to-eigenstate fluctuations of various observables decreases exponentially fast with increasing system size has also been presented in Refs. [159, 160, 170].

The results discussed so far suggest that, away from the edges of the spectrum and for sufficiently large system sizes, any strength of an integrability breaking perturbation ensures that the first term in Eq. (6.62) describes the diagonal matrix elements of physical observables. By sufficiently large system sizes, we mean the same conditions that were discussed for the

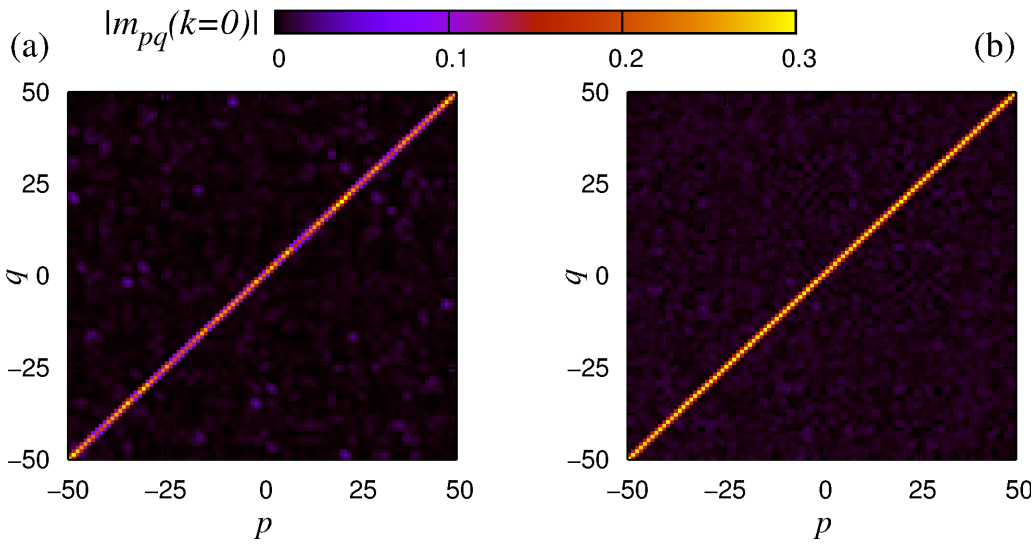

Figure 6.15: Off-diagonal matrix elements of $\hat{m}(k=0)$ in the eigenstates of the Hamiltonian for a system with $L=24$, $N=L/3$, and $J=V=1$ (unit of energy). (a) $J'=V'=0$ and (b) $J'=V'=0.32$. Results are shown for the matrix elements between the 100 eigenstates with energy closest to (a) $E/L=-0.16$ and (b) $E/L=-0.19$. Those energies were selected from canonical ensembles with $T=3$ in both systems. See also Ref. [158].

onset of quantum chaotic behavior in Sec. 6.3. Systems that exhibit a many-body localization transition do not conform with this expectation [51].

Off-diagonal matrix elements

In Fig. 6.15, we show the matrix elements of the zero momentum mode occupation $\hat{m}(k=0)$ between the 100 eigenstates whose energy is closest to the energy of the canonical ensemble with temperature[23] $T=3$. Figure 6.15(a) and 6.15(b) illustrates some of the most important properties of the off-diagonal matrix elements of few-body observables in integrable and non-integrable systems. They have been discussed in Refs. [28, 158, 70] for various lattice models in one and two dimensions and, recently, systematically studied in Refs. [154, 159, 164]. The first obvious property, seen in Fig. 6.15(a) and 6.15(b), is that no matter whether the system is integrable or not, the average value of the off-diagonal matrix elements is much smaller than the average value of the diagonal ones. In the integrable regime, Fig. 6.15(a), a few off-diagonal matrix elements can be seen to be relatively large, while many are seen to be zero [154, 164]. In the nonintegrable regime, Fig. 6.15(b), the (small) values of the off-diagonal matrix elements appear to have a more uniform distribution. Note that, in contrast to the integrable limit, no relatively large outliers can be identified among the off-diagonal matrix elements in the non-integrable regime. In the latter regime, the values of the off-diagonal matrix elements have been shown to exhibit a nearly Gaussian distribution with zero mean [159, 164], and to be exponentially small in system size [164].

A better quantitative understanding of the behavior of the off-diagonal matrix elements of observables can be gained by plotting them as a function of E_p-E_q for a small window of values $(E_p+E_q)/2$. This is done in Fig. 6.16 for a one-dimensional model of hard-core bosons

[23] $T=3$ was selected so that the eigenstates considered are not too close to the ground state and do not correspond to infinite temperature either. These results are relevant to the quenches discussed in Sec. 6.4.3.

with the Hamiltonian [154]

$$\hat{H} = -J \sum_{j=1}^{L-1} \left(\hat{b}_j^\dagger \hat{b}_{j+1} + \text{H.c.} \right) + V \sum_{j<l} \frac{\hat{n}_j \hat{n}_l}{|j-l|^3} + g \sum_j x_j^2 \, \hat{n}_j. \tag{6.81}$$

The number of bosons was set to be $L/3$. The three terms in this Hamiltonian describe, from left to right, hopping ($J = 1$ sets the energy scale), dipolar interactions, and a harmonic potential (x_j is the distance of site j from the center of the trap). We note that $\hat{H}$ in Eq. (6.81) is not translationally invariant so that the thermodynamic limit needs to be taken with care [33]. For $V = 0$, this model is integrable (mappable to noninteracting spinless fermions) irrespective of the value of J and g.

In Fig. 6.16(a), we show results at integrability ($V = 0$ and $g \neq 0$), while, in Fig. 6.16(b), we show results away from integrability ($V = 2$ and $g \neq 0$). For both cases, results are reported for two observables, the site occupation at the center of the trap and the zero momentum mode occupation. The off-diagonal matrix elements of both observables are qualitatively different in the integrable and nonintegrable regimes. In the integrable model, there is a small fraction of large outliers among the matrix elements (whose absolute value is orders of magnitude larger than that of the median of the nonvanishing absolute values). In addition, there is a large fraction of matrix elements that vanish. As a matter of fact, one can see in Fig. 6.16(a) that only a few off-diagonal matrix elements of the site occupation are nonzero (this observable is the same for hard-core bosons and for the noninteracting fermions to which they can be mapped [33]). For the zero momentum mode occupation (which is not the same for hard-core bosons and noninteracting fermions [33]), the histogram of the differences between the absolute values and their running average [inset in Fig. 6.16(a)] makes apparent that there is also a large fraction (increasing with system size [154]) of vanishing matrix elements. This demonstrates that, in the integrable model and for the observables shown, the off-diagonal matrix elements are not described by the ETH ansatz. In contrast, one does not find large outliers among the off-diagonal matrix elements in the nonintegrable model. In addition, the near flat histogram in the inset in Fig. 6.16(b) shows that there is no large fraction of them that vanish as in the integrable case. One can then conclude that the running average of the off-diagonal matrix elements, that is, the absolute value of the function $f_O(E, \omega)$ in Eq. (6.62), is a well-defined quantity in nonintegrable systems.

This function is studied in detail in Fig. 6.17 for the occupation at the center of the trap (see figure caption for a precise definition of the observable). Results are reported for the same system described above but with $L/2$ bosons. By selecting a narrow energy window in the center of the spectrum, and by comparing results for two different system sizes (including the largest we are able to solve numerically), it is possible to identify three qualitatively different regimes at large, intermediate, and small energy separation $\omega = E_p - E_q$ [in what follows, we drop "E" from $f_O(E, \omega)$, keeping in mind that E is that in the center of the spectrum]. These three regimes are shown in panels (a), (b), and (c). (a) For $\omega \gg 1$, the function $|f_O(\omega)|$ decays exponentially and the curves corresponding to different system sizes show an excellent collapse supporting the ETH ansatz (6.62). (b) At intermediate ω, $|f_O(\omega)|$ is proportional to $L^{1/2}$ and, around the point marked with a vertical dashed line, one can see a broad peak whose position scales with L^{-1}. (c) For $\omega \ll 1$, $|f_O(\omega)|$ exhibits a plateau. Our results suggest that $|f_O(\omega)|$ in the plateau is proportional to $L^{1/2}$, and that its width is proportional to L^{-2}. The results in panel (c) are noisier than in panels (a) and (b) because of poor statistics, which is the result of having only few pairs of eigenstates in the center of the spectrum such that $\omega = E_p - E_q \ll 1$.

The three regimes identified above, for large, intermediate, and small values of ω, determine what happens to the observable at short, intermediate, and long times during the dynamics (c.f., Sec. 6.6.8). In the fast, high-frequency, regime $|f_O(\omega)|$ is an exponentially decaying function

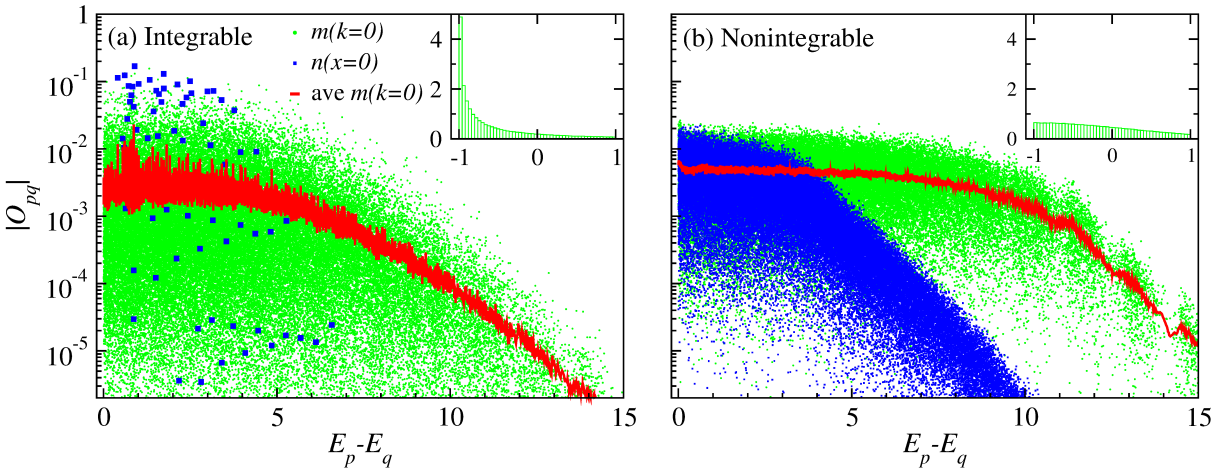

Figure 6.16: Absolute value of the off-diagonal matrix elements of the site occupation in the center of the system $[\hat{n}(x=0)]$ and of the zero momentum mode occupation $[\hat{m}(k=0)]$ in the eigenenergy basis vs the eigenenergy difference $E_p - E_q$, for a small window of energies $(E_p + E_q)/2$ (the center of the window was selected to be the energy of a canonical ensemble with $T = 5$). Results are shown for an integrable (a) and a nonintegrable (b) system with $L = 18$. Lines are running averages ($|O_{pq}|_{\text{avg}}$) for the matrix elements of $\hat{m}(k=0)$. The insets show histograms of the relative differences between the matrix elements of $\hat{m}(k=0)$ and the running averages. The relative difference is defined as $(|O_{pq}| - |O_{pq}|_{\text{avg}})/|O_{pq}|_{\text{avg}}$. The running averages were computed over 50 matrix elements for $L = 15$ and over 200 matrix elements for $L = 18$. Adapted from Ref. [154].

independent of the system size. In Sec. 6.6.8, we show that $|f_O(\omega)|^2$ is related to the spectral function of the observable $\hat{O}$ and to the dissipative part of the linear response susceptibility. Its exponential decay at high frequencies is expected on general grounds from perturbation theory, at least for systems with a bounded spectrum.[24] Such a high-frequency exponential tail was discussed, for example, in Ref. [173] for the conductivity, corresponding to the case where the observable $\hat{O}$ is the current operator. (ii) At intermediate times, the independence of $|f_O(\omega)|$ vs ωL on the system size indicates the existence of ballistic dynamics. (iii) At long times, the approximate collapse of $|f_O(\omega)|$ vs ωL^2 for different system sizes indicates diffusive dynamics. Remarkably, at frequencies smaller than a characteristic frequency $\omega_c \sim 1/L^2$ (corresponding to times longer than the diffusive time $t_c \sim L^2$), the function $|f_O(\omega)|$ saturates at a constant value proportional to $L^{1/2}$. It is in this regime that the ETH ansatz (6.62) becomes equivalent to the RMT ansatz.[25] As the diffusive time is the longest relaxation time scale in the system, one expects that in this regime physical observables do not evolve. The fact that $|f_O(\omega)|$ at the plateau is proportional to $L^{1/2}$ can be understood as follow. The function $|f_O(\omega)|^2$ is related to the nonequal-time correlation function of the observable $\hat{O}$, see Sec. 6.6.8. In particular, when evaluated at $\omega = 0$, we have

$$|f_O(\omega=0)|^2 \propto \int_0^{t_c} dt\, \langle \hat{O}(t)\hat{O}(0) + \hat{O}(0)\hat{O}(t)\rangle_c \propto \int_0^{t_c} \frac{dt}{\sqrt{t}} \propto \sqrt{t_c} \propto L, \tag{6.82}$$

where we have used that the diffusive time scale t_c sets an upper bound for the time integral, and that, assuming diffusive behavior, the nonequal-time correlation function of $\hat{O}$ is expected

[24] When the energy spectrum is bounded, in order to absorb energy $\omega \gg 1$, many-body processes are required. These processes appear only in high orders of perturbation theory, which leads to an exponential suppression of $|f_O(\omega)|$ for $\omega \gg 1$.

[25] It is likely that $t_c \approx L^2/D$, where D is the diffusion constant.

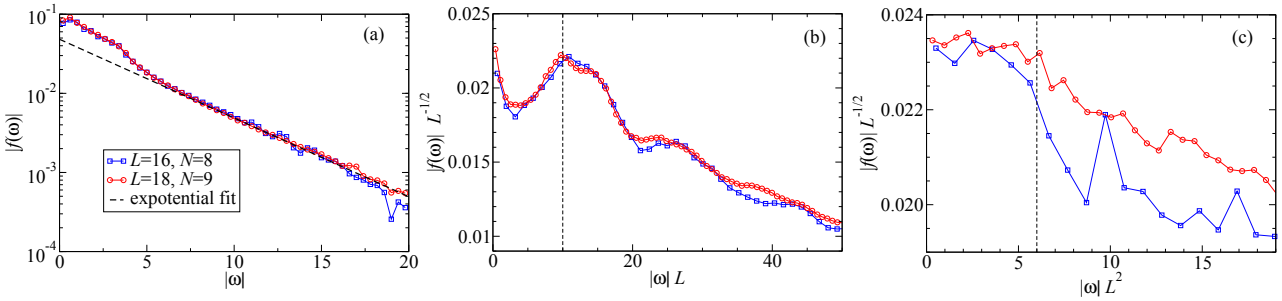

Figure 6.17: Plot of the function $|f_O(\omega)|$ vs the eigenenergy difference $\omega = E_p - E_q$ for a system of $L/2$ bosons described by the Hamiltonian (6.81) with parameters $J = 1$, $U = 1$ and $g = 16/(L-1)^2$. The observable $\hat{O}$ is the occupation at the center of the trap (more precisely, the average of the occupation of the two central sites, as the calculations were done in the even sector when taking into account reflection symmetry and the center of the trap is in the middle of two sites) and the function $|f_O(\omega)|$ is obtained in a small energy window centered around the middle of the spectrum. (a) At large ω, $|f_O(\omega)|$ decays exponentially. (b) At intermediate ω, $|f_O(\omega)|$ is proportional to $L^{1/2}$ and has a broad peak whose position scales as L^{-1}. (c) At small ω, $|f_O(\omega)|$ exhibits a plateau. $|f_O(\omega)|$ in the plateau is proportional to $L^{1/2}$, and the extension of the plateau is proportional to L^{-2}.

to be $\propto t^{-1/2}$. It then follows that $f_O(\omega = 0) \propto \sqrt{L}$. Remarkably, our results suggests that the scaling of $f_O(\omega)$ with $L^{1/2}$ is also valid at the intermediate frequencies that are relevant to ballistic transport [see Fig. 6.17(b)].

Quantum Quenches and Thermalization in Lattice Systems

Now, let us see what happens when systems such as those studied in Sec. 6.4.3 are taken out of equilibrium. Among the most common protocols for taking systems out of equilibrium are the so-called sudden quenches or, simply, quenches. As explained in Sec. 6.3.4, in a quench the system is assumed to be initially in equilibrium and then suddenly some parameter(s) is (are) changed. The dynamics proceeds without any further changes of parameters. For example, in ultracold gases experiments in optical lattices, one can suddenly change the depth of the optical lattice [34, 35, 36, 41, 37], displace the center of the trapping potential [174, 175, 176], or turn off a trapping potential while keeping the optical lattice on [177, 178, 43]. Theoretically, one can think of a quench as a protocol in which one starts with a stationary state of a given Hamiltonian, often the ground state, and then suddenly changes some Hamiltonian parameter(s). The initial state is not stationary in the new (time-independent) Hamiltonian, as a result of which it has a nontrivial unitary dynamics. Quenches in which one changes parameters throughout the system are called global quenches, while quenches in which parameters are only changed in a finite region are called local quenches. In the former class of quenches, one generally adds an extensive amount of the energy to the system, while, in the latter class, the change in energy is subextensive.

A remarkable property of quantum quenches involving local Hamiltonians is that one can actually prove, under very general conditions, that the width δE of the energy distribution after a quench scales with the square root of the volume (or of the number of particles) [28]. This behavior is expected from thermodynamics, and is essentially a consequence of the central limit theorem. This width sets the effective "microcanonical window" of the equivalent thermodynamic ensemble. It depends on the details of the initial state and the quench protocol.

To prove that after a global quench $\delta E \sim \sqrt{V}$, we consider, for concreteness, a lattice system prepared in an initial state $|\psi_I\rangle$ which is an eigenstate (not necessarily the ground state) of the

initial Hamiltonian $\hat{H}_0$. After the quench, the Hamiltonian is $\hat{H} = \hat{H}_0 + \hat{H}_1$, where $\hat{H}_1$ is a sum of local operators $\hat{H}_1 = \sum_j \hat{h}_j$. One can then write [28]

$$\delta E \equiv \sqrt{\langle\psi_I|\hat{H}^2|\psi_I\rangle - \langle\psi_I|\hat{H}|\psi_I\rangle^2} = \sqrt{\langle\psi_I|\hat{H}_1^2|\psi_I\rangle - \langle\psi_I|\hat{H}_1|\psi_I\rangle^2}$$
$$= \sqrt{\sum_{j_1,j_2}\Big[\langle\psi_I|\hat{h}_{j_1}\hat{h}_{j_2}|\psi_I\rangle - \langle\psi_I|\hat{h}_{j_1}|\psi_I\rangle\langle\psi_I|\hat{h}_{j_2}|\psi_I\rangle\Big]}. \tag{6.83}$$

From the expression above, one concludes that, in the absence of long-range *connected* correlations between $\hat{h}_j$ in the initial state, and if all matrix elements are finite,[26] the width δE scales at most as the square root of the number of lattice sites in the system, that is, $\delta E \sim \sqrt{V}$. Because the energy itself is extensive in the volume of the system, we see that the relative energy fluctuations are inversely proportional to the square root of the volume $\delta E/E \sim 1/\sqrt{V}$ as expected from equilibrium thermodynamics. This result is a consequence of the locality of the Hamiltonian and, hence, is unrelated to whether the system is integrable or nonintegrable. This scaling of energy fluctuations, in combination with eigenstate thermalization, ensures that in generic systems with local interactions thermalization occurs after a quench. Generalizing this proof to continuous systems is straightforward.

Next, we address two important questions whose precise answer depends on the specifics of the system and of the observable of interest, but whose qualitative answer has been found to be quite similar for several strongly correlated lattice models and observables studied. The first question is how long it takes for experimentally relevant observables to relax to the diagonal ensemble predictions. The second one is how large the system sizes need to be for the relative difference between the diagonal ensemble and the statistical mechanics predictions to be small. These questions have been mainly addressed in numerical experiments. We reproduce some results of these numerical experiments below.

Dynamics

We consider the dynamics of observables in the hard-core boson model (6.55). Some numerical results for this model were already discussed in Secs. 6.3.4 and 6.4.3. For the quench dynamics discussed here, the initial states are taken to be eigenstates of the Hamiltonian with $J_I = 0.5$, $V_I = 2$, $J' = V'$, and the time evolutions are studied under final Hamiltonians with $J = V = 1$ (unit of energy), and $J' = V'$ [157]. Hence, only the nearest neighbor parameters are changed during the quench. The strengths ($J' = V'$) of the integrability breaking terms remain unchanged. To characterize the dynamics of the entire momentum distribution function and of the kinetic energy (by comparing them to the diagonal ensemble results), the following relative differences are computed

$$\delta m(t) = \frac{\sum_k |m(k,t) - m_{\rm DE}(k)|}{\sum_k m_{\rm DE}(k)}, \quad \text{and} \quad \delta K(t) = \frac{|K(t) - K_{\rm DE}|}{|K_{\rm DE}|}, \tag{6.84}$$

respectively. In these expressions, t refers to time and the subscript "DE" refers to the diagonal ensemble prediction [recall Eq. (6.53)]. In order to be able to compare results for systems with different Hamiltonian parameters in a meaningful way, the initial state for each quench is selected to be the eigenstate of the initial Hamiltonian that, after the quench, has the closest energy to that of a system with temperature T, namely, $\langle\psi_I|\hat{H}|\psi_I\rangle = {\rm Tr}[\hat{H}\exp(-\hat{H}/T)]/{\rm Tr}[\exp(-\hat{H}/T)]$, where the Boltzmann constant is set to unity. For the quenches discussed in what follows, $T = 3$ as in Fig. 6.15. This temperature is such that eigenstate thermalization can be seen in these small systems and $O(\bar{E})$ is not featureless as expected in the center of the spectrum (i.e., at "infinite temperature").

[26] This is guaranteed if the operator norm of each $\hat{h}_j$ is finite

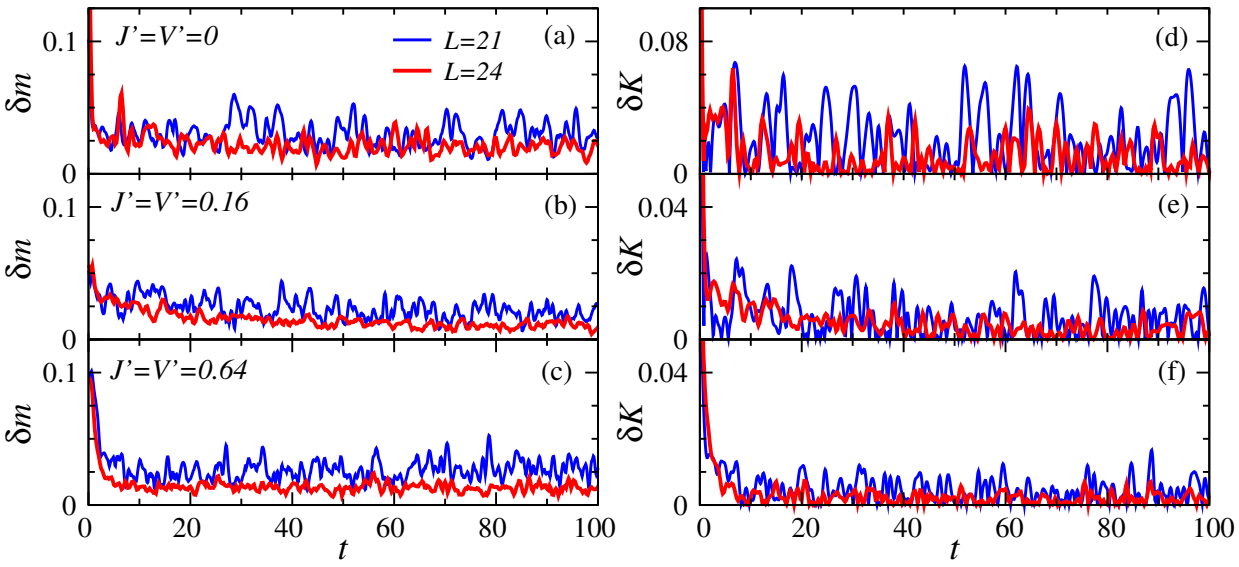

Figure 6.18: (a)–(c) Relative difference between the instantaneous momentum distribution function and the diagonal ensemble prediction (see text) as a function of time. (d)–(f) Relative difference between the instantaneous kinetic energy and the diagonal ensemble prediction (see text) as a function of time. The strength of the integrability breaking terms ($J' = V'$) increases from top to bottom: (a),(d) $J' = V' = 0$ (integrable point); (b),(e) $J' = V' = 0.16$; and (c),(f) $J' = V' = 0.64$. Results are reported for two system sizes ($L = 21$ and 24) and $N = L/3$. In all cases, $J = V = 1$ (unit of energy). Time is given in units of $\hbar/J$. See also Ref. [157].

In Fig. 6.18(a)–6.18(c), we show results for $\delta m(t)$ vs t for systems with $L = 21$ (blue lines) and $L = 24$ (red lines), and for three values of $J' = V'$. The behavior of $\delta m(t)$ vs t is qualitatively similar for all values of $J' = V'$. Namely, at $t = 0$, one can see that δm is large ($\gtrsim 10\%$, except for $J' = V' = 0.16$) and then it quickly decreases (in a time scale of the order of $\hbar/J$) and starts oscillating about a small nonzero value ($\sim 2\%$ for $L = 24$). With increasing system size, the value about which $\delta m(t)$ oscillates, as well as the amplitude of the oscillations, decrease. A qualitatively similar behavior, though with a significantly smaller mean and amplitude of the oscillations about the mean, can be seen during the time evolution of $\delta K(t)$ [Fig. 6.18(d)–6.18(f)]. Comparable results have been obtained for other nonintegrable models and observables [179, 180, 28, 181, 182, 157, 158, 183, 99, 184, 154, 185, 169]. All that numerical evidence makes clear that, despite the exponentially small (in system size) level spacing in many-body quantum systems, the relaxation of physically relevant observables to the diagonal ensemble results does not take exponentially long time. Furthermore, in accordance with our expectations based on the ETH ansatz, numerical experiments have also shown that the scaling of the variance of the time fluctuations of expectation values of observables is consistent with an exponential decrease with increasing system size [185].

Note that the results reported in Fig. 6.18 were obtained in systems in which there are only seven and eight hard-core bosons, for $L = 21$ and $L = 24$, respectively. Namely, the time fluctuations of the expectation values of observables can be very small even for systems with a very small number of particles (see Ref. [28] for an analysis of a two-dimensional system with only five hard-core bosons that exhibits a qualitatively similar behavior).

Post relaxation

After showing that even small finite systems relax to the predictions of the diagonal ensemble and remain close to them, we need to check how close the diagonal ensemble predictions are to those made by standard statistical mechanics. This is the final step needed to know

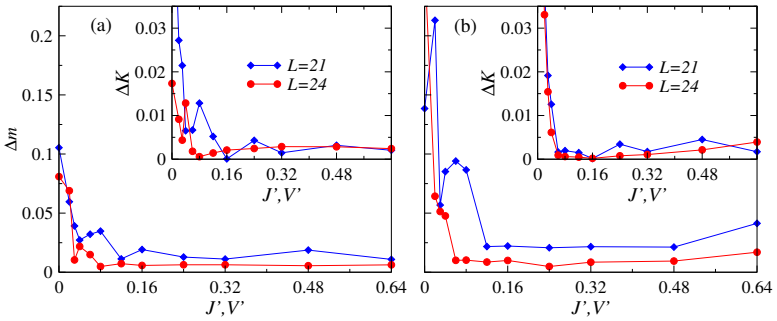

Figure 6.19: (Main panels) Relative difference between the predictions of the diagonal and microcanonical ensembles for the momentum distribution function (see text) as a function of the strength of the integrability breaking terms. (Insets) The same as the main panels but for the kinetic energy. Results are reported for hard-core bosons (a) and for spinless fermions (b), and for two system sizes $L = 21$ (blue lines) and $L = 24$ (red lines) with $N = L/3$. In all cases, $J = V = 1$ (unit of energy). See also Refs. [157, 158].

whether thermalization takes place. Since we are dealing with small systems, which ensemble is taken among the microcanonical, canonical, and grand canonical ensembles makes a difference. Considering that the systems of interest here are isolated, the most appropriate statistical ensemble is the microcanonical ensemble [28, 157]. Therefore, we compute the following relative differences to characterize whether the system thermalizes or not

$$\Delta m = \frac{\sum_k |m_{\rm DE}(k) - m_{\rm ME}(k)|}{\sum_k m_{\rm DE}(k)}, \quad \text{and} \quad \Delta K = \frac{|K_{\rm DE} - K_{\rm ME}|}{|K_{\rm DE}|}. \tag{6.85}$$

In these expressions, the subscripts "DE" and "ME" refer to the diagonal and microcanonical ensemble predictions, respectively.

The main panel (inset) in Fig. 6.19(a) depicts results for Δm (ΔK) in the hard-core boson systems whose dynamics was reported in Fig. 6.18. The corresponding results when the hard-core bosons are replaced by spinless fermions are shown in Fig. 6.19(b). One can see that the behavior of Δm (ΔK) is qualitatively similar for hard-core bosons and spinless fermions. The largest differences between the predictions of the diagonal and microcanonical ensembles are seen at (and close to) the integrable point. As one departs from the integrable point, the differences decrease. After a fast decrease, there is an interval of values of $J' = V'$ at which Δm (ΔK) becomes almost independent of the exact value of $J' = V'$ (up to finite-size fluctuations). In that interval, Δm (ΔK) can be seen to decrease as one increases system size (up to finite-size fluctuations). This is consistent with the expectation that those differences vanish in the thermodynamic limit. Numerical evidence that, in the thermodynamic limit, the predictions of the diagonal ensemble for observables after a quench to a nonintegrable model are identical to those from traditional statistical mechanics ensembles has been obtained in numerical linked cluster expansion studies [135, 130]. On the other hand, in quenches to integrable points in the thermodynamic limit, it was found that lack of thermalization is ubiquitous [135, 130] (see Sec. 6.8.3). For finite systems, it is striking that the differences between the diagonal and the microcanonical ensembles can be a fraction of a percent even for systems with less than 10 particles (which makes their experimental detection unlikely). Similar results have been obtained for other observables in Refs. [28, 157, 158, 99, 154, 169].

The results presented in this section support the expectation that nonintegrable quantum systems exhibit eigenstate thermalization and therefore thermalize in the strong sense as defined in this review.

6.5 Quantum Chaos and the Laws of Thermodynamics

If one assumes that a system is prepared in a Gibbs, or other equivalent ensemble, then one does not need assumptions about chaos and ergodicity to prove various statements of statistical mechanics and thermodynamics. For example, the fluctuation-dissipation relation can be straightforwardly proved using standard perturbation theory. Quantum chaos and ETH allow one to prove all the statements for individual eigenstates of chaotic Hamiltonians, and therefore for arbitrary stationary ensembles (with subextensive energy fluctuations). This distinction is at the heart of the importance of quantum chaos for the proper understanding of thermodynamics in isolated systems. In the earlier sections, we argued that eigenstate thermalization is generally needed for isolated quantum systems taken far from equilibrium to thermalize. Likewise, in the following sections, we will show that the same assumptions of quantum chaos together with ETH are sufficient for establishing thermodynamic relations in such isolated systems.

6.5.1 General Setup and Doubly Stochastic Evolution

Equilibrium thermodynamics studies transformations between equilibrium states of macroscopic systems. During such a transformation, thermodynamic quantities (such as the free energy, magnetization, and pressure) evolve in time. These changes are usually induced by either heat exchange with another macroscopic system or the work done on the system via changing some macroscopic parameters in time (like its volume or the applied magnetic field), or both. For example, consider a phase transformation from a solid to a liquid as temperature is changed, or the exchange of energy, in the form of heat and work, in heat engines. The laws of thermodynamics dictate which process are possible and which are not. They give bounds for engine efficiencies and provide relations between superficially different quantities (e.g., the Onsager relations, which will be discussed in the next section).

Since equilibrium thermodynamics provides relations between different equilibrium states, the concept of a quasi-static process is central to the development of the theory. A quasi-static process is one in which the state of the system is changed very slowly through a sequence of equilibrium states. However, it is important to stress that thermodynamics is not limited to quasi-static processes. For example, in one formulation of the second law of thermodynamics one considers an equilibrated isolated system that undergoes a dynamical process (which need not be quasi-static). As a result, the entropy difference between the final equilibrium state of the system and the initial equilibrium state is positive or zero independent of how rapidly the process is carried out. Moreover, this entropy difference is uniquely determined by the total energy change in the system, no matter how fast or slow the process of energy exchange is. Another remarkable example of thermodynamic relations are the recently discovered fluctuation theorems [20, 186, 25, 187], which make exact statements about work, heat, and free energy changes in arbitrary nonequilibrium processes.

To derive thermodynamic relations one needs to consider dynamical processes that start from a stationary state. To this end, we focus on an isolated system initially prepared in a stationary state, which undergoes a unitary evolution in response to an external change. The latter is modeled by a change in time of macroscopic parameters in the Hamiltonian according to a prescribed protocol. The protocol considered is such that the parameters are changed during a finite time, after which the Hamiltonian is time independent and the system is allowed to relax to equilibrium. As an example, one can think of a gas confined in a container by a piston (see Fig. 6.20). In this case, the macroscopic parameter is the position of the piston, which is changed in time from position $z = A$ to $z = B$ according to a protocol $z(t)$. At the end of the process, the piston is kept fixed at position $z = B$ and the gas is allowed to equilibrate. While we focus on isolated systems, our setup can also describe open systems. This is because, if the dynamical process involves changing parameters only in a part of the system (a local

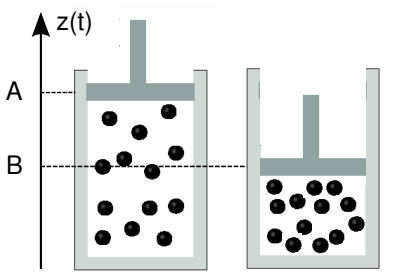

Figure 6.20: Schematic representation of a gas undergoing a compression

operation), the rest of the system can act as a thermal bath. If the bath is much larger than the part of the system in which the dynamical process is implemented, the intensive quantities characterizing the latter (such as the energy density defining the temperature or the pressure) after it relaxes to equilibrium will be identical to their initial values.

Mathematically, the assumption that the systems start in a stationary (i.e., a state that is translationally invariant in time) amounts to taking the initial density matrix to be diagonal in the basis of the initial Hamiltonian (if there are degeneracies in the spectrum, one just needs to find a basis where the density matrix is diagonal)

$$\rho^{(0)}_{nm} = \rho^{(0)}_{nn}\,\delta_{nm}. \tag{6.86}$$

It is important to note that, at the moment, we make no assumptions on the structure of the density matrix beyond stationarity. After the system undergoes a dynamical process, the density matrix in the basis of the final Hamiltonian, that is, the Hamiltonian at the end of the dynamical process, is not diagonal anymore. As discussed previously, the off-diagonal matrix elements dephase and, at long times, the expectation values of observables are solely determined by the diagonal matrix elements. The latter are given by

$$\rho_{\tilde{m}\tilde{m}} = \sum_n U_{\tilde{m}n}\rho^{(0)}_{nn}U^\dagger_{n\tilde{m}}, \tag{6.87}$$

where U_{nm} are the matrix elements of the evolution operator

$$\hat{U} = T_t \exp\left[-i\int_0^t dt'\hat{H}(t')\right],\ U_{\tilde{m}n} = \langle\tilde{m}|\hat{U}|n\rangle. \tag{6.88}$$

Here, T_t denotes time ordering, and the "tilde" indicates that the states $|\tilde{m}\rangle$ are eigenstates of the Hamiltonian after the evolution, while $|n\rangle$ are the eigenstates of the initial Hamiltonian. The two basis sets coincide only in the special case of cyclic processes.

Equation (6.87) can be rewritten as a master equation for the occupation probabilities of the microstates

$$\rho^{(1)}_{\tilde{m}\tilde{m}} = \sum_n \rho^{(0)}_{nn}\left(U_{\tilde{m}n}U^\dagger_{n\tilde{m}}\right) \equiv \sum_n \rho^{(0)}_{nn}\,p_{n\to\tilde{m}}, \tag{6.89}$$

where we have defined the transition probabilities between states $|n\rangle$ and $|\tilde{m}\rangle$ associated with the dynamical process to be[27]

$$p_{n\to\tilde{m}} = U_{\tilde{m}n}U^\dagger_{n\tilde{m}} = |U_{\tilde{m}n}|^2\ . \tag{6.90}$$

The last equality trivially follows from the identity $U^\dagger_{n\tilde{m}} = (U_{\tilde{m}n})^*$, where the star indicates complex conjugation.

[27]Note that the transition probabilities are conditional, i.e., they define the probability of a transition from state $|n\rangle$ to state $|\tilde{m}\rangle$ if the system is initially prepared in state $|n\rangle$.

From the unitarity of the evolution operator it follows that

$$\sum_{\tilde{m}} U_{\tilde{m}n} U^{\dagger}_{k\tilde{m}} = \delta_{nk}, \quad \text{and} \quad \sum_{n} U^{\dagger}_{n\tilde{k}} U_{\tilde{m}n} = \delta_{\tilde{k}\tilde{m}} \ . \tag{6.91}$$

Setting $k = n$ and $\tilde{k} = \tilde{m}$, we immediately see that

$$\sum_{\tilde{m}} p_{n\to\tilde{m}} = 1, \quad \sum_{n} p_{n\to\tilde{m}} = 1. \tag{6.92}$$

These conditions allow for a simple physical interpretation if we rewrite it changing the dummy indices n and m in the second sum, namely

$$\sum_{\tilde{m}\neq\tilde{n}} p_{n\to\tilde{m}} = \sum_{m\neq n} p_{m\to\tilde{n}}. \tag{6.93}$$

In other words, the sum of incoming probabilities to any given state $|\tilde{n}\rangle$ of the final Hamiltonian is equal to the sum of the outgoing probabilities from an equivalent, for example, adiabatically connected state $|n\rangle$ of the initial Hamiltonian. For a cyclic process, one can remove the tildes and simply say that the sum of incoming probabilities to any eigenstate is equal to the sum of outgoing probabilities from the same state.

The transition probabilities $p_{n\to\tilde{m}} = |U_{n\tilde{m}}|^2$ are positive semi-definite for any pair of states. This, combined with the constraints above, leads to

$$0 \leq p_{n\to\tilde{m}} \leq 1 \ , \tag{6.94}$$

as expected. Any semi-positive matrix p satisfying the constraints (6.92) and (6.94) is called doubly stochastic [188]. The corresponding evolution described by the master equation (6.89) is called a doubly stochastic evolution.

As it has been known for a long time, the constraints (6.92) have far-reaching consequences and, for example, play a prominent role in the formulation of the kinetic theory of gases [189]. Moreover, doubly stochastic evolution is the proper framework to discuss thermodynamic processes in isolated quantum systems since it emerges naturally based on the assumptions that: (i) the system starts from a stationary state, (ii) the system evolves unitarily, and (iii) the long-time behavior of the observables is determined only by the diagonal elements of the density matrix in the basis of the final Hamiltonian. With this in mind, we review some general properties of the master equation, and those associated with doubly stochastic matrices in particular.

Properties of Master Equations and Doubly Stochastic Evolution

Equation (6.89) is a discrete-time master equation. The matrix $\mathbf{p}$, with elements $p_{n,\tilde{m}} = p_{n\to\tilde{m}}$ satisfying the first of the two conditions in Eq. (6.92), is known as a Markov matrix or, equivalently, as a stochastic matrix. The action of $\mathbf{p}$ on a probability vector, in our case $\rho^{(0)}$ (with elements $\rho^{(0)}_{nn}$), gives a new probability vector $\rho^{(1)}$ (with elements $\rho^{(1)}_{\tilde{m}\tilde{m}}$), which is the result of stochastic transitions between the different states of the system. For completeness, we briefly review some of the properties of a Markov matrix that will be used in our discussion. More details and complete proofs can be found, for example, in Ref. [190].

We first note that the conservation of probability implies that the *outgoing* transition probabilities from any state must sum to one [first condition in Eq. (6.92)], so that the sum over each column of the Markov matrix is 1. This holds for any master equation. Indeed, from Eq. (6.89),

$$\sum_{\tilde{m}} \rho^{(1)}_{\tilde{m}\tilde{m}} = \sum_{\tilde{m}} \sum_{n} \rho^{(0)}_{nn}\, p_{n\to\tilde{m}} = \sum_{n} \rho^{(0)}_{nn} = 1. \tag{6.95}$$

In general, the matrix $\mathbf{p}$ is not symmetric and therefore admits separate left and right eigenvectors (the spectrum associated with left and right eigenvectors is the same). If one applies the matrix $\mathbf{p}$ many times on a probability vector one expects that the probability distribution relaxes to a steady state. This implies that the matrix $\mathbf{p}$ has one eigenvalue $\lambda_0 = 1$ whose corresponding right eigenvector is the steady-state probability distribution [190]. The existence of the eigenvalue $\lambda_0 = 1$ is straightforward to prove as the left vector $(1, 1, 1 \ldots)$ is always, by conservation of probability, the corresponding left eigenvector. One can show that if the Markov matrix does not have a block diagonal form, which implies that some states cannot be reached from others, then the right eigenvector corresponding to the eigenvalue 1 is unique [190]. Finally, we note that the relaxation to the steady-state following many applications of $\mathbf{p}$ is dictated by the other eigenvectors and their corresponding eigenvalues. One then expects that the eigenvalues λ_i satisfy $|\lambda_i| \leq 1$ (this can be proved rigorously [190]).

Next, we turn to the second condition in Eq. (6.92), which is associated with the doubly stochastic nature of $\mathbf{p}$. It states that the *incoming* transition probabilities to any state sum to one. This constraint is less trivial and does not generally hold for non-unitary evolution.[28] At the same time doubly stochastic evolution is more general than unitary evolution. In particular, the product of two doubly stochastic matrices is a doubly stochastic matrix [see Eq. (6.96)]. This implies that any projective measurement performed during the evolution, which breaks unitarity, keeps the transition matrix doubly stochastic. Moreover, any statistical mixture of doubly stochastic matrices is doubly stochastic. This implies that if, for example, one repeats slightly different dynamical protocols starting with the same density matrix and ending with the same final Hamiltonian, then the transition matrix describing the average effect of these dynamical protocols is still doubly stochastic. Because of this, various dephasing mechanisms (e.g., the presence of external noise or fluctuating waiting times between different pulses) keep the evolution doubly stochastic, even if they generally break its unitarity. The second condition in Eq. (6.92) is a direct consequence of the fact that any doubly stochastic matrix can be represented as $p_{n\to\tilde{m}} = |\langle\tilde{m}|\hat{U}|n\rangle|^2$ for *some* (maybe fictitious) unitary operator $\hat{U}$, see Ref. [191]. For a unitary process, one can always define its inverse. Therefore, the role of the initial and final states is interchangeable, and the same sum rule applies to both summations over n and $\tilde{m}$. The doubly stochastic condition is schematically illustrated in Fig. 6.21, where it is shown that the sum of the outgoing rates *from* a state $|2\rangle$ (red lines) is equal to the sum of the incoming probabilities *into* the state $|\tilde{2}\rangle$ (black lines).

The easiest way to satisfy the doubly stochastic constraint is to have identical transition probabilities between any two pair of energy levels, $p_{n\to\tilde{m}} = p_{\tilde{m}\to n}$. This condition is known as detailed balance for an isolated system.[29] Detailed balance is satisfied in: (i) two level systems, (ii) systems with more than two energy levels within first order of perturbation theory (e.g., a Fermi golden rule) [192], and (iii) systems with real Hamiltonians, which satisfy instantaneous time-reversal symmetry, subjected to symmetric cyclic protocols such that $\hat{H}(t) = \hat{H}(T - t)$, where T indicates the total duration of the dynamical process [193]. In general, however, pairwise transition probabilities are not the same, that is, the detailed balance condition $p_{n\to\tilde{m}} = p_{\tilde{m}\to n}$ is violated and only the sum rules (6.92) are satisfied.

In passing, we note that doubly stochastic matrices are intimately related to permutation matrices, as stated by Birkhoff's theorem, which is presented in Appendix 6.12. This theorem allows one to make physical predictions for arbitrary doubly stochastic evolution of systems with many degrees of freedom. For example, it allows one to rigorously bound the maximum

[28] For example, if the Markov process admits an absorbing state, this condition is violated since the sum of the incoming transition probabilities into the absorbing state is larger than one.

[29] For systems in contact with a thermal bath at temperature T, the detailed balance condition is $p_{n\to\tilde{m}} = p_{\tilde{m}\to n} \exp[\beta(E_n - E_{\tilde{m}})]$, where $\beta = (k_B T)^{-1}$ is the inverse temperature. In Sec.6.6.2, we show how this condition follows from the doubly stochastic transition rates.

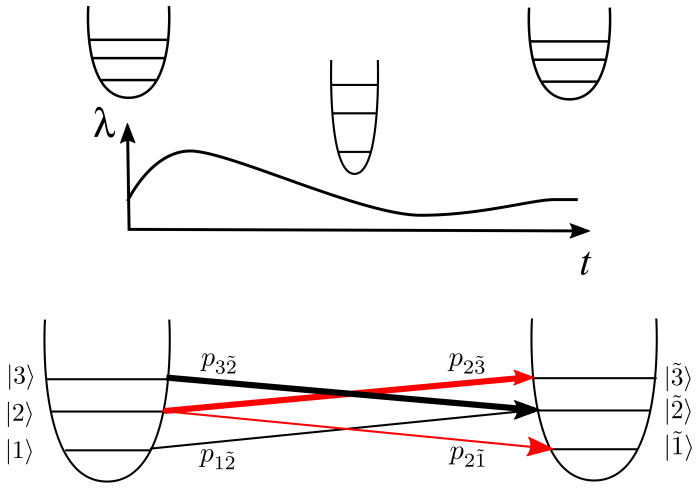

Figure 6.21: Schematic representation of a doubly stochastic evolution for a cyclic process. An isolated system undergoes some dynamical process where the control parameter λ changes in time in some arbitrary way (top). The cumulative effect of the evolution is given by the transition probabilities (bottom). Red arrows indicate the outgoing transition probabilities from the level $|2\rangle$ of the initial Hamiltonian to levels $|\tilde{1}\rangle$ and $|\tilde{3}\rangle$ of the final Hamiltonian (which in this case are the same as $|1\rangle$ and $|3\rangle$ because we consider a cyclic process). Black arrows describe the incoming transition probabilities to the level $|\tilde{2}\rangle$ of the final Hamiltonian: $|1\rangle \to |\tilde{2}\rangle$ and $|3\rangle \to |\tilde{2}\rangle$. Doubly stochastic evolution implies that $p_{2\tilde{1}} + p_{2\tilde{3}} = p_{1\tilde{2}} + p_{3\tilde{2}}$.

amount of work that can be extracted from a microcanonical bath [194].

Repeated processes. Next, we show that doubly stochastic matrices form a group under multiplication, that is, the product of two doubly stochastic matrices p and q is a doubly stochastic matrix s (the remaining group properties follow trivially):

$$s_{n\to k} \equiv \sum_m p_{n\to m} q_{m\to k} \Rightarrow \left\{ \begin{array}{l} \sum_n s_{n\to k} = \sum_m q_{m\to k} = 1 \\ \sum_k s_{n\to k} = \sum_m p_{n\to m} = 1 \end{array} \right. , \tag{6.96}$$

where, to simplicity the notation, we dropped the tilde over the state labels. Physically, Eq. (6.96) tells us that performing a sequence of two (or more) doubly stochastic processes on a system is again a doubly stochastic process. This property allows one to split any doubly stochastic process in a sequence of arbitrary many doubly stochastic processes. We now apply this result to a concrete setup in which an initially stationary density matrix $\rho^{(0)}_{nn}$ undergoes an arbitrary dynamical process that is interrupted by a sequence of ideal projective measurements, i.e., we consider the sequence:

$$\rho^{(0)}_{nn} \underbrace{\longrightarrow}_{U_1} M_1 \underbrace{\longrightarrow}_{U_2} M_2 \ldots \underbrace{\longrightarrow}_{U_N} M_N \tag{6.97}$$

where U_j represents an arbitrary dynamical process and M_j an arbitrary projective measurement. Immediately after each projective measurement, the density matrix is diagonal in the basis of the projection operator M_j. Hence the previous sequence is equivalent to:

$$\rho^{(0)}_{nn} \underbrace{\longrightarrow}_{U_1} \rho^{(1)}_{ll} \underbrace{\longrightarrow}_{U_2} \rho^{(2)}_{kk} \ldots \underbrace{\longrightarrow}_{U_N} \rho^{(N)}_{mm} \tag{6.98}$$

where $\rho^{(j)}$ is a diagonal matrix in the basis of the projection operator M_j.[30] Each fundamental

[30] To simplify the presentation, here we denote all basis states using the same notation. One needs to keep in mind that the initial state is always diagonal in the basis of the initial (measurement) Hamiltonian and the final state is always diagonal in the basis of the final (measurement) Hamiltonian.

block is a doubly stochastic process and is represented by a proper doubly stochastic matrix. For example:

$$\rho_{ll}^{(j-1)} \underbrace{\longrightarrow}_{U_j} \rho_{kk}^{(j)} \quad \Leftrightarrow \quad \rho_{kk}^{(j)} = \sum_l \rho_{ll}^{(j-1)}\, p_{l\to k}^{(j)}. \tag{6.99}$$

Using the group property discussed above, the sequence is described by a single doubly stochastic matrix s obtained as the (matrix) product of the doubly stochastic matrices of the fundamental processes:

$$\rho_{mm}^{(N)} = \sum_n \rho_{nn}^{(0)}\, s_{n\to m}, \quad \mathbf{s} = \mathbf{p}^{(N)} \dots \mathbf{p}^{(2)}\mathbf{p}^{(1)}\ , \tag{6.100}$$

where the bold symbols indicate matrices.

One can generally think of projective measurements as quenches to a measurement Hamiltonian and dephasing. For example, let us imagine we have a system of (possibly interacting) spins and we want to do a projective measurement of the z-magnetization of a given spin. Formally, we can simply say that we project this spin to the z-axis and read probabilities. Alternatively, one can think about the same process as a quench to a very strong local magnetic field along the z-axis, such that the remaining part of the Hamiltonian does not matter, and then dephasing (or time averaging) of the density matrix. Thus, this combination of quench and dephasing projects the local spin density matrix into a statistical mixture of "up" and "down" states. For this reason, the factorization property of the transition matrix (6.100) holds if we have a series of quenches with long random waiting times in between. These random waiting times are equivalent to the projection of the density matrix to the basis of the Hamiltonian after each quench or, formally equivalent, to the projective measurement of the energy of this intermediate Hamiltonian.

In ergodic systems, random waiting times are not needed, it is sufficient to wait times that are longer than the relevant relaxation time. As we discussed in the previous section, apart from small fluctuations, from the point of view of observables the density matrix is effectively dephased (see Ref. [195] for a more formal discussion of this point, and Ref. [196] for caveats). If the waiting time between quenches (random or not) is shorter than the relaxation time, then the transition matrix describing the whole dynamical process is doubly stochastic but it is not the product of the transition matrices corresponding to the individual quenches. For example, if one considers a large periodically driven ergodic system, one can anticipate that, if the driving period is longer than the relaxation time, the exact periodicity of the driving protocol is not important and the transition probability factorizes (in small ergodic systems the factorization can be violated even for long driving periods [196]). If the period is short compared to the relaxation time, one has to use the Floquet formalism (see, e.g., Ref. [197] for review) to accurately describe the time evolution after many periods. In this case, the dynamics between periods is coherent and the factorization property of the transition probability (6.100) does not apply. Still, the overall evolution remains doubly stochastic.

Let us now discuss the implications of doubly stochastic evolution for time-reversed processes. The two conditions (6.92) imply that one can define the transpose transition rate matrix $p^T_{\tilde{m}\to n} = p_{n\to\tilde{m}}$, which is also a doubly stochastic matrix that corresponds to a reversed process in which the role of initial and final states is swapped. For a unitary process (i.e., a process without projective measurements or dephasing), the time-reversal process corresponds to the transition matrix $\mathbf{p}^T$, that is, $\mathbf{p}^{\text{t.r.}} = \mathbf{p}^T$. Indeed, for the time-reversal process, the evolution operator is given by $\hat{U}^{-1} = \hat{U}^\dagger$. Therefore

$$p^{\text{t.r.}}_{\tilde{m}\to n} \equiv |U^\dagger_{n\tilde{m}}|^2 = |U_{\tilde{m}n}|^2 = p_{n\to\tilde{m}}. \tag{6.101}$$

In practice, time-reversal processes are very difficult to realize. They require either an overall change of sign of the Hamiltonian or taking the complex conjugate of the wave function, which

in the classical language is equivalent to changing the sign of the velocities of all particles. As noted in Ref. [25], the dynamics leading to the transition probabilities $p^{\mathrm{t.r.}}_{\tilde{m}\to n}$ can be achieved much more easily by using the so-called reversed protocol. To see the difference between the time-reversal and reversed processes, consider again a unitary evolution. The evolution operator and its time inverse are given by the time-ordered exponentials (such that later times t appear on the left):

$$\hat{U} = T_t \exp\left[-i\int_0^T \hat{H}(t)dt\right], \quad \hat{U}^\dagger = T_t \exp\left[i\int_0^T \hat{H}(T-t)dt\right] \tag{6.102}$$

Let us now define the reverse protocol as the forward time evolution with the Hamiltonian $H(T-t)$, that is, the Hamiltonian for which we simply reverse the dynamical protocol. The corresponding evolution operator is given by

$$\hat{U}^{\mathrm{r}} = T_t \exp\left[-i\int_0^T \hat{H}(T-t)dt\right]. \tag{6.103}$$

Note that $\hat{U}^{\mathrm{r}}$ and $\hat{U}^\dagger$ are very different. For example, $\hat{U}\hat{U}^\dagger$ is the identity while $\hat{U}\hat{U}^r$ is not. Nevertheless, if the Hamiltonian $\hat{H}(t)$ is real at each moment of time, that is, satisfies instantaneous time-reversal symmetry, then $\hat{U}^{\mathrm{r}}$ and $\hat{U}^\dagger$ lead to the same transition probabilities. Using this fact, the eigenstate $|n\rangle$ and $|\tilde{m}\rangle$ can be chosen to be real in that case, we find

$$\langle n|\hat{U}^r|\tilde{m}\rangle^* = \langle n^*|\left(\hat{U}^r\right)^*|\tilde{m}^*\rangle = \langle n|\hat{U}^\dagger|\tilde{m}\rangle. \tag{6.104}$$

Therefore

$$p^{\mathrm{r}}_{\tilde{m}\to n} = |U^{\mathrm{r}}_{n\tilde{m}}|^2 = |\langle n|U^\dagger|\tilde{m}\rangle|^2 = p^{\mathrm{t.r.}}_{\tilde{m}\to n}. \tag{6.105}$$

Unlike the time-reversal process, which generally exists only for unitary evolution, the reverse process is defined even if the forward protocol is not unitary. For example, if it involves projection measurements along the way. As we discussed, in this case the transition probability matrices factorize into products of transition probability matrices corresponding to processes between measurements. It is then straightforward to see that for the reversed process, which involves exactly the same sequence of measurement performed in the opposite order, one still has $p^r_{\tilde{m}\to n} = p_{n\to\tilde{m}}$. If the protocol is time symmetric, that is, $\hat{H}(T-t) = \hat{H}(t)$, then $\hat{U} = \hat{U}^{\mathrm{r}}$ and hence $p^{\mathrm{r}}_{m\to n} = p_{m\to n}$. Combining this condition with $p^r_{m\to n} = p_{n\to m}$, we see that for such symmetric protocols, detailed balance is automatically satisfied, i.e., $p_{n\to m} = p_{m\to n}$.

6.5.2 General Implications of Doubly Stochastic Evolution

We now derive the physical implications of doubly stochastic evolution. The results in this subsection rely *only* on doubly stochasticity and are therefore valid for both nonintegrable and integrable systems.

The Infinite Temperature State as an Attractor of Doubly-Stochastic Evolution

First, let us consider a cyclic process. In this case, the basis $\tilde{m}$ and m are identical and the master equation (6.89) becomes:

$$\rho^{(1)} = \boldsymbol{p}\rho^{(0)}, \tag{6.106}$$

where on the RHS we have a matrix vector multiplication. If we repeat the process N times, we obtain

$$\rho^{(N)} = \boldsymbol{p}^N\rho^{(0)}. \tag{6.107}$$

On physical grounds one expects that, after many applications of a dynamical process, all eigenstates of the Hamiltonian should have an equal occupation:

$$\lim_{N\to\infty} \rho_{mm}^{(N)} = \text{const.} = \frac{1}{\mathcal{D}}, \tag{6.108}$$

where $\mathcal{D}$ is the dimensionality of the Hilbert space. The state characterized by $\rho_{mm} = \text{const.}$ is often called an "infinite temperature state" since it is formally identical to a Gibbs distribution, $\rho_{nn} = e^{-\beta E_n}/Z$, in the limit $\beta \to 0$. The invariance of the infinite temperature state under doubly stochastic evolution trivially follows from the master equation. By substituting the infinite temperature state (which is the right eigenvector of $\mathbf{p}$ corresponding to $\lambda_0 = 1$) in the master equation, we obtain:

$$\rho_{mm}^{(N+1)} = \sum_n p_{n\to m}\rho_{nn}^{(N)} = \frac{1}{\mathcal{D}}\sum_n p_{n\to m} = \frac{1}{\mathcal{D}} = \rho_{nn}^{(N)}. \tag{6.109}$$

In Appendix 6.11, we prove that the infinite temperature state is an attractor of the doubly stochastic evolution. The approach to the steady state is controlled, as discussed in Sec. 6.5.1, by the eigenvalues of $\mathbf{p}$ whose absolute value is smaller than one.

Let us discuss in detail the three-level system depicted in Fig. 6.21. Besides providing a concrete example of the approach to infinite temperature, this example clarifies under which conditions the system always relaxes to the infinite temperature state. Instead of considering the most general doubly stochastic evolution (which is discussed in appendix 6.12 in connection with Birkhoff's theorem), we assume that: (i) the process is cyclic (therefore we can drop tilde signs over eigenstate labels of the final Hamiltonian), (ii) the transition probabilities satisfy the detailed balance condition $p_{n\to m} = p_{m\to n}$, and (iii) the only nonzero transition probabilities are between states 1 and 2 ($p_{12} = \gamma_{12}$) and states 2 and 3 ($p_{23} = \gamma_{23}$). From probability conservation, we must have $p_{11} = 1 - \gamma_{12}$, $p_{22} = 1 - \gamma_{12} - \gamma_{23}$ and $p_{33} = 1 - \gamma_{23}$

$$\mathbf{p} = \begin{pmatrix} 1-\gamma_{12} & \gamma_{12} & 0 \\ \gamma_{12} & 1-\gamma_{12}-\gamma_{23} & \gamma_{23} \\ 0 & \gamma_{23} & 1-\gamma_{23}. \end{pmatrix} \tag{6.110}$$

Note that $\mathbf{p}$ is symmetric because of the detailed balance condition. Its eigenvalues are:

$$\lambda_0 = 1,\ \lambda_1 = 1-\gamma_{12}-\gamma_{23}+\sqrt{\gamma_{12}^2+\gamma_{23}^2-\gamma_{12}\gamma_{23}},\ \lambda_2 = 1-\gamma_{12}-\gamma_{23}-\sqrt{\gamma_{12}^2+\gamma_{23}^2-\gamma_{12}\gamma_{23}} \tag{6.111}$$

One can then see that unless either $\gamma_{12} = 0$ or $\gamma_{23} = 0$, that is, unless the transition matrix is block diagonal, $|\lambda_1|, |\lambda_2| < 1$. As a result, for a repeated process, any probability distribution will relax to the eigenstate corresponding to the eigenvalue $\lambda_0 = 1$, which is nothing but the uniform probability distribution $(1/3, 1/3, 1/3)$.

Increase of the Diagonal Entropy Under Doubly Stochastic Evolution

As shown above, any initial state evolving under a repeated doubly stochastic process approaches the "infinite temperature state". This state is the one with the maximal spread in the eigenstates of any final Hamiltonian. As we discussed in Sec. 6.3.4, a natural measure of the spreading of states, in the basis of a given Hamiltonian, is the diagonal entropy:

$$S_d = -\sum_n \rho_{nn} \ln \rho_{nn}. \tag{6.112}$$

This entropy is maximized for the uniform occupation probability (which, as shown in Appendix 6.11, is an attractor) so one can anticipate that S_d can only increase under doubly stochastic evolution.

The diagonal entropy has many interesting properties. For example, it coincides with the usual von Neumann entropy for stationary density matrices. In addition, the diagonal entropy can be viewed as the entropy of the time averaged density matrix. The diagonal entropy also sets a natural "distance" between the density matrix ρ and the infinite temperature density matrix. Indeed given two discrete distributions P and Q a natural distance between them, also known as the Kullback-Leibler (KL) divergence [198], is[31]

$$D_{KL}(P||Q) = \sum_n P_n \ln(P_n/Q_n). \tag{6.113}$$

It is straightforward to see that this distance is non-negative and that it is zero only when the two distributions coincide, that is, only when $P_n = Q_n$ for all values of n. If we substitute $P_n \to \rho_{nn}$ and $Q_n \to 1/\mathcal{D}$ then

$$D_{KL}(\rho_{nn}||\rho^\infty) = S_\infty - S_d \geq 0, \tag{6.114}$$

where $S_\infty = \ln(\mathcal{D})$ is the entropy of the infinite temperature state (the highest possible entropy). Therefore, an increase of the diagonal entropy is equivalent to decreasing the distance between the actual and the infinite temperature energy distributions.

We prove next that doubly stochastic evolution leads to an increase of the diagonal entropy. First, recall that if a function is convex in a given interval then

$$f(x) \geq f(y) + (x-y)f'(y) \tag{6.115}$$

for any x, y in that interval. In particular, if we chose the function $f(x) = x\ln(x)$, which is convex for any $x \geq 0$, we obtain

$$x\ln(x) - y\ln(y) \geq (x-y)[\ln(y)+1]. \tag{6.116}$$

By replacing $x \to \rho^{(0)}_{nn}$ and $y \to \rho^{(1)}_{\tilde{m}\tilde{m}}$, we obtain

$$\rho^{(0)}_{nn}\ln\rho^{(0)}_{nn} - \rho^{(1)}_{\tilde{m}\tilde{m}}\ln\rho^{(1)}_{\tilde{m}\tilde{m}} \geq \left(\rho^{(0)}_{nn} - \rho^{(1)}_{\tilde{m}\tilde{m}}\right)\left(\ln\rho^{(1)}_{\tilde{m}\tilde{m}} + 1\right). \tag{6.117}$$

Multiplying both sides of the equation above by $p_{n\to\tilde{m}}$, and summing over n, leads to

$$\sum_n \left(p_{n\to\tilde{m}}\,\rho^{(0)}_{nn}\ln\rho^{(0)}_{nn}\right) - \rho^{(1)}_{\tilde{m}\tilde{m}}\ln\rho^{(1)}_{\tilde{m}\tilde{m}} \geq 0, \tag{6.118}$$

where we have used that $\sum_n p_{n\to\tilde{m}} = 1$ and $\sum_n \rho^{(0)}_{nn}\, p_{n\to\tilde{m}} = \rho^{(1)}_{\tilde{m}\tilde{m}}$. Finally, summing this inequality over $\tilde{m}$ and using that $\sum_{\tilde{m}} p_{n\to\tilde{m}} = 1$, one obtains

$$\Delta S_d \equiv S_d^{(1)} - S_d^{(0)} = \sum_n \rho^{(0)}_{nn}\ln\rho^{(0)}_{nn} - \sum_{\tilde{m}} \rho^{(1)}_{\tilde{m}\tilde{m}}\ln\rho^{(1)}_{\tilde{m}\tilde{m}} \geq 0. \tag{6.119}$$

This implies that, under *any* doubly stochastic evolution, the diagonal entropy can only increase or stay constant. Hence, the distance from the uniform or infinite temperature distribution monotonically decreases or stays constant. It is interesting that this statement is not tied in any way to quantum chaos. For example, if we take an arbitrary two level system in a stationary state and apply any sequence of pulses then the diagonal entropy cannot decrease. This statement, however, does not hold if the initial state is nonstationary. In that case, the evolution is not doubly stochastic and the diagonal entropy can decrease.

[31] Some caution is needed here as the Kullback-Leibler divergence is not symmetric and does not satisfy the triangular inequalities. Therefore, it is not a distance in the metric sense.

The increase of the diagonal entropy under doubly stochastic evolution should be contrasted with the exact conservation of von Neumann's entropy $S_{\rm vn} = -{\rm Tr}\,[\hat{\rho}\ln\hat{\rho}]$ under *any* unitary evolution. These two results do not contradict each other. In fact, the relation between these two results can be understood by considering a *unitary* evolution of an initially *stationary* density matrix. Then the following chain of relations hold:

$$S_d(0) = S_{\rm vn}(0) = S_{\rm vn}(t) \leq S_d(t)\ . \tag{6.120}$$

The first equality follows from the fact that, for a stationary density matrix, the von Neumann and the diagonal entropy are identical. The second equality reflects the obvious fact that under unitary evolution the von Neumann entropy is conserved. Finally, the last inequality follows from Eq. (6.119). This has a direct analogy in classical systems where Liouville's theorem conserves the volume in phase space while the total entropy of an isolated system increases or stays constant.

The fact that

$$S_d(t) \geq S_d(0), \tag{6.121}$$

means that, under unitary evolution starting from a stationary state, the diagonal entropy at any time $t > 0$ is larger than (or equal to) the initial diagonal entropy. This *does not* mean that the diagonal entropy increases continuously in time, that is, in general it is not true that $S_d(t_2) \geq S_d(t_1)$ for $t_2 > t_1 > 0$ because at intermediate times the system might retain coherence. A monotonic increase occurs if we consider repeated doubly stochastic processes, as discussed in Sec. 6.5.1. One can also prove a more general statement without assuming any dephasing, namely, that if one waits for a fixed long time between two pulses the probability that the diagonal entropy increases in time is higher (exponentially higher for many particles) than the probability that it decreases. The proof of this statement is beyond the scope of this review and can be found in Ref. [195].

The Second Law in the Kelvin Formulation for Passive Density Matrices

As shown above, under repeated doubly stochastic evolution that starts from a stationary density matrix, the diagonal entropy increases until it reaches its maximum value, corresponding to an "infinite temperature state".

Now, we take a step further and assume that the initial probabilities decrease monotonically in energy, that is, for any n and m

$$\left(\rho^{(0)}_{nn} - \rho^{(0)}_{mm}\right)(E_n - E_m) \leq 0, \tag{6.122}$$

where E_n and E_m are eigenenergies of the system. Relying on this assumption, one can prove that, for any doubly stochastic *cyclic* evolution (in particular, for any cyclic unitary process), the energy of the system can only increase or stay constant [188, 199]:

$$\sum_n E_n \rho^{(1)}_{nn} \geq \sum_n E_n \rho^{(0)}_{nn}. \tag{6.123}$$

By energy conservation, this difference must be equal to the average work done on the system during the cyclic process

$$\langle W\rangle = \sum_n E_n \rho^{(1)}_{nn} - \sum_n E_n \rho^{(0)}_{nn} \geq 0\ . \tag{6.124}$$

Diagonal density matrices satisfying the inequality (6.122) are termed passive [188] and are common. The Gibbs distribution for systems in thermal equilibrium, $\rho_{nn} = e^{-\beta E_n}/Z$, is a passive density matrix. Therefore, condition (6.124) is quite general and can be interpreted as a manifestation of the second law of thermodynamics in Kelvin's formulation – one cannot

extract work from a closed equilibrium system by carrying out a cyclic process. As all the results in Sec. 6.5.2, this statement is solely based on doubly stochastic evolution and on the passivity of the initial density matrix (and therefore, applies to both integrable and nonintegrable systems). In Sec. 6.7, we show explicitly how it works for a single particle driven in a chaotic cavity.

The proof of Eq. (6.124) relies on the fact that any doubly stochastic evolution tends to make the occupation probabilities uniform. In the case of an initial passive density matrix, this process requires a transfer of probability from low- to high-energy states causing the energy of the system to increase. If a stronger detailed balance condition is satisfied, that is, $p_{n\to m} = p_{m\to n}$ for any m, n, then the proof becomes particularly simple [192]:

$$\langle W\rangle = \sum_{n,m} E_n p_{n\to m}[\rho^{(0)}_{mm} - \rho^{(0)}_{nn}] = \frac{1}{2}\sum_{n,m} p_{n\to m}(E_n - E_m)[\rho^{(0)}_{mm} - \rho^{(0)}_{nn}] \geq 0. \tag{6.125}$$

The second equality follows from symmetrizing with respect to n and m and using the detailed balance condition. However, in general, pairwise transition probabilities are not the same and only the sum rule (6.92) is satisfied. In this case, the proof is more complicated but still straightforward [188]. For completeness, it is presented in Appendix 6.13.

6.5.3 Implications of Doubly-Stochastic Evolution for Chaotic Systems

In the previous three subsections we discussed three important results that are all manifestations of the second law of thermodynamics. In Sec. 6.5.2 (and Appendix 6.11), we showed that the "infinite temperature state" is the only generic attractor of a doubly stochastic evolution. In Sec. 6.5.2, we proved that under a repeated doubly stochastic evolution the diagonal entropy increases until it reaches its maximum value, which corresponds to that of the "infinite temperature state". Finally, in Sec. 6.5.2, we proved that any cyclic doubly stochastic evolution leads to an increase of the (average) energy of the system (provided the initial density matrix is passive). This statement is equivalent to the second law of thermodynamics in the Kelvin form.

All these statements rely only on doubly stochastic evolution and therefore apply to both integrable (and in particular noninteracting) and chaotic systems. In this section, we take a step further and assume that the system undergoing the dynamical process is chaotic.

The Diagonal Entropy and the Fundamental Thermodynamic Relation

The entropy of a system in thermal equilibrium is a unique function of its energy and other relevant extensive variables (denoted by λ). This fact implies the fundamental thermodynamic relation

$$dS = \frac{1}{T}\left(dE + F_\lambda d\lambda\right). \tag{6.126}$$

Here, F_λ is the generalized force conjugate to λ. Since this expression is directly derived from $S(E,\lambda)$, it applies to both reversible and irreversible processes. In the case of a reversible transformation, we can identify TdS as the heat transferred and $F_\lambda d\lambda$ as the work done by the system. In contrast, for an irreversible transformation, one cannot make these identifications. Equation (6.126) is then taken as a mathematical relation between thermodynamic functions. For example, if an isolated gas in a container is expanded by a volume $d\lambda$ by moving a partition very quickly (a Joule experiment), there is no work done and the energy change in the system is zero. The fundamental relation then implies that the change in entropy is given by $dS = F_\lambda d\lambda/T$ with F_λ being the pressure before the expansion. If one insists on giving an interpretation to the equation as describing a dynamical process, it can be thought of as a fictitious

reversible process (expansion with work and heat exchange) that is not related to the actual (irreversible) process that has taken place. As we show in this and the following subsection, thinking about the fundamental relation from a microscopic point of view is illuminating. The changes in the entropy can actually be assigned to underlying, in general irreversible, physical processes (which may result from work and/or heat exchange). The entropy change is then simply related to transitions between the energy levels of the system during the dynamical process.

From the microscopic point of view, the fundamental relation is not at all trivial (see, e.g., Ref. [200]). The energy and its change are uniquely defined by the density matrix and the energy eigenstates. The generalized force is also expressed through the density matrix and the Hamiltonian. Thus, for the fundamental relation to apply microscopically, we need to define an object, the entropy, which can also be expressed through the density matrix and possibly the Hamiltonian and ensure that Eq. (6.126) holds for any dynamical process both for open and isolated systems. Let us show that the diagonal entropy, which we defined earlier as the measure of delocalization in the energy space, satisfies the fundamental relation in chaotic systems [134, 125]. As we will see, S_d satisfies

$$dE = TdS_d - F_\lambda d\lambda, \tag{6.127}$$

for both reversible and irreversible processes. Once we identify S_d with the entropy, this constitutes the fundamental relation.

To derive the fundamental relation, let us first use standard statistical mechanics and come back to the role of quantum chaos later. We assume that the initial density matrix is described by a Gibbs distribution (the extension to other ensembles is straightforward)

$$\rho_{nm}(\lambda) = \frac{1}{Z(\lambda)} e^{-\beta E_n(\lambda)} \delta_{nm}. \tag{6.128}$$

Using that the energy of the system is given by $E(\lambda) = \sum_n \rho_{nn} E_n(\lambda)$, and calculating its change for an arbitrary 'small' dynamical process (we are not assuming here that the system is isolated or that the process is unitary), we find

$$dE(\lambda) = d\left(\sum_n \rho_{nn} E_n(\lambda)\right) = \sum_n \left[E_n(\lambda) d\rho_{nn} + \rho_{nn} \frac{dE_n}{d\lambda} d\lambda\right] = \sum_n E_n(\lambda) d\rho_{nn} - F_\lambda d\lambda, \tag{6.129}$$

where $F_\lambda = -\sum_n \rho_{nn} dE_n(\lambda)/d\lambda$. Next, we compute the change in the diagonal entropy for the same process. This gives

$$dS_d = -d\left[\sum_n \rho_{nn} \ln(\rho_{nn})\right] = -\sum_n d\rho_{nn} \ln(\rho_{nn}) - \sum_n d\rho_{nn} = \beta \sum_n E_n(\lambda) d\rho_{nn}, \tag{6.130}$$

where we used that, by conservation of probability, $\sum_n d\rho_{nn} = 0$. Comparing Eqs. (6.129) and (6.130), and noting that the generalized force can be also written as

$$F_\lambda = -\left.\frac{\partial E(\lambda)}{\partial \lambda}\right|_{S_d}, \tag{6.131}$$

we recover that the diagonal entropy indeed satisfies the fundamental thermodynamic relation, Eq. (6.127), for any dynamical process. Remarkably, under the assumption that the system is initially described by the Gibbs distribution, the fundamental relation applies exactly for both large and small systems whether they are open or closed during the dynamical process. Moreover, it applies to integrable and nonintegrable systems alike.

To see where quantum chaos enters, assume that an isolated system undergoes a quench (or any other dynamic process) protocol. Then, according to ETH, physical observables after relaxation are described by an equilibrium thermal ensemble. This is true despite the fact that the density matrix of the entire system is not that of the Gibbs ensemble. With this in mind, we want to prove that if the system is chaotic then the fundamental relation holds up to possible subextensive corrections. The easiest way to prove it without assuming a standard equilibrium density matrix is to show that the diagonal entropy, which is a function of the density matrix, coincides with the thermodynamic entropy up to subextensive corrections. Then, the fundamental relation and its generalization immediately follows. Recall that we already presented numerical evidence that the diagonal entropy coincides with the thermodynamic entropy in Sec. 6.3.4, when discussing implications of quantum chaos and RMT to delocalization in energy space (see Fig. 6.12).

We start our discussion by noticing that, for large system sizes (no matter whether they are in a pure or in a mixed state), the diagonal entropy can written as an integral over energies

$$S_d \simeq -\int dE\, \Omega(E)\, \rho(E)\, \ln[\rho(E)], \tag{6.132}$$

where $\rho(E)$ is an interpolating function satisfying $\rho(E_n) = \rho_{nn}$ and $\Omega(E)$ is the smoothed many-body density of states. We note that $\rho(E)\Omega(E) = P(E)$ is the energy distribution function in the system [see Eq. (6.56)], from which all moments of the energy can be computed. For example, the average energy is given by $\langle E\rangle = \int dE\, E\, P(E)$. One can rewrite the diagonal entropy as

$$S_d = -\int dE P(E) \ln\left[\frac{P(E)\delta E}{\Omega(E)\delta E}\right] = \int dE P(E) S_m(E) - \int dE P(E) \ln[P(E)\delta E], \tag{6.133}$$

where $S_m(E) = \ln[\Omega(E)\delta E]$ is the microcanonical entropy at energy E (δE is the width of the microcanonical energy window).

The last term in Eq. (6.133) is the one that exhibits a qualitatively different behavior in integrable and chaotic systems [125]. In nonintegrable systems, one expects $P(E)$ to be a smooth function of the energy (see, Sec. 6.3.4). As a result, $\int dE P(E) \ln P(E)$ is not extensive because $\int dE P(E)$ is normalized to one and the width of the energy distribution is not exponentially large in the system size (see Sec. 6.4.3). In integrable systems, on the other hand, $P(E)$ after a dynamical process (such as a quench) generally exhibits large fluctuations (see, e.g., left panels in Fig. 6.11). As a result, the last term in Eq. (6.133) can be extensive and, therefore, comparable to the contribution of the first term, that is, S_d can differ from the thermodynamic entropy. Numerical studies have indeed found that S_d agrees (disagrees) with the thermodynamic entropy in quenches in nonintegrable (integrable) systems [125, 135, 130] (for results at integrability, see Sec. 6.8.3).

Actually, if $P(E)$ after a dynamical process is well approximated by a smooth Gaussian (expected for sufficiently large nonintegrable systems, see Sec. 6.3.4)

$$P(E) \approx \frac{1}{\sqrt{2\pi\sigma^2}} \exp\left[-\frac{(E-\langle E\rangle)^2}{2\sigma^2}\right], \tag{6.134}$$

with σ^2 being, at most, extensive (for a discussion of σ^2 after a quench, see Sec. 6.4.3), then the fact that S_d agrees with the thermodynamic entropy follows straightforwardly. To show that, let us expand $S_m(E)$ around the mean energy $\langle E\rangle$

$$S_m(E) \approx S_m(\langle E\rangle) + \left.\frac{\partial S_m(E)}{\partial E}\right|_{\langle E\rangle} (E-\langle E\rangle) + \frac{1}{2}\left.\frac{\partial^2 S_m(E)}{\partial E^2}\right|_{\langle E\rangle} (E-\langle E\rangle)^2 + \dots\,. \tag{6.135}$$

By substituting Eqs. (6.134) and (6.135) into Eq. (6.133), and computing the Gaussian integrals, we obtain

$$S_d \approx S_m(\langle E\rangle) - \frac{1}{2}\left(\frac{\sigma^2}{\sigma_c^2} - 1\right), \tag{6.136}$$

where $S_m(\langle E\rangle) = \ln[\Omega(\langle E\rangle)\sqrt{2\pi}\sigma]$ is the von Neumann entropy of a microcanonical distribution with mean energy $\langle E\rangle$ and energy width $\delta E = \sqrt{2\pi}\sigma$. In the expression above

$$\sigma_c^{-2} = -\left.\frac{\partial\beta(E)}{\partial E}\right|_{\langle E\rangle}, \quad \text{with} \quad \beta(E) = \frac{\partial S(E)}{\partial E}. \tag{6.137}$$

We note that here the inverse temperature $\beta(E)$ is defined solely by the density of states at energy E, and that σ_c^2 is the variance of the energy in a canonical ensemble with inverse temperature $\beta(\langle E\rangle)$.[32] Since σ_c^2 is extensive, the last term in Eq. (6.136) is clearly non-extensive and can be ignored in large systems. We then see that, in chaotic systems, one can define a functional of the density matrix (the diagonal entropy) that coincides with the thermodynamic entropy both in open and closed systems after they are driven from equilibrium and allowed to relax. For closed systems, this is a nontrivial statement that relies on the assumption that the final Hamiltonian (the one after the dynamical process) is quantum chaotic (nonintegrable). From this result, the fundamental thermodynamic relation for chaotic systems follows without the assumption that the system is in thermal equilibrium.

To conclude this section, let us mention an apparent paradox that is frequently raised to argue that there is a deficiency in the diagonal entropy (or, for that matter, von Neumann's entropy) for quantum systems. A similar "paradox" can be argued to occur for Liouville's entropy for classical systems. If one starts a cyclic process from an eigenstate of an ergodic Hamiltonian, where von Neumann's entropy is zero by definition, after reaching the new equilibrium the energy change can be made arbitrarily small while the entropy change cannot. The latter will be the thermodynamic entropy. Hence, the equality $dE = TdS$ seems to be violated. There is, in fact, no paradox. The entropy of a single eigenstate is a singular quantity. Any arbitrarily small perturbation will immediately lead to mixing exponentially many eigenstates of the Hamiltonian and lead to the thermodynamic entropy (see, e.g., the discussion in Ref. [109]). In particular, any attempt to measure the temperature of the eigenstate, which is necessary to test the fundamental relation, will introduce an extensive thermodynamic entropy and thus the paradox is immediately removed.

The Fundamental Relation vs the First Law of Thermodynamics

It is interesting to put the results presented in the previous subsection in the context of the first law of thermodynamics:

$$dE = dQ + dW. \tag{6.138}$$

This law is a statement about energy conservation and implies that the energy of the system can change only due to heat (defined as the energy flow from one system to another at fixed macroscopic couplings) and work (defined as the energy change in the system due to a dynamical change of these couplings). Note that, as previously stressed, the fundamental relation (6.126) is a mathematical expression relating equilibrium quantities, while the first law only deals with the conservation of energy.

From the microscopic stand point it is convenient to split an infinitesimal energy change into two contributions [see Eq. (6.129)]:

$$dE = d\tilde{Q} + dW_{\text{ad}}. \tag{6.139}$$

[32] We assume that we are not at a phase transition, at which σ_c^2 might diverge.

The first one, $d\tilde{Q} = \sum_n E_n d\rho_{nn}$, results from changes in occupation numbers of the microscopic energy levels (and is not to be confused with the common definition of heat in the first law) and the second one, $dW_{\rm ad} = \sum_n dE_n \rho_{nn}$, results from the changes of the energy spectrum at fixed occupation numbers. This last term, as we discussed, can be written as the full derivative of the energy (assuming that the energy spectrum is differentiable) and thus represents the adiabatic work done on the system, $dW_{\rm ad} = -F_\lambda d\lambda$ [see Eq. (6.131)]. If the dynamical process is infinitesimally slow, changing the macroscopic parameter of the system does not change occupation probabilities. Formally, one can prove this statement using adiabatic perturbation theory, similarly to what was done for energy in Ref. [201]. We thus see that for infinitesimally slow processes $d\tilde{Q} = TdS = dQ$ and $dW = dW_{\rm ad}$, which is well known from thermodynamics. We note that in large systems the strict quantum-mechanical adiabatic limit requires exponentially slow processes in order to suppress transitions between many-body eigenstates. This is another way of saying that isolated eigenstates are very fragile. Thermodynamic adiabaticity on the other hand requires that the dynamical process is slow with respect to physical time scales, which are much shorter than the inverse level spacing. This is of course consistent with Eq. (6.139) as transitions between nearest eigenstates lead to exponentially small heating and essentially do not contribute to $d\tilde{Q}$ and hence to dE. So the only way to have significant heating is to introduce transitions across exponentially many energy levels, which requires much faster dynamics.

The situation becomes somewhat different in a setup where the process is not infinitesimally slow, even if it is still effectively quasi-static. For example, one can imagine a compression and expansion of a piston containing a gas (see Fig. 6.20) at some finite rate. At the end of the process, when the piston is back at its original position, the energy of the gas is higher than its initial energy. This is essentially the way microwave ovens function. There, the food heats up because of the non-adiabatic work performed by the time-dependent electromagnetic field. This process can still be quasi-static because if in each cycle the energy of the system increases by a small amount then it can be approximately described by local equilibrium. This "microwave heating" in ergodic systems is indistinguishable, at the end of the process, from conventional heating resulting from connecting the system to a thermal reservoir.

Therefore, from a microscopic standpoint, it is more natural to define $d\tilde{Q}$ (and not dQ) as heat. In the literature, $d\tilde{Q}$ has been called heat [192], excess heat [202], excess energy [203], non-adiabatic work [193], and others. We will not argue one way or another in terming $d\tilde{Q}$. We only note that, physically, it represents the heating of the system, that is, the energy change in the system caused by transitions between levels, independent of whether those transitions are induced by contact with another system or by changing non-adiabatically some coupling λ, or both. As we proved earlier [see Eq. (6.127)], for small changes in ergodic systems, one always has $d\tilde{Q} = TdS_d$, so this energy change is uniquely associated with the entropy change. If an isolated system starts in the stationary state then, as we proved, the entropy change is always non-negative and thus one always has $d\tilde{Q} \geq 0$. This, in turn, implies that $dW \geq dW_{\rm ad}$ (in the latter $dQ = 0$), in agreement with the results in Sec. 6.5.2.[33] If the system is not closed, then, by definition,

$$d\tilde{Q} = dQ + (dW - dW_{\rm ad}). \tag{6.140}$$

As a result, $d\tilde{Q} \geq dQ$ so that $TdS_d \geq dQ$, as expected from thermodynamics.

[33] For processes that are not infinitesimally slow, in the presence of unavoidable level crossings, there can be exceptions where $dW < dW_{\rm ad}$ [204]

6.6 Quantum Chaos, Fluctuation Theorems, and Linear Response Relations

The recently discovered fluctuation theorems are remarkable *equalities* involving thermodynamic variables. They are valid for systems initially prepared in equilibrium and then driven far from equilibrium in an arbitrary way (see, e.g., Refs. [25, 187] for reviews). These theorems effectively replace many thermodynamic inequalities by equalities (e.g., the second law of thermodynamics in the Kelvin form discussed previously). In many cases, the proof of the fluctuation theorems, as previously done for the fundamental relations, assumes that the initial state is described by a Gibbs distribution. When this is the case, one does not need any additional assumptions, such as quantum chaos. However, if the system is not weakly coupled to an equilibrium bath, then the assumption of a Gibbs distribution is often not justified and one has to rely on quantum chaos and ETH to prove these relations.

In this section, we derive the fluctuation theorems for individual eigenstates and hence extend them to arbitrary stationary distributions that are narrow in energy. Based on these fluctuation theorems, we derive energy drift-diffusion relations for both isolated and open systems, and discuss how they lead to nontrivial asymptotic energy distributions for driven isolated systems. For clarity, we derive these fluctuation relations in two ways. First we show a standard derivation for an initial Gibbs ensemble, and then, for quantum chaotic systems, we generalize this derivation to systems prepared in individual eigenstates. The latter approach clarifies in which situations fluctuation theorems apply to isolated systems. It also allows us to derive finite-size corrections and to extend them to open systems that are strongly coupled to a bath.

6.6.1 Fluctuation Theorems

Particularly simple proofs of fluctuation theorems are obtained by considering isolated quantum systems initially prepared in contact with a thermal bath at temperature T. The bath is then disconnected from the system which undergoes a unitary (or, more generally, doubly stochastic) evolution in response to an external protocol that changes some macroscopic parameter in time. The protocol has a specified duration after which the parameter is kept constant and the system is allowed to relax back to equilibrium.

Thermodynamics tell us that the average external work, W, done on the system during a thermodynamic protocol is bounded from below by the difference in the equilibrium free-energies (at the same temperature T) evaluated at the initial (A) and final (B) value of the control parameters. Specifically,

$$\langle W\rangle \geq \Delta F \equiv F_{B,T} - F_{A,T}. \tag{6.141}$$

Because the system is isolated, there is no heat flowing to the system, and according to the first law of thermodynamics $\langle W\rangle = W_{\rm ad} + \tilde{Q}$, where $\tilde{Q}$ [introduced in Eq. (6.139) in the previous section] is the irreversible work or, microscopically, the energy change associated with the transitions between different energy levels. Then Eq. (6.141) becomes

$$\tilde{Q} \geq 0. \tag{6.142}$$

For a cyclic process, $W_{\rm ad} = 0$. Therefore, $\langle W\rangle = \tilde{Q}$, and this inequality reduces to Kelvin's formulation of the second law. For an adiabatic process, $\tilde{Q} = 0$, and the inequality (6.142) becomes an equality.

By properly taking into account the fluctuations, the Jarzynski equality turns the inequality (6.141) into an equality even if the protocol drives the system far from equilibrium. This equality reads:

$$\langle e^{-W/k_BT}\rangle = e^{-\Delta F/k_BT}, \tag{6.143}$$

where the angular brackets denote the average over many experimental realizations of the same protocol. In particular, for cyclic processes (for which $A = B$), the Jarzynski equality reduces to

$$\langle e^{-W/k_BT} \rangle = 1, \tag{6.144}$$

which was first discovered by Bochkov and Kuzovlev [205, 206] as a nonlinear generalization of the fluctuation-dissipation theorem. Equation (6.144) is frequently referred to as the Bochkov-Kuzovlev work-fluctuation theorem [25].

To clarify the meaning of Eq. (6.143), it is better to refer to a concrete example, say, the compression of a gas by a moving piston (see Fig. 6.20). Initially, the gas is assumed to be in thermal equilibrium connected to a bath, with the piston at position $z(0) = A$. We assume that, during the protocol $z(t)$, the system is not connected the bath anymore, i.e., it can be regarded as isolated. At the end of the protocol, the control parameter reaches the value $z(t) = B$. We record the external work W, which is formally defined as the energy change of the piston. Note that the free energy $F_{B,T}$ is not the free energy of the system after the protocol. It is rather the equilibrium free energy evaluated at the initial temperature and the final value of the control parameter.[34] Upon repeating the protocol many times, the work will fluctuate around some average value. The Jarzynski equality (6.143) states that the exponential of the work done, averaged over many realizations of the same experiment, is equal to the exponential of the equilibrium free energy difference. Hence, the Jarzynski equality connects a dynamical quantity, work, which depends on the details of the protocol, and an equilibrium quantity, the free energy difference, which only depends on the initial and final values of the control parameter. In particular, this relation can be used to measure free energy differences in small systems by measuring the work. In large systems, the Jarzynski relation is generally not very useful unless W is small. This because the average of the function $\exp[-\beta W]$ will be dominated by rare events in which the work is negative. The assumption that the system is not connected to the bath during the protocol, which was present in the original work of Jarzynski [20] and which caused some confusion, is not necessary (see Ref. [207] and the proof below).

Equation (6.143) can be understood as a constraint on the work distribution $P(W)$. This constraint is independent of the details of the protocol $z(t)$, and depends only on the initial and final values of the macroscopic parameter, A and B, respectively, through the free energy difference $\Delta F \equiv F_{B,T} - F_{A,T}$. Note that the full distribution $P(W)$ depends on the details of $z(t)$. If we take the logarithm of Eq. (6.143), and perform the cumulant expansion, we obtain the expression:

$$\sum_{n\geq 1} \frac{(-1)^n}{n!} \frac{\langle W^n \rangle_c}{(k_BT)^n} = -\frac{\Delta F}{k_BT}. \tag{6.145}$$

We therefore see that the Jarzynski equality constraints different cumulants of the work. If the work is small, or if the temperature is high, then only a few cumulants effectively enter the sum. When this happens, the constraint has an important consequence and leads to standard thermodynamic relations. However, if many cumulants contribute to the expansion (as expected when W is large), then the constraint does not place strong restrictions to the moments of the work.

Note that, by combining the Jarzynski equality (6.143) and Jensen's inequality $\langle \exp[x] \rangle \geq \exp[\langle x \rangle]$, we recover the Clausius inequality (6.141). Let us emphasize that this inequality only applies to the average work. The work carried out in a single realization of the experiment can be smaller than ΔF. This can be the case especially in small systems, where fluctuations are large. The Jarzynski equality allows one to estimate the likelihood of such rare events [207].

[34] It would be the free energy of the system if it is reconnected to the same bath and allowed to re-equilibrate. Since no work is done on the system during its re-equilibration, such a process does not affect the Jarzynski equality.

Closely related to the Jarzynski equality is the Crooks theorem, which was originally formulated for classical systems [186] and then extended to quantum systems [23, 24]. The Crooks theorem relates the probability of performing a work W during the forward process, $P_F(W)$ $(A \to B)$, with the probability of performing a work $-W$ during the reverse process, $P_R(-W)$ $(B \to A$, in a time-reversed manner):

$$\frac{P_F(W)}{P_R(-W)} = e^{(W-\Delta F)/k_B T}. \tag{6.146}$$

The expression above can be interpreted as a symmetry of the distribution function between the forward and the reverse process. Note that this symmetry is with respect to $W = 0$ and not with respect to the average work. Rewriting the Crooks relation as

$$P_F(W)\, e^{-W/k_B T} = P_R(-W)\, e^{-\Delta F/k_B T}, \tag{6.147}$$

and integrating over W, one recovers the Jarzynski equality.

Fluctuation Theorems for Systems Starting from a Gibbs State

Here we derive the Jarzynski equality (6.143) and the Crooks theorem (6.146) for a system that is initially in a Gibbs state and is not coupled to a bath during its evolution. In this case, neither quantum chaos nor the limit of a large system size need to be invoked. The derivation relies exclusively on the symmetry of the doubly stochastic evolution between the forward and the reverse process [see Eq. (6.105)]:

$$p^r_{\tilde{m}\to n} = p_{n\to\tilde{m}}. \tag{6.148}$$

We recall, that a doubly stochastic evolution describes unitary dynamics of systems starting from stationary states and extends to some non-unitary processes involving projective measurements or dephasing.

Let us consider a system prepared in a state characterized by an initial energy E_A, corresponding to an initial value of the control parameter $\lambda(0) \equiv \lambda_A$, drawn from the Gibbs ensemble of the initial Hamiltonian. Then the system undergoes an arbitrary dynamical process described by a doubly stochastic evolution. At the end of the process, the system has an energy E_B, which is a random variable. The fluctuating work[35] is formally defined as $W = E_B - E_A$ [23, 24]. This work is characterized by the probability distribution:

$$P_F(W) = \sum_{n,\tilde{m}} \rho^{(0)}_{nn}\, p_{n\to\tilde{m}} \delta(\tilde{E}_{\tilde{m}} - E_n - W) = \sum_{n,\tilde{m}} \frac{\mathrm{e}^{-\beta E_n}}{Z_A}\, p_{n\to\tilde{m}}\, \delta(\tilde{E}_{\tilde{m}} - E_n - W), \tag{6.149}$$

where n and E_n ($\tilde{m}$ and $\tilde{E}_{\tilde{m}}$) refer to states and the spectrum of the initial (final) Hamiltonian, and Z_A is the partition function associated with the initial value of the control parameter λ_A. The probability of performing work $-W$ during the reverse process, starting from a Gibbs distribution, is

$$\begin{aligned} P_R(-W) &= \sum_{n,\tilde{m}} \frac{\mathrm{e}^{-\beta \tilde{E}_{\tilde{m}}}}{Z_B} p^r_{\tilde{m}\to n}\, \delta(E_n - \tilde{E}_{\tilde{m}} + W) \\ &= \sum_{n,\tilde{m}} \frac{\mathrm{e}^{-\beta(E_n+W)}}{Z_B}\, p_{n\to\tilde{m}}\, \delta(\tilde{E}_{\tilde{m}} - E_n - W) = P_F(W)\, e^{-\beta W}\, \frac{Z_A}{Z_B}, \end{aligned} \tag{6.150}$$

[35] There is an active discussion on how to define work in quantum systems, with many conflicting definitions. We use the definition due to Kurchan [23] and Tasaki [24], which has a transparent physical meaning, namely, the energy change in the system. By energy conservation, W is also the energy change of the macroscopic degree of freedom associated with the control parameter.

where Z_B is the partition function associated with the thermal equilibrium distribution at the final value of the control parameter, that is, λ_B. Writing the free energy difference as $\Delta F = F_B(T) - F_A(T)$, and using the relation between free energy and partition function, that is, $Z_{A,B} = e^{-\beta F_{A,B}}$, one sees that Eq. (6.150) is nothing but the Crooks theorem (6.146).

For cyclic symmetric protocols, for which the reverse process is identical to the forward process, the Crooks theorem simplifies to

$$P(W)e^{-\beta W} = P(-W), \tag{6.151}$$

where we suppressed the indexes F and R since, in this case, they are redundant. In turn, this relation can be recast in the form of a symmetry relation for the cumulant generating function $G(\zeta)$:

$$G(\zeta) = \ln\left[\int dW P(W)e^{-\zeta W}\right] = \sum_{n=1}^{\infty}\langle W^n\rangle_c \frac{(-\zeta)^n}{n!}. \tag{6.152}$$

To see this we multiply both sides of Eq. (6.151) by $e^{\zeta W}$:

$$P(W)e^{-\beta W}e^{\zeta W} = P(-W)e^{\zeta W}, \tag{6.153}$$

and integrate over W to obtain

$$G(\beta - \zeta) = G(\zeta). \tag{6.154}$$

The generating function formalism is a convenient tool for deriving various linear response relations, for example, Onsager relations and their nonlinear generalizations (see Ref. [208] and the discussion below).

Fluctuation Theorems for Quantum Chaotic Systems

Now, let us focus on eigenstates of many-body chaotic Hamiltonians and derive the corresponding fluctuation relations for isolated systems. The applicability of fluctuation relations to individual eigenstates allows one to extend them to arbitrary initial stationary distributions so long as they are sufficiently narrow. The approach based on individual eigenstates also allows us to derive the leading finite-size corrections to the cumulant expansion of these relations and prove these relations for open systems, even if they are strongly coupled to the bath throughout the dynamical process.

Let us analyze the probability of doing work W during the forward process starting from a given many-body energy eigenstate $|n\rangle$. By definition, this is given by

$$\begin{aligned} P_F(E_n \to E_n + W) \equiv P_F(E_n, W) &= \sum_{\tilde{m}} p_{n\to\tilde{m}}\, \delta(\tilde{E}_{\tilde{m}} - E_n - W) \\ &= \int d\tilde{E}\, \Omega_B(\tilde{E})\, p(E_n \to \tilde{E})\, \delta(\tilde{E} - E_n - W), \end{aligned} \tag{6.155}$$

where Ω_B is the density of states at the final value of the control parameter and we used the fact that, for chaotic systems, the probability $p_{n\to\tilde{m}} \approx p(E_n \to \tilde{E})$ is a smooth function of the energy $\tilde{E}_{\tilde{m}}$, up to a small Gaussian noise (c.f., Sec. 6.3.4). In non-chaotic systems, the transition probability $p_{n\to\tilde{m}}$ can fluctuate strongly between states that are close in energy, that is, changing the summation over $\tilde{m}$ by an integration over $\tilde{E}$ is not justified and, in general, is not valid. Integrating the expression above over the energy, we find

$$P_F(E_n \to E_n + W) = p(E_n \to E_n + W)\, \Omega_B(E_n + W). \tag{6.156}$$

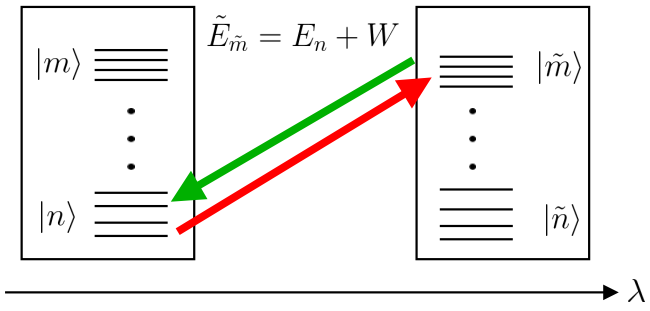

Figure 6.22: Illustration of relation (6.158). A system is composed of many closely spaced energy levels. In response to some dynamic process, during the forward process (red arrow) the system undergoes a transition from an initial state $|n\rangle$ to a final state $|\tilde{m}\rangle$ with the energy $\tilde{E}_{\tilde{m}} = E_n + W$. During the reverse process (green arrow), the opposite transition happens. The ratio of probabilities of doing work W for the red process and $-W$ for the green process is given by the ratio of the density of states of the corresponding final states [see Eq. (6.158)].

Using similar considerations, we find that the transition probability for doing work $-W$ during the reverse process starting from state $|\tilde{m}\rangle$ is:

$$\begin{aligned} P_R(\tilde{E}_{\tilde{m}} \to \tilde{E}_{\tilde{m}} - W) \equiv P_R(\tilde{E}_{\tilde{m}}, -W) &= \sum_n p^r_{\tilde{m}\to n}\, \delta(E_n - \tilde{E}_{\tilde{m}} + W) \\ &= \sum_n p_{n\to\tilde{m}}\, \delta(E_n - \tilde{E}_{\tilde{m}} + W) = \int dE\, \Omega_A(E)\, p(E \to \tilde{E}_m)\, \delta(E - \tilde{E}_{\tilde{m}} + W) \\ &= p(\tilde{E}_{\tilde{m}} - W \to \tilde{E}_{\tilde{m}}) \Omega_A(\tilde{E}_{\tilde{m}} - W). \end{aligned} \tag{6.157}$$

Comparing the expressions for the forward and backward processes, and substituting $E_n \to E$ and $\tilde{E}_{\tilde{m}} \to E + W$, we obtain

$$\frac{P_F(E, W)}{P_R(E + W, -W)} = \frac{\Omega_B(E + W)}{\Omega_A(E)} \equiv \mathrm{e}^{S_B(E+W) - S_A(E)}, \tag{6.158}$$

which is known as the Evans-Searles fluctuation relation [209] (for classical derivations of a similar nature, see Ref. [210]). This result tells us that the ratio of probabilities of doing work W in the forward process and $-W$ in the reverse process is simply equal to the ratio of the final and initial densities of states, that is, the ratio of the number of available microstates. Typically, as schematically illustrated in Fig. 6.22, the density of states is an exponentially increasing function of the energy (corresponding to positive temperature states). Hence, the number of available microstates is larger for processes corresponding to an energy increase. This asymmetry is the microscopic origin of the higher probability of doing positive work, despite the equivalence of the forward and backward microscopic rates. Note that these considerations are only valid for chaotic systems. For integrable systems, not all microstates might be accessible and one needs to refine the argument.

Relation (6.158) is very general. In particular, it contains fluctuation theorems and, in a sense, generalizes them. To see this, consider a total system with N particles and let us assume that a dynamical process is applied only to a small subsystem with N_1 particles, such that N_1 is kept fixed as $N \to \infty$ (N_1 can be arbitrarily small, e.g., just one particle, or can be macroscopic). If the subsystem is weakly coupled to the rest of the system, it is expected that the rest of the system will act as a thermal bath and, as discussed previously, from ETH we expect that the small subsystem is described by the Gibbs ensemble. In this case, we are back to the standard setup considered in Sec. 6.6.1. On the contrary, when the subsystem is strongly coupled to the rest of the system the assumption about the Gibbs distribution is not justified.

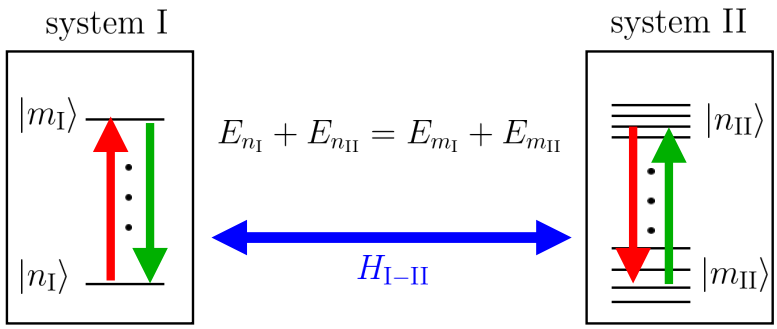

Figure 6.23: Schematic representation of the setup considered to prove the detailed balance condition, Eq. (6.167). A system I, which can be either quantum chaotic or not is coupled to another system II (bath), which is quantum chaotic. The two systems are weakly coupled and are allowed to exchange energy. The microscopic transition probabilities from a pair of states $|n_{\rm I}, n_{\rm II}\rangle$ to another pair of states $|m_{\rm I}, m_{\rm II}\rangle$ (red arrows) is the same as the probability of the reverse process (green arrows). However, if one is only interested in transition probabilities in system I, irrespective of the outcome in the bath, this symmetry is broken and one obtains the standard equilibrium detailed balance.

However, even in this case, the Crooks theorem (6.146) (and, hence, the Jarzynski equality) still applies. The proof is straightforward. Since W is at most proportional to N_1 and it is therefore non-extensive in N, we can expand the entropy in Eq. (6.158) to the leading order in W:

$$S_B(E+W) - S_A(E) = \frac{\partial S_B}{\partial E} W + S_B(E) - S_A(E) + \mathcal{O}(N_1/N) = \beta W - \beta \Delta F + \mathcal{O}(N_1/N), \tag{6.159}$$

where we used the standard thermodynamic result that at constant temperature

$$-\beta \Delta F = S(E, \lambda_B) - S(E, \lambda_A) \equiv S_B(E) - S_A(E). \tag{6.160}$$

Therefore, up to N_1/N corrections, Eq. (6.158) implies that

$$\frac{P_F(E,W)}{P_R(E+W,-W)} = \mathrm{e}^{\beta(W-\Delta F)}, \tag{6.161}$$

irrespective of whether the subsystem is described by the Gibbs ensemble or not. Note that the free energy difference here is that of the whole system. It becomes the free energy difference in the subsystem only for a weak coupling between the subsystem and the rest of the system.

If the work W is small but extensive, for example, coming from a global protocol, or if one does not take the thermodynamic limit, one can still perform a Taylor expansion of the entropy in Eq. (6.158) in powers of W. Then, corrections to the Crooks relation will be generally finite. In particular, in Sec. 6.6.3, we will discuss how such corrections affect the Einstein drift-diffusion relation for the energy current (as occurs, for example, in microwave heating) of a driven isolated system, and to the Onsager relations. In what follows, we discuss various implications of Eq. (6.158) to setups involving both isolated and open systems.

6.6.2 Detailed Balance for Open Systems

Let us use the general relation (6.158) to derive the familiar detailed balance condition for open systems. Imagine we have two weakly coupled systems I and II. We do not need to make

any assumption about system I. It can be arbitrarily small, for example, consisting of one spin, and can be either integrable or ergodic. We assume that system II is quantum chaotic. For convenience, we call system II a bath, but we emphasize that we do not assume that system II is much bigger than system I. The weak coupling assumption is made explicit by writing the Hamiltonian of the entire system as

$$H_{\rm tot} = H_{\rm I} + H_{\rm II} + \gamma H_{I-II}, \tag{6.162}$$

with γ small. Initially, the two systems are prepared in a stationary state with respect to the uncoupled Hamiltonian $H_{\rm I} + H_{\rm II}$ and then they are allowed to interact. The initial state can be the product of two Gibbs states with different temperatures or can be the product of two eigenstates. Because of the coupling, energy is allowed to flow between the two systems. If the coupling is weak, then the sum of the energies of systems I and II is (approximately) conserved. This implies that only microscopic transitions between states $|n_{\rm I}, n_{\rm II}\rangle$ and $|m_{\rm I}, m_{\rm II}\rangle$ satisfying the energy conservation $E^{\rm I}_{n_{\rm I}} + E^{\rm II}_{n_{\rm II}} = E^{\rm I}_{m_{\rm I}} + E^{\rm II}_{m_{\rm II}}$ are allowed (see the red arrows in Fig. 6.23). This setup is formally equivalent to a quench in the coupling γ. Therefore, the transition probabilities are doubly stochastic. Moreover, as we discussed in the previous section, within the Fermi golden rule (or because this quench can be viewed as a time-symmetric protocol) these probabilities satisfy the stronger global detailed balance condition

$$p_{n_{\rm I},n_{\rm II}\to m_{\rm I},m_{\rm II}} = p_{m_{\rm I},m_{\rm II}\to n_{\rm I},n_{\rm II}}. \tag{6.163}$$

Suppose that we are interested in the transition between microstates only in system I, irrespective of the outcomes in the bath II. Hence, we have to sum over all final states of the bath. Using that in quantum chaotic systems the transition probabilities are the same for nearby eigenstates

$$p_{\rm I}(n_{\rm I}\to m_{\rm I}) = \sum_{m_{\rm II}} p_{n_{\rm I},n_{\rm II}\to m_{\rm I},m_{\rm II}} = p_{n_{\rm I},n_{\rm II}\to m_{\rm I},m_{\rm II}}\Omega_{\rm II}(E^{\rm II}_{m_{\rm II}}). \tag{6.164}$$

This equation is a direct analogue of Eq. (6.156), with the solely difference being that only the density of states of the bath enters the RHS, as the sum is carried out over the final states of the bath. For the reverse process (green arrows in Fig. 6.23), using the same arguments, we find

$$p_{\rm I}(m_{\rm I}\to n_{\rm I}) = p_{m_{\rm I},m_{\rm II}\to n_{\rm I},n_{\rm II}}\Omega_{\rm II}(E^{\rm II}_{n_{\rm II}}) \tag{6.165}$$

Comparing these two results, using the conservation of energy together with the global detailed balance condition, and simplifying notations $E^{\rm II}_{n_{\rm II}} \to E^{\rm II}$ (6.163), we find

$$\frac{p_{\rm I}(n_{\rm I}\to m_{\rm I})}{p_{\rm I}(m_{\rm I}\to n_{\rm I})} = \frac{\Omega_{\rm II}(E^{\rm II} + E^{\rm I}_{n_{\rm I}} - E^{\rm I}_{m_{\rm I}})}{\Omega_{\rm II}(E^{\rm II})} = {\rm e}^{S_{\rm II}(E^{\rm II}+E^{\rm I}_{n_{\rm I}}-E^{\rm I}_{m_{\rm I}})-S_{\rm II}(E^{\rm II})}. \tag{6.166}$$

If the bath is large, or if the energy change $\delta E^{\rm I}_{mn} \equiv E^{\rm I}_{m_{\rm I}} - E^{\rm I}_{n_{\rm I}}$ is small compared to $E^{\rm II}$, as before, one can expand the entropy difference in the energy change. By doing that, one recovers the detailed balance condition in its most familiar form [211]:

$$\frac{p_{\rm I}(n_{\rm I}\to m_{\rm I})}{p_{\rm I}(m_{\rm I}\to n_{\rm I})} \approx {\rm e}^{-\beta_{\rm II}(E^{\rm II})\,\delta E^{\rm I}_{mn}}, \tag{6.167}$$

where $\beta_{\rm II}(E^{\rm II})$ is the temperature of the bath corresponding to the energy $E^{\rm II}$.

6.6.3 Einstein's Energy Drift-Diffusion Relations for Isolated and Open Systems

In Sec. 6.6.1, we showed that the Jarzynski equality can be viewed as a constraint on the cumulant expansion of the work generating function [see Eq. (6.145)]. Consider, for example,

the Jarzynski equality for a cyclic process applied to a small subsystem of a large system or to a system initialized in a Gibbs state. In these cases, the Jarzynski equality is exact and, given the fact that the process is cyclic, $\Delta F = 0$, so that

$$\langle e^{-\beta W}\rangle = 1. \tag{6.168}$$

Next, let us perform a cumulant expansion of this equality:

$$0 = \ln\langle e^{-\beta W}\rangle \;\; = \;\; -\beta\langle W\rangle + \frac{1}{2}\beta^2\langle W^2\rangle_c + \frac{1}{6}\beta^3\langle W^3\rangle_c + \dots \;\; . \tag{6.169}$$

where $\langle W^2\rangle_c = \langle W^2\rangle - \langle W\rangle^2$ and $\langle W^3\rangle_c = \langle W^3\rangle - 3\langle W^2\rangle\langle W\rangle + 2\langle W\rangle^3$. If the average work performed is small and its distribution is close to Gaussian or if temperature is high, then cumulants of order three and higher in the expansion above can be neglected leading to:

$$0 \approx -\beta\langle W\rangle + \frac{1}{2}\beta^2\langle W^2\rangle_c \Rightarrow \langle W\rangle = \frac{\beta}{2}\langle W^2\rangle_c\,. \tag{6.170}$$

The relation above can be interpreted as a fluctuation-dissipation relation for a system coupled to an external noise. $\langle W\rangle$ is the average work characterizing energy dissipation in the system and $\langle W^2\rangle_c$ characterizes the uncertainty in the work. Equation (6.170) can also be interpreted as an analogue of Einstein's drift-diffusion relation for the energy. Indeed, $\langle W\rangle$ is the average work done on the system during the cyclic process, which is the energy drift, and $\langle W^2\rangle_c$ represents the work fluctuations, which is the energy diffusion.

Next we consider a system prepared in a single eigenstate (hence, the results equally apply to a setup where we start from an arbitrary narrow stationary distribution). We focus on the general expression for the work probability distribution, Eq. (6.158). For simplicity, we focus once again on cyclic[36] and symmetric protocols.[37] Then

$$P(E,W)\,\mathrm{e}^{-S(E+W)+S(E)} = P(E+W,-W). \tag{6.171}$$

In order to proceed further, let us assume that the work W is small (though it can be extensive). Then, the probability $P(E,W)$ is a slow function of the first argument and a fast function of the second argument W. Similarly, the entropy is a slow function of W. Formally, the RHS of the equation above can be rewritten as

$$P(E+W,-W) = \mathrm{e}^{W\partial_E}P(E,-W), \tag{6.172}$$

where we used the notation $\partial_E = \partial/\partial E$. Finally, expanding the entropy $S(E+W)$ in Eq. (6.171) to second order in W, and integrating over W, we find

$$\langle \mathrm{e}^{-\beta W - \frac{W^2}{2}\frac{\partial\beta}{\partial E}}\rangle_E \approx \langle \mathrm{e}^{-W\partial_E}\rangle_E, \tag{6.173}$$

where $\langle\dots\rangle_E$ means that an average is taken with respect to the probability distribution $P(E,W)$ at fixed E. Taking the logarithm of both sides of this relation, and performing the cumulant expansion to the second order, one finds

$$-\beta\langle W\rangle_E + \frac{1}{2}\beta^2\langle W^2\rangle_{E,c} - \frac{1}{2}\partial_E\beta\,\langle W^2\rangle_E \approx -\partial_E\langle W\rangle_E + \frac{1}{2}\left[\partial^2_{EE}\langle W^2\rangle_E - (\partial_E\langle W\rangle_E)^2\right]. \tag{6.174}$$

[36] If the protocol is not cyclic the total work W is the sum of the adiabatic work W_{ad}, which is not fluctuating, and the non-adiabatic work $\tilde{Q}$ which is fluctuating. Then, the following derivation remains valid if one identifies W with $\tilde{Q}$.

[37] If the protocol is not symmetric one has to distinguish between forward and reverse processes.

Note that $\langle W^2\rangle_E = \langle W^2\rangle_{E,c} + \langle W\rangle_E^2$, where the first term on the RHS is linear and the second is quadratic in cumulants. By equating all linear terms in the cumulants[38] Eq. (6.174) reduces to:

$$-\beta\langle W\rangle_E + \frac{1}{2}\beta^2\langle W^2\rangle_{E,c} - \frac{1}{2}\partial_E\beta\,\langle W^2\rangle_{E,c} \approx -\partial_E\langle W\rangle_E + \frac{1}{2}\partial_{EE}^2\langle W^2\rangle_{E,c}\,. \tag{6.175}$$

Using that

$$\partial_E\beta\,\langle W^2\rangle_{E,c} = \partial_E(\beta\langle W^2\rangle_{E,c}) - \beta\partial_E\langle W^2\rangle_{E,c}\,, \tag{6.176}$$

and regrouping all the terms, one finds that the equation above simplifies to

$$-\beta\left(\langle W\rangle_E - \frac{\beta}{2}\langle W^2\rangle_{E,c} - \frac{1}{2}\partial_E\langle W^2\rangle_{E,c}\right) + \partial_E\left(\langle W\rangle_E - \frac{\beta}{2}\langle W^2\rangle_{E,c} - \frac{1}{2}\partial_E\langle W^2\rangle_{E,c}\right) = 0. \tag{6.177}$$

Therefore, the first and the second cumulant have to satisfy the relation:

$$\langle W\rangle_E = \frac{\beta}{2}\langle W^2\rangle_{E,c} + \frac{1}{2}\partial_E\langle W^2\rangle_{E,c}\,. \tag{6.178}$$

Equation (6.178) extends Einstein's drift-diffusion relation (6.170) connecting work and work fluctuations for a system prepared in a single eigenstate (and hence to a microcanonical shell). In large systems, the last term in (6.178) is a subleading correction since the energy is extensive. So, in the thermodynamic limit, this term can be dropped and one is back to Eq. (6.170). However, if one is dealing with a small chaotic system, then the last term cannot be neglected. As we will show in the next section, it has important implications for determining the correct asymptotic distribution of driven chaotic systems. Relation (6.178) was first obtained by C. Jarzynski for a single classical particle moving in a shaken chaotic cavity [212, 213], and then extended to arbitrary quantum or classical systems along the lines of our derivation in Ref. [193].

The exact same analysis can be carried out if, instead of a single driven system, one considers two weakly coupled systems I and II as illustrated in Fig. 6.23. For the purposes of this discussion, we will assume that both systems are ergodic. Let us assume that the two systems are initialized in eigenstates with energies $E_{\rm I}$ and $E_{\rm II}$ and then coupled weakly. This coupling leads to an energy exchange between the two systems. Since the dynamics is unitary, and after the assumption that each system is quantum chaotic, we can apply Eq. (6.171) to this setup. The only new ingredient is that the entropy S is replaced by the sum of entropies of the systems I and II (corresponding to the factorization of the densities of states of the uncoupled systems). Thus

$$\begin{aligned} P(E_{\rm I}\to E_{\rm I}+W, E_{\rm II}\to E_{\rm II}-W) &\equiv P(E_{\rm I},E_{\rm II},W)\\ &= \mathrm{e}^{S_{\rm I}(E_{\rm I}+W)+S_{\rm II}(E_{\rm II}-W)-S_{\rm I}(E_{\rm I})-S_{\rm II}(E_{\rm II})}P(E_{\rm I}+W,E_{\rm II}-W,-W). \end{aligned} \tag{6.179}$$

Note that, here, we use W to denote the energy exchange between systems I and II (even though now it means heat). As we will see shortly, for isolated chaotic systems an external drive is equivalent to a coupling to an infinite temperature bath $\beta_{\rm II}$. Therefore, we prefer to keep the same notation for both coupled and isolated driven systems. Repeating exactly the same steps as before, that is, expanding the two entropies and P with respect to W up to the second order and integrating over the distribution function $P(E_{\rm I},E_{\rm II},W)$, one obtains (see Appendix 6.15):

$$\langle W\rangle_{E_{\rm I},E_{\rm II}} = \frac{\beta_{\rm I}-\beta_{\rm II}}{2}\langle W^2\rangle_{E_{\rm I},E_{\rm II},c} + \frac{1}{2}\left(\partial_{E_{\rm I}} - \partial_{E_{\rm II}}\right)\langle W^2\rangle_{E_{\rm I},E_{\rm II},c}, \tag{6.180}$$

[38] Formally, this can be justified by introducing some parameter ε such that all cumulants are linear in ε. This parameter can be, for example, duration of the pulse $\varepsilon = dt$ or the size of the subsystem that is coupled to the driving term. Since the relation (6.171) is valid in all orders in ε, it is sufficient to verify it only to linear order.

where the symbol $\langle \dots \rangle_{E_{\rm I},E_{\rm II}}$ means that an average is taken with respect to the probability distribution $P(E_{\rm I}, E_{\rm II}, W)$ at fixed $E_{\rm I}$ and $E_{\rm II}$, the suffix "c" means connected, and $\beta_{\rm I} - \beta_{\rm II}$ is the difference in temperature between the two systems. If both systems are large, then the last term is again subextensive and can be dropped. It is interesting to note that Einstein's relation for coupled systems (6.180) reduces to the one for isolated systems (6.178) if the temperature of system II is infinite $\beta_{\rm II} = 0$ and $\langle W^2 \rangle_{E_{\rm I},E_{\rm II},c}$ is either negligible or independent of $E_{\rm II}$. Hence, from the point of view of energy flow, driving an isolated system by means of an external cyclic perturbation (like it happens, e.g., in microwave ovens) is equivalent to coupling it to an infinite temperature reservoir.

6.6.4 Fokker-Planck Equation for the Heating of a Driven Isolated System

The drift-diffusion relation (6.178) can be used to understand energy flow (or heating) in a driven ergodic system not coupled to a bath. Let us imagine that the process consists of many pulses, well separated in time, such that the system can relax between pulses to the diagonal ensemble. Then, after coarse-graining, one can view this as a continuous (in number of pulses) process. If the mean energy deposited in each pulse is small then both $\langle W \rangle$ and $\langle W^2 \rangle_c$ (as well as other cumulants of W) scale linearly with the number of pulses and, hence, with the coarse-grained time. Next, instead of a series of discrete processes, one can consider a single continuous process. Then, as long as the relaxation time is faster than the characteristic time for the energy change in the system, $\langle W \rangle$ and $\langle W^2 \rangle_c$ are approximately linear in time. It is well known that under such assumptions transport (energy transport in our case) can be described by the Fokker-Planck equation. The derivation of the Fokker-Planck equation is fairly standard (see, e.g., Ref. [190]) but we repeat it here for completeness. We start from the microscopic master equation (6.89). For simplicity, assuming a cyclic process and dropping the tildes:

$$\rho_n(t + \delta t) = \sum_m p_{m\to n}(\delta t)\rho_m(t), \tag{6.181}$$

where δt is a small interval of time. By assumption, $p_{m\to n}(\delta t) \propto \delta t$. Let us define the energy distribution function

$$\Pi(E_n, t) = \rho_n(t)\Omega(E_n). \tag{6.182}$$

Now, replacing the summation over m in the master equation by an integration over W (and multiplying by the density of states), recalling that the probability of performing work W is $P(E_n, W) = p_{n\to m}\Omega(E_m)$, where $E_m = E_n + W$, and dropping the index n in E_n, we can rewrite Eq. (6.181) as

$$\Pi(E, t + \delta t) = \int dW P(E - W, W)\Pi(E - W, t). \tag{6.183}$$

Note that $P(E - W, W)$ is a fast function of the second argument with the width $\delta W^2 \equiv \langle W^2 \rangle_c \propto \delta t$, but a slow function of the total energy of the system, that is, of the first argument. Similarly, the probability distribution $\Pi(E, t)$ is expected to be a slow function of E on the scale of δW. Hence, we can use the Taylor expansions:

$$\Pi(E - W, t) = \Pi(E, W) - W\partial_E\Pi(E, W) + \dots,$$
$$P(E - W, W) = P(E, W) - W\partial_E P(E, W) + \dots$$

By substituting these expansions in Eq. (6.183), and expanding to second order in the work W, we find:

$$\Pi(E,t+\delta t)-\Pi(E,t)=-\langle W\rangle_E\partial_E\Pi(E,t)-\partial_E\langle W\rangle_E\Pi(E,t)+\frac{1}{2}\langle W^2\rangle_E\partial^2_{EE}\Pi(E,t)$$
$$+\partial_E\langle W^2\rangle_E\partial_E\Pi(E,t)+\frac{1}{2}\partial^2_{EE}\langle W^2\rangle_E\Pi(E,t). \tag{6.184}$$

Dividing the equation above by δt, and using the notation

$$J_E=\frac{\langle W\rangle_E}{\delta t},\ D_E=\frac{\langle W^2\rangle_{E,c}}{\delta t}, \tag{6.185}$$

we find the Fokker-Planck equation

$$\frac{\partial\Pi(E,t)}{\partial t}=-\partial_E[J_E\Pi(E,t)]+\frac{1}{2}\partial^2_{EE}[D_E\Pi(E,t)]. \tag{6.186}$$

To obtain this result, we notice that the cumulants of the work are linear in transition probabilities and, hence, they are linear in δt. So, in the limit $\delta t\to 0$, one can substitute $\langle W^2\rangle_E\to\langle W^2\rangle_{E,c}$.

This Fokker-Planck equation for the energy drift and diffusion is completely general. Effectively, it describes the evolution of the energy distribution function under many small uncorrelated pulses or under a continuous slow driving such that, at each moment of time, the system is, approximately, in a stationary state. In general, the drift J_E and diffusion D_E coefficients are independent. However, in ergodic systems, they are related to each other by Eq. (6.178), which, after dividing by δt, reads [193]

$$J_E=\frac{\beta}{2}D_E+\frac{1}{2}\partial_E D_E. \tag{6.187}$$

Likewise, for open systems, Eq. (6.180) implies that [212, 213, 214]

$$J_E=\frac{\Delta\beta}{2}D_E+\frac{1}{2}\partial_E D_E \tag{6.188}$$

In the next section, we will see how powerful this result is for finding universal energy distributions in driven isolated and open systems. We note that the Fokker-Planck equation can be derived using a different approach, as done in Refs. [215, 216].

Interestingly, one can derive Eqs. (6.187) and (6.188) from a very simple argument [193]. Let us discuss it here only for an isolated setup, which is relevant to Eq. (6.187). It is straightforward to extend the discussion to open systems, relevant to Eq. (6.188). According to the discussion in Sec. 6.5.2, the only attractor for the probability distribution of a driven system is the infinite temperature distribution: $\rho^*_n=C_1$, where C_1 is a constant. This implies that $\Pi^*(E)=C_2\exp[S(E)]$, with C_2 another constant, should be stationary under the Fokker-Planck equation or, in other words, that

$$-\partial_E[J_E\Pi^*(E)]+\frac{1}{2}\partial^2_{EE}[D_E\Pi^*(E)]=0, \tag{6.189}$$

which, in turn, implies that

$$-J_E e^{S(E)}+\frac{1}{2}\partial_E[D_E e^{S(E)}]=C_3=0. \tag{6.190}$$

The integration constant C_3 has to be equal to zero because one can go to (typically, low) energies where there are no states and, hence, $J_E=D_E=0$. From Eq. (6.190), one immediately recovers the drift-diffusion relation (6.187).

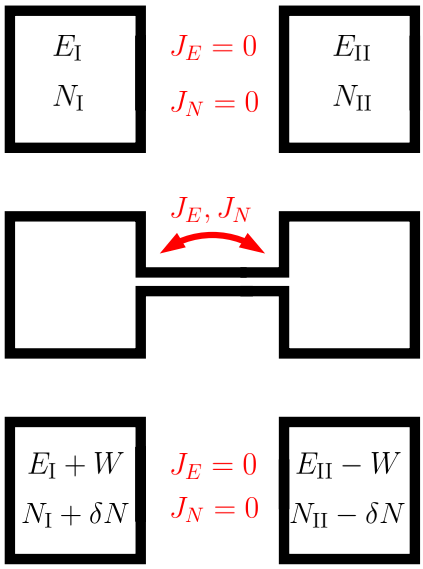

Figure 6.24: Two systems are connected and exchange energy and particles. (Top) Initially, the two systems have a well-defined energy and number of particles. (Middle) Then they are connected and allowed to exchange energy and particles. (Bottom) Finally they are disconnected and each system is allowed to equilibrate at the new fixed values of energy and particle numbers.

6.6.5 Fluctuation Theorems for Two (or More) Conserved Quantities

Until now we focused on systems with only one conserved quantity, the energy. Quite often one deals with situations where, in addition to the energy, there are other conserved quantities, such as the number of particles, magnetization, momentum, charge, and volume. In this section, we extend the fluctuation relations and their implications to such setups. To simplify our derivations, we will focus on systems with two conserved quantities: energy E and the number of particles N. At the end of Sec. 6.6.6, we comment on how to extend our results to an arbitrary (non-extensive) number of conserved quantities. We focus on a particular setup, where two initially separated chaotic systems I and II are weakly coupled allowing for energy and particle exchange (see Fig. 6.24). The expressions obtained in this setup can also be used to describe a single system, say, system I, coupled to an external driving by setting $\partial S_{\rm II}/\partial E_{\rm II} = \partial S_{\rm II}/\partial N_{\rm II} = 0$. We assume that the two systems are connected to each other for a short period of time τ and then detached again and allowed to equilibrate (i.e., reach a diagonal ensemble), see Fig. 6.24. It is intuitively clear that this assumption of connecting and disconnecting the systems is not needed if the coupling between them is weak and the two systems are in an approximate stationary state with respect to the uncoupled Hamiltonian at each moment of time. This intuition can be formalized using time-dependent perturbation theory (see Appendix 6.14).

Repeating the same steps as in Sec. 6.6.3, one can straightforwardly generalize Eq. (6.171) to:

$$\frac{P(E_{\rm I}, E_{\rm II}, N_{\rm I}, N_{\rm II}, W, \delta N)}{P(E_{\rm I}+W, E_{\rm II}-W, N_{\rm I}+\delta N, N_{\rm II}-\delta N, -W, -\delta N)} = \mathrm{e}^{S_{\rm I}(E_{\rm I}+W, N_{\rm I}+\delta N)+S_{\rm II}(E_{\rm II}-W, N_{\rm II}-\delta N)-S_{\rm I}(E_{\rm I}, N_{\rm I})-S_{\rm II}(E_{\rm II}, N_{\rm II})}, \tag{6.191}$$

where

$$P(E_{\rm I}, E_{\rm II}, N_{\rm I}, N_{\rm II}, W, \delta N) \equiv P(E_{\rm I} \to E_{\rm I} + W, E_{\rm II} \to E_{\rm II} - W, N_{\rm I} \to N_{\rm I} + \delta N, N_{\rm II} \to N_{\rm II} - \delta N).$$

If the energy and particle changes are small, one can expand the entropy and the probability distribution P in Taylor series. If W and δN are small and non-extensive, then only the leading derivatives of the entropy need to be kept and we find a Crooks-type relation for two conserved quantities:

$$P(E_{\rm I}, E_{\rm II}, N_{\rm I}, N_{\rm II}, W, \delta N) {\rm e}^{-\Delta\beta W - \Delta\kappa \delta N} \approx P(E_{\rm I}, E_{\rm II}, N_{\rm I}, N_{\rm II}, -W, -\delta N), \tag{6.192}$$

where $\Delta\beta = \beta_{\rm I} - \beta_{\rm II}$, and $\Delta\kappa = \kappa_{\rm I} - \kappa_{\rm II}$, with

$$\kappa_i = \frac{\partial S_i}{\partial N_i} = -\beta_i \mu_i, \quad i = {\rm I}, {\rm II} \tag{6.193}$$

As in Sec. 6.6.1, this relation is exact if the two systems I and II are described by grand canonical distributions. It is also asymptotically exact to order $1/N$ (with N of the order of the number of particles in each system) irrespective of the distribution, if the two systems are extensive while the energy and particle exchanges are not (which is, e.g., the typical setup if two large macroscopic systems are connected through a surface). For the specific case of effusion of an ideal gas between two reservoirs kept at different temperatures and chemical potentials, Eq. (6.192) was derived microscopically in Ref. [217]. Following Ref. [208], we can use the fluctuation relation (6.192) to derive the symmetry property of the cumulant generating function for W and δN, see Eq. (6.154). Namely, multiplying both sides of Eq. (6.192) by ${\rm e}^{\zeta W + \delta N}$

$$P(E_{\rm I}, E_{\rm II}, N_{\rm I}, N_{\rm II}, W, \delta N) {\rm e}^{-(\Delta\beta - \zeta) W - (\Delta\kappa - \eta)\delta N} = P(E_{\rm I}, E_{\rm II}, N_{\rm I}, N_{\rm II}, -W, -\delta N) {\rm e}^{\zeta W + \delta N} \tag{6.194}$$

for arbitrary ζ and η, and integrating over W and δN, we find

$$G(\Delta\beta - \zeta, \Delta\kappa - \eta) = G(\zeta, \eta) \tag{6.195}$$

together with the normalization condition $G(0,0) = 1$. For the particular choices of ζ and η the symmetry relation (6.195) is equivalent to two different Jarzynski-type relations:

$$\langle \exp[-\Delta\beta W - \Delta\kappa \delta N] \rangle = 1, \quad \langle \exp[-\Delta\beta W] \rangle = \langle \exp[-\Delta\kappa \delta N] \rangle, \tag{6.196}$$

where the left relation holds for $\zeta = \eta = 0$ and the right for $\zeta = 0$, $\eta = \Delta\kappa$. As in Sec. 6.6.3 the angular brackets imply averaging over W and δN starting at $E_{\rm I}, E_{\rm II}$ and $N_{\rm I}, N_{\rm II}$.

6.6.6 Linear Response and Onsager Relations

Continuing with the setup of the previous section, one can perform the cumulant expansion of Eq. (6.196) up to the second order, or, alternatively, perform a Taylor expansion of the cumulant generating function and using relation (6.195). One obtains:

$$-\Delta\beta \langle W \rangle - \Delta\kappa \langle \delta N \rangle + \frac{\Delta\beta^2}{2} \langle W^2 \rangle_c + \frac{\Delta\kappa^2}{2} \langle \delta N^2 \rangle_c + \Delta\beta\Delta\kappa \langle W \delta N \rangle_c = 0, \tag{6.197}$$

$$-\Delta\beta \langle W \rangle + \frac{\Delta\beta^2}{2} \langle W^2 \rangle_c = -\Delta\kappa \langle \delta N \rangle + \frac{\Delta\kappa^2}{2} \langle \delta N^2 \rangle_c. \tag{6.198}$$

First, we move all the terms to the left-hand side (LHS) of Eq. (6.198), then by adding and subtracting the resulting expression with Eq. (6.197), we obtain the two completely symmetric relations:

$$\langle W\rangle = \frac{\Delta\beta}{2}\langle W^2\rangle_c + \frac{\Delta\kappa}{2}\langle W\delta N\rangle_c, \qquad \langle \delta N\rangle = \frac{\Delta\kappa}{2}\langle \delta N^2\rangle_c + \frac{\Delta\beta}{2}\langle W\delta N\rangle_c. \tag{6.199}$$

If the coupling between the systems is weak, then either from Fermi's golden rule or using the same arguments as presented above Eq. (6.181), we conclude that $\langle W\rangle$ and $\langle \delta N\rangle$ (as well as other cumulants such as $\langle W^2\rangle_c$) are linear functions of the coupling time δt. Then one can define the energy and particle currents $J_E = \langle W\rangle/\delta t$ and $J_N = \langle \delta N\rangle/\delta t$; as well as $D_{WW} = \langle W^2\rangle_c/\delta t$, $D^2_{NN} = \langle \delta N^2\rangle_c/\delta t$, and $D_{WN} = \langle W\delta N\rangle_c/\delta t$. Equations (6.199) can then be rewritten in the matrix form [218]:

$$\begin{pmatrix} J_E \\ J_N \end{pmatrix} = \frac{1}{2}\begin{pmatrix} D_{WW} & D_{WN} \\ D_{WN} & D_{NN} \end{pmatrix}\begin{pmatrix} \Delta\beta \\ \Delta\kappa \end{pmatrix} \tag{6.200}$$

These equations are analogous to Eq. (6.170) and are known as the Onsager relations. On the LHS one has the energy and particle currents, while on the RHS one has the symmetric fluctuation matrix multiplied by the thermodynamic biases ($\Delta\beta$ and $\Delta\kappa$) that drive the energy and particle currents. Note that we obtained these relations as a cumulant expansion, not as a gradient expansion. This means that they remain valid for arbitrarily large $\Delta\beta$ and $\Delta\kappa$ as long as the distribution $P(W,\delta N)$ is approximately Gaussian. For this reason, the diffusion matrix in Eq. (6.200) does not have to be the one in equilibrium, that is, does not have to correspond to the one for $\Delta\beta = \Delta\kappa = 0$. When the temperature and the chemical potential gradients are small, contributions from higher order cumulants are suppressed because of the higher powers of $\Delta\beta$ and $\Delta\kappa$. As a result, the usual Onsager relations apply.

This derivation of the Onsager relations applies to large systems. As with the Einstein relation (6.180), there is a correction that can be important for small systems. The derivation of this correction is analogous to the derivation of Eq. (6.180). The starting point is now Eq. (6.191). One needs to expand the entropy and the probability distribution as a function of $E_{\rm I,II} \pm W$ and $N_{\rm I,II} \pm \delta N$ to second order in W and δN, and then to carry out a cumulant expansion with these additional corrections. We leave the details of the derivation to Appendix 6.15 and show only the final result, which is the natural extension of Eq. (6.180):

$$\begin{aligned} \langle W\rangle &= \frac{\Delta\beta}{2}\langle W^2\rangle_c + \frac{\Delta\kappa}{2}\langle W\delta N\rangle_c + \frac{1}{2}\partial_E\langle W^2\rangle_c + \frac{1}{2}\partial_N\langle W\delta N\rangle_c, \\ \langle \delta N\rangle &= \frac{\Delta\kappa}{2}\langle \delta N^2\rangle_c + \frac{\Delta\beta}{2}\langle W\delta N\rangle_c + \frac{1}{2}\partial_N\langle \delta N^2\rangle_c + \frac{1}{2}\partial_E\langle W\delta N\rangle_c. \end{aligned} \tag{6.201}$$

The terms with derivatives are clearly subextensive and not important for large systems, but they can play an important role in small or mesoscopic systems. It is interesting to note that the Onsager relations can still be written in the conventional form (6.200) if one redefines the energy and particle currents as

$$J_E = \frac{1}{\tau}\langle W\rangle - \frac{1}{2\tau}\partial_E\langle W^2\rangle_c - \frac{1}{2\tau}\partial_N\langle W\delta N\rangle_c, \quad J_N = \frac{1}{\tau}\langle \delta N\rangle - \frac{1}{2\tau}\partial_N\langle \delta N^2\rangle_c - \frac{1}{2\tau}\partial_E\langle W\delta N\rangle_c\,. \tag{6.202}$$

Let us comment that these results immediately generalize to more ($M \geq 3$) conserved quantities. For example, in the Onsager relation (6.200) one will need to use M-component vectors for the currents and the gradients and a symmetric $M \times M$ diffusion matrix. Similarly, one can generalize corrections to the currents (6.202) writing them using an M-component gradient form.

6.6.7 Nonlinear Response Coefficients

Along the lines of Refs. [208, 218], one can go beyond the Onsager relation and use the symmetry relation of the generating function (6.195) to constrain nonlinear response coefficients. It is convenient to work using a vector notation for M-conserved quantities $\delta\vec{N}$, where δN_1 stands for the energy, and $\delta N_2, \ldots, \delta N_M$ for other conserved quantities. Similarly, let us denote by $\Delta\vec{\kappa}$ the gradients of affinities (or thermodynamic forces) $\kappa_\alpha = \partial S/\partial N_\alpha$ (such that $\kappa_1 = \beta$) and $\Delta\kappa_\alpha$ is the difference in affinities between the systems I and II. Ignoring subextensive corrections, the symmetry relation (6.195) reads

$$G(\Delta\vec{\kappa} - \vec{\zeta}) = G(\vec{\zeta}), \tag{6.203}$$

where we recall that

$$\left\langle \exp\left[-\sum_\alpha \zeta_\alpha \delta N_\alpha\right]\right\rangle = \exp[G(\vec{\zeta})]. \tag{6.204}$$

Differentiating this equality with respect to ζ_α and using that $G(0) = 1$, we find

$$J_\alpha \equiv \langle \delta N_\alpha \rangle = -\left.\frac{\partial G(\vec{\zeta})}{\partial \zeta_\alpha}\right|_{\vec{\zeta}=0}. \tag{6.205}$$

To simplify the notation, we set $\tau = 1$ so that $\langle \delta N_\alpha \rangle = J_\alpha$ is the current of the α-th conserved quantity. The symmetry relation (6.203) thus implies that

$$J_\alpha = -\left.\frac{\partial G(\vec{\zeta})}{\partial \zeta_\alpha}\right|_{\vec{\zeta}=0} = -\left.\frac{\partial G(\Delta\vec{\kappa} - \vec{\zeta})}{\partial \zeta_\alpha}\right|_{\vec{\zeta}=0} = \left.\frac{\partial G(\vec{\zeta})}{\partial \zeta_\alpha}\right|_{\vec{\zeta}=\Delta\vec{\kappa}}. \tag{6.206}$$

Let us write explicitly the cumulant expansion of the generating function $G(\vec{\zeta})$:

$$G(\vec{\zeta}) = -\sum_\alpha \zeta_\alpha J_\alpha + \frac{1}{2}\sum_{\alpha\beta} D_{\alpha\beta}\zeta_\alpha\zeta_\beta - \frac{1}{3!}\sum_{\alpha\beta\gamma} M_{\alpha\beta\gamma}\zeta_\alpha\zeta_\beta\zeta_\gamma + \ldots, \tag{6.207}$$

where $D_{\alpha\beta} = \langle \delta N_\alpha \delta N_\beta \rangle_c$ is the covariance matrix (second-order joint cumulant matrix), $M_{\alpha\beta\gamma}$ is the third-order cumulant tensor, and so on. By substituting this expansion into Eq. (6.206), we find

$$2J_\alpha = \sum_\beta D_{\alpha\beta}\Delta\kappa_\beta - \frac{1}{2}\sum_{\beta\gamma} M_{\alpha\beta\gamma}\Delta\kappa_\beta\Delta\kappa_\gamma + \ldots \tag{6.208}$$

Using this expansion and the symmetry relations of joint cumulant tensors, such as $D_{\alpha\beta} = D_{\beta\alpha}$ and $M_{\alpha\beta\gamma} = M_{\beta\alpha\gamma}$, one can extend the Onsager reciprocity relations to higher order cumulants. As in the previous section, these results extend to externally driven systems by substituting $\Delta\vec{\kappa}$ by $\vec{\kappa}_{\rm I}$. Note that because we carry out a cumulant expansion, and not a gradient expansion, all cumulant tensors, such as $D_{\alpha,\beta}$ and $M_{\alpha\beta\gamma}$, are functions of $\Delta\vec{\kappa}$, that is, they are evaluated away from the global equilibrium corresponding to $\Delta\vec{\kappa} = 0$. If one further re-expands these tensors in gradients $\Delta\vec{\kappa}$, one obtains a more standard gradient expansion around equilibrium [208].

6.6.8 ETH and the Fluctuation-Dissipation Relation for a Single Eigenstate

In Sec. 6.4.2, we introduced the ETH ansatz for the matrix elements of physical operators in the eigenstates of a quantum chaotic Hamiltonian (6.62). This ansatz contains two smooth functions of the mean energy $\bar{E} = (E_n + E_m)/2$, and the energy difference $\omega = E_m - E_n$.

The first function, $O(\bar{E})$, is nothing but the microcanonical average of the observable $\hat{O}$. The second function, $f_O(\bar{E},\omega)$, contains information about the off-diagonal matrix elements of the operator $\hat{O}$. Let us elaborate on the second function here and show its relation to nonequal-time correlation functions of the observable $\hat{O}$ (see also Ref. [154]). In parallel, we will be able to prove the fluctuation-dissipation relation for individual eigenstates.

We begin by using the ETH ansatz (6.62) to analyze the quantum fluctuations of an observable $\hat{O}$ in the eigenstate $|n\rangle$:

$$\delta O_n^2 = \langle n|\hat{O}^2|n\rangle - \langle n|\hat{O}|n\rangle^2 = \sum_{m\neq n} |O_{nm}|^2 = \sum_{m\neq n} \mathrm{e}^{-S(E_n+\omega/2)} |f_O(E_n+\omega/2,\omega)|^2 |R_{nm}|^2, \quad (6.209)$$

where we used that $\bar{E} = (E_n + E_m)/2 = E_n + \omega/2$. For concreteness, we consider the most general case in which the matrix elements of observables are complex.

Because of the ETH requirement that the function f_O is smooth, the fluctuations of $|R_{nm}|^2$ average out in the sum and one can replace the summation over states m by an integration over ω: $\sum_m \to \int d\omega\, \Omega(E_n+\omega) = \int d\omega \exp[S(E_n+\omega)]$. To shorten the notation, we will drop the subindex n in E_n and, unless otherwise specified, will identify E with the energy of the energy eigenstate $|n\rangle$. Then

$$\delta O_n^2 = \sum_{m\neq n} \mathrm{e}^{-S(E+\omega/2)} |f_O(E+\omega/2,\omega)|^2 = \int_{-\infty}^{\infty} d\omega\, \mathrm{e}^{S(E+\omega)-S(E+\omega/2)} |f_O(E+\omega/2,\omega)|^2. \quad (6.210)$$

We are interested in expectation values of few-body (usually local) operators (such as the magnetization in a given region of space) or sums of those operators (such as the total magnetization). This kind of operators generally connect states that differ by non-extensive energies, implying that the function $f_O(E+\omega/2,\omega)$ rapidly decreases with the second argument ω [29, 154] (see Figs. 6.16 and 6.17). On the other hand, the entropy $S(E+\omega)$ and the function f_O as a function of the first argument can only change if ω changes by an extensive amount. This means that one can expand these functions in Taylor series around $\omega = 0$:

$$S(E+\omega) - S(E+\omega/2) = \frac{\beta\omega}{2} + \frac{\partial\beta}{\partial E}\frac{3\,\omega^2}{8} + \ldots,$$
$$f_O(E+\omega/2,\omega) = f_O(E,\omega) + \frac{\partial f_O(E,\omega)}{\partial E}\frac{\omega}{2} + \ldots.$$

By substituting this expansion in Eq. (6.210) and keeping terms up to the linear order in ω, one obtains

$$\delta O_n^2 \approx \int_{-\infty}^{\infty} d\omega\, \mathrm{e}^{\beta\omega/2} \left[|f_O(E,\omega)|^2 + \frac{\partial |f_O(E,\omega)|^2}{\partial E}\frac{\omega}{2} \right]. \quad (6.211)$$

The function $f_O(E,\omega)$ therefore determines the quantum fluctuations of the operator $\hat{O}$ in eigenstates of the Hamiltonian and, as a result, in the associated microcanonical ensembles.

In passing, we note that the result above shows that fluctuations of $\hat{O}$ within each eigenstate are slow functions of the energy. Combining this observation with an earlier discussion of fluctuations of observables in the diagonal ensemble (see Sec. 6.4.2), we can rewrite Eq. (6.73) as

$$\overline{\delta O^2} \approx \delta O_n^2 + \left(\frac{\partial \bar{O}}{\partial E}\right)^2 \delta E^2, \quad (6.212)$$

where n is the eigenstate corresponding to the mean energy: $E_n = \langle E\rangle$. We see that fluctuations of any observable in a diagonal ensemble have essentially two independent contributions, the first coming from fluctuations within each eigenstate and the second from the energy fluctuations. For extensive observables, these two contributions are of the same order but, for

intensive observables confined to a finite subsystem, the second contribution becomes subleading and all fluctuations are essentially coming from δO_n^2. This is nothing but a manifestation of equivalence of ensembles applied to the diagonal ensemble.

The previous derivation immediately extends to more general nonequal-time correlation functions:

$$C_O(t) \equiv \langle n|\hat{O}(t)\hat{O}(0)|n\rangle_c \equiv \langle n|\hat{O}(t)\hat{O}(0)|n\rangle - \langle n|\hat{O}(t)|n\rangle\langle n|\hat{O}(0)|n\rangle, \tag{6.213}$$

where $\hat{O}(t) = \mathrm{e}^{i\hat{H}t}\hat{O}\mathrm{e}^{-i\hat{H}t}$ is the operator in the Heisenberg picture. Repeating the same steps as before, one finds

$$C_O(t) \approx \int_{-\infty}^{\infty} d\omega\, \mathrm{e}^{\beta\omega/2 - i\omega t}\left[|f_O(E,\omega)|^2 + \frac{\partial |f_O(E,\omega)|^2}{\partial E}\frac{\omega}{2}\right]. \tag{6.214}$$

It is convenient to define the spectral density of the operator $\hat{O}$ as the Fourier transform of $C_O(t)$

$$\mathcal{S}_O(E,\omega) = \int_{-\infty}^{\infty} dt\; e^{i\omega t} C_O(t). \tag{6.215}$$

Substituting here the expression for $C_O(t)$, one obtains

$$|f_O(E,\omega)|^2 + \frac{\omega}{2}\frac{\partial |f_O(E,\omega)|^2}{\partial E} = \frac{\mathrm{e}^{-\beta\omega/2}}{2\pi}\mathcal{S}_O(E,\omega). \tag{6.216}$$

Noting that $|f_O(E,\omega)|^2$ is an even function of ω and $\omega|f_O(E,\omega)|^2$ is an odd function, changing $\omega \to -\omega$ in Eq. (6.216), and adding and subtracting the two resulting equations, one finds that

$$\begin{aligned} |f_O(E,\omega)|^2 &= \frac{1}{4\pi}\left[\mathrm{e}^{-\beta\omega/2}\mathcal{S}_O(E,\omega) + \mathrm{e}^{\beta\omega/2}\mathcal{S}_O(E,-\omega)\right] \\ &= \frac{1}{4\pi}\left[\cosh(\beta\omega/2)\mathcal{S}_O^+(E,\omega) - \sinh(\beta\omega/2)\mathcal{S}_O^-(E,\omega)\right], \\ \frac{\partial |f_O(E,\omega)|^2}{\partial E} &= \frac{1}{2\pi\omega}\left[\cosh(\beta\omega/2)\mathcal{S}_O^-(E,\omega) - \sinh(\beta\omega/2)\mathcal{S}_O^+(E,\omega)\right], \end{aligned} \tag{6.217}$$

where

$$\begin{aligned} \mathcal{S}_O^+(E,\omega) &= \mathcal{S}_O(E,\omega) + \mathcal{S}_O(E,-\omega) = \int_{-\infty}^{\infty} dt \mathrm{e}^{i\omega t}\langle n|\{\hat{O}(t),\hat{O}(0)\}|n\rangle_c, \\ \mathcal{S}_O^-(E,\omega) &= \mathcal{S}_O(E,\omega) - \mathcal{S}_O(E,-\omega) = \int_{-\infty}^{\infty} dt \mathrm{e}^{i\omega t}\langle n|[\hat{O}(t),\hat{O}(0)]|n\rangle_c, \end{aligned} \tag{6.218}$$

are the Fourier transforms of the symmetric and antisymmetric correlation functions, $\{\cdot,\cdot\}$ stands for the anti-commutator and $[\cdot,\cdot]$ stands for the commutator of two operators. The symmetric correlation function appears in the quantum fluctuations of physical observables and the antisymmetric correlation function appears in Kubo's linear response. We thus see that the absolute value of the function $f_O(E,\omega)$ and its derivative with respect to E are determined by the Fourier transforms of the symmetric and antisymmetric nonequal-time correlation functions of the operator $\hat{O}$ taken in the many-body eigenstate state $|n\rangle$, or, equivalently, in the microcanonical ensemble consisting of a single eigenstate with the energy $E = E_n$. The phase of this function is not uniquely defined because, in Eq. (6.62), the random function R_{nm} is defined up to a random phase. One can also invert the relations (6.217) and obtain

$$\begin{aligned} \mathcal{S}_O^+(E,\omega) &= 4\pi\left[\cosh(\beta\omega/2)|f_O(E,\omega)|^2 + \frac{\omega}{2}\sinh(\beta\omega/2)\frac{\partial |f_O(E,\omega)|^2}{\partial E}\right], \\ \mathcal{S}_O^-(E,\omega) &= 4\pi\left[\sinh(\beta\omega/2)|f_O(E,\omega)|^2 + \frac{\omega}{2}\cosh(\beta\omega/2)\frac{\partial |f_O(E,\omega)|^2}{\partial E}\right]. \end{aligned} \tag{6.219}$$

Let us recall that $\mathcal{S}(E,\omega)$ also determines Kubo's linear response susceptibility (see, e.g., Ref. [219]):

$$\chi_O(\omega) = i\int_0^\infty dt e^{i\omega t}\langle[\hat{O}(t),\hat{O}(0)]\rangle = i\int_0^\infty dt e^{i\omega t}[C_O(t) - C_O(-t)], \tag{6.220}$$

where we used that, for any stationary distribution (including an energy eigenstate), $\langle\hat{O}(0)\hat{O}(t)\rangle_c = \langle\hat{O}(-t)\hat{O}(0)\rangle_c = C_O(-t)$. Using Eq. (6.214), and that

$$\int_0^\infty dt e^{i\nu t} = \pi\delta(\nu) + i\mathcal{P}\left(\frac{1}{\nu}\right), \tag{6.221}$$

where $\mathcal{P}(1/\nu)$ stands for the principal value, we find

$$\begin{aligned}\chi_O(E,\omega) = 2\pi i\left[\sinh(\beta\omega/2)|f_O(E,\omega)|^2 + \cosh(\beta\omega/2)\frac{\omega}{2}\frac{\partial|f_O(E,\omega)|^2}{\partial E}\right]\\ + \mathcal{P}\int_{-\infty}^\infty d\nu\left[2|f_O(E,\nu)|^2\frac{\sinh(\beta\nu/2)}{\nu-\omega} + \frac{\partial|f_O(E,\nu)|^2}{\partial E}\frac{\nu\cosh(\beta\nu/2)}{\nu-\omega}\right]\end{aligned}$$

Hence, the imaginary part of Kubo's susceptibility is also determined by $|f_O(E,\omega)|^2$:

$$\mathcal{I}\left[\chi_O(E,\omega)\right] = 2\pi\left[|f_O(E,\omega)|^2\sinh(\beta\omega/2) + \frac{\omega}{2}\frac{\partial|f_O(E,\omega)|^2}{\partial E}\cosh(\beta\omega/2)\right] = \frac{1}{2}\mathcal{S}_O^-(E,\omega). \tag{6.222}$$

If $\hat{O}$ is a local operator, or a sum of local operators, then the terms with derivatives of the total energy become unimportant for very large systems, and Eqs. (6.219) and (6.222) simplify to:

$$\mathcal{S}_O^+(E,\omega) \approx 4\pi\cosh(\beta\omega/2)|f_O(E,\omega)|^2, \quad \mathcal{I}\left[\chi_O(E,\omega)\right] \approx 2\pi|f_O(E,\omega)|^2\sinh(\beta\omega/2), \tag{6.223}$$

which imply the famous fluctuation-dissipation relation [219]:

$$\mathcal{S}_O^+(E,\omega) \approx 2\coth\left(\frac{\beta\omega}{2}\right)\mathcal{I}\left[\chi_O(E,\omega)\right]. \tag{6.224}$$

We see that, as with the fluctuation theorems, the fluctuation-dissipation relation does not rely on the assumption of a Gibbs distribution. It is satisfied for every eigenstate of a chaotic Hamiltonian (away from the edges of the spectrum, where ETH is expected to hold), and hence for any stationary ensemble with non-extensive energy fluctuations.

For finite systems, one can calculate corrections to the fluctuation-dissipation relation. For example, combining the relations in Eq. (6.217), one finds that

$$\begin{aligned}\left[\sinh\frac{\beta\omega}{2}\left(1-\frac{\omega^2}{4\sigma_c^2}\right) + \frac{\omega}{2}\cosh\frac{\beta\omega}{2}\partial_E\right]\mathcal{S}_O^+(E,\omega)\\ = \left[\cosh\frac{\beta\omega}{2}\left(1-\frac{\omega^2}{4\sigma_c^2}\right) + \frac{\omega}{2}\sinh\frac{\beta\omega}{2}\partial_E\right]\mathcal{S}_O^-(E,\omega),\end{aligned} \tag{6.225}$$

which replaces the standard relation

$$\sinh\frac{\beta\omega}{2}\mathcal{S}_O^+(E,\omega) \approx \cosh\frac{\beta\omega}{2}\mathcal{S}_O^-(E,\omega), \tag{6.226}$$

valid for Gibbs ensembles or for individual eigenstates in very large systems. This more general fluctuation-dissipation relation for individual eigenstates (6.225) still connects the noise and the dissipative response but in a more complicated way.

6.6.9 ETH and Two-Observable Correlations Functions

In the previous section we established a relation between $f_O(E,\omega)$ and the Fourier transform $S_O(E,\omega)$ of the nonequal-time correlation function of $\hat{O}$, see Eq. (6.217). Here, we discuss how the ETH ansatz for two observables $\hat{O}^{(1)}$ and $\hat{O}^{(2)}$ are related to their nonequal-time (connected) correlation function $\langle n|\hat{O}^{(1)}(t)\hat{O}^{(2)}|n\rangle_c$. Because of its experimental relevance, a case of particular interest is when $\hat{O}^{(1)} \equiv \hat{O}(x_1)$ and $\hat{O}^{(2)} \equiv \hat{O}(x_2)$. This because $\langle n|\hat{O}(x_1,t)\hat{O}(x_2,0)|n\rangle_c$ determines the $\hat{O}$–$\hat{O}$ structure factor. Another commonly encountered situation correspond to $\hat{O}^{(1)}$ and $\hat{O}^{(2)}$ representing different components of some observable, such as the magnetization, the current, and the electric polarization.

We rewrite the ETH ansatz for the two observables [see Eq. (6.62)] as

$$O^{(j)}_{mn} = O^{(j)}(\bar{E})\delta_{mn} + \mathrm{e}^{-S(\bar{E})/2}\Upsilon^{(j)}_{mn}(E,\omega), \tag{6.227}$$

where $j = 1, 2$, and $\Upsilon^{(j)}_{mn}(E,\omega) \equiv f_{O^{(j)}}(E,\omega)\, R^{O^{(j)}}_{mn}$. This allows us to write

$$\langle n|\hat{O}_1(t)\hat{O}_2(0)|n\rangle_c = \int d\omega\, \mathrm{e}^{\beta\omega/2 - i\omega t} K_{12}(E+\omega/2,\omega), \tag{6.228}$$

where the noise kernel

$$K_{12}(E+\omega/2,\omega) \equiv \overline{\Upsilon^{(1)}_{nm}(E+\omega/2,\omega)\Upsilon^{(2)}_{mn}(E+\omega/2,\omega)}. \tag{6.229}$$

The overline indicates an average over states $|m\rangle$ within a narrow energy window, that is, at fixed E and ω (or, equivalently, an average over a fictitious Random Matrix ensemble).

It is apparent in the expressions above that the noise terms $R^{O^{(1)}}_{mn}$ and $R^{O^{(2)}}_{mn}$ must, in general, be correlated with each other, or else $\langle n|\hat{O}_1(t)\hat{O}_2(0)|n\rangle_c \equiv 0$. Hence, the assumption that they are random numbers with zero mean and unit variance is oversimplifying and only applicable if we are interested in $\langle n|\hat{O}(t)\hat{O}(0)|n\rangle_c$. In order to generalize ETH to deal with nonequal-time correlations of different observables, one can still take $\Upsilon^{(j)}_{mn}$ to be Gaussian with zero mean but its noise kernel with other observables generally needs to be nonvanishing.

Inverting Eq. (6.228), one has that

$$K_{12}(E+\omega/2,\omega) = \frac{\mathrm{e}^{-\beta\omega/2}}{2\pi} S_{12}(E,\omega), \tag{6.230}$$

where

$$S_{12}(E,\omega) = \int_{-\infty}^{\infty} dt\, \mathrm{e}^{i\omega t}\langle n|O_1(t)O_2(0)|n\rangle_c. \tag{6.231}$$

For nonequal-space correlation functions in translationally invariant systems, when indexes 1 and 2 represent spatial coordinates x_1 and x_2 for a given observable $\hat{O}$, one can write

$$K_{12}(E+\omega/2,\omega) \equiv K(E+\omega/2,\omega,x_1-x_2). \tag{6.232}$$

In this case it is convenient to define the spatial Fourier transform K and work in the momentum space, as one does with structure factors. If the system exhibits Lorentz or Galilean invariance one can further restrict the functional form of the noise kernel.

We note that, as we did in Sec. 6.6.8, one can further simplify Eq. (6.228) splitting the correlation function into its symmetric and antisymmetric parts and Taylor expanding the noise kernel $K_{1,2}(E+\omega/2,\omega)$ with respect to the first argument. However, we should stress that the extension of ETH that we have introduced in this section still needs to be verified numerically. In particular, one needs to understand the regime of validity of the Gaussian ansatz and its applicability to the study of higher order correlation functions. These important questions are left open to future investigations.

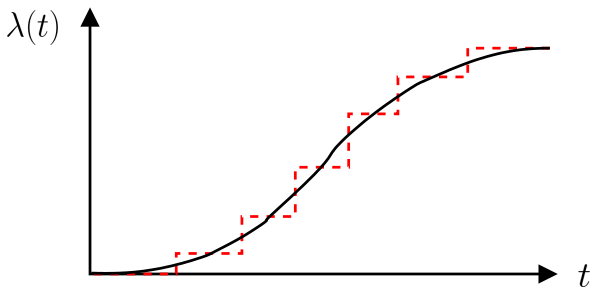

Figure 6.25: Schematic representation of a continuous process as a series of quenches followed by relaxation to the diagonal ensemble. This approximation is justified if the relevant relaxation time in the system is short compared to the characteristic time scale associated with the change of λ.

6.7 Application of Einstein's Relation to Continuously Driven Systems

In this section, we discuss several examples illustrating how one can use the Einstein relation to obtain nontrivial information about driven systems. We focus first on driven isolated systems which, in the absence of the drive, have only one conserved quantity (energy). We study the energy distribution obtained after a generic quasi-static process, where the driven system is approximately in equilibrium at each moment of time. Schematically, a quasi-static process in an isolated system can be represented as a series of small quenches and relaxation to the diagonal ensemble (see Fig. 6.25). As described in the previous section, the same setup applies to continuous driving protocols provided that the relevant relaxation time in the system is fast compared to time over which the energy of changes significantly.[39] As we will show, this setup, besides being common, allows one to take full advantage of the predictive power of the fluctuation theorems to derive results even if the overall energy change in the process is not small, and which, as we will see, might lead to energy distributions that are non-thermal. This setup is analogous to heating in a microwave oven. In the latter, heating occurs not due to the coupling to an external heat reservoir (like in the conventional oven) but rather due to the non-adiabatic work performed by the time-dependent electromagnetic field, see Fig. 6.26. Even though this field is periodic in time, the typical relaxation time in the system is much faster than the pulse frequency and therefore the process is quasi-static. Such a process is quasi-static but it is *not* adiabatic since each electromagnetic pulse performs irreversible work $d\tilde{Q}$ [see Eq. (6.139)] on the system. That work accumulates and leads to heating. This heating can be described by the Fokker-Planck drift-diffusion equation, where the drift and diffusion terms are connected by Einstein's relation (see Sec. 6.6.4).

In what follows, we apply these relations to several setups and show how they allow one to make nontrivial statements about the asymptotic energy distribution after long times. Moreover, one can even predict the existence of dynamical phase transitions. All the examples analyzed in this section are classical. The reason is that microscopic simulations of long-time dynamics in quantum chaotic systems are very difficult. It is expected, however, that the general expressions and the Fokker-Planck formalism apply equally to classical and quantum systems.

[39] In standard thermodynamics, by a quasi-static process one usually understands a process in which the irreversible work comes from heat exchange with a heat bath. However, such a definition is very restrictive.

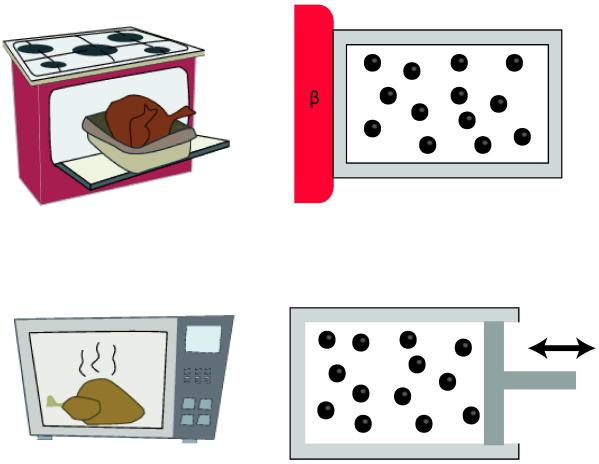

Figure 6.26: Schematic comparison between the usual thermal heating (traditional oven, top) and an energy increase due to non-adiabatic work (microwave oven, bottom).

6.7.1 Heating a Particle in a Fluctuating Chaotic Cavity

We start by considering a very simple problem, that of a classical particle bouncing elastically in a cavity in two spatial dimensions. When the cavity is stationary, the energy of the particle is conserved. If the cavity is chaotic, in the long-time limit, the particle reaches a uniform position distribution and an isotropic momentum distribution. We consider a process in which the system is repeatedly driven by deforming the cavity. At the end of each cycle, the cavity comes back to its original shape[40] and the system is allowed to relax in the sense described above (see Fig. 6.27). In a single collision with the moving wall, the particle's kinetic energy can either increase or decrease. However, it will always increase on average and eventually the particles velocity will become much greater than the velocity of the wall, so that the work per cycle automatically becomes small. The assumption that the cavity is chaotic implies that there are no correlations between consequent collisions. If this is the case, then one can consider a continuous driving protocol instead of repeated quenches and all the results will be the same. Such a setup was analyzed by Jarzynski [213] followed by other works [220, 221, 222, 193, 223, 224]. An interesting and nontrivial result that emerges from this analysis is a nonequilibrium exponential velocity distribution (to be contrasted with the Gaussian Maxwell distribution). Here, we analyze this problem in two ways. First, using standard kinetic considerations and then using the Einstein relation.

Let us denote the velocity of the particle as $\vec{v}$ and velocity of the wall as $\vec{V}$. Note that the wall velocity is perpendicular to the boundary and, by convention, it points outward, that is, $\vec{V} = V\hat{n}$, where $\hat{n}$ is the outward normal vector to the boundary. Since we assumed that the cavity deformations are volume preserving $\vec{V}$ averaged either over time, or over the boundary of the cavity, is zero. By elementary kinematics we know that, during a collision, the component of the relative velocity perpendicular to the boundary is reversed while the component parallel to the boundary is unchanged:

$$\vec{v} \to \vec{v}' = \vec{v} - 2\left(\vec{v}\cdot\hat{n} - \vec{V}\cdot\hat{n}\right)\hat{n} = \vec{v} - 2\left(\vec{v}_\perp - \vec{V}\right), \tag{6.233}$$

where, in the last equality, we have used that $\vec{V} = V\hat{n}$ and $\vec{v}_\perp \equiv v_\perp\,\hat{n} = (\vec{v}\cdot\hat{n})\,\hat{n}$. Note that for a collision to happen we need to have $v_\perp - V > 0$ indicating that the particle and the wall are

[40] This requirement can be further relaxed. It is only important that the cavity comes back to the original volume, as the density of states only depends on the volume.

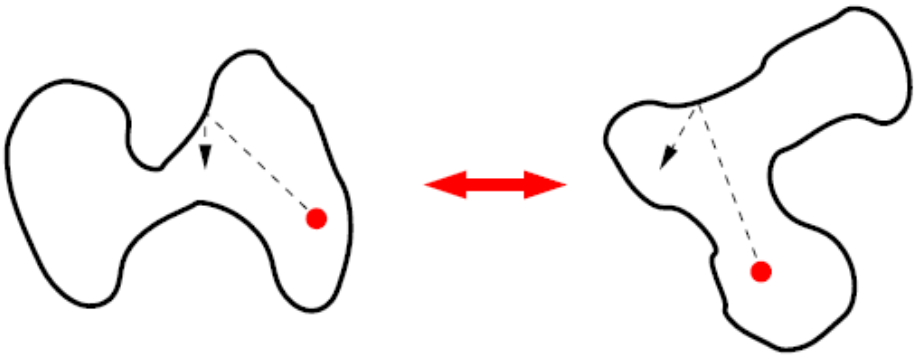

Figure 6.27: Schematic representation of a particle moving in a two-dimensional chaotic cavity with moving boundaries. The driving protocol consists in repeatedly deforming the cavity between the two shapes shown, while keeping its volume fixed.

approaching each other. As a check, we verify that when the boundary is stationary, that is, $\vec{V} = 0$, the update rule (6.233) simplifies to

$$\vec{v} \to \vec{v}\,' = \vec{v} - 2\vec{v}_\perp = \vec{v}_\parallel - \vec{v}_\perp \,, \tag{6.234}$$

where $\vec{v}_\parallel \equiv \vec{v} - \vec{v}_\perp$. As expected, this expression simply states that the perpendicular component of the velocity is reversed while the parallel component is unchanged.

The energy change of the particle during a collision is

$$\Delta E = \frac{m}{2}\left(|\vec{v}\,'|^2 - |\vec{v}|^2\right) = 2m\left(V^2 - V v_\perp\right). \tag{6.235}$$

We therefore see that the sign of the energy change depends on the sign of $V^2 - V v_\perp$. Combining this result with the constraint $v_\perp - V > 0$, which ensures that a collision takes place, we obtain that: i) the energy increases if the boundaries move inward, i.e., $V < 0$ and ii) the energy decreases if the boundaries move outward, i.e., $V > 0$. The probability of a collision per unit length, L, is proportional to the relative velocity between the particle and the wall $v_\perp - V$ (provided this is positive). For the collisions where the energy of the particle increases (i.e., $V < 0$) the latter is

$$p_> = \frac{c\,\delta t}{8L}(v_\perp - V)\;\theta\left(v_\perp - V\right) = \frac{c\,\delta t}{8L}(v_\perp + |V|)\;\theta\left(v_\perp + |V|\right), \tag{6.236}$$

where θ is the Heaviside step function, c is a proportionality constant (for many particles, c is proportional to the particle density), and 8 was introduced for convenience. On the other hand, for collisions in which the energy of particles decreases (i.e., $V > 0$) the probability of collision is

$$p_< = \frac{c\,\delta t}{8L}(v_\perp - V)\;\theta\left(v_\perp - V\right) = \frac{c\,\delta t}{8L}(v_\perp - |V|)\;\theta\left(v_\perp - |V|\right). \tag{6.237}$$

We are interested in the limit in which the wall moves slowly compared to the particle, i.e., $|v_\perp| \sim |v| \gg |V|$ and therefore the two-step functions above can be simplified to $\theta\left(v_\perp\right)$, indicating that $v_\perp > 0$. Rewriting expression (6.235) for the energy increasing (decreasing) collisions as

$$\Delta E_> = 2m\left(V^2 + |V||v_\perp|\right), \quad \Delta E_< = 2m\left(V^2 - |V||v_\perp|\right), \tag{6.238}$$

and using the expressions above for the collision probabilities, we find the average heating rate (energy drift) and the energy diffusion:

$$\begin{aligned} J_E &= \frac{1}{\delta t}\left[\Delta E_> p_> + \Delta E_< p_<\right] = c\, m\, V^2\, \overline{|v_\perp|}\, \theta(v_\perp), \\ D_E &= \frac{1}{\delta t}\left[(\Delta E_>)^2 p_> + (\Delta E_<)^2 p_<\right] \approx c\, m^2\, V^2\, \overline{|v_\perp|^3}\, \theta(v_\perp), \end{aligned} \tag{6.239}$$

where, in the second line, we have kept only the leading contribution in $|V|/v_\perp$. The overline indicates averaging over the velocity distribution. It is convenient to use polar coordinates, where $v_\perp = |\vec{v}|\cos(\phi)$ with $\phi \in [-\pi/2, \pi/2]$ to ensure $v_\perp > 0$. Using that the particle energy is $E = m|\vec{v}|^2/2$, we obtain

$$\begin{aligned} J_E &= \frac{c\, m\, V^2}{L}\left(\frac{2E}{m}\right)^{1/2} \frac{1}{2\pi}\int_{-\pi/2}^{\pi/2} d\phi \cos\phi, \\ D_E &= \frac{c\, m^2\, V^2}{L}\left(\frac{2E}{m}\right)^{3/2} \frac{1}{2\pi}\int_{-\pi/2}^{\pi/2} d\phi \cos\phi^3. \end{aligned} \tag{6.240}$$

Computing the integral over the angle ϕ, we obtain

$$J_E = C\sqrt{E}, \quad D_E = C\frac{4}{3}E^{3/2}, \tag{6.241}$$

where $C = c\, V^2\, \sqrt{2m}/(L\pi)$ is a constant with dimensions of $\sqrt{\text{energy}}/\text{time}$. Note that when computing the averages over $v_\perp$ in Eq. (6.240), we have used a uniform measure, that is, we took all angles ϕ to be equally probable. This is justified because the cavity is assumed to be chaotic. We note that the same analysis can be carried out in an arbitrary spatial dimension d. The only difference arises when computing the corresponding angular integrals. A straightforward generalization of the analysis above leads to:

$$J_E = C_d\sqrt{E}, \quad D_E = C_d\frac{4}{d+1}E^{3/2}, \tag{6.242}$$

where C_d is an overall constant that depends on the dimensionality d.

These coefficients satisfy the Einstein relation (6.187):

$$2J_E = \beta(E)D_E + \partial_E D_E. \tag{6.243}$$

To see this, we note that the single-particle density of states in d dimensions is $\Omega(E) \propto E^{(d-2)/2}$ and therefore

$$\beta(E) = \partial_E \ln[\Omega(E)] = \frac{d-2}{2E}. \tag{6.244}$$

Combining this with Eq. (6.242), it is easy to see that Einstein's relation is indeed satisfied. In fact, there was no need to carry out these relatively elaborate calculations. It was sufficient to note that J_E in all dimensions must be proportional to $\sqrt{E}$, which, for example, follows from the fact that the average number of collisions is proportional to $|v_\perp| \sim \sqrt{E}$. Then, the Einstein relation immediately fixes the energy diffusion D_E with respect to the energy drift J_E.

With relation (6.242) in hand, we can rewrite the Fokker-Planck equation describing the heating process in an arbitrary spatial dimension d as

$$\partial_t P(E,t) = -C_d\partial_E[\sqrt{E}P(E,t)] + \frac{2}{d+1}C_d\partial_{EE}[E^{3/2}P(E,t)]. \tag{6.245}$$

As a preliminary step, we define a new variable $t' = t\,C_d$ and write $\partial_t = C_d\,\partial_{t'}$ so that the constant C_d disappears from the Fokker-Plank equation for $P(E,t')$:

$$\partial_{t'} P(E,t') = -\partial_E[\sqrt{E}P(E,t')] + \frac{2}{d+1}\partial_{EE}[E^{3/2}P(E,t')] \tag{6.246}$$

We observe that, by a scaling analysis of this equation, $t' \sim \sqrt{E}$. Therefore, we can use the following scaling ansatz

$$P(E,t') = \frac{1}{2\alpha t'\sqrt{E}}\, f\left(\frac{\sqrt{E}}{\alpha t'}\right) \equiv \frac{1}{2t'\alpha\sqrt{E}}\, f(\xi). \tag{6.247}$$

where α is a constant of order one, which will be fixed later, and the prefactor $1/(2\alpha t'\sqrt{E})$ has been chosen so that the normalization condition becomes

$$1 = \int_0^\infty dE\, P(E,t') = \int_0^\infty \frac{dE}{2\alpha t'\sqrt{E}}\, f\left(\frac{\sqrt{E}}{\alpha t'}\right) = \int_0^\infty d\xi\, f(\xi). \tag{6.248}$$

By substituting ansatz (12.8) into the Fokker-Planck equation (6.246), we find:

$$2\alpha(1+d)f(\xi) + [2-d+2\alpha(1+d)\xi]\, f'(\xi) + \xi f''(\xi) = 0. \tag{6.249}$$

It is therefore convenient to choose $\alpha^{-1} = 2(1+d)$ so that the equation assumes a particularly simple form:

$$f(\xi) + (2-d+\xi)f'(\xi) + \xi f''(\xi) = 0 \quad \Rightarrow \quad f(\xi) = \frac{1}{(d-1)!}\, \xi^{d-1}\, e^{-\xi}, \tag{6.250}$$

where the normalization constant was fixed using Eq. (6.248).

Defining $\tau = \alpha t' = tC_d/[2(d+1)]$, we obtain the final result for the asymptotic energy distribution $P(E,\tau)$ (see also Refs. [223, 224]):

$$P(E,\tau) = \frac{1}{2(d-1)!}\frac{E^{\frac{d-2}{2}}}{\tau^d}\, e^{-\sqrt{E}/\tau}. \tag{6.251}$$

This distribution is *universal* in the sense that it does not depend on any details of the driving protocol. It is interesting to compare this result with the equilibrium canonical distribution at temperature β:

$$P_c(E,\beta) = \frac{1}{\Gamma[d/2]}\beta^{d/2}E^{\frac{d-2}{2}}\, e^{-\beta E}. \tag{6.252}$$

Clearly, these two distributions are different but share some properties. In particular, they both decay in energy faster than any power law so that all energy moments are well defined. However, $P(E,\tau)$ decay in energy is slower than the $P_c(E,\beta)$ one, that is, the former is "wider". To quantify this, we compute the first and second moments of the energy with respect both to $P(E,\tau)$ and $P_c(E,\beta)$:

$$\begin{aligned} \langle E\rangle_\tau &= \int_0^\infty dE\, EP(E,\tau) = d(d+1)\tau^2, \quad & \langle E^2\rangle_\tau &= d(d+1)(d+2)(d+3)\tau^4 \\ \langle E\rangle_c &= \int_0^\infty dE\, EP_c(E,\beta) = \frac{d}{2\beta}, & \langle E^2\rangle_c &= \frac{d(2+d)}{4\beta^2}, \end{aligned} \tag{6.253}$$

and define the relative energy width as a figure of merit to compare the width of the two distributions:

$$\frac{\sigma_\tau^2}{\langle E\rangle_\tau^2} \equiv \frac{\langle E^2\rangle_\tau}{\langle E\rangle_\tau^2} - 1 = \frac{6+4d}{d(d+1)}, \quad \frac{\sigma_c^2}{\langle E\rangle_c^2} \equiv \frac{\langle E^2\rangle_c}{\langle E\rangle_c^2} - 1 = \frac{2}{d}. \tag{6.254}$$

Clearly, the nonequilibrium distribution $P(E,\tau)$ is wider than $P_c(E,\beta)$ in any spatial dimension. In particular, as d increases from $d=1$ to $d=\infty$, the ratio of the relative energy widths changes from 2.5 to 2. In the analysis above, the dimensionality d only enters through the density of states. If we deal with a gas of weakly interacting particles in three dimensions, and the relaxation time of the gas is fast compared to the characteristic rate of energy change due to the cavity's motion, then the same analysis can be applied. The only difference is that $d \to 3N$, where N is the number of particles. Therefore, the result that the asymptotic width of the energy distribution of a driven gas is twice as large as the width of the Gibbs distribution applies to any weakly interacting many-particle gas in any spatial dimension. The gas asymptotically approaches a universal distribution (at least has universal energy fluctuations), but it is not the canonical distribution. In the examples that follow, we will show that a generalization of this result applies to arbitrary driven interacting systems.

Since the distribution $P(E,\tau)$ is a nonequilibrium distribution, it should also have lower entropy than the equivalent Gibbs distribution. The two entropies are

$$\begin{aligned} S_\tau &= -\int_0^\infty dE P(E,\tau) \ln\left[\frac{P(E,\tau)}{\Omega(E)}\right] = d(1+\ln\tau) + \ln\left(2\,\Gamma[d]\right), \\ S_c &= -\int_0^\infty dE P_c(E,\beta) \ln\left[\frac{P_c(E,\beta)}{\Omega(E)}\right] = \frac{d}{2}(1-\ln\beta) + \ln\left(\Gamma[d/2]\right). \end{aligned} \tag{6.255}$$

In order to compare these two entropies, we evaluate S_c at $\beta^{-1} = 2(d+1)\tau^2$ (so that the distributions $P(E,\tau)$ and $P_c(E,\beta)$ have identical average energy) and compute $S_c - S_\tau$:

$$S_c - S_\tau = \frac{d}{2}\ln\left[\frac{2(d+1)}{e}\right] + \ln\left(\frac{\Gamma[d/2]}{2\Gamma[d]}\right). \tag{6.256}$$

This function is positive and increases monotonically from 0.07 for $d=1$ to $(1-\ln 2)/2 \approx 0.15$ for $d \to \infty$. Note that, for large d, the first term of both entropies in Eq. (6.255) is proportional to d, so the relative difference between them decreases with the dimensionality.[41] According to our previous discussion, in a weakly interacting gas one has to substitute $d \to 3N$ so that, in the thermodynamic limit ($N \to \infty$), the driven gas has a thermal entropy up to subextensive corrections. If, conversely, we are dealing with a gas of noninteracting particles (implying that the their relaxation time is longer than the heating time) the entropy difference between the driven and the thermal gas will be extensive. This happens despite the fact that the total energy distribution of the noninteracting gas is still a Gaussian due to the central limit theorem. This extensive entropy difference can be used, for example, to build more efficient heat engines and even to beat the fundamental Carnot bound in some cases (see the discussion in Ref. [225]).

Let us note that the form of the distribution (6.251) was obtained under the assumption of constant driving, i.e., $V^2 = \text{const}$. If one uses feedback control mechanisms such that velocity of the wall is tied to the velocity of the particle, i.e., $V = V(E)$, then one can change the energy dependence of $J_E \propto V^2\sqrt{E}$ and, hence, change the resulting nonequilibrium distribution. One can even induce dynamical phase transitions (see the next example).

In passing, we note that the same results for the energy distribution have been derived in a the context of the Lorentz gas [226]. This gas is defined as a system of noninteracting light particles colliding with an interacting gas of heavy particles moving with an average velocity V. If the ratio of the masses is very large, then there is no effect of the collision on the heavy particles so the latter serve precisely the role of moving boundaries. In this case, the behavior of the light particles can be obtained exactly via the Lorentz-Boltzmann kinetic equation. It is interesting to note that the ensemble of heavy particles can be viewed as an infinite temperature heat bath. Indeed, the average energy of heavy particles $M\langle V^2\rangle/2$, which defines temperature,

[41] The β or τ independent terms in both entropies play no role in thermodynamics.

diverges in the limit $M \to \infty$ at fixed $\langle V^2 \rangle$. Thus, according to the general discussion of Sec. 6.6, this simple example shows that an external quasi-static driving of an isolated system is equivalent to the coupling to the infinite temperature bath.

While the single-particle example considered here is relatively simple, it teaches us several important lessons that can be extended to many-particle systems. In particular, it shows: (i) the possibility of nonequilibrium universal distributions, and (ii) that doubly stochastic evolution for quasi-static driving protocols is sufficiently constraining to predict such universality irrespective of the details of the driving protocol (in our example, the details are encoded in the overall constant C_d).

6.7.2 Driven Harmonic System and a Phase Transition in the Distribution Function

Next, we consider a driven single particle in a harmonic trap [193]. This particle is weakly coupled to a finite system composed of N identical particles, so that the overall system is ergodic. The details of the larger system define the density of states $\Omega(E)$, and therefore $\beta(E)$. Repeated impulses of short duration act on the particle and drive it away from equilibrium. The time scale between impulses is taken to be larger than the equilibration time of the particle. In addition, we assume that the coupling of the particle to the rest of the system is so weak that during the impulse it can be ignored. This setup can be easily generalized to impulses acting on an extensive number of particles. The energy of the particle ε (we use this notation to distinguish it from the total energy of the system E) between cycles is given by

$$\varepsilon = \frac{1}{2}kx^2 + \frac{p^2}{2}. \tag{6.257}$$

For simplicity, we work in one dimension. In Eq. (6.257), x is the coordinate of the particle, v its velocity, $m = 1$ its mass, and k is the spring constant. Because the system is ergodic and N is large, at any given energy of the system, the probability distribution for (x, v) before the impulse is Gibbs: $\rho(x, v) \propto \exp[-\beta(E)\varepsilon]$. We take the impulse magnitude to be $F(x)\delta t$, with δt short enough so that, during the impulse, the particle's position does not change appreciably and the coupling to the rest of the system can be ignored. Following the impulse, the momentum changes according to $p \to p + F(x)\,\delta t$. It is straightforward to calculate both the drift J_E and the diffusion constant D_E [193]:

$$J_E = \left\langle [F(x)]^2 \right\rangle \frac{\delta t^2}{\tau},$$
$$D_E = \frac{2}{\beta(E)} \left\langle [F(x)]^2 \right\rangle \frac{\delta t^2}{\tau},$$

where the angular brackets denote an average over $\rho(x, v)$ and τ is the time (or average time) between impulses. As in the previous example, one could have calculated J_E and deduced D_E from the Einstein relation. Note that here, in contrast to the single-particle example, the $\partial_E D_E$ term in the relation $2J_E = \beta(E)D_E + \partial_E D_E$ is a $1/N$ correction, which is negligible. Technically, this correction would amount to the fact that, at finite but large N, the single-particle distribution $\rho(x, v)$ slightly deviates from a Gibbs distribution.

Next, we consider the probability distribution for the energy of the system after the application of many impulses. To proceed, we have to assume a specific form for $\Omega(E)$ [or equivalently $\beta(E)$] and for $F(x)$. For simplicity, we take $\beta(E) \propto E^{-\alpha}$ and $F(x) \propto \mathrm{sign(x)}|\mathrm{x}|^{\mathrm{r}}$ so that

$$J_E \propto \langle x^{2r} \rangle \propto E^{\alpha r} \equiv E^s, \tag{6.258}$$

where we used $\langle x^2\rangle \propto \beta(E)^{-1} \propto E^{\alpha}$, with the first proportionality following from the equipartition theorem. For large N, due to the central limit theorem, the energy distribution is approximately Gaussian. Therefore, to characterize the distribution, it suffices to find the mean energy as a function of time and its variance as a function of the mean energy.

To find the relation between the mean energy and its variance, to leading order in $1/N$, we can multiply the Fokker-Planck equation (6.186) by E and E^2 and integrate over all energies. This yields the following differential equations describing the time evolution of $\langle E\rangle$ and $\sigma^2 = \langle E^2\rangle - \langle E\rangle^2$, where angular brackets stand for averaging over the probability distribution $P(E,t)$:

$$\begin{aligned}\partial_t\langle E\rangle &= \langle J_E\rangle \\ \partial_t\sigma^2 &= \langle D_E\rangle + 2\left(\langle J_E\, E\rangle - \langle J_E\rangle\,\langle E\rangle\right).\end{aligned}$$

Combining these equations yields

$$\frac{\partial\sigma^2}{\partial\langle E\rangle} = \frac{\langle D_E\rangle + 2\left(\langle J_E\, E\rangle - \langle J_E\rangle\,\langle E\rangle\right)}{\langle J_E\rangle}\,. \tag{6.259}$$

Moreover, if the energy distribution $P(E)$ is narrow, as is the case of large N, we can evaluate the averages within the saddle-point approximation. Using the Einstein relation $J_E = \beta(E)D_E/2$, we obtain:

$$\frac{\partial\sigma^2}{\partial\langle E\rangle} = \frac{2}{\beta(\langle E\rangle)} + 2\frac{\partial_E J_E(\langle E\rangle)}{J_E(\langle E\rangle)}\sigma^2(\langle E\rangle). \tag{6.260}$$

Integrating this equation between the initial energy of the system $\langle E\rangle_0$ and its final energy $\langle E\rangle$ gives

$$\sigma^2(\langle E\rangle) = \sigma_0^2\frac{J_E(\langle E\rangle)^2}{J_E(\langle E\rangle_0)^2} + 2J_E^2(\langle E\rangle)\int_{\langle E\rangle_0}^{\langle E\rangle}\frac{dE'}{J_E(E')^2\beta(E')} \tag{6.261}$$

where σ_0 is the initial width of the distribution and $\langle E\rangle_0$ is the initial mean energy.

We now use this equation in conjunction with the results obtained for the particle in a harmonic trap. In that case, the change of the mean energy of the system is given by

$$\partial_t\langle E\rangle = J_E(\langle E\rangle) = c\langle E\rangle^s\,. \tag{6.262}$$

Note that the values of α (recall that $\alpha r = s$), which define the specific heat exponents, are constrained by thermodynamic reasons to $0 < \alpha \leq 1$. The lower bound is required due to the positivity of the specific heat, and the upper bound assures that the entropy $[S(E) \propto E^{1-\alpha}]$ is an increasing unbounded function of the energy (the latter condition can be violated in systems with bounded energy spectrum). To prevent the energy of the system from diverging at finite time, we require $s \leq 1$ [as follows from integrating Eq. (6.262)].

For simplicity, we assume that $\sigma_0 \to 0$, that is, that we are starting from a very narrow microcanonical distribution. As done in Sec. 6.7.1, it is useful to compare the width σ^2 to the equilibrium canonical width $\sigma_c^2 = -\partial_\beta\langle E\rangle \sim \langle E\rangle^{1+\alpha}/\alpha$. This comparison reveals that, as the functional form of the impulse (specifically, the value of r) is changed, the system displays a *transition* between two behaviors. To see this, note that $\sigma^2(\langle E\rangle)$ is controlled by the exponent $\eta = 2\alpha r - \alpha - 1 = 2s - \alpha - 1$, which determines if the integral in Eq. (6.261) is controlled by its lower or upper bound: (i) When $\eta < 0$, the width is *Gibbs-like* with $\sigma^2/\sigma_c^2 \to 2\alpha/|\eta|$, that is, the ratio σ^2/σ_c^2 asymptotically approaches a constant value that can be either larger or smaller than one. Smaller widths correspond to protocols with large and negative s. Namely, protocols where J_E is a strongly decreasing function of the energy. (ii) When $\eta > 0$, there is a *run-away* regime. Here, the width increases with a higher power of the energy than the canonical width: $\sigma^2/\sigma_c^2 \sim E^{\eta}$. The resulting distribution is significantly wider than the canonical one. Given the

constraint on the value of s, this regime can only be reached if $\alpha < 1$ (in particular, this regime is unreachable for a driven classical ideal gas). The transition between the two regimes occurs when $\eta = 0$. In this case, $\sigma^2/\sigma_c^2 \sim 2\alpha \ln(\langle E\rangle/\langle E\rangle_0)$. One can show that close to this transition, when $|\eta| \ll 1$, there is a divergent time scale (in terms of the number of impulses) required to reach the asymptotic regime, see Ref. [193] for details. Therefore, this setup realizes a dynamical transition for the asymptotic energy distribution of the system, which is qualitatively similar to a continuous phase transition. The parameter η plays the role of the tuning parameter.

For concreteness, consider a system with $\alpha = 1/2$ (such as a Fermi liquid or the one-dimensional harmonic system above). When $r = 1$, we have $\eta = 2\alpha r - \alpha - 1 = -1/2$ and the resulting distribution is *Gibbs-like* with $\sigma^2/\sigma_c^2 = 2$. When $r = 3/2$, we are at the critical regime $\eta = 0$. Finally, for $r = 2$, one has $\eta = 1/2$ leading to the run-away regime with $\sigma^2/\sigma_c^2 \sim E^{1/2}$. Note that Eq. (6.261) implies that the existence of these three regimes is generic. In particular, depending on the functional form of $J_E(E)$ and $\beta(E)$, the variance of the distribution can be larger or, surprisingly, smaller than the width of the equilibrium Gibbs distribution at the same mean energy. Specifically, $\sigma^2(E)/\sigma_c^2(E)$ can be made arbitrarily small by a proper choice of $J_E(E)$. Also, the existence of the dynamical phase transition described for this simple model is only tied to whether the integral in Eq. (6.261) diverges or converges at high energy. The emergence of a nontrivial universal asymptotic behavior of the energy distribution is insensitive to the details of the driving protocol, such as the driving amplitude and shape of the pulse.

While in the examples in this section we focused on classical systems, the same conclusions apply to driven quantum systems (see Ref. [193] for specific examples). One can also anticipate nontrivial universal non-equilibrium distributions in driven systems with more than one conserved quantity. In this case, the Onsager relations will be responsible for constraining the mean flows of the conserved quantities and the flows of their fluctuations.

6.7.3 Two Equilibrating Systems

As a final example, we follow Ref. [214] and describe the equilibration of two weakly coupled systems, as those shown in Fig. 6.24, but with no particle exchange ($J_N = 0$). When one of the systems is much bigger than the other one, the bigger system serves as a heat bath for the small system and the two systems equilibrate at the temperature of the bath, which does not change during the equilibration process. The situation changes, however, when the two systems are comparable to each other, so that both systems are affected by the heat exchange. Assuming that the energy flow between the two systems is much slower than the characteristic relaxation time of each of the systems, and that the total energy $E_{\rm tot}$ is not fluctuating, we can again use the Fokker-Planck formalism and the analysis in the previous example. The only difference is that, instead of $\beta(E)$, we need to use $\Delta\beta(E) = \beta_{\rm I}(E_{\rm I}) - \beta_{\rm II}(E_{\rm II})$, where $\beta_{\rm I}$ and $\beta_{\rm II}$ are the temperatures of systems I and II, respectively, and $E_{\rm I}$ and $E_{\rm II}$ are their respective energies. The latter satisfy the constraint $E_{\rm I} + E_{\rm II} = E_{\rm tot} = \text{const}$. Then, instead of Eq. (6.261), we find the following expression for the energy fluctuations in system I:

$$\sigma_{\rm I}^2(\langle E_{\rm I}\rangle) = \sigma_{\rm I,0}^2 \frac{J_E(\langle E_{\rm I}\rangle)^2}{J_E(\langle E_{\rm I}\rangle_0)^2} + 2J_E(\langle E_{\rm I}\rangle)^2 \int_{\langle E_{\rm I}\rangle_0}^{\langle E_{\rm I}\rangle} \frac{1}{J_E(E')^2\,[\beta_{\rm I}(E') - \beta_{\rm II}(E_{\rm tot} - E')]} dE' \,, \quad (6.263)$$

where J_E is the rate of the heat flow into system I. This equation describes the evolution of the width of the energy distribution of system I. As the system equilibrates, one expects that

$$J_E = C(E - E_{\rm I}^{\rm eq}), \quad (6.264)$$

where $E_{\rm I}^{\rm eq}$ is the equilibrium steady-state mean energy of system I, for a given total energy $E_{\rm tot}$. Likewise

$$\beta_{\rm I}(E') - \beta_{\rm II}(E_{\rm tot} - E') \approx -\left(\frac{1}{\sigma_{\rm I,c}^2} + \frac{1}{\sigma_{\rm II,c}^2}\right)(E' - E_{\rm I}^{\rm eq}), \quad (6.265)$$

where $\sigma^2_{\mathrm{I},c} = -\partial E_{\mathrm{I}}/\partial\beta_{\mathrm{I}}$ is the variance of the energy distribution in the canonical ensemble of system I with mean energy $E^{\mathrm{eq}}_{\mathrm{I}}$ and, similarly, $\sigma^2_{\mathrm{II},c}$ is defined for system II. The two expressions above ensure that, in the steady state, when $E_{\mathrm{I}} = E^{\mathrm{eq}}_{\mathrm{I}}$, the (average) heat flux is zero and the temperatures of the two subsystems are identical. By substituting this expansion in Eq. (6.263), we find the asymptotic result for the energy fluctuations in system I after equilibration:

$$\sigma^2_{\mathrm{I}} = \sigma^2_{\mathrm{II}} \approx \frac{\sigma^2_{\mathrm{II},c}\sigma^2_{\mathrm{I},c}}{\sigma^2_{\mathrm{II},c} + \sigma^2_{\mathrm{I},c}}. \tag{6.266}$$

If one of the systems, say system I, is much smaller than the other, then this result simply implies that, after equilibration, the energy fluctuations in both systems are given by the canonical energy fluctuations of the *smallest* system. If the two systems are identical, then the energy fluctuations in either one of the systems are equal to one half of the canonical ones.

Equation (6.263) is, however, more general and can be used to study the full evolution of the distribution as the systems equilibrate (and not just the approach to the asymptotic result). Again, following Ref. [214], let us consider a specific example of a gas of hard spheres in a box. They are simulated using an event-driven molecular dynamics [227]. The gas has N_{I} particles of mass m_{I} and N_{II} particles of mass m_{II}, all of equal size. These groups of particles represent the two systems I and II. This setup is similar to the Lorentz gas analyzed in Sec. 6.7.1, which in turn is identical to a single particle in a chaotic cavity. The difference is that here the two masses are both finite while, in the Lorentz gas analyzed earlier, one type of atoms was infinitely heavier than the other. It is straightforward to check studying the collision between two particles that, if the two masses are very different, the energy transfer in each collision is small. In this case, a significant energy transfer occurs only over many collisions. Numerical simulations were repeated for many runs to evaluate the width of the distribution as a function of the average energy. In addition, during the evolution, the energy transfer between the two systems was evaluated and Eq. (6.263) was used to compute the width of the distribution. The results, shown in Fig. 6.28, indeed confirm the predictions of the Fokker-Planck derivation based on the Einstein relation for the open systems (6.188).

6.8 Integrable Models and the Generalized Gibbs Ensemble (GGE)

One of the focuses of this review has been understanding what happens in isolated nonintegrable quantum systems that are taken far from equilibrium by means of a sudden quench. We have discussed the relaxation dynamics of physical observables and their properties after relaxation. We explained that quantum chaos, through eigenstate thermalization, is the reason behind thermalization in those systems. In this section, we briefly discuss what happens in integrable systems. Such systems do not exhibit eigenstate thermalization.

We note that the very definition of quantum integrability is a topic of debate (see, e.g., Ref. [228, 229, 230]), but we will not touch upon that here. A rather standard definition of quantum integrability, based on the existence of an extensive number of local operators (or, more precisely, operators that are extensive sums of local operators) $\hat{I}_k$ that commute with the Hamiltonian and with each other, will be sufficient for the discussion here. The requirement that the conserved quantities are local/extensive is essential and it excludes the projection operators to the eigenstates of the Hamiltonian. In fact, for any quantum Hamiltonian, integrable or not, the projection operators to its eigenstates commute with the Hamiltonian and with each other, that is, they are conserved, but they are neither local nor extensive. As we have argued for quantum chaotic systems, the existence of those conserved quantities does not preclude the thermalization of physical observables. Exactly the same can be said about higher moments of the Hamiltonian, which are separately conserved but play no role both in equilibrium thermodynamics and in the thermalization of chaotic systems (see, e.g., the discussion in

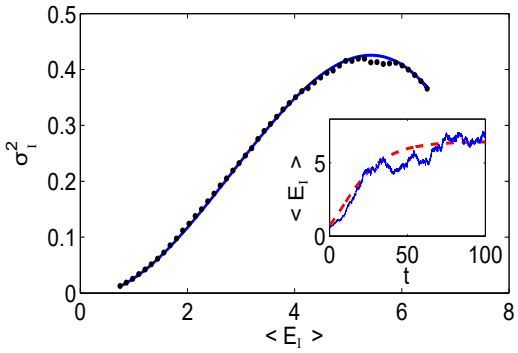

Figure 6.28: Equilibration of a system consisting of 50 particles with two different masses confined in a box. We plot results for $\langle E_{\rm I}\rangle$ vs σ^2 (dots), and compared them to the theoretical prediction in Eq. (6.263) (solid line). Inset: Energy $E_{\rm I}(t)$ in a single run (solid line), and the average energy $\langle E_{\rm I}\rangle(t)$ (dashed line). The particle numbers used in the simulations are $N_{\rm I} = 30$ and $N_{\rm II} = 20$. The initial velocities are sampled from a Maxwell-Boltzmann distribution with very different initial temperatures: $\beta_{\rm I} = 60$ and $\beta_{\rm II} = 3$. The total energy constraint is enforced by a (small) rescaling of the velocities of the $m_{\rm II}$-particles. The masses are chosen to be $m_{\rm I} = 10^{-4}$ and $m_{\rm II} = 1$ (in arbitrary units). The box is a unit cube with reflecting boundaries, and the added volume of the particles is taken to occupy a 5% of the volume of the box.

Sec. 6.4.3).

6.8.1 Constrained Equilibrium: the GGE

The main difference between chaotic and integrable systems becomes apparent already at the single-particle level, see Fig. 6.1. In the classical chaotic billiard any trajectory, after some time, uniformly fills the available phase space at a given energy. As a result, the long-time average and the microcanonical ensemble average of an observable agree with each other. In contrast, in the integrable cavity the particle's motion is constrained by other conserved quantities and the time average and the microcanonical ensemble average need not agree. Nevertheless, the particle might still uniformly fill the available phase space. This means that the long-time average could still be described by an ensemble average, but it needs to be a generalized microcanonical ensemble that accounts for all conserved quantities in the system [231].

In the quantum language, this amounts to saying that, in order to describe time averages of observables in integrable systems, one needs a constrained ensemble which is built using eigenstates of the Hamiltonian involved in the dynamics (they are selected by the initial state). As in classical systems, in which conserved quantities preclude the exploration of all phase space, the failure of integrable quantum systems to exhibit eigenstate thermalization can be traced back to the fact that they have an extensive number of nontrivial (local/extensive) conserved quantities $\{\hat{I}_k\}$, as opposed to the $\mathcal{O}(1)$ number of extensive conserved quantities in nonintegrable systems (energy, momentum, etc). Despite the existence of the conserved quantities $\{\hat{I}_k\}$, and because of dephasing (like in nonintegrable systems), observables in integrable systems are expected to relax to stationary values and remain close to those values at most later times.

Remarkably, in Ref. [232], the previous statements were shown to hold for an integrable model of hard-core bosons. Instead of a generalized microcanonical ensemble, a generalized grand canonical one was introduced in that work. It is now known as the GGE, whose density matrix:

$$\hat{\rho}_{\rm GGE} = \frac{\exp(-\sum_k \lambda_k \hat{I}_k)}{\mathrm{Tr}[\exp(-\sum_k \lambda_k \hat{I}_k)]}, \tag{6.267}$$

was obtained by maximizing the entropy [233, 234] under the constraints imposed by conserved quantities that make the system integrable. The values of the Lagrange multipliers were determined by requiring that, for all k's, $\mathrm{Tr}[\hat{\rho}_{\mathrm{GGE}}\hat{I}_k]$ equals the expectation value of $\hat{I}_k$ in the initial state. It is a priori not obvious that the exponential form in Eq. (6.267) is warranted. For extensive integrals of motion, one can justify the exponential form in the same way as it is done in traditional statistical mechanics, namely, noting that: (i) because of the equivalence of ensembles for subsystems, which is a direct consequence of the extensivity of the conserved quantities, the precise form of the distribution is not essential, and (ii) the exponential distribution leads to statistical independence of subsystems, which is naturally expected after relaxation in a system governed by a local Hamiltonian.

The fact that observables in integrable systems do not, in general, relax to the same values seen in thermal equilibrium, and that the GGE describes few-body observables after relaxation, has been verified in a large number of studies of integrable models. These can be either solved numerically for much larger system sizes than those accessible to full exact diagonalization or analytically solved in the thermodynamic limit [232, 235, 236, 237, 238, 239, 240, 131, 241, 242, 243, 244, 245, 246, 247, 248, 249, 250, 251, 252, 253, 254, 255, 133]. We should emphasize, however, that special initial states may still lead to nearly thermal expectation values of observables in integrable systems after relaxation [236, 256, 136, 145, 137, 257, 258, 259]. Hence, finding nearly thermal results for some initial states does not automatically mean that a system is nonintegrable. In what follows we discuss several examples for which the GGE can be used. These will highlight the reasons for its applicability.

Noninteracting Spinless Fermions

Noninteracting systems are possibly the simplest class of integrable systems. Let us discuss one particular noninteracting system that clarifies some important features of the GGE introduced above. We focus on noninteracting spinless fermions in a one-dimensional lattice (relevant to the hard-core boson system discussed in Sec. 6.8.1)

$$\hat{H}_{\mathrm{SF}} = -J\sum_{j=1}^{L-1}\left(\hat{f}_j^\dagger \hat{f}_{j+1} + \mathrm{H.c.}\right) + \sum_{j=1}^{L} u_j \hat{n}_j^f, \tag{6.268}$$

where $\hat{f}_j^\dagger$ ($\hat{f}_j$) is a fermionic creation (annihilation) operator at site j, $\hat{n}_j^f = \hat{f}_j^\dagger \hat{f}_j$ is the site j occupation operator, J is the hopping parameter, and u_j are arbitrary site potentials.

The single-particle Hamiltonian (6.268) can be straightforwardly diagonalized: $\hat{H}_{\mathrm{SF}}\hat{\gamma}_k^\dagger|0\rangle = \varepsilon_k\hat{\gamma}_k^\dagger|0\rangle$, where ε_k are the single-particle eigenenergies, $|k\rangle \equiv \hat{\gamma}_k^\dagger|0\rangle$ are the single-particle eigenstates, and $k = 1, 2, \ldots, L$. The occupations of the single-particle eigenstates $\hat{\eta}_k = \hat{\gamma}_k^\dagger\hat{\gamma}_k$ immediately form a set of L nontrivial *nonlocal* conserved quantities for a system consisting of many noninteracting spinless fermions. These conserved quantities *are not* extensive. However, carrying out the GGE analysis for this set of conserved quantities, imposing that $\mathrm{Tr}[\hat{\rho}_{\mathrm{GGE}}\hat{\eta}_k] = \langle\psi_I|\hat{\eta}_k|\psi_I\rangle \equiv \eta_k^I$, one finds that the Lagrange multipliers are given by the expression [232]

$$\lambda_k = \ln\left[\frac{1-\eta_k^I}{\eta_k^I}\right], \tag{6.269}$$

that is, the Lagrange multipliers are smooth functions of η_k^I.

In Fig. 6.29, we show results for η_k^I and λ_k after a quench in which a superlattice potential [$u_j = u(-1)^j$ in Eq. (6.268)] is turned off. In this quench the initial state is taken to be the ground state for $u_I \neq 0$ and the time evolution is carried out under a final Hamiltonian with $u = 0$. An important feature, made apparent by the results in Fig. 6.29, is that increasing the system size by a factor of 10 leads to essentially the same curve for η_k^I vs k but with

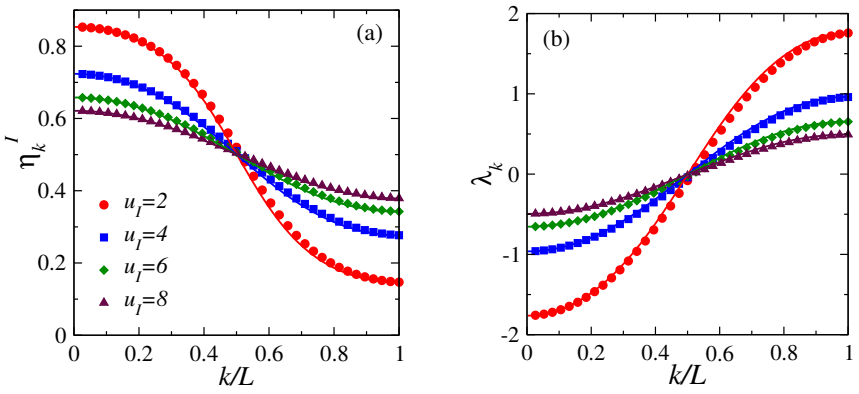

Figure 6.29: (a) Expectation value of the conserved quantities in quenches from $u_I \neq 0$ (as indicated in the figure) to $u = 0$. (b) The corresponding Lagrange multipliers. The conserved quantities are ordered such that ε_k increases with increasing k. The results denoted by symbols (lines) correspond to systems with $L = 38$ (380) sites at half-filling ($N = L/2$). Adapted from Ref. [136].

10 times the number of data points. This smooth dependence of λ on $k' = k/L$ allows one, for sufficiently large system sizes, to define extensive integrals of motion by taking the sum $\sum_{k' \in [k''-\delta k''/2, k''+\delta k''/2]} \lambda_{k'} \hat{\eta}_{k'}$ as being equal to $\lambda_{k''} \hat{\eta}'_{k''}$ where now $\hat{\eta}'_{k''} = \sum_{k' \in [k''-\delta k''/2, k''+\delta k''/2]} \hat{\eta}_{k'}$ is extensive. Hence, the mode occupations $\hat{\eta}_k$ can be thought of as being extensive in a coarse-grained sense and the justification of the GGE exponential form [see Eq. (6.267)] presented above remains valid [131, 136, 133]. The formal equivalence between the GGE constructed using occupation modes (as done here) and using extensive conserved quantities was established in Ref. [252]. It extends beyond noninteracting systems to integrable models that may or may not be mappable to noninteracting ones.

Having justified the applicability of the GGE to the occupation modes of the single-particle Hamiltonian of noninteracting many-particle systems, one can go a step further and prove that the GGE defined this way provides exact results for the time average of all one-body observables (without finite-size errors) [260, 132]. The proof, following Ref. [132], is straightforward. Projecting the many-body time-evolving wave function $\hat{\rho}(t) = |\psi(t)\rangle\langle\psi(t)|$ onto the one-body sector, and using the fact that all eigenstates of the many-body Hamiltonian are (antisymmetrized) direct products of the single-particle states $|k\rangle$, the time evolution of the one-body density matrix can be written as

$$\hat{\rho}_{\rm ob}(t) = \sum_{k,k'} c_{kk'} e^{-i(\varepsilon_k - \varepsilon_{k'})t} |k\rangle\langle k'|. \tag{6.270}$$

In the absence of degeneracies in the *single-particle* spectrum, the infinite-time average of $\hat{\rho}_{\rm ob}(t)$ can be written as

$$\overline{\hat{\rho}_{\rm ob}(t)} = \lim_{t' \to \infty} \frac{1}{t'} \int_0^{t'} dt\, \hat{\rho}_{\rm ob}(t) = \sum_k \eta_k^I |k\rangle\langle k|, \tag{6.271}$$

which is, by construction, the one-body density matrix within the GGE, as $\eta_k^I = \sum_n |\langle n|\psi_{\rm I}\rangle|^2 \eta_{k,n} \equiv {\rm tr}[\hat{\rho}_{\rm GGE}\, \hat{\eta}_k]$, where $\eta_{k,n} = 1$ ($\eta_{k,n} = 0$) if the single-particle state $|k\rangle$ is (is not) part of the particular many-body state $|n\rangle$, and ${\rm Tr}[\hat{\rho}_{\rm GGE}\, \hat{\gamma}_k^\dagger \hat{\gamma}_{k'}] \equiv 0$ for $k \neq k'$. We should emphasize at this point that this does not mean that all one-body observables equilibrate at their GGE values (they do not, see Refs. [238, 260, 132, 255]), but simply that their time average is given by the GGE prediction.

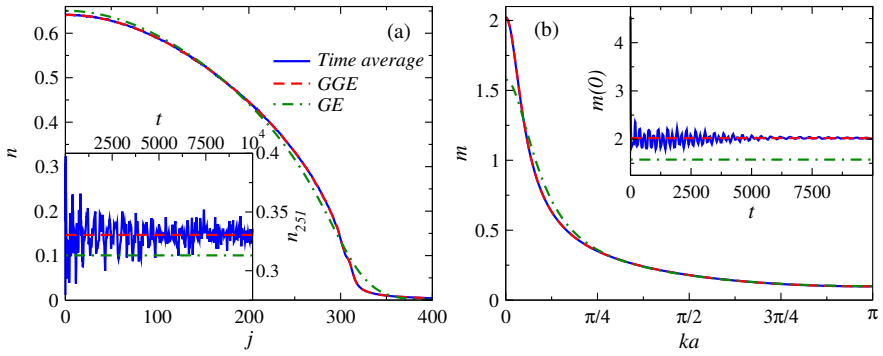

Figure 6.30: (Main panels) Site (a) and momentum (b) occupations in a trapped integrable system of hard-core bosons after a quench in which the initial state is the ground state of a trapped system ($v_I \neq 0$) in the presence of a superlattice potential ($u_I \neq 0$) and the dynamics is carried out in the presence of the same trap ($v = v_I$) but with no superlattice potential ($u = 0$), see text. Results are presented for the time average of the occupations after relaxation, as well as for the GGE and the grand canonical ensemble (GE) predictions. The insets show the dynamics of the occupation of site 251 (a) and of the zero momentum occupation (b). The horizontal lines correspond to the results in the GGE and grand canonical ensemble, as depicted in the main panels. The system has 900 sites and 299 hard-core bosons. Times are reported in units of $\hbar/J$, and k is reported in units of $1/a$, where a is the lattice spacing. See also Ref. [236].

Hard-Core Bosons

We now turn our attention to hard-core bosons, described by the Hamiltonian

$$\hat{H}_{\rm HCB} = -J\sum_{j=1}^{L-1}\left(\hat{b}_j^\dagger \hat{b}_{j+1} + \text{H.c.}\right) + \sum_{j=1}^{L} u_j \hat{n}_j^b, \tag{6.272}$$

where $\hat{b}_j^\dagger$ ($\hat{b}_j$) is the hard-core boson creation (annihilation) operator at site j, $\hat{n}_j^b = \hat{b}_j^\dagger \hat{b}_j$ is the site j occupation operator, J is the hopping parameter, and u_j are arbitrary site potentials. Hard-core bosons satisfy the same commutation relations as bosons but with the additional constraint that there cannot be multiple occupancy of any lattice site, i.e., $(\hat{b}_j^\dagger)^2 = \hat{b}_j^2 = 0$ [33].

The hard-core boson Hamiltonian above can be mapped onto a spin-1/2 chain through the Holstein-Primakoff transformation [261, 33] and the spin-1/2 chain onto the spinless fermion Hamiltonian in Eq. (6.268) via the Jordan-Wigner transformation [262, 33]

$$\hat{b}_j^\dagger \to \hat{f}_j^\dagger \prod_{\ell=1}^{j-1} e^{-i\pi \hat{f}_\ell^\dagger \hat{f}_\ell}, \quad \hat{b}_j \to \prod_{\ell=1}^{j-1} e^{i\pi \hat{f}_\ell^\dagger \hat{f}_\ell} \hat{f}_j, \quad \hat{n}_j^b \to \hat{n}_j^f. \tag{6.273}$$

This means that the dynamics of the hard-core boson site occupations is identical to that of the fermions, but the momentum distribution function of hard-core bosons, which involves a Fourier transform of one-body correlations in real space, is very different from that of the fermions. The hard-core momentum distribution function can be efficiently calculated for eigenstates of the Hamiltonian [263], for systems out of equilibrium [264], and in the grand canonical ensemble [265] using properties of Slater determinants. The conserved quantities to construct the GGE can be taken to be the same as for the noninteracting spinless fermions in Sec. 6.8.1, namely, single-particle mode occupations.

In Fig. 6.30, we show results for an integrable model of hard-core bosons in the presence of a harmonic trap after a quench in which a superlattice potential is turned off [236] – in this case, $u_j = v(j - L/2)^2 + u(-1)^j$, where v and u set the strength of the harmonic trap and the superlattice potential, respectively. In the main panels, one can see the time average of the

site (a) and momentum (b) occupation profiles after relaxation. They are clearly different from the predictions of a grand canonical ensemble for a system whose Hamiltonian is the one after the quench. The temperature and chemical potential of the grand canonical ensemble are fixed so that the mean energy and number of particles match those of the time-evolving state. We note that the system considered here is large enough so that the observed differences between the time-averaged profiles and the thermal predictions are not due to finite-size effects [236]. On the other hand, the predictions of the GGE, which like the grand canonical ensemble also has energy and particle number fluctuations, are indistinguishable from the results of the time average. The insets exemplify the relaxation dynamics by depicting the time evolution of the occupation of one site [Fig. 6.30(a)] and of the zero momentum mode [Fig. 6.30(b)]. They can both be seen to relax towards, and oscillate about, the GGE prediction. The grand canonical ensemble results are clearly incompatible with the results after relaxation. The amplitude of the fluctuations about the time average reveals another qualitative difference between nonintegrable and integrable systems. In quenches involving pure states in isolated integrable systems mappable to noninteracting models (and in the absence of localization), time fluctuations only decrease as a power law of the system size [131, 245, 266, 267, 260, 255]. This is to be contrasted to the exponential decrease of the amplitude of the time fluctuations as a function of the system size expected, and seen [185], in nonintegrable systems. In Ref. [185], it was argued based on numerical experiments that the time fluctuations of observables in integrable systems that are not mappable to noninteracting ones can also decrease exponentially fast with increasing system size.

6.8.2 Generalized Eigenstate Thermalization

One may ask at this point why is it that the GGE is able to describe observables after relaxation in isolated integrable systems following a quantum quench. After all, Eq. (6.60) is still dictating the dynamics and, once eigenstate thermalization does not occur, one might expect that the results after relaxation will depend on the *exponentially* large (in the system size) number of parameters $C_n \equiv \langle n|\psi_{\rm I}\rangle$ that are set by the initial state while the GGE depends only on a *polynomially* large number of parameters. As discussed in Ref. [131], the validity of the GGE can be understood in terms of a generalization of eigenstate thermalization in integrable systems. Namely, if eigenstates of integrable Hamiltonians with similar distributions of conserved quantities have similar expectation values of physical observables (we call this phenomenon generalized eigenstate thermalization[42]), then the GGE will describe those observables after relaxation following a quench. This can be understood as follows. In the diagonal ensemble (after quenches to integrable systems), the fluctuations of each extensive conserved quantity are expected to be subextensive for physical initial states – as we showed for the energy in Sec. 6.4.3. This, together with the fact that the GGE is constructed to have the same expectation values of conserved quantities as the diagonal ensemble and combined with generalized eigenstate thermalization, is what leads to the agreement between the GGE and the results after relaxation.

Numerical evidence for the occurrence of generalized eigenstate thermalization was presented in Refs. [131, 132] for integrable hard-core boson systems (similar to those in Fig. 6.30), and in Ref. [133] for the transverse field Ising model. In addition, for some observables, the occurrence of generalized eigenstate thermalization was proved analytically in Ref. [133]. In what follows, we review results for the transverse field Ising model.

The relation between the transverse field Ising model and the hard-core boson model in

[42] What changes from nonintegrable to integrable Hamiltonians is that, in the latter, the expectation values of few-body observables in any eigenstate are determined by the values of all conserved quantities and not just the energy.

Eq. (6.272) can be understood as follows. The hard-core boson chain can be mapped onto a spin-1/2 chain via:

$$\hat{S}_j^z = \hat{b}_j^\dagger \hat{b}_j - \frac{1}{2}, \quad \hat{S}_j^+ = \hat{b}_j^\dagger, \quad \hat{S}_j^- = \hat{b}_j. \tag{6.274}$$

After these substitutions, using that $\hat{S}_j^+ = \hat{S}_j^x + i\hat{S}_j^y$ and $\hat{S}_j^- = \hat{S}_j^x - i\hat{S}_j^y$, the Hamiltonian (6.272) reads

$$\hat{H}_{XX} = -2J \sum_{j=1}^{L-1} \left(\hat{S}_j^x \hat{S}_{j+1}^x + \hat{S}_j^y \hat{S}_{j+1}^y \right) + \sum_{j=1}^{L} u_j \left(\hat{S}_j^z + \frac{1}{2} \right), \tag{6.275}$$

This Hamiltonian is known as the isotropic XY model (or the XX model) in a transverse field. Its anisotropic version, for periodic boundary conditions in the presence of a uniform field of strength h, can be written as

$$\hat{H}_{XY} = -J\frac{(1+\gamma)}{2} \sum_{j=1}^{L} \hat{\sigma}_j^x \hat{\sigma}_{j+1}^x - J\frac{(1-\gamma)}{2} \sum_{j=1}^{L} \hat{\sigma}_j^y \hat{\sigma}_{j+1}^y + h \sum_{j=1}^{L} \hat{\sigma}_j^z, \tag{6.276}$$

where we used that $\hat{S}_j^\alpha = \hat{\sigma}_j^\alpha/2$, and γ is the anisotropy parameter. In the hard-core boson language, $\gamma \neq 0$ leads to non-number-conserving terms of the form $(\hat{b}_j^\dagger \hat{b}_{j+1}^\dagger + \text{H.c.})$. In the extreme anisotropic limit $\gamma = 1$, the model in Eq. (6.276) is known as the transverse field Ising model [268].

In Fig. 6.31, we show results for the weights of the many-body eigenstates of the transverse field Ising model (color coded in the scale on the right) as a function of the energy of the eigenstates and of the eigenstate expectation values of $\hat{\sigma}_j^x \hat{\sigma}_{j+2}^x$. In the top panels, we show weights in the diagonal ensemble and in the bottom panels we show weights in the GGE, in each case for three different system sizes. The black regions mark the existence of eigenstates with the corresponding eigenenergies and eigenstate expectation values, but with vanishing weight in the ensembles. The fact that those black regions do not narrow with increasing system size (they can be seen to slightly widen) is to be contrasted to the results in Fig. 6.13 for nonintegrable systems. The contrast makes apparent that in the transverse field Ising model eigenstate thermalization does not occur.

More remarkably, Fig. 6.31 shows that the eigenstates of the Hamiltonian with a significant weight in the diagonal ensemble and the GGE are located in approximately the same small region in the plane defined by the eigenstate energies and expectation values of $\hat{\sigma}_j^x \hat{\sigma}_{j+2}^x$ (see Ref. [133] for similar results for other observables). In Ref. [133], it was shown that, in both ensembles, the width of the energy distribution and of the distribution of expectation values of $\hat{\sigma}_j^x \hat{\sigma}_{j+2}^x$ vanishes as $1/\sqrt{L}$ with increasing system size. If one adds to this finding the fact that, in both ensembles, the mean value of the energy is the same by construction and the expectation value of $\hat{\sigma}_j^x \hat{\sigma}_{j+2}^x$ is found to agree, as in previous examples, one concludes that the eigenstates of the final Hamiltonian that determine the results in the diagonal ensemble and in the GGE in the thermodynamic limit are located at the same point in the aforementioned plane. Generalized eigenstate thermalization is reflected by the fact that the width of the distribution of eigenstate expectation values vanishes with increasing system size. These results make apparent that the exact distribution of weights in the diagonal ensemble and the GGE is irrelevant, the overwhelming majority of the states they sample have the same expectation values of the observable. This is why the GGE can predict the expectation values of observables in integrable systems after relaxation following a quench, even though the number of parameters required to construct the GGE increases polynomially with the system size while for the diagonal ensemble it increases exponentially with the system size. In this spirit, in Ref. [249] it was argued that a single representative state is sufficient to describe the relaxed state of integrable systems after a quench in the thermodynamic limit. This statement is indeed very reminiscent of ETH for nonintegrable systems.

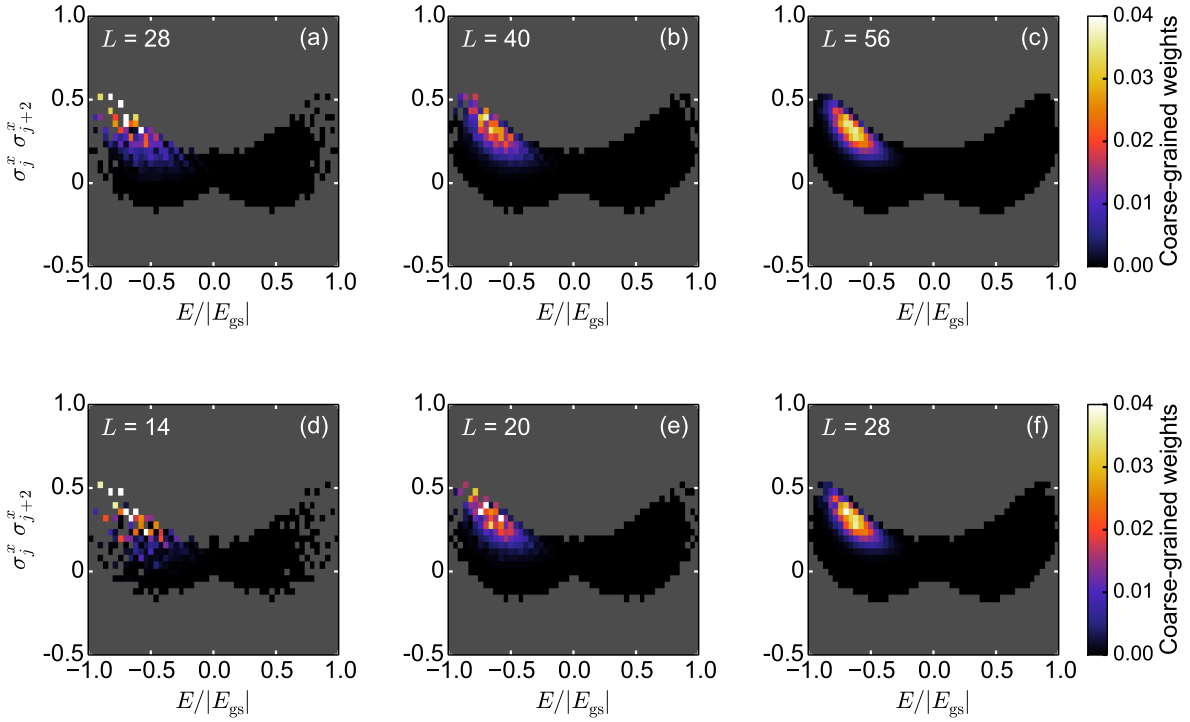

Figure 6.31: Density plots of the weights of the eigenstates of the transverse field Ising Hamiltonian [Eq. (6.276) with $\gamma = 1$ and $J = 1$] as a function of their eigenenergies and of the eigenstate expectation values of the next-nearest neighbor correlation function $\hat{\sigma}_j^x \hat{\sigma}_{j+2}^x$. Panels (a)-(c) depict the weights in the diagonal ensemble and panels (d)-(f) depict the weights in the GGE, in each case for three different system sizes. The initial state is the ground state for $h_I = 0.1$, and after the quench $h = 1.5$. Black pixels mark the presence of eigenstates (with vanishing weight), while gray pixels signal their absence. Colored pixels show the nonvanishing weights in the diagonal ensemble [panels (a)-(c)] and in the GGE [panels (d)-(f)]. These results were provided by Lev Vidmar (see also Ref. [133]).

Truncated GGE for the Transverse Field Ising Model

As for hard-core bosons, for the transverse field Ising model in Fig. 6.31 the GGE was constructed using occupations of single-particle fermionic quasiparticles (Bogoliubov fermions) [133]. Alternatively, one can construct a different equivalent set of integrals of motion, which are explicitly local and extensive. Following Ref. [252], these integrals of motion can be ordered according to their locality and come in pairs $\hat{I}_k^+$ and $\hat{I}_k^-$, such that $I_k^{+,-}$ contains sums of products of up to $k+2$ neighboring spin operators [252]. They can be written as

$$\begin{aligned}
\hat{I}_0^+ &= \hat{H} = -J \sum_j \hat{\mathcal{S}}_{j,j+1}^{xx} + h \sum_j \hat{\sigma}_j^z, \\
\hat{I}_1^+ &= -J \sum_j (\hat{\mathcal{S}}_{j,j+2}^{xx} - \hat{\sigma}_j^z) - h \sum_j (\hat{\mathcal{S}}_{j,j+1}^{xx} + \hat{\mathcal{S}}_{j,j+1}^{yy}), \\
\hat{I}_{n\geq 2}^+ &= -J \sum_j (\hat{\mathcal{S}}_{j,j+n+1}^{xx} + \hat{\mathcal{S}}_{j,j+n-1}^{yy}) - h \sum_j (\hat{\mathcal{S}}_{j,j+n}^{xx} + \hat{\mathcal{S}}_{j,j+n}^{yy}), \\
\hat{I}_n^- &= -J \sum_j (\hat{\mathcal{S}}_{j,j+n+1}^{xy} - \hat{\mathcal{S}}_{j,j+n+1}^{yx}),
\end{aligned} \tag{6.277}$$

where $\hat{\mathcal{S}}_{j,j+l}^{\alpha\beta} = \sigma_j^\alpha [\sigma_{j+1}^z \dots \sigma_{j+l-1}^z] \sigma_{j+l}^\beta$.

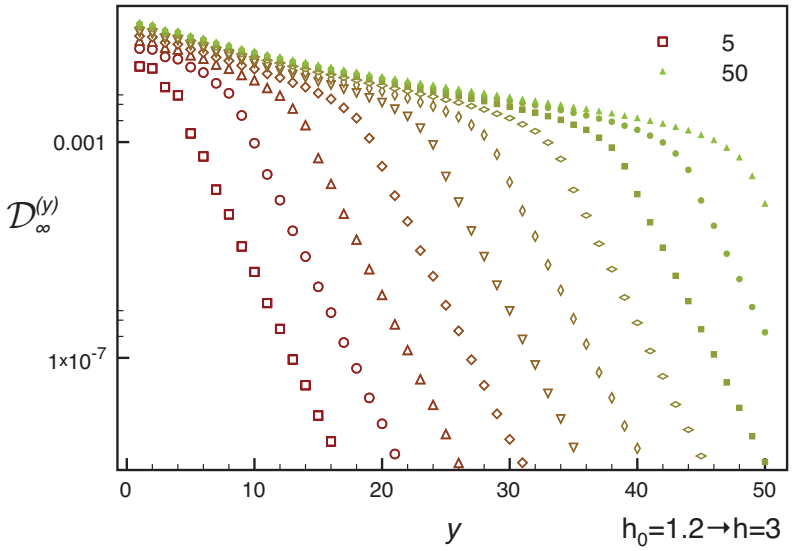

Figure 6.32: Norm distance $\mathcal{D}_\infty^{(y)}$, in the thermodynamic limit, between reduced density matrices in the GGE and in the truncated GGE obtained by imposing local conservation laws with support in at most $y+1$ consecutive sites, for a particular quench in the transverse Ising model. The subsystem size ranges from $l=5$ to $l=50$. The color and size of the symbols in the figure change gradually as a function of the subsystem size l. For $y>l$, the norm distance decays exponentially in y, with an l-independent decay constant. From Ref. [252].

An important question one might ask is, given a desired accuracy for some observable, how many conserved quantities are needed for the GGE to describe the result after relaxation. On this point, the locality of the observable and of the conserved quantities included in the GGE turn out to be crucial. For the model above, Fagotti et al. showed numerically that if one is interested in the reduced density matrix of a subsystem of size L', then only the first L' integrals of motion: $I_k^{+,-}$ with $k \lesssim L'$, that is, the integrals of motion that can "fit" on the subsystem, are important [252]. All other "less local" integrals of motion have an exponentially small effect on the subsystem (see Fig. 6.32). This is expected to be generic in integrable models, whether they are mappable or not to noninteracting ones.

6.8.3 Quenches in the XXZ model

An area of much current interest within the far from equilibrium dynamics of integrable systems is that of quenches in models that are not mappable to noninteracting ones. One model in this class, which is particularly important due to its relevance to experiments with ultracold bosons in one-dimensional geometries, is the Lieb-Liniger model. Studies of quenches within this model, in which repulsive interactions were suddenly turned on, revealed that the expectation values of conserved quantities diverge. As a result, a straightforward implementation of the GGE is not possible [269, 270]. A lattice regularization for this problem was discussed in Refs. [269, 254] (generalized eigenstate thermalization was argued to occur in this regularized model [254]). Despite progress in constructing GGEs for field theories [271], an explicit construction of the GGE for the Lieb-Liniger is still lacking.

Another model that has attracted much recent interest, and which is the focus of this subsection, is the XXZ model

$$\hat{H}_{XXZ} = -J \sum_{j=1}^{L} \left(\hat{\sigma}_j^x \hat{\sigma}_{j+1}^x + \hat{\sigma}_j^y \hat{\sigma}_{j+1}^y + \Delta\, \hat{\sigma}_j^z \hat{\sigma}_{j+1}^z \right). \tag{6.278}$$

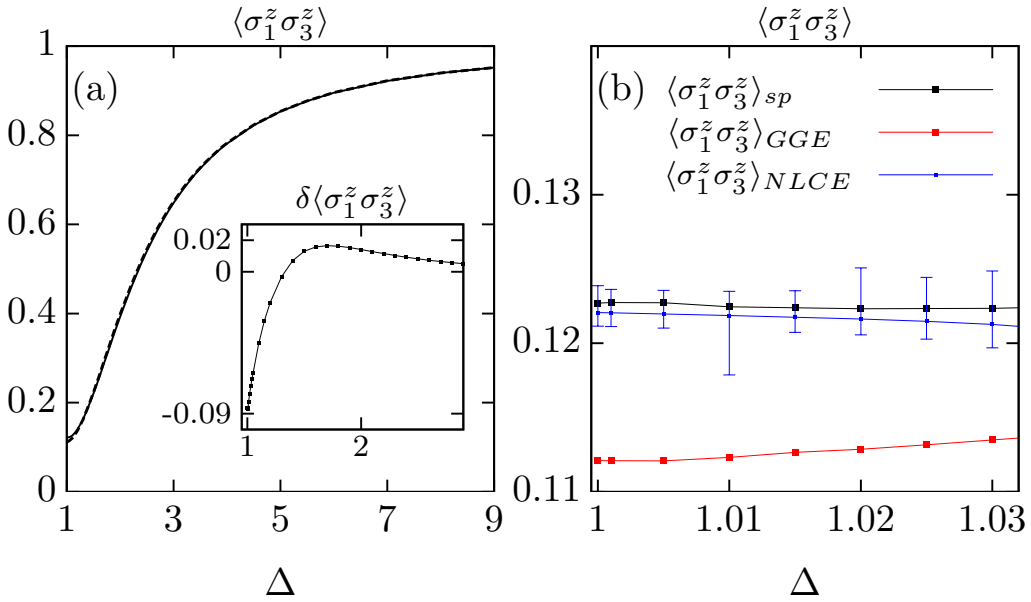

Figure 6.33: Quenches in the XXZ chain in the thermodynamic limit. (a) Next-nearest neighbor correlations $\langle\hat{\sigma}_1^z\hat{\sigma}_3^z\rangle$ following a quench starting from a Néel state to a finite value of the anisotropy parameter Δ. Results are reported for the expected steady state obtained using Bethe ansatz (solid line) and for the GGE prediction (dashed line). (b) Comparison between the steady state $\langle\hat{\sigma}_1^z\hat{\sigma}_3^z\rangle_{\rm sp}$, the GGE $\langle\hat{\sigma}_1^z\hat{\sigma}_3^z\rangle_{\rm GGE}$, and the NLCE for the diagonal ensemble $\langle\hat{\sigma}_1^z\hat{\sigma}_3^z\rangle_{\rm NLCE}$ results close to the isotropic point. The GGE results are seen to depart from the others. Error bars in the NLCE data display an interval of confidence. Inset in (a): Relative difference between the steady-state Bethe ansatz result and the GGE, $\delta\langle\hat{\sigma}_1^z\hat{\sigma}_3^z\rangle = (\langle\hat{\sigma}_1^z\hat{\sigma}_3^z\rangle_{\rm GGE} - \langle\hat{\sigma}_1^z\hat{\sigma}_3^z\rangle_{\rm sp}) / |\langle\hat{\sigma}_1^z\hat{\sigma}_3^z\rangle_{\rm sp}|$. From Ref. [272].

This model is, up to a possible boundary term, mappable onto the models in Eqs. (6.40) and (6.55) when $J' = V' = 0$. Studies of quenches in the XXZ model revealed that the GGE constructed using all known local conserved quantities at the time failed to describe few-body observables after relaxation [272, 273, 274, 275]. In Fig. 6.33(a), we show results for the next-nearest neighbor correlation $\langle\hat{\sigma}_1^z\hat{\sigma}_3^z\rangle$ in this model after a quench from an initial Néel state to a finite value of the anisotropy parameter Δ [equivalent to $V/(2J)$ in Eq. (6.55) for $J' = V' = 0$]. The results expected for that correlation in the steady state, which were obtained in the thermodynamic limit using Bethe ansatz, ($\langle\hat{\sigma}_1^z\hat{\sigma}_3^z\rangle_{\rm sp}$, continuous line) are almost indistinguishable from the GGE results ($\langle\hat{\sigma}_1^z\hat{\sigma}_3^z\rangle_{\rm GGE}$, dashed line). However, plotting the relative difference $\delta\langle\hat{\sigma}_1^z\hat{\sigma}_3^z\rangle = (\langle\hat{\sigma}_1^z\hat{\sigma}_3^z\rangle_{\rm GGE} - \langle\hat{\sigma}_1^z\hat{\sigma}_3^z\rangle_{\rm sp}) / |\langle\hat{\sigma}_1^z\hat{\sigma}_3^z\rangle_{\rm sp}|$, see the inset in Fig. 6.33(a), reveals that they are not identical. The differences are largest close to the isotropic Heisenberg point. Near that point, calculations using numerical linked cluster expansions (NLCEs) for the diagonal ensemble [135] after the same quench [276] agree with the steady-state predictions obtained using Bethe ansatz, see Fig. 6.33(b). The discrepancy between the GGE results and the others suggested that, given the set of conserved quantities selected, generalized eigenstate thermalization did not occur in this model (in Ref. [277], it was argued that it fails for integrable models that support bound states). Hence, other local conserved quantities (not known at the time) were expected to also be important. The extra conserved quantities needed were recently found [278, 279] and the GGE constructed using them has been shown to describe the steady state of observables after relaxation following the quench for the XXZ model described above [279].

It is important to emphasize at this point that we expect generalized eigenstate thermalization to be a generic phenomenon in integrable systems (as eigenstate thermalization is in

nonintegrable systems) and that, as a result, GGEs allow one to describe observables in integrable systems after relaxation. However, in contrast to nonintegrable systems in which the conserved quantities are trivial to find and, as a result, traditional statistical mechanics can be used almost as a black box, the same is not true in integrable systems. For the latter, a careful analysis needs to be done (specially for models that are not mappable to noninteracting ones) in order to identify the appropriate conserved quantities needed to construct the GGE.

In all quenches discussed so far for integrable systems, mappable or not mappable to noninteracting ones, the initial states were taken to be eigenstates (mostly ground states) of an integrable model. One may wonder whether the lack of thermalization we have seen in those quenches is a result of the special initial states selected. In order to address this question, NLCEs were used in Ref. [130] to study the diagonal ensemble results (in the thermodynamic limit) for observables in quenches to the $J' = V' = 0$ hard-core boson model in Eq. (6.55), which is the XXZ model (6.278) written in the hard-core boson language. The initial states for those quenches were taken to be thermal equilibrium states of Hamiltonian (6.55) for $\Lambda \equiv J'_I = V'_I \neq 0$, that is, thermal equilibrium states of a nonintegrable model. Those are the kind of initial states that one expects to have usually in experiments.

In Fig. 6.34, we show results for the relative entropy differences

$$\delta S_l = \frac{S_{18}^{\mathrm{GE}} - S_l^{\mathrm{DE}}}{S_{18}^{\mathrm{GE}}}, \tag{6.279}$$

between the grand canonical ensemble (GE) and the diagonal ensemble (DE) predictions, and the relative momentum distribution differences

$$\delta m_l = \frac{\sum_k \left| m_{k_l}^{\mathrm{DE}} - m_{k_{18}}^{\mathrm{GE}} \right|}{\sum_k m_{k_{18}}^{\mathrm{GE}}}, \tag{6.280}$$

also between the GE and the DE predictions, plotted as a function of the order l of the NLCE for the diagonal ensemble. The initial states were taken to have a temperature $T_I = 2J$ (the results for other initial temperatures are qualitatively similar [130]). After the quench, the temperature and chemical potential in the grand canonical ensemble were fixed so that the mean energy and number of bosons per site agree (up to machine precision) with those in the diagonal ensemble. The NLCE was carried out up to order $l = 18$. S_{18}^{GE} and $m_{k_{18}}^{\mathrm{GE}}$ were checked to be converged to the thermodynamic limit result up to machine precision (see Ref. [130] for details).

The results for δS_l and δm_l in Fig. 6.34 are qualitatively similar. For $\Lambda = 0$, that is, in the absence of a quench ($J'_I = V'_I = J' = V' = 0$), one can see that δS_l and δm_l vanish exponentially fast with increasing l, i.e., the convergence of the NLCE expansion to the thermodynamic limit result is exponential in l. However, as soon as $\Lambda \neq 0$, that is, as soon as there is a quench, the differences saturate to a nonzero value.[43] This means that the entropy and the momentum distribution function in the diagonal ensemble are different from their grand canonical counterpart in the *thermodynamic limit*. This is to be contrasted with the opposite quench, from integrable to nonintegrable points, for which the numerical results are consistent with vanishing $\delta S_{l\to\infty}$ and $\delta m_{l\to\infty}$ [130]. For quenches to the integrable point, the fact that $\delta S_{l\to\infty} \neq 0$ [as suggested by Fig. 6.34(a)] means that the energy distribution is not a smooth Gaussian function (or else $\delta S_{l\to\infty} = 0$, see Sec. 6.5.3). Hence, the sparseness of the energy density appears to be a generic feature in physically relevant quenches and not a consequence of specially fine-tuned initial states. This is why, after the quench, observables such as the

[43] The quantitative difference between the values at which each relative difference saturates is related to the fact that $\delta S_{l\to\infty} \propto \Lambda^2$ while $\delta m_{l\to\infty} \propto \Lambda$. This is something that was argued analytically and demonstrated numerically for $\delta S_{l=18}$ and $\delta m_{l=18}$ in Ref. [130], but that it is not important for the discussion here.

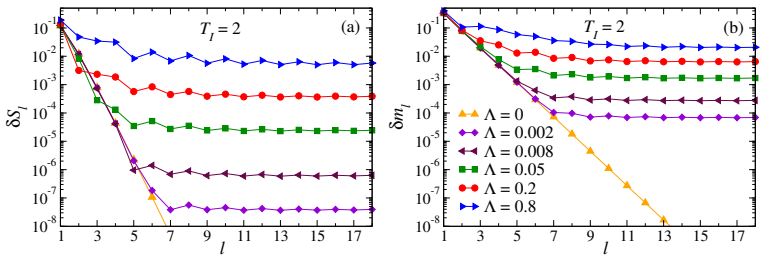

Figure 6.34: NLCE results after quenches in which the initial state is a thermal equilibrium state of the nonintegrable Hamiltonian (6.55) with $\Lambda \equiv J_I' = V_I' \neq 0$ and the system is quenched to $J' = V' = 0$, that is, to the integrable XXZ model written in the hard-core boson language. $J = V = 1$ remains unchanged during the quench. (a) Relative entropy differences δS_l [see Eq. (6.279)] and (b) relative momentum distribution differences δm_l [see Eq. (6.280)] vs the order l of the NLCE for the diagonal ensemble. Results are shown for $T_I = 2$ and six values of Λ. δS_l and δm_l for $\Lambda = 0$, that is, in the absence of a quench, decrease exponentially fast with the order l of the NLCE. All other differences saturate to a nonvanishing value reflecting lack of thermalization. Similar results were obtained in Ref. [130] for other initial temperatures and observables. Adapted from Ref. [130].

momentum distribution function do not thermalize [$\delta m_{l\to\infty} \neq 0$ as suggested by Fig. 6.34(b)]. The latter phenomenon also appears to be generic. These results highlight how careful one needs to be when using typicality arguments [142, 143, 144]. Those arguments might lead one to conclude that a fine-tuning of the initial state is needed for integrable systems not to thermalize after a quench, while this appears not to be the case in physically relevant situations.

6.8.4 Relaxation of Weakly Non-Integrable Systems: Prethermalization and Quantum Kinetic Equations

Integrable systems are unlikely to be found in nature. Nevertheless there are many examples of models which are nearly integrable, where the integrability breaking terms are irrelevant for relatively long times. As early as in 1834, Scott Russel observed the soliton created by a boat in a narrow canal near Edinburgh [280]. In our language, the solitary wave is an example of a macroscopic non-thermalizing perturbation. It was not until 30 years later that it was realized that this phenomenon can be attributed to the integrability of the Korteweg-de Vries (KdV) equation, which approximately describes water waves in narrow one-dimensional channels [281]. Since the KdV equation only provides an approximate description of the problem, one can expect that after long times the soliton will decay and the system will thermalize. Similarly, in a recent experiment with ultracold atoms [38], the lack of thermalization of the one-dimensional bosonic gas was attributed to the integrability of the Lieb-Liniger model that quite accurately describes those systems [33]. Like the KdV equation, the Lieb-Liniger model provides only an approximate description of the experimental system and there are various integrability breaking corrections that need to be taken into account at long times (see, e.g., Ref. [282]).

For nearly integrable systems, one can naturally expect a relatively fast relaxation to an approximate steady state determined by the integrable model, and then a much slower relaxation to the true thermal equilibrium. Such a scenario is now known under the name of prethermalization. This term was introduced by Berges et al. in the context of cosmology [283], though the ideas of multi-time thermalization are much older. Recently, several different prethermalization scenarios have been explored both theoretically and experimentally. Just to name a few: relaxation of weakly interacting fermions after an interaction quench [284, 285, 237, 183, 286, 287], prethermalization plateaus in various one-dimensional nonintegrable systems [288, 39, 289, 290,

291, 292, 293], prethermalization in interacting spin systems [294], two-dimensional superfluids with slow vortices and other topological defects [295, 296, 297], prethermalization after turning on a long-range interaction in a spinless Fermi gas in two dimensions [298], the emergence of nonthermal fixed points, and, in particular, the emergence of turbulence [299, 300, 301]. On the latter, it is actually interesting to note that a GGE based on momentum occupation numbers (for the limit of weakly interacting particles) can be used to explain Kolmogorov's law [299].

In few-particle classical systems, the KAM theorem ensures that chaotic motion does not appear immediately after one breaks integrability. Instead, one can have coexistence of regions of chaotic and regular motion. As the strength of integrability breaking perturbation increases, chaotic regions spread and eventually occupy all available phase space (see, e.g., Fig. 6.35). It is not known whether a similar scenario is realized in many-particle systems. If situations like that exist, so that an extensive number of integrals of motion can survive small integrability breaking perturbations then, instead of prethermalization, one can anticipate relaxation to a GGE defined with respect to deformed integrals of motion. Such deformations have been discussed in the literature for transitionally invariant integrable systems with small integrability breaking perturbations [302, 303, 292], and, in the context of many-body localization, for weakly interacting disordered systems [304, 305]. At the moment, it is unclear whether in non-disordered extended systems (either classical or quantum) in the thermodynamic limit there can be a finite threshold for ergodicity breaking. Thus, it is not clear whether the emerged deformed GGEs can only describe transient states (although potentially long lived) or can represent true steady states. The former scenario is probably more generic but we are not aware of any strong evidence for it.

Arguably, the most successful approach for describing relaxation of weakly interacting (i.e., weakly nonintegrable) systems to equilibrium is the kinetic theory (see, e.g., Ref. [189]). Recently, Stark and Kollar [306] derived kinetic equations using time-dependent perturbation theory applied to the GGE. These equations describe the relaxation from a prethermalized GGE to a thermal state. Below, we closely follow that work, extending it to arbitrary integrable systems.

Let us assume that we have an integrable system described by the Hamiltonian $\hat{H}_0$ and a weak integrability breaking perturbation $\hat{H}'$

$$\hat{H} = \hat{H}_0 + \hat{H}', \tag{6.281}$$

The Hamiltonian $\hat{H}_0$ commutes with a set of mutually commuting linearly independent integrals of motion $\hat{I}_k$, i.e., $[\hat{H}_0, \hat{I}_k] = 0$. For example, in the spirit of what was discussed in Sec. 6.8.1, in a system of interacting fermions or bosons, these integrals of motion can be the occupations of the single-particle eigenstates.

Let us now assume that the system is prepared in some nonequilibrium initial state, for example, by a quantum quench, and we are interested in its relaxation. If $\hat{H}'$ is a weak perturbation of $\hat{H}_0$, then, at short times after a quench, the system "does not know" that it is nonintegrable and the effect of $\hat{H}'$ on the dynamics is small and the system relaxes to an appropriate GGE, possibly described by deformed integrals of motion of $\hat{H}_0$. This was found to be the case numerically in several systems (see, e.g., Refs. [306, 292].) At long times, $\hat{H}'$ is expected to lead to relaxation to thermal equilibrium.

Since $\hat{H}'$ is assumed weak compared to $\hat{H}_0$, the dynamics generated by $\hat{H}'$ is slow compared to the dynamics generated by $\hat{H}_0$. This time scale separation translates into the fact that, at each moment of the evolution, the system is approximately stationary with respect to $\hat{H}_0$ so that it can be described by a GGE with *slowly* evolving Lagrange multipliers plus a *small*

correction $\delta\hat{\rho}(t)$. This leads to the following ansatz for the density matrix of the system:

$$\begin{aligned}\hat{\rho}(t) &\equiv \hat{\rho}_{\mathrm{GGE}}(t) + \delta\hat{\rho}(t),\\ \hat{\rho}_{\mathrm{GGE}}(t) &\equiv \frac{\exp(-\sum_k \lambda_k(t)\hat{I}_k)}{\mathrm{Tr}[\exp(-\sum_k \lambda_k(t)\hat{I}_k)]}.\end{aligned} \tag{6.282}$$

If the system thermalizes, one expects that the Lagrange multiplier associated with the energy approaches the inverse temperature β, while all others approach zero.

Since $\hat{H}'$ is small, it is convenient to go to the interaction picture with respect to $\hat{H}_0$:

$$\hat{\rho}_I(t) = \mathrm{e}^{-i\hat{H}_0 t}\hat{\rho}(t)\,\mathrm{e}^{i\hat{H}_0 t}, \qquad \hat{H}'(t) = \mathrm{e}^{i\hat{H}_0 t}\hat{H}'\mathrm{e}^{-i\hat{H}_0 t}. \tag{6.283}$$

where von Neumann's equation becomes:

$$i\partial_t\hat{\rho}_I(t) = [\hat{H}'(t), \hat{\rho}_I(t)]. \tag{6.284}$$

Our strategy will be to solve the von Neumann equation (6.284) using time-dependent perturbation theory with the GGE ansatz as the initial condition. This will allow us to find small changes in the expectation values of the integrals of motion $\langle\hat{I}_k\rangle$, which in turn define the Lagrange multipliers in the GGE (6.282). In this way, the slow evolution of $\hat{\rho}_{\mathrm{GGE}}$ is determined self-consistently:

$$d_t\langle\hat{I}_k\rangle = d_t\left(\mathrm{Tr}\left[\hat{I}_k\hat{\rho}_I(t)\right]\right) = \mathrm{Tr}\left(\hat{I}_k\partial_t[\hat{\rho}_I(t)]\right) = i\mathrm{Tr}\left(\hat{I}_k[\hat{\rho}_I(t), H'(t)]\right), \tag{6.285}$$

where we used Eq. (6.284), and that $\hat{I}_k$ is commute with $\hat{H}_0$ and thus remain time independent in the interaction picture. To leading order of perturbation theory in $\hat{H}'(t)$, we have $\hat{\rho}_I(t) \approx \hat{\rho}_{GGE}$,[44] and therefore

$$d_t\langle\hat{I}_k\rangle \approx i\mathrm{Tr}\left(\hat{I}_k\left[\hat{\rho}_{\mathrm{GGE}}, \hat{H}'(t)\right]\right) = 0. \tag{6.286}$$

The last equality follows from the cyclic property of trace and the fact that $\hat{\rho}_{\mathrm{GGE}}$ and $\hat{I}_k$ commute. Therefore, we have to go to the next order of perturbation theory: $\hat{\rho}_I(t) \approx \hat{\rho}_{GGE} + \delta\hat{\rho}_I(t)$, where from Eq. (6.284)

$$\delta\hat{\rho}_I(t) \approx i\int_{t_0}^{t} dt'[\hat{\rho}_{\mathrm{GGE}}, \hat{H}'(t')] = i\int_0^{t-t_0} d\tau[\hat{\rho}_{\mathrm{GGE}}, \hat{H}'(t-\tau)]. \tag{6.287}$$

Here, t_0 is some arbitrary time in the past. By substituting this correction to Eq. (6.285), we obtain

$$\begin{aligned}d_t\langle\hat{I}_k\rangle = i\mathrm{Tr}\left(\hat{I}_k[\delta\hat{\rho}_I(t), \hat{H}'(t)]\right) &\approx -\int_0^{t-t_0} d\tau\,\mathrm{Tr}\left(\hat{I}_k\left[\left[\hat{\rho}_{\mathrm{GGE}}, \hat{H}'(t-\tau)\right], \hat{H}'(t)\right]\right)\\ &= -\int_0^{t-t_0} d\tau\langle[[\hat{I}_k, \hat{H}'(t-\tau)], \hat{H}'(t)]\rangle_{\mathrm{GGE}},\end{aligned} \tag{6.288}$$

where, once again, we have used the cyclic property of the trace and the fact that $\hat{\rho}_{\mathrm{GGE}}$ and $\hat{I}_k$ commute. To simplify this expression further, we note that the correlation functions appearing in Eq. (6.288) depend only on time differences. Also, because the relaxation of nearly conserved integrals of motion is very slow compared to the time scales set by $\hat{H}_0$, the correlation functions appearing in the integral above decay fast so one can take the limit $t - t_0 \to \infty$. After these simplifications, one obtains the desired quantum kinetic equations for the integrals of motion

$$d_t\langle\hat{I}_k\rangle \approx -\int_0^{\infty} dt\langle[[\hat{I}_k, \hat{H}'(0)], \hat{H}'(t)]\rangle_{\mathrm{GGE}}. \tag{6.289}$$

[44] We note that the GGE density matrix is not affected by the transformation to the interaction picture.

Both the expectation value on the LHS and RHS of the equation above can be written in terms of the Lagrange multipliers specifying $\hat{\rho}_{\rm GGE}$ [see Eq. (6.282)]. Solving these equations, it is possible to determine the evolution of the Lagrange multipliers and therefore the slow relaxation of the GGE to the thermal equilibrium state. Being a set of coupled *scalar* equations, Eq. (6.289) is much simpler than the original von Neumann equation.

It is instructive to rewrite the kinetic equations using the Lehman representation in the basis of $\hat{H}_0$. Using the identity

$$\int_0^\infty dt e^{i(\epsilon_n-\epsilon_m)t} = \pi\delta(\epsilon_n-\epsilon_m) + \mathcal{P}\frac{i}{\epsilon_n-\epsilon_m}, \tag{6.290}$$

and, for simplicity, assuming that both the Hamiltonian and the integrals of motion are real, we rewrite Eq. (6.289) as

$$d_t\langle \hat{I}_k\rangle = 2\pi\sum_{nm}(\rho_{nn}^{GGE}-\rho_{mm}^{GGE})\langle n|\hat{I}_k|n\rangle|\langle n|\hat{H}'|m\rangle|^2\delta(\epsilon_n^0-\epsilon_m^0). \tag{6.291}$$

where ϵ_n^0 is the eigenvalue of $\hat{H}_0$ corresponding to eigenstate $|n\rangle$, i.e., $\hat{H}_0|n\rangle = \epsilon_n^0|n\rangle$. In this form, it becomes clear that the thermal distribution (where ρ_{nn} is only a function of energy) is a stationary solution of these kinetic equations, i.e., $d_t\langle\hat{I}_k\rangle = 0$ for any $\hat{I}_k$. Also, the delta function of $(\epsilon_n^0-\epsilon_m^0)$ ensures that $d_t\langle\hat{H}_0\rangle = 0$. So relaxation to thermal equilibrium occurs in the presence of energy conservation. Both properties are, of course, expected from general considerations.

Let us now apply the kinetic equation (6.288) to a common setup dealing with a gas of weakly interacting particles, bosons or fermions. For simplicity, we assume that they are spinless. Also, to shorten notations, we will use a scalar notation for the momentum modes, keeping in mind that this can be a vector index. Then the Hamiltonian reads

$$\hat{H}_0 = \sum_k \epsilon_k \hat{c}_k^\dagger \hat{c}_k \tag{6.292}$$

For the integrability breaking term, we take the usual (normal ordered) density-density interactions

$$\hat{H}' = \sum_{ij} V(i,j)\hat{c}_i^\dagger\hat{c}_j^\dagger\hat{c}_j\hat{c}_i = \sum_{k_1,k_2,k_3,k_4}\hat{c}_{k_1}^\dagger\hat{c}_{k_2}^\dagger V_{k_1,k_2,k_3,k_4}\hat{c}_{k_3}\hat{c}_{k_4}. \tag{6.293}$$

For translationally invariant interactions, V_{k_1,k_2,k_3,k_4} is nonzero only when $k_1+k_2 = k_3+k_4$, and it depends only on the transferred momentum $q = k_1 - k_3$. But, since our formalism applies even if translational invariance is broken, we will keep the interaction matrix element in the most general form. The obvious integrals of motion are the momentum occupation numbers $\hat{n}_k = \hat{c}_k^\dagger\hat{c}_k$. Let us first compute the commutator

$$[\hat{n}_{k'},\hat{H}'] = 2\sum_{k_2,k_3,k_4}[\hat{c}_{k'}^\dagger\hat{c}_{k_2}^\dagger V_{k',k_2,k_3,k_4}\hat{c}_{k_3}\hat{c}_{k_4} - \hat{c}_{k_2}^\dagger\hat{c}_{k_3}^\dagger V_{k_2,k_3,k',k_4}\hat{c}_{k'}\hat{c}_{k_4}], \tag{6.294}$$

where we used the invariance of the interaction matrix element with respect to permutation of k_1 with k_2 and k_3 with k_4. Plugging this into Eq. (6.289) and using Wick's theorem, which works for any GGE with quadratic integrals of motion, we find

$$\dot{n}_{k'} \approx 16\pi\sum_{k_2,k_3,k_4}(\tilde{n}_{k'}\tilde{n}_{k_2}n_{k_3}n_{k_4} - n_{k'}n_{k_2}\tilde{n}_{k_3}\tilde{n}_{k_4})|V_{k',k_2,k_3,k_4}|^2\delta(\epsilon_{k'}+\epsilon_{k_2}-\epsilon_{k_3}-\epsilon_{k_4}), \tag{6.295}$$

where $\tilde{n}_k = 1\pm n_k$ with a plus sign referring to bosons and a minus sign referring to fermions and $n_k = \langle\hat{n}_k\rangle$. Classical kinetic equations are obtained by taking the limit $n_k \ll 1$ and effectively

replacing $\tilde{n}_k$ by unity. Solving these kinetic equations can be tedious, but it is numerically feasible for very large systems. Let us check that the thermal distribution is a fixed point of these kinetic equations. For example, for fermions, the equilibrium distribution reads

$$n_k = \frac{1}{1+\exp[\beta(\epsilon_k-\mu)]} \tag{6.296}$$

then

$$\begin{aligned}\tilde{n}_{k'}\tilde{n}_{k_2}n_{k_3}n_{k_4} - n_{k'}n_{k_2}\tilde{n}_{k_3}\tilde{n}_{k_4} &= (1-n_{k'}-n_{k_2})n_{k_3}n_{k_4} - n_{k'}n_{k_2}(1-n_{k_3}-n_{k_4}) \\ &= \left[e^{\beta(\epsilon_{k'}+\epsilon_{k_2}-2\mu)} - e^{\beta(\epsilon_{k_3}+\epsilon_{k_4}-2\mu)}\right] n_{k'}n_{k_2}n_{k_3}n_{k_4} = 0, \end{aligned} \tag{6.297}$$

where the last equality relies on the total energy conservation. With more effort, one can show that the equilibrium fixed distribution is the attractor of the kinetic equations.

This example connects the ideas of GGE as a generic stationary state of integrable systems, prethermalized states as slowly evolving GGE states, and the kinetic theory as the perturbation theory in time describing the final evolution to thermal equilibrium. As previously mentioned, more work is needed to understand the generality of this approach and its applicability to systems other than those for which one can take the occupations of the single-particle eigenstates to be the nearly conserved quantities.

6.9 The Kicked Rotor

In this appendix, we discuss how chaos emerge in the simplest setup, namely, a driven single-particle system in one dimension. In the presence of driving there is no energy conservation and, as a result, the system is not integrable. The Hamiltonian of the *classical* kicked rotor reads

$$H(p,x,t) = \frac{p^2}{2} - K\cos(x)\sum_{n=-\infty}^{\infty}\delta(t-nT). \tag{6.298}$$

If one thinks of p as angular momentum and x as the canonically conjugate angle, this Hamiltonian describes a freely rotating particle that is periodically kicked at times $t = nT$. We choose the minus sign in front of K so that the time-averaged Hamiltonian reduces to a conventional pendulum with an energy minimum at $x = 0$ (there is no loss of generality as this sign can always be changed by $x \to x + \pi$). For simplicity, in what follows we refer to p and x as momentum and position, respectively.

The equations of motion for the kicked rotor are

$$\frac{dx}{dt} = \{x,H\} = \frac{\partial H}{\partial p} = p, \quad \frac{dp}{dt} = \{p,H\} = -\frac{\partial H}{\partial x} = -K\sin(x)\sum_{n=-\infty}^{\infty}\delta(t-nT). \tag{6.299}$$

These equations can be easily integrated between kicks. Let us denote by p_n and x_n the momentum and the position of the particle, respectively, just before the n-th kick, i.e., at time $t = nT - \epsilon$, where $\epsilon \to 0$. Then the equations of motion result in the following recursion relations

$$x_{n+1} = x_n + T\,p_{n+1}, \qquad p_{n+1} = p_n - K\sin(x_n). \tag{6.300}$$

These equations provide a discrete map (known as the Chirikov standard map) that allows one to uniquely determine the position and the momentum of the particle. If $nT < t < (n+1)T$, then $p(t) = p_{n+1}$ and $x(t) = x_n + p_{n+1}(t \bmod T)$. Note that one can confine momentum to any periodic interval of length $2\pi/T$. Indeed, from Eq. (6.300), it is obvious that shift of the momentum by $2\pi/T$ and the coordinate by 2π leaves the map invariant. Let us analyze the

time evolution that follows from this map. The dynamics is determined by the kick strength K, the period T, and the initial values of p and x. The map depends only on the product KT so we can set $T = 1$ and analyze the map as a function of K keeping in mind that $K \ll 1$ is equivalent to the short period limit.

If $K \ll 1$ and $p_0 \ll 1$, from Eqs. (6.300), one can see that both p and x change very little during each period. Hence, instead of solving discrete equations, one can take the continuum limit and write

$$\frac{\partial x}{\partial n} \approx p, \quad \frac{\partial p}{\partial n} = -K \sin(x) \ \rightarrow \frac{\partial^2 x}{\partial n^2} \approx -K \sin(x). \tag{6.301}$$

This equation describes the motion of a pendulum in a cosine potential, which is regular. Depending on the initial conditions there are two types of trajectories, corresponding to oscillations ($p \ll K$) and full rotations ($p \gg K$). A careful analysis shows that one does not need to assume that p is initially small, the only crucial assumption is that $K \ll 1$.

Next, one needs to check the stability of the obtained trajectories. It might happen that, if one includes corrections to the continuum approximation, chaos occurs. However, as proved by Kolmogorov, Arnold, and Moser (KAM) [62, 63, 64], this is not the case. As mentioned in the Introduction, the KAM theorem states that regular motion is stable against small perturbations. For the kicked rotor problem, one can check the stability of the solution above perturbatively. In particular, Eqs. (6.300) can be written as

$$x_{n+1} - 2x_n + x_{n-1} = -K \sin(x_n). \tag{6.302}$$

If K is small, we can assume that x is a nearly continuous variable. By expanding in Taylor series one gets

$$\frac{d^2x}{dn^2} + \frac{1}{12}\frac{d^4x}{dn^4} \approx -K \sin(x). \tag{6.303}$$

From the unperturbed solution, we see that (at least in the localized regime) the natural frequency of oscillations is $\sqrt{K}$. This means that, in Eq. (6.303), the term with the fourth derivative is proportional to K^2, that is, it is small when $K \ll 1$.

When K is large, the continuum approximation for the map fails. p and x "jump" from kick to kick. Since both are determined modulo 2π, one may guess that the motion is chaotic. A rigorous analytical proof that this is the case does not exist. Hence, we discuss indications for the occurrence of chaos for large values of K by analyzing the stability of the fixed points of the map:

$$x_{n+1} = x_n + p_{n+1} = x_n, \quad p_{n+1} = p_n - K \sin(x_n) = p_n. \tag{6.304}$$

There are only two possible solutions: $p_n = 0, x_n = 0$ and $p_n = 0, x_n = \pi$. Now, let us perturb the trajectories and see whether they remain stable. The linearized equations read

$$\delta x_{n+1} - 2\delta x_n + \delta x_{n-1} = -K \cos(x_n)\delta x_n = \mp K \delta x_n, \tag{6.305}$$

where the minus and plus signs refer to the fixed points $x = 0$ and $x = \pi$, respectively. In Eq. (6.305), one might recognize the equation of motion of coupled harmonic oscillators, where $\pm K$ plays the role of the frequency squared. For a harmonic chain, it is standard to introduce normal Fourier modes, i.e, $\lambda = \exp[iq]$. Here, we need to be careful because the frequency, $\sqrt{\pm K}$, can be imaginary. Because this is a translationally invariant system, we seek the solution of the form $\delta x_{n+1} = \lambda \delta x_n = \lambda^n \delta x_0$. Using our ansatz for the solution, Eq. (6.305) reduces to a simple quadratic equation

$$\lambda^2 - (2 \mp K)\lambda + 1 = 0, \tag{6.306}$$

which has two solutions

$$\lambda_{1,2} = 1 \mp \frac{K}{2} \pm \sqrt{\mp K + \frac{K^2}{4}}. \tag{6.307}$$

Let us analyze these solutions separately for the two fixed points. For $x = 0$, corresponding to the "$-$" sign, we have two solutions

$$\lambda_{1,2} = 1 - \frac{K}{2} \pm \sqrt{\frac{K^2}{4} - K}. \tag{6.308}$$

For $0 < K < 4$, the expression in the square root is negative leading to an imaginary contribution to λ. In the same range of K, the absolute value of the real part of λ is smaller than one. This means that the solution is stable. Indeed, if one introduces a small deviation to the stable position then, as the discrete time n increases, that deviation does not grow. Moreover, in this range, we can check that

$$|\lambda^2| = (1 - K/2)^2 + K - K^2/4 = 1 \tag{6.309}$$

implying that $\lambda = \exp[iq]$, as for a harmonic chain. This means that any small deviation leads to oscillations around the fixed point.

If $K > 4$, the outcome of introducing a small deviation is completely different. This is because now there are two real solutions for λ. The solution with the negative sign,

$$\lambda_2 = 1 - \frac{K}{2} - \sqrt{\frac{K^2}{4} - K}, \tag{6.310}$$

satisfies $|\lambda_2| > 1$. This means that any small deviation from the fixed point grows exponentially in time without bound, at least in the linearized regime. This exponential growth does not prove that the motion is chaotic, but is a strong indicator of it. The exponent characterizing the rate of growth, $\ln(\lambda)$, is called the Lyapunov exponent. In chaotic systems with many degrees of freedom, there are many Lyapunov exponents. Typically, the largest one determines the rate of divergence of nearby phase-space trajectories.

The analysis of the other fixed point, with $x = \pi$, is even simpler

$$\lambda_{1,2} = 1 + \frac{K}{2} \pm \sqrt{K + \frac{K^2}{4}}. \tag{6.311}$$

Clearly, for any positive K, there are two real solutions with one larger than one, that is, this point is always unstable. This is not surprising since this fixed point corresponds to the situation where a mass sits at a potential maximum. It is interesting that if, instead of δ kicks, one applies a fast periodic drive to the pendulum: $K = K_0 + a\sin(\nu t)$, one can stabilize $x = \pi$ to be an equilibrium position. This is known as the Kapitza effect (or Kapitza pendulum), and can be seen to occur in many physical systems [307, 66, 197].

In Fig. 6.35, we show phase-space portraits of the kicked rotor for different values of K. For small values of K (left panel), the motion is essentially regular everywhere except in the vicinity of the unstable fixed point $x = \pi$, $p = 0$. As K increases, chaotic regions gradually cover a larger and larger fraction of phase space. At $K = K_c$ (center panel), with $0.971635 \lesssim K_c < 63/64$ [309, 310, 311], there is a percolation transition. Isolated chaotic regions for $K < K_c$ percolate through phase space for $K > K_c$. This implies that the system can increase its energy without bound. For sufficiently large values of K, chaotic regions cover phase space almost entirely (right panel).

The Chirikov standard map can be quantized. A discussion of the quantum map can be found in Ref. [308], and references therein.

6.10 Zeros of the Riemann Zeta Function

Here, we discuss a remarkable manifestation of RMT, which highlights a connection between GUE statistics and prime numbers. There is no clear understanding of the origin of this

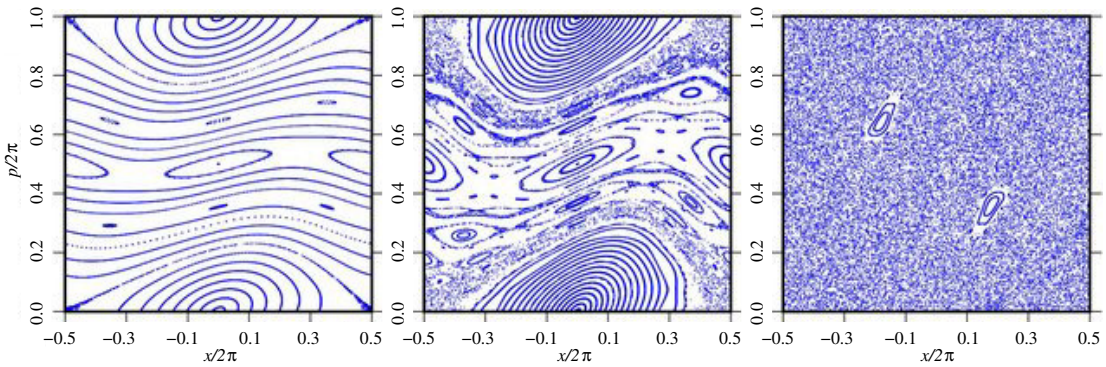

Figure 6.35: Phase-space portrait (Poincare cross-section) of the kicked rotor for different values of the parameter K. From left to right, $K = 0.5$, 0.971635, and 5. Images taken from scholarpedia [308].

connection and, at the moment, it represents one of the biggest mysteries associated with prime numbers. The Riemann zeta function $\zeta(s)$ is formally defined (for $\Re(s) > 1$) as

$$\zeta(s) = \sum_{n\geq 1} \frac{1}{n^s} \, . \tag{6.312}$$

For other values of s, it is defined by an appropriate analytic continuation through the integral:

$$\zeta(s) = \frac{1}{\Gamma(s)} \int_0^\infty \frac{x^{s-1}}{e^x - 1} \mathrm{d}x \tag{6.313}$$

As proved by Euler in 1859, the Riemann zeta function is related to prime numbers (again for $\Re(s) > 1$):

$$\zeta(s) = \prod_{p=\text{prime}} \frac{1}{1 - p^{-s}}. \tag{6.314}$$

The proof of this result is simple and elegant. Notice that we can construct a function $I_2(s)$

$$I_2(s) = \zeta(s) - \frac{1}{2^s}\zeta(s) = 1 + \frac{1}{3^s} + \frac{1}{5^s} + \dots \, , \tag{6.315}$$

which is a sum that lacks terms that are inverse powers of integer multiples of 2. Similarly, one can construct $I_3(s)$

$$I_3(s) = I_2(s) - \frac{1}{3^s} I_2(s) = \zeta(s) \left(1 - \frac{1}{2^s}\right) \left(1 - \frac{1}{3^s}\right) = 1 + \frac{1}{5^s} + \frac{1}{7^s} + \frac{1}{11^s} + \dots , \tag{6.316}$$

which is a sum that lacks terms that are inverse powers of integer multiples of 2 and 3. Continuing this exercise, and using the fundamental theorem of arithmetic, i.e., that any number has a unique decomposition into prime numbers, ones proves that, as $n \to \infty$, $I_n(s) \to 1$, and hence proves Eq. (6.314).

Equation (6.314) allows one to map $\zeta(s)$ onto the partition function of a noninteracting harmonic chain in which the frequencies of the normal modes are related to the prime numbers. The partition function for a single oscillator is

$$z_p(\beta) = \sum_n \exp[-\beta\omega_p n] = \frac{1}{1 - \exp[-\beta\omega_p]}. \tag{6.317}$$

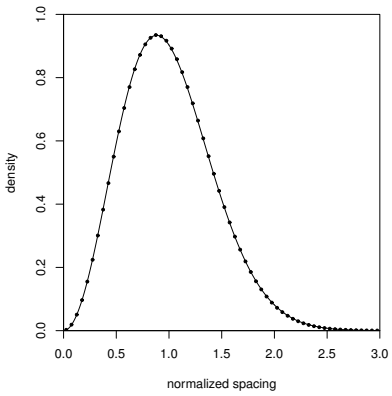

Figure 6.36: Distribution of the spacings between approximately one billion zeros of the Riemann zeta function near zero number $10^23+17,368,588,794$, and the statistics of level spacings in the Gaussian unitary ensemble (continuous line). These results were provided by Andrew Odlyzko (see also Ref. [316]).

If we associate prime numbers with normal modes, $\omega_p = \ln(p)$, and require that $\beta = s$, then

$$Z(\beta) = \prod_p z_p(\beta) = \zeta(\beta). \tag{6.318}$$

The (complex) zeros of the zeta function are thus the (complex) zeros of the partition function of this model. The zeros of the partition function are known as Fisher zeros [312], which are closely related to Yang-Lee zeros [313]. Condensation of these zeros near the real temperature axis is an indicator of a phase transition [312]. Recently, it was conjectured that concentration of Fisher zeros at complex infinity is related to the ergodicity of the system [314]. Physically, the Fisher zeros correspond to the zeros of the Fourier transform of the energy distribution function $P(E)$ (closely connected to the Loshmidt echo and zeros of the work distribution for the quench problems [315]). Indeed

$$P(E) = \frac{1}{Z(\beta)} \sum_n \exp[-\beta E_n] \delta(E_n - E) \tag{6.319}$$

where

$$Z(\beta) = \sum_n \exp[-\beta E_n] \tag{6.320}$$

is the partition function. Hence

$$\widetilde{W}(\tau) \equiv \int_{-\infty}^{\infty} dE\, P(E) \exp[iE\tau] = \frac{1}{Z(\beta)} \sum_n \exp[-(\beta - i\tau)E_n] = \frac{Z(\beta - i\tau)}{Z(\beta)}. \tag{6.321}$$

Thus, in the physics language, the complex zeros of the partition function $Z(\beta - i\tau)$ correspond to the zeros of the Fourier transform of the energy distribution for a system of phonons with normal modes given by the natural logarithm of the prime numbers.

Riemann's zeta function has many fascinating properties. One of them is that the nontrivial zeros of $\zeta(s)$, i.e., zeros that are nonnegative integers, lie on the line $\Re(s) = 1/2$. This conjecture is called the Riemann hypothesis and it remains one of the greatest unsolved problems in mathematics. By now, it has been checked for the first 10^{22} zeros [316]. Remarkably, the distribution of the normalized spacings of the zeros of Riemann's zeta function is the same as that of level spacings in the GUE (see Fig. 6.36). This agreement hints, as mentioned before, a deep connection between prime numbers and random numbers.

6.11 The Infinite Temperature State as an Attractor

To prove that the infinite temperature distribution is an attractor, let us recall that any stochastic matrix $\boldsymbol{M}$ or, equivalently, Markov matrix has one eigenvalue $\lambda_0 = 1$, while all the other eigenvalues have absolute value less or equal than one, i.e., $|\lambda_{\alpha>0}| \leq 1$ [190]. The eigenvalue $\lambda_0 = 1$ clearly corresponds to the steady state of the system while the others denote processes where the probability distribution decays to the steady state. The *left* and *right* eigenvectors corresponding to the eigenvalue $\lambda_0 = 1$ satisfy the relation

$$L_0 \boldsymbol{M} = L_0, \quad \boldsymbol{M} R_0 = R_0. \tag{6.322}$$

Note that, by construction, the right eigenvector R_0 is the steady-state probability distribution of the system so that its elements should, by normalization, sum to 1. By the conservation of probability, i.e., $\sum_m M_{n\to m} = 1$, and by direct substitution, it is easy to see that the *left* eigenvector is given by the constant vector $L_0 = (1, 1, \cdots, 1)$. Note that with this choice $L_0 \cdot R_0 = 1$. Of course, the *right* eigenvector R_0 depends on the details of the Markov matrix $\boldsymbol{M}$ and in general has a nontrivial structure.

To see this, let us decompose the vector of initial probabilities $\rho^{(0)}_{nn}$ in terms of the *right* eigenvectors as[45]

$$\rho^{(0)} = \sum_{\alpha=0}^{D} c_\alpha R_\alpha = R_0 + \sum_{\alpha>0}^{D} c_\alpha R_\alpha \tag{6.323}$$

where we have used the fact that the coefficients c_α are determined by projection on the *left* eigenvectors $c_\alpha = \sum_n \rho^{(0)}_{nn} (L_\alpha)_n$ and therefore $c_0 = 1$. Plugging the expression above into the master equation (6.107), we obtain

$$\rho^{(N)} = \sum_{\alpha=0}^{D} c_\alpha \left(\lambda_\alpha\right)^N R_\alpha \approx R_0 \tag{6.324}$$

where we have used that $c_0 = 1$, $\lambda_0 = 1$, and assumed that $|\lambda_{\alpha>0}| < 1$ so that $\lambda^N_{\alpha>0} \approx 0$. This equation shows that $\rho^{(N)}$ approaches the stationary state R_0 exponentially fast in the number of processes N. The only exception to this result is when the doubly stochastic matrix admits other eigenvalues with absolute value one. This situation, however, is not generic. It corresponds to systems that are not ergodic so that some portions of the configuration space cannot be accessed from others, see Appendix 6.12.

Doubly stochastic matrices $\boldsymbol{p}$ are a special subgroup of Markov matrices which, besides satisfying the conservation of probability $\sum_m p_{n\to m} = 1$, satisfy the additional constraint $\sum_n p_{n\to m} = 1$. This additional property allows one to prove that the *right* eigenvector corresponding to the $\lambda_0 = 1$ eigenvalue has the specific form $R^{\rm ds}_0 = (1/D, \cdots, 1/D)^T$, where D is the dimension of the matrix $\boldsymbol{p}$. Therefore, for a doubly stochastic matrix, the stationary state is the "infinite temperature state". To this end, we simply check explicitly that $\boldsymbol{p}\, R^{\rm ds}_0 = R^{\rm ds}_0$:

$$\boldsymbol{p}\ R^{\rm ds}_0 = \boldsymbol{p} \begin{pmatrix} 1/D \\ \vdots \\ 1/D \end{pmatrix} = \begin{pmatrix} D^{-1} \sum_m p_{1\to m} \\ D^{-1} \sum_m p_{2\to m} \\ \vdots \end{pmatrix} = \begin{pmatrix} D^{-1} \\ D^{-1} \\ \vdots \end{pmatrix} = R^{\rm ds}_0, \tag{6.325}$$

where the third equality follows directly from the doubly stochastic condition (6.92). Next, we prove that $|\lambda_\alpha| \leq 1$. Let us assume that there is an eigenvalue λ_α larger than one. Then, the corresponding eigenvector R_α grows exponentially under the repeated action of $\boldsymbol{p}$, that is,

[45] In this discussion, we ignore cases in which the Markov matrix cannot by diagonalized. The proof can be extended to these cases as well.

$\boldsymbol{p}^N R_\alpha = \lambda_\alpha^N R_\alpha$. This implies that there are entries of $\boldsymbol{p}^N$ that are larger than one. However, $\boldsymbol{p}^N$ is a product of doubly stochastic matrices so it is itself a doubly stochastic matrix (see Sec. 6.5.1). Therefore, all its entries need to be smaller than one, see Eq. (6.94). As a result, we conclude that there cannot be any eigenvalue larger than one.

6.12 Birkhoff's Theorem and Doubly Stochastic Evolution

Birkhoff's theorem [191] states that any doubly stochastic matrix is given by the convex sum of permutation matrices $\mathbf{\Pi}_\alpha$:

$$\mathbf{p} = \sum_\alpha k_\alpha \mathbf{\Pi}_\alpha, \quad \sum_\alpha k_\alpha = 1, \quad 0 \leq k_\alpha \leq 1. \tag{6.326}$$

We can then rewrite the doubly stochastic master equation (6.89) as

$$\rho^{(1)} = \mathbf{p}\,\rho^{(0)} = \sum_\alpha k_\alpha \mathbf{\Pi}_\alpha \rho^{(0)} \tag{6.327}$$

When only one permutation matrix contributes, the master equation simply describes a perfect transfer of population between two states. For example, for a three level system in which only one permutation matrix contributes, say, between states one and two, the permutation matrix is given by

$$\Pi_{1\leftrightarrow 2} = \begin{pmatrix} 0 & 1 & 0 \\ 1 & 0 & 0 \\ 0 & 0 & 1 \end{pmatrix} \tag{6.328}$$

and the master equation above simply reduces to:

$$\rho_{11}^{(1)} = \rho_{22}^{(0)}, \quad \rho_{22}^{(1)} = \rho_{11}^{(0)}, \quad \rho_{33}^{(1)} = \rho_{33}^{(0)} \tag{6.329}$$

If we apply the master equation with this transition matrix, the system will enter a cycle that will neither lead to an entropy increase nor to an energy increase.

In general, however, many permutation matrices contribute to the master equation. Using Birkhoff's theorem, it is easy to see that the most general doubly stochastic matrix for the three level system considered above is

$$\mathbf{p} = \begin{pmatrix} \delta+\beta & \alpha+\eta & \gamma+\mu \\ \alpha+\mu & \delta+\gamma & \beta+\eta \\ \gamma+\eta & \beta+\mu & \delta+\alpha \end{pmatrix}, \tag{6.330}$$

which describes the transfer of probabilities between states 1 and 2 with weight α, between states 2 and 3 with weight β, between states 1 and 3 with weight γ, no transfer of probabilities with weight δ, cyclic permutations $1 \to 2 \to 3 \to 1$ with probability η, and cyclic permutations $3 \to 2 \to 1 \to 3$ with probability μ. Note that the sum of the weights is one, that is, $\alpha+\beta+\gamma+\delta+\eta+\mu = 1$, so that the matrix above is doubly stochastic (i.e., the sum of each row and each column is one). Also note that, while $\mathbf{p}$ is not symmetric in general, it is symmetric when only pairwise permutation are present.

The most general master equation for a three level system, using $\mathbf{p}$ in Eq. (6.330), has the form:

$$\begin{aligned} \rho_{11}^{(1)} &= (\delta+\beta)\rho_{11}^{(0)} + (\alpha+\eta)\rho_{22}^{(0)} + (\gamma+\mu)\rho_{33}^{(0)} \\ \rho_{22}^{(1)} &= (\alpha+\mu)\rho_{11}^{(0)} + (\delta+\gamma)\rho_{22}^{(0)} + (\beta+\eta)\rho_{33}^{(0)} \\ \rho_{33}^{(1)} &= (\gamma+\eta)\rho_{11}^{(0)} + (\beta+\mu)\rho_{22}^{(0)} + (\delta+\alpha)\rho_{33}^{(0)}, \end{aligned} \tag{6.331}$$

and is already quite complicated when compared to the particular case in Eq. (6.329). The complexity increases as the number of states increases. However, as we discussed in the main text, the doubly stochastic form of the transition matrix leads to several important general consequences (see also Ref. [194]).

6.13 Proof of $\langle W\rangle \geq 0$ for Passive Density Matrices and Doubly-Stochastic Evolution

In this appendix, we prove that $\langle W\rangle \geq 0$ if the initial density matrix is passive and the evolution is doubly stochastic (see also Ref. [188]).

Let us arrange the energy levels in order of increasing energies and, hence, by passivity, decreasing occupation probabilities, that is, $E_1 \leq E_2 \leq \ldots E_D$ and $\rho^{(0)}_{11} \geq \rho^{(0)}_{22} \geq \ldots \rho^{(0)}_{DD}$. We also assume that the Hilbert space size D is finite (one can always take the limit $D \to \infty$ at the end). The general expression for the average work is

$$\begin{aligned}\langle W\rangle &= \sum_m \rho^{(1)}_{mm} E_m - \sum_n \rho^{(0)}_{nn} E_n \\ &= \sum_{m,n} \rho^{(0)}_{nn} p_{n\to m} E_m - \sum_n \rho^{(0)}_{nn} E_n = \sum_n \rho^{(0)}_{nn} \left[\sum_m p_{n\to m} E_m - E_n\right]\end{aligned} \tag{6.332}$$

where the sums over n and m go from 1 to D. Next, we define

$$\Delta^k_n \equiv \rho^{(0)}_{nn} - \rho^{(0)}_{D-k,D-k}. \tag{6.333}$$

Clearly, from the passivity condition (6.122), $\Delta^0_n = \rho^{(0)}_{nn} - \rho^{(0)}_{DD} \geq 0$. Then, we rewrite Eq. (6.332) as:

$$\langle W\rangle = \sum_{n=1}^{D} \Delta^0_n \left[\sum_{m=1}^{D} p_{n\to m} E_m - E_n\right] + K^0, \tag{6.334}$$

where, using the doubly stochastic condition for transition rates, that is, $\sum_{n=1}^{D} p_{n\to m} = 1$, one can show that

$$K^0 = \rho^{(0)}_{DD} \sum_{n=1}^{D} \left[\sum_{m=1}^{D} p_{n\to m} E_m - E_n\right] = 0. \tag{6.335}$$

Finally, noting that $\Delta^0_D = 0$, we rewrite (6.334) as

$$\langle W\rangle = \sum_{n=1}^{D-1} \Delta^0_n \left[\sum_{m=1}^{D} p_{n\to m} E_m - E_n\right]. \tag{6.336}$$

Next, we write Δ^0_n in terms of Δ^1_n, that is, $\Delta^0_n = \Delta^1_n + \rho^{(0)}_{D-1,D-1} - \rho^{(0)}_{D,D}$, and plug it in the equation above to obtain

$$\langle W\rangle = \sum_{n=1}^{D-1} \Delta^1_n \left[\sum_{m=1}^{D} p_{n\to m} E_m - E_n\right] + K^1, \tag{6.337}$$

where

$$K^1 = \left(\rho^{(0)}_{D-1,D-1} - \rho^{(0)}_{D,D}\right) \sum_{n=1}^{D-1} \left[\sum_{m=1}^{D} p_{n\to m} E_m - E_n\right] \geq 0. \tag{6.338}$$

To see why $K^1 \geq 0$ note that: (i) the passivity condition, Eq. (6.122), implies $\rho^{(0)}_{D-1,D-1} \geq \rho^{(0)}_{D,D}$, and that (ii) the remaining sum can be rewritten as

$$\begin{aligned}\sum_{n=1}^{D-1}\left[\sum_{m=1}^{D} p_{n\to m}E_m - E_n\right] &= \sum_{m,n=1}^{D} p_{n\to m}E_m - \sum_{m=1}^{D} p_{D\to m}E_m - \sum_{n=1}^{D-1} E_n \\ = \sum_{m=1}^{D} E_m - \sum_{n=1}^{D-1} E_n - \sum_{m=1}^{D} p_{D\to m}E_m &= E_D - \sum_{m=1}^{D} p_{D\to m}E_m \geq E_D - \sum_{m=1}^{D} p_{D\to m}E_D = 0,\end{aligned} \tag{6.339}$$

where we have used the doubly stochastic (6.92) condition multiple times. Finally, noting that $\Delta^1_{D-1} = 0$, we rewrite Eq. (6.337) as

$$\langle W\rangle \geq \sum_{n=1}^{D-2} \Delta^1_n \left[\sum_{m=1}^{D} p_{n\to m}E_m - E_n\right]. \tag{6.340}$$

Equation (6.340) is similar to Eq. (6.336) except that the external sum in Eq. (6.340) extends only up to $D-2$ and not to $D-1$ as in Eq. (6.336).

The proof continues iteratively. For example, in the next iteration, we write Δ^1_n in terms of Δ^2_n, that is, $\Delta^1_n = \Delta^2_n + \rho^{(0)}_{D-2,D-2} - \rho^{(0)}_{D-1,D-1}$ to obtain

$$\langle W\rangle \geq \sum_{n=1}^{D-2} \Delta^2_n \left[\sum_{m=1}^{D} p_{n\to m}E_m - E_n\right] + K^2 \tag{6.341}$$

where

$$K^2 = (\rho^{(0)}_{D-2,D-2} - \rho^{(0)}_{D-1,D-1}) \sum_{n=1}^{D-2}\left[\sum_{m=1}^{D} p_{n\to m}E_m - E_n\right] \tag{6.342}$$

The prefactor $(\rho^{(0)}_{D-2,D-2} - \rho^{(0)}_{D-1,D-1})$ is positive by the passivity condition, Eq. (6.122). Moreover, using similar steps as above, we rewrite the sum as

$$\begin{aligned}\sum_{n=1}^{D-2}\left[\sum_{m=1}^{D} p_{n\to m}E_m - E_n\right] &= E_D + E_{D-1} - \sum_{m=1}^{D} p_{(D-1)\to m}E_m - \sum_{m=1}^{D} p_{D\to m}E_m \\ &= E_D + E_{D-1} - 2E_{D-1} + \sum_{m=1}^{D}\left[p_{(D-1)\to m} + p_{D\to m}\right]\delta E_m \\ &\geq E_D + E_{D-1} - 2E_{D-1} + \left[p_{(D-1)\to D} + p_{D\to D}\right]\delta E_D \\ &\geq E_D + E_{D-1} - 2E_{D-1} + (E_{D-1} - E_D) = 0,\end{aligned} \tag{6.343}$$

where we have defined $\delta E_m \equiv E_{D-1} - E_m$. In the third line, we have used that $\delta E_m \geq 0$ for any $m \leq D-1$ and, in the fourth line, we have used that $p_{(D-1)\to D} + p_{D\to D} \leq 1$, which is guaranteed by the doubly stochastic condition $\sum_m p_{m\to D} = 1$. We therefore conclude that $K_2 \geq 0$. Finally, noting that $\Delta^2_{D-2} = 0$ we arrive at:

$$\langle W\rangle \geq \sum_{n=1}^{D-3} \Delta^2_n \left[\sum_{m=1}^{D} p_{n\to m}E_m - E_n\right] \tag{6.344}$$

where now the external sum extends only up to $D-3$.

Clearly, comparing Eqs. (6.336), (6.340) and (6.344), we see that at each iteration the upper limit of the external sum decreases by one and the index k in Δ^k_n increases by one. Continuing this iterative process, eventually, the external sum will include only one element proportional to Δ^{D-1}_1, which is zero by definition [see Eq. (6.333)]. Therefore one can conclude that $\langle W\rangle \geq 0$.

6.14 Derivation of the Drift Diffusion Relation for Continuous Processes

We already showed how one can derive the drift diffusion relation (6.178) by means of a cumulant expansion of the Evans-Searles fluctuation relation (6.158). Here, we show how the same result can be derived directly from the ETH ansatz (6.62) applied to continuous driving protocols. In particular, let us focus on a setup in which the external parameter λ, conjugate to the observable $\hat{O} = -\partial_\lambda \hat{H}$, changes in time at a constant rate. For example, this parameter can be the position of a macroscopic object moving in some media (quantum or classical).

Within leading order in adiabatic perturbation theory (see Ref. [201] for further details), the energy dissipation in the system is given by (we have set $\hbar = 1$ so that the energy has dimension of time^{-1}):

$$\frac{d\tilde{Q}}{dt} \approx \dot{\lambda}^2 \sum_{n,m} \frac{\rho_n - \rho_m}{E_m - E_n} \langle n|\hat{O}|m\rangle\langle m|\hat{O}|n\rangle \delta(E_n - E_m), \tag{6.345}$$

where ρ_n and ρ_m are the stationary probabilities to occupy the many-body eigenstates $|n\rangle$ and $|m\rangle$ corresponding to the energies E_n and E_m, respectively. All matrix elements and energies here correspond to the instantaneous value of λ. For the Gibbs distribution, $\rho_n \propto \exp[-\beta E_n]$, it is easy to see that

$$\frac{\rho_n - \rho_m}{E_m - E_n}\delta(E_n - E_m) = \beta\rho_n \delta(E_n - E_m) \tag{6.346}$$

and Eq. (6.345) reduces to the standard expression for the energy dissipation (see, e.g., Ref. [317]). As in many places in this review, let us focus instead on the dissipation from a single many-body energy eigenstate, $\rho_n = \delta_{n,n_0}$. If the relation holds for any eigenstate, it holds for any stationary distribution with subextensive energy fluctuations. For a single eigenstate, Eq. (6.345) becomes

$$\frac{d\tilde{Q}}{dt} = 2\dot{\lambda}^2 \sum_{m\neq n_0} \frac{1}{E_m - E_{n_0}} \langle n_0|\hat{O}|m\rangle\langle m|\hat{O}|n_0\rangle \delta(E_{n_0} - E_m), \tag{6.347}$$

Let us now use the ETH ansatz (6.62) and, as usual, replace the summation over the eigenstates by an integration over $\omega = E_m - E_{n_0} \equiv E_m - E$: $\sum_m \to \int d\omega \exp[S(E+\omega)]$ (for simplicity, we drop the index n_0 in the energy). Then

$$\frac{d\tilde{Q}}{dt} = 2\dot{\lambda}^2 \mathcal{P}\int d\omega \, \frac{\mathrm{e}^{S(E+\omega)-S(E+\omega/2)}}{\omega} |f_O(E+\omega/2,\omega)|^2 \delta(\omega), \tag{6.348}$$

where $\mathcal{P}\int$ stands for the principal value of the integral. Noting that

$$\begin{aligned} \mathrm{e}^{S(E+\omega)-S(E+\omega/2)} &\approx \mathrm{e}^{\beta\omega/2} = 1 + \frac{\beta\omega}{2} + \ldots, \\ |f_O(E+\omega/2,\omega)|^2 &= |f_O(E,\omega)|^2 + \frac{\omega}{2}\partial_E |f_O(E,\omega)|^2 + \ldots, \end{aligned} \tag{6.349}$$

and using the fact that $|f_O(E,\omega)|^2$ is an even function of ω, we find

$$\frac{d\tilde{Q}}{dt} \equiv J_E = \dot{\lambda}^2[\beta|f_O(E,0)|^2 + \partial_E|f_O(E,0)|^2]. \tag{6.350}$$

We note that, formally, the function $|f_O(E,0)|^2$ diverges in the thermodynamic limit (see Fig. 6.17). However, physically, this divergence is cutoff by the inverse relaxation time in the system, which defines the broadening of the δ-function in Eq. (6.345).

Similarly, from adiabatic perturbation theory, one can show that

$$\frac{d(\delta E^2)}{dt} \equiv D_E = 2\dot{\lambda}^2 \sum_{m\neq n_0} \langle n_0|\hat{O}|m\rangle\langle m|\hat{O}|n_0\rangle \delta(E_{n_0} - E_m) = 2\dot{\lambda}^2 |f_O(E,0)|^2. \tag{6.351}$$

Comparing Eqs. (6.350) and (6.351), we recover the desired drift-diffusion relation (6.178).

6.15 Derivation of Onsager Relations

In this appendix, we derive Eqs. (6.180) and (6.201). Since Eq. (6.201) is more general, we show its derivation first and then obtain Eq. (6.180) as a special case. First, in the Crooks relation (6.201), we expand the entropy and the probability distribution as a function of $E_{\rm I,II}\pm W$ and $N_{\rm I,II} \pm \delta N$ to second order in W and δN to obtain

$$\begin{aligned} P(E_{\rm I}, E_{\rm II}, N_{\rm I}, N_{\rm II}, W, \delta N) \exp\Bigg[&-\Delta\beta W - \Delta\kappa \delta N - \frac{W^2}{2}\partial_E \Delta\beta - \frac{\delta N^2}{2}\partial_N \Delta\kappa \\ &- \frac{W\delta N}{2}(\partial_N \Delta\beta + \partial_E \delta\kappa)\Bigg] = \exp\left[W\partial_E + \delta N \partial_N\right] P(E_{\rm I}, E_{\rm II}, N_{\rm I}, N_{\rm II}, -W, -\delta N), \end{aligned} \tag{6.352}$$

where $\Delta\beta = \beta_{\rm I} - \beta_{\rm II}$, $\Delta\kappa = \kappa_{\rm I} - \kappa_{\rm II}$, $\beta_{\rm I} = \partial_{\rm E_I} S_{\rm I}$, $\kappa_{\rm I} = \partial_{\delta \rm N_I} S_{\rm I}$, and similarly for II (I $\to$ II). The partial derivatives ∂_E and ∂_N are understood as derivatives with respect to energy and particle exchange: $\partial_E f(E_{\rm I}, E_{\rm II}) \equiv \partial_{E_{\rm I}} f(E_{\rm I}, E_{\rm II}) - \partial_{E_{\rm II}} f(E_{\rm I}, E_{\rm II})$. Next, one needs to integrate over W and δN and perform the cumulant expansion to second order. Following the discussion after Eq. (6.174), we keep only the terms linear in the cumulants to obtain

$$\begin{aligned} &-\Delta\beta\langle W\rangle - \Delta\kappa\langle\delta N\rangle - \frac{\langle W^2\rangle_c}{2}\partial_E\Delta\beta - \frac{\langle\delta N^2\rangle_c}{2}\partial_N\Delta\kappa - \frac{\langle W\delta N\rangle_c}{2}\left(\partial_N\Delta\beta + \partial_E\Delta\kappa\right) \\ &+ \frac{(\Delta\beta)^2}{2}\langle W^2\rangle_c + \frac{(\Delta\kappa)^2}{2}\langle\delta N^2\rangle_c + \Delta\beta\Delta\kappa\langle W\delta N\rangle_c \\ &= -\partial_E\langle W\rangle - \partial_N\langle\delta N\rangle + \frac{1}{2}\partial^2_{EE}\langle W^2\rangle_c + \frac{1}{2}\partial^2_{NN}\langle\delta N^2\rangle_c + \partial^2_{EN}\langle W\delta N\rangle_c\,. \end{aligned} \tag{6.353}$$

Using the following identities:

$$\begin{aligned} \langle W^2\rangle_c\partial_E\Delta\beta =& \partial_E\left(\Delta\beta\langle W^2\rangle_c\right) - \Delta\beta\partial_E\langle W^2\rangle_c, \\ \langle\delta N^2\rangle_c\partial_N\Delta\kappa =& \partial_N\left(\Delta\kappa\langle\delta N^2\rangle_c\right) - \Delta\kappa\partial_N\langle\delta N^2\rangle_c, \\ \langle W\delta N\rangle_c\left(\partial_N\Delta\beta + \partial_E\Delta\kappa\right) =& \partial_N(\Delta\beta\langle W\delta N\rangle_c) - \Delta\beta\partial_N\langle W\delta N\rangle_c \\ &+ \partial_E(\Delta\kappa\langle W\delta N\rangle_c) - \Delta\kappa\partial_E\langle W\delta N\rangle_c, \end{aligned}$$

we can rewrite Eq. (6.353) as

$$\begin{aligned} &(\Delta\beta - \partial_E)\left[-\langle W\rangle + \frac{\Delta\beta}{2}\langle W^2\rangle_c + \frac{\Delta\kappa}{2}\langle W\delta N\rangle_c + \frac{1}{2}\partial_E\langle W^2\rangle_c + \frac{1}{2}\partial_N\langle W\delta N\rangle_c\right] + \\ &(\Delta\kappa - \partial_N)\left[-\langle\delta N\rangle + \frac{\Delta\kappa}{2}\langle\delta N^2\rangle_c + \frac{\Delta\beta}{2}\langle W\delta N\rangle_c + \frac{1}{2}\partial_N\langle\delta N^2\rangle_c + \frac{1}{2}\partial_E\langle W\delta N\rangle_c\right] = 0\,. \end{aligned} \tag{6.354}$$

Since this relation holds for any value of $\Delta\beta$ and $\Delta\kappa$, each term in the square brackets must be zero, leading to Eq. (6.201). By assuming that the systems do not exchange particles, that is, that $\delta N = 0$, we recover Eq. (6.180).

7 Quench dynamics and relaxation in isolated integrable quantum spin chains by Essler, Fagotti

Abstract

We review the dynamics after quantum quenches in integrable quantum spin chains.

We give a pedagogical introduction to relaxation in isolated quantum systems, and discuss the description of the steady state by (generalized) Gibbs ensembles.

We then turn to general features in the time evolution of local observables after the quench, using a simple model of free fermions as an example.

In the second part we present an overview of recent progress in describing quench dynamics in two key paradigms for quantum integrable models, the transverse field Ising chain and the anisotropic spin-1/2 Heisenberg chain.

(compare this with Vidmar's article!)

7.1 Introduction

An isolated many-particle quantum system is characterized by the absence of any coupling to its environment. According to the laws of quantum mechanics its time evolution is unitary and governed by the time dependent Schrödinger equation. In order to specify the state $|\Psi(t)\rangle$ of the system at a given time t, it is then sufficient to know its Hamiltonian H and its state at an earlier time

$$|\Psi(t)\rangle = e^{-iHt}|\Psi(0)\rangle. \tag{7.1}$$

In spite of this purely unitary evolution, macroscopic systems are expected to eventually "relax" in some way and be amenable to a description by quantum Statistical Mechanics [1]. For many-particle systems it is convenient to focus on the time evolution of the expectation values of particular observables of interest rather than the state itself, i.e. one considers

$$\langle\Psi(t)|\mathcal{O}|\Psi(t)\rangle \ . \tag{7.2}$$

Historically, studies of many-particle quantum systems such as electronic degrees of freedom in solids mainly focussed on equilibrium properties at zero and finite temperature. This is because in the context of solids, the many-body system of interest is typically coupled to an "environment", i.e. other degrees of freedom, the presence of which is felt after very short time scales. The situation changed dramatically about a decade ago, when it became possible to experimentally investigate the non-equilibrium dynamics of clouds of ultra-cold, trapped atoms[2, 4, 3, 5, 6, 7, 8, 9, 10, 11, 12, 13, 14, 15, 16, 17] (see also the review by T. Langen, T. Gasenzer and J. Schmiedmayer in this volume[18]).

(????)

These are by design almost isolated. Moreover the natural energy scale underlying the dynamics is incredibly small, so that there is a long time window (on the order of seconds) for conducting experiments. The main effect of the coupling to the environment is particle loss through heating. This eventually becomes significant, but over an intermediate time window the dynamics is to a good approximation unitary. It is important to note in view of the following discussion that finite size effects are often important in cold atom systems, and as a result of the trapping potential these systems are not translationally invariant. They are however highly tuneable both with regards to Hamiltonian parameters and their effective dimensionality. This was exploited in the seminal Quantum Newton's Cradle experiments by Kinoshita, Wenger and Weiss[3]. These investigated the non-equilibrium evolution of one, two and three dimensional Bose gases that were initially driven out of equilibrium. While the two and three dimensional

systems were seen to relax very quickly towards an equilibrium state, the behaviour in the one dimensional case was very different. In Ref. [3] this was attributed to the presence of approximate conservation laws. Neglecting the trap, the Hamiltonian is well approximated by the Lieb-Liniger model[19]

$$H_{\mathrm{LL}} = -\frac{\hbar^2}{2m}\sum_{j=1}^{N}\frac{\partial^2}{\partial x_j^2} + c\sum_{j<k}\delta(x_j - x_k)\ . \tag{7.3}$$

The Hamiltonian (7.3) is integrable and as a result has an infinite number of conservation laws I_n[20, 21] such that

$$[H, I_n] = [I_n, I_m] = 0. \tag{7.4}$$

It is intuitively clear that conservation laws will affect the quantum dynamics, because they impose constraints of the form

$$\langle\Psi(t)|I_n|\Psi(t)\rangle = \text{const.} \tag{7.5}$$

The difference in behaviours between the one and three dimensional Quantum Newton's Cradle experiments suggested that the non-equilbirium dynamics of integrable models is unusual. This was one of the motivations for the recent intense theoretical efforts aimed at understanding the non-equilibrium dynamics of integrable quantum many-particle systems. Integrable models come in a variety of guises, the two main classes being

- Lattice models:

  These include non-interacting fermion and boson theories [22, 23, 24], models that can be mapped to free fermions like the transverse-field Ising [25, 26, 27, 28, 29, 30, 31, 32, 33, 34, 35, 36, 37, 38, 39, 40, 41, 42, 43] and XY chains [44, 45, 46, 47, 48, 49, 51, 52, 50], spin models like the Heisenberg chain [53, 54, 55, 56, 57, 58, 59, 60, 61, 62, 63, 64, 65, 66, 67, 69, 68, 70, 71, 72] and electronic theories like the Hubbard model[73, 74, 75, 76, 77].

- Continuum models:

  These include free field theories like the Klein-Gordon[80, 78, 79] and Luttinger models[81, 82, 83, 84, 85, 86, 53] (see the review by M. Cazalilla and M.-C. Chung [87] in this volume), conformal field theories[89, 90, 80, 91, 92, 93] (see the review by P. Calabrese and J. Cardy [88] in this volume), massive relativistic field theories like the sine-Gordon[94, 95, 96], sinh-Gordon[97, 98, 99, 100] and nonlinear sigma models[101], and non-relativistic field theories like the Lieb-Liniger model[102, 103, 104, 105, 106, 107, 108, 109, 110, 111, 112, 113, 114]. In continuum models the spectrum of elementary excitations is unbounded, which leads to certain differences as compared to lattice models.

In this review we focus on the equilibrium dynamics in integrable lattice models. We moreover restrict our discussion to a particular protocol for inducing out of equilibrium dynamics, the so-called quantum quench. We note that other protocols have been studied in the literature. One example are ramps[115, 116], which are of interest in relation to the Kibble-Zurek mechanism [117].

The outline of this review is as follows. In section 7.2 we define what we mean by a quantum quench. This is followed by a discussion in section 7.3, of how isolated many-particle quantum systems relax, and of how to describe their late time behaviour. In section 7.4 we provide a simple example that shows these ideas at work. Having established a framework for the late time behaviour after a quantum quench, section 7.5 turns to the discussion of general features of the evolution of observables at finite times, such as how correlations spread through the system. Section 7.6 is concerned with one of the key paradigms of quantum quenches, the transverse field Ising chain (TFIC). This constitutes a non-trivial example, for which it is nevertheless

possible to obtain exact results in closed form. From the point of view of quantum integrability the TFIC is quite special, because it can be mapped onto a non-interacting fermionic theory by means of a (nonlocal) Jordan-Wigner transformation. The case of fully interacting integrable models (defined as having scattering matrices that are different from ± 1) is discussed in section 10.3.2. We conclude with an outlook on some open problems of current interest in section 7.8.

Apart from the other contributions to this Special Issue, there have been several previous reviews[116, 118, 120, 119, 121] on closely related topics. They differ considerably in perspective, focus, scope and style, and are therefore largely complementary to ours.

7.2 The essence of a global quantum quench

Our starting point is an isolated many-particle quantum system characterized by a time-independent, translationally invariant Hamiltonian $H(h)$ with only short-range interactions. Here h is a system parameter such as a magnetic field, or an interaction strength. An example we will return to frequently throughout this review is the transverse field Ising chain (TFIC)

$$H(h) = -J \sum_{j=1}^{L} \sigma_j^x \sigma_{j+1}^x + h\sigma_j^z \ , \tag{7.6}$$

where σ_j^α are Pauli matrices acting on a spin-1/2 on site j of a one dimensional ring, and $\sigma_{L+1}^\alpha \equiv \sigma_1^\alpha$ ($\alpha = x, y, z$). The short-ranged nature of $H(h)$ is an essential condition, and it is known that models with infinite range interactions such as the BCS problem [122] exhibit very different behaviours when driven out of equilibrium. Let us imagine that we somehow prepare our system in the ground state $|\Psi(0)\rangle$ of $H(h_0)$. This state is highly non-generic in the sense that it has low entanglement [123, 124, 125]. At time $t = 0$ we then suddenly "quench" the system parameter to a new value h, and then consider subsequent unitary time evolution with our new Hamiltonian $H(h)$. As the change of Hamiltonian is assumed to be instantaneous, the system remains in state $|\Psi(0)\rangle$ ("sudden approximation"). At times $t > 0$ the state of the system is found by solving the time-dependent Schrödinger equation

$$|\Psi(t)\rangle = e^{-iH(h)t}|\Psi(0)\rangle. \tag{7.7}$$

We are interested in the cases where in a large, finite volume the initial state $|\Psi(0)\rangle$ has non-zero overlaps with an exponentially large number of the eigenstates of $H(h)$. The case where $|\Psi(0)\rangle$ has non-zero overlaps with only a finite, system-size independent number of eigenstates is equivalent to the one discussed in undergraduate Quantum Mechanics courses. In terms of energy eigenstates

$$H(h)|n\rangle = E_n|n\rangle \ , \quad E_n \geq E_0 \ , \tag{7.8}$$

we can express the state of the system at time t as

$$|\Psi(t)\rangle = \sum_n \langle n|\Psi(0)\rangle \ e^{-iE_n t}|n\rangle \ . \tag{7.9}$$

Our objective is the description of expectation values of a certain class of operators $\mathcal{O}$, that will be defined in detail later, in the state $|\Psi(t)\rangle$

$$\langle\Psi(t)|\mathcal{O}|\Psi(t)\rangle = \sum_{n,m} \langle\Psi(0)|n\rangle \ \langle m|\Psi(0)\rangle \ \langle n|\mathcal{O}|m\rangle e^{-i(E_m - E_n)t} \ . \tag{7.10}$$

All the interesting phenomena after a quantum quench arise from the presence of the oscillatory factors $e^{-i(E_m - E_n)t}$, which induce quantum mechanical interference effects [126], in the double sum over exponentially (in system size) many terms. We note that focussing on expectation

values is not as restrictive as it may first appear, as it still allows us to consider the full probability distributions of the observables we are interested in.

A crucial property of a global quantum quench is that energy is conserved at all $t > 0$, and that the post-quench energy density is larger than the ground state energy per site

$$e = \lim_{L\to\infty} \frac{1}{L}\langle\Psi(t)|H(h)|\Psi(t)\rangle > \lim_{L\to\infty} \frac{E_0}{L}. \tag{7.11}$$

This means that through the quantum quench we explore a region of Hilbert space that is macroscopically different from the sector containing the ground state and low-lying excitations.

In practice one often considers more general "quench protocols", where for example $H(h)$ and/or $|\Psi(0)\rangle$ are invariant only under translations by $2, 3, ...$ sites [51, 127, 63], and initial states that are not necessarily pure [78], but are described by a density matrix $\rho(0)$. Considering $\rho(0)$ to be a thermal density matrix provides a simple way of varying the energy density e "injected" into the system. It is essential for our purposes that the initial density matrix $\rho(0)$ has a cluster decomposition property[128]

$$\lim_{|x-y|\to\infty} \mathrm{Tr}\left[\rho(0)\mathcal{O}(x)\mathcal{O}(y)\right] = \mathrm{Tr}\left[\rho(0)\mathcal{O}(x)\right]\mathrm{Tr}\left[\rho(0)\mathcal{O}(y)\right], \tag{7.12}$$

and we elaborate on this point in Appendix 7.9. Invariance of the initial density matrix under translations is another key requirement. Inhomogeneous initial conditions have been considered by many authors in the literature, see e.g. Refs [44, 129, 130, 131, 132, 54, 133, 134, 135, 55, 136, 137, 106, 138, 139, 141, 140, 142, 143, 144, 145, 146, 147, 148, 149, 150, 151, 152, 153], and the reviews by D. Bernard and B. Doyon [154] and by R. Vasseur and Joel E. Moore [155] in this volume, but we will not consider them here.

7.3 Relaxation in isolated quantum systems

Given that we are considering an isolated quantum system, an obvious question is in what sense it may relax to a stationary state at late times after we have driven it out of equilibrium. In order to sharpen the following argument, let us revisit the case discussed in Section 7.2, namely an isolated system initially prepared in a pure state $|\Psi(0)\rangle$, that is not an eigenstate of the (time independent) Hamiltonian $H(h)$ describing the time evolution after our quantum quench. Let us now consider the following class of hermitian operators

$$\mathcal{O}_{jk} = |j\rangle\langle k| + |k\rangle\langle j| \ . \tag{7.13}$$

Their expectation values in the state $|\Psi(t)\rangle$ can be expressed using (7.9) as

$$\langle\Psi(t)|\mathcal{O}_{jk}|\Psi(t)\rangle = e^{i(E_j-E_k)t}\langle\Psi(0)|j\rangle\langle k|\Psi(0)\rangle + \text{c.c.} \tag{7.14}$$

We see that generically the right hand side exhibits periodic oscillatory behaviour in time. Hence the observables $\mathcal{O}_{jk}$ typically do not relax at late times. A crucial point is that $\mathcal{O}_{jk}$ are generally very nonlocal in space. As locality is an important concept in quantum quenches it is useful to define what we mean by a local operator.

Definition 1. *Local Operators.*

In lattice models an operator $\mathcal{O}$ is called local if in the thermodynamic limit $\mathcal{O}$ acts non-trivially only on a finite number of sites separated by a finite distance. For a quantum spin-1/2 chain with L sites examples of local operators are

$$\sigma_j^\alpha \ , \quad \sigma_j^\alpha\sigma_{j+k}^\beta, \quad \prod_{j=1}^{k}\sigma_j^{\alpha_j} \ , \qquad k \text{ fixed}, \tag{7.15}$$

where σ_j^α ($\alpha = x, y, z$) are Pauli matrices acting on site j. On the other hand operators such as

$$\sigma_1^x \sigma_{L/2}^x \ , \qquad \prod_{j=1}^{L/2} \sigma_j^{\alpha_j} \tag{7.16}$$

are nonlocal. Acting with a local operator on a state $|\psi\rangle$ does not change its macroscopic properties (e.g. its energy per volume in the thermodynamic limit).

Definition 2. *Range of a local operator.*

The range of a local operator $\mathcal{O}$ is the size of the largest interval on which it acts non-trivially. For the examples above we have

$$\text{range}(\sigma_j^\alpha) = 1 \ , \quad \text{range}(\sigma_j^\alpha \sigma_{j+k}^\beta) = k+1 \ , \quad \text{range}\Big(\prod_{j=1}^{k} \sigma_j^{\alpha_j}\Big) = k \ . \tag{7.17}$$

7.3.1 Local Relaxation

The previous argument shows that an isolated quantum system prepared in a pure state cannot relax in its entirety. However, it can and does relax locally in space[126, 156, 157, 26, 28, 158]. To explain this concept let us consider the example of a one-dimensional spin system with Hamiltonian H with only short-range interactions. An example would be the TFIC (7.6). We partition the entire system into an arbitrary but finite subsystem B and its complement A. Eventually we will take the thermodynamic limit while keeping B fixed. Let us prepare our spin system at time $t = 0$ in some initial density matrix $\rho(0)$ that is not an eigenstate of H. At later times the entire system is characterized by the density matrix

$$\rho(t) = e^{-iHt} \rho(0) e^{iHt}. \tag{7.18}$$

The reduced density matrix of the subsystem B is obtained by tracing out the degrees of freedom in A

$$\rho_B(t) = \text{Tr}_A \rho(t). \tag{7.19}$$

It is instructive to give an explicit representation of the reduced density matrix for our spin

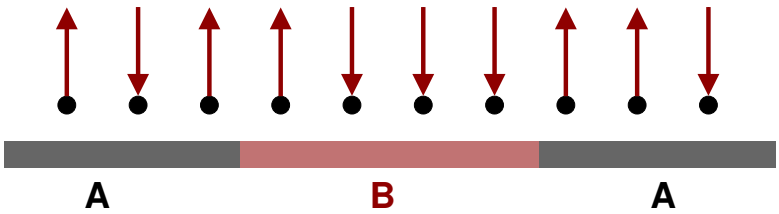

Figure 7.1: Local relaxation in an isolated many-particle quantum system: we partition the entire system into an arbitrary finite subsystem B and its complement A. We then take the thermodynamic limit while keeping B fixed. Expectation values of all operators that act non-trivially only in B will relax to stationary values at late times.

chain example, cf. Fig. 7.1. An orthonormal basis of states is given by

$$|\sigma_1, \sigma_2, \ldots, \sigma_L\rangle = \bigotimes_{j=1}^{L} |\sigma_j\rangle_j \ , \quad \sigma_j = \pm 1, \tag{7.20}$$

where $|\sigma_j\rangle_j$ denote the two eigenstates of S_j^z. Let us take our subsystem B to consist of sites $1, 2, \cdots \ell$ for simplicity. The reduced density matrix is then

$$\begin{aligned}\rho_B(t) &= \sum_{\sigma_{\ell+1},\ldots,\sigma_L} \left(\bigotimes_{k=\ell+1}^{L} {}_k\langle\sigma_k| \right) \rho(t) \left(\bigotimes_{n=\ell+1}^{L} |\sigma_n\rangle_n \right) \\ &= 2^{-\ell} \sum_{\alpha_1,\ldots,\alpha_\ell=0,x,y,z} \mathrm{Tr}\left[\rho(t)\sigma_1^{\alpha_1}\sigma_2^{\alpha_2}\ldots\sigma_\ell^{\alpha_\ell}\right]\ \sigma_1^{\alpha_1}\sigma_2^{\alpha_2}\ldots\sigma_\ell^{\alpha_\ell}\ , \end{aligned} \tag{7.21}$$

where we have defined $\sigma_j^0 = \mathbb{1}_j$. Eqn (7.21) shows that the matrix elements of $\rho_B(t)$ are equal to particular correlation functions of local operators acting non-trivially only on B, and that $\rho_B(t)$ in fact encodes all such correlators.

Definition 3. *Local Relaxation.*

We say that our system relaxes locally if the limit

$$\lim_{t\to\infty}\lim_{L\to\infty} \rho_B(t) = \rho_B(\infty) \tag{7.22}$$

exists for any finite subsystem B.

Definition 4. *Stationary State.*

Consider a system that relaxes locally in the sense just defined. Then its stationary state is defined as a time-independent density matrix ρ^{SS} for the full system such that for any finite subsystem B

$$\lim_{L\to\infty} \mathrm{Tr}_A\left(\rho^{\mathrm{SS}}\right) = \rho_B(\infty), \tag{7.23}$$

where A is the complement of B. We stress that this equivalence applies only at the level of finite subsystems in the thermodynamic limit and not for the density matrices of the full system.

Definition 5. *Local equivalence of ensembles.*

Let ρ_1 and ρ_2 be two density matrices. We call the corresponding two ensembles locally equivalent, if in the thermodynamic limit the reduced density matrices for any finite subsystem B coincide, i.e.

$$\lim_{|A|\to\infty} \mathrm{Tr}_A\left(\rho_1\right) = \lim_{|A|\to\infty} \mathrm{Tr}_A\left(\rho_2\right). \tag{7.24}$$

Here A is the complement of B and $|A|$ denotes its volume. We denote local equivalence by

$$\rho_1 =_{\mathrm{loc}} \rho_2. \tag{7.25}$$

A key problem in the field of non-equilibrium dynamics is the determination of the stationary state density matrix. A crucial role is played by symmetries of the Hamiltonian. In translationally invariant systems there are essentially two paradigms for local relaxation, and we turn to their respective descriptions next. Before doing so an important comment is in order. By design our focus is on local operators, which in turn leads us to define local relaxation in the sense formulated above. In practice one might be interested in observables that are formally not captured by our framework, and yet might relax to stationary values. An example would be expectation values of the momentum distribution function, which is the Fourier transform of the single particle Green's function[24, 159]. The relaxational properties of such quantities are at present not understood in general, and further investigation is called for.

7.3.2 Thermalization

As we are dealing with an isolated system, energy is always a conserved quantity

$$E = \mathrm{Tr}\left(\rho(t)H\right) = \mathrm{Tr}\left(e^{-iHt}\rho(0)e^{iHt}H\right) = \mathrm{Tr}\left(\rho(0)H\right) \ . \tag{7.26}$$

In absence of other conserved quantities isolated systems are believed to locally relax to thermal equilibrium. This is known as thermalization [1, 160, 161]. In the framework we have set up, this means that our stationary state is described by a Gibbs ensemble

$$\rho^{\mathrm{SS}} =_{\mathrm{loc}} \rho^{\mathrm{Gibbs}} = \frac{e^{-\beta_{\mathrm{eff}}H}}{\mathrm{Tr}\left(e^{-\beta_{\mathrm{eff}}H}\right)} \ . \tag{7.27}$$

Here the inverse effective temperature β_{eff} is fixed by the initial value of the energy density

$$e \equiv \lim_{L\to\infty}\frac{1}{L}\mathrm{Tr}\left(\rho(0)H\right) = \lim_{L\to\infty}\frac{1}{L}\mathrm{Tr}\left(\rho^{\mathrm{Gibbs}}H\right) \ . \tag{7.28}$$

We once again stress that (7.27) implies only that in the thermodynamic limit the stationary state is locally indistinguishable from a Gibbs ensemble in the sense that expectation values of all operators that act non-trivially only in a finite subsystem are identical to the corresponding thermal expectation values. The physical picture underlying thermalization is that the infinitely large complement of our subsystem acts like a heat bath with an effective inverse temperature β_{eff}.

We note that β_{eff} defined in this way can be either positive or negative. The meaning of a negative temperature in this context is as follows. Let us consider a Hamiltonian with bounded spectrum (e.g. a quantum spin model). Then the average energy associated with H is

$$\bar{e} = \lim_{L\to\infty}\frac{1}{L}\mathrm{Tr}\left(H\right) \ . \tag{7.29}$$

Depending on our initial density matrix we now have two possibilities

$$\begin{aligned} e < \bar{e} &\Rightarrow \beta_{\mathrm{eff}} > 0 \ , \\ e > \bar{e} &\Rightarrow \beta_{\mathrm{eff}} < 0 \ . \end{aligned} \tag{7.30}$$

We note that negative temperature ensembles have been observed experimentally in Ref. [162].

7.3.3 Generalized Gibbs Ensembles (GGE)

We now turn to the case of systems with additional local conservation laws $I^{(n)}$. These are operators that commute with the Hamiltonian

$$[H, I^{(n)}] = 0, \tag{7.31}$$

and have the property that their densities are local operators. In most of the cases of interest these conservation laws also commute with one another

$$[I^{(n)}, I^{(m)}] = 0, \tag{7.32}$$

and we will assume this to be the case in the following. We note that exceptions to (7.32) are known [51, 93, 92] (see also Sec. 7.3.3). What we mean by local conservation laws is best

explained by an example. The TFIC (7.6) has infinitely many local conservation laws in the thermodynamic limit [163]

$$\begin{aligned} I^{(1,+)} &= H(h) \ , \\ I^{(n,+)} &= -J\sum_j \left(S^{xx}_{j,j+n} + S^{yy}_{j,j+n-2}\right) + h\left(S^{xx}_{j,j+n-1} + S^{yy}_{j,j+n-1}\right) \equiv \sum_j \mathcal{I}^{(n,+)}_j \ , \\ I^{(n,-)} &= -J\sum_j \left(S^{xy}_{j,j+n} - S^{yx}_{j,j+n}\right) \equiv \sum_j \mathcal{I}^{(n,-)}_j \ , \end{aligned} \tag{7.33}$$

where $n \geq 1$ and we have defined

$$S^{\alpha\beta}_{j,j+\ell} = \sigma^\alpha_j \left[\prod_{k=1}^{\ell-1} \sigma^z_{j+k}\right] \sigma^\beta_{j+\ell} \ , \quad S^{yy}_{j,j} = -\sigma^z_j \ . \tag{7.34}$$

The conservation laws themselves are extensive, but their densities $\mathcal{I}^{(n,\pm)}_j$ involve only finite numbers of neighbouring sites ($n+1$ sites for $I^{(n,\pm)}$). As a consequence of (7.31), expectation values of the conservation laws as well as their densities are time independent

$$\frac{1}{L}\mathrm{Tr}\left(\rho(t) I^{(n,\pm)}\right) = \mathrm{Tr}\left(\rho(t)\mathcal{I}^{(n,\pm)}_j\right) = \frac{1}{L}\mathrm{Tr}\left(\rho(0) I^{(n,\pm)}\right) \equiv \frac{E^{(n,\pm)}}{L} \ , \tag{7.35}$$

where in the first step we used translational invariance. An obvious question at this point is why we insist on conservation laws to be local. The answer lies in the simple fact that any Hamiltonian has at least as many nonlocal conservation laws as there are basis states in the Hilbert space. Let us consider one-dimensional projectors on energy eigenstates

$$H|n\rangle = E_n|n\rangle \ , \quad P_n = |n\rangle\langle n|. \tag{7.36}$$

Then we clearly have

$$[P_n, P_m] = 0 = [P_n, H] \ , \tag{7.37}$$

which imply that the expectation values of all P_n are time independent. Importantly, these conservation laws are not local, and as they exist for any Hamiltonian they are not expected to have any profound effect. In contrast, local conservation laws are rather special and, as is clear from (7.35), have important consequences for local relaxation after quantum quenches.

An immediate consequence of (7.35) is that systems with local conservation laws cannot thermalize after a quantum quench, because the system retains memory of the initial expectation values of all conserved quantities at all times. The maximum entropy principle [164] then suggests that the stationary state density matrix should be given by a GGE [8]

$$\rho^{\mathrm{GGE}} = \frac{e^{-\sum_n \lambda_n I^{(n)}}}{\mathrm{Tr}\left(e^{-\sum_n \lambda_n I^{(n)}}\right)}. \tag{7.38}$$

Here λ_n are Lagrange multipliers that are fixed by the initial conditions (7.35), as we require that

$$\lim_{L\to\infty} \frac{E^{(n,\pm)}}{L} = \lim_{L\to\infty} \frac{1}{L}\mathrm{Tr}\left(\rho^{\mathrm{GGE}} I^{(n)}\right) . \tag{7.39}$$

Local conservation laws vs mode occupation numbers

In free theories GGEs are often formulated using conserved mode occupation numbers[8]. This is usually equivalent to our formulation in terms of local conservation laws in these cases

[28] as we now demonstrate for a simple example. Let us consider a fermionic tight binding model

$$H = -J\sum_j c_j^\dagger c_{j+1} + c_{j+1}^\dagger c_j - \mu \sum_j c_j^\dagger c_j \ , \quad \{c_j, c_n^\dagger\} = \delta_{j,n}. \tag{7.40}$$

The Hamiltonian is easily diagonalized by going to momentum space

$$H = \sum_k \left[-2J\cos(k) - \mu\right] c^\dagger(k)c(k) \ . \tag{7.41}$$

The mode occupation operators $n(k) = c^\dagger(k)c(k)$ commute with the Hamiltonian and with one another. However, the $n(k)$ are neither local nor extensive. An equivalent set of local, extensive conserved quantities is easily found

$$\begin{aligned} I^{(n,+)} &= 2J\sum_k \cos(nk)\ c^\dagger(k)c(k) = J\sum_j c_j^\dagger c_{j+n} + c_{j+n}^\dagger c_j \ , \\ I^{(n,-)} &= 2J\sum_k \sin(nk)\ c^\dagger(k)c(k) = iJ\sum_j c_j^\dagger c_{j+n} - c_{j+n}^\dagger c_j \ . \end{aligned} \tag{7.42}$$

The crucial point is that these conservation laws are linearly related to the mode occupation numbers. This implies that the GGE describing the stationary state after a quantum quench to the Hamiltonian H can be constructed either from the local conservation laws, or from the mode occupation numbers

$$\rho^{\mathrm{GGE}} = \frac{e^{-\sum_n \lambda_{n,+} I^{(n,+)} + \lambda_{n,-} I^{(n,-)}}}{\mathrm{Tr}\left(e^{-\sum_n \lambda_{n,+} I^{(n,+)} + \lambda_{n,-} I^{(n,-)}}\right)} = \frac{e^{-\sum_k \mu_k\ n(k)}}{\mathrm{Tr}\left(e^{-\sum_k \mu_k\ n(k)}\right)}. \tag{7.43}$$

At this point a word of caution is in order. There are cases in which local conservation laws exist that cannot be expressed in terms of mode occupation operators. In non-interacting theories this occurs if the dispersion relation in the finite volume has additional symmetries. An example is provided by setting $\mu = 0$ in our tight-binding model (7.40), in which case the dispersion has the symmetry $\epsilon(p) = -\epsilon(\pi - p)$. In this case the following operator commutes with the Hamiltonian

$$\sum_j (-1)^j \left[c_j c_{j+1} - c_j^\dagger c_{j+1}^\dagger\right] = \sum_k e^{-ik} c(\pi - k)c(k) + \mathrm{h.c.} \qquad (\mu = 0)\,, \tag{7.44}$$

but is clearly neither expressible in terms of mode occupation operators, nor does it commute with the latter. In cases like this the stationary state is not always locally equivalent to a GGE of the form (7.43) since the constraints arising from the additional local charges must be imposed as well [51, 93, 166].

7.3.4 Generalized Microcanonical Ensemble (GMC)

In equilibrium Statistical Physics it is well known that in the thermodynamic limit the Gibbs ensemble becomes equivalent to the microcanonical ensemble. In the quench context analogous equivalences of ensembles hold, and we now turn to their discussion.

Generic Systems

We have stated above that generic systems thermalize when their stationary state density matrix is equal to a Gibbs ensemble in the sense of (7.23), (7.27), where the effective temperature is fixed by the energy density e given by (7.28). There is strong numerical evidence [161, 167,

168, 169, 170, 171, 172, 173, 174, 175, 176] that an equivalent microcanonical ensemble can be constructed in the form

$$\rho^{\mathrm{MC}} = |n\rangle\langle n| \ , \tag{7.45}$$

where $|n\rangle$ is any energy eigenstate (of the post-quench Hamiltonian) with energy density e. Importantly, no averaging over a microcanonical energy shell is required. This implies that in generic systems all energy eigenstates at a given energy density are locally indistinguishable and thermal. The microcanonical description for the stationary state of a thermalizing system is then

$$\rho^{\mathrm{SS}} =_{\mathrm{loc}} \rho^{\mathrm{MC}} \ . \tag{7.46}$$

Systems with local conservation laws

If a system has local conservation laws other than energy the above construction needs to be modified. This was first discussed in the non-interacting case by Cassidy et.al. [22] and subsequently generalized to interacting integrable models by Caux and Essler [177]. Let us recall that the "initial data" for a (post quench) system with local conservation laws $I^{(n)}$ and Hamiltonian $H = I^{(1)}$ is

$$e^{(n)} = \lim_{L\to\infty} \frac{1}{L} \mathrm{Tr}\left(\rho(0) I^{(n)}\right) \ . \tag{7.47}$$

The stationary state is then locally equivalent to the density matrix

$$\rho^{\mathrm{SS}} =_{\mathrm{loc}} \rho^{\mathrm{GMC}} = |\Phi\rangle\langle\Phi| \ , \tag{7.48}$$

where $|\Phi\rangle$ is a simultaneous eigenstate of all local conservation laws such that

$$\lim_{L\to\infty} \left[\frac{1}{L} I^{(n)} - e^{(n)}\right] |\Phi\rangle = 0 \ . \tag{7.49}$$

Conditions (7.49) ensure that all $I^{(n)}$ have the correct expectation values (7.47) in the stationary state. An obvious question is how to construct $|\Phi\rangle$ in practice. For non-interacting lattice models this is often straightforward as we now discuss. In free theories the Hamiltonian is diagonalized in terms of mode occupation operators $n(k) = c^\dagger(k)c(k)$

$$H = \sum_k \epsilon(k) n(k) \ , \quad [n(k), n(q)] = 0 = [n(k), H]. \tag{7.50}$$

As discussed above the $n(k)$ are in one-to-one correspondence with local conservation laws and can therefore be used to construct GGEs. The initial conditions (7.47) therefore fix the densities $\rho(k)$ of particles with momentum k

$$\mathrm{Tr}\left(\rho(0) n(k)\right) = \rho(k) \ . \tag{7.51}$$

In a large, finite volume L, the state $|\Phi\rangle$ can then be taken as a Fock state

$$|\Phi\rangle = \prod_{j=1}^{N} c^\dagger(k_j)|0\rangle \ , \quad c(q)|0\rangle = 0 \ . \tag{7.52}$$

The k_j need to be chosen to reproduce the correct particle density $\rho(k)$ in the thermodynamic limit $N, L \to \infty$, $n = N/L$ fixed. Noting that $\Delta n = \rho(k)\Delta k$ we see that a possible choice is

$$k_{j+1} = k_j + \frac{1}{L\rho(k_j)}. \tag{7.53}$$

In practice we can determine $\rho(k)$ from (7.51), construct the state $|\Phi\rangle$ from (7.52), (7.53), and then use it to form ρ^{GMC}. In interacting theories the construction is analogous but considerably more involved and will be discussed in Section 10.3.2.

In contrast to the non-integrable case, energy eigenstates at a given energy density e are not all locally indistinguishable and thermal. While the typical state at a given e is thermal in this case as well, there exist other, non-thermal, macro-states at a given e. However, their entropies are smaller than the one of the thermal equilibrium state. A more detailed discussion is given in Appendix 7.10.

7.3.5 Time averaged relaxation and Diagonal Ensemble

In the literature a different definition of relaxation after quantum quenches in finite systems is widely used [118, 121]. Let us for simplicity consider a one-dimensional system on a ring of length L, which is initially prepared in a state with density matrix $\rho(0)$. The time average of an operator $\mathcal{O}$ is then defined as

$$\bar{\mathcal{O}}_L = \lim_{T\to\infty} \frac{1}{T}\int_0^T dt\ \mathrm{Tr}\left(\rho(t)\ \mathcal{O}\right), \tag{7.54}$$

where we have introduced the subscript L to indicate that the system size is kept fixed at L, and where we assumed the limit $T\to\infty$ to exist. The operator $\mathcal{O}$ is then said to relax if its expectation value is very close to its time average most of the time, i.e. if

$$\frac{1}{T}\int_0^T dt \left[\mathrm{Tr}\left(\rho(t)\ \mathcal{O}\right) - \bar{\mathcal{O}}_L\right]^2 \ll \bar{\mathcal{O}}_L^2. \tag{7.55}$$

Physically this way of thinking about relaxation is very different from ours. This is most easily understood for a non-interacting system, which by construction features stable particle and hole excitations. Let us denote their maximal group velocity by v_{max}. In time averaged relaxation one considers times t such that $v_{\mathrm{max}}t \gg L$, i.e. the stable excitations traverse the entire system many times. In contrast, our way of defining relaxation is based on taking the thermodynamic limit first, and then considering late times.

A natural question to ask is what statistical ensemble describes the averages $\bar{\mathcal{O}}$. To see this let us consider time evolution with a Hamiltonian H that has non-degenerate eigenvalues E_n. Expanding the density matrix in the basis of energy eigenstates gives

$$\rho(t) = \sum_{n,m}\langle n|\rho(0)|m\rangle\ e^{-i(E_n-E_m)t}|n\rangle\langle m|\ . \tag{7.56}$$

Substituting this back into (7.54) and using that the energy eigenvalues are non-degenerate we arrive at

$$\bar{\mathcal{O}}_L = \sum_n \langle n|\rho(0)|n\rangle\ \langle n|\mathcal{O}|n\rangle. \tag{7.57}$$

This shows that time averages involve only the diagonal elements (in the energy eigenbasis) of the density matrix. The description (7.57) is known as diagonal ensemble. Is there a relation between the subsystem view of relaxation and the time-averaged one? It is believed that for local operators $\mathcal{O}$ the two viewpoints are in fact equivalent in the sense that

$$\lim_{L\to\infty}\bar{\mathcal{O}}_L = \mathrm{Tr}\left[\rho^{SS}\mathcal{O}\right]\ . \tag{7.58}$$

In the case of the TFIC this has been shown in Appendix E of Ref. [26] and elaborated on in Ref. [30].

7.3.6 Symmetry restoration

An interesting question in the quantum quench context concerns problems where the Hamiltonian is invariant under a symmetry operation, but the initial state after the quench is not. If we denote the symmetry operation by U, then we have

$$[H, U] = 0 \ , \qquad U|\Psi(0)\rangle \neq |\Psi(0)\rangle. \tag{7.59}$$

The question is then, whether or not the symmetry associated with U is restored in the stationary state

$$[\rho^{\mathrm{SS}}, U] \stackrel{?}{=} 0. \tag{7.60}$$

The answer to this is quite straightforward for the stationary states we have considered here, which are described by (generalized) Gibbs ensembles

$$\rho^{\mathrm{SS}} =_{\mathrm{loc}} \rho_{\mathrm{GGE}} = \frac{1}{Z_{\mathrm{GGE}}} e^{-\sum_n \lambda_n I^{(n)}} \ . \tag{7.61}$$

Clearly, if U is a symmetry of all local conservation laws

$$[I^{(n)}, U] = 0 \ , \quad \forall n \ , \tag{7.62}$$

the symmetry associated with U will be restored in the stationary state. Conversely, if there is at least one conservation law for which $[I^{(s)}, U] \neq 0$, then the symmetry will remain broken in the stationary state. It is useful to consider some explicit examples.

Spin-flip symmetry

The TFIC Hamiltonian (7.6) is invariant under rotations in spin space around the z-axis by 180 degrees

$$U\sigma_\ell^\alpha U^\dagger = -\sigma_\ell^\alpha \ , \quad \alpha = x, y, \qquad U\sigma_\ell^z U^\dagger = \sigma_\ell^z \ . \tag{7.63}$$

A quantum quench of the transverse field starting in the ordered phase $h < 1$ leads to an initial state that breaks this symmetry. However, the local conservation laws (7.33) that characterize the stationary state are invariant with respect to spin reflection. As a result the spin flip symmetry is restored in the stationary state [28], as will be shown in Section 7.6.

Parity symmetry

The Hamiltonian of the tight-binding model (7.40) is invariant under the parity transformation (reflection across a link)

$$U c_\ell^\dagger U^\dagger = c_{1-\ell}^\dagger \, . \tag{7.64}$$

On the other hand, the set of charges $I^{(n,-)}$ in (7.42) is odd under U, and hence a quantum quench from a state that is not parity even does not generally result in a parity-symmetric stationary state. As an example we may consider the time evolution of the ground state $|\Psi(0)\rangle$ of the following Hamiltonian

$$H_0 = \sum_\ell \frac{i}{4} \left(3c_\ell^\dagger c_{\ell+1} - 3c_{\ell+1}^\dagger c_\ell - c_\ell^\dagger c_{\ell+1}^\dagger + c_{\ell+1} c_\ell \right) + \mu_0 c_\ell^\dagger c_\ell \, . \tag{7.65}$$

For $|\mu_0| < \sqrt{2}$, $|\Psi(0)\rangle$ is not parity-symmetric and the expectation value of $I^{(n,-)}$ is nonzero

$$\langle \Psi(0)|I^{(n,-)}|\Psi(0)\rangle = J \frac{1-(-1)^n}{2} \frac{\cos\left(n \arcsin(\frac{|\mu_0|}{\sqrt{2}})\right)}{\pi n} \neq 0. \tag{7.66}$$

As $I^{(n,-)}$ are conserved we must have

$$\lim_{L\to\infty}\frac{1}{L}\mathrm{Tr}\big(\rho^{\mathrm{SS}}\ I^{(n,-)}\big)=\lim_{L\to\infty}\frac{1}{L}\langle\Psi(0)|I^{(n,-)}|\Psi(0)\rangle, \tag{7.67}$$

and consequently the stationary state cannot be not symmetric under (7.64). We note that the above symmetry argument does not guarantee a non-zero value for the expectation value in (7.66), as there could be other symmetries that force it to vanish.

Translational symmetry

If we allow the initial state to partially break translational symmetry the situation can become significantly more complicated. An interesting example is provided by the quantum XY model [178]

$$H_{\mathrm{XY}}=J\sum_{\ell=1}^{L}\frac{1+\gamma}{4}\sigma_\ell^x\sigma_{\ell+1}^x+\frac{1-\gamma}{4}\sigma_\ell^y\sigma_{\ell+1}^y\ , \tag{7.68}$$

where we take L to be even. As long as we consider quenches from translationally invariant initial states, the stationary behaviour is described by a GGE constructed from local conservation laws $Q^{(n,\pm)}$ along the lines described above. The situation changes for initial states $|\Psi_2(0)\rangle$ that are invariant only under translations by two sites. One might naively expect that translational symmetry gets restored in the stationary state, but this is in fact not the case [51]. This can be understood by noting that H has local conservation laws that are not translationally invariant, an example being

$$J_1^+=\sum_{\ell=1}^{L}(-1)^\ell\Big[\frac{1+\gamma}{4}\sigma_\ell^x\sigma_{\ell+1}^x-\frac{1-\gamma}{4}\sigma_\ell^y\sigma_{\ell+1}^y\Big],\quad [J_1^+,H_{\mathrm{XY}}]=0. \tag{7.69}$$

Generically one will have $\langle\Psi_2(0)|J_1^+|\Psi_2(0)\rangle\neq 0$, and as J_1^+ is conserved, translational invariance must remain broken at all times. The construction of a GGE in this case is complicated by the fact that J_1^+ does not commute with all $Q^{(n,\pm)}$, and involves an initial state dependent selection of mutually commuting local conservation laws.

7.3.7 Truncating Generalized Gibbs Ensembles

As we have seen above, GGEs in integrable models involve infinite numbers of conservation laws in the thermodynamic limit. A natural question to ask is whether all of these are equally important for the description of the stationary state, or whether certain classes are more important than others. A general framework for investigating this question was developed in Ref. [28] and then applied to the specific example of quenches in the TFIC. The main findings are conjectured to apply much more generally to quenches in integrable models. A key measure of importance of a given conservation law is its degree of locality[28] D_{loc}. This is straightforward to quantify for conservation laws like (7.33), which have densities that act non-trivially only on a fixed number of $n+1$ neighbouring sites,

$$I^{(n)}=\sum_j\mathcal{I}_j^{(n)}\ ,\quad \mathrm{range}(\mathcal{I}_j^{(n)})=n+1\qquad\Rightarrow D_{\mathrm{loc}}\big(I^{(n)}\big)=n+1. \tag{7.70}$$

The idea of Ref. [28] was to select various finite subsets $\{J_m|m=1,\ldots,y\}\subset\{I^{(n)}\}$, and ask how well the density matrices

$$\rho^{\mathrm{pGGE,y}}=\frac{e^{-\sum_{n=1}^{y}\lambda_n^{(y)}J_n}}{\mathrm{Tr}\left(e^{-\sum_{n=1}^{y}\lambda_n^{(y)}J_n}\right)} \tag{7.71}$$

approximate the full GGE density matrix. Here the Lagrange multipliers $\lambda_n^{(y)}$ are fixed by imposing the appropriate initial conditions

$$\lim_{L\to\infty} \frac{\langle\Psi(0)|J_n|\Psi(0)\rangle}{L} = \lim_{L\to\infty} \frac{1}{L}\mathrm{Tr}\left(\rho^{\mathrm{pGGE,y}} J_n\right) \ , \quad n = 1, \ldots, y. \tag{7.72}$$

A useful way of comparing the full ρ^{GGE} and partial $\rho^{\mathrm{pGGE,y}}$ GGEs is through a distance $\mathcal{D}(\rho_\ell, \rho'_\ell)$ on the space of reduced density matrices on an interval of length ℓ. In order for $\rho^{\mathrm{pGGE,y}}$ to be a good approximation to ρ^{GGE} it should be possible to make the distance between their respective reduced density matrices arbitrarily small

$$\mathcal{D}\big(\rho_\ell^{\mathrm{GGE}}, \rho_\ell^{\mathrm{pGGE,y}}\big) \stackrel{!}{<} \epsilon \ , \quad \forall \ell. \tag{7.73}$$

The findings of Ref. [28] show that if even a single conservation law with small degree of locality is excluded, the approximation (7.71) immediately becomes very poor, and the only way to achieve (7.73) is by retaining all conservation laws with the smallest degrees of locality (7.70), i.e. by considering "truncated GGEs" of the form

$$\rho^{\mathrm{tGGE,y}} = \frac{e^{-\sum_{n=1}^{y} \lambda_n^{(y)} I^{(n)}}}{\mathrm{Tr}\left(e^{-\sum_{n=1}^{y} \lambda_n^{(y)} I^{(n)}}\right)} \ . \tag{7.74}$$

The value of y is then determined by the required degree of accuracy ϵ in (7.73). A consequence of these findings is that the full GGE can in fact be defined as the limit of truncated GGEs

$$\rho^{\mathrm{GGE}} \equiv \lim_{y\to\infty} \rho^{\mathrm{tGGE,y}} \ . \tag{7.75}$$

The limiting procedure (7.75) was originally introduced in a non-interacting model (the transverse-field Ising)[28], and has since proved very useful for the construction of GGEs and the calculation of the stationary state values of local observables in interacting integrable models[58, 59, 17, 64, 179].

To exhibit the above ideas more explicitly it is useful to consider the example of a transverse field quench in the disordered phase of the TFIC[28]. Fig. 7.2 shows results for an appropriately defined distance between the reduced density matrices of the full and truncated GGEs as a function of the number y of conservation laws retained in (7.74). Ten different subsystem sized $\ell = 5, 10, \ldots, 50$ are shown.

We see that for a given subsystem size ℓ the distance $\mathcal{D}\big(\rho_\ell^{\mathrm{GGE}}, \rho_\ell^{\mathrm{pGGE,y}}\big)$ starts decaying exponentially in y above an ℓ-dependent value. This means that conservation laws $I^{(n)}$ with $n \gg \ell$ play a negligible role in describing stationary state properties in a subsystem of size ℓ. The main message is then as follows:

> The smaller the degree of locality of a conservation law is, the more important it is for describing the stationary properties of local observables.

7.3.8 Dynamical properties in the stationary state

It is clearly of interest to go beyond the equal time correlators we have discussed so far and consider dynamical (non equal time) correlations. In particular one can envisage using them to characterize the stationary state in the same way they are used in thermal equilibrium. An example would be the measurement of dynamical response functions in the stationary state by e.g. photoemission spectroscopy[180]. For such purposes the objects of interest are of the form

$$\lim_{t\to\infty} \langle\Psi(t)|\mathcal{O}_1(t_1)\cdots\mathcal{O}_n(t_n)|\Psi(t)\rangle \, , \qquad \mathcal{O}_j(t) = e^{iHt}\mathcal{O}_j e^{-iHt} \, , \tag{7.76}$$

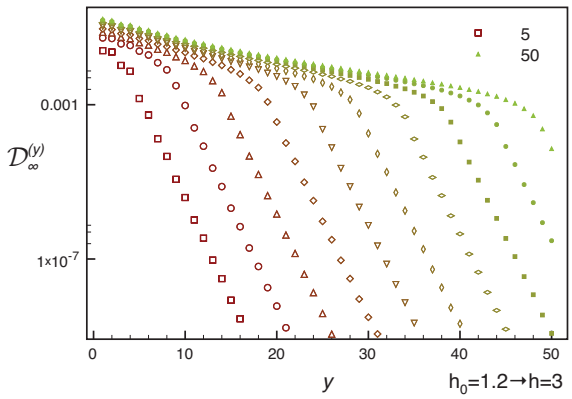

Figure 7.2: Distance $\mathcal{D}_\infty^{(y)} = \mathcal{D}(\rho_\ell^{\rm GGE}, \rho_\ell^{\rm tGGE,y})$, as defined in (7.156), between the GGE and the truncated GGEs obtained by taking into account local conservation laws with densities involving at most $y+1$ consecutive sites. The quench is from $h_0 = 1.2$ to $h = 3$ and the subsystem size ranges from $\ell = 5$ to $\ell = 50$. Colors and sizes change gradually as a function of the size ℓ. For $y > \ell$, the distance starts decaying exponentially in y, with an ℓ-independent decay rate. [Figure taken from Ref. [28]]

where $\mathcal{O}_j$ are local observables. The problem one is faced with is that the descriptions of the stationary state by statistical ensembles (GGE, GMC) a priori hold only at the level of finite subsystems in the thermodynamic limit. On the other hand, time dependent operators act by construction non-trivially on the entire system, which moves them beyond the remit of applicability of the framework set out above. This issue was addressed in Ref. [29], which established that the stationary state density matrix $\rho^{\rm SS}$ that describes the local relaxation in fact provides a correct description of dynamical correlations as well, i.e.

$$\lim_{t\to\infty} \langle \Psi(t)|\mathcal{O}_1(t_1)\cdots\mathcal{O}_n(t_n)|\Psi(t)\rangle = {\rm Tr}[\rho^{\rm SS}\mathcal{O}_1(t_1)\cdots\mathcal{O}_n(t_n)]\,. \tag{7.77}$$

The proof of this statement is based on the Lieb-Robinson bound (see Sec. 7.5.1) and more specifically on a theorem by Bravyi, Hastings, and Verstraete [181], who showed that time-evolving operators (in the Heisenberg picture) are well approximated by local operators with a range that increases linearly in time. We stress that (7.77) does not depend on which statistical ensemble describes the local relaxation in the stationary state, i.e. for generic systems $\rho^{\rm SS}$ would be a Gibbs or a microcanonical density matrix, while for integrable systems it would be that of a GGE or GMC.

The issue of whether or not a fluctuation dissipation relation (FDR) holds in the stationary state was investigated in Refs [38, 41, 29, 182]. In thermal equilibrium, the FDR connects the imaginary part of the linear response function $\chi_{AB}(\omega,\vec{q}|\rho)$ of two observables A, B to the corresponding spectral function $S_{AB}(\omega,\vec{q}|\rho)$

$$-\frac{1}{\pi}{\rm Im}\;\chi_{AB}\big(\omega,\vec{q}\,|\rho^{\rm Gibbs}(\beta)\big) = (1-e^{-\beta\omega})S_{AB}\big(\omega,\vec{q}\,|\rho^{\rm Gibbs}(\beta)\big)\,. \tag{7.78}$$

Here we have defined

$$\begin{aligned}
\chi_{AB}(\omega,\vec{q}\,|\rho) &= -\frac{i}{L}\sum_{j,\ell}\int_0^\infty {\rm d}t\; e^{i\omega t - i\vec{q}\cdot(\vec{r}_j-\vec{r}_\ell)}{\rm Tr}\Big(\rho\;[A_j(t),B_\ell]\Big)\,,\\
S_{AB}(\omega,\vec{q}\,|\rho) &= \frac{1}{L}\sum_{j,\ell}\int_{-\infty}^\infty \frac{{\rm d}t}{2\pi}\; e^{i\omega t - i\vec{q}\cdot(\vec{r}_j-\vec{r}_\ell)}{\rm Tr}\Big(\rho\;A_j(t)B_\ell\Big)\,.
\end{aligned} \tag{7.79}$$

In the derivation of (7.78) one uses that in thermal equilibrium the spectral function for negative and positive frequencies are related in a simple way

$$S_{BA}\big(-\omega,-\vec{q}\,|\rho^{\rm Gibbs}(\beta)\big)=e^{-\beta\omega}S_{AB}\big(\omega,\vec{q}\,|\rho^{\rm Gibbs}(\beta)\big). \tag{7.80}$$

Let us now turn to FDRs in the steady state after quantum quenches. Clearly, if the system thermalizes (7.27), the equilibrium FDR (7.78) with inverse temperature $\beta_{\rm eff}$ applies. If on the other hand the system locally relaxes to a GGE, the imaginary part of the linear response function ceases to be proportional to the spectral function[38, 41, 29]. This can be traced back to the absence of a simple relationship between the spectral functions at positive and negative frequencies. However, the basic form of the FDR still holds[29]

$$-\frac{1}{\pi}{\rm Im}\;\chi_{AB}\big(\omega,\vec{q}\,|\rho^{\rm GGE}\big)=S_{AB}\big(\omega,\vec{q}\,|\rho^{\rm GGE}\big)-S_{BA}\big(-\omega,-\vec{q}\,|\rho^{\rm GGE}\big)\,. \tag{7.81}$$

7.4 A simple example

In order to see the ideas presented above at work, we now consider the specific example of a one dimensional fermionic pairing model

$$H(\Delta,\mu)=-J\sum_{j=1}^{L}c_j^\dagger c_{j+1}+c_{j+1}^\dagger c_j-\mu\sum_{j=1}^{L}c_j^\dagger c_j+\Delta\sum_{j=1}^{L}c_j^\dagger c_{j+1}^\dagger+c_{j+1}c_j\;. \tag{7.82}$$

Here $c_j^\dagger$, c_j are canonical fermion creation and annihilation operators at site j and $\{c_j,c_n^\dagger\}=\delta_{j,n}$. In momentum space we have

$$H(\Delta,\mu)=\sum_k\epsilon_0(k)\;c^\dagger(k)c(k)-i\Delta\sin(k)\big(c^\dagger(k)c^\dagger(-k)-c(-k)c(k)\big)\;, \tag{7.83}$$

where we have defined $\epsilon_0(k)=-2J\cos(k)-\mu$ and

$$c_j=\frac{1}{\sqrt{L}}\sum_k e^{-ikj}c(k)\;. \tag{7.84}$$

The Hamiltonian (7.83) is diagonalized by a Bogoliubov transformation

$$\begin{pmatrix}\alpha(k)\\ \alpha^\dagger(-k)\end{pmatrix}=\begin{pmatrix}\cos(\Theta_k/2) & -i\sin(\Theta_k/2)\\ -i\sin(\Theta_k/2) & \cos(\Theta_k/2)\end{pmatrix}\begin{pmatrix}c(k)\\ c^\dagger(-k)\end{pmatrix},\quad k\neq 0, \tag{7.85}$$

where

$$\epsilon(k)=\sqrt{(2J\cos(k)+\mu)^2+4\Delta^2\sin^2(k)}\;,\quad e^{i\Theta_k}=\frac{-2J\cos(k)-\mu+2i\Delta\sin(k)}{\epsilon(k)}. \tag{7.86}$$

Defining $\alpha(0)=c^\dagger(0)$ we find

$$H(\Delta,\mu)=\sum_k\epsilon(k)\;\alpha^\dagger(k)\alpha(k)+{\rm const}\;. \tag{7.87}$$

Let us now implement a quantum quench by initially preparing our system in the ground state of $H(\Delta,\mu)$, and at $t=0$ quenching the pairing amplitude from Δ to zero. The initial state is the Bogoliubov fermion vacuum

$$|\Psi(0)\rangle=|0\rangle\;,\quad \alpha(k)|0\rangle=0\;\forall k. \tag{7.88}$$

The time evolution of the fermion annihilation operators is obtained by solving the Heisenberg equations of motion $\frac{d}{dt}c(k,t) = i[H(0,\mu), c(k,t)] = -i\epsilon_0(k)c(k,t)$, which gives

$$c(k,t) = e^{-i\epsilon_0(k)t}c(k) = e^{-i\epsilon_0(k)t}\left[\cos(\Theta_k/2)\ \alpha(k) - i\sin(\Theta_k/2)\ \alpha^\dagger(-k)\right]. \tag{7.89}$$

The fermion two-point functions at $t > 0$ are thus equal to

$$\begin{aligned}\langle\Psi(t)|c^\dagger(k)c(q)|\Psi(t)\rangle &= \langle 0|c^\dagger(k,t)c(q,t)|0\rangle = \delta_{k,q}\sin^2\left(\Theta_k/2\right),\\ \langle\Psi(t)|c(k)c(q)|\Psi(t)\rangle &= \delta_{k,-q}\frac{i}{2}\sin\Theta_k\ e^{-2i\epsilon_0(k)t}.\end{aligned} \tag{7.90}$$

In position space we obtain

$$\begin{aligned}\langle\Psi(t)|c^\dagger_{j+\ell}c_j|\Psi(t)\rangle &= \frac{1}{L}\sum_k e^{ik\ell}\sin^2\left(\Theta_k/2\right) = f_L(\ell),\\ \langle\Psi(t)|c_{j+\ell}c_j|\Psi(t)\rangle &= \frac{1}{L}\sum_k e^{-ik\ell}\frac{i}{2}\sin\Theta_k\ e^{-2i\epsilon_0(k)t} = g_L(\ell,t).\end{aligned} \tag{7.91}$$

Importantly, multi-point correlation functions can be calculated by Wick's theorem, e.g.

$$\langle\Psi(t)|c^\dagger_j c^\dagger_k c_n c_m|\Psi(t)\rangle = g^*_L(k-j,t)g_L(n-m,t) - f_L(j-n)f_L(k-m) + f_L(k-n)f_L(j-m). \tag{7.92}$$

In the limit $L\to\infty$ we can turn the sums in (7.91) into integrals, which at late times can be evaluated by a stationary phase approximation. At infinite times we obtain

$$\begin{aligned}\lim_{L\to\infty} f_L(\ell) &= \int_0^{2\pi}\frac{dk}{2\pi}\ e^{ik\ell}\ \sin^2\left(\Theta_k/2\right),\\ \lim_{t\to\infty}\lim_{L\to\infty} g_L(\ell,t) &= 0.\end{aligned} \tag{7.93}$$

Importantly the "anomalous" average $\langle\Psi(t)|c_{j+\ell}c_j|\Psi(t)\rangle$ vanishes in this limit. We can now immediately conclude that our system relaxes locally to some steady state: any operator $\mathcal{O}$ acting non-trivially only on a given, finite subsystem B can be expressed in terms of fermionic creation and annihilation operators acting only on sites in B. We then can use Wick's theorem to express the expectation value of $\langle\Psi(t)|\mathcal{O}|\Psi(t)\rangle$ in terms of the functions $f_L(\ell)$ and $g_L(\ell,t)$. After taking the infinite volume limit $L\to\infty$, the limit $t\to\infty$ of the resulting expression exists. This argument shows that the steady state is completely characterized by the two-point functions (7.93) and the fact that Wick's theorem holds.

7.4.1 Generalized Gibbs Ensemble

According to our previous discussion the steady state should be described by the GGE (7.43), where the Lagrange multipliers are fixed by

$$\mathrm{Tr}\left[\rho^{\mathrm{GGE}}c^\dagger(k)c(k)\right] = \frac{1}{1+e^{\mu_k}} = \langle\Psi(0)|c^\dagger(k)c(k)|\Psi(0)\rangle = \sin^2\left(\Theta_k/2\right). \tag{7.94}$$

As the GGE density matrix is Gaussian a Wick's theorem holds, and as a consequence of (7.94) the two-point functions in the GGE coincide with those of our steady state. As we have a Wick's theorem in the steady state as well, the GGE correctly reproduces all multi-point correlation functions. This proves that the steady state in our example is locally equivalent to the GGE (7.43), (7.94).

7.5 Spreading of correlations after a quantum quench

Let us now turn to the time dependence of the expectation values of local operators after a quantum quench. As an example we consider the connected correlation function of the fermionic density $n_j = c_j^\dagger c_j$ in our example of section 7.4

$$S_L(\ell, t) = \langle \Psi(t)|n_{j+\ell} n_j|\Psi(t)\rangle - \langle \Psi(t)|n_{j+\ell}|\Psi(t)\rangle\langle \Psi(t)|n_j|\Psi(t)\rangle \ . \tag{7.95}$$

Application of Wick's theorem gives

$$S_L(\ell, t) = |g_L(-\ell, t)|^2 - |f_L(\ell)|^2. \tag{7.96}$$

It is convenient to isolate the time dependent part $|g_L(-\ell, t)|^2$, which is shown in Fig. 7.3 for a quantum quench, where we start in the ground state of $H(\Delta = 2J, \mu = -J)$ and time evolve with $H(0, \mu = -J)$. At a fixed value of ℓ the connected correlator is exponentially small (in ℓ)

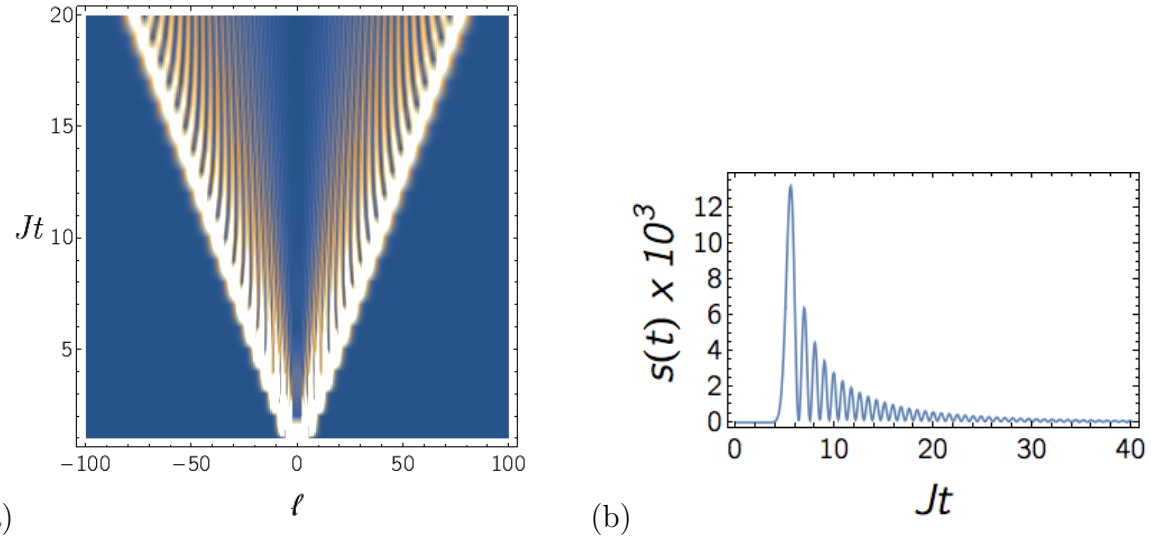

Figure 7.3: (a) Time dependent part $S_\infty(\ell, t) + |f_\infty(\ell)|^2$ of the connected density-density correlator after a quantum quench where the system is initialized in the ground state of $H(\Delta = 2J, \mu = -J)$, and time evolved with $H(0, \mu = -J)$. A light cone effect is clearly visible. (b) $s(t) = S_\infty(\ell = 20, t) + |f_\infty(20)|^2$ as a function of time.

until a time

$$t_F = \frac{\ell}{2v_{\max}} \ , \tag{7.97}$$

where in our example $v_{\max} = 2J$ is the maximal group velocity of elementary particle and hole excitations of our post-quench Hamiltonian $H(0, \mu = -J)$. At $t \approx t_F$ the connected correlator increases substantially, goes through a maximum, and then decays in an oscillating fashion. A physical explanation for the light cone effect was provided by Calabrese and Cardy[89, 80]. For a non-interacting, non-relativistic theory like the one in our example it goes as follows, cf. Fig. 7.4. We focus on connected correlation functions of local operators, e.g.

$$G_{\mathcal{O}\mathcal{O}}(r_1, r_2; t) = \langle \Psi(t)|\mathcal{O}(r_1)\mathcal{O}(r_2)|\Psi(t)\rangle - \langle \Psi(t)|\mathcal{O}(r_1)|\Psi(t)\rangle\langle \Psi(t)|\mathcal{O}(r_2)|\Psi(t)\rangle \ . \tag{7.98}$$

This is the average of the simultaneous measurement of the observables $\mathcal{O}(r_j)$ minus the product of the averages of separate measurements of $\mathcal{O}_j$ at time t after the quench. The initial state in our case is characterized by a finite correlation length ξ

$$G_{\mathcal{O}\mathcal{O}}(r_1, r_2; t = 0) \propto e^{-|r_1 - r_2|/\xi} \ , \tag{7.99}$$

and is therefore extremely small at large spatial separations. At time $t = 0$ the quantum quench generates a finite density of stable quasiparticle excitations throughout the system. Their dispersion relation is $\epsilon_0(p)$ as our post-quench Hamiltonian is simply $H(0, \mu) = \sum_k \epsilon_0(k) n(k)$. The maximal group velocity of these free fermionic excitations is

$$v_{\max} = \max_p \frac{d\epsilon_0(p)}{dp} = 2J. \tag{7.100}$$

At times $t > 0$ the quasi-particles created by the quench propagate through the system.

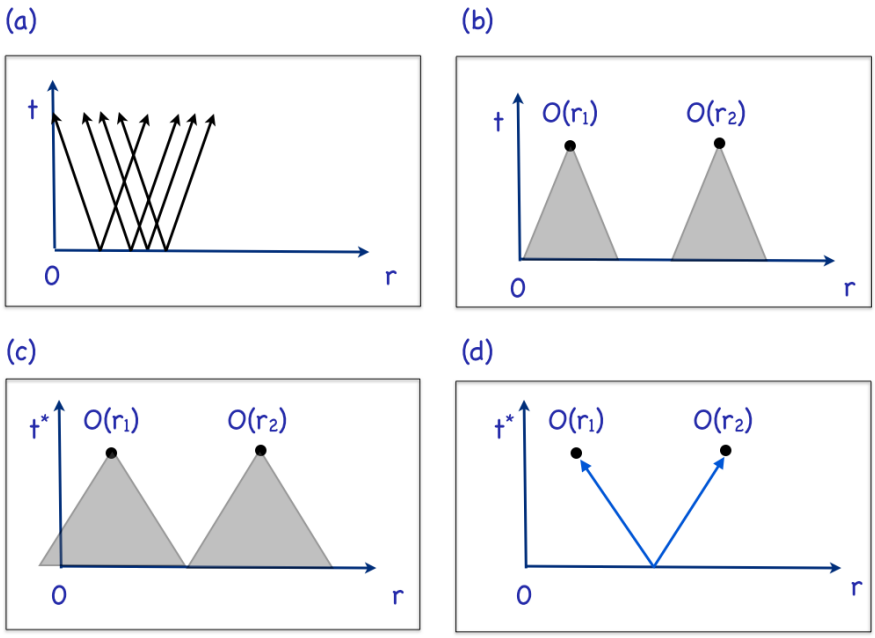

Figure 7.4: "Quasi-particle picture" for the light cone effect [89]: (a) At time $t = 0$ the quantum quench creates quasi-particle excitations throughout the system. (b) At time t quasi-particles from within the "backward light cone" $[r_j - v_{\max} t, r_j + v_{\max} t]$ will affect a measurement at position r_j. This leads to de-phasing of 1-point functions $\langle \Psi(t) | \mathcal{O}(r_j) | \Psi(t) \rangle$. (c) At time $t^* = \frac{|r_2 - r_1|}{2 v_{\max}}$ the backwards light cones touch, and measurements at r_1 and r_2 become correlated. (d) Connected correlations are induced by quasi-particle pairs created at time $t = 0$ and propagating with group velocities $v_{\max}$ in opposite directions.

A measurement at r_j will be influenced by quasi-particles from within the "backwards light cone" $[r_j - v_{\max} t, r_j + v_{\max} t]$. At all times $t > 0$ this will affect the value of the 1-point functions $\langle \Psi(t) | \mathcal{O}(r_j) | \Psi(t) \rangle$, but the effect cancels in the connected two-point function. At time $t^* = \frac{|r_2 - r_1|}{2 v_{\max}}$ the backwards light cones emanating from r_1 and r_2 touch, and the average of measurements at r_1 and r_2 becomes correlated. These connected correlations are induced by quasi-particle pairs created at time $t = 0$ and propagating with group velocities $v_{\max}$ in opposite directions.

Since the work of Calabrese and Cardy light cone effects after quantum quenches have been analyzed in a number of lattice models [183, 184, 48, 185, 25, 26, 27, 186] and observed in experiments on systems of ultra-cold atomic gases [9, 10] and trapped ions [16, 17]. The experimental work raises the poignant theoretical issue of which velocity underlies the observed light cone effect in non-relativistic systems at finite energy densities. Here there is no unique velocity of light, and quasi-particles in interacting systems will generally have finite life times depending on the details of the initial density matrix. For the case of the spin-1/2 Heisenberg

XXZ chain, an integrable model, it was shown in Ref. [56] that the light cone propagation velocity in general depends on the energy density of the initial state, and an explanation for this effect in terms of properties of stable excitations at finite energy densities was put forward. More recent theoretical works address the influence of long-range interactions on the spreading of correlations [188, 187, 189, 190, 191, 192]. Sufficiently long-range interactions lead to a destruction of light cone effects. Non-relativistic continuum models are also known to exhibit modifications to light cone behaviour [110].

It is useful to contrast the above discussion to the spreading of correlations in equilibrium and after "local quantum quenches" [193]. In the latter context one is concerned with the spreading of a local perturbation that has been imposed on an equilibrium state. Light cone effects are observed in such situations as well, but the spreading occurs at the maximum group velocity of elementary excitations over the equilibrium state that is being considered. In other words, unlike for global quantum quenches, there is no factor of two.

7.5.1 Relation to Lieb-Robinson bounds

As shown by Lieb and Robinson [194, 195], the velocity of information transfer in quantum spin chains is effectively bounded. More precisely, there exists a causal structure in commutators of local operators at different times

$$\|[\mathcal{O}_A(t), \mathcal{O}_B(0)]\| \leq c \, \min(|A|, |B|) \, \|\mathcal{O}_A\| \, \|\mathcal{O}_B\| \, e^{-\frac{L-vt}{\xi}} \, . \tag{7.101}$$

Here $\mathcal{O}_A$ and $\mathcal{O}_B$ are local operators acting non-trivially only in two subsystems A and B that are spatially separated by a distance L, $\|.\|$ denotes the operator norm and $|A|$ the number of sites in subsystem A. Finally, c, v and ξ are constants. More recently, the Lieb-Robinson bounds have been refined [196, 197] and extended to mixed state dynamics in open quantum systems [198, 197].

The Lieb-Robinson bound has important consequences for quantum quenches starting in initial states with finite correlation lengths, and time evolving under a short-ranged Hamiltonian. It was shown in Ref. [181] that (7.101) implies a bound on the connected two-point correlation functions after such quenches

$$\langle \Psi(t)|\mathcal{O}_A \, \mathcal{O}_B|\Psi(t)\rangle_{\rm conn} < \bar{c}\big(|A| + |B|\big) \, e^{-\frac{L-2vt}{\chi}} \, . \tag{7.102}$$

Here $\bar{c}$, v and χ are constants. The bound (7.102) shows that connected two-point functions of local operators after quantum quenches in spin chains are exponentially small up to times $t = L/2v$. This tallies very nicely with the light cone effects discussed above. We note that the bound does not provide values for the velocity v or the length χ.

7.5.2 Finite-size effects

Throughout our discussion we have stressed that we are ultimately interested in taking the thermodynamic limit. In a large but finite system local observables can never truly relax. There always will be recurrences[199] such that the return amplitude $\mathcal{F}(t) = |\langle\Psi(0)|\Psi(t)\rangle|$ is arbitrarily close to 1

$$|1 - \mathcal{F}(t)| < \epsilon \, . \tag{7.103}$$

However, in many-particle systems these typically occur only at astronomically late times. The exception to this rule are cases in which the spectrum of the post-quench Hamiltonian in a (large) finite volume for some reason has a highly commensurate structure. A very simple example are Hamiltonians with equidistant energy levels $E_n = E_0 + n\delta$, for which we have $\mathcal{F}(2\pi j/\delta) = 1$.

A more relevant effect in practice are revivals, which refers to situations where $\mathcal{F}(t) = \mathcal{O}(1)$. This again requires the finite size energy spectrum to have a certain regularity, as is the case for example in conformal field theories [91, 88].

A different finite-size effect affects all observables and is related to the light cone repeatedly traversing the system [104, 106, 37, 50]. We refer to this effect as a traversal. As an example we consider the connected two point function (7.95) on a finite ring. A density plot is shown for a system of size $L = 100$ in Fig. 7.5. We see that the light cone traverses the system and

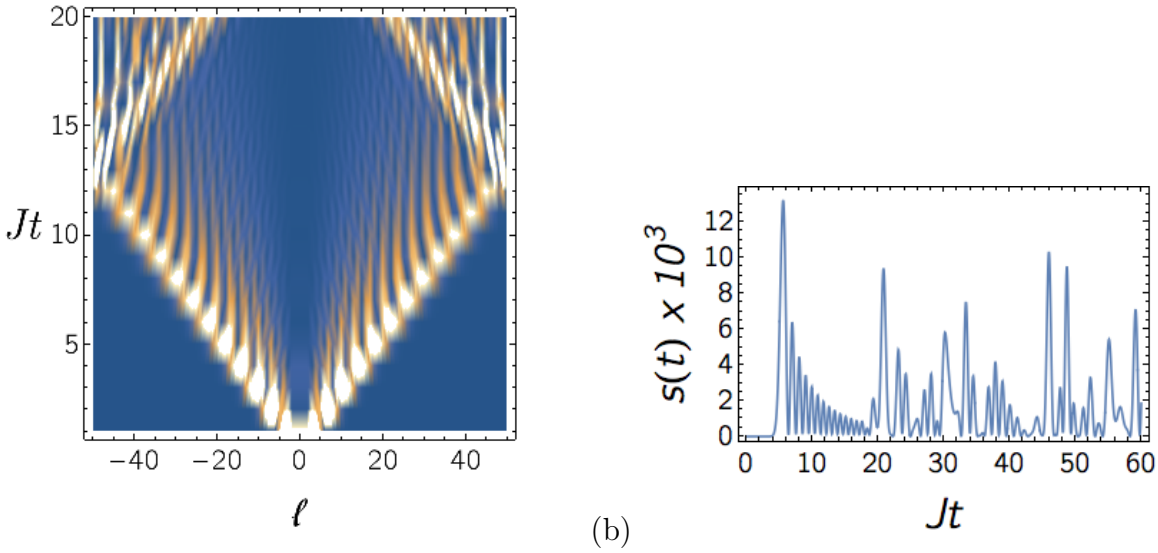

Figure 7.5: (a) Same as Fig. 7.3 but for a finite system with $L = 100$ sites and periodic boundary conditions. At times $Jt > 12.5$ the light cone has traversed the system and eventually causes a revival of the connected correlation function at a given separation ℓ. This is strictly a finite-size effect and has no analog in the thermodynamic limit. (b) $s(t) = S_L(\ell = 20, t) + |f_L(20)|^2$ for $L = 100$ as a function of time.

induces a signal in $S_L(\ell, t)$ at a time $(L - |\ell|)/2v_{\max}$ after the light cone first reaches. Clearly at times $t > (L - |\ell|)/2v_{\max}$ correlation functions of the finite system look very different from the ones in the thermodynamic limit. As is shown in Fig. 7.6, the traversal in not associated with any revival, because the return amplitude remains exponentially small in the system size.

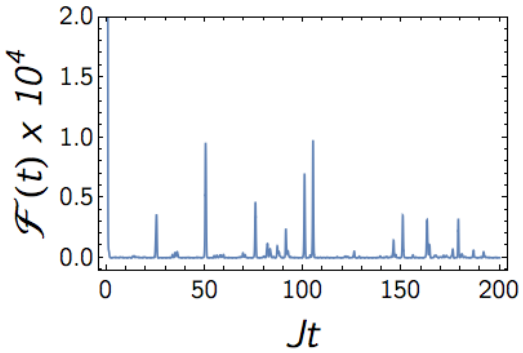

Figure 7.6: The return probability for the same quench as in Fig. 7.3 with $L = 100$ sites and periodic boundary conditions. The overlap with the initial state remains negligible at any time $t > 0$.

7.6 Transverse-field Ising chain (TFIC)

We now turn our attention to a key paradigm for quantum quenches, the transverse-field Ising chain

$$H(h) = -J \sum_{\ell=1}^{L} \sigma_\ell^x \sigma_{\ell+1}^x + h\sigma_\ell^z \,. \tag{7.104}$$

Here we impose periodic boundary conditions $\sigma_{L+1}^\alpha \equiv \sigma_1^\alpha$, L even, $h \geq 0$ and $J > 0$. We note that the signs of h and J can be reversed by unitary transformations with respectively

$$U_1 = \prod_{\ell=1}^{L} \sigma_\ell^x \;, \quad U_2 = \prod_{\ell=1}^{L/2} \sigma_{2\ell-1}^x \sigma_{2\ell}^y. \tag{7.105}$$

The Hamiltonian (7.104) has a $\mathbb{Z}_2$ symmetry of rotations by π around the z-axis. The ground state phase diagram of the TFIC features a paramagnetic (for $h > 1$) and a ferromagnetic (for $h < 1$) phase, in which the $\mathbb{Z}_2$ symmetry is spontaneously broken. The two phases are separated by a quantum critical point at $h = 1$, which is described by the Ising conformal field theory with central charge $c = 1/2$, cf. Ref. [200].

It is well known that the TFIC admits a representation in terms of non-interacting fermions. However, the Jordan-Wigner transformation between spins and fermions is nonlocal. This renders the TFIC an ideal testing ground for relaxation ideas, in particular in relation to the crucial role played by locality.

The study of non-equilibrium dynamics in the TFIC was initiated in a seminal paper by Barouch, McCoy and Dresden in 1970[45]. They analyzed the time evolution of the transverse magnetization $\langle\Psi(t)|\sigma_\ell^z|\Psi(t)\rangle$ and observed that it relaxes to a non-thermal value at late times. The focus of research on the TFIC and its two-dimensional classical counterpart then shifted to the determination of equilibrium properties, and it took thirty years before the issue of relaxation after quantum quenches returned to centre stage[34, 35]. A combination of experimental advances in cold atom systems and the theoretical insights gained through the study of quantum quenches in conformal field theories[89, 90, 80] revitalized the quest for obtaining a complete understanding of the quench dynamics in the TFIC. Exact closed form expressions for the time evolution of the entanglement entropy after a global quench were obtained in Ref. [48]. By combining free-fermion techniques with numerical methods important insights on thermalization issues were gained[33], and finite-size effects like traversals were analyzed in detail[37]. Exact results for the time evolution of order parameter correlations were finally obtained in Refs [25, 26, 27, 40], and it was demonstrated that the stationary state is described by a generalized Gibbs ensemble. The time evolution of reduced density matrices was studied in Ref. [28], and the question of which conservation laws are most important for characterizing the stationary state with a given accuracy was resolved. Refs [39, 50] introduced a semi-classical approach to quantum quenches by generalizing a method developed by Sachdev in the context of equilibrium dynamics[200]. Dynamical (non-equal time) correlations were studied in Refs [39, 50, 29] in relation to the question whether the stationary state fulfils a fluctuation-dissipation theorem. Progress on experimental studies of non-equilibrium evolution in TFICs has been more limited. Ref. [11] reported results on quantum quenches in a cold atom system described by one dimensional Bose Hubbard chains, which map onto the TFIC in a particular limit. Refs [201] proposed a realization of the TFIC with a time-dependent magnetic field in the framework of circuit QED.

7.6.1 Fermionic form of the Hamiltonian

Spin chains that can be mapped to free fermions differ in two important aspects from free fermion models like the one we considered in Section 7.4:

- two-point functions of spin operators map onto n-point correlation functions of fermions, where n is related to the distance between the two spins and can be arbitrarily large;
- The ground state of the TFIC in the ordered phase is not a Fock state (as a result of spontaneous symmetry breaking).

The Hamiltonian (7.104) can be mapped to a fermionic theory by a Jordan-Wigner transformation

$$\sigma_\ell^z = i a_{2\ell} a_{2\ell-1} \ , \quad \sigma_\ell^x = \left(\prod_{j=1}^{\ell-1} (i a_{2j} a_{2j-1}) \right) a_{2\ell-1} \ , \quad \sigma_\ell^y = \left(\prod_{j=1}^{\ell-1} (i a_{2j} a_{2j-1}) \right) a_{2\ell}, \tag{7.106}$$

Here a_ℓ are Majorana fermions satisfying the anti-commutation relations $\{a_\ell, a_n\} = 2\delta_{\ell n}$. The usual spinless fermions are obtained by taking linear combinations $c_\ell^\dagger = (a_{2\ell-1} + i a_{2\ell})/2$. It is now straightforward to see that spin-spin correlation functions map onto expectation values of strings of fermions, e.g.

$$\langle \sigma_\ell^x \rangle = (-i)^{\ell-1} \langle \prod_{j=1}^{2\ell-1} a_j \rangle \qquad \langle \sigma_\ell^x \sigma_{\ell+n}^x \rangle = (-i)^n \langle \prod_{j=2\ell}^{2\ell+2n-1} a_j \rangle \, . \tag{7.107}$$

Application of the Jordan-Wigner transformation to the TFIC Hamiltonian (7.104) results in a fermion Hamiltonian of the form

$$\begin{aligned} H &= \frac{\mathrm{I} - e^{i\pi\mathcal{N}}}{2} H_{\mathrm{R}} + \frac{\mathrm{I} + e^{i\pi\mathcal{N}}}{2} H_{\mathrm{NS}} \, , \\ H_{\mathrm{NS/R}} &= iJ \sum_{j=1}^{L-1} a_{2j} \left[a_{2j+1} - h a_{2j-1} \right] - iJ a_{2L} \left[h a_{2L-1} \mp a_1 \right] . \end{aligned} \tag{7.108}$$

Here $e^{i\pi\mathcal{N}}$ is the fermion parity operator with eigenvalues ± 1

$$e^{i\pi\mathcal{N}} = \prod_{\ell=1}^{L} \sigma_\ell^z = (-i)^L \prod_{j=1}^{2L} a_j \ , \qquad e^{i\pi\mathcal{N}} a_j = -a_j e^{i\pi\mathcal{N}} \, . \tag{7.109}$$

$H_{\mathrm{R,NS}}$ commute with the fermion parity operator, and the full Hamiltonian (7.108) is therefore block-diagonal: H_{R} (H_{NS}) describes the action on states with an odd (even) number of fermions. We note that the free fermion Hamiltonians $H_{\mathrm{NS/R}}$ are closely related to the pairing model (7.83) considered earlier

$$H_{\mathrm{R}} = -H(-J, -2hJ) + JhL \ . \tag{7.110}$$

Ground states

The Hamiltonians $H_{\mathrm{NS/R}}$ can be diagonalized by Bogoliubov transformations to canonical momentum space fermion operators b_p (details can be found in e.g. Appendix A of Ref. [25])

$$H_{\mathrm{a}}(h) = \sum_{p \in \mathrm{a}} \varepsilon_h(p) \left(b_p^\dagger b_p - \frac{1}{2} \right) , \quad \mathrm{a} = \mathrm{R}, \ \mathrm{NS} \ , \tag{7.111}$$

where the single-particle energy is given by

$$\varepsilon_h(k) = 2J\sqrt{1 + h^2 - 2h\cos k}. \tag{7.112}$$

The difference between R and NS sectors enters via the allowed values of the momenta, which are $p = \frac{\pi n}{L}$, where n are even/odd integers for R and NS fermions respectively. The ground states of $H_{\mathrm{R,NS}}(h)$ are the fermionic vacua

$$b_p|GS\rangle_{\mathrm{a}} = 0 \ \forall p \in \mathrm{a}\ , \quad \mathrm{a} = \mathrm{R}, \mathrm{NS}. \tag{7.113}$$

These vacuum states are also eigenstates of the fermion parity operator

$$e^{i\pi\mathcal{N}}|GS\rangle_{\mathrm{NS}} = |GS\rangle_{\mathrm{NS}}\ , \qquad e^{i\pi\mathcal{N}}|GS\rangle_{\mathrm{R}} = \mathrm{sgn}(h-1)|GS\rangle_{\mathrm{R}}\,. \tag{7.114}$$

From (7.108) it follows that in the ferromagnetic phase $h < 1$ both fermion vacua are eigenstates of the full Hamiltonian H. Their respective energies are exponentially (in system size) close, and they become degenerate in the thermodynamic limit. Spin-flip symmetry then gets spontaneously broken, and the ground state is either the symmetric or the antisymmetric combination of the two vacuuum states. In the paramagnetic phase $h > 1$ the ground state of H is given by the NS vacuum state. In summary, we have

$$|GS\rangle = \begin{cases} \frac{|GS\rangle_{\mathrm{NS}} \pm |GS\rangle_{\mathrm{R}}}{\sqrt{2}} & h < 1 \\ |GS\rangle_{\mathrm{NS}} & h > 1\,. \end{cases} \tag{7.115}$$

This shows that for $h < 1$ the ground state of H is not a Fock state.

7.6.2 Quantum quench of the transverse field

We now consider the following quench protocol. We prepare the system in the ground state of $H(h_0)$, and at time $t = 0$ quench the transverse field to a new value h. At times $t > 0$ we time evolve with the new Hamiltonian $H(h)$. All local operators in spin basis can be classified according to their fermion parity, and this turns out to be very useful. We have

$$e^{i\pi\mathcal{N}}\mathcal{O}_{e/o}e^{-i\pi\mathcal{N}} = \pm\mathcal{O}_{e/o}. \tag{7.116}$$

Quenches originating in the paramagnetic phase

For a quench starting in the paramagnetic phase it follows from (7.115), (7.108) and (7.114) that the state of the system at times $t > 0$ is given by

$$|\Psi(t)\rangle = e^{-iHt}|GS\rangle \equiv e^{-iH_{\mathrm{NS}}t}|GS\rangle_{\mathrm{NS}}\,. \tag{7.117}$$

This is even under fermion parity. Hence expectation values of odd operators must vanish

$$\langle\Psi(t)|O_o|\Psi(t)\rangle = 0. \tag{7.118}$$

By virtue of the simple form of both the time evolution operator H_{NS} and the initial state $|\mathrm{GS}\rangle_{\mathrm{NS}}$ in (7.117), expectation values of even operators can be calculated by applying Wick's theorem. This allows the reduction of expectation values of strings of fermion operators to Pfaffians involving only the two-point functions $\langle a_i a_j\rangle$ [202, 46, 47]. For example we have

$$\begin{aligned}\langle\sigma^x_\ell\sigma^x_{\ell+2}\rangle &= -\langle a_{2\ell}a_{2\ell+1}a_{2\ell+2}a_{2\ell+3}\rangle \\ &= -\langle a_{2\ell}a_{2\ell+1}\rangle\langle a_{2\ell+2}a_{2\ell+3}\rangle + \langle a_{2\ell}a_{2\ell+2}\rangle\langle a_{2\ell+1}a_{2\ell+3}\rangle - \langle a_{2\ell}a_{2\ell+3}\rangle\langle a_{2\ell+1}a_{2\ell+2}\rangle\end{aligned} \tag{7.119}$$

Quenches originating in the ferromagnetic phase

As a result of spontaneous symmetry breaking in the ground state, the situation for quenches originating in the ferromagnetic phase $h_0 < 1$ is more complicated. The time evolved initial state is

$$|\Psi(t)\rangle = \frac{e^{-iH_{\rm NS}t}|GS\rangle_{\rm NS} \pm e^{-iH_{\rm R}t}|GS\rangle_{\rm R}}{\sqrt{2}}\,. \tag{7.120}$$

The expectation values of even operators can be expressed in the form

$$\begin{aligned}\langle\Psi(t)|\mathcal{O}_e|\Psi(t)\rangle &= \frac{1}{2}\sum_{\mathrm{a}\in\{\mathrm{R},\mathrm{NS}\}} {}_{\mathrm{a}}\langle GS|e^{iH_{\rm NS}t}\mathcal{O}_e e^{-iH_{\rm NS}t}|GS\rangle_{\mathrm{a}} \\ &\xrightarrow[L\to\infty]{} {}_{\rm NS}\langle GS|e^{iH_{\rm NS}t}\mathcal{O}_e e^{-iH_{\rm NS}t}|GS\rangle_{\rm NS}\,. \end{aligned}\tag{7.121}$$

In the last line we have used that the expectation values in the R and NS sectors become equal in the thermodynamic limit. The last line in (7.121) can again be evaluated by application of Wick's theorem.

In contrast, expectation of odd operators cannot be simplified in this way. Instead we have

$$\langle GS|e^{iHt}\mathcal{O}_o e^{-iHt}|GS\rangle = \pm\mathrm{Re}[{}_{\rm NS}\langle GS|e^{iH_{\rm NS}t}\mathcal{O}_o e^{-iH_{\rm R}t}|GS\rangle_{\rm R}]\,. \tag{7.122}$$

Wick's theorem does not apply here, and in order to proceed one commonly resorts to one of the following methods[203]:

1. Using the cluster decomposition property we can obtain (7.122) from the expectation value of an even operator by considering the limit

$$|\langle GS|e^{iHt}\mathcal{O}_o e^{-iHt}|GS\rangle| = \lim_{d\to\infty}\sqrt{{}_{\rm NS}\langle GS|e^{iH_{\rm NS}t}O_o(r)\mathcal{O}_o(r+d)e^{-iH_{\rm NS}t}|GS\rangle_{\rm NS}}\,. \tag{7.123}$$

2. One imposes open boundary conditions on the spins (in that case the Hamiltonian is mapped into a purely quadratic form of fermions) and considers the expectation value of $\mathcal{O}_o$ asymptotically far away from the boundaries.

An alternative method that applies more generally to integrable models was developed in Refs [25, 26, 27]. It is based on the observation that the initial state after the quench can be expressed in a squeezed state form, e.g.

$$|\Psi(0)\rangle = \exp\Big[i\sum_{0<p\in\mathrm{NS}} K(p)b_p^\dagger b_{-p}^\dagger\Big]|GS\rangle_{\rm NS}\,. \tag{7.124}$$

Here $K(p)$ is a function that depends on the quench (cf. (7.132)), $b_p^\dagger$ are the aforementioned momentum space Bogoliubov fermion operators. Two point correlation functions can then be written in a Lehmann representation based on energy eigenstates. The matrix elements ("form factors") in the Lehmann representation are known[204], and it is possible to obtain explicit results in the framework of a low-density expansion. We refer the reader to Refs [26, 27] for further details and the explicit calculations. Here we only review and discuss the main results.

7.6.3 Stationary state properties

Stationary state properties were analyzed in detail in Ref. [27]. An important simplification at late times is that expectation values of odd operators go to zero. As discussed above, for quenches originating in the paramagnetic phase they vanish identically because the $\mathbb{Z}_2$ symmetry remains unbroken. On the other hand, for quenches originating in ferromagnetic phase

($h_0 < 1$) their expectation value is generally nonzero (cf. (7.122)). However, as shown in Ref. [28], expectation values of all odd local operators decay exponentially in time to zero. This leaves us with expectation values for even operators, which can be analyzed by standard free fermion methods. The basic object is the fermion two-point function, which in the thermodynamic limit can be written in the form (cf. (7.91))

$$i\langle a_\ell a_n\rangle\Big|_{\ell\neq n} = \int_{-\pi}^{\pi}\frac{\mathrm{d}k}{2\pi}\left[A_{\ell-n}(k) + B_{\ell-n}(k)e^{2i\varepsilon_h(k)t} + B^*_{\ell-n}(k)e^{-2i\varepsilon_h(k)t}\right]. \tag{7.125}$$

Here $A(k)$ and $B(k)$ are smooth functions (we are considering noncritical quenches) that depend on the quench details and $\varepsilon_h(k)$ is the dispersion relation (7.112). By the Riemann-Lebesgue lemma, in the infinite time limit the fermion two-point functions approach stationary values

$$\lim_{t\to\infty} i\langle a_\ell a_n\rangle\Big|_{\ell\neq n} = \int_{-\pi}^{\pi}\frac{\mathrm{d}k}{2\pi}A_{\ell-n}(k)\,. \tag{7.126}$$

Since the expectation value of any even local operator can always be written as a finite sum of finite products of fermion two-point functions (cf. (7.119)), the infinite time limit exists and is obtained by replacing (7.125) with (7.126). Courtesy of Wick's theorem, the stationary properties of all other even operators can be expressed in terms of (7.126).

Description of the steady state by a GGE

Since expectation values of odd operators vanish at infinite times, the steady state can be constructed in complete analogy to our fermionic example considered in Sec. 7.4. The appropriate GGE density matrix is of the form

$$\rho_{\mathrm{GGE}} = \frac{e^{-\sum_{j=1}^{\infty}\lambda_n^+ I^{(n,+)}+\lambda_n^- I^{(n,-)}}}{Z_{\mathrm{GGE}}}\,, \tag{7.127}$$

where the conservation laws $I^{(n,\pm)}$ have been reported earlier in (7.33). The Lagrange multipliers for transverse field quenches were determined in Ref. [28]

$$\lambda_j^+ = \left\{\frac{\mathrm{sgn}[(h-1)(h_0-1)]}{\varepsilon_h(0)} + \frac{(-1)^j}{\varepsilon_h(\pi)}\right\}\frac{2}{j}\,, \qquad \lambda_j^- = 0. \tag{7.128}$$

The local equivalence of the steady state density matrix to this GGE was demonstrated in Refs [25, 28]

$$\lim_{t\to\infty}|\Psi(t)\rangle\langle\Psi(t)| =_{\mathrm{loc}} \rho_{\mathrm{GGE}}. \tag{7.129}$$

The GGE can be interpreted as a Gibbs ensemble at inverse temperature $\beta = J^{-1}$ for an effective "GGE Hamiltonian", defined as

$$H_{\mathrm{GGE}} \equiv J\sum_{j=1}^{\infty}\lambda_j^+ I_j^+\,. \tag{7.130}$$

By virtue of (7.128) this "Hamiltonian" is long-ranged. It can be diagonalized by combined Jordan-Wigner and Bogoliubov transformations [28], which for a quench from h_0 to h results in

$$H_{\mathrm{GGE}} = \int_{-\pi}^{\pi}\frac{dp}{2\pi}J\log\left(K^2(p)\right)\left[b^\dagger(p)b(p) - \frac{1}{2}\right], \tag{7.131}$$

where

$$K^2(p) = \frac{\sin^2(p)\ (h-h_0)^2}{(\varepsilon_{h_0}(p)\varepsilon_h(p)\big(2J\big)^{-2} + 1 + hh_0 - (h+h_0)\cos(p))^2}\,. \tag{7.132}$$

The "dispersion relation" $J \log K^2(p)$ diverges logarithmically at momenta zero and π. This is related to the fact that the mode occupation numbers at these momenta are independent of h, and ultimately produces the algebraic decay (7.128) of the Lagrange multipliers. These logarithmic singularities do not compromise the cluster decomposition properties of the steady state.

Connected spin-spin correlation functions

In the stationary state the connected two-point correlators decay exponentially with distance[26]

$$\rho_c^{\alpha\alpha}(\ell) = \langle \sigma_j^\alpha \sigma_{j+\ell}^\alpha \rangle - \langle \sigma_j^\alpha \rangle \langle \sigma_{j+\ell}^\alpha \rangle \simeq C^\alpha(\ell) e^{-\ell/\xi_\alpha} \,. \tag{7.133}$$

The correlation lengths are given by[26]

$$\xi_z^{-1} = |\ln h_0| + \min(|\ln h_0|, |\ln h|) \,, \tag{7.134}$$

$$\xi_x^{-1} = \theta_H(h-1)\theta_H(h_0-1) \ln\left[\min(h_0, h_1)\right] - \ln\Big[x_+ + x_- + \theta_H((h-1)(h_0-1))\sqrt{4x_+x_-}\Big] \tag{7.135}$$

where $\theta_H(x)$ is the Heaviside step function and

$$x_\pm = \frac{[\min(h, h^{-1}) \pm 1][\min(h_0, h_0^{-1}) \pm 1]}{4} \,, \quad h_1 = \frac{1 + hh_0 + \sqrt{(h^2-1)(h_0^2-1)}}{h + h_0} \,. \tag{7.136}$$

The prefactors $C^\alpha(\ell)$ depend on the details of the quench and are listed in Appendix 7.11.

7.6.4 Time dependence

Having established the stationary behaviour of spin correlations, we now turn to their dynamics at late times. The first question of interest is how they relax towards their stationary values.

For even operators we can use Wick's theorem to express spin-spin correlators in terms of the fermion two-point functions (7.125). At late times the resulting expression can be evaluated by a stationary phase approximation, which gives

$$\langle \mathcal{O}_e \rangle \simeq \langle \mathcal{O}_e \rangle_{\rm GGE} + O(t^{-\frac{n[\mathcal{O}_e]}{2}}) \,. \tag{7.137}$$

Here the exponent $n[\mathcal{O}_e]$ is an integer that depends on the particular even operator under consideration.

Expectation values of odd operators were argued in Ref. [28] to decay exponentially in time

$$\langle \mathcal{O}_o \rangle \simeq O(e^{-t/\tau[\mathcal{O}_o]}) \,, \tag{7.138}$$

where $\tau[\mathcal{O}_o]$ denotes a relaxation time. Having established the gross structure of the late time dynamics, we now turn to a more quantitative description.

One-point functions

Longitudinal spin operator.

The longitudinal spin operator $\sigma_j^x = (-i)^{\ell-1} \prod_{j=1}^{2\ell-1} a_j$ is the simplest and most important example of an odd operator. Its expectation value is the order parameter in the ferromagnetic phase. As we are dealing with an odd operator, its expectation value is identically zero for

quenches originating in the paramagnetic phase. For quenches from the ferromagnetic phase ($h_0 < 1$) it was shown in Ref. [25, 26] that

$$\langle\Psi(t)|\sigma_j^x|\Psi(t)\rangle \simeq C^x(t)e^{-t/\tau_x}\,, \qquad h_0 < 1\,, \tag{7.139}$$

where the inverse decay time is given by

$$\tau_x^{-1} = \int_0^\pi \frac{\mathrm{d}k}{\pi}\varepsilon_h'(k)\ln\left|\frac{1-K^2(k)}{1+K^2(k)}\right|. \tag{7.140}$$

Here the function $K^2(k)$ has been previously defined in (7.132). The prefactor $C^x(t)$ was calculated in Ref. [26]

$$C^x(t) = \begin{cases} \sqrt{\frac{1-hh_0+\sqrt{(1-h^2)(1-h_0^2)}}{2\sqrt{1-hh_0}(1-h_0^2)^{\frac{1}{4}}}} & h<1 \\ \left[\frac{h\sqrt{1-h_0^2}}{h+h_0}\right]^{\frac{1}{4}}\left[1+\cos(2\varepsilon_h(k_0)t+\alpha)+\ldots\right]^{\frac{1}{2}} & h>1\,. \end{cases} \tag{7.141}$$

The oscillatory behaviour for $h > 1$ can be related to the presence of a gapless mode with momentum k_0 in the GGE Hamiltonian (7.130) ($K^2(k_0) = 1$). It was noted in Ref. [42] that the period of the oscillations in (7.141) coincides with cusps in the time evolution of the logarithm of the return probability per unit length $f(t) = -\lim_{L\to\infty}\frac{1}{L}\log|\langle\Psi(0)|e^{-iHt}|\Psi(0)\rangle|^2$ after quenches between the phases. The result (7.139) has been derived in the late time limit $Jt \gg 1$. However, it gives an excellent account of the full answer except at very short times. This can be shown by comparing (7.139) to a numerical solution based on free fermion methods[26]. The latter works directly in the thermodynamic limit and does not suffer from finite-size effects. Fig. 7.7 shows such comparisons for two different quenches within the ferromagnetic phase, and for two quenches from the ferromagnetic to the paramagnetic phase. The agreement is visibly excellent even at moderate times.

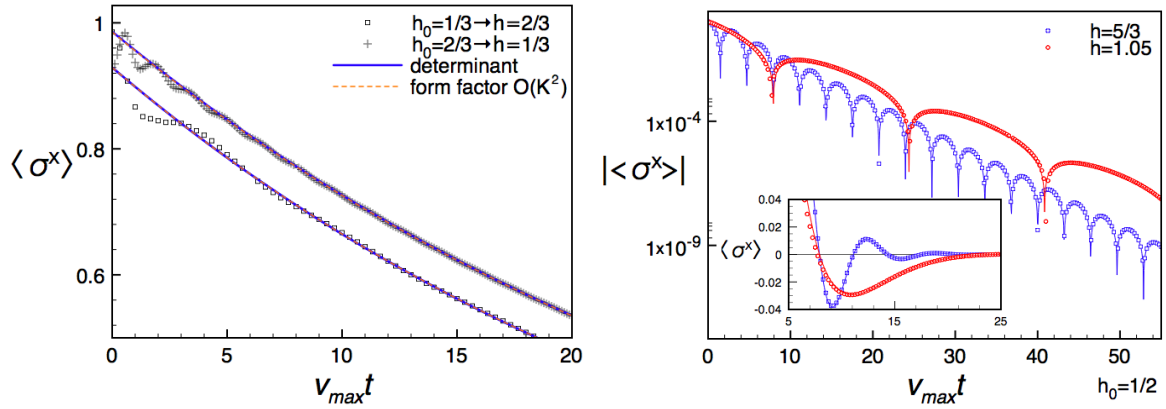

Figure 7.7: Expectation value of the order parameter after two quenches within the ferromagnetic phase (left) and two quenches across the critical point (right). Numerical results obtained in the thermodynamic limit are compared with the asymptotic predictions (7.139) (labelled as "determinant"). In the left panel analytic results obtained by form factor methods[26] are shown as well (labelled as "form factor"). The agreement in all cases is excellent even at the short times depicted. [Figures taken from Ref. [26]]

At first sight the exponential decay (7.139) of the order parameter for quenches within the ferromagnetic phase may look surprising. Even a very small quench will lead to the eventual disappearance of the order parameter. A simple way of understanding this is to note that the

ferromagnetic order persists only at zero temperature $T = 0$, and melts for any $T > 0$. By means of our quantum quench we deposit a finite energy density into the system, which is very similar to imposing a finite temperature. This consideration provides an intuitive explanation for why even small quenches wipe out the long range order present in the initial state. We note that this behaviour is specific to one dimensional systems, where discrete symmetries can be spontaneously broken only at $T = 0$. In higher dimensional systems we expect order parameters to be generally stable when subjected to sufficiently small quantum quenches.

Finally we note that the expectation value $\langle \sigma_j^y(t) \rangle$ can be obtained in a simple way by considering the Heisenberg equations of motion for σ_j^x, and is given by

$$\langle \Psi(t)|\sigma_j^y|\Psi(t)\rangle = \frac{\partial}{\partial t} \frac{\langle \Psi(t)|\sigma_j^x|\Psi(t)\rangle}{2Jh} \,. \tag{7.142}$$

Transverse spin operator.

The spin operator $\sigma_j^z = i a_{2j} a_{2j-1}$ is even and its expectation value can be straightforwardly calculated with free-fermion techniques [45, 47]. It decays like a $t^{-3/2}$ power law in time towards its stationary value $\langle \cdot \rangle_{\rm GGE}$

$$\langle \Psi(t)|\sigma_l^z|\Psi(t)\rangle\Big|_{Jt\gg 1} = \langle \sigma_l^z \rangle_{\rm GGE} + \frac{h_0 - h}{4\sqrt{\pi}(2hJt)^{\frac{3}{2}}} \Big[\frac{\sin(4J|1-h|t + \pi/4)}{\sqrt{|1-h|}|1-h_0|} - \frac{\sin(4J(1+h)t - \pi/4)}{\sqrt{1+h}(1+h_0)} \Big] + O((Jt)^{-\frac{5}{2}}) \,. \tag{7.143}$$

The relaxation to the stationary value is only algebraic, in agreement with (7.137).

Spin-spin correlators in the "space-time scaling limit"

A particularly useful way of describing the time dependence of two-point functions after a quantum quench is by considering an asymptotic expansion around the so-called space-time scaling limit[25, 26]. The latter refers to the behaviour along a particular ray in space-time

$$t, \ell \to \infty \,, \quad \frac{v_{\rm max} t}{\ell} = \kappa = \text{fixed.} \tag{7.144}$$

Here $v_{\rm max} = \max_k \frac{d\varepsilon_h(k)}{dk}$ is the maximal group velocity of elementary excitations of the post-quench Hamiltonian.

Transverse spin-spin correlator

In the space-time scaling limit, the asymptotic behavior of $\rho_c^{zz}(\ell, t)$ can be evaluated by means of Wick's theorem, followed by a stationary phase approximation. The leading behaviour is a t^{-1} power-law decay, and the subleading corrections are power laws as well[26]

$$\rho_c^{zz}\big(\ell = \frac{v_{\rm max} t}{\kappa}, t\big) \sim \frac{D^z(t)}{\kappa^2 t} + o\big(t^{-1}\big) \,. \tag{7.145}$$

Here $D^z(t)$ is the sum of a constant contribution and oscillatory terms with constant amplitudes.

Longitudinal spin-spin correlator

In the space-time scaling limit the order parameter two-point function $\rho^{xx}(\ell, t)$ takes the form

$$\rho^{xx}(\ell, t) \simeq \mathcal{C}^x(\ell, t) \exp\Big[\int_0^\pi \frac{{\rm d}k}{\pi} \ln \Big| \frac{1 - K^2(k)}{1 + K^2(k)} \Big| \min\big(2\varepsilon_h'(k) t, \ell\big) \Big] \,. \tag{7.146}$$

The function $\mathcal{C}^x(\ell, t)$ has been determined in Ref. [26].

1. For quenches within the ferromagnetic phase, $h_0, h < 1$, $\mathcal{C}^x(\ell,t)$ equals the constant denoted by $\mathcal{C}^x_{\rm FF}$ in (7.245). For times smaller than the Fermi time

$$t_F = \frac{\ell}{2v_{\max}}\,, \tag{7.147}$$

(7.146) equals the square of the one-point function (7.139). Thus, in the space-time scaling limit, connected correlations *vanish identically* for times $t < t_F$ and begin to form only after the Fermi time. We stress that this does not imply that the connected correlations are exactly zero for $t < t_F$: in any model, both on the lattice or in the continuum there are exponentially suppressed terms (in ℓ), which however vanish in the scaling limit.

2. For quenches from the ferromagnetic phase to the paramagnetic phase the prefactor is given by

$$\mathcal{C}^x(\ell,t) = \mathcal{C}^x_{\rm FP}\Big[1+\theta_H(t_F-t)\Big(\cos(2\varepsilon_h(k_0)t+\alpha)+\dots\Big)\Big]\,, \tag{7.148}$$

where $\mathcal{C}^x_{\rm FP}$ is the constant defined in (7.246), while k_0 and α are the constants appearing in the one-point function (7.141). For $t < t_F$, (7.146) is simply the square of the corresponding one-point function, which ensures that connected correlations vanish for $t < t_F$ in the space-time scaling regime. We note that the expression for $t < t_F$ is a conjecture[26].

3. For quenches within the paramagnetic phase one has

$$\mathcal{C}^x(\ell,t) \simeq \mathcal{C}^x_{\rm PP}(\ell) + (h^2-1)^{\frac{1}{4}}\sqrt{4J^2h}\int_{-\pi}^{\pi}\frac{dk}{\pi}\frac{K(k)}{\varepsilon_k}\sin(2t\varepsilon_k - k\ell)+\dots\,, \tag{7.149}$$

where $\mathcal{C}^x_{\rm PP}(\ell)$ is the function defined in (7.248). Eq. (7.149) constitutes the leading order in a low-density expansion computed within the form-factor formalism. The exact expression for a generic (not small) quench is not known.

4. For quenches from the paramagnetic to the ferromagnetic phase, for $t > t_F$, $\mathcal{C}^x(\ell,t)$ is independent of time and is given by $\mathcal{C}^x_{\rm PF}(\ell)$ of (7.247). For $t < t_F$ the correlator is exponentially small and, to the best of our knowledge, there are no analytic predictions for its behaviour.

Long time asymptotics of connected spin-spin correlators at a fixed separation ℓ

The late time asymptotics of spin-spin correlation functions at a fixed separation ℓ between the spin operators was analyzed in Ref. [26].

1. In the late time regime at fixed, large ℓ, $\rho^{zz}_c(\ell,t)$ decays in a power law fashion to its stationary value

$$\rho^{zz}_c(\ell,t) \sim \rho^{zz}_c(\ell,\infty) + \frac{E^z(t)\ell e^{-\ell/\tilde\xi_z}}{t^{3/2}} + o\big(t^{-3/2}\big)\,. \tag{7.150}$$

Here $E^z(t) = \sum_{q=0,\pi} A_q\cos\big(2t\varepsilon_h(q)+\varphi_q\big)$ and the steady state value is exponentially small in ℓ: $\rho^{zz}_c(\ell,\infty) \propto e^{-\ell/\xi_z}$. Crucially one has (cf. (7.134))

$$\tilde\xi_z^{-1} = \min(|\log h_0|, |\log h|) < \xi_z^{-1}\,. \tag{7.151}$$

This implies that the time scale after which the stationary behaviour becomes apparent is in fact exponentially large in the separation ℓ. This makes the stationary behaviour difficult to observe in practice.

2. For quenches originating in the ferromagnetic phase, the stationary value of $\rho^{xx}(\ell,t)$ emerges at a time scale
$$\tau_{\rm F}^{\rm x} \sim v_{\rm max}^{-1}\ell^{4/3}\,, \tag{7.152}$$
where $v_{\rm max}$ is the maximal velocity at which information propagates. This makes the approach to the steady state straightforward to observe.

3. For quenches within the paramagnetic phase, $\rho_c^{xx}(\ell,t)$ exhibits an oscillatory power-law decay in time towards its stationary value, which is exponentially small in ℓ. Hence, in complete analogy to the case of the transverse two-point function, the time scale $\tau_{\rm PP}^{\rm x}$ after which the stationary behavior reveals itself is exponentially large
$$\tau_{\rm PP}^{\rm xx} \propto e^{2\ell/3\xi_x}, \tag{7.153}$$
and very difficult to observe in practice.

7.6.5 Reduced density matrices

As we have seen above, the quench dynamics of one and two point functions of quantum spins is rich and interesting. However, these are nonetheless very special observables. Ideally one would like to have access to the full reduced density matrix for a given subsystem size, as its matrix elements encode the time evolution of all correlation functions, cf. (7.21). In practice this is only possible in very simple non-interacting examples, or for very small subsystem sizes. An example are quenches in the disordered phase of the TFIC[177, 28]. Here the reduced density matrix on the interval $[1,\ell]$ is given by
$$\rho_\ell(t) = \frac{1}{Z}\exp\Big(\frac{1}{4}\sum_{\ell,n} a_l W_{lm} a_m\Big)\,, \tag{7.154}$$
where a_{2n} and a_{2n-1} are the Majorana fermion operators (7.106) and the factor Z ensures $\mathrm{Tr}(\rho_\ell(t)) = 1$. The matrix W is related to the two-point function of Majorana fermions by[123, 205, 124]
$$\tanh\frac{W}{2} = \Gamma\,, \qquad \Gamma_{jk} = \langle\Psi(t)|a_k a_j|\Psi(t)\rangle - \delta_{j,k} = -\Gamma_{kj}, \tag{7.155}$$
where the time evolved initial state $|\Psi(t)\rangle$ is given by (7.117). The matrix elements of the correlation matrix are simple (single) integrals and can be found in Ref. [26].

As we have argued above, at late times after global quantum quenches isolated quantum systems relax locally towards some steady states $\rho^{\rm SS}$. How quickly this relaxation occurs can be efficiently measured by considering the distance of the time evolving reduced density matrix $\rho_B(t)$ from its steady state value $\rho_B^{\rm SS}$, where B is a subsystem of a given size. This diagnostic can be implemented quite generally numerically as long as the subsystem size is small[206]. For models that can be mapped to non-interacting theories, it is possible to go considerably further. An example is the TFIC, which was considered in Ref. [28]. The first step is to introduce a measure of distance on the space of RDMs on a given subsystem. A convenient choice was introduced in Ref. [28]
$$\mathcal{D}(\rho_1,\rho_2) = \sqrt{\frac{\mathrm{Tr}[(\rho_1-\rho_2)^2]}{\mathrm{Tr}[(\rho_1)^2]+\mathrm{Tr}[(\rho_1)^2]}}\,. \tag{7.156}$$
Fig. 7.8 shows results for the distance between the RMDs for the time-evolving and stationary states for quantum quenches within the disordered and ordered phases in the TFIC. Subsystems consisting of ℓ neighbouring sites are considered, where ℓ ranges from 10 to 150. In both cases

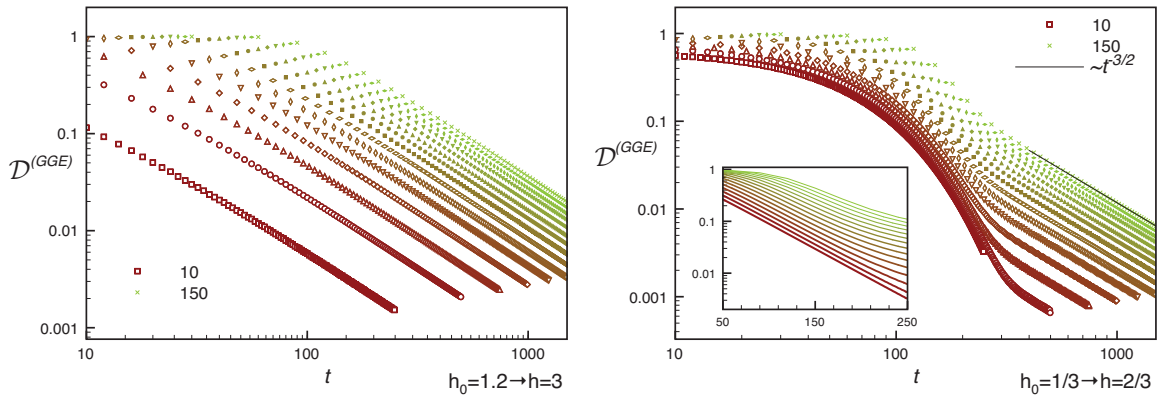

Figure 7.8: Normalized distance $\mathcal{D}^{(\mathrm{GGE})} = \mathcal{D}(\rho_\ell(t), \rho_\ell^{\mathrm{GGE}})$ after a quench within the paramagnetic (left) and ferromagnetic (right) phase for subsystem sizes $\ell = 10, 20, \ldots, 150$. As ℓ increases, the color changes from brown to green, the symbols become smaller and the curves narrower. At late times $D(\rho_\ell(t), \rho_\ell^{(GGE)})$ tends to zero in a universal power-law fashion $\propto (Jt)^{-3/2}$. For quenches in the ordered phase there is an intermediate time regime, in which the distance decays exponentially (inset). This stems from the non-vanishing spontaneous magnetization in the initial state for this quench. [Figures taken from Ref. [28]]

the distance is seen to eventually decay as a power law in time

$$\mathcal{D}(\rho_\ell(t), \rho_\ell^{\mathrm{GGE}}) \propto \ell^2 (Jt)^{-\frac{3}{2}} . \tag{7.157}$$

The power-law decay of the distance in time can be interpreted by relating it to expectation values of local operators in the subsystem. Using (7.21) one can show that

$$\mathcal{D}(\rho_1, \rho_2) = \big(\overline{R(\mathcal{O})^2}\big)^{\frac{1}{2}} , \qquad R(\mathcal{O}) = \frac{|\mathrm{Tr}[(\rho_1 - \rho_2)\mathcal{O}]|}{\sqrt{\mathrm{Tr}[\rho_1 \mathcal{O}]^2 + \mathrm{Tr}[\rho_2 \mathcal{O}]^2}} , \tag{7.158}$$

where the bar denotes an average on the space of operators acting on the spins in the subsystem, taken with respect to the probability distribution

$$P(\mathcal{O}) = \frac{\mathrm{Tr}[\rho_1 \mathcal{O}]^2 + \mathrm{Tr}[\rho_2 \mathcal{O}]^2}{\sum_{\mathcal{O}'} \mathrm{Tr}[\rho_1 \mathcal{O}']^2 + \mathrm{Tr}[\rho_2 \mathcal{O}']^2} . \tag{7.159}$$

Here the sum is over all operators $\sigma_1^{\alpha_1} \sigma_2^{\alpha_2} \ldots \sigma_\ell^{\alpha_\ell}$, where $\alpha_j = 0, x, y, z$ and where we have assumed for simplicity that the subsystem is the interval $[1, \ell]$. The contribution from a given operator $\mathcal{O}$ to the distance is weighted by the square of its expectation value. This shows that (7.158) measures a mean relative difference between the expectation values of local operators in the two states.

As $\overline{R(\mathcal{O})} \leq (\overline{R(\mathcal{O})^2})^{1/2} = \mathcal{D}(\rho_\ell(t), \rho_\ell^{\mathrm{GGE}})$ we may use (7.158) to identify a time scale t^*_{rms} associated with the relaxation of the "typical" operator (with respect to the probability distribution (7.159))

$$J t^*_{\mathrm{rms}} \sim \ell_B^{\frac{4}{3}} . \tag{7.160}$$

The time scale t^*_{rms} is very different from the ones governing the time evolution of the two-point functions of spin operators.

7.6.6 Entanglement entropy

The von Neumann entropy (also known as entanglement entropy) of a density matrix ρ is defined as

$$S_{\mathrm{vN}}[\rho] = -\mathrm{Tr}[\rho \log \rho] . \tag{7.161}$$

If ρ is a reduced density matrix in a system that is in a pure state, $S_{\rm vN}$ measures the entanglement between the subsystem and its complement. Entanglement entropies have become a standard diagnostic for detecting and identifying quantum phase transitions. In the context of quantum quenches the time evolution of the von Neumann entropy and other entanglement measures provides very useful information about the spreading of correlations[89, 48, 183, 184, 16, 127, 109, 31, 207, 208, 209, 210]. A key result obtained in Ref. [48] is that after quenches to conformal field theories the von Neumann entropy of a subsystem of length ℓ increases linearly in time until it eventually saturates (see the review by P. Calabrese and J. Cardy [88] in this volume)

$$S_{\rm vN}[\rho] \sim \begin{cases} \frac{\pi c v t}{6\epsilon} & v t < \frac{\ell}{2} \\ \frac{\pi c \ell}{12\epsilon} & v t \gtrsim \frac{\ell}{2} \,. \end{cases} \tag{7.162}$$

Here c is the central charge of the CFT, ϵ is a constant with dimensions of length that depends on the initial state and v is the speed of light. The two behaviours in (7.162) connect smoothly over a region $|vt - \frac{\ell}{2}| \sim \epsilon$. A physical interpretation of the result (7.162) is provided by the Calabrese-Cardy quasi-particle picture[89] we already encountered in Section 7.5. Its application to the time evolution of the entanglement entropy in integrable models initialized in squeezed states with finite correlation lengths proceeds as follows. The idea is that in a squeezed state correlations spread via the propagation of pairs of quasi-particles with equal but opposite momenta. At time $t = 0$ the quantum quench generates such quasi-particles pairs throughout the system. Correlations between quasi-particles produced at a distance larger than the correlation length in the initial state can be neglected. The entanglement between a given region B and its complement is generated by quasi-particle pairs. The entanglement entropy is interpreted as a measure of the number of correlated pairs such that, at a given time, one quasi-particle is inside B and one outside, see Fig. 7.9. Entanglement is initially generated at the boundaries of B, and the entangled region spreads outwards in the form of two light cones. This picture suggests the following semiclassical expression for the von Neumann entropy

$$S_{\rm vN}[\rho_B] \stackrel{\rm sc}{=} \int \mathrm{d}k \; f(k) \min\Big(\ell_B, 2|v(k)|t\Big) \,. \tag{7.163}$$

Here $v(k)$ is the semiclassical group velocity $v(k) = \frac{\mathrm{d}\varepsilon(k)}{\mathrm{d}k}$, $\varepsilon(k)$ is the dispersion relation of the quasiparticles and $f(k)$ is an unknown function that contains information on the initial state.

This behaviour has been observed in a variety of lattice and continuum models [89, 48, 183, 184, 127, 109, 31, 210, 207], including non-integrable cases [184], in which the quasi-particle picture does not apply by virtue of the finite quasi-particle life time. The semiclassical interpretation has been generalized to prethermalized regimes in models with weak integrability breaking[127].

The linear entanglement growth after quantum quenches has important ramifications. It is a crucial limiting factor for applying matrix-product state methods such as t-DRMG [211] and i iTEBD [212] algorithms to the computation of the dynamics after global quantum quenches. We note that translational invariance is essential for the quasi-particle picture to hold, and the time evolution of the entanglement entropy in e.g. disordered models [207] is very different.

Exact results for the evolution of the entanglement entropy after quenches in the transverse field Ising chain[48] are in accordance with the structure (7.163) suggested by the quasi-particle picture. In the limit $1 \ll \ell, Jt$, the entanglement entropy of a block of ℓ neighbouring spins is

$$S_{\rm vN}[\rho_B] \simeq \int_{\pi}^{\pi} \frac{\mathrm{d}k}{2\pi} \; w(\langle\Psi(0)|n(k)|\Psi(0)\rangle) \; \min\Big(\ell, 2|\varepsilon'(k)|t\Big) + o(\ell) \,, \tag{7.164}$$

where $w(x) = -x \log x - (1-x)\log(1-x)$ is the entropy per site (cf. Appendix 7.10), and $\langle\Psi(0)|n(k)|\Psi(0)\rangle$ is the (conserved) density of elementary excitations of the post-quench Hamil-

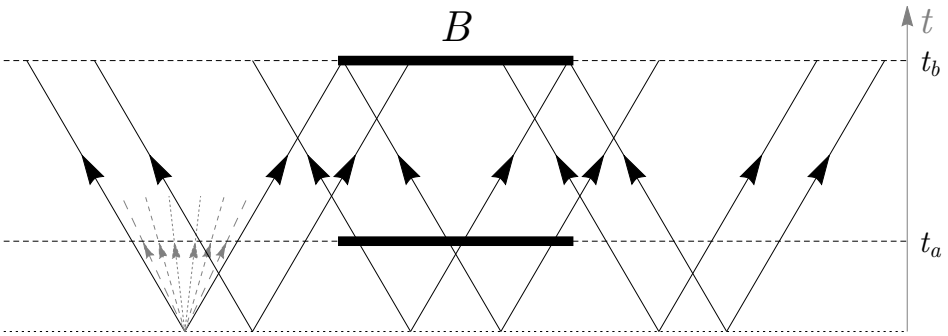

Figure 7.9: Space-time picture illustrating the semiclassical interpretation of entanglement entropy growth after a global quantum quench[89]. Quasi-particles moving at the maximal group velocity are indicated by thick black arrows, and are initially generated throughout the system by the quantum quench. Slower quasi-particles are shown only on the left (short dashed gray arrows). At time t_a the entanglement entropy of B is still increasing linearly in time, as there are still trajectories such that maximum velocity quasi-particle pairs are incident inside B. At times $t = t_b$ the entanglement entropy starts saturating because any maximum velocity quasi-particle incident in B generates entanglement with the rest of the system.

tonian H with momentum k at times $t > 0$. It is given by

$$\langle\Psi(0)|n(k)|\Psi(0)\rangle = \frac{K^2(k)}{1+K^2(k)}\,, \tag{7.165}$$

where $K^2(k)$ was defined previously in (7.132). It follows from (7.164) that the entanglement entropy increases linearly until the Fermi time (7.147), and then slowly approaches its stationary value set by the GGE. The latter equals the entropy per site of the GGE for the entire system [109]

$$\int_{\pi}^{\pi} \frac{\mathrm{d}k}{2\pi}\; w(\langle\Psi(0)|n(k)|\Psi(0)\rangle) = \lim_{L\to\infty} \frac{1}{L} S_{vN}[\rho^{\mathrm{GGE}}]\,. \tag{7.166}$$

These observations persist for quantum quenches in the TFIC starting in excited states [31].

Interestingly, the stationary value of the entropy density in the diagonal ensemble differs from that in the GGE[30, 213]. This is not a problem, because the entropy per site is a global property of the system, while the equivalence between ensembles only holds for (finite) subsystems in the thermodynamic limit. A detailed explanation of the origin of this difference for the case of the TFIC was provided in Ref. [30].

7.6.7 Dynamical spin-spin correlation functions

We now turn to dynamical correlation functions

$$\rho^{\alpha\alpha}(\ell, t+t_1, t+t_2) = \langle\Psi(t)|\sigma^{\alpha}_{j+\ell}(t_1)\sigma^{\alpha}_{j}(t_2)|\Psi(t)\rangle\,. \tag{7.167}$$

The transverse correlator ($\alpha = z$ in (7.167)) can be calculated by elementary means [45], as σ^z_j is quadratic in Jordan-Wigner fermions. The order parameter correlator ($\alpha = x$ in (7.167)) is much more difficult to evaluate. In Ref. [29] it was determined by means of a generalization of the form factor methods developed in Ref. [26], and by exploiting exact results in particular limits[27]. These methods are so far restricted to quenches within either the paramagnetic or

the ferromagnetic phase, and lead to answers of the form[29]

$$\rho^{xx}(\ell, t+\tau, t+t_2) \simeq C^x(\ell,\tau,t)\exp\left[\int_0^\pi \frac{\mathrm{d}k}{\pi}\log\left|\frac{1-K^2(k)}{1+K^2(k)}\right|\min\left\{\max\left[\varepsilon_h'(k)\tau,\ell\right],\varepsilon_h'(k)(2t+\tau)\right\}\right]. \tag{7.168}$$

Here the functions $\epsilon_h(k)$ and $K^2(k)$ are given in (7.112) and (7.132) respectively, and h_0 and h are the initial and final values of the transverse field. The function $C^{(x)}(\ell,\tau,t)$ depends on the phase in which the quench is performed:

1. In the ferromagnetic phase, $h_0, h < 1$, $C^x(\ell,\tau,t)$ equals the constant $\mathcal{C}^x_{\mathrm{FF}}$ in (7.245).

2. In the paramagnetic phase ($h_0, h > 1$) $C^x(\ell,\tau,t)$ is given (to leading order in the form factor expansion) by[29]

$$C^x(\ell,\tau,t) = \int_{-\pi}^{\pi}\frac{\mathrm{d}k}{2\pi}\frac{Je^{i\ell k}}{\varepsilon_h(k)}\left[e^{-i\varepsilon_h(k)t} + 2iK(k)\cos(2\varepsilon_h(k)(2t+\tau))\mathrm{sgn}(\ell-\varepsilon_h'(k)\tau)\right] \times \frac{hh_0 - 1 + \sqrt{(h^2-1)(h_0^2-1)}}{\sqrt{h_0-1/h}\sqrt[4]{h_0^2-1}}, \qquad \ell < v_{\max}(2t+\tau). \tag{7.169}$$

   In the complementary regime $v_{\max}(2t+\tau) < \ell$ the correlator is exponentially small and this expression no longer applies.

The form factor result gives an excellent approximation to the exact answer (which can be computed numerically using free fermion techniques) for "small" quenches[29]. These are defined as being characterized by having low densities of excitations in the initial state.

It is possible to obtain some of these results in an alternative way by generalizing the semiclassical approach of Ref. [39] to the non-equal time case, and then elevating it using exact limiting results derived in Refs [25, 26]. This method fails to reproduce the result for quenches in the disordered phase outside the light cone $v_{\max}\tau < \ell$, but is significantly simpler.

7.7 Relaxation in interacting integrable models

We now turn to interacting integrable models that are solvable by the Bethe Ansatz[20, 214, 215]. By "interacting" we mean theories in which the scattering matrix is momentum dependent. Most of our discussion will focus on the example of the spin-1/2 Heisenberg chain.

7.7.1 The "initial state problem"

Integrability allows the construction of a basis of simultaneous eigenstates of the Hamiltonian and all its conservation laws. Unlike in the non-interacting case these states have a very complicated structure described by the Bethe Ansatz[20, 214, 215]. When we consider a quench between two integrable Hamiltonians $H(h_0) \to H(h)$, we are thus faced with the problem of how to translate between the eigenbases of the two integrable theories. This is a difficult undertaking[216, 217], and no general formalism for achieving it is currently known. Progress has however been made in cases where the initial state has a simpler structure, in particular for (matrix) product states in either position[58, 63, 66, 68, 65, 69] or momentum/rapidity space[97, 95, 105, 107, 111, 113, 114]. There are two main methods for encoding the relevant information contained in the initial state.

1. Let us denote the eigenstates of the post-quench Hamiltonian $H(h)$ by $|n\rangle$. One way to implement the initial conditions is via the overlaps $\langle n|\Psi(0)\rangle$[67]. If these are known, the

initial state can be translated into the eigenbasis of the time evolution operator. This method is used in the Quench Action Approach[177] (see the review by J.-S. Caux [218] in this volume).

2. Let us denote the local conservation laws of $H(h)$ by $\{I^{(n)}\}$. If the set $\{I^{(n)}\}$ is in some sense complete[219, 112, 220], then the initial conditions can be encoded in the constraints

$$\lim_{L\to\infty} \frac{\langle\Psi(0)|I^{(n)}|\Psi(0)\rangle}{L} = \lim_{L\to\infty} \frac{\mathrm{Tr}\big(\rho^{\mathrm{SS}} I^{(n)}\big)}{L} \ , \tag{7.170}$$

where ρ^{SS} is one of the density matrices (GGE, GMC, diagonal ensemble) that describes the local properties of the stationary state.

In the following we will discuss implementations of the second approach.

7.7.2 On mode occupation operators

In free theories a convenient way for constructing the GGE is by exploiting the linear relation between the local conservation laws and the mode occupation operators, cf. (7.42). In interacting integrable models the situation is different. Like free theories they feature stable excitations. In the thermodynamic limit these can be described by creation and annihilation operators $Z_a^\dagger(\lambda)$, $Z_a(\lambda)$ (the index a labels different particle species) fulfilling the Faddeev-Zamolodchikov algebra[221, 222]

$$\begin{aligned} Z_a(\lambda_1)Z_b(\lambda_2) &= S_{ab}^{cd}(\lambda_1,\lambda_2)Z_d(\lambda_2)Z_c(\lambda_1), \\ Z_a(\lambda_1)Z_b^\dagger(\lambda_2) &= 2\pi\delta(\lambda_1-\lambda_2)\delta_{a,b} + S_{bc}^{da}(\lambda_2,\lambda_1)Z_d^\dagger(\lambda_2)Z_c(\lambda_1). \end{aligned} \tag{7.171}$$

Here λ parametrizes the momenta $p_a(\lambda)$ and $S_{ab}^{cd}(\lambda_1,\lambda_2)$ is the purely elastic two-particle S-matrix. The generalized mode occupation operators $N_a(\lambda) = Z_a^\dagger(\lambda)Z_a(\lambda)$ then indeed provide a set of mutually commuting conserved charges. The problem is that, due to the interacting nature of the stable excitations, there is no simple way of defining such operators in the finite volume[95], which is the standard way of making the theory well defined (working directly in the thermodynamic limit requires the regularization of very complicated singularities[223, 40, 95], which appears impractical in general). The problem lies in the nature of the quantization conditions in the finite volume, which on a ring of length L read

$$e^{iLp_a(\lambda_j^{(a)})} = -\prod_{b,k} S_{ab}(\lambda_j^{(a)},\lambda_k^{(b)}) \ . \tag{7.172}$$

The solutions to this complicated system of coupled equations are such that the possible values of $\lambda_j^{(a)}$, and hence $p_a(\lambda_j^{(a)})$, depend in a very sensitive way on all the other particles present in a given excitation. This is fundamentally different from the non-interacting case, where the momenta are simply given by

$$p_a(\lambda_j^{(a)}) = \frac{2\pi}{L} \times \text{integer}, \tag{7.173}$$

and are independent of the particle content of a given excitation. This makes it clear that defining finite volume analogues of $N_a(\lambda)$ is difficult.

7.7.3 The spin-1/2 Heisenberg model

Our paradigm for an interacting integrable model will be the spin-1/2 Heisenberg XXZ chain. Its Hamiltonian on a ring with L sites is

$$H_{\mathrm{XXZ}} = \frac{J}{4}\sum_{j=1}^{L} \sigma_j^x\sigma_{j+1}^x + \sigma_j^y\sigma_{j+1}^y + \Delta\left[\sigma_j^z\sigma_{j+1}^z - 1\right] \ , \tag{7.174}$$

where we will assume for definiteness that

$$\Delta = \cosh(\eta) \geq 1. \tag{7.175}$$

From now on we set $J = 1$.

Generalized microcanonical ensemble

For interacting integrable models the GMC is easier to work with than the GGE. It is based on working with macro-states obtained by taking the thermodynamic limit of eigenstates constructed from the Bethe Ansatz. This procedure is an essential ingredient of the Thermodyamic Bethe Ansatz and is reviewed in several monographs[226, 214]. A very brief summary is given in Appendix 7.10.2. The upshot is that macro-states in integrable models are characterized by an (infinite) set of densities $\{\rho_{n,p}(\lambda)|n = 1, 2, \dots\}$, where n labels all distinct stable species of excitations in the model. A given macro-state corresponds to a set of micro-states $|\Phi\rangle$, called representative states in Ref. [177]. These are by construction simultaneous eigenstates of all local conservation laws. For the macro-state describing the stationary state after our quench, they satisfy the initial conditions

$$\lim_{L\to\infty} \frac{\langle \Phi^{\rm SS}|I^{(n)}|\Phi^{\rm SS}\rangle}{L} = \lim_{L\to\infty} \frac{\langle \Psi(0)|I^{(n)}|\Psi(0)\rangle}{L} \ . \tag{7.176}$$

The GMC density matrix is then defined[177] in terms of a single such "representative" micro-state $|\Phi^{\rm SS}\rangle$

$$\rho^{\rm GMC} = |\Phi^{\rm SS}\rangle\langle\Phi^{\rm SS}| \ . \tag{7.177}$$

Here we have assumed that the stationary state is given in terms of a single macro-state constructed from the Bethe Ansatz. In principle it is possible that the steady state has a more complicated structure and requires a description in terms of a sum of several density matrices of the form (7.177).

Transfer matrix and "ultra-local" conservation laws

According to our general discussion, local observables should relax to an appropriate GGE after quenches to the XXZ chain. In order to construct this GGE, we need to know the required set of local conservation laws of (7.174). One family of conservation laws has been known for a long time and is most conveniently constructed by exploiting the relation of the Heisenberg Hamiltonian to the transfer matrix of the six-vertex model [224, 225, 20]. The fundamental building block of the six-vertex model is the L-operator

$$L_n(\lambda) = \frac{1}{\sinh(\eta + i\lambda)}\Big[\sinh(\tfrac{\eta}{2}+i\lambda)\cosh(\tfrac{\eta}{2})+\cosh(\tfrac{\eta}{2}+i\lambda)\sinh(\tfrac{\eta}{2})\tau^z\sigma_n^z+\sinh(\eta)(\tau^-\sigma_n^+ + \tau^+\sigma_n^-)\Big], \tag{7.178}$$

which acts on the tensor product $\mathbb{C}^2 \otimes \mathbb{C}^2$ of "auxiliary" and "quantum" spaces through the Pauli matrices τ^α and σ^α respectively. Matrix elements in the auxiliary/quantum spaces are denotes by Roman/Greek letters respectively, e.g.

$$\big(\tau^-\sigma_n^+\big)^{ab}_{\alpha\beta} = \tau^-_{ab}\big(\sigma_n^+\big)_{\alpha\beta}. \tag{7.179}$$

The vertex weights of the six-vertex model are obtained by taking matrix elements $L(\lambda)^{ab}_{\alpha\beta}$ and have a graphical representation as shown in Fig. 7.10 (a). The row-to-row transfer matrix is obtained as shown in Fig. 7.10 (b)

$$\big(\tau_{\frac{1}{2}}(\lambda)\big)^{\beta_1\dots\beta_L}_{\alpha_1\dots\alpha_L} = \big(L_1(\lambda)\big)^{a_1a_2}_{\alpha_1\beta_1}\big(L_2(\lambda)\big)^{a_2a_3}_{\alpha_2\beta_2}\dots\big(L_L(\lambda)\big)^{a_La_1}_{\alpha_L\beta_L} \ . \tag{7.180}$$

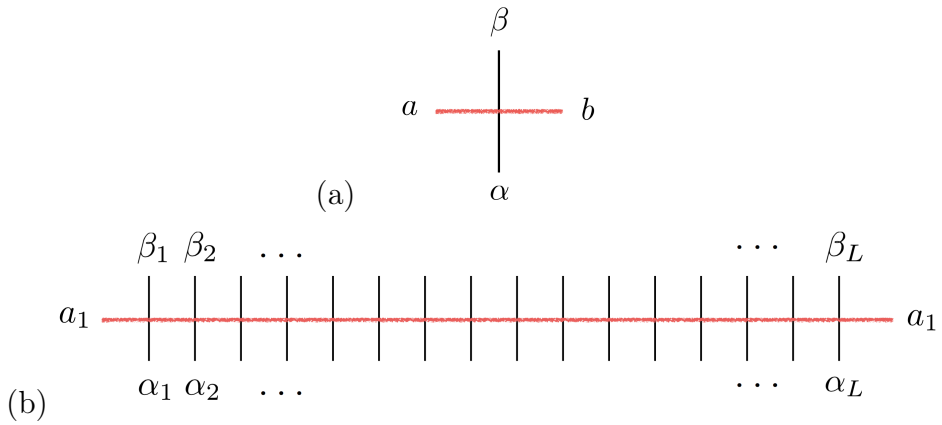

Figure 7.10: (a) Vertex with weight $[L_n(\lambda)]^{ab}_{\alpha\beta}$. The horizontal and vertical lines are associated with the "auxiliary" and "quantum" spaces respectively. (b) Transfer matrix element $\tau_{\frac{1}{2}}(\lambda)^{\beta_1\dots\beta_L}_{\alpha_1\dots\alpha_L}$.

The partition function of the 6-vertex model on an $L \times M$ rectangular lattice with periodic boundary conditions is then

$$Z_{6-\text{vertex}} = \text{Tr}\left[\left(\tau_{\frac{1}{2}}(\lambda)\right)^M\right], \tag{7.181}$$

where the trace is over the quantum space. As a consequence of the Yang-Baxter relation for the L-operators [20], the transfer matrices form a commuting family

$$[\tau_{\frac{1}{2}}(\lambda), \tau_{\frac{1}{2}}(\mu)] = 0. \tag{7.182}$$

The Heisenberg Hamiltonian is related to the transfer matrix by taking a logarithmic derivative

$$H_{\text{XXZ}} = -i\frac{\sinh\eta}{2}\frac{\partial}{\partial\lambda}\Big|_{\lambda=0} \ln\left[\tau_{\frac{1}{2}}(\lambda)\right]. \tag{7.183}$$

By virtue of the commutation relations (7.182) it is clear that a set of mutually commuting operators can be obtained by taking higher derivatives, i.e.

$$H^{(\frac{1}{2},k)} = i\left(-\frac{\sinh\eta}{2}\frac{\partial}{\partial\lambda}\right)^k\Big|_{\lambda=0} \ln\left[\tau_{\frac{1}{2}}(\lambda)\right]. \tag{7.184}$$

Crucially, these conservation laws have the form

$$H^{(\frac{1}{2},k)} = \sum_j H^{(\frac{1}{2},k)}_{j,j+1,\dots,j+k}\ , \tag{7.185}$$

where the densities $H^{(\frac{1}{2},k)}_{j,j+1,\dots,j+k}$ act non-trivially only on the $k+1$ consecutive sites $j, j+1, \dots, j+k$. These conservation laws are sometimes referred to as ultra-local. They have been studied extensively in the literature [20, 229, 227, 228]. We note that the above construction is not restricted to Heisenberg models, but works much more generally [20].

"Ultra-local" GGE

According to our general discussion, the GGE describing the steady state after a quench to the Heisenberg model should contain all of the conservation laws (7.184). An important question is whether these conservation laws are also sufficient. This was investigated in Refs [59, 58, 63]. The basic idea is as follows. One considers time evolution induced by the Hamiltonian (7.174)

starting from an initial state $|\Psi(0)\rangle$. The quantities of interest are the matrix elements of the reduced density matrix on a short interval in the steady state, cf. (7.21)

$$g_{\alpha_1,\ldots,\alpha_n} = \lim_{t\to\infty}\lim_{L\to\infty}\langle\Psi(t)|\sigma_1^{\alpha_1}\sigma_2^{\alpha_2}\ldots\sigma_n^{\alpha_n}|\Psi(t)\rangle\ . \tag{7.186}$$

The question is whether these expectation values can be obtained, to a given accuracy, from a GGE density matrix of the form

$$\rho^{(y)}_{\rm ulGGE} = \frac{1}{Z_{\rm ulGGE}}\exp\Big(-\sum_{k=1}^{y}\lambda_k^{(y)}H^{(k,\frac{1}{2})}\Big)\ , \tag{7.187}$$

which takes into account the first y conservation laws in the series (7.184). The Lagrange multipliers $\lambda_k^{(y)}$ are in principle fixed by the requirements

$$\langle\Psi(0)|H^{(k,\frac{1}{2})}|\Psi(0)\rangle = {\rm Tr}\left(\rho^{(y)}_{\rm ulGGE}H^{(k,\frac{1}{2})}\right)\ ,\quad k=1,\ldots,y. \tag{7.188}$$

In practice it is very difficult to determine the Lagrange multipliers from these conditions, even for very simple initial states $|\Psi(0)\rangle$. A method to circumvent this problem was developed in Ref. [58]. The idea is to define a generating function for the initial values (7.188)

$$\begin{aligned}\Omega^{(\frac{1}{2})}_{\Psi(0)}(\lambda) &= \lim_{L\to\infty}\frac{i}{L}\langle\Psi(0)|\tau'_{\frac{1}{2}}(\lambda)\tau^{-1}_{\frac{1}{2}}(\lambda)|\Psi(0)\rangle\\ &= \lim_{L\to\infty}\frac{1}{L}\sum_{k=1}\left(-\frac{2}{\sinh\eta}\right)^k\frac{\lambda^{k-1}}{(k-1)!}\frac{\langle\Psi(0)|H^{(k,\frac{1}{2})}|\Psi(0)\rangle}{L}.\end{aligned} \tag{7.189}$$

For large L (and real λ) the inverse of the transfer matrix becomes

$$\tau^{-1}_{\frac{1}{2}}(\lambda)\simeq\Big(\tau_{\frac{1}{2}}(\lambda)\Big)^\dagger = \left[\frac{\sinh\big(-i\lambda\big)}{\sinh\big(\eta-i\lambda\big)}\right]^L\tau_{\frac{1}{2}}(\lambda+i\eta). \tag{7.190}$$

Using the expression (7.180) of the transfer matrix as a product of L-operators, the generating function can thus be expressed in the form

$$\Omega^{(\frac{1}{2})}_{\Psi(0)}(\lambda) = \lim_{L\to\infty}\frac{i}{L}\frac{\partial}{\partial x}\Big|_{x=\lambda}{\rm Sp}\langle\Psi(0)|V_L(x,\lambda)\ldots V_1(x,\lambda)|\Psi(0)\rangle, \tag{7.191}$$

where $V_n(x,\lambda)$ are 4×4 matrices with entries $(V_n(x,\lambda))^{ab}_{cd}$ that are operators acting on the 2-dimensional quantum space at site n, and Sp denotes the usual trace for 4×4 matrices. The explicit expression is

$$\Big[(V_n(x,\lambda))^{ab}_{cd}\Big]_{\alpha_n\beta_n} = \frac{\sinh\big(-i\lambda\big)}{\sinh\big(\eta-i\lambda\big)}\sum_{\gamma_n}\big(L_n(x)\big)^{ab}_{\alpha_n\gamma_n}\big(L_n(\lambda+i\eta)\big)^{cd}_{\gamma_n\beta_n}\ . \tag{7.192}$$

The advantage of representation (7.191) is that it can be efficiently evaluated for initial states $|\Psi(0)\rangle$ of matrix product form [58, 63]. To understand the principle behind this let us consider a translationally invariant product state

$$|\Psi(0)\rangle = \otimes_{j=1}^L|\psi\rangle_j\ . \tag{7.193}$$

In this case the generating function is obtained from the eigenvalues of the 4×4 matrix $U(x,\lambda) = {}_1\langle\psi|V_1(x,\lambda)|\psi\rangle_1$ as

$$\Omega^{(\frac{1}{2})}_{\Psi(0)}(\lambda) = \lim_{L\to\infty}\frac{i}{L}\frac{\partial}{\partial x}\Big|_{x=\lambda}{\rm Sp}\left(U(x,\lambda)^L\right). \tag{7.194}$$

An efficient algorithm for calculating $\Omega^{(\frac{1}{2})}_{\Psi(0)}(\lambda)$ for matrix-product states was given in Ref. [63]. Having encoded the "initial data" of our quantum quench in the generating function $\Omega^{(\frac{1}{2})}_{\Psi(0)}(\lambda)$, we now move on to the calculation of expectation values of local operators in the state given by (7.187). A very useful observation is that $\rho^{(y)}_{\rm ulGGE}$ can be viewed as a Gibbs ensemble for the "Hamiltonian"

$$H_{\rm eff} = \sum_{k=1}^{y} \lambda_k^{(y)} H^{(k,\frac{1}{2})} \tag{7.195}$$

at an effective inverse temperature $\beta = 1$. As all $H^{(k,\frac{1}{2})}$ commute and are obtained by taking logarithmic derivatives of the transfer matrix, finite temperature properties of (7.195) can be studied by standard methods[227, 230]. The Quantum Transfer Matrix approach (QTM)[231] is particularly useful in this regard, as it provides an efficient way to obtain explicit results for thermal averages of local operators[233, 232] (see also Ref. [234]). Refs [59, 58, 63] employed the QTM approach to the calculation of steady state properties of the density matrix (7.187) for quenches from simple initial states. By employing the generating function (7.189), it is possible to take into account all ultra-local conservation laws, and arrive at explicit results for local observables without having to determine the Lagrange multipliers $\lambda_k^{(\infty)}$[58]. In the QTM approach the stationary state is described in terms of the solution of a system of coupled, nonlinear integral equations. Remarkably, the information on the initial state enters this system only via the function $\Omega^{(\frac{1}{2})}_{\Psi(0)}(\lambda)$. Results for spin correlators obtained in this way were compared to t-DMRG computations for quenches from a variety of initial states in Ref. [63], and found to be compatible within the limitations of the numerical analysis.

The subsequent application of the Quench Action Approach[177] (reviewed by J.-S. Caux [218] in this volume) to the same problem revealed that the ultra-local GGE in fact does not correctly describe the steady state for quenches to the spin-1/2 Heisenberg chain[66, 68, 65, 69, 70], although it does provide a very good approximation for e.g. quenches from the Néel state. This suggested the existence of hitherto unknown conservation laws in the Heisenberg chain, which need to be taken into account in the construction of the GGE.

"Quasi-local" GGE

The "missing" conservation laws for the spin-1/2 Heisenberg XXZ chain were discovered in Refs [235, 64] (see the review by E. Ilievski, M. Medenjak, T. Prosen, and L. Zadnik [236] in this volume). Their structure is quite different from that of the ultra-local conservation laws discussed above: their densities are not local in the sense that they act non-trivially only on a finite number of neighbouring sites, but quasi-local. Similar conservation laws had been identified earlier in relation to transport properties of the Heisenberg chain[237]. In order to define the concept of quasi-locality one introduces an inner product on the space of operators by

$$(A, B) = \langle A^\dagger B\rangle_\infty \ , \qquad \langle A\rangle_\infty = \frac{1}{2^L}{\rm Tr}\big(A\big). \tag{7.196}$$

Definition 6. *Quasi-local operators[235].*

Let us consider an operator Q and expand it in terms of mutually orthogonal local operators $q_{j,r}$ of range r

$$Q = \sum_j \sum_r q_{j,r}. \tag{7.197}$$

Q is called quasi-local if it fulfils the following three conditions:

$$\begin{aligned} &\text{(QL1)}: && \lim_{L\to\infty}\frac{1}{L}(Q-\langle Q\rangle_\infty, Q-\langle Q\rangle_\infty)=\text{const};\\ &\text{(QL2)}: && \lim_{L\to\infty}(Q,B_k)\ \text{exists}\ ,\\ &\text{(QL3)}: && (q_{j,r},q_{j,r})<Ce^{-r/\xi}\ , \end{aligned} \tag{7.198}$$

where B_k is any operator that acts non-trivially only on a fixed number of k sites, and ξ and C are positive constants.

In the anisotropic Heisenberg chain quasi-local charges can be constructed as follows[235, 64]. It is well known that the six-vertex model transfer matrix (7.180) is part of a much larger family, built from the L-operators

$$L_n^{(S)}(\lambda)=\frac{1}{\sinh\left(\frac{\eta}{2}(1+s)+i\lambda\right)}\Big[\sinh(\frac{\eta}{2}+i\lambda)\cosh(\eta\mathcal{S}^z)+\cosh(\frac{\eta}{2}+i\lambda)\sinh(\eta\mathcal{S}^z)\sigma_n^z \\ +\sinh(\eta)(\mathcal{S}^-\sigma_n^++\mathcal{S}^+\sigma_n^-)\Big), \tag{7.199}$$

which again acts on the tensor product of auxiliary and quantum spaces, but now the auxiliary space is $2S+1$ dimensional. Here S is an arbitrary half integer. The operators $\mathcal{S}^\alpha$ obey a q-deformed SU(2) algebra

$$[\mathcal{S}^+,\mathcal{S}^-]=[2\mathcal{S}^z]_q\ ,\qquad [\mathcal{S}^z,\mathcal{S}^\pm]=\pm\mathcal{S}^\pm\ , \tag{7.200}$$

where $[x]_q=\sinh(\eta x)/\sinh(\eta)$, and act on a q-deformed spin-S representation as

$$\mathcal{S}^z|k\rangle=k|k\rangle,\qquad \mathcal{S}^\pm|k\rangle=\sqrt{[S+1\pm k]_q[S\mp k]_q}|k\pm1\rangle\ ,\quad k=-S,\dots,S. \tag{7.201}$$

A family of row-to-row transfer matrices is then obtained as

$$\big(\tau_S(\lambda)\big)_{\alpha_1\dots\alpha_L}^{\beta_1\dots\beta_L}=\big(L_1^{(S)}(\lambda)\big)_{\alpha_1\beta_1}^{a_1a_2}\big(L_2^{(S)}(\lambda)\big)_{\alpha_2\beta_2}^{a_2a_3}\dots\big(L_L^{(S)}(\lambda)\big)_{\alpha_L\beta_L}^{a_La_1}\ . \tag{7.202}$$

All $\tau_S(\lambda)$ are operators on the same quantum space (a tensor product of L spin-1/2's), and as a consequence of the Yang-Baxter relation form a commuting family

$$[\tau_S(\lambda),\tau_{S'}(\mu)]=0. \tag{7.203}$$

By virtue of the commutation relations (7.182) it is clear that a set of mutually commuting operators can be obtained by taking higher derivatives, i.e.

$$H^{(S,k)}=i\left(C_S\frac{\partial}{\partial\lambda}\right)^k\Big|_{\lambda=0}\ln\left[\tau_S(\lambda)\right], \tag{7.204}$$

where C_S are some normalization constants that can be conveniently chosen. As a consequence of (7.203) we have

$$[H^{(S,k)},H^{(S',k')}]=0. \tag{7.205}$$

Apart from the special case $S=1/2$ these conservation laws are quasi-local. This means that (in the infinite volume) their general structure is

$$H^{(S>\frac{1}{2},k)}=\sum_{j=-\infty}^{\infty}\sum_{k\geq1}\sum_{\alpha_1,\dots,\alpha_k}f^{(k)}_{\alpha_1\alpha_2\dots\alpha_k}\sigma_j^{\alpha_1}\sigma_{j+1}^{\alpha_2}\dots\sigma_{j+k-1}^{\alpha_k}\ , \tag{7.206}$$

where $\alpha_j = 0, x, y, z$, and the coefficient functions $f^{(k)}_{\alpha_1 \dots \alpha_k}$ decay sufficiently fast with k so that the conservation laws are extensive. As shown in Ref. [64], the initial data of the quantum quench can again be encoded in suitably chosen generating functions, which are generalizations of (7.189)

$$\Omega^{(S)}_{\Psi(0)}(\lambda) = \lim_{L\to\infty} \frac{i}{L} \langle \Psi(0)|\tau_S'(\lambda)\tau_S^{-1}(\lambda)|\Psi(0)\rangle = \lim_{L\to\infty} \frac{i}{L} \left[\frac{\sinh\left(\frac{\eta}{2}(1-2S)-i\lambda\right)}{\sinh\left(\frac{\eta}{2}(1+2S)-i\lambda\right)}\right]^L \langle \Psi(0)|\tau_S'(\lambda)\tau_S(\lambda-\eta)|\Psi(0)\rangle \tag{7.207}$$

The generating functionals $\Omega^{(S)}_{\Psi(0)}(\lambda)$ can be evaluated for matrix product states by the same method discussed above (although the computational effort increases with the value of S).

The most convenient description of the stationary state turns out to be in terms of the generalized microcanonical ensemble discussed above. The steady state is characterized by the set $\{\rho^{\rm SS}_{n,p}(\lambda)|n = 1, \dots\}$ of particle densities or the equivalent set of hole densities $\{\rho^{\rm SS}_{n,h}(\lambda)|n = 1, \dots\}$. Ultimately this set must be determined by the initial conditions, which are encoded in (7.207). We now use that $X_S(\lambda) = \tau_S'(\lambda)\tau_S^{-1}(\lambda)$ can be diagonalized by Algebraic Bethe Ansatz [20, 239]. The eigenvalues of $X_S(\lambda)$ for M-particle states with $M \sim L$ are of the form

$$\nu_S(\lambda) = \sum_{k=1}^{M} \frac{2\sinh(2S\eta)}{\cos(2\lambda+2\lambda_k)-\cosh(2S\eta)} + o(L) \ , \tag{7.208}$$

where the λ_k are solutions to the Bethe Ansatz equations[239]

$$\left(\frac{\sin(\lambda_j+i\eta S)}{\sin(\lambda_j-i\eta S)}\right)^L = \prod_{k\neq j=1}^{M} \frac{\sin(\lambda_j-\lambda_k+i\eta)}{\sin(\lambda_j-\lambda_k-i\eta)} \ , \quad j = 1, \dots, M. \tag{7.209}$$

In the thermodynamic limit this can be simplified by following through the usual logic of the string hypothesis and the Thermodynamic Bethe Ansatz[226, 214, 215]. Rather than with solutions to the Bethe equations (7.209) one then works with macro-states $|\boldsymbol{\rho}\rangle$, which are described by sets $\{\rho_{n,p}(\lambda)|n = 1, \dots\}$ of particle densities or the equivalent set of hole densities $\{\rho_{n,h}(\lambda)|n = 1, \dots\}$. The eigenvalue equation (7.208) then becomes[64]

$$\lim_{L\to\infty} \frac{1}{L} \langle \boldsymbol{\rho}|X_S(\mu)|\boldsymbol{\rho}\rangle = \sum_{k\in\mathbb{Z}} \frac{e^{-i2k\mu}}{\cosh(k\eta)} \left(\int_{-\pi/2}^{\pi/2} {\rm d}\lambda \, e^{2ik\lambda} \rho_{2S,h}(\lambda) - e^{-2S|k|\eta} \right) . \tag{7.210}$$

For $|\boldsymbol{\rho}\rangle = |\boldsymbol{\rho}^{\rm SS}\rangle$ the right hand side of (7.210) must agree with the initial values after the quench (7.207). This is achieved by setting[64]

$$\rho^{\rm SS}_{2S,h}(\lambda) = a_{2S}(\lambda) + \frac{1}{2\pi} \left[\Omega^{(S)}_{\Psi(0)}\big(\lambda + i\tfrac{\eta}{2}\big) + \Omega^{(S)}_{\Psi(0)}\big(\lambda - i\tfrac{\eta}{2}\big) \right] , \tag{7.211}$$

where $a_{2S}(\lambda)$ is a function independent of the initial state that is defined in Appendix 7.10.2. This shows that the initial data (7.207), which involves both ultra-local and quasi-local conservation laws, completely determines the macro-state that defines the generalized microcanonical ensemble. We note that the derivation did not invoke the maximum entropy principle. For the particular case of quenches from the Néel state (7.211) agrees with the one obtained by the Quench Action Approach[66, 68, 65, 69].

The generalization of the approach discussed above for quenches to particular values of Δ with $-1 < \Delta < 1$ in the Heisenberg model (7.174) was achieved in Ref. [240] .

7.8 Outlook

We have given an introduction to quantum quenches in many-particle systems and then reviewed recent developments, focussing in particular on the role played by conservation laws. In spite of the impressive progress of the last few years, many important questions remain largely open. Let us list a few of them in no particular order.

1. In the spin-1/2 Heisenberg XXZ chain quasi-local conservation laws have been shown to play a prominent role in determining the stationary state. It is believed that this holds quite generally in interacting integrable models. The construction used in the XXZ case can in principle be generalized to the $sl(M|N)$ family of integrable graded quantum "spin" chains, see e.g. Refs [241], and it would be interesting to investigate the role of quasi-local charges in such models. The Hubbard model is another very interesting case, but is like to be more difficult to handle due to its non standard structure[214].

2. So far only particularly simple classes of initial states can be accommodated, cf. Section 7.7.1. It would be highly desirable to have a more general method for capturing the information on the initial state.

3. In interacting theories the focus has so far been on stationary state properties. The study of the full time evolution of observables is much less developed[95, 113, 242, 243]. A promising method for analyzing the time dependence of the expectation values of local operators after a quantum quench in an interacting integrable theory is the Quench Action approach[177]. So far it has been implemented only in a very small number of cases[95, 113], and further studies are sorely needed.

4. As we have seen, the non-equilibrium dynamics of integrable and non-integrable models is quite different. This poses the question of what happens, when one adds a small perturbation to an integrable model. This has been investigated in a number of theoretical works [244, 245, 246, 247, 248, 249, 251, 250, 252, 253, 254, 255, 256, 257, 51, 127, 258, 259, 260, 261, 262, 263, 264], and is of immediate experimental relevance[265, 266] (see also the review by T. Langen, T. Gasenzer and J. Schmiedmayer in this volume[18]). The generic effect of adding a small integrability breaking term appears to be the generation of an intermediate "prethermalization" time scale, below which the system retains information about being proximate in parameter space to an integrable model. At late times thermalization seems to set in[259]. So far the theoretical analyses are restricted to weak interactions and/or short times, and it is crucial to go beyond these limitations.

7.9 Requirements on the initial state

7.9.1 Cluster decomposition

We have defined our quench protocol such that it results in initial states $|\Psi(0)\rangle$ that have a cluster decomposition property (7.12). This requirement is often relaxed in both numerical and analytical investigations, and in some cases $|\Psi(0)\rangle$ is taken to be a Schrödinger cat state, see e.g. Refs [65, 66, 69, 68]. An example is provided by quenches where the system is initialized in a classical Néel state $|\uparrow\downarrow\uparrow\downarrow\ldots\rangle$. This breaks translational invariance and it can be calculationally convenient to work instead with a translationally invariant cat state

$$\frac{1}{\sqrt{2}}\left(|\uparrow\downarrow\uparrow\downarrow\uparrow\ldots\rangle + |\downarrow\uparrow\downarrow\uparrow\downarrow\ldots\rangle\right). \tag{7.212}$$

While for specific calculations such replacements can be useful, they significantly affect the steady state behaviour in general. This can be seen by considering a $\mathbb{Z}_2$ symmetric pre-quench

Hamiltonian H_0 with a ground state that spontaneously breaks the $\mathbb{Z}_2$ symmetry. An example is provided by the transverse-field Ising chain (7.104) with $h < 1$. In the thermodynamic limit H_0 has two ground states $|\Psi_\pm\rangle$, both of which have a cluster decomposition property. We now consider a general linear combination

$$|\Psi(0)\rangle = \cos\theta|\Psi_+\rangle + e^{i\phi}\sin\theta|\Psi_-\rangle\,. \tag{7.213}$$

As $|\Psi_\pm\rangle$ are macroscopically distinct (as they lead to different order parameters), we conclude that expectation values of local operators $\mathcal{O}$ are given by

$$\langle\Psi(0)|\mathcal{O}|\Psi(0)\rangle = \cos^2\theta\langle\Psi_+|\mathcal{O}|\Psi_+\rangle + \sin^2\theta\langle\Psi_-|\mathcal{O}|\Psi_-\rangle\,. \tag{7.214}$$

As the Hamiltonian of our system is short ranged, this decomposition persists at all finite times, i.e.

$$\langle\Psi(t)|\mathcal{O}|\Psi(t)\rangle = \cos^2\theta\langle\Psi_+(t)|\mathcal{O}|\Psi_+(t)\rangle + \sin^2\theta\langle\Psi_-(t)|\mathcal{O}|\Psi_-(t)\rangle \tag{7.215}$$

To see this, we may use a result derived in Ref. [181] for the time evolution of local operators with short-ranged Hamiltonians: restricting $\mathcal{O}(t) = e^{iHt}\mathcal{O}e^{-iHt}$ to a subsystem S of size $|S|$ gives an error that scales as $e^{(2vt-|S|)/\zeta}$, where ζ is a constant and v is the Lieb-Robinson velocity. This means that it is possible to approximate $\mathcal{O}(t)$ to a given accuracy by a local operator of a "size" that scales as $2vt$. This in turn implies that $\langle\Psi_+|\mathcal{O}(t)|\Psi_-\rangle = 0$, because $|\Psi_\pm\rangle$ are macroscopically distinct.

On the other hand, our system relaxes locally by construction if we initialize it in $|\Psi_\pm(0)\rangle$, i.e.

$$\lim_{t\to\infty}|\Psi_\pm(t)\rangle\langle\Psi_\pm(t)| =_{\rm loc} \rho^{\rm SS}_\pm. \tag{7.216}$$

Putting everything together we conclude that

$$\lim_{t\to\infty}|\Psi(t)\rangle\langle\Psi(t)| =_{\rm loc} \rho^{\rm SS} = \cos^2\theta\rho^{\rm SS}_+ + \sin^2\theta\rho^{\rm SS}_-\,. \tag{7.217}$$

The problem is that this form of the stationary state can be different from what one would expect on the basis of local relaxation to (generalized) Gibbs ensembles. To be specific, we consider the example of a quench to an anisotropic spin-1/2 Heisenberg chain

$$H = \frac{J}{4}\sum_\ell \sigma^y_\ell\sigma^y_{\ell+1} + \sigma^z_\ell\sigma^z_{\ell+1} + \Delta\sigma^x_\ell\sigma^x_{\ell+1} + g\sigma^x_\ell\sigma^x_{\ell+2}\,. \tag{7.218}$$

Imposing $\Delta, g \neq 0$ renders this model non-integrable, but is has one local conservation law

$$Q = \sum_\ell \sigma^x_\ell\ , \quad [H,Q] = 0. \tag{7.219}$$

Our initial state is of the form (7.213), where $|\Psi_\pm(0)\rangle$ are the two ground states of the TFIC in the thermodynamic limit at $h < 1$. We note that the energy density e of (7.218) is the same in both $|\Psi_+\rangle$ and $|\Psi_-\rangle$. As these states have a cluster decomposition property, it follows from our general discussion that the respective stationary states are locally equivalent to grand canonical ensembles

$$\lim_{t\to\infty}|\Psi_\pm(t)\rangle\langle\Psi_\pm(t)| =_{\rm loc} \rho^{\rm GC}_\pm = \frac{e^{-\beta_\pm H-\mu_\pm Q}}{Z_\pm}\,, \tag{7.220}$$

where the values for $\beta_\pm$ and $\mu_\pm$ are obtained by fixing the energy density e and charge density $q_\pm$ to agree with their initial values at time $t = 0$. Eqn (7.217) tells us that the correct stationary state in this example is then

$$\rho^{\rm SS} =_{\rm loc} \cos^2\theta\rho^{\rm GC}_+ + \sin^2\theta\rho^{\rm GC}_-\ . \tag{7.221}$$

Crucially, while the density matrices $\rho_{\pm}^{\rm GC}$ have the cluster decomposition property, $\rho^{\rm SS}$ does not. This can be seen as follows. The local conservation law distinguishes between the two states $|\Psi_{\pm}\rangle$

$$q_+ = \langle\Psi_+|\sigma_\ell^x|\Psi_+\rangle \neq \langle\Psi_-|\sigma_\ell^x|\Psi_-\rangle = q_- \ . \tag{7.222}$$

Using the cluster decomposition property of $\rho_{\pm}^{\rm GC}$ we have

$$\lim_{|n-\ell|\to\infty} {\rm Tr}\left(\rho_{\pm}^{\rm GC}\sigma_\ell^x\sigma_n^x\right) = q_\pm^2, \tag{7.223}$$

which in turn establishes that $\rho^{\rm SS}$ does not have the cluster decomposition property

$$\lim_{|n-\ell|\to\infty}\left[{\rm Tr}\left(\rho^{\rm SS}\sigma_\ell^x\sigma_n^x\right) - {\rm Tr}\left(\rho^{\rm SS}\sigma_\ell^x\right){\rm Tr}\left(\rho^{\rm SS}\sigma_n^x\right)\right] = \frac{(q_+-q_-)^2}{4}\sin^2(2\theta) \neq 0. \tag{7.224}$$

On the other hand, if we were to apply our formalism of local relaxation blindly to our Hamiltonian (7.218), we would conclude that the stationary state is locally equivalent to a grand canonical ensemble, which is expected to have a cluster decomposition property [268].

Our discussion can be summarized as follows: If there exists at least one integral of motion that distinguishes $|\Psi_-\rangle$ from $|\Psi_+\rangle$, the stationary state associated with the time evolution of the cat state (7.213) does not possess the cluster decomposition property (7.12) and hence is not described by a standard generalized Gibbs ensemble.

7.9.2 Probability distributions of energy and conservation laws

Let us consider a post-quench Hamiltonian H with a set of local conservation laws $I^{(n)}$, cf. (7.31), (7.32). In our basic definition of a quantum quench we initialize the system in a pure state $|\Psi(0)\rangle$. Then the cluster decomposition property implies that the probability distribution of energy and all local conservation laws approach delta-functions in the thermodynamic limit, e.g.

$$P_n(\epsilon) = \lim_{L\to\infty}\frac{1}{L}{\rm Tr}\left[\rho(0)\delta(I^{(n)}-L\epsilon)\right] = \delta(\varepsilon - i^{(n)}) \ , \quad i^{(n)} = \lim_{L\to\infty}\frac{1}{L}{\rm Tr}\left[\rho(0)I^{(n)}\right], \tag{7.225}$$

where $\rho(0) = |\Psi(0)\rangle\langle\Psi(0)|$. As we have pointed out, it is sometimes desirable to consider initial density matrices $\rho(0)$ that are not pure states. When doing so one must ensure that (7.225) continues to hold. In cases where it does not it is clearly impossible for the system to locally relax to a GGE, because there the probability distributions of all conservation laws approach delta functions in the thermodynamic limit. Generalizations of GGE ideas to such cases have been explored in Ref. [267] .

7.10 "Atypical" macro-states in integrable models

Integrable models have the unusual property of having atypical finite entropy eigenstates at finite energy densities. This is well known for non-interacting theories and we discuss this case first.

7.10.1 Free fermions

Let us consider a model of free fermions with Hamiltonian

$$H = \sum_k \epsilon(k)n(k) \ , \tag{7.226}$$

where $n(k) = c^\dagger(k)c(k)$. Imposing periodic boundary conditions quantizes the allowed momenta

$$k_n = \frac{2\pi n}{L} \ , \quad n = -\frac{L}{2} + 1, \ldots, \frac{L}{2}. \tag{7.227}$$

We now focus on a special class of Fock states $\prod_{j=1}^N c^\dagger(k_j)|0\rangle$, for which the particle densities

$$\rho_p(k_j) = \frac{1}{L(k_{j+1} - k_j)} \tag{7.228}$$

approach smooth functions in the thermodynamic limit $N, L \to \infty$, $n = N/L$ fixed. For such states, the number of particles in the interval $[k_n, k_n + \Delta k]$ for large L is given by

$$\rho_p(k_n)\Delta k \ . \tag{7.229}$$

It is convenient to define a hole density by $\rho_h(k_j) = \frac{1}{2\pi} - \rho_p(k_j)$. In the thermodynamic limit many different choices of $\{k_j\}$ lead to the same macro-state described by a given particle density. To enumerate them we note that the number of different states in the interval $[k, k + \Delta k]$, that give rise to a given density in the thermodynamic limit, is obtained by distributing $\rho_p(k)L\Delta k$ particles among $\big(\rho_p(k) + \rho_h(k)\big)L\Delta k$ vacancies. This follows a binomial distribution. For large L the latter may be approximated by Stirling's formula, and in the thermodynamic limit one obtains the well-known expression for the entropy per site

$$s[\rho_p] = \int_{-\pi}^{\pi} dk \left[\big(\rho_p(k) + \rho_h(k)\big) \ln\big(\rho_p(k) + \rho_h(k)\big) - \rho_p(k) \ln\big(\rho_p(k)\big) - \rho_h(k) \ln\big(\rho_h(k)\big)\right] \ . \tag{7.230}$$

Let us now investigate what kind of macro-states exist for a given energy density e. The most likely (maximum entropy) macro-state can be constructed using equilibrium statistical mechanics. Extremizing the free energy per site

$$f[\rho_p] = \int_{-\pi}^{\pi} \frac{dk}{2\pi} \epsilon(k)\rho_p(k) - Ts[\rho_p] \tag{7.231}$$

with respect to the particle density ρ_p gives

$$\rho_p^{\rm eq}(k) = \frac{1}{2\pi} \frac{1}{1 + e^{\epsilon(k)/T}}. \tag{7.232}$$

The "temperature" T is related to the energy density e by

$$e = \int_{-\pi}^{\pi} \frac{dk}{2\pi} \frac{\epsilon(k)}{1 + e^{\epsilon(k)/T}}. \tag{7.233}$$

The entropy per site of this equilibrium state is

$$s[\rho_p^{\rm eq}] = \frac{\partial}{\partial T} T \int_{-\pi}^{\pi} \frac{dk}{2\pi} \ln\left[1 + e^{-\epsilon(k)/T}\right]. \tag{7.234}$$

By construction the macro-state (7.232) is the typical state at energy density (7.233): if we randomly pick an energy eigenstate with energy density e for a very large system size L, the probability for this state to have particle density (7.232) is exponentially close (in L) to one. On the other hand, there are atypical finite entropy macro-states characterized by their respective particle densities $\rho_p(k)$. As a particular example we consider our tight-binding model (7.40) for $\mu = 0$, which gives a dispersion $\epsilon(k) = -2J\cos(k)$. We fix the particle density to be $1/2$ and

the energy density to be $e = -0.405838J$, which corresponds to temperature $T = J$ in (7.232), (7.233), i.e.

$$\rho_p^{\rm eq}(k) = \frac{1}{2\pi}\frac{1}{1+e^{-2\cos(k)}}. \tag{7.235}$$

The entropy of the equilibrium state is $s_{\rm eq} = 0.511571$. Let us now consider the family of macro-states described by the particle density

$$\rho_p^{(\lambda)}(k) = \frac{1}{2\pi}\frac{1}{1+e^{-4\cos(k)-\lambda\cos(3k)}} \ . \tag{7.236}$$

Fixing $\lambda = 2.43096..$ gives us the same particle and energy densities as for the equilibrium state, i.e. $n = 1/2$ and $e = -0.405838J$. The entropy density $s = 0.396781$ is of course lower than that of the (maximum entropy) equilibrium state. This means that if we randomly select an energy eigenstate with particle density $n = 1/2$ and energy density $e = -0.405838J$ for a very large system size L, we are exponentially more likely by a factor $e^{L(s_{\rm eq}-s)}$ to end up with a state described by (7.235) than one described by (7.236). Unsurprisingly, expectation values of local operators are generally different in the two macro-states. As an example, let us consider

$$\mathcal{O}_j = c_j^\dagger c_{j+3} + c_{j+3}^\dagger c_j \ . \tag{7.237}$$

Setting again $\lambda = 2.43096..$ and taking the thermodynamic limit we have

$$\langle\rho_p^{\rm eq}(k)|\mathcal{O}_j|\rho_p^{\rm eq}(k)\rangle = -0.0271229 \neq \langle\rho_p^{(\lambda)}(k)|\mathcal{O}_j|\rho_p^{(\lambda)}(k)\rangle = 0.215148 \ . \tag{7.238}$$

Here the expectation values may be taken with regards to any micro-state that gives rise to the appropriate macro-state in the thermodynamic limit.

7.10.2 Interacting theories: anisotropic spin-1/2 Heisenberg model

The situation in integrable models is analogous to what we just discussed for free fermions. The main difference arises from the more complicated structure and interacting nature of the elementary excitations in integrable models. For the sake of definiteness we consider the particular example of the spin-1/2 Heisenberg model (7.174) with $\Delta \geq 1$. Energy eigenstates $|\lambda_1, \ldots, \lambda_M\rangle$ on a ring of length L are parametrized by M rapidity variables λ_j, which fulfil the quantization conditions[226]

$$\left(\frac{\sin(\lambda_j + i\frac{\eta}{2})}{\sin(\lambda_j - i\frac{\eta}{2})}\right)^L = \prod_{k\neq j=1}^{M}\frac{\sin(\lambda_j-\lambda_k+i\eta)}{\sin(\lambda_j-\lambda_k-i\eta)} \ , \quad j = 1, \ldots, M. \tag{7.239}$$

Each λ_j is associated with an elementary "magnon" excitation over the ferromagnetic state with all spins up, and the total energy and momentum of the eigenstate are additive $E = \sum_{j=1}^M e(\lambda_j)$, $P = \sum_{j=1}^M p(\lambda_j)$. As a result of interactions, magnons form bound states. These correspond to "string solutions" of the quantization conditions (7.239)

$$\lambda_\alpha^{n,j} = \lambda_\alpha^n + i\frac{\eta}{2}(n+1-2j) + i\delta_\alpha^{n,j} \ , \qquad j = 1, \ldots, n \ , \tag{7.240}$$

where $\delta_\alpha^{n,j}$ are deviations from "ideal" strings that become negligible when we take the thermodynamic limit at finite densities of magnons and bound states, cf. 6.2.A of Ref. [269]. As a consequence of integrability these bound states are stable excitations. The generalization of particle density description of macro-states in free theories to interacting integrable models is then clear: macro-states are characterized by an (infinite) set of densities $\{\rho_{n,p}(\lambda)|n = 1, 2, \ldots\}$ for magnons ($n = 1$) and bound states of all lengths ($n \geq 2$). Just as in the case of free fermions,

we can define corresponding hole densities $\rho_{n,h}(\lambda)$. The relation between particle and hole densities is fixed by the quantization conditions (7.239)

$$\rho_{n,t}(\lambda) \equiv \rho_{n,p}(\lambda) + \rho_{n,h}(\lambda) = a_n(\lambda) - \sum_{m=1}^{\infty} \int_{-\frac{\pi}{2}}^{\frac{\pi}{2}} d\mu \; A_{nm}(\lambda-\mu)\rho_{m,p}(\mu) \; , \tag{7.241}$$

where $A_{nm}(\lambda) = (1-\delta_{n,m})a_{|n-m|}(\lambda) + 2a_{|n-m|+2}(\lambda) + \cdots + 2a_{n+m-2}(\lambda) + a_{n+m}(\lambda)$ and $a_n(\lambda) = \frac{1}{2\pi}\frac{2\sinh(n\eta)}{\cosh(n\eta)-\cos(2\lambda)}$. Eqn (7.241) allows one to express the hole densities in terms of the particle densities and vice versa, but in contrast to the non-interacting case the relationship is non-trivial. The energy and entropy per site of a macro-state are given by

$$\begin{aligned} e[\{\rho_{n,p}\}] &= -J\sinh(\eta)\sum_{n=1}^{\infty}\int_{-\frac{\pi}{2}}^{\frac{\pi}{2}} d\lambda \; \rho_{n,p}(\lambda)\; a_n(\lambda) \; , \\ s[\{\rho_{n,p},\rho_{n,h}\}] &= \sum_{n=1}^{\infty}\int_{-\frac{\pi}{2}}^{\frac{\pi}{2}} d\lambda \left[\rho_{n,t}(\lambda)\ln\big(\rho_{n,t}(\lambda)\big) - \rho_{n,p}(\lambda)\ln\big(\rho_{n,p}(\lambda)\big) - \rho_{n,h}(\lambda)\ln\big(\rho_{n,h}(\lambda)\big)\right] \end{aligned} \tag{7.242}$$

The typical state at a given energy density is then obtained by extremizing the free energy per set $f[\{\rho_{n,p}\}] = e[\{\rho_{n,p}\}] - Ts[\{\rho_{n,p},\rho_{n,h}\}]$ with respect to particle and hole densities under the constraints (7.241). This results in the so-called Thermodynamic Bethe Ansatz equations[226]. By construction this state is thermal, i.e. corresponds to a standard Gibbs distribution.

Atypical finite entropy states can be constructed by specifying a set of particle densities $\{\rho_{n,p}(\lambda)\}$. The corresponding hole densities are then obtained by solving equations (7.241). The entropy per site of the resulting macro-state can be calculated from (7.242), and will by construction be smaller than that of the maximum entropy state.

7.11 Stationary state correlators in the TFIC

In this appendix we summarize results for the amplitudes $C^{\alpha}(\ell)$ describing the subleading behaviour of stationary state spin-spin correlators in the TFIC, cf. Eqn (7.133).

Transverse spin correlator.

Here the amplitude is of the form[26]

$$C^z(\ell) = \bar{C}^z \ell^{-\alpha^z} \; , \qquad \alpha^z = \begin{cases} 1 & \text{if } \; |\ln h| > |\ln h_0| \; , \\ 0 & \text{if } \; h_0 = 1/h \; , \\ 1/2 & \text{if } \; |\ln h| < |\ln h_0| \, , \end{cases} \tag{7.243}$$

where the constant is known exactly

$$C^z = \begin{cases} \frac{|h_0-1/h_0|}{4\pi}\frac{h_0-h}{hh_0-1} & \text{if } \; |\ln h| > |\ln h_0| \; , \\ -\frac{(h-1/h)^2}{2\pi} & \text{if } \; h_0 = 1/h \; , \\ \frac{(h-1/h)\sqrt{|h_0-1/h_0|}(h_0-h)}{8\sqrt{\pi}h}\sqrt{\frac{h_0-h}{h_0(hh_0-1)}}\frac{e^{\mathrm{sgn}(\ln h)|\ln h_0|/2}}{\sinh\frac{|\ln h|+|\ln h_0|}{2}} & \text{if } \; |\ln h| < |\ln h_0| \, . \end{cases} \tag{7.244}$$

Longitudinal spin correlator.

Here the large-ℓ asymptotics of prefactor $C^x(\ell)$ are as follows.

1. Quench within the ferromagnetic phase ($h_0, h < 1$).

$$C^x(\ell) \equiv \mathcal{C}^x_{\mathrm{FF}} = \frac{1 - hh_0 + \sqrt{(1-h^2)(1-h_0^2)}}{2\sqrt{1-hh_0}\sqrt[4]{1-h_0^2}} \, . \tag{7.245}$$

2. Quench from the ferromagnetic to the paramagnetic phase ($h_0 < 1 < h$).

$$C^x(\ell) \equiv \mathcal{C}^x_{\rm FP} = \sqrt{\frac{h\sqrt{1-h_0^2}}{h+h_0}}. \tag{7.246}$$

3. Quench from the paramagnetic to the ferromagnetic phase ($h_0 > 1 > h$).

$$C^x(\ell) \equiv \mathcal{C}^x_{\rm PF}(\ell) = \sqrt{\frac{h_0-h}{\sqrt{h_0^2-1}}}\cos\Big(\ell \arctan\frac{\sqrt{(1-h^2)(h_0^2-1)}}{1+h_0h}\Big)\,. \tag{7.247}$$

4. Quench within the paramagnetic phase ($1 < h_0, h$).

$$C^x(\ell) \equiv \mathcal{C}^x_{\rm PP}(\ell) = \begin{cases} -\frac{h_0\sqrt{h}\left(hh_0-1+\sqrt{(h^2-1)(h_0^2-1)}\right)^2}{4\sqrt{\pi}(h_0^2-1)^{3/4}(h_0h-1)^{3/2}(h-h_0)}\ \ell^{-3/2} & \text{if } 1<h_0<h\,, \\ \sqrt{\frac{h(h_0-h)\sqrt{h_0^2-1}}{(h+h_0)(hh_0-1)}} & \text{if } 1<h<h_0. \end{cases} \tag{7.248}$$

8 Generalized Gibbs ensembles in weakly interacting dissipative systems and digital quantum computers by Ulčakar, Lenarčič

Abstract

Digital quantum computers promise to solve important and challenging problems in many-body quantum physics. However, at least for the superconducting platforms, their current limitation is the noise level. It thus seems more reasonable to presently use them to model dissipative systems, where platforms' native noise is not that crucial. Here, we propose using a digital quantum computer to showcase the activation of integrability by realizing exotic generalized Gibbs ensembles in weakly dissipative integrable systems. Dissipation is realized by coupling system's qubits to periodically reset ancilla ones, like in the protocol [45] recently used to realize dissipative cooling. We derive the effective equations of motion for trotterized dynamics and contrast such a setup to the usual Lindblad continuous evolution. For simplicity, we consider and compare different approaches to calculating steady-states of non-interacting integrable systems weakly coupled to baths, where thermodynamic results can be obtained via a generalized scattering theory between the Bogoliubov quasiparticles. Corresponding quantum computer implementation would illuminate the possibilities of realizing similar exotic states in nearly integrable quantum materials.

8.0.1 Main ideas and formulas

(?? I'll summarize the article later here)

$$\chi_{q,q'}(t) := \langle n_q n_{q'}\rangle_{\rho_{\boldsymbol{\mu}}(t)} - \langle n_q\rangle_{\rho_{\boldsymbol{\mu}}(t)}\langle n_{q'}\rangle_{\rho_{\boldsymbol{\mu}}(t)};$$

$$\dot\mu_q(t) = -\sum_{q'}(\chi^{-1})_{q,q'}(t)\,\langle \dot n_{q'}\rangle(t).$$

$$\langle \dot n_q\rangle(t) \approx \mathrm{Tr}\left[n_q\hat{\mathcal{D}}[\rho]\right].$$

or actually this one: (??)
$\chi_{q,q'}(t) = \delta_{q,q'}\, e^{-\mu_q(t)}/(1+e^{-\mu_q(t)})^2$

$$\langle \dot n_m\rangle = \epsilon\sum_j \langle L_j^\dagger n_m L_j\rangle - \langle L_j^\dagger L_j n_m\rangle; \qquad L_j = \sum_{q,q'}\frac{e^{-ij(q-q')}}{L}(1+e^{iq'})c_q^\dagger c_{q'}; \qquad c_q := u_q d_q - v_q d_{-q}^\dagger.$$

8.0.2 Introduction

Most of the quantum simulators and computers strive to eliminate any elements of openness, however, to some extent, it is unavoidable: atom loss and dipolar coupling in cold atoms, light leakage in cavities, heating, dephasing and other errors on gates, etc. In the pioneering experiments with trapped ions [44] and also in some more recent experiments with superconducting qubit platform [45] (???), there have been propositions on how to actually use engineered dissipation [3, 4] to prepare target/ground states [5, 6] or to measure phase transitions [7] (???). Such protocols might also be more resilient to the inherent platforms' noise. For example, in a recent implementation of trotterized transverse field Ising model with the superconducting circuit [45], a dissipative cooling towards the ground state has been implemented by coupling the system's qubits to ancilla ones that are periodically reset. This realization builds on a series of theoretical works [8, 9, 10, 11, 12, 13, 14, 15] proposing cooling in quantum computers by coupling to low entropy baths (ancilla qubits), involving tuning the Hamiltonian of the ancilla qubits and its coupling to the system qubits. While the above mentioned cooling protocols might be more naturally and efficiently implemented with an ergodic system [8], considering non-interacting models can assist to get more exact/analytical insight into the conditions required [16].

(???) In many cases, non-interacting many-body models are the cornerstone of our understanding and description of many-body physics. The fact that they are exactly diagonalizable via the Bogoliubov transformation makes them also a rare and appealing platform to study non-equilibrium many-body physics [4, 3, 19]. In the context of thermalization or its failure, non-interacting systems are an example of models with extensively many conserved quantities [4, 3]. The conserved quantities of translationally invariant models are simply the mode occupation operators of Bogoliubov quasiparticles [3] and one can use those to construct extensively many local conserved quantities [4]. The existence of macroscopically many conserved quantities places non-interacting many-body systems on the same footing as more general interacting integrable systems, in the sense that they fail to thermalize due to the presence of additional conservation laws, or equivalently, limited quasiparticle scattering [3, 4, 19]. Non-interacting models have been among the first for which the applicability of generalized Gibbs ensembles (GGEs) [1] as a local description of steady states reached after a sudden quench has been demonstrated [67, 69, 68, 24, 25, 37, 27]. Introducing additional Lagrange parameters, associated with the mode occupation operators or the local conserved operators, proved to be a successful way to take into account constraints on equilibration. More recent studies showed that a GGE description applies not only to quenches in isolated models but also to weakly dissipative integrable systems, including the non-interacting ones [26, 18, 25, 28, 29, 33, 30, 32, 33, 34, 35, 39]. In that case, GGE gives the zeroth order approximation to the dynamics and the steady state density matrix. The main difference between the closed and open setup is that for the former, the Lagrange multipliers are determined by the post-quench state, while in the open setup, they are determined by the dissipation operator [26, 18, 25, 28, 29, 33]. Only if the dissipators obeys detailed balance condition, the stabilized steady-state is thermal [18, 16]. In any other situations, such weakly dissipative, nearly integrable systems tend to converge to highly non-thermal GGEs. This explains why a careful tuning of parameters is necessary for preparation of thermal states on a quantum computer modelling an integrable system [45, 16].

In this work, we marry the two topics and show that for generic weak couplings between integrable system and periodically reset ancilla qubits, highly non-thermal generalized Gibbs ensembles would be stabilized with quantum computers. We focus on the non-interacting (those, which can be diagonalized) integrable (those, which have conserved quantities, so all non-interacting are integrable right?) systems, for which we also review and compare different

approaches to thermodynamically large systems. In Sec. 8.0.3, description of weakly open integrable systems in terms of (time dependent) generalized Gibbs ensembles is introduced in general.

In Sec. 8.0.4, we first present time evolution in terms of GGEs in a traditional weakly dissipative continuous Lindblad model with transverse field Ising model coupled to Lindblad baths. We show how within the generalized Gibbs ensemble descriptions, equations of motion simplify into a generalized scattering problem between the Bogoliubov quasiparticles what is ment by this???. In Sec. 8.0.5 we highlight that superconducting circuit platforms [45] or digital trapped ion quantum computers [40] would be ideal implementations why ideal? of all elements required to show that highly non-thermal and possibly exotic GGEs emerge in weakly open nearly integrable systems. We extend our formalism to such a Floquet time evolution Floquet time evolution???? with reset of ancilla qubits. To obtain equations of motion for the occupation of Bogoliubov quasiparticles, we derive the Lindblad master equation for a weakly dissipative trotterized setup. In the end, we propose how reviving of integrability can be detected via measurement of anomalously slow decay of certain spatial correlations. In a more technical Sec. 8.0.6, different approaches to non-interacting weakly dissipative systems are compared. In Sec. 8.0.7, we conclude that an actual experimental realization would prove the concept of GGEs to be applicable also for other platforms and, ultimately, for nearly integrable materials [22, 42].

8.0.3 Setup

We first review the structure of the density matrix perturbation theory using the example of a traditional Lindblad setup with a continuous model. In the next section, we generalize this to a trotterized implementation with a reset protocol relevant to digital quantum computers. Within the continuous implementations, we consider a system with dominant unitary dynamics described by a non-interacting translationally invariant Hamiltonian H_0, which has a diagonal form in terms of mode occupation operators n_q of Bogoliubov quasiparticles,

$$H_0 = \sum_q \varepsilon_q n_q + E_0 \tag{8.1}$$

where ε_q is the dispersion of a single particle excitation with momentum q and E_0 is a constant shift in energy. In addition, the system is weakly coupled in bulk to baths described by the dissipator $\hat{\mathcal{D}}$,

$$\hat{\mathcal{L}}\rho = -i[H_0, \rho] + \hat{\mathcal{D}}[\rho], \qquad \hat{\mathcal{D}}[\rho] = \epsilon \sum_i L_i \rho L_i^\dagger - \frac{1}{2}\{L_i^\dagger L_i, \rho\}. \tag{8.2}$$

Here, $\epsilon \ll 1$ is a weak coupling parameter, and L_i are the Lindblad operators acting around site i.

In our previous works [26, 25, 28, 18], we showed that the zeroth order (in ϵ) approximation to the steady state and the slow evolution towards the steady state has the form of a generalized Gibbs ensemble (GGE). For the non-interacting translationally invariant H_0 one can build a GGE using the local extensive conserved quantities C_i, $[H_0, C_i] = 0$, or the mode occupation operators n_q,

$$\rho_{\boldsymbol{\mu}}(t) = \frac{e^{-\sum_q \mu_q(t) n_q}}{\mathrm{Tr}[e^{-\sum_q \mu_q(t) n_q}]}. \tag{8.3}$$

Here, μ_q are the associated Lagrange multipliers. Since the dissipator weakly breaks the integrability properties of H_0, mode occupations are slowly changing, in the lowest order described

by the rate equations

$$\langle \dot{n}_q \rangle(t) \approx \mathrm{Tr}\left[n_q \hat{\mathcal{D}}[\rho_{\boldsymbol{\mu}}(t)] \right], \tag{8.4}$$

where contribution of order ϵ^2 and higher are neglected. This is how the distribution function is changed over time. Equivalently, the Langrange multipliers μ_q will be changing on the timescale $\mathcal{O}(1/\epsilon)$ according to the following equation derived in Ref. [25],

$$\dot{\mu}_q(t) = -\sum_{q'} (\chi^{-1})_{q,q'}(t)\, \langle \dot{n}_{q'} \rangle(t). \tag{8.5}$$

Here, $\chi_{q,q'}(t) = \langle n_q n_{q'} \rangle_{\rho_{\boldsymbol{\mu}(t)}} - \langle n_q \rangle_{\rho_{\boldsymbol{\mu}(t)}} \langle n_{q'} \rangle_{\rho_{\boldsymbol{\mu}(t)}}$ is the $\{q, q'\}$ entry of matrix χ and

$$\langle O \rangle_{\rho_{\boldsymbol{\mu}}} := \mathrm{Tr}[O \rho_{\boldsymbol{\mu}}].$$

In the case of free fermions, matrix χ is of a diagonal form

$$\chi_{q,q'}(t) = \delta_{q,q'}\, e^{-\mu_q(t)} / (1 + e^{-\mu_q(t)})^2.$$

Proof: The $\langle n \rangle$ can be 0 or 1, since we have fermions. Thus $\langle n^2 \rangle = \langle n \rangle$. For $q \neq q'$ there is $\langle n_q n_{q'} \rangle_{\rho_{\boldsymbol{\mu}(t)}} = \langle n_q \rangle_{\rho_{\boldsymbol{\mu}(t)}} \langle n_{q'} \rangle_{\rho_{\boldsymbol{\mu}(t)}}$, so $\chi_{q,q'}(t) = 0$. For $q = q'$ we have

$$\chi_{q,q'}(t) = \langle n^2 \rangle - \langle n \rangle^2 = \langle n \rangle - \langle n \rangle^2 = \frac{1}{1 + e^{-\mu}} - \frac{1}{(1 + e^{-\mu})^2} = \frac{e^{-\mu_q(t)}}{(1 + e^{-\mu_q(t)})^2}$$

(???? see again the derivation of Fermi-Dirac distribution!!)

We use $\dot{\mu}_q(t) = -\sum_{q'} (\chi^{-1})_{q,q'}(t)\, \langle \dot{n}_{q'} \rangle(t)$ to perform time evolutions from simple thermal initial states in the following sections.

Detailed balance (???)

(??? why this Lindbladian do not obey the detailed balance???)

8.0.4 GGE for TFI model

We consider the transverse field Ising model

$$H_0 = \sum_i J \sigma_i^x \sigma_{i+1}^x + h \sigma_i^z, \tag{8.6}$$

as a paradigmatic non-interacting integrable model, which can be (at least approximately) realized with quantum simulators [43, 44, 45, 46, 47, 48]. In order to obtain its mode occupation operators, we perform the Jordan-Wigner tranformation from spin-$\frac{1}{2}$ degrees of freedom to spinless fermions maybe I'll check it soon!!!

$$\sigma_j^z = 2 c_j^\dagger c_j - 1, \qquad \sigma_j^+ = e^{i\pi \sum_{l<j} n_j} c_j^\dagger, \tag{8.7}$$

and the Fourier transform from the positional basis to the momentum basis

$$c_j = \frac{e^{-i\pi/4}}{\sqrt{L}} \sum_q e^{iqj} c_q. \tag{8.8}$$

Here L without index is the number of the lattice cites. Finally, the Bogoliubov transformation

$$c_q = u_q d_q - v_q d_{-q}^\dagger, \tag{8.9}$$

$$u_q := \frac{(\varepsilon_q + a_q)}{\sqrt{2\varepsilon_q(\varepsilon_q + a_q)}}, \qquad v_q := \frac{b_q}{\sqrt{2\varepsilon_q(\varepsilon_q + a_q)}},$$

$$a_q := 2(J \cos q + h), \qquad b_q := 2J \sin q, \qquad \varepsilon_q := 2\sqrt{J^2 + 2hJ \cos q + h^2}. \tag{8.10}$$

brings the Hamiltonian into a diagonal form

$$H = \sum_q \varepsilon_q \left(n_q - \frac{1}{2} \right), \qquad n_q = d_q^\dagger d_q. \tag{8.11}$$

(????) Therefore, the Hamiltonian and all the local conserved charges, $C_i = \sum_q \mathfrak{c}_q^{(i)} n_q$, $\mathfrak{c}$ is cos or sin (???) can be expressed in terms of mode occupation operators. One should note that periodic boundary conditions in the spin picture are translated to periodic boundary conditions in the fermion picture for an odd number of particles and anti-periodic for an even number of particles. Consequently, the two cases are diagonalized by a different set of wave vectors, $\mathcal{K}^+ = \{\frac{2\pi}{L}(q+\frac{1}{2}), q = 0, \dots L-1\}$ for the even sector and $\mathcal{K}^- = \{\frac{2\pi}{L} q, q = 0, \dots L-1\}$ for the odd sector what is it???. The two symmetry sectors are uncoupled by the Hamiltonian dynamics and should be treated separately.

If the following Lindblad operator

$$L_j = \sigma_j^+ \sigma_{j+1}^- + \frac{1}{2}\left(\sigma_j^z + \mathbb{1}_j\right). \tag{8.12}$$

accounts for coupling of two baths, the stable state will be a nontrivial steady states.

why other Lindblad operators don't work???

In terms of d operators the Lindblad operator has a form:

$$L_j = \sum_{q,q'} \frac{e^{-ij(q-q')}}{L} (1 + e^{iq'}) c_q^\dagger c_{q'}; \qquad c_q := u_q d_q - v_q d_{-q}^\dagger. \tag{8.13}$$

We rind that here L without index is the number of the lattice cites.

Proof.

$$L_j = e^{i\pi \sum_{l<j} n_l} c_j^+ e^{-i\pi \sum_{l<j+1} n_l} c_{j+1} + c_j^+ c_j = c_j^+ c_{j+1} e^{-i\pi n_j} + c_j^+ c_j$$

We have fermions, so j-th state can be occupied or not, so n_j can be 1 or 0. If it is zero, then $c_j^+ c_{j+1} e^{-i\pi n_j} |0_j\rangle = c_j^+ c_{j+1} |0_j\rangle$. Otherwise, c_j^+ will act on it and give zero, so $c_j^+ c_{j+1} e^{-i\pi n_j} |1_j\rangle = -c_{j+1} e^{-i\pi} c_j^+ |1_j\rangle = 0 |0_j\rangle \equiv c_j^+ c_{j+1} |1_j\rangle$,

$$L_j = c_j^+ c_{j+1} + c_j^+ c_j = \frac{1}{L} \sum_{k,k'} \left(e^{-ij(k-k')} e^{ik'} c_k^+ c_{k'} + e^{-ij(k-k')} c_k^+ c_{k'} \right) = \frac{1}{L} \sum_{k,k'} e^{-ij(k-k')} c_k^+ c_{k'} \left(e^{ik'} + 1 \right).$$

□

However, due to the form of dissipator with L_i and $L_i^\dagger$ pairs, Eq. (8.2), analysis is not much more complicated in the presence of string operators as well.

These Lindblad operators preserve the parity, i.e., some terms preserve the number of fermions while others change it by two why?. Therefore, we get two steady states, one for the even and one for the odd parity sector. Thermodynamically, the two solutions behave the same. We consider only the even sector in the following and work with momenta $\mathcal{K}^+$ why?.

To calculate the time evolution as described in Sec. 8.0.3, the central object to be evaluated is the expression $\langle \dot{n}_q \rangle(t) \approx \mathrm{Tr}\left[n_q \hat{\mathcal{D}}[\rho_{\boldsymbol{\mu}}(t)] \right]$. It can be written as

$$\langle \dot{n}_q \rangle = \epsilon \sum_j \langle L_j^\dagger n_q L_j \rangle - \langle n_q L_j^\dagger L_j \rangle \tag{8.14}$$

Proof.

$$\langle \dot{n}_q \rangle = \epsilon \mathrm{Tr}\left[n\Big(\sum L_i \rho L_i^\dagger - \frac{1}{2}\{L_i^\dagger L_i, \rho\}\Big)\right] = \epsilon \sum \mathrm{Tr}\Big[nL_i\rho L_i^\dagger - \frac{1}{2} nL_i^\dagger L_i \rho - \frac{1}{2} n\rho L_i^\dagger L_i\Big] =$$
$$= \epsilon \sum \mathrm{Tr}\Big[nL_i\rho L_i^\dagger\Big] - \epsilon \sum \mathrm{Tr}\Big[\frac{1}{2} nL_i^\dagger L_i \rho\Big] - \epsilon \sum \mathrm{Tr}\Big[\frac{1}{2} n\rho L_i^\dagger L_i\Big] =$$
$$= \epsilon \sum \mathrm{Tr}\Big[L_i^\dagger n L_i \rho\Big] - \frac{1}{2}\epsilon \sum \mathrm{Tr}\Big[nL_i^\dagger L_i \rho\Big] - \frac{1}{2}\epsilon \sum \mathrm{Tr}\Big[L_i^\dagger L_i n\rho\Big].$$

We know that there is a real expression under trace, so Lindblad operators are such that

$$\mathrm{Tr}\Big[L_i^\dagger L_i n\rho\Big] = \mathrm{Tr}\Big[L_i^\dagger L_i n\rho\Big]^\dagger = \mathrm{Tr}\Big[\rho^\dagger n^\dagger L_i^\dagger L_i\Big] = \mathrm{Tr}\Big[\rho n L_i^\dagger L_i\Big] = \mathrm{Tr}\Big[nL_i^\dagger L_i \rho\Big]$$

and this is two last sums are the same.

□

Due to the diagonal form of the GGE, only the combinations of creation $d_q^\dagger$ and annihilation d_q operators, which are in total diagonal in the mode occupation operators, contribute to the expectation values with respect to the GGE Ansatz. After extracting the contributing Wick contractions and simplifying the remaining terms, Eq. (8.14) obtains a compact and meaningful form

$$\langle \dot{n}_q \rangle = \frac{2\epsilon}{N} \sum_{q'} f_{q',q}\langle n_{q'}\rangle(1-\langle n_q\rangle) - f_{q,q'}\langle n_q\rangle(1-\langle n_{q'}\rangle) + \tilde{f}_{q',q}(1-\langle n_{q'}\rangle)(1-\langle n_q\rangle) - \tilde{f}_{q,q'}\langle n_q\rangle\langle n_{q'}\rangle. \tag{8.15}$$

$$f_{q',q} := u_q^2 u_{q'}^2(1+\cos q') + v_q^2 v_{q'}^2(1+\cos q) - u_q v_q u_{q'} v_{q'}(1+\cos q' + \cos q + \cos(q+q')), \tag{8.16}$$

$$\tilde{f}_{q',q} := v_q^2 u_{q'}^2(1+\cos q) + u_q^2 v_{q'}^2(1+\cos q') - u_q v_q u_{q'} v_{q'}(1+\cos q' + \cos q + \cos(q-q')). \tag{8.17}$$

this is the wrong equation. In the program there was another formula

Proof. We start with

$$\langle \dot{n}_m \rangle = \epsilon \sum_j \langle L_j^\dagger n_m L_j\rangle - \langle L_j^\dagger L_j n_m\rangle; \qquad L_j = \sum_{q,q'} \frac{e^{-ij(q-q')}}{L}(1+e^{iq'}) c_q^\dagger c_{q'}; \qquad c_q := u_q d_q - v_q d_{-q}^\dagger.$$

In the first term we have:

$$\langle L_j^\dagger n_m L_j\rangle = \Big\langle \sum_{q,q'} \frac{e^{ij(q-q')}(1+e^{-iq'})}{L} c_{q'}^\dagger c_q d_m^\dagger d_m \sum_{p,p'} \frac{e^{-ij(p-p')}(1+e^{ip'})}{L} c_p^\dagger c_{p'}\Big\rangle =$$
$$= \sum_{q,q',p,p'} \frac{e^{ij(q-q')}e^{-ij(p-p')}(1+e^{-iq'})(1+e^{ip'})}{L^2} \langle c_{q'}^\dagger c_q d_m^\dagger d_m c_p^\dagger c_{p'}\rangle.$$

And here we have

$$\langle c_{q'}^\dagger c_q d_m^\dagger d_m c_p^\dagger c_{p'}\rangle = \langle (u_{q'} d_{q'}^\dagger - v_{q'} d_{q'})(u_q d_q - v_q d_{-q}^\dagger) d_m^\dagger d_m (u_p d_p^\dagger - v_p d_{-p})(u_{p'} d_{p'} - v_{p'} d_{-p'}^\dagger)\rangle =$$

$$= \begin{aligned} &\langle u_{q'} d_{q'}^\dagger u_q d_q\ n_m\ u_p d_p^\dagger u_{p'} d_{p'}\ +\ u'_{q'} d_{q'}^\dagger u_q d_q\ n_m\ v_p d_{-p} v_{p'} d_{-p'}^\dagger\ + \\ &+ v_{q'} d_{-q'} v_q d_{-q}^\dagger\ n_m\ u_p d_p^\dagger u_{p'} d_{p'}\ +\ v_{q'} d_{-q'} v_q d_{-q}^\dagger\ n_m\ v_p d_{-p} v_{p'} d_{-p'}^\dagger\ + \ = \\ &+ u_{q'} d_{q'}^\dagger v_q d_{-q}^\dagger\ n_m\ v_p d_{-p} u_{p'} d_{p'}\ +\ v_{q'} d_{-q'} u_q d_q\ n_m\ u_p d_p^\dagger v_{p'} d_{-p'}^\dagger\rangle \end{aligned}$$

$$= \begin{aligned} &u_{q'} u_q u_p u_{p'} \langle d_{q'}^\dagger d_q\ n_m\ d_p^\dagger d_{p'}\rangle\ +\ u_{q'} u_q v_p v_{p'} \langle d_{q'}^\dagger d_q\ n_m\ d_{-p} d_{-p'}^\dagger\rangle\ + \\ &+ v_{q'} v_q u_p u_{p'} \langle d_{-q'} d_{-q}^\dagger\ n_m\ d_p^\dagger d_{p'}\rangle\ +\ v_{q'} v_q v_p v_{p'} \langle d_{-q'} d_{-q}^\dagger\ n_m\ d_{-p} d_{-p'}^\dagger\rangle\ + \\ &+ u_{q'} v_q v_p u_{p'} \langle d_{q'}^\dagger d_{-q}^\dagger\ n_m\ d_{-p} d_{p'}\rangle\ +\ v_{q'} u_q u_p v_{p'} \langle d_{-q'} d_q\ n_m\ d_p^\dagger d_{-p'}^\dagger\rangle. \end{aligned}$$

All signs are taken into account and finally we have only pluses.

Now, let us analyze the second term because some subterms might cancel. For the second term, we have:

$$\langle L_j^\dagger L_j n_m\rangle = \Big\langle \sum_{q,q'} \frac{e^{ij(q-q')}}{L}(1+e^{-iq'})c_{q'}^\dagger c_q \sum_{p,p'} \frac{e^{-ij(p-p')}}{L}(1+e^{ip'})c_p^\dagger c_{p'} n_m\Big\rangle =$$
$$= \sum_{q,q',p,p'} \frac{e^{ij(q-q')}e^{-ij(p-p')}(1+e^{-iq'})(1+e^{ip'})}{L^2}\langle c_{q'}^\dagger c_q c_p^\dagger c_{p'} n_m\rangle$$

Again, here we have

$$\langle c_{q'}^\dagger c_q c_p^\dagger c_{p'} n_m\rangle = \langle (u_{q'}d_{q'}^\dagger - v_{q'}d_{-q'})(u_q d_q - v_q d_{-q}^\dagger)(u_p d_p^\dagger - v_p d_{-p})(u_{p'}d_{p'} - v_{p'}d_{-p'}^\dagger)n_m\rangle =$$

$$= \begin{array}{l} \big\langle u_{q'}d_{q'}^\dagger u_q d_q u_p d_p^\dagger u_{p'}d_{p'}n_m + u_{q'}d_{q'}^\dagger u_q d_q v_p d_{-p} v_{p'}d_{-p'}^\dagger n_m + \\ + v_{q'}d_{-q'}v_q d_{-q}^\dagger u_p d_p^\dagger u_{p'}d_{p'}n_m + v_{q'}d_{-q'}v_q d_{-q}^\dagger v_p d_{-p} v_{p'}d_{-p'}^\dagger n_m + = \\ + u_{q'}d_{q'}^\dagger v_q d_{-q}^\dagger v_p d_{-p} u_{p'}d_{p'}n_m + v_{q'}d_{-q'}u_q d_q u_p d_p^\dagger v_{p'}d_{-p'}^\dagger n_m\big\rangle \end{array}$$

$$= \begin{array}{l} u_{q'}u_q u_p u_{p'}\langle d_{q'}^\dagger d_q d_p^\dagger d_{p'}n_m\rangle + u_{q'}u_q v_p v_{p'}\langle d_{q'}^\dagger d_q d_{-p}d_{-p'}^\dagger n_m\rangle + \\ + v_{q'}v_q u_p u_{p'}\langle d_{-q'}d_{-q}^\dagger d_p^\dagger d_{p'}n_m\rangle + v_{q'}v_q v_p v_{p'}\langle d_{-q'}d_{-q}^\dagger d_{-p}d_{-p'}^\dagger n_m\rangle + \\ + u_{q'}v_q v_p u_{p'}\langle d_{q'}^\dagger d_{-q}^\dagger d_{-p}d_{p'}n_m\rangle + v_{q'}u_q u_p v_{p'}\langle d_{-q'}d_q d_p^\dagger d_{-p'}^\dagger n_m\rangle \end{array}$$

Here in both terms from the initial expression the indexes are in general different, because these are just two different sums. But we label it the same and the structures of the sum are the same, so we if we put all sums in front of all terms, we will get the same equation. So, we treat indices from two sums with the same label as they are the same index from the general sum.

So we see that all prefactors are the same and we should think about subtraction of each term at each position (we kept the position of terms without changes).

Let us transform the subterm $\langle d_{q'}^\dagger d_q\ n_m\ d_p^\dagger d_{p'}\rangle$ to make it look like the subterm from the second term $\langle d_{q'}^\dagger d_q\ d_p^\dagger d_{p'}\ d_m^\dagger d_m\rangle$, we write:

$$\langle d_{q'}^\dagger d_q\ n_m\ d_p^\dagger d_{p'}\rangle = \langle d_{q'}^\dagger d_q\ d_m^\dagger d_m\ d_p^\dagger d_{p'}\rangle = \langle d_{q'}^\dagger d_q\ d_m^\dagger(\delta_{mp} - d_p^\dagger d_m)d_{p'}\rangle = \langle d_{q'}^\dagger d_q\ d_m^\dagger d_{p'}\rangle\delta_{mp} + \langle d_{q'}^\dagger d_q\ d_m^\dagger d_p^\dagger d_{p'}d_m\rangle =$$

$$= \langle d_{q'}^\dagger d_q\ d_m^\dagger d_{p'}\rangle\delta_{mp} + \langle d_{q'}^\dagger d_q\ (-d_p^\dagger d_m^\dagger)d_{p'}d_m\rangle = \langle d_{q'}^\dagger(\delta_{mq} - d_m^\dagger d_q)d_{p'}\rangle\delta_{mp} - \langle d_{q'}^\dagger d_q\ d_p^\dagger(\delta_{m,p'} - d_{p'}d_m^\dagger)d_m\rangle =$$

$$= \langle d_{q'}^\dagger d_{p'}\rangle\delta_{mq}\delta_{mp} - \langle d_{q'}^\dagger d_m^\dagger d_q d_{p'}\rangle\delta_{mp} - \langle d_{q'}^\dagger d_q\ d_p^\dagger d_m\rangle\delta_{m,p'} + \langle d_{q'}^\dagger d_q\ d_p^\dagger d_{p'}d_m^\dagger d_m\rangle =$$

$$= \langle d_{q'}^\dagger d_{p'}\rangle\delta_{mq}\delta_{mp} - \langle d_{q'}^\dagger d_m^\dagger d_q d_{p'}\rangle\delta_{mp} + \langle d_{q'}^\dagger d_p^\dagger\ d_q d_m\rangle\delta_{m,p'} - \langle d_{q'}^\dagger d_m\rangle\delta_{q,p}\delta_{m,p'} + \langle d_{q'}^\dagger d_q\ d_p^\dagger d_{p'}d_m^\dagger d_m\rangle$$

Here the last term cancels with the last term form the second part of the whole expression. We are left with subterm that we will denote as $\mathcal{O}_1$

$$\mathcal{O}_1 := \langle d_{q'}^\dagger d_{p'}\rangle\delta_{mq}\delta_{mp} - \langle d_{q'}^\dagger d_m^\dagger d_q d_{p'}\rangle\delta_{mp} + \langle d_{q'}^\dagger d_p^\dagger\ d_q d_m\rangle\delta_{m,p'} - \langle d_{q'}^\dagger d_m\rangle\delta_{q,p}\delta_{m,p'}.$$

Here by the definition of distribution function $\langle n_q\rangle := \langle d_q^\dagger d_q\rangle$ and Wick's theorem we have:

$$\begin{aligned} \langle d_{q'}^\dagger d_{p'}\rangle &= \langle n_{q'}\rangle\ \delta_{q',p'};\\ \langle d_{q'}^\dagger d_m^\dagger d_q d_{p'}\rangle &= \langle d_{q'}^\dagger d_{p'}\rangle\langle d_m^\dagger d_q\rangle - \langle d_{q'}^\dagger d_q\rangle\langle d_m^\dagger d_{p'}\rangle = \langle n_{q'}\rangle\langle n_q\rangle\delta_{q',p'}\delta_{m,q} - \langle n_{q'}\rangle\langle n_m\rangle\delta_{q',q}\delta_{m,p'};\\ \langle d_{q'}^\dagger d_p^\dagger\ d_q d_m\rangle &= \langle d_{q'}^\dagger d_m\rangle\langle d_p^\dagger d_q\rangle - \langle d_{q'}^\dagger d_q\rangle\langle d_p^\dagger d_m\rangle = \langle n_{q'}\rangle\langle n_q\rangle\delta_{q',m}\delta_{p,q} - \langle n_{q'}\rangle\langle n_m\rangle\delta_{q',q}\delta_{m,p};\\ \langle d_{q'}^\dagger d_m\rangle &= \langle n_{q'}\rangle\ \delta_{q',m}. \end{aligned}$$

And totally we have:

$$\mathcal{O}_1 := \langle n_{q'}\rangle\ \delta_{q',p'}\delta_{mq}\delta_{mp} - \big(\langle n_{q'}\rangle\langle n_q\rangle\delta_{q',p'}\delta_{m,q} - \langle n_{q'}\rangle\langle n_m\rangle\delta_{q',q}\delta_{m,p'}\big)\delta_{mp} +$$
$$+ \big(\langle n_{q'}\rangle\langle n_q\rangle\delta_{q',m}\delta_{p,q} - \langle n_{q'}\rangle\langle n_m\rangle\delta_{q',q}\delta_{m,p}\big)\delta_{m,p'} - \langle n_{q'}\rangle\ \delta_{q',m}\delta_{q,p}\delta_{m,p'} =$$

$$= \langle n_{q'}\rangle\big(\delta_{q',p'}\delta_{mq}\delta_{mp} - \delta_{q',m}\delta_{q,p}\delta_{m,p'}\big) + \langle n_{q'}\rangle\langle n_q\rangle\big(\delta_{q',m}\delta_{p,q}\delta_{m,p'} - \delta_{q',p'}\delta_{m,q}\delta_{mp}\big) +$$
$$+ \underbrace{\langle n_{q'}\rangle\langle n_m\rangle\big(\delta_{q',q}\delta_{m,p'}\delta_{mp} - \delta_{q',q}\delta_{m,p}\delta_{m,p'}\big)}_{=0}.$$

In the result, this expression will give the following term in the initial equation:

$$\epsilon \sum_j \sum_{q,q',p,p'} \frac{e^{ij(q-q')}e^{-ij(p-p')}(1+e^{-iq'})(1+e^{ip'})}{L^2} u_{q'}u_q u_p u_{p'} \mathcal{O}_1 = [1]+[2]+[3]$$

$$[1] := \epsilon \sum_j \sum_{q,q',p,p'} \frac{e^{ij(q-q')}e^{-ij(p-p')}(1+e^{-iq'})(1+e^{ip'})}{L^2} \langle n_{q'}\rangle u_{q'}u_q u_p u_{p'} \left(\delta_{q',p'}\delta_{mq}\delta_{mp} - \delta_{q',m}\delta_{q,p}\delta_{m,p'}\right) =$$
$$= \frac{2\epsilon}{L}\sum_{q'} u_{q'}^2 u_m^2 (1+\cos(q'))\langle n_{q'}\rangle - \frac{2\epsilon}{L}\sum_q u_q^2 u_m^2 (1+\cos(m))\langle n_m\rangle =$$
$$= \frac{2\epsilon}{L}\sum_{q'} u_{q'}^2 u_m^2 \Big((1+\cos(q'))\langle n_{q'}\rangle - (1+\cos(m))\langle n_m\rangle\Big)$$

(????)

□

In the expression $\langle \dot{n}_q\rangle = \frac{2\epsilon}{N}\sum_{q'} f_{q',q}\langle n_{q'}\rangle\langle 1-n_q\rangle - f_{q,q'}\langle n_q\rangle\langle 1-n_{q'}\rangle + \tilde{f}_{q',q}\langle 1-n_{q'}\rangle\langle 1-n_q\rangle - \tilde{f}_{q,q'}\langle n_q\rangle\langle n_{q'}\rangle$, the first two terms correspond to the transitions between q' and q momenta, and the last two terms correspond to creation/annihilation of q' and q modes.

Terms with $\langle 1-n_q\rangle$, corresponding to transitions into the q mode, have a positive sign. On the other hand, terms with $\langle n_q\rangle$, where q mode is annihilated, have a negative sign. In the GGE, the expectation value of the mode occupation operator is given by $\langle n_q\rangle = e^{-\mu_q}/(1+e^{-\mu_q})$. The rate equation (8.15) thus has the structure of the Boltzmann equation but without the usual assumption of thermal Fermi functions. this is a complicated equation...

We should note that $f_{q',q}$ and $\tilde{f}_{q',q}$ can be factorized over variables q, q' and therefore summation over q' in Eq. (8.15) can be performed independent of q. The complexity of evaluating $\langle \dot{n}_q\rangle$ for all q thus scales as $\mathcal{O}(L)$. A similar factorization property should also hold for other choices of Lindblad operators, implying that $\langle \dot{n}_q\rangle$ is calculated in $\mathcal{O}(L)$ generically.

We perform calculations of time-dependent Lagrange parameters $\mu_q(t)$ from $\dot{\mu}_q(t) = -\sum_{q'}(\chi^{-1})_{q,q'}(t)\,\langle \dot{n}_{q'}\rangle(t)$ by summation over discrete momenta on $L = 10^5$ sites.

Fig. 8.1(a) shows how the momentum distributions change from an initial thermal Gaussian distribution around $q = \pi$ (where the minimum of dispersion ϵ_q, Eq. (8.9), lies for our choice $J = 1$, $h = 0.6$), to a highly non-thermal distribution, double-peaked around some non-trivial momenta.

This result is the main message of our example: since our Lindblad operators L_i, Eq. (8.13), do not obey detailed balance (why????), a highly non-thermal steady state is stabilized even if the coupling to the baths is only weak.

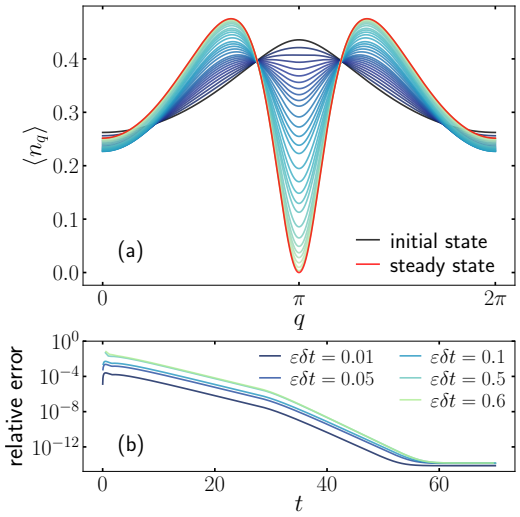

Figure 8.1: (a) Time evolution from an initial thermal mode occupation with $\beta = 0.323$ to a highly non-thermal steady state distribution, stabilized by our choice of Lindblad operators, Eq. (8.13). (b) Relative error $\sum_q |(\langle n_q \rangle(t) - \langle n_q \rangle_0(t))/\langle n_q \rangle_0(t)|$ of the occupations $\langle n_q \rangle(t)$ obtained with Euler method with time steps $\epsilon\delta t = 0.01, ..., 0.6$ and the reference $\langle n_q \rangle_0(t)$ evaluated with smallest $\epsilon\delta t = 0.005$. At late times differences are tiny. Parameters: $J = 1, h = 0.6, L = 10^5$.

Physically the system is just as was before, the only difference is that there are strange big influence of one spin to another (this is the increased correlation length). right???

The calculation is performed using the Euler method with time step $\delta t\epsilon = 0.6$, which is sufficiently small that errors do not affect the dynamics significantly and the system converges to the right the steady-state. Namely, Fig. 8.1(b) shows the difference between calculations done at chosen $\epsilon\delta t = [0.01, 0.05, 0.1, 0.5, 0.6]$ with respect to the smallest $\epsilon\delta t = 0.005$ time step tested. In an absolute sense, the relaxation time is given by the strength of the coupling to the bath. i.e., the distributions relax to the steady state on $1/\epsilon$ timescale since the rate of change for the mode occupations is proportional to ϵ, Eqs. (8.14, 8.15). However, for the same reason, we can use scaled $\epsilon\delta t$ in our discrete-time propagation scheme.

Numerical calculations

```
import numpy as np
from datetime import datetime

def uq2(q, J, h):
    e = 2*np.sqrt(h**2 + 2*h*J*np.cos(q) + J**2)
    a = 2*(J*np.cos(q) + h)
    return (e+a)/(2*e)


def vq2(q, J, h):
    e = 2*np.sqrt(h**2 + 2*h*J*np.cos(q) + J**2)
    a = 2*(J*np.cos(q) + h)
    b = 2*(J*np.sin(q))
    return b**2/(2*e*(e+a))


def uvq(q, J, h):
    e = 2*np.sqrt(h**2 + 2*h*J*np.cos(q) + J**2)
    a = 2*(J*np.cos(q) + h)
    b = 2*J*np.sin(q)
    return b/(2*e)


def nmdot_fromn(nqji, momenta, J, h):

    L = len(nqji)

    uq2ji = np.array([uq2(q, J, h) for q in momenta])
```

```
    uvqji = np.array([uvq(q, J, h) for q in momenta])
    vq2ji = np.array([vq2(q, J, h) for q in momenta])

    cosqji = np.cos(momenta)
    sinqji = np.sin(momenta)

    nqdot = (1-nqji) * (uq2ji*np.sum(nqji*uq2ji*(1+cosqji)) +
    vq2ji*(1+cosqji)*np.sum(nqji*vq2ji)
            - uvqji*np.sum(nqji*uvqji*(1+cosqji)) - uvqji*cosqji*np.sum(nqji*uvqji)
            - uvqji*cosqji*np.sum(nqji*uvqji*cosqji) +
    uvqji*sinqji*np.sum(nqji*uvqji*sinqji))

    nqdot += (1-nqji) * (vq2ji*(1+cosqji)*np.sum((1-nqji)*uq2ji) +
    uq2ji*np.sum((1-nqji)*vq2ji*(1+cosqji))
            - uvqji*np.sum((1-nqji)*uvqji*(1+cosqji)) - uvqji*cosqji*np.sum((1-nqji)*uvqji)
            - uvqji*cosqji*np.sum((1-nqji)*uvqji*cosqji) -
    uvqji*sinqji*np.sum((1-nqji)*uvqji*sinqji))

    nqdot -= nqji * (uq2ji*(1+cosqji)*np.sum((1-nqji)*uq2ji) +
    vq2ji*np.sum((1-nqji)*vq2ji*(1+cosqji))
            - uvqji*np.sum((1-nqji)*uvqji*(1+cosqji)) - uvqji*cosqji*np.sum((1-nqji)*uvqji)
            - uvqji*cosqji*np.sum((1-nqji)*uvqji*cosqji) +
    uvqji*sinqji*np.sum((1-nqji)*uvqji*sinqji))

    nqdot -= nqji * (vq2ji*np.sum(nqji*uq2ji*(1+cosqji)) +
    uq2ji*(1+cosqji)*np.sum(nqji*vq2ji)
            - uvqji*np.sum(nqji*uvqji*(1+cosqji)) - uvqji*cosqji*np.sum(nqji*uvqji)
            - uvqji*cosqji*np.sum(nqji*uvqji*cosqji) -
    uvqji*sinqji*np.sum(nqji*uvqji*sinqji))

    return 2/L*nqdot

L = 50

J = 1; h = 0.698989

ti = 0; tf = 5; dt = 0.05
N = int((tf-ti)/dt)

beta = 3

momenta = 2*np.pi/L * (np.arange(1, L+1))

nq = lambda muq: np.exp(-muq)/(1 + np.exp(-muq))
nqji = np.empty((N+1, len(momenta)))
nqji[0] = nq(beta*2*np.sqrt(h**2 + 2*h*J*np.cos(momenta) + J**2))

for n in range(N):
    ndot = nmdot_fromn(nqji[n], momenta, J, h)
    nqji[n+1] = nqji[n] + ndot * dt
```

The only important feature is that there are here different functions, not the $f_{q,q'}$!! this is because there is a mistake in the formulas for them.

So, here we got the array `nqji`, where for each element there is a distribution of the $\langle n \rangle$. One can see the plot at different time for example, by `plt.plot(nqji[30])` (at time `(tf-ti)/dt`).

We could also define for odd sector: `momenta␣=␣2*np.pi/L␣*␣(np.arange(1,␣L+1)-1/2)`, but it does not matter, since the result is nearly the same. Actually, for momenta with `-1/2`, there is a little peak in the center. I have no idea why someone bothers about it? And is this is important?

Also, there should not be such coefficients h and J that "a" and "e" would be zero, since we divide by them.

8.0.5 Digital quantum computer protocol

We continue by discussing a contemporary possible implementation of the previous example using a digital quantum computer. There, dissipation can be realized by coupling system's qubits to auxiliary ones and resetting the latter to, e.g., spin down state every T steps [45]. A sketch of possible realization is shown in Fig. 8.2. While Ref. [45] used the reset protocol for an approximate ground state preparation by dissipative cooling for the transverse field Ising model, we would like to point out that due to the proximity to integrability such a weakly

dissipative setup is prone to realize highly non-thermal GGEs, with the steady state mode occupation fixed by the form of coupling to the ancilla qubits. so this happens in Ref. [45]???

As the integrable system we again consider a transverse field Ising model, now realized via trotterized gate propagation with gate duration chosen to be $\pi/2$,

$$U_S = e^{-i\frac{\pi J}{2}\sum_j \sigma_j^x \sigma_{j+1}^x} e^{-i\frac{\pi h}{2}\sum_j \sigma_j^z} \equiv e^{-iH_{\mathrm{FTFI}}}, \tag{8.18}$$

where H_{FTFI} is the corresponding Floquet Hamiltonian derived below. Ancilla qubits are propagated by simple

$$U_A = e^{-i\frac{\pi h_A}{2}\sum_j \tilde{\sigma}_j^z}, \tag{8.19}$$

where $\tilde{\sigma}_j^\alpha$ represent operators acting on ancilla qubits. In addition, at each time step $\tau \leq T$ before the reset, system and ancilla qubits are coupled by

$$U_{SA,\tau} = \prod_j e^{-i\lambda_\tau Q_j \otimes A_j}. \tag{8.20}$$

We use coupling operators resembling the Lindblad operators (8.13) from the previous section,

$$Q_j = S_j^+ S_{j+1}^- + S_j^- S_{j+1}^+, \quad A_j = \tilde{\sigma}_j^x, \tag{8.21}$$

where Q_j operators act on the system's qubits, while A_j operators act on the ancilla qubits. Applying multi-qubit gates has been relized before [49]. One cycle contains T system-ancilla-coupling propagations

$$U_T = U_{SA,T} U_A U_S \cdots U_{SA,1} U_A U_S, \tag{8.22}$$

followed by the reset of ancilla qubits to the down spin state. maybe I'll check that it works so...

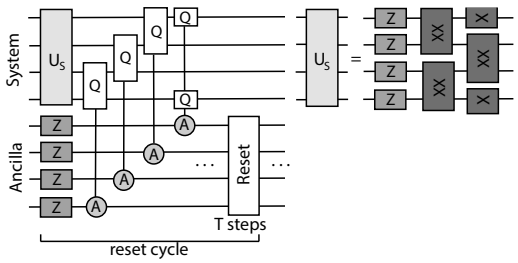

Figure 8.2: Scheme of our dissipative transverse field Ising realization, similar to Refs. [45, 8] and realistic to implement with a digital quantum computer. In this setup, the system's qubits are coupled to ancillary ones. After every T system-ancilla-coupling propagations, ancilla qubits are reset to the spin-down state.

We again use periodic boundary conditions for the system's gates under which the system's propagation operator factorizes over momenta

$$U_S = \prod_{q\geq 0} e^{-i\Phi_q^\dagger X_q \Phi_q} e^{-i\Phi_q^\dagger Z_q \Phi_q}, \tag{8.23}$$

with $\Phi_q = \{c_q, c_{-q}^\dagger\}^T$ representing the bispinor of fermionic operators in momentum space, Eq. (8.8). X_q and Z_q are 2x2 matrices, derived by representing the first and the second term in U_S, Eq. (8.18), with fermionic operators in the momentum space, using relations (8.7, 8.8). Explicit expressions for X_q, Z_q are given in App. 8.0.8, where we also derive that Floquet quasi-energy dispersion $\tilde{\epsilon}_q$ takes the form

$$\cos(\tilde{\epsilon}_q) = \cos(\pi J)\cos(\pi h) - \sin(\pi J)\sin(\pi h)\cos(q). \tag{8.24}$$

Coefficients $\tilde{u}_q, \tilde{v}_q$, connecting fermionic operators to the Bogoliubov ones via relation $c_q = \tilde{u}_q d_q - \tilde{v}_q^* d_{-q}^\dagger$, are for the trotterized transverse field Ising model of the form

$$\begin{aligned}
\tilde{u}_q &= \frac{(\xi_q + \tilde{a}_q)}{\sqrt{2\xi_q(\xi_q + \tilde{a}_q)}}, \ \tilde{v}_q = \frac{\tilde{b}_q}{\sqrt{2\xi_q(\xi_q + \tilde{a}_q)}}, \\
\tilde{a}_q &= \sin(\pi J)\cos(\pi h)\cos(q) + \cos(\pi J)\sin(\pi h), \\
\tilde{b}_q &= -e^{-i\pi h}\sin(\pi J)\sin(q), \\
\xi_q &= \sqrt{\tilde{a}_q^2 + |\tilde{b}_q|^2},
\end{aligned} \tag{8.25}$$

$\tilde{a}_q, \tilde{b}_q$ are different now. I'll rederive them later which is very similar to the original (8.9). See App. 8.0.8 for the derivation. Finally,

$$H_{\text{FTFI}} = \sum_q \tilde{\epsilon}_q \left(n_q - \frac{1}{2} \right), \ n_q = d_q^\dagger d_q. \tag{8.26}$$

Following Ref. [50], we derive the system's density matrix evolution for one reset cycle, from cycle number N_c to $N_c + 1$. As in the previous section, we approximate the system's density matrix with a generalized Gibbs ensemble, $\rho_{\boldsymbol{\mu}}(N_c) = (1/Z)e^{-\sum_q \mu_q(N_c) n_q}$, which should well approximate the exact density matrix time evolution for a weak system-ancilla coupling $\lambda_\tau \ll 1$, see also [16],

$$\begin{aligned}
&\rho_{\boldsymbol{\mu}}(N_c + 1) - \rho_{\boldsymbol{\mu}}(N_c) \\
&\approx \sum_{j,\omega,\omega'} -i\,\mathrm{Im}(\mathcal{A}_{\omega,\omega'})[\mathrm{Q}_{\mathrm{j},\omega'}^\dagger \mathrm{Q}_{\mathrm{j},\omega}, \rho_{\boldsymbol{\mu}}(\mathrm{N_c})] \\
&+ \mathfrak{a}_{\omega,\omega'} \left(Q_{j,\omega} \rho_{\boldsymbol{\mu}}(N_c) Q_{j,\omega'}^\dagger - \frac{1}{2}\{Q_{j,\omega'}^\dagger Q_{j,\omega}, \rho_{\boldsymbol{\mu}}(N_c)\} \right).
\end{aligned} \tag{8.27}$$

Above we introduced

$$\begin{aligned}
\mathfrak{a}_{\omega,\omega'} &= \sum_{\tau=1}^{T} \lambda_\tau e^{i\tau(\omega' - \pi h_A)} \sum_{\tau'=1}^{T} \lambda_{\tau'} e^{-i\tau'(\omega - \pi h_A)}, \\
\mathcal{A}_{\omega,\omega'} &= \sum_{\tau=1}^{T} \sum_{\tau'=1}^{\tau} \lambda_\tau \lambda_{\tau'} e^{i(\omega'\tau - \omega\tau' + \pi h_A(-\tau + \tau'))},
\end{aligned} \tag{8.28}$$

and $Q_{j,\omega}$, which represents Q_j operator (8.21) projected between many-body eigenstates of H_{FTFI} that differ in quasi-energy for ω, $Q_{j,\omega} = \sum_{\alpha,\beta,\tilde{E}_\beta - \tilde{E}_\alpha = \omega} |\alpha\rangle\langle\alpha|Q_j|\beta\rangle\langle\beta|$. A more detailed derivation of the system's density matrix time evolution is given in App. 8.0.9 and 8.0.10. I'll look later and re-do it!

In the case of weak coupling to ancilla qubits, $\lambda_\tau \ll 1$, changes within one reset cycle are small. Therefore, one can still use the Euler propagation method to calculate the time-dependent Lagrange multipliers, parametrizing $\rho_{\boldsymbol{\mu}}(N_c)$, from the rate equations for the H_{FTFI} mode occupation operators. The latter obtains a compact and meaningful form, similar to the continuous model,

$$\begin{aligned}
&\langle n_q(N_c + 1)\rangle - \langle n_q(N_c)\rangle \\
&= \frac{2}{N} \sum_{q'} g_{q',q} \big(\langle n_{q'}\rangle\langle 1 - n_q\rangle \mathfrak{a}_{\epsilon_{q'} - \epsilon_q} - \langle n_q\rangle\langle 1 - n_{q'}\rangle \mathfrak{a}_{\epsilon_q - \epsilon_{q'}} \big) \\
&+ \tilde{g}_{q',q} \big(\langle 1 - n_{q'}\rangle\langle 1 - n_q\rangle \mathfrak{a}_{-\epsilon_{q'} - \epsilon_q} - \langle n_q\rangle\langle n_{q'}\rangle \mathfrak{a}_{\epsilon_{q'} + \epsilon_q} \big).
\end{aligned} \tag{8.29}$$

For a GGE form of the density matrix, Eq. (8.27) gets simplified in such a way that only the diagonal contributions $\mathfrak{a}_\omega \equiv \mathfrak{a}_{\omega,\omega}$ survive, while the term with $\mathcal{A}_{\omega,\omega'}$ drops out completely. One

should note that the periodicity $\mathfrak{a}_\omega = \mathfrak{a}_{\omega+n2\pi}$ is consistent with quasienergies $\tilde{\epsilon}_q$ being defined up to shift in multiples of 2π. Transitions caused by the coupling to the ancillas are thus well behaved in the Floquet sense. While function $\mathfrak{a}_\omega$ captures the type of coupling to the ancilla qubits, positive real functions

$$g_{q',q} = (1+\cos(q+q'))|\tilde{u}_{q'}\tilde{u}_q - \tilde{v}^*_{q'}\tilde{v}_q|^2, \tag{8.30}$$

$$\tilde{g}_{q',q} = (1+\cos(q'-q))|\tilde{u}_{q'}\tilde{v}_q - \tilde{v}^*_{q'}\tilde{u}_q|^2, \tag{8.31}$$

take into account the transverse field Ising parameters.

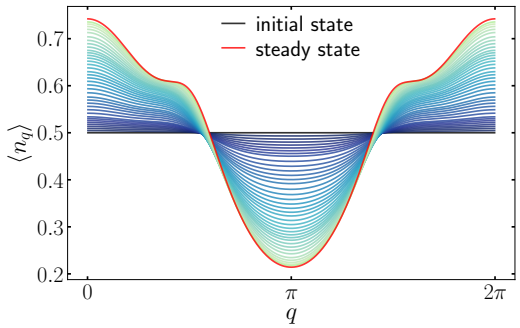

Figure 8.3: Time evolution of the mode occupation from an initial infinite temperature state. A highly non-thermal steady-state distribution is reached, which could be stabilized by the system-ancilla coupling in a digital quantum computer. Parameters: $J = 0.8, h = 0.45, h_A = 0.8, T = 6$, $L = 500, \lambda_\tau = \sqrt{\epsilon} = 0.1$.

We consider a time evolution from an initial infinite temperature state with $\mu_q = 0$, which could be in the digital quantum computer prepared by applying a few layers of (translationally invariant) random two-site gates on some product state [29]. In Fig. 8.3, we show the (zeroth order) GGE evolution from this state for parameters $J = 0.8$, $h = 0.45$, $h_A = 0.8$, $T = 6$, $L = 500$ and constant $\lambda_\tau = \sqrt{\epsilon} = 0.1$ for which $\mathfrak{a}_\omega = \epsilon \sin^2(\frac{T}{2}(\omega - \pi h_A))/\sin^2(\frac{1}{2}(\omega - \pi h_A))$. If the exact density matrix was considered, subleading correction of order $\mathcal{O}(\epsilon^2)$ would be present. We see that out of a featureless infinite temperature state, some non-thermal features quickly start to appear, and the steady state is reached after approximately $N_c \sim 100$ reset cycles for the above parameters. The steady-state itself has a clearly non-thermal occupation of eigenmodes, which depends on the system parameters J, h via function $g_{q',q}$, $\tilde{g}_{q',q}$ and on the parameters of system-ancilla coupling h_A, T via function $\mathfrak{a}_\omega$. Our main observation is that without a careful shaping of the coupling strength done for the purpose of approximate cooling to the ground state [45, 16], weak constant coupling $\lambda_\tau = \sqrt{\epsilon} \ll 1$ of integrable evolution to the ancilla qubits stabilizes a highly non-thermal population of eigenmodes, which depends on the choice of model parameters J, h, h_A, T.

While mode occupation clearly exposes the non-thermal nature of the stabilized state, it cannot be measured directly in a digital quantum computer, which has access only to local observables in the spin language. Local observables, which can expose the non-thermal nature of the stabilized state, are observables that strongly overlap with the local conserved quantities of the transverse field Ising model in the spin language [4, 43], still don't understand how to derive it. however, in many articles these formulas are written.

$$\begin{aligned} C_0 &= H_0 \\ C_2 &= \sum_j J S^{xx}_{j,j+2} - h S^{yy}_{j,j+1} - h S^{xx}_{j,j+1} - J\sigma^z_j \\ C_{2\ell>2} &= \sum_j J S^{xx}_{j,j+\ell+1} - h_x S^{yy}_{j,j+\ell} - h_x S^{xx}_{j,j+\ell} + J S^{yy}_{j,j+\ell-1} \\ C_{2\ell-1} &= J \sum_j S^{yx}_{j,j+\ell} - S^{xy}_{j,j+\ell}. \end{aligned} \tag{8.32}$$

where $S^{\alpha\beta}_{i,j} = \sigma^{\alpha}_i \sigma^z_{i+1} \dots \sigma^z_{j-1} \sigma^{\beta}_j$. this def should be changed by including the case of interaction through periodic boundary conditions.

Observables $S^{xx}_{i,j}$ and $S^{yy}_{i,j}$ are experimentally accessible and have been measured also in Ref. [45]. soon I'll understand, what are they?

In Fig. 8.4(a), we plot $|\langle S^{yy}_{i,i+\ell}\rangle|$ in the GGE steady state as a function of ℓ and compare it to expectation values in the ground state ($\langle n_q\rangle = 0$). Because we choose a non-critical set of system parameters, $J = 0.8, h = 0.45$, ground state and steady state correlations are decaying exponentially. The smoking gun for the GGE stabilization is a slow decay of spatial correlations in the steady state,

$$|\langle S^{yy}_{i,i+\ell}\rangle| \sim e^{-\ell/\xi},$$

which is even slower than the ground state ones, $\xi > \xi_{gs}$ why?. For the chosen Ising parameters J and h, $\xi_{gs} \approx 1$, which is not true generically. In Fig. 8.4(b) we show that with different choices of system-ancilla coupling parameters, one can tune the correlation length ξ. Quite generically, a larger number of system-ancilla couplings T induces slower (more non-thermal) decay of spatial correlations. However, this requires a larger number of gates and in total a longer circuit, which comes with a stronger influence of the inherent noise.

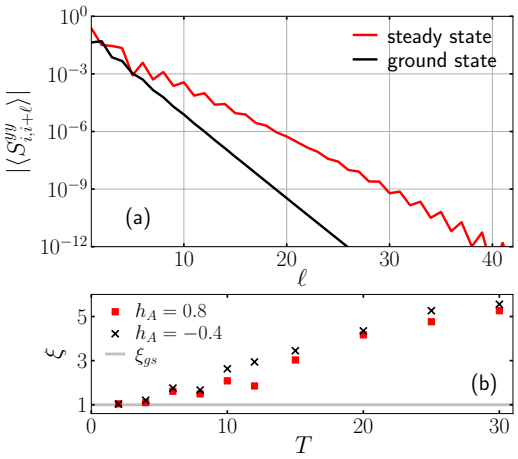

Figure 8.4: (a) Decay of correlations $|\langle S^{yy}_{i,i+\ell}\rangle|$, Eq. (8.32), as a function of ℓ in the steady-state GGE and the ground state for $h_A = 0.8, T = 6$. As a signature of the stabilized non-thermal GGE, operators that overlap with local conserved quantities of transverse field Ising models show a slower decay of spatial correlations compared to the ground state. (b) Different choices of system-ancilla coupling parameters (field h_A and cycle duration T) yield different correlation lengths ξ. Quite generically, longer cycles lead to slower decay of spatial correlations and thus more non-thermal states. Parameters: $J = 0.8, h = 0.45, L = 500$.

A slow decay of correlations in the steady-state for the operators that are overlapping with the conserved quantities of the transverse field Ising model is a direct consequence of reviving effects of integrability (????). In this case, the integrability is perturbed but also revived due to the dissipative coupling to ancilla qubits(why?). Same would hold in the presence of weak additional unitary integrability breaking or additional native noise: while steady-state would change quantitatively, its non-thermal nature would persist. In that sense these results are rather stable. okay, but why?

8.0.6 Comparison of approaches for steady-state calculation

maybe I'll see myself why such algorithms have such properties, for now I believe that it is so and it is not important for now. It will be important at the stage of computing numerically.

Since different approaches to nearly integrable, weakly dissipative system are still rather new [26, 18, 25, 33, 33, 34, 35, 30, 39] and not necessarily fully optimal, we return to the continuous model in this more technical section and compare the performance and complexity of different approaches. A reader not interested in the technical aspects of thermodynamically large calculations for non-interacting models can skip this section and proceed to the Conclusions.

In addition to previously mentioned time evolution from a given initial state, there are other possible approaches to calculating steady-states.
(1) Direct steady-state calculation: If aiming directly for the steady state, one can find the steady state Lagrange parameters $\mu_q(t\to\infty)$ from the stationarity condition Eq. (8.4), $\langle \dot{n}_q\rangle = 0$ for all momenta. If considering a system of L sites with L mode occupation operators, the complexity of such a root finding procedure is $\mathcal{O}(L^{b+1})$, where $\mathcal{O}(L)$ is the complexity of evaluating the expression $\langle \dot{n}_q\rangle$ and $\mathcal{O}(L^b)$ is the complexity of finding the root for L variables. For example, $b = 2$ for Powell method [55].
(2) Iterative steady state calculation: In Ref. [33], we developed an alternative approach, which avoids considering the stationarity conditions for all $\sim L$ conserved quantities (or mode occupation operators) by iteratively constructing the conserved quantities $\tilde{C}_k$ which play the leading role in a truncated generalized Gibbs ensemble description of the steady state, $\rho^{(k)}_{\tilde{\boldsymbol{\lambda}}} \propto e^{-\sum_{k'=0}^{k}\tilde{\lambda}^{(k)}_{k'}\tilde{C}_{k'}}$. As the zeroth approximation to the steady state a Gibbs ensemble is taken, $\rho^{(0)}_{\tilde{\boldsymbol{\lambda}}} \propto e^{-\tilde{\lambda}^{(0)}_0 H_0}$, with the zeroth iterative conserved quantity being the Hamiltonian, $\tilde{C}_0 = H_0$. In the next iterative steps, the kth iterative conserved quantity is constructed in some operator basis, which is for non-interacting systems most naturally the basis of mode occupation operators n_q,

$$\tilde{C}_k = \sum_q w^{(k)}_q n_q,\ \ w^{(k)}_q \propto \mathrm{Tr}[n_q \hat{\mathcal{D}}\rho^{(k-1)}_{\tilde{\boldsymbol{\lambda}}}], \tag{8.33}$$

see App. 8.0.12 for details. The approximation to the steady state is established by finding Lagrange parameters $\{\tilde{\lambda}^{(k)}_{k'}\}$ for $\rho^{(k)}_{\tilde{\boldsymbol{\lambda}}} \propto e^{-\sum_{k'=0}^{k}\tilde{\lambda}^{(k)}_{k'}\tilde{C}_{k'}}$ from the set of $k+1$ stationarity conditions $\langle \dot{\tilde{C}}_{k'}\rangle = 0$, Eq.(8.4), for $\{\tilde{C}_{k'}\}_{k'=0}^{k}$. The complexity of the procedure scales as $\mathcal{O}(k^3 L)$ for the Powell method. If $k\sim\mathcal{O}(1)$ and small, for thermodynamically large systems, the iterative method is clearly advantageous to the previous approach.
(3) Truncated GGE (most local conserved quantities): In principle, another possibility is the truncation in the Fourier modes of $\langle n_q\rangle$ or in the number of local conserved quantities C_i of the spin model that are considered [26, 25, 28, 36, 37, 4, 38]. C_i are for the transverse field Ising model linearly related to the mode occupation operators as $C_{2\ell} = \sum_q \cos(q\ell)\epsilon_q n_q$ for even ones ($C_0 = H_0$) and as $C_{2\ell-1} = 2J\sum_q \sin(q\ell) n_q$ for odd ones [37]. If one includes only N_i most local ones, $2\ell < N_i$, then the complexity of finding the truncated steady state GGE scales as $\mathcal{O}(LN_i^2)$.
(4) Time propagation: As done in the previous sections, one can calculate the whole time evolution from some initial $\mu_q(0)$, using a discretized version of $\dot{\mu}_q(t) = -\sum_{q'}(\chi^{-1})_{q,q'}(t)\,\langle \dot{n}_{q'}\rangle(t)$ and, for example, the Euler method. The complexity of such a calculation is $\mathcal{O}(N_t L)$, where N_t is the number of steps needed to reach the steady state. If we aim to calculate the steady state, the initial $\mu_q(0)$ can be a guess for the steady state. On the other hand, if we aim to describe a realistic time evolution from a state $|\psi_0\rangle$, the initial $\mu_q(0)$ are given by the initial state through the condition $\langle\psi_0|n_q|\psi_0\rangle = \mathrm{Tr}\left[n_q \frac{e^{-\sum_{q'}\mu_{q'}(0)n_{q'}}}{\mathrm{Tr}[e^{-\sum_{q'}\mu_{q'}(0)n_{q'}}]}\right]$. However, this itself is a root-finding procedure which requires $\mathcal{O}(L^{b+1})$ steps.

The approach (1) is clearly disadvantageous to others and will not be considered. Below we compare approach (4) to the iterative approach (2) from Ref. [33]. We perform the comparison for the model introduced in Sec. 8.0.4, where the time-dependent calculation (4) has already been performed.

Fig. 24.2 shows results for the iterative steady-state calculation, Eq. (8.33). We start with an initial approximation in the form of a Gibbs ensemble, with Hamiltonian being the only conserved quantities. Then, we perform our iterative procedure for constructing a truncated GGE steady-state description. The leading conserved quantities $\tilde{C}_k$, Eq. (8.33), are a linear superposition of the basis mode occupation operators n_q with weights selected by the dissipator. Fig. 24.2 shows momentum distributions obtained after k iterative steps. The initial $k = 0$ distribution corresponds to the thermal ensemble at a temperature that best represents the steady state, as obtained from a steady state rate equation for the energy. We observe that

convergence to the steady state is obtained in a finite number of $k = 8$ steps when we cannot discern this distribution from the ones of the following iterative steps. In Fig. 24.2(b), we push the number of iterative steps further, even though this is not needed for practical purposes. We observe that improvement is obtained only up to $k = 18$ iterative steps. The reason might be that with further steps, we are not adding new direction to the GGE manifold or that we are dealing with extremely small weights in (8.33) that can be numerically unstable and prone to errors. However, this problematic behavior appears in, for all practical purposes, an irrelevant regime.

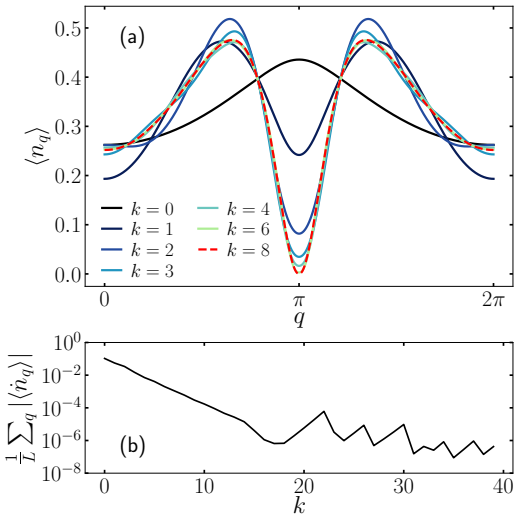

Figure 8.5: (a) Convergence to the steady state mode occupation at different iterative steps k. In the $k = 0$ step, the steady state is approximated by a thermal state. In the following iterative steps, additional leading conserved operators are added to a truncated GGE. A decent convergence is obtained in finite number of steps. (b) After the initial improvement of results with increasing number of iterative steps, for chosen parameters, $k > 18$ iterative steps fail to improve the results further. However, this happens in the regime where results are converged for all practical purposes. Parameters: $J = 1, h = 0.6, L = 10^5$.

In Fig. 8.6 we compare the efficiency of the direct time propagation, Eq. (8.4), and the iterative approach, Eq. (8.33) by plotting the ratio of CPU times for the former vs the latter. We show that as a function of the average remaining flow of the mode occupations, $(1/L)\sum_q |\langle \dot{n}_q \rangle|$, characterizing how far from the steady state is the approximate description at a given iterative or finite time step. Fig. 8.6 reveals that the two methods are comparable, as anticipated from the scaling arguments. Namely, the numerical complexity of time propagation scales as $\mathcal{O}(N_t L)$, where N_t is the number of propagation steps, while the iterative method scales as $\mathcal{O}(k^3 L)$, where k is the number of needed iterative steps. For the case studied, direct propagation can be performed at rather large $\epsilon \delta t = 0.6$ time steps, meaning that the direct propagation is rather efficient. We could have gained some efficiency for the iterative method by not converging the steady state equations at intermediate iterative steps, however, we did not play with that knob. Which approach is quantitatively advantageous depends on the choice of parameters J, h.

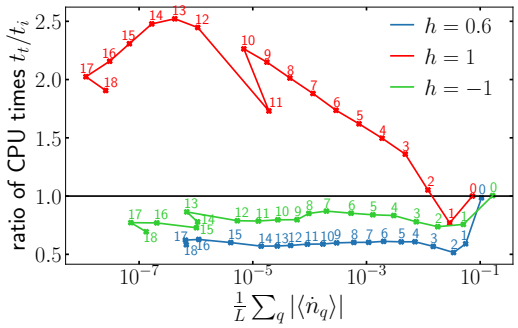

Figure 8.6: Ratio of computing times t_t/t_i, where t_t corresponds to time evolution with $\epsilon\delta t = 0.6$ and t_i to calculation with the iterative scheme, as a function of $(1/L)\sum_q |\langle \dot{n}_q \rangle|$, characterizing the accuracy of steady state calculation. Points are labeled by the number of iterative step taken for t_i calculation. The two methods are comparable. Which one is more efficient in absolute terms depends on parameters. Parameters: $J = 1, L = 10^5$.

In Fig. 8.7, we plot the steady state expectation values of local conserved quantitites $\langle C_i \rangle$, Eq. (8.32). Since the steady state mode occupation is symmetric, $\langle n_q \rangle = \langle n_{-q} \rangle$, only parity-even conserved quantities have finite expectation values. Fig. 8.7 reveals exponentially decaying contribution with growing support, which indicates that also more standard truncation (3) using the most local conserved quantities is meaningful. If N_i conserved quantities are used, the complexity of calculating the steady state scales as $\mathcal{O}(LN_i^2)$. Because we expect that our iterative construction is more efficient, we do not perform a detailed comparison.

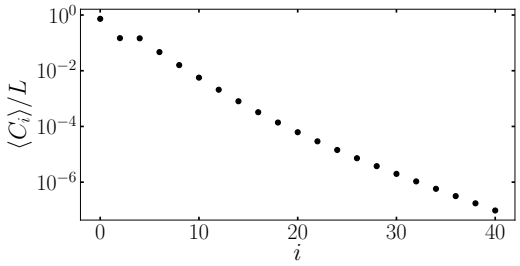

Figure 8.7: Steady state expectation values of local conserved quantities (8.32). With increasing support, the importance of even conserved quantities decays exponentially. Expectation values of odd observables are zero due to symmetry. Parameters: $J = 1$, $h = 0.6$, $L = 10^5$.

Our main conclusion from this analysis is that a direct, steady-state calculation (1) of all Lagrange parameters for all the mode occupation operators from the stationarity condition of Eq. (8.4) is the most costly ($\mathcal{O}(L^3)$) and should be avoided. Other approaches are comparable; which one is the most efficient depends on the model parameters. Regardless of the method, our first important message is that a weak coupling to non-thermal (Lindblad) baths can stabilize a highly non-thermal steady-state mode occupation. Our second messages is that thermodynamically large calculations can be performed if the GGE ansatz is used as an approximation to the full density matrix description of non-interacting systems weakly coupled to baths.

8.0.7 Conclusions

We benchmarked different approaches to non-interacting integrable many-body systems that are weakly coupled to baths and discussed how they could be realized with digital quantum computers, such as superconducting circuits [45] or trapped ions [40].

After mapping the non-interacting model to free fermions, GGEs in terms of mode occupation operators offer a compact interpretation of time evolution and stabilized steady states. Namely, weak integrability breaking perturbations cause scattering between Bogoliubov quasiparticles, and we derived a generalized scattering theory, reminiscent of the Boltzmann equations, which yields the time-dependent eigenmode population, see also [30, 34, 35, 39, 16]. The

non-thermal nature of the stabilized steady state can be inferred from the non-Gaussian, structured distribution over eigenmodes, which is related to the transition rates between different quasiparticles caused by the integrability-breaking bath coupling.

We discussed the numerical complexity of different approaches: (1) direct, steady-state calculation, (2) iterative steady-state truncated GGE construction, (3) traditional truncated GGE approximation, and (4) time evolution towards the steady state. We conclude that approach (1) is more expensive than others and should be avoided. We compare (2) and (4) on the example of transverse field Ising model coupled to non-thermal baths and find that they are comparable, in agreement with scaling argument expectations. Which of the two is quantitatively more efficient depends on the model and precise form of coupling to baths. A similar benchmarking for interacting integrable models remains a future challenge.

Notably, we proposed how to realize highly non-thermal GGEs due to proximity to integrability with a digital quantum computer. There, driven-dissipative effects can be implemented by weakly coupling system and ancilla qubits and resetting the latter at the end of every cycle [45]. We derived the effective system's density matrix time evolution for such a Floquet-reset protocol. By shaping the system-ancilla coupling strength, Ref. [45] recently prepared nearly thermal ensembles with very low temperatures, pushing the system close to the ground state. With our work, we stress that in their case, stabilized states are actually generalized Gibbs ensembles where temperature dominates over other Lagrange parameters due to a particular choice of time-dependent system-ancilla coupling strength. Our example shows that integrable systems that are weakly but generically coupled to ancilla qubits are prone to relax to highly non-thermal GGEs. We comment on how such a highly non-thermal nature could be detected by measuring the decay of correlations that are slower than in the ground state. Additional native noise of the proposed platform should not be a problem and would only slightly alter the time evolution and the steady state while preserving its highly non-thermal nature. A digital quantum computer realization of our proposal would be the first to support a series of theory works [26, 18, 25, 28, 29, 33] revealing a peculiar nature of nearly integrable models that can show a strong non-linear response to weak coupling to non-thermal baths.

Note: During the preparation of this manuscript, a related work appeared on arXiv [16], interpreting the dissipative steady state preparation of Ref. [45] in terms of the scattering theory equivalent to ours.

8.0.8 Floquet transverse field Ising model

In this section, we discuss the generalized Bogoliubov rotation for the Floquet transverse field Ising model,

$$U_S = e^{-i\frac{\pi J}{2}\sum_j \sigma_j^x\sigma_{j+1}^x} e^{-i\frac{\pi h}{2}\sum_j \sigma_j^z} = e^{-iH_{\mathrm{FTFI}}}, \tag{8.34}$$

so what is different with Ising model??? relevant for a digital quantum computer realization, Sec. 8.0.5. Using the Jordan-Wigner transformation, Eq. (8.7), the Fourier transform, Eq. (8.8), and periodic boundary conditions, system's time evolution factorizes over momenta as

$$U_S = \prod_{q\geq 0} e^{-i\Phi_q^\dagger X_q \Phi_q} e^{-i\Phi_q^\dagger Z_q \Phi_q}, \tag{8.35}$$

with $\Phi_q = \{c_q, c_{-q}^\dagger\}^T$ representing the bispinor of fermionic operators in momentum space, Eq. (8.8) and 2x2 matrices

$$X_q = \pi J \begin{bmatrix} \cos(q) & -\sin(q) \\ -\sin(q) & -\cos(q) \end{bmatrix}, \quad Z_q = \pi h \begin{bmatrix} 1 & 0 \\ 0 & -1 \end{bmatrix}. \tag{8.36}$$

Factorization (8.35) is possible since X_q commute amongst each other for positive momenta but not necessarily with their negative momenta counterparts. Dispersion relation $\tilde{\epsilon}_q$ and the Bogoliubov transformation are obtained by diagonalizing each q-block $e^{-iX_q}e^{-iZ_q}$ separately,

$$P^{-1}e^{-iX_q}e^{-iZ_q}P = \mathrm{diag}[e^{-i\tilde{\epsilon}_q}, e^{-i\tilde{\epsilon}_{-q}}], \tag{8.37}$$

yielding

$$\cos(\tilde{\epsilon}_q) = \cos(\pi J)\cos(\pi h) - \sin(\pi J)\sin(\pi h)\cos(q). \tag{8.38}$$

The Bogoliubov transformation, $\Phi_k^\dagger P = (d_k^\dagger, d_{-k})$, then takes a similar form as in the continuous-time propagation

$$
\begin{aligned}
c_q &= \tilde{u}_q d_q - \tilde{v}_q^* d_{-q}^\dagger, \\
\tilde{u}_q &= \frac{(\xi_q + \tilde{a}_q)}{\sqrt{2\xi_q(\xi_q + \tilde{a}_q)}},\ \tilde{v}_q = \frac{\tilde{b}_q}{\sqrt{2\xi_q(\xi_q + \tilde{a}_q)}}, \\
\tilde{a}_q &= \sin(\pi J)\cos(\pi h)\cos(q) + \cos(\pi J)\sin(\pi h), \\
\tilde{b}_q &= -e^{-i\pi h}\sin(\pi J)\sin(q), \\
\xi_q &= \sqrt{\tilde{a}_q^2 + |\tilde{b}_q|^2}.
\end{aligned}
\tag{8.39}
$$

it was already written?

The system's unitary time propagator in the diagonal form then equals

$$
U_S = e^{-i\sum_q \tilde{\varepsilon}_q (d_q^\dagger d_q - \frac{1}{2})}. \tag{8.40}
$$

Above we were able to consider the diagonalization of one q-block as a matrix, $e^{-iX_q}e^{-iZ_q} = e^{-iH_{q,\mathrm{FTFI}}}$ Eq. (8.37), and not as an operator, $e^{-i\Phi_q^\dagger X_q \Phi_q} e^{-i\Phi_q^\dagger Z_q \Phi_q} = e^{-i\hat{H}_{q,\mathrm{FTFI}}}$, since we can show that $\hat{H}_{q,\mathrm{FTFI}} = \Phi_q^\dagger H_{q,\mathrm{FTFI}} \Phi_q$. This is shown by realizing that for any matrices $\Phi_q^\dagger A \Phi_q$ and $\Phi_q^\dagger B \Phi_q$, where $\Phi_q = \{c_q, c_{-q}^\dagger\}^T$ is the fermionic bispinor in momentum space, the following commutation relation holds: $[\Phi_q^\dagger A \Phi_q, \Phi_q^\dagger B \Phi_q] = \Phi_q^\dagger [A, B] \Phi_q$. From this, it follows that finding the effective Floquet transverse field Ising Hamiltonian for momentum q in the operator form is equivalent to finding it in the matrix form (e.g., via the Baker-Hausdorff-Campbell formula) and applying bispinor operator $\Phi_q^\dagger$ left and Φ_q right of the Floquet Hamiltonian matrix.

8.0.9 Lindblad evolution of system's density matrix in a digital quantum computer propagation

looks like a good place for practice by re-deriving the results. But now I need to do other topics.

Here, we derive the discrete time evolution of the system's density matrix, Eq. (8.27), for the trotterized gate propagation in a digital quantum computer, where dissipation is due to the coupling and reset of ancillary qubits.

As written in Sec. 8.0.5, the system's time evolution is for one step given by

$$
U_S = e^{-i\frac{\pi J}{2}\sum_j \sigma_j^x \sigma_{j+1}^x} e^{-i\frac{\pi h}{2}\sum_j \sigma_j^z} \equiv e^{-iH_{\mathrm{FTFI}}}. \tag{8.41}
$$

One step of ancilla qubits time propagation is given by

$$
U_A = e^{-i\frac{\pi h_A}{2}\sum_j \tilde{\sigma}_j^z}, \tag{8.42}
$$

where $\tilde{\sigma}_j^\alpha$ denotes operators acting on ancilla qubits. This is always followed by a weak hermitian system-ancilla coupling

$$
\begin{aligned}
U_{SA,\tau} &= \prod_j e^{-i\lambda_\tau Q_j \otimes A_j} \\
&\approx e^{-i\lambda_\tau \sum_j Q_j \otimes A_j - \frac{1}{2}\lambda_\tau^2 \sum_{j,j'} [Q_j, Q_{j'}] \otimes A_j A_{j'}} \\
&\equiv e^{-iW_\tau},
\end{aligned}
\tag{8.43}
$$

where we have introduced W_τ to denote the first and second order of an effective coupling Hamiltonian at time step $\tau \leq T$ before the reset. One cycle contains T system-ancilla-coupling propagations

$$
U_T = U_{SA,T} U_A U_S \cdots U_{SA,1} U_A U_S, \tag{8.44}
$$

followed by a reset of ancilla qubits to spin down state

$$\tilde{P}_{\downarrow} = \hat{\mathbb{1}} \otimes \prod_j \frac{1}{2}\left(\tilde{\mathbb{1}} - \tilde{\sigma}_j^z\right). \tag{8.45}$$

Following Ref. [50], we derive the system's density matrix time evolution in the interaction picture, which is slightly non-standard due to the trotterized nature of the setup. The interaction picture propagator for one cycle (before the reset) equals

$$\mathcal{U}_T \equiv U_0^{-T} U_T = \hat{\mathcal{T}} e^{-i\sum_{\tau=1}^{T} W_{I\tau}},\ U_0 = U_A U_S, \tag{8.46}$$

where $W_{I\tau} = U_0^{-\tau} W_\tau U_0^{\tau}$ is the first and second order of the effective coupling Hamiltonian (8.43) propagated in the interaction picture for τ steps and $\hat{\mathcal{T}}$ is the time ordering operator. In App. 8.0.10, we prove Eq. (8.46).

Due to the projection (8.45), the whole density matrix operator has a product form at the end of each cycle,

$$\rho_I(N_c) = \rho_{S,I}(N_c) \otimes \prod_j \frac{1}{2}\left(\tilde{\mathbb{1}} - \tilde{\sigma}_j^z\right). \tag{8.47}$$

One cycle evolution of the system's density matrix $\rho_{S,I}$, obtained by tracing out the ancilla qubits, is approximated to second order in coupling strength λ_τ by

$$\begin{aligned}
&\rho_{S,I}(N_c+1) - \rho_{S,I}(N_c) && (8.48)\\
&= \mathrm{Tr}_A\Big(\mathcal{U}_T \rho_I(N_c) \mathcal{U}_T^\dagger\Big) - \rho_{S,I}(N_c)\\
&\approx -i\mathrm{Tr}_A\Big(\sum_{\tau=1}^{T}[W_{I\tau}, \rho]\Big) && (8.49)\\
&\quad - \mathrm{Tr}_A\Big(\sum_{\tau=1}^{T}\sum_{\tau'=1}^{\tau}[\lambda_\tau V_{I\tau}, [\lambda_{\tau'} V_{I\tau'}, \rho_I(N_c)]]\Big) && (8.50)\\
&= \sum_{\tau=1}^{T}\sum_{\tau'=1}^{\tau}\sum_j \lambda_\tau \lambda_{\tau'} && (8.51)\\
&\quad \times \Big(\big(Q_{j,I\tau} Q_{j,I\tau'} \rho_{S,I}(N_c) - Q_{j,I\tau'} \rho_{S,I}(N_c) Q_{j,I\tau}\big)\mathcal{A}_{\tau,\tau'}\\
&\quad + \big(\rho_{S,I}(N_c) Q_{j,I\tau'} Q_{j,I\tau} - Q_{j,I\tau} \rho_{S,I}(N_c) Q_{j,I\tau'}\big)\mathcal{A}^*_{\tau,\tau'}\Big).
\end{aligned}$$

The linear term (8.49) vanishes for our choice $A_j = \tilde{\sigma}_j^x$ since $\mathrm{Tr}_A\big(U_0^{-\tau} A_j U_0^{\tau}(\tilde{\mathbb{1}} - \tilde{\sigma}_j^z)\big) = 0$. Generically, it can be set to zero by shifting the A_j operators [50]. In a compact notation, the result of resetting and tracing over the ancilla qubits is represented by $\mathcal{A}_{\tau,\tau'}$, which for our choice $A_j = \tilde{\sigma}_j^x$ simplifies to

$$\begin{aligned}
\mathcal{A}_{\tau,\tau'}\delta_{i,j} &= \mathrm{Tr}_A\Big[\prod_k \frac{1}{2}\left(\tilde{\mathbb{1}} - \tilde{\sigma}_k^z\right) A_{j,I\tau} A_{i,I\tau'}\Big]\\
&= e^{-i\pi h_A(\tau-\tau')}\delta_{i,j}
\end{aligned} \tag{8.52}$$

Furthermore, we define

$$\begin{aligned}
\mathcal{A}_{\omega,\omega'} &= \sum_{\tau=1}^{T}\sum_{\tau'=1}^{\tau} \lambda_\tau \lambda_{\tau'} e^{i\omega'\tau - i\omega\tau'} \mathcal{A}_{\tau,\tau'} = \mathfrak{a}_{\omega,\omega'} - \mathcal{A}^*_{\omega',\omega}\\
\mathfrak{a}_{\omega,\omega'} &= \sum_{\tau=1}^{T} \lambda_\tau e^{i(\omega' - \pi h_A)\tau} \sum_{\tau'=1}^{T} \lambda_{\tau'} e^{-i(\omega - \pi h_A)\tau'}
\end{aligned} \tag{8.53}$$

and

$$Q_{j,\omega} = \sum_{\alpha,\beta,\tilde{E}_\beta-\tilde{E}_\alpha=\omega} |\alpha\rangle\langle\alpha|Q_j|\beta\rangle\langle\beta|, \tag{8.54}$$

which represents Q_j operator projected between many-body eigenstates of H_{FTFI} that differ in energy for ω, such that

$$Q_{j,I\tau} = \sum_\omega U_0^{-\tau} Q_{j,\omega} U_0^\tau, = \sum_\omega e^{-i\omega\tau} Q_{j,\omega}, \tag{8.55}$$

Putting all these together, we derive a compact form

$$\begin{aligned} &\rho_{S,I}(N_c+1) - \rho_{S,I}(N_c) \\ &\approx \sum_{j,\omega,\omega'} -i\,\mathrm{Im}(\mathcal{A}_{\omega,\omega'})[Q^\dagger_{j,\omega'}Q_{j,\omega}, \rho_{S,I}(N_c)] \\ &+ \mathfrak{a}_{\omega,\omega'}\Big(Q_{j,\omega}\rho_{S,I}(N_c)Q^\dagger_{j,\omega'} - \frac{1}{2}\{Q^\dagger_{j,\omega'}Q_{j,\omega}, \rho_{S,I}(N_c)\}\Big). \end{aligned} \tag{8.56}$$

To obtain the propagation equation (8.27) presented in the main text, we approximate the system's density matrix with a GGE ansatz that, notably, does not evolve under U_0, making the transformation back to the Schrödinger picture trivial.

8.0.10 Floquet interaction picture time propagator

In this section, we show that $\mathcal{U}_T$, Eq. (8.46), is really the interaction picture propagator for one cycle consisting of T system-ancilla-coupling propagations.

The Schrödinger picture propagator (8.44) can be written as

$$\begin{aligned} U_T &= U_{SA,T}U_A U_S \cdots U_{SA,1}U_A U_S, \\ &= U_{SA,T}U_0 U_{SA,T-1}U_0 \cdots U_{SA,1}U_0 \\ &= \mathbb{1}U_{SA,T}U_0\mathbb{1}U_{SA,T-1}U_0 \cdots \mathbb{1}U_{SA,1}U_0 \\ &= U_0^T \prod_{\tau=1}^{T} U_{I,SA,\tau}, \end{aligned} \tag{8.57}$$

where the leftmost identity is $U_0^T U_0^{-T}$, next one $U_0^{T-1}U_0^{-(T-1)}$ and the rightmost $U_0 U_0^{-1}$. Above we also introduce the interaction picture coupling propagator $U_{I,SA,\tau} = U_0^{-\tau}U_{SA,\tau}U_0^\tau \approx e^{-iW_{I\tau}}$ at step τ. The interaction picture time propagator for one reset cycle of length T is then

$$\mathcal{U}_T = U_0^{-T}U_T = \prod_{\tau=1}^{T} e^{-iW_{I\tau}} = \hat{\mathcal{T}} e^{-i\sum_{\tau=1}^{T} W_{I\tau}} \tag{8.58}$$

In the last step, we used the following property of the time ordering operator: $e^{-i\hat{O}(t_2)}e^{-i\hat{O}(t_1)} = \hat{\mathcal{T}}e^{-i(\hat{O}(t_2)+\hat{O}(t_1))}$ for any operator $\hat{O}(t)$, if $t_2 > t_1$. Thus, we have shown that Eq. (8.46) holds.

8.0.11 Examples and symmetries in the trotterized setup

In order to illustrate the great variety of different non-thermal steady states stabilized, we show here a few examples of steady state mode occupations that were considered to demonstrate anomalously long spatial correlations in the main text, Fig. 8.4(b). In Fig. 8.8, we show the full time evolution of the mode occupation from the initial infinite temperature state, for $J = 0.8, h = 0.45, h_A = -0.4, T = 6$. write the model again here! It is interesting to observe that even though these parameters yield a comparable correlation length ξ for the decay of spatial correlations in Fig. 8.4(b) as $h_A = 0.8$, the steady state distribution is completely different from the distribution at $h_A = 0.8$ shown in the main text, Fig. 8.3. (??!!! what is

exactly the meaning of mode occupations?? how exactly they look in basic statistical physics examples???)

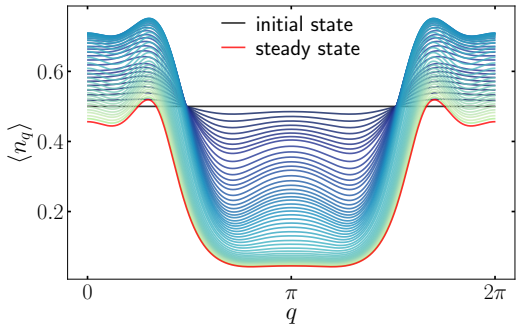

Figure 8.8: Time evolution of the mode occupation from an initial infinite temperature state. Evolution correspond to the system-ancilla coupling in a digital quantum computer at parameters: $J = 0.8, h = 0.45, h_A = -0.4, T = 6,\ L = 500, \lambda_\tau = \sqrt{\epsilon} = 0.1$.

In Fig. 8.9, we show the steady state distributions of momentum occupations at three different lengths of the reset cycle, $T = 2, 6, 30$, again for parameters $J = 0.8, h = 0.45, h_A = 0.8, L = 500, \lambda_\tau = \sqrt{\epsilon} = 0.1$ shown in the main text in Fig. 8.4(b). Consistently with results from the main text, longer reset-cycles lead to more clearly non-thermal steady states yielding longer spatial correlations in $|\langle S^{yy}_{i,i+\ell}\rangle|$.

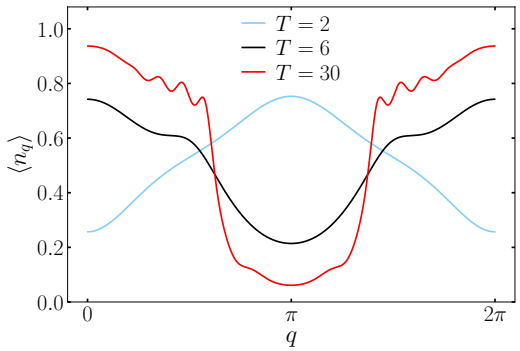

Figure 8.9: Steady state distributions of the mode occupation for different lengths of the reset cycle T. Parameters: $J = 0.8, h = 0.45, h_A = 0.8, L = 500, \lambda_\tau = \sqrt{\epsilon} = 0.1$ and $T = 2, 6, 30$.

The equations of motion for the mode occupation,

$$\begin{aligned} &\langle n_q(N_c+1)\rangle - \langle n_q(N_c)\rangle \\ &= \frac{2}{N}\sum_{q'} g_{q',q}\big(\langle n_{q'}\rangle\langle 1-n_q\rangle \mathfrak{a}_{\epsilon_{q'}-\epsilon_q} - \langle n_q\rangle\langle 1-n_{q'}\rangle \mathfrak{a}_{\epsilon_q-\epsilon_{q'}}\big) \\ &\quad + \tilde{g}_{q',q}\big(\langle 1-n_{q'}\rangle\langle 1-n_q\rangle \mathfrak{a}_{-\epsilon_{q'}-\epsilon_q} - \langle n_q\rangle\langle n_{q'}\rangle \mathfrak{a}_{\epsilon_{q'}+\epsilon_q}\big), \end{aligned} \tag{8.59}$$

have certain symmetries, which imply symmetric relations also for the steady state occupations. Since $\mathfrak{a}_\omega(-h_A) = \mathfrak{a}_{-\omega}(h_A)$, the steady state occupations at $-h_A$ are inverted around the infinite temperature value, $\langle n_q\rangle(-h_A) = 1/2 - \langle n_q\rangle(h_A)$, with respect to the occupations at h_A, see Fig. 8.10. This is a consequence of the exchanged roles of $\mathfrak{a}_\omega$ between the first and the second, as well as between the third and the fourth term in Eq. (8.59). Also, $\langle S^{yy}_{i,i+\ell}\rangle(-h_A) = -\langle S^{yy}_{i,i+\ell}\rangle(h_A)$. The second symmetry comes from reflecting the Ising parameter $h \to 1/2 - h$. Taking into account the form of functions $g_{q',q}, \tilde{g}_{q',q}$, Eq. (8.31), one gets $\langle n_q\rangle(1/2-h) = 1/2 - \langle n_{q+\pi}\rangle(h)$, see Fig. 8.10. Under this transformation only the correlations between even distances get a minus sign, $\langle S^{yy}_{i,i+2\ell}\rangle(1/2-h) = -\langle S^{yy}_{i,i+2\ell}\rangle(h)$. Same properties hold for the $J \to 1/2 - J$ transformation. In addition to the symmetries discussed above, the equations of motion are invariant under shifting Ising parameters J, h and bath field h_A by multiples of 2.

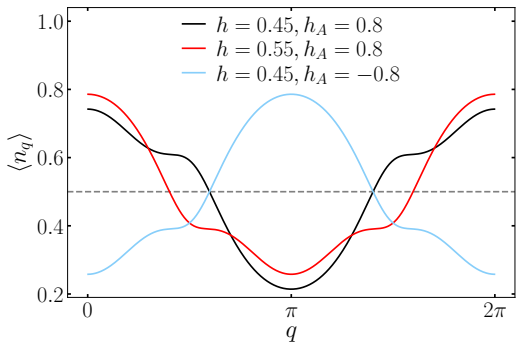

Figure 8.10: Steady-state mode occupations under different symmetry transformations of the model. Taking $h_A \to -h_A$ will invert the steady state population, whereas $h \to 1/2 - h$ will invert the population and shift momentum by π. Parameters: $J = 0.8, T = 6, L = 500$, $\lambda_\tau = \sqrt{\epsilon} = 0.1$.

8.0.12 Iterative construction of the leading conserved quantities

I have no idea how to use this approach, Iris didn't tell much yet about it.

In Ref. [33], we developed an iterative approach for constructing the conserved quantities $\tilde{C}_k$, which play the leading role in a truncated generalized Gibbs ensemble description of the steady state, $\rho^{(k)}_{\tilde{\boldsymbol{\lambda}}} \propto e^{-\sum_{k'=0}^{k} \tilde{\lambda}^{(k)}_{k'} \tilde{C}_{k'}}$. As the zeroth approximation to the steady state a Gibbs ensemble is taken, $\rho^{(0)}_{\tilde{\boldsymbol{\lambda}}} \propto e^{-\tilde{\lambda}^{(0)}_0 H_0}$, with the zeroth iterative conserved quantity being the Hamiltonian, $\tilde{C}_0 = H_0$. In next iterative steps, the kth iterative conserved quantity is constructed in the basis Q_m, $[H_0, Q_m] = 0$ as

$$\begin{aligned} \tilde{C}_k &= \mathcal{N}_k^{-1} \sum_m w^{(k)}_m Q_m, \\ w^{(k)}_m &= -\sum_n \left(\chi^{-1}_{(k-1)}\right)_{mn} \mathrm{Tr}[Q_n \hat{\mathcal{D}} \rho^{(k-1)}_{\tilde{\boldsymbol{\lambda}}}]. \end{aligned} \tag{8.60}$$

For the non-interacting H_0, a natural choice of basis is the basis of mode occupation operators, $Q_m = n_m$. In this case, the susceptibility matrix $(\chi_{(k)})_{m,n} = \langle Q_m Q_n \rangle_{\rho^{(k)}_{\tilde{\boldsymbol{\lambda}}}} - \langle Q_m \rangle_{\rho^{(k)}_{\tilde{\boldsymbol{\lambda}}}} \langle Q_n \rangle_{\rho^{(k)}_{\tilde{\boldsymbol{\lambda}}}}$ is diagonal $(\chi_{(k)})_{m,n} = e^{-\mu^{(k)}_m}/(1+e^{-\mu^{(k)}_m})^2 \delta_{m,n}$ which further reduces the complexity of performing the iterative procedure. Here, $\mu^{(k)}_m$ is an effective Lagrange parameter associated to the mode occupation operator n_m at kth iterative step, $\mu^{(k)}_m = \tilde{\lambda}^{(k)}_0 \varepsilon_m + \sum_{k'=1}^{k} \mathcal{N}^{-1}_{k'} \tilde{\lambda}^{(k)}_{k'} w^{(k')}_m$, and ε_m is the dispersion. The approximation to the steady state is established by finding $\{\tilde{\lambda}^{(k)}_{k'}\}$ for $\rho^{(k)}_{\tilde{\boldsymbol{\lambda}}} \propto e^{-\sum_{k'=0}^{k} \tilde{\lambda}^{(k)}_{k'} \tilde{C}_{k'}}$ from the set of $k+1$ conditions $\langle \dot{\tilde{C}}_{k'} \rangle = 0$, Eq.(8.4), for $\{\tilde{C}_{k'}\}^{k}_{k'=0}$. We set normalization $\mathcal{N}_k$ to be 1, thereby absorbing it into the corresponding Lagrange parameters.

8.0.13 General important left questions about "GGE in weakly-int dissip. syst. ..." by Ulčakar, et al.

What to do with steady state, based on "GGE in weakly-int dissip. syst. ..." by Ulčakar, Lenarčič?

we got a steady state plots, so what does it tell us about physics?

Why GGE is useful, based on "GGE in weakly-int dissip. syst. ..." by Ulčakar, Lenarčič?

so the main idea was that we can reduce the number of parameters that describe the system and it was proven that results are the same as for long hard direct calculation, right? If so, I'll write explicitly that it is so. Currently, I don't see it.

9 Time-dependent generalized Gibbs ensembles in open quantum systems by Lange, Lenarčič, Rosch

this article presents the results. not so much explanation about technical steps is given. also, the codes are essential to understand how plots were obtained?

Abstract

Generalized Gibbs ensembles have been used as powerful tools to describe the steady state of integrable many-particle quantum systems after a sudden change of the Hamiltonian. Here we demonstrate numerically, that they can be used for a much broader class of problems. We consider integrable systems in the presence of weak perturbations which both break integrability and drive the system to a state far from equilibrium. Under these conditions, we show that the steady state and the time-evolution on long time-scales can be accurately described by a (truncated) generalized Gibbs ensemble with time-dependent Lagrange parameters, determined from simple rate equations. We compare the numerically exact time evolutions of density matrices for small systems with a theory based on block-diagonal density matrices (diagonal ensemble) and a time-dependent generalized Gibbs ensemble containing only small number of approximately conserved quantities, using the one-dimensional Heisenberg model with perturbations described by Lindblad operators as an example.

9.1 Introduction

below again a good literature review, I'll look at these articles later

In recent years the thermalization of closed quantum systems has been intensively studied [7, 2, 19]. A typical setup is the quantum quench: a system, initialized in the ground state of a Hamiltonian H_i, undergoes a non-equilibrium dynamics due to evolution with another Hamiltonian H_f. In the long time limit generic ergodic many-particle systems are expected to reach a thermal Gibbs state, $\rho \sim e^{-\beta H_f}$ [6]. The approach to this state can, however, be slow and is generically characterized by power-laws [110, 111, 112].

In integrable systems, in contrast, the existence of macroscopically many local conserved quantities restricts the dynamics and prohibits conventional thermalization [4, 3, 10, 11]. It has, however, been conjectured [1] that generalized Gibbs ensembles (GGEs) provide an accurate thermodynamic description of steady states in this case, at least for local observables. For each (quasi-)local conserved quantity a Lagrange parameter is introduced, generalizing the concept of temperature or chemical potential. The Lagrange parameters are thereby determined from the value of conserved quantities in the initial state. Exact local equivalence of GGEs and diagonal ensembles can be proven only after a complete set of local conserved quantities is included into the GGE, and is for non-interacting models equivalent to including all mode occupation numbers [1, 37]. For the Heisenberg model, as a prototypical interacting quantum integrable model, quenches have been fist studied by [36, 25]. A vast improvement in agreement has been achieved [2] only after the discovery of additional quasi-local conserved quantities [47, 22, 48], by systematically including families of quasi-local conservation laws. Using the quenched action

approach [5, 54], it was possible to demonstrate that GGEs indeed destribe the steady state at least for certain initial conditions [60, 15, 16, 63, 66].

When only a few most local (or even all strictly local) conservation laws are included into the GGE, a correct qualitative behavior with some discrepancies is typically observed interesting, I'll look later [37, 36, 55, 15, 2]. It has also been suggested that convergent approximations to the steady state are obtained when more and more conservation laws are included [38].

Using ultracold atoms integrable models can be realized with such a high precision, that one can neglect integrability breaking terms at least up to some time [17, 29, 30, 92]. In spectacular experiments, Langen *et al.* [19] succeeded to demonstrate that a truncated GGE can describe high-order steady-state correlation functions of an interacting Bose gas after a quench with a high precision. Integrability breaking perturbations can also be controllably tuned [23] to display the crossover from integrable dynamics to thermalization.

In condensed matter systems, one can realize approximately integrable systems for example in spin-chain materials. In this case, however, one cannot neglect integrability breaking terms arising, e.g., from phonons, intra-chain coupling or other terms not described by simple spin-1/2 one-dimensional Heisenberg model. Due to the proximity to integrable points, the heat conductivity in such systems can be strongly enhanced [19, 20], but the steady state is expected to become thermal after a quantum quench. Nevertheless, it was shown that a static weak integrability breaking induces thermalization only on the longest time scale [41, 37, 38, 96, 98, 11, 42, 43], while the transient dynamics dwells on the so-called prethermal plateaux [40, 95] that can be described by a GGE with Lagrange multipliers fixed by the initial state using approximately conserved quantities, possibly perturbatively readjusted according to the weak integrability breaking [52].

After a quantum quench, all exotic concerved quantities decay in the presence of integrability breaking perturbation. The situation is, however, completely different for another class of problems: (weakly) driven systems. These are systems, where time-dependent perturbations or the coupling to non-thermal reservoirs drive the system towards a non-equilibrium state. For example, we considered in Ref. [26] the coupling of a spin-chain to laser light and phonons. In this case, the decay of conserved quantities due to integrability breaking can be balanced by gain terms arising from the driving terms. Generically, a macroscopic set of approximate conservation laws is activated despite the presence of integrability breaking. Contrary to the case of quench problems, the value of the conserved quantities in the steady state is not determined by initial conditions but by the balance of driving terms, the coupling to thermal and non-thermal baths, and other integrability breaking terms. We argued in [26] that the resulting states are far from equilibrium and one can use a GGE to describe them quantitatively as long as all driving and integrabilty breaking terms are weak. We showed that one can use this ideas to realize novel types of spin or heat pumps.

The main goal of the present paper is to demonstrate numerically that GGEs with time-dependent Lagrange parameters accurately describe both the time-evolution and the steady state of weakly driven approximately integrable many-particle quantum systems. As an example we chose a one-dimensional spin-1/2 Heisenberg model coupled to a non-thermal bath described by Lindblad operators. We have chosen this model because it is better suited for numerical analysis compared to the much more complicated case considered in Ref. [26]. Our approach based on time-dependent GGEs covers both the physics of prethermalization and the relaxation towards a steady state potentially far from thermal equilibrium. The concept of time-dependent GGE has been suggested earlier, to our knowledge in Refs. [38, 48, 49]. Ref. [38] uses it only implicitly while constructing an effective quantum Boltzmann equation that captures prethermal-to-thermal regime for weakly interacting systems (a Boltzmann equation was also analyzed by us in Ref. [33, 18]). Ref. [48] addresses quenches from superintegrable (con-

taining additional symmetries) to post-quench noninteracting integrable models (that weakly break those symmetries). Observed prethermalization and subsequent equilibration to a GGE spanned by the conservation laws of the final model was also captured by a time-dependent GGE. Unlike in our setup, in this case integrability is preserved throughout the whole evolution and the time-dependence arises because the additional symmetries do not commute with the local conserved quantities of the final Hamiltonian. A similar condition also applies for [49], which studied weakly interacting integrable models with and without weak integrability breaking and showed that mean-field equation capture the dynamics at intermediate times. Technically, the formulation used in Refs. [48, 49] appears to be different from ours.

In the following, we will first introduce our model, a Heisenberg model with small perturbations described by Lindblad operators. Then we derive equations of motion for a time-dependent GGE and similar equations for block-diagonal density matrices. We then compare three types of approaches: the exact evolution of the density matrix, an approximate time-evolution in the subspace of block-diagonal density matrices and the evolution described by truncated GGEs.

9.2 Model

we state that we will work only in the model below. why was it chosen so - unknown We consider the one-dimensinal spin-1/2 Heisenberg model

$$H_0 = J \sum_j \boldsymbol{S}_j \cdot \boldsymbol{S}_{j+1} \tag{9.1}$$

arguably the most studied integrable system. In [26] we investigated the case where a Heisenberg model was coupled to Hamiltonian perturbations arising from phonons and oscillating fields. This situation was, however, too complicated for a detailed numerical study on the validity of GGEs. Therefore we consider a numerically more tractable case and describe the (weak) integrability breaking by the coupling to non-equilibrium Markovian baths described by Lindblad dissipators $\hat{\mathcal{D}}^{(i)}$ acting on the density matrix ρ prepared at time $t = 0$ in some initial $\rho(0)$

$$\begin{aligned} &\partial_t \rho = (\hat{\mathcal{L}}_0 + \hat{\mathcal{L}}_1)\,\rho \\ &\hat{\mathcal{L}}_0 \rho = -i[H_0, \rho], \qquad \hat{\mathcal{L}}_1 \rho = \epsilon \left(\gamma \hat{\mathcal{D}}^{(1)} + (1-\gamma)\hat{\mathcal{D}}^{(2)}\right) \rho \end{aligned} \tag{9.2}$$

with

$$\hat{\mathcal{D}}^{(i)} = J \sum_k \left(L_k^{(i)} \rho L_k^{(i)\dagger} - \frac{1}{2} \{ L_k^{(i)\dagger} L_k^{(i)}, \rho \} \right) \tag{9.3}$$

where L_k are so-called Lindblad operators and the prefactor J has been included to obtain a dimensionless ϵ. As Lindblad operators we chose

$$L_k^{(1)} = S_k^z \quad \text{and} \quad L_k^{(2)} = \frac{1}{2}(S_k^+ S_{k+1}^- + i S_{k+1}^- S_{k+2}^+) \tag{9.4}$$

$L_k^{(1)}$ represents dephasing and, considered alone, heats up the system to an infinite temperature state. $L_k^{(2)}$ has been chosen to break all relevant symmetries (up to S^z conservation) as we want to study below the generation of heat currents. It also provides a cooling mechanism. We have checked that similar agreement is also obtained for other Lindblad operators. Our analysis will be performed as a function of the relative strength of both terms, $\gamma \in [0, 1]$. Using the conservation of the total magnetization S^z, we study in the following only the sector with $S^z = 0$.

Here we choose a Lindblad setup for convinience since it allows to determine the zeroth order of the non-equilibrium steady state (NESS) density matrix in first order of perturbation theory in ϵ.
(???)

9.3 Time-dependent generalized Gibbs ensembles

The main goal of our paper is to provide numerical evidence for the following claim: The time evolution of a translationally-invariant integrable many-particle system not only for the stated model?? in the presence of weak integrability-breaking perturbation is generically described by a generalized Gibbs ensemble

$$\lim_{\epsilon\to 0}\rho(t) \overset{\text{loc}}{=} \rho_{GGE}(t) \quad \text{for } t=\frac{1}{\epsilon J}\tau \tag{9.5}$$

$$\rho_{GGE}(t) = \frac{e^{-\sum_i \lambda_i(t) C_i}}{\mathrm{Tr}[e^{-\sum_i \lambda_i(t) C_i}]} \tag{9.6}$$

where C_i are the (quasi-)local conservation laws of the integrable system [52, 48]. Eq. (9.5) holds only in the thermodynamic limit and the $\overset{\text{loc}}{=}$ symbol is used to indicate that it applies only to local observables A for which $\lim_{\epsilon\to 0}\mathrm{Tr}[A\,\rho(t)] = \mathrm{Tr}[A\,\rho_{GGE}(t)]$. We assume that at $t=0$ the dynamics is switched on and we have introduced the dimensionless time $\tau>0$ to indicate that the relation holds only for times of the order of $1/\epsilon$ and larger. The $\lambda_j(t)$ are determined from Eq. (9.8) derived below. For the validity of Eq. (9.5) we furthermore demand that Eq. (9.8) is well-behaved, leading to a unique steady state, see below.

In the limit $\tau \ll 1$ (with $\tau/\epsilon \gg 1$ such that $t \gg 1/J$), the effect of the perturbation can be ignored and one recovers the standard quench problem for an integrable system, for which the emergence of a GGE has been firmly established, see e.g. [2] I'll study this article if needed. sounds important. The initial values of the $\langle C_i\rangle = \mathrm{Tr}[C_i\,\rho(0)]$ determine the value of the initial Lagrange parameters $\lambda_j(\tau\to 0)$. This regime is closely associated to the so-called prethermalization plateau, where approximate conservation laws fix a transient state before perturbations set in, see e.g. [41]. The dynamics for $\tau>0$ is the focus of our study.

Derivation 1

I'LL THINK A LOT ABOUT IT LATER

The dynamics of the Lagrange parameters is obtained by demanding that

$$\mathrm{Tr}[C_i\,\dot\rho(t)] \overset{!}{=} \mathrm{Tr}[C_i\,\dot\rho_{GGE}(t)] \tag{9.7}$$

up to corrections which vanish for small ϵ. Approximating on the left-hand side of the equation $\dot\rho = (\hat{\mathcal{L}}_0+\hat{\mathcal{L}}_1)\rho \approx (\hat{\mathcal{L}}_0+\hat{\mathcal{L}}_1)\rho_{GGE} = \hat{\mathcal{L}}_1\rho_{GGE}$ and using $\dot\rho_{GGE}(t) = -\sum \dot\lambda_j \rho_{GGE}(t)\,(C_j - \langle C_j\rangle_{GGE})$ with $\langle A\rangle_{GGE} = \mathrm{Tr}[A\,\rho_{GGE}(t)]$ on the right-hand side, one obtains a simple differential equation

$$\dot\lambda_i = F_i(t) \tag{9.8}$$

where the generalized forces $F_i(t)$ are functions of $\lambda_j(t)$ obtained from

$$\begin{aligned} F_i(t) &\approx -\sum_j (\chi(t)^{-1})_{ij}\mathrm{Tr}[C_j\hat{\mathcal{L}}_1\rho_{GGE}(t)] \\ &= -\sum_j (\chi^{-1})_{ij}\langle \dot C_j\rangle_{GGE} \\ \chi_{ij}(t) &= \langle C_iC_j\rangle_{GGE} - \langle C_i\rangle_{GGE}\langle C_j\rangle_{GGE} \end{aligned} \tag{9.9}$$

Note that the forces F_i are of order ϵ (correction to Eq. (9.8) are of order ϵ^2). Therefore the time evolution after the initial prethermalization is slow and set by a time scale of order $1/\epsilon$. More precisely, this is valid for perturbations of the Lindblad type studied in this paper. For Hamiltonian perturbations, the linear order perturbation theory vanishes. As is well-known from Fermi's golden rule, transition rates arise only in second order perturbation theory. The formulas given above can easily be generalized to this case, see Methods section of Ref. [26].

Derivation 2

I'LL THINK A LOT ABOUT IT LATER

An alternative, slightly more formal derivation of Eq. (9.8) is obtained by setting $\rho(t) = \rho_{GGE}(t) + \delta\rho(t)$ where $\rho_{GGE}(t)$ has to be chosen in such a way that $\delta\rho \sim \epsilon$ vanishes in the limit $\epsilon \to 0$. The essential idea is now to separate the slow dynamics within the GGE manifold arising from $\hat{\mathcal{L}}_1 \sim \epsilon$ from the fast dynamics in the perpendicular space. One therefore introduces a projection operator [18, 36, 37, 38, 42, 43]

$$\hat{P}(t)X := -\sum_{i,j} \frac{\partial \rho_{GGE}(t)}{\partial \lambda_i} (\chi(t)^{-1})_{ij} \mathrm{Tr}[C_j X] \tag{9.10}$$

which projects density matrices onto the space tangential to the GGE manifold, spanned by $\partial\rho_{GGE}(t)/\partial\lambda_i$. We apply $\hat{P}(t)$ to Eq. (9.2) and use that $\hat{P}(t)\dot{\rho}_{GGE}(t) = \dot{\rho}_{GGE}(t)$, $\hat{\mathcal{L}}_0\rho_{GGE} = 0$, $\hat{P}(t)\hat{\mathcal{L}}_0\delta\rho = 0$, and $\hat{\mathcal{L}}_1\delta\rho \sim \epsilon^2$. From this we obtain

$$\hat{P}(t)\delta\dot{\rho} + \dot{\rho}_{GGE} = \hat{P}(t)\hat{\mathcal{L}}_1\rho_{GGE} + \mathcal{O}(\epsilon^2) \tag{9.11}$$

Demanding that $\hat{P}(t)\delta\dot{\rho}$ is of order ϵ^2 leads to $\dot{\rho}_{GGE} = \hat{P}(t)\hat{\mathcal{L}}_1\rho_{GGE}$ which is equivalent to Eq. (9.8).

The arguments given above, strongly suggest that the GGE ansatz fulfills the time evolution equation (9.2) projected on the conservation laws up to corrections of order ϵ^2. This does, however, not yet guarantee the validity of the much stronger claim that the time-dependent GGE is also valid in the long-time limit. For this we have to demand that errors don't pile up during time evolution but decay exponentially. This is the case in situations where Eq. (9.8) predicts a unique and stable steady state, see Appendix 9.8. In all examples considered by us so far, we have never found that this condition is violated.

We will show that in practical implementations it is not necessary to take all $O(N)$ (quasi-)local conservation laws into account. Accurate results can already be obtained for a truncated GGE (tGGE), including only a small number of approximately conserved quantities and Lagrange parameters. I'll see, how???

9.4 Time-dependent block-diagonal density matrices

The GGE approach is only valid in the thermodynamic limit where the (quasi-)local approximately conserved C_i determine the dynamics. For smaller systems, one has, however, to take into account that the set of conservation laws of H_0 is much larger, and given by $\mathcal{Q} = \{|n\rangle\langle m|$ with $E_n^0 = E_m^0\}$ where $|n\rangle$ and $|m\rangle$ are eigenstates of H_0 with the same energy. Note that the elements of $\mathcal{Q}$ are in general non-commuting and highly non-local operators. In the limit of small ϵ, one can, however, derive the dynamics in the space spanned by the elements of $\mathcal{Q}$. Such approaches are well described in literature [43] and we briefly sketch the relevant formulas, emphasizing the analogy to the GGE approach. So, I'll just study later [43]. Didn't learn it yet from there...

The role of the GGE density matrix is taken over by the block-diagonal density matrix

$$\rho_{BD}(t) = \sum_{E_n=E_m} \lambda_{nm}(t)\, |n\rangle\langle m| \tag{9.12}$$

with normalization $\sum_n \lambda_{nn} = 1$. In analogy to Eq. (9.7), we demand that $\mathrm{Tr}[|m\rangle\langle n|\, \dot\rho(t)] \stackrel{!}{=} \mathrm{Tr}[|m\rangle\langle n|\, \dot\rho_{BD}(t)]$ up to corrections vanishing for $\epsilon \to 0$. Using $\dot\rho(t) \approx \hat{\mathcal{L}}_1 \rho_{BD}(t)$, we obtain a linear (!) differential equation for $\lambda_{nm}(t)$

$$\dot\lambda_{nm}(t) = \sum_{E_{n'}=E_{m'}} M_{nm,n'm'}\, \lambda_{n'm'}(t) \tag{9.13}$$

where M is an effective Liouvillian acting on the space of block-diagonal density matrices ($E_n = E_m$, $E_{n'} = E_{m'}$)

$$M_{nm,n'm'} = \mathrm{Tr}[\, |m\rangle\langle n|\, \hat{\mathcal{L}}_1\, |n'\rangle\langle m'|\,] \tag{9.14}$$

M is linear in ϵ and therefore all ϵ dependence can be absorbed in a rescaling of the time axis within this approximation which is valid only for small ϵ and covers the dynamics after prethermalization. The initial condition for the time evolution is simply set by $\lambda_{nm}(0) = \langle n|\rho(0)|m\rangle$.

Compared to the GGE approach which uses only a few (maximally $O(N)$) Lagrange parameters, the block-diagonal matrix uses $O(2^N)$ parameters and is therefore much less efficient. For $N = 14$ and $S^z = 0$ we have to use 6752 parameters where does this number come from?. The block-diagonal approach is, however, numerically much more efficient than an approach using the full density matrix which has $O(4^N)$ parameters.

9.5 Numerical Results

To test the validity of the GGE approach we have to face the problem that the GGE approach is only valid in the thermodynamic limit what is this limit??? while the exact results for driven nonequilibrium systems at finite ϵ can only be obtained for tiny systems. We therefore use the following two-step approach: We first show numerically that for small systems ($N = 8$) the numerically exact results obtained from the exact time-dependent density matrices for small ϵ are well-described by time-dependent block-diagonal density matrices. We then compare for larger systems (up to $N = 14$) the block-diagonal density matrices to truncated GGEs based on only a small number of approximately conserved quantities.

9.5.1 Time evolution for small systems

As an initial state, we consider a classical Néel configuration. In Fig. 9.1 we show the time evolution of the nearest-neighbor spin correlation, $\langle \sigma_i^z \sigma_{i+1}^z \rangle$, and of the heat current,

$$J_H = J^2 \sum_j (\boldsymbol{S}_j \times \boldsymbol{S}_{j+1}) \cdot \boldsymbol{S}_{j+2} \tag{9.15}$$

for a small system with $N = 8$ sites. why this formula is such?

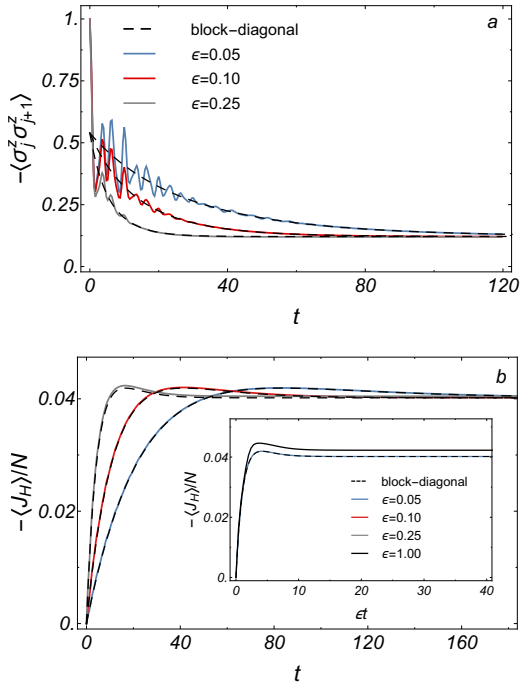

Figure 9.1: Exact time evolution of a weakly perturbed Heisenberg model ($N = 8$, $\gamma = 0.8$, $J = 1$) for three small values of ϵ. The dashed lines show the result for the time evolution of the block-diagonal density matrix using Eqs. (9.12,9.13). (a) Decay of the nearest-neighbor spin-correlation. (b) For the heat current rapid oscillations on a time scale of order $1/J = 1$ are absent as J_H is a conservation law of H_0. For the values of ϵ shown in the plot the dashed lines follow the solid lines: the block-diagonal density matrices correctly describe the time evolution with high precision. Inset: At large $\epsilon = 1.0$ discrepancies are visible.

We compare the numerically exact results, calculated from the exact density matrix evolution, to the approximate results based on the block-diagonal density matrix. Starting from 1 at $t = 0$ the spin correlation rapidly decays on a time scale of order $1/J = 1$ to a value around 0.45. Due to the smallness of the system, rapid oscillations persist and get only slowly damped. Subsequently both the average value of the spin-correlation and the oscillations decay on a time scale set by $1/\epsilon$. The block-diagonal density matrix correctly captures the decay of the spin-correlations quantitatively. The time-dependence of the heat current, in contrast, is much smoother as the heat current is a conserved quantity, $[J_H, H_0] = 0$. The initial state has not heat current but a large heat current builds up on a time scale set by $1/\epsilon$. The heat current obtained in the long-time limit is large and the system is therefore far out of equilibrium. Its value is approximately independent of ϵ for small ϵ and is predicted by the time-dependent block-diagonal density matrices and the GGE approach, see below. The main result of this section is, however, that for small ϵ the time evolution for times large compared to $1/J$ is accurately described by the block-diagonal ensemble.

9.5.2 Time evolution of truncated GGE

For a system with $N = 14$ sites, we compare in Fig. 9.2 the time evolution of the block-diagonal ensemble with the results obtained for a truncated GGE based on only $N_c = 4$ conserved quantities, $C_2, \ldots, C_5$, where $C_2 = H_0$ is the Hamiltonian, $C_3 = J_H$ is the heat current and $C_4 = [O_b, C_3]$, $C_5 = [O_b, C_4]$ are conservation laws involving products of 4 and 5 spins. Here $O_b = -i\sum_j j\boldsymbol{S}_j \cdot \boldsymbol{S}_{j+1}$ is the so-called boost operator [52]. $C_1 = S^z$, the total spin in z-direction, does not play a role in our study which focuses on the $S^z = 0$ sector. The heat

current operator C_3 and C_5 have the same symmetry properties. Despite of the rather small system size, the small number of conservation laws and the omission of quasi-local conservation laws [47, 48], a surprisingly accurate description of the time evolution is obtained. Note that the block-diagonal matrix approach keeps track of 6752 approximately conserved quantities to be compared to just 4 approximately conserved quantities in the truncated GGE!

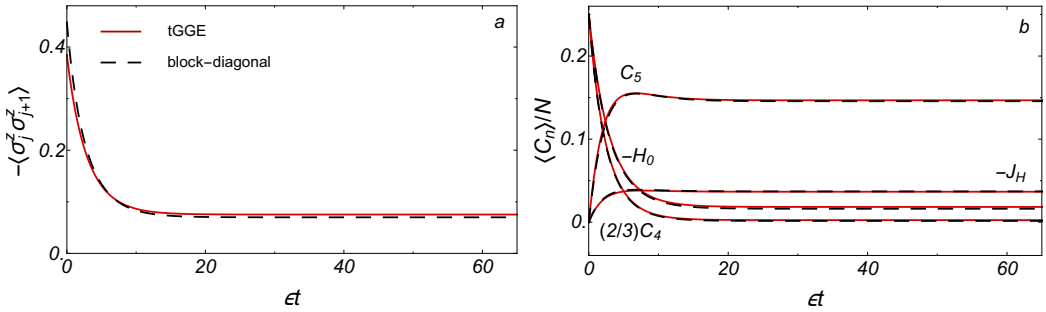

Figure 9.2: Comparision of the results obtained from the truncated GGE (solid line) and the block-diagonal density matrix (dashed). (a) Antiferromagnetic nearest neighbor spin correlations, (b) Approximate conservation laws, C_5, $-J_H$, $-H_0$, and $(2/3)C_4$. All quantities change on a time scale of order $1/\epsilon$. Parameters: $\gamma = 0.8$, $J = 1$, $N = 14$.

The largest discrepancies are visible for the spin-spin correlation function at $t = 0$. Note that this limit is completely independent of the integrability breaking perturbations. It only tests whether diagonal ensemble and GGE coincide after a quantum quench of the pure Heisenberg model. It therefore tests the ability of the GGE to describe the steady state after a quantum quench in an integrable system. Many previous numerical and analytical studies have shown that for this problem the GGE approach applies, e.g. [2, 15, 66].

The lower panel of Fig. 9.2 shows the time evolution of the conserved quantities. In this case by construction the value at $t = 0$ are the same for the truncated GGE and the block-diagonal approach. All conserved quantities change on time scales of order $1/\epsilon$ compared to their prethermalized value and show an exponential decay towards their steady-state value. Note that features like the small overshooting of C_5 at intermediate times are well reproduced by the numerical approach.

Let us remind that $\hat{\mathcal{L}}_1\rho = \epsilon\left(\gamma\hat{\mathcal{D}}^{(1)} + (1-\gamma)\hat{\mathcal{D}}^{(2)}\right)\rho$. The agreement obtained for $\gamma = 0.8$ in Fig. 9.2 is also observed for other values of the parameter γ controlling the nature of the dissipative terms. This is shown in Fig. 9.3, where the steady-state value of the conservation laws is shown as function of γ. The largest deviations are visible for γ close to 1.

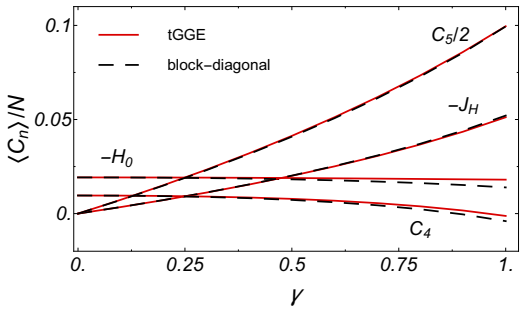

Figure 9.3: Expectation values of conservation laws in the stationary state ($t \to \infty$) as a function of γ, which controls the nature of the dissipative terms ($N = 14$, $J = 1$). As in Fig. 9.2, a comparison of the truncated GGE (solid lines) the block-diagonal density matrix (dashed) is shown. For $\gamma = 0$ the system heats up to infinite temperatue and all conservation laws vanish in the thermodynamic limit. Due to finite size effects small finite values are obtained form H and C_4.

9.5.3 Finite-size, finite-ϵ, and truncation effects

Formally, the description of the driven many-particle quantum system by a time-dependent GGE is only accurate in the limit of weak perturbations, $\epsilon \to 0$, for large systems, $N \to \infty$, and taken all (quasi-)local conservation laws into account, $N_c \to \infty$. The results presented above already suggest that one can, nevertheless, obtain surprisingly accurate results for moderate values of ϵ, rather small system sizes and a tiny number of conservation laws.

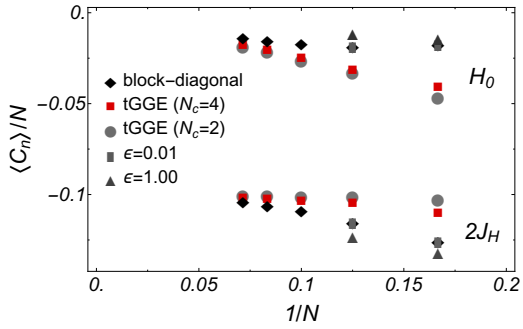

Figure 9.4: Steady-state expectation value of the energy, $\langle H_0 \rangle$, and the heat current, $\langle J_H \rangle$, as function of the inverse system size, $1/N$ ($N = 6, 8, 10, 12, 14$), for the truncated GGE with 2 and 4 conservation laws and the block-diagonal ensemble. For the smallest system size, $N = 6, 8$, we also show the exact results for $\epsilon = 0.01$, which practially coincides with the the block-diagonal ensemble, and for $\epsilon = 1.0$ ($\gamma = 1$). so ϵ doesn't matter much??

In Fig. 9.4 the expectation value of the energy density and the heat current in the steady state ($t \to \infty$) are shown as function of $1/N$ for the exact density matrix, for the block-diagonal ensemble (exact for $\epsilon \to 0$) and for two truncated GGEs with $N_c = 2$ and $N_c = 4$. One clearly sees that in the thermodynamic limit the truncated GGEs become more and more accurate. Already for the largest system ($N = 14$) for which we were able to evaluate the block-diagonal ensemble, a satisfactory agreement is obtained. Also $N_c = 4$ is more accurate than $N_c = 2$ but the errors arising from finite-size effects are dominating. We are therefore not showing results for larger values of N_c as those are spoiled by finite-size effects which tend to become more severe for more complicated approximate conservation laws which involve a large number of neighboring spins.

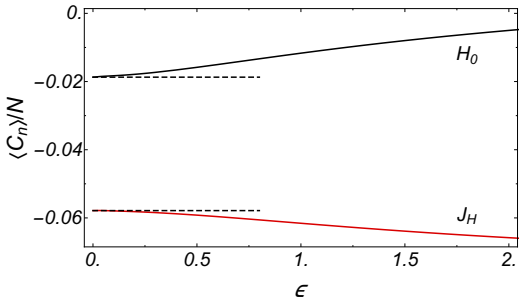

Figure 9.5: Steady-state expectation value of the energy, $\langle H_0 \rangle$, and the heat current, $\langle J_H \rangle$ as function of the strength ϵ of the integrability-breaking Lindblad terms ($N = 8$, $J = 1$, $\gamma = 1$). For $\epsilon \to 0$ the result of the block-diagonal ensemble (dashed line) is recovered.

The effects of finite ϵ for steady-state expectation values are displayed in Fig. 9.5 for $N = 8$. We find that the ϵ dependence of the steady state is not strongly pronounced and is described by a smooth function. In the $\epsilon \to 0$ limit the block-diagonal ensemble is exact (as expected from the analytical arguments). It also captures with high accuracy the properties for small ϵ.

The results obtained in the limit $\epsilon \to 0$ can be systematically improved using perturbation theory in ϵ, developed for the steady state in Ref. [18]. Here it is important to distinguish the perturbation theory for finite size systems (ϵ smaller than the dimensionless level-spacing $1/N$ or even 2^{-N}) from the perturbation theory in the thermodynamic limit ($1/N \ll \epsilon \ll 1$). The numerical results show indeed a different behavior in the regime $\epsilon \lesssim 0.1$ and $0.1 \lesssim \epsilon \lesssim 1$ but the system size is too small to extract reliable results for the perturbation theory in the thermodynamic limit. A more detailed discussion of this issue can be found in the Appendix 9.7.

9.6 Conclusion and Outlook

We have demonstrated that time-dependent generalized Gibbs ensembles can be used to describe quantitatively the dynamics of approximately integrable systems where small perturbations drive the system far from equilibrium. While the present study has focused on perturbations arising from Lindblad operators describing the coupling to Markovian baths, it can also be used to investigate Hamiltonian perturbations. Our example, a Heisenberg model coupled to two types of Lindblad disspators was chosen for numerical convenience but one can think of a wide range of experimental systems where our approach is applicable. In practically all cold-atom experiments there are atomic loss processes. An interesting question is therefore how atomic loss processes affect experimental ultracold-atom realization integrable models, e.g., of the fermionic Hubbard model in one dimension. It is reasonable to assume that the loss processes will activate some of the exotic conservation laws of this model. An experimental setup, particularly suitable for our theoretical proposal, is also that of trapped ions where openness can be directly simulated [44] by realizing Lindblad driving [8], currently using a few tens of atoms [60]. Another interesting class of systems are spin-chain materials, well-described by one-dimensional Heisenberg models. Here phonons and the coupling to lasers take over the role of the integrability breaking perturbations. We have studied steady-state properties of such models in Ref. [26].

We have used exact diagonalization of Lindblad operators to compare the time-dependent GGE approach to exact results. A main advantage of the time-dependent GGE approach is that it can be combined with other, more powerful numerical approaches how????. For Markovian dynamics it is sufficient to evaluate simple expectation values of operators to calculate effective forces. Many different numerical or analytical methods can therefore be used to obtain the non-

equlibrium dynamics. This includes Monte-Carlo approaches, transfer-matrix DMRG methods, or high-temperature expansions. For the model considered by us all Lagrange parameters remain rather small during time evolution. Therefore it should be possible to calculate the dynamics of a truncated GGE using a rather straightforward high-temperature expansion (or, more precisely, small-Lagrange-parameter expansion) directly in the thermodynamic limit, $N = \infty$.

There are many interesting open question. For example, the solution of the rate equation for the analyzed Lindblad driving, Eq. (9.8), shows a simple exponential relaxation to a single steady state. Out of equilibrium, however, other types of behavior can also occur: several steady states, cyclic solutions, or even chaotic solutions. It is an interesting open question how our approach has to be modified in these cases. Another interesting class or problems concern situations which are not translationally invariant and where Lagrange parameters depend on space and time. For exactly integrable models such a hydrodynamics description has recently be developed [10, 9, 63], and we expect that it can be generalized in a straightforward way to models where integrability is broken by small perturbations which drive the system out of equilibrium.

9.7 Perturbation theory for steady state

We have argued that in the limit of small but finite perturbation strength ϵ a time-dependent GGE or an approach based on block-diagonal density matrices correctly describes both the dynamics and the steady state of the perturbed integrable model.

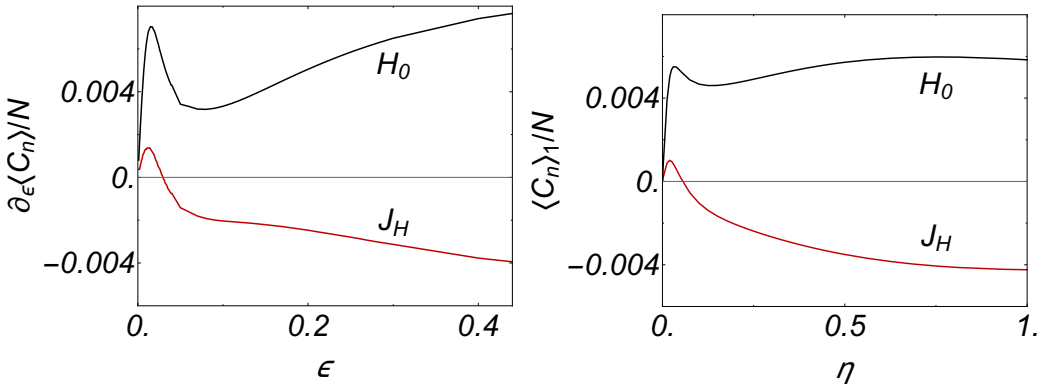

Figure 9.6: Left panel: Derivative of energy and heat current, $\frac{d\langle H\rangle}{d\epsilon}$ and $\frac{d\langle J_H\rangle}{d\epsilon}$, as function of the strength of perturbation ϵ calculated for $\gamma = 1$, $J = 1$ and $N = 8$. Right panel: Calculation of the coefficient linear in ϵ from perturbation theory [18] as function of the broadening η for the same parameters.

In this Appendix we discuss the leading order correction to the steady state for finite ϵ. In Ref. [18] we have shown how one can formulate a perturbation theory in powers of ϵ around such a state. Here it is important to distinguish the perturbation theory in the thermodynamic limit from the perturbation theory for finite-size systems. The latter is only valid for ϵ small compared to the level spacing $\Delta = \delta J$ of the system, where δ is the dimensionless level spacing. We are mainly interested in the opposite limit $\delta \ll \epsilon \ll 1$.

As is well known from standard perturbation theory (Kubo formula) it is essential to include a small imaginary decay rate $i\eta$ in all calculations. For $\eta \ll \Delta$ one recovers the perturbation theory for a finite-size system while in the thermodynamic limit one choses $\eta \gg \Delta$ but smaller than all other relevant energy scales.

As our goal is to compare numerically exact results with the formulas of Ref. [18], we have to face the problem that exact results are only available for rather small system sizes and therefore the regime $\delta \ll \epsilon \ll 1$ and $\Delta \ll \eta \ll J$ are difficult to achieve.

As we are interested in the correction linear in ϵ, we plot in Fig. 9.6 (left panel) the derivative of energy and heat-current, $d\langle H\rangle/d\epsilon$ and $\overline{d\langle J_H\rangle/d\epsilon}$. This is compared to the perturbation theory result to linear order in ϵ (based on the formulas derived in Ref. [18]) shown in the right panel as function of the broadening η. Both panels show that the linear slope vanishes in a finite size system. For finite N and in the steady state the leading correction is of order ϵ^2/δ. In the analytic treatment this can be shown by observing that the corrections to the steady state are proportional to the imaginary part of $\frac{1}{E_n - E_m - i\eta}$ with $E_n \neq E_m$ [18] which vanishes for $\eta \ll \Delta$.

In the thermodynamic limit, $1 \gg \epsilon \gg \delta$, we expect instead that a linear correction does exist. Unfortunately, we cannot extract a well-defined linear slope from the exact result shown in Fig. 9.6 (left panel) due to the small size of the system. The same issue arises also in the dependence of the perturbative result of η. The fact that qualitatively similar results are obtained for the η and ϵ dependencies is not an accident but reflects that the Lindblad coupling effectively leads to a broadening of levels.

In conclusion, our analysis has shown that it is very important to distinguish perturbations for finite size systems and in the thermodynamics limit. At least semi-quantitatively, the analysis also confirms the perturbative approach suggested in Ref. [18].

9.8 Effective forces and γ dependence of steady-state expectation values

In Fig. (9.7) we show the effective forces which determine the dynamics of the time-dependent GGE according to Eq. (9.8). For the chosen Lindblad dynamics we find that the system is always attracted to a unique, well-defined fixed point. Therefore also small errors in, e.g., the initial state do not grow over time but are damped out.

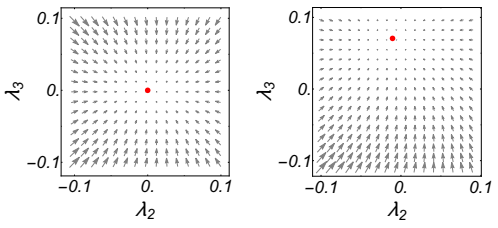

Figure 9.7: Effective force field (F_2, F_3) in the vicinity of the steady state (red point) in the plane spanned by the Lagrange parameters $\lambda_2 = \beta$ and λ_3 using $e^{-\beta H - \lambda_3 J_H}$ as an ansatz for ρ_{GGE} $(N = 8)$. Left: For $\gamma = 0$ the system approaches an infinite temperature state since the Lindblad operator $L^{(1)}$ is constantly heating the system up. Right: At $\gamma = 1$ the system is attracted towards a non-equilibrium state with finite stationary values of both λ_2 and λ_3.

In Fig. (9.8) we show the steady-state expectation value of the energy and the heat current as function of γ. The figure shows that the block-diagonal density matrix quantitatively describes for all values of γ the steady state for moderate values of ϵ.

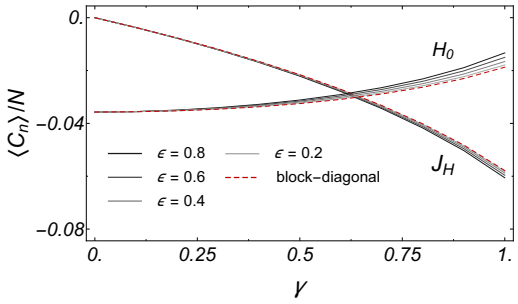

Figure 9.8: Steady state expectation values of the energy and the heat current J_H as a function of γ parametrizing the type of Markovian coupling. For a system of $N = 8$ sites the steady state is shown at $J = 1$ for several values of ϵ and also for the limit $\epsilon \to 0$ where the block-diagonal ensemble becomes exact.

10 Thermalization at Low Temperatures via Weakly-Damped Multi-Site Baths by Zanoci, Yoo, Swingle

Abstract

We study the thermalization properties of one-dimensional open quantum systems coupled to baths at their boundary. The baths are driven to their thermal states via Lindblad operators, while the system undergoes Hamiltonian dynamics. We specifically consider multi-site baths and investigate the extent to which the late-time steady state resembles a Gibbs state at some controllable temperature set by the baths. We study three models: a non-interacting fermion model accessible via free-fermion technology, and two interacting models, the XZ model and the chiral clock model, which are accessible via tensor network methods. We show that, by tuning towards the weak coupling and slow relaxation limits, one can engineer low temperatures in the bulk of the system provided the bath size is big enough. We use this capability to study energy transport in the XZ model at lower temperatures than previously reported. Our work paves the way for future studies of interacting open quantum systems at low temperatures.

10.1 Introduction

Open many-body quantum systems are fundamentally different from closed systems and their dynamics displays a wide variety of phenomena not found in equilibrium setups [1]. For instance, current-carrying non-equilibrium steady states play a major role in deriving the transport properties of the system [2]. The coupling to an environment can also significantly alter existing properties of the system, such as its phase of matter [46, 4, 5]. Despite their rich physics, open systems remain vastly understudied, due to both computational and conceptual challenges associated with describing the quantum many-body system and modeling its interaction with the environment.

Quantum many-body systems are inherently difficult to study due to the exponential growth of their Hilbert space with system size. The computational complexity is further increased for open systems, since we are now dealing with density matrices, instead of wavefunctions. Additional care is necessary to preserve the positivity and hermiticity of the state. We therefore require methods that are specifically tailored to this setup [6]. Some of the most popular choices include tensor networks [7, 8, 9, 10, 11], quantum trajectories [12], and neural networks [13, 14, 15, 16, 17, 18]. In the context of one-dimensional systems, matrix product state methods [19,

20, 21, 22, 23, 24, 25] have proven particularly powerful for describing large-scale open systems. However, even these techniques can suffer from slow convergence to the steady state if the open system dynamics are not properly designed.

Efficiently modeling the system's interaction with the environment remains a major challenge within the field. One way to approach this problem is by viewing the target system together with the infinitely large environment as a closed system undergoing Hamiltonian evolution. The evolution of the target system is then recovered by tracing out the environment degrees of freedom. However, the resulting master equations are usually non-local in time and involve a complicated memory kernel [26, 27, 1]. The master equation simplifies significantly within the Born-Markov approximation, leading to the Redfield equation [28], which is unfortunately not guaranteed to preserve the positivity of the density matrix. A further secular approximation is necessary to mitigate this problem, resulting in a global Lindblad master equation [29, 43, 1]. Nevertheless, identifying the correct global Lindblad operators leading to the desired dynamics can be computationally impractical for large systems, since it usually requires knowledge of the full energy eigenbasis.

Due to these limitations, the majority of studies on open many-body quantum systems rely on a local Lindblad description of the dynamics. In this approach, the interaction with the environment is modeled by Lindblad jump operators acting locally on the boundary of the system [31, 32, 33, 34, 35, 36, 37, 38, 39, 40, 41], such that the bulk dynamics is still coherent and governed by the system's Hamiltonian. In the thermodynamic limit, the bulk properties should not depend on the details of the boundary driving, given that the system is sufficiently ergodic. However, the local Lindblad equation can sometimes fail to describe the correct steady state, as reported for integrable systems [32, 39], in the weak coupling limit [42, 43, 44, 45, 46], and in the presence of multiple baths [47, 48]. Moreover, it is also not clear whether the boundary driving can thermalize the system to arbitrarily low temperatures.

The issue of thermalization in open quantum systems has been previously studied in Ref. [49], in the context of both interacting and non-interacting fermionic systems with particle number conservation. Their results, based on a perturbative expansion in the limit of zero system-bath coupling, suggest that both models thermalize if the baths are infinitely large and weakly damped. In this paper, we extend these results to strongly interacting spin chains, whose steady states admit a tensor network representation. Furthermore, we show that a system coupled to a thermal bath at its boundary typically reaches a temperature far above the one imposed by the bath. We then pinpoint the conditions under which the system thermalizes to the desired bath temperature.

We consider three different one-dimensional systems in our analysis. The first one is the complex Sachdev-Ye-Kitaev (SYK) model describing fermions with random all-to-all 2-body interactions [50, 51, 52, 53, 54, 55, 56, 57, 58, 59, 60, 61]. This Hamiltonian is quadratic in the fermionic operators and its steady state can be computed exactly [11, 63]. We use this model to test the validity of the previous results and to determine the conditions under which the system can be cooled to low temperatures by an external bath. The second system is described by a spin-1/2 XZ Hamiltonian in a transverse field [64]. This model is interacting and non-integrable, and we expect its behavior to be fairly representative of one-dimensional gapped systems. Finally, the third model is known as the chiral clock model and can be tuned to a gapless non-integrable quantum critical point [65, 66, 67, 68, 69, 70, 71, 72, 73, 74, 75, 76, 77]. In the absence of an analytical solution, the steady states for both of these models are computed via tensor network methods [19, 20, 68, 69, 80]. The final temperature of the system is extracted using our previously developed thermometry technique [41].

Our results show that the system thermalizes even at low temperatures, as long as the bath is extremely large, weakly coupled to the system, and infinitely damped, in agreement with previous findings [49, 81]. In practice, however, taking these limits is often unnecessary. We

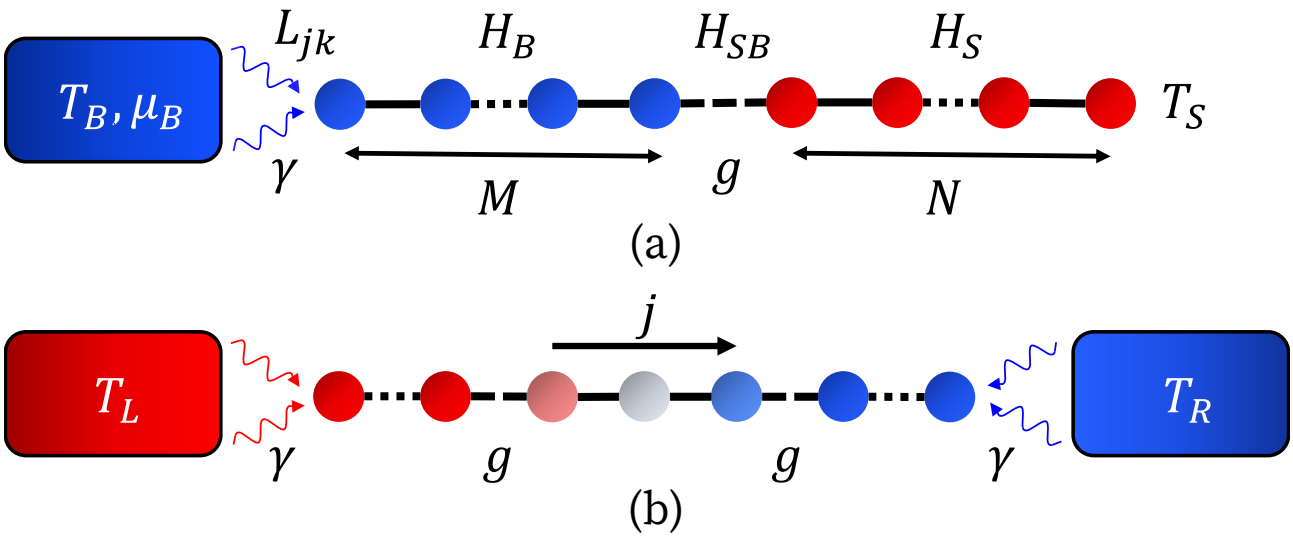

Figure 10.1: Schematic diagram of our (a) thermalization and (b) transport setups. The system is connected to baths at its boundary. The Lindblad operators L_{jk} drive the baths to their thermal states. In non-equilibrium, a homogeneous current j flows through the bulk of the system.

find that convergence to within 1% of the target bath temperature can already be achieved with leads that are a fraction of the system size by lowering the system-bath coupling g and the bath driving strength γ by an order of magnitude. This observation has important implications for models whose dynamics is not exactly solvable, where we rely on approximate time-evolution methods to find the steady state.

As an immediate practical application, we study energy transport by attaching two boundary baths and imposing a temperature gradient across the system. The temperature bias is small, such that the system is only weakly perturbed from equilibrium. This results in a constant energy gradient and current across the chain. By adjusting the average bath temperature, we are able to extract the temperature dependence of the transport coefficients. In particular, we focus on the low-temperature behavior of the diffusivity in the XZ model and are now able to reach regimes that were previously inaccessible with conventional open system setups [41]. We find that the energy diffusivity increases exponentially at low temperatures, in agreement with the predictions of a semi-classical kinetic theory for gapped systems [82, 83, 41].

The ultimate limiting factor in our study is the minimal temperature below which the baths can no longer reliably cool the system on the timescales accessible numerically. We conjecture that this temperature is set by the smallest energy scale in the problem – either the model's gap or its interaction strength. Other methods beyond the Lindblad master equation might be able to circumvent this limitation.

The outline of this paper is as follows. In Sec. 10.2 we present our open system setup and describe some key properties of the steady states and the relaxation dynamics towards them. In Sec. 10.3 we introduce our models and show the thermalization results for each of them. We also analyze the low-temperature transport properties of the XZ model. Finally, we comment on our findings and discuss possible extensions in Sec. 10.4.

10.2 Setup

We begin by presenting the general setting of our thermalization studies, which is depicted in Fig. 23.1(a). The setup consists of a system S of size N coupled to a bath B of size M at

its boundary. The environment only acts upon the bath. The full Hamiltonian is given by

$$H = H_S + H_B + gH_{SB}, \tag{10.1}$$

where H_S, H_B, and H_{SB} are the Hamiltonians describing the system, bath, and their interaction, respectively, while g is a dimensionless parameter controlling the system-bath coupling strength. The state of the entire open quantum system at time t is characterized by its density matrix $\rho(t)$. The evolution of this density matrix is governed by the local Lindblad equation [29, 43]

$$\frac{d\rho}{dt} = \mathcal{L}(\rho) \equiv -i[H,\rho] + \sum_{jk}\left(L_{jk}\rho L_{jk}^\dagger - \frac{1}{2}\{L_{jk}^\dagger L_{jk},\rho\}\right), \tag{10.2}$$

where L_{jk} are jump operators acting only on the bath degrees of freedom and describing their interaction with the environment. These operators are chosen such that, when decoupled from the system ($g = 0$), the bath is driven to its thermal state ρ_B at temperature T_B and chemical potential μ_B. The strength of this damping introduces a new energy scale γ into the picture. A generic construction for the Lindblad operators L_{jk} that thermalize baths of any size is described in Appendix 10.5.

Initially, the system starts in an arbitrary (usually infinite temperature) state, while the bath is in its thermal state ρ_B. Once the coupling g between the two is turned on, the baths are still continuously driven towards their decoupled thermal state, but the coupling with the system causes the steady state of the bath to differ from its target thermal state. The system also begins to exchange energy and particles with the bath while converging to its steady state. The operator $\mathcal{L}$ capturing this time evolution in Eq. (10.2) is called the Liouvillian super-operator and it acts on the space of density matrices. For Lindblad equations, this map is completely positive and trace-preserving [29, 43]. The steady state ρ_∞ is given by the fixed point of this map $\mathcal{L}\rho_\infty = 0$. The relaxation time to this steady state depends on the gap in the Liouvillian spectrum. Assuming that the fixed point of the Lindblad equation is unique, the gap $\Delta_\mathcal{L}$ is equal to the negative real part of the second largest eigenvalue of $\mathcal{L}$ [11, 31, 84].

Formally, the solution of the Lindblad equation is given by the right eigenvector of $\mathcal{L}$ with eigenvalue zero. While closed-form exact solutions exist in the case of non-interacting systems [11, 63] and for certain strongly-driven interacting systems [85, 86, 87, 88, 89, 90, 91, 92, 93], one usually has to resort to approximate methods when dealing with generic interacting systems and arbitrary driving. This is because the dimensions of the Liouvillian grow exponentially with system size. In practice, it is more feasible to directly simulate the time evolution and look for a converged final state $\rho_\infty = \lim_{t\to\infty}\rho(t) = \lim_{t\to\infty} e^{\mathcal{L}t}\rho(0)$. To achieve this, we employ a tensor network representation of the density matrix [19, 20] and perform an approximate time evolution under the Liouvillian super-operator using the Time Evolving Block Decimation (TEBD) algorithm [68, 69, 80]. We represent the states and operators in vectorized form [20, 6, 1] and use a second-order Suzuki-Trotter decomposition [94] of the time-evolution operator $e^{\mathcal{L}t}$. We should mention that alternative approaches, such as variational algorithms targeting the ground state of the Hermitian operator $\mathcal{L}^\dagger\mathcal{L}$ [21, 22, 23], could also be used to find steady state ρ_∞ more directly.

The limiting factor in reaching the steady state is the size of the spectral gap $\Delta_\mathcal{L}$. If the gap is finite, the distance between the time-evolved state $\rho(t)$ and the steady state ρ_∞ will decrease exponentially in time, with a relaxation rate set by $\Delta_\mathcal{L}$. For systems that are only subject to boundary dissipation, a generic bound on the gap as a function of system size $\Delta_\mathcal{L} \lesssim 1/N$ is known [84]. In integrable systems, one typically observes a scaling $\Delta_\mathcal{L} \sim 1/N^3$, as is the case for nearest-neighbor hopping free-fermion models [84, 81]. On the other hand, for non-integrable models, one usually has a faster relaxation rate which saturates the bound $\Delta_\mathcal{L} \sim 1/N$. The gap can also be exponentially small in localized systems [84, 81]. Furthermore, perturbation

theory calculations in the limit of small system-bath coupling ($g \to 0$) or small driving ($\gamma \to 0$) reveal the following scaling [95, 84, 96]

$$\Delta_{\mathcal{L}} \sim \gamma g^2, \quad \text{as} \quad g, \gamma \to 0. \tag{10.3}$$

In practice, this implies that we cannot use traditional time-evolution methods to study the regime where these parameters are infinitesimally small, as the convergence to steady state would be prohibitively slow. It turns out that this limit is precisely the one required to observe thermalization [49]. Nevertheless, we will show in Sec. 10.3.2 that even moderate values of g and γ accessible numerically for small systems are sufficient to reach states that are close to thermal.

Once we find the steady state, we have to evaluate how well the system resembles a Gibbs state at some temperature and whether this temperature is close to the bath's driving temperature T_B. The state of the system alone is obtained by tracing out the bath degrees of freedom $\rho_S = \mathrm{tr}_B(\rho_\infty)$. Assigning a global temperature to this state requires access to reference Gibbs states of the same size, which is unfeasible for large systems. Moreover, we expect the system to deviate from thermal equilibrium near the boundary where it is coupled to the bath. Therefore, it is more suitable to assign a local temperature for different parts of the system [97, 98, 99, 100, 101, 102]. To accomplish this, we use the thermometry method introduced in Ref. [41]. The local temperature of a region A is derived by minimizing the trace distance between the reduced density matrices of that region in the steady state ρ_S^A and in a thermal state $\rho^A(T)$

$$D\left(\rho_S^A, \rho^A(T)\right) = \frac{1}{2}\mathrm{tr}\left(\sqrt{\left(\rho_S^A - \rho^A(T)\right)^2}\right). \tag{10.4}$$

The trace distance between the two states is a meaningful metric because it places an upper bound on the difference between the corresponding expectation values of any local observable [39]. We usually choose the region A to be comprised of two consecutive sites $(i, i+1)$ in the system, which is consistent with our definition of local energy. For the models we studied, we found good thermalization and a uniform local temperature away from the boundaries. Therefore, we define the temperature of the system T_S in a steady state as the local temperature at its center

$$T_S = arg\, min_T D\left(\rho_S^{\left(\frac{N}{2}, \frac{N}{2}+1\right)}, \rho^{\left(\frac{N}{2}, \frac{N}{2}+1\right)}(T)\right). \tag{10.5}$$

10.3 Results

The framework described above can in principle be applied to any system. In this work, we consider three prototypical examples of non-interacting and interacting systems in one dimension. We start with a non-interacting SYK2 model, since it has a simple description in terms of single-particle eigenstates and its steady state is exactly solvable even for large system sizes. We use this model to find the precise limits in which the bath thermalizes the system and verify that they agree with previous predictions [49]. We then extend our analysis to interacting XZ and chiral clock chains, which do not have analytical solutions, and find that the same thermalization behavior persists for these systems. Additionally, we show how to apply the lessons learned from the equilibrium setup to study low-temperature energy transport in the XZ model. Our numerical results focus on the intermediate ($T_B = 1$) and low ($T_B = 0.1$) temperatures, since we expect thermalization to be especially challenging in these regimes [41]. However, we checked that our conclusions hold for a wide range of temperatures, including the high-temperature limit. Lastly, we set $\mu_B = 0$ for the remainder of this paper.

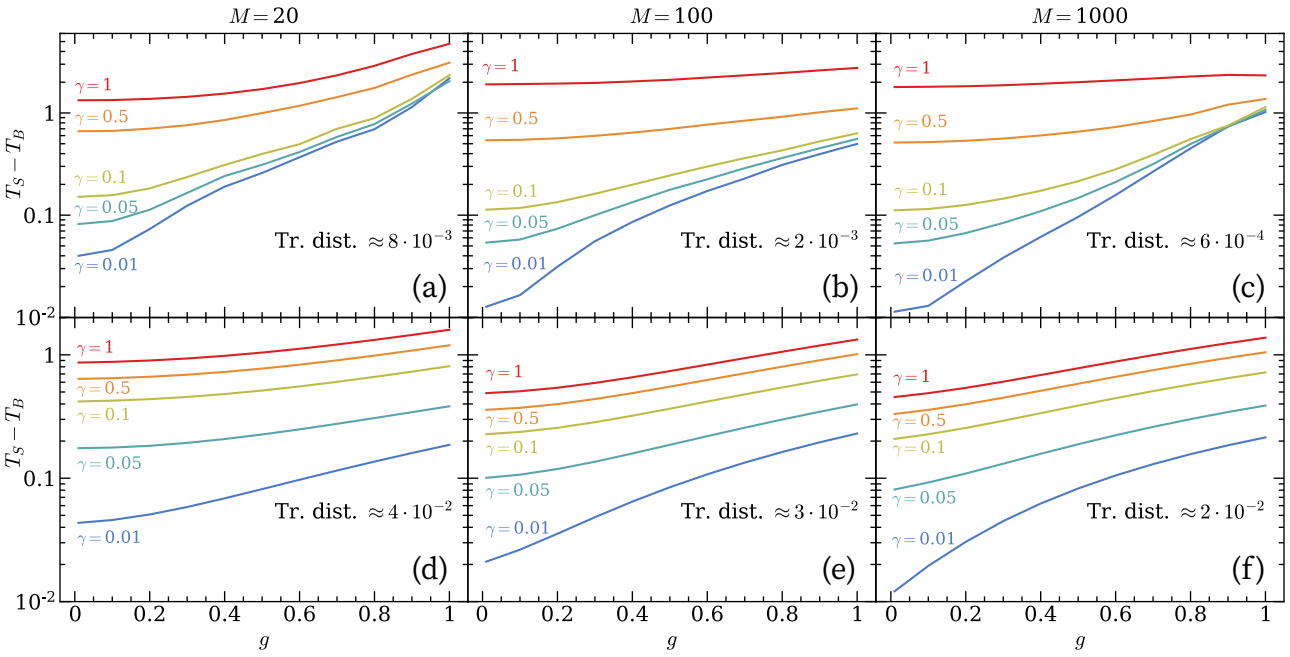

Figure 10.2: Thermalization results for the SYK2 model coupled to a boundary bath at temperatures (a-c) $T_B = 1$ and (d-f) $T_B = 0.1$. The system temperature T_S approaches the bath temperature T_B in the limit of weak system-bath coupling g and damping γ. The trace distances shown are for the steady states with the lowest temperature.

10.3.1 Non-interacting SYK2 Model

Our first model is a complex SYK2 cluster with random all-to-all 2−body interactions among spinless fermions [50, 51, 52, 53, 54, 55, 56, 57, 58, 59, 60, 61]. Both the bath and the system are described by similar Hamiltonians

$$H_B = \sum_{1\le i,j\le M} J^B_{ij} c^\dagger_i c_j, \tag{10.6}$$

$$H_S = \sum_{M+1\le i,j\le M+N} J^S_{ij} c^\dagger_i c_j. \tag{10.7}$$

The fermions obey the standard anti-commutation relations $\{c^\dagger_i, c_j\} = \delta_{ij}$. The SYK couplings are complex, independent Gaussian random variables with zero mean obeying

$$J^{B,S}_{ij} = (J^{B,S}_{ji})^*, \tag{10.8}$$

$$\langle |J^B_{ij}|^2 \rangle = \frac{J_B^2}{M}, \quad \langle |J^S_{ij}|^2 \rangle = \frac{J_S^2}{N}, \tag{10.9}$$

where the factors of M and N ensure that the energy is extensive. The SYK2 model describes free fermions, since it can be diagonalized in the energy eigenbasis

$$H_{B,S} = \sum_k \epsilon^{B,S}_k c^\dagger_k c_k. \tag{10.10}$$

It is also integrable and non-chaotic [56]. The coupling between the system and the bath is simply given by

$$H_{SB} = J_{SB}(c^\dagger_M c_{M+1} + c^\dagger_{M+1} c_M), \tag{10.11}$$

since we wanted to keep the interaction local and restricted to the boundary of the system. One could also choose an SYK2 interaction between the two sides and recover the same results.

In the non-interacting case, the Lindblad equation is quadratic in the fermionic operators and can be solved analytically using the third quantization technique [11, 63]. This method allows us to study fairly large systems with extremely high accuracy. The main idea is to write the Liouvillian $\mathcal{L}$ in terms of adjoint Majorana maps and diagonalize it in the basis of normal master modes, which represent anticommuting super-operators acting on the Fock space of density operators. The steady state is then given by the zero-mode eigenvector of an antisymmetric matrix of size $4(M+N)$. The reduced density matrix of the system is diagonal in the third quantization eigenbasis

$$\rho_S = \prod_{k=1}^{N} \left(n_k c_k^\dagger c_k + (1-n_k) c_k c_k^\dagger \right), \tag{10.12}$$

where the occupation numbers n_k are sorted in descending order and modes c_k are computed numerically [81]. In the thermal state of the decoupled system, the occupation numbers are expressed in terms of the Fermi-Dirac distribution

$$f_k = \frac{1}{1+e^{(\epsilon_k-\mu)/T}}. \tag{10.13}$$

However, in the limit of weak system-bath coupling, we expect the occupation numbers n_k to be close to the thermal values f_k. Therefore, in order to determine the temperature T_S associated with ρ_S, we minimize the average trace distance between the single-particle density matrices in the steady state and in thermal equilibrium

$$D(\rho_S, \rho(T)) = \frac{1}{N} \sum_{k=1}^{N} |n_k - f_k|. \tag{10.14}$$

This metric closely matches the one introduced in Eq. (10.4).

Our results are shown in Fig. 23.2. We set $J_B = J_S = J_{SB} = 1$, $N = 100$, and average over 100 realizations of the interaction matrices $J^{B,S}$. We consider three different bath sizes $M = 20, 100, 1000$, which are representative of small, large, and infinite reservoirs, respectively. The absolute deviation of the system's temperature from the target bath temperature is plotted as a function of system-bath coupling g for several rates γ. We observe that T_S monotonically increases with both of these parameters. At $g = 1$, the system temperature can be up to an order of magnitude larger than T_B. In the limit of zero coupling g, the temperature deviation converges to a finite value with a substantial $\gamma-$dependence. In order for the system to thermalize at the desired temperature, one must additionally take the limit $\gamma \to 0$.

The error in approximating the steady state solution with a Gibbs state is quantified by Eq. (10.14). Based on this metric (see Fig. 23.2), we see that achieving good thermalization at low temperatures can be challenging. The trace distance is almost independent of g, but does decrease with γ. Moreover, larger baths lead to steady states that are much closer in trace distance to thermal states. For $M = 1000$, we effectively have an infinite bath, which provides very little improvement over the configuration with $M = 100$. Somewhat surprisingly, the system does not attain perfect thermalization solely in the infinite bath limit. The reason for this becomes more clear in the perturbative expansion discussed below [49]. We should emphasize that our findings here do not contradict our previous results showing that SYK2 clusters thermalize when connected to infinitely large reservoirs with no backreaction [103, 104, 105], which were derived in quite a different setup not involving Lindblad open system dynamics.

In order to gain an analytical understanding of the interplay between various parameters in the problem, we seek a perturbative solution for the steady state at small g and γ [95, 84, 96].

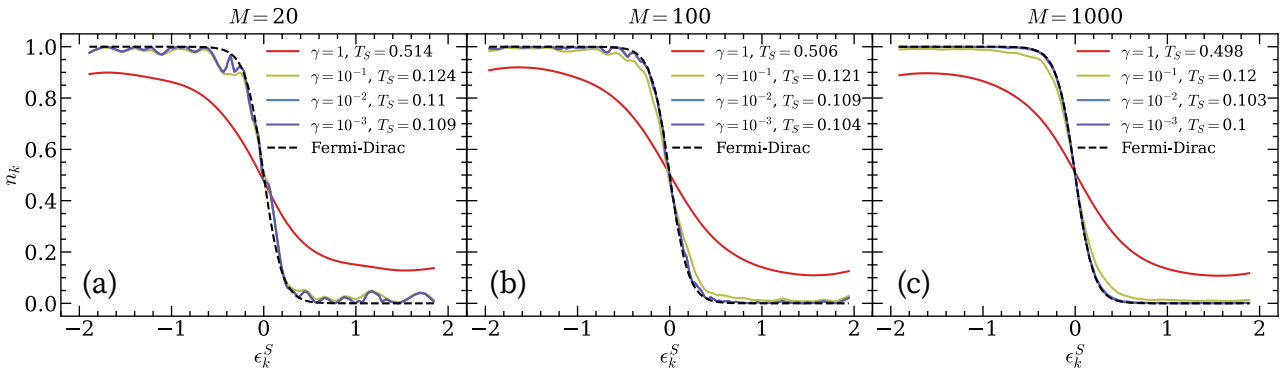

Figure 10.3: Perturbation theory for the SYK2 system in the limit of $g \to 0$ and at low temperature $T_B = 0.1$. Steady state occupation numbers n_k of the single-particle energy levels ϵ_k^S match the Fermi-Dirac distribution in Eq. (10.13) if $\gamma \ll T_B$. In this limit, the fit improves substantially for larger bath sizes M.

As argued in Ref. [49], it is more natural to take the limit of $g \to 0$ first. Following their derivation, the system's reduced density matrix is of the form introduced in Eq. (10.12) with occupations

$$n_k = \frac{\sum_{l=1}^{M} |J_{lk}^{SB}|^2 Q_{lk} f_l}{\sum_{l=1}^{M} |J_{lk}^{SB}|^2 Q_{lk}}, \tag{10.15}$$

where Q_{lk} is a Lorentzian

$$Q_{lk} = \frac{\gamma}{(\epsilon_l^B - \epsilon_k^S)^2 + \gamma^2/4}, \tag{10.16}$$

and f_l is the bath's thermal occupation of the eigenmode with energy ϵ_l^B at temperature T_B. The matrix elements J_{lk}^{SB} are defined by re-writing the system-bath interaction in the energy eigenbasis

$$H_{SB} = \sum_{l=1}^{M} \sum_{k=1}^{N} J_{lk}^{SB} c_l^\dagger c_k + \text{h.c.}. \tag{10.17}$$

Next, we take $\gamma \to 0$. In this limit, the exchange rate with the bath simply becomes a delta function $Q_{lk} \to 2\pi\delta(\epsilon_l^B - \epsilon_k^S)$. This in turn collapses the sum in Eq. (10.15) to a single term and we recover perfect thermalization $n_k = f_k$, as long as there is an energy mode of the bath that matches each one in the system $\epsilon_l^B = \epsilon_k^S$. The size of the bath plays a crucial role here, since a larger bath is more likely to have a broad enough energy spectrum that contains all the energy levels in the system [49]. Moreover, it is usually beneficial to make the bath's Hamiltonian identical to the one describing the system, since this guarantees that their spectrums will have significant overlap. Any finite γ broadens Q_{lk} into a Lorentzian, which is more forgiving of energy mismatches, but also introduces a small deviation from thermal occupation numbers.

We numerically verify our claims in the case of low temperature $T_B = 0.1$, which is the hardest setup for thermalization. Our results are presented in Fig. 23.3. First, we see that for our smallest bath, there are significant deviations in the occupation numbers even as $\gamma \to 0$. Second, we notice that the increase in bath size at large values of γ does almost nothing for thermalization. This suggests that lowering γ should be a priority over increasing the bath size in actual simulations. In fact, having good convergence to T_B requires making $\gamma \ll T_B$. The same conclusion was reached in Ref. [49].

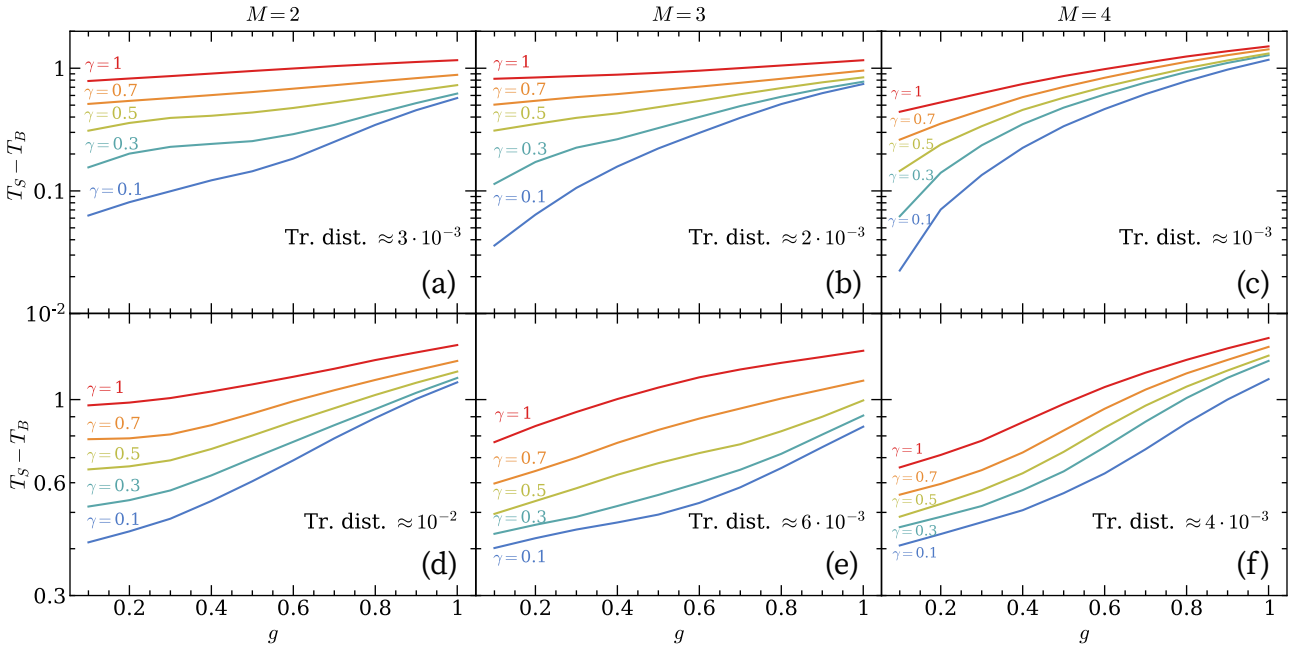

Figure 10.4: Thermalization results for the XZ model coupled to a boundary bath at temperatures (a-c) $T_B = 1$ and (d-f) $T_B = 0.1$. For intermediate bath temperatures (top), the system approaches a temperature close to T_B in the limit of weak system-bath coupling g and damping γ. At low bath temperatures (bottom), the system's final temperature is limited by its gap $\Delta = 0.51$. The reference trace distances correspond to the steady states with the lowest temperature.

Unfortunately, taking the limit of both g and γ to zero can be problematic for models that do not have closed-form analytic solutions and rely on time-evolution methods to find the steady state. We verified numerically that the Liouvillian gap scales according to Eq. (10.3). Furthermore, the average spectral gap depends on system size as $\Delta_{\mathcal{L}} \sim 1/N^2$, which is better than the expected $1/N^3$ scaling for integrable models [84]. This is likely due to the non-local all-to-all interactions of SYK2. Therefore, the convergence rate to a steady state solution would be extremely slow for large systems with small parameters g and γ. However, for most practical purposes, such as quantum transport, reaching perfect thermalization at low temperatures is not essential. In fact, it is often sufficient to cool down the system to a temperature in the ballpark of T_B and then use a thermometry procedure to determine the exact T_S [41]. Moreover, temperatures of interest can be on the order of J_S, which are significantly easier to achieve with this setup.

10.3.2 Interacting Models

Gapped XZ Model

Our second model is a uniform XZ spin chain in a transverse magnetic field

$$H_B + H_S = \sum_{i \neq M} \left(J_x \sigma_i^x \sigma_{i+1}^x + J_z \sigma_i^z \sigma_{i+1}^z \right) + h_x \sum_{i=1}^{M+N} \sigma_i^x, \tag{10.18}$$

$$H_{SB} = J_x \sigma_M^x \sigma_{M+1}^x + J_z \sigma_M^z \sigma_{M+1}^z, \tag{10.19}$$

where $\sigma_i^{x,z}$ denote Pauli matrices at site i. We choose $(J_x, J_z, h_x) = (1, 0.75, 0.21)$, which places the model in a non-integrable, quantum chaotic regime [64]. The model is known to have a small,

but finite energy gap equal to $\Delta = 0.51$ [41]. In order to thoroughly investigate thermalization in this model, we restrict ourselves to small systems $N = 20$ and baths $M = 2, 3, 4$, such that we can reliably reach the steady state without convergence issues.

As mentioned in Sec. 10.2, we simulate the time evolution of our density matrix using the TEBD algorithm [68, 69, 8, 80]. During the evolution, we restrict the amount of built-up entanglement by truncating the matrices to a maximum bond dimension of χ. We start with a larger bond dimension $\chi = 256$ during the early stages, when we have rapid entanglement growth, and then slowly decrease it to $\chi = 64$ as we approach the steady state. We choose a time step of $\delta t = 0.05$, which is small enough so as to not dominate over the truncation error, and evolve up to late times $t = 4000$ for the smallest values of g and γ. Additionally, we implement an annealing procedure which saves a lot of computational time when sweeping these parameters. We use the steady state results from larger values of g and γ as the starting point of the time evolution at lower parameter values.

We present our findings in Fig. 23.4. Qualitatively, they are similar to the non-interacting case. The temperature is uniform throughout the system, away from the boundaries. At $g = \gamma = 1$, the local temperature is much larger than the driving temperature, which is consistent with previous studies [32, 33, 39, 40, 41]. Its value decreases continuously with g and γ. For intermediate bath temperatures $T_B = 1$, the system's temperature T_S can be within 1% of the target at the smallest $g = \gamma = 0.1$. On the other hand, for low temperatures $T_B = 0.1$, the final bulk temperature is strictly limited by the model's gap $T_S \approx \Delta$. Notice that this was not the case for the SYK2 model, where the gap is of order $1/N$ and still below the bath temperature. Although we only increase M by a few sites, it has a substantial effect on the trace distance (see Fig. 23.4). Larger baths lead to faster and more robust convergence to the steady state. However, they are not helpful in lowering the system's temperature below Δ.

Gapless $\mathbb{Z}_3$ Chiral Clock Model

As our third model, we investigate a $\mathbb{Z}_3$ chiral clock model in a one-dimensional chain [76, 77] whose Hamiltonian can be written as

$$H_B + H_S = -J \sum_{i \neq M} \sigma_i \sigma_{i+1}^\dagger e^{i\theta} - f \sum_{i=1}^{M+N} \tau_i e^{i\phi} + \text{h.c.}, \tag{10.20}$$

$$H_{SB} = -J \sigma_M \sigma_{M+1}^\dagger e^{i\theta} + \text{h.c.}, \tag{10.21}$$

where τ_i and σ_i are the local three-state 'spin' operators at site i in the following matrix representations:

$$\tau = \begin{pmatrix} 1 & 0 & 0 \\ 0 & \omega & 0 \\ 0 & 0 & \omega^2 \end{pmatrix}, \quad \sigma = \begin{pmatrix} 0 & 1 & 0 \\ 0 & 0 & 1 \\ 1 & 0 & 0 \end{pmatrix}, \quad \omega = e^{\frac{2\pi i}{3}}. \tag{10.22}$$

These operators satisfy $\tau^3 = \sigma^3 = I$ and $\sigma\tau = \omega\tau\sigma$. Notice that the local Hilbert space dimension is now $d = 3$, which significantly increases the computational complexity of the problem. As a result, we limit our analysis to small systems of size $N = 16$ and $M = 2, 3$. As our Hamiltonian parameters, we choose $(J, f, \theta, \phi) = (0.5373, 0.4627, \pi/8, 0)$ such that the model is at a quantum phase transition, which has been revealed by various numerical techniques [74, 75, 76]. Consequently, the model becomes gapless and is therefore a good target for investigating the performance of our multi-site bath scheme, with possible applications to quantum critical transport near zero temperature.

The general approach to obtaining the steady state for this model is similar to that of the XZ spin chain. We employ the same annealing procedure and set the minimal bond dimension to $\chi = 81$. The convergence is noticeably slower, so we evolve the initial state up to $t =$

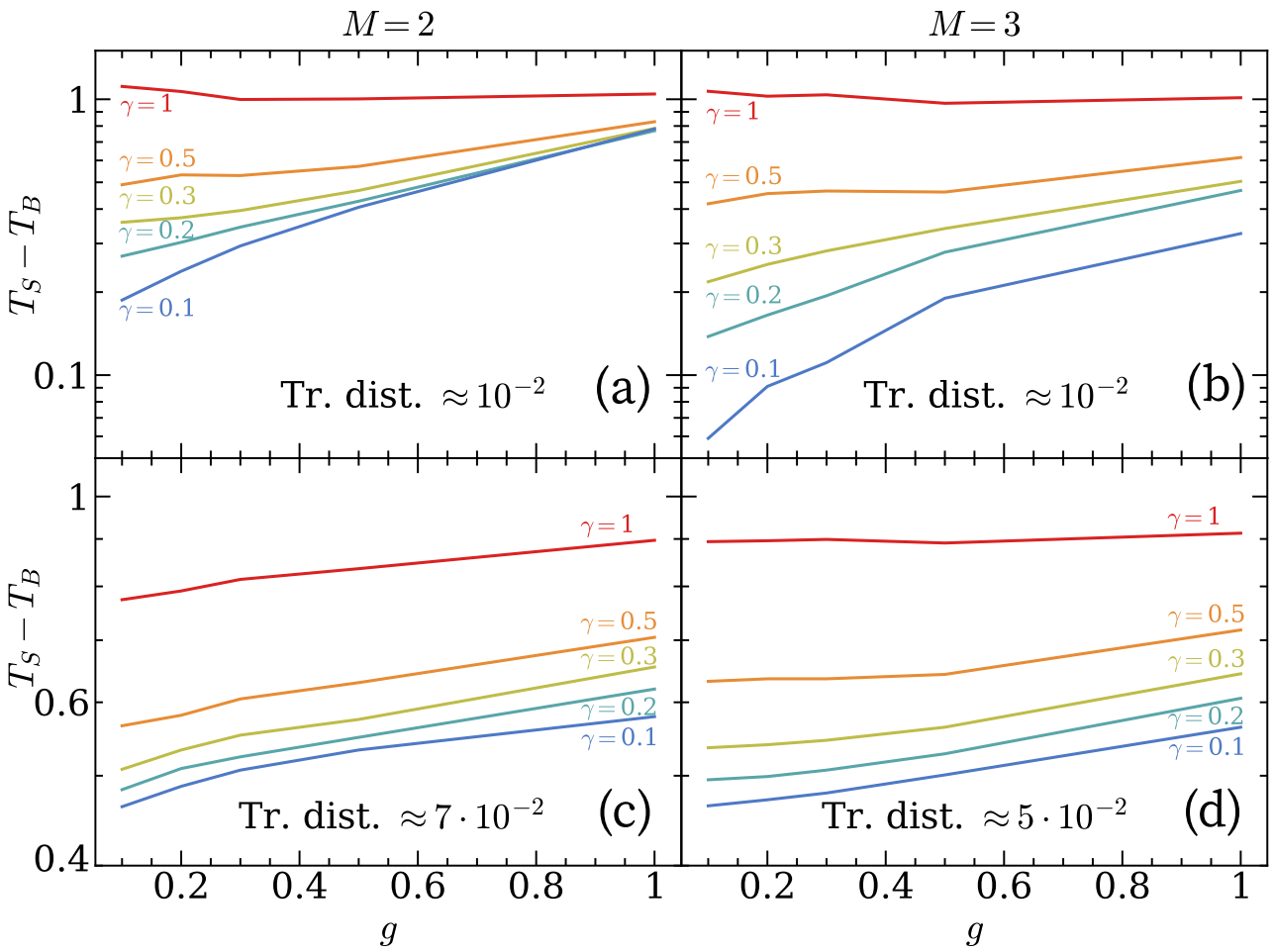

Figure 10.5: Thermalization results for the chiral clock model coupled to a boundary bath at temperatures (a-b) $T_B = 1$ and (c-d) $T_B = 0.1$. For intermediate bath temperatures (top), the system approaches a temperature close to T_B in the limit of weak system-bath coupling g and damping γ. At low driving temperatures (bottom), the system's final temperature is significantly above T_B. The trace distances indicated in each panel are for the steady states with the lowest temperature.

$2 \cdot 10^4$ for the smallest values of g and γ. The results for the chiral clock model are displayed in Fig. 23.5. In terms of final bulk temperature, they resemble our observations for the XZ model at intermediate temperature $T_B = 1$. However, in the low temperature $T_B = 0.1$ case, the final bulk temperature does not improve past $T_S \approx 0.5$, even though the system is gapless. Nevertheless, there are slight improvements in the trace distance when expanding the bath from $M = 2$ sites to $M = 3$ sites. It is quite possible that cooling a gapless model may require much larger baths and longer convergence times, beyond what is accessible numerically with the current setup. Another explanation is that there may be an emergent energy scale that prohibits the Lindblad operators from cooling the system below that scale. We elaborate more on this in Sec. 10.4.

10.3.3 Application to Low-Temperature Transport

In this section, we put to use the lessons learned about thermalization in open systems to explore some previously inaccessible physics of the XZ model. More specifically, we study its energy transport at low temperatures. The boundary-driven setup consists of a system

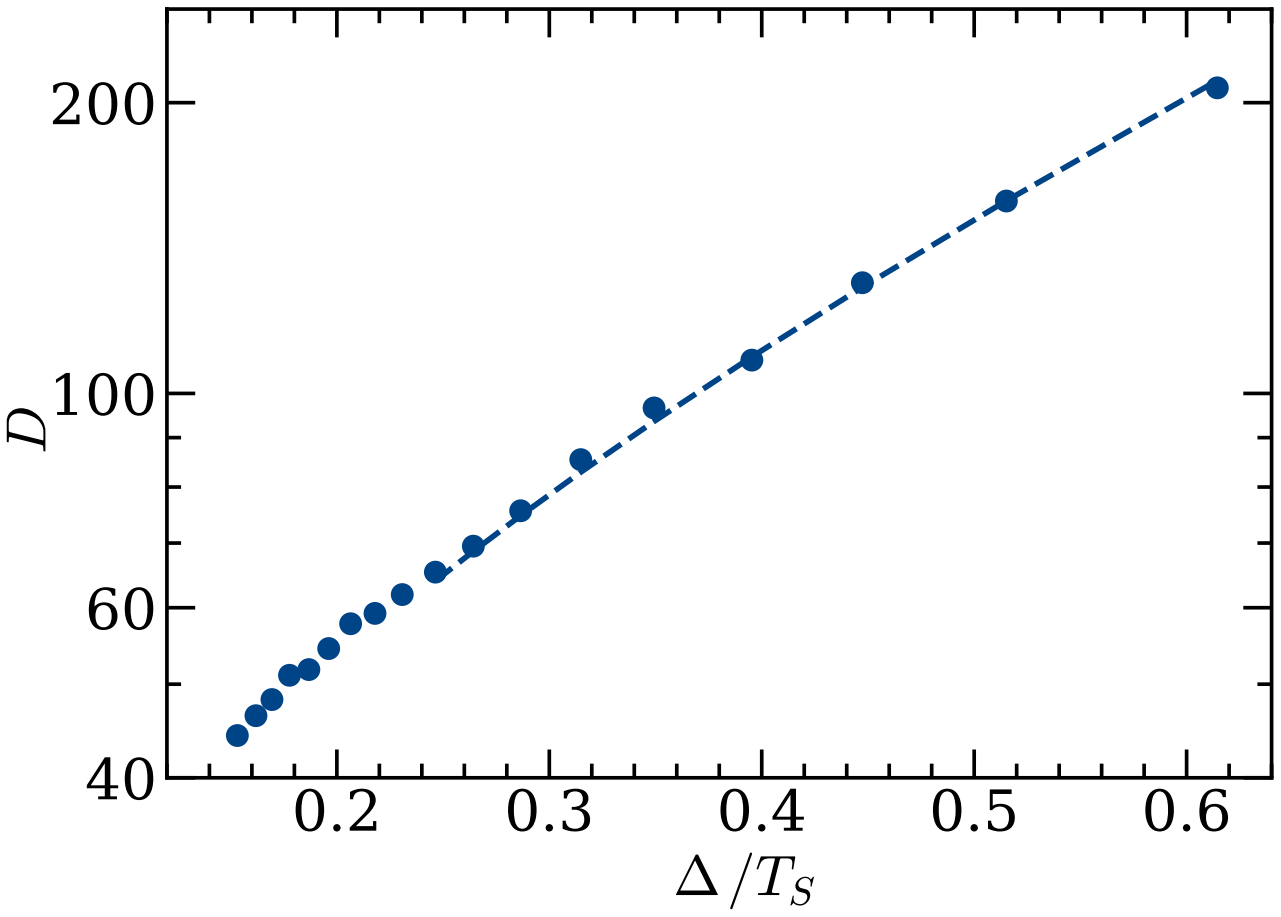

Figure 10.6: Temperature dependence of the energy diffusion constant D for the XZ model. Symbols represent numerical values obtained via our open system setup and the dashed line is fit to Eq. (10.24). At low temperatures, the diffusivity grows exponentially with inverse temperature.

coupled to two baths at its ends (see Fig. 23.1(b)), which imposes a temperature imbalance driving the system out of equilibrium. The left and right baths are maintained at temperatures $T_{L,R} = T_B \pm \delta T$ using the same Lindblad operators as before. The temperature offset is taken to be small $\delta T = 0.1 T_B$, so that we remain in the linear-response regime. Under this assumption, we can assign a local temperature for the system weakly perturbed from equilibrium. This temperature varies slowly and linearly in the bulk, as investigated in more detail in our previous work [41], and hence the system's temperature T_S can still be defined according to Eq. (10.5).

The system evolves while coupled to the baths until it reaches a non-equilibrium steady state (NESS) characterized by a uniform current flowing through the chain

$$\begin{aligned} j = {} & 2J_x J_z \langle (\sigma^x_{i-1}\sigma^y_i\sigma^z_{i+1} - \sigma^z_{i-1}\sigma^y_i\sigma^x_{i+1})\rangle \\ & - h_x J_z \langle (\sigma^z_{i-1}\sigma^y_i - \sigma^y_i\sigma^z_{i+1})\rangle. \end{aligned} \tag{10.23}$$

The XZ model exhibits diffusive energy transport $j = -D\nabla E$, where ∇E is the energy density gradient and D is the diffusivity. The temperature dependence of this diffusion constant has been previously studied in the regime of intermediate and high temperatures [41]. At low temperatures, the semi-classical kinetic theory predicts an exponential increase in diffusivity for gapped one-dimensional systems

$$D \sim \frac{e^{2\Delta/T_S}}{\sqrt{T_S}}. \tag{10.24}$$

Unlike spin diffusion, which only relies on two-body collisions [82, 83], energy transport requires three-body collisions to relax the current [41] and therefore doubles the exponent. Strictly speaking, this scaling is derived for the regime $T_S \ll \Delta$. However, since the gap for our model is so small, we find that it correctly describes the increase in diffusivity even at temperatures slightly above the gap.

Our numerical results for a system of size $N = 51$ and bath temperatures between $T_B = 0.4$ and $T_B = 2$ are showcased in Fig. 10.6. The diffusion constant at low temperatures matches the semi-classical prediction in Eq. (10.24) remarkably well, with the only fitting parameter being the overall prefactor. In our previous studies, we managed to attain a minimum local temperature of $T_S = 2.1$ in the bulk [41]. Now we have decreased this value to $T_S = 0.8$. We should point out that g cannot be too small, since it would decrease the current and energy gradient to the point where they can be affected by the numerical precision of our simulations. We also emphasize that γ should not be taken to zero, since it may cause the bulk to decouple from the boundary, resulting in a different scaling of the current [88]. Therefore, we choose $g = \gamma = 0.4$, which strikes a good balance between having well-converged NESS and reaching low temperatures.

10.4 Discussion

In this paper, we studied thermalization in open quantum systems coupled to a bath at their boundary. We investigated the emergent steady state in these systems and determined whether its associated temperature matches the driving temperature of the bath. Our analysis was based on three models: a free-fermion SYK2 cluster, a gapped XZ spin chain, and a gapless chiral clock model. For all these models, we found that the system's temperature in the default parameter regime was much higher than the target bath temperature. However, upon increasing the bath size M and lowering the system-bath coupling g and the bath relaxation rate γ, we saw that the two temperatures start to agree. In fact, using perturbation theory for the SYK2 model, we were able to show that the system reaches perfect thermalization at our desired temperature in the limit $g, \gamma \to 0$ and $M \gg N$. These results carry over to the interacting models as well, where we found that even baths comprised of a few sites can approximately impose the correct temperature on the system in the limit of weak coupling and damping.

We demonstrated the applicability of our method by computing the low-temperature energy diffusion constant of the XZ model in an open system setup. We were able to reach temperatures much lower than in our previous work [41] and showed that the diffusivity scales exponentially with inverse temperature, as predicted by a semi-classical calculation for gapped one-dimensional systems [82, 83, 41].

Although our approach can successfully thermalize the system under the aforementioned conditions, there is still a minimal temperature below which the system cannot be cooled with the current setup. For the XZ model, this temperature seems to exactly match its energy gap. However, this is not true for all models. For example, we have shown that an Ising model in a mixed field, which has a relatively large gap, can be cooled far below this energy scale [41]. At present, we do not fully understand what determines this minimal temperature, but we conjecture that it is on the order of $\min(\Delta, J)$, where Δ is the energy gap and J is the typical interaction strength of the model. Moreover, it is unclear whether the limiting gap is that of the system or the bath, since both are represented by the same Hamiltonian in this case. It is difficult to distinguish between the two scenarios, because changing the bath Hamiltonian usually leads to significantly less efficient cooling at low temperatures and hence a larger minimal temperature, even if the gap of the bath Hamiltonian stays roughly the same. This is in agreement with our findings for the non-interacting model, where we showed that the energy spectra of the system and bath must closely match. Surprisingly, we also found

a minimal accessible temperature for the gapless chiral clock model. A possible explanation involves the emergence of a new energy scale in the system, defined in terms of Luttinger liquid parameters [106], which sets its effective temperature under Lindblad dynamics. A direction of future research would be to formulate a general framework for constructing efficient baths and dynamics that could circumvent this limitation.

Our study also highlights some other shortcomings of the Lindblad approach. One has to take the limit of weak coupling and damping, in addition to making the baths a substantial fraction of the system. This can become impractical for larger and more complex systems. Recently, there has been a lot of progress towards engineering mesoscopic leads with better thermalization properties. Refs. [25, 107] described tensor network algorithms for boundary-driven thermal machines, where mesoscopic baths are systematically approximated by a finite number of damped fermionic modes. Concurrently, Refs. [108, 109] introduced a mixed spatial-energy basis for fermionic systems coupled to mesoscopic leads, which significantly lowers the required bond dimension in tensor network simulations. Tensor network methods have also been developed to implement other quantum master equations, such as the Redfield equation [110], although only for short evolution times. Given this abundance of new methods, it would be interesting to apply them to larger scale problems of interest, such as low-temperature transport, and compare them to our approach.

10.5 Multi-site Lindblad Operators

Our goal is to construct a super-operator $\mathcal{L}_B$ from a set of Lindblad operators $\{L_{jk}\}$ such that it drives the $M-$site bath to a Gibbs state at temperature T_B and chemical potential μ_B, i.e., $\mathcal{L}_B(\rho_B) = 0$ where

$$\rho_B = \frac{e^{-(H_B - \mu_B N_B)/T_B}}{\mathrm{tr}\left(e^{-(H_B - \mu_B N_B)/T_B}\right)}, \tag{10.25}$$

and N_B is the total spin or particle number operator of the bath. We therefore require that ρ_B is a unique eigenvector of $\mathcal{L}_B$ with eigenvalue 0. However, this condition does not fully fix the jump operators, as it only ensures that the steady state is correct. One can additionally require that all the other modes decay at the same rate [31], which results in the fastest convergence to ρ_B. Alternatively, one could impose the detailed-balance condition between the energy levels of H_B, which may lead to better thermalization in certain regimes [111]. For our models, we find that both approaches work equally well even at low temperatures.

In the case of free fermions, the number of Lindblad operators required to thermalize the bath scales linearly with its size, while for a generic spin system, this number scales exponentially with M. This may seem problematic at first, since it would severely restrict the size of the bath that can be implemented in practice. However, as we show in the main text, even a relatively small bath can result in good thermalization under the right conditions. The real bottleneck is in designing a compact tensor network representation of the Liouvillian $\mathcal{L}_\mathcal{B}$, which can be efficiently applied to the bath without generating too much entanglement during time evolution. A potential avenue of research would be to leverage the Product Spectrum Ansatz [112, 113] to design dissipators that only approximately thermalize larger baths.

10.5.1 Non-interacting Hamiltonian

If the bath Hamiltonian is quadratic in the fermion creation and annihilation operators, the jump operators can be made linear [114, 81, 49]. We first write the Hamiltonian (Eq. (10.6)) in the energy eigenbasis by diagonalizing the interaction matrix $J^B = V^\dagger \epsilon^B V$, where $\epsilon^B = \mathrm{diag}(\epsilon_1^B, \epsilon_2^B, \ldots, \epsilon_M^B)$ and V is unitary. We recover Eq. (10.10) with $c_k = \sum_{j=1}^M V_{kj} c_j$. Note that

the new operators also satisfy the canonical anti-commutation relations $\{c_k^\dagger, c_l\} = \delta_{kl}$. The thermal density matrix can be written in this basis as well

$$\rho_B = \prod_{k=1}^{M} \left(f_k c_k^\dagger c_k + (1 - f_k) c_k c_k^\dagger \right), \tag{10.26}$$

where f_k are the equilibrium occupation numbers defined in Eq. (10.13). For each mode k, we introduce two jump operators that either add a fermion at a rate γf_k or remove a fermion at a rate $\gamma(1 - f_k)$

$$L_{\text{in},k} = \sqrt{\gamma f_k} c_k^\dagger, \tag{10.27}$$

$$L_{\text{out},k} = \sqrt{\gamma(1 - f_k)} c_k. \tag{10.28}$$

The rates are chosen to satisfy the detailed-balance condition $f_k/(1 - f_k) = e^{-(\epsilon_k^B - \mu_B)/T_B}$. We can further check that all the terms in the Lindblad equation exactly cancel

$$\begin{aligned} &L_{\text{in},k} \rho_B L_{\text{in},k}^\dagger = L_{\text{out},k}^\dagger L_{\text{out},k} \rho_B = \rho_B L_{\text{out},k}^\dagger L_{\text{out},k} \\ &= \gamma f_k (1 - f_k) c_k^\dagger c_k \prod_{l \neq k} \left(f_l c_l^\dagger c_l + (1 - f_l) c_l c_l^\dagger \right), \end{aligned} \tag{10.29}$$

$$\begin{aligned} &L_{\text{out},k} \rho_B L_{\text{out},k}^\dagger = L_{\text{in},k}^\dagger L_{\text{in},k} \rho_B = \rho_B L_{\text{in},k}^\dagger L_{\text{in},k} \\ &= \gamma f_k (1 - f_k) c_k c_k^\dagger \prod_{l \neq k} \left(f_l c_l^\dagger c_l + (1 - f_l) c_l c_l^\dagger \right). \end{aligned} \tag{10.30}$$

Thus we conclude that ρ_B is indeed a fixed point under the dynamics generated by these jump operators.

10.5.2 Interacting Hamiltonian

For interacting spin systems, we extend the two-site Lindblad operators construction in Refs. [31, 33, 39, 40, 41] to systems of arbitrary size. Consider the general case where each of the M spins has a local Hilbert space dimension d. We begin by diagonalizing the density matrix $\rho_B = V^\dagger W V$, where $W = \text{diag}(W_0, W_1, \ldots, W_{d^M-1})$ and V is unitary. Define a set of d^{2M} operators $\tilde{L}_{jk} \in \mathbb{R}^{d^M \times d^M}$

$$\tilde{L}_{jk} = \sqrt{\gamma W_j} E_{jk}, \quad 0 \leq j, k < d^M, \tag{10.31}$$

where E_{ab} is the matrix unit with a 1 in row a and column b as its only non-zero entry. Here γ quantifies the overall strength of the bath damping. It is easy to verify that

$$\tilde{L}_{jk} W \tilde{L}_{jk}^\dagger = \gamma W_j W_k E_{jj}, \tag{10.32}$$

$$\tilde{L}_{jk}^\dagger \tilde{L}_{jk} W = W \tilde{L}_{jk}^\dagger \tilde{L}_{jk} = \gamma W_j W_k E_{kk}. \tag{10.33}$$

Therefore we have

$$\begin{aligned} \tilde{\mathcal{L}}_B(W) &= \sum_{j,k=0}^{d^M-1} \left(\tilde{L}_{jk} W \tilde{L}_{jk}^\dagger - \frac{1}{2} \tilde{L}_{jk}^\dagger \tilde{L}_{jk} W - \frac{1}{2} W \tilde{L}_{jk}^\dagger \tilde{L}_{jk} \right) \\ &= \gamma \sum_{j,k=0}^{d^M-1} W_j W_k \left(E_{jj} - E_{kk} \right) = 0, \end{aligned} \tag{10.34}$$

and we can multiply this expression by $V^\dagger$ and V on the left and right sides, and use the identity $VV^\dagger = I$ to deduce that

$$\sum_{j,k=0}^{d^M-1} \left(L_{jk}\rho_B L_{jk}^\dagger - \frac{1}{2} L_{jk}^\dagger L_{jk}\rho_B - \frac{1}{2}\rho_B L_{jk}^\dagger L_{jk} \right) = 0, \tag{10.35}$$

with $L_{jk} = V^\dagger \tilde{L}_{jk} V$. Hence we can use these new Lindblad operators L_{jk} to construct a super-operator satisfying $\mathcal{L}_B(\rho_B) = 0$. Moreover, since V is unitary, the eigenvalues of $\mathcal{L}_B$ will be the same as those of $\tilde{\mathcal{L}}_B$. We can compute the latter using the vectorized representation of the Liouvillian [20, 6, 1]

$$\tilde{\mathcal{L}}_B = \sum_{j,k=0}^{d^M-1} \left(\tilde{L}_{jk}^* \otimes \tilde{L}_{jk} - \frac{1}{2} I \otimes \tilde{L}_{jk}^\dagger \tilde{L}_{jk} - \frac{1}{2} \tilde{L}_{jk}^T \tilde{L}_{jk}^* \otimes I \right), \tag{10.36}$$

where

$$\tilde{L}_{jk}^* \otimes \tilde{L}_{jk} = \gamma W_j E_{j(d^M+1),k(d^M+1)}, \tag{10.37}$$

$$I \otimes \tilde{L}_{jk}^\dagger \tilde{L}_{jk} = \gamma W_j \sum_{i=0}^{d^M-1} E_{k+i\cdot d^M, k+i\cdot d^M}, \tag{10.38}$$

$$\tilde{L}_{jk}^T \tilde{L}_{jk}^* \otimes I = \gamma W_j \sum_{i=0}^{d^M-1} E_{i+k\cdot d^M, i+k\cdot d^M}, \tag{10.39}$$

and I denotes the $d^M \times d^M$ identity matrix. It is straightforward to check that $\tilde{\mathcal{L}}_B$ has exactly one zero eigenvalue and the remaining eigenvalues are equal to $-\gamma$, since $\sum_{j=0}^{d^M-1} W_j = \mathrm{tr}(\rho_B) = 1$. Hence our construction leads to the fastest relaxation to the target density matrix [31].

A different set of dissipators, satisfying detailed-balance relations, has also been proposed [111]. Using our notation above, these operators take the form

$$\tilde{L}_{jk} = \sqrt{\frac{\gamma W_j}{W_j + W_k}} E_{jk}, \quad 0 \le j \ne k < d^M. \tag{10.40}$$

We can again verify that they drive the bath to its correct thermal state

$$\tilde{\mathcal{L}}_B(W) = \gamma \sum_{j,k=0}^{d^M-1} \frac{W_j W_k}{W_j + W_k} (E_{jj} - E_{kk}) = 0, \tag{10.41}$$

since

$$\tilde{L}_{jk} W \tilde{L}_{jk}^\dagger = \gamma \frac{W_j W_k}{W_j + W_k} E_{jj}, \tag{10.42}$$

$$\tilde{L}_{jk}^\dagger \tilde{L}_{jk} W = W \tilde{L}_{jk}^\dagger \tilde{L}_{jk} = \gamma \frac{W_j W_k}{W_j + W_k} E_{kk}. \tag{10.43}$$

The final jump operators are given by $L_{jk} = V^\dagger \tilde{L}_{jk} V$.

Part V
Old, Fundamental Articles

11 Chaos and Quantum Thermalization by Srednicki

Abstract

We show that a bounded, isolated quantum system of many particles in a specific initial state will approach thermal equilibrium if the energy eigenfunctions which are superposed to form that state obey Berry's conjecture. Berry's conjecture is expected to hold only if the corresponding classical system is chaotic, and essentially states that the energy eigenfunctions behave as if they were gaussian random variables. We review the existing evidence, and show that previously neglected effects substantially strengthen the case for Berry's conjecture. We study a rarefied hard-sphere gas as an explicit example of a many-body system which is known to be classically chaotic, and show that an energy eigenstate which obeys Berry's conjecture predicts a Maxwell-Boltzmann, Bose-Einstein, or Fermi-Dirac distribution for the momentum of each constituent particle, depending on whether the wave functions are taken to be nonsymmetric, completely symmetric, or completely antisymmetric functions of the positions of the particles. We call this phenomenon eigenstate thermalization. We show that a generic initial state will approach thermal equilibrium at least as fast as $O(\hbar/\Delta)t^{-1}$, where Δ is the uncertainty in the total energy of the gas. This result holds for an individual initial state; in contrast to the classical theory, no averaging over an ensemble of initial states is needed. We argue that these results constitute a new foundation for quantum statistical mechanics.

11.1 I. Introduction

Take some helium atoms, put them in one corner of a well insulated box, and let them go. Wait a while, then punch a small hole in the side of the box. As the atoms emerge, one by one, measure their momenta. Make a histogram, plotting the fraction of atoms with magnitude of momentum between p and $p + dp$.

Every physicist knows what the result of this experiment will be. The histogram will be very well approximated by the Maxwell-Boltzmann distribution

$$f_{\rm MB}(\mathbf{p}, T) = (2\pi mkT)^{-3/2} e^{-\mathbf{p}^2/2mkT} \tag{1.1}$$

multiplied by $4\pi F p^2 dp$, where $F = (\pi/8mkT)^{1/2} p$ is a flux factor. Here m is the mass of a helium atom, k is Boltzmann's constant, and T is the "temperature," a number which will depend on how the atoms were originally put into the corner of the box, how much space they occupied, and other details of the initial conditions. The challenge is to derive this result from first principles.

The biggest problem with a theoretical analysis of this particular experiment is the need to treat the hole in the box in a reasonable way. It is much easier to study the following thought experiment instead. Suppose, after preparing the system in its initial state, we are able to measure the momentum of one atom at a specific (but arbitrary) time t. Suppose further that, after having made this measurement, we can empty out the box, and then start it off again with the system in exactly the same initial state. We now do this repeatedly, each time measuring the momentum of one atom after exactly the same amount of time t has passed. We make a histogram of the results.

Let us analyze this experiment, beginning with classical mechanics as the underlying theory. We take the hamiltonian for N atoms to be

$$H = \sum_{i=1}^{N} \frac{\mathbf{p}_i^2}{2m} + \sum_{i<j} V\left(|\mathbf{x}_i - \mathbf{x}_j|\right) \tag{1.2}$$

where we take $V(r)$ to be a hard-sphere potential:

$$V(r) = \begin{cases} +\infty & \text{for } r < 2a \\ 0 & \text{for } r > 2a \end{cases} \tag{1.3}$$

We assume perfectly reflecting boundary conditions at the walls of the box. The atoms initially have some definite total energy U. The phase space of this system is known to be fully chaotic, with no invariant tori for any value of U [1]. Thus the motion in phase space on any constant energy surface is ergodic and mixing. (For a review of classical chaos theory, see, e.g., [2-4].)

However, this is entirely irrelevant if we always start out with exactly the same initial state, and always make the measurement after exactly the same amount of time has elapsed. The momentum of the measured atom (assuming that it is always the same atom) is determined exactly by the initial conditions, and so will always be the same. To have any hope of getting a distribution of momenta, we must average over either the initial conditions or the times of measurement or both.

If we keep the initial conditions fixed, ergodicity implies that the system wanders all over the constant energy surface. (This assumes that we have not started the system off at a point located on a periodic orbit; such points form a set of measure zero.) If we divide the constant energy surface into many patches of equal area (and that area is not too small) then after a certain finite time the system will, to a very good approximation, be equally likely to be in any one of these patches at any later time. Conversely, if we permit a range of initial conditions, mixing implies that, if the measurement time is fixed but not too early, the system will once again, to a very good approximation, be equally likely to be in any one of the equal-area patches. The rule that equal-area patches are equally likely is just the usual formulation of the microcanonical ensemble, which after a little work leads to eq. (1.1) for the fraction of atoms with momentum in a range of d^3p around $\mathbf{p}$, with the temperature T simply given by the ideal gas formula $U = \frac{3}{2}NkT$. In short, if we do a modest average over either the initial conditions or the times of measurement, then classical chaos results in classical thermalization. (For an elementary review of chaos theory as it applies to classical statistical mechanics, see [5].)

On the other hand, if we have a weakly perturbed integrable system (for example, harmonic oscillators with small nonlinear couplings), then according to the Kolmogorov-Arnol'd-Moser theorem [6], its phase space is foliated by invariant tori almost everywhere, and we do not expect it to thermalize. If it is partially integrable, with some invariant tori embedded in an otherwise chaotic phase space, then the system may or may not thermalize, depending on the initial state.

These results from classical mechanics are clear and powerful, and provide a satisfying explanation of statistical behavior in classical systems which exhibit chaos. However, we know that the real world is ultimately described by quantum mechanics, and we so should seek the quantum analog of the classical analysis. We would like to know, for example, what property a quantum system must possess, analogous to classical chaos, so that "most" of its initial states thermalize, in the sense discussed above. Furthermore if a quantum system does possess this property (whatever it may be), then we might hope that the inherent uncertainties in quantum mechanics lead to a thermal distribution for the momentum of a single atom, even if we always start with exactly the same initial state, and make the measurement at exactly the same time. If this is true, then quantum mechanics automatically provides the "coarse graining" which is missing [3,7] in the classical theory.

I will argue that the property needed for thermalization of a quantum system is the validity of Berry's conjecture [8-10]. For a quantum gas of hard spheres, Berry's conjecture states that each energy eigenfunction appears to be a superposition of plane waves (in the $3N$ dimensional coordinate space) with random phase and gaussian random amplitude, but fixed wavelength. In general, Berry's conjecture is expected to hold only for systems which exhibit classical chaos in all or at least most of the classical phase space. As already noted, a hard sphere gas meets this condition.

We will see that Berry's conjecture leads to either Bose-Einstein, Fermi-Dirac, or Maxwell-Boltzmann statistics, depending on whether the wave functions are chosen to be completely symmetric, completely antisymmetric, or nonsymmetric functions of the positions of the N atoms. Furthermore we will find that any nonthermal features of the initial distribution of momenta decay away at least as fast as $O(h/\Delta)t^{-1}$, where h is Planck's constant and Δ is the uncertainty in the total energy. Thermal behavior thus appears for a very wide range of possible initial states, without assuming that the system interacts with an external heat bath, or any other environmental variables. We also do not need to take any averages over initial states, times of measurement, or hamiltonians, or make any unjustifiable approximations to the quantum equation of motion, such as truncation of the BBGKY hierarchy.

The rest of this paper is organized as follows. In Sect. II, we review Berry's conjecture for a system of hard spheres in a box. In Sect. III, we show how Berry's conjecture leads, in the limit of low density and high energy, to a Maxwell-Boltzmann distribution for the momentum of a single atom in the gas, with a temperature that is related to the total energy by the ideal gas law. In this section we treat the atoms as distinguishable, making no assumptions about the symmetry of the wave function of the gas under exchange of individual atoms. In Sect. IV, we evaluate the effects of certain corrections to Berry's conjecture known as "scars," and reconsider some of the numerical results on Berry's conjecture which have appeared in the literature. In Sect. V, we examine time evolution beginning with a nonthermal initial state, and study the approach to equilibrium. In Sect. VI, we consider wave functions which are completely symmetric or antisymmetric under exchange of atoms, and see that these lead to Bose-Einstein or Fermi-Dirac distributions for individual momenta, respectively. Conclusions, speculations, and possible extensions are presented in Sect. VII.

11.2 II. Berry's Conjecture

Consider a system of N hard spheres, each of radius a, in a cubic box with edge length $L + 2a$. Call the energy eigenvalues U_α and the corresponding eigenfunctions $\psi_\alpha(\mathbf{X})$, where $\mathbf{X} = (\mathbf{x}_1, \ldots, \mathbf{x}_N)$ denotes the $3N$ coordinates, and $\mathbf{P} = (\mathbf{p}_1, \ldots, \mathbf{p}_N)$ will denote the $3N$ conjugate momenta. We take the wave functions to be defined on the domain

$$D = \left\{ \mathbf{x}_1, \ldots, \mathbf{x}_N \,\middle|\, -\frac{1}{2}L \le x_{i1,2,3} \le +\frac{1}{2}L; |\mathbf{x}_i - \mathbf{x}_j| \ge 2a \right\} \tag{2.1}$$

with the boundary condition that each $\psi_\alpha(\mathbf{X})$ vanish on the boundary of D. For now we assume that $\psi_\alpha(\mathbf{X})$ has no symmetries under exchange of individual $\mathbf{x}_i$.

The energy eigenfunctions $\psi_\alpha(\mathbf{X})$ can always be chosen to be everywhere real, and can be written as

$$\psi_\alpha(\mathbf{X}) = \mathcal{N}_\alpha \int d^{3N_P} A_\alpha(\mathbf{P}) \delta\left(\mathbf{P}^2 - 2mU_\alpha\right) \exp(i\mathbf{P}\cdot\mathbf{X}/\hbar) \tag{2.2}$$

where $\mathcal{N}_\alpha$ is a constant to be determined by the normalization condition

$$\int_D d^{3N} X \psi_\alpha^2(\mathbf{X}) = 1 \tag{2.3}$$

and where $A^*_\alpha(\mathbf{P}) = A_\alpha(-\mathbf{P})$. For this system, Berry's conjecture is equivalent to assuming that $A_\alpha(\mathbf{P})$ can be treated as a gaussian random variable with a two-point correlation function given by

$$\langle A_\alpha(\mathbf{P}) A_\beta(\mathbf{P}')\rangle_{\mathrm{EE}} = \delta_{\alpha\beta}\delta^{3N}(\mathbf{P}+\mathbf{P}')/\delta\left(\mathbf{P}^2-\mathbf{P}'^2\right) \tag{2.4}$$

Here $\delta^{3N}(\mathbf{P})$ is the $3N$-dimensional Dirac delta function and $\delta(x)$ is the one-dimensional Dirac delta function. The subscript EE stands for "eigenstate ensemble." This is a fictitious ensemble which describes the properties of a typical energy eigenfunction. Individual eigenfunctions behave as if they were selected at random from the eigenstate ensemble. Berry's conjecture also asserts that the eigenstate ensemble is gaussian, so that all multipoint correlation functions are given in terms of the two-point correlation function; e.g.,

$$\begin{aligned}\langle A_\alpha(\mathbf{P}_1) A_\beta(\mathbf{P}_2) A_\gamma(\mathbf{P}_3) A_\delta(\mathbf{P}_4)\rangle_{\mathrm{EE}} &= \langle A_\alpha(\mathbf{P}_1) A_\beta(\mathbf{P}_2)\rangle_{\mathrm{EE}} \langle A_\gamma(\mathbf{P}_3) A_\delta(\mathbf{P}_4)\rangle_{\mathrm{EE}} \\ &+ \langle A_\alpha(\mathbf{P}_1) A_\gamma(\mathbf{P}_3)\rangle_{\mathrm{EE}} \langle A_\delta(\mathbf{P}_4) A_\beta(\mathbf{P}_2)\rangle_{\mathrm{EE}} \\ &+ \langle A_\alpha(\mathbf{P}_1) A_\delta(\mathbf{P}_4)\rangle_{\mathrm{EE}} \langle A_\beta(\mathbf{P}_2) A_\gamma(\mathbf{P}_3)\rangle_{\mathrm{EE}} .\end{aligned} \tag{2.5}$$

Of course, each $A_\alpha(\mathbf{P})$ must give back a $\psi_\alpha(\mathbf{X})$ which vanishes on the boundary of D; this is not a stringent requirement on $A_\alpha(\mathbf{P})$ at high energy, where $\psi_\alpha(\mathbf{X})$ has many wavelengths between any two segments of the boundary. We will say more about the requirement of high energy shortly. Meanwhile, for a more general but less transparent definition of Berry's conjecture, see sect. 4; for related mathematical results, see [11,12].

Berry's conjecture is based on semiclassical reasoning, and is manifestly untrue for systems whose classical phase space is foliated almost everywhere by invariant tori [13]. It has been investigated numerically for simple systems which are fully chaotic classically, such as a single particle in a two-dimensional stadium-shaped box [14-18], or a single particle on a two-dimensional surface with constant negative curvature and periodic boundary conditions [19, 20]. In these systems, Berry's conjecture is found to be valid for eigenstates of sufficiently high energy, and its validity has even been suggested as a good definition of
chaos in a quantum system [21]. However, an important caveat is the existence of "scars" on some energy eigenfunctions, regions of enhanced value of $\psi_\alpha(\mathbf{X})$ which follow the paths of the most stable classical periodic orbits [14,15]. For now we will ignore the scars, since their presence will not alter any of our conclusions. We will discuss them in more detail in sect. 4. Also, there we will argue that some numerical results which have been interpreted as evidence against Berry's conjecture actually provide evidence for it.

Even in a system which is fully chaotic classically (like a hard-sphere gas), Berry's conjecture will certainly not be valid for eigenfunctions which are too low in energy. The low-lying states necessarily have specific structure: the ground state, for example, is nodeless. A rough criterion for the validity of Berry's conjecture is that the average wavelength of each particle be small enough to "see" the features which produce classical chaos [16]. For the hard-sphere gas, the relevant feature is the nonzero radius a of each particle. Anticipating a bit and defining a temperature T_α for each energy eigenvalue U_α via the ideal gas formula $U_\alpha = \frac{3}{2}NkT_\alpha$, and further defining a "thermal" wavelength $\lambda_\alpha = (2\pi\hbar^2/mkT_\alpha)^{1/2}$, then the criterion for the validity of Berry's conjecture is $\lambda_\alpha \lesssim a$. Numerically, this becomes $T_\alpha \gtrsim (300/ma^2)$ Kelvin, where a is in angstroms and m is in amu.

It turns out that getting explicit results will also require us to work at low density, $Na^3 \ll L^3$. Combining this with $\lambda_\alpha \lesssim a$, we see that we need to have $N\lambda_\alpha^3 \ll L^3$, a condition which is also required, in quantum statistical mechanics, for the Bose-Einstein and Fermi-Dirac distributions to be well approximated by the Maxwell-Boltzmann distribution.

Let us now consider the eigenfunctions in momentum space:

$$\begin{aligned}\widetilde{\psi}_\alpha(\mathbf{P}) &\equiv h^{-3N/2}\int_D d^{3N}X\psi_\alpha(\mathbf{X})\exp(-i\mathbf{P}\cdot\mathbf{X}/\hbar)\\ &= h^{3N/2}\mathcal{N}_\alpha\int_{-\infty}^{+\infty} d^{3N}KA_\alpha(\mathbf{K})\delta\left(\mathbf{K}^2-2mU_\alpha\right)\delta_D^{3N}(\mathbf{K}-\mathbf{P}),\end{aligned} \tag{2.6}$$

where we have defined

$$\delta_D^{3N}(\mathbf{K}) \equiv h^{-3N}\int_D d^{3N}X\exp(i\mathbf{K}\cdot\mathbf{X}/\hbar) \tag{2.7}$$

If the condition needed for Berry's conjecture is satisfied ($\lambda_\alpha \lesssim a$), and we are in the low density regime ($Na^3 \ll L^3$), then we can make the substitutions

$$\begin{aligned}\delta_D^{3N}(0) &\to (L/h)^{3N}\\ \delta_D^{3N}(\mathbf{P}) &\to \delta^{3N}(\mathbf{P})\\ \left[\delta_D^{3N}(\mathbf{P})\right]^2 &\to (L/h)^{3N}\delta^{3N}(\mathbf{P}).\end{aligned} \tag{2.8}$$

Now using eqs. (2.2), (2.4), (2.6), and (2.8), we find that (for $\lambda_\alpha \lesssim a$ and $Na^3 \ll L^3$),

$$\left\langle\widetilde{\psi}_\alpha^*(\mathbf{P})\widetilde{\psi}_\beta\left(\mathbf{P}'\right)\right\rangle_{\mathrm{EE}} = \delta_{\alpha\beta}\mathcal{N}_\alpha^2 h^{3N}\delta\left(\mathbf{P}^2-2mU_\alpha\right)\delta_D^{3N}\left(\mathbf{P}-\mathbf{P}'\right), \tag{2.9}$$

which will play a key role in the next section.

11.3 III. Eigenstate Thermalization

Let us now put our gas of N hard spheres into some initial state specified by the momentum-space wave function

$$\widetilde{\psi}(\mathbf{P},0) = \sum_\alpha C_\alpha\widetilde{\psi}_\alpha(\mathbf{P}) \tag{3.1}$$

We take the energy eigenfunctions to be orthonormal, and also assume $\widetilde{\psi}(\mathbf{P},0)$ to be normalized, so that $\sum_\alpha |C_\alpha|^2 = 1$. The expectation value of the energy is then

$$\bar{U} = \sum_\alpha |C_\alpha|^2 U_\alpha, \tag{3.2}$$

and the uncertainty in the energy is Δ, where

$$\Delta^2 = \sum_\alpha |C_\alpha|^2\left(U_\alpha-\bar{U}\right)^2 \tag{3.3}$$

We will assume that $\Delta \ll \bar{U}$. The initial wave function will evolve in time according to the Schrodinger equation:

$$\widetilde{\psi}(\mathbf{P},t) = \sum_\alpha C_\alpha\exp\left(-iU_\alpha t/\hbar\right)\widetilde{\psi}_\alpha(\mathbf{P}) \tag{3.4}$$

Now return to the thought experiment in which the system is repeatedly prepared in the same initial state (specified by the C_α 's), and the momentum of one atom is repeatedly measured after the same elapsed time t. The theoretical prediction for the fraction of atoms with momentum in a range d^3p around $\mathbf{p}$ is $f_{\mathrm{QM}}(\mathbf{p},t)d^3p$, where

$$\begin{aligned} f_{\rm QM}\left(\mathbf{p}_1,t\right) &= \int d^3p_2\ldots d^3p_N|\widetilde{\psi}(\mathbf{P},t)|^2 \\ &= \sum_{\alpha\beta} C_\alpha^* C_\beta e^{i\left(U_\alpha-U_\beta\right)t/\hbar}\int d^3p_2\ldots d^3p_N\widetilde{\psi}_\alpha^*(\mathbf{P})\widetilde{\psi}_\beta(\mathbf{P}) \\ &= \sum_{\alpha\beta} C_\alpha^* C_\beta e^{i\left(U_\alpha-U_\beta\right)t/\hbar}\Phi_{\alpha\beta}\left(\mathbf{p}_1\right) \end{aligned} \tag{3.5}$$

In the last line we have introduced

$$\Phi_{\alpha\beta}\left(\mathbf{p}_1\right) \equiv \int d^3p_2\ldots d^3p_N\widetilde{\psi}_\alpha^*(\mathbf{P})\widetilde{\psi}_\beta(\mathbf{P}) \tag{3.6}$$

which obeys the normalization condition

$$\int d^3p_1\Phi_{\alpha\beta}\left(\mathbf{p}_1\right) = \delta_{\alpha\beta}. \tag{3.7}$$

If the system thermalizes, then after some time has passed, $f_{\rm QM}\left(\mathbf{p}_1,t\right)$ should be equal to the Maxwell-Boltzmann distribution of eq. (1.1), although (as in the classical case) some modest averaging over either the initial conditions (the C_α 's) or the times of measurement (the value of t) might first be necessary. Furthermore the temperature $\bar{T}$ should be given at least approximately by the ideal gas law $\bar{U} = \frac{3}{2}Nk\bar{T}$, with a fractional uncertainty of order $\Delta/\bar{U}$.

To practice on a simple example, let us study the case where the initial state is a single energy eigenstate. This is, of course, unphysical: we cannot actually prepare such a state in a time less than $O(\hbar/\delta)$, where δ is the mean energy level spacing near U_α [22]. This is fantastically small in any realistic case [$\delta_\alpha = 1/n_\alpha$, where n_α is given by eq. (4.6)], so that $\hbar/\delta_\alpha$ is much longer than the age of the universe. Nevertheless taking the initial state to be an energy eigenstate will turn out to be an instructive exercise.

In this case, eq. (3.5) becomes simply $f_{\rm QM}\left(\mathbf{p}_1,t\right) = \Phi_{\alpha\alpha}\left(\mathbf{p}_1\right)$, which is independent of time. We now study the properties of $\Phi_{\alpha\alpha}\left(\mathbf{p}_1\right)$ in the eigenstate ensemble introduced in the previous section. Assuming high energy ($\lambda_\alpha \lesssim a$) and low density ($Na^3 \ll L^3$), it follows from eqs. (2.8), (2.9), and (3.6) that

$$\left\langle\Phi_{\alpha\alpha}\left(\mathbf{p}_1\right)\right\rangle_{\rm EE} = \mathcal{N}_\alpha^2 L^{3N}\int d^3p_2\ldots d^3p_N\delta\left(\mathbf{P}^2-2mU_\alpha\right) \tag{3.8}$$

We introduce the useful formula

$$\begin{aligned} I_D(x) &\equiv \int d^DP\delta\left(\mathbf{P}^2-x\right) \\ &= \frac{(\pi x)^{D/2}}{\Gamma(D/2)x} \end{aligned} \tag{3.9}$$

and use it to fix $\mathcal{N}_\alpha^{-2} = L^{3N}I_{3N}\left(2mU_\alpha\right)$ via eq. (3.7). We then find

$$\begin{aligned} \left\langle\Phi_{\alpha\alpha}\left(\mathbf{p}_1\right)\right\rangle_{\rm EE} &= \frac{I_{3N-3}\left(2mU_\alpha-\mathbf{p}_1^2\right)}{I_{3N}\left(2mU_\alpha\right)} \\ &= \frac{\Gamma(3N/2)}{\Gamma((3N-3)/2)}\left(\frac{1}{2\pi mU_\alpha}\right)^{3/2}\left(1-\frac{\mathbf{p}_1^2}{2mU_\alpha}\right)^{(3N-5)/2}. \end{aligned} \tag{3.10}$$

If we now set $U_\alpha = \frac{3}{2}NkT_\alpha$ and take the large N limit, we get

$$\left\langle\Phi_{\alpha\alpha}\left(\mathbf{p}_1\right)\right\rangle_{\rm EE} = \left(2\pi mkT_\alpha\right)^{-3/2}e^{-\mathbf{p}_1^2/2mkT_\alpha} \tag{3.11}$$

which is precisely $f_{\mathrm{MB}}(\mathbf{p}_1, T_\alpha)$.
Let us note first that, given eq. (3.8) as a starting point, eqs. (3.9-11) simply recapitulate a standard derivation of the canonical ensemble from the microcanonical [23].

More importantly, we must study the fluctuations of $\Phi_{\alpha\alpha}(\mathbf{p}_1)$ about its average value in the eigenstate ensemble. We begin by defining

$$[\Delta\Phi_{\alpha\beta}(\mathbf{p}_1)]^2 \equiv \left\langle \left|\Phi_{\alpha\beta}(\mathbf{p}_1)\right|^2 \right\rangle_{\mathrm{EE}} - \left|\langle \Phi_{\alpha\beta}(\mathbf{p}_1)\rangle_{\mathrm{EE}}\right|^2 \tag{3.12}$$

Using eqs. (2.5), (2.8), (2.9), and (3.6), we find

$$\begin{aligned}[\Delta\Phi_{\alpha\beta}(\mathbf{p}_1)]^2 =& \mathcal{N}_\alpha^2 \mathcal{N}_\beta^2 (Lh)^{3N} \int d^3p_2 \ldots d^3p_N d^3p'_2 \ldots d^3p'_N \\ & \times \delta\left(\mathbf{P}^2 - 2mU_\alpha\right) \delta\left(\mathbf{P}'^2 - 2mU_\beta\right) \delta_D^{3N}(\mathbf{P} - \mathbf{P}')\end{aligned} \tag{3.13}$$

Before evaluating eq. (3.13) explicitly, we can see that it will be very small: if we replace $\delta_D^{3N}(\mathbf{P} - \mathbf{P}')$ by its maximum value $(L/h)^{3N}$ everywhere, the right-hand side of eq. (3.13) becomes $\langle \Phi_{\alpha\alpha}(\mathbf{p}_1)\rangle_{\mathrm{EE}} \langle \Phi_{\beta\beta}(\mathbf{p}_1)\rangle_{\mathrm{EE}}$ [cf. eq. (3.8)]. Of course this replacement results in a huge overestimate of $[\Delta\Phi_{\alpha\beta}(\mathbf{p}_1)]^2$, since in fact $\delta_D^{3N}(\mathbf{P} - \mathbf{P}')$ is close to zero almost everywhere. Thus we will have, in particular, $\Delta\Phi_{\alpha\alpha}(\mathbf{p}_1) \ll \langle \Phi_{\alpha\alpha}(\mathbf{p}_1)\rangle_{\mathrm{EE}}$. Furthermore we see why $\Delta\Phi_{\alpha\alpha}(\mathbf{p}_1)$ is so small: $\widetilde{\psi}_\alpha(\mathbf{P})$ has fluctuations of order one in the eigenstate ensemble, but these are washed out when we integrate over most of the momenta. (In Sect. IV we will see that the same fate befalls the "scars" mentioned in Sect. II.)

We now turn to the evaluation of eq. (3.13), to find out just how small it is. We will need to know a bit more detail about $\delta_D^{3N}(\mathbf{P} - \mathbf{P}')$ than the substitution rules of eq. (2.8). We therefore approximate it with a gaussian:

$$\delta_D^{3N}(\mathbf{P} - \mathbf{P}') \simeq (L/h)^{3N} \exp\left[-(\mathbf{P} - \mathbf{P}')^2 L^2/4\pi\hbar^2\right] \tag{3.14}$$

In the low density regime ($Na^3 \ll L^3$), using eq. (3.14) instead of eq. (2.7) changes the result only by an overall constant of order one. Substituting eq. (3.14) into eq. (3.13), setting $\alpha = \beta$, and taking the large N limit yields

$$\Delta\Phi_{\alpha\alpha}(\mathbf{p}_1) = O(1) N^{1/2} e^{-3N/4} (L/\lambda_\alpha)^{-(3N-6)/2} e^{+\mathbf{p}_1^2/4mkT_\alpha} f_{\mathrm{MB}}(\mathbf{p}_1, T_\alpha)\,. \tag{3.15}$$

Since we have $L \gg \lambda_\alpha$, we see that the fluctuations in $\Phi_{\alpha\alpha}(\mathbf{p}_1)$ about $f_{\mathrm{MB}}(\mathbf{p}_1, T_\alpha)$ are negligibly small for large N. That is to say, an energy eigenstate which satisfies Berry's conjecture predicts a thermal distribution for the momentum of a single constituent particle. We will refer to this remarkable phenomenon as eigenstate thermalization.

Given a system which exhibits eigenstate thermalization, it is not hard to understand why almost any initial state will thermalize. In fact, the problem now is primarily to prevent the system from having a thermal distribution for the momentum of each particle at all times. To do so at $t = 0$, we must carefully superpose energy eigenstates in order to construct an initial state with whatever nonthermal features we might want. Once this superposition is prepared, however, the delicate phase relationships we have set up to avoid thermal behavior will gradually be destroyed by hamiltonian time evolution, and the system will equilibrate. We will see how this works in more detail in Sect. V. First, however, we digress briefly to discuss the scars, and check to see that they do not change any of our conclusions so far.

11.4 IV. Faded Scars

The theory of scar formation has been developed by Heller [15,18], Bogomolny [24], and Berry [25, 10]. We will be rather schematic here; readers unfamiliar with scar theory should consult the cited references for more details.

We first consider any system governed by a hamiltonian $H(\mathbf{P},\mathbf{X})$ which is time-reversal invariant and which results in classical chaos. For consistency of notation with the previous sections, we take $\mathbf{P}$ and $\mathbf{X}$ to be vectors with $3N$ components.

We begin by introducing the Wigner density for an eigenstate,

$$\rho_\alpha(\mathbf{P},\mathbf{X}) = h^{-3N}\int d^{3N}S\exp(i\mathbf{P}\cdot\mathbf{S}/\hbar)\psi_\alpha\left(X+\frac{1}{2}\mathbf{S}\right)\psi_\alpha\left(X-\frac{1}{2}\mathbf{S}\right) \tag{4.1}$$

where $\psi_\alpha(\mathbf{X})$ is real. The Wigner density has the useful properties that

$$\begin{aligned}\int d^{3N}P\rho_\alpha(\mathbf{P},\mathbf{X}) &= \psi_\alpha^2(\mathbf{X})\\ \int d^{3N}X\rho_\alpha(\mathbf{P},\mathbf{X}) &= \left|\widetilde{\psi}_\alpha(\mathbf{P})\right|^2\end{aligned} \tag{4.2}$$

which imply the normalization condition

$$\int d^{3N}Pd^{3N}X\rho_\alpha(\mathbf{P},\mathbf{X}) = 1 \tag{4.3}$$

Scar theory begins with a semiclassical formula for $\rho_\alpha(\mathbf{P},\mathbf{X})$:

$$\rho_\alpha(\mathbf{P},\mathbf{X}) = n_\alpha^{-1}h^{-3N}\delta\left(H(\mathbf{P},\mathbf{X})-U_\alpha\right)\left\{1+\sum_p A_p e^{iS_p/\hbar}\exp\left[(i/\hbar)\mathbf{Z}_p\cdot\mathbf{W}_p\left(T_p\right)\cdot\mathbf{Z}_p\right]\right\} \tag{4.4}$$

The sum is over all periodic orbits on the surface with constant energy U_α; S_p is the action of the orbit; T_p is a coordinate in phase space along the orbit; $\mathbf{Z}_p$ are the $6N-2$ coordinates in the energy surface which are perpendicular to the orbit; and A_p and $\mathbf{W}_p\left(T_p\right)$ are purely classical quantities which depend on the monodromy matrix of the orbit. The constant n_α is fixed by the normalization condition, eq. (4.3), and can be interpreted physically as the energy eigenvalue density near U_α. If we ignore the sum over periodic orbits in eq. (4.5), we obtain the "Weyl rule" for n_α:

$$n_\alpha = h^{-3N}\int d^{3N}Pd^{3N}X\delta\left(H(\mathbf{P},\mathbf{X})-U_\alpha\right) \tag{4.5}$$

In the case of a hard-sphere gas of $3N$ distinguishable particles, this becomes

$$n_\alpha = \frac{1}{\Gamma(3N/2)U_\alpha}\left(\frac{mL^2U_\alpha}{2\pi\hbar^2}\right)^{3N/2} \tag{4.6}$$

For bosons or fermions, the right-hand side should be divided by N !. Even so, n_α is fantastically large in any realistic case [22].

The key point for scar theory is that the periodic-orbit terms in eq. (4.4) have no $\hbar$ dependent prefactors; the peak height of each term is controlled by the classical quantity A_p. A short periodic orbit can have an A_p which is greater than one; this produces an obvious "scar" in phase space along the path of the orbit.

We are interested, however, in $\Phi_{\alpha\alpha}\left(\mathbf{p}_1\right)$, and so we must integrate $\rho_\alpha(\mathbf{P},\mathbf{X})$ over all $3N$ components of $\mathbf{X}$, and all but three of the $3N$ components of $\mathbf{P}$. If we consider isolated periodic orbits, we see from eq. (4.4) that an integral over one of the $6N-2$ components of $\mathbf{Z}_p$ yields a prefactor of $\hbar^{1/2}$. Thus the contribution of each isolated periodic orbit to $\Phi_{\alpha\alpha}\left(\mathbf{p}_1\right)$ is suppressed, relative to the leading term, by $\hbar^{(6N-3)/2}$, which means that each individual scar on $\Phi_{\alpha\alpha}\left(\mathbf{p}_1\right)$ is totally negligible.

Nonisolated periodic orbits are a little more complicated, since moving off a nonisolated orbit in some directions in phase space merely puts the system onto another nonisolated orbit in the same "family"; there are a finite number of these families. For the hard-sphere gas, the nonisolated orbits consist of motions where the spheres bounce off the walls but never collide with each other [26]. A given nonisolated orbit of this type can in general be deformed into another one by moving in any direction in coordinate space. Thus when integrating $\rho_\alpha(\mathbf{P},\mathbf{X})$ over the $3N$ components of $\mathbf{X}$, we do not get any factors of $\hbar^{1/2}$. We do, however, get a net factor of $\hbar^{(3N-3)/2}$ from integrating over $3N-3$ components of $\mathbf{P}$. Thus, while the contribution of a family of nonisolated orbits to $\Phi_{\alpha\alpha}(\mathbf{p}_1)$ is much larger than the contribution of a single isolated orbit, it is still negligible. These conclusions are supported by the much more detailed calculation of Gaspard [26] for the periodic-orbit corrections to n_α for the hard-sphere gas.

Therefore, in computing $\Phi_{\alpha\alpha}(\mathbf{p}_1)$, we can safely ignore the short isolated orbits and all of the nonisolated orbits. The most modern version of Berry's conjecture [10] then assigns the origin of the gaussian fluctuations in $\psi_\alpha(\mathbf{X})$ to the long isolated orbits. Thus $\psi_\alpha(\mathbf{X})$ is conjectured to behave like a gaussian random variable with a two-point correlation function embodied by the elegant formula [8, 11]

$$\langle \rho_\alpha(\mathbf{P},\mathbf{X})\rangle_{\mathrm{EE}} = n_\alpha^{-1} h^{-3N} \delta\left(H(\mathbf{P},\mathbf{X}) - U_\alpha\right) \tag{4.7}$$

There has been important progress recently [27] in bringing the long isolated orbits under analytic control, but so far Berry's conjecture remains just that. Even if a rigorous proof is eventually found, it is likely to apply only for asymptotically high energies. We turn, therefore, to a discussion of the existing numerical evidence.

Berry's conjecture has been studied numerically in some two-dimensional systems, such as a particle in a stadium-shaped box [14-18]. One popular object to study is the correlation function [8]

$$\begin{aligned}\mathcal{C}_\alpha(\mathbf{s}) &\equiv \int d^2x \psi_\alpha\left(\mathbf{x}+\frac{1}{2}\mathbf{s}\right)\psi_\alpha\left(\mathbf{x}-\frac{1}{2}\mathbf{s}\right)\\ &= \int d^2p d^2x \exp(-i\mathbf{p}\cdot\mathbf{s}/\hbar)\rho_\alpha(\mathbf{p},\mathbf{x})\end{aligned} \tag{4.8}$$

where in the simplest case the integral over x covers the entire box, whose area we will call L^2. For a particular eigenstate, the numerically computed $\mathcal{C}_\alpha(\mathbf{s})$ is compared to its expectation value in the eigenstate ensemble:

$$\begin{aligned}\langle \mathcal{C}_\alpha(\mathbf{s})\rangle_{\mathrm{EE}} &= \int d^2p d^2x \exp(-i\mathbf{p}\cdot\mathbf{s}/\hbar)\,\langle\rho_\alpha(\mathbf{p},\mathbf{x})\rangle_{\mathrm{EE}}\\ &= n_\alpha^{-1}h^{-2}L^2\int d^2p\,\delta\left(\mathbf{p}^2/2m - U_\alpha\right)\\ &= J_0\left(k_\alpha s\right)\end{aligned} \tag{4.9}$$

where $J_0(z)$ is a Bessel function, $k_\alpha = (2mU_\alpha/\hbar^2)^{1/2}$, and $s = |\mathbf{s}|$. In [16], only moderately good agreement was found with this prediction, with discrepancies of approximately 0.1 for $k_\alpha = 65$ and $L = \sqrt{\pi}$; see fig. 7 of [16]. However, these discrepancies are entirely explained by consideration of the fluctuations in $\mathcal{C}_\alpha(\mathbf{s})$ which are predicted by the eigenstate ensemble:

$$
\begin{aligned}
\left[\Delta\mathcal{C}_\alpha(\mathbf{s})\right]^2 \equiv & \left\langle \mathcal{C}_\alpha^2(\mathbf{s})\right\rangle_{\mathrm{EE}} - \left\langle \mathcal{C}_\alpha(\mathbf{s})\right\rangle_{\mathrm{EE}}^2 \\
= & \int d^2x d^2y \left[\left\langle \psi_\alpha\left(\mathbf{x}+\frac{1}{2}\mathbf{s}\right)\psi_\alpha\left(\mathbf{y}+\frac{1}{2}\mathbf{s}\right)\right\rangle_{\mathrm{EE}} \left\langle \psi_\alpha\left(\mathbf{x}-\frac{1}{2}\mathbf{s}\right)\psi_\alpha\left(\mathbf{y}-\frac{1}{2}\mathbf{s}\right)\right\rangle_{\mathrm{EE}} \right. \\
& \left. + \left\langle \psi_\alpha\left(\mathbf{x}+\frac{1}{2}\mathbf{s}\right)\psi_\alpha\left(\mathbf{y}-\frac{1}{2}\mathbf{s}\right)\right\rangle_{\mathrm{EE}} \left\langle \psi_\alpha\left(\mathbf{x}+\frac{1}{2}\mathbf{s}\right)\psi_\alpha\left(\mathbf{y}-\frac{1}{2}\mathbf{s}\right)\right\rangle_{\mathrm{EE}} \right] \\
= & L^{-4}\int d^2x d^2y \left[J_0^2\left(k_\alpha|\mathbf{x}-\mathbf{y}|\right) + J_0\left(k_\alpha|\mathbf{x}-\mathbf{y}+\mathbf{s}|\right) J_0\left(k_\alpha|\mathbf{x}-\mathbf{y}-\mathbf{s}|\right)\right]
\end{aligned}
\tag{4.10}
$$

The first term in the last line dominates over the second for all $\mathbf{s}$, and is $O\left(1/k_\alpha L\right)$. That is, we expect discrepancies of roughly $\left(k_\alpha L\right)^{-1/2}$ between $\mathcal{C}_\alpha(\mathbf{s})$ as computed numerically for a particular eigenstate and $\left\langle \mathcal{C}_\alpha(\mathbf{s})\right\rangle_{\mathrm{EE}}$ as given by eq. (4.9). This is exactly what is seen in fig. 7 of [16]. Similar comments apply to figs. $14-17$ of [20]. The fact that these discrepancies are predicted by the eigenstate ensemble does not seem to have been noticed previously.

We note finally that the gaussian nature of the eigenstate ensemble [which is used crucially in eq. (4.10)] has also been directly tested. The prediction is that

$$
\left\langle \psi_\alpha^{2n}(\mathbf{x})\right\rangle_{\mathrm{EE}} = (2n-1)!!\left\langle \psi_\alpha^2(\mathbf{x})\right\rangle_{\mathrm{EE}}^n = (2n-1)!!L^{-2n} \tag{4.11}
$$

but this just means that the probability distribution for the amplitude ψ at any point is

$$
P(\psi) = \frac{L}{\sqrt{2\pi}}\exp\left[-\frac{1}{2}L^2\psi^2\right] \tag{4.12}
$$

which is well supported by the numerical results [16, 19, 20].

11.5 V. Time Evolution And Equilibration

In Sect. III, we saw that an individual energy eigenstate which satisfies Berry's conjecture predicts a thermal distribution for the momentum of each constituent particle. Now we must see what happens when we consider more general states. We will once again express the initial state as a wave function in momentum space, and expand it in energy eigenfunctions, as in eq. (3.1). We assume that the uncertainty Δ in the total energy, eq. (3.3), is much smaller than the average energy $\bar{U}$, eq. (3.2). This is easy to arrange in practice.

The predicted momentum distribution of a single particle at time t is $f_{\mathrm{QM}}\left(\mathbf{p}_1,t\right)$, as given by eq. (3.5). Now take the average of eq. (3.5) in the eigenstate ensemble. From eq. (2.4), it is immediately obvious that $\left\langle \Phi_{\alpha\beta}\left(\mathbf{p}_1\right)\right\rangle_{\mathrm{EE}} = 0$ if $\alpha \neq \beta$, and so we get

$$
\begin{aligned}
\left\langle f_{\mathrm{QM}}\left(\mathbf{p}_1,t\right)\right\rangle_{\mathrm{EE}} &= \sum_\alpha \left|C_\alpha\right|^2 \left\langle \Phi_{\alpha\alpha}\left(\mathbf{p}_1\right)\right\rangle_{\mathrm{EE}} \\
&= \sum_\alpha \left|C_\alpha\right|^2 \left(2\pi m k T_\alpha\right)^{-3/2} e^{-\mathbf{p}_1^2/2mkT_\alpha}
\end{aligned}
\tag{5.1}
$$

where we have used eq. (3.11) in the second line. Now, since $\Delta \ll \bar{U}$, we can with negligible error replace each T_α in this sum with $\bar{T}$, where $\bar{U} = \frac{3}{2}Nk\bar{T}$, and then $\sum_\alpha \left|C_\alpha\right|^2 = 1$ gives us

$$
\left\langle f_{\mathrm{QM}}\left(\mathbf{p}_1,t\right)\right\rangle_{\mathrm{EE}} = f_{\mathrm{MB}}\left(\mathbf{p}_1,\bar{T}\right)\left[1+O(\Delta/\bar{U})\right] \tag{5.2}
$$

the desired result.

Once again, though, we must study the fluctuations of $f_{\mathrm{QM}}\left(\mathbf{p}_1,t\right)$ that are predicted by the eigenstate ensemble. We can write

$$
f_{\mathrm{QM}}\left(\mathbf{p}_1,t\right) = f_{\mathrm{MB}}\left(\mathbf{p}_1,\bar{T}\right) + \sum_{\alpha\beta} C_\alpha^* C_\beta e^{i\left(U_\alpha-U_\beta\right)t/\hbar}\widetilde{\Phi}_{\alpha\beta}\left(\mathbf{p}_1\right) \tag{5.3}
$$

where we have defined

$$\widetilde{\Phi}_{\alpha\beta}(p_1) \equiv \Phi_{\alpha\beta}(\mathbf{p}_1) - \langle \Phi_{\alpha\beta}(\mathbf{p}_1) \rangle_{\mathrm{EE}} . \tag{5.4}$$

Our problem is to understand the double-sum term on the right-hand side of eq. (5.3). For a fixed value of $\mathbf{p}_1$, each $\left|\widetilde{\Phi}_{\alpha\beta}(\mathbf{p}_1)\right|$ is given roughly by its RMS value in the eigenstate ensemble, which is $\Delta\Phi_{\alpha\beta}(\mathbf{p}_1)$ as given by eq. (3.13). We have already seen that $\Delta\Phi_{\alpha\alpha}(\mathbf{p}_1)$ is extremely small, and $\Delta\Phi_{\alpha\beta}(\mathbf{p}_1)$ is not going to be any bigger when $\alpha \neq \beta$. In fact, using the gaussian approximation of eq. (3.14) in eq. (3.13), we find

$$[\Delta\Phi_{\alpha\beta}(\mathbf{p}_1)]^2 \simeq [\Delta\Phi_{\alpha\alpha}(\mathbf{p}_1)]^2 \exp\left[-m(U_\alpha - U_\beta)^2 L^2/8\pi\hbar^2 U_\alpha\right] \tag{5.5}$$

We see that we will have $\Delta\Phi_{\alpha\beta}(\mathbf{p}_1) \ll \Delta\Phi_{\alpha\alpha}(\mathbf{p}_1)$ if $|U_\alpha - U_\beta|/U_\alpha$ is much bigger than $(\hbar^2/mU_\alpha L^2)^{1/2} \sim \lambda_\alpha/N^{1/2}L$, a very small number. [Note, though, that the precisely gaussian form of the falloff is an artifact of eq. (3.14).] For simplicity, let us assume that $\Delta/\bar{U} \lesssim \bar{\lambda}/N^{1/2}L$, where $\bar{\lambda} = \left(2\pi\hbar^2/mk\bar{T}\right)^{1/2}$. Then for the range of α and β of interest, each $\Delta\Phi_{\alpha\beta}(\mathbf{p}_1)$ is given by the right-hand-side of eq. (3.15) with U_α replaced by $\bar{U}$. We will need only the crudest approximations here, and so we write

$$\left|\widetilde{\Phi}_{\alpha\beta}(\mathbf{p}_1)\right| \sim \Delta\Phi_{\alpha\beta}(\mathbf{p}_1) \sim (L/\bar{\lambda})^{-3N/2} \tag{5.6}$$

However, we expect that the phase of $\widetilde{\Phi}_{\alpha\beta}(\mathbf{p}_1)$ varies wildly with α and β.
Let N_{C} be the number of nonnegligible C_α 's which appear in eq. (5.3); N_{C} can be defined precisely via $N_{\mathrm{C}}^{-1} = \sum_\alpha |C_\alpha|^4$, and crudely estimated as $N_{\mathrm{C}} \sim \bar{n}\Delta$, where $\bar{n}$ is the energy level density near $U = \bar{U}$ [cf. eq. (4.6)]. The order of magnitude of each nonnegligible $|C_\alpha|$ is then $N_{\mathrm{C}}^{-1/2}$ (so that $\sum_\alpha |C_\alpha|^2 = 1$).

Now consider doing the double sum in eq. (5.3). If the phases of the C_α 's are not carefully correlated with those of the $\widetilde{\Phi}_{\alpha\beta}(\mathbf{p}_1)$'s, then each of the two sums will yield a random-walk result: the square root of the number of "steps", $N_{\mathrm{C}}^{1/2}$, times the size of each step, $C_\alpha \sim N_{\mathrm{C}}^{-1/2}$. With an overall factor of $(L/\bar{\lambda})^{-3N/2}$ from eq. (5.6), we get

$$\sum_{\alpha\beta} C_\alpha^* C_\beta e^{i(U_\alpha - U_\beta)t/\hbar} \widetilde{\Phi}_{\alpha\beta}(\mathbf{p}_1) \sim (L/\bar{\lambda})^{-3N/2} \tag{5.7}$$

which is again extremely small. If we let $\Delta/\bar{U}$ be bigger than $\bar{\lambda}/N^{1/2}L$, then the result is even smaller.

On the other hand, we can certainly set up an initial state which is very far from thermal. For example, we could give each particle the same initial value (to within quantum uncertainties) for its individual momentum, leading to an $f_{\mathrm{QM}}(\mathbf{p}_1, 0)$ which is sharply peaked at that value. In this case, though, the phases of the C_α 's must be correlated with those of the $\widetilde{\Phi}_{\alpha\beta}(\mathbf{p}_1)$'s in exactly the right way to produce the desired nonthermal distribution $f_{\mathrm{QM}}(\mathbf{p}_1, 0)$. In this case, we want to see what happens as time evolves.

Let us begin with eq. (5.3) at $t = 0$, with the phases of the C_α 's carefully chosen to give us a nonthermal distribution. Now let the clock run. Each of the off-diagonal ($\alpha \neq \beta$) terms in the double sum begins acquiring an extra phase; there are roughly N_{C}^2 off-diagonal terms in all. The growing phase of each individual term will cause its contribution to the sum to have a random orientation in the complex plane once $|U_\alpha - U_\beta|\, t/\hbar \gtrsim 2\pi$. We will say that such a term has decohered. The first terms to decohere (those with the largest difference between U_α and U_β) do so at a time $t \sim h/\Delta$. The fraction of terms which have decohered at later times is given roughly by $(\Delta - h/t)^2/\Delta^2$. Thus the fraction of still coherent terms at this time is roughly $1 - (\Delta - h/t)^2/\Delta^2 \sim (h/\Delta)/t$ for $t \gg h/\Delta$.

Now, each of the coherent terms should give its usual contribution to the sum, since its phase is still (almost) properly aligned, but the net contribution of all the coherent terms will be suppressed by a factor of $O(h/\Delta)t^{-1}$ due to their reduced population. On the other hand, the terms which have decohered will contribute with random phases. Since almost all terms have decohered for $t \gg h/\Delta$, their total contribution will be given by eq. (5.6), and is negligibly small. Thus, overall we expect that any nonthermal features present in the initial distribution $f_{\rm QM}(\mathbf{p}_1, 0)$ will decay away with time like $O(h/\Delta)t^{-1}$.

We can test this conclusion with a very simple example. The system we will analyze is classically integrable, and so chaos plays no role in the following discussion.

Consider a single particle with mass $m = 100$ in a two-dimensional circular box with radius $R = 1$; we also set $\hbar = 1$. The initial wave function for the particle is taken to be

$$\psi(\mathbf{x}, 0) = \pi^{-1/2} a^{-1} \exp(i\mathbf{p}_0 \cdot \mathbf{x}) \exp\left(-\mathbf{x}^2/2a^2\right) \tag{5.8}$$

This is a gaussian wave packet of width a at the center of the box, moving with momentum $\mathbf{p}_0$. If we Fourier transform into momentum space, we get

$$\widetilde{\psi}(\mathbf{p}, 0) = \pi^{-1/2} a \exp\left[-\frac{1}{2}a^2 (\mathbf{p} - \mathbf{p}_0)^2\right]. \tag{5.9}$$

We will take $a = 0.1$ and $p_0 = 100$. Classically, the particle has energy $E = p_0^2/2m = 50$, and just bounces back and forth, changing directions at times $t = 1, 3, 5, \ldots$ Quantum mechanically, the uncertainty in the particle's energy is $\Delta = p_0/\sqrt{2}ma \simeq 7$. We can solve this problem exactly by expanding $\widetilde{\psi}(\mathbf{p}, 0)$ in the energy eigenstate basis and using eq. (3.4). Then we can compute the probability density for the particle to have its initial momentum at time t; that is, we compute $\left|\widetilde{\psi}(\mathbf{p}_0, t)\right|^2$. Let us see what we should expect for this quantity, based on the general arguments outlined above.

First of all, note that the infinite time average of $\left|\widetilde{\psi}(\mathbf{p}_0, t)\right|^2$ is given by

$$\lim_{\tau\to\infty} \frac{1}{\tau} \int_0^\tau dt \left|\widetilde{\psi}(\mathbf{p}_0, t)\right|^2 = \sum_\alpha |C_\alpha|^2 \left|\widetilde{\psi}_\alpha(\mathbf{p}_0)\right|^2 \tag{5.10}$$

where $\widetilde{\psi}_\alpha(\mathbf{p}_0)$ is an energy eigenfunction in momentum space. We expect $\left|\widetilde{\psi}(\mathbf{p}_0, t)\right|^2$ to approach its infinite time average at late times, with late-time fluctuations of the same order of magnitude. If $\left|\widetilde{\psi}(\mathbf{p}_0, t)\right|^2$ does not start out close to its infinite time average at $t = 0$, then it should decay towards that value like $O(h/\Delta)t^{-1}$.

The exact result for $\left|\widetilde{\psi}(\mathbf{p}_0, t)\right|^2$, normalized to its value at $t = 0$, is shown in fig. 1. We clearly see the classical bounces, as the probability to have the initial momentum drops to zero at the first turning point, $t = 1$, then returns at $t = 3$, etc. However, the quantum probability does not return to its initial value, but follows the $(h/\Delta)/t$ envelope predicted by the general argument outlined above. It finally drops down to its infinite time average, with fluctuations of the expected size. Thus we see that the simple phase decoherence argument works very well for this example.

If we now compare the right-hand sides of eqs. (5.1) and eq. (5.10), we see the analogy between the infinite time average of $\left|\widetilde{\psi}(\mathbf{p}_0, t)\right|^2$ and the eigenstate ensemble average of $f_{\rm QM}(\mathbf{p}_1, t)$. The main difference is that, because we have integrated out almost all the degrees of freedom, the fluctuations of $f_{\rm QM}(\mathbf{p}_1, t)$ about its average value are very small.

There is more we can learn from our simple example, however. First, we have seen that the classical motion is reflected in the quantum probabilities, a fact which is expected to be

true for classically chaotic systems as well [28]. This means that quantum initial states which can be understood as representing classical initial conditions may thermalize even faster, due to the effects of classical chaos. If we can follow classical trajectories (with initial quantum uncertainties) for some time, and classical chaos spreads these out over a constant energy surface in phase space, then the system has thermalized classically. This argument may be needed in cases where the initial distribution is so far from thermal that the quantum $O(h/\Delta)t^{-1}$ decay of its nonthermal features seems to take too long. It also shows that the $O(h/\Delta)t^{-1}$ rule need not be related to more traditional diffusion times, which are more likely to reflect classical physics.

Second, consider fig. 2, which shows the $|C_\alpha|$'s for this problem plotted against the corresponding energy eigenvalues, E_α. While they form a nice envelope, with mean energy $\bar{E} = 50$ and uncertainty $\Delta = 7$, there is a great deal of fine structure. This is needed to get the very special initial state, localized at the origin and moving in the x direction at a particular speed. We cannot, therefore, think of replacing C_α by a smooth function of E_α. This is unfortunate, since if we average eq. (4.4) over a smooth distribution of energy eigenvalues, the contributions of the long periodic orbits are suppressed [24,25,10], and the problem becomes much more tractable. However, as we see in fig. 2, such smoothing is physically far too restrictive, since it would prevent us from considering a wide variety of initial states which we could actually prepare in a real experiment.

Let us summarize the results of this section. If we construct a particular initial state for the hard-sphere gas at low density by superposing energy eigenstates, each of which individually satisfies Berry's conjecture, then we find that, at sufficiently late times, the quantum mechanical prediction for the probability that any one particle has momentum $\mathbf{p}$ is simply given by the Maxwell-Boltzmann distribution of eq. (1.1). The probability that this will not be the case is negligible, if we wait long enough. Any nonthermal features of the initial distribution for a single particle's momentum will decay away at least as fast as $O(h/\Delta)t^{-1}$, where Δ is the quantum uncertainty in the total energy. Faster decays are possible, and likely if the initial state has a classical interpretation. Absolutely no averaging over initial states or times of measurement is needed, in contrast with the classical case.

This concludes our analysis of the high energy, low density, hard-sphere gas in the case that we assume no symmetries of the wave function on exchange of individual particles. We will return to discuss lower energies and higher densities in Sect. VII. Now, though, we turn our attention to wave functions which are either completely symmetric or completely antisymmetric functions of the positions of the N particles.

11.6 VI. Bosons And Fermions

The detailed analysis in Sects. II and III required the assumptions of high energy ($\lambda_\alpha \lesssim a$) and low density ($Na^3 \ll L^3$), which combine to give $N\lambda_\alpha^3 \ll L^3$. In Sect. II we noted that this is precisely the condition needed for the Bose-Einstein and Fermi-Dirac distributions to be well approximated by the Maxwell-Boltzmann distribution. Nevertheless, even though the corrections due to quantum statistics may be numerically small, a valid formalism should be able to reproduce them. In this section we will see that the present formalism meets this test.

Define a symmetrization operator $\mathcal{P}_\pm$via

$$\mathcal{P}_\pm f(\mathbf{p}_1 \ldots \mathbf{p}_N) = \frac{1}{N!} \sum_{\text{perms}} (\pm 1)^P f(\mathbf{p}_{i_1}, \ldots, \mathbf{p}_{i_N}) \tag{6.1}$$

where the sum is over the permutations of the indices, and P is even (odd) if the permutation is even (odd). Now we can construct completely symmetric and antisymmetric energy eigenfunctions analogous to those of eq. (2.2):

$$\psi_\alpha^\pm(\mathbf{X}) = \mathcal{N}_\alpha^\pm \int d^{3N_P} A_\alpha(\mathbf{P}) \delta\left(\mathbf{P}^2 - 2mU_\alpha\right) \mathcal{P}_\pm \exp(i\mathbf{P}\cdot\mathbf{X}/\hbar) \tag{6.2}$$

We will need the generalization of eq. (2.9). Using the same assumptions as in Sect. III, namely $\lambda_\alpha \lesssim a$ and $Na^3 \ll L^3$, we get

$$\left\langle \widetilde{\psi}_\alpha^{\pm *}(\mathbf{P}) \widetilde{\psi}_\beta^{\pm}(\mathbf{P}') \right\rangle_{\mathrm{EE}} = \delta_{\alpha\beta} \left(\mathcal{N}_\alpha^\pm\right)^2 h^{3N} \delta\left(\mathbf{P}^2 - 2mU_\alpha\right) \mathcal{P}_\pm \delta_D^{3N}(\mathbf{P} - \mathbf{P}') \tag{6.3}$$

We now want to compute

$$\left\langle \Phi_{\alpha\alpha}^\pm(\mathbf{p}_1) \right\rangle_{\mathrm{EE}} = \int d^3p_2 \ldots d^3p_N \left\langle \widetilde{\psi}_\alpha^{\pm *}(\mathbf{P}) \widetilde{\psi}_\alpha^{\pm}(\mathbf{P}) \right\rangle_{\mathrm{EE}} \tag{6.4}$$

For nonsymmetric wave functions, we found in Sect. III that $\langle \Phi_{\alpha\alpha}(\mathbf{p}_1) \rangle_{\mathrm{EE}}$ was equal to a Maxwell-Boltzmann distribution at a temperature T_α related to the energy eigenvalue U_α by the ideal gas formula $U_\alpha = \frac{3}{2} N k T_\alpha$. We therefore expect to find that $\langle \Phi_{\alpha\alpha}^\pm(\mathbf{p}_1) \rangle_{\mathrm{EE}}$ is given by a Bose-Einstein distribution $f_{\mathrm{BE}}(\mathbf{p}_1, T_\alpha) \equiv f^+(\mathbf{p}_1, T_\alpha)$ or a Fermi-Dirac distribution $f_{\mathrm{FD}}(\mathbf{p}_1, T_\alpha) \equiv f^-(\mathbf{p}_1, T_\alpha)$. In statistical mechanics, these are usually computed using the grand canonical ensemble, but in our case the number of particles is firmly fixed at N. Thus we expect to find that $\langle \Phi_{\alpha\alpha}^\pm(\mathbf{p}_1) \rangle_{\mathrm{EE}}$ is equal to $f^\pm(\mathbf{p}_1, T_\alpha)$ as given by the canonical, rather than the grand canonical, ensemble. Relevant formulae from the less familiar canonical ensemble are gathered in the Appendix.

Let us warm up by computing $\mathcal{N}_\alpha^\pm$. The normalization condition we need is

$$\int d^3p_1 \ldots d^3p_N \left\langle \widetilde{\psi}_\alpha^{\pm *}(\mathbf{P}) \widetilde{\psi}_\alpha^{\pm}(\mathbf{P}) \right\rangle_{\mathrm{EE}} = 1 \tag{6.5}$$

We must first evaluate

$$\mathcal{P}_\pm \delta_D^{3N}(\mathbf{P} - \mathbf{P}')\big|_{\mathbf{P}'=\mathbf{P}} = \frac{1}{N!} \sum_{\text{perms}} (\pm 1)^P \delta_D^3(\mathbf{p}_1 - \mathbf{p}_{i_1}) \ldots \delta_D^3(\mathbf{p}_N - \mathbf{p}_{i_N}) \tag{6.6}$$

where $\delta_D^3(\mathbf{p})$ is assumed to satisfy the substitution rules of eq. (2.8) with $N \to 1$. Now examine a particular term in this sum. If a particular momentum is paired with itself, we will say that it comprises a "1-cluster." If a particular momentum is not paired with itself, it will be part of an " m-cluster" of momenta which are all set equal to each other by the (approximate) delta functions. For each term, let m_l be the number of momenta in the l th cluster, with $m_1 \leq \ldots \leq m_C$. Also let C_m be the number of m-clusters, and C be the total number of clusters. Obviously, we have the relations

$$\begin{aligned} m_1 + \ldots + m_C &= N, \\ C_1 + \ldots + C_N &= C \\ C_1 + 2C_2 + \ldots + NC_N &= N \end{aligned} \tag{6.7}$$

Each term in the sum in eq. (6.6) can now be labeled by a set of nondecreasing integers $\{m\} \equiv \{m_1, \ldots, m_C\}$. The number of terms with the same label is

$$A_{\{m\}} \prod_{l=1}^{C} (m_l - 1)! \tag{6.8}$$

where $(m_l - 1)$! counts the number of ways momenta in the l th cluster can be rearranged without breaking it into smaller clusters, and

$$A_{\{m\}} = \frac{N!}{(m_1! \ldots m_C!)\,(C_1! \ldots C_N!)} \tag{6.9}$$

counts the number of inequivalent ways of assigning momenta to clusters. Each cluster has one redundant delta function, which results in a factor of $(L/h)^{3C}$. Furthermore the l th cluster contributes a factor of $(\pm 1)^{m_l - 1}$ to $(\pm 1)^P$. Now from eqs. (6.3) and (6.5) we see that to determine $\mathcal{N}_\alpha^\pm$we must multiply each term in eq. (6.6) by $\delta\left(\mathbf{P}^2 - 2mU_\alpha\right)$ and then integrate over all the momenta. Under the integral, when multiplied by a term labeled by $\{m\}$, we can make the replacement

$$\delta\left(\mathbf{P}^2 - 2mU_\alpha\right) \to \delta\left(m_1\mathbf{p}_1^2 + \ldots + m_C\mathbf{p}_C^2 - 2mU_\alpha\right), \tag{6.10}$$

All together, then, we have

$$\begin{aligned}\left(\mathcal{N}_\alpha^\pm\right)^{-2} = h^{3N} \sum_{\{m\}} A_{\{m\}} (L/h)^{3C} \int d^3p_1 \ldots d^3p_C \\ \times \delta\left(m_1\mathbf{p}_1^2 + \ldots + m_C\mathbf{p}_C^2 - 2mU_\alpha\right) \prod_{l=1}^{C} (\pm 1)^{m_l - 1}\,(m_l - 1)!\end{aligned} \tag{6.11}$$

The sum is over all $\{m\}$ with fixed N. We now make the change of variable $\mathbf{p}_i \to m_i^{-1/2}\mathbf{k}_i$, which yields

$$\left(\mathcal{N}_\alpha^\pm\right)^{-2} = h^{3N} \sum_{\{m\}} A_{\{m\}} (L/h)^{3C} I_{3C}\left(2mU_\alpha\right) \prod_{l=1}^{C} (\pm 1)^{m_l - 1}\,(m_l - 1)! m_l^{-3/2} \tag{6.12}$$

where $I_D(x)$ is defined in eq. (3.9). It turns out that terms with $C \gg 1$ dominate, and so we can use the large- C formula

$$h^{3N}(L/h)^{3C} I_{3C}\left(2mU_\alpha\right) \simeq \lambda_\alpha^{3N}\left(L/\lambda_\alpha\right)^{3C} I_{3N}\left(2mU_\alpha\right) \tag{6.13}$$

where $\lambda_\alpha = \left(2\pi\hbar^2/mkT_\alpha\right)^{1/2}$, to rewrite eq. (6.12) as

$$\left(\mathcal{N}_\alpha^\pm\right)^{-2} = \lambda_\alpha^{3N} I_{3N}\left(2mU_\alpha\right) \sum_{\{m\}} A_{\{m\}} \prod_{l=1}^{C} \left(L/\lambda_\alpha\right)^3 (\pm 1)^{m_l - 1}\,(m_l - 1)! m_l^{-3/2} \tag{6.14}$$

Now we can apply the Mayer cluster-expansion theorem [29], which can be written as

$$\sum_{\{m\}} A_{\{m\}} \prod_{l=1}^{C} W_{m_l} = \frac{\partial^N}{\partial z^N} \left\{ \exp\left[\sum_{m=1}^{\infty} \frac{z^m}{m!} W_m \right] \right\} \Bigg|_{z=0} \tag{6.15}$$

where, in our case,

$$W_m = \left(L/\lambda_\alpha\right)^3 (\pm 1)^{m-1} (m-1)! m^{-3/2}. \tag{6.16}$$

From eq. (A.3) of the Appendix, we have

$$\sum_{m=1}^{\infty} \frac{z^m}{m!} W_m = \left(L/\lambda_\alpha\right)^3 g_{5/2}^\pm(z) \tag{6.17}$$

So putting all of this together, we find

$$\begin{aligned}\left(\mathcal{N}_\alpha^{\pm}\right)^{-2} &= \lambda_\alpha^{3N} I_{3N}\left(2mU_\alpha\right) \frac{\partial^N}{\partial z^N}\left\{\exp\left[\left(L/\lambda_\alpha\right)^3 g_{5/2}^{\pm}(z)\right]\right\}\Big|_{z=0} \\ &= \lambda_\alpha^{3N} I_{3N}\left(2mU_\alpha\right) N! Z_{\mathrm{C}}^{\pm} \end{aligned} \tag{6.18}$$

where $Z_{\mathrm{C}}^{\pm}$is the canonical partition function for a gas of noninteracting bosons (+)or fermions (−) at a temperature T_α in a box of volume L^3 [cf. eq. (A.8)].

Clearly we are on the right track! Now we have to do it all over again, this time leaving one of the N momenta unintegrated.

Following the same logic which led us to eq. (6.12), we get

$$\begin{aligned}\left\langle \Phi_{\alpha\alpha}^{\pm}\left(\mathbf{p}_1\right)\right\rangle_{\mathrm{EE}} = \left(\mathcal{N}_\alpha^{\pm}\right)^2 h^{3N} \sum_{\{m\}} A_{\{m\}} (L/h)^{3C} \sum_{i=1}^{C} \left(m_i/N\right) I_{3C-3}\left(2mU_\alpha - m_i \mathbf{p}_1^2\right) \\ \times (\pm 1)^{m_i-1}\left(m_i-1\right)! \prod_{l\neq i} (\pm 1)^{m_l-1}\left(m_l-1\right)! m_l^{-3/2}\end{aligned} \tag{6.19}$$

The differences from eq. (6.12) arise as follows. First, we must choose which cluster contains the unintegrated momentum $\mathbf{p}_1$; this gives the sum over $i = 1$ to C. Then we must choose which of the m_i momenta in the i th cluster is unintegrated; this gives the factor of m_i. Now we have overcounted by N, which results in the factor of $1/N$. The change to the subscript and argument of I results from not integrating $\mathbf{p}_1$, and the factor of $m_i^{-3/2}$ is missing because we did not have to rescale $\mathbf{p}_1$.

Again, terms with $C \gg 1$ dominate, and so we have

$$I_{3C-3}\left(2mU_\alpha - m_i\mathbf{p}_1^2\right) \simeq \left(2\pi mkT_\alpha\right)^{-3/2} \exp\left(-m_i\mathbf{p}_1^2/2mkT_\alpha\right) I_{3C}\left(2mU_\alpha\right) \tag{6.20}$$

Then using eq.(6.13), we get

$$\left\langle \Phi_{\alpha\alpha}^{\pm}\left(\mathbf{p}_1\right)\right\rangle_{\mathrm{EE}} = \left(\mathcal{N}_\alpha^{\pm}\right)^2 \lambda_\alpha^{3N} I_{3N}\left(2mU_\alpha\right) \sum_{\{m\}} A_{\{m\}} \sum_{i=1}^{C} V_{m_i} \prod_{l\neq i} W_{m_l} \tag{6.21}$$

where W_m is given by eq. (6.16), and

$$V_k = \left(L^3/Nh^3\right)(\pm 1)^{k-1} k! \left[\exp\left(-\mathbf{p}_1^2/2mT_\alpha\right)\right]^k \tag{6.22}$$

Starting with eq. (6.15), it is not hard to prove a generalization of it which reads

$$\sum_{\{m\}} A_{\{m\}} \sum_{i=1}^{C} V_{m_i} \prod_{l\neq i} W_{m_l} = \frac{\partial^N}{\partial z^N}\left\{\left[\sum_{k=1}^{\infty} \frac{z^k}{k!} V_m\right] \exp\left[\sum_{m=1}^{\infty} \frac{z^m}{m!} W_m\right]\right\}\Big|_{z=0} \tag{6.23}$$

In the present case, we have

$$\sum_{k=1}^{\infty} \frac{z^k}{k!} V_m = \frac{L^3}{Nh^3} \frac{z}{\exp\left(\mathbf{p}_1^2/2mT_\alpha\right) \mp z} \tag{6.24}$$

Combining eqs. (6.17), (6.18), (6.21), (6.23), and (6.24), we finally get

$$\begin{aligned}\left\langle \Phi_{\alpha\alpha}^{\pm}\left(\mathbf{p}_1\right)\right\rangle_{\mathrm{EE}} &= \frac{1}{Z_{\mathrm{C}}^{\pm}} \frac{1}{N!} \frac{\partial^N}{\partial z^N}\left\{\exp\left[\left(L/\lambda\right)^3 g_{5/2}^{\pm}(z)\right] \frac{L^3}{Nh^3} \frac{z}{\exp\left(\mathbf{p}_1^2/2mT_\alpha\right) \mp z}\right\}\Big|_{z=0} \\ &= f^{\pm}\left(\mathbf{p}_1, T_\alpha\right)\end{aligned} \tag{6.25}$$

where $f^{\pm}(\mathbf{p}_1, T_\alpha)$ is the Bose-Einstein (+) or Fermi-Dirac (-) distribution as predicted by the canonical ensemble [cf. eq. (A.12)]. As expected, then, symmetrization or antisymmetrization of the wave function changes the statistics from Maxwell-Boltzmann to Bose-Einstein or Fermi-Dirac .

For the last time, we must study the fluctuations of $\Phi_{\alpha\alpha}(\mathbf{p}_1)$ that are predicted by the eigenstate ensemble. The relevant object is $\Delta\Phi^{\pm}_{\alpha\beta}(\mathbf{p}_1)$, defined by the obvious replacements in eq. (3.12). $\Delta\Phi^{\pm}_{\alpha\beta}(\mathbf{p}_1)$ is then given by eq. (3.13) with $\mathcal{P}_{\pm}$acting on $\delta^{3N}_D(\mathbf{P}-\mathbf{P}')$. Explicit evaluation of $\Delta\Phi^{\pm}_{\alpha\beta}(\mathbf{p}_1)$ is a fearsome combinatoric problem, but luckily a simple variation of the general argument presented after eq. (3.13) still applies, and can be used to show that $\Delta\Phi^{\pm}_{\alpha\beta}(\mathbf{p}_1)$ is very small compared to $\langle\Phi^{\pm}_{\alpha\alpha}(\mathbf{p}_1)\rangle_{\mathrm{EE}}\langle\Phi^{\pm}_{\beta\beta}(\mathbf{p}_1)\rangle_{\mathrm{EE}}$. Therefore eigenstate thermalization still holds, and the previous analysis (in Sect. V) of time evolution still applies.

11.7 VII. Discussion And Speculation

Let us begin with a brief recap of the central results. Berry's conjecture, as applied to a gas of N hard spheres in a box, states that each energy eigenfunction appears to be a superposition of plane waves with wavelength fixed by the energy eigenvalue, but with random phases and gaussian random amplitudes. It is expected to apply only to systems which are classically chaotic, and has been found to be valid (with corrections that do
not affect our conclusions) in simple chaotic systems. Given Berry's conjecture for the hard-sphere gas, we have discovered the phenomenon of eigenstate thermalization: each energy eigenstate predicts a thermal distribution for the momentum of each constituent particle. This distribution is Maxwell-Boltzmann, Bose-Einstein, or Fermi-Dirac, depending on whether the energy eigenfunctions are nonsymmetric, completely symmetric, or completely antisymmetric functions of the N particle positions. Then, a superposition of energy eigenstates with a small fractional uncertainty in the total energy will also appear to be thermal, unless the amplitudes and phases of the superposition coefficients are carefully selected to avoid thermal behavior. If this is done initially, then the usual phase changes produced by hamiltonian time evolution destroy the needed coherence, and any nonthermal features disappear as $O(h/\Delta)t^{-1}$, where Δ is the uncertainty in the total energy. However, classical effects which are reflected in the quantum theory can result in faster thermalization.

All of the analysis in Sects. II, III, and VI was done in the limits of low density: $Na^3 \ll L^3$, where a is the radius of a hard sphere and L^3 is the volume of the box, and high energy: $\lambda_\alpha \lesssim a$, where $\lambda_\alpha = (2\pi\hbar^2/mkT_\alpha)^{1/2}$ is the typical wavelength of one particle when the energy eigenvalue is $U_\alpha = \frac{3}{2}NkT_\alpha$; numerically this means $T_\alpha \gtrsim (300/ma^2)$ Kelvin, where a is in angstroms and m is in amu. But what happens if we relax these constraints?

There are no fundamental difficulties with carrying out the analysis for moderately higher densities. All we need to do is use the exact formula for the smeared delta function in momentum space, eq. (2.7). In practice, though, this greatly complicates the calculations. It would be very interesting to try to develop some sort of perturbative (in $a/N^{1/3}L$) analysis, and compare the results with more standard treatments of the hard-sphere Bose or Fermi gas [30].

Lower energies present an entirely different problem, since if we go low enough in energy, Berry's conjecture will break down. The question is, how low can we go? The generic expectation is that Berry's conjecture will be valid if the relevant wavelengths are small enough to "see" the features which produce classical chaos [16]. For the hard-sphere gas, the relevant feature is the nonzero radius a of each particle, which leads to $\lambda_\alpha \lesssim a$. However, this may not be good enough at high density [31]. Classically, if the density is large enough to result in very slow diffusion of the particles, then their positions will be correlated over long times; the Lyapunov exponents are all very small. We would then naturally expect that these correlations are reflected in the quantum energy eigenfunctions, which would mean that Berry's conjecture

is not valid. In this case, a possible alternative criterion for the validity of Berry's conjecture is $\lambda_\alpha \lesssim \ell$, where ℓ is the classical mean free path of a particle, which can be much less than a.

Whatever the correct criterion turns out to be, at a low enough energy Berry's conjecture will break down, and we must ask what happens at lower energies. One possibility is that eigenstate thermalization will still be valid for a wide range of energy eigenvalues, even though Berry's conjecture is not. The reason for this speculation appears in the results of eqs. (3.15) and Sect. IV. In eq. (3.15), we see that the fluctuations about the mean, thermal value of $\Phi_{\alpha\alpha}(\mathbf{p}_1)$ in the eigenstate ensemble are extremely small; experimentally, we can tolerate much larger fluctuations. Thus, we may also be able to tolerate significant violations of Berry's conjecture without destroying eigenstate thermalization. In Sect. IV, this speculation receives some more support. Scars represent violations of Berry's conjecture which are quite obvious when one looks at the Wigner density of an energy eigenstate in phase space, since there the scars appear with a "signal-to-noise" ratio of 1:1. Once we integrate out all of the coordinates and most of the momenta, however, the scars fade away almost completely. The same should be true of more generic violations of Berry's conjecture. Thus, eigenstate thermalization may still be valid at energies well below the threshold for the validity of Berry's conjecture.

If we go even lower in energy, though, presumably eigenstate thermalization will eventually cease to be valid. If the system is this low in energy, it will not be able to thermalize itself. To find thermal behavior in a system below its threshold for eigenstate thermalization, we must couple it to an external heat bath, such as the refrigeration apparatus in a low-temperature experiment. Of course, once we have contact with a large, pre-existing heat bath, all the usual results of statistical mechanics can be applied without further worry.

The basic question we have been trying to address in this paper is how such a heat bath might form in the first place. We have seen that this will happen for a hard-sphere gas, provided that Berry's conjecture is satisfied by the energy eigenstates which are superposed to form the initial state. Whether or not other mechanisms exist for self-thermalization of isolated quantum systems is an open question, one to which we hope to return. Meanwhile we believe that the present results constitute a new foundation for quantum statistical mechanics. In particular, we have at least one answer to the question of which quantum systems will approach thermal equilibrium. It is satisfying that this answer (those systems which obey Berry's conjecture) is closely related to the answer from classical physics (those systems which exhibit chaos). In fact the situation in the quantum theory is even better than it is in the classical theory, because we no longer need to consider an ensemble of initial states. Each and every superposition of energy eigenstates obeying Berry's conjecture will eventually yield a thermal distribution for the momentum of a constituent particle, provided that we wait long enough. Absolutely no averaging of any kind is needed: not over initial states, not over times of measurement, and not over hamiltonians.

Finally we would like to comment on the much-discussed question of an appropriate definition for quantum chaos. Some time ago, van Kampen suggested that quantum chaos be defined as "that property that causes a quantum system to behave statistically" [32]. If we replace "behave statistically" with "obey the laws of statistical mechanics," then we have seen that the key feature is Berry's conjectured properties of the energy eigenstates. In particular, properties of the energy eigenvalues (such as GOE rather than Poisson statistics for the unfolded level spacings [33]) have played no role at all in the present work. Steiner has suggested [21] that Berry's conjecture be elevated to the status of the best definition of quantum chaos, a proposal which we see to be equivalent to (our version of) van Kampen's. More generally, in quantum mechanics, where time evolution is always linear and therefore essentially trivial, the only place to encode the complexities of the classical limit is in the energy eigenfunctions: that is where quantum chaos, like thermal behavior, must be sought.

I am grateful to Walter Kohn, Jim Langer, Joe Polchinski, Andy Strominger, and especially Doug Scalapino for helpful discussions. I also thank Matthew Foulkes for pointing out an error in the original version of this paper, and the anonymous referee for several suggested improvements. This work was supported in part by NSF Grant PHY-91-16964.

11.8 Appendix. The Canonical Ensemble For Bosons And Fermions

We will use a notation close to that of [5]. We ignore spin degrees of freedom.
The canonical partition function for N noninteracting bosons or fermions in a box is given by

$$Z_{\mathrm{C}}^{\pm} = \prod_{l=0}^{\infty} \sum_{n_l=0}^{N_{\pm}} e^{-\beta n_l E_l} \delta_{N, n_1+n_2+\ldots} \tag{A.1}$$

where $\beta = 1/kT$, E_l is the l th energy eigenvalue for a single particle in the box, and $N_+ = \infty$ for bosons and $N_- = 1$ for fermions.

Introducing the fugacity z, the grand canonical partition function for N noninteracting bosons or fermions in a box is given by

$$\begin{aligned} Z_{\mathrm{GC}}^{\pm} &= \prod_{l=0}^{\infty} \sum_{n_l=0}^{N_{\pm}} z^{n_l} e^{-\beta n_l E_l} \\ &= \exp\left[\mp \sum_{l=0}^{\infty} \log\left(1 \mp z e^{-\beta E_l}\right) \right] \\ &= \exp\left[\mp L^3 h^{-3} \int d^3p \log\left(1 \mp z e^{-\beta \mathbf{p}^2/2m}\right) \right] \\ &= \exp\left[(L/\lambda)^3 g_{5/2}^{\pm}(z) \right] \end{aligned} \tag{A.2}$$

In the third line, we have replaced the sum over levels by an integral over momenta (without separating out the zero mode, which would be necessary for a discussion of

Bose condensation). In the fourth line, we have introduced the thermal wavelength $\lambda \equiv (2\pi\hbar^2/mkT)^{1/2}$, and the Lerch transcendents

$$g_{\nu}^{\pm}(z) \equiv \sum_{m=1}^{\infty} \frac{(\pm)^{m-1} z^m}{m^{\nu}} \tag{A.3}$$

$Z_{\mathrm{GC}}^{\pm}$must be supplemented with the condition

$$\begin{aligned} N &= z \frac{\partial}{\partial z} \log Z_{\mathrm{GC}}^{\pm} \\ &= (L/\lambda)^3 g_{3/2}^{\pm}(z) \end{aligned} \tag{A.4}$$

which can be thought of as fixing the value of z. We will call the positive real solution of this equation z_0.

The relation between $Z_{\mathrm{C}}^{\pm}$and $Z_{\mathrm{GC}}^{\pm}$can be found by writing the Kronecker delta in eq. (A.1) as

$$\delta_{N, n_1+n_2+\ldots} = \frac{1}{2\pi i} \oint dz z^{-N-1} z^{n_1+n_2+\ldots}, \tag{A.5}$$

where the contour encloses the origin. Substituting this into eq. (A.1) and using the first and fourth lines of eq. (A.2) yields

$$Z_{\rm C}^{\pm} = \frac{1}{2\pi i}\oint dz z^{-N-1} Z_{\rm GC}^{\pm} = \frac{1}{2\pi i}\oint dz z^{-N-1} \exp\left[(L/\lambda)^3 g_{5/2}^{\pm}(z)\right] \tag{A.6}$$

Evaluating this integral approximately by stationary phase, treating both N and $(L/\lambda)^3$ as large, results in

$$Z_{\rm C}^{\pm} = \left[2\pi (L/\lambda)^3 g_{1/2}^{\pm}(z_0)\right]^{-1/2} Z_{\rm GC}^{\pm} \tag{A.7}$$

where $Z_{\rm GC}^{\pm}$is to be evaluated at $z = z_0$. The fractional error in this approximate equality is of order $1/N$. Note also that, using Cauchy's theorem, we can rewrite eq. (A.6) as

$$Z_{\rm C}^{\pm} = \frac{1}{N!}\frac{\partial^N}{\partial z^N}\left\{\exp\left[(L/\lambda)^3 g_{5/2}^{\pm}(z)\right]\right\}\Big|_{z=0} \tag{A.8}$$

We would now like to compute the expected fraction $\langle f^{\pm}(\mathbf{p})\rangle\, d^3p$ of particles with momentum in a range d^3p around $\mathbf{p}$. The expected fraction of particles with energy E_l is given in either formalism by

$$\left\langle f_l^{\pm}\right\rangle = \left\langle n_l^{\pm}\right\rangle / N = -\frac{1}{N\beta}\frac{1}{Z^{\pm}}\frac{\partial Z^{\pm}}{\partial E_l} \tag{A.9}$$

where $Z^{\pm}$is either $Z_{\rm C}^{\pm}$or $Z_{\rm GC}^{\pm}$. Then converting to the normalization required for continuous momenta gives $\langle f^{\pm}(\mathbf{p})\rangle = (L/h)^3 \left\langle f_l^{\pm}\right\rangle$with $E_l = \mathbf{p}^2/2m$. In the grand canonical case this gives the well-known result

$$\left\langle f^{\pm}(\mathbf{p})\right\rangle_{\rm GC} = \frac{L^3}{Nh^3}\frac{z_0}{e^{\beta \mathbf{p}^2/2m} \mp z_0} \tag{A.10}$$

In the canonical case, this procedure gives

$$\left\langle f^{\pm}(\mathbf{p})\right\rangle_{\rm C} = \frac{1}{Z_{\rm C}^{\pm}}\frac{1}{2\pi i}\oint dz z^{-N-1} \exp\left[(L/\lambda)^3 g_{5/2}^{\pm}(z)\right] \frac{L^3}{Nh^3}\frac{z}{e^{\beta \mathbf{p}^2/2m} \mp z} \tag{A.11}$$

Approximate evaluation of this integral by stationary phase gives $\left\langle f^{\pm}(\mathbf{p})\right\rangle_{\rm C} = \left\langle f^{\pm}(\mathbf{p})\right\rangle_{\rm GC}$, again with a fractional error of order $1/N$. Also, we can again use Cauchy's theorem to write

$$\left\langle f^{\pm}(\mathbf{p})\right\rangle_{\rm C} = \frac{1}{Z_{\rm C}^{\pm}}\frac{1}{N!}\frac{\partial^N}{\partial z^N}\left\{\exp\left[(L/\lambda)^3 g_{5/2}^{\pm}(z)\right] \frac{L^3}{Nh^3}\frac{z}{e^{\beta \mathbf{p}^2/2m} \mp z}\right\}\Big|_{z=0} \tag{A.12}$$

In the main text, we simplify the notation a bit via $\left\langle f^{\pm}(\mathbf{p})\right\rangle_{\rm C} \to f^{\pm}(\mathbf{p}, T)$.

11.9 Figure Captions

Fig. 1. Solid line: $\left|\widetilde{\psi}\left(\mathbf{p}_0, t\right)\right|^2 / \left|\widetilde{\psi}\left(\mathbf{p}_0, 0\right)\right|^2$ vs t for a single particle in a two-dimensional circular box; the initial wave function is a narrow gaussian at the center with momentum $\mathbf{p}_0$. Classically, the particle bounces off the wall at $t = 1, 3, 5, \ldots$ Dashed line: $(2\pi\hbar/\Delta)/t$, where Δ is the uncertainty in the energy. Dotted line: the infinite time average of the solid line.

Fig. 2. Expanding the wave function of fig. 1 in energy eigenstates yields expansion coefficients C_α; here $|C_\alpha|$ is plotted vs the energy eigenvalues E_α. There are 1736 energy

eigenvalues in the plotted range, $20 \leq E \leq 90$.

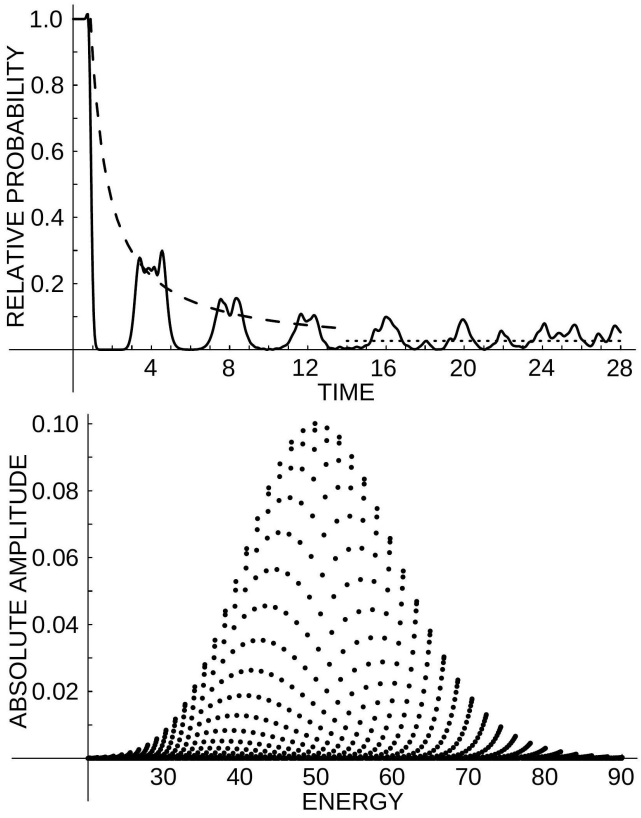

12 A new class of completely integrable quantum spin chains by Prosen

Abstract

A large (infinitely-dimensional) class of completely integrable (possibly non-autonomous) spin chains is discovered associated to an infinite-dimensional Lie Algebra of infinite rank. The complete set of integrals of motion is constructed explicitly, as well as their eigenstates and spectra. As an example we outline kicked Ising model: Ising chain periodically kicked with transversal magnetic field.

In the past three decades intricate algebraic techniques (under the names quantum inverse scattering or algebraic Bethe Ansatz) have been developed [1] in order to construct Integrable Quantum Many-body (IQM) dynamical systems and the associated complete sets of integrals of motion. Integrability of a quantum many-body dynamical systems is defined in a generalized Liouvilean sense; namely by the existence of an infinite set of (independent and local) conservation laws. All the so far discovered IQM systems are 1-dimensional, typically SU(2) spin chains or related systems. Quantum integrability is nongeneric but, however, of great importance since it has been shown recently [2] that the existence of nontrivial conservation laws generically leads to ideal transport properties with infinite Kubo transport coefficients, and deviation from quantum ergodicity in general.

In this Letter we present a new and elementary approach to the construction of IQM 1-dim lattice systems. It is based on the particular infinite dimensional dynamical Lie algebra (DLA) generated and represented by the essential dynamical observables (in our case it is generated by the Ising Hamiltonian $\sum_j \sigma_j^x \sigma_{j+1}^x$ and the interaction with the transversal external field $\sum_j \sigma_j^z$) and for which the 'transfer matrix' can be explicitly constructed from the commutativity condition. We show that any element H of DLA may be considered as a

Hamiltonian of IQM system and construct an analytic DLA valued function $T(\vec{\lambda})$ of possibly vectorial spectral parameter $\vec{\lambda} \in \mathbb{C}^N$ (for some $N \geq 1$), comuting with H, $[H, T(\vec{\lambda})] \equiv 0$. $T(\vec{\lambda})$ is a formal analog of logarithm of the transfer matrix. The integrals of motion (conserved charges and currents) are derived as coefficients of Taylor expansion of $T(\vec{\lambda})$ around $\vec{\lambda} = 0$. Therefore we have an infinite-dimensional class of IQM Hamiltonian systems. Furthermore, real DLA of self-adjoint observables generates infinite dimensional unitary dynamical Lie group of even larger class of integrable quantum many-body propagators of possibly non-Hamiltonian (non-autonomous, e.g. periodically kicked) IQM systems. As an example we work out kicked 1-dim Ising chain periodically kicked with transversal external field. Moreover, we explicitly calculate the complete set of eigenstates and spectra of the conserved charges (including the Hamiltonian).

We start with Lie algebra $\mathfrak{U}$ over an infinite spin chain spanned by the spatially homogeneous local observables

$$Z_{[s_1 s_2 \ldots s_p]} = \sum_j \sigma_j^{s_1} \sigma_{j+1}^{s_2} \ldots \sigma_{j+p-1}^{s_p}, \tag{12.1}$$

where $\sigma_j^s, s \in \{1 = x, 2 = y, 3 = z\}$, are the spin variables (Pauli matrices) of spin j obeying the standard commutation relations $[\sigma_j^p, \sigma_k^r] = 2\delta_{jk}\sigma_j^p\sigma_k^r = 2i\delta_{jk}\sum_s \epsilon_{prs}\sigma_j^s$, and $\sigma_j^0 = 1$. The order of the local observable A is defined as the maximal number of digits p of some observable (12.1) in the expansion of A in terms of basis (12.1). We are interested in nontrivial infinite dimensional subalgebras of $\mathfrak{U}$ for which the number of elements with order smaller than p grows algebraically (as a function of p) and not exponentially ($\sim 4^p$) as for $\mathfrak{U}$ [3]. Indeed we found subalgebra $\mathfrak{S}$, which we call dynamical Lie algebra (DLA) (essentially generated by $Z_{[3]}$ and $Z_{[11]}$), and spanned by two infinite sequences of selfadjoint observables U_n and V_n,

$$U_n = \begin{cases} Z_{[1(3^{n-1})1]}, & n \geq 1, \\ -\ Z_{[3]}, & n = 0, \\ Z_{[2(3^{-n-1})2]}, & n \leq -1, \end{cases} \tag{12.2}$$

$$V_n = \begin{cases} Z_{[1(3^{n-1})2]}, & n \geq 1, \\ Z_{[0]}, & n = 0, \\ -\ Z_{[2(3^{-n-1})1]}, & n \leq -1, \end{cases}$$

for $-\infty < n < \infty$ ((3^n) indicates digit 3 being repeated n times), which satisfy the following commutation relations

$$\begin{aligned} [U_m, U_n] &= 2i(V_{m-n} - V_{n-m}), \\ [V_m, V_n] &= 0, \\ [U_m, V_n] &= 2i(U_{m+n} - U_{m-n}). \end{aligned} \tag{12.3}$$

The order of observables U_n and V_n is $|n| + 1$. The covering algebra $\mathfrak{U}$ is equiped with the Euclidean metric associated to the bilinear form (scalar product)

$$(A|B) = \lim_{L\to\infty} \frac{1}{L2^L} \operatorname{tr}_L(A^\dagger B), \tag{12.4}$$

(tr_L is a trace for a finite system of size L) with respect to which (12.1) is an ortho-normal (ON) basis. Further, U_n and V_n form ON basis of DLA $\mathfrak{S}$ in the same metric. Note that (12.4) is invariant with respect to adjoint map, $(\operatorname{ad}A)B = [A, B]$, namely $((\operatorname{ad}A^\dagger)B|C) = (B|(\operatorname{ad}A)C)$.

Conservation laws in general autonomous case: Let us assume that the Hamiltonian H and the logarithm of the transfer matrix T belong to DLA $\mathfrak{S}$. We write

$$H = \sum_{m=-m_-}^{m_+} (h_m U_m + g_m V_m), \tag{12.5}$$

$$T = \sum_{m=-\infty}^{\infty} (a_m U_m + b_m V_m). \tag{12.6}$$

where the Hamiltonian H has a finite order $M := \max\{m_+, m_-\}$. The commutativity relation $[H, T] = 0$ gives the system of difference equations

$$\begin{aligned} &\sum_m h_m (a_{-n+m} - a_{n+m}) = 0, \\ &\sum_m [h_m (b_{n-m} - b_{-n+m}) + g_m (a_{n+m} - a_{n-m})] = 0, \end{aligned} \tag{12.7}$$

which can be solved with an ansatz

$$\begin{aligned} a_n &= a_+ \lambda^n, \quad b_n = b_+ \lambda^n, \\ a_{-n} &= a_- \lambda^n, \quad b_{-n} = b_- \lambda^n, \end{aligned} \tag{12.8}$$

for $n \geq 0$. Quite surprisingly, the resulting homogeneous system

$$\begin{pmatrix} h(\lambda) & -h(\lambda^{-1}) & 0 & 0 \\ g_a(\lambda) & 0 & h(\lambda^{-1}) & -h(\lambda^{-1}) \\ 0 & g_a(\lambda) & h(\lambda) & -h(\lambda) \end{pmatrix} \begin{pmatrix} a_+ \\ a_- \\ b_+ \\ b_- \end{pmatrix} = 0 \tag{12.9}$$

has rank 2 for any value of the spectral parameter λ, where $h(\lambda)$ and $g_a(\lambda) := g(\lambda) - g(\lambda^{-1})$ are the polynomials

$$h(\lambda) = \sum_{m=-m_-}^{m_+} h_m \lambda^m, \quad g(\lambda) = \sum_{m=-m_-}^{m_+} g_m \lambda^m.$$

Hence, there are two linearly independent solutions of (12.9) (up to an arbitrary common prefactor), namely

$$\begin{aligned} a_+(\lambda) &= h(\lambda^{-1}), \quad b_+(\lambda) = g(\lambda^{-1}), \\ a_-(\lambda) &= h(\lambda), \quad\quad b_-(\lambda) = g(\lambda), \end{aligned} \tag{12.10}$$

and

$$a_+(\lambda) = a_-(\lambda) \equiv 0, \quad b_+(\lambda) = b_-(\lambda) \equiv 1. \tag{12.11}$$

(i) Let us first consider the case where the solutions $a_\pm(\lambda), b_\pm(\lambda)$ are given by (12.10). The global uniform solution (for all $n \in \mathbb{Z}$) is given by a linear combination of $N := m_+ + m_- + 1$ solutions (12.10)

$$a_n = \sum_{m=1}^{N} c_m a_+(\lambda_m) \lambda_m^n, \quad b_n = \sum_{m=1}^{N} c_m b_+(\lambda_m) \lambda_m^n, \tag{12.12}$$

for $n \geq 0$, and

$$a_n = \sum_{m=1}^{N} c_m a_-(\lambda_m) \lambda_m^{-n}, \quad b_n = \sum_{m=1}^{N} c_m b_-(\lambda_m) \lambda_m^{-n}, \tag{12.13}$$

for $n \leq 0$. $N-$tuple of spectral parameters $\vec{\lambda} = (\lambda_1 \dots \lambda_N)$ is an arbitrary subset of a complex unit disk $|\lambda_m| < 1$ (in order to ensure convergence of T) while the coefficients c_m are determined by gluing the solutions (12.12) and (12.13) on $m_+ + m_- = N - 1$ sites around $n = 0$, giving a homogeneous system of $N - 1$ linear equations

$$\sum_{m=1}^{N} (\lambda_m^n - \lambda_m^{-n}) c_m = 0, \ n = 1 \dots N, \tag{12.14}$$

with a general (polynomial) solution

$$c_m(\vec{\lambda}) = (-1)^m \lambda_m^{N-1} \prod_{j \leq k}^{j,k \neq m} (1 - \lambda_j \lambda_k) \prod_{j<k}^{j,k \neq m} (\lambda_j - \lambda_k) \tag{12.15}$$

Logarithmic transfer matrix $T(\vec{\lambda})$ is a holomorphic function in $\vec{\lambda}$, and the coefficients of its Taylor expansion around $\vec{\lambda} = 0$ also commute with H. After some simple series manipulations we easily find an infinite sequence of independent integrals of motion, namely the conserved charges $Q_k, \ k \geq 0, \ [H, Q_k] = 0$, (note that $Q_0 = 2H$)

$$Q_k = \sum_{m=-m_-}^{m_+} \left[h_m (U_{k+m} + U_{-k+m}) + g_m (V_{k+m} + V_{-k+m}) \right]. \tag{12.16}$$

(ii) In the other case, the solutions $a_\pm(\lambda), b_\pm(\lambda)$ are given by (12.11) and aready solve (12.7) globally (so $N = 1$). The logarithmic transfer matrix is now rather trivial, $T(\lambda) = \sum_{m=1}^{\infty} (V_m + V_{-m}) \lambda^m$, giving the conserved currents $C_k, \ k \geq 0, \ [H, C_k] = 0$,

$$C_k = V_{k+1} + V_{-k-1} = Z_{[1(3^k)2]} - Z_{[2(3^k)1]}. \tag{12.17}$$

C_0 is the particle current of the associated spinless fermion model (via Wigner-Jordan transformation), C_1 is the energy current, etc.

It can be easily verified directly that $[T_{(i)}(\vec{\lambda}), T_{(i)}(\vec{\mu})] \equiv 0$, $[T_{(i)}(\vec{\lambda}), T_{(ii)}(\mu)] \equiv 0$, and $[T_{(ii)}(\lambda), T_{(ii)}(\mu)] \equiv 0$. Hence all the conservation laws are in involution $[Q_k, Q_l] = [Q_k, C_l] = [C_k, C_l] = 0$. For example, for the Ising model in a transversal magnetic field, $H = JU_1 + hU_0$, one recovers well known conservation laws $Q_k = J(U_{k+1} + U_{1-k}) + h(U_k + U_{-k})$ and C_k (12.17) which required more involved methods in the literature [4].

Conservation laws in non-autonomous case, kicked-Ising model: Next we study more general possibly non-autonomous quantum spin chains which are propagated by members of a unitary Lie group generated by DLA $\mathfrak{S}$ which in general cannot be written in terms of some Hamiltonian H, as $\exp(-iH)$. For simplicity, we consider periodically kicked systems which correspond to time-dependent Hamiltonian

$$H(t) = H_0 + \delta_p(t) H_1 \tag{12.18}$$

where $\delta_p(t)$ is a periodic delta function of period 1, and $H_0, H_1 \in \mathfrak{S}$ are the generators — the kinetic energy and the potential, respectively. Using the adjoint representation of DLA, the (linear) Heisenberg map $U^{\,\mathrm{ad}}$ of an observable $A \in \mathfrak{S}$ for one time step is factorized as

$$A(t+1) = U^{\mathrm{ad}} A(t) = U_1^{\mathrm{ad}} U_0^{\mathrm{ad}} A(t) \tag{12.19}$$

where $U_p^{\mathrm{ad}} A = \exp(i \,\mathrm{ad} H_p) A = \exp(iH_p) A \exp(-iH_p)$, is the propagation by the kinetic energy and the potential, for $p = 0, 1$, respectively. Transfer matrix is now sought by the invariance condition

$$U^{\,\mathrm{ad}} T(\vec{\lambda}) = T(\vec{\lambda}) \tag{12.20}$$

in the form (12.6). The method of solution is analogous to (12.7-12.15) whereas the difference equations for a_n, b_n are now obtained by means of adjoint representation of propagators which can be derived explicitly by means of eqs. (12.3) and series expansion of exponential function; say if generated by U_m

$$\exp(i\alpha\,\mathrm{ad}U_m)U_n = c^2U_n + s^2U_{2m-n} + cs(V_{n-m} - V_{m-n}),$$
$$\exp(i\alpha\,\mathrm{ad}U_m)V_n = c^2V_n + s^2V_{-n} - cs(U_{m+n} - U_{m-n}),$$

where $c = \cos(2\alpha), s = \sin(2\alpha)$.

Here the general procedure cannot be written as explicitly as in the autonomous case, so we work out in detail an example of kicked Ising (KI) model where the kinetic generator is the usual 1-dim. Ising Hamiltonian, $H_0 = JU_1 = \sum_j J\sigma_j^x\sigma_{j+1}^x$, and the kick potential is the transversal magnetic field, $H_1 = hU_0 = \sum_j h\sigma_j^z$. Condition (12.20) results in the system of second order difference equations for a_n, a_{-n}, b_n, b_{-n} which is solved thru the ansatz (12.8) giving the solution (again for any $|\lambda| < 1$)

$$\begin{aligned} a_+(\lambda) &= s_Jc_h + c_Js_h\lambda^{-1}, \quad & b_+(\lambda) &= s_Js_h(\lambda - \lambda^{-1})/4, \\ a_-(\lambda) &= s_Jc_h + c_Js_h\lambda, & b_-(\lambda) &= -b_+(\lambda) \end{aligned} \tag{12.21}$$

where $s_J = \sin(2J), c_J = \cos(2J), s_h = \sin(2h), c_h = \cos(2h)$, and the trivial solution (12.11). In order to obtain the global solution (a_n, b_n) we again glue together a linear combination of partial solutions for positive and negative n at the two points (since the system is of second order), say at $n = 0, 1$. We obtain the system (12.14) for the three coeficients c_m, $N = 3$, depending on a triple of spectral parameters $\vec{\lambda} = (\lambda_1, \lambda_2, \lambda_3)$ with the solution (12.15). Collecting the terms with different powers of λ_m in the power series expansion of the logarithmic transfer matrix $T(\vec{\lambda})$ we obtain two infinite sets of conservation laws, namely the charges Q_k, $k \geq 0$, $U^{\,\mathrm{ad}}Q_k = Q_k$,

$$\begin{aligned} Q_k = {} & c_Js_h(U_{k+1} + U_{-k+1}) + s_Jc_h(U_k + U_{-k}) \\ & - s_Js_h(V_{k+1} + V_{-k+1} - V_{k-1} - V_{-k-1}), \end{aligned} \tag{12.22}$$

and currents (12.17), C_k, $k \geq 0$, $U^{\,\mathrm{ad}}C_k = C_k$. The conservation laws of KI model (12.22) are identical to invariants (12.16) of an autonomous IQM system with the Hamiltonian $H_{\mathrm{KI}} = Q_0/2 = c_Js_hU_1 + s_Jc_hU_0 - s_Js_h(V_1 - V_{-1})/2$. Note, however, that the full dynamics are not identical, $\exp(i\,\mathrm{ad}H_{\mathrm{KI}}) \neq U^{\,\mathrm{ad}}$.

Structure of DLA and diagonalization of conserved charges: Let us now analyze the structure of DLA $\mathfrak{S}$ more carefully. The current invariants C_k are rather trivial; they span a maximal ideal $\mathfrak{I}$ of DLA $\mathfrak{S}$, $[\mathfrak{S}, \mathfrak{I}] = 0$. The derived (semi-simple) DLA $\mathfrak{S}' = [\mathfrak{S}, \mathfrak{S}] = (\,\mathrm{ad}\mathfrak{S})^\infty\mathfrak{S} = \mathfrak{S}/\mathfrak{I}$ is spanned by $U_m \pm U_{-m}$ and $V_m - V_{-m}$, for $m \geq 0$, or in terms of real non-local Fourier transformed basis

$$\begin{aligned} J^1(\kappa) &= \frac{i}{8\pi}\sum_{m=-\infty}^{\infty} e^{i\kappa m}(U_m - U_{-m}), \\ J^2(\kappa) &= \frac{i}{8\pi}\sum_{m=-\infty}^{\infty} e^{i\kappa m}(V_m - V_{-m}), \\ J^3(\kappa) &= -\frac{1}{8\pi}\sum_{m=-\infty}^{\infty} e^{i\kappa m}(U_m + U_{-m}), \end{aligned} \tag{12.23}$$

for $0 \le \kappa < \pi$, where the commutation relations read

$$[J^p(\kappa), J^r(\kappa')] = i\delta(\kappa - \kappa') \sum_s \epsilon_{prs} J^s(\kappa). \tag{12.24}$$

Therefore, derived DLA is isomorphic to an infinite direct sum $\mathfrak{S}' \sim \bigoplus_{n=1}^{\infty} \mathfrak{su}_2$. It has an infinite rank, Cartan subalgebra is spanned by a continuous root basis $J^3(\kappa)$ and Chevalley generators are $J^{\pm}(\kappa) = J^1(\kappa) \pm iJ^2(\kappa)$. Now we construct the vacuum state $|\emptyset\rangle$ by the condition $J^-(\kappa)|\emptyset\rangle \equiv 0$, which is is equivalent to $(U_m - U_{-m} - iV_m + iV_{-m})|\emptyset\rangle \equiv 0$, and also $\sigma_j^-|\emptyset\rangle \equiv 0$. Hence the vacuum is the state with all spins down. Let us write the Fourier transform of the currents and charges as, $C(\kappa) = \sum_n \exp(i\kappa m) C_m$ and $Q(\kappa) = \sum_m \exp(i\kappa m) Q_m = Q(-\kappa)$, respectively. Note that $Q(\kappa) = Q(-\kappa)$ since $Q_m = Q_{-m}$. Using explicit form (12.16) we compute

$$\begin{aligned} Q(\kappa) &= -8\pi \vec{q}(\kappa) \cdot \vec{J}(\kappa) + g_r(\kappa) C(\kappa), \\ \vec{q}(\kappa) &= (h_i(\kappa), g_i(\kappa), h_r(\kappa)), \end{aligned} \tag{12.25}$$

where $h_r(\kappa) = \text{Re}\, h(\exp(i\kappa))$, $h_i(\kappa) = \text{Im}\, h(\exp(i\kappa))$, $g_r(\kappa) = \text{Re}\, g(\exp(i\kappa))$, $g_i(\kappa) = \text{Im}\, g(\exp(i\kappa))$. The structure (12.24) is invariant with respect to arbitrary local (κ-dependent) rotation (non-abelian gauge transformation) of the vector field $\vec{J}(\kappa)$. Particularly interesting is the rotation $\text{R}(\kappa)$ around axis $\vec{a}(\kappa)$,

$$\vec{a}(\kappa) = \frac{(g_i(\kappa), -h_i(\kappa), 0)}{\sqrt{g_i^2(\kappa) + h_i^2(\kappa)}}, \quad \vec{a}(\kappa) \cdot \vec{q}(\kappa) \equiv 0,$$

for an angle $\varphi(\kappa)$,

$$\varphi(\kappa) = \arctan \frac{\sqrt{g_i^2(\kappa) + h_i^2(\kappa)}}{h_r(\kappa)},$$

namely, $\text{R}\vec{r} = (\vec{a} \cdot \vec{r})\vec{a} + \frac{\vec{q} \cdot \vec{r}}{|\vec{q}|}\vec{k} + \frac{(\vec{a} \times \vec{q}) \cdot \vec{r}}{|\vec{a} \times \vec{q}|} \frac{\vec{a} \times \vec{k}}{|\vec{a} \times \vec{k}|}$, where $\vec{k} = (0, 0, 1)$, which has the property $\text{R}(\kappa)\vec{q}(\kappa) = |\vec{q}(\kappa)|\vec{k}$. The unitary transformation of the vector field

$$\vec{W}(\kappa) = \text{R}(\kappa)\vec{J}(\kappa) = \exp(i\textstyle\int_0^{\pi} d\kappa \varphi \vec{a} \cdot \vec{J}) \vec{J} \exp(-i\int_0^{\pi} d\kappa \varphi \vec{a} \cdot \vec{J}),$$

makes the the conserved charges $Q(\kappa)$ proportional to the new root basis $W_3(\kappa) = \vec{q}(\kappa) \cdot \vec{J}(\kappa)/|\vec{q}(\kappa)|$, namely

$$Q(\kappa) = -8\pi |\vec{q}(\kappa)| W^3(\kappa) + g_r(\kappa) C(\kappa). \tag{12.26}$$

Using the same rotation we construct a new vacuum state $|\emptyset\rangle_W$ relative to the field $\vec{W}(\kappa)$, $W^-(\kappa)|\emptyset\rangle_W \equiv 0$, namely,

$$|\emptyset\rangle_W = \exp\left(i \int_0^{\pi} d\kappa \varphi(\kappa) \vec{a}(\kappa) \cdot \vec{J}(\kappa) \right) |\emptyset\rangle.$$

Let us now discretize the momentum κ to L bins what corresponds to (but is not identical to) a finite chain of L spins, and define

$$W_k^p := \int_{\pi(k-1)/L}^{\pi k/L} d\kappa W^p(\kappa), \quad 1 \le k \le L.$$

Then we have $[W_k^p, W_l^r] = i\delta_{kl} \sum_s \epsilon_{prs} W_k^s$. The eigenstates of conserved charges $Q(\kappa)$ (and of root basis W_k^3 since $[Q(\kappa), W^3(\kappa')] \equiv 0$) can be labeled by L binary quantum numbers $c_k \in \{0, 1\}, k = 1 \dots L$, and are constructed by means of creation operators

$$|c_k\rangle = \prod_{1 \le k \le L}^{c_k = 1} W_k^+ |\emptyset\rangle_W, \tag{12.27}$$

with $W_l^3|c_k\rangle = (c_l - 1/2)|c_k\rangle$. Hence, for smooth $|\vec{q}(\kappa)|$ and large L, all the charges (12.26) are diagonal in the eigenbasis (12.27). Of course, the eigenvalues are finite (for the infinite system $L = \infty$) only for the charge densities $Q'_m = \lim_{L\to\infty}(1/L)Q_m|_L$ and not for the extensive charges Q_m. The eigenvalues of invariant densities are computed by taking the limit $L \to \infty$ and the inverse cosine transform

$$Q'_m|c(\kappa)\rangle = -\frac{8}{\pi}\int_0^\pi d\kappa' \cos(\kappa' m)|\vec{q}(\kappa')|\left[c(\kappa') - \frac{1}{2}\right]|c(\kappa)\rangle.$$

Label $c(\kappa)$ is an arbitrary (measurable) index function $c : [0,\pi) \to \{0,1\}$, (for finite L, $c(\kappa) = c_k, \pi(k-1)/L \le \kappa < \pi k/L$) and $|c(\kappa)\rangle$ is the corresponding eigenstate which should be properly defined by some limiting procedure $L \to \infty$ of (12.27). It seems that the spectrum of Q'_m is purely continuous. On the other hand, for the currents we have $C_m|c(\kappa)\rangle \equiv 0$, since $[C(\kappa), \vec{W}_l] \equiv 0$. Having such a transparent structure (12.24-12.27) it should be an easy task to compute physically interesting correlation functions.

In this Letter we have introduced an infinitely dimensional space of completely integrable quantum many-body systems (spin-chains or chains of spinless fermions), the so called Dynamical Lie Algebra, as opposed to few-parameter families of completely integrable quantum many body systems known so far in the literature. The model is an infinitely dimensional extension of Ising model in transversal field (equivalent to XY-model [4] and to 1-dimensional free fermion theory). For every element of the algebra being interpreted as a Hamiltonian, or any propagator from the associated unitary Lie group being generated by a finite number of elements of the algebra (e.g. Ising model periodically kicked by transversal magnetic field), we construct two infinite sets of quantum invariants of motion, the conserved charges and the conserved currents. Is is shown heuristically how to diagonalize these conservation laws. Explicit expressions of the conserved charges are quite simple (much simpler than in general Heisenberg (XYZ) or Hubbard model[5], for example) though nontrivial.

13 Statistical Mechanics of the XY Model. by Barouch, McCoy, Dresden

13.0.1 Introduction

There is extensive literature on the general aspects of nonequilibrium statistical mechanics. There are many different approaches and procedures, and it is not at all trivial to decide what procedures and approximations, if any, are appropriate in given circumstances. The lack of nontrivial examples, in which the Liouville equation can be solved exactly and the time dependence explicitly obtained, has been keenly felt. With such an exactly soluble example, one can compare the effectiveness and legitimacy of the many approximate procedures. This makes the construction and analysis of such systems especially important.

A considerable amount of success has been achieved in the exact discussion of various one-dimensional spin systemsThe general type of system studied is a onedimensional chain with nearestneighbor interactionsMost of the studies start from a Hamiltonian of the form

$$H = \sum_{j=1}^{N}\left(\alpha S_i^x S_{i+1}^x + \beta S_i^y S_{i+1}^y + \gamma S_i^z S_{i+1}^z\right), \tag{1.1}$$

where the $\vec{S}_i$ are $\frac{1}{2}$ of the Pauli spin matricesand $\alpha\beta\gamma$ are the coupling constants

In spite of the idealization involved in repre senting an actual magnetic substance by the Ha miltonian11the analysis of such systems is of considerable difficulty

From a physical viewpointthese models are all highly contrivedWhatever interest they might possess depends on the information and insight they yield about the general character and structure of manybody theory and statistical mechanics There is always the hope that methods which yield exact information about idealized systems will be helpful in discussing more realistic onesThere is also the suspicion that the inability to solve simple systems means that one is poorly prepared to discuss more realistic ones

Various special cases of11have been ana lyzed in detailSome of these cases areiα = β = 0 the Ising modelstudied by Ising[1] Onsager[2] and many othersiiα = β = γ the Heisenberg modelstudied by Bethe [3] and Hulthen [4] iiiα = β ≠ γ the HeisenbergIsing model studied by Yang and Yang [5] ivα ≠ β; γ = 0 the XY modelstudied by LiebSchultzand Mattis [6]LSMand others[7−11]

LSM diagonalized the Hamiltonian of the XY mod elfound its spectrum and eigenstatesand studied its thermodynamic propertiesIt is the purpose of this paper to study the nonequilibrium proper ties of this model

In the timedependent casethe eigenvalues of 11are not of primary interestThe discussion here is concerned with the manner in which a sys tem responds to external disturbances and the way that appropriate observables behave for infinite times

To study such questionsit is useful to introduce an explicitly timedependent term in the Hamil tonianIn general$H$ has the form

$$H = H_{ss} + h(t)H_{sh}, \tag{1,2}$$

$$\text{where} \quad H_{sh} = \sum_j S_j^z, \tag{1,3}$$

where H_{ss} is given by11and $h(t)$ is the time dependent magnetic fieldIn the case

$$[H_{ss}, H_{sh}] = 0, \tag{1.4}$$

the density matrix of the system has a trivial time dependencePhysically this means that the spin spin interaction energy and the spinfield interac tion energy are separately conservedThusno
energy transfer can take place between the two systemsHenceit is not surprising that the change of an external fieldin this casedoes not result in an interesting time evolution of the spin systemThe simplest system for which14is not satisfied is
$H = \sum_{j=1}^{N} \left[(1+\gamma)S_j^x S_{j+1}^x + (1-\gamma)S_j^y S_{j+1}^y - h(t)S_j^z\right]$ 15
This is the XY model [$\gamma \neq 0$ since $\gamma = 0$ results in 14
This system was chosen for our detailed study In order to obtain an understanding of the time evolution of this systemthe timedependent density matrix has to be computedOnce this is accom plishedit is possible to calculate the time evolu tion of physical observables such as the magneti zationwhich is discussed in this paperThe in stantaneous correlation functions are of physical interestbut their calculation is quite involved and will be dealt within a separate paper-From the explicit expression for the magnetization the limit $t \to \infty$ is obtainedThe somewhat surprising result of the detailed analysis is thatalthough this limit existsit does not approach its equilibrium value This may well be connected with the observation of Mazur [12] that the magnetization is not an ergodic observable in this model
The paper is divided into eight sectionsSection II contains a recapitulation of the diagonalization procedure of LSMThe main point is thatby means of an appropriate unitary transformation the Hamiltonian is transformed into $\Sigma_p H_p$ where each H_p acts in an independent subspace In Sec IIIit is shown that the density matrix has a direct product structure

$$\rho(t) = \rho_1(t) \otimes \cdots \rho_p(t) \otimes \cdots \rho_{N/2}(t), \tag{1,6}$$

where each ρ_p is a 4×4 matrix satisfying

$$i\frac{d}{dt}\rho_p(t) = [H_p(t), \rho_p(t)]\,. \tag{1.7}$$

The initial condition chosen at $t = 0$ is thermal equilibrium of the system at that timenamely

$$\rho_p(0) = e^{-\beta H_p(0)}; \quad \beta = (kT)^{-1}. \tag{1.8}$$

The matrix elements of ρ_p are obtained by ele mentary means from a function V which satisfies

$$\frac{d^2}{dt^2}V + \left[\Lambda^2 + \psi(t)\right] V = 0 \tag{1,9}$$

Here ψ is an explicitly given functional of $h(t)$ while Λ depends on the parameters of the system and the value of the magnetic field

In SecIVthe solutions of19are used to compute the magnetization

Sections VVII contain the detailed evaluation
and analysis for three examples of external fields. The general results of these sections is that the asymptotic behavior of $m(t)$ is identical for large times, the specific coefficients depend on the details of $h(t)$, and there is no approach to equilibrium, no matter how slow the field varies.

The conclusions are collected in Sec. VIII, and Appendixes A-C give details of the various asymptotic expansions and some solutions of (1.9).

13.0.2 II. Formulation

The equilibrium properties of the XY model in one dimension, have been derived many times. [6–10] We choose to outline the basic steps used by LSM for sake of completeness.

The XY Hamiltonian is

$$\begin{aligned} H =& J\sum_{j=1}^{N}\left\{(1+\gamma)S_j^x S_{j+1}^x \right. \\ & \left. +(1-\gamma)S_{j+1}^y - [\mu h(t)/J]S_j^z\right\}. \end{aligned} \tag{2.1}$$

This Hamiltonian represents a chain of interacting spins, with nearest-neighbor interaction only. The boundary condition is cyclic, namely, $\overrightarrow{\mathrm{S}}_{N+1} = \overrightarrow{\mathrm{S}}_1 . S_j^x, S_j^y, S_j^z$, are the spin- $\frac{1}{2}$ operators at the j th lattice site (they are $\frac{1}{2}$ the Pauli spin matrices), γ is the anistropy measure, μ is the magnetic moment, $h(t)$ is the time-dependent magnetic field, and J is the coupling constant. We set $J = 1$ and $\mu = 1$ for convenience, and write them explicitly only when necessary.

Define new operators $b_j, b_j^\dagger$, which are neither Fermi nor Bose operators, by

$$\begin{aligned} S_j^x &= \frac{1}{2}\left(b_j^\dagger + b_j\right), \quad S_j^y = \left(b_j^\dagger - b_j\right)/2i, \\ S_j^z &= b_j^\dagger b_j - \frac{1}{2}. \end{aligned} \tag{2.2}$$

These operators are expressed in terms of Fermi operators $c_K, c_K^\dagger$ by

$$b_j = \exp\left(-\pi i \sum_{K=1}^{j-1} c_K^\dagger c_K\right) c_j, \tag{2,3}$$
$$b_j^+ = c_j^+ \exp\left(\pi i \sum_{K=1}^{j-1} c_K^\dagger c_K\right)$$

Following LSM, we substitute (2.3) in (2.1) and obtain

$$H = \frac{1}{2}\sum_{j=1}^{N}\Big[\Big(c_j^\dagger c_{j+1} + \gamma c_j^\dagger c_{j+1}^\dagger + \text{ H. c. }\Big) - 2h c_j^\dagger c_j\Big] + \frac{1}{2}Nh \tag{2.4}$$

with the boundary condition [13] $c_1 \equiv c_{N+1}$.
The diagonalization of (2.1) for $h(t)$ independent of t is completed by using two more transformations: (i) Fourier transformation, and (ii) Bogoliubov transformation.

We can still carry out the Fourier transform
for a general $h(t)$ Define

$$c_j^+ = \frac{1}{\sqrt{N}} \sum_{p=-N/2}^{N/2} \exp(ij\phi_p)\, a_p^\dagger$$
$$c_j = \frac{1}{\sqrt{N}} \sum_{p=-N/2}^{N/2} \exp(-ij\phi_p)\, a_p \tag{2,5}$$

where $\phi_p = 2\pi p/N$
Substituting $(2,5)$ in (2.4), one obtains

$$H = \frac{1}{2}\sum_{p=1}^{N/2}\Big\{\alpha_p(t)\left[a_p^\dagger a_p + a_{-p}^\dagger a_{-p}\right] + \frac{1}{2}i\delta_p\left[a_p^\dagger a_{-p}^\dagger + a_p a_{-p}\right] + 2h(t)\Big\}, \tag{2.7}$$
$$\text{with} \quad \alpha_p(t) = 2\left[\cos\phi_p - h(t)\right], \tag{2.8}$$
$$\delta_p = -2\gamma \sin\phi_p, \tag{2,9}$$

and a_p and $a_p^\dagger$ are again Fermi operators.
The Bogoliubov transformation that would diagonalize (2.7) in terms of new Fermi operators would have no meaning, since the coefficients of this transformation would be explicitly time dependent. However, we can write (2.7) as

$$H = \sum_{p=1}^{N/2} \tilde{H}_p \tag{2.10}$$

where $\tilde{H}_p = \frac{1}{2}\Big\{\alpha_p(t)\left(a_p^\dagger a_p + a_{-p}^\dagger a_{-p}\right) + \frac{1}{2}i\delta_p\left[a_p^\dagger a_{-p}^\dagger + a_p a_{-p}\right] + 2h(t)\Big\}$ (2,11)

Clearly, we obtain $\left[\tilde{H}_p, \tilde{H}_p\right] = 0,$
which means the space upon which $\tilde{H}$ acts decomposes into noninteracting subspaces, each of four dimensions. No matter what $h(t)$ is, there will be no transitions among those subspaces.

It is convenient to use the following basis for the p th subspace:

$$\left(|0\rangle; a_p^\dagger a_{-p}^\dagger|0\rangle; a_p^\dagger|0\rangle; a_{-p}^\dagger|0\rangle\right) \tag{2.13}$$

This is the Heisenberg picture. The Hamiltonian (2.10) with the basis (2.13) becomes the matrix

$$\bar{H}(t) \sum_{p=1}^{N/2} \left[I \otimes I \otimes \cdots \otimes \bar{H}_p(t) \otimes \cdots \otimes I\right] \tag{2.14}$$

where we have explicitly

$$\bar{H}_p(t) = \begin{bmatrix} h(t) & \frac{1}{2}i\delta_p & 0 & 0 \\ -\frac{1}{2}i\delta_p & 2\cos\phi_p - h(t) & 0 & 0 \\ 0 & 0 & \cos\phi_p & 0 \\ 0 & 0 & 0 & \cos\phi_p \end{bmatrix} \tag{2.15}$$

and I is the 4×4 unit matrix.

13.0.3 III. Liouville equation

In this section, we reduce the Liouville equation for the density matrix of the system (2.7) to a sec-
ond-order ordinary differential equation.
Let $U_p(t)$ be the time-evolution matrix in the p th subspace, namely, ($\hbar = 1$):

$$i\frac{d}{dt}U_p(t) = U_p(t)\bar{H}_p(t) \tag{3.1}$$

with the boundary condition

$$U_p(0) = I. \tag{3.2}$$

Then, the Hamiltonian of the system $H^s(t)$ in the Schrdinger picture is

$$H^s(t) = \sum_{p=1}^{N/2} \left[I \otimes I \otimes \cdots \otimes H_p^s(t) \otimes \cdots \otimes I\right] \tag{3.3}$$

where $H_p^s(t) = U_p(t)\bar{H}_p(t)U_p(t)^\dagger$,
and $\bar{H}_p(t)$ is given by (2.15)
Let $\rho(t)$ be the density matrix of the system. The Liouville equation of the system is

$$i\frac{d}{dt}\rho(t) = \left[H^s(t), \rho(t)\right]. \tag{3.5}$$

To complete the specification of $\rho(t)$, we need to provide the differential equation (3.5) with an initial condition. For the purposes of this paper, we will consider only systems which at time $t = 0$ are in thermal equilibrium at temperature T. Since we obtain

$$H^s(0) = \bar{H}(0) \tag{3,6}$$

we have $\rho(0) = e^{-\beta H^s(0)} = e^{-\beta \bar{H}(0)}$,
where $\beta = 1/kT$ and k is the Boltzmann constant.
The boundary condition (3.6), by using (3.3), can be written explicitly

$$\begin{aligned}\rho(0) &= \prod_{p=1}^{N/2} \left(I \otimes I \otimes \cdots \otimes e^{-\beta H_p(0)} \otimes I \cdots \otimes I\right) \\ &= e^{-\beta \bar{H}_1(0)} \otimes e^{-\beta \bar{H}_2(0)} \otimes \ldots \otimes e^{-\beta \bar{H}_{N/2}(0)}\end{aligned} \tag{3.8}$$

This particular algebric form, together with (2.12), suggests the solution of (3.1):

$$\rho(t) = \rho_1(t) \otimes \rho_2(t) \otimes \cdots \otimes \rho_{N/2}(t) \tag{3.9}$$

By substitution of (3.9) and (3.3) in (3.5), one obtains

$$\begin{aligned}\sum_{p=1}^{N/2} [\rho_1(t) \otimes \rho_2(t) \cdots \otimes \Bigg(& i\frac{d}{dt}\rho_p(t) \\ & - \left[H_p^s(t), \rho_p(t)\right]\Bigg) \otimes \cdots \otimes \rho_{N/2}(t)\Big] = 0.\end{aligned} \tag{3.10}$$

From (3.10), we conclude that if for every integer $p, 1 \leqslant p \leqslant \frac{1}{2}N, \rho_p$ satisfies

$$i\frac{d}{dt}\rho_p(t) = \left[H_p^s(t), \rho_p(t)\right] \tag{3.11}$$

with the initial condition

$$\rho_p(0) = e^{-\beta H_p(0)}; \tag{3.12a}$$

then (3.9) is the unique solution (3.5) under the condition (3.6). Furthermore, because of (3.1) and (3.4), the solution of (3.11) is

$$\rho_p(t) = U_p(t)\rho_p(0)U_p(t)^\dagger \tag{3.12b}$$

and $\rho_p(0)$ is given explicitly

$$\rho_p(0) = \begin{bmatrix} k_{11}^p & k_{12}^p & 0 & 0 \\ k_{21}^p & k_{22}^p & 0 & 0 \\ 0 & 0 & e^{-\beta\cos\phi_p} & 0 \\ 0 & 0 & 0 & e^{-\beta\cos\phi_p} \end{bmatrix}, \tag{3.13}$$

where (we omit here the index p for convenience)

$$\Lambda[h(0)] \equiv \left\{\gamma^2 \sin^2\phi + [h(0) - \cos\phi]^2\right\}^{1/2} \tag{3.14}$$

$$q = -\Lambda[h(0)]^{-1} e^{-\beta\cos\phi} \sinh[\beta\Lambda(h(0))] \tag{3.15}$$

$$r = -\frac{1}{2}\delta q \tag{3.16}$$

$$\begin{aligned}P = & \frac{[\cos\phi + \Lambda(h(0))]e^{-\beta[\cos\phi + \Lambda(h(0))]}}{2\Lambda[h(0)]} \\ & - \frac{[\cos\phi - \Lambda(h(0))]e^{-\beta[\cos\phi - \Lambda(0))]}}{2\Lambda[h(0)]}\end{aligned} \tag{3.17}$$

$$k_{12} = k_{21}^* = -ir \tag{3,18}$$

$$k_{11} = h(0)q + P \tag{3.19}$$

$$k_{22} = P + q[2\cos\phi - h(0)] \tag{3.20}$$

Because $\bar{H}_p$ is in block form it is clear that

$$U_p(t) = \begin{bmatrix} U_{11,p}(t) & U_{12,p}(t) & 0 & 0 \\ U_{21,p}(t) & U_{22,p}(t) & 0 & 0 \\ 0 & 0 & e^{-it\cos\phi_p} & 0 \\ 0 & 0 & 0 & e^{-it\cos\phi_p} \end{bmatrix} \tag{3.21}$$

where the upper-left block is determined from
$i\frac{d}{dt}\begin{bmatrix} U_{11} & U_{12} \\ U_{21} & U_{22} \end{bmatrix} = \begin{bmatrix} U_{11} & U_{12} \\ U_{21} & U_{22} \end{bmatrix}\begin{bmatrix} h(t) & \frac{1}{2}i\delta \\ -\frac{1}{2}i\delta & 2\cos\phi - h(t) \end{bmatrix}$.
This matrix equation contains two independent systems of coupled differential equations. By straightforward algebra, we obtain
$i\frac{d^2}{dt^2}U_{11}(t) = 2\cos\phi\frac{d}{dt}U_{11}(t)$

$$+\left(\frac{dh(t)}{dt} - i\frac{1}{4}\delta^2 + i[2\cos\phi - h(t)]h(t)\right)U_{11} \tag{3.23}$$

with boundary conditions

$$U_{11}(0) = 1 \text{ and } \frac{d}{dt}U_{11}(0) = -ih(0) \tag{3.24}$$

Let $h(t) = b + h_1(t)$,
while $\lim_{t\to\infty} h_1(t) = 0$,

$$U_{11}(t) = V(t)e^{-it\cos\Phi} \tag{3.26}$$

Then (3.22) becomes

$$\frac{d^2}{dt^2}V(t) + \left[\Lambda^2(b) + \psi(t)\right]V(t) = 0 \tag{3.28}$$

where $\Lambda(b)$ is given by (3.14),

$$\psi(t) = h_1^2(t) - 2(\cos\phi - b)h_1(t) + i\frac{d}{dt}h_1(t), \tag{3.29}$$

and from (3.23), $V(t)$ satisfies the initial conditions

$$V(0) = 1, \frac{d}{dt}V(0) = i[\cos\phi - h(0)]. \tag{3.30}$$

From a well-known theorem, [14] we deduce that all solutions of (3.28) are bounded as $t \to \infty$ provided the following conditions are fulfilled:

$$\lim_{t\to\infty}\psi(t) = 0, \int_0^\infty |\psi'(t)|\,dt < \infty \tag{3.31}$$

Let W_1 and W_2 be two independent solutions of (3.26). Because of (3.31), we know that $\lim_{t\to\infty} V \cong \mu_1 e^{i\Lambda(b)t} + \mu_2 e^{-i\Lambda(b)t}$, where μ_1 and μ_2 are constants to be determined. Accordingly we specify $W_i, i = 1, 2$, by

$$\lim_{t\to\infty} W_1(t) \sim e^{it\Lambda(b)}, \quad \lim_{t\to\infty} W_2(t) \sim e^{-it\Lambda(b)}. \tag{3.32}$$

Using (3.22), (3.28), and (3.32), we have "immediately'

$$V_{11}(t) = A_1 W_1(t) + A_2 W_2(t), \tag{3.33}$$
$$V_{21}(t) = B_1 W_1(t) + B_2 W_2(t), \tag{3.34}$$

with initial conditions

$$V_{21}(0) = 0 \text{ and } \frac{d}{dt} V_{21}(0) = -\frac{1}{2}\delta. \tag{3,35}$$

The constants A_1, A_2, B_1, B_2 are easily determined from (3.35) to be

$$\begin{aligned} A_1 &= \frac{(d/dt)W_2(0) - i[\cos\phi - h(0)]W_2(0)}{W(0)}, \\ A_2 &= \frac{iW_1(0)[\cos\phi - h(0)] - (d/dt)]\, W_1(0)}{W(0)}, \\ B_1 &= -\frac{\frac{1}{2}\delta W_2(0)}{W(0)}, \quad B_2 = \frac{\frac{1}{2}\delta W_1(0)}{W(0)}, \end{aligned} \tag{3.36}$$

where $W(t)$ is the Wronskian of the two independent solutions W_1, W_2, namely,

$$W(t) = W_1(t)\frac{d}{dt}W_2(t) - W_2(t)\frac{d}{dt}W_1(t) \tag{3.37}$$

13.0.4 IV. Magnetization

We derive a general expression for the z-direction magnetization in terms of the solutions of
(3.28), and obtain its asymptotic behavior.

The magnetization operator per spin is defined

$$M = \frac{1}{N}\sum_j S_j^z \tag{4.1}$$

M can be written in terms of the operators $a_p, a_p^\dagger$, defined in (2.5) and (2.6) as

$$M = \frac{1}{N}\sum_{p=1}^{N/2} M_p, \tag{4.2}$$

where $M_p = a_p^\dagger a_p + a_{-p}^\dagger a_{-p} - 1$.
Clearly, we obtain

$$[M_p, M_{p'}] = 0. \tag{4.4}$$

Since (4.3) and (4.4) are conditions similar to (2.10) and (2.12), we conclude that M has the same algebric structure as H.

Let $M_z(t)$ be the average magnetization per spin, namely,

$$M_z(t) = \frac{1}{N}\frac{\mathrm{Tr}[M\rho]}{\mathrm{Tr}[\rho]} = \frac{1}{N}\sum_{p=1}^{N/2}\frac{\mathrm{Tr}\left[M_p U_p \rho_p(0) U_p^\dagger\right]}{\mathrm{Tr}\left[\rho_p(0)\right]} \tag{4.5}$$

Using (2.13), (3.13), (4.3), and (3.21) in (4.5) we obtain explicitly

$$M_z(t) = -\frac{1}{N}\sum_p \Big(k_{11}^p + k_{22}^p + 2e^{-\beta\cos\varphi_p)^{-1}} \times \Big[(k_{11}^p - k_{22}^p)\left(2\left|U_{11}^p\right|^2 - 1\right) - 4r_p \operatorname{Im}\left(U_{12}^p U_{11}^{p*}\right)\Big]. \tag{4.6}$$

One can replace the U_{ij} in (4.6) by the V_{ij} of (3.33) and (3.34). Using the constants (3.36), (4.6) becomes

$$\begin{aligned} M_z(t) = \frac{1}{N}\sum_{p=1}^{N/2} \frac{\tanh\left[\frac{1}{2}\beta\Lambda(h(0))\right]}{\Lambda(h(0))} \{[h(0) - \cos\phi_p] \\ \times \Bigg(2\left|\frac{W_2'(0) - i\left[\cos\phi_p - h(0)\right]W_2(0)}{W(0)}W_1(t)\right. \\ \left. + \frac{iW_1(0)\left[\cos\phi_p - h(0)\right] - W_1'(0)}{W(0)}W_2(t)\right|^2 - 1\Bigg) \\ + (-2\gamma\sin\phi_p)^2 \operatorname{Im}\Bigg[\Bigg(\frac{W_2'(0) - i\left[\cos\phi_p - h(0)\right]W_2(0)}{W(0)} \\ \times W_1(t) + \frac{iW_1(0)\left[\cos\phi_p - h(0)\right] - W_1'(0)}{W(0)}W_2(t)\Bigg) \\ \times\left(-\frac{\frac{1}{2}W_2(0)}{W(0)}W_1(t) + \frac{\frac{1}{2}W_1(0)}{W(0)}W_2(t)\right)\Bigg]\Bigg\}. \end{aligned} \tag{4.7}$$

This is the exact expression for all N for the magnetization in the z directions in terms of the solutions $W_1(t)$ and $W_2(t)$ of (3.28) with conditions (3.32). However, our major interest is in the thermodynamic limit $N \to \infty$. This limit is easily obtained from (4.7) by using the definition of integral to replace ϕ_p by ϕ and $\frac{1}{N}\sum_{p=1}^{N/2}$ by $\frac{1}{2\pi}\int_0^\pi d\phi$.

13.0.5 V. Step-function magnetic field

A step function in the magnetic field provides us with the easiest example of the above formalism. Let

$$\begin{aligned} h(t) &= a, \quad t \leqslant 0 \\ &= b, \quad t > 0; \end{aligned} \tag{5.1}$$

then the solution of (3, 22) is readily found to be

$$\begin{aligned} \begin{bmatrix} U_{11} & U_{12} \\ U_{21} & U_{22} \end{bmatrix} &= e^{-it\cos\phi}\begin{bmatrix} V_{11} & V_{12} \\ -V_{12}^* & V_{11}^* \end{bmatrix} \\ &= e^{-it\cos\phi}\begin{bmatrix} i\frac{(\cos\phi - b)}{\Lambda(b)} & \sin[t\Lambda(b)] + \cos[t\Lambda(b)] \\ -\frac{\delta}{2}\frac{\sin[t\Lambda(b)}{\Lambda(b)} & \end{bmatrix} \end{aligned} \tag{5,2}$$

The explicit density matrix for the p th subspace is also obtained by straightforward matrix multiplication as

$$\rho_p(t) = \begin{bmatrix} K_{11}^p(t) & K_{12}^p(t) & 0 & 0 \\ K_{12}^*(t) & k_{11}^p + k_{22}^p - K_{11}^p(t) & 0 & 0 \\ 0 & 0 & e^{-\beta\cos\phi_p} & 0 \\ 0 & 0 & 0 & e^{-\beta\cos\phi_p} \end{bmatrix} \tag{5.3}$$

where

$$K_{11}^p(t) = k_{11}^p \left[(\cos\phi_p - b)^2 \left(\tfrac{\sin[t\Lambda(b)]}{\Lambda(b)} \right)^2 + \cos^2[t\Lambda(b)] \right] + r_p\delta_p (\cos\phi_p - b) \left(\tfrac{\sin[t\Lambda(b)]}{\Lambda(b)} \right)^2 + k_{22}^p \tfrac{\delta_p^2}{4} \left(\tfrac{\sin[t\Lambda(b)]}{\Lambda(b)} \right)^2, \tag{5.4}$$

$$K_{12}^p(t) = (k_{22}^p - k_{11}^p) \frac{\delta_p}{2} \frac{\sin[t\Lambda(b)]}{\Lambda(b)} \left(i \frac{\cos\phi_p - b}{\Lambda(b)} \sin[t\Lambda(b)] + \cos[t\Lambda(b)] \right)$$
$$-ir_p \left[\cos^2[t\Lambda(b)] + i\tfrac{\cos\phi_p - b}{\Lambda(b)} \sin[2t\Lambda(b)] - (\cos\phi_p - b)^2 \left(\tfrac{\sin[t\Lambda(b)]}{\Lambda(b)} \right)^2 + \tfrac{\delta^2}{4} \left(\tfrac{\sin[t\Lambda(b)]}{\Lambda(b)} \right)^2 \right], \tag{5.5}$$

and $r_p, k_{11}^p, k_{22}^p, \Lambda(b)$ are the same as before (3.14)-(3.20).
By direct substitution of the matrix elements of (5.2) in the general formula for the magnetization (4.7) one obtains

$$m_z(t) = \tfrac{1}{N} \sum_p \frac{\tanh\left[\frac{1}{2}\beta\Lambda(a)\right]}{\Lambda(a)} \left(\frac{\cos 2\Lambda(b)t}{\Lambda^2(a)} \gamma^2 (a-b) \sin^2\phi_p - \frac{(\cos\phi_p - b)\left[(\cos\phi_p - b)(\cos\phi_p - a) + \gamma^2 \sin^2\phi_p\right]}{\Lambda^2(b)} \right) \tag{5.6}$$

We proceed to take the thermodynamic limit $N \to \infty$ The sum (5.6) becomes an integral. In other words, only the first term in the Poisson summation formula survives, and the others are exponentially small. It is interesting to note that (5.6) does not approach a limit as $t \to \infty$ This is not the case if the thermodynamic limit is taken first. Explicitly, (5.6) becomes [15]

$$\lim_{N\to\infty} m_z(t) = \frac{1}{2\pi} \int_0^\pi d\phi \frac{\tanh\left[\frac{1}{2}\beta\Lambda(a)\right]}{\Lambda(a)\Lambda^2(b)} \times \left\{ \cos[2\Lambda(b)t]\gamma^2(a-b)\sin^2\phi - (\cos\phi - b) \times [\cos\phi - a)(\cos\phi - b) + \gamma^2 \sin^2\phi] \right\} \tag{5.7}$$

One would like to check (5.7) for several limiting cases. Since we have

$$\left[\sum_i S_i^z, \sum_j \left(S_j^x S_{j+1}^x + S_j^y S_{j+1}^y \right) \right] = 0 \tag{5.8}$$

we expect no time dependence of $m_z(t)$ when $\gamma = 0$, and the time-dependent term of (5.7) is proportional to γ^2. The limit $a = b$ corresponds to a constant field, and should agree with $m_z(0)$ which is the wellknown statistical equilibrium formula, namely,

$$m_z(0) = \frac{1}{2\pi} \int_0^\pi d\phi \frac{\tanh\left[\frac{1}{2}\beta\Lambda(a)\right]}{\Lambda(a)} (a - \cos\phi). \tag{5.9}$$

On the other hand, the infinite-time limit is
$m_z(\infty) = \frac{1}{2\pi} \int_0^\pi d\phi \frac{\tanh\left[\frac{1}{2}\beta\Lambda(a)\right]}{\Lambda(a)}$

$$\times \frac{(b - \cos\phi)}{\Lambda^2(b)} \left[(\cos\phi - a)(\cos\phi - b) + \gamma^2 \sin^2\phi \right] \tag{5.10}$$

$m_z(\infty)$ depends on a, but for a general value of b this does not mean that $m_z(\infty)$ is not in thermal equilibrium, since the temperature of the finite state could depend on how much the magnetic field had changed. However, when $b = 0, m_z(\infty)$ does not vanish. From (5.9), we see that there is no value of T for which the equilibrium magnetization will be different from zero if no external field is applied. Therefore, we conclude that as $t \to \infty$ the system does not approach thermal equilibrium when $h(t)$ is given by (5.1). In Fig 1 we plot $m_z(\infty)$ as a function of the initial field a. We see that it is a monotonic function of a and as $a \to \infty$ it saturates at a value smaller than $\frac{1}{2}$, where $\frac{1}{2}$ is the saturation value of the initial magnetization.

In Appendix B, we perform a detailed study of the asymptotic behavior of (5.7) for large t. This expansion is valid for $t = 0(N)$ for taking the thermodynamic limit and then letting $t \to \infty$.

The result of this expansion is given in terms of three cases, [16] where

$$f_j(t) = m_z(t) - m_z(\infty), \quad j = 1, 2, 3. \tag{5.11}$$

Case (i): $|\mu b/J| > (1 - \gamma^2)$; $f_1(t)$ is given up to second order by

$$f_1(t) \sim -\frac{(a-b)\gamma^2\mu}{2\pi J}\left[(\frac{2tJ}{\hbar})^{-3/2}\left\{-\left[\frac{|\mu b - J|}{\mu b - J\,(1-\gamma^2)}\right]^{1/2}\right.\right.$$

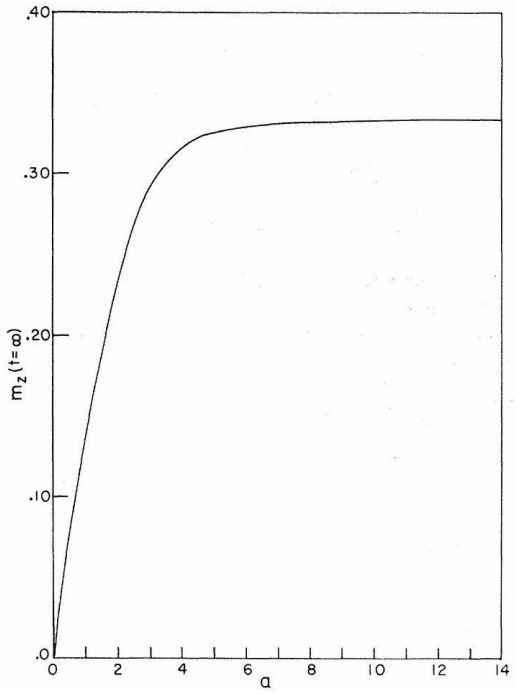

FIG. 1. Final magnetization versus initial field a for step function case: a - jumps to 0 .

$$\times\Gamma\left(\frac{3}{2}\right)E_1\left(\left|\frac{\mu b}{J}-1\right|\right)\quad\cos\left[\frac{2t}{\hbar}|b\mu-J|-\frac{1}{4}\pi\right]$$
$$+\left[\frac{|\mu b+J|}{\mu b+J\left(1-\gamma^2\right)}\right]^{1/2}\Gamma\left(\frac{3}{2}\right)E_1\left(\left|\frac{\mu b}{J}+1\right|\right)$$
$$\times\cos\left[\frac{2t}{\hbar}|b\mu+J|+\frac{1}{4}\pi\right]\Bigg\}$$
$$+\left(\frac{2tJ}{\hbar}\right)^{-5/2}\Bigg\{\left[\frac{|\mu b-J|}{\mu b-J\left(1-\gamma^2\right)}\right]^{1/2}\Gamma\left(\frac{5}{2}\right)$$
$$\times E_1'\left(\left|\frac{b\mu}{J}-1\right|\right)\cos\left(\frac{2t}{\hbar}|b\mu-J|+\frac{1}{4}\pi\right)$$
$$-\left[\frac{|\mu b+J|}{\mu b+J\left(1-\gamma^2\right)}\right]^{1/2}\Gamma\left(\frac{5}{2}\right)E_1'\left(\left|\frac{b\mu}{J}+1\right|\right)$$
$$\times\cos\left(\frac{2t}{\hbar}|b\mu+J|-\frac{1}{4}\pi\right)\Bigg\}\Bigg]. \tag{5.12}$$

E_1 and E_1' are given by (B25) and (B26), respectively.
Case (ii): $|\mu b/J|<\left(1-\gamma^2\right)$; $f_2(t)$ is given up to second order by

$$f_2(t)\sim\frac{(a-b)\gamma^2\mu}{2\pi J}\Bigg\{(t\alpha)^{-1/2}\cos\left[\frac{2t}{\hbar}\gamma\right.$$
$$\left.\times\left(J^2-\frac{b^2\mu^2}{1-\gamma^2}\right)^{1/2}+\frac{1}{4}\pi\right]E_3\left(\frac{b}{1-\gamma^2}\right)\Gamma\left(\frac{1}{2}\right)\Bigg\}$$
$$+\Bigg\{\frac{(a-b)\gamma^2\mu}{4\pi J}(t\alpha)^{-3/2}\Gamma\left(\frac{3}{2}\right)E_3''\left(\frac{b}{1-\gamma^2}\right)$$
$$\times\cos\left[\frac{2t}{\hbar}\gamma\left(J^2-\frac{b^2\mu^2}{1-\gamma^2}\right)^{1/2}-\frac{1}{4}\pi\right]$$
$$+[\text{ first-order terms of } f_1(t)]\Bigg\} \tag{5.13}$$

α, E_3, E_3'' are given by (B34), (B41), and (B43), respectively.
Case (iii): $|b|=1-\gamma^2$; f_3 is given up to second order by

$$f_3(t)\sim\frac{(a-b)\gamma^2\mu}{2\pi J}\left[\frac{1}{2}\Gamma\left(\frac{3}{4}\right)(mt)^{-3/4}E_4(0)\right.$$
$$\times\cos\left(\frac{2t}{\hbar}|\mu b-J|+\frac{3\pi}{8}\right)+\frac{1}{2}\Gamma\left(\frac{5}{2}\right)(mt)^{-5/4}$$
$$\left.\times E_4'\cos\left(\frac{2t}{\hbar}|\mu b-J|+\frac{5\pi}{8}\right)\right] \tag{5.14}$$

where m is given by (B48) and $E_4(0)$ by (B46).
In Fig. 2, we exhibit the numerical analysis of (5.7) together with its appropriate asymptotic formula (5.12). We obtain the interference of two collective frequencies, which are understood from (5.12) to be "Larmor type" and "spin-exchange type." We cannot give an intuitive interpretation of the other collective frequency in (5.13).

13.0.6 VI. Exponentially decaying magnetic field

Section V raises the suspicion that nonergodic behavior found in the system is due to the special case (5.1). In other words, when initial field a jumps to a final field b at a very fast rate,

the system does not approach equilibrium. However, one might hope that a continuous very slow change of the magnetic field would result in an equilibri-

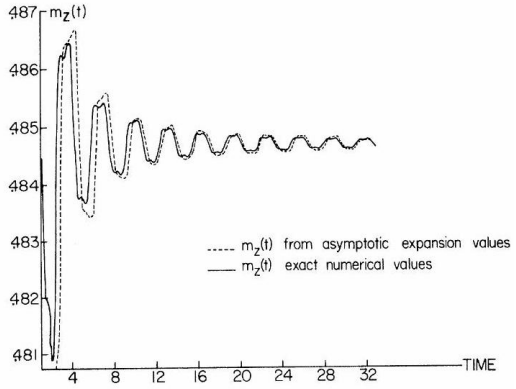

FIG. 2. $m_z(t)$ exact (numerical) and asymptotic for large t. $a = 10, b = 2, \gamma = \frac{1}{2}, \beta = 1$

um result.

To demonstrate this hope to be wrong we define a new field, which we can control to change as slow as we please:

$$h(t) = \begin{cases} a, & t \leqslant 0 \\ b + (a-b)e^{-Kt}, & t \geqslant 0 \end{cases} \tag{6.1}$$

where $a > b$.

The two solutions $W_1(t), W_2(t)$ [Eq. (3.32)] of Eq. (3.28) are obtained in Appendix A to be

$$\begin{aligned} W_1 = &\exp\left(i\Lambda(b)t + i\frac{a-b}{K}e^{-Kt}\right) {}_1F_1\left(\frac{i}{K}[-\Lambda(b)\right. \\ &\left. +b - \cos\phi]; 1 - \frac{2i\Lambda(b)}{K}; -\frac{2i(a-b)}{K}e^{-Kt}\right), \end{aligned} \tag{6.2}$$

$$\begin{aligned} W_2 = &\exp\left(-i\Lambda(b)t + i\frac{(a-b)}{K}e^{-Kt}\right) {}_1F_1\left(\frac{i}{K}[\Lambda(b)\right. \\ &\left. +b - \cos\phi]; 1 + \frac{2i\Lambda(b)}{K}; -\frac{2i(a-b)}{K}e^{-Kt}\right), \end{aligned} \tag{6.3}$$

where ${}_1F_1(a, c, x)$ is the confluent hypergeometric function [17] (Kummer series), and $\Lambda(b)$ is again given by (3.14).

One obtains the values of the constants (3.36) by direct substitution of (6.2) and (6.3) in (3.36) at $t = 0$:

$$\begin{aligned} W_1(0) = &{}_1F_1\left(\frac{i}{K}[-\Lambda(b) + b - \cos\phi];\right. \\ &\left. 1 - \frac{2i\Lambda(b)}{K}; -\frac{2i(a-b)}{K}\right), \\ W_2(0) = &{}_1F_1\left(\frac{i}{K}[\Lambda(b) + b - \cos\phi];\right. \\ &\left. 1 + \frac{2i\Lambda(b)}{K}; -\frac{2i(a-b)}{K}\right), \\ \frac{d}{dt}W_1(0) = &[i\Lambda(b) - i(a-b)]{}_1F_1\left(\frac{i}{K}[-\Lambda(b)\right. \\ &\left. +b - \cos\phi]; 1 - \frac{2i\Lambda(b)}{K}; -\frac{2i(a-b)}{K}\right) \end{aligned}$$

$$-2(a-b)\frac{-\Lambda(b)+b-\cos\phi}{K-2i\Lambda(b)}$$

$$\times{}_1F_1\left(1+\frac{i}{K}[-\Lambda(b)+b-\cos\phi];\right.$$

$$\left.2-\frac{2i\Lambda(b)}{K};-\frac{2i(a-b)}{K}\right)$$

$$\frac{d}{dt}W_2(0)=[-i\Lambda(b)-i(a-b)]_1F_1\left(\frac{i}{K}[\Lambda(b)\right.$$

$$\left.+b-\cos\phi];1+\frac{2i\Lambda(b)}{K};-\frac{2i(a-b)}{K}\right),$$

$$-2(a-b)\frac{\Lambda(b)+b-\cos\phi}{K+2i\Lambda(b)}$$

$$\times{}_1F_1\left(1+\frac{i}{K}[\Lambda(b)+b-\cos\phi]\right. \tag{6.10}$$

$$\left.2+\frac{2i\Lambda(b)}{K};-\frac{2i(a-b)}{K}\right) \tag{6.4d}$$

$$W(0)=W_1(0)\frac{d}{dt}W_2(0)$$

$$-W_2(0)\frac{d}{dt}W_1(0)=-2i\Lambda(b).$$

$$\times\left((a-\cos\phi)\left(2|A|^2+|B|^2-1\right)\right.$$

$$\left.+\frac{\gamma^2\sin^2\phi}{\Lambda(b)}\,\mathrm{Re}\,(BW_1+AW_2)\right)$$

This expression is an explicit function of K, which means that the final magnetization explicitly depends on how fast the field decays. For example, as $K\to\infty$

$$\lim_{K\to\infty}m(a,b,K)=\tfrac{1}{2\pi}\int_0^\pi d\phi\frac{\tanh\left[\frac{1}{2}\beta\Lambda(a)\right]}{\Lambda(a)}\frac{(b-\cos\phi)}{\Lambda^2(b)} \tag{6.11}$$
$$\times[\cos\phi-a)(\cos\phi-b)+\gamma^2\sin^2\phi]\cdot(6.11)$$

This is identical with (5.10) - a result which is expected, since when $K\to\infty$, (6.1) reduces to (5.1).

The hope stated at the beginning of this section is that as $K^{-1}\to\infty, m(a,b,K)$ will approach the value it would have in thermal equilibrium at some temperature T_1. To study this limit let $K^{-1}=s$. As $s\to\infty$ the asymptotic expansion of $W_1[a,b,s,\Lambda(b)]$ is found in Appendix C to be

$$W_1(a,b,s,\Lambda(b))\sim\frac{[2\Lambda(b)(\Lambda(b)-b+\cos\phi)]^{1/2}}{2(a-b)+(\Lambda(b)-b+\cos\phi)}$$

$$\times\exp\left(i\left\{\frac{1}{2}\pi-s(\Lambda-b+\cos\phi)\right.\right.$$

$$+s(\Lambda-b+\cos\phi)\ln[s(\Lambda-b+\cos\phi)+2s\Lambda$$

$$-2s(a-b)-2s\Lambda\ln(2s\Lambda)+s(\Lambda+b-\cos\phi)$$

$$\left.\left.\times\ln[2s(a-b)+s(\Lambda-b+\cos\phi)]\}\right) \tag{6.12}$$

$$W_2(a,b,s,\Lambda(b))\sim W_1(a,b,s,-\Lambda(b)). \tag{6.13}$$

By substitution of (6.12) and (6.13) in (6.10), and taking the limit $s \to \infty$, one obtains the final magnetization for this case. Clearly, only terms containing $|W_1|^2$ and $|W_2|^2$ will survive. Otherwise we again have the conditions of the RiemannLebesque lemma.

Explicitly, the final magnetization is

$$m(a,b) = \frac{1}{2\pi}\int_0^\pi d\phi \frac{\tanh\left[\frac{1}{2}\beta\Lambda(a)\right]}{\Lambda(a)}\left[(\cos\phi - a) + \left(\frac{3(b-\cos\phi)^2(a-\cos\phi)}{\Lambda(b)} + \frac{\gamma^2\sin^2\phi(a-\cos\phi)}{2\Lambda(b)} + \frac{\gamma^2\sin^2}{}\right.\right.$$
$$\times \frac{2\left[4(a-b)^2+\gamma^2\sin^2\phi\right]}{4(a-b)^2 - 4(a-b)(b-\cos\phi) - \gamma^2\sin^2\phi} + \left\{2(a-\cos\phi) - \gamma^2\sin^2\phi\right\}$$
$$\left.\times \frac{(b-\cos\phi)[2(a-b)-(b-\cos\phi)]^2 + 4\Lambda^2[2(a-b)-(b-\cos\phi)] + 2\Lambda^2(b-\cos\phi)}{4(a-b)^2 - 4(a-b)(b-\cos\phi) - \gamma^2\sin^2\phi}\right] \tag{6.14}$$

This magnetization shares with the $t \to \infty$ magnetization of the step function case, the unpleasant feature of failing to vanish when $b = 0$. Hence, we conclude that the $t \to \infty$ system is not in thermal equilibrium. Therefore, the nonergodic behavior of m_ε found in Sec. V does not depend on the rate at which $h(t)$ approaches its $t \to \infty$ limit.

13.0.7 VII. General properties of $m_z(t)$ for large t

The final question of interest is the generality of the asymptotic approach of (4.7) to its final value, and its relation to the asymptotic behavior of (5.7).

To understand this point we consider the general field:

$$\begin{aligned} &h(t) = a, && t \leqslant 0 \\ &h(t) = g(t), && 0 \leqslant t \leqslant t_0 \\ &h(t) = b, && t_0 \leqslant t < \infty. \end{aligned} \tag{7.1}$$

The evolution matrix for $t \leqslant t_0$ is, in general,

$$\begin{bmatrix} U_{11}(t) & U_{12}(t) \\ U_{21}(t) & U_{11}(t) \end{bmatrix} = e^{-it\cos\phi}\begin{bmatrix} V_{11}(t) & -V_{21}^*(t) \\ V_{21}(t) & V_{11}^*(t) \end{bmatrix}, \tag{7.2}$$

where V_{11} and V_{21} are given by (3.31) and (3.32), with constants A_1, A_2, B_1, B_2 given by (3.34). A_1 and A_2 are, in general, independent of δ, and B_1 and B_2 are proportional to $\frac{1}{2}\delta$.

The evolution matrix for $t \geqslant t_0$ is obtained as

$$Ut = \begin{bmatrix} U_{11}(t) & U_{12}(t) \\ U_{21}(t) & U_{22}(t) \end{bmatrix} = e^{-it_0\cos\phi}\begin{bmatrix} V_{11}(t_0) & -V_{21}^*(t_0) \\ V_{21}(t_0) & V_{11}^*(t_0) \end{bmatrix} \exp\left[i(t-t_0)\begin{pmatrix} b & \frac{1}{2}i\delta \\ -\frac{1}{2}i\delta & 2\cos\phi - b \end{pmatrix}\right]. \tag{7.3}$$

Using (3.36), (6.3) becomes

$$U(t) = e^{-it\cos\phi}\begin{bmatrix} V_{11}(t_0) & -\frac{1}{2}\delta\bar{V}_{21}^*(t_0) \\ \frac{1}{2}\delta\bar{V}_{21}(t_0) & V_{11}^*(t_0) \end{bmatrix}$$
$$\times \begin{bmatrix} i\frac{\cos\phi - b}{\Lambda(b)} - \sin[(t-t_0)\Lambda(b)] + \cos[(t-t_0)\Lambda(b)] & \frac{1}{2}\delta\frac{\sin[(t-t_0)\Lambda(b)]}{\Lambda(b)} \\ -\frac{1}{2}\delta\frac{\sin[(t-t_0)\Lambda(b)]}{\Lambda(b)} & -i\frac{(\cos\phi - b)}{\Lambda(b)} \qquad \sin[(t-t_0)\Lambda(b)] + \cos[(t-t_0)\Lambda(b)] \end{bmatrix} \tag{7.4}$$

where $V_{21} \equiv \frac{1}{2}\delta\bar{V}_{21}$ and $\bar{V}_{21}$ is δ independent. The magnetization for this case is obtained by substitution of the appropriate elements (7.4) in formula (4.6).

The asymptotic expansion of $m_g(t)$ is very similar to that of Sec. V and Appendix B. There are three cases.
(i) $|\mu b/J| < 1-\gamma^2$. In this case, $\Lambda(b)$ has an extremal point in the range $0 \leqslant \phi \leqslant \pi$ and the asymptotic expansion may be performed as a stationary phase integral. We find that the leading term of $m_g(t) - m_g(\infty)$ is given by the leading term of (5.13), where E_3 is replaced by an expression which depends explicitly on $V_{j,k}(t_0)$.
(ii) $|\mu b/J| > 1-\gamma^2$. In this case, $\Lambda(b)$ is monotonic for $0 \leqslant \phi \leqslant \pi$, and the asymptotic expansion comes from the endpoint contribution near 0 and π. Because of the presence of the factor δ^2 (note that r is proportional to δ) these contributions are similar to those seen in Sec. V, and we find that the leading terms of $m_g(t) - m_g(\infty)$ are given by the leading term of (5.12), where E_1 and E_2 are re-
placed by expressions which depend explicitly on $V_{j,k}(t_0)$.
(iii) $|\mu b/J| = 1-\gamma^2$. In this case, the extremal point of $\Lambda(b)$ occurs at 0 or π depending upon the sign of b. Again, because of the factor δ^2 this expansion is the same as that of Sec. V and we find the leading term of $m_g(t) - m_g(\infty)$ is given by the leading term of (5.14), where E_4 now depends on $V_{i,j}(t_0)$.

In summary, the form of the t dependence of the asymptotic behavior of $m_g(t) - m_g(\infty)$ is the same for all fields of the form (7.1). Only the constants depend on the details of the function $g(t)$.

13.0.8 VIII. Conclusion and summary

Since the considerations of this paper of necessity involve rather detailed and lengthy calculations, it may be worth while to summarize the various results and comment on their physical significance.
(i) Once the time-independent solutions are known, the time-dependent evolution is described by (1.7). The character of the system is described
by the normal modes Λ_p of the time-independent system relevant to the field $h(t)$. Thus, the nonequilibrium description requires an analysis of Eq. (3.28), over and above the solution of the equilibrium problem.
(ii) The explicit result for the time dependence of the magnetization for the step-function case $m_s(a,b,t)$ has the feature, that for a finite system (N finite) the limit $t \to \infty$ does not exist. The nonexistence of this time limit for physically meaningful observables is the generally known fact that the thermodynamic limit must be taken before an "approach to equilibrium" as $t \to \infty$ can be expected.
(iii) The main result of this study is the realization that the magnetization $m(a,b,t)$ as $t \to \infty$ does not approach an equilibrium value. This is indicated by the fact that $m(a,o,t)$ does not go to zero at infinite time. The fact that even as $a \to \infty$, the limiting value of m is less than $\frac{1}{2}$ is also surprising and shows that this model is not in agreement with the obvious physical intuition. The analysis of the exponentially decaying case, where the change from an external field a to b was carried out as slow as desired, results in the same "nonapproach" to equilibrium. This behavior is not a pecularity of the particular external field. It must be expected that this nonapproach is a general feature of the system at hand.
(iv) In connection with this nonapproach to equilibrium, Mazur [12] formulated a necessary and sufficient condition for a variable X to be ergodic in a classical system. This condition can be expressed in terms of the autocorrelation function as

$$R \equiv \lim \frac{1}{T} \int_0^T \langle X(0)X(t)\rangle dt = \left\langle \bar{X}^2(E) \right\rangle \tag{8.1}$$

Here $\langle X \rangle$ is the canonical average of X and $\bar{X}(E)$ is the microcanonical average of X. It is possible to obtain a generally valid inequality for R (i.e., its validity is independent of

the ergodic character of the system or the nature of the variable X). This inequality can be expressed as

$$R \geqslant Q. \tag{8.2}$$

The quantity Q can be expressed exclusively of the canonical average. Thus from the relations (8.1) and (8.2) one can see that a system cannot be ergodic if

$$Q\rangle \left\langle \bar{X}^2(E)\right\rangle . \tag{8.3}$$

Mazur has found a condition guaranteeing the nonergodic character of a variable. This is a useful condition since both Q and $\left\langle \bar{X}^2(E)\right\rangle$ are cononical averages, and as such can be obtained without explicit knowledge of the time dependence. Using this inequality for X, the magnetization, Mazur showed that it is not ergodic for the XY model.

Thus, harmony exists with the results obtained in this paper. The only point of concern, in a direct application of Mazur's result, is the fact that his analysis is classical, while the spin system is as quantum mechanical as it can be. The results obtained here indicate that there is good reason to expect Mazur's ingenious analysis to be valid in the quantum case, but it would be highly desirable to give a formal proof of Mazur's work for general quantum systems.

(v) The detailed formula for the asymptotic time dependence (for the step function and for the general case) indicates interesting and suggestive beat phenomena which are, as noted, dependent on a and b, but not on $g(t)$. It would be interesting if these various frequencies could be understood in an immediate intuitive fashion. It is believed that this is possible because the results are general, but so far this has not been done. It would be even more interesting if these were experimental situations in which these oscillations could be observed. Perhaps spin-echo experiments might show some of these features. In this connection a detailed examination of the oscillatory approach to the final state would be interesting. Furthermore, the case $h(t) = a + b\cos wt$, should be further analyzed.

(vi) It is possibly not too surprising that equilibrium in the conventional sense is not approached in this system. The system considered is quite simple and reminiscent of a system of coupled oscillators, and it is well known that these are peculiar phenomena associated with the approach to the equipartition of energy for such systems. The system is perhaps not complex enough to produce the mixing between the various degrees of freedom necessary for an approach to equilibrium. Even so, it would be interesting to see whether this system possesses any ergodic observables. [18]

13.0.9 Appendix A

We analyze here Eq. (3.26) for two cases of interest.

A. Exponential Decay

$$\begin{aligned} & h(t) && = b + (a-b)e^{-Kt}, \qquad t > 0 \\ \text{Let} \quad & && = a, \\ & && t \leq 0, K > 0 \end{aligned} \tag{A2}$$

and $\quad h_1(t) = (\mathrm{a} - b)e^{-Kt}$.

Equation (3.26) for $t > 0$ becomes

$$\frac{d^2}{dt^2}V + [\left[\Lambda^2(b) + (a-b)^2 e^{-2Kt}\right. \\ \left. -2(\cos\phi - b)e^{-Kt} - iKe^{-Kt}\right] V = 0. \tag{A3}$$

Let $y(z) = z^R e^{ibz/K} y_z(z) = V(t)$,
where $z = e^{-Kt}$,

$$R = \pm i\Lambda(b)/K \tag{A5}$$

Equation (A3) becomes

$$\begin{aligned} z\frac{d^2}{dz^2}y_2(z) + \left[z\left(\pm\frac{zi(a-b)}{K}\right)\right. & \\ \left. + \left(1 \pm \frac{2i\Lambda(b)}{K}\right)\right]\frac{d}{dz} & \quad y_2(z) + \left[-i\frac{a-b}{K}\right. \\ + \frac{2(a-b)(b-\cos\phi)}{K^2} \pm \frac{i(a-b)}{K} & \\ \left. \times \left(1 \pm \frac{2i\Lambda(b)}{K}\right)\right] y_2(z) = 0 & \end{aligned} \tag{A7}$$

Change the variable once more, and let

$$x = -[2i(a-b)/K]z \tag{A8}$$

One obtains confuent hypergeometric equation in Kummer's form, [17] and the two solutions $W_1(z)$ and $W_2(z)$ are

$$\begin{aligned} W_1(z) =& z^{(i/K)\Lambda} e^{\lfloor (b-a)/K \rfloor z}\, {}_1F_1\left(\frac{i}{K}[\Lambda + b - \cos\phi];\right. \\ & \left. 1 + 2i\Lambda/K; -[2i(a-b)/K]z\right), \end{aligned} \tag{A9}$$

$$\begin{aligned} W_2(z) =& z^{-(i/K)\Lambda} e^{i[(b-a)/K]z}\, {}_1F_1\left(\frac{i}{K}[-\Lambda + b - \cos\phi];\right. \\ & \left. 1 - 2i\Lambda/K; -[2i(a-b)/K]z\right), \end{aligned} \tag{A10}$$

with z given by (A5).

B. Hyperbolic Decay

Let $h(t) = a, \quad t \le 0$

$$= b + \frac{a-b}{t+1}, \quad t \ge 0 \tag{A11}$$

$$h_1(t) = (a-b)/(t+1) \tag{A12}$$

Let $t + 1 = s$ in (3.26) and $V(t) = y(s)$. We obtain

$$\begin{aligned} s^2\tfrac{d^2}{ds^2}y + [\Lambda^2(b)s^2 + 2(a-b)(b-\cos\phi)s & \\ +(a-b)(a-b-i)]y = 0 & \end{aligned} \tag{A13}$$

Let $y(s) = s^K e^{i\Lambda s} y_1(s)$,
where
$K = \frac{1}{2}\left\{1 + [1 - 4(a-b)(a-b-i)]^{1/2}\right\} = -i(a-b)$.(A15)
Equation (A13) becomes

$$\begin{aligned} s\frac{d^2}{ds^2}y_1(s) + (2i\Lambda s + 2K)\frac{d}{ds}y_1(s) & \\ + [2iK\Lambda + 2(a-b)(b-\cos\phi)]y_1(s) = 0 & \end{aligned} \tag{A16}$$

This equation is similar to (A7) with different constants, and the solutions are again Kummer function with $-2i\Lambda(t+1)$ as a variable.

There are other cases of interest for $h_1(t)$, for instance an attenuated periodic field $h_1(t) = (a-b)e^{-Kt}\cos\omega t$. To treat such cases, one should substitute his $h_1(t)$ in (3.26) and use the general theory of second-order ordinary differential equations.

13.0.10 Appendix B

We perform the asymptotic expansion of (5.8). In the integral (5.8), $\cos\phi$ changes monotonically between $[0,\pi]$, so we can always change the variable.
Let $y=\cos\phi$ and $d\phi=-\frac{dy}{(1-y^2)^{1/2}}$.
Let $f(t)=A\,\mathrm{Re}\int_{-1}^{1}dy\frac{\left(1-y^2\right)^{1/2}\tanh\left[\frac{1}{2}\beta\Lambda(a,y)\right]}{\Lambda(a,y)\Lambda^2(b,y)}$

$$\times e^{2it\Lambda(b,y)} \tag{B1}$$

This is the time-dependent part of the magnetization m_{xy}. Assume $|\gamma|<1, b>0$. Let $A\equiv(a-b)\gamma^2\ /2\pi$; then

$$\begin{aligned} f(t) &= A \\ &\times \mathrm{Re}\left(\int_{-1}^{1}dy\frac{(1-y^2)^{1/2}\tanh\left\{\frac{1}{2}\beta\left[\dot{\gamma}^2(1-y^2)+(a-y)^2\right]^{1/2}\right\}}{\left[\gamma^2(1-y^2)+(a-y)^2\right]^{1/2}\left[\gamma^2(1-y^2)+(b-y)^2\right]}\right. \\ &\left.\times\exp\left\{2it\left[\gamma^2\left(1-y^2\right)+(b-y)^2\right]^{1/2}\right\}\right). \end{aligned} \tag{B2}$$

Case (I) $b>1-\gamma^2$;
Case (II) $b<1-\gamma^2$;
Case (III) $b=1-\gamma^2$.
Clearly, in these regions, there will be contributions from the end points. The important question is whether $\left[\gamma^2(1-y^2)+(b-y)^2\right]^{1/2}$ has an extremum point for $y\in[-1,1]$, or not.

Our method of evaluating the integral $f(t)$ for large t is somewhat similar to the method used to evaluate asymptotically Bessel functions. We are going to the complex y plane. Doing so, it appears as if we introduce a serious difficulty:

$$p(y)=\frac{\tanh\left\{\frac{1}{2}\beta\left[\gamma^2(1-y^2)+(a-y)^2\right]^{1/2}\right\}}{\left[\gamma^2(1-y^2)+(a-y)^2\right]^{1/2}}. \tag{B3}$$

The function $p(y)$ has an infinite number of poles in the complex y plane. By integrating along a properly chosen contour, one might have to include an infinite sum of the residues of these poles. However, we domonstrate that for large t, these poles decay exponentially; therefore, they do not contribute to the asymptotic expansion for large t.

To demonstrate this last assertion we use the partial fraction decomposition of $p(y)$:

$$\begin{aligned} \frac{2}{\beta}p(y) &= \frac{\tanh\left[\frac{1}{2}\beta\Lambda(a,y)\right]}{\frac{1}{2}\beta\Lambda(a,y)} \\ &= 2\sum_{n=0}^{\infty}\frac{1}{\left[\frac{1}{2}\beta\Lambda(a,y)\right]^2-\left[\frac{1}{2}\beta\Lambda_n\right]^2} \end{aligned} \tag{B4}$$

where $\cosh\left[\frac{1}{2}\beta\Lambda_n\right]=0$
or

$$\Lambda_n=i\pi(2n+1)/\beta \tag{B5}$$

Substituting these values in $p(y)$, one obtains

$$p(y)=\frac{4}{\beta}\sum_{n=0}^{\infty}\left[\left(1-\gamma^2\right)y^2-2ay+\gamma^2+a^2+\pi^2(2n+1)^2/\beta^2\right]^{-1} \tag{B7}$$

An important feature of $p(y)$ is that $p(y)$ does not have any pole in the interval $[-1,1]$. This is seen immediately from $\gamma^2(1-y^2)+(a-y)^2 \geqslant 0$ in $[-1,1]$, and the square root is always real, therefore (B5) has no solution for $-1 \leqslant y \leqslant 1$.

Poles of $p(y)$ are at the points

$$y_n^{\pm} = \frac{a^{\pm}\left[a^2-(1-\gamma^2)\left(\gamma^2+a^2+\pi^2(2n+1)^2/\beta^2\right)\right]^{1/2}}{1-\gamma^2} \tag{B8}$$

Two possibilities for these poles are: (a) y_n is real so these poles, which must obey $|y_n|>1$, do not contribute anything; (b) y_n is complex. Let $\left[(1-\gamma^2)\,y_n^2-2by_n+b^2+\gamma^2\right]^{1/2} \equiv \xi+i\psi$, with $\psi \neq 0$. Then $\xi+i\psi$ is complex unless $a=b$. But the case $a=b$ is trivial, since the integral $f(t)$ is proportional to $a-b$. By calculation of the residue,
for the simple poles y_n of $p(y)$, we obtain contributions to the value of $f(t)$ of the form

$$\text{const } e^{2it(\xi+i\phi)} = \text{ const } e^{-2\phi t}e^{2it\xi}.$$

This means that possibly a-dependent oscillation frequencies of the magnetization decay exponentially, which is very fast compared to decay of the type t^{-a}, where we have $\alpha>0$. We conclude that for large t, the contribution to $f(t)$ from the poles y_n is negligible.

Case (I) $b>1-\gamma^2$; assume $b \neq 1$. (The case $b=1$ does not introduce any major difficulty. The result for this case would be sum of two descending series. One series vanishes for $b=1$.) We further assume $a \neq 1$. Having $a=1$, $\tanh\left[\frac{1}{2}\beta\Lambda\right]/\Lambda$ becomes $\frac{1}{2}\beta$ at the endpoints. Define

$$F(t) \equiv \int_{-1}^{1} dy \frac{(1-y^2)^{1/2}\tanh\left\{\frac{1}{2}\beta\left[\gamma^2(1-y^2)+(a-y)^2\right]^{1/2}\right\}}{\left[\gamma^2(1-y^2)+(a-y)^2\right]^{1/2}\left[\gamma^2(1-y^2)+(b-y)^2\right]} \exp\left\{2it\left[\gamma^2\left(1-y^2\right)+(b-y)^2\right]^{1/2}\right\}$$

namely, $f(t) = A\,\mathrm{Re}\,F(t)$. One can change the variables

$$\left[\gamma^2\left(1-y^2\right)+(b-y)^2\right]^{1/2} = x \tag{B10}$$

or

$$y = \frac{b-\left[b^2-(1-\gamma^2)\left(b^2+\gamma^2-x^2\right)\right]^{1/2}}{1-\gamma^2} \equiv B(x), \tag{B11}$$

where

$$B(|b+1|) = -1, \quad B(|b-1|) = 1 \tag{B12}$$

and

$$dy = -\frac{x\,dx}{\left[b^2-(1-\gamma^2)\left(b^2+\gamma^2-x^2\right)\right]^{1/2}} \tag{B13}$$

$$F(t) = \int_{|b-1|}^{|b+1|} \frac{dx}{x} e^{2itx} \frac{\left[1-B^2(x)\right]^{1/2}\tanh\left\{\frac{1}{2}\beta\left[\gamma^2(1-B^2(x)+(a-B(x))^2\right]\right\}}{\left\{\gamma^2\left[1-B^2(x)\right]+\left[a-B(x)\right]^2\right\}^{1/2}\left[b^2-(1-\gamma^2)\left(b^2+\gamma^2-x^2\right)\right]^{1/2}}. \tag{B14}$$

Let $I(t)$ be the following contour integral in the complex x plane;

$$I(t) = \oint_C \frac{dx}{x} \frac{\left[1-B^2(x)\right]^{1/2}\tanh\left\{\frac{1}{2}\beta\left[\gamma^2(1-B^2(x)+(a-B(x))^2\right]^{1/2}\right\}}{\left\{\gamma^2(1-B^2(x)+\left[a-B(x)\right]^2\right\}^{1/2}\left[b^2-(1-\gamma^2)\left(b^2+\gamma^2-x^2\right]^{1/2}\right.} \tag{B15}$$

where the contour C_1 is shown in Fig. 3. Apart from possible poles of $\left[\tanh \frac{1}{2}\beta\Lambda(x,a)\right]/\Lambda(x,a)$,
which were shown to be negligible for large t, the integral $I(t)$ along the contour C_1 vanishes. The
integral along $z_1 z_2$ vanishes as $\operatorname{Im} x \to \infty$, especially for t going to infinity. So we are left with

$$F(t) = \int_{b-1}^{z_1} - \int_{b+1}^{z_2} \equiv P_1(t) - P_2(t). \tag{B16}$$

Evaluation of $P_1(t)$:

$$\begin{aligned} P_1(t) = \int_{|b-1}^{|b-1|+i\infty} \Bigg(& \frac{dx}{x} \tanh \left\{ \frac{1}{2}\beta \left[\gamma^2 \left(1 - B^2(x)\right) \right.\right. \\ & \left.\left. +(a - B(x))^2\right]^{1/2} \right\} \left[(1 + B(x))(1 - B(x))\right]^{1/2} \\ & \times \exp(2itx) \left[\gamma^2 \left(1 - B^2(x)\right) + (a - B(x))^2\right]^{-1/2} \\ & \times \left[b^2 - \left(1 - \gamma^2\right)\left(b^2 + \gamma^2 - x^2\right)\right]^{-1/2} \Bigg) \end{aligned}$$

$$\text{Let} \quad |b-1| + i\xi = x \tag{B18}$$

and $id\xi = dx$.

$$\begin{aligned} P_1(t) = i \int_0^\infty & d\xi([1 + B(|b-1|) \\ & + i\xi)]^{1/2}(|b-1| + i\xi)^{-1/2} \\ & \times \tanh \left\{ \frac{1}{2}\beta \left[\gamma^2 \left(1 - B^2(|b-1| + i\xi)\right) \right.\right. \\ & \left.\left. +(a - B(|b-1| + i\xi))^2\right]^{1/2} \right\} \\ & \times \left[\gamma^2 \left(1 - B^2(|b-1| + i\xi)\right) + (a - B(|b-1| + i\xi))^2\right]^{-1/2} \end{aligned}$$

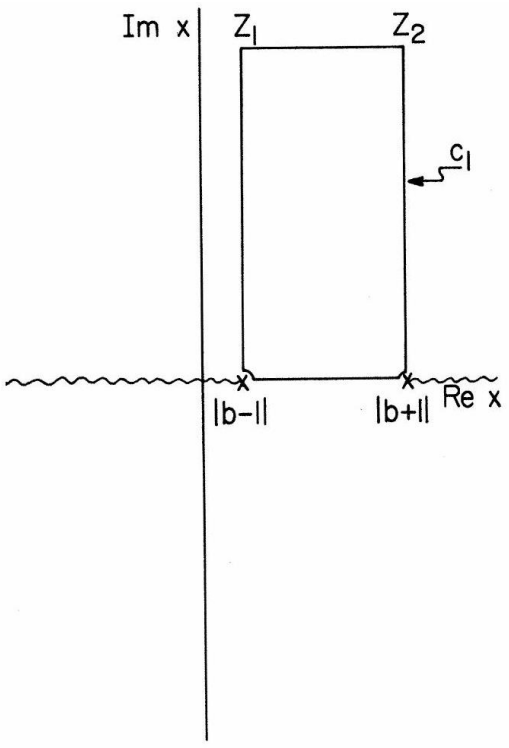

FIG. 3. Contour C_1.

$$\times \left[b^2 - \left(1-\gamma^2\right)\left(b^2+\gamma^2 - (|b-1|+i\xi)^2\right)\right]^{-1/2}$$
$$\times [1 - B(|b-1|+i\xi)]^{-1/2} \exp[2it(|b-1|+i\xi)]\Big) \tag{B19}$$

Define next the function $E_1(|b-1|+i\xi)$ such that

$$P_1(t) = ie^{2it|b-1|}\int_0^\infty d\xi \times E_1(|b-1|+i\xi)$$
$$\times e^{-2t\xi} \times [1+B(|b-1|+i\xi)]^{1/2}, \tag{B20}$$

where $E_1(|b-1|+i\xi) \simeq E_1(|b-1|)$

$$+E_1'(|b-1|)(i\xi) - E_1''(|b-1|)\xi^2 + \cdots \tag{B21}$$

exists around $\xi = 0$:

$$B(|b-1|+i\xi) \simeq \frac{b}{1-\gamma^2}$$
$$-\frac{b-(1-\gamma^2)}{1-\gamma^2}\left(1+\frac{i|b-1|\,(1-\gamma^2)}{\left[b-(1-\gamma^2)\right]^2}\xi\right)$$
$$= 1 - \frac{i|b-1|}{b-(1-\gamma^2)}\xi, \tag{B22}$$
$$[1-B(|b-1|+i\xi)]^{1/2} \simeq e^{i\pi/4}$$
$$\times \left[\frac{(b-1)}{b-(1-\gamma^2)}\right]^{1/2}\xi^{1/2}, \tag{B23}$$
$$P_1(t) \simeq ie^{i\mp/4}\left(\frac{b-1}{b-(1-\gamma^2)}\right)^{1/2} e^{2it|b-1|}$$
$$\times \left(E_1(|b-1|)\int_0^\infty d\xi e^{-2tt^{1/2}}\right.$$
$$+ iE_1'(|b-1|)\int_0^\infty d\xi \times \xi^{3/2}e^{-2t\xi}$$
$$\left.-\frac{E_1''}{2!}\int_0^\infty d\xi \times \xi^{5/2}e^{-2tt}\right)$$
$$= -e^{-i\pi/4}\left(\frac{|b-1|}{b-(1-\gamma^2)}\right)^{1/2} e^{2it|b-1|}$$
$$\times \left(\frac{E_1(|b-1|)\Gamma\left(\frac{3}{2}\right)}{(2t)^{3/2}} + \frac{iE_1'(|b-1|)\Gamma\left(\frac{5}{2}\right)}{(2t)^{5/2}} + \cdots\right), \tag{B24}$$

and

$$E_1(b-1) = \frac{\sqrt{2}\tanh\left[\frac{1}{2}\beta|a-1|\right]}{|a-1|\times|b-1|\left[b-(1-\gamma^2)\right]}, \tag{B25}$$
$$E_1'(|b-1|) = \frac{\sqrt{2}\left\{1-\tanh^2\left[\frac{1}{2}\beta|a-1|\right]\right\}\left\{\frac{1}{2}\beta\left[a-(1-\gamma^2\right]\right\}}{|a-1|^2\left[b-(1-\gamma^2)\right]^2}$$
$$-\frac{\sqrt{2}\tanh\left[\frac{1}{2}\beta|a-1|\right]}{|a-1|^2\left[b-(1-\gamma^2\right]}\left(\frac{1}{|b-1|^2} + \frac{(1-\gamma^2)}{\left[b-(1-\gamma^2)\right]^2}\right.$$

$$+\frac{1}{|a-1|^2\left[b-(1-\gamma^2)\right]}+\frac{1}{4\left[b-(1-\gamma^2)\right]}\Bigg) \tag{B26}$$

so $P_1(t)$ is calculated asymptotically for large t, up to second order. It can be done, in principle, to any order desired. In order to obtain $P_2(t)$, we see by close inspection, or better by repeating the above method, that replacing $a-1, b-1,\ b-(1-\gamma^2), -\frac{1}{4}i\pi$, by $a+1, b+1, b+1-\gamma^2, \frac{1}{4}i\pi$, respectively, in $P_1(t)$ gives the correct formula for $P_2(t)$:

$$\begin{aligned} P_2(t) \cong & -e^{i\pi/4}\left(\frac{|b+1|}{b+(1-\gamma^2)}\right)^{1/2} e^{2it|b+1|} \\ & \times\left(\frac{E_2(|b+1|)\Gamma\left(\frac{3}{2}\right)}{(2t)^{3/2}}+\frac{iE_2'(|b+1|)\Gamma\left(\frac{5}{2}\right)}{(2t)^{5/2}}+\cdots\right), \end{aligned} \tag{B27}$$

where $E_2(|b+1|)=\frac{2\tanh\left[\frac{1}{2}\beta|a+1|\right]}{|a+1||b+1|[b+(1-\gamma^2)]}$, (B28)

$$\begin{aligned} & E_2'(|b+1|) \\ & =\frac{\sqrt{2}\left[1-\tanh^2\left(\frac{1}{2}\beta|a+1|\right)\right]\left\{\frac{1}{2}\beta\left[a+(1-\gamma^2)\right]\right\}}{|a+1|^2\left[b+(1-\gamma^2)\right]^2} \\ & -\frac{\sqrt{2}\tanh\left[\frac{1}{2}\beta|a+1|\right]}{|a+1|\left(b+(1-\gamma^2)\right)}\Bigg(\frac{1}{|b+1|^2} \\ & +\frac{1-\gamma^2}{\left(b+1-\gamma^2\right)^2}+\frac{1}{|a+1|^2\left(b+1-\gamma^2\right)}+\frac{1}{4\left(b+1-\gamma^2\right)}\Bigg). \end{aligned} \tag{B29}$$

Case II: $b<1-\gamma^2$; We compute $f(t)$ for this case up to second order. The existence of a stationary phase in the integrand will contribute the first-order term. The second-order term will consist of two parts, the second-order stationary phase, and the endpoint integration, calculated for $b>1-\gamma^2$.

Here we cannot go to the complex x plane, since $\Lambda(b,y)$ is not a monotonic function of y.

We find a stationary phase at the point $y=b/\ (1-\gamma^2)$, and expand the two parts of the integral around this point. Rewrite $f(t)$:

$$\begin{aligned} f(t) &= A\,\mathrm{Re}\int_{-1}^{1}dy\frac{(1-y^2)^{1/2}\tanh\left[\frac{1}{2}\beta\left[\gamma^2\left(1-y^2\right)+(a-y)^2\right]^{1/2}\right]\exp\left\{2it\left[\gamma^2\left(1-y^2\right)+(b-y)^2\right]^{1/2}\right\}}{\left[\gamma^2\left(1-y^2\right)+(a-y)^2\right]^{1/2}\left[\gamma^2\left(1-y^2\right)+(b-y)^2\right]} \\ &\equiv A\,\mathrm{Re}\int_{-1}^{1}dyE_3(y)\exp\left\{2it\left[\gamma^2\left(1-y^2\right)+(b-y)^2\right]^{1/2}\right\}, \end{aligned} \tag{B30}$$

$$f(t)\simeq A\,\mathrm{Re}\int_{-1}^{1}E_3(y)\exp\left\{2it\left[\gamma\left(1-\frac{b^2}{1-\gamma^2}\right)^{1/2}+\frac{1-\gamma^2}{2\gamma}\left(1-\frac{b^2}{1-\gamma^2}\right)^{-1/2}\left(y-\frac{b}{1-\gamma^2}\right)^2\right]\right\} \tag{B31}$$

We estimate this last integral in the complex y place, along the contour C_2 (Fig. 4). We have introduced two more branch cuts, to define the sign of the square root in the exponent. It is necessary to mention that these branch points do not contribute any factor to the answer.

To complete the estimate of $f(t)$ for this case, one needs to compute the line integral $P_3(t)$ along AB.

Let $E_3(y)=E_3\left(\frac{b}{1-\gamma^2}\right)+E_3'\left(\frac{b}{1-\gamma^2}\right)\left(y-\frac{b}{1-\gamma^2}\right)$

$$+\frac{1}{2!}E_3''\left(\frac{b}{1-\gamma^2}\right)\left(y-\frac{b}{1-y^2}\right)^2+\cdots \tag{B32}$$

$$P_3(t)\cong A\,\mathrm{Re}\exp\left[2it\gamma\left(1-\frac{b^2}{1-\gamma^2}\right)^{1/2}\right]$$

$$\times\left[E_3\left(\frac{b}{1-\gamma^2}\right)\int_{AB}dye^{+it\alpha\left[y-b/\left(1-\gamma^2\right)\right]^2}\right.$$

$$\left.+E_3''\left(\frac{b}{1-\gamma^2}\right)\int_{AB}dye^{it\alpha\left[y-b/\left(1-\gamma^2\right)\right]^2}\left(y-\frac{b}{1-\gamma^2}\right)^2\right], \tag{B33}$$

where $\alpha=\frac{1-\gamma^2}{2\gamma}\left(1-\frac{b^2}{1-\gamma^2}\right)^{-1/2}$.

Let $y-\frac{b}{1-\gamma^2}=e^{i\pi/4}z,\quad dy=e^{i\pi/4}dz,$

$$P_3(t)\cong A\,\mathrm{Re}\exp\left[2it\gamma\left(1-\frac{b^2}{1-\gamma^2}\right)^{1/2}\right] \tag{B35}$$

$$\times\left[-E_3\left(\frac{b}{1-\gamma^2}\right)\int_{-\infty}^{\infty}e^{i\pi/4}dze^{-t\alpha\varepsilon^2}\right.$$

$$\left.-\frac{1}{2}E_3''\left(\frac{b}{1-\gamma^2}\right)\int_{-\infty}^{\infty}e^{i\pi/4}iz^2e^{-t\alpha z^2}dz\right] \tag{B36}$$

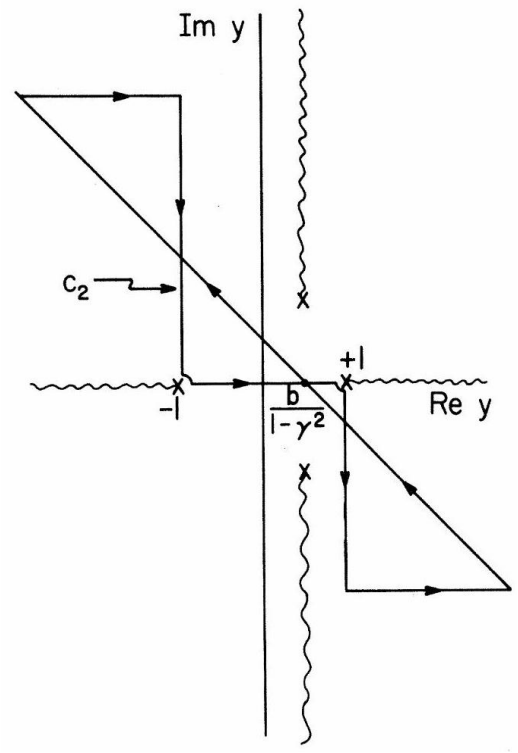

FIG. 4. Contour C_2.

we have

$$P_3(t) \cong A \operatorname{Re} \exp\left[2it\gamma\left(1-\frac{b^2}{1-\gamma^2}\right)^{1/2}\right] \times\left(-\frac{E_3\left[b/\left(1-\gamma^2\right)\right]\Gamma\left(\frac{1}{2}\right)}{(t\alpha)^{1/2}}e^{i\pi/4} +\frac{E_3''\left[b/\left(1-\gamma^2\right)\right]\Gamma\left(\frac{3}{2}\right)}{2(t\alpha)^{3/2}}e^{-i\pi/4}\right), \tag{B39}$$

$$f(t) \simeq -P_3(t) - P_2(t) + P_1(t), \tag{B40}$$

$$E_3\left(\frac{b}{1-\gamma^2}\right) = \left(1-\frac{b^2}{\left(1-\gamma^2\right)^2}\right)^{1/2} \times\tanh\left\{\frac{1}{2}\beta\left[\gamma^2\left(1-\frac{b^2}{\left(1-\gamma^2\right)^2}\right)+\left(a-\frac{b}{1-\gamma^2}\right)^2\right]^{1/2}\right\} \times\left[\gamma^2\left(1-\frac{b^2}{\left(1-\gamma^2\right)^2}\right)+\left(a-\frac{b}{1-\gamma^2}\right)^2\right]^{-1/2} \times\left[\gamma^2\left(1-\frac{b^2}{\left(1-\gamma^2\right)^2}\right)+\left(a-\frac{b}{1-\gamma^2}\right)^2\right]^{-1}. \tag{B41}$$

Because of its complexity, $E_3{}''\left[b/\left(1-\gamma^2\right)\right]$ is expressed in terms of the following constants:

$$Y \equiv \frac{b}{1-\gamma_2}, \tag{B42a}$$

$$S \equiv \left[1-b^{-2}\left(1-\gamma^2\right)^{-2}\right]^{1/2}, \tag{B42b}$$

$$B \equiv \gamma\left[1-b^{-2}\left(1-\gamma^2\right)^{-1}\right]^{1/2}, \tag{B42c}$$

$$D \equiv \left[b^{-2}\left(1-\gamma^2\right)^{-1}-2ab\left(1-\gamma^2\right)^{-1}+a^2+\gamma^2\right]^{1/2} \tag{B42d}$$

$$Q \equiv (b-a), \tag{B42e}$$

$$\begin{aligned} E_3''(Y) = &-Y - S^{-1}QD^{-2}B^{-2}\left[1-\tanh^2\left(\frac{1}{2}\beta D\right)\right]\frac{1}{2}\beta - S^{-1}D^{-1}B^{-2}\tanh\left(\frac{1}{2}\beta D\right) - Y^2S^{-3/2}D^{-1}B^{-2}\,\mathrm{ta} \\ &- YS^{-1}D^{-2}B^{-2}Q\left[1-\tanh^2\left(\frac{1}{2}\beta D\right)\right]^{\frac{1}{2}\beta+YS^{-1}D^{-3}B^{-2}Q\tanh\left(\frac{1}{2}\beta D\right)} \\ &- SB^{-2}D^{-3}\left(\frac{1}{2}\beta\right)^2Q^2 2\tanh\left(\frac{1}{2}\beta D\right)\left[1-\tanh^2\left(\frac{1}{2}\beta D\right)\right] + SD^{-2}B^{-2}\frac{1}{2}\beta\left(1-\gamma^2\right)\left[1-\tanh^2\right. \\ &+ YS^{-1}D^{-3}B^{-2}Q\tanh\left(\frac{1}{2}\beta D\right) - 2S\left(\frac{1}{2}\beta\right)Q^2B^{-2}D^{-4}\left[1-\tanh^2\left(\frac{1}{2}\beta D\right)\right] \\ &+ 3SD^{-5}B^{-2}Q^2\tanh\left(\frac{1}{2}\beta D\right) - \left(1-\gamma^2\right)SB^{-2}D^{-3}\tanh\left(\frac{1}{2}\beta D\right) \\ &- SQ^2\left(\frac{1}{2}\beta\right)B^{-2}D^{-4}\left[1-\tanh^2\left(\frac{1}{2}\beta D\right)\right] - \left(1-\gamma^2\right)SD^{-1}B^{-4}\tanh\left(\frac{1}{2}\beta D\right). \end{aligned} \tag{B43}$$

This completes the calculations for this case. Next we perform the asymptotic expansion for the interesting case $b = 1-\gamma^2$. This point is the boundary between these two regions.

Case III: $b = 1 - \gamma^2$. Having the leading term $\sim t^{-1/2}$ in case II, and $t^{-3/2}$ in case I, one would expect $t^{-\alpha}$ as a leading term for this boundary case, with $\frac{1}{2} \leqslant \alpha \leqslant \frac{3}{2}$. We indeed find $\alpha = \frac{3}{4}$. We perform the first-order calculation for large t. The interesting feature here is that the endpoint coincides with the stationary phase point. $\Lambda(b, y)$ will have now the following form: $[by^2 - 2by + b^2 + 1 - b]^{1/2} = \Lambda(b, y)$, and using the notation of cases I and II, one obtains

$$f(t) = A \operatorname{Re} \int_{-1}^{1} dy \left(1 - y^2\right)^{1/2}$$
$$\times \frac{\tanh\left[\frac{1}{2}\beta\left[(1-\gamma^2)\, y^2 - 2ya + a^2 + \gamma^2\right]^{1/2}\right] \exp\left\{i2t\left[by^2 - 2by + b^2 + 1 - b\right]^{1/2}\right\}}{\left[(1-\gamma^2)\, y^2 - 2ay + a^2 + \gamma^2\right]^{1/2}\left[by^2 - 2by + b^2 + 1 - b\right]}. \tag{B44}$$

Near $y = -1$, one obtains same endpoint integral as case I, but we will see that this gives a contribution, higher than second order. So we concentrate on the endpoint $y = 1$ (Fig. 5):

$$f(t) = A \operatorname{Re} e^{i3\pi/8} \int_0^\infty d\xi \xi^{1/2} E_4\left(e^{i\pi/4}\xi\right)$$
$$\times \exp\left[2it\left(\gamma^2 + \frac{1-\gamma^2}{2\gamma^2} e^{i\pi/2}\xi^2\right)\right] \tag{B45}$$

where

$$E_4\left(e^{i\pi/4}\xi\right) = \left(2 + e^{i\pi/4}\xi\right)^{1/2} \tanh\left[\frac{1}{2}\beta\Lambda\left(a, e^{i\pi/4}\xi\right)\right]$$
$$\times \left[\Lambda\left(a, e^{i\pi/4}\xi\right)\left(\gamma^2 + \frac{1-\gamma^2}{2\gamma^2}\left(e^{i\pi/4}\xi\right)^2\right)\right]^{-1} \tag{B46}$$

Using same method as before one obtains

$$f(t) = A \operatorname{Re} e^{i3\pi/8} e^{2itr^2}\left[E_4(0)\frac{1}{2}(mt)^{-3/4}\Gamma\left(\frac{3}{4}\right)\right.$$
$$\left. + e^{i\pi/4} E_4'(0) \times \frac{1}{2}(mt)^{-5/4}\Gamma\left(\frac{5}{4}\right)\right], \tag{B47}$$

where $E_4(0)$ and $d/dz\,[E_4(z)]$ for $z = e^{ir/4}\xi = 0$ can be

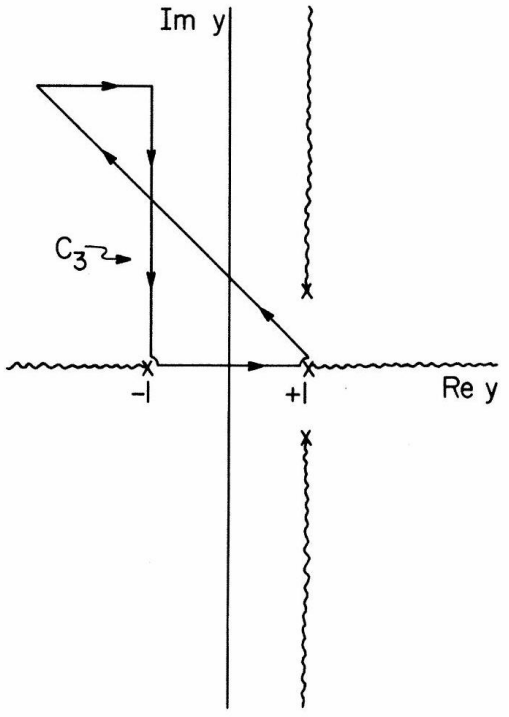

FIG. 5. Contour C_3.

easily determined from (B46) and

$$m = \left(1-\gamma^2\right)/\gamma^2 \tag{B48}$$

13.0.11 Appendix C

We perform the basic steps of the asymptotic expansion of $W_1(0)$ for large s, where $s = 1/K$:

$$\begin{aligned} W_1(0) =& {}_1F_1[is(-\Lambda + b - \cos\phi); \\ & 1 - 2is\Lambda; -2is(a-b)]. \end{aligned} \tag{C1}$$

We use the integral representation [17]

$$\begin{aligned} W_1(0) = & -\frac{\Gamma(1-2is\Lambda)\Gamma[1-is(-\Lambda+b\overline{\qquad}\cos\phi)]}{2\pi i\Gamma[1-is(\Lambda+b-\cos\phi)]} \\ & \times \int_C e^{-2is(a-b)t}(-t)^{-[1-is(-\Lambda+b-\cos\phi)]} \\ & \times (1-t)^{-is(\Lambda+b-\cos\phi)}dt \end{aligned} \tag{C2}$$

where C is the contour shown in Ref. 17. Since the asymptotic expansion of the Γ function is well known, [17] it is sufficient to study the asymptotic expansion of the integral in (C2). Let

$$\begin{aligned} \Phi = & \int_C e^{-2is(a-b)t}(-t)^{-[1-is(-\Lambda+b-\cos\phi)]} \\ & \times (1-t)^{-is(\Lambda+b-\cos\phi)}dt \end{aligned} \tag{C3}$$

Since the major contribution of Φ, for large s, is coming from the vicinity of the endpoint $t = 1$ in the lower half of the complex t plane, we deform the contour and approximate Φ by a line integral.

$$\begin{aligned} & \text{Let } t = 1 - iy, \quad dt = -idy \\ \Phi \sim & e^{-i\pi[1-is(-\Lambda+b-\cos\phi)]}(-i) \\ & \times e^{i(\pi/2)[-is(\Lambda+b-\cos\phi)]}e^{-2is(a-b)} \\ & \times \int_0^\infty e^{-2s(a-b)y}(1-iy)^{-1+is(-\Lambda+b-\cos\phi)} \\ & \times y^{-is(\Lambda+b-\cos\phi)}dy \end{aligned}$$

Let $2s(a-b)y = \zeta$.

Φ becomes

$$\begin{aligned} \Phi_{s\to\infty} \sim & ie^{s\pi(\Lambda-b+\cos\phi)+(\pi/2)s(\Lambda+b-\cos\phi)}e^{-2isi(\xi-b)} \\ & \times [2s(a-b)]^{is(\Lambda+b-\cos\phi)-1} \\ & \times \int_0^\infty e^{-\zeta}\left(1+\frac{\zeta}{i2s(a-b)}\right)is(-\Lambda+b-\cos\phi) \\ & \times \zeta^{-is(\Lambda+b-\cos\phi)}d\zeta \\ \simeq & ie^{s\pi(\Lambda-b+\cos\phi)+(\pi/2)s(\Lambda+b-\cos\phi)} \\ & \times e^{-2is(a-b)}[2s(a-b)]^{is(\Lambda+b-\cos\phi)}\frac{1}{2s(a-b)} \\ & \times \int_0^\infty \exp\left[-\zeta\left(1+\frac{\Lambda-b+\cos\phi}{2(a-b)}\right)\right]\zeta^{-is(\Lambda+b-\cos\phi)}d\zeta. \end{aligned} \tag{C6}$$

Finally, we obtain

$$\Phi \cong ie^{s\pi(\Lambda-b+\cos\phi)+(\pi/2)s(\Lambda+b-\cos\phi)}e^{-2is(a-b)}$$
$$\times\left[2s(a-b)\left(1+\frac{\Lambda-b+\cos\phi}{2(a-b)}\right)\right]^{is(\Lambda+\bar{b}-\cos\phi)}$$
$$\times\left[2s(a-b)\left(1+\frac{\Lambda-b+\cos\phi}{2(a-b)}\right)\right]^{-1}$$
$$\times\Gamma[1-is(\Lambda+b-\cos\phi)] \tag{C7}$$

Combining (C'7) with the asymptotic expansions for $\Gamma(1-2is\Lambda)$ and $\Gamma[1-is(-\Lambda+b-\cos\phi)]$, one obtains (6.12).

*Present address: Department of Mathematics, M.I. T., Cambridge, Mass. 02139.

† Supported in part by U. S. Atomic Energy Commission, under Contract No. AT(30-1)-3668A.

[1] E. Ising, Z. Phyzik 31, 253 (1925).
[2] L. Onsager, Phys. Rev. 65, 117 (1944).
[3] H. Bethe, Z. Phyzik 71, 205 (1931).
[4] L. Hulthn, Arkiv. Mat. Astron. Fysik 26A, Na11 (1938).
[5] C. N. Yang and C. P. Yang, Phys. Rev. 147, 303 (1966); 150, 321 (1966); 150, 327 (1966); 151, 258 (1966)
[6] E. Lieb, T. Schultz, and D. Mattis, Ann. Phys. (N. Y.) 16, 407 (1961). This paper will be referred to as LSM.
[7] Th. Niemeijer, Physica 36, 377 (1967); 39, 313 (1968).
[8] B. M. McCoy, Phys. Rev. 173, 531 (1968).
[9] S. Katsura, Phys. Rev. 127, 1507 (1962).
[10] E. Barouch and M. Dresden, Phys. Rev. Letters 23, 114 (1969).
[11] H. A. W. Van Vianen and J. A. Tjon (unpublished). In this work, the authors study the validity of the KuboTomita linear response theory.
[12] P. Mazur, Physica 43, 533 (1969).
[13] This boundary condition is called c cyclic by LSM. It is not the same boundary condition that was imposed on (2.1). In the thermodynamic limit the change of boundary condition is not expected to be significant. See LSM for further discussion.
[14] R. Bellman, Stability Theory of Differential Equations (McGraw-Hill, New York, 1953), p. 112. We would like to remark that somewhat weaker conditions can be imposed on $h_1(t)$. However, the conditions (3.29) provide us with sufficiently large class of time-dependent forces. The examples that are explicitly solved in Appendix A obey restrictions (3.31).
[15] We remark that example (5.7) was derived in an independent way by Niemeijer. However, he did not study the interesting consequences of this formula, and inaccurately stated that in all cases, the long-time behavior of $m_z(t)$ is proportional to $t^{-1/2}$
[16] At this point we perform the following substitutions: $t \to tJ/\hbar; \beta \to \beta J; a \to a\mu/J; b \to b\mu/J$.
[17] Bateman Manuscript Project, Higher Transcendental Functions, edited by A. Erdelyi (McGraw-Hill, New York, 1953).
[18] M. L. Girardeau, Phys. Letters 30A, 442 (1969).

14 Statistical Behavior in Deterministic Quantum Systems with Few Degrees of Freedom by Jensen, Shankar

Abstract

Numerical studies of the dynamics of finite quantum spin chains are presented which show that quantum systems with few degrees of freedom ($N = 7$) can be described by equilibrium statistical mechanics. The success of the statistical description is seen to depend on the interplay between the initial state, the observable, and the Hamiltonian. This work clarifies the impact of integrability and conservation laws on statistical behavior. The relation to quantum chaos is also discussed.

Until recently it was believed that the laws of statistical mechanics were applicable only to systems with many degrees of freedom. This view has been revised by recent studies in classical nonlinear dynamics which show that classical mechanical systems with very few degrees of freedom can exhibit dynamical behavior which is indistinguishable from a random process. [1,2] Here we ask whether the deterministic evolution of quantum systems with a few degrees of freedom can also exhibit statistical behavior. Specifically, we ask whether the expectation values of observables approach equilibrium and whether the equilibrium values can be predicted by the methods of quantum statistical mechanics, namely the use of the microcanonical and canonical ensembles. [3] We emphasize that these predictions do not require full knowledge of the initial wave function but only the gross features (such as the mean energy) necessary to specify the ensemble. We will refer to deterministic systems which can be described with this limited information as statistical. By studying the quantum mechanisms which give rise to statistical behavior in small quantum systems, we hope to gain a better understanding of the foundations of quantum statistical mechanics. Finally, we comment on the relation of our work to quantum chaos.

We studied the deterministic dynamics of a finite, spin- $\frac{1}{2}$, quantum chain in a magnetic field described
by the Hamiltonian

$$H = \alpha \sum_{n=1}^{N} \sigma_3(n)\sigma_3(n+1) + \lambda \sum_{n=1}^{N} \sigma_1(n) + \gamma \sum_{n=1}^{N} \sigma_3(n) \tag{1}$$

Here $\sigma_1(n)$ and $\sigma_3(n)$ are Pauli matrices at the site n of a cyclic chain of N spins, α is the nearest-neighbor coupling, and λ and γ are components of an external magnetic field.

The use of such models for investigation of statistical behavior in quantum systems has several important advantages. First, since the Hilbert space has a finite dimension, $d = 2^N$, numerical calculations of the energy spectra and the time evolution of arbitrary initial states can be performed to machine precision. Although much recent work has been devoted to the study of coupled nonlinear oscillators, numerical simulation of these systems must also restrict the Hilbert space to a finite dimensionality at the expense of introducing truncation errors. Second, by varying the parameters in H we can easily explore the effect of additional constants of motion as well as complete integrability on the statistical behavior. In particular, when $\gamma = 0$, the Hamiltonian is integrable and can be diagonalized by the fermion method of Schultz,
Mattis, and Lieb. [4]
To test for statistical behavior, we evolved various initial states with seven spins by numerically integrating the Schrödinger equation and plotted the expectation values of several observables as functions of time. We looked for an approach to equilibrium and compared the equilibrium values with the mean values computed on a microcanonical ensemble. Our main conclusion from these numerical studies is that both integrable and nonintegrable quantum systems with as few as seven degrees of freedom can exhibit statistical behavior for finite times.

Figure 1 shows typical results for the evolution of $M_1 = \sum_n \sigma_1(n)$ for a nonintegrable Hamiltonian with $\alpha = 0.5, \lambda = 1$, and $\gamma = 0.5$.M_1 exhibits an oscillatory decay to an equilibrium

value around 2.5 from an initial value of 0 . Of course a true equilibrium is never achieved since the system is quasiperiodic with a relatively long recurrence time.

The average value of M_1 over the corresponding microcanonical ensemble was determined by numerically computing the energy eigenvalues and eigenvectors and averaging the expectation values of M_1 over the eigenstates in the interval $E \pm \Delta E$ with equal weights, where E is the mean energy of the initial state and ΔE is a small interval in energy which must be large enough to span many energy levels of the system. (The results should not and did not depend on the precise value of ΔE.) In Fig. 2(a) the magnetization is plotted against energy for each of the energy eigenstates along with the microcanonical average computed with $\Delta E = 2.0$. For the state depicted in Fig. 1, which had a mean energy $E = 4.0$, this calculation predicts an equilibrium magnetization of $M_1 = 2.5$ which is in ex-

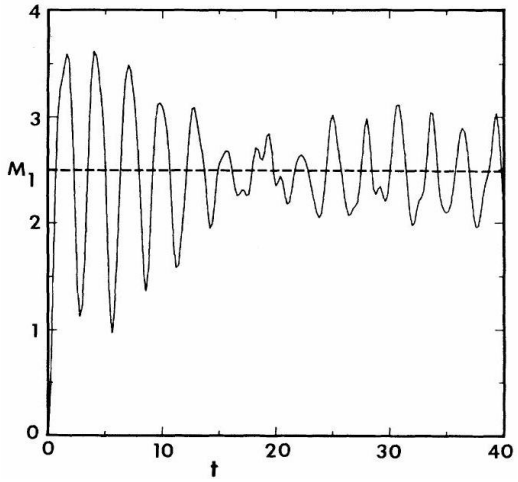

FIG. 1. The expectation value of the magnetization, M_1, as a function of time for a typical initial condition evolved by the spin Hamiltonian, Eq. (1). The dashed line shows the statistical prediction for the equilibrium magnetization.

cellent agreement with the numerical experiment.

Figure 2(a) also shows the equilibrium values of the magnetization calculated by evolving a number of different initial states. [5] The associated error bars indicate the level of fluctuations from the short-time average. Not only does the magnetization for this system with seven degrees of freedom approach equilibrium but the equilibrium values are correctly predicted by the microcanonical ensemble. The fact that the short-time average of $M_1(t)$, which is computed using the full knowledge of the wave function, is accurately predicted by the ensemble calculation, based only on the knowledge of the mean energy, is what justifies our characterization of the dynamics as statistical.

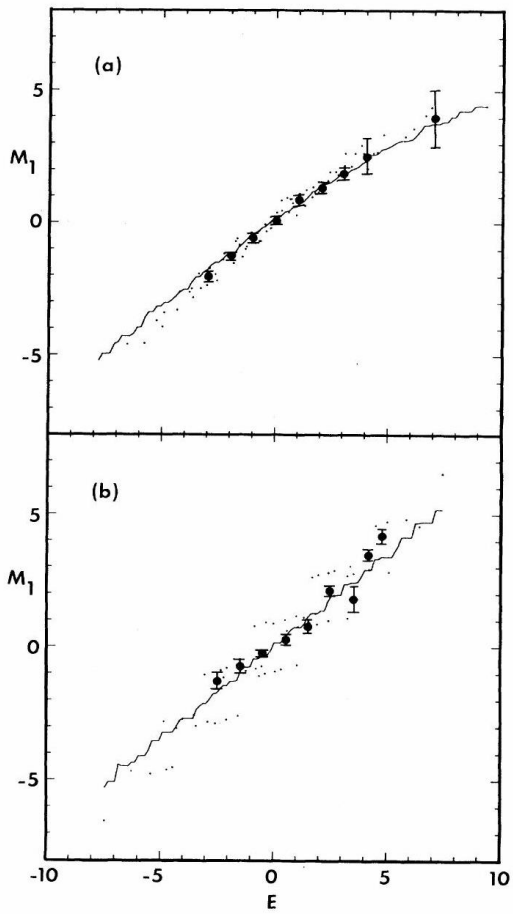

FIG. 2. The magnetization, M_1, plotted against energy for each of energy eigenstates (small dots) for (a) a nonintegrable Hamiltonian and (b) an integrable Hamiltonian; the solid curves represent the microcanonical average of the magnetization as functions of energy, and the large dots show the equilibrium values approached in numerical experiments performed with a variety of initial states. The associated error bars represent an estimate of the typical fluctuations from equilibrium.

Although lattice momentum was conserved because of the translational invariance of the Hamiltonian, it apparently had little influence on the dynamics of generic initial states. Only if the initial state were an eigenstate of momentum did we find a difference. In this case, the evolution of the initial state was restricted by selection rules and the appropriate ensemble was restricted to energy eigenstates with that momentum. Similarly, when the spin system was completely integrable the microcanonical ensemble was found to be applicable as long as the initial state was not an eigenstate of any of the conserved quantities. For generic initial states the constants of motion generally impose very mild constrains on the evolution of the wave function in the 2^N-dimensional Hilbert space. This is in contrast to the classical case where all dynamical variables are sharply defined in any initial state and the conserved quantities impose very severe restrictions on the dynamics.

In Fig. 2(b) the equilibrium values of M_1 for a number of different initial states evolved by an integrable Hamiltonian with $\alpha = 0.5, \lambda = 1.0$, and $\gamma = 0$ are compared with the statistical predictions. Deviations from equilibrium tend to be larger than in the nonintegrable case partly because of degeneracies which reduce the number of distinct frequencies in the problem and partly because the observable, M_1, is not a function of the energy alone but also of the other conserved quantities that label the state. This latter consideration is apparent in Fig. 2(b) where the magnetization for each of the energy eigenstates increases in an oscillatory manner over a series of steps in contrast to the nonintegrable case shown in Fig. 2(a) where the magnetization is a fairly smooth and monotonic function of energy.

An additional test of statistical behavior on the fact that if an isolated system is well described by the microcanonical ensemble, then a small subsystem should
be described by the canonical ensemble. [3] We choose spin 7 to be our subsystem, weakly coupled to the reservoir composed of the remaining spins. Given the postulate of equal a priori probabilities for the eigenstates for the combined system, it follows that P_+/P_-, the ratio of the probablities that spin 7 is in its upper or lower energy eigenstate with energy $\pm\epsilon$, is

$$P_+/P_- = N(E-\epsilon)/N(E+\epsilon) \tag{2}$$

where E is the energy of the combined system, $\pm\epsilon$ are the eigenvalues of the single spin Hamiltonian, $H_7 = \lambda\sigma_1(7) + \gamma\sigma_3(7)$, and $N(E \pm \epsilon)$ is the density of energy eigenstates of the reservoir, determined by numerically diagonalizing the Hamiltonian for the reservoir and constructing a coarse-grained density of states by smoothing over an interval ΔE. Since the density of states for this system was too irregular to replace the right-hand side of Eq. (2) by a Boltzmann factor $e^{-2\beta\epsilon}$, Eq. (2) was used directly to test the postulate of equal a priori probabilities. Numerical solutions for the evolution of $P_+$for both integrable and nonintegrable reservoirs once again showed an oscillatory approach to equilibrium which was accurately predicted by Eq. (2).

Numerous attempts have been made to extend the concept of chaos to quantum systems. [6–8] However, these efforts have led to much controversy because the linearity of the Schrödinger equation precludes the mixing behavior which characterizes chaos in classical systems. [1] Nevertheless, we find that the solutions of Schrödinger's equation are rich enough to exhibit statistical behavior. Moreover, we conclude that the applicability of statistical mechanics depends in the following way on the three interrelated factors: the initial state, the observable, and the Hamiltonian. [9]

The expectation of any observable, Ω, can be expressed as the sum of a time-independent and a timedependent term:

$$\langle\Omega\rangle(t) = \sum_n |c_n(0)|^2 \langle n|\Omega|n\rangle + \sum_{n\neq m}\sum_n c_n^*(0)c_m(0)\exp\left[i\left(E_n - E_m\right)t\right]\langle n|\Omega|m\rangle \tag{3}$$

where $c_n(0)$ are the coefficients of expansion of the initial state in terms of the energy eigenstates $|n\rangle$. The approach to equilibrium is a consequence of the phase-mixing decay of the time-dependent piece of $\langle\Omega\rangle(t)$. Although the initial state will recur as a large fluctuation, this recurrence time is long, $\tau_r \sim$ [minimum level spacing] $^{-1}$, compared with the decay time, $\tau_d \sim$ [energy spread of initial state] $^{-1}$, unless the initial state is an exact eigenstate or very close to one.

The equilibrium value of the observable is given by the time-independent part of $\langle\Omega\rangle$. For a generic initial state with given values of $c_n(0)$ the agreement with the equilibrium values predicted by the microcanonical average (with all c_n equal for eigenstates in
the interval $E \pm \Delta E$) depends on the observable. If the expectation values are smooth functions of the energy as in Fig. 2(a), then the short-time average of the observable will be very close to the ensemble average. In fact, it is clear from Fig. 2(a) that the statistical behavior will be obtained for any initial state with a reasonably narrow spread in energy. Even an initial energy eigenstate will exhibit a constant value for the observable which is very close to that predicted by the statistical theory. An observable which exhibits this property for a particular system could be called a "good" statistical quantity for that system. [10]
If the expectation value of the observable is not
principally determined by the energy, if other state labels exist and play an important role such that nearby energy eigenstates have very different expectation values, then the equilibrium approached in the dynamic evolution of a given initial state may not agree with statistical predictions based on the assumption of equal a priori probabilities. Nevertheless, although

the expectation value of M_1 for the integrable system shown in Fig. 2(b) does not show the smooth dependence on energy that is required of "good" observables, the time average is in good agreement with the predictions of statistical mechanics. This can be attributed to the fact that the generic initial states were nearly uniformly distributed over all the eigenstates of H in the interval $E \pm \Delta E$.[11] As a result, the time-independent part of the expectation of the observable in Eq. (3) was very close to the equal weight average.

Finally, we come to the role of the spectrum of the Hamiltonian. A number of different criteria have been suggested to define quantum chaos by distinguishing between the regularity of the energy level spacing of integrable and nonintegrable Hamiltonians. [6–8,12,13] However, depsite the fact that our small quantum system had a distribution of energy levels which was peaked at zero separation (Poisson type) for integrable Hamiltonians and exhibited level repulsion for nonintegrable Hamiltonians (Wigner-Dyson type), we observed statistical behavior in both cases.

This work was supported by the Alfred P. Sloan Foundation, the Department of Energy under Contract No. DE-AC02-76ER03075, the National Science Foundation under Contract No. PHY-8308280, and the Office of Naval Research under Contract No.

N00014-82-K-0184.

[1] A. J. Lichtenberg and M. A. Lieberman, Regular and Stochastic Motion (Springer, New York, 1983).
[2] J. Ford, Physics Today 36, No. 4, 40 (1983).
[3] R. C. Tolman, The Principles of Statistical Mechanics (Oxford, London, 1938).
[4] T. D. Schultz, D. C. Mattis, and E. H. Lieb, Rev. Mod. Phys. 36, 856 (1964).
[5] The initial states were typically chosen to be eigenstates of $M_3 = \Sigma_n \sigma_3(n)$; however, random superpositions of energy eigenstates gave similar results.
[6] G. M. Zaslavskii, Phys. Rep. 80, 157 (1981).
[7] D. W. Noid, M. L. Koszykowski, and R. A. Marcus, Annu. Rev. Phys. Chem. 32, 267 (1981).
[8] Chaotic Behavior in Quantum Systems, edited by G. Casati (Plenum, New York, 1984).
[9] Our criteria for statistical behavior do not constitute a definition of quantum chaos, unless chaos is permitted to have a weaker meaning in quantum mechanics than in classical mechanics, since integrable classical systems can also exhibit statistical behavior with phase-mixing decay to equilibrium for finite times. However, a stronger definition is precluded since the Schrödinger equation is linear for both integrable and nonintegrable quantum systems. B. V. Chirikov, F. M. Israilev, and D. L. Shepelyansky, Sov. Sci. Rev. 2C, 209 (1981).
[10] This definition of "good" statistical observables is related to the "pseudorandom" property of the matrix representations of observables introduced by A. Peres, Phys. Rev. A 30, 504 (1984).
[11] K. S. Nordholm and S. A. Rice, J. Chem. Phys. 61, 203 (1974).
[12] I. C. Percival, J. Phys. B 6, L229 (1973).
[13] M. V. Berry and M. Tabor, Proc. Roy. Soc. London, Ser. A 365, 75 (1977).

15 Thermalization and its mechanism for generic isolated quantum systems by Rigol, Dunjko, Olshanii

Abstract

Time dynamics of isolated many-body quantum systems has long been an elusive subject. Very recently, however, meaningful experimental studies of the problem have finally become possible [17, 24], stimulating theoretical interest as well [1, 4, 5, 6, 60]. Progress in this field is perhaps most urgently needed in the foundations of quantum statistical

mechanics. This is so because in generic isolated systems, one expects [8, 88] nonequilibrium dynamics on its own to result in thermalization: a relaxation to states where the values of macroscopic quantities are stationary, universal with respect to widely differing initial conditions, and predictable through the time-tested recipe of statistical mechanics. However, it is not obvious what feature of many-body quantum mechanics makes quantum thermalization possible, in a sense analogous to that in which dynamical chaos makes classical thermalization possible [10]. For example, dynamical chaos itself cannot occur in an isolated quantum system, where time evolution is linear and the spectrum is discrete [11]. Underscoring that new rules could apply in this case, some recent studies even suggested that statistical mechanics may give wrong predictions for the outcomes of relaxation in such systems [4, 5]. Here we demonstrate that an isolated generic quantum many-body system does in fact relax to a state well-described by the standard statistical mechanical prescription. Moreover, we show that time evolution itself plays a merely auxiliary role in relaxation and that thermalization happens instead at the level of individual eigenstates, as first proposed by J. M. Deutsch [72] and M. Srednicki [73]. A striking consequence of this *eigenstate thermalization* scenario, confirmed below for our system, is that the knowledge of a *single* many-body eigenstate suffices to compute thermal averages—any eigenstate in the microcanonical energy window will do, as they all give the same result.

15.1 Theory

If we pierce an inflated balloon inside a vacuum chamber, very soon we find the released air uniformly filling the enclosure and the air molecules attaining the Maxwell velocity distribution whose width depends only on their total number and energy. Different balloon shapes, placements, or piercing points all lead to the same spatial and velocity distributions. Classical physics explains this *thermodynamical universality* as follows [10]: almost all particle trajectories quickly begin looking alike, even if their initial points are very different, because nonlinear equations drive them to explore ergodically the constant-energy manifold, covering it uniformly with respect to precisely the microcanonical measure. However, if the system possesses further conserved quantities *functionally independent* from the Hamiltonian and each other, then time evolution is confined to a highly restricted hypersurface of the energy manifold. Hence, microcanonical predictions fail and the system does not thermalize.

On the other hand, in isolated quantum systems not only is dynamical chaos absent due to the linearity of time evolution and the discreteness of spectra [11], but it is also not clear under what conditions conserved quantities provide independent constraints on relaxation dynamics. To begin with, any operator commuting with a generic and thus nondegenerate Hamiltonian is functionally dependent on it [383], implying that the conservation of energy is the only independent constrain. On the other hand, even when operators are functionally dependent, their expectation values—considered as functionals of states—generally are not: for example, two states may have the same mean energies but different mean square-energies. For nondegenerate Hamiltonians a maximal set of constants of motion with functionally independent expectation values is as large as the dimension of the Hilbert space; examples include the projectors $\widehat{P}_\alpha = |\Psi_\alpha\rangle\langle\Psi_\alpha|$ to the energy eigenstates [383] and the integer powers of the Hamiltonian [5].

The current numerical and analytic evidence from integrable systems suggests that there exists a minimal set of independent constraints whose size is much smaller than the dimension of the Hilbert space but may still be much greater than one. In our previous work [1] (with V. Yurovsky) we showed that an integrable isolated one-dimensional system of lattice hard-core bosons relaxes to an equilibrium characterized not by the usual but by a *generalized* Gibbs ensemble. Instead of just the energy, the Gibbs exponent contained a linear combination of conserved quantities—the occupations of the eigenstates of the corresponding Jordan-Wigner fermions—whose number was still only a tiny fraction of the dimension of the Hilbert space. Yet

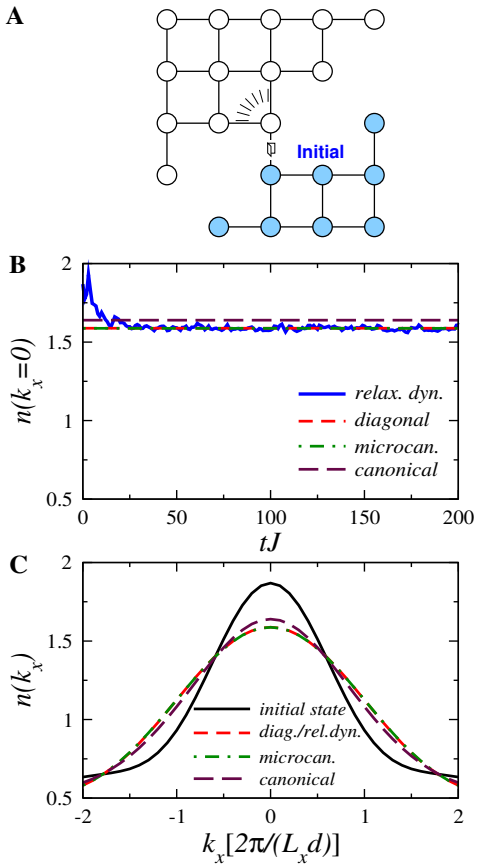

Figure 15.1: **Relaxation dynamics**. **a**, Two-dimensional lattice on which five hard-core bosons propagate in time. The bosons are initially prepared in the ground state of the sublattice in the lower-right corner and released through the indicated link. **b**, The corresponding relaxation dynamics of the marginal momentum distribution center $[n(k_x = 0)]$ compared with the predictions of the three ensembles. In the microcanonical case, we averaged over all eigenstates whose energies lie within a narrow window (see Supplementary Discussion) $[E_0 - \Delta E, E_0 + \Delta E]$, where $E_0 \equiv \langle\psi(0)|\widehat{H}|\psi(0)\rangle = -5.06J$, $\Delta E = 0.1J$, and J is the hopping parameter. The canonical ensemble temperature is $k_{\mathrm{B}}T = 1.87J$, where k_{B} is the Boltzmann constant, so that the ensemble prediction for the energy is E_0. **c**, Full momentum distribution function in the initial state, after relaxation, and in the different ensembles. Here d is the lattice constant and $L_x = 5$ the lattice width.

this ensemble works, while the usual one does not, for a wide variety of initial conditions [36] as well as for a fermionic system [39]; it also explains a recent experimental result, the absence of thermalization in the Tonks-Girardeau gas [17]. Thus, while at least some constraints beyond the conservation of energy must be kept, it turns out one needs only a relatively limited number of additional conserved quantities with functionally independent expectation values; adding still further ones is redundant.

Since it is not clear which sets of conserved quantities—and some are always present—constrain relaxation and which do not, it becomes even more urgent to determine whether isolated generic quantum systems relax to the usual thermal state. The theoretical attention to this question has in fact been increasing recently, because of the high levels of isolation [17, 24, 17] and control [20, 19] possible in experiments with ultracold quantum gases. However, despite numerous studies of specific models there is not yet consensus on how or even if relaxation to the usual thermal values occurs for nonintegrable systems [60]. Common wisdom says that it does [8, 88], but some recent numerical results suggest otherwise, either under certain conditions [4] or in general [5].

In order to study relaxation of an isolated quantum systems, we considered the time evolution of five hard-core bosons with additional weak nearest-neighbor repulsions, on a 21-site two-dimensional lattice, initially confined to a portion of the lattice and prepared in their ground state there. Figure 24.1a shows the exact geometry (see also Supplementary Discussion); the relaxation dynamics begins when the confinement is lifted. Expanding the initial state wavefunction in the eigenstate basis of the final Hamiltonian $\widehat{H}$ as $|\psi(0)\rangle = \sum_\alpha C_\alpha |\Psi_\alpha\rangle$, the many-body wavefunction evolves as $|\psi(t)\rangle = e^{-i\widehat{H}t}|\psi(0)\rangle = \sum_\alpha C_\alpha e^{-iE_\alpha t}|\Psi_\alpha\rangle$, where the E_α's are the eigenstate energies. Thus obtaining numerically-exact results for all times required the full diagonalization of the 20,349-dimensional Hamiltonian. The quantum-mechanical mean of any observable $\widehat{A}$ evolves as

$$\langle \widehat{A}(t)\rangle \equiv \langle\psi(t)|\widehat{A}|\psi(t)\rangle = \sum_{\alpha,\,\beta} C^\star_\alpha C_\beta e^{i(E_\alpha - E_\beta)t} A_{\alpha\beta}\,, \tag{15.1}$$

with $A_{\alpha\beta} = \langle\Psi_{\alpha'}|\widehat{A}|\Psi_\alpha\rangle$. The long-time average of $\langle\widehat{A}(t)\rangle$ is then

$$\overline{\langle\widehat{A}\rangle} = \sum_\alpha |C_\alpha|^2 A_{\alpha\alpha}\,. \tag{15.2}$$

Note that if the system relaxes at all, it must be to this value. We find it convenient to think of Eq. (15.2) as stating the prediction of a "diagonal ensemble," $|C_\alpha|^2$ corresponding to the weight $|\Psi_\alpha\rangle$ has in the ensemble. In fact, this ensemble is precisely the generalized Gibbs ensemble introduced in Ref. [1] if as integrals of motion one takes all the projection operators $\widehat{P}_\alpha = |\Psi_\alpha\rangle\langle\Psi_\alpha|$. Using these as constraints on relaxation dynamics, the theory gives $\hat{\rho}_c = \exp\left(-\sum_{\alpha=1}^{D}\lambda_\alpha \hat{P}_\alpha\right)$, with $\lambda_\alpha = -\ln(|C_\alpha|^2)$, and D the dimension of the Hilbert space. (Notice, however, that for the integrable system treated in Ref. [1], the generalized Gibbs ensemble was defined using a different, *minimal* set of independent integrals of motion, whose number was equal to the number of lattice sites $N \ll D$.)

Now if the quantum-mechanical mean of an observable behaves thermally it should settle to the prediction of an appropriate statistical-mechanical ensemble. For our numerical experiments we chose to monitor the marginal momentum distribution along the horizontal axis $n(k_x)$ and its central component $n(k_x = 0)$ (see Supplementary Discussion). Figures 24.1b and 24.1c demonstrate that both relax to their microcanonical predictions. The diagonal ensemble predictions are indistinct from these, but the canonical ones, although quite close, are not. This is an indication of the relevance of finite size effects, which may be the origin of some of the apparent deviations from thermodynamics seen in the recent numerical studies of Refs. [4] and [5].

The statement that the diagonal and microcanonical ensembles give the same predictions for the relaxed value of $\widehat{A}$ reads

$$\begin{aligned}\sum_\alpha |C_\alpha|^2 A_{\alpha\alpha} \;&=\; \langle A\rangle_{\text{microcan.}}(E_0)\\ &\overset{\text{def.}}{=} \frac{1}{\mathcal{N}_{E_0,\,\Delta E}} \sum_{\substack{\alpha\\ |E_0 - E_\alpha|<\Delta E}} A_{\alpha\alpha}\,,\end{aligned} \tag{15.3}$$

where E_0 is the mean energy of the initial state, ΔE is the half-width of an appropriately chosen (see Supplementary Discussion) energy window centered at E_0, and the normalization $\mathcal{N}_{E_0,\,\Delta E}$ is the number of energy eigenstates with energies in the window $[E_0 - \Delta E,\, E_0 + \Delta E]$. Thermodynamical universality is evident in this equality: while the left hand side depends on the details of the initial conditions through the set of coefficients C_α, the right hand side

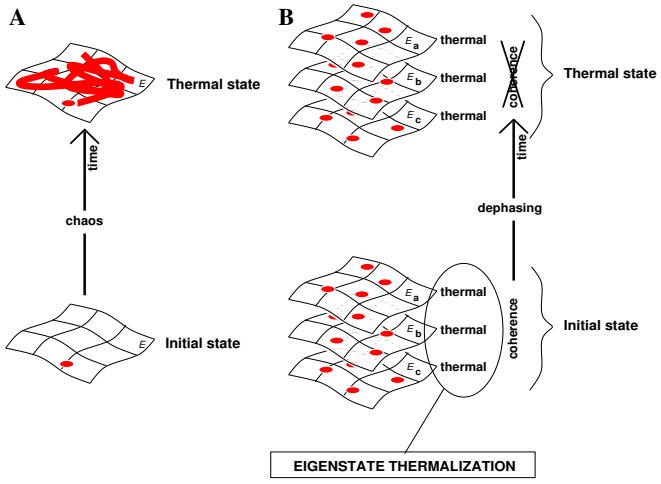

Figure 15.2: **Thermalization in classical vs quantum mechanics**. **a**, In classical mechanics, time evolution constructs the thermal state from an initial state that generally bears no resemblance to the former. **b**, In quantum mechanics, according to the eigenstate thermalization hypothesis, every eigenstate of the Hamiltonian always implicitly contains a thermal state. The coherence between the eigenstates initially hides it, but time dynamics reveals it through dephasing.

depends only on the total energy, which is the same for many different initial conditions. Three mechanisms suggest themselves as possible explanations of this universality (assuming the initial state is sufficiently narrow in energy, as is normally the case—see Supplementary Discussion):

(i) Even for eigenstates close in energy, there are large eigenstate-to-eigenstate fluctuations of both the eigenstate expectation values $A_{\alpha\alpha}$ and of the eigenstate occupation numbers $|C_\alpha|^2$. However, for physically interesting initial conditions, the fluctuations in the two quantities are uncorrelated. A given initial state then performs an unbiased sampling of the distribution of the eigenstate expectation values $A_{\alpha\alpha}$, resulting in Eq. (15.3).

(ii) For physically interesting initial conditions, the eigenstate occupation numbers $|C_\alpha|^2$ practically do not fluctuate at all between eigenstates that are close in energy. Again, Eq. (15.3) immediately follows.

(iii) The eigenstate expectation values $A_{\alpha\alpha}$ practically do not fluctuate at all between eigenstates that are close in energy. In that case Eq. (15.3) holds for literally *all* initial states narrow in energy.

J. M. Deutsch and M. Srednicki have independently proposed the scenario (iii), dubbed the

> Eigenstate thermalization hypothesis (ETH) [Deutsch[72] (1991), Srednicki[73] (1994)].
> The expectation value $\langle\Psi_\alpha|\widehat{A}|\Psi_\alpha\rangle$ of a few-body observable $\widehat{A}$ in an eigenstate of the Hamiltonian $|\Psi_\alpha\rangle$, with energy E_α, of a large interacting many-body system equals the thermal (microcanonical in our case) average $\langle A\rangle_{\text{microcan.}}(E_\alpha)$ of $\widehat{A}$ at the mean energy E_α:
>
> $$\langle\Psi_\alpha|\widehat{A}|\Psi_\alpha\rangle = \langle A\rangle_{\text{microcan.}}(E_\alpha). \tag{15.4}$$

The ETH suggests that classical and quantum thermal states have very different natures, as depicted in Fig. 24.2. While at present there are no general theoretical arguments supporting the ETH, some results do exist for restricted classes of systems. To begin with, Deutsch [72] showed that the ETH holds in the case of an integrable Hamiltonian weakly perturbed by a single matrix taken from a random Gaussian ensemble. Next, nuclear shell model calculations have shown that individual wavefunctions reproduce thermodynamic predictions [20]. Then there are rigorous proofs that some particular quantum systems, whose classical counterparts are chaotic, satisfy the ETH in the semiclassical limit [21, 22, 23, 24]. More generally, for low

density billiards in the semiclassical regime, the ETH follows from Berry's conjecture [73, 25], which in turn is believed to hold in semiclassical classically-chaotic systems [26]. Finally, at the other end of the chaos-integrability continuum, in systems solvable by Bethe ansatz, observables are smooth functions of the integrals of motion. This allows the construction of single energy eigenstates that reproduce thermal predictions [27].

In Figs. 24.3a-c we demonstrate that the ETH *is* in fact the mechanism responsible for thermal behavior in our nonintegrable system. Fig. 24.3c additionally shows that scenario (ii) mentioned above plays no role, because the fluctuations in the eigenstate occupation numbers $|C_\alpha|^2$ are large. Thermal behavior also requires that both the diagonal and the chosen thermal ensemble have sufficiently narrow energy distributions $\rho(E)$ [= probability distribution $\times$ the density of states], so that in the energy region where the energy distributions $\rho(E)$ are appreciable, the derivative of the curve eigenstate expectation value $A_{\alpha\alpha}$ vs the energy (here $n(k_x = 0)$ vs the energy) does not change much; see Supplementary Discussion. As shown in Fig. 24.3b, this holds for the microcanonical and diagonal ensembles but not for the canonical ensemble, explaining the failure of the latter to describe the relaxation in Fig. 24.1. Note that the fluctuations of the eigenstate occupation numbers $|C_\alpha|^2$ in Fig. 24.3b are lowered by the averaging involved in the computation of the density of states (compare with Fig. 24.3c).

To strengthen the case for the ETH, we tested another observable. We chose it with the following consideration in mind: in our system interactions are local in space, and momentum distribution is a global, approximately spatially additive property. Thus one might wonder if the ETH for momentum distribution arises through some spatial averaging mechanism (we thank the anonymous referee 2 for bringing this point to our attention). It does not: for our final test of the ETH we chose an observable that is manifestly local in space, the expectation value of the occupation of the central site of the lattice. We again found that the ETH holds true (3% relative standard deviation of eigenstate-to-eigenstate fluctuations).

On the other hand, Figs. 24.3d-f show how the ETH *fails* for an isolated one-dimensional *integrable* system. The latter consists of five hard-core bosons initially prepared in their ground state in an 8-site chain, one of the ends of which we then link to one of the ends of an adjoining (empty) 13-site chain to trigger relaxation dynamics. As Fig. 24.3e shows, $n(k_x)$ as a function of energy is a broad cloud of points, meaning that the ETH is not valid; Fig. 24.3f shows that scenario (ii) does not hold either.

Nevertheless, one may still wonder if in this case scenario (i) might hold—if the averages over the diagonal and the microcanonical energy distributions shown in Fig. 24.3e might agree. Figure 24.3d shows that this does not happen. This is so because, as shown in Fig. 24.3f, the values of $n(k_x = 0)$ for the most-occupied states in the diagonal ensemble (the largest values of eigenstate occupation numbers $|C_\alpha|^2$) are always smaller than the microcanonical prediction, and those of the least-occupied states, always larger. Hence, the usual thermal predictions fail because the correlations between the values of $n(k_x = 0)$ and $|C_\alpha|^2$ preclude unbiased sampling of the latter by the former. These correlations have their origin in the nontrivial integrals of motion that make the system integrable and that enter the *generalized* Gibbs ensemble, which was introduced in Ref. [1] as appropriate for formulating statistical mechanics of isolated integrable systems. In the nonintegrable case shown in Fig. 24.3c, $n(k_x = 0)$ is so narrowly distributed that it does not matter whether or not it is correlated with $|C_\alpha|^2$ (we have in fact seen no correlations in the nonintegrable case).

The thermalization mechanism outlined thus far explains why long-time averages converge to their thermal predictions. A striking aspect of Fig. 24.1b, however, is that the time fluctuations are so small that after relaxation the thermal prediction works well at every instant of time. Looking at Eq. (15.1), one might think this is so because the contribution of the off-diagonal terms gets attenuated by temporal dephasing, which results from the generic incommensurability of the frequencies of the oscillating exponentials. However, this attenuation

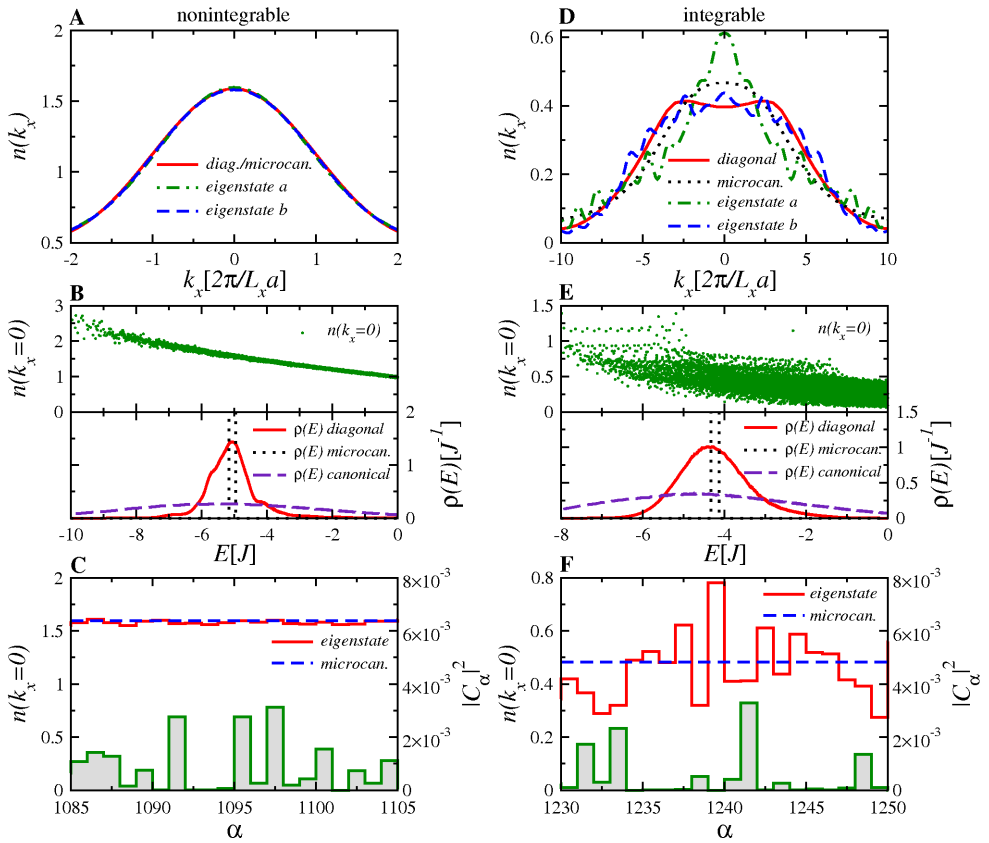

Figure 15.3: **Eigenstate thermalization hypothesis**. **a**, In our nonintegrable system, the momentum distribution $n(k_x)$ for two typical eigenstates with energies close to E_0 is identical to the microcanonical result, in accordance with the ETH. **b**, Upper panel: $n(k_x = 0)$ eigenstate expectation values as a function of the eigenstate energy resemble a smooth curve. Lower panel: the energy distribution $\rho(E)$ of the three ensembles considered in this work. **c**, Detailed view of $n(k_x = 0)$ (left labels) and $|C_\alpha|^2$ (right labels) for 20 eigenstates around E_0. **d**, In the integrable system, $n(k_x)$ for two eigenstates with energies close to E_0 and for the microcanonical and diagonal ensembles are very different from each other, i.e., the ETH fails. **e**, Upper panel: $n(k_x = 0)$ eigenstate expectation value considered as a function of the eigenstate energy gives a thick cloud of points rather than resembling a smooth curve. Lower panel: energy distributions in the integrable system are similar to the nonintegrable ones depicted in **b**. **f**, Correlation between $n(k_x = 0)$ and $|C_\alpha|^2$ for 20 eigenstates around E_0. It explains why in **d** the microcanonical prediction for $n(k_x = 0)$ is larger than the diagonal one.

only scales as the root of the number of dephasing terms, and is exactly compensated by their larger number: if the number of eigenstates that have a significant overlap with the initial state is N_{states}, then typical $C_\alpha \sim 1/\sqrt{N_{\text{states}}}$, and the sum over off-diagonal terms in Eq. (15.1) finally does not scale down with N_{states}:

$$\sum_{\substack{\alpha,\beta \\ \alpha\neq\beta}} \frac{e^{i(E_\alpha - E_\beta)t}}{N_{\text{states}}} A_{\alpha\beta} \sim \frac{\sqrt{N_{\text{states}}^2}}{N_{\text{states}}} A_{\alpha\beta}^{\text{typical}} \sim A_{\alpha\beta}^{\text{typical}} \tag{15.5}$$

Hence, were the magnitude of the diagonal and off-diagonal terms comparable, their contributions would be comparable as well, and time fluctuations of the average would be of the order of the average. However, this is not the case and thus

$$A_{\substack{\alpha\beta \\ \alpha\neq\beta}}^{\text{typical}} \ll A_{\alpha\alpha}^{\text{typical}}. \tag{15.6}$$

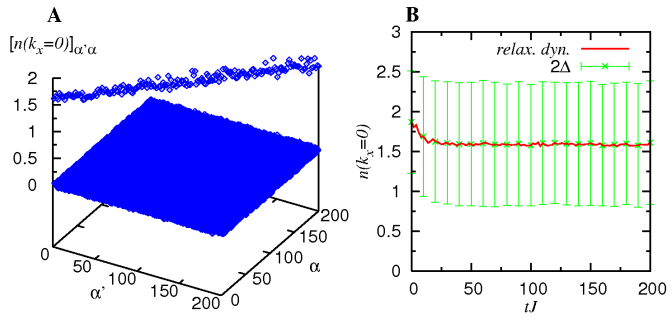

Figure 15.4: **Temporal vs quantum fluctuations**. **a**, Matrix elements of the observable of interest, $n(k_x = 0)$, as a function of state indices; the eigenstates of the Hamiltonian are indexed in the order of diminishing overlap with the initial state. The dominance of the diagonal matrix elements is apparent. **b**, The same time evolution as in Fig. 24.1b with the error bars showing the quantum fluctuations $n(k_x = 0) \pm \Delta$ with $\Delta = [\langle \widehat{n}^2(k_x = 0)\rangle - \langle \widehat{n}(k_x = 0)\rangle^2]^{1/2}$, which are clearly much larger than the temporal fluctuations of $n(k_x = 0)$.

Figure 24.4a confirms this inequality for the matrix elements of the momentum distribution in our system. We should mention that there is an *a priori* argument—admittedly in part dependent on certain hypotheses about chaos in quantum billiards—in support of this inequality for the case when the mean value of $\widehat{A}$ in an energy eigenstate is comparable to the quantum fluctuation of $\widehat{A}$ in that state [28].

On the other hand, the thermalization we see appears to be working a bit *too well*: in a system as small as ours, one would expect measurement-to-measurement fluctuations to be much larger than what Fig. 24.1b suggests. Indeed, as we show in Figure 24.4b, the fluctuations that one would actually measure would be dominated by the quantum fluctuations of the time-dependent state. The rather large size of the quantum fluctuations relative to the thermal mean value is of course particular to small systems; however, the dominance of the quantum fluctuations over the temporal fluctuations of quantum expectation values is not and is actually expected for generic systems in the thermodynamic limit [29].

We have demonstrated that, in contrast to the integrable case, the nonequilibrium dynamics of a generic isolated quantum system does lead to standard thermalization. We verified that this happens through the eigenstate thermalization mechanism, a scenario J. M. Deutsch [72] demonstrated for the case of an integrable quantum Hamiltonian weakly perturbed by a single matrix taken from a random Gaussian ensemble and M. Srednicki [73] compellingly defended for the case of rarefied semiclassical quantum billiards, and which both authors conjectured to be valid in general. Our results, when combined with the others we mentioned [72, 20, 21, 22, 23, 24, 73, 25, 26, 27], constitute strong evidence that eigenstate thermalization indeed generally underlies thermal relaxation in isolated quantum systems. Therefore, to understand the existence of universal thermal time-asymptotic states, one should study operator expectation values in individual eigenstates. This is a problem that is linear, time-independent, and conceptually far simpler than any arising in the research—currently dominating the field—on the nonlinear dynamics of semiclassical systems. Among the fundamental open problems of statistical mechanics that could benefit from the linear time-independent perspective are the nature of irreversibility, the existence of a KAM-like threshold [30] in quantum systems, and the role of conserved quantities in the approach to equilibrium. Finally, having a clear conceptual picture for the origins of thermalization may make it possible to engineer new, "unthermalizable" states of matter [72], with further applications in quantum information and precision measurement.

We thank A. C. Cassidy, K. Jacobs, A. P. Young, and E. J. Heller for helpful comments. We

acknowledge financial support from the National Science Foundation and the Office of Naval Research. We are grateful to the USC HPCC center where our numerical computations were performed.

15.2 Supplementary Discussion

15.2.1 1. The Hamiltonian and the numerical calculations.

In a system of units where $\hbar = 1$ the Hamiltonian reads

$$\widehat{H} = -J \sum_{\langle i,j \rangle} \left(\hat{b}_i^\dagger \hat{b}_j + \text{h.c.} \right) + U \sum_{\langle i,j \rangle} \hat{n}_i \hat{n}_j \tag{15.7}$$

where $\langle i, j \rangle$ indicates that the sums run over all nearest-neighbor pairs of sites, J is the hopping parameter, and U the nearest-neighbor repulsion parameter that we always set to $0.1J$. The hard-core boson creation ($\hat{b}_i^\dagger$) and annihilation ($\hat{b}_j$) operators commute on different sites, $[\hat{b}_i, \hat{b}_j^\dagger] = [\hat{b}_i, \hat{b}_j] = [\hat{b}_i^\dagger, \hat{b}_j^\dagger] = 0$ for all i and $j \neq i$, while the hard-core condition imposes the canonical anticommutation relations on the same site, $\{\hat{b}_i, \hat{b}_i^\dagger\} = 1$, and $(\hat{b}_i)^2 = (\hat{b}_i^\dagger)^2 = 0$ for all i. Here $\hat{n}_i = \hat{b}_i^\dagger \hat{b}_i$ is the density operator.

An exact study of the nonequilibrium dynamics for *all* time scales requires a full diagonalization of the many-body Hamiltonian (15.7). We are able to fully diagonalize—essentially to machine precision—matrices of dimension $D \sim 20,000$, and so we consider $N = 5$ hard-core bosons on a 5×5 lattice with four sites missing ($D = 20,349$); see Fig. 15.5. All the eigenstates of the Hamiltonian are used for the time evolution

$$|\psi(t)\rangle = \exp\left[-i\widehat{H}t\right]|\psi(0)\rangle = \sum_\alpha C_\alpha \exp\left[-iE_\alpha t\right]|\Psi_\alpha\rangle\,,$$

where $|\psi(t)\rangle$ is the time-evolving state, $|\psi(0)\rangle$ the initial state, $|\Psi_\alpha\rangle$ the eigenstates of the Hamiltonian with the energies E_α, and $C_\alpha = \langle\Psi_\alpha|\psi(0)\rangle$. Our initial state is the ground state of the five bosons when they are confined to the lower part of the lattice (the colored part in Fig. 15.5. The time evolution begins with the opening of the link shown in Fig. 15.5, which allows the bosons to expand over the whole lattice. The position of the missing sites was chosen so that we only open a single link to start the relaxation dynamics. The motivation for this will become apparent in the last paragraph below.

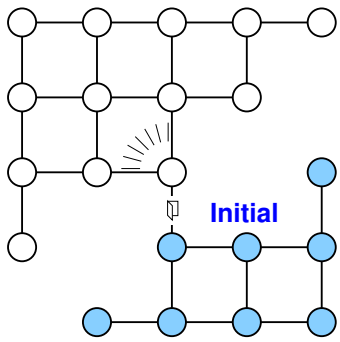

Figure 15.5: **The lattice for the dynamics**. Two-dimensional lattice on which the particles propagate in time. The initial state is the ground state of 5 hard-core bosons confined to the sub-lattice in the lower right-hand corner, and the time evolution starts after the opening of the link indicated by the door symbol.

As the principal observables of interest we chose the marginal momentum distribution along the horizontal axis $n(k_x) = \sum_{k_y} n(k_x, k_y)$ and in particular its central component $n(k_x = 0)$,

quantities readily measurable in actual experiments with ultracold quantum gases [19]. Here the full two-dimensional momentum distribution is $n(k_x, k_y) = 1/L^2 \sum_{i,j} e^{-i2\pi \mathbf{k}(\mathbf{r}_i - \mathbf{r}_j)/L} \langle \hat{b}_i^\dagger \hat{b}_j \rangle$, where $L = L_x = L_y = 5$ are the linear sizes of the lattice. The position $\mathbf{r}_i = (i_x\, d\,, i_y\, d)$ involves the lattice constant d.

15.2.2 2. The microcanonical ensemble in a small system.

To compute the microcanonical ensemble predictions, we have averaged over all eigenstates whose energies lie within a narrow window $[E_0 - \Delta E, E_0 + \Delta E]$, with $E_0 \equiv \langle \psi(0)|\widehat{H}|\psi(0)\rangle = \langle \psi(t)|\widehat{H}|\psi(t)\rangle = -5.06J$. Since our systems are small there is generally no meaning to the limit $\Delta E \to 0$, because small enough windows may fail to contain even a single eigenstate. Instead, one should show that the microcanonical predictions are robust with respect to the choice of the width of the energy window. In Fig. 15.6 we demonstrate this robustness in a neighborhood of $\Delta E = 0.1J$, a value that seems to be an appropriate choice given the data presented in the inset of the same figure. There we show the dependence on ΔE of the predictions for $n(k_x = 0)$ given by the "left-averaged" and the "right-averaged" microcanonical ensembles, by which we mean that the microcanonical windows are chosen as $[E_0 - \Delta E, E_0]$ and $[E_0, E_0 + \Delta E]$, respectively. We see that for $\Delta E \lesssim 0.1J$, the two microcanonical predictions are almost independent of the value of ΔE. The main panel in Fig. 15.6 shows that the microcanonical values of $n(k_x)$ for $\Delta E = 0.05J$ and for $\Delta E = 0.1J$ are indistinguishable.

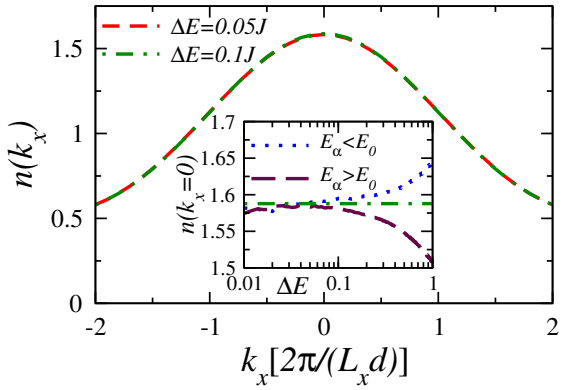

Figure 15.6: **Microcanonical ensemble**. Microcanonical momentum distribution function for two different values of ΔE. Inset: Microcanonical predictions for $n(k_x = 0)$ calculated using the left ($[E_0 - \Delta E, E_0]$) and the right ($[E_0, E_0 + \Delta E]$) averages as functions of ΔE.

15.2.3 3. Eigenstate thermalization and the width of the energy distribution.

The eigenstate thermalization alone is not sufficient to ensure an agreement between the predictions of the diagonal and thermal ensembles. As discussed in Ref. [73], it is also necessary that both distributions be sufficiently narrow. More specifically, one must require for both ensembles

$$(\Delta E)^2 \, |A''(E)/A(E)| \ll 1, \tag{15.8}$$

where ΔE is the width of the energy distribution in the ensemble, and $A(E)$ is the dependence of the expectation value of the observable $A_{\alpha\alpha} = \langle \Psi_\alpha | \widehat{A} | \Psi_\alpha \rangle$ on the energy E_α of the Hamiltonian-operator eigenstate $|\Psi_\alpha\rangle$. Note that because of eigenstate thermalization, $A(E)$ is a smooth function of energy. For the thermodynamical ensembles the condition (15.8) is always satisfied

in the thermodynamic limit. We now show that it is also satisfied for the diagonal ensemble in the thermodynamic limit.

If one considers an observable a that is the intensive counterpart of A, all conclusions obtained for a can be extended to the original observable A via trivial rescaling. For example, for our principal observable of interest, $n(k_x)$, the corresponding intensive variable is the momentum density $\xi(p_x)$ normalized as $\int dp_x\, \xi(p_x) = 1$. Notice that in this case $\xi(p_x) = n(k_x)L_x d/(2\pi N)$.

For a, the condition in (15.8) reduces to

$$(\Delta\epsilon)^2 |a''(\epsilon)/a(\epsilon)| \ll 1, \tag{15.9}$$

where $\epsilon \equiv E/N$. For sufficiently large systems the dependence of a on ϵ is independent of the system size. Hence, in order to justify the validity of (15.9) it is sufficient to prove that the width of the distribution of the energy per particle in the diagonal ensemble converges to zero for large linear sizes L of the system:

$$\Delta\epsilon \overset{L\to\infty}{\longrightarrow} 0\,. \tag{15.10}$$

Suppose that initially our system is prepared in an eigenstate $|\Psi_0\rangle$ of a Hamiltonian $\widehat{H}_0$ and that at time $t = 0$ the Hamiltonian is suddenly changed to $\widehat{H}$:

$$\widehat{H}_0 \to \widehat{H} = \widehat{H}_0 + \widehat{W},$$

where $\widehat{W}$ is the difference between the new and the old Hamiltonians. Within this scenario, the energy width

$$\Delta E = \sqrt{\sum_\alpha E_\alpha^2 |C_\alpha|^2 - \left(\sum_\alpha E_\alpha |C_\alpha|^2\right)^2}$$

of the diagonal ensemble becomes equal to the variance of the new energy in the state $|\Psi_0\rangle$:

$$\Delta E = \Delta H \equiv \sqrt{\langle\Psi_0|\widehat{H}^2|\Psi_0\rangle - \langle\Psi_0|\widehat{H}|\Psi_0\rangle^2}\,.$$

It is now straightforward to show that the variance of $\widehat{H}$ equals the variance of $\widehat{W}$:

$$\Delta H = \Delta W.$$

In order to deduce how ΔW scales in the thermodynamic limit, we assume that $\widehat{W}$ is a sum of local operators $\hat{w}(j)$ over some region of the lattice σ (a single point, a straight line, the whole lattice, etc.):

$$\widehat{W} = \sum_{j\in\sigma} \hat{w}(j).$$

Here $\hat{w}(j)$ is a polynomial of creation and annihilation operators localized at the points $j + \Delta j$, where $|\Delta j|$ is limited from the above by a finite number that does not scale with the system size. The mean square of $\widehat{W}$ can be written as

$$\begin{aligned}\langle\Psi_0|\widehat{W}^2|\Psi_0\rangle = \langle\Psi_0|\widehat{W}|\Psi_0\rangle^2 &\\ + \sum_{j_1,j_2\in\sigma} &[\langle\Psi_0|\hat{w}(j_1)\hat{w}(j_2)|\Psi_0\rangle \\ &- \langle\Psi_0|\hat{w}(j_1)|\Psi_0\rangle\langle\Psi_0|\hat{w}(j_2)|\Psi_0\rangle]\,.\end{aligned} \tag{15.11}$$

In the absence of long-range correlations the expression in brackets tends to zero for large distances between j_1 and j_2. Therefore, the whole second term on the right-hand-side of (15.11)

scales as L^{d_σ}, where d_σ is the dimensionality of the sublattice σ and L is the linear size of the lattice. The variance of $\widehat{W}$ scales the same way:

$$(\Delta W)^2 \overset{L\to\infty}{\propto} L^{d_\sigma}.$$

Retracing our steps, we arrive at the conclusion that the energy width $\Delta\epsilon$ indeed tends to zero in the thermodynamic limit:

$$\Delta\epsilon \overset{L\to\infty}{\propto} \frac{1}{L^{d_L - d_\sigma/2}},$$

where $d_L \geq d_\sigma$ is the dimensionality of the whole lattice.

Note that for the two-dimensional lattice considered in this paper the role of $\widehat{W}$ is played by the hopping energy of the "door" link. An analysis similar to the one above shows that increasing the number of "door" links will lead to an increase in the width $\Delta\epsilon$, proportional to the square root of the number of "door" links. This is why in our 2D experiment, we have chosen the position of the missing sites to be the one in Fig. 15.5, so that only a single link is opened during the time evolution.

References

[1] Kinoshita, T., Wenger, T. & Weiss, D. S. A quantum Newton's cradle. Nature **440**, 900–903 (2006).

[2] Hofferberth, S., Lesanovsky, I., Fischer, B., Schumm, T. & Schmiedmayer, J. Non-equilibrium coherence dynamics in one-dimensional Bose gases. Nature **449**, 324–327 (2007).

[3] Rigol, M., Dunjko, V., Yurovsky, V. & Olshanii, M. Relaxation in a completely integrable many-body quantum system: An ab initio study of the dynamics of the highly excited states of 1d lattice hard-core bosons. Phys. Rev. Lett. **98**, 050405 (2007).

[4] Kollath, C., Läuchli, A. & Altman, E. Quench dynamics and nonequilibrium phase diagram of the Bose-Hubbard model. Phys. Rev. Lett. **98**, 180601 (2007).

[5] Manmana, S. R., Wessel, S., Noack, R. M. & Muramatsu, A. Strongly correlated fermions after a quantum quench. Phys. Rev. Lett. **98**, 210405 (2007).

[6] Burkov, A. A., Lukin, M. D. & Demler, E. Decoherence dynamics in low-dimensional cold atom interferometers. Phys. Rev. Lett. **98**, 200404 (2007).

[7] Calabrese, P. & Cardy, J. Quantum quenches in extended systems. J. Stat. Mech. P06008 (2007).

[8] Sengupta, K., Powell, S. & Sachdev, S. Quench dynamics across quantum critical points. Phys. Rev. A **69**, 053616 (2004).

[9] Berges, J., Borsányi, S. & Wetterich, C. Prethermalization. Phys. Rev. Lett. **93**, 142002 (2004).

[10] Gallavotti, G. Statistical Mechanics: A Short Treatise (Springer, Berlin, 1999).

[11] Krylov, N. S. Works on the Foundation of Statistical Physics (Princeton Univ. Press, Princeton, 1979).

[12] Deutsch, J. M. Quantum statistical mechanics in a closed system. Phys. Rev. A **43**, 2046–2049 (1991).

[13] Srednicki, M. Chaos and quantum thermalization. Phys. Rev. E **50**, 888–901 (1994).

[14] Sutherland, B. Beautiful Models (World Scientific, Singapore, 2004).

[15] Rigol, M., Muramatsu, A. & Olshanii, M. Hard-core bosons on optical superlattices: Dynamics and relaxation in the superfluid and insulating regimes. Phys. Rev. A **74**, 053616 (2006).

[16] Cazalilla, M. A. Effect of suddenly turning on interactions in the Luttinger model. Phys. Rev. Lett. **97**, 156403 (2006).

[17] Jin, D. S., Ensher, J. R., Matthews, M. R., Wieman, C. E. & Cornell, E. A. Collective excitations of a Bose-Einstein condensate in a dilute gas. Phys. Rev. Lett. **77**, 420–423 (1996).

[18] Greiner, M., Mandel, O., Esslinger, T., Hänsch, T. W. & Bloch, I. Quantum phase transition from a superfluid to a Mott insulator in a gas of ultracold atoms. Nature **415**, 39–44 (2002).

[19] Mandel, O. et al. Controlled collisions for multi-particle entanglement of optically trapped atoms. Nature **425**, 937–940 (2003).

[20] Horoi, M., Zelevinsky, V. & Brown, B. A. Chaos vs thermalization in the nuclear shell model. Phys. Rev. Lett. **74**, 5194–5197 (1995).

[21] Shnirelman, A. I. Ergodic properties of eigenfunctions. Usp. Mat. Nauk **29**, 181–182 (1974).

[22] Voros, A. Stochastic Behavior in Classical and Quantum Hamiltonian Systems (Springer, Berlin, 1979).

[23] de Verdière, Y. C. Ergodicité et fonctions propres du Laplacien. Commun. Math. Phys. **102**, 497–502 (1985).

[24] Zelditch, S. Uniform distribution of eigenfunctions on compact hyperbolic surfaces. Duke Math. J. **55**, 919–941 (1987).

[25] Heller, E. J. & Landry, B. R. Statistical properties of many particle eigenfunctions. J. Phys. A **40**, 9259–9274 (2007).

[26] Berry, M. V. Regular and irregular semiclassical wavefunctions. J. Phys. A **10**, 2083–2091 (1977).

[27] Korepin, V. E., Bogoliubov, N. M. & Izergin, A. G. Quantum Inverse Scattering Method and Correlation Functions (Cambridge Univ. Press, Cambridge, 1993).

[28] Srednicki, M. Does quantum chaos explain quantum statistical mechanics? Preprint at ⟨http://arxiv.org/abs/cond-mat/9410046⟩ (1994).

[29] Srednicki, M. Thermal fluctuations in quantized chaotic systems. J. Phys. A **29**, L75–L79 (1996).

[30] José, J. V. & Saletan, E. J. Classical Dynamics: A Contemporary Approach (Cambridge Univ. Press, Cambridge, 1998).

16 Complete Generalized Gibbs Ensemble in an Interacting Theory by Ilievski et al.

Abstract

In integrable many-particle systems, it is widely believed that the stationary state reached at late times after a quantum quench can be described by a generalized Gibbs ensemble (GGE) constructed from their extensive number of conserved charges. A crucial issue is then to identify a complete set of these charges, enabling the GGE to provide exact steady state predictions. Here we solve this long-standing problem for the case of the spin-1/2 Heisenberg chain by explicitly constructing a GGE which uniquely fixes the macrostate describing the stationary behaviour after a general quantum quench. A crucial ingredient in our method, which readily generalizes to other integrable models, are recently discovered quasi-local charges. As a test, we reproduce the exact post-quench steady state of the Néel quench problem obtained previously by means of the Quench Action method.

16.0.1 Introduction.

Understanding and describing the equilibration of isolated many-particle systems is one of the main current challenges of quantum physics. The presence of higher conserved charges (above the Hamiltonian) is linked to the absence of full relaxation to a thermalized state; the conjectured appropriate framework to characterize the steady state properties in such a situation is the Generalized Gibbs Ensemble (GGE) [1], in which all available charges are ascribed an individual 'chemical potential' set by the initial conditions, and the steady state is the maximal entropy state fulfilling all the constraints associated to the conserved charges [2, 3, 4, 5, 6, 7, 8, 9, 10, 11, 12, 13, 14, 15, 16, 17, 18, 19, 20, 21, 22, 23, 24, 25, 26, 27]. The basic idea underlying the GGE is as follows. Let $H \simeq H^{(1)}$ be the Hamiltonian of an integrable model, and $\{H^{(n)}\}$ a set of conserved charges fulfilling $[H^{(n)}, H^{(m)}] = 0$. The situation we are interested in is that of a quantum quench, where we initially prepare our system in the ground state $|\Psi(0)\rangle$ of a local Hamiltonian H_0 and then consider unitary time evolution with respect to our integrable Hamiltonian

$$|\Psi(t)\rangle = e^{-iHt}|\Psi(0)\rangle. \tag{16.1}$$

We assume that we are dealing with a generic case, where in the thermodynamic limit $|\Psi(0)\rangle$ cannot be expressed as a linear combination of any finite number of eigenstates of H why????. At late times after the quench expectation values of local operators approach stationary values

$$\langle\mathcal{O}\rangle_\Psi = \lim_{t\to\infty}\langle\Psi(t)|\mathcal{O}|\Psi(t)\rangle. \tag{16.2}$$

The GGE hypothesis asserts that these expectation values can be calculated as $\langle\mathcal{O}\rangle_\Psi = \mathrm{Tr}(\hat{\varrho}_{\mathrm{GGE}}\mathcal{O})$ from a statistical ensemble with a density matrix

$$\hat{\varrho}_{\mathrm{GGE}} = \frac{1}{Z}\exp\left[-\sum_n \beta_n H^{(n)}\right]. \tag{16.3}$$

Here Z is a normalization, and the Lagrange multipliers β_n are fixed by the initial conditions

$$\lim_{\mathrm{th}}\frac{\mathrm{Tr}(\hat{\varrho}_{\mathrm{GGE}}H^{(n)})}{N} = \lim_{\mathrm{th}}\frac{\langle\Psi(0)|H^{(n)}|\Psi(0)\rangle}{N}, \tag{16.4}$$

where N is the system size and $\lim_{\mathrm{th}}$ denotes the thermodynamic limit $N\to\infty$. Eqns. (16.4) are a direct consequence of the fact that $H^{(n)}$ are conserved charges.

below there is a good literature review While the GGE hypothesis has been successfully verified for many systems mappable to free particles, in interacting theories such as the spin-1/2 Heisenberg XXZ chain the question arises, precisely which charges need to be included in (16.3). In Refs. [17, 18, 20] a GGE based on the known conserved local charges [28] was constructed and used to determine steady-state averages of observables [20]. Subsequent analyses [21, 22] by the Quench Action (QA) approach [14] demonstrated that this GGE fails to predict the correct steady state properties. This failure was shown to be related to the existence of bound states [21] (see also [29, 30]), which are known to be a generic feature in quantum integrable models. These results posed the question whether the GGE is conceptually faulty, or whether there could exist hitherto unknown charges that need to be taken into account in its construction.

In this Letter, we settle this issue by explicitly showing how to repair the GGE in Heisenberg chains, by complementing it with recently-discovered additional families of conserved charges [31] [31] is a complicated article . Crucially, these "quasi-local" charges fulfil a weaker form of locality than the previously known ones. We derive a set of fundamental identities between the initial-state expectation values of these charges, and the density functions characterizing the steady state. An explicit test of our construction is provided by a quantum quench from the Néel state to the XXZ chain: we demonstrate that our GGE correctly recovers the stationary state, the form of which is known exactly from the QA approach [21, 32]. In this way we completely resolve the above-mentioned conundrum. Our construction shows that quasi-local conserved charges are in fact crucial for understanding the non-equilibrium dynamics of quantum integrable models.

16.0.2 Anisotropic spin-1/2 Heisenberg chain.

We shall consider a completely generic quench protocol from an initial pure wavefunction $|\Psi_0\rangle$, which is unitarily time evolved according to the Hamiltonian

$$H = \frac{J}{4}\sum_{j=1}^{N}\left[\sigma_j^x\sigma_{j+1}^x + \sigma_j^y\sigma_{j+1}^y + \Delta(\sigma_j^z\sigma_{j+1}^z - 1)\right]. \tag{16.5}$$

Here $J > 0$, σ_j^α, $\alpha = x, y, z$ are Pauli matrices acting on spin-1/2 degrees of freedom, and we consider anisotropy values in the regime $\Delta = \cosh(\eta) \geq 1$. The Hamiltonian (16.5) can be diagonalized by Bethe Ansatz [33, 34]. Imposing periodic boundary conditions, energy eigenstates $|\boldsymbol{\lambda}\rangle$ with magnetization $S^z_{\rm tot} = \frac{N}{2} - M$ are labeled by a set of rapidities $\boldsymbol{\lambda} = \{\lambda_k\}_{k=1}^M$ satisfying the Bethe equations $\left(\frac{\sin(\lambda_j+i\eta/2)}{\sin(\lambda_j-i\eta/2)}\right)^N = -\prod_{k=1}^M \frac{\sin(\lambda_j-\lambda_k+i\eta)}{\sin(\lambda_j-\lambda_k-i\eta)}$, $j = 1, \ldots, M$. The momentum and energy of a Bethe state are $P_{\boldsymbol{\lambda}} = \sum_{j=1}^M p(\lambda_j)$, $\omega_{\boldsymbol{\lambda}} = \sum_{j=1}^M e(\lambda_j)$ where $p(\lambda) = i\ln\left[\frac{\sin(\lambda-i\eta/2)}{\sin(\lambda+i\eta/2)}\right]$ and $e(\lambda) = -J\pi\sinh(\eta)a_1(\lambda)$, where

$$a_n(\lambda) = \frac{1}{2\pi}\frac{2\sinh(n\eta)}{\cosh(n\eta) - \cos(2\lambda)}. \tag{16.6}$$

Solutions $\boldsymbol{\lambda}$ to the Bethe equations are closed under complex conjugation and consist of so-called strings $\lambda_\alpha^{n,a} = \lambda_\alpha^n + \frac{i\eta}{2}(n+1-2a) + i\delta_\alpha^{n,a}$, $a = 1, \ldots, n$ and $\lambda_\alpha^n \in \mathbb{R}$. Here index α enumerates a string, n is the string length, a counts rapidities inside a given string and deviations $\delta_\alpha^{n,a}$ are (for the majority of states) exponentially small in system size [35, 28, 36]. The string centers λ_α^n lie in the interval $[-\pi/2, \pi/2)$. In the thermodynamic limit $N \to \infty$ with M/N fixed one can describe a state not in terms of individual rapidities, but rather in terms of a set of functions $\boldsymbol{\rho} = \{\rho_n\}_{n=1}^\infty$ representing string densities (see Supplementary Material (SM) for more info).

Ultra-local GGE treatment.

Exactly-solvable Hamiltonians such as (16.5) can be embedded [28] in a commuting family $[T(\lambda), T(\lambda')] = 0$ of transfer matrices (defined in (16.15)). The Hamiltonian and an infinite number of mutually commuting conserved charges are obtained by

$$H^{(n)} = \frac{i}{n!}\partial_\lambda^n \ln T(-i\lambda)\Big|_{\lambda=\frac{i\eta}{2}} \tag{16.7}$$

with the Hamiltonian reading $H = \frac{J\sinh(\eta)}{2}H^{(1)}$. These charges are ultra-local in the sense that they can be written as $H^{(m)} = \sum_{j=1}^{N} h_j^{(m)}$, where the operators $h_j^{(m)}$ act nontrivially on a block of at most m sites adjacent to j. The GGE constructed in [17, 18] was of the form (16.3), (16.4) with charges (16.7). The initial values $h^{(n)} = \lim_{\rm th} N^{-1}\langle\Psi(0)|H^{(n)}|\Psi(0)\rangle$ of the conserved charges are conveniently encoded in the generating function [18]

$$\begin{aligned}\Omega^{\Psi_0}(\lambda) &= \lim_{\rm th}\frac{i}{N}\langle\Psi_0|T^{-1}\big(\lambda+\tfrac{i\eta}{2}\big)\,\partial_\lambda T\big(\lambda+\tfrac{i\eta}{2}\big)\,|\Psi_0\rangle,\\ &= \sum_{k=0}^{\infty}\frac{\lambda^k}{k!}h^{(k+1)}.\end{aligned} \tag{16.8}$$

Given the GGE density matrix, a "microcanonical" description of the steady state can be obtained by performing a generalized Thermodynamic Bethe Ansatz (GTBA) [37, 11], see SM for a brief summary. This results in a representative eigenstate $|\boldsymbol{\rho}_{\rm GGE}^{\Psi_0}\rangle$ labeled by root density functions $\boldsymbol{\rho}_{\rm GGE}^{\Psi_0}$, which has the property that for any local operator $\mathcal{O}$

$$\mathrm{Tr}(\mathcal{O}\hat{\varrho}_{\rm GGE}) = \big\langle\boldsymbol{\rho}_{\rm GGE}^{\Psi_0}\big|\mathcal{O}\big|\boldsymbol{\rho}_{\rm GGE}^{\Psi_0}\big\rangle. \tag{16.9}$$

Within the GTBA formalism macrostates can be described either by root densities of particles, or by densities of holes. Holes can be, loosely speaking, understood as analogues of unoccupied states in models of free fermions. In terms of the latter the state $|\boldsymbol{\rho}_{\rm GGE}^{\Psi_0}\rangle$ is parametrized in terms of the set of positive functions $\{\rho_{n,h}^{\Psi_0}\}$. In [21, 32] it was found that the initial data (16.4) directly determines the hole density of 1-strings (i.e. vacancies of unbound states), according to the remarkable identity

$$\rho_{1,h}^{\Psi_0}(\lambda) = a_1(\lambda) + \frac{1}{2\pi}\left[\Omega^{\Psi_0}(\lambda+\tfrac{i\eta}{2}) + \Omega^{\Psi_0}(\lambda-\tfrac{i\eta}{2})\right]. \tag{16.10}$$

All other hole densities are fixed by the maximum entropy principle under the constraints (16.4).

16.0.3 Quench Action treatment.

The above GGE treatment should be compared to an independent calculation using the QA method [14]. For a generic quench problem, given an initial state $|\Psi_0\rangle$, the time-dependent expectation value of a generic local observable $\mathcal{O}$ can be expressed as a double Hilbert space summation

$$\langle\Psi(t)|\,\mathcal{O}\,|\Psi(t)\rangle = \sum_{\boldsymbol{\lambda},\boldsymbol{\lambda}'} e^{-S_{\boldsymbol{\lambda}}^* - S_{\boldsymbol{\lambda}'}} e^{i(\omega_{\boldsymbol{\lambda}}-\omega_{\boldsymbol{\lambda}'})t}\langle\boldsymbol{\lambda}|\mathcal{O}|\boldsymbol{\lambda}'\rangle, \tag{16.11}$$

where $S_{\boldsymbol{\lambda}} = -\ln\langle\boldsymbol{\lambda}|\Psi_0\rangle$. Here, $|\boldsymbol{\lambda}\rangle$ are eigenstates of the Hamiltonian driving the post-quench time evolution. Exploiting the fact that in the themodynamic limit, the summation over eigenstates can be written as a functional integral over root densities, which can be evaluated in a

saddle-point approximation (becoming exact in the thermodynamic limit), one finds in particular that the steady-state expectation values of observables a long time after the quench can be obtained as

$$\lim_{t\to\infty}\lim\nolimits_{\rm th}\,\langle\Psi(t)|\,\mathcal{O}\,|\Psi(t)\rangle=\big\langle\boldsymbol{\rho}_{\rm QA}^{\Psi_0}\big|\mathcal{O}\big|\boldsymbol{\rho}_{\rm QA}^{\Psi_0}\big\rangle. \tag{16.12}$$

Here $\big|\boldsymbol{\rho}_{\rm QA}^{\Psi_0}\big\rangle$ is an eigenstate minimizing the QA $S_{\rm QA}[\boldsymbol{\rho}]=2S[\boldsymbol{\rho}]-S_{\rm YY}[\boldsymbol{\rho}]$, where $S[\boldsymbol{\rho}]=\lim_{\rm th}\mathrm{Re}\,S_{\boldsymbol{\lambda}}$ is the extensive real part of the overlap coefficient in the thermodynamic limit and $S_{\rm YY}[\boldsymbol{\rho}]$ is the Yang-Yang entropy of the state [35, 28, 36]. For the Néel to XXZ quench, the exact overlaps were obtained in [38] and used in [21, 32] to obtain the exact saddle-point densities $\boldsymbol{\rho}_{QA}^{\Psi_0}$ representing the steady state. Crucially, one finds [21, 22] that $\boldsymbol{\rho}_{\rm GGE}^{\Psi_0}\neq\boldsymbol{\rho}_{\rm QA}^{\Psi_0}$, which in turn leads to different predictions for physical properties such as spin-spin correlators. This demonstrated that the ultra-local GGE does not correctly describe the steady state after a generic quantum quench in the XXZ chain.

16.0.4 Constructing a "quasi-local" GGE.

Very recently [31] (see also [39, 40, 41, 42, 43, 44]) hitherto unknown conserved charges of the isotropic ($\Delta=1$) Heisenberg model were discovered. These operators are not local in the sense that they cannot be represented as a spatially homogeneous sum of finitely supported densities, but rather quasi-local, meaning [31] that their Hilbert–Schmidt norms scale linearly with system size and their overlaps with locally-supported operators become independent of N in the limit of large system size. Moreover, they are linearly independent from the known local charges generated from the spin-1/2 transfer matrix. Until now, the impact of these charges on local physical observables has not been quantified.

Our first step is to construct a family of quasi-local conserved charges for $\Delta\geq 1$ by generalizing the procedure of [31]. The starting point is the q-deformed L-operator,

$$\begin{aligned}L(z,s)=\frac{1}{\sinh\eta}\Big(&\sinh(z)\cosh\left(\eta s^z\right)\otimes\sigma^0\\&+\cosh(z)\sinh\left(\eta s^z\right)\otimes\sigma^z+\sinh(\eta)(s^-\otimes\sigma^+ + s^+\otimes\sigma^-)\Big),\end{aligned} \tag{16.13}$$

whose auxiliary-space components are given by q-deformed spin-s representations with $s=\frac{1}{2},1,\frac{3}{2},\ldots$, obeying commutation relations $[s^+,s^-]=[2s^z]_q$, $[s^z,s^\pm]=\pm s^\pm$ and acting in a $(2s+1)$-dimensional irreducible representation $\mathcal{V}_s\cong\mathbb{C}^{2s+1}=\mathrm{lsp}\{|k\rangle\,;k=-s,\ldots,s\}$,

$$s^z\,|k\rangle=k\,|k\rangle\,,\quad s^\pm\,|k\rangle=\sqrt{[s+1\pm k]_q[s\mp k]_q}\,|k\pm1\rangle\,, \tag{16.14}$$

with $[x]_q=\sinh\left(\eta x\right)/\sinh(\eta)$. By means of higher-spin auxiliary (fused) transfer matrices defined via ordered products of L-operators

$$T_s(z)=\mathrm{Tr}_a\left[L_{a,1}(z,s)\ldots L_{a,N}(z,s)\right], \tag{16.15}$$

(where $T_{1/2}(z)\equiv T(z)$ was used in (16.7)) we define families of conserved operators

$$X_s(\lambda)=\tau_s^{-1}(\lambda)\{T_s(z_\lambda^-)T_s'(z_\lambda^+)\},\quad z_\lambda^\pm=\pm\frac{\eta}{2}+i\lambda, \tag{16.16}$$

with $T_s'(z)\equiv\partial_z T_s(z)$ and $\{\bullet\}$ denoting the traceless part. The normalization reads $\tau_s(\lambda)=f(-(s+\frac{1}{2})\eta+i\lambda)f((s+\frac{1}{2})\eta+i\lambda)$ with $f(z)=(\sinh\left(z\right)/\sinh\left(\eta\right))^N$. In [31] it was shown for the isotropic case that these charges are quasi-local for all $s=\frac{1}{2},1,\frac{3}{2},\ldots$ and $\lambda\in\mathbb{R}$. A rigorous proof for general $\Delta>1$ is currently under construction [46].

[46] M. Medenjak, E. Ilievski and T. Prosen, to be published

A central piece of our work is the extraction of the thermodynamically leading part of the quasi-local charges $\{X_s\}_{s=1/2}^{\infty}$ when operating on an arbitrary Bethe state. It proves useful to resort to the so-called fusion relations [46, 47, 48, 49] (T-system) for higher-spin transfer matrices,

$$T_s(z+\tfrac{\eta}{2})T_s(z-\tfrac{\eta}{2}) = f(z+(s+\tfrac{1}{2})\eta)f(z-(s+\tfrac{1}{2})\eta) + T_{s-1/2}(z)T_{s+1/2}(z), \tag{16.17}$$

with the initial condition $T_0(z) \equiv f(z)$. There exists a closed-form solution to the above recurrence relation in terms of Baxter's Q-operators [47]

$$T_s(z) = Q(z+(s+\tfrac{1}{2})\eta)Q(z-(s+\tfrac{1}{2})\eta) \times \sum_{\ell=0}^{2s} \frac{f(z+(\ell-s)\eta)}{Q(z+(\ell-s-\tfrac{1}{2})\eta)Q(z+(\ell-s+\tfrac{1}{2})\eta)}. \tag{16.18}$$

The eigenvalues of the Q-operators (in what follows, in view of commutations $[T_s(z_1), Q(z_2)] = 0\ \forall s, z_i \in \mathbb{C}$, we slightly abuse notation by using the same symbol for an operator and its eigenvalue) are determined by the position of Bethe roots $Q(z) = \prod_{k=1}^{M} \sinh(z+i\lambda_k)$. A key observation is that, in the thermodynamic limit, the spin-s transfer matrix evaluated at z_λ^- (z_λ^+) is simply given by the $\ell = 0$ ($\ell = 2s$) term in the sum in Eq. (16.18). This then gives

$$\lim_{\rm th} T_s(z_\lambda^\pm) = \lim_{\rm th} f(\pm(s+\tfrac{1}{2})\eta + i\lambda)\frac{Q(\mp s\eta + i\lambda)}{Q(\pm s\eta + i\lambda)}. \tag{16.19}$$

The latter analysis is consistent with $\lim_{\rm th} \tau_s^{-1}(\lambda)T_s(z_\lambda^-)T_s(z_\lambda^+) = \mathbb{1}$, representing a thermodynamic version of an inversion identity (see [31]) that can be proven in an entirely operatorial way, without making reference to the Bethe eigenstates. At this point it is convenient to define modified conserved operators

$$\widehat{X}_s(\lambda) := T_s^{(-)}(z_\lambda^-)T_s^{(+)\prime}(z_\lambda^+), \tag{16.20}$$

where $T_s^{(\pm)}(z)$ have the same structure as (16.15) but involve L-operators $L^{(\pm)}(z,s) = L(z,s)\sinh(\eta)/[\sinh(z \pm s\eta)]$. In thermodynamic limit a quasi-local conserved operator $\widehat{X}_s(\lambda)$ only differs from $X_s(\lambda)$ by a multiple of identity, $\widehat{X}_s(\lambda) = X_s(\lambda) + t_s(\lambda)\mathbb{1}$, with $t_s(\lambda) = \frac{2s}{2s+1}\frac{\sinh((2s+1)\eta)}{\sinh^2(\eta)}\tau_s^{-1}(\lambda)$. We can now define a two-parameter family of conserved charges

$$H_s^{(n+1)} = \frac{1}{n!}\partial_\lambda^n \widehat{X}_s(\lambda)\Big|_{\lambda=0}. \tag{16.21}$$

By construction we have $[H_s^{(n)}, H_{s'}^{(m)}] = 0$ and $\{H_{1/2}^{(n)}\}_{n=1}^{\infty}$ precisely recover the ultra-local conservation laws (16.7). We are thus in a position to define the density matrix of our GGE. It is given by

$$\hat{\varrho}_{\rm GGE} = \frac{1}{Z}\exp\left[-\sum_{n,s=1}^{\infty}\beta_n^s H_{s/2}^{(n)}\right], \tag{16.22}$$

where the Lagrange multipliers β_n^s are fixed by initial conditions of the form (16.4). Our assertion is that (16.22) provides a correct description of the stationary behaviour after a general quench to the spin-1/2 XXZ chain (in the regime $\Delta \geq 1$). In order to prove this it suffices to establish that the initial values of our conserved charges uniquely specify a macrostate.

Let us now derive the main result of our Letter. Analogously to what was found in [21, 32] for the ultra-local charges, the values of the quasi-local charges associated with a spin-s transfer matrix are in 1-to-1 correspondence with functions $\rho^{\Psi_0}_{2s,h}(\lambda)$, which in turn specify (see SM) a unique macrostate (namely the GGE saddle-point state).

Our starting point is the following expression for the spectrum of $\{\widehat{X}_s\}_{s=1/2}^{\infty}$, valid for large system size (cf. Eq. (16.19))

$$\begin{aligned}\widehat{X}_s(\lambda) &= -i\partial_\lambda \log \frac{Q(-s\eta + i\lambda)}{Q(s\eta + i\lambda)} + o(N) \\ &= \sum_{k=1}^{M} \frac{2\sinh(2s\eta)}{\cos(2(\lambda_k + \lambda)) - \cosh(2s\eta)} + o(N),\end{aligned} \tag{16.23}$$

Starting from Eq. (16.23), working in the thermodynamic limit under the string hypothesis and making use of Bethe equations, one arrives at (see SM)

$$\rho^{\Psi_0}_{2s,h}(\lambda) = a_{2s}(\lambda) + \frac{1}{2\pi}\left[\Omega^{\Psi_0}_s(\lambda + \tfrac{i\eta}{2}) + \Omega^{\Psi_0}_s(\lambda - \tfrac{i\eta}{2})\right], \tag{16.24}$$

where $s = \frac{1}{2}, 1, \frac{3}{2}, \ldots$. The right-hand side of (16.24) is determined by the expectation values of the quasi-local charges on the initial state,

$$\Omega^{\Psi_0}_s(\lambda) = \lim_{\text{th}} \frac{\langle\Psi_0|\widehat{X}_s(\lambda)|\Psi_0\rangle}{N}. \tag{16.25}$$

This is a generalization of Eq. (16.10) to arbitrary spin. Note the remarkable fact that this correspondence is valid for a generic initial state $|\Psi_0\rangle$. As a consequence, the family of quasi-local charges $\{\widehat{X}_s\}_{s=1/2}^{\infty}$ completely determines the postquench stationary state through the GGE and gives the latter's predictions identical to those coming from the QA.

16.0.5 Néel quench.

An explicit example of our construction if provided by the quench from the Néel state

$$|\Psi_0\rangle = \frac{1}{\sqrt{2}}\left(|\uparrow\downarrow\uparrow\downarrow\ldots\rangle + |\downarrow\uparrow\downarrow\uparrow\ldots\rangle\right). \tag{16.26}$$

Here the root distributions characterizing the stationary state have been previously determined by a QA calculation [21, 32]. In order to demonstrate that our GGE recovers these known results we need to compute the generating functions (16.25). Here we can repeat the logical steps from the calculation for $s = 1/2$ in [18, 20] by studying the spectrum of associated auxiliary transfer matrices. This calculation can be found in the SM. Substituting the results obtained in this way into (16.24) gives perfect agreement with the known QA results.

16.0.6 Towards a truncated GGE.

In [10] it was argued that for the purpose of describing finite subsystems in the thermodynamic limit ultra-local GGEs can be truncated by retaining only a finite number of the "most local" conserved charges. An obvious question is whether a similar logic can be applied to our quasi-local GGE. As a first step towards understanding this issue, we have calculated the next-nearest spin correlation function in the steady state after a Néel-to-XXZ quench for several GGEs truncated in the s direction. In Fig. 16.1 we show the results of these calculations for $\Delta \gtrsim 1$. The data clearly shows that adding subsequent families of quasi-local charges results in a rapid convergence of the corresponding truncated GGE result to the exact value.

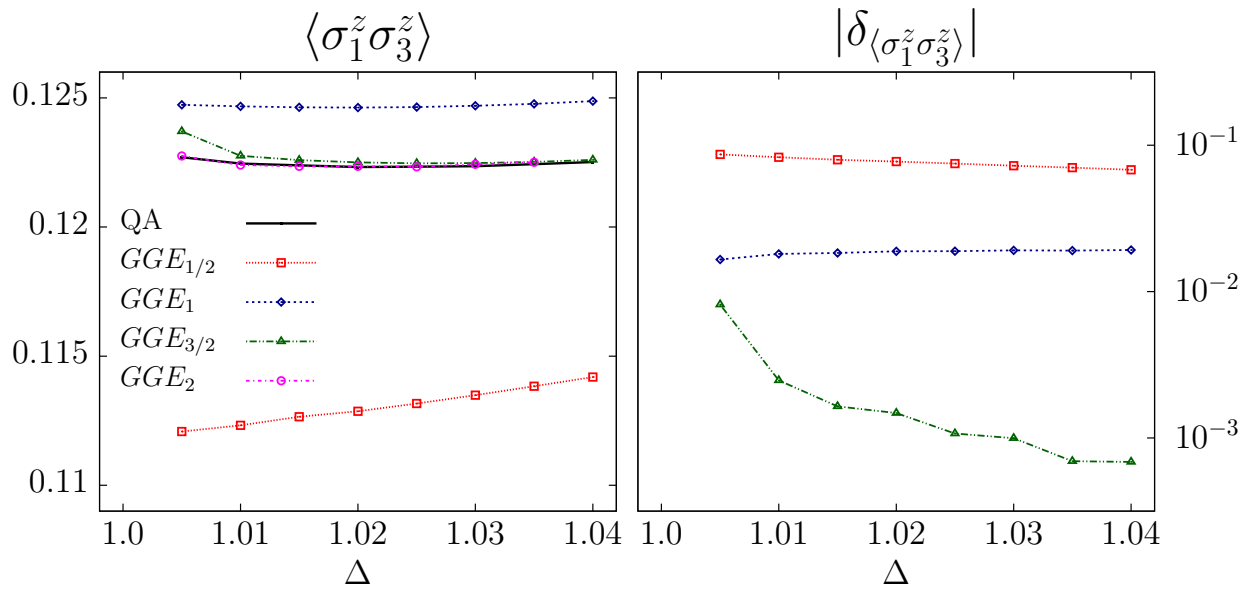

Figure 16.1: Comparison of methods: QA method versus improved GGE predictions. Colored lines pertain to the refined GGE calculation with systematic addition of higher-spin families of quasi-local charges $\{H_s^{(n)}\}$ for the local correlation function $\langle\sigma_1^z\sigma_3^z\rangle$ in the regime $\Delta \gtrsim 1$ (left panel). Labels in $GGE_{\bar{s}}$ indicate the maximal auxiliary spin $\bar{s}$ for the charges $\{H_s^{(n)}\}$ being included in the GGE computation. The right panel displays the relative differences $\delta_{\langle\sigma_1^z\sigma_3^z\rangle} = (\langle\sigma_1^z\sigma_3^z\rangle_{QA} - \langle\sigma_1^z\sigma_3^z\rangle_{GGE_{\bar{s}}})/\langle\sigma_1^z\sigma_3^z\rangle_{QA}$ in logarithmic scale. We used the mapping between correlation functions and the set of densities $\boldsymbol{\rho}$ given in [50].

16.0.7 Conclusions.

We have shown how to construct an exact GGE describing the stationary state after generic quantum quenches to the spin-1/2 Heisenberg XXZ chain. Our GGE is built from an extended set of local and quasi-local charges. We have shown that our construction resolves previously observed discrepancies between predictions for steady state expectation values by an exact QA treatment on the one hand, and a GGE restricted to ultra-local charges obtained from the transfer matrix of the spin-1/2 chain on the other hand. Our results provide unambiguous proof that the recently discovered quasi-local charges have a non-negligible impact on the relaxation processes of strongly-interacting many-body quantum systems in one dimension.

16.1 Thermodynamic limit of Bethe equations

We begin by recalling some of the fundamental equations of the Bethe Ansatz solution of the XXZ chain, together with few results obtained in [21, 32] which are used in the bulk of our paper.

In the thermodynamic limit, the Bethe equations for the XXZ chain read [35, 28, 36]

$$\rho_{n,t}(\lambda) \;=\; a_n(\lambda) - \sum_{m=1}^{\infty} (a_{nm} * \rho_m)(\lambda), \tag{16.27}$$

for $n \geq 1$, where $\rho_{n,t}(\lambda) = \rho_n(\lambda) + \rho_{n,h}(\lambda)$ and $\rho_n, \rho_{n,h}$ are respectively the particle and hole densities of n-strings. The convolution is defined by $(f * g)(\lambda) = \int_{-\pi/2}^{\pi/2} \mathrm{d}\mu\, f(\lambda-\mu)\, g(\mu)$. The

kernels are

$$a_{nm}(\lambda) = (1-\delta_{nm})a_{|n-m|}(\lambda) + 2a_{|n-m|+2}(\lambda) + \ldots \\ + 2a_{n+m-2}(\lambda) + a_{n+m}(\lambda), \tag{16.28}$$

with a_n defined in (16.6) in the main part of the manuscript. A convenient rewriting is in the decoupled form [36]

$$\rho_n(1+\eta_n) = s * (\eta_{n-1}\rho_{n-1} + \eta_{n+1}\rho_{n+1}), \tag{16.29}$$

for $n \geq 1$, where $\eta_n \equiv \rho_{n,h}/\rho_n$. The λ-dependence is left implicit and we use the conventions $\eta_0(\lambda) = 1$ and $\rho_0(\lambda) = \delta(\lambda)$. The kernel in (16.29) reads

$$s(\lambda) = \frac{1}{2\pi}\sum_{k\in\mathbb{Z}} \frac{e^{-2ik\lambda}}{\cosh(k\eta)} \,. \tag{16.30}$$

The set $\boldsymbol{\rho} = \{\rho_n\}_{n=1}^{\infty}$ represents an ensemble of states with Yang-Yang entropy

$$S_{YY}[\boldsymbol{\rho}] = N\sum_{n=1}^{\infty}\int_{-\pi/2}^{\pi/2} \mathrm{d}\lambda \,[\rho_{n,t}(\lambda)\ln\rho_{n,t}(\lambda) \\ -\rho_n(\lambda)\ln\rho_n(\lambda) - \rho_{n,h}(\lambda)\ln\rho_{n,h}(\lambda)] \,. \tag{16.31}$$

An important point to bear in mind is that the Bethe equations (16.29) relate the set of densities $\boldsymbol{\rho}$ to the set of hole densities $\boldsymbol{\rho}_h$. Knowing one of these two sets is thus sufficient to completely determine a given state. This point is crucial to understand the effects of constraints coming from ultra-local and quasi-local charges, as is explained below.

16.2 GTBA for the GGE

The generalized TBA for the GGE based on local charges proceeds as a standard TBA, but now with the effect of additional charges beyond the Hamiltonian being taken into account by additional parameters β_n (chemical potentials) in the GGE density matrix. By applying the standard maximal entropy reasoning using these constraints results in the GTBA equations [21, 32]

$$\ln(\eta_n) = -\delta_{n,1}(s*d) + s*[\ln(1+\eta_{n-1}) + \ln(1+\eta_{n+1})] \,, \tag{16.32}$$

for $n \geq 1$, where $\eta_0(\lambda) = 0$ and $s(\lambda)$ is defined in (16.30). The driving term originating from ultra-local charges is remarkably only present in the first integral equation and is specified by the chemical potentials β_m, $m \geq 2$,

$$d(\lambda) = \sum_{k\in\mathbb{Z}} e^{-2ik\lambda}\sum_{m=2}^{\infty}\beta_m \sinh^{m-1}(\eta)(ik)^{m-2} \,. \tag{16.33}$$

As shown in [21, 32], the ultra-local charges associated to the spin-1/2 transfer matrix completely fix the density of holes of 1-strings to $\rho_{1,h}^{\Psi_0}$, but leave all higher hole density functions $\boldsymbol{\rho}_{n,h}$, with $n \geq 2$, undetermined. As explained in detail in [32], the GTBA system of (16.32) and (16.29) for the GGE can then be solved (using the constraint $\rho_{1,h} = \rho_{1,h}^{\Psi_0}$ to eliminate the unknown driving term in (16.32)).

16.3 GTBA for the Quench Action

In the case of the QA treatment, the GTBA equations take the form

$$\ln(\eta_n) = d_n + s*\big[\ln(1+\eta_{n-1}) + \ln(1+\eta_{n+1})\big] \,, \tag{16.34}$$

where $n \geq 1$. The driving terms are given by the exact overlaps of Bethe states with the initial state. In the specific case of the Néel quench, these are given by

$$\begin{aligned} d_n(\lambda) &= \sum_{k\in\mathbb{Z}} e^{-2ik\lambda} \frac{\tanh(k\eta)}{k} \left[(-1)^n - (-1)^k\right] \\ &= (-1)^n \ln\left[\frac{\vartheta_4^2(\lambda)}{\vartheta_1^2(\lambda)}\right] + \ln\left[\frac{\vartheta_2^2(\lambda)}{\vartheta_3^2(\lambda)}\right] , \end{aligned} \tag{16.35}$$

where ϑ_j, $j = 1, \ldots, 4$, are Jacobi's ϑ-functions with nome $e^{-2\eta}$.

Note the difference between this GTBA and the one associated to the ultra-local GGE: from the exact QA treatment one obtains GTBA equations with driving terms at all string lengths n, as a result yielding a different set of the steady state densities.

16.4 Relating quasi-local charges and hole densities

In the main text in (16.23) we provided the expectation values of the quasi-local charges on Bethe eigenstates in the limit of large system size. Strictly in the thermodynamic limit one obtains

$$\begin{aligned} &\lim_{\text{th}} \frac{1}{N} \langle \boldsymbol{\lambda}| \widehat{X}_s(\mu) |\boldsymbol{\lambda}\rangle \\ &= \lim_{\text{th}} \frac{1}{N} \sum_{k=1}^{M} \frac{2\sinh(2s\eta)}{\cosh(2(z_k - i\mu)) - \cosh(2s\eta)} \qquad (16.36) \\ &= -2\pi \sum_{n=1}^{\infty} \int_{-\pi/2}^{\pi/2} d\lambda\, \rho_n(\lambda) \sum_{j=1}^{\min(n,2s)} a_{|n-2s|-1+2j}(\lambda+\mu), \qquad (16.37) \end{aligned}$$

with a_n defined in (16.6). In the last equality we accounted for $z_k = -i\lambda_k$, used the string hypothesis and the fact that the expectation values can be written as

$$\begin{aligned} &\langle \boldsymbol{\lambda}| \widehat{X}_s(\mu) |\boldsymbol{\lambda}\rangle \\ &= -i\,\partial_\mu \ln\left(\prod_{k=1}^{M} \frac{\sin(\lambda_k + \mu + is\eta)}{\sin(\lambda_k + \mu - is\eta)}\right) + o(N). \end{aligned} \tag{16.38}$$

Using conventions for the Fourier transform

$$\hat{f}(k) = \int_{-\pi/2}^{\pi/2} \mathrm{d}\lambda\, e^{2ik\lambda} f(\lambda)\,, \quad k \in \mathbb{Z}\,, \tag{16.39}$$

$$f(\lambda) = \frac{1}{\pi} \sum_{k\in\mathbb{Z}} e^{-2ik\lambda} \hat{f}(k)\,, \quad \lambda \in [-\tfrac{\pi}{2}, \tfrac{\pi}{2})\,, \tag{16.40}$$

one can map Eq. (16.37) to Fourier space,

$$\begin{aligned} &\lim_{\text{th}} \frac{1}{N} \langle \boldsymbol{\lambda}| \widehat{X}_s(\mu) |\boldsymbol{\lambda}\rangle \qquad (16.41) \\ &= -2 \sum_{k\in\mathbb{Z}} e^{-i2k\mu} \sum_{n=1}^{\infty} \hat{\rho}_n(k) \sum_{j=1}^{\min(n,2s)} e^{-|k|\eta(|n-2s|-1+2j)}, \end{aligned}$$

using that $\hat{a}_n(k) = e^{-|k|\eta n}$. By performing the sum over j and using that $|n-2s|+2\min(n,2s) = n+2s$, one finds

$$\begin{aligned} &\lim_{\text{th}} \frac{1}{N} \langle \boldsymbol{\lambda}| \widehat{X}_s(\mu) |\boldsymbol{\lambda}\rangle \\ &= \sum_{k\in\mathbb{Z}} \frac{e^{-i2k\mu}}{\sinh(|k|\eta)} \sum_{n=1}^{\infty} \hat{\rho}_n(k) \left(e^{-|k|\eta(n+2s)} - e^{-|k|\eta|n-2s|}\right). \end{aligned} \tag{16.42}$$

Using the thermodynamic Bethe equations (cf. (16.29)) in Fourier space,

$$\hat{\rho}_{n,t}(k) = \frac{1}{2\cosh(k\eta)} \left(\hat{\rho}_{n-1,h}(k) + \hat{\rho}_{n+1,h}(k)\right), \tag{16.43}$$

where $\hat{\rho}_{0,h}(k) = 1$, one can observe a cancellation of all terms with an exception of an expression given solely in terms $\rho_{2s,h}$:

$$\begin{aligned} &\lim_{\text{th}} \frac{1}{N} \langle \boldsymbol{\lambda}| \widehat{X}_s(\mu) |\boldsymbol{\lambda}\rangle \\ &= \sum_{k\in\mathbb{Z}} \frac{e^{-i2k\mu}}{\cosh(k\eta)} \left(\hat{\rho}_{2s,h}(k) - e^{-2s|k|\eta}\right). \end{aligned} \tag{16.44}$$

The quasi-local conservation laws make the left-hand side of Eq. (16.44) equal to the generating function of the charges on the initial state as stated previously in (16.25), leading to

$$\hat{\Omega}_s^{\Psi_0}(k) \frac{\cosh(k\eta)}{\pi} = \hat{\rho}_{2s,h}(k) - e^{-2s|k|\eta}. \tag{16.45}$$

Taking the inverse Fourier transform produces the main result of our Letter, namely the identification given by (16.24).

16.5 Truncated GGE

For practical reasons it is useful to determine a GGE ensemble by including only a finite number $\bar{s}$ of quasi-local charges $\{\widehat{X}_s\}_{s=1}^{\bar{s}}$. Using Eq. (16.24) for $s = 1, \ldots, \bar{s}$ we fix the distributions of holes $\rho_{n,h} = \rho_{n,h}^{\Psi_0}$ for string of lengths $n = 1, \ldots, 2\bar{s}$. These restrictions can be in turn used as a driving term for the following GTBA equations (analogously to what has been done for the case $\bar{s} = 1/2$ in [21, 32, 29])

$$\ln(\eta_n) = s * \left[\ln(1+\eta_{n-1}) + \ln(1+\eta_{n+1})\right] \qquad n > 2\bar{s}\,, \tag{16.46}$$

with

$$\eta_n = \frac{\rho_{n,h}^{\Psi_0}}{\rho_n} \qquad n \leq 2\bar{s}\,, \tag{16.47}$$

where the functions ρ_n solve the Bethe equations (16.29). For any $\bar{s} \geq 1/2$ we then apply an iterative procedure to find a solution for all the $\{\eta_n^{\bar{s}}\}_{n=1}^{\infty}$ and all the $\{\rho_n^{\bar{s}}\}_{n=1}^{\infty}$, ultimately leading to the results shown in figure 16.1.

16.6 Néel initial state

As the Néel state is a simple product state we can evaluate all scalar products in the "quantum" spaces pertaining to the physical spin-1/2 degrees of freedom. This leaves us with a staggered product of diagonal components of an auxiliary two-channel L-matrix $\mathbb{L}_s(z_1, z_2) =$

$L^{(-)}_{a_1}(z_1,s)L^{(+)}_{a_2}(z_2,s)$, producing a transfer matrix $\mathbb{T}_s(z_1,z_2)$ operating on two copies of auxiliary spin-s spaces $\mathcal{V}_s\otimes\mathcal{V}_s$,

$$\mathbb{T}_s(z_1,z_2)=\mathbb{L}_s^{\uparrow\uparrow}(z_1,z_2)\mathbb{L}_s^{\downarrow\downarrow}(z_1,z_2). \tag{16.48}$$

This is a local unit of the 'boundary partition function' $Z_s(z_1,z_2)=\lim_{\rm th}N^{-1}\mathrm{Tr}_a\mathbb{T}_s(z_1,z_2)^{N/2}$, whose large-$N$ limit on $\mathcal{D}:=\{(z_\lambda^-,z_\lambda^+);\lambda\in\mathbb{R}\}\subset\mathbb{C}^2$ is dominated by a non-degenerate unit eigenvalue $\Lambda_s(z_\lambda^-,z_\lambda^+)=1$ of $\mathbb{T}_s(z_1,z_2)|_{\mathcal{D}}$, implying

$$\Omega_s^{\rm N\acute{e}el}(\lambda)=\partial_{z_2}Z_s(z_1,z_2)|_{\mathcal{D}}=\frac{1}{2}[\partial_{z_2}\Lambda_s(z_1,z_2)]_{\mathcal{D}}. \tag{16.49}$$

It also helps noticing that $\mathbb{T}_s(z_1,z_2)$ enjoys a $U(1)$-symmetry, with the leading eigenvalue always residing in the largest $(2s{+}1)$-dimensional subspace. Closed-form results can be readily obtained in the cases $s=\frac{1}{2},1$

$$\Omega_{1/2}^{\rm N\acute{e}el}(\lambda)=\frac{-\sinh(2\eta)}{1-2\cos(2\lambda)+\cosh(2\eta)}, \tag{16.50}$$

$$\Omega_{1}^{\rm N\acute{e}el}(\lambda)=\frac{2\sinh(3\eta)}{3\cos(2\lambda)-\cosh(\eta)-2\cosh(3\eta)}. \tag{16.51}$$

suppressing $\Omega_s^{\rm N\acute{e}el}(\lambda)$ for higher spins $s\geq 3/2$ which become quickly cumbersome expressions. For practical implementation of the truncated GGE it however suffices to evaluate them numerically. For a class of initial states which are given in the Matrix Product State form this can be done efficiently by e.g. employing the method outlined in [20].

17 Understanding many-body physics in one dimension from the Lieb-Liniger model by Jiang, Chen, Guan

Abstract

This article presents an elementary introduction on various aspects of the prototypical integrable model the Lieb-Liniger Bose gas ranging from the cooperative to the collective features of many-body phenomena. In 1963 Lieb and Liniger first solved this quantum field theory many-body problem using the Bethe's hypothesis, i.e. a particular form of wave function introduced by Bethe in solving the one-dimensional Heisenberg model in 1931. Despite the Lieb-Liniger model is arguably the simplest exactly solvable model, it exhibits rich quantum many-body physics in terms of the aspects of mathematical integrability and physical universality. Moreover, the Yang-Yang grand canonical ensemble description for the model provides us with a deep understanding of quantum statistics, thermodynamics and quantum critical phenomena at the many-body physics level. Recently, such fundamental physics of this exactly solved model has been attracting growing interest in experiments. Since 2004, there have been more than 20 experimental papers that report novel observations of different physical aspects of the Lieb-Liniger model in the lab. So far the observed results to date are seen to be in excellent agreement with results obtained using the analysis of this simplest exactly solved model. Those experimental observations reveal the unique beauty of integrability.

17.1 Introduction

Mathematical principles play significant roles in understanding quantum physics. The concept "exact integrability" originally came from the early study of the classical dynamical systems which were described by some differential equations. Usually, the solutions of those differential equations are tantamount to the determination of enough integration constants, i.e., the

integrals of motions. In this sense, classical integrability is synonymous with exact solution. However, conceptual understanding of quantum integrability should trace back to Hans Bethe's seminal work to obtain the energy eigenstates of the one-dimensional Heisenberg spin chain with the nearest interaction in 1931.[1] He proposed a special form of the wavefunction — superposition of all possible permutations of plane waves in a ring of size L, namely,

$$\chi = \sum_{\mathcal{P}} A(\mathcal{P}) \mathrm{e}^{\mathrm{i}(k_{\mathcal{P}_1} x_1 + \cdots + k_{\mathcal{P}_N} x_N)},$$

where N is the number of down spins and $\mathcal{P}_1, \ldots, \mathcal{P}_N$ stand for a permutation $\mathcal{P}$ of 1, 2, ..., N. The $N!$ plane waves are N-fold products of individual exponential phase factors $\mathrm{e}^{\mathrm{i}k_i x_j}$. Here the N distinct wave numbers k_i are permuted among the N distinct coordinates x_j. Each of the $N!$ plane waves has an amplitude coefficient which can be in turn determined by solving the eigenvalue problem of the Heisenberg Hamiltonian.

The Bethe's ansatz appeared to be escaped from physicists' attention that time. It was only 30 years later that in 1963 Lieb and Liniger[2] first solved the one-dimensional (1D) many-body problem of delta-function interacting bosons by Bethe's hypothesis. The exact solution for the delta-function interacting Bose gas was given in terms of the wave numbers k_i $(i = 1, \ldots, N)$ satisfying a set of Bethe ansatz equations, called the Lieb–Liniger equations. The spectrum was given by summing up all k_i^2. In fact, the Bethe ansatz equations describe the roles of individual particles in many-body corrections. The significance of quantum integrability is such that the roles of individual particles enable one to precisely access full aspects of many-body physics for a particular university class of many-body systems, for example, spin chains, interacting quantum gases, strongly correlated electronic systems, Kondo impurity problems, Gaudin magnets, etc. Once concerning ensemble statistics, we have to properly distinguish physical origin of distinguishable and indistinguishable particles. At room temperature, the molecules in the air can be treated as billard balls that occasionally collide with each other. The size of those molecules is much smaller than the mean distance between them. The particles are distinguishable. However, according to de Broglie matter wave theory, the thermal wavelength of a moving particle is given by a simple formula: $\lambda_{\mathrm{dB}} = \sqrt{2\pi\hbar^2/(mk_{\mathrm{B}}T)}$, where m is the mass of the particle, $\hbar$ is the Plank constant, k_{B} is the Boltzmann constant, and T is the temperature. The temperature becomes very low, the thermal wave length increases, and the wave packets start to overlap. Thus, the particles are indistinguishable below the degenerate temperature. The quantum statistics play an essential role under such a degenerate temperature. Below the degenerate temperature, there are thus fundamental differences between the properties of fermions (with spins of 1/2, 3/2, ...) and bosons (with spins of 0, 1, 2, ...). All fermions must obey the Pauli exclusion principle, which means that they cannot occupy the same quantum state. However, as bosons are not subject to the same restrictions, they can collapse under suitable conditions into the same quantum ground state, known as a Bose–Einstein condensate. The Lieb–Linger model provides an ideal ensemble to understand the physics resulting from the distinguishable and indistinguishable nature of classical and quantum particles.

Towards a deeper understanding of the physics of the Lieb–Liniger gas, a significant next step was made by Yang C N and Yang C P on the thermodynamics of this many-body problem in 1969.[3] They for the first time present a grand canonical description of the model in equilibrium. In fact, there are many microscopic states for an equilibrium state of the system at finite temperatures. The minimization of Gibbs free energy gives rise to the so-called Yang–Yang equation that determines the true physical state in an analytical way. In the grand canonical ensemble, the total number of particles can be associated with chemical potential μ. The temperature is associated with the entropy S, counting thermal disorder. This canonical Yang–Yang approach marks a significant step to the exact solutions of finite temperature many-body physics. It shows the subtlety of vacuum fluctuation, interaction effect, excitation modes, criticality, quantum statistics, thermalization, dynamics, correlations, and Luttinger liquid.

The name Bethe's hypothesis was coined by Yang C N and Yang C P in the study of the Heisenberg spin chain. The Bethe ansatz is now well accepted as a synonym of quantum integrability. >From solving eigenvalue problem of spin-1/2 delta-function interacting Fermi gas, Yang[4] found that the many-body scattering matrix can be reduced to a product of many two-body scattering matrices, i.e., a necessary condition for solvability of the 1D many-body systems. The two-body scattering matrix satisfies a certain intertwined relation, called Yang–Baxter equation. This seminal work has inspired a great deal of developments in physics and mathematics. The Yang–Baxter relation was independently shown by Baxter as the conditions for commuting transfer matrices in two-dimensional statistical mechanics.[5, 6] For such exactly solved models, the energy eigen-spectrum of the model Hamiltonian can be obtained exactly in terms of the Bethe ansatz equations, from which physical properties can be derived via mathematical analysis. The Lieb–Liniger Bose gas[2] and Yang–Gaudin model[4, 7] are both notable Bethe ansatz integrable models.

Yang–Baxter solvable models have flourished into majority in physics since last 70's. Later it turned out that the Yang–Baxter integrability plays an important role in physical and mathematical studies.[8, 9, 10, 11, 12, 13, 14, 15] The Bethe ansatz approach has also found success in the realm of condensed matter physics, such as Kondo impurity problems, BCS pairing models, strongly correlated electron systems and spin ladders, cold atoms, quantum optics, quantum statistical mechanics, etc. The Yang–Baxter equation has led to significant developments in mathematics, such as 2D conformal field theory, quantum croups, knot theory, 2D statistical problems, lattice loop models, random walks, etc. Recent research showed that there exists a remarkable connection between conformal field theory and Yang–Baxter integrability of 2D lattice models. Remarkably, conformal field theory has led to the theory of vertex operator algebras, modular tensor categories, and algebraic topology in connection to new states of matter with topological order, such as fractional quantum Hall effect, topological insulators, etc. In this elementary introduction to the exactly solvable Lieb–Liniger model, we will discuss the rigorousness of mathematical integrability and the novelty of quantum many-body effects that comprise the beautiful cold world of many-body systems in the lab. The content of this article involves understanding the fundamental many-body physics through the model of Lieb–Liniger Bose gas.

The paper is organized as follows. In Section 2, we present a rigorous derivation of the Bethe ansatz for the Lieb–Liniger Bose gas. In this section we show how a field theory problem reduces to a quantum-mechanical many-body systems following the Lieb–Liniger's derivation. In Section 3, the properties of the ground state are discussed, including ground-state energy, excitations, cooperative and collective features, Luttinger parameter, etc. In Section 4, we introduce the Yang–Yang grand canonical approach to the finite temperature physics of the Lieb–Linger gas. In this section, we demonstrate how the Yang–Yang equation encode the subtle Bose–Einstein statistics, Fermi–Dirac statistics, and Boltzmann statistics. In particular, we give an insightful understanding of quantum criticality. In Section 5, we briefly review some of recent experimental measurements related to the Lieb–Liniger Bose gas from which one can conceive the beauty of the integrability.

17.2 Bethe ansatz for the Lieb–Liniger Bose gas

17.2.1 Wavefunction

We start with introduction of canonical quantum Bose fields $\hat{\psi}(x)$ satisfying the following commutation relations:

$$\begin{aligned}\left[\hat{\psi}(x), \hat{\psi}^\dagger(y)\right] &= \delta(x-y),\\ \left[\hat{\psi}(x), \hat{\psi}(y)\right] &= \left[\hat{\psi}^\dagger(x), \hat{\psi}^\dagger(y)\right] = 0.\end{aligned}$$

The Hamiltonian of the 1D single component bosonic quantum gas of N particles in a 1D box with length L is given by[2]

$$\hat{H} = \frac{\hbar^2}{2m}\int_0^L \mathrm{d}x\ \partial_x\hat{\psi}^\dagger\partial_x\hat{\psi} + \frac{g_{1\mathrm{D}}}{2}\int_0^L \mathrm{d}x\ \hat{\psi}^\dagger\hat{\psi}^\dagger\hat{\psi}\hat{\psi}, \tag{17.1}$$

where m is the mass of the bosons, $g_{1\mathrm{D}}$ is the coupling constant which is determined by the 1D scattering length $g_{1\mathrm{D}} = -2\hbar^2/ma_{1\mathrm{D}}$. The scattering length is given by $a_{1\mathrm{D}} = (-a_\perp^2/2a_\mathrm{s})\left[1 - C\left(a_\mathrm{s}/a_\perp\right)\right]$.[16, 17, 18] Here the numerical constant $C \approx 1.4603$. The model (17.1) presents the second-quantized form of the Lieb–Liniger Bose gas with contact interaction.[2]

In order to process Lieb and Liniger's solution, we first define the vacuum state in the Fock space as $\hat{\psi}(x)|0\rangle = 0,\ x \in \mathbb{R}$ with $\langle 0|0\rangle = 1$. The equation of motion for the field $\hat{\psi}(x)$ is given by the Heisenberg equation $\mathrm{i}\partial_t\hat{\psi}(x) = [\hat{H}, \hat{\psi}(x)]$. It follows that the corresponding equation of the motion for this model reads

$$\mathrm{i}\partial_t\hat{\psi}(x) = -\partial_x^2\hat{\psi}(x) + 2c\hat{\psi}^\dagger(x)\hat{\psi}(x)\hat{\psi}(x). \tag{17.2}$$

Considering $\hat{\psi}(x)$ as a classical field, this equation of motion reduces to a non-linear Schrödinger equation of the classical field theory. Moreover, it is easy to show that the particle number operator $\hat{N}$ and the momentum operator $\hat{P}$

$$\hat{N} = \int_0^L \hat{\psi}^\dagger\psi\mathrm{d}x, \quad \hat{P} = -\frac{\mathrm{i}}{2}\int_0^L \left\{\left[\partial_x, \hat{\psi}^\dagger(x)\right]\hat{\psi}(x)\right\}\mathrm{d}x \tag{17.3}$$

are commutative with the Hamiltonian (17.1), i.e., $[\hat{H}, \hat{N}] = 0$ and $[\hat{H}, \hat{P}] = 0$. They are among the conserved quantities of this model. The eigenfunction of the N-particle state $|\Psi\rangle$ for the operators $\hat{H}$, $\hat{N}$, and $\hat{P}$ is given by

$$|\Psi\rangle = \frac{1}{\sqrt{N!}}\int_0^L \mathrm{d}^N\boldsymbol{x}\ \Psi(\boldsymbol{x})|\boldsymbol{x}\rangle, \tag{17.4}$$

where $\boldsymbol{x} = \{x_1, x_2, \ldots, x_N\}$ and

$$|\boldsymbol{x}\rangle = \hat{\psi}^\dagger(x_1)\hat{\psi}^\dagger(x_2)\cdots\hat{\psi}^\dagger(x_N)|0\rangle.$$

Here x_j is the coordinate position of the j-th particle. For the bosons, the first quantized wavefunction Ψ is symmetric with respect to any exchange of two particles in space $\boldsymbol{x}$, namely,

$$\Psi(\ldots, x_\xi, \ldots, x_\eta, \ldots) = \Psi(\ldots, x_\eta, \ldots, x_\xi, \ldots). \tag{17.5}$$

In the following discussion, we set $\hbar = 2m = 1$ and $c = mg_{1\mathrm{D}}/\hbar^2$. After some algebra, one can find that the eigenvalue problem of the Schrödinger equation $\hat{H}|\Psi\rangle = E|\Psi\rangle$ in N-particle sector reduces to the quantum-mechanical many-body problem which is described by the Schrödinger equation $H\Psi(\boldsymbol{x}) = E\Psi(\boldsymbol{x})$ with the first quantized form of the Hamiltonian

$$H = -\sum_{i=1}^N \frac{\partial^2}{\partial x_i^2} + 2c\sum_{i<j}^N \delta(x_i - x_j). \tag{17.6}$$

This many-body Hamiltonian describes N bosons with δ-function interaction in one dimension, called the Lieb–Liniger model. This is a physical realistic model in quantum degenerate gases with s-wave scattering potential. In the dilute quantum gases, when the average distance

between particles is much larger than the scattering length, the s-wave scattering between two particles at x_ξ and x_η have the following short distance behavior:[19]

$$\Psi'(0^+) - \Psi'(0^-) = -\tfrac{1}{a_{1\mathrm{D}}}[\Psi(0^+) + \Psi(0^-)], \tag{17.7}$$

where $\Psi(x)$ is the relative wavefunction of the two particles and x is the relative distance between the two particles, i.e., $x = x_\eta - x_\xi$. In the above equation, the prime denotes the derivative with respect to x.

In the model (17.6), the interaction only occurs when two particles contact with each other. Following the Bethe ansatz,[1] we can divide the wavefunction into $N!$ domains according to the positions of the particles $\Theta(\mathcal{Q}) : x_{\mathcal{Q}_1} < x_{\mathcal{Q}_2} < \cdots < x_{\mathcal{Q}_N}$, where $\mathcal{Q}$ is the permutation of number set $\{1, 2, \ldots, N\}$. The wavefunction can be written as $\Psi(\boldsymbol{x}) = \sum_{\mathcal{Q}} \Theta(\mathcal{Q})\psi_{\mathcal{Q}}(\boldsymbol{x})$. Considering the symmetry of bosonic statistics, all the ψ in different domain $\mathcal{Q}$ should be the same, i.e., $\psi_{\mathcal{Q}} = \psi_{\mathbf{1}}$, where we denote the unitary element of the permutation group as $\mathbf{1} = \{1, 2, \ldots, N\}$. Lieb and Linger wrote the wavefunction for the model (17.6) as the superposition of $N!$ plane waves[2]

$$\psi_{\mathbf{1}} = \sum_{\mathcal{P}} A(\mathcal{P}) \mathrm{e}^{\mathrm{i}(k_{\mathcal{P}_1} x_1 + \cdots + k_{\mathcal{P}_N} x_N)}, \tag{17.8}$$

where k's are the pseudo-momenta carried by the particles under a periodic boundary condition.

Indeed, after solving Schrödinger equation $H\Psi(\boldsymbol{x}) = E\Psi(\boldsymbol{x})$, we can obtain the same s-wave scattering boundary condition (17.7) that provides the two-body scattering relation among the coefficients $A(\mathcal{P})$

$$A(\mathcal{P}') = \frac{k_{\mathcal{P}_j} - k_{\mathcal{P}_{j+1}} + \mathrm{i}c}{k_{\mathcal{P}_j} - k_{\mathcal{P}_{j+1}} - \mathrm{i}c} A(\mathcal{P}), \tag{17.9}$$

where $\mathcal{P}'$ is a permutation obtained by exchanging $\mathcal{P}_j$ and $\mathcal{P}_{j+1}$, i.e., $\mathcal{P}' = \{\mathcal{P}_1, \ldots, \mathcal{P}_{j-1}, \mathcal{P}_{j+1}, \mathcal{P}_j, \mathcal{P}_{j+2}, \ldots, \mathcal{P}_N\}$. The scattering process in Eq. (17.9) implies that any two-body scattering with momenta k_a and k_b leads to an anti-symmetric phase shift $A(\mathcal{P}') = \mathrm{e}^{-\mathrm{i}\theta(k_{\mathcal{P}_j} - k_{\mathcal{P}_{j+1}})} A(\mathcal{P})$,

$$\theta(k_\mathrm{a} - k_\mathrm{b}) = 2\arctan\left(\frac{k_\mathrm{a} - k_\mathrm{b}}{c}\right). \tag{17.10}$$

When $c \neq 0$, all the quasi-momenta are different. If there are two equal pseudo momenta $k_\mathrm{a} = k_\mathrm{b}$, we can prove that the wavefunction $\psi_{\mathbf{1}} = 0$.

In general, equation (17.9) gives the two-body scattering matrix $\hat{S}$, $A(\mathcal{P}') = \hat{S}A(\mathcal{P})$ for a quantum many-body system. Yang[4] proved that, if the two-body scattering matrix $\hat{S}$ satisfies the following equation:

$$\hat{S}_{12}(\lambda - \mu)\hat{S}_{13}(\lambda)\hat{S}_{23}(\mu) = \hat{S}_{23}(\mu)\hat{S}_{13}(\lambda)\hat{S}_{12}(\lambda - \mu), \tag{17.11}$$

then the system is integrable. This relation was independently found by Baxter[5, 6] in studying two-dimensional statistical models. Nowadays, equation (17.11) is called Yang–Baxter equation. The Yang–Baxter equation guarantees that the multi-body scattering process can be factorized as the product of many two-body scattering processes. This factorization reveals the nature of the integrability, i.e., no diffraction in outgoing waves. For the Lieb–Linger model (17.6), $\hat{S}$ matrix is a scalar function so that the scattering matrix satisfies the Yang–Baxter equation trivially. In the scattering process from $\mathbf{1}$ to $\mathcal{P}$, the multi-body scattering matrix is defined by $A(\mathcal{P}) = \hat{S}(\mathcal{P}\boldsymbol{k})A(\mathbf{1})$. By using Eq. (17.9), the multi-body scattering matrix of this model is given by

$$\hat{S}(\mathcal{P}\boldsymbol{k}) = \prod_{\mathcal{P}_j < \mathcal{P}_l} \frac{k_{\mathcal{P}_j} - k_{\mathcal{P}_l} - \mathrm{i}c}{k_{\mathcal{P}_j} - k_{\mathcal{P}_l} + \mathrm{i}c}. \tag{17.12}$$

With the help of Eq. (17.12), the eigen wavefunction of the system is given by

$$\Psi(\boldsymbol{x}) = \sum_{\mathcal{Q},\mathcal{P}} \Theta(\mathcal{Q}) \Bigg(\prod_{\mathcal{P}_j<\mathcal{P}_l} \frac{k_{\mathcal{P}_j} - k_{\mathcal{P}_l} - \mathrm{i}c}{k_{\mathcal{P}_j} - k_{\mathcal{P}_l} + \mathrm{i}c} \Bigg) \mathrm{e}^{\mathrm{i}\mathcal{Q}\boldsymbol{x}\cdot\mathcal{P}\boldsymbol{k}}. \tag{17.13}$$

17.2.2 Bethe ansatz equations

Submitting the periodic boundary conditions $\Psi(\ldots, x_\xi = 0, \ldots) = \mathrm{e}^{\mathrm{i}\alpha}\Psi(\ldots, x_\xi = L, \ldots)$ into the wavefunction (17.13), we can find that the pseudo momenta k_l satisfies the following Bethe ansatz equations (BAE):

$$\mathrm{e}^{\mathrm{i}k_i L} = -\mathrm{e}^{-\mathrm{i}\alpha} \prod_{j=1}^{N} \frac{k_i - k_j + \mathrm{i}c}{k_i - k_j - \mathrm{i}c}, \quad i = 1, 2, \ldots, N, \tag{17.14}$$

which are called the Lieb–Liniger equations. When $\alpha = \pi$, the wavefunction is anti-periodic; while when $\alpha = 0$, it is periodic. In the following discussion, we only consider the periodic boundary conditions.

Since partial number $\hat{N}$ and momentum $\hat{P}$ are conversed quantities of the Lieb–Liniger model, the Hamiltonian together with $\hat{N}$ and $\hat{P}$ can be simultaneously diagonalized. For the eigenstate (17.13), the corresponding particle number $\langle \hat{N} \rangle = N$. For a given set of quasi-momenta $\{k_j\}$, the total momentum and the energy of the system are obtained as

$$P = \langle \hat{P} \rangle = \sum_{j}^{N} k_j, \quad E = \langle \hat{H} \rangle = \sum_{j}^{N} k_j^2. \tag{17.15}$$

The solutions to the BAE (17.14) provide complete spectra of the Lieb–Linger model. The physical solutions to the Bethe ansatz equations require that all the pseudo momenta are distinct to each other. The BAE (17.14) can be written in the form of phase shift function $\theta(k)$ as

$$2\pi \frac{I_i}{L} = k_i + \frac{1}{L} \sum_{j=1}^{N} \theta\left(\frac{k_i - k_j}{c} \right), \tag{17.16}$$

where $\{I_i\}$ are the quantum numbers of pseudo momenta. If N is odd, these quantum numbers are integers, whereas they are half odd integers when N is even. For a given set of quantum numbers $\{I_i\}$, there is a unique set of real values $\{k_i\}$ for $c > 0$. These quantum numbers are independent of coupling constant c. The total momentum can be expressed as

$$P = \frac{2\pi}{L} \sum_{i=1}^{N} I_i = 2\ell\pi/L, \ \ell = 0, \pm 1, \pm 2, \ldots \tag{17.17}$$

For the ground state, $P = 0$, where all quasi-momenta $\{k_i\}$ are located in an interval $(-Q, Q)$. Here Q is the cut-off. For the ground state, the quantum numbers are given by

$$I_j = -\frac{N-1}{2} + j - 1, \ \ j = 1, \ldots, N. \tag{17.18}$$

17.3 Ground-state energy, excitations, and correlations

In the thermodynamic limit, i.e., $N, L \to \infty$ and the particle density $n = N/L$ is a constant, the BAE (17.16) can be written in the integral form

$$\rho(k) = \frac{1}{2\pi} + \int_{-Q}^{Q} a(k-q)\rho(q)\mathrm{d}q, \quad |k| < Q, \tag{17.19}$$

where $\rho(k)$ is the density distribution function of the quasi-momenta defined by the particle numbers in a small interval of $(k, k+\Delta k)$, i.e.,

$$\rho(k) = \lim_{\Delta k \to 0} \frac{1}{L\Delta k}.$$

Here the cut-off Q is the "Fermi point" of the pseudo momenta. It is determined by the particle density $n = \int_{-Q}^{Q} \rho(k)\mathrm{d}k$. Energy per length can also be written as

$$\frac{E}{L} = \int_{-Q}^{Q} \rho(k)k^2\mathrm{d}k. \tag{17.20}$$

For the ground state, the energy depends on the dimensionless scale $\gamma = Lc/N$. Let us make a scaling transformation

$$k = Qx,\ c = Q\lambda,\ \rho(Qx) = g(x), \tag{17.21}$$

we find the ground-state energy per particle,

$$\frac{E}{N} = \frac{\hbar^2 n^2}{2m} e_0(\gamma), \tag{17.22}$$

with $e_0(\gamma) = \frac{\gamma^3}{\lambda^3}\int_{-1}^{1} x^2 g_0(x)\mathrm{d}x$. Here the distribution function $g_0(x)$ is determined by

$$g_0(x) = \frac{1}{2\pi} + \frac{\lambda}{\pi}\int_{-1}^{1} \frac{g_0(y)}{\lambda^2 + (x-y)^2}\mathrm{d}y, \tag{17.23}$$

with the cut-off condition $\gamma\int_{-1}^{1} g_0(x)\mathrm{d}x = \lambda$. Equation (17.23) is the standard inhomogeneous Fredholm equation, which is well understood in mathematics. The Fredholm equation can be numerically solved. We will further study the ground-state energy later.

17.3.1 Ground state: from cooperative to collective

For the ground state, the competition of kinetic energy and interaction energy is represented by the dimensionless coupling strength γ. When $\gamma = 0$, the system is free bosons, and all the particles are condensed at the zero momentum state; while if there is a small coupling constant, all the k's are distinct. At the limit $\gamma = \infty$, the strong repulsion makes the quasi-momentum distribution the same as the one of the free fermions.

Weak coupling limit: semicircle law

It is very insightful to examine the physics of the model in weak coupling limit. In this case the Bethe ansatz roots comprise the semi-circle law. Gaudin firstly noticed such a kind of distribution,[20] followed by several groups.[21, 22] The Fredholm equation (17.23) is known as the Love equation for the problem of the circular disk condenser. By using Hutson's method, Gaudin found the density distribution function and energy density

$$\begin{aligned} g_0(t) &\approx \frac{Q}{2\pi c}\left(1-t^2\right)^{1/2} \\ &\quad + \frac{1}{4\pi^2}\left(1-t^2\right)^{-1/2}\left(t\ln\frac{1-t}{1+t} + \ln\frac{16\pi eQ}{c}\right), \\ e &= n^3\left(\gamma - \frac{4}{3\pi}\gamma^{3/2}\right). \end{aligned} \tag{17.24}$$

This result coincides with the perturbative calculation by using the Bogoliubov method.

This problem can also be solved from the original BAE (17.14). In the weak coupling limit, i.e., $Lc \ll 1$, the quasi-momenta k_j are proportional to the square root of c and $c/(k_j - k_l)$ is a small value. Up to the second order of c, the BAE (17.14) is expanded as[22]

$$q_j = \sum_{l \neq j}^{N} \frac{1}{q_j - q_l}, \tag{17.25}$$

where $q_j = k_j\sqrt{L/2c}$. If we define a function $H_N(q) = \prod_{i=1}^{N}(q - q_j)$, we can find that $F(q_j) = 0$ for the polynomial $F(q) \equiv H_N''(q) - 2qH_N'(q)$. Both $F(q)$ and $H_N(q)$ are the polynomial of degree N and $F(q_j) = H_N(q_j) = 0$, and $F(q)$ and $H_N(q)$ are proportional to each other. At the large order of q, $H(q) = q^N + \cdots$ and $F(q) = -2Nq^N + \cdots$, so that we have $F(q) = 2NH_N(q)$. It follows that

$$H_N''(q) - 2qH_N'(q) + 2NH_N(q) = 0. \tag{17.26}$$

The solution of this differential equation is a Hermite polynomial and q_j is the root of the corresponding polynomial of degree N, i.e., $H_N(q) = 0$. We set the order of q_j as $q_j < q_{j+1}$, then we have $(2N + 1 - q_j^2)^{1/2} > \pi/(q_{j+1} - q_j) > (2N + 1 - q_{j+1}^2)^{1/2}$. The distribution function, $\rho(k) = \lim_{L,N\to\infty} \frac{1}{L(k_{j+1}-k_j)}$, is thus determined by[23]

$$\rho(k) \approx \frac{1}{\pi}\sqrt{\frac{n}{c}}\left(1 - \frac{k^2}{Q^2}\right)^{1/2} + O\left(\frac{1}{Lnc}\right), \tag{17.27}$$

where the cut-off $Q = 2\sqrt{nc}$ is obtained by $\int_{-Q}^{Q}\rho(k)\mathrm{d}k = n$. We can see that the quasi-momentum distribution function satisfies the semi-circle law where the cut-off is the radius of this circle (see Fig. 17.3.1(a)). The leading order of energy (17.24) was also found based on the pseudo momentum distribution (17.27).

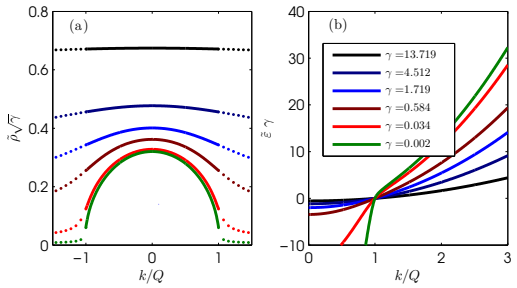

Fig. 1. Densities and dressed energies of pseudo momenta for the ground state. (a) Solid lines: the dimensionless densities of the pseudo momenta, $\tilde{\rho}(k) = \rho(k)/c$ obtained from Eq. (17.23); dotted lines: the corresponding dimensionless hole densities, $\tilde{\rho}_{\mathrm{h}}(k) = \rho_{\mathrm{h}}(k)/c$. When the coupling strength is small, the distribution function $\tilde{\rho}$ meets a semi-circle law (17.27). For the strong coupling limit, i.e., $\gamma \gg 1$, the distribution function gradually becomes flatter and flatter, and approaches $\rho(k) \approx 1/2\pi$. (b) Dimensionless dressed energy is defined by $\tilde{\varepsilon}(k) = \varepsilon(k)/c^3$, which is obtained from the dressed energy equation (17.64).

Strong coupling limit: fermionzation

In the strong repulsion limit, the gas is known as the Tonks–Girardeau (TG) gas. In realistic experiment with cold atoms, it is practicable to observe the quantum degenerate gas with the strong coupling regime.[24, 25] In the regime $\gamma \to \infty$, the Bose–Fermi mapping method[19] can map out the ground-state properties of the Bose gas through the wavefunction of the non-interacting fermions. For finitely strong interaction, $\gamma \gg 1$, we can obtain the ground-state pseudo momenta from the Bethe asnatz equations (17.14)[26, 27]

$$k_j = 2\pi \frac{I_j}{L}\left(1 - \frac{2}{\gamma} + \frac{4}{\gamma^2} - \frac{8}{\gamma^3}\right) + \frac{4\pi^3}{3c^3L^4}\left[\left(N + \frac{1}{2} - j\right)^4 - \left(\frac{1}{2} - j\right)^4\right] + O\left(\frac{1}{c^5}\right), \tag{17.28}$$

where I_j take the ground-state quantum numbers $I_j = -\frac{N-1}{2} + j - 1,\ \ j = 1, \ldots, N$. With the help of Eq. (17.28), the ground-state energy of the strong repulsive gas is given by

$$\frac{E}{L} \approx \frac{\pi^2}{3} n^3 \left[1 - \frac{4}{\gamma} + \frac{12}{\gamma^2} + \frac{32}{\gamma^3}\left(\frac{\pi^2}{15} - 1\right)\right]. \tag{17.29}$$

This asymptotic result fits well with the numerical result obtained by solving the integral BAE (17.19) (see Fig. 17.3.1(a)). The ground-state energy (17.29) can also be obtained from the integral BAE (17.19) by strong coupling expansion method.[26, 28] We see that for $\gamma \to \infty$ the leading order of the ground-state energy reduces to that of the free fermions $e_{\mathrm{f}} = \pi^2 n^3/3$. One can also calculate other important properties such as compressibility, sound velocity, and Luttinger parameter, once we know the dimensionless function $e_0(\gamma)$.

Very recently, Ristivojevic obtained high-precision ground-state distribution function for the strong coupling regime[29]

$$\rho(k) = \frac{1}{2\pi} + \frac{1}{\pi^2\lambda} + \frac{2}{\pi^3\lambda^2} + \frac{12 - \pi^2}{3\pi^4\lambda^3} + \frac{8 - 2\pi^2}{\pi^5\lambda^4} - \frac{k^2}{Q^2}\left(\frac{1}{\pi^2\lambda^3} + \frac{1}{\pi^3\lambda^4}\right) + \mathcal{O}(\lambda^{-5}). \tag{17.30}$$

The ground-state energy per unit length and particle density are given by

$$\frac{E}{L} = \frac{\lambda^3}{3\pi c^3}\left(1 + \frac{2}{\pi\lambda} + \frac{4}{\pi^2\lambda^2} + \frac{120 - 28\pi^2}{15\pi^3\lambda^3} + \frac{80 - 26\pi^2}{5\pi^4\lambda^4}\right), \tag{17.31}$$

$$n = \frac{\lambda}{c\pi}\left(1 + \frac{2}{\pi\lambda} + \frac{4}{\pi^2\lambda^2} + \frac{24 - 4\pi^2}{3\pi^3\lambda^3} + \frac{48 - 14\pi^2}{3\pi^4\lambda^4}\right), \tag{17.32}$$

where $\lambda = (\gamma + 2)/\pi - 4\pi/(3\gamma^2) + 16\pi/(3\gamma^3)$. The result $e_0 = E/(Ln^3)$ is plotted in Fig. 17.3.1.

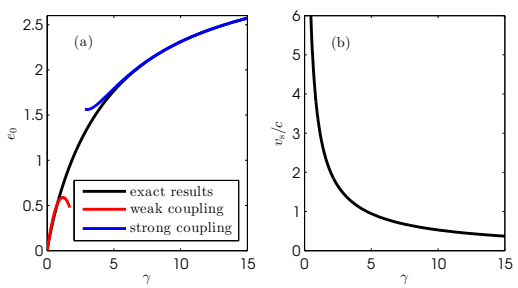

Fig. 2. The ground state energy and sound velocity for different coupling strength γ. (a) The ground energy density is a monotonic increasing function of γ when the linear density is fixed. Black line: the exact numerical result from Eq. (17.23). Red line: the weakly coupling expansion result (17.24). Blue line: the result obtained by the strongly coupling expansion (17.31). (b) The sound velocity is a monotonic decreasing function of γ. In the weakly coupling limit, the ratio turns to be infinite, while in the strong coupling limit, $v_s/c \to= 2\pi/\gamma$ (see Eq. (17.45)).

Elementary excitations: collective motion

As discussed in previous section, the eigenstates of the model are described by the quantum numbers $\{I_j\}$. We define I_j as a function of the psudomomenta, i.e., $I(k_j) = I_j$, thus we have

$$\frac{I(k)}{L} = \frac{k}{2\pi} + \frac{1}{L}\sum_{j=1}^{N} \frac{\theta(k-k_j)}{2\pi}. \tag{17.33}$$

Usually we define the occupied Bethe ansatz roots as particles, while the unoccupied roots as holes. For a hole quasimomentum k_h, the quantum number $I_h = I(k_h) \in \mathbb{Z} + (N+1)/2$. We demonstrate the quantum numbers I_j for the ground state and excited states in Figs. 17.3.1(a)–17.3.1(d). For the ground state, there is no hole below the quasi-Fermi momentum, i.e., $|k| < Q$, whereas the quantum numbers I's for the holes site outside the interval $[I_1, I_N]$ (see Fig. 17.3.1(a)).

In the thermodynamic limit, the pseudo momentum distribution function $\rho_0(k)$ for the ground state is determined by Eq. (17.19) with the cut-off of Q. The ground-state energy and the particle density can be regarded as the function of the cut-off Q, i.e., $e(Q)$ and $n(Q)$. The changes over the configuration of quantum numbers for the ground state give rise to excited states. Figure 17.3.1(d) shows such an excitation where the particle with a quasimomentum k_h below the pseudo Fermi point is excited outside the Fermi point with a new quasimomentum k_e.

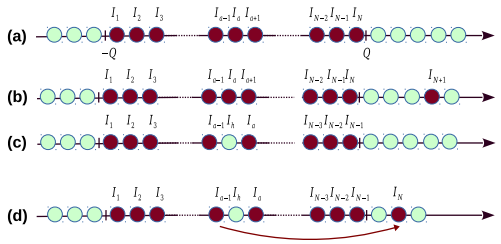

Fig. 3. Schematic diagrams of the ground state and elementary excitations. (a) Quantum numbers for the ground state. The quantum numbers for the ground state are symmetric around the the origin. The largest quasi-momentum denotes the "Fermi points" $\pm Q$. (b) Configuration of adding a particle near the right Fermi point with the quantum number I_{N+1}, so that the total number of particles is $N+1$. (c) A hole excitation. The hole at $I_{\rm h}$ is created so that the total number of particles is $N-1$. In panels (b) and (c), the parities of their quantum numbers are changed from half-odd (or integers) to integer (or half-odds) due to the changes of particle numbers. (d) A single particle–hole excitation. A particle at the position $I_{\rm h}$ is excited out of the pseudo Fermi sea. In this case, the total number of particles is still N, and the parity of quantum numbers dose not change.

For a single-particle excitation, we decompose the pseudo momentum density into two parts, $\rho_t(k) = \bar{\rho}(k) + \frac{1}{L}\delta(k-k_{\rm e})$, where the delta function term attributes to the excited particle and $\bar{\rho}(k)$ stands for the density below the cut-off pseudo momenta, i.e., $|k| < Q$. In the thermodynamic limit, $\bar{\rho}(k)$ satisfies the following integral equation:

$$\bar{\rho}(k) = \frac{1}{2\pi} + \int_{-Q}^{Q} a(k-k')\bar{\rho}(k')\mathrm{d}k' + \frac{1}{L}a(k-k_{\rm e}). \tag{17.34}$$

Here we choose a state which satisfies Eq. (17.19) with cut-off Q as a reference state, i.e.,

$$\rho_0(k) = \frac{1}{2\pi} + \int_{-Q}^{Q} a(k-k')\rho_0(k')\mathrm{d}k' + \frac{1}{L}a(k-k_{\rm e}). \tag{17.35}$$

The addition of the excited particle leads to a collective rearrangement of the distribution of the pseudo momenta of the $N-1$ particles. We denote the difference of the pseudo momentum distribution functions between the excited and the reference state as $\Delta\rho(k) = \bar{\rho}(k) - \rho_0(k)$, where $\rho_0(k)$ is the pseudo momentum distribution of the reference state within $|k| < Q$. By comparing the integral BAE (17.34) and (17.19), we can find that $\Delta\rho$ satisfies the following equation:

$$\Delta\rho(k) = \frac{1}{L}a(k-k_{\rm e}) + \int_{-Q}^{Q} a(k-k')\Delta\rho(k'). \tag{17.36}$$

The addition of the particle also leads to a shift of the cut-off over the psuado-Fermi point of the ground state of N-particle, i.e., $\Delta Q = Q - Q_{\rm G}$. Here, $Q_{\rm G}$ is the cut-off for the ground state with the particle number $N = Ln_{\rm G}(Q_{\rm G})$, and Q is that for the excited state with $N = Ln_{\rm G}(Q) + L\int_{-Q}^{Q}\mathrm{d}k\Delta\rho(k) + 1$. In the thermodynamic limit, ΔQ is a small value. By comparing the formulas of particle numbers between the ground state and the excited state, $\Delta Q n'_{\rm G}(Q_{\rm G}) = -[\int_{-Q}^{Q}\Delta\rho(k)\mathrm{d}k + 1/L]$. The prime denotes the derivative with respect to the the cut-off Q. The corresponding excited energy

$$\begin{aligned}\Delta E(k_{\rm c}) &= L\int_{-Q}^{Q}\Delta\rho(k)k^2\mathrm{d}k + k_{\rm e}^2 + Le'(Q)\Delta Q \\ &= L\int_{-Q}^{Q}\Delta\rho(k)(k^2-\mu)\mathrm{d}k + (k_{\rm e}^2-\mu),\end{aligned} \tag{17.37}$$

where μ is the chemical potential, and $\mu = \mathrm{d}E/\mathrm{d}N = e'_{\mathrm{G}}(Q_{\mathrm{G}})/n'_{\mathrm{G}}(Q_{\mathrm{G}})$. Later we will further prove that the dressed energy can be expressed as

$$\varepsilon(k) = k^2 - \mu + \int_{-Q}^{Q} a(k-k')\varepsilon(k'). \tag{17.38}$$

For convenience, we introduce a useful relation between the dressed energy and density. Assuming that two functions $f(k)$ and $g(k)$ satisfy the following equations:

$$\begin{aligned} f(k) &= f_0(k) + \int_{-Q}^{Q} a(k-k')f(k')\mathrm{d}k', \quad |k| < Q, \\ g(k) &= g_0(k) + \int_{-Q}^{Q} a(k-k')g(k')\mathrm{d}k', \quad |k| < Q, \end{aligned} \tag{17.39}$$

where $f_0(k)$ and $g_0(k)$ are the driving terms of these integral equations. Then we have the useful relation

$$\int_{-Q}^{Q} f(k)g_0(k)\mathrm{d}k = \int_{-Q}^{Q} g(k)f_0(k)\mathrm{d}k. \tag{17.40}$$

By using Eq. (17.40), from Eqs. (17.38) and (17.39), we thus prove that the dressed energy is nothing but the excitation energy of a particle,

$$\begin{aligned} &\varepsilon(k_{\mathrm{e}}) = k_{\mathrm{e}}^2 - \mu + \textstyle\int_{-Q}^{Q} a(k_{\mathrm{e}} - k')\varepsilon(k') \\ &= k_{\mathrm{e}}^2 - \mu + L\int_{-Q}^{Q} (k_{\mathrm{e}}^2 - \mu)\Delta\rho(k') = \Delta E(k_{\mathrm{e}}). \end{aligned} \tag{17.41}$$

On the other hand, the hole excitations impose an additional condition, namely, the maximum momentum is $n\pi$. Similarly, one can prove that the excited energy reads

$$\Delta E(k_{\mathrm{h}}) = -\varepsilon(k_{\mathrm{h}}). \tag{17.42}$$

We plot the dressed energies for different coupling strengths in Fig. 17.3.1(b). In order to see clearly excitation spectra, we need to calculate the total momentum using Eq. (17.17). For both the particle–hole excitation and the Type-II hole excitation, the total particle numbers of particles do not change, as shown in Figs. 17.3.1(d) and 17.3.1(b). Therefore, the total momenta of the excited states are given by

$$P = n\pi - 2\pi\int_{0}^{k_{\mathrm{e,h}}} \rho_0(k)\mathrm{d}k. \tag{17.43}$$

For the low-energy excitations, $k_e - Q$ is a very small value. Therefore, the low-lying behavior can be described by a linear dispersion relation

$$\Delta E = \varepsilon'_{\mathrm{G}}(Q)|k \pm Q| = v_{\mathrm{s}}|P|, \quad v_{\mathrm{s}} = \frac{\varepsilon'_{\mathrm{G}}(Q)}{2\pi\rho_{\mathrm{G}}(Q)}, \tag{17.44}$$

where v_{s} is the sound velocity of the system. In the above equation, $\pm$ corresponds to the excitations at left/right Fermi point, respectively. Nevertheless, for $|k| > Q$, the relation (17.44) is the dispersion relation for particle–hole excitations. This linear spectra uniquely determine the universal Luttinger liquid behaviour at the low temperatures. The essential feature resulted from the dispersion relation (17.44) is such that the system exhibits the conformal invariant in low energy sector. We will further discuss this universal nature of the 1D many-body physics.

For the strong coupling, we can obtain the sound velocity from the ground-state energy through the relation $v_s = \sqrt{\frac{L}{mn}\frac{\partial^2 E}{\partial L^2}}$, namely,

$$v_s \approx 2\pi n\left[1 - \frac{4}{\gamma} + \frac{12}{\gamma^2} + \frac{16}{\gamma^3}\left(\frac{\pi^2}{3} - 2\right)\right]. \tag{17.45}$$

In Figs. 17.3.1(a) and 17.3.1(b), we present the analytical and numerical results for the dimensionless energy $\bar{e}(\gamma) = e/n^3$ and v_s/c, respectively.

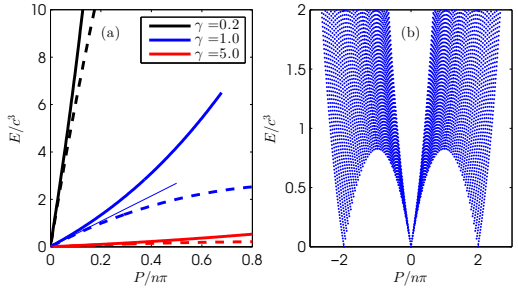

Fig. 4. Dispersion relations in elementary excitations: adding one particle and adding one hole excitation. (a) Solid lines: the spectra for adding one particle to the ground state corresponding to the configuration presented in Fig. 17.3.1(b). Dashed lines: the dispersion relations for the hole excitation, see the configuration shown in Fig. 17.3.1(c). For $\gamma = 1$, the thin blue line is calculated by using Eq. (17.44). We see that both the particle and hole excitations comprise the dispersion relations with the same velocity. (b) The particle–hole excitation spectra, see Fig. 17.3.1(d). The linear dispersion relation is seen for the long-wavelength limit, i.e., the momentum tends to be zero.

The super Tonks–Girardeau gas-like phase

In regard of the strong interacting bosons in 1D, the super Tonks–Girardeau gas is particularly interesting. It describes a gas-like phase of the attractive Bose gas which was first proposed in a system of attractive hard rods by Astrakharchik et al.[30] Batchelor and his coworkers showed its existence of such a novel state in the Lieb–Liniger model with a strong attraction.[31] Due to the large kinetic energy inherited from the repulsive Tonks–Girardeau gas, the hard-core behavior of the particles with Fermi-like pressure prevents the collapse of the super TG phase after the switch of interactions from repulsive to attractive interactions.[32, 33, 34, 35] In fact, the energy can be continuous in the limits $c \to \pm\infty$. >From the Bethe ansatz equations (17.14), near $c \to \pm\infty$, the compressibility is given by

$$\frac{1}{\kappa} = 2\pi^2 n - \frac{16\pi^2}{c}n^2 + \frac{80\pi^2}{c^2}n^3 + \left(\frac{64}{3}\pi^2 - 320\right)\frac{n^4}{c^3}. \tag{17.46}$$

However, for the Lieb–Liniger gas with weak repulsive interaction ($0 < c \ll 1$), compressibility is given by

$$\frac{1}{\kappa} = 2c - \frac{1}{\pi\sqrt{n}}c^{3/2}. \tag{17.47}$$

In contrast, the energy for the gas-like phase (super Tonks–Girardeau gas) in weak attractive interaction limit ($-1 \ll c < 0$) is given by

$$E = \frac{2\pi^2}{3}n^2 - |c|\,n^2. \tag{17.48}$$

Thus, the compressibility of the super Tonks–Giraread gas with weak attraction is given by

$$\frac{1}{\kappa} = 4\pi^2 n - 2\,|c|\,. \tag{17.49}$$

Such different forms of compressibility reveal an important insight into the root patterns of the quasi-momenta. We now show the subtlety of the Bethe ansatz roots for the super Tonks–Girardeau state[32] in Fig. 17.3.1.

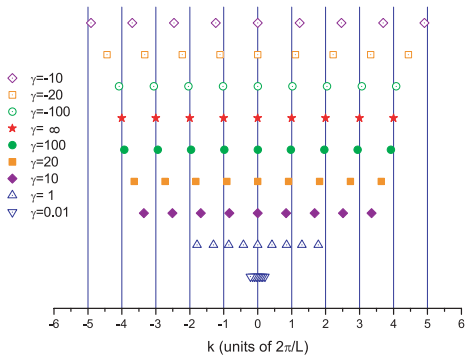

Fig. 5. Quasi-momenta for the ground state of the Lieb–Liniger gas with the strong repulsion and the supper Tonks–Girardeau gas of the attractive Bose gas for a large value of γ. It is obvious that the super Tons–Girardeau gas has a larger kinetic energy than the free Fermion momentum. Thus the quantum statistics of the super Tonks–Girardeau gas is more exclusive than the free fermion statistics.

17.3.2 Luttinger parameter and correlation functions

The 1D integrable system gives rise to the power law behavior of long distance or long time asymptotics of correlation functions for the ground state. The effective Hamiltonian can be approximately described by the conformal Hamiltonian which can be written in terms of the generators of the underlying Virasoro algebra with the central charge $C = 1$. The low-lying excitations present the phonon dispersion $\Delta E(p) = v_s p$ in the long-wavelength limit. In this limit, all particles participate in the excitations and form a collective motion of bosons which is called the Luttinger liquid.[36] The Lieb–Liniger field theory Hamiltonian can be rewritten as an effective Hamiltonian in long-wavelength limit, which essentially describes the low-energy physics of the Lieb–Linger Bose gas

$$H = \int \mathrm{d}x \left(\frac{\pi v_\mathrm{s} K}{2} \Pi^2 + \frac{v_\mathrm{s}}{2\pi K} \left(\partial_x \phi\right)^2 \right), \tag{17.50}$$

where the canonical momenta Π conjugate to the phase ϕ obeying the standard Bose commutation relations $[\phi(x), \Pi(y)] = \mathrm{i}\delta(x-y)$. $\partial_x \phi$ is proportional to the density fluctuations. In this effective Hamiltonian, v_s/K fixes the energy for the change of density. In this approach, the density variation in space is viewed as a superposition of harmonic waves.

For example, the leading order of one-particle correlation $\langle \psi^\dagger(x)\psi(0)\rangle \sim 1/x^{1/2K}$ is uniquely determined by the Luttinger parameter K. The Luttinger parameter is defined by the ratio of sound velocity to stiffness, namely,

$$K = \frac{v_\mathrm{s}}{v_N} = \frac{\pi}{\sqrt{3e_0(\gamma) - 2\gamma \frac{\mathrm{d}e_0(\gamma)}{\mathrm{d}\gamma} + \frac{1}{2}\gamma^2 \frac{\mathrm{d}^2 e_0(\gamma)}{\mathrm{d}\gamma^2}}}, \tag{17.51}$$

where v_s is the sound velocity and v_N is the stiffness and defined as

$$v_N = \frac{L}{\pi\hbar}\frac{\partial^2 E}{\partial N^2}, \quad v_s = \sqrt{\frac{L^2}{mN}\frac{\partial^2 E}{\partial L^2}}. \tag{17.52}$$

In Eq. (17.51), the second expression of the Luttiger parameter is used for numerical calculation with the help of Eq. (17.22).

Using the asymptotic expansion result of the ground-state energy (17.24) for weak counting and (17.29) for the strong counting regimes, we find the asymptotic forms of the Luttinger parameter K for the two limits

$$K|_{\gamma\ll 1} = \pi\left(\gamma - \frac{1}{2\pi}\gamma^{3/2}\right)^{-1/2}, \tag{17.53}$$

$$K|_{\gamma\gg 1} = 1 + \frac{4}{\gamma} + \frac{4}{\gamma^2} - \frac{16\pi^2}{3\gamma^3}. \tag{17.54}$$

In Fig. 17.3.2, we show that these asymptotic forms of the Luttinger parameters provide a very accurate expression throughout the whole parameter space. The correlation functions can be calculated by the conformal field theory.[11, 36, 37, 38, 39]

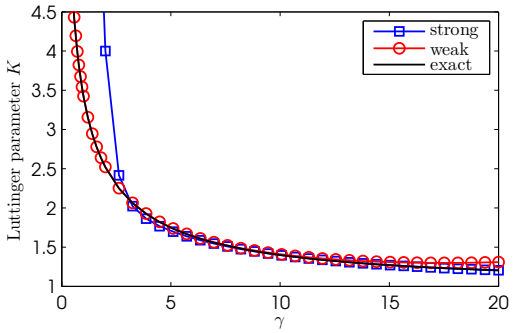

Fig. 6. Luttinger parameter K versus interaction strength γ. Blue dashed line: the result obtained from Eq. (17.54) for the strong coupling limit; red dashed line: result obtained from Eq. (17.53) for weak coupling regime; black solid line: the numerical result obtained from Eq. (17.51). The analytical result of the Luttinger parameter is in a good agreement with the numerical result.

Usually, the long-distance or long-time asymptotics of correlation functions of the 1D critical systems can be calculated by using the canonical field theory (CFT).[11] >From the CFT, the two-point correlation function for primary fields with the conformal dimensions $\Delta^{\pm}$ is given by[40]

$$G_O(y,\tau) = \sum \frac{A e^{-2\pi i(N\Delta D)y/L}}{(v\tau + iy)^{2\Delta^+}(v\tau - iy)^{2\Delta^-}}, \tag{17.55}$$

where τ is the Euclidean time, v is the velocity of light, $G_O(x,t) = \langle G|\hat{O}^\dagger(x,t)\hat{O}(0,0)|G\rangle$ is the correlator for the field operators $\hat{O}(0,0)$ and $\hat{O}^\dagger(x,t)$. Equation (17.55) involves the contributions of the excited states which are characterized by numbers ΔD, $N^{\pm}$, and ΔN. Here N^- (or N^+) describes the elementary particle–hole excitations by moving atoms close to the left (or right) pseudo Fermi point outside the Fermi sea with adding N^- (or N^+) holes below the left (or right) Fermi point. ΔN is the change of particle number and it characterizes

the elementary excitations by adding (or removing) particles over the ground state. $N^{\pm}$ and ΔN are not enough to describe all elementary excitations. It is necessary to introduce the quantum number $2\Delta D$ to denote the particle number difference between the right- and left-going particles. >From the analysis of finite-size corrections of the BAE, the total momentum and excited energy of the low-lying excitations in terms of these quantum numbers $N^{\pm}$, ΔN, and D are given by

$$\Delta P = \frac{2\pi}{L}\left[\Delta N \Delta D + N^{+} - N^{-}\right] + 2\Delta D k_{\mathrm{F}}, \tag{17.56}$$

$$\Delta E = \frac{2\pi v}{L}\left[\frac{1}{4}(\Delta N/Z)^2 + (\Delta D Z)^2 + N^{+} + N^{-}\right], \tag{17.57}$$

where $Z = 2\pi\rho(Q)$ is the dressed charge at the pseudo Fermi point for the ground state. >From the conformal field theory, the excited energy and momentum are given by

$$\Delta E = \frac{2\pi v}{L} v(\Delta^{+} + \Delta^{-}), \tag{17.58}$$

$$\Delta P = \frac{2\pi}{L}\sum_{\alpha}(\Delta^{+} - \Delta^{-}) + 2\Delta D k_{\mathrm{F}}, \tag{17.59}$$

By comparison between the two results obtained from finite-size corrections (17.56), (17.57), and CFT (17.58), (17.59), the conformal dimensions are analytically obtained as a function of $N^{\pm}$, ΔN, ΔD, and the dressed charge Z as well, namely,

$$2\Delta^{\pm} = 2N^{\pm} \pm \Delta N \Delta D + (\Delta D Z)^2 + \frac{1}{4}(Z^{-1}\Delta N)^2. \tag{17.60}$$

It turns out that only the low-energy excitations determine the long distance or time asymptotic behavior of the correlation functions. Given that the operator $\hat{\psi}(x)$ is a prime operator of this $U(1)$ symmetric system, the correlation functions of the prime field have a universal power law decay in distance

$$\langle\hat{\psi}^{\dagger}(\tau, y)\hat{\psi}(0,0)\rangle = \frac{\exp(2\mathrm{i}\Delta D k_{\mathrm{F}} y)}{(v\tau + \mathrm{i}y)^{2\Delta^{+}}(v\tau - \mathrm{i}y)^{2\Delta^{-}}}. \tag{17.61}$$

We find that the Luttinger parameter $K = Z^2$ by comparing with the result of the Luttinger theory, $\langle\hat{\psi}^{\dagger}(y)\hat{\psi}(0)\rangle \sim 1/y^{1/2K}$. For example, in the strong coupling regime, the dressed charge $Z = 1 + 2/\gamma - 8\pi^2/3\gamma^3$ from the dressed charge equation.[11] Submitting it into $K = Z^2$, we obtain the same result as Eq. (17.54).

17.4 Yang–Yang thermodynamics and quantum criticality

In 1969, Yang C N and Yang C P presented a grand canonical ensemble to describe finite-temperature thermodynamics for the Lieb–Linger model.[3] The Yang–Yang method has led to significant developments in quantum integrable systems.[12, 13, 41] This approach allows one to access full finite temperature physics of the models in terms of the thermodynamic Bethe ansatz (TBA) equations.[12] In the grand canonical ensemble, we usually convert the TBA equations in terms of the dimensionless chemical potential $\tilde{\mu} = \mu/c^2$ and the dimensionless temperature $\tilde{T} = T/c^2$ with the interaction strength c. It is also convenient to use the degenerate temperature as an energy unit, i.e., $T_{\mathrm{d}} = \hbar^2 n^2/2m$.[42, 43] It is very insightful to discuss the critical phenomena of the models in terms of the dimensionless units. We first discuss the Yang–Yang grand canonical ensemble below.

17.4.1 The Yang–Yang grand canonical ensemble

For the ground state, the set of quantum numbers (17.18) provides the lowest energy. However, at finite temperatures, any thermal equilibrium state involves many microscopic eigenstates. As discussed in previous section, these eigenstates are characterized by different quantum numbers $\{I_j\}$, see Eq. (17.16). In the thermodynamic limit, $I(k)$ is a monotonic function of pseudo momenta k.[11] We define $\mathrm{d}I(k)/(L\mathrm{d}k) = \rho(k) + \rho_\mathrm{h}(k)$, where ρ_h is the density of the holes. >From Eq. (17.16), we can obtain the integral BAE for arbitrary eigenstate as

$$\rho(k) + \rho_\mathrm{h}(k) = \frac{1}{2\pi} + \int_{-\infty}^{\infty} a(k-k')\rho(k')\mathrm{d}k'. \tag{17.62}$$

Here we should notice that integral interval can extend to the whole real axis, i.e., particles can occupy any real quasimomentum.

In order to understand the equilibrium states of the model, it is essential to introduce the entropy. In a small interval $\mathrm{d}k$, the number of total vacancies is $L[\rho(k) + \rho_\mathrm{h}(k)]\mathrm{d}k$ with a number of $L\rho(k)\mathrm{d}k$ particles and a number of $L\rho_\mathrm{h}(k)\mathrm{d}k$ holes. These particles and holes give rise to microscopic states

$$\mathrm{d}W = \frac{[L(\rho(k) + \rho_\mathrm{h}(k))\mathrm{d}k]!}{[L\rho(k)\mathrm{d}k]![L\rho_\mathrm{h}(k)\mathrm{d}k]!}.$$

In the thermodynamic limit, $[L(\rho(k) + \rho_\mathrm{h}(k))\mathrm{d}k] \gg 1$ and $\mathrm{d}k \to 0$, with the help of Stirling's formula, the entropy in this small interval is given by

$$\mathrm{d}S = \ln \mathrm{d}W \approx L\{\rho \ln[1+\eta] + \rho_\mathrm{h} \ln[1+\eta^{-1}]\}\mathrm{d}k,$$

where $\eta(k) = \rho_\mathrm{h}(k)/\rho(k)$. The total entropy is $S = \int \mathrm{d}S$. It can be understood from this procedure that the entropy involves the disorder of mixing the particles and holes in the pseudo momentum space. For regions with zero $\rho(k)$ or zero $\rho_\mathrm{h}(k)$, no disorder occurs, i.e., $\mathrm{d}S = 0$. Therefore, the entropy for the ground state is zero. It is worth noting that the above discussion is valid only in the equilibrium state.

The Gibbs free energy Ω is the thermodynamic potential of grand canonical ensemble for this model,

$$\Omega = E - TS - \mu N, \tag{17.63}$$

where μ is the chemical potential, and the particle number is given by $N = L\int \rho(k)\mathrm{d}k$. In thermal equilibrium, the true physical state is determined by the conditions of minimizing the Gibbs free energy. Making a virtual change $\delta\rho, \delta\rho_\mathrm{h}$ in the thermal equivalent state, we take the variation of the free energy such that

$$\delta\Omega = \delta E - T\delta S - \mu\delta N = 0.$$

Here we should notice that the variations $\delta\rho$ and $\delta\rho_\mathrm{h}$ are not independent in view of the integral BAE (17.62). This minimization condition leads to the TBA equations in terms of the dressed energy[3]

$$\varepsilon(k) = k^2 - \mu + \int_{-\infty}^{\infty} a(k-k')\varepsilon_-(k')\mathrm{d}k', \tag{17.64}$$

where the dressed energy is defined by $\varepsilon(k) = T\ln\eta(k)$. In the above equation, we also denote $\varepsilon_-(k) = -T\ln[1+\mathrm{e}^{-\varepsilon(k)/T}]$. Using the TBA equation (17.64), we further obtained the grand thermodynamic potential $\Omega = \frac{L}{2\pi}\int \varepsilon_-(k)\mathrm{d}k$. It follows that the pressure is given by

$$p = -\left(\frac{\partial\Omega}{\partial L}\right)_{\mu,c,T} = -\frac{1}{2\pi}\int \varepsilon_-(k)\mathrm{d}k. \tag{17.65}$$

This serves as the equation of state (17.65) from which we can calculate the thermodynamics of this model at finite temperatures. We can obtain the zero-temperature and finite-temperature phase diagrams of the Lieb–Liniger model. In the zero-temperature limit, the TBA equation (17.64) reduces to the dressed energy equation (17.38) in the limit $T \to 0$. From the standard thermodynamic relations, one can calculate the particle density $n = \partial_\mu p|_{c,T}$, entropy density $s = \partial_T p|_{\mu,c}$, compressibility $\kappa^* = \partial_\mu^2 p|_{c,T}$, specific heat $c_\mathrm{v} = T\partial_T^2 p|_{\mu,c}$ in a straightforward way.

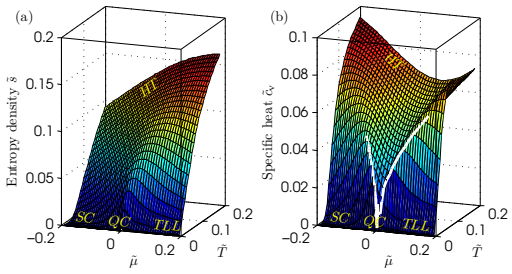

Fig. 7. Quantum critical regimes for the Lieb–Liniger model. (a), (b) Dimensionless entropy and specific heat in the $\tilde{T}$–$\tilde{\mu}$ plane, respectively. For $\tilde{T} \gg 1$, it is the HT regime. The TLL with the dynamical exponent $z = 2$ and correlation length exponent $\nu = 1$ lies in the region $\tilde{T} \ll 1$ and $\mu > \mu_\mathrm{c}$. For $\tilde{T} \gg |\mu - \mu_\mathrm{c}|$, the QC regime with $z = 2$, $d = 1$, and $\nu = 1/2$ fans out near the quantum phase transition point $\tilde{\mu}_\mathrm{c} = 0$. It is obvious that the entropy and the specific heat have singularity properties near the critical point $\mu_\mathrm{c} = 0$.

In view of the grand canonical ensemble, there exists a quantum phase transition at the chemical potential $\mu_\mathrm{c} = 0$ at zero temperature. Universal thermodynamics is expected for the temperature under the quantum degenerate regime $T \lesssim T_\mathrm{d}$, where $T_\mathrm{d} = \hbar^2 n^2/2m$.[42, 43] At high temperatures (HT), i.e., $T \gg T_\mathrm{d}$, the system behaves like a classical Boltzmann gas. For $\mu < \mu_\mathrm{c} = 0$ and at low temperatures, the density is very low and the gas becomes de-coherent. This phase is semiclassical (SC). Whereas for $\mu > \mu_\mathrm{c}$ and the temperature $T < |\mu - \mu_\mathrm{c}|$, it shows the Tomonaga–Luttinger liquid (TLL) phase. The quantum critical regime lies between SC and TLL for the temperature $T \gg |\mu - \mu_\mathrm{c}|$. We show such different regimes through the entropy and specific heat in Fig. 17.4.1.

17.4.2 The Yang–Yang equation and quantum statistics

Dynamical interaction and thermal fluctuation drive Lieb–Liniger model from one phase into another. In particular, under the degenerate temperature T_d, the model has three distinct phases: semi-classical, quantum critical, and the TTL critical phases. At high temperatures, there does not exhibit universal behaviour. When the temperature tends to be infinity, the system reaches the Boltzmann gas. Therefore, the Yang–Yang equation (17.64) encodes different quantum statistics. For example, when the coupling strength $\gamma \to 0$, the system behaves as the free bosons; for the strong coupling limit, it behaves like free fermions; at high temperatures, the system becomes the Boltzmann gas. In the following, we rigorously derive such quantum statistics in an analytical way.

When the coupling strength γ turns to be zero, the integral kernel $a(k) \to \delta(x)$. The dressed energy in this limit can be expressed as

$$\lim_{c\to 0} \varepsilon(k) = T \ln\left[\mathrm{e}^{(k^2-\mu)/T} - 1\right], \tag{17.66}$$

from which we obtain the thermal potential per length $\lim_{c\to 0}\Omega/L=\int_0^\infty 2\sqrt{\epsilon}/[\mathrm{e}^{(\epsilon-\mu)/T}-1]\,\mathrm{d}\epsilon$. Thus, the distribution function satisfies the Bose–Einstein statistics

$$\lim_{c\to 0} g(\epsilon)=\frac{1}{\mathrm{e}^{(\epsilon-\mu)/T}-1}. \tag{17.67}$$

If $\gamma\to\infty$, the dressed energy reads

$$\lim_{c\to\infty}\varepsilon(k)=k^2-\mu. \tag{17.68}$$

In this limit, the Bethe ansatz equation (17.62) naturally reduces to the form

$$\rho(k)=\frac{1}{2\pi(1+\rho_{\mathrm{h}}(k)/\rho(k))}, \tag{17.69}$$

which indicates the Fermi–Dirac statistics. Consequently, the thermal potential per unit length is given by $\lim_{c\to\infty}\Omega/L=\int_0^\infty 2\sqrt{\epsilon}/[\mathrm{e}^{(\epsilon-\mu)/T}+1]\,\mathrm{d}\epsilon$. This result gives rise to the Fermi–Dirac statistics

$$\lim_{c\to\infty} g(\epsilon)=\frac{1}{\mathrm{e}^{(\epsilon-\mu)/T}+1}. \tag{17.70}$$

We further remark that equations (17.66)–(17.70) are valid for arbitrary temperature. If the system is under the quantum degeneracy, the quantum statistical interaction is important. Thus, the particles are indistinguishable. At high temperatures, the Yang–Yang equation (17.64) gives rise to the Maxwell–Boltzmann statistic such that the particles are distinguishable. In the weak coupling limit and high-temperature limits, it is very convenient to consider Viral expansions with the Yang–Yang equation (17.64), namely,

$$\mathrm{e}^{-\epsilon(k)/T}=\mathcal{Z}\mathrm{e}^{-k^2/T}\mathrm{e}^{\int_{-\infty}^{\infty}\mathrm{d}q a(k-q)\ln\left(1+\mathcal{Z}\mathrm{e}^{-q^2/T}\right)}. \tag{17.71}$$

Here $\mathcal{Z}=\mathrm{e}^{\mu/T}$ is fugacity. After some algebra, we find that the pressure up to the second Viral coefficient is given by

$$p=p_0+\frac{T^{3/2}}{\sqrt{2\pi}}\mathcal{Z}^2 p_2, \tag{17.72}$$

where $p_2=-\frac{1}{2}+\int_{-\infty}^{\infty}\mathrm{d}q' a(2q')\mathrm{e}^{-2q'^2/T}$ reveals the two-body interaction effect. In the above equation, $p_0=-\frac{T}{2\pi}\int_{-\infty}^{\infty}\mathrm{d}k\ln\left(1-\mathcal{Z}\mathrm{e}^{-k^2/T}\right)$ is the pressure of the free bosons. The result (17.72) gives the Maxwell–Boltzmann statistics in the limit of $T\to\infty$.

It is remarkable to discover the universal low temperature behavior of the Lieb–Liniger model with the Bose–Einstein statistic and Fermi–Dirac statistic. The Yang–Yang equation (17.64) provides full physics of the Lieb–Liniger model which goes beyond that can be found by Bose–Fermi mapping.[19] In fact, for strong coupling limit, i.e., $\gamma\gg 1$, the system can be viewed as an ideal gas with the fractional statistics.[44] When the coupling strength is very weak, the ground state behaves like a quasi BEC. The Bogoliubov approach is valid in the weak coupling limit $\tilde{T}\ll\sqrt{\gamma}\ll 1$.[28, 42, 43] The result (17.72) is also a good approximation for the weak coupling Lieb–Liniger gas.

17.4.3 Luttinger liquid and quantum criticality

Equation of state

In low-energy physics, $T\ll T_{\mathrm{d}}$, low-lying excitations form a collective motion of bosons. The linear relativistic dispersion near the Fermi points results in the TLL behavior. At finite

temperatures, the TLL can be sustained in a region of $T < |\mu - \mu_c|$ in the T–μ plane (see Fig. 17.4.1). In the TLL phase, we can take the Sommerfeld expansion with the TBA equation (17.64). By iterations, the pressure with the leading order temperature correction is given by

$$p = p_0 + \frac{\pi^2 T^2}{3}\frac{\rho_0(Q)}{\varepsilon'(Q)} = p_0 + \frac{\pi T^2}{6v_s}, \tag{17.73}$$

which gives the free energy per unit length as the field theory prediction

$$F(T)/L = \mu n - p \approx E_0 - \frac{\pi C (k_B T)^2}{6\hbar v_s}, \tag{17.74}$$

with the central charge $C = 1$. Here we took $k_B = 1$, so that in TLL phase the specific heat is linear temperature-dependent

$$c_v = \frac{\pi T}{3v_s}. \tag{17.75}$$

This is a universal signature of the TLL.

However, for the temperature beyond the crossover temperature, i.e., $T > T^* \sim |\mu - \mu_c|$, the excitations give a non-relativistic dispersion, i.e., $\Delta E \sim p^2$. The crossover temperature T^* can be also determined by the breakdown of linear temperature-dependent relation given by Eq. (17.75).[26] The crossover is also evidenced by the correlation length.[45]

For strong coupling and low temperatures, i.e., $\gamma \gg 1$ and $\tilde{T} \ll 1$, the pressure is given by[26]

$$p = -\frac{T^{3/2}}{2\sqrt{\pi}}\mathrm{Li}_{3/2}\big(-\mathrm{e}^{A/T}\big)\left[1 + \frac{T^{3/2}}{2\sqrt{\pi}c^3}\mathrm{Li}_{3/2}\big(-\mathrm{e}^{A/T}\big)\right], \tag{17.76}$$

where $A = \mu + 2p/c + (T^{5/2}/2\sqrt{\pi}c^3)\mathrm{Li}_{3/2}(-\mathrm{e}^{A/T})$ and the polylogarithm function is given by $\mathrm{Li}_n(x) = \sum_{k=1}^{\infty}\frac{x^k}{k^n}$. In the above equation, the pressure p gives a close form of the equation of state. Using the standard thermodynamical relations, we can analytically calculate the particle density, compressibility, and the specific heat

$$\begin{aligned} n = &-\frac{1}{2\sqrt{\pi}}T^{1/2}f_{1/2}\left\{1 - \frac{1}{\sqrt{\pi}c}T^{1/2}f_{1/2} + \frac{T}{\pi c^2}f_{1/2}^2\right. \\ &\left. + \frac{1}{\sqrt{\pi}c^3}T^{3/2}\left[-\frac{1}{\pi}f_{1/2}^3 + \frac{3}{2}f_{3/2}\right]\right\}, \end{aligned} \tag{17.77}$$

$$\begin{aligned} \kappa^* \approx &-\frac{1}{2\sqrt{\pi}}T^{-1/2}f_{-1/2} + \frac{3}{2\pi c}f_{-1/2}f_{1/2} \\ &- \frac{2}{\pi^{3/2}c^2}T^{1/2}f_{-1/2}f_{1/2}^2 - \frac{1}{\pi c^3}Tf_{-1/2}f_{3/2} \\ &+ \frac{5}{\pi^2 c^3}Tf_{-1/2}f_{1/2}^3 - \frac{3}{4\pi c^3}Tf_{1/2}^2, \end{aligned} \tag{17.78}$$

$$\begin{aligned} \frac{c_v}{T} = \left(\frac{\partial s}{\partial T}\right)_{\mu,c} = &-\frac{3}{8\sqrt{\pi}}T^{-1/2}f_{3/2} + \frac{1}{2\sqrt{\pi}}T^{-1/2}\frac{A}{T}f_{1/2} \\ &- \frac{1}{2\sqrt{\pi}}T^{-\frac{1}{2}}\left(\frac{A}{T}\right)^2 f_{-1/2} + O\left(\frac{1}{c}\right), \end{aligned} \tag{17.79}$$

respectively. Here $f_n = \mathrm{Li}_n(-\mathrm{e}^{A/T})$.

Quantum criticality

At zero temperature, the quantum phase transition from the vacuum phase into the TLL at the critical point $\mu_c = 0$ occurs in the Lieb–Liniger Bose gas. According to the renormalized group theory, universal scaling properties are expected in the critical regime at low temperatures (see Fig. 17.4.1). In 2011, Guan and Batchelor investigated the quantum criticality of the Bose gas and found that the equation of state (17.76) reveals the universal scaling behavior of quantum criticality in terms of the polylogarithm functions.[26] It is straightforward from the equation of the state to derive the universal scaling form of the density as

$$n(T,\mu) \approx n_0 + T^{d/z+1-1/\nu z}\mathcal{F}\left(\frac{\mu-\mu_c}{T^{1/\nu z}}\right), \tag{17.80}$$

where the background density $n_0 = 0$. The scaling function $\mathcal{F}(x) = -\frac{1}{2\sqrt{\pi}}\mathrm{Li}_{1/2}(-e^x)$ read off the dynamic critical exponent $z = 2$, and the correlation length exponent $\nu = 1/2$. It is particularly interesting that the finite temperature density profiles of the 1D trapped gas can map out the quantum criticality with these universal exponents for the Lieb–Liniger gas. The density curves at different temperatures intersect at the critical point, see Fig. 17.4.3(a). The universal scaling behavior of compressibility κ^* is given by

$$\kappa^* = \kappa_0 + T^{d/z+1-2/\nu z}\mathcal{K}\left(\frac{\mu-\mu_c}{T^{1/\nu z}}\right), \tag{17.81}$$

where $\kappa_0 = 0$ and $\mathcal{Q}(x) = -\frac{1}{2\sqrt{\pi}}\mathrm{Li}_{-1/2}(x)$. This scaling function again reads out the dynamic critical exponent $z = 2$, and the correlation length exponent $\nu = 1/2$. The intersection at the critical point for different temperatures attributes to the universal scaling form (17.81) (see Fig. 17.4.3(b)).

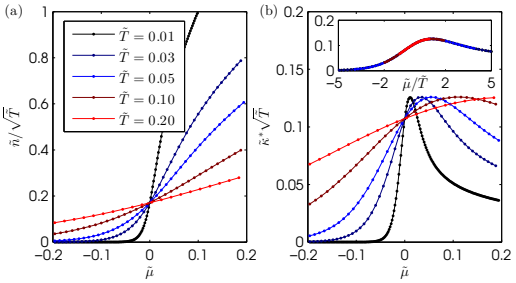

Fig. 8. Universal scaling behaviors of the density and compressibility at quantum criticality. (a) Density shows the universal scaling behavior given by (17.80). (b) Compressibility presents the universal scaling behavior (17.81). The inset in (b) shows the collapse of temperature-rescaled compressibility $\tilde{\kappa}^*\sqrt{\tilde{T}}$ with respect to the argument $(\tilde{\mu} - \tilde{\mu_c})/\tilde{T}$.

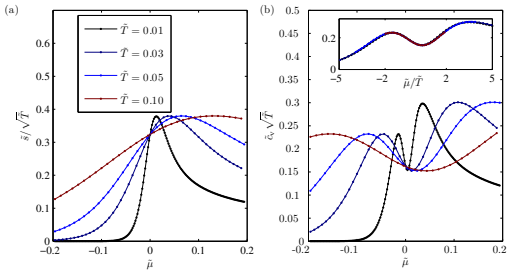

Fig. 9. Quantum critical behaviour of the entropy and specific heat. (a) The entropy divided by temperature $\tilde{s} = s/c$ has a universal scaling bahavior at the quantum criticality. (b) Specific heat divided by temperature $\tilde{c}_{\rm v} = c_{\rm v}/T$ has a universal scaling bahavior at the quantum criticality. The inset in (b) shows the collapse of $\tilde{c}_{\rm v}\sqrt{\tilde{T}}$ with respect to the argument $(\tilde{\mu} - \tilde{\mu}_{\rm c})/\tilde{T}$.

Near the critical point, the specific heat divided by the temperature $\tilde{c}_v \equiv c_{\rm v}/T$ obeys the following scaling form:

$$\tilde{c}_{\rm v} = -T^{-1/2}\left[\frac{3}{8\sqrt{\pi}}{\rm Li}_{3/2}\left(-{\rm e}^{\mu/T}\right) - \frac{1}{2\sqrt{\pi}}\frac{\mu}{T}{\rm Li}_{1/2}\left(-{\rm e}^{\mu/T}\right) + \frac{1}{2\sqrt{\pi}}\left(\frac{\mu}{T}\right)^2{\rm Li}_{-1/2}\left(-{\rm e}^{\mu/T}\right)\right]. \tag{17.82}$$

The specific heat at different temperatures has two round peaks near the critical point $\mu_{\rm c} = 0$. These peaks mark the crossover temperatures that distinguish the TLL and semi-classical gas phases from the quantum critical regime. This is a very robust signature for the existence of the crossover temperatures in the 1D Bose gas. This scaling law of the entropy and specific heat is shown in Fig. 17.4.3.

17.4.4 The local pair correlations and Tan's contact

In the study of the interacting Bose gas in one dimension, an important property is the local two-body correlation function g_2. Physically speaking, this function describes the rates of inelastic collision between pairs of particles.[46, 47, 48] This quantity reflects the probability that the two particles site at the same size. It is also known as contact that strikingly captures the universality of ultracold atoms. This has been described by Tan's relations.[49, 50, 51] Tan's contact, which measures the two-body correlations at short distances in dilute systems, is a central quantity to ultra-cold atoms. It builds up universal relations among thermodynamic quantities such as the large momentum tail, energy, and dynamic structure factor, through the renowned Tan's relations, see recent developments in this research.[52]

Knowing that the two-body correlation can lead to the classification of physically distinct regimes, for example, the Tonks–Girardeau regime with $g_2 \to 0$, the Gross–Pitaevskii regime with $g_2 = 1$ and the very weak coupling or fully decoherent regime with $g_2 = 2$. The two-body correlation function can be calculated for these different regimes by expression $g_2 = \langle\hat{\Psi}^\dagger(x)\hat{\Psi}^\dagger(x)\hat{\Psi}(x)\hat{\Psi}(x)\rangle$. where $\hat{\Psi}$ is the field operator in second quantization. At $T = 0$, we have ${\rm d}E_0/{\rm d}c = Lg_2$, where E_0 is the ground-state energy. For weak coupling limit, the local pair correlation $g_2/n^2 = 1 - 2\sqrt{\gamma}/\pi$. For strong coupling limit, $g_2/n^2 = 4\pi^2/3\gamma^2\,(1 - 6/\gamma)$. In general, the local pair correlation can be used to study phase coherence behavior at finite temperatures. Introducing the free energy per particle, i.e., $f(\gamma, T) = F/N$, the normalized two-particle local correlation is defined as

$$g_2 = \frac{\langle\hat{\Psi}^\dagger(x)\hat{\Psi}^\dagger(x)\hat{\Psi}(x)\hat{\Psi}(x)\rangle}{n^2} = \frac{2m}{\hbar^2 n^2}\left(\frac{\partial f(\gamma, T)}{\partial\gamma}\right)|_{n,T}. \tag{17.83}$$

For strong coupling regime, the local pair correlation function is obtained from the equation of state[47, 48, 53, 54]

$$g_2 = \frac{4\pi^2}{3\gamma^2}\left(1 - \frac{6}{\gamma} + \frac{T^2}{4\pi^2 T_d^2}\right). \tag{17.84}$$

On the other hand, in one dimension the fundamental thermodynamic relation in a harmonic trap is given by[52]

$$\mathrm{d}p = n\mathrm{d}\mu + s\mathrm{d}T - \frac{\rho_\mathrm{s}}{2}\mathrm{d}w^2 - \mathcal{C}\mathrm{d}a_{1\mathrm{D}}, \tag{17.85}$$

where ρ_s and $\mathcal{C}$ are the densities of superfluid and contact, respectively. In this relation, $w = v_\mathrm{s} - v_\mathrm{n}$ is the difference between the velocity of the superfluid and normal components. Maxwell relations build the general connections between the contact and other physical quantities such as

$$\left(\frac{\partial \mathcal{C}}{\partial \mu}\right)_{T,a_{1\mathrm{D}}} = -\left(\frac{\partial n}{\partial a_{1\mathrm{D}}}\right)_{\mu,T},$$
$$\left(\frac{\partial \mathcal{C}}{\partial T}\right)_{\mu,a_{1\mathrm{D}}} = -\left(\frac{\partial s}{\partial a_{1\mathrm{D}}}\right)_{\mu,T}.$$

Furthermore, we can obtain the contact through the following relations:

$$\mathcal{C} = -\frac{1}{c^2}\left(\frac{\partial p}{\partial c}\right)_{\mu,T} \approx \frac{1}{2\pi}T^2 f_{1/2} f_{3/2} \times \left(1 - \frac{1}{\sqrt{\pi}c}T^{1/2} f_{1/2}\right). \tag{17.86}$$

The Tan's contact of the Lieb–Liniger gas does not have the usual scaling behavior which was found for the interacting Fermi gas in Ref. [52]. This is mainly because the critical field $\mu_\mathrm{c} = 0$ which does not depend on the scattering length $a_{1\mathrm{D}}$ (see Fig. 17.4.4).

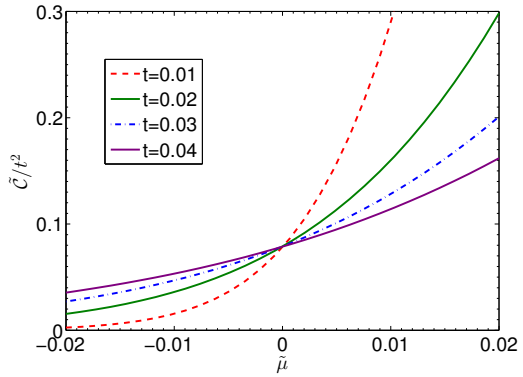

Fig. 10. Contact divided by $\tilde{T}^2$ versus chemical potential. The critical scaling behavior of the contact for the Lieb–Liniger gas is different from that for the 1D interacting Fermi gas.[28]

17.5 Experimental development related to the Lieb–Liniger gas

Over the past few decades, experimental achievements in trapping and cooling ultra-cold atomic gases have revealed beautiful physics of the cold quantum world. In particular, recent breakthrough experiments on trapped ultracold bosonic and fermionic atoms confined to one dimension have provided a precise understanding of significant quantum statistical and strong correlation effects in quantum many-body systems. The particles in the waveguides are tightly confined in two transverse directions and weakly confined in the axial direction. The transverse excitations are fully suppressed by the tight confinements. Thus, the atoms in these waveguides can be effectively characterised by a quasi-1D system. Thus, 1D effective interaction potentials can be controlled in the whole interacting regime by the underlying 3D scattering with

tight confinements in the two transverse directions.[16, 17, 18] In such a way, these 1D many-body systems ultimately relate to the integrable models of interacting bosons and fermions. It is now possible to realize effectively one-dimensional quantum Bose gases, in which the interaction strength between ultracold atoms is tunable, see recent reviews.[37, 41] These experiments have successfully demonstrated the anisotropic confinements of atoms to one dimension by optical waveguides, see a feature review article.[55] Particularly striking examples involve the measurements of momentum distribution profiles,[24, 52] the ground state of the Tonks–Girardeau gas,[25] quantum correlations,[56, 57, 58, 59, 60, 61] Yang–Yang thermodynamics,[62, 63] the super Tonks–Girardeau gas,[64] quantum phonon fluctuations,[65, 66, 67] elementary excitations and dark solitons,[68, 69] thermolization and quantum dynamics.[70, 71, 72] More experimental developments of the Lieb–Liniger model are listed in Table 17.5.[73]

Table 1. Experiments of Lieb–Liniger gas.

quantum dynamics	^{87}Rb[61, 71, 74, 75, 76]
thermalization	^{87}Rb[61, 70, 74, 75]
solitons	^{87}Rb[68, 77]
fermionization	^{39}K[57, 72]
YY thermodynamics	^{87}Rb[56, 61, 62, 65, 66, 67, 78]
strong coupling	^{87}Rb[24, 25]
phase diagram	Cs[79]
3-body correlations	^{87}Rb,[58, 63] Cs[60]
excited state	Cs[64]

The early experimental studies of the Lieb–Linger gas with cold atoms were made in the laboratory by Bloch's group[24] and Weiss's group.[25] In particular, the observation of the ground state energy of the Tonks–Girardeau gas provides deep insights into understanding fermionization effect induced by a strong repulsive interaction, see Fig. 17.5. Loading the ^{87}Rb ultracold atoms into a 2D array of 1D tubes, where the atoms were kept in the lowest energy state in the two transverse directions. Thus, the systems were realized in quasi-1D systems within axial harmonic traps. The essential feature of the Tonks–Girardeau gas was observed through the ground-state energy T_{1D} of such waveguided ensembles.

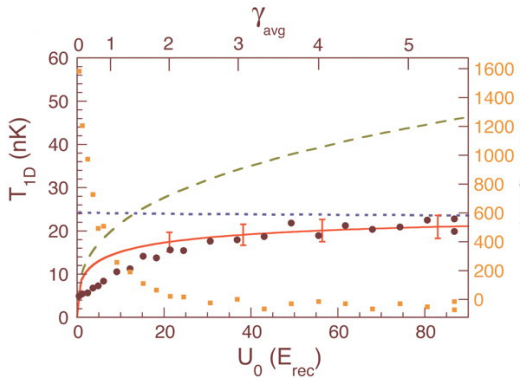

Fig. 11. The 1D ground-state energy T_{1D} versus transverse confinement depth of the lattice. For the confinement potential $U_0 > 0$ (or the effective interaction $\gamma \gg 1$), the energy T_{1D} well presents the ground-state energy of the Lieb–Liniger gas in strong coupling regime within the local density approximation.[17]

The experimental measurement of the metastable highly excited state — the super Tonks–Girardeau gas was achieved by Haller[64] in 2009. They made a new experimental breakthrough

with a stable highly excited gas-like phase in the strongly attractive regime of bosonic Cesium atoms across a confinement-induced resonance, see Fig. 17.5. This particular state was first predicted theoretically by Astrakharchik et al.[30] Using the Monte Carlo method and by ANU group from the integrable interacting Bose gas with attractive interactions.[31] This model has improved our understanding of quantum statistics and dynamical interaction effect in many-body physics. It turns out that a highly excited state of gas-like gas could be stable as the interaction is switched from strongly repulsive into strongly attractive interactions due to the the existence of Fermi-like pressure.[32, 33, 34] This phenomenon has triggered much attention in theory.[80]

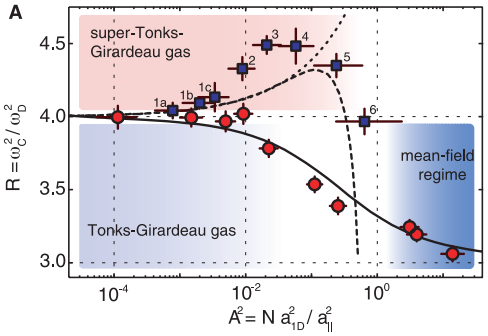

Fig. 12. The ratio of compress mode over the trapping frequency $R = \omega_c^2/\omega_D^2$ versus the interaction parameter A^2. The squares show the experimental measurements in strong attractive regime. The circles show the experimental data ranging from weak coupling to strong TG regimes. The black solid line stands for the exact result from the Lieb–Linger gas with a repulsion. The dashed lines present the theoretical data from the result.[30] Further study of the Tonks–Girardeau gas can be found in Ref. [32].

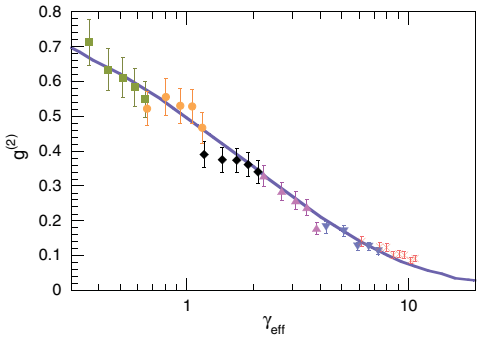

Fig. 13. The local pair correlation function versus the effective coupling constant. The solid line is obtained from the exactly solved model of Lieb–Linger gas at zero temperature. The symbols show the experimental data.[56]

In fact, many experiments have successfully demonstrated the confinements of atoms to one dimension by optical waveguides. Another particularly interesting example involves the measurement of photoassociation rates in one-dimensional Bose gases of ^{87}Rb atoms to determine the local pair correlation function $g^{(2)}(0)$ over a range of interaction strengths, see Fig. 17.5. This experiment provides a direct observation of the fermionization of bosons with increasing interaction strength. It sheds light on the phase coherence behavior.[29, 34, 42, 43, 81] At zero

temperature, the local pair correlation is $g^{(2)}(0) \sim 1$ for the weakly interacting Bose gas and $g^{(2)}(0) \to 0$ as the system enters into the Tonks–Girardeau regime.

As discussed in previous sections, the finite-temperature problem of the Lieb–Liniger Bose gas was solved by Yang and Yang in 1969.[3] It turns out that the Yang–Yang thermodynamic equation is an elegant way to analytically access the thermodynamics, quantum fluctions, and quantum criticality. The Yang–Yang thermodynamics have been confirmed in the recent experiments through various thermodynamical properties[62, 63] and quantum fluctuations.[65, 66, 67] A typical example is the measurement of the Yang–Yang thermodynamics on the atom chip, see Fig. 17.5.

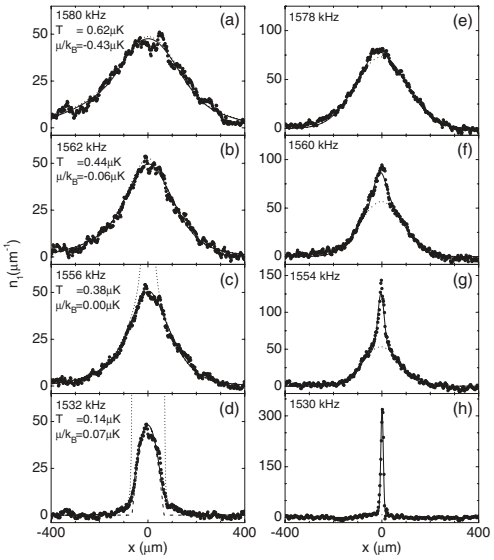

Fig. 14. The in situ axial density profiles for the weakly interaction Bose gas of ^{87}Rb atoms at different temperatures. The solid lines show the result obtained from the Yang–Yang equations. The values of the chemical potentials are indicated by the harmonically trapping potentials. The experimental data show a good agreement with the theoretical prediction from the Yang–Yang equation.[55]

Moreover, recent experimental simulations with ultracold atoms provide promising opportunities to test quantum dynamics of many-body systems. In particular, nonequilibrium evolution of an isolated system involves transport and quench dynamics beyond the usual thermal Gibbs mechanism where the ground state and low lying excitation play an essential role. The experimental study[70, 71] of thermalization of 1D ensemble of cold atoms has led to significant developments in this field.[82, 83] In these experiments, it was demonstrated that quenching the dynamics into the isolated systems can lead to non-thermal distributions if conserved laws exist. So far a generalized Gibbs ensemble is believed to present the non-thermal distributions in the isolated systems with conserved laws. The many-body density matrix is written as

$$\hat{\rho} = \frac{1}{Z} \exp\left(- \sum_m \lambda_m \hat{\mathcal{I}}_m \right) \tag{17.87}$$

in terms of conserved quantities $\hat{\mathcal{I}}_m$. Here $Z = \mathrm{Tr} \exp\left(- \sum_m \lambda_m \hat{\mathcal{I}}_m \right)$ is the partition function. The Lagrange multipliers λ_m acting for maximization of the entropy are determined by the associated conserved laws. Figure 17.5 shows the quantum Newton's cradle that provides an insightful signature of such a generalized Gibbs ensemble. It shows that the 1D systems with many-conserved laws do not approach the thermal equilibrium.

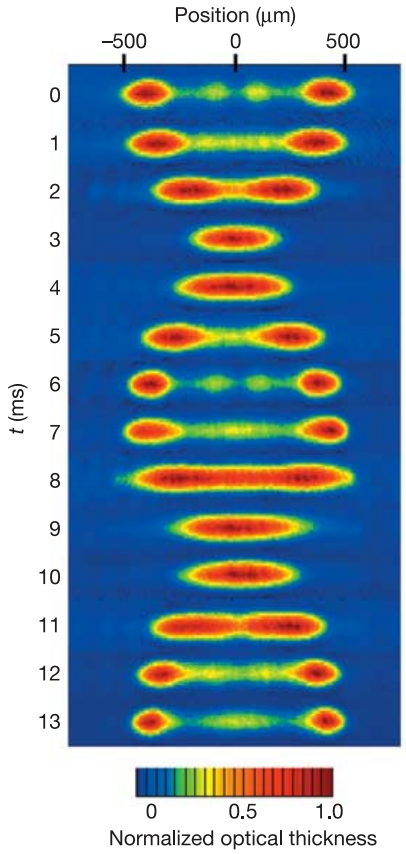

Fig. 15. The time series of absorption images of the first oscillation cycle for initial average peak coupling strength $r_0 = 1$. The two groups of the cold atoms were confined in one dimension and initially separated by grating pulses. They evolved from time to time and collided twice in the centre of the harmonic 1D trap in each full cycle. The oscillations in 1D Bose gas last for a long time, even without approaching equilibrium.[70]

Recently, Langen et al.[76] showed that a degenerate 1D Bose gas relaxes to a state that can be described by such a generalized Gibbs ensemble. By splitting a 1D Bose gas into two halves, they prepared a non-equilibrium system of ^{87}Rb atoms trapped in an atomic chip. They measured the local relative phase profile $\varphi(z)$ between the two halves. It was shown that most of the experimentally reachable initial states evolve in time into the steady states which can be determined within a reasonable precision by far less than N Lagrange multipliers. It was particularly interesting to see that the experimental data of the reduced χ^2 values can be well fitted with about 10 modes although there exist a much larger number of conserved quantities in the system. This research further opens the study of the generalized Gibbs ensemble for the quantum systems out of equilibrium.

17.6 Outlook

We have introduced a fundamental understanding of many-body phenomena in the Lieb–Liniger model. The exact results for various physical properties of the Lieb–Liniger model at $T = 0$ and at finite temperature were obtained by using the Bethe ansatz equations. In particular, we have presented a precise understanding of the excitation modes, Luttinger liquid, quantum statistics, quantum criticality, correlations, and dynamics in the context of Bethe ansatz. In fact, there have been great developments in the study of the Lieb–Liniger model in Refs. [11, 15, 37] via various methods, such as field theory methods,[34, 84] Luttinger liquid

theory and bosonization, etc.[36, 85] It was shown that the repulsive Lieb-Liniger Bose gas can be obtained as the nonrelativistic limit of the sinh-Gordon model.[86, 87, 88] Moreover, the study of the non-thermal distributions for the isolated systems with many conserved laws has attracted much attention. In this scenario, the generalized Gibbs ensemble[83, 89, 90, 91, 92] has been used to study the thermalization of the isolated systems. More recently, there has been growing interest on quench dynamics in terms of the generalized Gibbs Ensemble.[93, 94, 95, 96, 97, 98] This research has been becoming a new frontier in cold atoms and condensed matter physics. It turns out that the integrable systems of this kind thus provide a promising platform to advance the basic understanding of new quantum effects in many-body physics, such as few-body problems, universal thermodynamics, universal contact, quench dynamics, and correlation functions. These studies will further place mathematical theories of exactly solvable models into the laboratory for a wide range of physical phenomena.

Part VI
Special Effects: Useful, Selected Articles

Part VII
Localization: Main Articles

18 Stark many-body localization by Schulz, Hooley, Moessner, Pollmann

Abstract

We consider spinless fermions on a finite one-dimensional lattice, interacting via nearest-neighbor repulsion and subject to a strong electric field. In the non-interacting case, due to Wannier-Stark localization, the single-particle wave functions are exponentially localized even though the model has no quenched disorder. We show that this system remains localized in the presence of interactions and exhibits physics analogous to models of conventional many-body localization (MBL). In particular, the entanglement entropy grows logarithmically with time after a quench, albeit with a slightly different functional form from the MBL case, and the level statistics of the many-body energy spectrum are Poissonian. We moreover predict that a quench experiment starting from a charge-density wave state would show results similar to those of Schreiber *et al.* [*Science* **349**, 842 (2015)].

18.1 Main theory

Introduction.

In the latter half of the twentieth century, pioneering work by Anderson [350] and collaborators [2] established that the eigenfunctions of a quantum particle moving in a disordered potential landscape in one or two dimensions are exponentially localized. In the beginning of the twenty-first century, it was shown [3, 359, 5] that this localization can persist even for finite densities of fermions with repulsive interparticle interactions, a phenomenon now termed many-body localization (MBL) [6].

Subsequent theoretical work has explored the disorder-driven transition from ergodic to MBL behavior in a variety of mostly one-dimensional models. Key results include the 'l-bit' picture of the MBL regime [7], the logarithmic growth of entanglement entropy following a quench into it [8, 9, 10], and subdiffusive transport of spin and energy in the approach to the MBL transition from the ergodic side [11, 12, 13, 14]. Significant progress has also been made in the experimental study of MBL in one- and two-dimensional systems of cold atoms [15, 16, 13].

It is natural to ask whether disorder is at all an essential ingredient for observing MBL phenomenology, or whether it is possible for thermalization to fail for reasons due to interactions alone. This can happen when the system is integrable [18, 13], but such cases constitute isolated points in parameter space, with arbitrarily small generic variations in the Hamiltonian parameters restoring ergodicity. An important question is then whether there can be *robust* non-ergodic phases in models without quenched disorder. There have so far been several proposals for this, ranging from models inspired by classical glassy physics [37, 21] to variants of the Bose Hubbard model [22, 359] and models with mixed species [23]; however, there are also counterarguments that the localization in some of these systems is a long-lived intermediate-time phenomenon which eventually yields to thermalization at very long times [24, 25].

Here, we approach the question of MBL without disorder from a different angle, by introducing interactions into a single-particle model that exhibits Wannier-Stark localization [2]. It is instructive to compare the resulting physics, which we call Stark many-body localization, with the well known many-body disorder localized (MBL) case. The comparison is interesting because in both cases the single-particle eigenfunctions are exponentially localized in space,

and thus one might expect at least some MBL signatures also to be present in the disorder-free Stark-MBL case.

Specifically, we study the properties of spinless fermions on a finite one-dimensional lattice. The fermions interact via nearest-neighbor repulsion, and we subject them to a strong electric field: either a strictly spatially uniform one, for which the non-interacting many-body spectrum contains many exact degeneracies, or a field with a slight spatial gradient, for which these degeneracies are lifted. The setup is depicted in Fig. 18.1.

For fields with slight spatial gradients, we find that Stark-MBL is robust and shares many similarities with MBL. Specifically, the entanglement entropy grows logarithmically with time after a quench (Fig. 18.2), and the many-body eigenenergies of the Stark-MBL problem generically show Poissonian level statistics (Fig. 18.3). We moreover predict the results in our Stark-MBL system of a quench experiment starting from a charge-density wave state of the type conducted in [15], and we obtain graphs similar to those seen in the MBL case. Interestingly, for a strictly uniform field [27], entropy and level statistics deviate from MBL phenomenology, which we attribute to exact degeneracies in the non-interacting spectrum.

Model.

The Hamiltonian of our model is

$$\hat{H} = \frac{J}{2}\sum_{j=0}^{L-2}\left(c_j^\dagger c_{j+1} + \text{h.c.}\right) + \sum_{j=0}^{L-1} W_j\left(n_j - \frac{1}{2}\right) + V\sum_{j=0}^{L-2}\left(n_j - \frac{1}{2}\right)\left(n_{j+1} - \frac{1}{2}\right). \quad (18.1)$$

Here the operator $c_j^\dagger$ creates a fermion on lattice site j, and the associated number operator $n_j = c_j^\dagger c_j$. $J/2$ is the hopping matrix element between neighboring sites, V is the strength of the nearest-neighbor repulsion, and L is the number of sites of the lattice, the boundary conditions of which we take to be open.

W_j is the on-site potential energy due to the applied electric field. For a uniform field γ, it takes the form $W_j = -\gamma j$. For a non-uniform field, it acquires some curvature, $W_j = -\gamma j + \alpha j^2/(L-1)^2$. This means that the potential has the same value and slope as the linear one at $j = 0$, but differs at the other end of the chain by α from the purely linear case (see the inset of Fig. 18.2).

Entanglement entropy growth.

A quantity that is often used to diagnose and characterize MBL is the entanglement entropy. To calculate this, a spatial bipartition into two halves is made by cutting a particular bond. The reduced density matrix of the subsystem, ρ_{red}, is calculated, and the entropy determined via $S = -\text{tr}\left(\rho_{\text{red}}\log(\rho_{\text{red}})\right)$. Serbyn *et al.* [10] argued, on the basis of the general physical picture of 'l-bits' in the MBL regime, that at long times the entropy should grow logarithmically with time, i.e. that $S(t) \sim S_0 \ln(Vt)$.

This argument uses the fact that the density profiles of the individual l-bits are exponentially localized. We now show that the long-time entanglement growth in the Stark-MBL system behaves similarly, though with some modification reflecting the fact that the tails of Wannier-Stark-localized wave functions are not pure exponentials.

The functional form of these tails may be obtained from a semiclassical argument [28] in which the wave function is approximated by a WKB-like expression $\psi(x) \sim \exp\left(i\int^x k(x')dx'\right)$, with $k(x)$ obtained from the condition of local energy conservation, $J\cos(ka) + V(x) = E$,

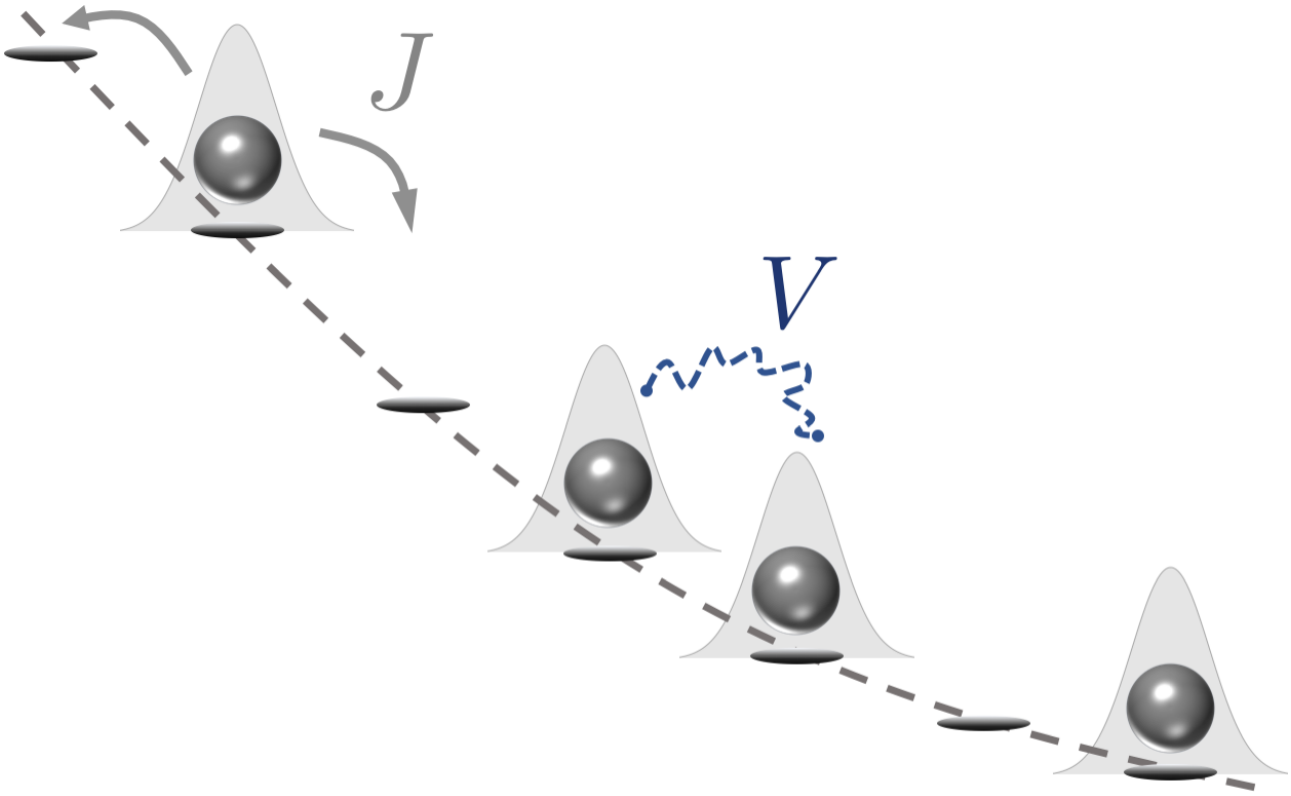

Figure 18.1: Schematic illustration of our model. On a *finite* lattice in one dimension, the single particle states of spinless fermions, which can delocalize via hopping J, are exponentially localized via a strong electric field. For a purely uniform field (i.e. a linear electric potential), this is usually referred to as Wannier-Stark localization [2]. When the particles interact via nearest-neighbor interactions V, they share many properties with the well studied MBL phenomenology.

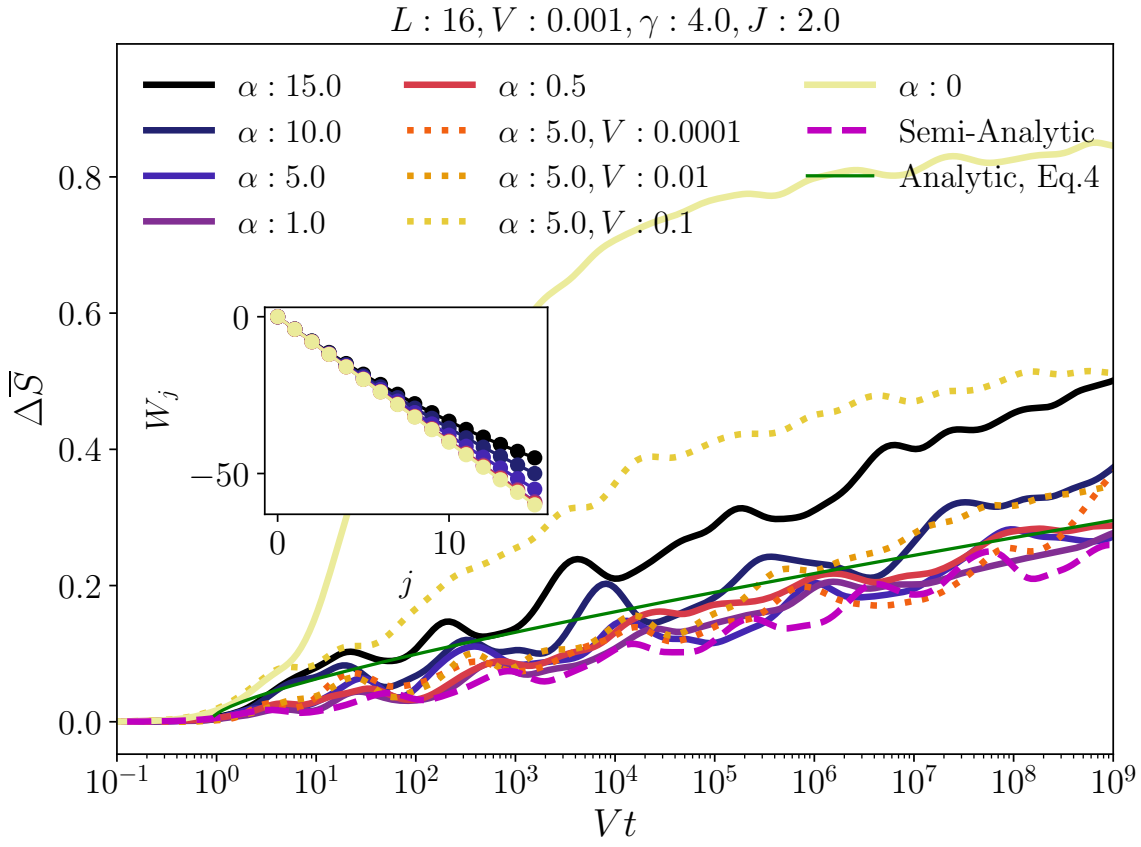

Figure 18.2: Difference ΔS between the bipartite entanglement in the interacting and non-interacting cases. The parameter α denotes the cumulative effect of field non-uniformity on the potential at the end site. For sufficiently small α and suitably large field γ there is good qualitative agreement with our semi-analytic calculation (magenta dashed line) and full analytic calculation (green line and Eq. (18.4)). For larger α, the entanglement growth becomes stronger than predicted due to the progressive delocalization of some of the single-particle orbitals as the position-dependent field gets weaker at the right-hand end of the chain (see right of inset). For the purely uniform field, there is an initial steep rise which we attribute to additional degeneracies of the many-body spectrum. The numerical curves have been smoothed by convolution with a Gaussian, $w(n) = e^{-(n/\sigma)^2/2}$, with $\sigma = 4$. Inset: Potential used in the respective main curves.

where a is the lattice spacing. Our potential is to a good approximation $V(x) = -\gamma x$, and hence $k(x) = \frac{1}{a}\arccos\left(\frac{\gamma x + E}{J}\right)$. Taking x to be large and positive, the exponent in the WKB wave function is thus given by $-\frac{1}{a}\int^x \ln\left(\frac{\gamma x'}{J}\right) dx' \approx -\frac{x}{a}\ln\left(\frac{\gamma x}{J}\right)$, where we have dropped a linear-in-x term that does not have a logarithm. Hence the form of the tail of the wave function is

$$\psi(x) \sim \exp\left[-\frac{x}{a}\ln\left(\frac{\gamma x}{J}\right)\right]. \tag{18.2}$$

We now use (18.2) to derive the form of the entanglement entropy $S(t)$ at long times, in analogy to Ref. [10]. The matrix element of the nearest-neighbor repulsion between a pair of localized particles at distance x is approximately $V\exp\left[-\frac{x}{a}\ln\left(\frac{\gamma x}{J}\right)\right]$, corresponding to a dephasing time of

$$t_{\text{deph}} \approx V^{-1}\exp\left(\frac{x}{a}\ln\left(\frac{\gamma x}{J}\right)\right). \tag{18.3}$$

This is the timescale on which the entanglement entropy due to this pair will rise from zero to its maximum value.

Now consider the total entanglement entropy of the subsystem. This can be thought of as an entanglement front moving through the system from the cut as t increases. At time t, this front will have moved a distance $x(t)$, which is obtained by solving (18.3) for x. The entanglement entropy will thus be $S(t) = S_{\max}\frac{x(t)}{L}$, where L is the length of the subsystem to the left of the cut. Solving (18.3) for $x(t)$, we obtain as entanglement entropy:

$$S(t) = \frac{S_{\max}}{L}\frac{a\ln(Vt)}{p\left(\frac{a\gamma\ln(Vt)}{J}\right)}, \tag{18.4}$$

where $p(u)$ is the solution of the equation $p\,e^p = u$.

We supplement this analytic approach by computing a 'semi-analytic' form for the entanglement entropy. For strong fields, $\gamma \gg J$, we may assume that the single-particle eigenfunctions of the Stark-localized states are restricted to three sites. We can thus write any initial state with fixed particle number M in fixed positions as

$$|\psi(t=0)\rangle = \sum_{\{Q\}} f_Q \beta^\dagger_{Q(j_M)}\beta^\dagger_{Q(j_{M-1})}\cdots\beta^\dagger_{Q(j_2)}\beta^\dagger_{Q(j_1)}|0\rangle, \tag{18.5}$$

where $\beta^\dagger_j$ creates a fermion in the single-particle Stark-localized state centered at position j. Here Q is an operation that, for each original site label j_i, either moves it one place to the left, moves it one place to the right, or leaves it alone. The factor f_Q is given approximately by

$$f_Q \approx \left(\frac{J}{\gamma}\right)^{\lambda_Q+\rho_Q}, \tag{18.6}$$

where λ_Q counts the number of original site labels that are shifted to the left by Q, and ρ_Q the number that are shifted to the right.

The energy E_Q of every state-component Q is composed of two parts: the electric potential energy, and the repulsive interaction energy of each pair of its constituent particles:

$$E_Q \approx E_0 + \gamma\left(\rho_Q - \lambda_Q\right) + \frac{V}{2}\sum_k\sum_{p\neq k}\left(\frac{J}{\gamma}\right)^{2|Q(j_k)-Q(j_p)|-2}, \tag{18.7}$$

where E_0 is the energy of some reference state and the sums over k and p run from 1 to M.

Combining (18.5) and (18.7), we obtain the initial state time-evolved to arbitrary times:

$$|\psi(t)\rangle = \sum_Q f_Q e^{-iE_Q t}\beta^\dagger_{Q(j_M)}\beta^\dagger_{Q(j_{M-1})}\cdots\beta^\dagger_{Q(j_2)}\beta^\dagger_{Q(j_1)}|0\rangle. \tag{18.8}$$

This allows us to calculate the time-evolved reduced density matrix of any subsystem, from which we obtain $S(t)$ via diagonalization. The results can be found in Fig. 18.2 and further details on the above calculation are found in [29].

Numerical simulations.

We now compare the above results against numerical simulations of the model (18.21). Hopping is set to $J = 2$ and we consider an $L = 16$ chain at half-filling. The field on one end has strength γ and decreases uniformly, so that the value of the potential on the final site of the chain differs by an amount α from its value in the purely linear case. We use all possible initial product states that do not have a particle on the two sites directly adjacent to the cut, which we choose to be at the middle bond. For $L = 16$, this amounts to 1225 states. Using exact diagonalization, we compute the time-evolution for a given initial state, and obtain the entanglement entropy $S(t)$ for an equal bipartition of the lattice. We then average over all of the abovementioned initial states.

Our results for $\gamma = 4$ and various values of α are shown in Fig. 18.2. In order to show the effect of interactions, we display $\Delta\overline{S}(t) \equiv \overline{S}(t) - \overline{S}_0(t)$, where $S_0(t)$ is the entropy in the non-interacting case, and the bar denotes an average over the initial conditions as discussed above. Consistent with previous findings, the entanglement growth due to many-body dephasing effects commences at times $Vt \sim 1$. The curves scale as a function of Vt, until the interactions become strong enough to alter the eigenstates significantly.

For sufficiently nonuniform field, this growth continues logarithmically up to a maximum value , which is finite for a finite system size. This growth agrees qualitatively with our semi-analytic calculation presented above, confirming our intuition that the physics of this system is well described by (18.5) and (18.7). We have also compared the pure analytic calculation (18.4) against the numerics. Here $S_{\max}$ is taken to be as the diagonal entropy S_{diag} resulting from the reduced density matrix obtained by (18.8). S_{diag} denotes the maximum achievable entropy for a given initial state, assuming that the interactions do not significantly change the form of the eigenstates [30, 10].

In the case of a strictly linear potential, there is instead a steep rise of the entanglement entropy followed by slow growth. We attribute this to the many exact degeneracies in the non-interacting version of the problem, which arise from the fact that all two-particle states with the same center of mass are degenerate, and can therefore hybridize strongly.

The logarithmic entanglement growth given by (18.4) can thus fail for two different reasons: too little non-uniformity, or too small a local field. The former allows delocalization of the two-particle states into a broad band, with a correspondingly short dephasing time, leading to steep initial growth of $\Delta\overline{S}(t)$. On the other hand, the latter causes the localization to weaken in parts of the chain, in turn making the accumulation of entanglement in that part stronger. The former case is shown in Fig. 18.2 for $\alpha = 0$, while the latter can be observed in the same panel for $\alpha = 15$. However, in between them there is a large range of curvature values for which an MBL-like entanglement growth is observed.

Many-body level statistics.

A powerful and basis-independent diagnostic to determine whether a model is localized is its spectral statistics [9, 32]. Fig. 18.3 shows our exact diagonalization results for the gap-ratio parameter in a chain of length $L = 16$ with open boundary conditions, for a range of field strengths γ and gradients α in the half-filled sector. The gap-ratio parameter is defined as $r_n = \min(\delta_n/\delta_{n+1}, \delta_{n+1}/\delta_n)$, where δ_n is the gap between the n^{th} and $(n-1)^{\text{th}}$ energy eigenvalues. Plotting a histogram of the gap-ratio parameter eliminates a dependence on the density of states, such that we can use the whole spectrum as long as there is no mobility edge

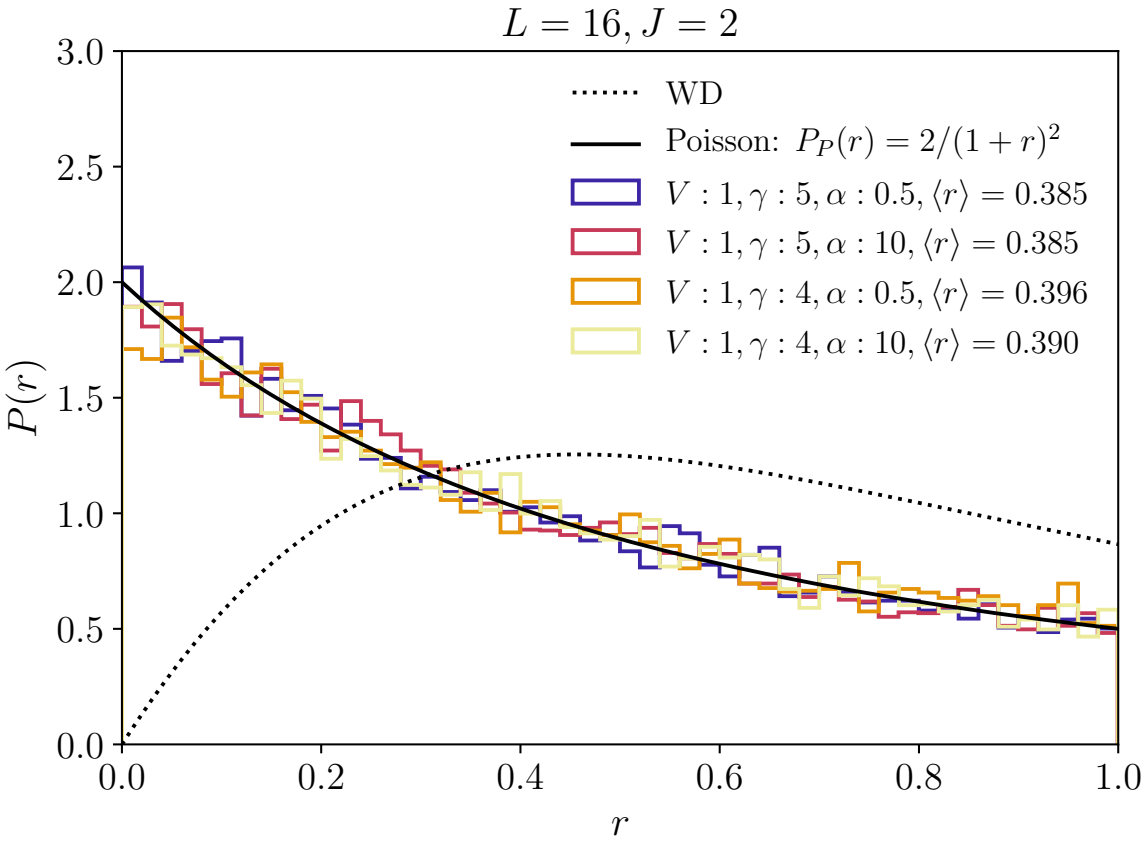

Figure 18.3: The many-body level statistics for the case of nonzero α in the half-filled sector. For all displayed values of γ and α the probability distribution of the gap-ratio parameter, $r_n = \min(\delta_n/\delta_{n+1}, \delta_{n+1}/\delta_n)$ (where δ_n is the gap between the n^{th} and $(n-1)^{\text{th}}$ energy eigenvalues), agrees with the prediction for Poisson level statistics expected for integrable or localized models. The predicted average gap-ratio parameter in this case is $\langle r\rangle_P = 0.3863$. For comparison we have included the prediction for Wigner-Dyson (WD) statistics.

present. We have verified this and the results are qualitatively the same for all ranges and energy densities used.

The probability distribution for Poisson statistics reads $P_P(r) = 2/(1+r)^2$, which is in excellent agreement with our results over most of our parameter range. In the case of very small or zero field gradient α however, we find results that are consistent neither with Poissonian nor with Wigner-Dyson (WD) statistics. We attribute this to the many exact degeneracies in the non-interacting problem creating a disproportionally large weight for small r_n in the many body spectrum. Interestingly we may further observe a cross-over to WD level statistics for small uniform field strength γ. Results for both of these cases can be found in the Supplemental Material [29].

Quench from charge-density wave.

While the entanglement and spectral statistics are experimentally difficult to extract, there are other indicators of localization. One of the simplest setups consists of monitoring the relaxation of an initial charge-density wave (CDW) order, in which all even sites are occupied [15]. An associated observable is the imbalance $\mathcal{I}$ between the occupation on odd and even

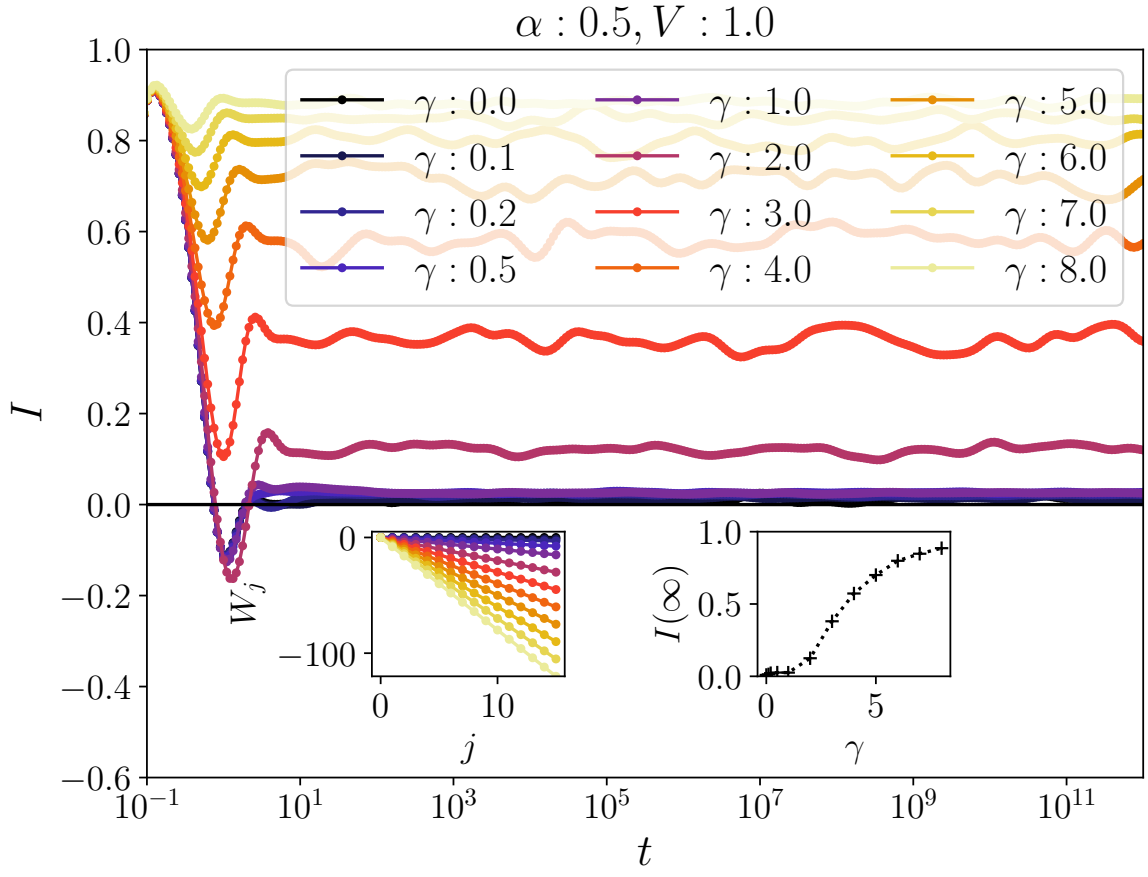

Figure 18.4: The $L = 16$ study of a hypothetical imbalance experiment, where an initial charge-density wave relaxes under unitary time-evolution. The different curves represent different field strengths γ with $\alpha = 0.5$. Inset left: Visualization of the corresponding potential. Inset right: Average imbalance $\mathcal{I}$ at times $10^{13} \geq t/J \geq 10^{11}$. The numerical curves have been smoothed by convolution with a Gaussian, $w(n) = e^{-(n/\sigma)^2/2}$, with $\sigma = 4$.

sites, N_o and N_e respectively,

$$\mathcal{I} = \frac{N_\mathrm{e} - N_\mathrm{o}}{N_\mathrm{e} + N_\mathrm{o}}. \tag{18.9}$$

In the ergodic, thermalizing case it should quickly decay to zero, which it does in the case $\gamma = 0$ when there is no Wannier-Stark localization. For a many-body localized system, on the other hand, the value of the imbalance should remain non-zero up to infinite times.

In Fig. 18.4, we show exact diagonalization results of the time-evolution of an initial CDW state under unitary time-evolution of (18.21). After initial transient behavior, the imbalance (18.9) remains non-zero for arbitrarily long times for sufficiently large fields.

Discussion.

In summary, we have shown that the experimentally natural case of a finite system in an electric field, a simple Wannier-Stark-localized system, shows properties that coincide with those of the MBL phase. While the case of a purely uniform field, $\alpha = 0$, remarkably turns out to be a non-generic limit, even moderate curvature gives consistent and robust MBL-like features. The bipartite entanglement entropy $S(t)$ exhibits a slow, logarithmic growth to a value much larger than that obtained in the non-interacting case. The spectral statistics, a dynamics-independent measure for localization, are Poissonian. And finally, localization seems

equally persistent in a now standard imbalance experiment, where the relaxation of CDW order is measured.

In the limit of large system sizes, the energy density can grow without bound on account of the unbounded potential implied by a uniform compound of the electric field. This precludes an asymptotic definition of exponential localization, which should however not pose a problem in practice given the attainability of short localization lengths. While the set-up of Stark-MBL is quite different from conventional disorder MBL, the similar phenomenology is quite striking. The MBL phase is described in terms of l-bits, while other disorder-free localized systems have also identified integrals of motion. Here, l-bits emerge naturally and robustly as Stark locators, again without the use of any quenched disorder. While finalizing this manuscript, we became aware of the related work by van Nieuwenburg *et al.* [33].

18.2 Supplementary material

18.2.1 Semi-analytic calculation of entanglement entropy

Model and initial condition

In the following we develop an approximate analytical description of the entanglement entropy growth in Stark-MBL from a specific product-state initial condition, which allows us to circumvent full diagonalization of the Hamiltonian, Eq. (1) of the main text. We shall assume that the number of sites, L, is even, and that the entanglement entropy is calculated across a cut between sites $(L/2)-1$ and $L/2$. We choose our zero of potential energy to lie in the middle of that bond. We shall often ignore the V-term, assuming that it is too weak to modify the form of the many-body eigenfunctions significantly, i.e. we consider the leading effect of V on energies, not wave functions.

Our initial condition involves placing fermions at the sites $S = \{j_k\}$, where $k = 1, 2, \ldots, M$, and M is the total number of fermions. Let $M = M_L + M_R$, where M_L and M_R are respectively the number of fermions to the left and right of the cut, and let us assume that the list S is in order from left to right (i.e. that $j_k < j_{k+1}$ for all relevant k). This initial condition can be written in second-quantized form as

$$|\psi\rangle = c^\dagger_{j_M} c^\dagger_{j_{M-1}} \ldots c^\dagger_{j_2} c^\dagger_{j_1} |0\rangle, \tag{18.10}$$

where $|0\rangle$ is the fermionic vacuum. Let us note that the electric potential energy of this state is given by

$$E_0 = \gamma \sum_{k=1}^{M} j_k, \tag{18.11}$$

where we have neglected the contribution of α.

Writing the initial condition in the many-body eigenbasis

Clearly we can only do this analytically if we ignore V, so we shall do that for now. In that case, we just need to know how to write the on-site creation operator in terms of creation operators for the Stark-localized states. If we assume the strong-field limit, i.e. that $\gamma \gg J$, then we may suppose that

$$c^\dagger_j = \sqrt{1 - 2\left(\frac{J}{\gamma}\right)^2}\, \beta^\dagger_j + \frac{J}{\gamma}\left(\beta^\dagger_{j+1} + \beta^\dagger_{j-1}\right), \tag{18.12}$$

where $\beta^\dagger_j$ creates a fermion in the single-particle Stark-localized state centered at position j. This assumes that the Stark-localized states are restricted to three sites (the central, or 'locator',

site and its two nearest neighbors). It also does not account for the mutual orthogonality of the different Stark-localized states, and it does not work at the very ends of the chain.

Substituting (18.12) into (18.10), we obtain the following:

$$|\psi\rangle = \sum_Q f_Q \beta^\dagger_{Q(j_M)} \beta^\dagger_{Q(j_{M-1})} \dots \beta^\dagger_{Q(j_2)} \beta^\dagger_{Q(j_1)} |0\rangle. \tag{18.13}$$

Here Q is an operation that, for each original site label, either moves it one place to the left, moves it one place to the right, or leaves it alone. The factor f_Q is given approximately by

$$f_Q \approx \left(\frac{J}{\gamma}\right)^{\lambda_Q + \rho_Q}, \tag{18.14}$$

where λ_Q counts the number of original site labels that are shifted to the left by Q, and ρ_Q the number that are shifted to the right.

Calculating the many-body energies of the components of the state

In order to time-evolve (18.13), we attach to each many-body state in the sum a factor of $e^{-iE_Q t}$, where E_Q is the state's energy. As we know from Ref. [10], we need to be more precise about the tails of the single-particle wave functions at this stage if we want to capture the entanglement evolution at late times.

The energy E_Q is composed of two parts: the electric potential energy, and the repulsive interaction energy of each pair of its constituent particles. The electric potential energy can be calculated by noting which particles have moved compared to the reference state:

$$E_{Q,\text{elec}} = E_0 + \gamma\left(\rho_Q - \lambda_Q\right). \tag{18.15}$$

The repulsive interaction energy may be roughly calculated by taking the probability density in the tail of one Stark-localized state at the center of the other and multiplying it by V. For two Stark-localized states with locators separated by ξ lattice sites, this gives an energy of approximately

$$V\left(\frac{J}{\gamma}\right)^{2\xi-2}. \tag{18.16}$$

Thus the complete energy of the state-component Q is given approximately by

$$E_Q \approx E_0 + \gamma\left(\rho_Q - \lambda_Q\right) + \frac{V}{2}\sum_k \sum_{p\neq k} \left(\frac{J}{\gamma}\right)^{2|Q(j_k) - Q(j_p)|-2}, \tag{18.17}$$

where the sums over k and p run from 1 to M.

Calculating the entanglement entropy as a function of time

We can thus approximate the state of the M-fermion system at an arbitrary time t as

$$|\psi(t)\rangle = \sum_Q f_Q e^{-iE_Q t} \beta^\dagger_{Q(j_M)} \beta^\dagger_{Q(j_{M-1})} \dots \beta^\dagger_{Q(j_2)} \beta^\dagger_{Q(j_1)} |0\rangle, \tag{18.18}$$

where f_Q is given by (18.14) and E_Q is given by (18.17). To turn this into a density operator it is more convenient to write it in first-quantized notation:

$$|\psi(t)\rangle = \sum_Q f_Q e^{-iE_Q t} \Big[|Q(j_1)\rangle \otimes |Q(j_2)\rangle \otimes \dots \tag{18.19}$$

$$\otimes |Q(j_{M-1})\rangle \otimes |Q(j_M)\rangle \Big], \tag{18.20}$$

where $|j\rangle$ is the single-particle state in which the particle is on site j. From this we obtain the density operator. We trace out the states on the right-hand side of the cut to construct the reduced density matrix on the left, and then use that to calculate the entanglement entropy $S(t)$. The results can be see in Fig. 2 of the main text.

18.2.2 Level statistics in the case of too little field non-uniformity

In this section we present the case in which the field non-uniformity is not strong enough, hence in which case α is too small. We recall from the main text that the model reads

$$\hat{H} = \frac{J}{2}\sum_{j=0}^{L-2}\left(c_j^\dagger c_{j+1} + \text{h.c.}\right) + \sum_{j=0}^{L-1} W_j\left(n_j - \frac{1}{2}\right) + V\sum_{j=0}^{L-2}\left(n_j - \frac{1}{2}\right)\left(n_{j+1} - \frac{1}{2}\right). \quad (18.21)$$

Here the operator $c_j^\dagger$ creates a fermion on lattice site j, and the associated number operator $n_j = c_j^\dagger c_j$. $J/2$ is the hopping matrix element between neighboring sites, V is the strength of the nearest-neighbor repulsion, and L is the number of sites of the lattice, the boundary conditions of which we take to be open.

W_j is the on-site potential energy due to the applied electric field. For a uniform field γ, it takes the form $W_j = -\gamma j$. For a non-uniform field, it acquires some curvature, $W_j = -\gamma j + \alpha j^2/L^2$. This means that the potential has the same value and slope as the linear one at $j = 0$, but differs at the other end of the chain by α from the purely linear case.

Numerically diagonalizing (18.21), and then obtaining the level-statistics and more specifically the gap-ratio parameter, $r_n = \min(\delta_n/\delta_{n+1}, \delta_{n+1}/\delta_n)$ (where δ_n is the gap between the n^{th} and $(n-1)^{\text{th}}$ energy eigenvalues) allows us to make predictions about the existence of a localized phase. In Fig. 18.5 we show the case for small and zero α in which the system exhibits neither Poisson nor Wigner-Dyson level statistics. The disproportionately large weight for small r_n in this case is in line with our reasoning that this failure to exhibit Poisson or Wigner-Dyson level statistics is due to the many exact degeneracies in the non-interacting problem.

18.2.3 The cross-over from Wigner-Dyson to Poisson

In this section we present additional results on the cross-over from Wigner-Dyson (WD) to Poisson statistics in the case of vanishing field γ with fixed α. In this *finite* lattice setup this means that as $\gamma \to 0$, the localization length of the single particles will grow larger than the length of the chain, thus making the system effectively delocalized. We note that this relies on α being chosen small enough such that it does not provide any effective single-particle localization itself. The level statistics in this case were obtained as described in the previous section. The results are shown in Fig. 18.6. We clearly see the cross-over from WD to Poisson statistics for increasing field strength. The inset illustrates this particularly well, displaying the average gap-ratio parameter $\langle r\rangle$ as a function of γ. As a reminder we note that the expected value for Poisson statistics is $\langle r\rangle_{\text{P}} = 0.39$, while for WD statistics, $\langle r\rangle_{\text{GOE}} = 0.53$ (in the symmetry class of the Gaussian Orthogonal Ensemble) is the expected value.

We may further investigate the finite-size scaling of the gap-ratio parameter r. The results of this are shown in Fig. 18.7. As can be seen from the finite-size scaling of small systems in Fig. 18.7, there is no significant flow towards either the Poisson or the WD limit when the system is made larger. As such we expect the phenomenology of Stark MBL, including the cross-over to WD statistics to be visible in realistic finite size experimental setups. It remains

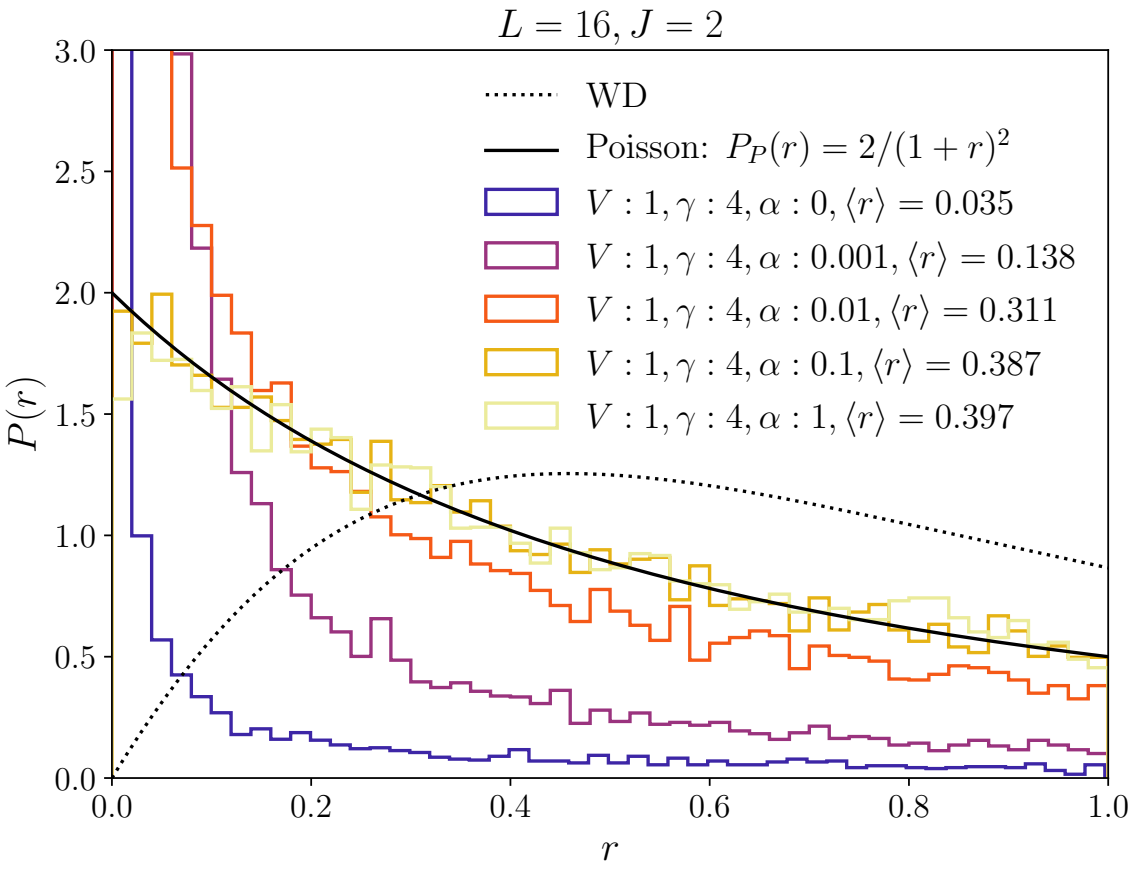

Figure 18.5: Illustration of the many-body energy level statistics for the half-filled sector as shown in Fig. 3 of the main text. Again, we study the probability distribution of the gap-ratio parameter, $r_n = \min(\delta_n/\delta_{n+1}, \delta_{n+1}/\delta_n)$ (where δ_n is the gap between the n^{th} and $(n-1)^{\text{th}}$ energy eigenvalues). Here we illustrate the case of small or zero α in which Stark MBL is absent, which we attribute to the many exact degeneracies in the non-interacting problem. This creates a disproportionately large weight for small r_n in the many body spectrum clearly illustrated in the case of small or zero α.

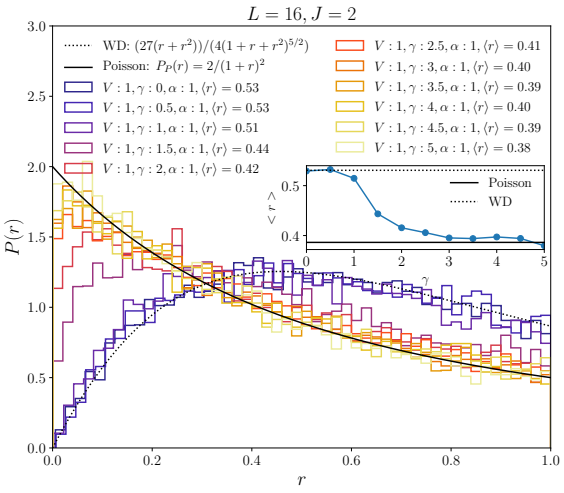

Figure 18.6: Illustration of the many-body energy level statistics for the half-filled sector as shown in Fig. 3 of the main text. Again, we study the probability distribution of the gap-ratio parameter, $r_n = \min(\delta_n/\delta_{n+1}, \delta_{n+1}/\delta_n)$ (where δ_n is the gap between the n^{th} and $(n-1)^{\text{th}}$ energy eigenvalues). Here we illustrate the cross-over from Wigner-Dyson to Poisson level statistics for fixed α but changing uniform field strength γ. The crossover is clearly visible with the inset showing the average gap-ratio parameter $\langle r \rangle$ as a function of γ.

an interesting open question how the gap-ratio parameter would behave in the limit of very large system size.

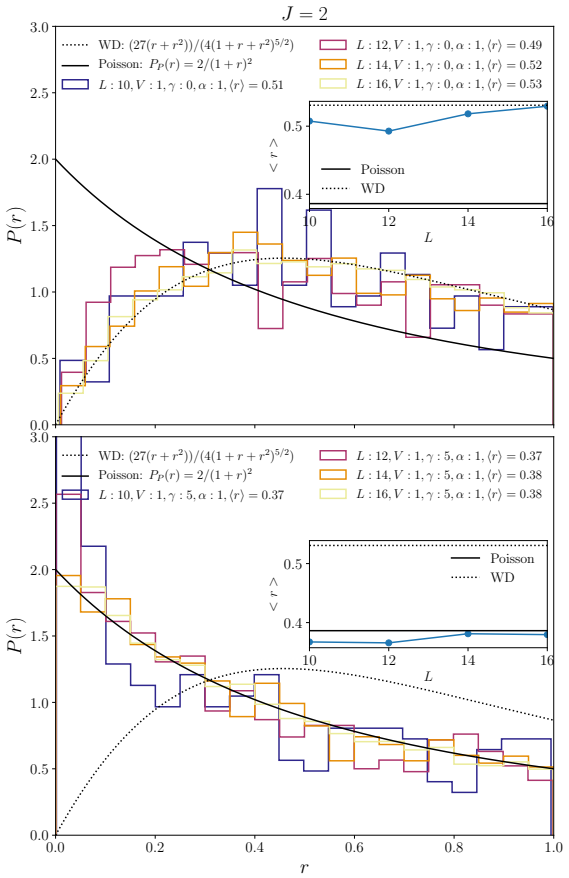

Figure 18.7: Finite-size scaling of the gap-ratio parameter as described in previous figures. The two panels show the distribution of the gap-ratio parameter for two different values of the field-strength γ, namely $\gamma = 0$ and $\gamma = 5$, for different system sizes L. As far as the presented system sizes are concerned, we do not observe any significant flow towards the Poisson or Wigner-Dyson limit as the system size L grows and therefore we expect the presented physics to be observable in any realistic finite experimental setup. The insets shows the average gap-ratio parameter as a function of system size L.

19 From Bloch Oscillations to Many Body Localization in Clean Interacting Systems by van Nieuwenburg, Baum, Refael

Abstract

In this work we demonstrate that non-random mechanisms that lead to single-particle localization may also lead to many-body localization, even in the absence of disorder. In particular, we consider interacting spins and fermions in the presence of a linear potential. In the non-interacting limit, these models show the well known Wannier-Stark localization. We analyze the fate of this localization in the presence of interactions. Remarkably, we find that beyond a critical value of the potential gradient, these models exhibit non-ergodic behavior as indicated by their spectral and dynamical properties. These models, therefore, constitute a new class of generic non-random models that fail to thermalize. As such, they suggest new directions for experimentally exploring and understanding the phenomena of many-body localization. We supplement our work by showing that by employing machine learning techniques, the level statistics of a system may be calculated without generating and diagonalizing the Hamiltonian, which allows a generation of large statistics.

19.1 Introduction

Since the phenomenon of many-body-localization (MBL) was re-postulated more than a decade ago [1, 2, 3], it has attracted a great deal of attention. It provides an example of a generic quantum many-body system that cannot reach thermal equilibrium [4, 5, 6, 7]. In recent years, an enormous theoretical effort was invested in understanding the nature of the MBL transition [8, 9, 10], the dynamical [11, 12, 13] and entanglement [14, 15, 16, 17] properties of these systems and their response to external probes [18, 19] and periodic driving [20, 21, 22]. Also the experimental community [23, 24, 25, 26, 27] has found interest in this field, in particular, because these systems have the potential of storing information about initial states for long times, and hence may implement quantum memory devices. These systems may also be useful for dynamical quantum control, as they allow the application of driving protocols without heating the system to an infinite temperature.

A key ingredient for achieving the MBL phase is disorder (randomness). The roots of this phase lie within the phenomenon of Anderson localization [1], where non-interacting particles form a localized non-ergodic phase. Questioning the fate of Anderson localization in the presence of interactions led to the discovery of the MBL phase.

In this work we ask whether randomness is indeed an essential ingredient in achieving generic non-ergodic interacting phases. Viewing MBL as a competition between single-particle localization and interactions, one may wonder whether a localizing mechanism that does not require disorder may produce similar results. It was suggested that quasi-many-body localization may exist in a translationally invariant quantum system such as a quantum disentangled liquid [28, 29, 30, 31], where light particles evade thermalization (for long times) by localizing on heavy particles [32, 33, 34, 35, 36]. Moreover, it was shown that clean 1D systems with quasi-periodic potentials may host an MBL phase [37, 38, 39]. While quasi periodic systems are not considered disordered, they do not respect exactly the discrete translational symmetry of the lattice either and can not be treated in momentum space. Other proposals (Ref. [40]) suggested the appearance of non-ergodic dynamics for a large portion of states belonging to the low energy subspace of the cubic code Hamiltonian which involves eight-spin interaction terms. The model we propose in this work respects the crystal symmetry exactly, and hence, in that regard it is a realizable and a truly discrete translational invariant model. We show

that this model supports a phase that is indistinguishable from the MBL phase based on all the standard characteristics.

A well known mechanism for localizing single particles is the Wannier-Stark effect [41], in which particles living on a lattice become localized in the presence of a linear potential. We refer to this phenomenon as Bloch localization. Notice that beside lacking randomness, such systems also preserve translation-invariance as the linear potential represents a uniform force and may be replaced by a time-dependent vector potential. One may consider Wannier-Stark effect as a particular case of dynamical localization [42] with linear-in-time vector potential. While no physical difference is expected between the different gauges, the thermodynamic limit in the time-dependent gauge avoids the existence of an infinite energy difference between the edges of the system. Nevertheless, we chose to work in the static gauge since in this work we are only interested in static forces and since it dramatically reduces the numerical effort. In the appendices we show that our numerical method is, as expected, indifferent to the choice of gauge. The fate of dynamical-localization in the case of time dependent fields has been discussed in Refs. [43, 44]. The interplay between interactions and linear fields has been investigated in the past. It was shown that the oscillatory part of the current, i.e. Bloch oscillations (BO), decays as the interaction strength increases [45, 46]. It was also shown that the presence of a uniform force changes the nature of the evolution of an initial state under the non-linear Schrödinger equation (NLSE) as the non-linearity increases, e.g., for a large non-linearity the dynamics is localized. Yet, the ergodic properties and the generality (stability) of these phases can not be inferred from these works. The absence of BO does not necessarily signify ergodicity and the dynamics of generic interacting models can not be captured by the NLSE, which is generally valid only as a mean field description of weakly interacting Bosons [47]. Moreover, only the evolution of low energy (near ground state) states have been considered and the stability of the above phenomenon was not analyzed. In this work we show that single-particle-localization that is not necessarily due to disorder, results in a state that is indistinguishable from the MBL state based on the typical tools of assessment. We analyze the spectral and the dynamical properties of one-dimensional interacting fermions and spins in the presence of both disorder and a linear potential. We show that by considering these two different localizing mechanisms, i.e., disorder (W) and linear fields (F), one may construct a two-dimensional phase diagram in the (F, W)-space which hosts a connected non-ergodic (MBL) phase. We find that above a critical value F_c, the MBL phase extends down to the clean limit, i.e., the $W = 0$ line.

It is worth mentioning that integrable models, such as the 1D Heisenberg and transverse field Ising models, are known examples of clean models that fail to thermalize. While these models fail to thermalize, they are sensitive to the existence of small integrability-breaking terms such as disorder or longer range interactions and hopping. In this sense the model we suggest is more generic, since the addition of disorder and/or weak longer range hopping and interactions does not lead to thermalization.

The existence of generic clean models that fail to thermalize may have important implications both theoretically and experimentally. From the theory side, it can simplify dramatically the numerical effort in analyzing these interacting systems. Moreover, the lack of randomness gives hope that the nature of the MBL transition, the emergent conserved quantities and the generalization to higher dimensions may be approached analytically. From the experimental side the necessity of strong disorder is a major drawback. In intrinsic systems it is not clear whether such strong disorder generically exists. In controlled systems, such as optical lattices, only quasi-random disorder or correlated disorder, e.g. speckle potentials, may be implemented and a repetition over many realizations is needed due to the small size of the systems [48, 49]. In stark contrast, linear field (tilt in optical lattices) may be implemented relatively easily and it provides the ability to experimentally realize these systems in a highly reproducible way, and without the necessity of many repetitions. Unlike integrable models, the inevitable existence

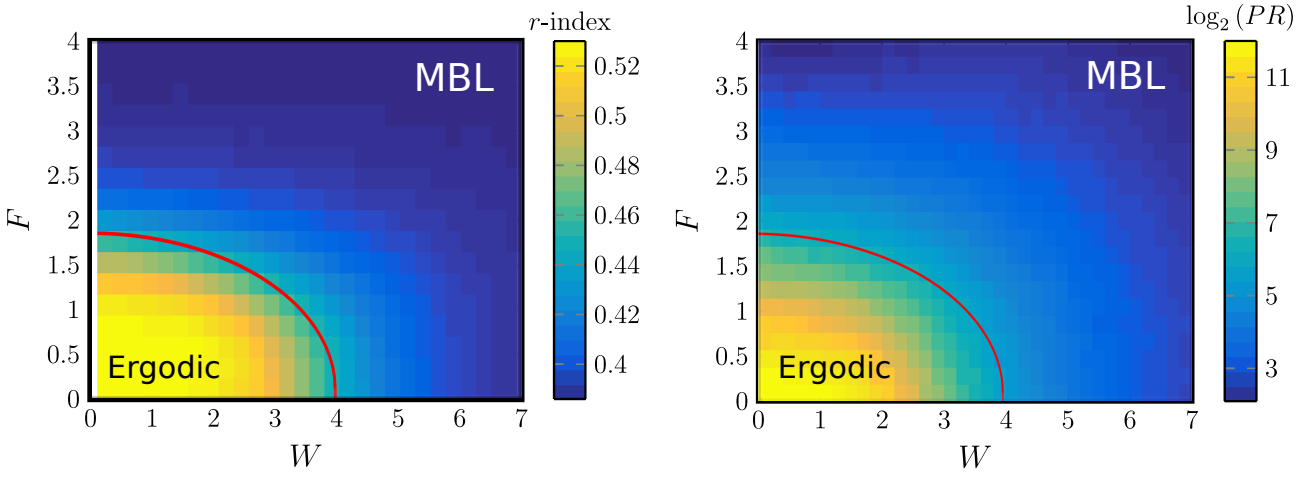

Figure 19.1: These plots constitute the main results of the paper and demonstrate the existence of a potential-gradient induced MBL phase. (a) The r-index as a function of disorder and field strength as calculated for the Hamiltonian in Eq. (19.5) with $L = 16$ and $J_0 = J_z = 1$ (averaged over 125 realizations). Evidently, a phase boundary exists between a region with $r = 0.53$ (Wigner-Dyson) for small values of W and F (the ergodic dome) to a region with $r = 0.386$ (Poisson). (b) The averaged participation ratio ($PR = 1/IPR$) as a function of disorder and field strength for the same system as in (a). Consistently with the level statistics, inside the ergodic dome the PR is proportional to the Hilbert space dimension ($\mathcal{D}$), while outside the dome it becomes small and independent of $\mathcal{D}$. Notice that in (b) the line $W = 0$ is included in the data. In both cases the red line serves only as a guide to eye and is a contour or $r \approx 0.46$.

of unwanted terms such as weak disorder, should not have a dramatic effect on the dynamics.

19.2 Background and Model Definition

19.2.1 Bloch localization

Our ultimate goal is to understand the fate of Bloch localization in the presence of interactions. In this section we briefly review the properties of non-interacting particles in the presence of a uniform force (linear potential). Consider a 1D lattice model in the presence of a linear potential,

$$H_0 = \sum_j t(c_j^\dagger c_{j+1} + h.c) - Fjc_j^\dagger c_j, \tag{19.1}$$

where c_j annihilates a particle from lattice site j, t is the nearest neighbor hopping amplitude, and F is the uniform force. The Hamiltonian can be diagonalized by the following transformation,

$$b_m = \sum_j \mathcal{J}_{j-m}(x)\, c_j, \tag{19.2}$$

with $\mathcal{J}_n$ being the Bessel functions of the first kind and $x = 2t/F$. Under this transformation Eq. (19.1) becomes,

$$H_0 = -\sum_m Fm\, b_m^\dagger b_m. \tag{19.3}$$

Since $|\mathcal{J}_n(x)| < e^{-|n|}$ for $x \ll n$, all the eigenstates are localized for any $F \neq 0$. Each eigenstate, $b_m^\dagger|vac\rangle$, is localized around site m with an inverse localization length given by $\xi^{-1} \approx 2\sinh^{-1}(1/x)$.

Unlike for Anderson localization, where the localization length is energy dependent (smaller near the middle of the energy band), for Bloch localization case the localization length is an energy independent quantity. Another prominent difference between the two is the form of the density of states, where in the case of Bloch localization the spectrum forms an ordered ladder even deep in the localized phase.

19.2.2 Model Definition

The basic model we wish to analyze concerns the interplay between the two mechanisms of single particle localization (disorder and linear field) and interactions. For that, we consider a 1D lattice of interacting spinless fermions in the presence of disorder and a uniform force,

$$H = \sum_j t(c_j^\dagger c_{j+1} + h.c) - Fjn_j + h_j n_j + U n_j n_{j+1}, \tag{19.4}$$

where c_j annihilates a particle from lattice site j, $n_j = c_j^\dagger c_j$ is the density, t is the nearest-neighbor (nn) hopping amplitude, F is the uniform force, $h_j \in [-W, W]$ is a random on-site potential with strength W and U is the nn interaction strength.

The above fermionic Hamiltonian may be mapped, via a Jordan-Wigner transformation, into an equivalent spin-1/2 chain (Heisenberg),

$$H = \sum_j J_0(S_j^x S_{j+1}^x + S_j^y S_{j+1}^y) + J_z S_j^z S_{j+1}^z + FjS_j^z + h_j S_j^z, \tag{19.5}$$

with $J_0 = 2t$ and $J_z = U$ while F and $h_j \in [-W, W]$ defined as before. In the rest of this paper we will analyze the localization and dynamical properties of these Hamiltonians as a function of the interaction strength, force and disorder strength. Since the particle-number (fermionic model) or the total S_z (spin model) are conserved, we focus our analysis on the half-filled ($S_z = 0$) sector. Regardless, the results do not depend much on the specific sector.

19.3 Results and Discussion

19.3.1 Level statistics

A well established signature for the transition from ergodic to non-ergodic dynamics is the level statistics of the many body spectrum. In particular, generic ergodic Hamiltonians belong to the Gaussian Orthogonal Ensemble (GOE) [50, 51] and their level-spacings, $\delta_n = \epsilon_{n+1} - \epsilon_n$, typically obey the Wigner-Dyson distribution. On the other hand, for non-ergodic systems the level-spacings typically obey the Poisson distribution. It should be pointed out that in both cases, symmetries may add high level of degeneracies which lead to deviation from the Wigner-Dyson distribution (non-ergodic) and from perfect Poisson distribution (ergodic). Yet, level spacing obtained from symmetry sectors should not have these additional degeneracies. As in the case of the disordered Heisenberg chain within the sector of zero total magnetization, the transition from ergodic to non-ergodic is accompanied by a transition from Wigner-Dyson to Poisson level statistics [9].

Both distributions are often characterized by a single parameter, $r = \langle \min(\delta_n, \delta_{n+1}) / \max(\delta_n, \delta_{n+1}) \rangle$, which conveniently avoids the need for unfolding the spectrum. For the Wigner-Dyson distribution $r \approx 0.530$ and $r = \ln 4 - 1 \approx 0.386$ for the Poisson distribution.

We diagonalize the Hamiltonian in Eq. (19.5) for $L = 12, 14, 16, 18$ spins using exact diagonalization, with $J_0 = J_z = 1$ and for different values of F and W. In the appendices we show

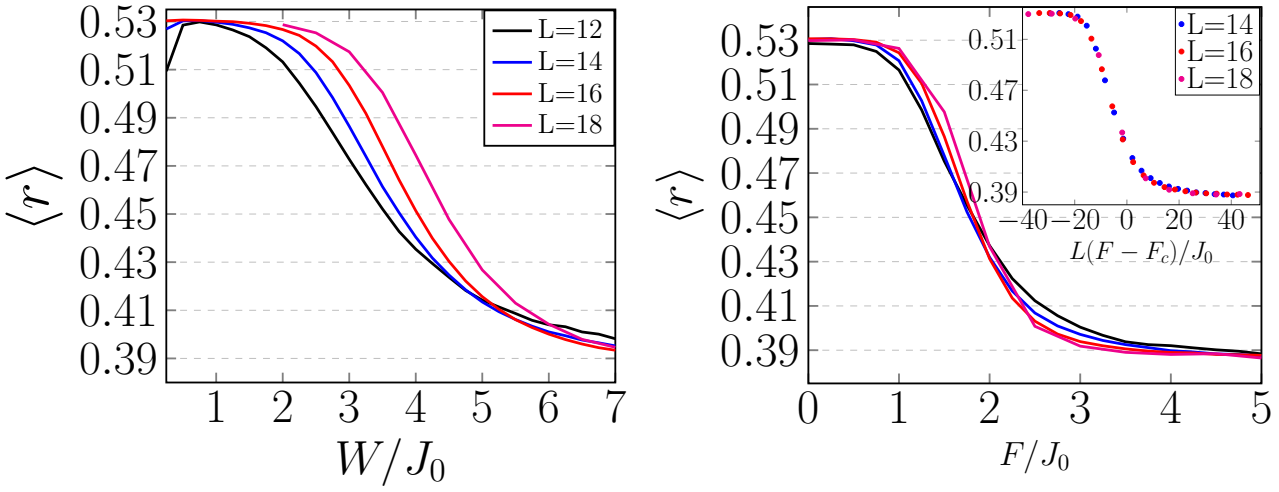

Figure 19.2: The r-index as calculated for the Hamiltonian in Eq. (19.5) with $J_0 = J_z = 1$ for different system sizes, $L = 12, 14, 16, 18$. In (a) the r-index is plotted as a function of W for zero linear field. In (b) the r-index is plotted as a function of F for a fixed disorder strength $W = 0.5$, where in the inset we plotted the data as a function of $L(F - F_c)$ with $F_c = 2.2$.

that by employing machine learning techniques, statistics for the r-value may be generated from h_j directly without the need of diagonalizing the Hamiltonian.

In Fig. 19.1(a) we show the r value (averaged over different disorder realizations) in the space of (F, W). We find that the ergodic phase lives in a dome-shaped region near the origin of the (F, W) space. The line $F = 0$ corresponds to the often discussed MBL transition near the critical disorder strength W_c. As F increases, the value of W_c decreases. Above a critical value of F, the critical disorder appears to go to zero and the non-ergodic phase appears also in the clean non-disordered limit.

In Fig. 19.2 we show the r value for different system sizes as a function disorder (zero field) and as a function of the field (for a fixed weak disorder). The critical values may be extracted by finite size scaling through a scaling collapse. The case of zero field was analyzed in several works [8, 52, 53, 54] in which the critical disorder was found to be in the range $W_c \sim 7.5 \pm 0.5$ (notice a factor of 2 due to a different definition of the spin matrices). For the weak disorder case we plot the data, Fig. 19.2 (inset), as a function of $L^{1/\nu}(F - F_c)$. We find that the critical exponent is $\nu \approx 1$ and the critical field is $F_c \approx 2.2$, for which the data collapse on one curve. In the appendices we provide more details regarding the finite size scaling, and show that the above results are not sensitive to integrability-breaking terms such as next-next-nearest-neighbor hopping and interactions.

Notice that in this part, we always considered $W > 0.2$, since for small enough disorder, small systems behave as clean systems which leads to symmetry related degeneracies in the spectrum.

19.3.2 Inverse participation ratio

Analyzing level statistics of clean systems requires a separation of the Hilbert space into momentum sectors, since degeneracies due to symmetries have to be removed. For finite systems and below a critical disorder strength, the system behaves similar to a clean system. Therefore, the level statistics becomes a less reliable measure for small disorder strengths since degeneracies start to appear due to the emergence of translation symmetry. A quantity which is less sensitive

to symmetries is the inverse participation ratio (IPR). The IPR is also a measure of the long-time return probability of arbitrary initial states. To see that, consider the return probability of a state $|\psi_0\rangle$,

$$P(t) = \left|\langle\psi_0|\hat{U}(t)|\psi_0\rangle\right|^2, \tag{19.6}$$

where $\hat{U}(t)$ is the time evolution operator. The state $|\psi_0\rangle$ may be expanded in terms of the Hamiltonian eigenstates, $|\psi_0\rangle = \sum_n c_n|\phi_n\rangle$ which allows to write the IPR (long-time limit of the return probability) as,

$$IPR = \lim_{T\to\infty}\frac{1}{T}\int_0^T dtP(t) = \sum_{n,m}|c_n|^2|c_m|^2\delta_{\epsilon_n,\epsilon_m}. \tag{19.7}$$

In the absence of degeneracies, Eq. (19.7) becomes $IPR = \sum_n |c_n|^4$. Clearly, if the initial state is an eigenstate then $IPR = 1$, while if the initial states is an equal-superposition of all the eigenstates then $IPR = 1/\mathcal{D}$, where $\mathcal{D}$ is the Hilbert space dimension which generically is exponential in the system size. In the following we average the IPR over different initial states which we choose to be eigenstates of some local operators, e.g., s_j^z. For ergodic systems, the IPR should be exponentially small in the system size and the system should lose its memory of the initial state. In stark contrast, in the localized phase the IPR converges to a positive system size independent constant.

In Fig. 19.1(a) we present the averaged and normalized participation ratio, $\langle PR\rangle = \mathcal{D}/IPR$, in the space of (F, W). While the IPR is a smooth function, there is a transition between a region where the IPR is exponentially small to a region where the IPR is independent of system size. These regions agree with the results obtained in the previous section. Here also the line $W = 0$ behaves in a similar way (c.f. Fig. 19.1(b)), where the IPR becomes independent of system size as a function of F.

19.3.3 Dynamics and experimental measurables

The distinction between ergodic and non-ergodic dynamics is well-captured by the level-statistics and the participation ratio. Yet both these measures are hard to access in experiments. As shown in Refs. [24, 25, 27], the nature of the dynamics is examined by tracking the dynamics of an initially prepared out-of-equilibrium density configuration. We numerically show that the existence of a linear field prevents thermalization. For concreteness, we consider a similar out-of-equilibrium initial state as in Ref. [24]. The system is prepared in a anti-ferromagnetic configuration (or charge density wave for the fermions), where the spins on odd sites point down (empty) and on even sites point up (full). We then track the time evolution of the odd-even imbalance, $I = (S^e_{z,\uparrow} - S^o_{z,\uparrow})/(S^o_{z,\uparrow} + S^e_{z,\uparrow})$. We use a numerical method based on Krylov-subspaces via a re-orthogonalized Lanczos implementation to do so (see the appendices for more information).

In the inset of Fig. 19.3 we show the resulting long time limit as a function of F. Below a critical value $F \lesssim F_c$ the long time limit of $\mathcal{I}$ tends to zero, while above that value the long time limit tends to a finite value that increases with the field. Computational costs limit the available times we can access, and we remark that not each of these curves have converged yet. Extrapolating the available curves will move the estimated critical field to higher values than suggested by the inset.

In ergodic systems, $\mathcal{I}$ is expected to decay to zero with a typical relaxation time τ. We show that while indeed this is the case when the linear field is small, both for the clean case and for weak disorder, beyond a critical field strength, the long time limit of $\mathcal{I}$ is different from zero. In Fig. 19.3 we show the imbalance $\mathcal{I}$ in a system of 24 spins (sites) as a function of

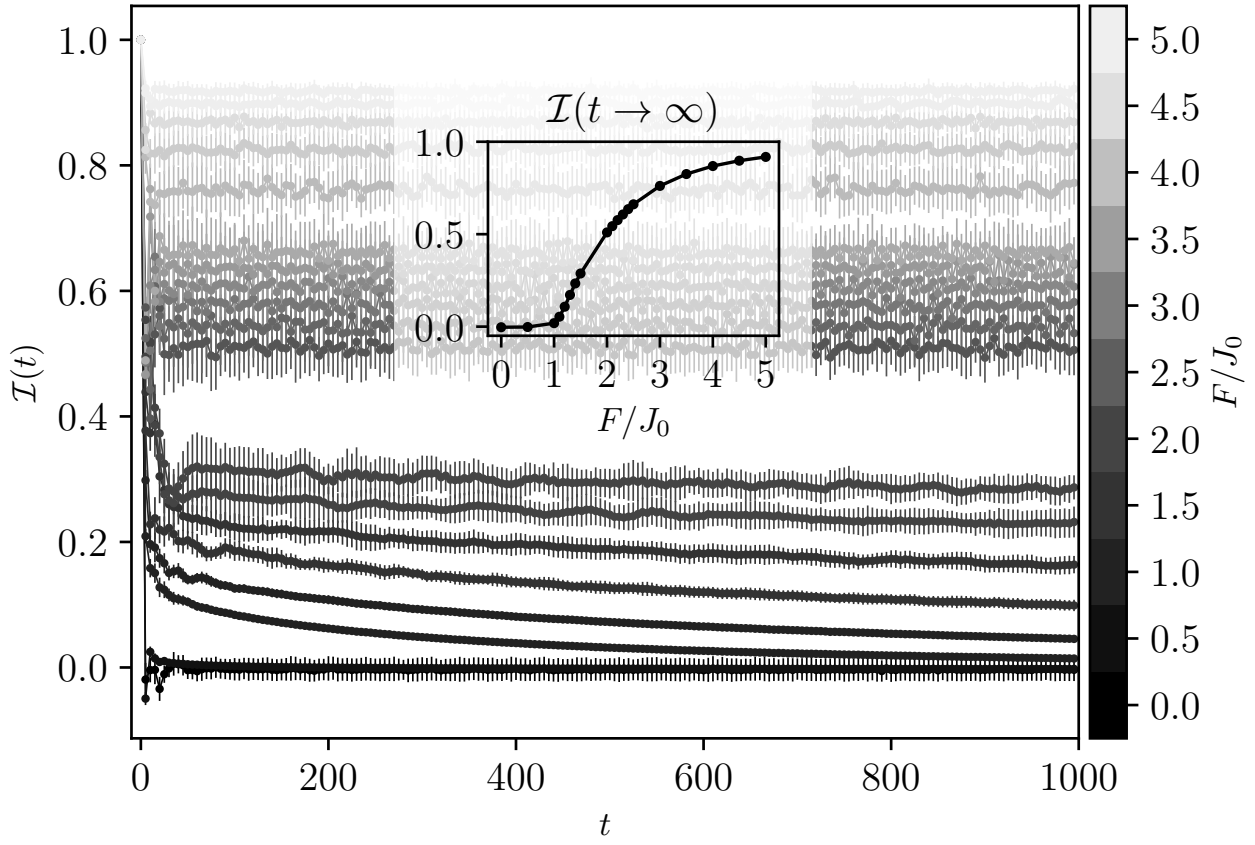

Figure 19.3: The imbalance $\mathcal{I}$ as a function of time for different field strength and for fixed weak disorder $W = 0.2$, where $L = 24$, $J_z = J_0 = 1$. At $t = 0$, the imbalance for each field strength starts at $\mathcal{I}(t = 0) = 1$. For field strengths above (and including) $F = 2.0$ we can not identify decaying behavior at these time-scales. Error bars show statistical variance over 32 realizations of disorder. The inset shows the long time limit of the imbalance as a function of the field (averaged over the last 50 timesteps). Below a critical value $F \lesssim F_c$ the long time limit of $\mathcal{I}$ tends to zero, while above that value the long time limit tends to a finite value that increases with the field. Notice that some of the lower F curves have not yet reached their final value.

time for different values of the field F and for a fixed weak disorder strength ($W = 0.2$). It is worth noticing that energetics gives an upper bound to this relaxation process. In the fermionic language, the charge density wave (CDW) configuration and the uniform configuration differ in their dipole moment $D = \sum_j j n_j$ by an extensive amount $\Delta D = N/4$. In the absence of a field, the many-body bandwidth of the Heisenberg model with all $J = 1$ is $\log(2)N$. Hence, in the presence of a field, if $F\Delta D > \log(2)N$ or $F > 4\log(2) \approx 2.77$ the CDW configuration can not evolve into a uniform configuration at any time. In practice, the critical field obtained from the the level statistics is around $F \sim 2.2$ while it seems that the dynamics suggests a slightly lower value (notice that not all of the imbalance curves have converged yet). Yet, while the the true critical field (if it exists) should limit the dynamics of all processes, specific processes like the one considered here may show non-ergodic dynamics at lower values. Moreover, one may consider the presence of a pre-localized phase (or pre-thermal for that matter) that appears in the dynamics. Our numerical data cannot confirm or disprove the existence of such a phase. An analysis of larger systems, and more importantly, much longer times, may resolve that issue.

19.4 MBL in two-dimensions

The lesson we learned about the effect of interaction on the Anderson localized (AL) phase in 1D can not be trivially extended to higher dimensions. The nature, and even the existence, of a many-body-localized phase in $D > 1$ is a hotly debated subject. While theoretical works [55, 56, 57] showed that locally thermal regions in systems with true random disorder can destabilize the MBL phase in two dimensions, experimental works [24, 26, 27] have shown indications for such a phase in $D > 1$.

Similar questions may be posed in the context of the uniform field as a cause for single particle localization. In stark contrast to the AL phase, this phase is not sensitive to rare regions. In particular, if the field is applied at an irrational angle, the field is non-zero along all lattice directions. This field can indeed be arbitrarily small for specific lattice directions, but can be chosen such that lattice sites along directions at which the field is below the critical value are separated by multiple hops. Since each of these hopping processes has a component against a strong field, and since the bare interaction is local, both the effective hopping coefficient and the effective interaction along these directions may be extremely small. How these renormalized hopping coefficients and interactions scale with the field along these direction, and whether it is possible to choose the field such that along each lattice direction the field is larger than the 1D critical field, is an interesting question worth further investigation. Additionally, along these same lattice directions the linear potential is not perfect and can be regarded as a combination of a linear field and weak quasi-periodic disorder. This quasi-periodic disorder may also help the localization along directions where the field is small. Finally, the absence of rare regions (which are a main reason to exclude MBL in high dimensions [56]) may help the survival of the non-ergodic behavior in the thermodynamic limit.

To further speculate on the existence of MBL in 2D, Fig. 19.4 shows the level statistics (r index) of a 2D Heisenberg model as a function of the uniform force $\mathbf{F} = F(\sqrt{2}, 1)$ and disorder. Similar to the 1D case, we see a clear transition from a Wigner-Dyson distribution to Poisson distribution. Since we are restricted to very small system sizes (4×4 lattice), these results should not be taken as a claim of the existence of a two dimensional MBL phase. However, we hope that these ideas will stimulate further works in this directions.

19.5 Dipole moment analysis

Single-particle Wannier-Stark localization may be thought of in terms of energetic constraints imposed by the field. In the many-body case, one may wonder whether interactions can help overcome energetic constraints by reordering of particles. Heuristically, a many-body configuration can be described by its dipole moment D (see section 19.3.3), which in the presence of a field F is associated with an energy FD. In order for such a configuration to evolve into a different configuration with dipole moment $\tilde{D}$, the internal structure of the system, i.e., hopping and interaction, must be able to supply the energy difference $F(D - \tilde{D})$. This condition is captured in the dipole moment structure of the eigenstates. Clearly, in the infinite field limit of our model, the dipole moment becomes an exactly conserved quantity. In that case an analogy with Ref. [58] can be made, where it was shown that non-ergodic dynamics arises in a one dimensional random quantum circuit model which is constrained to conserve both a $U(1)$ charge and the dipole moment of this charge.

The main question is to what extent the dipole moment may be considered as a conserved quantity for finite fields. In the appendices we show the results of exact diagonalization of a half-filled fermionic system where each point represents an eigenstate in the space of energy and dipole-moment. As expected, in a given energy window and for large field the many body wave functions have well-defined dipole moment. Each dipole moment sector is further split into subsectors of doublon (occupied neighboring sites) number. Hence the dynamics is

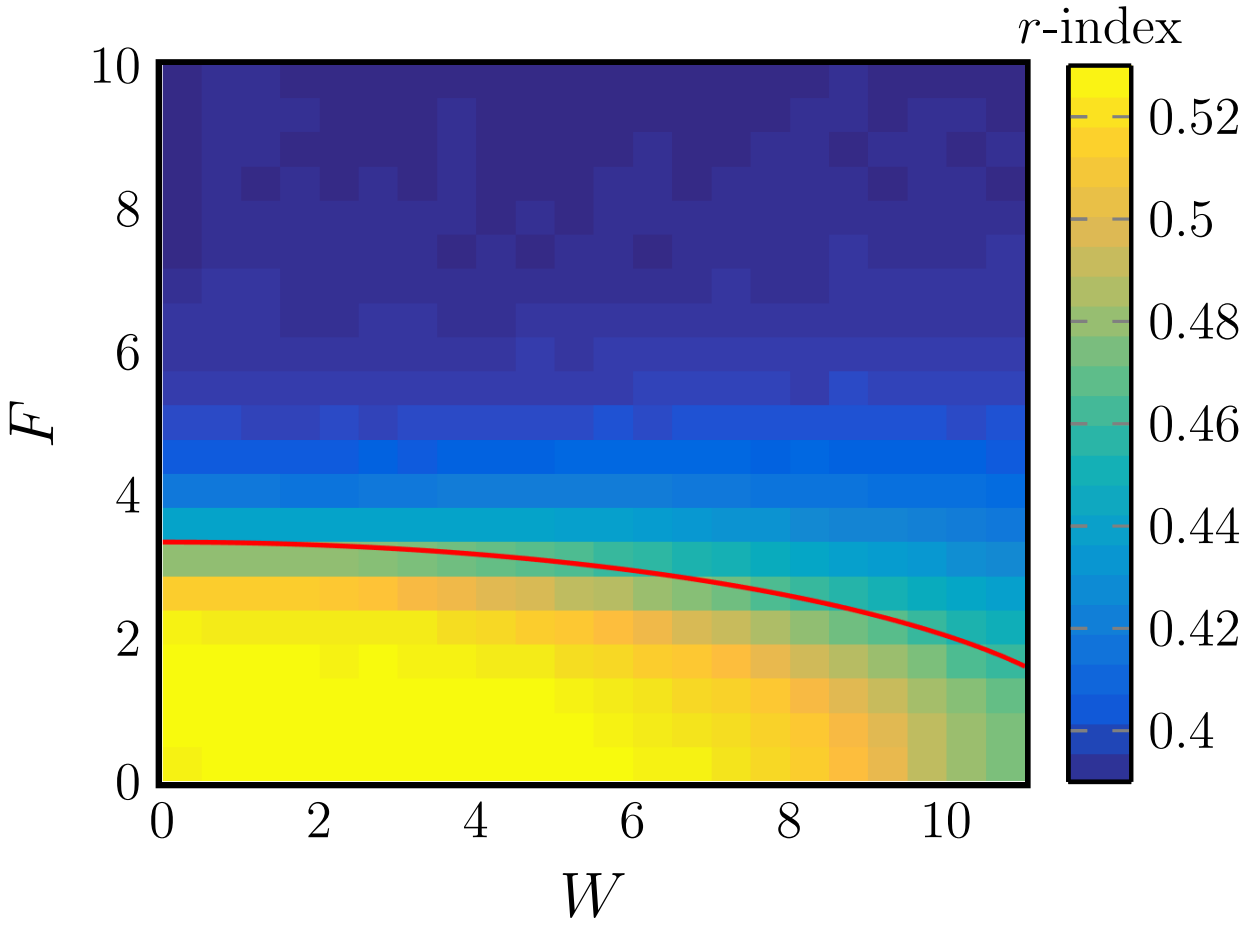

Figure 19.4: The level statistics (r-value) as a function of the field strength, F, and disorder strength, W, for a disordered 2D system of 4×4 spins with an incommensurate force $\mathbf{F} = F(\sqrt{2}, 1)$ (averaged over 32 realizations). The red line is a guide to the eye and is given by a contour of $r \approx 0.46$.

effectively restricted to preserve the initial dipole moment and the initial doublon number, which is predicted to yield non-ergodic dynamics [58]. For a weak field however, this is not the case. The eigenstates in a given energy window span a range of dipole moments and doublon numbers. Around the critical field, we observe that while the eigenstates in a given energy have a finite spread in the dipole moment, the different sectors become distinct and the integer part of the dipole moment behaves as a conserved quantity. Beyond this critical field we also observe a separation into the subsectors of doublon number. While it is hard to pinpoint the exact value of the transition using this approach, the transition can be bounded and is consistent with the value we obtained from the level spacing statistics.

19.6 Conclusions

In this work we analyzed the effect of interactions on single particle localization that arise both from disorder, W, and from the existence of linear potentials F. With that, we showed that the notion of a many-body localized (MBL) phase may be generalized also to a class of clean (non-integrable) systems. In particular, we find that a phase boundary in the space (F, W) exists, beyond which the resulting phase fails to thermalize. We find that, unlike in clean integrable models, this non-ergodic phase is stable to perturbations, and shares all the familiar fingerprints of the well studied MBL phase in the presence of disorder.

The existence of such a phase demonstrates that randomness is not an essential ingredient for the emergence of stable non-ergodic interacting phases. Such a conclusion may have an impact on the realization of these non-ergodic phases. Unlike disorder potentials, linear potentials are relatively easy to implement, and are highly tunable and may be controlled dynamically. The ability to realize stable and generic non-ergodic phases is an important step toward the realization of quantum memory devices that may store information for long times. Moreover, the lack of randomness and the low sensitivity to dimensionality may render these systems more accessible to a further theoretical investigation, both numerically and analytically. It came to our knowledge that simultaneously to our work, the entanglement-entropy grows in the presence of linear field has been studied in Refs. [59]. The results presented in Refs. [59] are in agreement with the conclusions we presented in this work.

The C++ code we developed for this is available online at `https://www.github.com/everthemore/krylov-cpp`, and the data for Fig. 19.3 is available at `https://data.caltech.edu/records/1089`.

19.7 Data augmentation using machine learning

The different disorder realizations we study in this manuscript differ only in the values for the on-site potentials. Given the on-site potentials, there exists a procedure that results in the value for the r-statistics. Namely, one builds the corresponding Hamiltonian matrix and diagonalizes it to obtain the eigenvalues ϵ_n. The r-statistics is obtained by looking at neighboring eigenvalue differences $\delta_n = \epsilon_{n+1} - \epsilon_n$ and computing the ratio $r = \langle \min(\delta_n, \delta_{n+1}) / \max(\delta_n, \delta_{n+1}) \rangle$ as discussed in the main text.

Here, however, we ask whether or not a more direct (approximate) map exists from the on-site potentials to r. Rather than trying to explicitly construct it, we attempt to train a neural network to perform this map for us. Hence we generate a large data-set of pairs $(\mathbf{h}, r)$, where $\mathbf{h}$ is a vector of the on-site potentials augmented with the value of W from which they were drawn, and r is the resulting r-statistics for this particular realization. These serve as the input and output respectively for the machine learning model.

Provided that such a mapping exists and that the network is capable of learning it, the resulting network can be used to generate more r-values by using it to predict on more realizations. This allows one to generate statistics much faster compared to running the full exact diagonalization. It must be noted that this procedure cannot take away the inherent statistical uncertainty due to the finite size of the system. Particularly, for disorder strengths near the transitions point, the exact r-values of systems with different realizations drawn from the same distribution, lie within a relatively large window. As the system becomes larger this window becomes smaller. For example, already by including a few hundreds of realizations, for $L = 16$, the error bars near the transition are dominated by the intrinsic finite size effect and cannot be improved by adding more realizations.

In Fig. 19.5 we demonstrate the above procedure for the $L = 16$ data, for which the data-set consists of $\sim$ 15k entries (25 values of W spread over $\sim$ 550 realizations). We split off 10% of the data as a validation set, and train a network with the following architecture. First, two convolutional layers with 32 filters and kernel sizes 6 and 3, followed by a maximum pooling of size 3. Then a convolutional layer with 64 filters and kernel size 2, followed by a global average pooling. Next, two fully connected sigmoid layers with 256 and 128 neurons respectively, and dropout 0.5. And finally an output layer with a single sigmoid neuron.

We train the network with the Adam [60] optimizer to minimize the mean-squared-error loss function, and achieve a validation loss of $\sim 2 \cdot 10^{-5}$ in 100 epochs of batchsize 32. In our experiments, we have found no particular reason for the above network to work better than others, but we found that considerably simpler networks (e.g. just fully connected layers)

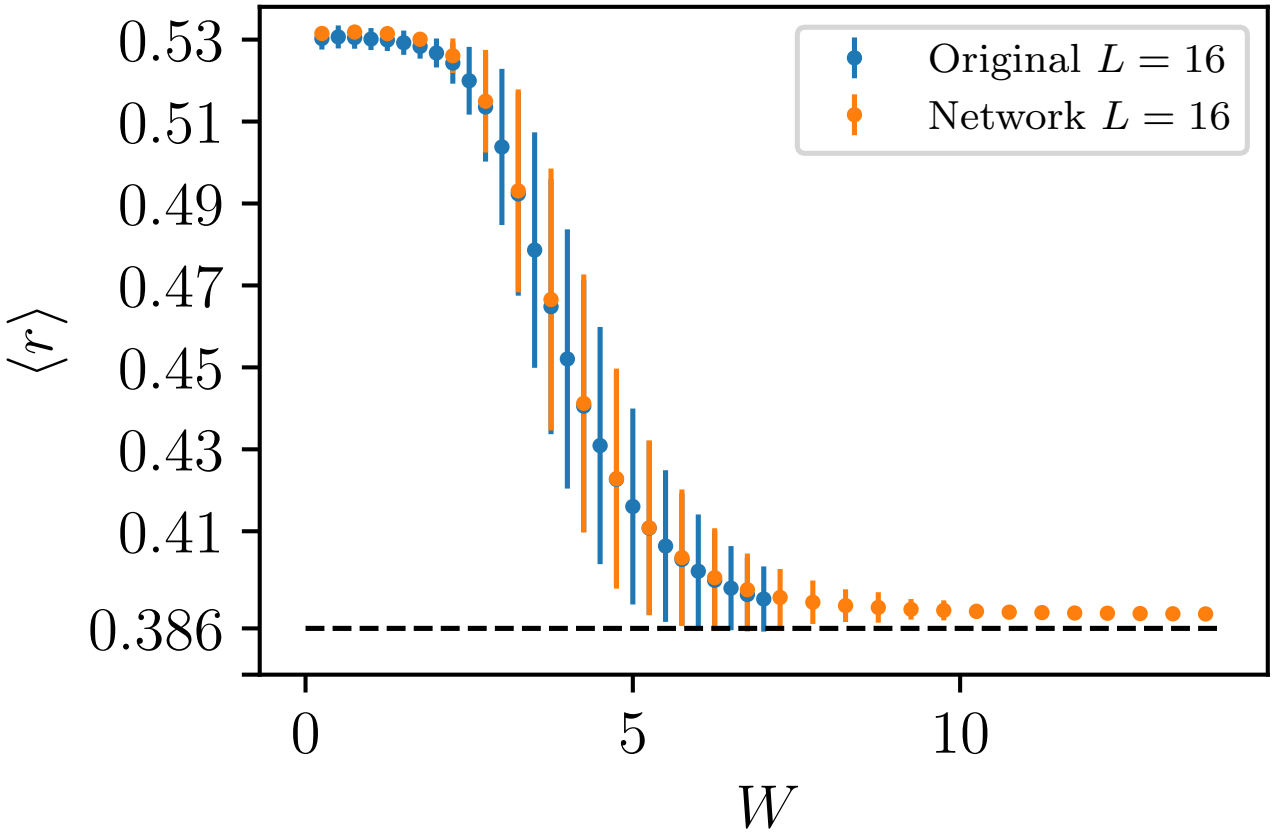

Figure 19.5: The original $L = 16$ data and the machine learned map from the disorder realization h_1 through h_{16} to the resulting r-statistics. With the network we are able to generate considerably more realizations (10^6 versus 10^3) in a much shorter timespan, provided that the network is capable of learning and generalizing. The sigmoid output neuron rather than linear for optimizing the mean-squared-error ensures convergence of the output as a function of W. Error bars indicate the standard deviation over the number of realizations, and the black dashed horizontal line indicates the Poissonian r-value of $\ln 4 - 1$.

converge much slower. For the purpose of extracting the mapping, our chosen network might be hard to interpret. It would be an interesting research direction however to see if the approximate mapping can be extracted from a network, or whether a single network can be trained on different system sizes to extract finite size behavior. Both would potentially allow predictions to be made on larger system sizes than trained on, although further investigation into this question is required.

19.7Finite size scaling

In this appendix we discuss the transition from the ergodic to the non-ergodic phase as a function of the linear field f. To do so, we fix $W = 0.5$ and perform a finite size scaling analysis attempting to collapse the curves for different system sizes. We consider a universal function $g\left((f - f_c)\, L^{1/\nu}\right)$ for the r-statistics, and optimize the parameters f_c and ν so that the rescaled r-statistics curves for the different sizes collapse.

Each of the curves is first rescaled with proposed f_c and ν after which we use spline interpolation to numerically minimize the cost function $C(f_c, \nu) = \sum_{i<j} \int_x (y_i(x) - y_j(x))^2$, where i, j both run over system sizes $L = 12, 14, 16, 18$ and $y_i(x)$ represents the spline-interpolated data. The integration regime x is taken to be centered around the transition (i.e. $x = 0$) and has a width $2w$ that we vary to obtain statistics on f_c and ν. In the collapse including the system size

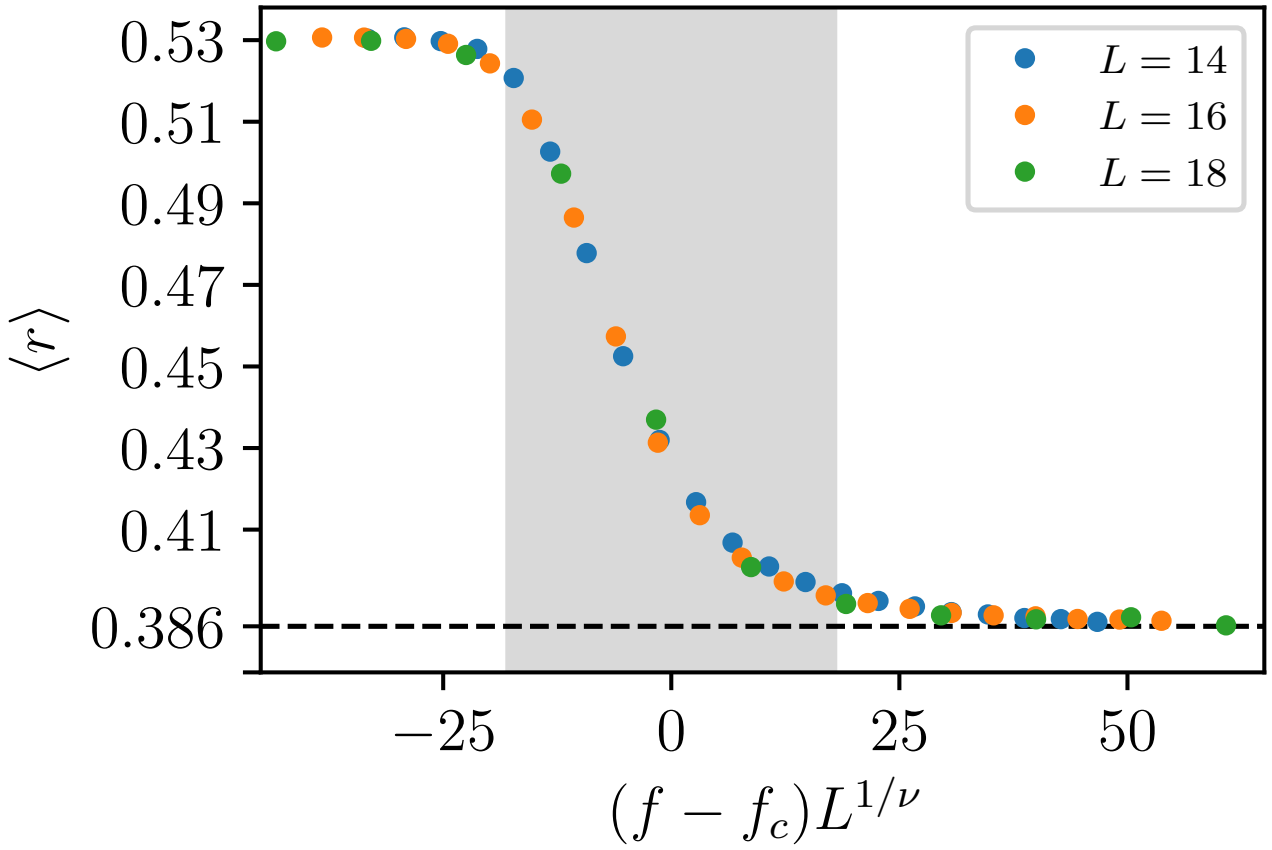

Figure 19.6: Collapse of the $W = 0.5$ data for system sizes $L = 14, 16, 18$, as a function of the field strength f. The collapse is obtained by rescaling the fields according to $f \to (f - f_c)L^{1/\nu}$ with $f_c = 2.08$ and $\nu = 0.952$. The gray area indicates the width w that was used to make the curves collapse, and is the width at which the collapse is most stable against inclusion or removal of the $L = 12$ data.

$L = 12$ data, the $L = 12$ curve is consistently the most off. In the spirit of Ref. [52] we consider the width w for which the extracted parameters are least sensitive to the inclusion/removal of the $L = 12$ data. This results in the parameters $f_c = 2.08 \pm 0.10$ and $\nu = 0.952(5)$. The resulting collapse for this set of parameters is shown in Fig. 19.6.

19.8 Choice of gauge for numerics

We chose to work with a time-independent Hamiltonian for which the linear field is added via the dipole term, rather than as a time-dependent phase factor for the hopping. This interpretation brings with it the potential issue of having an infinite energy difference between the endpoints of our system as one scales up to the thermodynamic limit. The physics in these two gauges is evidently invariant, but since we consider (rather small) finite size systems the infinite energies are not a concern. Working in the time-independent gauge is numerically considerably more convenient, since the time evolution operator over a period T, i.e. $U(T)$, can be constructed by a single exponentiation through as $U(T) = \exp(-iH_{\text{static}}T)$. For the time-dependent case, one would have to compute the time ordered integral $U(T) = \mathcal{T}\exp\left(-i\int \mathrm{d}t H(t)\right)$ by breaking it down into many small $\mathrm{d}t$-sized steps and exponentiating $H(t)$ for each. The resulting differences in the spectra $\lambda_{i,\text{static}}$ and $\lambda_{i,\text{time}}$ are only of the order of $\mathcal{O}(\mathrm{d}t)$. An interesting phenomenon for future investigation is the observed clustering of the eigenvalues for field $F > F_c$, shown in Fig. 19.7.

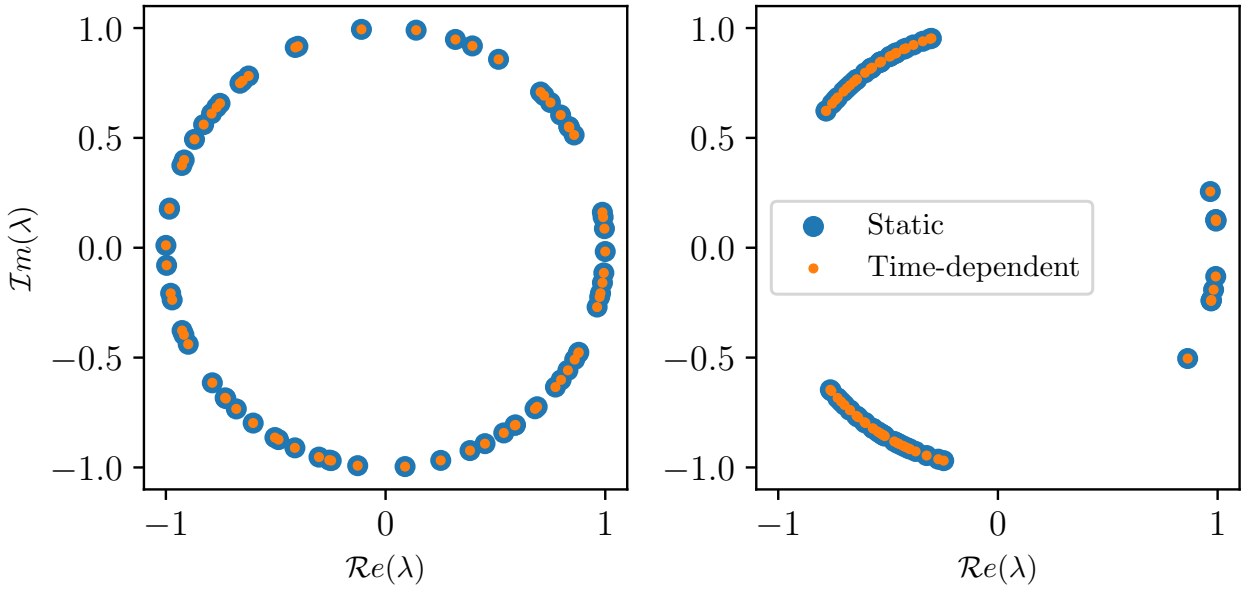

Figure 19.7: The (real and imaginary parts of the) spectrum of $U(T)$ computed in the static gauge (larger blue dots) versus the spectrum of $U(T)$ computed in the time-dependent gauge (smaller orange dots), for field strengths $F = 0.5$ (left panel) and $F = 3.0$ (right panel). The difference between the spectra $\sum_i |\lambda_{i,\text{static}} - \lambda_{i,\text{time}}|$ is of order $\mathrm{d}t$ used to calculate the latter.

19.9 Sensitivity to integrability-breaking terms

We now consider an extended version of Eq. 5 of the main text,

$$H = \sum_j t(c_j^\dagger c_{j+1} + h.c) - Fjn_j + h_j n_j + Un_j n_{j+1} \\ + \zeta \left(c_j^\dagger c_{j+2} + h.c + n_j n_{j+2} \right). \tag{19.8}$$

In the absence of both disorder and linear field, the above model is integrable for $\zeta = 0$. We show that also in the presence of the integrability-breaking terms, the application of linear field (with or without disorder) leads to a transition from a Wigner-Dyson level statistics (ergodic) to a Poisson level statistics (non-ergodic). While the value of the critical field depends on ζ and the disorder strength, the qualitative behavior is indifferent to these terms. In Fig. 19.8 we show the r-index as a function of the linear field strength. Different curves represent different values of ζ.

19.10 Time-evolution using the re-orthogonalized Lanczos algorithm

In this appendix we discuss algorithmic details of simulating the time-evolution of a wavefunction using a Krylov-subspace method. In particular, we have used the so-called Lanzcos algorithm with re-orthogonalization to obtain the results presented in Fig. 3 of the main text.

We wish to numerically perform the time-evolution of a wavefunction, i.e., to compute $|\psi(t_0 + t)\rangle = e^{-iHt}|\psi(t_0)\rangle$. To do this exactly would require the full diagonalization of the Hamiltonian H, which becomes impossible for large system sizes due to memory requirements. An improvement can be made by using a sparse matrix implementation of the Hamiltonian and iteratively simulating

$$|\psi(t_0 + \mathrm{d}t)\rangle = e^{-iH\mathrm{d}t}|\psi(t_0)\rangle \tag{19.9}$$

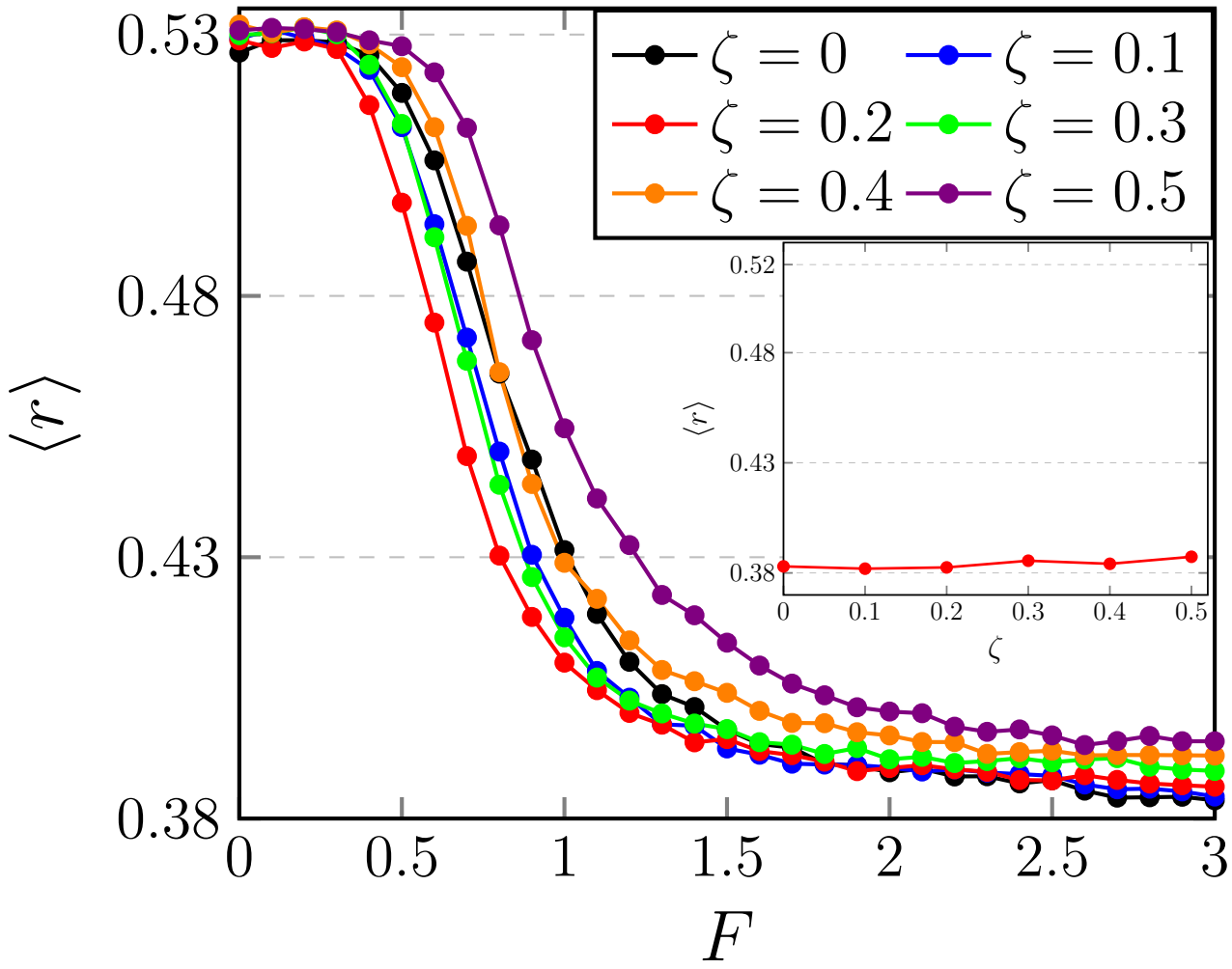

Figure 19.8: The level statistics (r-index) as a function of the linear field for different values of the integrability-breaking strength, ζ. The calculation was done for a system of 14 sites (half-filled) with a fixed weak disorder $W = 0.2$ (averaged over 50 realizations),$t = 1/2$ and $U = 1$. Inset: the r-index of a clean system of 16 sites with fixed field $F = 3$ as a function of ζ.

for small time-steps $\mathrm{d}t$. A naive implementation of this iterative algorithm quickly accumulates numerical errors and becomes unstable, however, a more stable variant can be constructed using Krylov-subspaces [61]. A Krylov-subspace of dimension m, $\mathcal{K}_m(H, |\psi\rangle)$, is defined as the span of the vectors $(|\psi\rangle, H|\psi\rangle, H^2|\psi\rangle, \ldots, H^{m-1}|\psi\rangle)$. The vector $|\psi(t_0 + \mathrm{d}t)$, after expanding the exponent on right-hand side of Eq. 19.9, is approximated well by a vector in this Krylov subspace.

The vectors in $\mathcal{K}_m(H, |\psi(t_0)\rangle)$ first need to be orthonormalized (discussed in more depth shortly), after which we store them as the columns of a new matrix Q_m of dimension $\mathcal{N} \times m$, where $\mathcal{N}$ is the size of the Hilbert space. After obtaining Q_m, we project the Hamiltonian into the spanned subspace to obtain $h_m = Q_m^\dagger H Q_m$. This is a much smaller $m \times m$ matrix that can be easily exponentiate, and allows us to compute

$$\begin{aligned} |\psi(t_0 + \mathrm{d}t)\rangle &= e^{-iH\mathrm{d}t}|\psi(t_0)\rangle \\ &\approx \text{the first column of } Q_m e^{-ih_m \mathrm{d}t}. \end{aligned} \tag{19.10}$$

In all of the above, the Krylov subspace dimension m can either be systematically increased until convergence is obtained, or changed adaptively during the orthogonalization procedure described next.

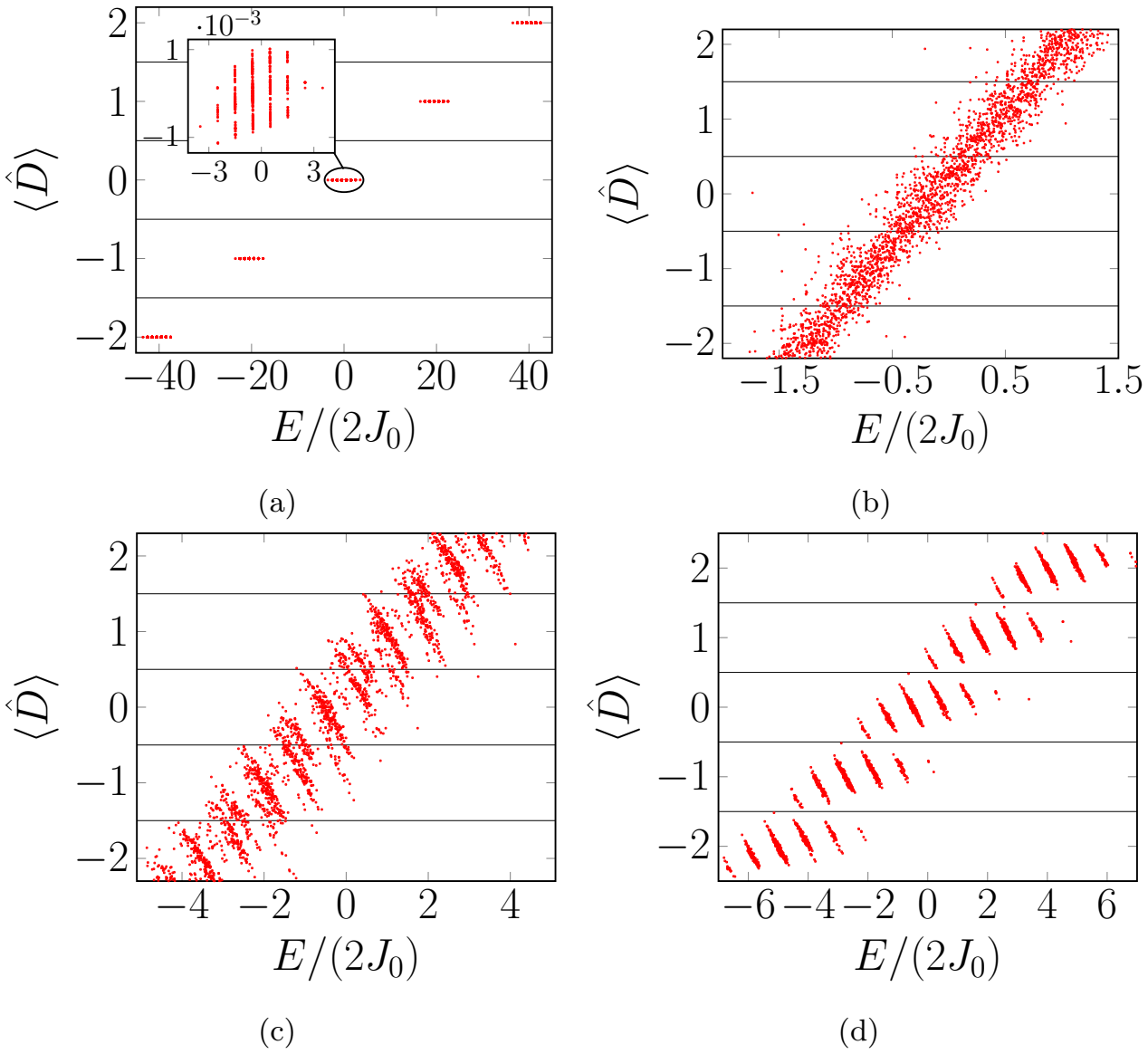

Figure 19.9: Eigenstates dipole moment (expectation value) as a function of their energy for 16 sites half filled chain with $J_0 = 1/2$, $U = 1$ and different fields: (a) $F = 20$, (b) $F = 0.5$, (c) $F = 1.5$, (d) $F = 2.2$. For presentational reasons we show only the expectation value of the dipole moment and omit the fluctuations. The mean fluctuations are (a) $\sigma_F \approx 0.04$, (b) $\sigma_F \approx 3.2$, (c) $\sigma_F \approx 1$, (d) $\sigma_F \approx 0.6$. Above a critical field, the eigenstates in a given energy window have a well define dipole moment which restrict the dynamics.

The numerically most challenging step in this algorithm is obtaining the orthonormalized set of vectors for Q_m from $\mathcal{K}_m(H, |\psi(t)\rangle)$. A standard Gram-Schmidt procedure for orthonormalizing a set of vectors loses the orthogonality between successive vectors simply due to rounding errors (i.e. finite precision of floating point numbers). The modified Gram-Schmidt procedure does considerably better, but we have found it insufficient for our purpose. The set of vectors we wish to orthonormalize is a special set, in which each vector is generated from the previous one by application of a matrix. This means we can generate the vectors during the Gram-Schmidt procedure instead of having them given to use beforehand. This small but important difference leads to this algorithm often being called the Arnoldi method. The resulting projected matrix is in general an upper Hessenberg matrix (upper triangular plus the first lower off-diagonal). If the matrix is Hermitian as it is in our case, the projected matrix is therefore tri-diagonal. The Arnoldi algorithm with a Hermitian matrix is called the Lanczos algorithm, and provides an

improvement in terms of computational effort.

Regardless of using modified Gram-Schmidt, Arnoldi or Lanczos, the orthogonality between successive vectors is gradually lost. A significant improvement, at computational cost of course, can be made by simply re-orthogonalizing the set of obtained (semi-)orthogonal vectors. It turns out that for the re-orthogonalization "twice is enough" for non-singular cases [62]. For the numerics presented in Fig. 3 of the main text, we have checked the convergence of the curves with respect to the timestep dt and the Krylov-subspace dimension m. The values we have used are $\mathrm{dt} = 0.02$ and $m = 15$.

19.11 Dipole moment analysis

We show in Fig. 19.9 the results of exact diagonalization of a half-filled fermionic system where each point represents an eigenstate in the space of energy and dipole-moment. As expected, in a given energy window and for large field (Fig. 19.9a) the many body wave functions have well-defined dipole moment. For a weak field however (Fig. 19.9b), this is not the case. The eigenstates in a given energy window span a range of dipole moments. Around the critical field (Fig. 19.9c,d), while the eigenstates in a given energy have a finite spread in the dipole moment, the different sectors become distinct and the integer part of the dipole moment behaves as a conserved quantity.

Part VIII
Main Experiments

20 Stable Quantum-Correlated Many Body States through Engineered Dissipation by Google Collaboration

Abstract

Engineered dissipative reservoirs (what are they??) have the potential to steer many-body quantum systems toward correlated steady states (how does it look?) useful for quantum simulation of high-temperature superconductivity or quantum magnetism (why is it used there?).

Using up to 49 superconducting qubits, we prepared low-energy states of the transverse-field Ising model through coupling to dissipative auxiliary qubits.

In one dimension, we observed long-range quantum correlations and a ground-state fidelity (what is fidelity?) of 0.86 for 18 qubits at the critical point (which?).

In two dimensions, we found mutual information (what is it?) that extends beyond nearest neighbors.

Lastly, by coupling the system to auxiliaries emulating reservoirs with different chemical potentials, we explored transport in the quantum Heisenberg model.

Our results establish engineered dissipation as a scalable alternative to unitary evolution for preparing entangled many-body states on noisy quantum processors.

20.1 Theory

A major effort in quantum simulation and computation is devising scalable algorithms for preparing correlated states, such as the ground state of interacting Hamiltonians. On analog quantum simulators, states are often prepared via adiabatic unitary evolution from an initial Hamiltonian to a desired Hamiltonian [1, 2, 3]. On digital quantum processors supporting more flexible unitary dynamics, variational quantum algorithms have also gained popularity in recent years [4]. Both methods, however, have inherent limitations: Adiabatic state preparation is fundamentally difficult across quantum phase transitions where the many-body energy gaps close, whereas variational quantum algorithms involve large optimization overheads and are challenged by the so-called barren plateaus [5]. The lifetimes of states prepared through unitary evolution are also limited by the coherence times of physical qubits, hindering their use as basis for noise-biased qubits [6] or topological quantum computation [7].

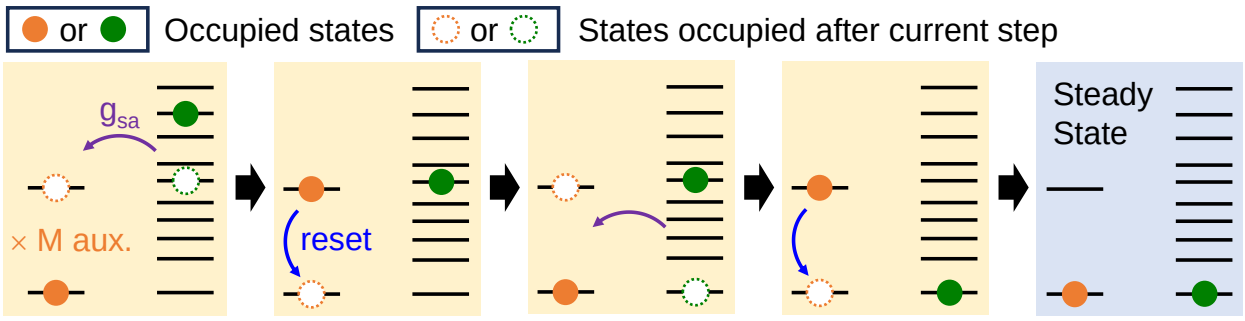

Figure 20.1: Dissipative cooling of a many-body system (green dot) to its ground state via a reservoir comprising M auxiliary two-level systems (orange dot), schematically illustrated as a sequence of steps.

An alternative and more robust route toward quantum state preparation is through engineered dissipation [8, 6, 1, 31, 12, 13]. In such schemes, the quantum system is coupled to a dissipative reservoir that is repeatedly entangled (why entangled?) with the system and projected to a chosen state (how is projected?).

Over time, the system is steered toward a steady state of interest by the reservoir (concrete example?).

A concrete example is dissipative cooling (Fig. 20.1). Here the reservoir is represented by M two-level "auxiliary" qubits, each with an energy splitting close to the energy of low-lying excitations of a many-body quantum system [41, 42].

The entangling operation, having a rate g_{sa}, transfers excitations from the system into the auxiliaries, which are then removed via controlled dissipation ("reset") that brings the auxiliaries to their ground states.

The process therefore cools the system toward its ground state.

Even after the completion of the cooling process, the continued reset cycles of the auxiliaries stabilize the cooled state against environmental decoherence, extending its lifetime beyond the coherence times of physical qubits.

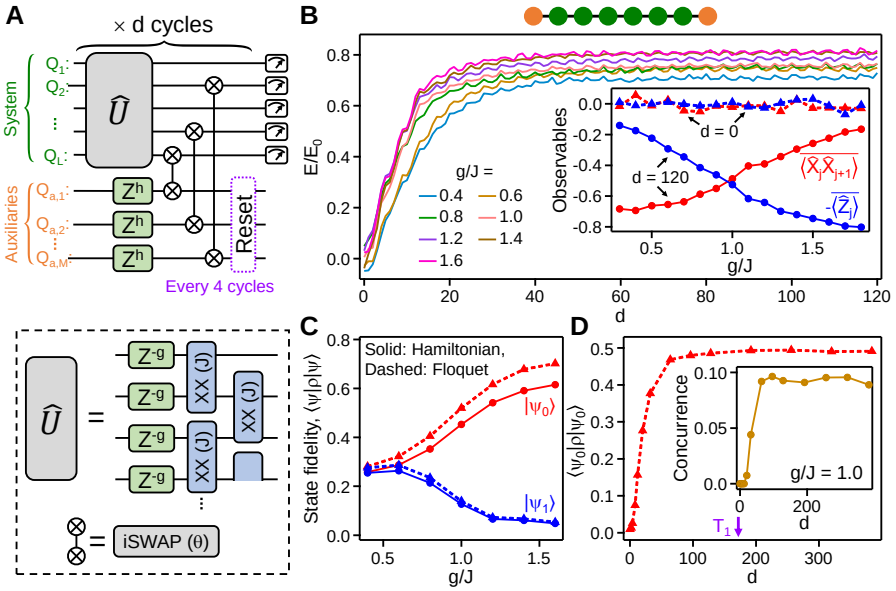

Figure 20.2: Dissipative cooling and stabilization of a 1D TFIM. (A) A periodic quantum circuit used to implement dissipative cooling on a quantum processor. Here the $XX(J)$ and iSWAP(θ) gates are composed from tunable CPHASE and fermionic simulation (fSim) gates (see SM). (B) E/E_0 as a function of d for different relative transverse field strengths, g/J. Here E is the experimentally obtained energy and E_0 is the ground state energy. Inset shows the site-averaged observables $\overline{\langle \hat{X}_j \hat{X}_{j+1} \rangle}$ and $-\overline{\langle \hat{Z}_j \rangle}$ as functions of g/J, measured at $d = 0$ and $d = 120$. (C) Fidelity of steady state ($d = 100$) with respect to the ground state of the TFIM, $|\psi_0\rangle$ (red), and the first excited state $|\psi_1\rangle$. Data are computed from experimental 6-qubit density matrices ρ. Here the solid lines correspond to eigenstates of the TFIM Hamiltonian and the dashed lines correspond to the Floquet eigenstates of the cycle unitary $\hat{U}$. (D) Floquet ground state fidelity $\langle \psi_0 | \rho | \psi_0 \rangle$ as a function of d for $g/J = 1.0$. Inset shows site-averaged nearest-neighbor concurrence as a function of d. The typical single-qubit $T_1 = 22\ \mu$s corresponds to $d \approx 170$.

Past experimental works have demonstrated the dissipative preparation of few-qubit states of trapped ions [25, 36] and superconducting qubits [37], as well as an 8-qubit Mott insulator state in an analog quantum simulator [19]. Dissipative preparation of many-body quantum states, however, has remained experimentally challenging due to increased environmental de-

coherence which threatens to overwhelm the impact of the auxiliaries. Open questions also remain on whether dissipatively prepared states with more than a few qubits in fact possess any non-classical characteristics. Dissipatively preparing many-body states and measuring their quantum correlation or entanglement entropy are therefore crucial for assessing the practical importance of engineered dissipation to current quantum hardware.

In this article, we report the preparation of many-body quantum states via dissipative cooling on a superconducting transmon quantum processor [20]. We provide experimental evidence of entanglement and long-range quantum correlations in the steady state, and demonstrate a favorable scaling of dissipative state preparation over system sizes when compared to unitary evolution algorithms. Furthermore, we extend the use of engineered dissipation beyond cooling and explore the non-equilibrium physics arising from coupling a many-body quantum system to two different reservoirs. This work is enabled by two technical advances: (i) Continuously tunable quantum gates with simultaneously operated two-qubit gate fidelities reaching 99.7% in 1D and 99.6% in 2D. Details of gate calibration are described in the Supplementary Materials (SM). (ii) A fast reset protocol comparable to unitary gates in duration, which reduces errors from qubit idling [21, 22].

We first perform a benchmarking experiment using a 6-site 1D transverse-field Ising model (TFIM) connected to two auxiliaries at the edges. The 1D TFIM is chosen since it is analytically solvable and has a quantum-entangled ground state. The Hamiltonian describing the system is:

$$\hat{H}_{\mathrm{TFIM}} = -g \sum_{j=1}^{L} \hat{Z}_j + J \sum_{j=1}^{L-1} \hat{X}_j \hat{X}_{j+1} \tag{20.1}$$

Here $\hat{X}$ and $\hat{Z}$ are Pauli operators whereas g and J denote control parameters. For $J > 0$, the model exhibits two quantum phases: an antiferromagnetic phase ($g/J < 1$) with two nearly degenerate ground states ($\sim |{+}{-}\rangle^{\otimes L/2} \pm |{-}{+}\rangle^{\otimes L/2}$, where $|\pm\rangle = |0\rangle \pm |1\rangle$) and a paramagnetic phase ($g/J > 1$) with a unique ground state ($\sim |0\rangle^{\otimes L}$). At the critical point $g/J = 1$, the ground state is most entangled, having an entanglement entropy that grows logarithmically with subsystem size, and quantum correlations that decay as a power law over distance.

The dissipative cooling described in Fig. 20.1 is implemented via d cycles of a periodic quantum circuit on a system of qubits, Q_1 through Q_{L} (Fig. 20.2A). The quantum circuit includes a Trotter-Suzuki approximation of the time-evolution operator $\hat{U}_{\mathrm{TFIM}}(\frac{\pi}{2}d) \approx \hat{U}^d$, where:

$$\hat{U} = e^{-\frac{i\pi J}{2}\sum_{j=1}^{L-1} \hat{X}_j \hat{X}_{j+1}} e^{\frac{i\pi g}{2}\sum_{j=1}^{L} \hat{Z}_j}. \tag{20.2}$$

Unless otherwise stated, we use $J = 0.25$ for $g/J < 0.6$ and $J = 0.2$ for $g/J \geq 0.6$. Within every cycle, each auxiliary ($Q_{\mathrm{a},1}$ through $Q_{\mathrm{a,M}}$) is also rotated with a phase gate Z^h, where the exponent h effectively controls its energy splitting as illustrated in Fig. 20.1. Lastly, the auxiliaries are coupled to the system via a partial iSWAP gate with a tunable angle θ, iSWAP(θ) $= e^{i\frac{\theta}{2}(\hat{X}\hat{X}+\hat{Y}\hat{Y})}$, where $\hat{Y}$ is another Pauli operator [23]. Here θ controls the system-reservoir coupling g_{sa} in Fig. 20.1. The auxiliaries are reset every 4 circuit cycles to allow sufficient time for energy exchange between the system and the reservoir [41]. In the SM, we present additional experimental characterization that is used to determine the optimal values of h and θ. To demonstrate that our protocol may be applied to any initial state, all initial states used in the TFIM experiments are scrambled states prepared using random circuits having 50 cycles of CZ and single-qubit gates [24].

We begin by characterizing the energy of the system, $E = \langle \hat{H}_{\mathrm{TFIM}} \rangle$, as a function of d and across the two phases of the TFIM. Figure 20.2B shows the time-dependent E/E_0 for different values of g/J, where E_0 is the ground state energy. We observe that E/E_0 increases from 0 at $d = 0$ to a stable value at $d > 50$, which ranges from 0.7 deep in the antiferromagnetic phase ($g/J = 0.4$) to 0.8 deep in the paramagnetic phase ($g/J = 1.8$). The site-averaged observables,

$\overline{\langle \hat{X}_j \hat{X}_{j+1} \rangle}$ and $-\overline{\langle \hat{Z}_j \rangle}$, show an expected crossing around the critical point of the TFIM, $g/J = 1.0$ (inset to Fig. 20.2B). These data are preliminary indications that our dissipative cooling protocol is robust across quantum phase transitions, where the nature of the ground state qualitatively changes.

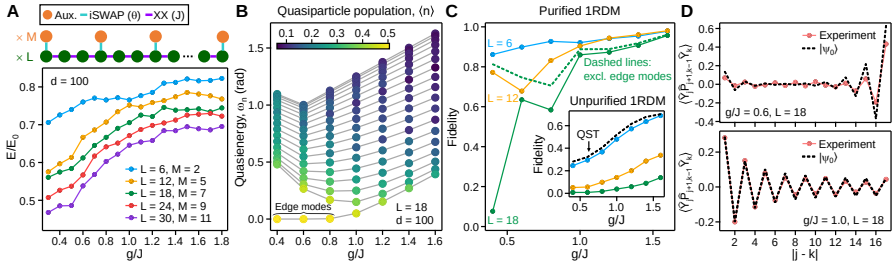

Figure 20.3: Observation of long-range quantum correlations. (A) Steady state ($d = 100$) energy ratio E/E_0 for a TFIM chain with system sizes up to $L = 30$ qubits, plotted as a function of g/J. The number of auxiliaries, M, is proportionally increased with L. (B) Quasienergies ω_n of the L non-interacting quasiparticles describing $\hat{U}$, as a function of g/J. The color of each point corresponds to an experimentally measured quasiparticle population $\langle n \rangle$ at $d = 100$. Here $L = 18$. (C) Ground state fidelities as functions of g/J for system sizes $L = 6$, 12 and 18, constructed from the purified 1RDM. The dashed line refers to $L = 18$ fidelities computed excluding contribution from the edge modes. Inset shows the fidelities without purification. The values obtained from QST in the $L = 6$ case (Fig. 20.2C) are also included and show close agreement with 1RDM estimates for the same system size. (D) Long-ranged correlator $\langle \hat{Y}_j \hat{P}_{j+1,k-1} \hat{Y}_k \rangle$ as a function of $|j-k|$ for $g/J = 0.6$ (upper panel) and $g/J = 1.0$ (lower panel). Results are constructed from the purified 1RDM and exact calculations for the ground state are also shown for comparison.

To further understand the structure of the steady states, we perform quantum state tomography (QST) and obtain the density matrices ρ of the 6-qubit system at $d = 100$. The results are then used to compute the fidelities with respect to the ground state $|\psi_0\rangle$ and the first excited state $|\psi_1\rangle$ of the TFIM (Fig. 20.2C). We find that $\langle \psi_0|\rho|\psi_0\rangle$ and $\langle \psi_1|\rho|\psi_1\rangle$ assume an approximately equal value of 0.26 deep in the antiferromagnetic phase $g/J = 0.4$, indicating that the system cools to an equal mixture of the two nearly degenerate states. As the system approaches the paramagnetic phase, the degeneracy is lifted and $\langle \psi_0|\rho|\psi_0\rangle$ increases to 0.61 while $\langle \psi_1|\rho|\psi_1\rangle$ decreases to 0.05 at $g/J = 1.6$. Alternatively, the state fidelities are also computed by choosing $\langle \psi_0|$ ($\langle \psi_1|$) to be the "ground" ("first excited") eigenstate of the cycle unitary $\hat{U}$, defined as the state having 0 (1) low-energy quasiparticle excitation (see later discussion). The resulting values are found to be higher, due to the fact that the digital cooling process here is fundamentally governed by time-periodic (a.k.a. Floquet) dynamics rather than a time-independent Hamiltonian. The fixed points of the dissipative evolution are therefore closer to the Floquet eigenstates of the cycle unitary than those of $\hat{H}_{\mathrm{TFIM}}$. A detailed theoretical treatment of Floquet cooling is presented in the SM.

A key advantage of dissipatively prepared quantum states is that their lifetime extends beyond the coherence times of physical qubits. To test this, we measure the Floquet ground state fidelity $\langle \psi_0|\rho|\psi_0\rangle$ up to $d = 384$, corresponding to a time duration of 49 μs ($\gg$ single-qubit $T_1 = 22$ μs). As shown in Fig. 20.2D, the fidelity exhibits no sign of decay up to this time scale. Furthermore, we find that the nearest-neighbor concurrence increases from 0 to a steady-state value of 0.1 over time, indicating the generation and preservation of entanglement by the cooling process [25].

We now test the scalability of the dissipative cooling protocol by extending it to larger system sizes in 1D. A natural starting point is measuring the steady state ($d = 100$) energy

with respect to $\hat{H}_{\mathrm{TFIM}}$, E, as a function of g/J (Fig. 20.3A). Here the number of auxiliaries is increased for longer qubit chains to overcome the higher decoherence rates. For an auxiliary-to-qubit ratio of $\frac{M}{L} \approx 0.4$, we observe only weak degradation in E/E_0 as the system scales up. In particular, E/E_0 retains a value of 0.65 for $L = 30$ compared to a value of 0.76 for $L = 6$ at the critical point $g/J = 1.0$. This result suggests that our protocol is capable of maintaining a low energy density for large 1D quantum systems.

For practical applications of the steady state, it is desirable to improve its fidelity via error-mitigation. One such strategy is purification, which projects a mixed-state experimental density matrix to the closest pure state before computing observables [26]. Although this is generally challenging for non-integrable quantum systems due to the $O(e^L)$ measurement overhead of full QST, the integrability of the 1D TFIM renders an efficient description of the eigenspectrum of $\hat{U}$ in terms of L non-interacting Bogoliubov fermionic quasiparticles. The many-body spectrum of $\hat{U}$ is represented by the filling or emptying of each quasiparticle level, and each many-body eigenstate belongs to a class of Gaussian states. Such states can be fully characterized through the one-particle reduced density matrix (1RDM) of the quasiparticles, which requires measuring only $O(L^2)$ multiqubit operators (see SM for the exact compositions of these operators).

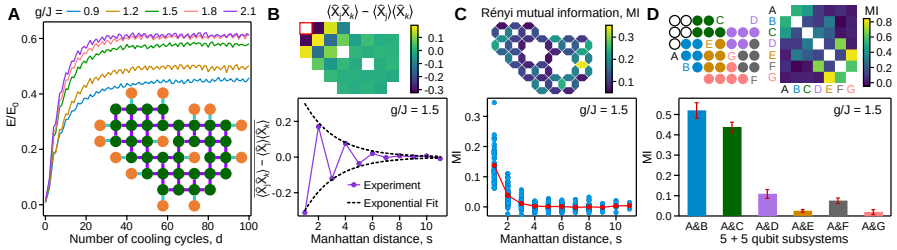

Figure 20.4: Dissipative cooling of a 2D TFIM and many-body mutual information. (A) E/E_0 of a 2D TFIM as a function of d for different values of g/J. Inset shows the experimental geometry, where 35 coupled qubits in 2D are connected to 14 auxiliaries. E_0 is calculated using the density matrix renormalization group. Here J is chosen to be 0.15 to reduce the Trotter error. (B) Upper panel: Correlator $\langle \hat{X}_j \hat{X}_k \rangle - \langle \hat{X}_j \rangle \langle \hat{X}_k \rangle$ between the top-left qubit (red square) and every other qubit in the system, at the critical point $g/J = 1.5$. Lower panel: $\overline{\langle \hat{X}_j \hat{X}_k \rangle - \langle \hat{X}_j \rangle \langle \hat{X}_k \rangle}$ as a function of the Manhattan distance s between qubits, obtained from the upper panel. The overline denotes averaging over data with the same s. Dashed lines show an exponential fit $\sim e^{-\frac{s}{2.3}}$ to the decaying envelope. (C) Upper panel: Rényi mutual information (MI) between all nearest-neighbor qubits. Lower panel: MI between all possible pairs of qubits in the system (blue) as a function of s. Red symbols indicates the average values. (D) Upper panel: MI between different partitions of the system, each containing 5 qubits. Lower: MI between subsystem A and every other subsystem. Error bars indicate standard errors estimated from jacknife resampling.

Using experimental 1RDMs, we first construct the steady state population $\langle n \rangle$ for each quasiparticle level across the two different phases. In Fig. 20.3B, the numerically computed quasienergy ω_n is shown as a function of g/J, where the colors of the data points represent measured values of $\langle n \rangle$. Here the ground state $|\psi_0\rangle$ of the system corresponds to a state where $\langle n \rangle = 0$ for all quasiparticle levels whereas a trivial depolarized state yields $\langle n \rangle = 0.5$ for all levels. In comparison, we find that the experimental populations follow a clear distribution whereby $\langle n \rangle$ increases as ω_n decreases. In particular, $\langle n \rangle \approx 0.5$ for the levels associated with the localized edge modes in the antiferromagnetic phase ($g/J < 1$) [27, 28]. This dependence is theoretically understood to be a result of the optimal auxiliary energy splitting matching the upper quasiparticle band edge and thus being detuned from the lower band edge (see SM). The quasiparticle populations provide an error budget to the overall cooling performance from each

quasiparticle level and allow the ground state fidelity to be estimated, since the probability of finding the system in $|\psi_0\rangle$ is $\prod_{n=1}^{L}(1-\langle n\rangle)$.

We then numerically perform a purification of the 1RDMs using a method akin to McWeeny purification used in e.g. quantum chemistry [29] (see SM). The ground state fidelities, constructed from the quasiparticle populations $\langle n\rangle$ after purification, are shown in Fig. 20.3C. At the critical point $g/J = 1.0$, we observe fidelities of 0.92 ($L = 6$), 0.90 ($L = 12$) and 0.86 ($L = 18$), which degrade only weakly over system size. In contrast, the fidelities from the unpurified 1RDMs decay exponentially over L, as shown in the inset of Fig. 20.3C. The dramatic increase of fidelity through the purification process indicates that despite its mixed nature, the steady state has a large overlap with the ground state of the TFIM in its dominant eigenvector. We note that the fidelity decrease in the antiferromagnetic regime is due to the ∼0.5 populations of the edge modes which lead to high purification uncertainties. This interpretation is confirmed by the $L = 18$ fidelities calculated without the edge modes, where the degradation is much reduced (Fig. 20.3C).

Having error-mitigated the steady state, we now demonstrate its topological and quantum-critical behaviors through measuring the long-ranged correlator (Fig. 20.3D):

$$\langle \hat{C}_{jk}\rangle = \langle \hat{Y}_j \hat{P}_{j+1,k-1} \hat{Y}_k\rangle, \tag{20.3}$$

where the parity operator $\hat{P}_{j+1,k-1} = \prod_{n=j+1}^{k-1} \hat{Z}_n$. In the Majorana-fermion formulation of the 1D TFIM, $\langle \hat{C}_{jk}\rangle$ is the correlation between Majorana operators on sites j, k of the chain (see SM). We first show $\langle \hat{C}_{jk}\rangle$ in the antiferromagnetic regime $g/J = 0.6$ (upper panel of Fig. 20.3D). Here we observe that $\langle \hat{C}_{jk}\rangle$ is nearly zero at short range ($|j-k| \leq 12$) but suddenly increases for $|j-k| > 12$. This is a manifestation of the correlation between the exponentially localized edge modes at the ends of the open chain, which map onto the topological phase of a Majorana chain [27, 28]. At $g/J = 1.0$ (lower panel of Fig. 20.3D), we observe that $\langle \hat{C}_{jk}\rangle$ has a maximum at $|j-k| = 1$ instead and decays as a power law over distance, consistent with the critical behavior of the TFIM and in close agreement with ground state calculations. In the SM, we also present $\langle \hat{C}_{jk}\rangle$ in the paramagnetic regime where it decays exponentially due to the ground state resembling a product state (Fig. S6), and entanglement entropy measurements showing logarithmic growth at the critical point (Fig. S7 and Fig. S11).

Although we have thus far focused on exactly solvable models to develop physical insights into dissipative cooling, the experimental protocol is also applicable to non-integrable models where the ground states are not known *a priori*. Figure 20.4A shows the dissipative cooling of a 2D TFIM, implemented with 35 qubits connected to 14 auxiliaries. Besides its large size, the 2D model is challenging to cool since each application of $\hat{U}$ includes four layers of parallel two-qubit $XX(J)$ gates, compared to only two layers in 1D. Nevertheless, we find that the system still stabilizes to a low-energy state of the 2D TFIM from a scrambled initial state, with a steady-state energy ratio $E/E_0 = 0.58$ at the critical point ($g/J = 1.5$ for this particular geometry). The antiferromagnetic behavior of the steady state is visible through measurements of the connected correlator $\langle \hat{X}_j \hat{X}_k\rangle - \langle \hat{X}_j\rangle\langle \hat{X}_k\rangle$ between a corner qubit and every other qubit (Fig. 20.4B). We observe that the correlation persists over a Manhattan distance of ∼6 sites, with a characteristic decay length of ∼2.3.

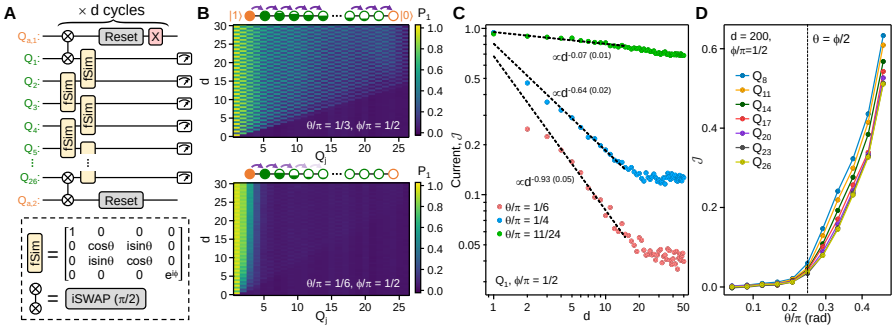

Figure 20.5: Non-equilibrium transport driven by different reservoirs. (A) Quantum circuit for realizing a boundary-driven Floquet XXZ model. Here a 1D chain of 26 qubits are driven by fSim gates and connected to two auxiliaries on the edges that are reset after every cycle. An X gate is applied to $Q_{\mathrm{a},1}$ after each reset to stabilize it in the $|1\rangle$ state. (B) $|1\rangle$ state population P_1 for different qubits Q_j as a function of d, measured with $\phi/\pi = 1/2$ and two different values of θ. Mid-cycle (i.e. $d + 0.5$) data for P_1 are also included, which are taken between the two layers of fSim gates within each cycle. (C) Current flow $\mathcal{J}$ from $Q_{\mathrm{a},1}$ to Q_1, extracted via $\mathcal{J}(d) = P_1(d+0.5) - P_1(d)$ where P_1 is measured at Q_1, as a function of d. Dashed lines are fits to early-time ($d \leq 15$) data using the function form Ad^{α}, where A and α are free parameters. The fitted results for α are shown as exponents of d, along with their standard errors in parentheses. (D) Steady state ($d = 200$) $\mathcal{J}$ as a function of θ, shown for different qubits along the chain. $\mathcal{J}$ represents the population transfer from Q_{j-1} to Q_j in each cycle and is extracted by $\mathcal{J}(d) = P_1(d+0.5) - P_1(d)$ for Q_j with odd j and $\mathcal{J}(d) = P_1(d+1) - P_1(d+0.5)$ for Q_j with even j. Dashed line indicates the isotropic point $\theta = \phi/2$.

To probe the entanglement structure of the steady state, we adopt the second-order Rényi mutual information:

$$\mathrm{MI} = S_{\mathrm{A}}^{(2)} + S_{\mathrm{B}}^{(2)} - S_{\mathrm{AB}}^{(2)}, \tag{20.4}$$

where $S^{(2)} = -\log_2 \mathrm{Tr}\rho^2$ denotes the second-order Rényi entropy of a subsystem (A, B or AB) with density matrix ρ. MI includes contributions from both classical and quantum correlations and is relatively insensitive to classical entropy coming from imperfect cooling or measurement errors [30]. In 2D, the MI is generally inaccessible to quantum simulators in which measurements are limited to a single basis [12, 32]. Leveraging the universal gate set of the quantum processor, we obtain MI between all possible partitions of the system through a single set of randomized measurements [33] (see SM).

The upper panel of Fig. 20.4C shows the MI between nearest-neighbor qubits, where values between 0.06 and 0.35 are observed throughout the system. The MI between all qubit pairs is shown in the lower panel of Fig. 20.4C, where it is seen to decay over distance. Despite the spatial decay, MI is finite between qubits separated by $s \approx 3$. We note that the fluctuation of MIs between qubits separated by the same Manhattan distance is likely due to inhomogeneous cooling across the system due to, e.g., different qubit decoherence rates. The randomized measurements also allow us to extract the many-body MI between seven 5-qubit partitions of the system, as shown in the upper panel of Fig. 20.4D. Here we again observe a large MI between contiguous 5-qubit subsystems, which decays as the subsystems become more separated (lower panel of Fig. 20.4D). Notably, we still observe finite MIs between some non-neighboring subsystems, such as A and D. The behavior of MI above shows that the cooling protocol is capable of steering models of quantum magnetism into correlated steady states. Further improvements of qubit coherence times will allow preparation of a large variety of magnetic states with longer-ranged quantum correlations.

The dissipative dynamics investigated thus far has focused on coupling a many-body system to a single reservoir. It is natural to ask whether quantum-coherent behavior may also

arise from coupling the system to different reservoirs, which induces non-equilibrium transport through a chemical potential difference. We explore this possibility using another paradigmatic model of quantum magnetism, the 1D XXZ spin chain [34], which is currently the subject of intense theoretical [35] and experimental [36, 37, 38] investigations due to its rich magnetic transport properties. A Floquet version of the XXZ model [39, 40] is readily implementable using consecutive applications of fSim gates parameterized by a conditional phase ϕ and iSWAP angle θ, as shown in Fig. 20.5A. Here the qubit $|0\rangle$ ($|1\rangle$) state mimics the spin-up (spin-down) state. A pair of boundary auxiliaries ($Q_{\mathrm{a},1}$ and $Q_{\mathrm{a},2}$), stabilized to $|1\rangle$ and $|0\rangle$ states, are coupled to the chain via iSWAP gates. We then measure $|1\rangle$ state probability, P_1, of the system qubits (initialized in $|0\rangle^{\otimes L}$) over d.

Within the linear response regime [41, 42], the XXZ chain is predicted to show different transport regimes depending on the anisotropy parameter $\Delta = \frac{\phi}{2\theta}$. In our experiment, the strong driving from the boundary auxiliaries unveils transport phenomena in a highly non-equilibrium regime far away from linear response. The initial spreading of qubit excitations in the system up to $d = 30$ is illustrated in Fig. 20.5B. In the easy-plane regime ($\Delta < 1$), we observe a ballistic propagation consistent with the existence of freely propagating magnon quasiparticles. In contrast, in the easy-axis ($\Delta > 1$) regime, qubit excitations fail to propagate into the system. Instead, a relatively sharp domain wall is formed between a few excited qubits adjacent to Q_1 and the other qubits which remain in the $|0\rangle$ state. The observed domain wall is due to the fact that n adjacent qubit excitations form a heavy bound state with a group velocity exponentially suppressed by n, hence inhibiting transport [40].

We next characterize details of the quantum transport through the local current $\mathcal{J}$, which corresponds to the difference between qubit populations in the middle and at the end of each cycle d. Compared to P_1, $\mathcal{J}$ is less sensitive to readout errors. Figure 20.5C shows the time-dependent $\mathcal{J}$ at Q_1, corresponding to the population pumped into the system from $Q_{\mathrm{a},1}$ per cycle [43]. At early cycles ($d \leq 15$) where qubit decoherence plays a minor role in transport, we observe different dynamical exponents depending on Δ: In the easy-plane regime, the current is nearly constant at early times and scales as $\propto d^{-0.07}$. In the easy-axis regime, we find a dependence $\mathcal{J}(d) \propto d^{-0.93}$, which corresponds to a total population transfer approximately scaling as $\sim\log d$. The unusual logarithmic scaling was found in a recent Bethe ansatz solution for the Hamiltonian case [44]. At the isotropic point ($\Delta = 1$) where no exact solution is available, we observe a power-law scaling $\mathcal{J}(d) \propto d^a$ with a sub-diffusive exponent $a \approx -0.64$. The dynamical exponent found at the isotropic point agrees well with noise-free numerical simulation of larger system sizes shown in the SM, which finds a similar value of $a \approx -0.72$. This result qualitatively differs from recent experiments in closed quantum systems which observed super-diffusive ($a = -1/3$) transport at the isotropic point [36, 37], providing evidence for a previously unknown transport regime of the XXZ model outside linear response.

Lastly, we focus on the long-time behavior of the local currents after their saturation at $d \gtrsim 30$. The saturation corresponds to the formation of a non-equilibrium steady state (NESS) which is stable up to an experimental limit of $d = 200$. Interestingly, despite the spreading of qubit decoherence at this late cycle, we observe that $\mathcal{J}$ still depends sharply on the coupling anisotropy and serves as a dynamical order parameter for the different transport regimes (Fig. 20.5D): In the easy-plane regime, we observe finite current flow through qubits away from $Q_{\mathrm{a},1}$. At the isotropic point, $\mathcal{J}$ is greatly suppressed but retains a finite value throughout the chain. In the easy-axis regime, we find that $\mathcal{J}$ is nearly 0 for all qubits. Our results complement early theoretical investigations of a boundary-driven XXZ model and indicate that the insulating behavior of the XXZ model persists even in the presence of qubit decoherence [45].

In summary, our work highlights engineered dissipation as a promising method for preparing quantum many-body states. Compared to state preparation algorithms based on unitary evolution, our protocol has several advantages, including long lifetimes of the prepared states,

robustness across quantum phase transitions and a better scaling at larger system sizes (see Section S4 of the SM). Even against variational quantum algorithms which may achieve similar performance at current system sizes, the dissipative protocol is advantageous owing to its minimal optimization overhead and the ability to capture long-range quantum correlation. Despite these advantages, we note that cooling generic Hamiltonians may require complex system-bath couplings that are too challenging to implement in practice. The development of error-mitigation schemes for non-integrable models such as the 2D TFIM remains another open question.

Beyond cooling, we find that our platform may also be applied to study non-equilibrium dynamics that is difficult to access via closed quantum systems. Using the XXZ chain as an example, we have already made the experimental discovery of a new transport regime in this well-known quantum spin model. Our work therefore broadly enhances the functionality of quantum processors by introducing engineered dissipative channels as fundamental building blocks, with applications to open-system quantum simulation [46], quantum transport [47] and stabilization of topological quantum states [4, 49, 50].

Data availability – Xiao Mi, Data for "Stable Quantum-Correlated Many Body States via Engineered Dissipation," Zenodo (2023); https://doi.org/10.5281/zenodo.8187929.

20.2 Supplementary Materials for "Stable Quantum-Correlated Many Body States through Engineered Dissipation"

20.3 Experimental details and additional data

20.3.1 CPHASE and fSim gates

The quantum processor used in our experiment is similar to those used in recent works [28, 20] and consists of 68 frequency-tunable transmons with tunable couplings. The median T_1 of the qubits is 22 μs. Two main improvements have been made to the calibration of tunable CPHASE gates and tunable fSim gates to enable dissipative cooling and XXZ non-equilibrium transport: (i) The errors of the CPHASE gates are reduced by more than two-fold compared to past implementations [51]. (ii) The tunability of the fSim gates is enhanced [40], allowing nearly all combinations of iSWAP angles and conditional phases to be accessed with low control errors. We briefly outline the technical progress that enabled these improvements below.

The CPHASE gates are implemented by flux pulses that bring two transmons to a relative frequency detuning of ϵ_{2p} between the $|11\rangle$ and $|02\rangle$ states, while ramping the coupler to enact a $XX+YY$ coupling with a maximum value of $g_{\max}$. After a pulse duration $t_p \approx \frac{1}{\sqrt{8g_{\max}^2+\epsilon_{2p}^2}}$, qubit leakage (i.e. $|2\rangle$ state population) returns to $\sim$0 and a conditional phase ϕ is accumulated. By keeping t_p fixed while adjusting $g_{\max}$ and ϵ, ϕ may be tuned between 0 and 2π. The gate fidelities were found to be $\sim$99.0% in our earlier works [51], limited by both coherence times and a parasitic iSWAP angle $\theta \approx 0.02$ rad.

In the current work, we have reduced the parasitic iSWAP angles to a lower level of $\sim$0.003 rad. This is accomplished by smoothing the coupler pulses to better maintain an adiabatic condition between the $|01\rangle$ and $|10\rangle$ states of the qubits during gate implementation. The reduced iSWAP errors also allow us to remove the qubit detuning pulses (a.k.a. "physical" Z gates) before the coupler pulses and replace them with virtual Z rotations, which further reduce gate errors [52]. Furthermore, improved frequency-selection algorithms along with careful monitoring of system stability allow avoidance of two-level system (TLS) defects in large quantum systems, reducing the number of outlier gates [53, 54]. Lastly, we have also optimized the fidelity of single-qubit gates by reducing their pulse lengths.

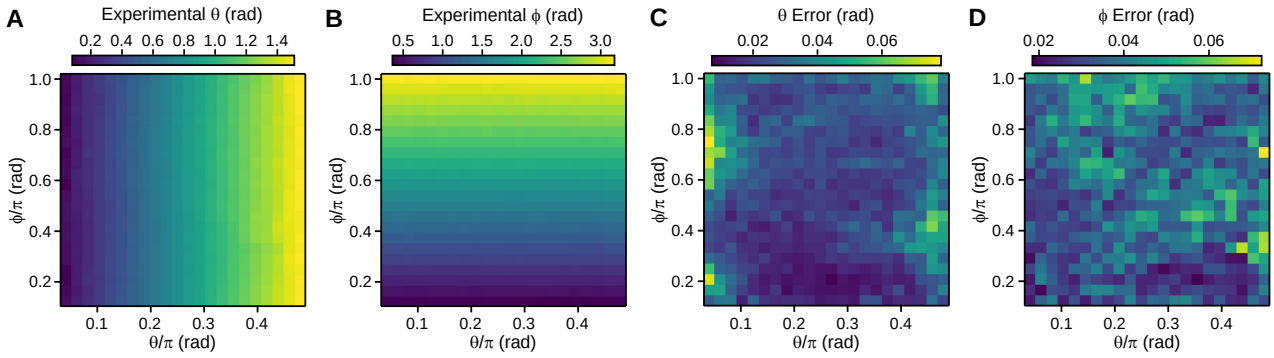

Figure 20.7: Continuously tunable fSim gates. (A) The experimentally measured values of θ as a function of target θ and ϕ, averaged over 25 qubit pairs in a chain of 26 qubits. (B) Same as panel A but with experimentally measured values of ϕ plotted. (C) Root-mean-squared differences between target and measured values of θ, averaged over all 25 qubit pairs. (D) Same as panel C but with the error in ϕ shown.

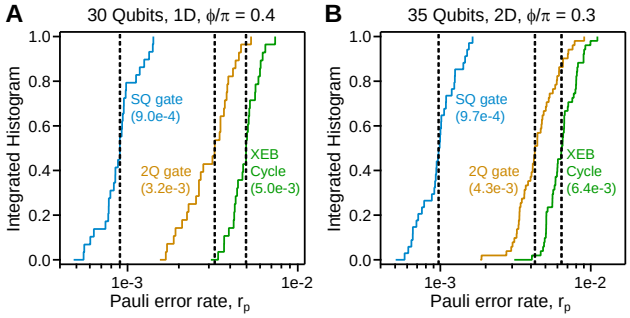

Figure 20.6: Single-qubit and CPHASE gate fidelities. (A) Integrated histograms of Pauli error rates r_{p} associated with single-qubit $\sqrt{X}$ and $\sqrt{Y}$ rotations (blue), two-qubit CPHASE gate with $\phi/\pi = 0.4$ (brown) and an XEB cycle (green). Median value of each histogram is listed within the figure and also indicated with a vertical dashed line. The results are obtained with a 1D chain of 30 qubits and gates executed in parallel. (B) Same as panel **a** but with $\phi/\pi = 0.3$ and 35 qubits in 2D. Gates are also executed in parallel.

The fidelities of single-qubit gates and two-qubit CPHASE gates are shown in Fig. 20.6. Here we show the gate errors associated with the 30-qubit 1D chain used in Fig. 3A and the 35-qubit 2D grid used in Fig. 4 of the main text, along with the conditional phases ϕ used in these two figures. In 1D, we achieve single-qubit gate errors that have both a median and a mean of 9.0×10^{-4}, characterized through simultaneous randomized benchmarking. The two-qubit CPHASE gate errors, characterized through simultaneous cross-entropy benchmarking [55], have a median (mean) error of 3.2×10^{-3} (3.1×10^{-3}). In 2D, the single-qubit gate errors have a median (mean) value of 9.7×10^{-3} (9.9×10^{-3}). The two-qubit CPHASE gate errors have a median (mean) error of 4.3×10^{-3} (4.6×10^{-3}). For both 1D and 2D, the two-qubit XEB cycle errors (which include contributions from two single-qubit gates and one CPHASE gate) are also included for reference. The entangling gate fidelity is among the lowest for experimentally reported quantum processors of this size.

In contrast to the CPHASE gates, the tunable fSim gates are implemented primarily through the resonant interaction between the $|01\rangle$ and $|10\rangle$ states of the two qubits [40]. In our past works, independent tuning of ϕ and θ is achieved by exploiting the different scaling of each angle with respect to the strength of the interqubit coupling g_{max}, i.e. $\theta \propto g_{\mathrm{max}}$ whereas $\phi \propto g_{\mathrm{max}}^2$. However, achieving full coverage over the entire range of ϕ and θ is difficult, since certain combinations of the two angles require either excessively long pulses or large g_{max} where either

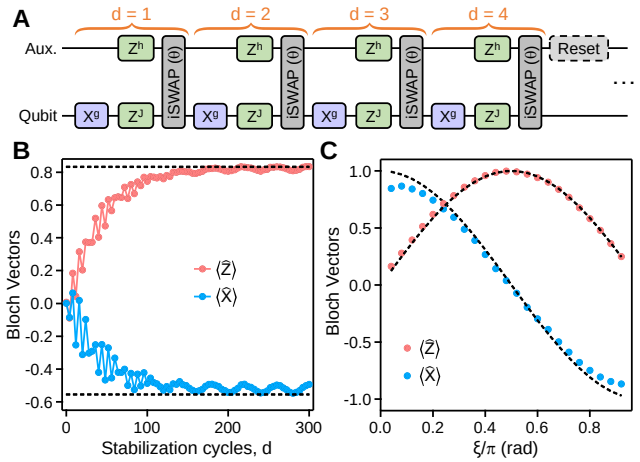

Figure 20.8: Stabilization of single-qubit states. (A) Circuit schematic for stabilizing states of a single qubit using a single auxiliary. (B) Bloch vectors of the single qubit, $\langle\hat{Z}\rangle$ and $\langle\hat{X}\rangle$, as a function of number of stabilization cycles d. Here $J = 0.18$, $g = -0.12$, $\theta = 0.09$ rad and $h = \sqrt{g^2 + J^2}$. Dashed lines indicate the Bloch vectors corresponding to an eigenstate of the single-qubit Hamiltonian $\hat{H}_{1q} = g\hat{X} + J\hat{Z}$. Readout errors have been corrected in the data via experimentally obtained readout errors. (C) Bloch vectors (averaged between $d = 280$ and $d = 300$) as a function of ξ, where $J = A\sin\xi$, $g = A\cos\xi$ and $A = \frac{0.3}{|\sin\xi|+|\cos\xi|}$. $\theta = 0.09$ rad in this plot. Dashed lines indicate the Bloch vectors corresponding to an eigenstate of the single-qubit Hamiltonian at each ξ.

decoherence or leakage becomes an issue. To circumvent these constraints, we have added a third tuning parameter to the fSim gate, namely a variable detuning ϵ_{1p} between the $|01\rangle$ and $|10\rangle$ states. The detuning parameter allows θ to be varied while leaving ϕ largely constant, allowing coverage of previously unachievable angles.

In Fig. 20.7A and Fig. 20.7B, we show experimentally measured values of θ and ϕ over a nearly complete coverage of all possible target angles, $\theta \in [\frac{\pi}{24}, \frac{23\pi}{48}]$ and $\phi \in [\frac{\pi}{8}, \pi]$, averaged over the 26-qubit chain used in Fig. 5 of the main text. The results are obtained from unitary tomography measurements [40]. The control errors associated with each angle are shown in Fig. 20.7C and Fig. 20.7D. The average error in θ is 0.026 rad and the average error in ϕ is 0.037 rad. These errors may be reduced in future experiments using Floquet calibration [56]. We also note that the control errors in θ are larger for $\theta \to 0$ or $\theta \to \pi/2$, which may be a result of their higher sensitivities to state preparation and measurement (SPAM) errors in unitary tomography.

20.3.2 Stabilization of single-qubit states

While we have primarily focused on the stabilization of multiqubit systems in the main text, the dissipative scheme is straightforwardly applicable to single-qubit stabilization as well. Past works on this topic have employed superconducting resonators with tailored shot-noise spectrum or parametrically modulated coupling to stabilize the states of a transmon qubit [57, 58]. Here we utilize the same setup as Fig. 1 of the main text and seek to stabilize a single qubit to an eigenstate of the Hamiltonian, $\hat{H}_{1q} = g\hat{X} + J\hat{Z}$, by coupling it to a dissipative auxiliary (Fig. 20.8A). The single qubit is evolved via a Trotterized implementation of $e^{-i\hat{H}_{1q}t}$ using alternating layers of X^g and Z^J gates. The auxiliary is evolved by a phase gate Z^h with an exponent $h = \sqrt{g^2 + J^2}$ that matches the energy splitting of the auxiliary to the qubit. Similar to the TFIM, the qubit and auxiliary are coupled by a weak partial-iSWAP gate having an angle $\theta = 0.09$ rad. A reset is applied to the auxiliary every 4 stabilization cycles, d.

The time dependence of the Bloch vectors of the qubit is shown in Fig. 20.8B, where we have averaged over 20 random initial states. We observe that, on average, the Bloch vectors $\langle \hat{Z} \rangle$ and $\langle \hat{X} \rangle$ increase and reach steady state values close to the calculated values for an eigenstate of $\hat{H}_{1q}$. To see how the steady state Bloch vectors compare to the idealized values across different Hamiltonian parameters, we vary the ratio of g/J by sweeping the parameter $\xi = \tan^{-1}(J/g)$ and measure the steady state values of the Bloch vectors. The results, plotted in Fig. 20.8C, show close agreement between the idealized values and the experimentally measured values over a wide range of ξ.

20.3.3 Circuit optimization and comparison with quantum trajectory simulations

As illustrated by Fig. 1 of the main text, to maximize the efficiency of the dissipative cooling protocol, the energy splitting of the auxiliaries needs to match excitation energies of the quantum system. At the same time, the auxiliary-system coupling needs to be strong enough to remove system excitations at a high rate but weak enough to avoid dressing the energy spectrum of the system and modifying its Hamiltonian. We perform an experimental optimization procedure by measuring the energy of the system $E = \langle \hat{H}_{\mathrm{TFIM}} \rangle$ at a late time $d = 100$, while sweeping circuit parameters θ and h. The normalized energy, E/E_0, where E_0 is the numerically calculated energy of the ground state, is shown in Fig. 20.9A. A maximum ratio of $E/E_0 \approx 0.8$ is observed at $h = 1.65$ and $\theta/\pi = 0.11$, indicating that the system is closest to the ground state for these circuit parameters. This optimization process is performed for each value of g/J and each different geometry in Fig. 2 to Fig. 4 of the main text.

To confirm that our system is indeed performing as expected, we compare experimentally obtained energies E against numerical simulations of the exact same quantum circuits via quantum trajectory methods. Both experimental results and noisy simulation results are shown in Fig. 20.9B. Here we have used single-qubit $T_1 = 21$ μs and $T_2 = 8$ μs, which are close to the typical coherence times of our qubits. The gate times used in the numerical simulations are also identical to those used in experiments. We find excellent agreements between the numerically simulated time-dependent energies and experimental values, indicating that relatively simple error channels including qubit relaxation and dephasing are sufficient to account for the experimental performance.

Figure 20.9C shows the steady state energy ratio E/E_0 as a function of g/J, from both experimental results and noisy simulation. We again observe close agreement between the two cases. To identify the limitation of the cooling performance from decoherence alone, we also simulate the experiment without qubit relaxation and dephasing. The results, also plotted in Fig. 20.9C, show an improved steady state energy ratio of $E/E_0 \approx 0.9$. The energy ratio in the noiseless simulation is primarily limited by the relatively large Trotter angle, $J = 0.2$ or $J = 0.25$, in these experiments, which is chosen to ensure sufficiently fast motion of quasiparticles such that they are removed by the auxiliaries within a time scale $\ll T_1, T_2$. This is confirmed by reducing the value of J to $1/12$ and rerunning the noiseless simulation, the result of which is also shown in Fig. 20.9C. Here the energy ratio E/E_0 is higher and averages to 0.98. As observed in the experiments, the limitation imposed by large J can be mitigated by comparing the steady state to the Floquet eigenstates instead. The fidelities of the steady state with respect to the two low-lying states of the TFIM, for the noiseless simulation with $J = 1/12$, are also shown in Fig. 20.9D. We observe a total fidelity of $\langle \psi_0 | \rho | \psi_0 \rangle + \langle \psi_1 | \rho | \psi_1 \rangle > 0.97$ throughout the different phases of the model, with a nearly equal mixture of the two states deep in the anti-ferromagnetic phase ($g/J = 0.4$) owing to the near-degeneracy of the two low-lying states. These results indicate that the cooling protocol can yield high-fidelity results in the idealized case of no decoherence and small Trotter steps.

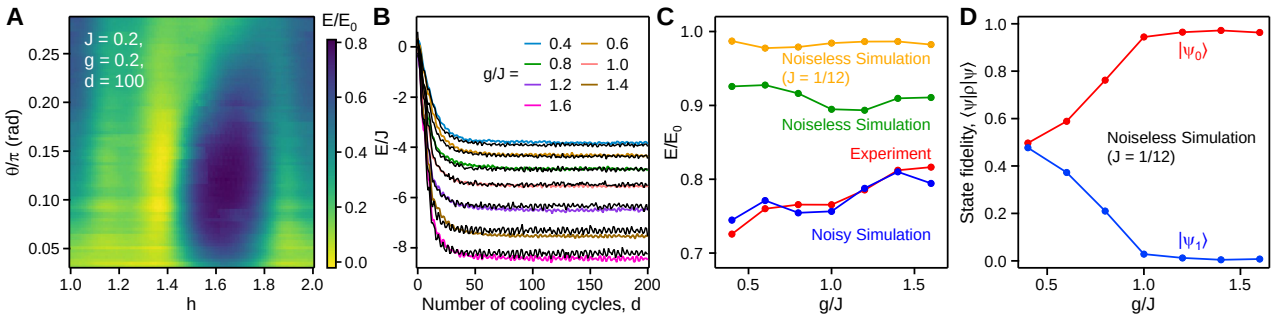

Figure 20.9: Circuit parameter optimization and comparison with quantum trajectory simulations. (A) Experimentally measured ratio between the energy E at $d = 100$ and the ground state energy E_0, as a function of gate parameters θ and h (see Fig. 2 of the main text). $L = 6$ in this plot. (B) Experimentally obtained (colored lines) and numerically simulated (black dashed lines) energies E of the 6-site TFIM as a function of d and for different values of g/J. (C) Steady state energy ratio E/E_0 as a function of g/J, obtained through experiment (red), noisy simulation (blue) and noiseless simulation (green). Noiseless simulation results using a smaller Trotter angle $J = 1/12$ are also shown, where the auxiliary reset is applied every 12 cycles. (D) Steady state fidelities with respect to the ground ($|\psi_0\rangle$) and excited ($|\psi_1\rangle$) states of the 6-site TFIM, computed from noiseless simulation and $J = 1/12$.

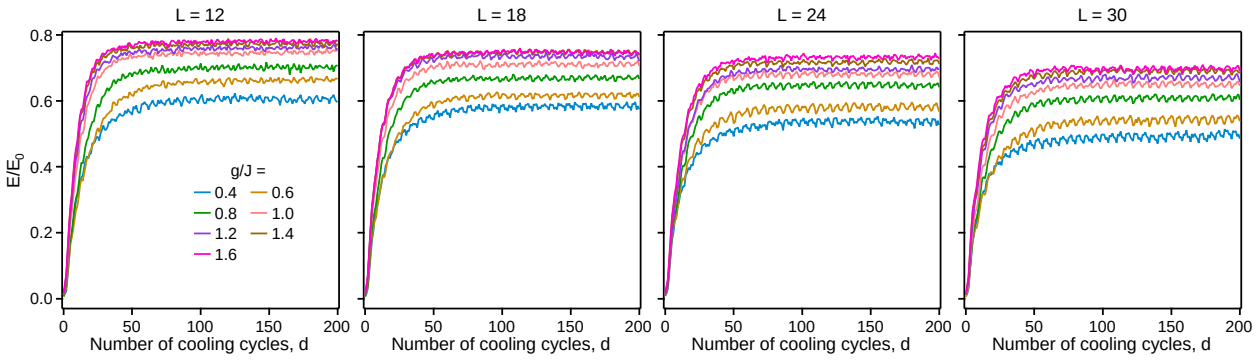

Figure 20.10: **Time-dependence of energy for large 1D TFIM chains.** Ratio between the measured energy $E = \langle \hat{H}_{\mathrm{TFIM}} \rangle$ and the ground state energy E_0 as a function of the number of cooling cycles d. Data are shown for chain lengths of $L = 12$, 18, 24 and 30.

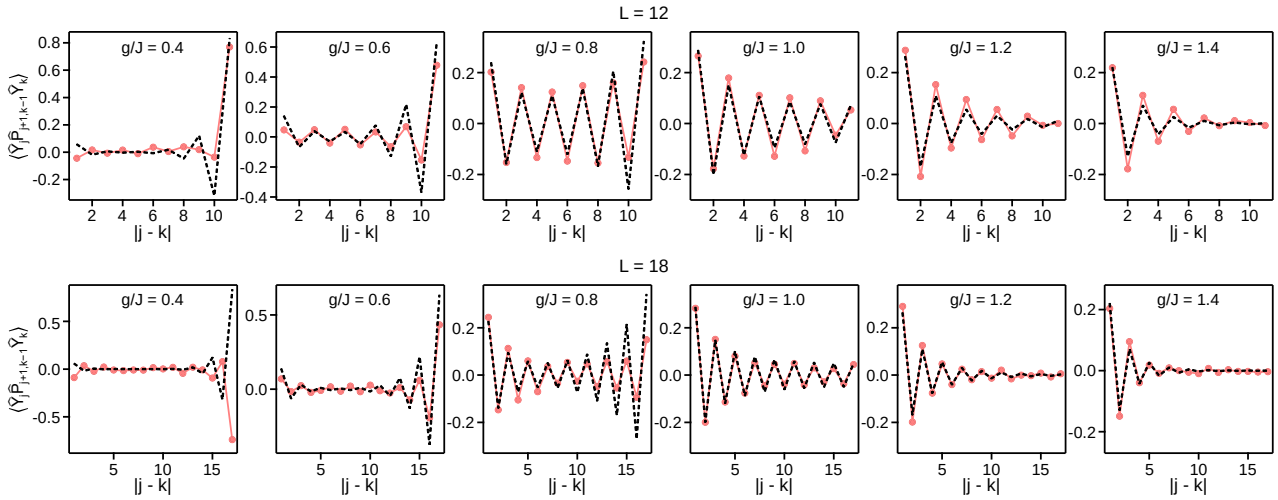

Figure 20.11: Detailed experimental data of quantum correlations $\langle \hat{Y}_j \hat{P}_{j+1,k-1} \hat{Y}_k \rangle$ for $L = 12$ and $L = 18$, across the quantum phase transition. Solid symbols are experimental results constructed from purified 1RDMs and dashed lines are exact ground state calculations.

20.3.4 Time-dependent energy for large 1D TFIM

The experimental data showing the detailed time dependence of the ratio between measured energy E of the system and the numerically calculated ground state energy E_0 of the 1D TFIM is plotted in Fig. 20.10. Data for each system size L is also shown for different values of g/J spanning the anti-ferromagnetic regime ($g/J < 1.0$), critical point ($g/J = 1.0$) and the paramagnetic regime ($g/J > 1.0$). For each case, we observe that the system reaches a steady state at $d \approx 100$, beyond which E/E_0 is approximately constant.

20.3.5 Additional quantum correlation data

Experimentally measured values of the long-range quantum correlator $\langle \hat{Y}_j \hat{P}_{j+1,k-1} \hat{Y}_k \rangle$, constructed using the purified 1RDMs, are shown in Fig. 20.11 for different values of g/J across different phases of the 1D TFIM. Results for both $L = 12$ and $L = 18$. We observe that for $L = 12$, results are in good agreement with the ground state. For $L = 18$, we observe equally good agreement except at $g/J = 0.4$, where the experimental data show oscillations with an opposite sign compared to the ground state, at large $|j - k|$. This is due to the small energy splitting between the two edge modes at this system size and g/J, which makes distinguishing them difficult in experiment. Consequently, the mixed-state 1RDM of the steady state is projected to the first excited state rather than the ground state by the purification process (see Section 20.5).

20.3.6 Rényi entropy and entanglement structure of the steady state

In addition to quantum correlations, the ground state entanglement structure of the 1D TFIM can also be detected via measurements of the second-order Rényi entropy, defined as $S^{(2)} = -\log_2 \mathrm{Tr}\rho^2$ where ρ is the reduced density matrix of a given subsystem. To measure $S^{(2)}$, we adopt the randomized measurement protocol [33] which has more favorable scaling in the number of measurement shots required compared to full QST. The results for the dissipatively cooled steady state of a $L = 16$ qubit chain is shown in Fig. 20.12A. Here we observe that $S^{(2)}$ increases nearly monotonically with system size. This is a consequence of an extensive

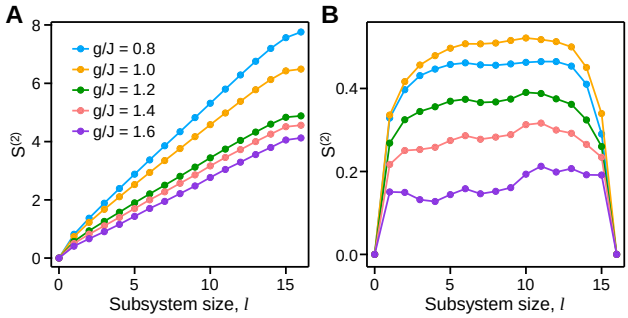

Figure 20.12: Rényi entropy and entanglement structure of the steady state. (A) Second-order Rényi entropy $S^{(2)}$ for different subsystem sizes l, measured on a 16-qubit chain after it has been dissipatively cooled with $d = 100$ cycles. For each subsystem size, the data are averaged over all possible chains of length l. To scramble the steady state, we use 30 sets of randomly chosen single-qubit Clifford gates and perform 3 million measurement shots on each set. (B) Error-mitigated values of $S^{(2)}$ as a function of l.

background classical entropy due to the mixed-state nature of the steady state and measurement errors.

Despite the background entropy, past works have shown that it is still possible to extract the entanglement scaling of a quantum state [59, 60]. This is because background classical entropy such as measurement error typically scales linearly, with a slope $S^{(2)}_{BG}$, against the subsystem size. Since the entanglement entropy is expected to be 0 at the full system size for a pure state, $S^{(2)}_{BG} = S^{(2)}_{L}/L$ where $S^{(2)}_{L}$ is $S^{(2)}$ measured at $l = L$ and has contributions only from the background entropy. The error-mitigated entanglement entropy $S^{(2)}$ for each subsystem is then extracted by subtracting $(l/L)S^{(2)}_{BG}$ from the unmitigated value of $S^{(2)}$. The error-mitigated values of $S^{(2)}$ are shown in Fig. 20.12B. Here we see that the $S^{(2)}$ exhibits area-law scaling while in the paramagnetic phase ($g/J > 1.0$). At the critical point $g/J = 1.0$, $S^{(2)}$ has the largest value and the strongest dependence on system size l, consistent with the expected logarithmic scaling of entanglement. In the antiferromagnetic regime ($g/J = 0.8$), $S^{(2)}$ starts to decrease and approach an area law again. These results indicate the entanglement structure of the 1D TFIM is preserved in the dissipatively cooled steady state. An alternative method of extracting entanglement entropy using purified 1RDMs is presented in Fig. 20.16, where a similar transition from area-law to logarithmic scaling of entanglement is observed.

20.4 Mechanism of dissipative cooling

Here, we discuss the mechanism of dissipative cooling, focusing on the example of the Trotterized, or Floquet TFIM. First, for completeness we provide expressions for the eigenmodes of the Floquet TFIM, obtained by mapping it onto a kicked Kitaev fermionic chain. Second, we introduce an auxiliary at the edge. Assuming a weak coupling between the auxiliary qubit and the chain, we derive a perturbative expression for system's evolution. Adopting secular approximation, we analyze time evolution of quasiparticle occupation numbers. This allows us to identify the parameter values where cooling protocol is optimal and lowest quasiparticle occupations are reached in the steady state. Finally, we illustrate the validity of the secular approximation for a broad range of auxiliary-system couplings, by comparing predicted quasiparticles occupations to exact numerical results.

20.4.1 Eigenmodes of the Floquet transverse-field Ising model

We start by considering the Floquet TFIM described in the main text, which is specified by a cycle unitary operator:

$$\hat{U} = e^{-\frac{i\pi J}{2}\sum_{j=1}^{L-1}\hat{X}_j\hat{X}_{j+1}} e^{\frac{i\pi g}{2}\sum_{j=1}^{L}\hat{Z}_j}. \tag{20.5}$$

This model can be mapped onto a quadratic fermionic chain by the Jordan-Wigner transformation. We define Majorana operators on site j as follows:

$$\hat{a}_{2j-1} = \left[\prod_{k=1}^{j-1}\hat{Z}_k\right]\hat{X}_j, \quad \hat{a}_{2j} = \left[\prod_{k=1}^{j-1}\hat{Z}_k\right]\hat{Y}_j. \tag{20.6}$$

These operators obey standard Majorana anti-commutation relations, and are related to complex fermion operators $\hat{c}_j, \hat{c}_j^\dagger$ via

$$\hat{a}_{2j-1} = \hat{c}_j^\dagger + \hat{c}_j, \quad \hat{a}_{2j} = i\left(\hat{c}_j^\dagger - \hat{c}_j\right).$$

We note that the fermionic vacuum defined with respect to operators $\hat{c}_j, \hat{c}_j^\dagger$, corresponds to $|1\rangle$ state of the qubits/spins.

The spin operators that enter the expression for the Floquet unitary (20.5) are related to the Majorana operators as follows,

$$\hat{Z}_j = -i\hat{a}_{2j-1}\hat{a}_{2j}, \quad \hat{X}_j\hat{X}_{j+1} = -i\hat{a}_{2j}\hat{a}_{2j+1}. \tag{20.7}$$

Thus, $\hat{U}$ is a quadratic evolution operator in terms of fermions, and the Majorana operators are linearly transformed under it:

$$\hat{U}^\dagger\hat{a}_k\hat{U} = \sum_{l=1}^{2L} K_{kl}\hat{a}_l. \tag{20.8}$$

We look for the eigenmodes of the Floquet TFIM, specified by the annihilation/creation operators $\hat{\eta}, \hat{\eta}^\dagger$ such that $\hat{U}^\dagger\hat{\eta}\hat{U} = e^{-i\phi}\hat{\eta}$ (ϕ being the quasienergy), in the following form:

$$\hat{\eta} = \sum_{j=1}^{L}\psi_{2j-1}\hat{a}_{2j-1} + \psi_{2j}\hat{a}_{2j}. \tag{20.9}$$

In an infinite system, the solutions have a plane-wave form with quasimomentum q, with quasienergy dispersion relation specified by

$$\cos\phi_q = \cos(\pi J)\cos(\pi g) - \sin(\pi J)\sin(\pi g)\cos q. \tag{20.10}$$

In Fig. 20.13, we plot the quasienergy bands as a function of q for an infinitely long chain.

We are interested in the case of a finite chain. In this case, the eigenmodes are given by a superposition of two plane waves with $\pm q$. The boundary conditions yield a transcendental equation for quasimomentum quantization that determines L quasimomenta values, q_α. The corresponding quasienergies are specified by Eq. (20.10). These eigemodes are derived as follows:

For the Floquet TFIM, the action of K on vectors is given by $\underline{v}' = K\underline{v}$, where

$$\begin{aligned}
v'_{2j-1} &= -\sin(\pi J)\sin(\pi g)v_{2j-3} + \sin(\pi J)\cos(\pi g)v_{2j-2} + \cos(\pi J)\cos(\pi g)v_{2j-1} + \cos(\pi J)\sin(\pi g)v_{2j},\\
v'_{2j} &= -\cos(\pi J)\sin(\pi g)v_{2j-1} + \cos(\pi J)\cos(\pi g)v_{2j} - \sin(\pi J)\cos(\pi g)v_{2j+1} - \sin(\pi J)\sin(\pi g)v_{2j+2},
\end{aligned} \tag{20.11}$$

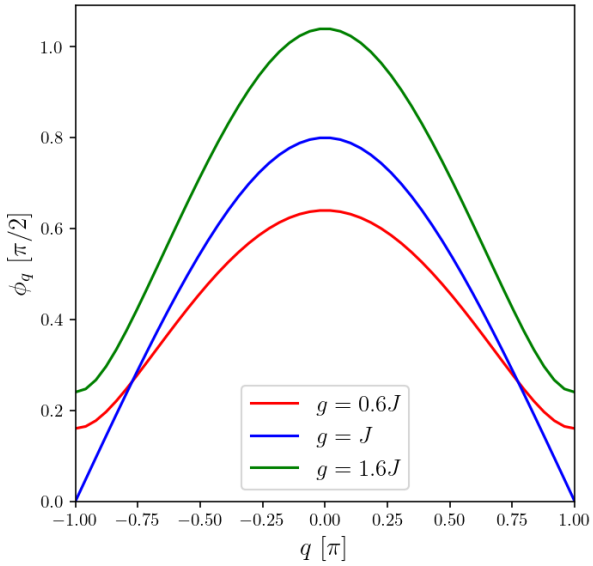

Figure 20.13: The quasienergy band spectrum ϕ_q defined in (20.10) as a function of the quasimomentum q, for $J = 0.2$, g within antiferromagnetic phase ($g = 0.6J$), at critical point ($g = J$) and within paramagnetic phase ($g = 1.6J$). At the critical point the band gap closes.

for $1 < 2j - 1 \leq 2L - 1$ and the open boundary conditions fix

$$v_1' = \cos(\pi g)v_1 + \sin(\pi g)v_2, \tag{20.12}$$

$$v_{2L}' = -\sin(\pi g)v_{2L-1} + \cos(\pi g)v_{2L}. \tag{20.13}$$

We look for the L eigenvectors of K with non-negative quasienergy $\phi_q \geq 0$ such that $\underline{\psi}'^q = e^{-i\phi_q}\underline{\psi}^q$. Here q labels the quasimomentum. Due to particle-hole symmetry the eigenvectors of K with negative quasienergy are related to those of positive quasienergy by the conjugation $\underline{\varphi}^q = (\underline{\psi}^q)^*$, $\underline{\varphi}'^q = e^{i\phi_q}\underline{\varphi}^q$. First we derive the plane waves $\underline{v}$ satisfying the eigenvalue equation in the bulk (20.11), but not the the boundary conditions (20.12, 20.13).

The Bloch ansatz

$$\begin{pmatrix} v_{2j-1}^q \\ v_{2j}^q \end{pmatrix} = \frac{e^{iq(j-1)}}{\sqrt{L}} \begin{pmatrix} \chi_1^q \\ \chi_2^q \end{pmatrix}, \tag{20.14}$$

reduces the bulk equations (20.11) to the secular equation

$$\begin{pmatrix} \cos(\pi J)\cos(\pi g) - \sin(\pi J)\sin(\pi g)e^{-iq} & \cos(\pi J)\sin(\pi g) + \sin(\pi J)\cos(\pi g)e^{-iq} \\ -\cos(\pi J)\sin(\pi g) - \sin(\pi J)\cos(\pi g)e^{iq} & \cos(\pi J)\cos(\pi g) - \sin(\pi J)\sin(\pi g)e^{iq} \end{pmatrix} \begin{pmatrix} \chi_1^q \\ \chi_2^q \end{pmatrix} = e^{-i\phi_q} \begin{pmatrix} \chi_1^q \\ \chi_2^q \end{pmatrix}. \tag{20.15}$$

The two eigenvalues are $e^{-i\phi_q}$ and $e^{+i\phi_q}$ and taking the matrix trace yields Eq. (20.10). The matrix transformation (20.15) can be viewed as an $SU(2)$ rotation by angle $2\phi_q$ about the axis defined by the unit vector

$$\underline{n}(q) = \begin{pmatrix} \sin(2\mu_q)\cos\xi_q \\ \sin(2\mu_q)\sin\xi_q \\ \cos(2\mu_q) \end{pmatrix} \equiv \frac{1}{\sin(\phi_q)} \begin{pmatrix} \sin(\pi J)\cos(\pi g)\sin q \\ -\cos(\pi J)\sin(\pi g) - \sin(\pi J)\cos(\pi g)\cos q \\ -\sin(\pi J)\sin(\pi g)\sin q \end{pmatrix}, \tag{20.16}$$

where we have parameterized by polar and azimuthal angles μ_q and ξ_q, which depend on the quasimomentum. The eigenvector with eigenvalue $e^{-i\phi_q}$ is given by

$$\begin{pmatrix} \chi_1^q \\ \chi_2^q \end{pmatrix} = \begin{pmatrix} \cos\mu_q \\ e^{i\xi_q}\sin\mu_q \end{pmatrix}. \tag{20.17}$$

Each quasienergy ϕ_q is degenerate with its quasimomentum-reversed partner ϕ_{-q} (with the exception of $q = 0$ and $q = \pi$, which must be treated separately). The boundary lifts this degeneracy. We then form standing waves $\underline{\psi}^q$ as linear combinations of $\underline{v}^q$ and $\underline{v}^{-q}$, with $\underline{\psi}^q$ satisfying the boundary equations. Introducing the phase shift δ_q, the standing waves take the form

$$\begin{pmatrix} \psi^q_{2j-1} \\ \psi^q_{2j} \end{pmatrix} = \frac{1}{\sqrt{L}} \begin{pmatrix} e^{i\delta_q}\chi_1^{-q} & \chi_1^q \\ e^{i\delta_q}\chi_2^{-q} & \chi_2^q \end{pmatrix} \begin{pmatrix} e^{-iq(j-1)} \\ e^{iq(j-1)} \end{pmatrix}, \tag{20.18}$$

where δ_q is chosen so as to satisfy the left boundary condition (20.12),

$$e^{i\delta_q} = \frac{-(e^{-i\phi_q} - \cos(\pi J)) + e^{i\xi_q}\sin(\pi g)\tan\mu_q}{(e^{-i\phi_q} - \cos(\pi J))\tan\mu_q + \sin(\pi g)e^{-i\xi_q}}. \tag{20.19}$$

The right boundary condition (20.13) yields a transcendental equation for the quasimomenta quantization:

$$e^{2iq(L-1)} = -\left[\frac{(e^{-i\phi_q} - \cos(\pi J)) - e^{i\xi_q}\tan\mu_q\sin(\pi g)}{(e^{i\phi_q} - \cos(\pi J))e^{i\xi_q}\tan\mu_q + \sin(\pi g)}\right]^2. \tag{20.20}$$

In the limit of large L and small quasimomentum $q \ll \pi$, Eq. (20.20) can be replaced by the usual formula

$$q_\alpha \sim \frac{\pi(\alpha - 1)}{L}, \quad \alpha \in (1, L). \tag{20.21}$$

The standing wave solutions $\underline{\psi}^q$ are the operator coefficients appearing in Eq. (20.9), for the eigenmode $\hat{\eta}^q$.

20.4.2 Perturbation theory for Floquet evolution

Here, we provide a perturbative expression for the state of a Floquet system coupled to an auxiliary, assuming that the auxiliary-system coupling is weak. We start by considering a general setup, where the system and auxiliary first undergo M periods of unitary evolution, specified by an operator

$$\hat{\mathcal{U}} = \hat{U}_{\rm SA}\hat{U}_{\rm A}\hat{U}_{\rm S}, \tag{20.22}$$

followed by the reset of auxiliary to a state $\rho^0_{\rm A}$. The auxiliary-system coupling is chosen to be in the form

$$\hat{U}_{\rm SA} = e^{i\theta\hat{K}}, \tag{20.23}$$

with $\hat{K}$ being system-auxiliary coupling Hamiltonian. We will be interested in the limit of weak coupling, $\theta \ll 1$.

To find the density matrix of the system after one dissipative cycle ($\mathcal{U}^M$ followed by auxiliary reset), it is convenient to use interaction representation for operators:

$$\hat{A}_I(s) = \hat{U}_0^{-s}\hat{A}\hat{U}_0^s, \tag{20.24}$$

where s is the discrete time (number of unitary evolution periods within one dissipative cycle, such that $s \in [0; M]$) and $\hat{U}_0 = \hat{U}_{\rm A}\hat{U}_{\rm S}$ is the unperturbed evolution operator. The unitary evolution operator can be written as

$$\hat{\mathcal{U}}^M = \hat{U}_0\mathcal{T}\prod_{s=1}^{M} e^{i\theta\hat{K}_I(s)}, \tag{20.25}$$

where $\mathcal{T}$ denotes time-ordering.

Next, we focus on the system's density matrix after one dissipative cycle. At the beginning of the cycle, the system and auxiliary are described by a density matrix $\rho^{(n)} \otimes \rho^0_A$, where ρ^0_A

is the state to which the auxiliary is reset. Expanding the evolution operator in Eq.(20.25) to second order in θ, and tracing out the auxiliary, we obtain system density matrix in the interaction representation:

$$\hat{U}_{\rm S}^{-M}\rho^{(n+1)}\hat{U}_{\rm S}^{M}=\rho^{(n)}-\theta^2\sum_{\substack{s_2=1\\ s_1<s_2}}^{M}{\rm Tr}_A[\hat{K}_I(s_2),[\hat{K}_I(s_1),\rho^{(n)}\otimes\rho^0_{\rm A}]]-\frac{\theta^2}{2}\sum_{s=1}^{M}{\rm Tr}_A[\hat{K}_I(s),[\hat{K}_I(s),\rho^{(n)}\otimes\rho^0_{\rm A}]]. \tag{20.26}$$

Next, we define the density matrix in the interaction representation with respect to system only evolution, to describe system's state after many dissipative cycles:

$$\rho^{(n)}_{\rm int}\equiv\hat{U}_{\rm S}^{-Mn}\rho^{(n)}\hat{U}_{\rm S}^{Mn}. \tag{20.27}$$

The advantage of considering the density matrix in the interaction representation is that the change of $\rho_{\rm int}$ over one dissipative cycle is proportional to θ^2, and therefore small provided $\theta\ll 1$. This change is obtained from Eqs.(20.26,20.27).

20.4.3 Application to the Floquet TFIM: secular approximation

Next, we analyze the cooling of the Floquet TFIM, described in the main text. In this case,

$$\hat{U}_{\rm A}=e^{i\frac{\pi h}{2}\hat{Z}_a},\quad \hat{K}=\frac{1}{2}\left(\hat{X}_a\hat{X}_1+\hat{Y}_a\hat{Y}_1\right). \tag{20.28}$$

Since our purpose here is mostly to illustrate the cooling mechanism, for simplicity we consider an auxiliary coupled to the first site of the chain.

We perform Jordan-Wigner transformation, described above, arriving at the following Floquet operator, written in terms of fermionic eigenmodes of the chain $\hat{\eta}_k$ with quasienergies ϕ_k (see above), and in terms of fermionic operator $\hat{d}$ acting on the auxiliary site:

$$\hat{U}_{\rm S}=e^{-i\sum_k\phi_k\hat{\eta}_k^\dagger\hat{\eta}_k},\quad \hat{U}_{\rm A}=e^{-i\pi h\hat{d}^\dagger\hat{d}},\quad \hat{K}=\hat{d}^\dagger\hat{c}_1+\hat{c}_1^\dagger\hat{d}, \tag{20.29}$$

where $\hat{c}_1$ is the annihilation operator on the first site of the chain, introduced above. We further express the operator $\hat{c}_1$ via eigenmode operators $\hat{\eta}_k,\hat{\eta}_k^\dagger$:

$$\hat{c}_1=\sum_k\alpha_k\hat{\eta}_k+\beta_k\hat{\eta}_k^\dagger,\quad \hat{c}_1^\dagger=\sum_k\alpha_k^*\hat{\eta}_k^\dagger+\beta_k^*\hat{\eta}_k. \tag{20.30}$$

The coefficients α_k,β_k are obtained from the expressions for the eigenmode wave functions.

In the experiment, we reset the auxiliary to $|0\rangle$ state, which corresponds to the occupied d-level in the fermionic language. Thus,

$${\rm Tr}_A(\hat{d}^\dagger\hat{d}\rho_{\rm A}(0))=1,\quad {\rm Tr}_A(\hat{d}\hat{d}^\dagger\rho_{\rm A}(0))=0. \tag{20.31}$$

From Eqs.(20.30,20.29), we obtain the expression for the operator $\hat{K}$ in the interaction picture,

$$\hat{K}_I(s)=\sum_k\alpha_k e^{i(\pi h-\phi_k)s}\hat{d}^\dagger\hat{\eta}_k+\beta_k e^{i(\pi h+\phi_k)s}\hat{d}^\dagger\hat{\eta}_k^\dagger+{\rm h.c.}, \tag{20.32}$$

where h.c. denotes hermitian conjugate. Combining this equation with Eq.(20.26) and Eq.(20.31), we obtain system's density matrix evolution.

Further, we consider the density matrix in the interaction representation (20.27). This leads to dressing of the fermionic operators $\hat{\eta}_k^\dagger,\hat{\eta}_k$ entering the equation for the change of density matrix, $\Delta\rho_{\rm int}=\rho^{(n+1)}_{\rm int}-\rho^{(n)}_{\rm int}$, by phases $e^{\pm iMn\phi_k}$, respectively.

Next, we adopt the standard secular approximation: assuming $\theta^2 \ll \delta\phi$, where $\delta\phi$ is the quasienergy level spacing, we coarse-grain the time evolution of $\rho_{\rm int}^{(n)}$ over a number of dissipative cycles of order $(M\delta\phi)^{-1}$, and observe that the terms of the form $\hat{\eta}_k^\dagger \hat{\eta}_q$ with $k \neq q$ can be neglected due to their oscillating phases. Thus, we are left only with the contributions where $k = q$. This results in a simplified equation for the density matrix evolution (over one dissipative cycle):

$$\frac{d\rho_{\rm int}^{(n)}}{dn} - i\left[\rho_{\rm int}^{(n)}, \Delta H_{\rm S}\right] =$$

$$+\sum_{k=1}^{L} W^{+}(q_k)\left(\eta_k^\dagger \rho_{\rm int}\eta_k - \frac{1}{2}\left\{\eta_k\eta_k^\dagger, \rho_{\rm int}\right\}\right) + W^{-}(q_k)\left(\eta_k \rho_{\rm int}\eta_k^\dagger - \frac{1}{2}\left\{\eta_k^\dagger\eta_k, \rho_{\rm int}\right\}\right), \quad (20.33)$$

where $\{A, B\}$ denotes anticommutator of the operators A and B , the sum in the r.h.s. is over L fermionic eigenmodes. $W^{+}(q)$ and $W^{-}(q)$ are probabilities to, respectively, create and annihilate a fermion mode k with an absolute value of the quasimomentum q_k over one dissipative cycle. We express these quantities via the properties of the eigenmodes of the Floquet TFIM described above, by relating the coefficients α_k, β_k in Eq. (20.30) to the eigenmode amplitudes $\psi_{2j-1}^q, \psi_{2j}^q$:

$$W^{\pm}(q) \equiv 2\pi M\theta^2 \ |\psi_1^q \pm i\psi_2^q|^{\,2}\delta_M(\phi_q \pm \pi h), \quad (20.34)$$

$$|\psi_1^q \pm i\psi_2^q|^2 = \frac{1}{L}f_q^{\pm}, \qquad f_q^{\pm} = 4\left|\cos(\mu_q)\cos\left(\frac{\delta_q}{2}\right) \mp \sin(\mu_q)\sin\left(\xi_q - \frac{\delta_q}{2}\right)\right|^2. \quad (20.35)$$

where μ_q , ξ_q are defined via Eq. (20.16) and the phase shifts δ_q are is given in Eq. (20.19).

The equation (20.33) takes the form of the Lindblad equation quadratic in fermion operators. It has a simple physical meaning: the first term in the r.-h.s. describes quasiparticles being removed from the system, with a rate $W^{-}(q)$ that depends on the weight of the quasiparticle wave function with momentum q on the site coupled to the auxiliary, and on the phase difference $\pi h + \phi_q$. Similarly, the second term describes processes where quasiparticles are being excited from the vacuum.

In Eq. (20.33) $\Delta H_{\rm S}$ is effective Hamiltonian correction (collective "Lamb shift") of the system produced by the auxiliary qubits

$$\Delta H_{\rm S} = \frac{M\theta^2}{L}\sum_{k=1}^{L}\Delta(q_k)\,\eta_k^\dagger\eta_k - \Delta_0$$

$$\Delta(q) = \sum_{\sigma=\pm} f_q^{\sigma}\mathcal{P}_M\left(\frac{1}{\phi_q + \sigma\pi h}\right), \qquad \Delta_0 = \frac{M\theta^2}{L}\sum_{\mu=1}^{L} f_q^{+}\mathcal{P}_M\left(\frac{1}{\mathcal{E}_\mu + \pi h}\right)$$

The functions $\delta_M(x)$ and $\mathcal{P}_M(x)$ above approximate delta function and principle value function in the limit $M \to \infty$

$$\delta_M(x) = \frac{1}{2\pi M}\frac{\sin\left(\frac{Mx}{2}\right)^2}{\sin\left(\frac{x}{2}\right)^2}, \qquad \mathcal{P}_M\left(\frac{1}{x}\right) = \frac{1}{M}\sum_{m=1}^{M}\sum_{l=1}^{m-1}\sin(xl)$$

(for brevity we omit the explicit form of the double sum). From the fermionic Lindblad equation (20.33) one can n obtain the steady-state population of the quasiparticle levels given by:

$$n_k = \left\langle \eta_k^\dagger\eta_k \right\rangle = \left(1 + \frac{f_q^-}{f_q^+}\frac{\delta_M(\pi h - \phi_q)}{\delta_M(\pi h + \phi_q)}\right)^{-1} \quad (20.36)$$

This analytical expression allows one to theoretically identify the optimal value of the parameter h, for which the steady-state quasiparticle number is minimal. As a test, we calculate an optimal value of $h = 1.60$ for the model parameters in Fig. 20.9a, close to the experimentally determined value of $h = 1.65$. This coincides with the upper edge of the quasiparticle band.

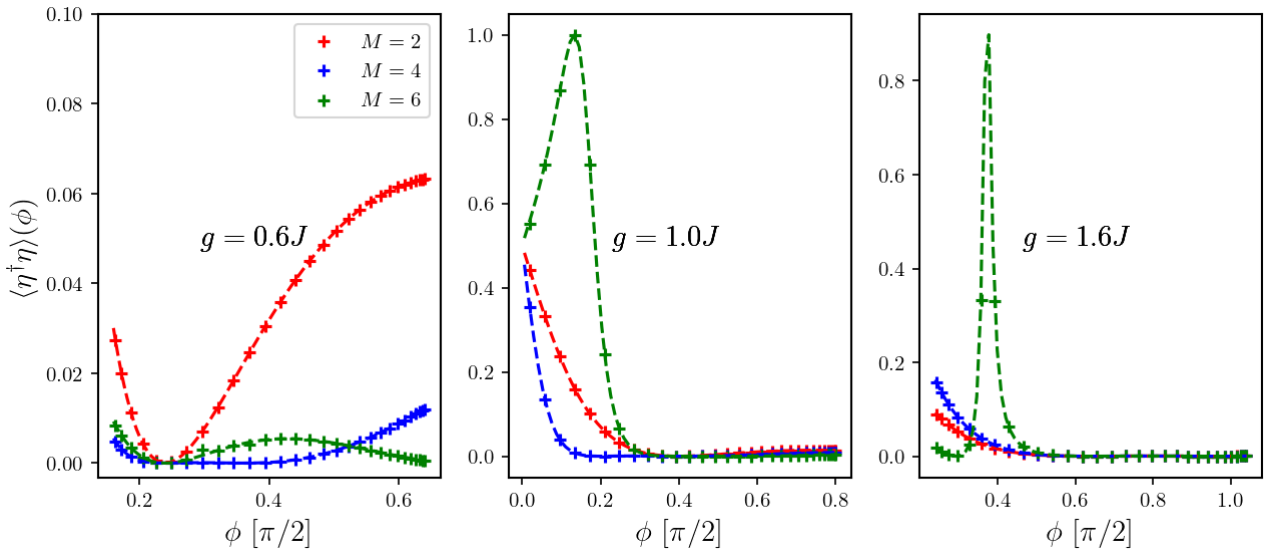

Figure 20.14: Quasiparticle occupations in the steady state, as a function of the quasiparticle quasienergy ϕ: a comparison of secular approximation prediction (dashed lines) and numerical results (crosses). The coupling of auxiliary and the system is chosen to be weak, $\theta/\pi = 0.001$, and M denotes a number of cycles before auxiliary is reset. The ancilla field h is tuned to the approximately optimal upper band edge, $h = J + g$. The system size is $L = 30$ sites. Parameter $J = 0.2$. We observe a quantitative agreement between the two approaches, with the lowest quasiparticle population achieved for $M = 4$. We note that the quasiparticle population at zero quasienergy remains large at the critical point (middle panel).

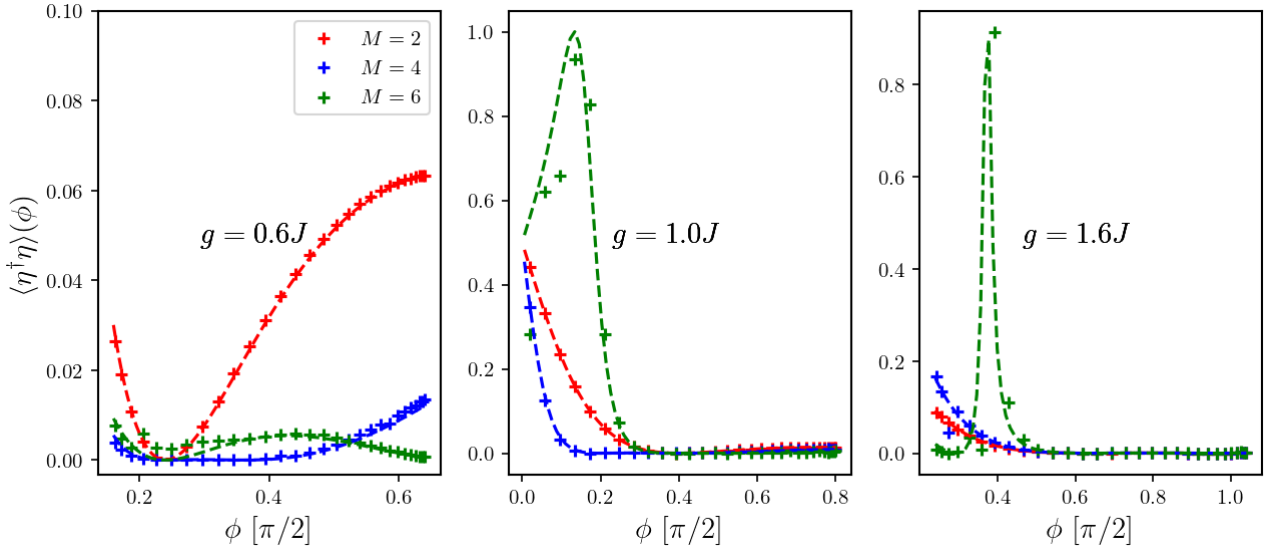

Figure 20.15: Same as in Fig. 20.14, but with stronger auxiliary-system coupling $\theta/\pi = 0.01$. Despite visible deviations from an exact result, the secular approximation qualitatively captures the behavior of quasiparticle population in the steady state.

As a next step, it is instructive to verify the validity of the secular approximation. To this

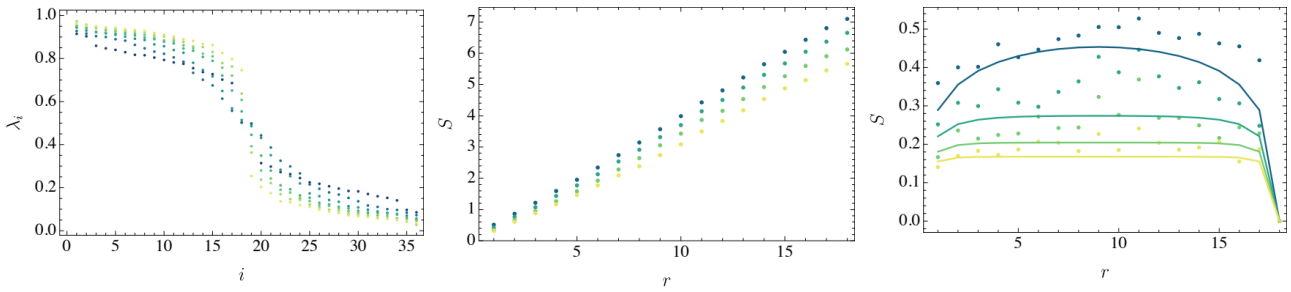

Figure 20.16: Left panel: Eigevalues of the 1RDM, D, in the NESS of the Kicked Ising model for $L = 18$ qubits. The parameters are $(g, J) = (0.08, 0.2)$ and $g = (0.6, 0.8, \ldots 1.6)J$ for $J = 0.25$. Lighter colours denote increasing g. Middle panel: The dependence of entanglement entropy for a quadratic fermionic system described by the experimental 1RDM, D. We only plot the parameters $g/J \geq 1$. Right panel: Same as before for the purified 1RDM, D_{pure}. Full lines correspond to the values for the exact vacuum of the Kicked Ising model, Eq. (20.5).

end, we first compare the analytical prediction (20.36) with the exact numerical calculation. The result for weak auxiliary-system coupling, $\theta/\pi = 0.001$, is illustrated in Fig. 20.14. We use the value $h = J + g$ for ancilla field, which agrees with the optimal value above. We observe excellent agreement in all regions of the phase diagram and for different values of unitary evolution periods M before a reset.

Further, we study the case of stronger coupling $\theta/\pi = 0.01$ (Fig. 20.15). Interestingly, at the critical point $g = J$, the secular approximation remains accurate. In the two gapped phases, the approximation captures qualitative features, but significant deviations from exact results are visible, especially near the band edges. Nevertheless, secular approximation provides a good guide for identifying optimal auxiliary parameters.

20.5 1RDM of the Ising chain and purification

In this section we describe the one-body density matrix (1RDM) formalism and the corresponding purification scheme. Due to the quadratic nature of the Floquet transverse-field Ising model, Eq. (20.5), all the information about its many-body eigenstates is contained in the two-body fermionic correlation functions. The latter require a polynomial number of measurements in the system size ($\propto L^2$). The $2L \times 2L$ matrix of such correlation functions is referred to as 1RDM. It is conveniently expressed via Majorana operators defined in Eq. (20.6):

$$D = \frac{1}{2}\begin{pmatrix} D^{oo} & D^{oe} \\ D^{eo} & D^{ee}, \end{pmatrix}, \quad D^{oo}_{i,j} = \langle a_{2i-1}a_{2j-1}\rangle, \quad D^{oe}_{i,j} = \langle a_{2i-1}a_{2j}\rangle, \quad D^{eo}_{i,j} = \langle a_{2i}a_{2j-1}\rangle, \quad D^{ee}_{i,j} = \langle a_{2i}a_{2j}\rangle, \quad i \tag{20.37}$$

Here the averaging is taken over the system's state, described by a density matrix ρ: $\langle\cdot\rangle \equiv \mathrm{tr}(\cdot\rho)$. For quadratic states there is a one-to-one relation between the many-body density matrix of the system and 1RDM [61]. For many-body states the 1RDM is just a correlation matrix, however we keep the terminology unchanged for clarity.

The experimentally extracted 1RDM can be written in the basis of eigenmode operators, related to the Majorana operators via Eq. (20.9):

$$F_{ij} = \begin{pmatrix} F^{+-} & F^{--} \\ F^{++} & F^{-+}, \end{pmatrix}, \quad F^{+-}_{i,j} = \langle \eta_i^\dagger \eta_j\rangle, \quad F^{++}_{i,j} = \langle \eta_i^\dagger \eta_j^\dagger\rangle, \quad F^{-+}_{i,j} = \langle \eta_i \eta_j^\dagger\rangle, \quad F^{--}_{i,j} = \langle \eta_i \eta_j\rangle, \tag{20.38}$$

In particular, the quasiparticle occupations are given by $F^{+-}_{i,i} = \langle \eta_i^\dagger \eta_i\rangle$.

To purify a 1RDM, we approximate it by the 1RDM, D_{pure}, of the closest pure quadratic fermionic state, i.e. a Slater determinant wavefunction. Taking into account the fact that the

1RDM of a Slater determinant wavefunction is a projector, we can express the purification as a constrained minimization problem,

$$\min|D - D_{pure}|_F, \quad \mathrm{tr}D_{pure} = L, D_{pure}^2 = D_{pure}, \tag{20.39}$$

where$|\cdot|_F$ denotes the Frobenius norm. The minimization constraints for the matrix are fixed trace and being a projector. In our approach, we use a purification scheme which is equivalent to the purification proposed by McWeeny [29]. The purified 1RDM has the form $D_{pure} = \sum_{i=1}^{L} |i\rangle\langle i|$, corresponding to the projector to the space spanned by the eigenvectors associated to the L largest eigenvalues of the original 1RDM,

$$\mathrm{spec}(D) = \lambda_i, \quad i \in \{1, 2L\}, \quad \lambda_i \geq \lambda_{i+1}. \tag{20.40}$$

The purified state can be thought of as a state with occupied fermionic modes $\tilde{\eta}_i, \tilde{\eta}_i^\dagger$, which correspond to the L eigenvectors of 1RDM with the largest eigenvalues. The many-body fidelity of the purified state with respect to the ground state, shown in Fig.3C of the main text, is then given by an overlap of two Slater determinant states, defined by sets of modes $\{\tilde{\eta}_i\}_{i=1}^{L}$ and $\{\eta_i\}_{i=1}^{L}$, respectively. This procedure is used to obtain the fidelity illustrated in Fig.3C of the main text.

In Fig. 20.16, we illustrate the effect of purification on the experimentally measured steady state 1RDM for the Floquet TFIM defined in Eq. (20.5). We first discuss the properties of the experimentally measured 1RDM, D, including eigenvalue spectrum (left panel in Fig. 20.16) and entanglement entropy, computed for a quadratic state that corresponds to D (middle panel of Fig. 20.16). In the paramagnetic phase $g/J > 1$, a clear "jump" in the eigenvalue magnitude at $i = L$ indicates the proximity to a pure state. In the anti-ferromagnetic phase $g/J < 1$, we observe the close degeneracy of the eigenvalues $\lambda_L \sim \lambda_{L-1}$. This reflects the presence of a degenerate ground state manifold due to the presence of a Majorana edge mode. The cooling algorithm leads to a steady state in which the steady state contains a mixture of the two nearly degenerate ground states; this corresponds to the Majorana edge mode being occupied with probability close to 1/2. To exclude the effect of the Majorana edge modes, we divide the full fidelity by the contribution of the Lth mode: Fidelity $\rightarrow$ Fidelity$/\langle\eta_L\eta_L^\dagger\rangle$. This leads to an improved fidelity in the antiferromagnetic phase, illustrated by dashed lines in Fig.3C of the main text.

We note that the high fidelity of the purified state indicates that the modes $\tilde{\eta}_i$ are close to the true quasiparticle modes η_i of the system. In other words, 1RDM in Bogoliubov-de-Gennes basis, Eq. (20.38), is almost diagonal. The near-diagonal nature of the density matrix in the quasiparticle basis is justified in the limit of the weak system-ancilla coupling θ, (see discussion about the validity of the secular approximation, Eq. (20.33), in the previous section).

Next we focus on entanglement entropy $S_A = -\mathrm{tr}\rho_B \log \rho_B$, where $\rho_B = \mathrm{tr}_A\rho$ is the reduced density matrix for a partition of the system $A \bigcup B = \{1, 2, \ldots, r\} \bigcup \{r+1, \ldots, L\}$. Experimentally determining the full many-body density matrix of the system is prohibitively expensive for large systems, as it scales exponentially with the number of qubits. On the other hand, the 1RDM can be efficiently extracted as it just involves two-point correlation functions. For this reason, by only using experimental data, we calculate the entanglement entropy of a quadratic system with the same 1RDM as the experimental steady state [61]. Even though the exact entanglement entropy of the NESS can be significantly different from our calculation, the 1RDM entanglement entropy nicely illustrates the effect of purification: The volume-law entanglement scaling, $S \propto r$ of the original 1RDM, arising due to decoherence, changes to an area-law scaling, $S \propto$ const., for the purified 1RDM, for all parameters except at the critical point, $g \neq J$. Additionally we see that the value of the entropy is close to that of the exact vacuum of the TFIM, even at the critical point. This means that critical properties such as the long-range order shown in the main text are also captured by D_{pure}.

20.6 Comparison between dissipative and unitary state preparation protocols

In this section we compare the dissipative cooling protocol to the unitary preparation protocol for fermionic Gaussian states proposed by Jiang et al. [62]. In the absence of decoherence, the unitary protocol efficiently prepares the exact vacuum state of a given quadratic fermionic system. However, weak decoherence present in NISQ devices leads to errors in the prepared state. We explore how the states prepared using the unitary protocol ρ_U compare to the dissipatively cooled states, ρ_D.

The Gaussian state preparation protocol for a system of L fermions consists of $O(L)$ layers of one- and two-body gates as illustrated in Fig. 20.17A. The gates have the form,

$$G_n(\theta_n, \phi_n) = e^{i\frac{\phi_n}{2}\hat{Z}_{i_n}} e^{-i\frac{\theta_n}{2}\left(\hat{X}_{i_n}\hat{Y}_{i_{n+1}} - \hat{Y}_{i_n}\hat{X}_{i_{n+1}}\right)}, \qquad B = \hat{X}_L, \tag{20.41}$$

where the gate index $n \in [1, L(L-1)/2]$, and i_n denotes the position of the corresponding qubit in the system. The angles (θ_n, ϕ_n) are determined from the TFIM unitary $\hat{U}$ (Eq. (20.5)) by employing the algorithm proposed in [62]. The weak decoherence in the system is modeled according to Eq. (20.49). Since the decoherence strength is proportional to the experimental time required to apply the quantum circuit, we apply $\mathcal{D}(\gamma_\theta, \gamma_\phi)$ after every layer of unitary gates. The decoherence rates are set to the qubit coherence rates $\gamma_\theta = 1/T_2 \sim 0.016$, $\gamma_\phi = 1/T_1 \sim 0.006$, which were previously shown (Fig. 20.9.B) to match the experimental data.

In order to explore large system sizes we perform the state preparation protocols using tensor-networks techniques. The state is represented by a matrix product density operator (MPDO) [66]. The time integration is performed by a time-evolving block decimation (TEBD) algorithm [64], implemented using ITensor library [70]. The bond dimension is set to $\chi = 300$, as this value is found to give converged numerical results for all cases studied.

We focus on the critical point $J = g = 0.2$ of the TFIM, since the long-range order present in the critical ground state is expected to be most susceptible to noise effects, challenging the performance of the preparation protocols. In Fig. 20.17B we compare the energy convergence of the numerically simulated dissipative cooling protocol and the experimental data (Fig. 20.10). We observe a close agreement for system sizes $L = 12, 18, 24$ and a slightly worse agreement for $L = 30$. The agreement of these results provides a justification for the choice of the decoherence strength in the protocol comparison.

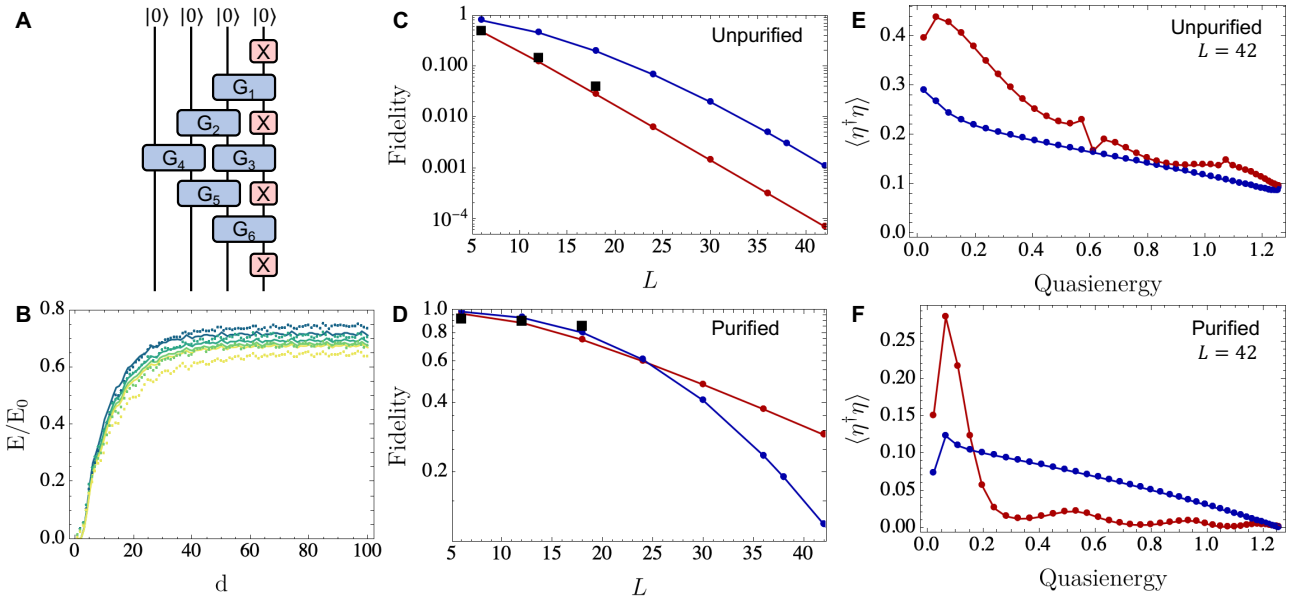

Figure 20.17: (A) Illustration of the state preparation protocol [62], for a system of $L = 4$ qubits. Every qubit is initialized in its ground state. (B) Comparison of energy convergence between experimental data (points) and simulations (lines) at the critical point ($g = J = 0.2$) of the Floquet TFIM (Eq. (20.5)). System sizes $L = \{12, 18, 24, 30\}$ are represented by blue to yellow colors. (C) Fidelity between the exact vacuum state of Floquet TFIM unitary $\hat{U}$ at the aforementioned critical point, and the states prepared by simulating the dissipative (red) and unitary (blue) protocols. Black squares denote the experimental values for $\{6, 12, 18\}$ qubits. (D) Same as (C), for the purified states according to the method described in Section 20.5. (E,F) Unpurified and purified quasiparticle occupations for the simulated protocols. We observe that the purified states generated by the dissipative protocol have considerably lower high-energy quasiparticle occupations.

In Fig. 20.17C we show the fidelity between the prepared state and the vacuum state. The unitary preparation yields higher fidelity for the available system sizes, $\langle \rho_D \rangle < \langle \rho_U \rangle$. However, we expect that for larger system sizes, where the number of layers required for the unitary protocol requires running times that are much longer than the qubit coherence times, the dissipative protocol will become more efficient. Next, in Fig. 20.17D we present the fidelities following purification (see Section 20.5) of the states, ρ_D^P, ρ_U^P. We observe that $\langle \rho_U^P \rangle$ decays considerably faster than $\langle \rho_D^P \rangle$ and for $L \geq 25$ onward, $\langle \rho_D^P \rangle > \langle \rho_U^P \rangle$, illustrating a better performance of the dissipative cooling algorithm.

To further understand the structure of the approximate vacuum states prepared by the two protocols, we calculate the density of quasiparticle excitations in the system, Fig. 20.17E,F. The density of quasiparticles in ρ_D depends strongly on the quasiparticle quasienergy, while for ρ_U this is not the case. In addition, we observe that excitations at sufficiently high quasienergies are suppressed by purification more efficiently for ρ_D. This is a result of the different 1RDM structure in the quasiparticle basis, Eq. (20.38), for the two protocols. The dissipatively prepared state ρ_D is close to a diagonal mixture of different quasiparticle states. In contrast, the density matrix ρ_U reached by the unitary protocol features larger off-diagonal matrix elements. For this reason, the purification scheme performs considerably better on ρ_D.

20.7 Transport in Floquet XXZ under maximal pumping

In this section of the Supplementary Material (SM), we provide numerical simulations of the non-equilibrium quantum transport in the Floquet XXZ chain and compare them to the

experimental results.

20.7.1 Model and setup

For the driving protocol we use two auxiliary qubits coupled to the boundaries of the system of L qubits. We label the qubits according to the definitions of Fig. 1 of the main text: The left and right auxiliaries are denoted by $Q_{a,1}$ and $Q_{a,2}$, respectively. The qubits of the system are denoted as $Q_{s,1}, \ldots, Q_{s,N-2}$. The system size is therefore $N = L + 2$.

Our system is inspired by the XXZ-Hamiltonian,

$$H_{XXZ} = \sum_{i=1}^{L-1} h_i, \quad h_i = \theta \left(\sigma_i^+ \sigma_{i+1}^- + \text{h.c.}\right) + \phi n_i n_{i+1}, \tag{20.42}$$

where i denotes the position of the system qubit in the chain, $n = |1\rangle\langle 1|$ is the particle density and $\sigma^\pm$ are the hardcore boson creation/annihilation operators. Similarly to the Floquet system (see main text), the anisotropy parameter $\Delta = \frac{\phi}{2\theta}$ controls the transport properties of the Hamiltonian system [45, 35].

The Floquet XXZ chain is realized by a trotterization of the Hamiltonian evolution,

$$U_{XXZ} = U_{even} U_{odd}, \qquad U_{even} = \prod_{i=1}^{N/2} \text{FSim}_{2i,2i+1}, \qquad U_{odd} = \prod_{i=1}^{N/2-2} \text{FSim}_{2i+1,2i+2}, \qquad . \tag{20.43}$$

where the two-qubit gates are generated by the Hamiltonian density as

$$\text{FSim}_{i,i+1}(\theta, \phi) = \exp\left(i h_i(\theta, \phi)\right). \tag{20.44}$$

The Floquet XXZ chain retains the integrable structure of the Hamiltonian model, and therefore, features a macroscopic number of conserved quantities [39]. In addition, the total number of particles $N_{tot} = \sum_i n_i$ in the system is conserved.

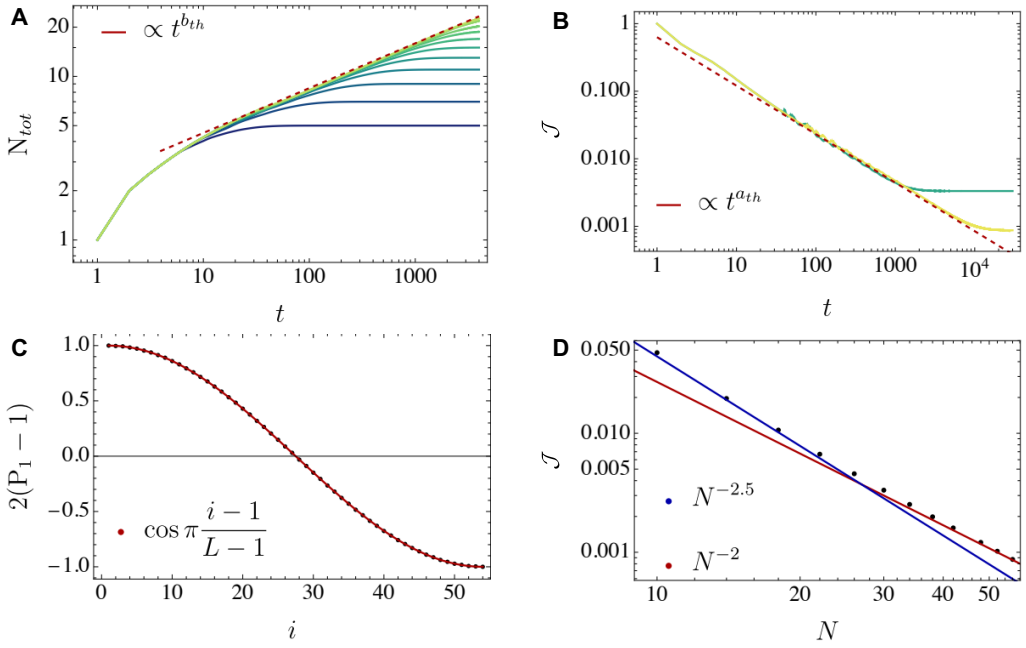

Figure 20.18: Numerical simulations of quantum transport in the boundary-driven Floquet XXZ chain at the isotropic point $\phi = 2\theta = \pi/2$, in the absence of external decoherence. The bond dimension of the MPDO is truncated to $\chi = 128$. (A) Time dependence of the total number of particles into the system $N_{tot} = \sum_{i=2}^{N-1} n_i$ for system sizes of $N = 10 - 56$ qubits (blue to yellow colors), as a function of the number of driving cycles. We find a power-law scaling law with an exponent $b_{th} \sim 0.2746$ which develops after an initial transient. (B) Pumping current as a function of time for $N = 30, 56$ qubits exhibits an exponent $a_{th} = -0.7178 \approx b_{th} - 1$. (C) A normalized local particle number in the NESS as a function of qubit position for $N = 56$. The cosine function is the strong driving limit prediction for the case of solvable boundaries, at the isotropic point of the XXZ Hamiltonian [45]. (D) NESS current scaling with the system size. We observe that for larger system sizes $\mathcal{J} \propto N^{-2}$ while for smaller sizes the exponent is slightly larger.

The driving of the system is realized by a trace-preserving operation, where the auxiliary qubits are reset to a $|0\rangle$ or $|1\rangle$ state. The local quantum channel that corresponds to this operation can be formally expressed with a set of two Kraus operators,

$$K^1_{1,i} = \frac{n_i + \sigma_i^+}{\sqrt{2}} \quad K^1_{2,i} = \frac{n_i - \sigma_i^+}{\sqrt{2}} \qquad K^0_{1,i} = \frac{1 - n_i + \sigma_i^-}{\sqrt{2}} \quad K^0_{2,i} = \frac{1 - n_i - \sigma_i^-}{\sqrt{2}}, \tag{20.45}$$

where,

$$\sum_{l=1}^{2} K^1_{l,i}\rho(K^1_{l,i})^\dagger = |1_i\rangle\langle 1_i|\mathrm{tr}_i\rho \equiv \mathcal{K}^1_i(\rho), \qquad \sum_{l=1}^{2} K^0_{l,i}\rho(K^0_{l,i})^\dagger = |0_i\rangle\langle 0_i|\mathrm{tr}_i\rho \equiv \mathcal{K}^0_i(\rho), \tag{20.46}$$

and satisfy $\sum_{l=1}^{2}(K^m_{l,i})^\dagger K^m_{l,i} = 1_{2\times 2}$. The index i denotes the auxiliary qubit $i = 1, 2$ which is reset by the operation. We use the calligraphic letters to denote the action of the quantum channel on a state. We additionally denote the reset channel at both boundaries by $\mathcal{K}^{m_1 m_2} = \mathcal{K}^{m_1}_1 \otimes \mathcal{K}^{m_2}_2$. Following the reset operation, we couple the auxiliary qubit to the system using swap gates,

$$U_B = \mathrm{iSWAP}_{(a,1),1}\mathrm{iSWAP}_{(a,2),L}, \qquad \mathrm{iSWAP}_{(a,i),j} = \mathrm{FSim}_{(a,i),j}\left(\frac{\pi}{2}, 0\right). \tag{20.47}$$

A stroboscopic time step, in the absence of decoherence, starts with the reset of the auxiliary qubits to states m_1, m_2, followed by the auxiliary-system coupling, Eq. (20.47), and is completed by the unitary evolution according to Eq. (20.43),

$$\rho(d+1) = U_{XXZ} U_B \mathcal{K}^{m_1 m_2} (\rho(d)) U_B^\dagger U_{XXZ}^\dagger. \tag{20.48}$$

We consider an initial product state with qubits initialized in the state $\rho(0) = |0 \dots 0_N\rangle\langle 0 \dots 0_N|$. For the pumping protocol we will assume that the first qubit, resets to state $|1\rangle$, $m_1 = 1$, while the last qubit resets to state $|0\rangle$, $m_2 = 0$. It is evident by construction that our protocol generates maximal pumping of particles in the system, as at the start of each driving cycle the left-most auxiliary qubit, $Q_{a,1}$ is always in state $|1\rangle$.

To study the transport properties of the system, we measure local occupations $\langle n_i \rangle$ at half-integer times (that is, after an integer number of cycles and also in the middle of cycles, see main text). This allows us to obtain the local currents.

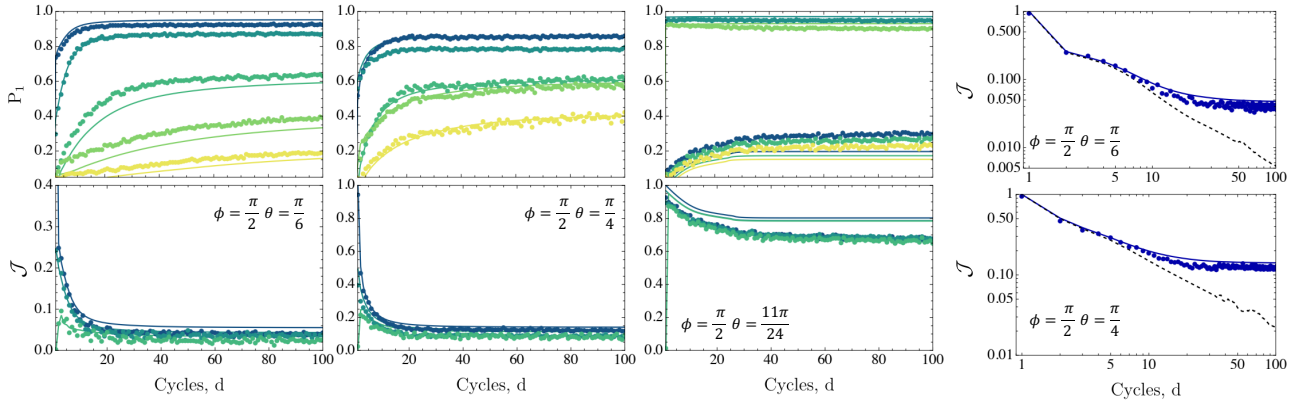

Figure 20.19: Left three columns: A comparison between the experimental data and tensor-network simulations in the presence of weak decoherence. For the numerical simulations we used MPDO parametrization of the density matrix with bond dimension $\chi = 500$. The top 3 plots show the particle numbers of the five system qubits closest to the left auxiliary, where color varies according to position, $1 \to 5$ corresponding to blue $\to$ yellow. The bottom plots illustrate the three local currents closest to the auxiliary site. The values of decoherence are $(\gamma_\theta, \gamma_\phi) = (0.01, 0.03), (0.016, 0.038), (0.016, 0.038)$ for the three values of parameters $\theta = \pi/6, \pi/4, 11\pi/24$, respectively. Right column: The decay of the pumping current $\mathcal{J} = \mathcal{J}_{in}$ as a function of time for different parameters. The points denote experimental data and the solid lines are the result of the simulation in the presence of the weak decoherence specified above. The dashed line shows the decoherence-free simulation.

For the numerical evolution of the state, we employ tensor-network description of the density matrix known as matrix product density operator (MPDO) [66]. The time integration is performed by a time-evolving block decimation (TEBD) algorithm [64], implemented using ITensor library [70].

Furthermore, we model the (uncontrolled) decoherence as a product of local quantum channels,

$$\mathcal{D} = \bigotimes_{i=1}^{N} \mathcal{D}_i, \qquad \mathcal{D}_i \begin{pmatrix} \rho_{1,1} & \rho_{1,0} \\ \rho_{0,1} & \rho_{0,0} \end{pmatrix} = \begin{pmatrix} e^{-\gamma_\theta}\rho_{1,1} & e^{-\gamma_\phi - \gamma_\theta/2}\rho_{1,0} \\ e^{-\gamma_\phi - \gamma_\theta/2}\rho_{0,1} & (1 - e^{-\gamma_\theta})\rho_{1,1} + \rho_{0,0} \end{pmatrix}, \tag{20.49}$$

where $\gamma_\theta/\gamma_\phi$ are the decay and dephasing noise rates, respectively. The local quantum channel $\mathcal{D}_i$ can be equivalently defined by jump operators $l_1 = \sqrt{\gamma_\theta}\sigma^-$, $l_2 = \sqrt{\frac{\gamma_\phi}{2}}\sigma^z$, time-integrated using the standard Lindblandian formalism over one unit of time. The decoherence map is applied to the system at the end of every Floquet step, Eq. (20.48).

20.7.2 Dynamics and steady state in the absence of decoherence at the isotropic point

We start by analyzing the transport properties in the absence of external decoherence, focusing on the isotropic point $\phi = 2\theta$. In Fig. 5 of the main text we showed the power-law temporal dependence of current through the system, with a dynamical exponent that corresponds to a subdiffusive phase. We perform large-scale tensor-network simulations to verify the presence of a sub-diffusive dynamical exponent for various system sizes and at all timescales. The results are shown in Fig. 20.18A and Fig. 20.18B. Here we find that the number of particles in the system follows a universal dynamical exponent $b_{th} \approx 0.2746$ and the rate of pumping particles displays a dynamical exponent $a_{th} = -0.7178 \approx b_{th} - 1$. As we will later see, the small deviation from the experimental value $a_{ex} \sim -0.64$ can be attributed to the presence of weak decoherence. We note that the total number of particles is not directly equivalent to the rate of pumping particles. It is the time integrated difference between the rate of pumping and the rate of dissipating particles from the other end of the chain, $N_{tot} = \int_t dt\,(\mathcal{J}_{in}(t) - \mathcal{J}_{out}(t))$. We have explicitly checked that for times sufficiently smaller than the saturation timescale, defined by the approach to the NESS, the outgoing current is weak ($\mathcal{J}_{in} \gg \mathcal{J}_{out}$).

Furthermore, in Fig. 20.18C and Fig. 20.18D, we extract the properties of the non-equilibrium steady state (NESS). We observe that for large system sizes the local current scales with the system size as $\mathcal{J} \propto N^{-2}$ and a particle profile follows a relation $\langle n_i \rangle \sim \frac{1}{2}\cos\pi\frac{i-1}{L-1} + 1$. These predictions are in agreement with the strong driving limit prediction, for the case of solvable boundaries, at the isotropic point of the XXZ Hamiltonian [45]. However, the dynamical exponent a_{th} of the transient regime does not have a clear connection to the current exponent $c = 2$ of the NESS. The reason for that is the large deviation from linear response. However, it is worth noting that linear response arguments [66] would lead to a relation between the two exponents $b_{LR} = \frac{1}{1+c} = 1/3$ and therefore $a_{LR} = -2/3$. Interestingly the theoretical exponents we observe are relatively close to these values.

20.7.3 Effects of decoherence on the dynamics and the steady state

In this subsection, we investigate the effects of external decoherence on transport. We use a simplified model of decoherence described by Eq. 20.49, and assume uniform strength of decoherence across the device. In Fig. 20.19 we illustrate that across all dynamical regimes, both polarization and currents are in a good qualitative agreement with numerical simulations where dephasing noise and decay rates are chosen to be $\gamma_\phi \sim 0.03$ to 0.04, $\gamma_\theta \sim 0.01$ to 0.015. The agreement is worse for the ballistic regime $\theta = 11\pi/24$. We attribute this to the fact that the steady state in this regime depends very strongly on the precise values of θ, ϕ. Small fluctuations of the order of $2-3\%$ are sufficient to explain the observed difference. The experimental errors on θ and ϕ are also larger for θ values closer to $\pi/2$ (Fig. 20.7). In addition, we explicitly illustrate that the deviation of the observed pumping current $\mathcal{J} = \mathcal{J}_{in}$ from the decoherence-free numerical results can be accurately explained by decoherence both at finite times and the NESS.

21 An Open-System Quantum Simulator with Trapped Ions by Barreiro et al.

Abstract

The control of quantum systems is of fundamental scientific interest and promises powerful applications and technologies. Impressive progress has been achieved in isolating the

systems from the environment and coherently controlling their dynamics, as demonstrated by the creation and manipulation of entanglement in various physical systems. However, for open quantum systems, engineering the dynamics of many particles by a controlled coupling to an environment remains largely unexplored. Here we report the first realization of a toolbox for simulating an open quantum system with up to five qubits. Using a quantum computing architecture with trapped ions, we combine multi-qubit gates with optical pumping to implement coherent operations and dissipative processes. We illustrate this engineering by the dissipative preparation of entangled states, the simulation of coherent many-body spin interactions and the quantum non-demolition measurement of multi-qubit observables. By adding controlled dissipation to coherent operations, this work offers novel prospects for open-system quantum simulation and computation.

Every quantum system is inevitably coupled to its surrounding environment. Significant progress has been made in isolating systems from their enviroment and coherently controlling the dynamics of several qubits [1, 2, 3, 4]. These achievements have enabled the realization of high-fidelity quantum gates, the implementation of small-scale quantum computing and communication devices as well as the measurement-based probabilistic preparation of entangled states, in atomic [5, 6], photonic [7] and solid-state setups [8, 9, 10]. In particular, successful demonstrations of quantum simulators [11, 12], which allow one to mimic and study the dynamics of complex quantum systems, have been reported [13].

In contrast, controlling the more general dynamics of open systems amounts to engineering both the Hamiltonian time evolution of the system as well as the coupling to the environment. Although open-system dynamics in a many-body or multi-qubit system are typically associated with decoherence [14, 15, 16], the ability to design dissipation can be a useful resource. For example, controlled dissipation allows the preparation of a desired entangled state from an arbitrary state [17, 18, 19] or an enhanced sensitivity for precision measurements [20]. In a broader context, by combining suitably chosen coherent and dissipative time steps, one can realize the most general non-unitary open-system evolution of a many-particle system. This engineering of the system-environment coupling generalizes the concept of Hamiltonian quantum simulation to open quantum systems. In addition, this engineering enables the dissipative preparation and manipulation of many-body states and quantum phases [21], and also quantum computation based on dissipation [22].

Here we provide the first experimental demonstration of a complete toolbox, through coherent and dissipative manipulations of a multi-qubit system, to control the dynamics of open systems. In a string of trapped ions, each ion encoding a qubit, we subdivide the qubits into "system" and "environment". The system-environment coupling is then engineered through the universal set of quantum operations available in ion-trap quantum computers [23, 24] and a dissipative mechanism based on optical pumping.

We first illustrate this engineering by dissipatively preparing a Bell state in a 2+1 ion system, such that an initially fully mixed state is pumped into a given Bell state. Similarly, with 4+1 ions, we also dissipatively prepare a 4-qubit GHZ-state, which can be regarded as a minimal instance of Kitaev's toric code [6]. Besides the dissipative elements, we show coherent n-body interactions by implementing the fundamental building block for 4-spin interactions. In addition, we demonstrate a readout of n-particle observables in a non-destructive way with a quantum-nondemolition (QND) measurement of a 4-qubit stabilizer operator. Altogether, our work demonstrates all essential coherent and dissipative elements for controlling general open-system dynamics.

21.1 Open-System Quantum Dynamics and Bell-State "Cooling"

The dynamics of an open quantum system S coupled to an environment E can be described by the unitary transformation $\rho_{SE} \mapsto U\rho_{SE}U^\dagger$, with ρ_{SE} the joint density matrix of

the composite system S + E. Thus, the reduced density operator of the system will evolve as $\rho_S = \mathrm{Tr}_E U \rho_{SE} U^\dagger$. The time evolution of the system can also be described by a completely positive Kraus map

$$\rho_S \mapsto \mathcal{E}(\rho_S) = \sum_k E_k \rho_S E_k^\dagger \tag{21.1}$$

with E_k operation elements satisfying $\sum_k E_k^\dagger E_k = 1$ [26]. If the system is decoupled from the environment, the general map (21.1) reduces to $\rho_S \mapsto U_S \rho_S U_S^\dagger$, with U_S the unitary time evolution operator acting only on the system.

Control of both coherent and dissipative dynamics is then achieved by finding corresponding sequences of maps (21.1) specified by sets of operation elements $\{E_k\}$ and engineering these sequences in the laboratory. In particular, for the example of dissipative quantum state preparation, pumping to an entangled state $|\psi\rangle$ reduces to implementing appropriate sequences of dissipative maps. These maps are chosen to drive the system to the desired target state irrespective of its initial state. The resulting dynamics have then the pure state $|\psi\rangle$ as the unique attractor, $\rho_S \mapsto |\psi\rangle\langle\psi|$. In quantum optics and atomic physics, the techniques of optical pumping and laser cooling are successfully used for the dissipative preparation of quantum states, although on a *single-particle* level. The engineering of dissipative maps for the preparation of entangled states can be seen as a generalization of this concept of pumping and cooling in driven dissipative systems to a *many-particle* context. To be concrete, we focus on dissipative preparation of stabilizer states, which represent a large family of entangled states, including graph states and error-correcting codes [27].

We start by outlining the concept of Kraus map engineering for the simplest non-trivial example of "cooling" a system of two qubits into a Bell state. The Hilbert space of two qubits is spanned by the four Bell states defined as $|\Phi^\pm\rangle = \frac{1}{\sqrt{2}}(|00\rangle \pm |11\rangle)$ and $|\Psi^\pm\rangle = \frac{1}{\sqrt{2}}(|01\rangle \pm |10\rangle)$. Here, $|0\rangle$ and $|1\rangle$ denote the computational basis of each qubit, and we use the short-hand notation $|00\rangle = |0\rangle_1|0\rangle_2$, for example. These maximally entangled states are stabilizer states: the Bell state $|\Phi^+\rangle$, for instance, is said to be *stabilized* by the two stabilizer operators Z_1Z_2 and X_1X_2, where X and Z denote the usual Pauli matrices, as it is the only two-qubit state being an eigenstate of eigenvalue $+1$ of these two commuting observables, i.e. $Z_1Z_2|\Phi^+\rangle = |\Phi^+\rangle$ and $X_1X_2|\Phi^+\rangle = |\Phi^+\rangle$. In fact, each of the four Bell states is uniquely determined as an eigenstate with eigenvalues ± 1 with respect to Z_1Z_2 and X_1X_2. The key idea of cooling is that we can achieve dissipative dynamics which pump the system into a particular Bell state, for example $\rho_S \mapsto |\Psi^-\rangle\langle\Psi^-|$, by constructing two dissipative maps, under which the two qubits are irreversibly transfered from the $+1$ into the -1 eigenspaces of Z_1Z_2 and X_1X_2.

The dissipative maps are engineered with the aid of an ancilla "environment" qubit [28, 29] and a quantum circuit of coherent and dissipative operations. The form and decomposition of these maps into basic operations are discussed in Box 1. The cooling dynamics are determined by the probability of pumping from the $+1$ into the -1 stabilizer eigenspaces, which can be directly controlled by varying the parameters in the employed gate operations. For pumping with unit probability ($p = 1$), the two qubits reach the target Bell state — regardless of their initial state — after only one cooling cycle, i.e., by a single application of each of the two maps. In contrast, when the pumping probability is small ($p \ll 1$), the process can be regarded as the infinitesimal limit of the general map (21.1). In this case, the system dynamics under a repeated application of the cooling cycle are described by a master equation [30]

$$\begin{aligned} \dot{\rho}_S &= -i[H_S, \rho_S] \\ &\quad + \sum_k \left(c_k \rho_S c_k^\dagger - \frac{1}{2} c_k^\dagger c_k \rho_S - \rho_S \frac{1}{2} c_k^\dagger c_k \right). \end{aligned} \tag{21.2}$$

Here, H_S is a system Hamiltonian, and c_k are Lindblad operators reflecting the system-environment coupling. For the purely dissipative maps discussed here, $H_S = 0$. Quantum

jumps from the +1 into the -1 eigenspace of Z_1Z_2 and X_1X_2 are mediated by a set of *two-qubit* Lindblad operators (see box 1 for details); here the system reaches the target Bell state asymptotically after many cooling cycles.

21.2 Experimental Bell-State Cooling

The dissipative preparation of n-particle entangled states is realized in a system of n+1 $^{40}Ca^+$ ions confined to a string by a linear Paul trap and cooled to the ground state of the axial centre-of-mass mode [31]. For each ion, the internal electronic Zeeman levels $D_{5/2}(m = -1/2)$ and $S_{1/2}(m = -1/2)$ encode the logical states $|0\rangle$ and $|1\rangle$ of a qubit. For coherent operations, a laser at a wavelength of 729 nm excites the quadrupole transition connecting the qubit states ($S_{1/2} \leftrightarrow D_{5/2}$). A broad beam of this laser couples to all ions (see Fig. 21.1a) and realizes the collective single-qubit gate $U_X(\theta) = \exp(-i\frac{\theta}{2}\sum_i X_i)$ as well as a Mølmer-Sørensen [32] (MS) entangling operation $U_{X^2}(\theta) = \exp(-i\frac{\theta}{4}(\sum_i X_i)^2)$ when using a bichromatic light field [33]. Shifting the optical phase of the drive field by $\pi/2$ exchanges X_i by Y_i in these operations. As a figure of merit of our entangling operation, we can prepare 3 (5) qubits in a GHZ state with 98% (95%) fidelity [8]. These collective operations form a universal set of gates when used in conjuction with single-qubit rotations $U_{Z_i}(\theta) = \exp(-i\frac{\theta}{2}Z_i)$, which are realized by an off-resonant laser beam that can be adjusted to focus on any ion.

For engineering dissipation, the key element of the mapping steps, shown as (i) and (iii) in Box 1, is a single MS operation. The two-qubit gate, step (ii), is realized by a combination of collective and single-qubit operations. The dissipative mechanism, step (iv), is here carried out on the ancilla qubit by a reinitialization into $|1\rangle$, as shown in Fig. 21.1b. Another dissipative process [35] can be used to prepare the system qubits in a completely mixed state by the transfer $|0\rangle \rightarrow (|0\rangle + |S'\rangle)/\sqrt{2}$ followed by optical pumping of $|S'\rangle$ into $|1\rangle$, where $|S'\rangle$ is the electronic level $S_{1/2}(m = 1/2)$.

Qubit read-out is accomplished by fluorescence detection on the $S_{1/2} \leftrightarrow P_{1/2}$ transition. The ancilla qubit can be measured without affecting the system qubits by applying hiding pulses that shelve the system qubits in the $D_{5/2}$ state manifold during fluoresence detection [36].

We use these tools to implement up to three Bell-state cooling cycles on a string of 2+1 ions. Starting with the two system qubits in a completely mixed state, we cool towards the Bell state $|\Psi^-\rangle$. Each cooling cycle is accomplished with a sequence of 8 entangling operations, 4 collective unitaries and 6 single-qubit operations; see the Supplementary Information. The cooling dynamics are probed by quantum state tomography of the system qubits after every half cycle. The reconstructed states are then used to map the evolution of the Bell-state populations.

In a first experiment, we set the pumping probability at $p = 1$ to observe deterministic cooling, and we obtain the Bell-state populations shown in Fig. 21.2a. As expected, the system reaches the target state after the first cooling cycle. Regardless of experimental imperfections, the target state population is preserved under the repeated application of further cooling cycles and reaches up to 91(1)% after 1.5 cycles (ideally 100%). In a second experiment towards the simulation of master-equation dynamics, the probability is set at $p = 0.5$ to probe probabilistic cooling dynamics. The target state is then approached asymptotically (Fig. 21.2b). After cooling the system for 3 cycles with $p = 0.5$, up to 73(1)% of the initially mixed population cools into the target state (ideally 88%). In order to completely characterize the Bell-state cooling process, we also perform a quantum process tomography [26]. As an example, the reconstructed process matrix for $p = 1$ after 1.5 cycles (Fig. 21.2c) has a Jamiolkowski process fidelity [3] of 87.0(7)% with the ideal dissipative process $\rho_S \mapsto |\Psi^-\rangle\langle\Psi^-|$ which maps an arbitrary state of the system into the Bell state $|\Psi^-\rangle$.

21.3 Four-Qubit Stabilizer Pumping

The engineering of the system-environment coupling, as demonstrated by Bell-state cooling above, can be readily extended to larger n-qubit open quantum systems. We illustrate such an engineering experimentally with the dissipative preparation of a four-qubit Greenberger-Horne-Zeilinger (GHZ) state $(|0000\rangle + |1111\rangle)/\sqrt{2}$. This state is uniquely characterized as the simultaneous eigenstate of the four stabilizers Z_1Z_2, Z_2Z_3, Z_3Z_4 and $X_1X_2X_3X_4$, all with eigenvalue $+1$ (see Fig. 21.3a). Therefore, cooling dynamics into the GHZ state are realized by four consecutive dissipative steps, each pumping the system into the $+1$ eigenspaces of the four stabilizers. In a system of 4+1 ions, we implement such cooling dynamics in analogy with the Bell-state cooling sequence. Here, however, the circuit decomposition of one cooling cycle involves 16 five-ion entangling operations, 20 collective unitaries and 34 single-qubit operations; further details in the Supplementary Information.

In order to observe this deterministic cooling process into the GHZ state, we begin by preparing the system ions in a completely mixed state. The evolution of the state of the system after each pumping step is characterized by quantum state tomography. The reconstructed density matrices shown in Fig. 21.3b for the initial and subsequent states arising in each step have a fidelity, or state overlap [5], with the expected states of {79(2),89(1),79.7(7),70.0(7),55.8(4)}%; see Supplementary Information for further details. Since the final state has a fidelity with the target GHZ state greater than 50%, the initially mixed state is cooled into a genuinely four-particle entangled state [39]. The pumping dynamics is clearly reflected by the measured expectation values of the stabilizers Z_iZ_j $(ij = 12, 23, 34, 14)$ and $X_1X_2X_3X_4$ at each step, as shown in Fig. 21.3c.

Although the simulation of a master equation requires small pumping probabilities, as an exploratory study, we implement up to five consecutive $X_1X_2X_3X_4$-stabilizer pumping steps with two probabilities $p = 1$ and 0.5, for the initial state $|1111\rangle$. The measured expectation values of all relevant stabilizers for pumping with $p = 1$ are shown in Fig. 21.3d. After the first step, the stabilizer $X_1X_2X_3X_4$ reaches an expectation value of -0.68(1); after the second step and up to the fifth step, it is preserved at -0.72(1) regardless of experimental imperfections.

For $X_1X_2X_3X_4$-stabilizer pumping with $p = 0.5$, the four-qubit expectation value increases at each step and asymptotically approaches -0.54(1) (ideally -1, fit shown in Fig. 21.3d). A state tomography after each pumping step yields fidelities with the expected GHZ-state of {53(1), 50(1), 49(1), 44(1), 41(1)}%. From the reconstructed density matrices we determine that the states generated after one to three cycles are genuinely multi-partite entangled [40].

21.4 Coherent Four-Particle Interactions

The coupling of the system to an ancilla particle, as used above for the engineering of dissipative dynamics, can also be harnessed to mediate effective coherent n-body interactions between the system qubits [26, 29]. The demonstration of a toolbox for open-system quantum simulation is thus complemented by adding unitary maps $\rho_S \mapsto U_S\rho_S U_S^\dagger$ to the dissipative elements described above. Here, $U_S = \exp(-i\tau H_S)$ is the unitary time evolution operator for a time step τ, which is generated by a system Hamiltonian H_S. In contrast to the recent achievements [41, 42] of small-scale analog quantum simulators based on trapped ions, where two-body spin Hamiltonians have been engineered directly [43], here we pursue a gate-based implementation following the concept of Lloyd's digital quantum simulator [12], where the time evolution is decomposed into a sequence of coherent (and dissipative) steps.

In particular, the available gate operations enable an experimentally efficient simulation of n-body spin interactions [9], which we illustrate by implementing time dynamics of a four-body Hamiltonian $H_S = gX_1X_2X_3X_4$. This example is motivated by the efforts to experimentally realize Kitaev's toric code Hamiltonian [6], which is a sum of commuting four-qubit stabilizer

operators representing four-body spin interactions. This paradigmatic model belongs to a whole class of spin systems, which have been discussed in the context of topological quantum computing [45] and quantum phases exhibiting topological order [46].

The elementary unitary operation U_S can be decomposed into a compact sequence of three coherent operations, as explained in Fig. 21.4a. In an experiment carried out with 4+1 ions, we apply U_S for different values of τ to the system ions initially prepared in $|1111\rangle$. We observed coherent oscillations in the subspace spanned by $|0000\rangle$ and $|1111\rangle$, as shown in Fig. 21.4b. We characterize our implementation of U_S by comparing the expected and measured states, determined by quantum state tomography, for each value of τ. The fidelity between the expected and measured states is on average 85(2)%.

21.5 QND Measurement of Four-Qubit Stabilizer Operators

Our toolbox for quantum simulation of open systems is extended by the possibility of reading out n-body observables in a nondestructive way, which we illustrate here for a 4-qubit stabilizer operator $X_1X_2X_3X_4$. As above, we first coherently map the information about whether the system spins are in the +1(-1) eigenspace of the stabilizer operator onto the logical states $|0\rangle$ and $|1\rangle$ of the ancilla qubit. In contrast to the engineering of coherent and dissipative maps above, where this step was followed by single-and two-qubit gate operations, here we proceed instead by measuring the ancilla qubit.

Thus, depending on the measurement outcome for the ancilla, the system qubits are projected onto the corresponding eigenspace of the stabilizer: $\rho_S \mapsto P_+\rho_S P_+/N_+$ ($P_-\rho_S P_-/N_-$) for finding the ancilla in $|0\rangle$ ($|1\rangle$) with the normalization factor $N_\pm = \mathrm{Tr}(P_\pm\rho_S P_\pm)$. Here, $P_\pm = \frac{1}{2}(1 \pm X_1X_2X_3X_4)$ denote the projectors onto the ±1 eigenspaces of the stabilizer operator. Note that our measurement is QND in the sense that (superposition) states within one of the two eigenspaces are not affected by the measurement.

In the experiment with 4+1 ions, we prepare different four-qubit system input states (tomographically characterize in additional experiments), carry out the QND measurement and tomographically determine the resulting system output states.

To characterize how well the measurement device prepares a definite state, we use as input $|1111\rangle$, which is a non-eigenstate of the stabilizer. In this case, when the ancilla qubit is found in $|0\rangle$ or $|1\rangle$ the system qubits are prepared in the state $(|0000\rangle \pm |1111\rangle)/\sqrt{2}$ by the QND measurement. Experimentally we observe this behaviour with a quantum state preparation (QSP) fidelity [12] of $F_{\mathrm{QSP}} = 73(1)\%$. On the other hand, for a stabilizer eigenstate, the QND measurement preserves the stabilizer expectation value. Experimentally, for the input state $(|0011\rangle - |1100\rangle)/\sqrt{2}$, we observe a QND fidelity [12] of $F_{\mathrm{QND}} = 96.9(6)\%$. For more details see the Supplementary Information.

Our measurement of n-body observables is an essential ingredient in quantum error correction and quantum computing protocols. In contrast to the *open-loop* experiments presented here [28], this ability also enables an alternative approach for system-environment engineering: The outcome from measurements of the environment can be classically processed and used for feedback operations on the system. This procedure paves the way to *closed-loop* simulation scenarios in open quantum systems.

21.6 Outlook

Our experimental demonstration of a toolbox of elementary building blocks in a system of trapped ions should be seen as a first, and conceptual step towards the realization of an open quantum system simulator, with dynamics governed by the interplay of coherent and dissipative evolution. Such a quantum device has applications in various fields [13] including

condensed-matter physics and quantum chemistry, and possibly in modelling quantum effects in biology [48]. In addition to quantum simulation, it enables alternative approaches to quantum computing [22].

Although the present experiments were performed with a linear ion-trap quantum computer architecture, the ongoing development of two-dimensional trap arrays [49] promises scalable implementations of Kitaev's toric code [6] and related spin models, as discussed in the context of topological quantum computing. Following our original proposal [50], these ideas can be realized with neutral atoms in optical lattices and can be easily adapted to other physical platforms ranging from optical, atomic and molecular systems to solid-state devices.

21.7 Bell-state cooling

21.7.1 Implemented Kraus maps

The Bell state $|\Psi^-\rangle$ is not only uniquely determined as the simultaneous eigenstate with eigenvalue -1 of the two stabilizer operators X_1X_2 and Z_1Z_2 (as mentioned in the text), but also by X_1X_2 and Y_1Y_2. In the experiment, we implemented cooling into $|\Psi^-\rangle$ by engineering the two Kraus maps $\rho_S \mapsto E_1\rho_S E_1^\dagger + E_2\rho_S E_2^\dagger$ and $\rho_S \mapsto E_1'\rho_S {E_1'}^\dagger + E_2'\rho_S {E_2'}^\dagger$, where

$$
\begin{aligned}
E_1 &= \sqrt{p}\, Y_1 \frac{1}{2}\left(1 + X_1X_2\right), \\
E_2 &= \frac{1}{2}\left(1 - X_1X_2\right) + \sqrt{1-p}\,\frac{1}{2}\left(1 + X_1X_2\right), \\
E_1' &= \sqrt{p}\, X_1 \frac{1}{2}\left(1 + Y_1Y_2\right), \\
E_2' &= \frac{1}{2}\left(1 - Y_1Y_2\right) + \sqrt{1-p}\,\frac{1}{2}\left(1 + Y_1Y_2\right),
\end{aligned}
$$

which generate pumping into the -1 eigenspaces of X_1X_2 and Y_1Y_2 (instead of pumping into the eigenspaces of X_1X_2 and Z_1Z_2 as explained in Box 1 of the main text). The reason for pumping into the eigenspaces of X_1X_2 and Y_1Y_2 is that the mapping and unmapping steps, shown as (i) and (iii) in Box 1, are realized by a single MS gate $U_{X^2}(\pi/2)$ and $U_{Y^2}(\pi/2)$, respectively.

21.7.2 Circuit decomposition

The map for pumping into the -1 eigenspace of X_1X_2 was implemented by the unitary

$$
U_{X^2(\pi/2)}\, C(p)\, U_{X^2(\pi/2)} \tag{21.3}
$$

(corresponding to steps (i) - (iii) in Box 1) followed by an optical pumping of the ancilla qubit to $|1\rangle$. Here, the two-qubit controlled gate is

$$
\begin{aligned}
C(p) &= |0\rangle\langle 0|_0 \otimes \exp(i\alpha Z_1) + |1\rangle\langle 1|_0 \otimes \mathbb{1} \\
&= \exp\left[\frac{1}{2}(1 + Z_0) i\alpha Z_1\right] \\
&= U_{Z_1}(-\alpha)\, U_Y(\pi/2)\, U_{X^2}^{(0,1)}(-\alpha)\, U_Y(-\pi/2)
\end{aligned} \tag{21.4}
$$

where $U_{X^2}^{(0,1)}(-\alpha) = \exp(i(\alpha/2)X_0X_1)$ denotes an MS gate acting only on the ancilla and the first system qubit. This two-qubit MS gate operation was implemented in the experiment by the use of refocusing techniques [10]. In more detail, the gate $U_{X^2}^{(0,1)}$ was realized by interspersing two of the available three-qubit MS gate operations with single-ion light shifts on the second system qubit which induces a π-phase shift between the qubit states. Alternatively, this refocusing

could be avoided, and the sequences further simplified, by hiding the population of individual ions (here the second system ion) which are not supposed to participate in collective coherent operations in electronic levels decoupled from the driving laser excitation. More details on how to systematically decompose Kraus maps into the experimentally available ion-trap gate operations, in particular the multi-ion MS entangling gate, can be found in [9].

The circuit decompositions for the experimental implementation of the two maps are shown in Fig. 21.5. We note that the circuits have been simplified at the expense of implementing in addition in each dissipative map a flip operation Y_1Y_2 on the two system qubits. However, as this additional unitary corresponds to one of the stabilizers into whose -1 eigenspace cooling is performed, this does not interfere with the cooling dynamics.

Cooling with unit pumping probability $p = 1$ corresponds to $\alpha = \pi/2$, whereas $p = 0.5$ is realized with by setting $\alpha = \pi/4$. In the experiment, the "fundamental" MS gate was calibrated to implement $U_{X^2}(\alpha/2)$. The fully entangling operation $U_{X^2}(\pi/2)$ at the beginning and the end of the sequence Fig. 21.5a was then implemented by applying the $U_{X^2}(\alpha/2)$ operation twice (for $p = 1$) or four times (for $p = 0.5$). The fully entangling operations $U_{Y^2}(\pi/2)$ in Fig. 21.5b were implemented by two- and four-fold application of the "fundamental" MS gate with a shifted optical phase of the driving laser (cf. Section 2 in the main text).

21.7.3 Additional data

The initially mixed state was prepared with a fidelity of F=99.6(3)% with respect to the ideal state $\frac{1}{4}\mathbb{1}_{4\times4}$.

Physical process matrices were reconstructed with maximum likelihood techniques [4]. An error analysis was carried out via Monte Carlo simulations over the multinomially distributed measurement outcomes of the state and process tomography. For each process and state, 200 Monte Carlo samples were generated and reconstructed via maximum-likelihood estimation.

21.8 Four-qubit stabilizer pumping

Expectation values of the stabilizer operators Z_1Z_2, Z_2Z_3, Z_3Z_4 and $X_1X_2X_3X_4$ were not determined from the reconstructed density matrices of the system qubits. Instead, we performed fluorescence measurements in the X and Z basis on 5250 copies of the corresponding quantum states (for $p = 0.5$ cooling, 2100 copies were measured). The error bars were then determined from the multinomially distributed raw data.

21.8.1 Cooling

Cooling into the GHZ state $(|0000\rangle + |1111\rangle)/\sqrt{2}$ was realized by a pumping cycle where the four system qubits were deterministically pumped into the +1 eigenspaces of the stabilizers Z_1Z_2, Z_2Z_3, Z_3Z_4 and $X_1X_2X_3X_4$.

Pumping into the -1 eigenspace of Z_1Z_2 in the first cooling step could be achieved in complete analogy with Bell state cooling, i.e. by implementing a dissipative map, which only involves operations on the ancilla qubit and the system qubits #1 and #2, whereas the system qubits #3 and #4 remain completely unaffected. This could either be achieved through refocusing techniques or by hiding system ions #3 and #4 in electronically decoupled states for the duration of the dissipative circuit.

In the experiment, however, we used a few simplications, which are schematically shown in Fig. 21.6 and listed below:

- For deterministic cooling ($p = 1$), the inverse mapping step (shown in Box 1) is not necessary and has been taken out.

- In the coherent mapping step (shown in Box 1) the information about whether the system ions are in a ± 1 eigenstate of Z_1Z_2 is mapped onto the logical states of the ancilla qubit. This step ideally only involves the ancilla and the system qubits #1 and #2. One way to achieve this three-qubit operation without affecting the system qubits #3 and #4, is to combine the available five-ion MS gate with appropriately chosen refocusing pulses, i.e. light shift operations on individual ions. Those would have to be chosen such that ions #0, #1 and #2 become decoupled from ions #3 and #4, and furthermore residual interactions between ions #3 and #4 cancel out. However, it turns out that residual interactions between ions #3 and #4 can be tolerated: although not required for the Z_1Z_2-pumping dynamics, they are not harmful, as they do not alter the expectation values of the other two-qubit stabilizers Z_2Z_3 and Z_3Z_4. In our experiment the decoupling of ions #0, #1 and #2 from the ions #3 and #4 was achieved by the circuit shown in Fig. 21.6b.

  The additional interactions in the pumping of the two-qubit stabilizer operators Z_iZ_j affect the state of the system qubits with respect to the four-qubit stabilizer $X_1X_2X_3X_4$. However, this effect is not detrimental to the cooling, provided the pumping into the eigenspace of $X_1X_2X_3X_4$ is performed as the final step in the cooling cycle.

- In the employed sequence, the number of single-qubit rotations was reduced wherever possible. Essential single-qubit light shift operations, such as those needed for re-focusing operations, were kept.

- Local rotations of the system ions at the end of a cooling step, which would be compensated at the beginning of the subsequent cooling step, were omitted when several dissipative maps were applied in a row. The corresponding gates of the sequences are displayed in blue in Steps 1-3.

These simplifications allowed us to significantly reduce the length and complexity of the employed gate sequences for one stabilizer pumping step. The compressed gate sequences as used in the experiment are explicitly given below.

Step 1 (pumping into the $+1$ eigenspace of Z_1Z_2):

$$
\begin{aligned}
&U_Y(-\pi/2)\,U_{Z_2}(-\pi/2)\\
&U_X(\pi/2)\,U_{Z_2}(-\pi/2)\,U_X(-\pi/2)\\
&U_{Z_1}(\pi)\,U_{X^2}(\pi/4)\,U_{Z_2}(\pi)\,U_{Z_0}(\pi)\,U_{X^2}(\pi/4)\\
&U_X(-\pi/2)\,U_{Z_2}(-\pi/2)\,U_{Z_0}(-\pi/2)\,U_X(\pi/2)\\
&U_{X^2}(\pi/4)\,U_{Z_4}(\pi)\,U_{Z_3}(\pi)\,U_{X^2}(\pi/4)\\
&U_Y(\pi/2)\,U_X(-\pi/2)\,U_{Z_0}(-\pi/2)\,U_X(\pi/2)
\end{aligned}
$$

Step 2 (pumping into the $+1$ eigenspace of Z_2Z_3):

$$
\begin{aligned}
&U_Y(-\pi/2)\,U_{Z_3}(-\pi/2)\\
&U_X(\pi/2)\,U_{Z_3}(-\pi/2)\,U_X(-\pi/2)\\
&U_{Z_2}(\pi)\,U_{X^2}(\pi/4)\,U_{Z_3}(\pi)\,U_{Z_0}(\pi)\,U_{X^2}(\pi/4)\\
&U_X(-\pi/2)\,U_{Z_3}(-\pi/2)\,U_{Z_0}(-\pi/2)\,U_X(\pi/2)\\
&U_{X^2}(\pi/4)\,U_{Z_4}(\pi)\,U_{Z_1}(\pi)\,U_{X^2}(\pi/4)\\
&U_Y(\pi/2)\,U_X(-\pi/2)\,U_{Z_0}(-\pi/2)\,U_X(\pi/2)
\end{aligned}
$$

Step 3 (pumping into the +1 eigenspace of Z_3Z_4):

$$\begin{aligned} &U_Y(-\pi/2)\, U_{Z_4}(-\pi/2) \\ &U_X(\pi/2)\, U_{Z_4}(-\pi/2)\, U_X(-\pi/2) \\ &U_{Z_3}(\pi)\, U_{X^2}(\pi/4)\, U_{Z_4}(\pi)\, U_{Z_0}(\pi)\, U_{X^2}(\pi/4) \\ &U_X(-\pi/2)\, U_{Z_4}(-\pi/2)\, U_{Z_0}(-\pi/2)\, U_X(\pi/2) \\ &U_{X^2}(\pi/4)\, U_{Z_2}(\pi)\, U_{Z_1}(\pi)\, U_{X^2}(\pi/4) \\ &U_Y(\pi/2)\, U_X(-\pi/2)\, U_{Z_0}(-\pi/2)\, U_X(\pi/2) \end{aligned}$$

Step 4 (pumping into the +1 eigenspace of $X_1X_2X_3X_4$):

$$\begin{aligned} &U_X(-\pi/2) \\ &U_{Z_4}(-\pi/2)\, U_X(\pi/2)\, U_{Z_4}(-\pi/2) \\ &U_{X^2}(\pi/4)\, U_{Z_4}(\pi)\, U_{Z_0}(\pi)\, U_{X^2}(\pi/4) \\ &U_{Z_4}(-\pi/2)\, U_X(-\pi/2)\, U_{Z_0}(-\pi/2)\, U_X(\pi/2) \\ &U_{X^2}(\pi/4)\, U_{X^2}(\pi/4) \end{aligned}$$

Figure 21.14 shows the reconstructed density matrices (real and imaginary parts) for every step of the cooling cycle. The complete circuit decomposition of one cooling cycle involves 16 five-ion entangling operations, 28 (20) collective unitaries and 36 (34) single-qubit operations with (without) optional operations in blue. The reset operation involves further pulses not accounted for above.

21.8.2 Repeated four-qubit stabilizer pumping

To study the robustness of the dissipative operation, we prepared the initial state $|1111\rangle$ and subsequently applied repeatedly the dissipative map for pumping into the +1 eigenspace of the four-qubit stabilizer $X_1X_2X_3X_4$. We observed that after a single dissipative step a non-zero expectation value of $X_1X_2X_3X_4$ built up and stayed constant under subsequent applications of this dissipative map. However, due to imperfections in the gate operations, the expectation values of the two-qubit stabilizers decreased, ideally they should not be affected by the $X_1X_2X_3X_4$-pumping step (see Fig. 21.7). Interestingly, the expectation values of Z_1Z_4 and Z_3Z_4 decayed significantly faster than those for Z_1Z_2 and Z_2Z_3. This decay can be explained by the fact that in the gate sequence used for pumping into the +1 eigenspace of $X_1X_2X_3X_4$, step 4 above, single-ion light-shift operations are applied only to the fourth system qubit and the ancilla. This indicates that errors in the single-qubit gates applied to the fourth system ion accumulate under the repeated application of the dissipative step, and thus affect the stabilizers Z_1Z_4 and Z_3Z_4 which involve this system qubit more strongly than the others. This destructive effect can be minimized by alternating the roles of the system qubits.

Such optimization has been done for the dissipative dynamics shown in Fig. 21.8. Here, starting from the initial state $|1111\rangle$, repeated pumping into the -1 eigenspace of $X_1X_2X_3X_4$ has been implemented by the sequence

$$\begin{aligned} &U_{X^2}(\pi/8)\, U_{X^2}(\pi/8)\, U_{X^2}(\pi/8)\, U_{X^2}(\pi/8) \\ &U_X(-\pi/2) \\ &U_{Z_4}(-\pi/2 \times p)\, U_X(\pi/2)\, U_{Z_4}(\pi) \\ &U_{Y^2}(\pi/4 \times p)\, U_{Z_0}(\pi)\, U_{Z_4}(\pi)\, U_{Y^2}(\pi/4 \times p) \\ &U_Y(\pi/2)\, U_{Z_0}(-\pi/2)\, U_Y(-\pi/2) \\ &U_{X^2}(\pi/8)\, U_{X^2}(\pi/8)\, U_{X^2}(\pi/8)\, U_{X^2}(\pi/8) \end{aligned}$$

Here, we observed that indeed the expectation values of all two-qubit stabilizers decreased at the same pace and at a slightly slower rate (see Fig. 21.8). Upon repeating the sequence above 1,2,3,4, and 5 times, we changed the operations shown in red to act on qubits 4,3,2,1, and 1, respectively. The stabilizer expectation values for deterministic cooling, or $p = 1$, are shown in Fig. 21.8.

21.8.3 Pushing "anyons" around

In Kitaev's toric code [6], spins are located on the edges of a two-dimensional square lattice. The Hamiltonian

$$H = -g(\sum_p A_p + \sum_v B_p) \tag{21.5}$$

is a sum of mutually commuting four-qubit stabilizers $A_p = \prod_{i\in p} X_i$ and $B_v = \prod_{i\in v} Z_i$, which describe four-spin interactions between spins located around plaquettes p and vertices v of the lattice. The ground state of the Hamiltonian is the simultaneous $+1$ eigenstate of all stabilizer operators. The model supports two types of excitations that obey anyonic statistics under exchange (braiding), and they correspond to -1 eigenstates of either plaquette or vertex stabilizers.

For a minimal instance of this model, represented by a single plaquette of four spins located on the edges, the Hamiltonian contains a single four-qubit interaction term $X_1X_2X_3X_4$ and pairwise two-spin interactions Z_iZ_j of spins sharing a corner of the plaquette. The ground state as the simultaneous $+1$ eigenstate of these stabilizers is the GHZ-state $(|0000\rangle + |1111\rangle)/\sqrt{2}$. States corresponding to -1 eigenvalues of a two-qubit stabilizer Z_iZ_j can be interpreted as a configuration with an excitation located at the corner between the two spins i and j. Similarly, a four-qubit state with an eigenvalue of -1 with respect to $X_1X_2X_3X_4$, would correspond to an anyonic excitation located at the center of the plaquette.

In the experiment we prepared an initial state $|0111\rangle$ and then performed the cooling cycle of four deterministic pumping steps into the $+1$ eigenspaces of Z_1Z_2, Z_2Z_3, Z_3Z_4 and $X_1X_2X_3X_4$, using the sequences for Steps 1 to 4 given in section 21.8.1. The expectation values of the stabilizer operators for the initial state and the four spins after each pumping step are shown in Fig. 21.9. The dissipative dynamics can be visualized as follows: For the initial state with $\langle Z_1Z_2\rangle = -1$ and $\langle Z_1Z_4\rangle = -1$ a pair of excitations is located on the upper left and right corners of the plaquette, whereas $\langle X_1X_2X_3X_4\rangle = 0$ implies an anyon of the other type is present at the center of the plaquette with a probability 50%. In the first cooling step, where the first two spins are pumped into the $+1$ eigenspace of Z_1Z_2, the anyon at the upper right corner is dissipatively pushed to the lower right corner of the plaquette. In the third step of pumping into the $+1$ eigenspace of Z_3Z_4, the two excitations located on the upper and lower lefts corners fuse and disappear from the system. In the final step of pumping into the $+1$ eigenspace of $X_1X_2X_3X_4$, the anyon with a probability of 50% at the center of the plaquette is pushed out from the plaquette.

However, we'd like to stress that borrowing concepts from topological spin models, such as anyonic excitations, here is merely a convenient language to phrase and visualize the dissipative dynamics. In the present work with up to five ions, we do *not* explore the physics of topological spin models, since (i) in a minimal system of four spins the concepts developed for larger lattice models become questionable, and more importantly, (ii) during the implemented cooling dynamics the underlying (four-body) Hamiltonian of the model was not present. We rather demonstrate the basic tools which will allow one to explore this physics once larger, two-dimensional systems become available in the laboratory.

We note that photon experiments have reported the observation of correlations compatible with the manipulations of "anyons" in a setup representing two plaquettes [7, 11]. Such ex-

periments are based on postselection of measurements [as in teleportation by 2], which should be contrasted to our deterministic implementation of open system dynamics to prepare and manipulate the corresponding quantum state [as in deterministic teleportation by 13, 1].

21.8.4 Pumping into "excited" states

Starting from an initially fully mixed state of four qubits, we also implemented cooling into a different GHZ-type state, $(|0010\rangle - |1101\rangle)/\sqrt{2}$, by a sequence of four dissipative steps: 1) pumping into the +1 eigenspace of Z_1Z_2, 2) pumping into the -1 eigenspace of Z_2Z_2, 3) pumping into the -1 eigenspace of Z_3Z_4 and 4) pumping into the -1 eigenspace of $X_1X_2X_3X_4$. In the context of Kitaev's toric code, this state would correspond to an excited state. However, as above, we point out that the underlying Hamiltonian was not implemented in the cooling dynamics.

The measured expectation values of the stabilizers are shown in Fig. 21.10. The final density matrix, as determined from quantum state tomography after the four cooling steps, is shown in Fig. 21.11. This cooling cycle was implemented with the same sequences as given for Step 1 to 4 in section 21.8.1, with the only difference that the sign of the phase shift operations displayed in red was changed in Steps 2, 3, and 4. This allowed us to invert the pumping direction from the +1 into -1 eigenspaces of Z_2Z_2, Z_3Z_4 and $X_1X_2X_3X_4$.

21.9 QND measurement of a four-qubit stabilizer

21.9.1 Further details

As shown in Fig. 21.12, the QND measurement involves a mapping step where the information about whether the system described by an input density matrix ρ^{in} is in the +1 / -1 eigenspace of $A = X_1X_2X_3X_4$ is coherently mapped onto the internal states $|0\rangle$ and $|1\rangle$ of the ancilla qubit, which is initially prepared in $|1\rangle$. Subsequently the ancilla qubit is measured in its computational basis, leaving the system qubits in a corresponding output state ρ^{out}.

The coherent mapping $M(X_1X_2X_3X_4)$ was realized by the sequence

$$\begin{aligned} & U_X(\pi/4)U_{Z_0}(\pi)\,U_X(-\pi/4) \\ U_{X^2}(\pi/4)\,U_{X^2}(\pi/4)\,U_{Z_0}(-\pi/2)\,U_{X^2}(\pi/4)\,U_{X^2}(\pi/4) & \\ & U_Y(-\pi/4)\,U_{Z_0}(\pi)\,U_Y(\pi/4) \end{aligned}$$

which implements

$$\begin{aligned} M(X_1X_2X_3X_4) = & -\frac{i}{\sqrt{2}}(X_0 + Y_0) \otimes P_+ \\ & +\frac{1}{\sqrt{2}}(1 - iZ_0) \otimes P_-, \end{aligned} \tag{21.6}$$

with $P_\pm = \frac{1}{2}(1 \pm X_1X_2X_3X_4)$ the projectors onto the ± 1 eigenspaces of $X_1X_2X_3X_4$. Equation (21.6) shows that for the system qubits being in a state belonging to the +1 eigenspace of the stabilizer operator, the ancilla is flipped from $|1\rangle$ to $|0\rangle$, whereas it remains in its initial state $|1\rangle$ otherwise.

Subsequently, the ancilla as well as the four system qubits were measured. This was done by measuring the five ions simultaneously. Alternatively, we first hid the four system qubits in electronic levels decoupled from the laser excitation, performed the fluorescence measurement of the ancilla qubit, then recovered the state of the system qubits and tomographically measured the state of the four system qubits. The second approach, where the state of the system is not affected by the measurement of the ancilla, is of importance if the information from the ancilla measurement is to be used for feedback operations on the state of the system.

21.9.2 Quantitative analysis of the performance

To characterize the performance of a QND measurement for a (multi-)qubit system, a set of requirements and corresponding fidelity measures have been discussed in the literature [12].

(1) First of all, the measurement outcomes for the ancilla qubit should agree with those that one would expect from a direct measurement of the observable A on the input density matrix. This property can be quantified by the measurement fidelity,

$$F_{\mathrm{M}} = \left(\sqrt{p^{\mathrm{in}}_{+} p^{\mathrm{m}}_{|0\rangle}} + \sqrt{p^{\mathrm{in}}_{-} p^{\mathrm{m}}_{|1\rangle}}\right)^2 , \tag{21.7}$$

which measures the correlations of the distribution of measurement outcomes $p^{\mathrm{m}} = \{p^{\mathrm{m}}_{|0\rangle}, p^{\mathrm{m}}_{|1\rangle}\}$ of the ancilla qubit with the expected distribution $p^{\mathrm{in}} = \{p^{\mathrm{in}}_{+}, p^{\mathrm{in}}_{-}\}$ directly obtained from ρ^{in}, where $p^{\mathrm{in}}_{\pm} = \mathrm{Tr}\{\frac{1}{2}(1 \pm A)\rho^{\mathrm{in}}\}$.

(2) The QND character, reflected by the fact that the observable A to be measured should not be disturbed by the measurement itself, becomes manifest in ideally identical probability distributions p^{in} and p^{out}, which are determined from the input and output density matrices. These correlations are quantified by the QND fidelity

$$F_{\mathrm{QND}} = \left(\sqrt{p^{\mathrm{in}}_{+} p^{\mathrm{out}}_{+}} + \sqrt{p^{\mathrm{in}}_{-} p^{\mathrm{out}}_{-}}\right)^2 , \tag{21.8}$$

where $p^{\mathrm{out}}_{\pm} = \mathrm{Tr}\{\frac{1}{2}(1 \pm A)\rho^{\mathrm{out}}\}$.

(3) Finally, by measuring the ancilla qubit the system qubits should be projected onto the corresponding eigenspace of the measured observable A. Thus the quality of the QND measurement as a quantum state preparation (QSP) device is determined by the correlations between the ancilla measurement outcomes and the corresponding system output density matrices. It can be described by the QSP fidelity

$$F_{\mathrm{QSP}} = p^{\mathrm{m}}_{+} p^{\mathrm{out}}_{|0\rangle,+} + p^{\mathrm{m}}_{-} p^{\mathrm{out}}_{|1\rangle,-} , \tag{21.9}$$

where $p^{\mathrm{out}}_{|0/1\rangle,\pm}$ denotes the conditional probability of finding the system qubits in the +1 (-1) eigenspace of A, provided the ancilla qubit has been previously measured in $|0\rangle$ ($|1\rangle$).

The probability distributions for the system input and output states, the ancilla measurement outcome distributions, and the resulting fidelity values are summarized in Tables I to IV. The input states had a fidelity [5] with the ideal states $(|0000\rangle + |1111\rangle)/\sqrt{2}$, $(|0000\rangle - |1111\rangle)/\sqrt{2}$ and $(|0011\rangle - |1100\rangle)/\sqrt{2}$ of $75.3(9), 77.3(8), 93.2(4)\%$.

We observe that we obtain higher values for the measurement and QND fidelities than for the QSP fidelities. The latter is relevant in the context of quantum error correction or closed-loop simulation protocols or more generally whenever the information from the ancilla measurement is used for further processing of the system output state.

With the additional hiding and unhiding pulses before and after the measurement of the ancilla we observe a loss of fidelity of a few percent in the QSP fidelities.

Box 1: Engineering dissipative open-system dynamics

Dissipative dynamics which cool two qubits from an arbitrary initial state into the Bell state $|\Psi^-\rangle$ are realized by two maps that generate pumping from the $+1$ into the -1 eigenspaces of the stabilizer operators Z_1Z_2 and X_1X_2:

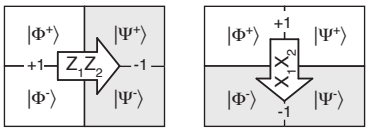

For Z_1Z_2, the dissipative map pumping into the -1 eigenspace is $\rho_S \mapsto \mathcal{E}(\rho_S) = E_1\rho_S E_1^\dagger + E_2\rho_S E_2^\dagger$ with

$$E_1 = \sqrt{p}\, X_2 \frac{1}{2}\left(1 + Z_1Z_2\right),$$
$$E_2 = \frac{1}{2}\left(1 - Z_1Z_2\right) + \sqrt{1-p}\,\frac{1}{2}\left(1 + Z_1Z_2\right).$$

The map's action as a uni-directional pumping process can be seen as follows. Since the operation element E_1 contains the projector $\frac{1}{2}(1 + Z_1Z_2)$ onto the $+1$ eigenspace of Z_1Z_2, the spin flip X_2 can then convert $+1$ into -1 eigenstates of Z_1Z_2, e.g., $|\Phi^+\rangle \mapsto |\Psi^+\rangle$. In contrast, the -1 eigenspace of Z_1Z_2 is left invariant. In the limit $p \ll 1$, the repeated application of this map reduces the process to a master equation with Lindblad operator $c = \frac{1}{2}X_2(1 - Z_1Z_2)$.

We implement the two dissipative maps by quantum circuits of three unitary operations (i)-(iii) and a dissipative step (iv). Both maps act on the two system qubits S and an ancilla which plays the role of the environment E:

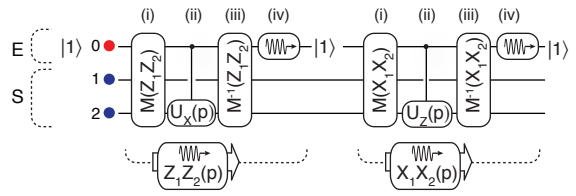

Cooling Z_1Z_2 proceeds as follows:

(i) Information about whether the system is in the $+1$ or -1 eigenspace of Z_1Z_2 is mapped by $M(Z_1Z_2)$ onto the logical states $|0\rangle$ and $|1\rangle$ of the ancilla (initially in $|1\rangle$).

(ii) A controlled gate $C(p)$ converts $+1$ into -1 eigenstates by flipping the state of the second qubit with probability p, where

$$C(p) = |0\rangle\langle 0|_0 \otimes U_{X_2}(p) + |1\rangle\langle 1|_0 \otimes \mathbb{1},$$

with $U_{X_2}(p) = \exp(i\alpha X_2)$ and $p = \sin^2\alpha$.

(iii) The initial mapping is inverted by $M^{-1}(Z_1Z_2)$. At this stage, in general, the ancilla and system qubits are entangled.

(iv) The ancilla is dissipatively reset to $|1\rangle$, which carries away entropy to "cool" the two system qubits.

The second map for cooling into the -1 eigenspace of X_1X_2 is obtained from interchanging the roles of X and Z above.

The engineering of dissipative maps can be readily generalized to systems of more qubits. As an example, dissipative preparation of n-qubit stabilizer states can be realized by a sequence of n dissipative maps (e.g. for Z_1Z_2 and $X_1X_2X_3X_4$ pumping), which are implemented in analogy to the quantum circuits for Bell state cooling discussed above:

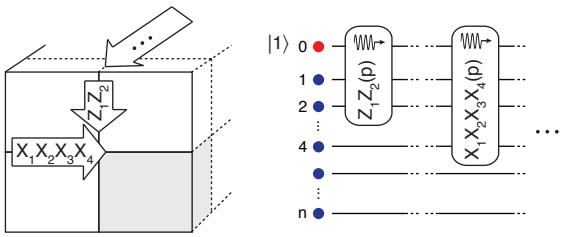

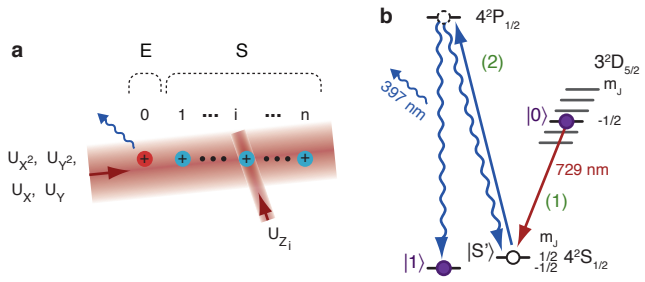

Figure 21.1: **Experimental tools for the simulation of open quantum systems with ions. a,** The coherent component is realized by collective $(U_X, U_Y, U_{X^2}, U_{Y^2})$ and single-qubit operations (U_{Z_i}) on a string of $^{40}Ca^+$ ions which consists of the environment qubit (ion 0) and the system qubits (ions 1 through n). **b,** The dissipative mechanism on the ancilla qubit is realized in the two steps shown on the Zeeman-split $^{40}Ca^+$ levels by (1) a coherent transfer of the population from $|0\rangle$ to $|S'\rangle$ and (2) an optical pumping to $|1\rangle$ after a transfer to the $4^2P_{1/2}$ state by a circularly-polarised laser at 397 nm.

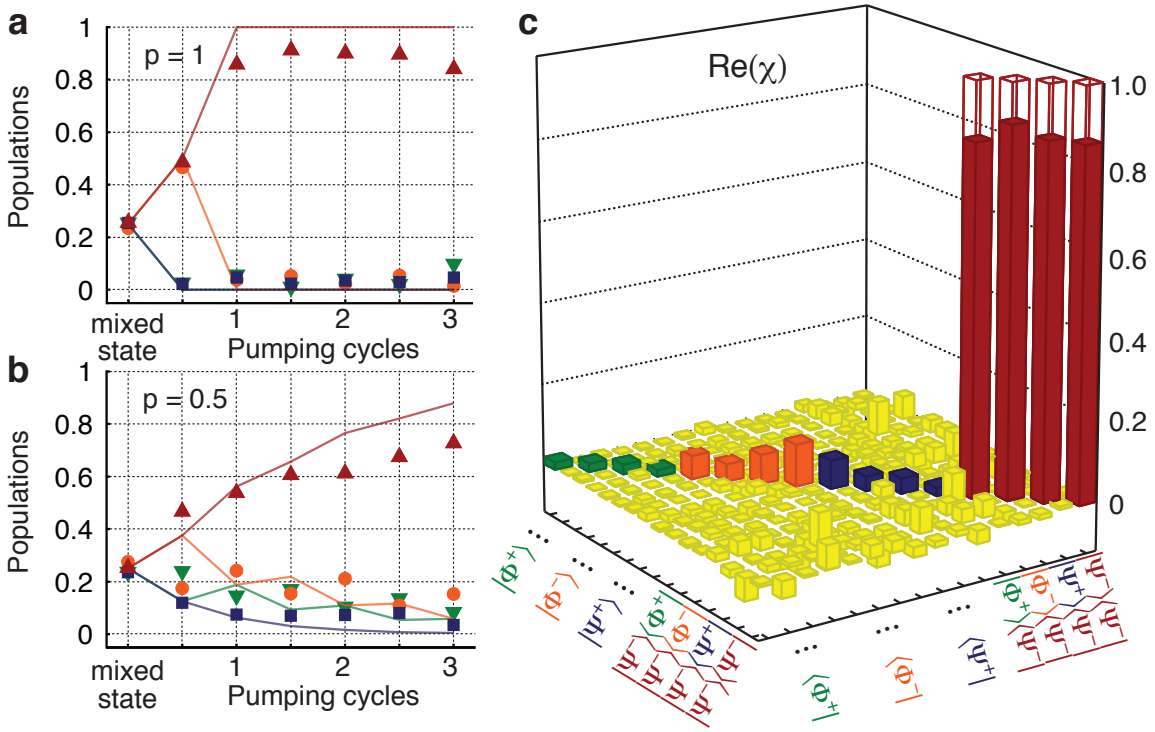

Figure 21.2: **Experimental signatures of Bell-state cooling.** Evolution of the Bell-state populations $|\Phi^+\rangle$ (down triangles), $|\Phi^-\rangle$ (circles), $|\Psi^+\rangle$ (squares) and $|\Psi^-\rangle$ (up triangles) of an initially mixed state under a cooling process with probability **a,** $p = 1$ or deterministic and **b,** $p = 0.5$. Error bars, not shown, are smaller than 2% (1σ). **c,** Reconstructed process matrix χ (real part), displayed in the Bell-state basis, describing the deterministic cooling of the two ions after one and a half cycles. The ideal process mapping any input state into the state $|\Psi^-\rangle$ has as non-zero elements only the four transparent bars shown. The imaginary elements of χ, ideally all zero, have an average magnitude of 0.004 and a maximum of 0.03. The uncertainties in the elements of process matrix are smaller than 0.01 (1σ).

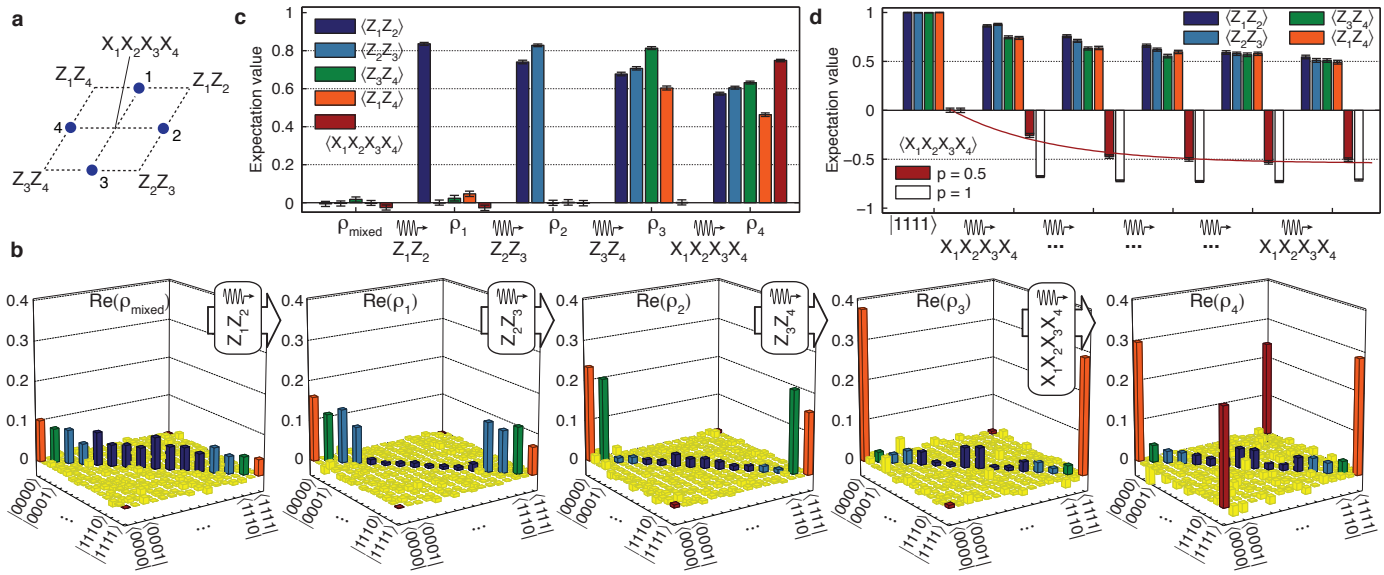

Figure 21.3: **Experimental signatures of four-qubit stabilizer pumping. a,** Schematic of the four system qubits to be cooled into the GHZ state $(|0000\rangle + |1111\rangle)/\sqrt{2}$, which is uniquely characterized as the simultaneous eigenstate with eigenvalue $+1$ of the shown stabilizers. **b,** Reconstructed density matrices (real part) of the initial mixed state ρ_{mixed} and subsequent states $\rho_{1,2,3,4}$ after sequentially pumping the stabilizers Z_1Z_2, Z_2Z_3, Z_3Z_4 and $X_1X_2X_3X_4$. Populations in the initial mixed state with qubits i and j antiparallel, or in the -1 eigenspace of the Z_iZ_j stabilizer, disappear after pumping this stabilizer into the $+1$ eigenspace. For example, populations in dark blue dissappear after Z_1Z_2-stabilizer pumping. A final pumping of the stabilizer $X_1X_2X_3X_4$ builds up the coherence between $|0000\rangle$ and $|1111\rangle$, shown as red bars in the density matrix of ρ_4. **c,** Measured expectation values of the relevant stabilizers; ideally, non-zero expectation values have a value of $+1$. **d,** Evolution of the measured expectation values of the relevant stabilizers for repetitively pumping an initial state $|1111\rangle$ with probability $p = 0.5$ into the -1 eigenspace of the stabilizer $X_1X_2X_3X_4$. The incremental cooling is evident by the red line fitted to the pumped stabilizer expectation value. The evolution of the expectation value $\langle X_1X_2X_3X_4\rangle$ for deterministic cooling ($p = 1$) is also shown. The observed decay of $\langle Z_iZ_j\rangle$ is due to imperfections and detrimental to the pumping process (see Supplementary Information). Error bars in **c** and **d**, $\pm 1\sigma$.

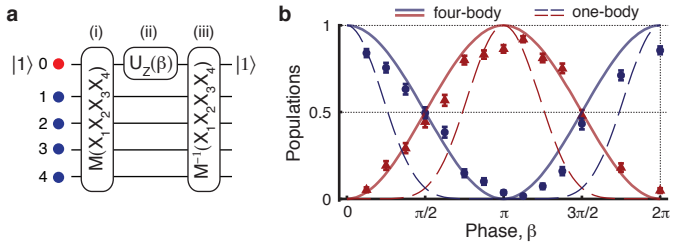

Figure 21.4: **Coherent simulation of 4-body spin interactions. a,** The elementary building block for the simulation of coherent evolution $U_S = \exp(-i\tau H_S)$ corresponding to the four-body Hamiltonian $H_S = gX_1X_2X_3X_4$ is implemented by a circuit of three operations: (i) First, a 5-qubit operation $M(X_1X_2X_3X_4)$, here realized by a single entangling 5-ion MS gate $U_{S_x^2}(\pi/2)$, coherently maps the information, whether the four system spins are in the +1(-1) eigenspace of $X_1X_2X_3X_4$ onto the internal states $|0\rangle$ and $|1\rangle$ of the ancilla qubit. (ii) Due to this mapping, all +1 (-1) eigenstates of $X_1X_2X_3X_4$ acquire a phase $\beta/2$ $(-\beta/2)$ by the single-qubit rotation $U_Z(\beta)$ on the ancilla ion. (iii) After the mapping is inverted, the ancilla qubit returns to its initial state $|1\rangle$ and decouples from the four system qubits, which in turn have evolved according to U_S. The simulation time step τ is related to the phase by $\beta = 2g\tau$. **b,** Experimentally measured populations in state $|0000\rangle$ (up triangles) and $|1111\rangle$ (circles) as a function of β for a single application of U_S to the initial state $|1111\rangle$ of the four system qubits (error bars, $\pm 1\sigma$). The solid lines show the ideal behavior. For comparison, the dashes lines indicate these populations for simultaneous single-qubit (one-body) oscillations, each driven by the rotation $\exp(-i\frac{\beta}{2}X_i)$.

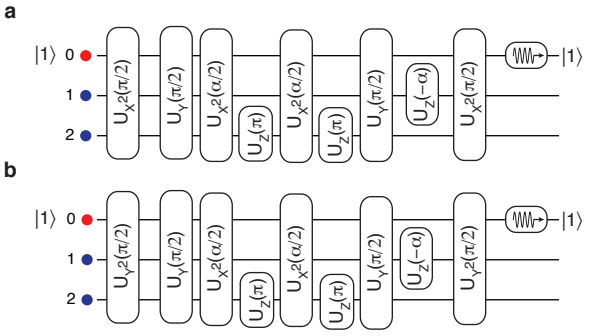

Figure 21.5: **Experimental sequences for Bell-state cooling.** Pumping into the eigenspaces of eigenvalue -1 of X_1X_2 (circuit **a,**) and Y_1Y_2 (circuit **b,**) occurs with a probability p in each step, where $\sin^2\alpha = p$.

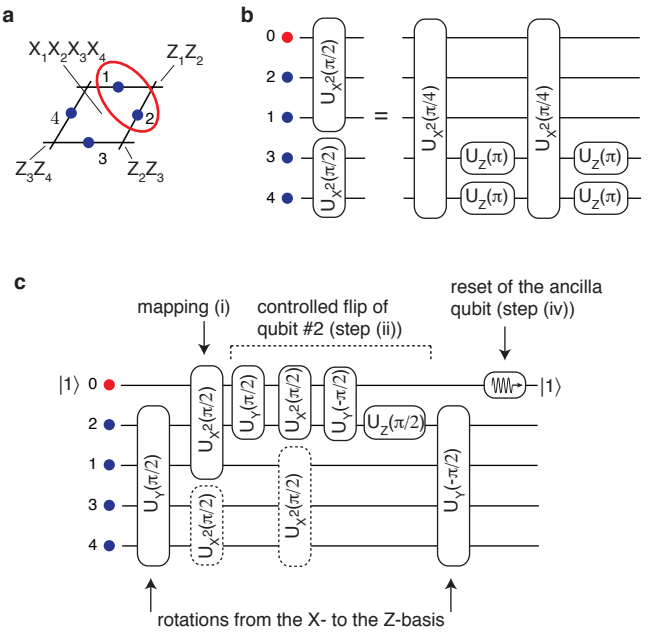

Figure 21.6: **Pumping into the +1 eigenspace of the Z_1Z_2 stabilizer operator a,** Ideally, only the ancilla qubit and the two system qubits #1 and #2 are involved in the circuit. **b,** An entangling gate acting on these three ions can be achieved by a refocusing technique, where ions #3 and #4 decouple from the dynamics. However, the latter ions still become entangled. However, these residual interactions are not harmful to the cooling, as they do not affect the expectation values of the other two-qubit stabilizer operators. **c,** Dashed operations in the quantum circuit indicate such residual entangling operations.

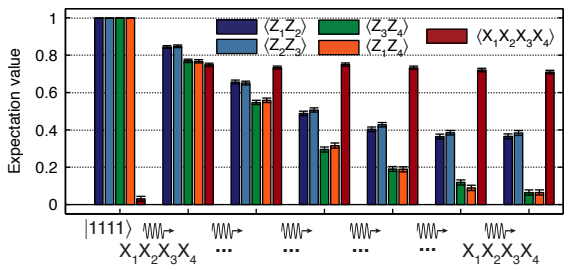

Figure 21.7: **Measured expectation value of stabilizers for repeated pumping without sequence optimization.** The expectation values of Z_1Z_4 and Z_3Z_4 show a significantly faster decay than those for Z_1Z_2 and Z_2Z_3. In every step of the cooling, most single-ion light-shift operations are applied to the fourth system qubit.

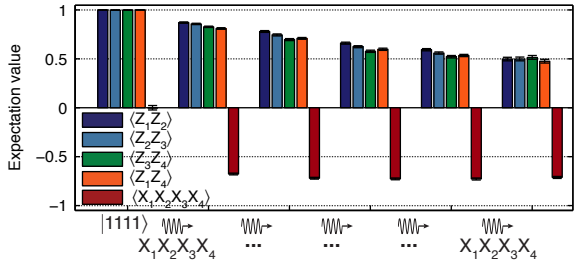

Figure 21.8: **Measured expectation value of stabilizers for repeated pumping with sequence optimization.** All two-qubit stabilizers decay at the same rate during cooling. In step 1,2,3,4, and 5 the single-qubit light-shift operations were applied on the system qubits 4,3,2,1, and 1, respectively.

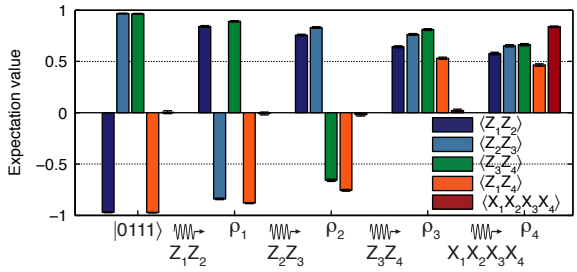

Figure 21.9: **Pushing "anyons" around by dissipation.** Measured expectation values of stabilizer operators for cooling dynamics of pumping into the $+1$ eigenspaces of Z_1Z_2, Z_2Z_3, Z_3Z_4 and $X_1X_2X_3X_4$, starting in the state $|0111\rangle$.

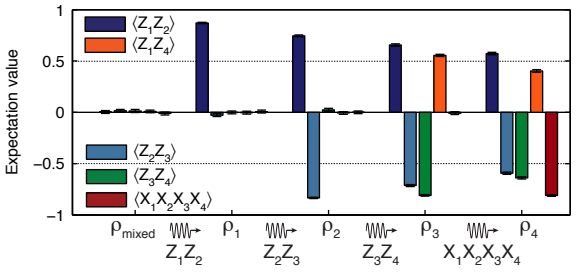

Figure 21.10: **Cooling into an "excited" state.** Measured expectation values of two- and four-qubit stabilizer operators for pumping into the state $(|0010\rangle - |1101\rangle)/\sqrt{2}$, starting from an initially four-qubit mixed state.

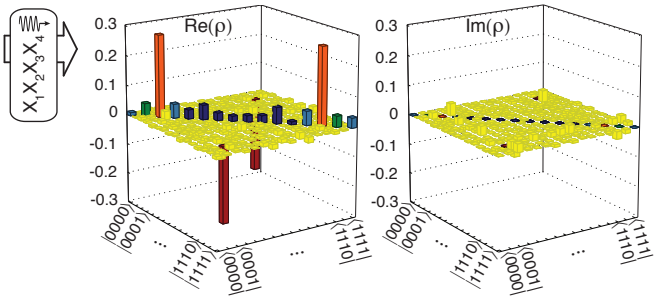

Figure 21.11: **Reconstructed density matrix after the full cooling cycle for dissipative preparation of the state** $(|0010\rangle - |1101\rangle)/\sqrt{2}$**.** This final state has a fidelity of 60(2)% with the expected state. This fidelity was determined from parity and coherence measurements and analysed with bayesian inference techniques as done in [8].

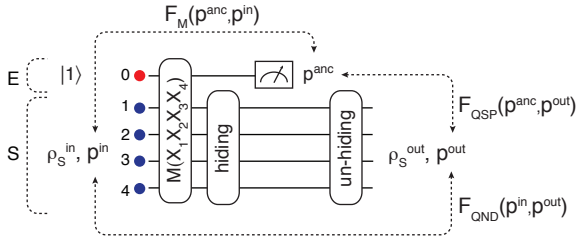

Figure 21.12: **QND measurement of the four-qubit stabilizer operator** $X_1X_2X_3X_4$**.** After the coherent mapping $M(X_1X_2X_3X_4)$, the ancilla qubit is measured. This measurement was performed both with and without applying additional pulses to hide the populations of the system qubits in electronically uncoupled states for the duration of the fluorescence measurement on the ancilla.

Table 2: QND probability distributions. Obtained from measurements **with** hiding of the system ions during the measurement of the ancilla.

input state	eigenspace	p^m_{in}	p^m_{out}	p^{in}	$p^{in}_{m=0}$	$p^{in}_{m=1}$	p^{out}	$p^{out}_{m=0}$	$p^{out}_{m=1}$
$\|0000\rangle + \|1111\rangle$	$+1$	0.959(1)	0.847(3)	0.817(9)	0.822(9)	0.618(34)	0.689(12)	0.736(12)	0.359(34)
	-1	0.041(1)	0.153(3)	0.183(9)	0.178(9)	0.382(34)	0.311(12)	0.264(12)	0.641(34)
$\|0000\rangle - \|1111\rangle$	$+1$	0.955(1)	0.169(3)	0.191(10)	0.187(9)	0.328(36)	0.310(11)	0.640(26)	0.242(12)
	-1	0.045(1)	0.831(3)	0.809(10)	0.813(9)	0.672(36)	0.690(11)	0.360(26)	0.758(12)
$\|0011\rangle - \|1100\rangle$	$+1$	0.978(1)	0.103(2)	0.041(4)	0.035(4)	0.412(47)	0.137(9)	0.476(36)	0.097(7)
	-1	0.022(1)	0.897(2)	0.959(4)	0.965(4)	0.588(47)	0.863(9)	0.524(36)	0.903(7)

Table 3: QND probability distributions. Obtained from measurements **without** hiding of the system ions during the measurement of the ancilla.

input state	eigenspace	p^m_{out}	p^{out}	$p^{out}_{m=0}$	$p^{out}_{m=1}$
$\|0000\rangle + \|1111\rangle$	$+1$	0.850(3)	0.713(11)	0.789(11)	0.336(30)
	-1	0.150(3)	0.287(11)	0.211(11)	0.664(30)
$\|0000\rangle - \|1111\rangle$	$+1$	0.188(3)	0.265(12)	0.504(28)	0.220(11)
	-1	0.812(3)	0.735(12)	0.496(28)	0.780(11)
$\|0011\rangle - \|1100\rangle$	$+1$	0.099(2)	0.073(7)	0.416(35)	0.038(5)
	-1	0.901(2)	0.927(7)	0.584(35)	0.962(5)

Table 4: QND figures of merit. Determined from measurements **with** hiding of the system ions during the measurement of the ancilla. Since the state $|0011\rangle - |1100\rangle$ is particularly robust against decoherence, the fidelity F_{QSP} is higher, as shown for 8 ions in [8].

input state	eigenspace	p^{in}	p^{out}	p^{m}	$p^{\mathrm{out}}_{\mathrm{QND}=+}$	$p^{\mathrm{out}}_{\mathrm{QND}=-}$	$F_{\mathrm{M}}(p^{\mathrm{in}}, p^{\mathrm{m}})$	$F_{\mathrm{QND}}(p^{\mathrm{in}}, p^{\mathrm{out}})$	$F_{\mathrm{QSP}}(p^{\mathrm{m}}, p^{\mathrm{out}}_{\mathrm{QND}})$
$\|0000\rangle + \|1111\rangle$	$+1$	0.82(1)	0.69(1)	0.85	0.74(1)		0.998(1)	0.978(5)	0.72(1)
	-1	0.18(1)	0.31(1)	0.15		0.64(3)			
$\|0000\rangle - \|1111\rangle$	$+1$	0.19(1)	0.31(1)	0.17	0.64(3)		0.999(1)	0.980(5)	0.74(1)
	-1	0.81(1)	0.69(1)	0.83		0.76(1)			
$\|0011\rangle - \|1100\rangle$	$+1$	0.041(4)	0.14(1)	0.10	0.48(4)		0.985(3)	0.969(6)	0.86(1)
	-1	0.959(4)	0.86(1)	0.90		0.90(1)			
$\|1111\rangle$	$+1$	0.5	0.47(1)	0.50049	0.70(1)		1	0.9992(6)	0.73(1)
	-1	0.5	0.53(1)	0.49951		0.76(1)			

Table 5: QND figures of merit. Determined from measurements **without** hiding of the system ions during the measurement of the ancilla. Since the state $|0011\rangle - |1100\rangle$ is particularly robust against decoherence, the fidelity F_{QSP} is higher, as shown for 8 ions in [8].

input state	eigenspace	p^{out}	p^{m}	$p^{\mathrm{out}}_{\mathrm{QND}=+}$	$p^{\mathrm{out}}_{\mathrm{QND}=-}$	$F_{\mathrm{M}}(p^{\mathrm{in}}, p^{\mathrm{m}})$	$F_{\mathrm{QND}}(p^{\mathrm{in}}, p^{\mathrm{out}})$	$F_{\mathrm{QSP}}(p^{\mathrm{m}}, p^{\mathrm{out}}_{\mathrm{QND}})$
$\|0000\rangle + \|1111\rangle$	$+1$	0.71(1)	0.85	0.79(1)		0.998(1)	0.984(4)	0.77(1)
	-1	0.29(1)	0.15		0.66(3)			
$\|0000\rangle - \|1111\rangle$	$+1$	0.26(1)	0.19	0.50(3)		1.0000(1)	0.992(3)	0.73(1)
	-1	0.74(1)	0.81		0.78(1)			
$\|0011\rangle - \|1100\rangle$	$+1$	0.07(1)	0.10	0.42(3)		0.986(2)	0.996(2)	0.91(1)
	-1	0.93(1)	0.90		0.96(1)			
$\|1111\rangle$	$+1$	0.52(1)	0.5078	0.75(1)		0.99994	0.9996(5)	0.74(1)
	-1	0.48(1)	0.4922		0.73(1)			

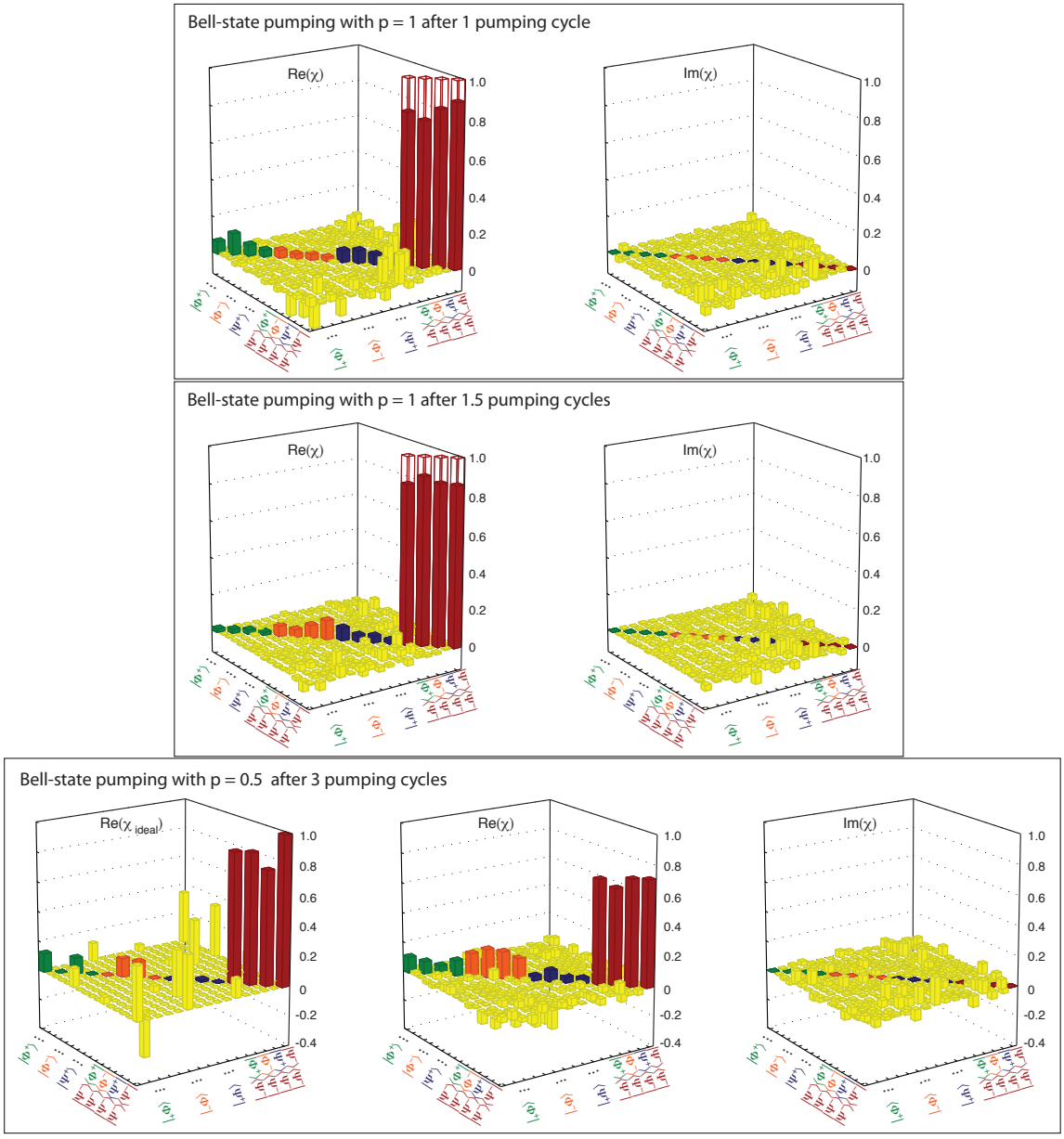

Figure 21.13: **Reconstructed process matrices of experimental Bell-state cooling.** The reconstructed process matrix for $p = 1$ after 1 (1.5) cycles has a Jamiolkowski process fidelity [3] of 83.4(7)% (87.0(7)%) with the ideal dissipative process $\rho_S \mapsto |\Psi^-\rangle\langle\Psi^-|$ which maps an arbitrary state of the system into the Bell state $|\Psi^-\rangle$. This ideal process has as non-zero elements only the four transparent bars shown. The reconstructed process matrix for $p = 0.5$ after 3 cycles has a Jamiolkowski process fidelity of 60(1)% with the ideal process χ_{ideal} shown [$\text{Im}(\chi_{\text{ideal}}) = 0$].

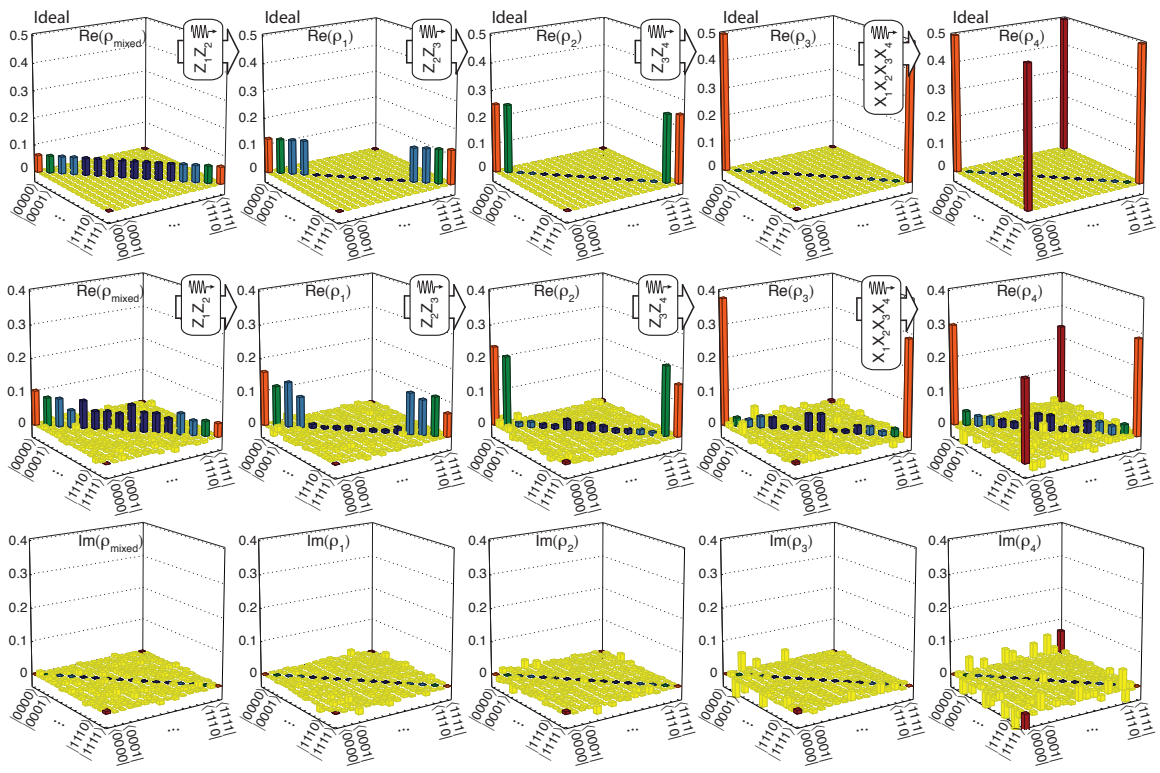

Figure 21.14: **Ideal and reconstructed density matrices of plaquette cooling.** An inital mixed state ρ_{mixed} is sequentially pumped by the stabilizers Z_1Z_2, Z_2Z_3, Z_3Z_4 and $X_1X_2X_3X_4$ driving the system into the states $\rho_{1,2,3,4}$.

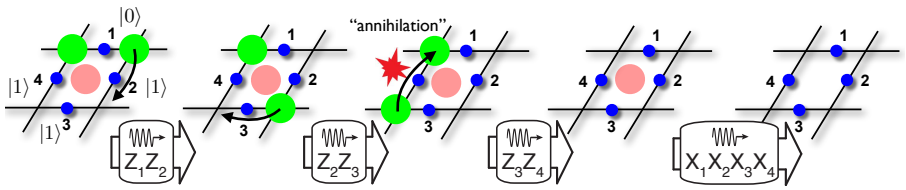

Figure 21.15: **Pushing "anyons".** Cartoon of the dissipative dynamics. The pumping dynamics can be visualized by dissipative pushing of excitations (green and red dots) between adjacent corners of the plaquette.

22 A quantum Newton's cradle by Kinoshita, Wenger, Weiss

22.1 Theory

It is a fundamental assumption of statistical mechanics that a closed system with many degrees of freedom ergodically samples all equal energy points in phase space. To understand the limits of this assumption, it is important to find and study systems that are not ergodic, and thus do not reach thermal equilibrium. A few complex systems have been proposed that are expected not to thermalize because their dynamics are integrable [1,2]. Some nearly integrable systems of many particles have been studied numerically, and shown not to ergodically sample phase space [3]. However, there has been no experimental demonstration of such a system with many degrees of freedom that does not approach thermal equilibrium. Here we report the preparation of out-of-equilibrium arrays of trapped one-dimensional (1D) Bose gases, each containing from 40 to 250 ^{87}Rb atoms, which do not noticeably equilibrate even after thousands of collisions. Our results are probably explainable by the well-known fact that a homogeneous 1D Bose gas with point-like collisional interactions is integrable. Until now, however, the time evolution of out-of-equilibrium 1D Bose gases has been a theoretically unsettled issue [4–6], as practical factors such as harmonic trapping and imperfectly point-like interactions may compromise integrability. The absence of damping in 1D Bose gases may lead to potential applications in force sensing and atom interferometry.

To see qualitatively why 1D gases might not thermalize, consider the elastic collision of two isolated, identical mass classical particles in one dimension. Energy and momentum are conserved only if they simply exchange momenta. Clearly, the momentum distribution of a 1D ensemble of particles will not be altered by such pairwise collisions. The well-known behaviour of Newton's cradle (see Fig. 1a) is most easily understood in this way. Even when several balls are simultaneously in contact, particles in an idealized Newton's cradle just exchange specific momentum values, though the explanation is more subtle [7]. Generalization of the Newton's cradle to quantum mechanical particles lends it a ghostly air. Rather than just reflecting off each other, colliding particles can also transmit through each other. When the particles are identical, the final states after transmission and reflection are indistinguishable.

In general, correlations and overlap among 1D Bose gas wavefunctions complicate the picture of independent particles colliding as in a Newton's cradle. In fact, there are circumstances in which 1D momentum distributions are known to change in time. For example, when weakly coupled bosons are released from a trap, the conversion of mean field energy to kinetic energy changes the momentum distribution. In the Tonks-Girardeau limit of infinite strength interactions [8], although the 1D bosons interact locally like noninteracting fermions, their momentum distribution is not fermionic [9,10]. When a Tonks-Girardeau gas is released from a trap and expands in one dimension, its momentum distribution evolves into that of a trapped Fermi gas [11–13]. The quantum Newton's cradle view of particles colliding with each other and either reflecting or transmitting can only be applied when the kinetic energy of the collision greatly exceeds the energy per atom at zero temperature at
the prevailing density [14]. The collisions that we study satisfy this criterion well. Our observations extend from the Tonks-Girardeau regime, where only pairwise collisions can occur [15], to the intermediate coupling regime, where there can be three- (or more) body collisions [15–17]. In both regimes, atoms that are set oscillating and colliding in a trap do not appreciably thermalize during our experiment.

We start our experiments with a Bose-Einstein condensate (BEC) loaded into the combination of a blue-detuned two-dimensional (2D) optical lattice and a red-detuned crossed dipole trap

(see Methods). The combination of light traps makes a 2D array of distinct, parallel Bose gases, with the 2D lattice providing tight transverse confinement and the crossed dipole trap providing weak axial trapping [11]. The dynamics within each tube of the 2D array are strictly 1D because the lowest transverse excitation, $\hbar\omega_r$ (where $\omega_r/2\pi = 67$kHz is the transverse oscillation frequency), far exceeds all other energies in

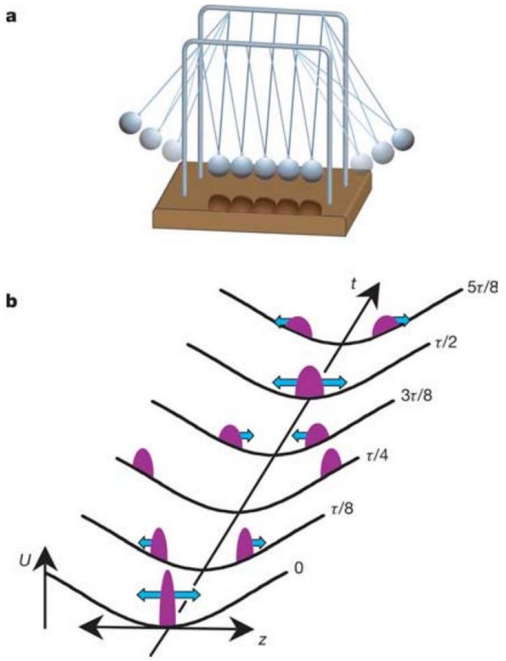

Figure 1 | Classical and quantum Newton's cradles. a, Diagram of a classical Newton's cradle. b, Sketches at various times of two out of equilibrium clouds of atoms in a 1 D anharmonic trap, $U(z)$. At time $t = 0$, the atoms are put into a momentum superposition with $2\hbar$k to the right and $2\hbar$k to the left. The two parts of the wavefunction oscillate out of phase with each other with a period τ. Each atom collides with the opposite momentum group twice every full cycle, for instance, at $t = 0$ and $\tau/2$. Anharmonicity causes each group to gradually expand, until ultimately the atoms have fully dephased. Even after dephasing, each atom still collides with half the other atoms twice each cycle.

the problem, and there is negligible tunnelling among the tubes. We can vary the weighted average number of atoms per tube, $N_{\rm tube}$, and the axial oscillation period, τ. For a given array, τ is the same to within 6% for all $1,000 - 8,000$ tubes. The 1D coupling strength is given by $\gamma = |2/a_{\rm 1D}n_{\rm 1D}|$, where $n_{\rm 1D}$ is the 1 D density, $|a_{\rm 1D}| \approx a_r^2/2a$ is the 1 D scattering length, $a = 5.3$ nm is the three-dimensional (3D) scattering length, $a_r = (\hbar/m\omega_r)^{1/2} = 41.5$ nm is the transverse oscillator width, and m is the Rb mass [18].

To study the 1D Bose gases, we turn off the crossed dipole trap and allow the atoms to expand in one dimension for 27 ms before taking an absorption image from the transverse direction. When we integrate the image transverse to the tubes, we get a 1D spatial distribution that corresponds to the momentum distribution after expansion, $f\,(p_{\rm ex})$. Although the individual 1D gases have ThomasFermi or Tonks-Girardeau $f\,(p_{\rm ex}\,)$ profiles, we measure gaussian $f\,(p_{\rm ex}\,)$ distributions, as expected when the $f\,(p_{\rm ex}\,)$ for many 1D Bose gases with different $N_{\rm tube}$ are summed.

To create non-equilibrium momentum distributions, we pulse on a 3.2 THz detuned 1D lattice along the tubes, which acts as a phase grating for the atoms. Two pulses, with intensity 11 W cm^{-2} and pulse widths of 23μ s separated in time by 33μ s, can deplete the

[461] Department of Physics, The Pennsylvania State University, 104 Davey Laboratory, University Park, Pennsylvania 16802, USA

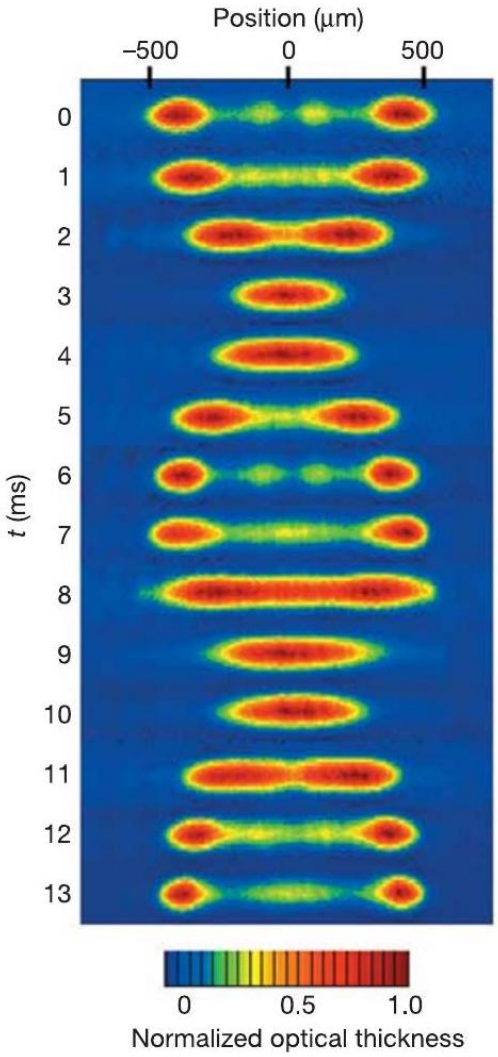

Figure 2 | Absorption images in the first oscillation cycle for initial average peak coupling strength $\gamma_o = 1$. Atoms are always confined to one dimension, in this case in 3,000 parallel tubes, with a weighted average of 110 atoms per tube. After grating pulses put each atom in a superposition of $\pm 2\hbar k$ momentum, they are allowed to evolve for a variable time t in the anharmonic 1D trap (crossed dipole trap), before being released and photographed 27 ms later. The false colour in each image is rescaled to show detail. These pictures are used to determine $f(p_{\mathrm{ex}})$. The first image shows that some atoms remain near $p_{\mathrm{ex}} = 0$ at $t = 0$. How many remain there depends on $n_{1\mathrm{D}}$, implying that these remnant atoms do not result from an imperfect pulse sequence, but rather from interactions during the grating pulses or evolution of the momentum distribution during expansion. The relative narrowness of the peaks in the last image compared to the first is indicative of the reduction in spatial density that results from dephasing (Fig. 1b). The transverse spatial width of each of the 14 image frames is 70μ m. Horizontal in the figure corresponds to vertical in the experiment, a minor distinction because a magnetic field gradient cancels gravity for the atoms.

zero momentum state and transfer atoms to $\pm 2\hbar k$ peaks [19,20] where k is the wavevector of the 1D lattice light. We wait after the grating pulses for a variable time, t, before measuring $f(p_{\mathrm{ex}})$. Figure 2 shows a time series of absorption images spanning a full oscillation in the crossed dipole trap, when the weighted average of the initial peak γ in each tube, γ_0, is 1.0. The two momentum groups collide with each other in the centre of the crossed dipole trap twice each full cycle, for instance at $t = 0$ and $\tau/2$, as illustrated in Fig. 1b. The total collision energy is $8(\hbar k)^2/2m = 0.45\hbar\omega_{\mathrm{r}}$, less than one-quarter the energy needed for transverse vibrational excitation [21], so the colliding gases remain 1D.

The first and last images in Fig. 2 differ because the oscillating atoms dephase. Illustrated conceptually in Fig. 1b, there is dephasing due to the gaussian crossed dipole trap anharmonicity, which gives an $\sim 8\%$ spread of τ across the full-width at half-maximum of each of the colliding clouds. The top curves in Fig. 3a-c show the time-averaged $f\,(p_{\rm ex}\,)$ over the first cycle for different $\gamma_{\rm o}$. Differences in shape among them reflect the initial energy per particle, which increases with $n_{\rm 1D}$, and hence γ_o^{-1}. Within 10τ to 15τ, $f\,(p_{\rm ex})$ stops changing noticeably during an oscillation period. The central observations in this letter are of the evolution of $f\,(p_{\rm ex})$ that are dephased, like the lower curves of Fig. 3a-c. Comparing only dephased distributions avoids the complication of how the momentum distribution in the trap evolves into $f\,(p_{\rm ex})$ during expansion, which may slightly depend on the initial spatial distributions. As atoms have clearly dephased within each tube, dephasing among tubes is irrelevant.

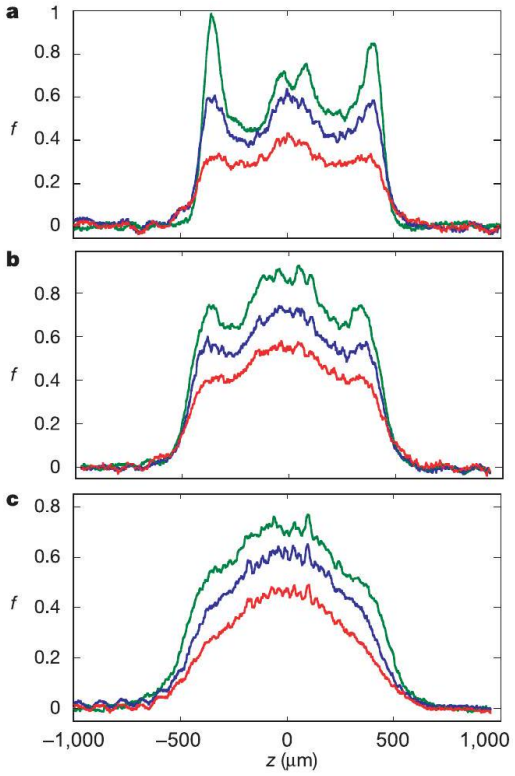

Figure 3 | The expanded momentum distribution, $f\,(p_{\rm ex}\,)$, for three values of γ_0. The curves are obtained by transversely integrating absorption images like those in Fig. 2. The spatial position, z, is approximately proportional to the expanded momentum, $p_{\rm ex}$. The vertical scale is arbitrary, but consistent among the curves. **a**, $\gamma_o = 4$; **b**, $\gamma_o = 1$; and c, $\gamma_{\rm o} = 0.62$. The highest (green) curve in each set is the average of $f\,(p_{\rm ex})$ from the first cycle, that is, from the images like those in Fig. 2. The lower curves in each set are $f\,(p_{\rm ex})$ taken at single times, t, after the atoms have dephased: **a**, $\tau = 34$ ms, $t = 15\tau$ (blue) and 30τ (red); **b**, $\tau = 13$ ms, $t = 15\tau$ (blue) and 40τ (red); and c, $\tau = 13$ ms, $t = 15\tau$ (blue) and 40τ (red). The changes in the distribution with time are attributable to known loss and heating. (See Supplementary Information for a discussion of the fine spatial structure in these curves.)

All the curves in Fig. 3 are non-gaussian. For comparison, we have created equilibrium 1D Bose gases with the same r.m.s. momentum as the non-equilibrium distributions we study here. To do so, we start with an equilibrium 3D Bose gas at an elevated temperature and adiabatically turn on the 2D lattice. The resultant $f\,(p_{\rm ex}\,)$ are nearly perfectly gaussian. Thus, to the extent that an observed $f\,(p_{\rm ex})$ is not gaussian, it has not thermalized.

Heating and loss affect the evolution of the distribution. We have studied these processes by watching how $f\,(p_{\rm ex})$ evolves without any grating pulses (see Supplementary Information). Some loss (20% or less, depending on γ_o) comes in the first couple of hundred milliseconds from three-body inelastic collisions. There is also 15% per second loss to background gas collisions.

Spontaneous emission caused by the lattice light heats some atoms, and by leaving some atoms in unlevitated magnetic sublevels, causes a 30% per second loss. This last loss in turn causes most of the heating, as exiting atoms transfer some of the momentum they pick up on their way out to atoms that remain.

To account for loss and heating in the time evolution shown in Fig. 3, we project how already dephased distributions would evolve

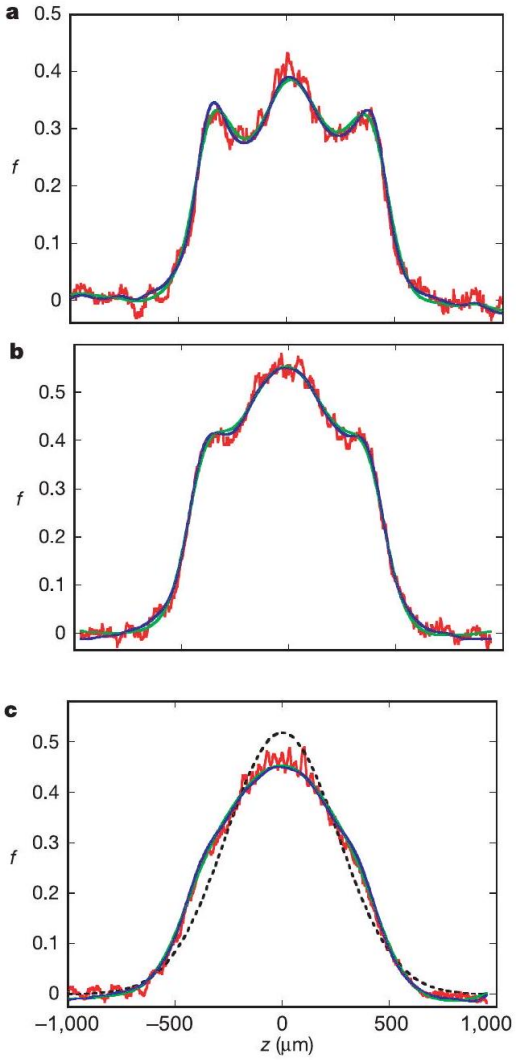

Figure 4 | Projected versus actual $f\,(p_{ex})$ for various γ_d, the dephased average peak coupling strength. The blue and green curves are $f\,(p_{\rm ex}\,)$ for $t_{\rm o} = 15\tau$, rescaled to account for loss and convolved with the known heating during $t_{\rm obs.}$. The blue curve's heating model is more sophisticated than that of the green curve, but the results are insensitive to the details. The red curves are the actual distributions at $t_{\rm o} + t_{\rm obs} \cdot \mathbf{a}, \gamma_{\rm d} = 18$ and $t_{\rm obs} = 15\tau$. $\mathbf{b}, \gamma_{\rm d} = 3.2$ and $t_{\rm obs} = 25\tau$. $\mathbf{c}, \gamma_{\rm d} = 1.4$ and $t_{\rm obs} = 25\tau$. The dashed line in **c** is a gaussian with the same number of atoms and r.m.s. width as the actual distribution. To the extent that the actual distribution conforms to the projected distribution rather than to a gaussian, the atoms have not thermalized.

without thermalization. Specifically, we take $f\,(p_{\rm ex}\,)$ at a time $t_{\rm o} = 15\tau$, rescale it to account for loss during an observation time, $t_{\rm obs}$, and convolve it with gaussian widths to capture the effect of the independently measured heating during $t_{\rm obs}$ (see Supplementary Information). The blue curves in Fig. 4 were projected with a twocomponent model that accurately reflects the measured heating, for $\gamma_{\rm o}\,(\gamma_{\rm d}) = 4(18), 1\ (3.2)$ and $0.62(1.4)$, where the coupling strength after dephasing, $\gamma_{\rm d}$, is calculated using the reduced $n_{\rm 1D}$ that prevails at $t_{\rm o}$. The green curves are the result of a simpler single-component projection. The similarity of the blue and green lines

illustrates the robustness of our projections (see Supplementary Information). The red curves show the actual distributions after $t_{\rm obs}$.

The actual and projected curves overlap reasonably well, with reduced χ^2 values of 1.2, 1.35 and 2.5 for Fig. 4a, b and c, respectively (using the blue curves). In each case, the difference between the projected and actual curves is far smaller than the difference between either of them and a thermal distribution. To highlight the nongaussian shape of Fig. 4c, we have superimposed a gaussian with the same atom number and r.m.s. width as the data. The slight discrepancies that exist between the actual and projected curves may result from the $\sim 25\%$ loss of atoms during $t_{\rm obs}$, which reduces the interaction energy contribution to $f\left(p_{\rm ex}\right)$. By assuming that any deviation between the projected and actual distributions is a step along the way to thermalization, we conservatively determine a lower bound on the thermalization time constant, $\tau_{\rm th}$ (see Methods). $\tau_{\rm th}$ is at least 390τ, $1,910\tau$ and 200τ for $\gamma_{\rm d} = 18, 3.2$ and 1.4, respectively. The data imply that each atom continues to oscillate in the trap with the same peak momentum it was given initially, as if there were no collisions.

Although collisions have no dynamical effect, we would like to roughly keep track of how many have occurred. Each atom passes $N_{\rm tube}/2$ atoms every half cycle. The probability of reflection, R, in a pairwise collision of 1D bosons with centre of mass momentum $2\hbar k$ was calculated in ref. 22. In the limit where $\left(2ka_{\rm 1D}\right)^2 \gg 1$, $R = \left(2ka_{\rm 1D}\right)^{-2}$. For our confinement parameters, $R = 1/22$. Therefore, in the first full cycle, the number of $2\hbar k$ collisions is $N_{\rm tube}$, with $r = N_{\rm tube}/22$ reflections. After dephasing within a tube, each atom has as many collisions, but at centre of mass momenta that range from $2\hbar k$ to near 0 . As the relative velocity decreases, R increases quadratically (until it saturates), but the ability of a collision to redistribute momentum is reduced roughly quadratically. Accordingly, we use the r derived above to keep track of reflections even after the atoms have dephased. For the conditions in Fig. 4a, b and c, the average number of collisions that have occurred per atom during $t_{\rm obs}$ are $600, 2,750$ and 6,250 , respectively, and the average number of reflections are 27, 125 and 285. Using the results from Fig. 4, we can set lower limits on the number of reflections required for thermalization of $710, 9,600$ and 2,300 for $\gamma_d = 18, 3.2$ and 1.4 , respectively. These limits are obviously much larger than the 2.7 collisions that characterize thermalization in a 3 D gas [23].

To experimentally confirm the existence of collisions in this system, despite their lack of consequence in one dimension, we apply the grating pulses without ever having turned on the 2D optical lattice, and so create non-equilibrium momentum distributions in three dimensions. Two BECs with different centre of mass velocities collide every half cycle. At the quarter cycle times, the two BECs are well separated spatially. This implies that collisions occur well above the Landau critical velocity, allowing particles to scatter out of the macroscopically occupied states [24]. We observe thermalization in a two-step process. Atoms first scatter into a spherical shell in velocity, which corresponds to the outgoing s-wave. They then scatter into a broad range of final states. Even though the 3D densities are nearly an order of magnitude lower than in the 1D tubes, thermalization occurs on a $< 2\tau$ timescale.

The absence of damping in 1D Bose gases has several potential applications. Atoms undergoing Bloch oscillations in quantum degenerate gases are candidate force sensors [25]. Fermions have emerged as better for this purpose than bosons, because the absence
of $s$wave collisions prevents instabilities in the Bloch oscillations [26] allowing for longer observation times [25] Howeverthe larger fermion momentum spreads reduce device sensitivityThe addition of 1D confinement for bosons could allow for narrow momentum spreads while avoiding dampingrelated instabilities

Atom interferometers can be sensitive gyroscopes [27] and work is in progress to achieve greater sensitivity using atom waveguides [20,28] To datethese experiments have been performed outside the strictly 1D regimeThe absence of thermalizing collisions promises potentially large sensitivity gains from reaching one dimension in the Thomas Fermi regime

Integrable systemsrare though they areare central to our under standing of nonlinear dynamicsThe KAM theorem [1] which underlies much of nonlinear dynamicsdescribes the effect of weak nonintegrability on system dynamicsAny weak nonintegrability in our system is apparently insufficient for thermalizationwhich confronts theory with a clear and rare manybody experimental observation in this areaIn the futurewe can allow tunnelling among the tubes by simply lowering the intensity of one or both of the 2D lattice beamsand so continuously change the system from one with 1 D to one with 2 D or 3 D collisional characterThe manybody systems integrability can thus be compromised in a controlled way presenting a new type of experimental model for the onset of chaos The possibility of direct control of τ_{th} may have further applications in the study of nonequilibrium quantum dynamics [29]

In summarywe have watched the time evolution of nonequi librium trapped 1D Bose gaseswhich are almost integrable systems We find no evidence of redistribution of momentumfrom the Tonks Girardeau gas limit to the intermediate coupling regimeThat iswe observe thousands of parallel 1D Bose gaseseach with hundreds of atoms colliding thousands of times without approaching equilibrium

22.2 Methods

Trapping detailsWe adiabatically load an ^{87}Rb BoseEinstein condensate BECproduced by alloptical means [30] and consisting of 2.5×10^5 atoms into the 2D latticecrossed dipole trap combinationA vertical magnetic field gradient cancels the effect of gravity on the $F = 1, m_F = 1$ atomsWe vary τ from 13 to 34 ms by changing the power and width of the crossed dipole trapN_{tube} depends on the value of τ when the 2D lattice is turned onand ranges from 40 to 250We vary $n_{1\mathrm{D}}$ in a range from 1.7×10^6 to 1.2×10^7 atoms m^{-1} by varying N_{tube} and by varying τ during the observations

Determination of a lower limit on τ_{th} To determine a lower limit on τ_{th} we calculate χ^2_{ap} the reduced χ^2 obtained from comparing the actual $f(p_{\mathrm{ex}})$ to the projected $f(p_{\mathrm{ex}})$ and χ^2_{ag} the reduced χ^2 obtained from comparing the actual $f(p_{\mathrm{ex}})$ to a gaussian with the same rmswidth and number of atomsWe take χ^2_{ag} as a measure of the extent to which the gas is not thermalizedIf we then assume that the entire χ^2_{ap} represents the small first step in an exponential approach of the actual distribution to a gaussianthen $\tau_{\mathrm{th}} = t_{\mathrm{obs}} \left(\chi^2_{\mathrm{ag}} + \chi^2_{\mathrm{ap}}\right)/\chi^2_{\mathrm{ap}}$ Note that even if the agreement between the projected and actual curves was statistically perfect so that $\chi^2_{\mathrm{ap}} = 1$ we would still only be able to set a finite lower limit on τ_{th}

We obtain the variance that normalizes χ^2_{ap} and χ^2_{ag} using the tails of the measured $f(p_{\mathrm{ex}})$ Fluctuations in the absorption probe beam dominate the noise along with the fine spatial structures discussed in Supplementary Information The spatial frequencies of these noise sources are higher than the spatial frequencies in the projected $f(p_{\mathrm{ex}})$ so they do not contribute to χ^2_{ap} But they do reduce χ^2_{ag} in a physically meaningless wayTo get a more appropriate measure of the relative sizes of these two χ^2 we apply a point spread filter function to the actual $f(p_{\mathrm{ex}})$ We increase the number of points used until the χ^2_{ap} for the filtered distribution is 10% larger than for the unfiltered functionThis is approximately when filtering starts to change the shape of the actual distribution on a scale relevant to the projected distributionThe projected distributions are unaffected by such point spread filteringas the projection operation smooths those curvesComparisons of the projected distributions and the filtered actual distributionssimilar to Fig4are shown in Supplementary Fig 2.

For $\gamma_{\mathrm{d}} = 18, 3.2$ and 14respectivelythe number of points in the filter function is 11,17 and 8; χ^2_{ap} is 1.29, 1.47 and 2.8; χ^2_{ag} is 32,111 and 19.5 and the lower limit on τ_{th} is $390\tau, 1,910\tau$ and 200τ These are the results we use in setting the lower limitsPerforming the same analysis with the single component heating projectionsthe number of points in the filter function is 17,19 and 9 χ^2_{ap} is 1.5, 1.8 and 2.7; χ^2_{ag} is 47,125 and 21 and the lower limit on τ_{th} is 470τ

$1,690\tau$ and 220τ The differences in the lower limits obtained using three different data analysesdiscussed in Supplementary Informationare in all cases less than 25% We consider this to be the approximate systematic uncertainty in the lower limits

23 Subdiffusion and heat transport in a tilted 2D Fermi-Hubbard system by Guardado-Sanchez, Morningstar et al.

Abstract

Using quantum gas microscopy we study the late-time effective hydrodynamics of an isolated cold-atom Fermi-Hubbard system subject to an external linear potential (a "tilt"). The tilt is along one of the principal directions of the two-dimensional (2D) square lattice and couples mass transport to local heating through energy conservation. We study transport and thermalization in our system by observing the decay of prepared initial density waves as a function of wavelength λ and tilt strength and find that the associated decay time τ crosses over as the tilt strength is increased from characteristically diffusive to subdiffusive with $\tau \propto \lambda^4$. In order to explain the underlying physics we develop a hydrodynamic model that exhibits this crossover. For strong tilts, the subdiffusive transport rate is set by a thermal diffusivity, which we are thus able to measure as a function of tilt in this regime. We further support our understanding by probing the local inverse temperature of the system at strong tilts, finding good agreement with our theoretical predictions. Finally, we discuss the relation of the strongly tilted limit of our system to recently studied 1D models which may exhibit nonergodic dynamics.

Introduction.—While non-interacting particles in a tilted lattice potential have been studied for almost a century [1, 2, 3, 4], the dynamics of strongly tilted and isolated many-body systems with strong interactions have been relatively unexplored. Characterizing the late-time behavior of such closed quantum many-body systems away from equilibrium is a topic of fundamental interest. In a series of recent papers [5, 6, 7, 8, 9, 10, 11] it was shown how irreversible dissipative dynamics can emerge from the unitary evolution of closed quantum systems. Thus generically we expect the transport of conserved quantities in such systems to behave hydrodynamically at late times as long as the system does thermalize. On the experimental front, advances in quantum simulation with cold atoms and other platforms have allowed for unprecedented control of quantum many-body systems, and for the controlled study of their dynamics [12, 13, 14, 15, 16, 17, 18]. For example, in a recent study diffusive charge transport was observed in an isolated strongly-interacting 2D Fermi-Hubbard system [18]. Here we follow that work by observing the dynamics of the same cold-atom Fermi-Hubbard system subject to a strong external linear potential, or "tilt", and find a crossover to qualitatively different subdiffusive behavior at strong tilts.

The dynamics of a weakly tilted 2D Fermi-Hubbard model were studied in Ref. [19] using semiclassical methods. That work formulated an understanding of the dynamics in which regions with positive local temperature heat up and transport charge "up" the tilt, and regions with negative local temperature [20, 21] transport charge "down" the tilt as the system approaches global equilibrium. Notably, if a tilted quantum system of particles in a lattice does approach thermal equilibrium within a band, that equilibrium is characterized by an infinite temperature [19]. In contrast, recent theoretical works [22, 23] explored the prospect of a transition to a localized phase in strongly tilted interacting 1D systems. While some evidence for this was found, it was suggested that this was the result of energetically-imposed local kinetic constraints that conserve the center of mass (COM)—a phenomenon later referred to as "Hilbert

space fragmentation" [24, 25]. This mechanism for nonergodicity at strong tilts depends on factors such as the range of interactions, the dimensionality of the system, and the direction of the tilt. In what follows, we explore a system which does not exhibit such nonergodicity. Thus this work is most directly related to Refs. [18, 19], although initial motivation for this study was derived from Refs. [22, 23], and investigating any nonergodic aspects of tilted systems is an interesting avenue for future work.

In this work we study the effect of an external tilt on the late-time emergent hydrodynamics of a 2D cold-atom system. This is done by varying the tilt strength and observing the relaxation of prepared initial density waves of various wavelengths λ. We observe a crossover from a diffusive regime at weak tilts, where the relaxation time τ scales like $\tau \propto \lambda^2$, to a subdiffusive regime at stronger tilts, where $\tau \propto \lambda^4$. We then construct a hydrodynamic model that exhibits the same crossover and discuss the underlying physics that leads to the subdiffusive transport. Using the hydrodynamic model we extract the tilt-dependent thermal diffusivity of this system. We further verify our understanding of the underlying physics by measuring the local inverse temperature profile of the system, thus confirming a prediction of our theoretical model that this profile should correspond to local equilibrium and be displaced by a quarter wavelength relative to the density profile.

System.—Our system is well-described by the tilted Fermi-Hubbard Hamiltonian $\hat{H} = \hat{H}_{\mathrm{FH}} - F\hat{N}_f\hat{x}_{\mathrm{COM}}$ where $\hat{H}_{\mathrm{FH}}$ is the conventional Fermi-Hubbard Hamiltonian on a square lattice, F is the tilt strength, $\hat{N}_f$ is the total number of fermions, and $\hat{x}_{\mathrm{COM}}$ is the x component of the COM. The repulsive on-site interaction energy is denoted by U, and the single-particle hopping energy by t_h. We emphasize that the system is tilted in only one of the lattice directions, which we denote with x.

We realize our tilted 2D Fermi-Hubbard model by loading a balanced mixture of two hyperfine ground states of ^{6}Li into an optical lattice [26]. The tilt is generated by an off-centered 1064 nm Gaussian beam of waist $\sim$ 180 µm, as depicted in Fig. 23.1(a). The resulting potential is linear to within 10% across a region of length 40 a_{latt} (30 µm), where a_{latt} is the spacing of the optical lattice, and the strength of the potential gradient can be tuned from 0 to $\sim h \times 5.5\,\mathrm{kHz}/a_{\mathrm{latt}}$ [27]. The beam is oriented such that the gradient is aligned with one of the two principal axes of the square lattice. A spatial light modulator (SLM) is used to project sinusoidal potentials of tunable wavelength along the direction of the gradient, and also remove any harmonic confinement from trapping potentials in the region of interest, similar to what was done in [18]. This allows us to prepare initial density modulations of tunable wavelength. We also add "hard walls" in the direction perpendicular to the gradient in order to contain the atoms in that direction and keep the average density constant over the experimental runtime (see Fig. 23.1(a)).

The atoms are adiabatically loaded into the lattice plus SLM potential at zero gradient (no tilt). The sinusoidal component of the SLM potential is chosen such that the resulting atom-density wave varies spatially with $0.0 \lesssim \langle \hat{n}_i \rangle \lesssim 1.2$ (see Fig. 23.1(b-c)), where $\hat{n}_i = \hat{n}_{i,\uparrow} + \hat{n}_{i,\downarrow}$. We also performed experiments with smaller-amplitude density waves and found no qualitative difference in our results [27]. Once the initial density wave is prepared we suddenly turn off the sinusoidal component of the potential created by the SLM, and turn on the tilt potential, thus initiating the dynamics. We focus on a square region of interest with a size of 35×35 lattice sites and measure only the single spin component $\langle \hat{n}_{i,\uparrow} \rangle$ using fluorescence imaging [26] since in a spin-balanced system $\langle \hat{n}_i \rangle = 2 \langle \hat{n}_{i,\uparrow} \rangle$.

We performed all experiments at an optical lattice depth of $7.4(1)E_R$, where $E_R/h = 14.66\,\mathrm{kHz}$ is the recoil energy and h is Planck's constant. This leads to a hopping rate of $t_h/h = 820(10)\,\mathrm{Hz}$. We work at a magnetic field of 595.29(4) G nearby a Feshbach resonance centered on 690 G. This leads to a scattering length of 472.0(9) a_0, where a_0 is a Bohr radius, which translates to an interaction energy of $U/t_h = 3.9(1)$ in the Fermi-Hubbard Hamiltonian.

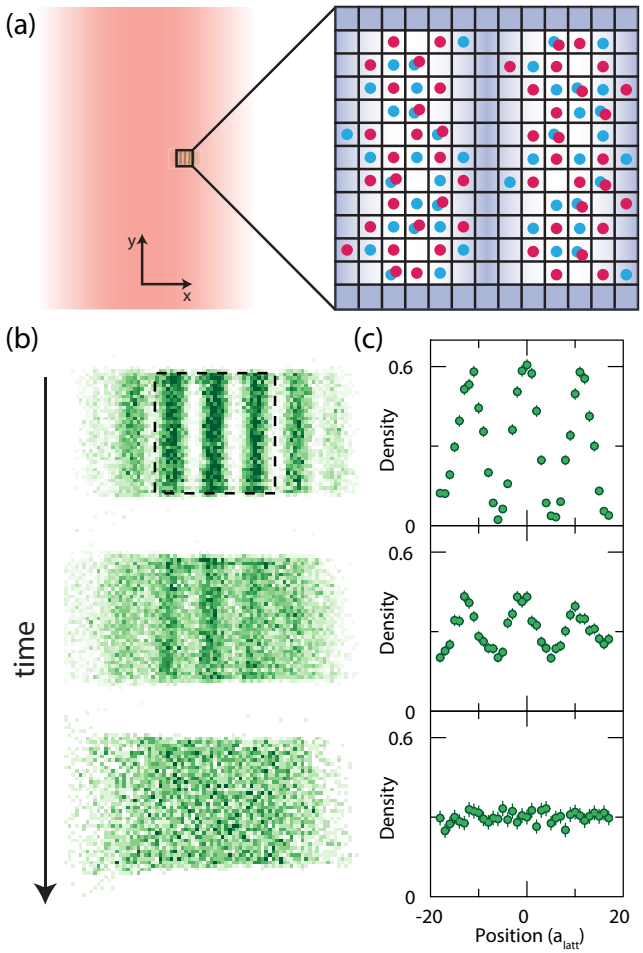

Figure 23.1: **Experimental setup and measurements.** (a) An off-centered beam generates a potential at the atoms that is approximately linear in x and independent of y. Blue-detuned light projected through a spatial light modulator is used to prepare the initial density waves of our experiments, with tunable wavelength in the direction of the tilt and hard walls a distance of 35 a_{latt} apart in the perpendicular direction. The figure is a schematic intended to portray the experimental setup and is not to scale. (b) Density of a single spin component *vs.* time averaged over ~ 10 images. The dotted square denotes the region of interest (ROI) in which our measurements were taken. (c) Evolution of the y-averaged density in the ROI of (b) as a function of x. The data corresponds to a system with interaction energy $U/t_h = 3.9(1)$, tilt strength $Fa_{\mathrm{latt}}/t_h = 0.99(3)$, and an initial density modulation of wavelength $\lambda/a_{\mathrm{latt}} = 11.46(3)$. The density profile is shown at times 0 ms (0 $\hbar/t_h$), 0.5 ms (2.6 $\hbar/t_h$), and 15 ms (36 $\hbar/t_h$) from top to bottom.

We tune the tilt strength F to values of up to $Fa_{\mathrm{latt}}/t_h \approx 6$ which allows us to explore tilts well above the crossover from diffusive to subdiffusive dynamics.

It is of note that we do not reach tilt strengths so strong that it would be accurate to describe our system over the experimental runtime using an effective Hamiltonian which exactly conserves the COM. Therefore we emphasize that this work does not focus on the physics of fracton-like systems with a strictly conserved dipole moment, nor does it explore the possible nonergodic dynamics in such systems, although these topics are an interesting direction for future research [22, 23, 24, 25, 28, 29, 30]. However, our tilted system does show an *emergent* conservation of the COM in the long wavelength limit where the potential energy of the tilt dominates the conserved total energy.

Results.—Our experimental protocol consists of preparing initial density waves of various wavelengths in a potential with tilt F and imaging the system's density profile after it has evolved under its own unitary dynamics for some time t. We analyze our data by averaging all measurements from a certain wavelength, tilt, and time, and we also average the density in the direction perpendicular to the tilt. This yields the averaged density profile along the tilted direction as a function of time, as shown in Fig. 23.1(c). For each wavelength, tilt, and time we fit the density profile to a sinusoid, $n(x,t) = \bar{n} + A(t)\cos\left(\phi(t) + 2\pi x/\lambda\right)$, after adjusting for any small amount of atom loss, with the wavelength being fixed by the fit to the initial profile. We extract both the phase ϕ and amplitude A of the sinusoidal fit as a function of time, normalizing the amplitude by its initial value $A(0)$. The main results of this paper are derived from tracking the decay of the amplitude $A(t)$ with time.

Any change in the phase with time is a result of the distance the center of mass "falls down" the tilt as the system heats up in the first band of the lattice potential. More precisely, an initial state with energy density corresponding to a finite temperature in the non-tilted Fermi-Hubbard system will evolve down the gradient of the tilted potential. As this happens the tilt does work $\sim F\Delta x_{\mathrm{COM}}$ per particle for a bulk shift of Δx_{COM}, and this work gets converted locally to kinetic and interaction energy in the system (the t_h and U terms) [19]. Since the t_h and U terms can only accommodate up to an energy of order $\sim t_h + U$ per particle before reaching infinite temperature, the shift of the COM of the system cannot be more than $\sim (t_h + U)/F$. We observe phase changes during the dynamics that are consistent with this approximate bound. We corroborate that the atoms are not excited to higher bands using a technique described in [31].

At late times we observe an approximately exponential decay of the density modulation (see Fig. 23.2). We fit an exponential to these curves to extract decay times as a function of λ and F. This is done at tilts $Fa_{\mathrm{latt}}/t_h \in \{0, 0.39(1), 0.99(3), 2.00(3), 3.88(9), 6.1(2)\}$ and for initial density waves with wavelengths $\lambda/a_{\mathrm{latt}} \in \{11.46(3), 15.16(5), 19.33(7), 23.3(2)\}$. We also use $\lambda/a_{\mathrm{latt}} = 7.69(3)$ for $Fa_{\mathrm{latt}}/t_h \approx 6$ as the decay time of the longest-wavelength modulation becomes very large for this tilt. Decay times that we observe vary increasingly with the tilt strength F, from $1{-}5\ \hbar/t_h$ at zero gradient up to $10^3{-}10^4\ \hbar/t_h$ for $Fa_{\mathrm{latt}}/t_h \approx 6$. At each value of the tilt strength we fit a power law of the form $\tau \propto \lambda^\alpha$ to our measured decay times. Diffusive relaxation has a characteristic $\tau \propto \lambda^2$ dependence ($\alpha = 2$), while values of $\alpha > 2$ indicate slower subdiffusive dynamics. Fig. 23.2 shows the full analysis for two of the values of F. From the extracted exponents α we observe a crossover from diffusive relaxation at weak tilts, where $\alpha \approx 2$, to subdiffusive behavior with an exponent of $\alpha \approx 4$ at stronger tilts. This crossover is shown in Fig. 23.3 along with the theoretical prediction of our hydrodynamic model.

Our observation of diffusive dynamics at weak tilts is consistent with the analysis of Ref. [19], and with the diffusive transport observed in previous experiments on the same system at $F = 0$ [18], albeit at lower temperatures. The crossover to subdiffusion with $\alpha \approx 4$ at strong tilts was, until now, previously unobserved, and its observation and explanation is the main result of this work. Below, and more completely in the Supplement, we construct a hydrodynamic

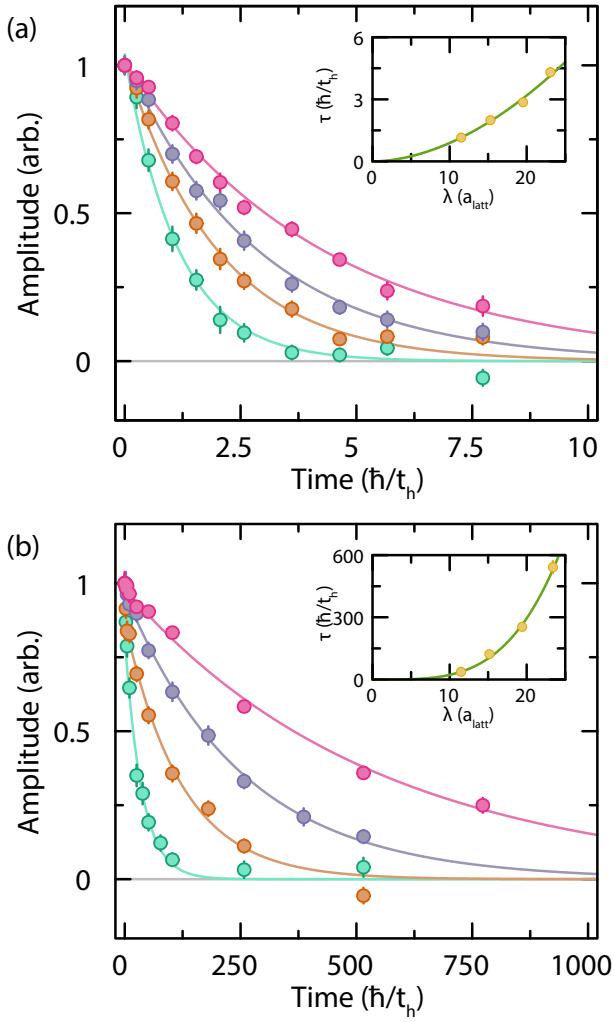

Figure 23.2: **Time decay of density waves.** Fitted normalized relative amplitudes of the periodic density modulation (circles) *vs.* time for wavelengths 11.46(3) (green), 15.16(5) (orange), 19.33(7) (purple), and 23.3(2) (pink) in units of a_{latt}. The lines are exponential fits to the decay at late times after any initial average heating (phase change). (Insets) Fitted decay times *vs.* wavelength (yellow circles) and a power law fit of the form $\tau \propto \lambda^{\alpha}$ (green line). (a) Dataset for tilt strength $Fa_{\mathrm{latt}}/t_h = 0$. (b) Dataset for tilt strength $Fa_{\mathrm{latt}}/t_h = 2.00(3)$.

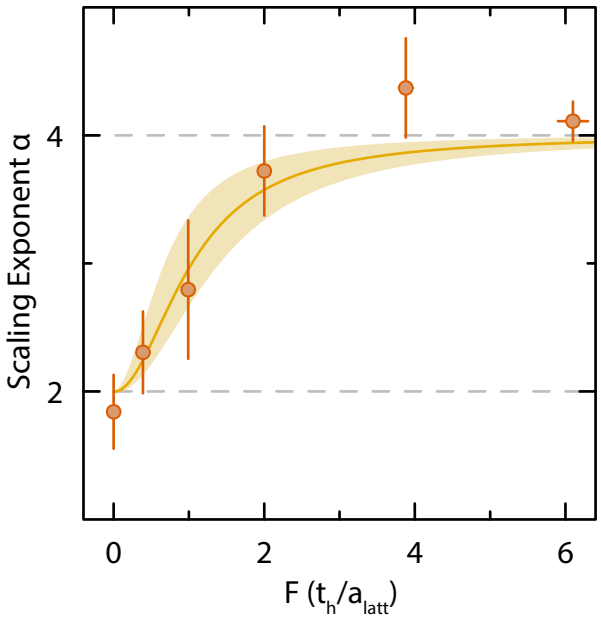

Figure 23.3: **Diffusive to subdiffusive crossover.** Extracted scaling exponent α for $\tau \propto \lambda^\alpha$ from datasets at different tilts (orange circles). As the tilt is increased from $Fa_{\mathrm{latt}}/t_h = 0$ to $Fa_{\mathrm{latt}}/t_h \approx 6$ the relaxation of initial density waves crosses over from characteristically diffusive ($\alpha = 2$) to subdiffusive with $\alpha \approx 4$. The shaded curve is a prediction of our hydrodynamic model which is derived in detail in the Supplement [27].

model of our system to help explain these observations. We also further test our understanding of the mechanism behind the subdiffusive transport by experimentally verifying our model's predictions for the local temperature profile.

Hydrodynamic model.— We denote the non-tilt energy density due to t_h and U terms by $e(x,t)$, and the number density of fermions by $n(x,t)$. Our system is, on average, uniform along the y direction, so e and n are assumed to only depend on x and t. n is a conserved density and so is $\epsilon = e - Fxn$, the total energy density including the tilted potential.

For nonzero tilt, our system heats up to near infinite temperature within the lowest band, where the thermodynamic properties are readily calculated using the high-temperature expansion. There are then three unknown transport coefficients in the most general formulation of our model: diffusivities for each of the two conserved densities and a thermopower coefficient which might be significant for this system since the energy and atom transport are strongly coupled by the tilt. Our data does not have enough detail to allow us to estimate all three of these transport parameters. However, in the stronger-tilt regime where $\tau \sim \lambda^4$, a tilt-dependent thermal diffusivity is the only transport coefficient that enters in the relaxation, and thus this one parameter can be determined from our measurements. We therefore present a less general version of our model for this strong-tilt regime here, leaving the more general model to the Supplement.

Let us first consider the infinite temperature equilibrium that our system thermalizes to at late times. This is a limit of zero inverse temperature ($\beta \to 0$) and infinite chemical potential ($\mu \to \infty$), with a finite spatially uniform $\beta\mu$; we call this equilibrium value $\bar{\beta}\bar{\mu}$. This uniform equilibrium has atom number density $\bar{n} = 2e^{\bar{\beta}\bar{\mu}}/(1 + e^{\bar{\beta}\bar{\mu}})$ per site. It is convenient when separating the energy into tilt and nontilt terms to choose the interaction term at each site to be $U(n_\uparrow - (\bar{n}/2))(n_\downarrow - (\bar{n}/2))$. This choice amounts to changing the total energy and potential $V(x)$ by constants, so it does not change the physics. With this choice, the equilibrium nontilt energy density vanishes: $\bar{e} = 0$.

The density profile at finite time has an additional sinusoidal component: $n(x,t) = \bar{n} + A_0 e^{-t/\tau} \cos kx$ with $k = 2\pi/\lambda$ (choosing the origin so there is no added phase in the argument of the cosine). In the strong tilt, small k regime we are considering now, this density profile is at *local* equilibrium with a time-dependent and spatially nonuniform inverse temperature $\beta(x,t)$. We assume the system is also near global equilibrium, so we work to lowest order in A_0 and β. Near position x, if we have local equilibrium in the tilted potential $V(x) = -Fx$ in this high temperature limit, the density is given by $n(x) = 2e^{\beta(\mu+Fx)}/(1+e^{\beta(\mu+Fx)})$. So, in the long wavelength limit we are considering here, the density gradient is $dn/dx = Fn(1-(n/2))\beta(x)$. Thus to leading order the temperature profile is given by $-A_0 k e^{-t/\tau} \sin kx = F\bar{n}(1-(\bar{n}/2))\beta(x,t)$. Using this result along with a high temperature expansion to write e as a function of β to leading order, we obtain the nontilt energy profile

$$e(x,t) = \frac{A_0}{F}\left(4t_h^2 + U^2\frac{\bar{n}}{4}\left(1-\frac{\bar{n}}{2}\right)\right) k e^{-t/\tau} \sin kx \tag{23.1}$$

at local equilibrium to lowest order in A_0 and k. Now that we have determined the profiles of n and e assuming local equilibrium, next we consider the dynamics and use energy and number conservation to determine the relaxation time τ. In the regime we are now considering, the rate-limiting bottleneck is the transport of nontilt energy (heat) through the system. This limits the rate at which tilt energy can be converted to heat and dissipated to the rest of the system, and thus the rate at which the whole system relaxes.

The relaxation of the number density implies, via the continuity equation for atom number, an atom number current density of

$$j_n(x,t) = \frac{A_0}{k\tau} e^{-t/\tau} \sin kx \ . \tag{23.2}$$

This current flows along the tilt direction, locally converting tilt energy to nontilt energy. In addition, there is a heat current $j_h(x,t) = -D_{\rm th}\nabla e(x,t)$ flowing due to the temperature gradients, where $D_{\rm th}(F)$ is a tilt-dependent thermal diffusivity. Conservation of energy is then

$$\dot{e} = D_{th}\nabla^2 e + F j_n \ , \tag{23.3}$$

showing the contribution of heat diffusion and the conversion of energy from tilt to nontilt due to the atom current j_n. In the strong tilt regime we are considering, the two terms on the RHS of Eqn. 23.3 are each much larger in magnitude than the LHS: the motion of the atoms converts tilt energy to nontilt energy and this is dissipated by thermal transport, while the amplitude of the inhomogeneities decays slowly ($D_{\rm th}k^2\tau \gg 1$). In this strong tilt regime, the decay rate is

$$\frac{1}{\tau} = \frac{D_{\rm th}k^4}{F^2}\left(4t_h^2 + U^2\frac{\bar{n}}{4}\left(1-\frac{\bar{n}}{2}\right)\right) \ll D_{\rm th}k^2 \ , \tag{23.4}$$

and the condition for the validity of this regime is

$$k^2\left(4t_h^2 + U^2\frac{\bar{n}}{4}\left(1-\frac{\bar{n}}{2}\right)\right) \ll F^2 \ . \tag{23.5}$$

We use Eqn. 23.4 to extract the thermal diffusivity $D_{\rm th}$ as a function of tilt strength in the regime consistent with $\tau \propto \lambda^4$ and plot the result in Fig. 23.4. From the validity condition of Eqn. 23.5 we can also estimate the location of the crossover shown in Fig. 23.3. Plugging in the experimental values of $U/t_h = 4$ and $\bar{n} = 0.6$, and any value of k from the experimental range $ka_{\rm latt} \in [2\pi/24, 2\pi/12]$, we get the condition that $\alpha \approx 4$ when $Fa_{\rm latt}/t_h \gg 1$, which is consistent with the data shown in Fig. 23.3. A more complete model is detailed in the Supplement, and this model is used to derive the superimposed curve of Fig. 23.3 which agrees quantitatively

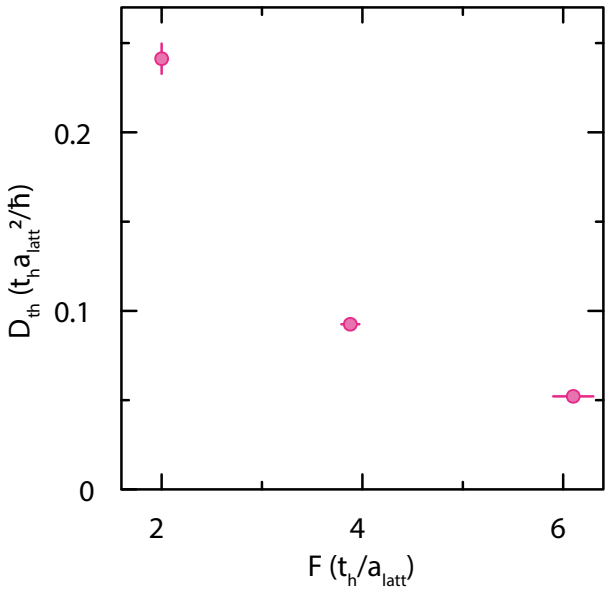

Figure 23.4: **Thermal diffusivity.** Extracted thermal diffusivity (circles) *vs.* gradient. The values were extracted by doing a fit of our hydrodynamic model to all wavelengths of each gradient simultaneously [27].

with our experimental results. This more detailed model also gives the thermal diffusivity D_{th} in terms of all of the transport coefficients, including the thermopower. We therefore conclude that our hydrodynamic model captures the essential physics leading to the main observation of this paper: the crossover from diffusive to subdiffusive relaxation with $\tau \propto \lambda^4$ as the tilt becomes strong.

The picture we have laid out in this section is one where, at strong tilts and long wavelengths, the system quickly achieves local equilibrium, locking the local inverse temperature to the density profile. As the density profile decays, local number density currents flow, and by conservation of energy this necessitates the flow of nontilt energy in the system. It is this flow of nontilt energy that we claim bottlenecks the relaxation in the large F regime, and thus D_{th} sets the relaxation rate of the system. A prediction of this understanding is *local* equilibrium between $\beta(x,t)$ and $n(x,t)$. We verify this prediction by measuring the single component density and singlon occupancy profiles in our system and solving for the inverse temperature in the atomic limit, which is an effective method of thermometry at such high temperatures. In Fig. 23.5(a) and (b) we show both the density and local inverse temperature profiles, the decay of both of their amplitudes, and the phase difference between them in time (inset). From this we see that the β profile is at local equilibrium, locked at a quarter wavelength phase shift from the density profile, and both profiles decay together in time, as predicted by our understanding of the subdiffusive regime of this system.

Summary and outlook.—We studied a new regime of thermalization in a square-lattice cold-atom Fermi-Hubbard system subject to an external linear potential. Our system was effectively closed and evolved under its own unitary dynamics starting from prepared initial density waves of various wavelengths λ. By observing how the amplitude of these initial density modulations evolved in time we found two qualitatively different hydrodynamic regimes and a crossover between them: At weak tilts the system relaxes diffusively, in accordance with previous theory [19] and experiments [18]. At strong tilts, we found a new regime where the system relaxes subdiffusively with a decay time τ that scales as $\tau \propto \lambda^4$. We argued that this subdiffusive behavior is a result of having to "drain" the large reservoir of tilt energy via the bottleneck of heat transport

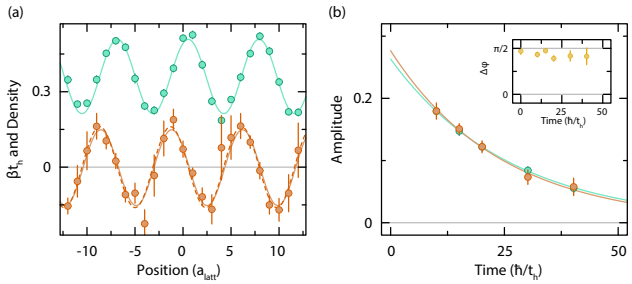

Figure 23.5: **Local inverse temperature.** Near infinite temperature, the density of singles can be used for thermometry. For a tilt strength of $Fa_{\mathrm{latt}}/t_h = 3.4(1)$ and periodic modulation of wavelength 7.69(3) a_{latt}, we measure the average single component density (green) and the density of singles (not shown) in order to extract the local inverse temperature of the cloud (orange). (a) The measured average single component density (green circles) and extracted inverse temperature βt_h (orange circles) with sinusoid fits (solid lines) after a decay time of 15.1 $\hbar/t_h$. In the case of the inverse temperature, the dashed line is the predicted inverse temperature profile from the density fit and local equilibrium. (b) The amplitude of the density (green) and inverse temperature (orange) modulations *vs.* time (circles) with exponential decay fits (solid lines). (inset) Shows the phase difference of the sinusoid fits between the single component density and the extracted local inverse temperature *vs.* time (yellow circles).

en route to *global* equilibrium, and is captured effectively by a hydrodynamic description with the system remaining near *local* equilibrium. To test this understanding we measured the local temperature profile and do indeed find that the system remains near local equilibrium as it relaxes in this subdiffusive regime. In the Supplement, we also develop and present a more complete and detailed hydrodynamic model that quantitatively captures the crossover between the diffusive and subdiffusive regimes (Fig. 23.3). In the strongly tilted regime we used our model to extract the tilt-strength-dependent thermal diffusivity that bottlenecks the relaxation of the system. One perspective on why this novel subdiffusive regime appears is that in the strong-tilt and long-wavelength limit the center-of-mass potential energy is the dominant part of the total energy, so energy conservation becomes an emergent almost-conservation of the center of mass.

In contrast to recent theoretical studies of potential ergodicity breaking in tilted 1D systems [22, 23], in this work we focused on the novel effects of a tilt on the approach to equilibrium in an isolated system that does indeed thermalize. This thermalization was robust because our system had a tilt potential along only one of the two principal axes of the lattice, and the resulting unconstrained motion of atoms in the perpendicular direction produced good thermal baths in each such row of the lattice. To arrest this thermalization more microscopically, one avenue of future exploration will be to apply tilt potentials along both axes of the lattice to suppress such local thermalization.

Acknowledgments.—We thank Vedika Khemani for helpful discussions. This work was supported by the NSF (grant no. DMR-1607277), the David and Lucile Packard Foundation (grant no. 2016-65128), and the AFOSR Young Investigator Research Program (grant no. FA9550-16-1-0269). W.S.B. was supported by an Alfred P. Sloan Foundation fellowship. A.M. acknowledges the support of the Natural Sciences and Engineering Research Council of Canada (NSERC). D.A.H. was supported in part by the DARPA DRINQS program.

23.1 Supplemental material

The experimental setup and basic parameters are already described in detail in the supplement of Ref. [26]. The spatial light modulator calibration is also explained in the supplement

of Ref [18].

23.1.1 Tilt potential calibration

To calibrate the gradient and characterize its homogeneity across the region of interest, we used the SLM to prepare an initial state consisting of three thin stripes of width $\sim 1\ a_{\mathrm{latt}}$ and a separation of $\sim 20\ a_{\mathrm{latt}}$, with their long direction oriented orthogonal to the tilt direction. Each stripe consists of a spin-polarized gas of the lowest hyperfine ground state of ^{6}Li.

For weak tilts, we are able to directly measure Bloch oscillations of these non-interacting particles. We do so by fitting a Gaussian profile to the density profile integrated along the direction perpendicular to the tilt which is used to quantify the "breathing" oscillation of the width of the stripes. This is similar to what was done in [32]. From the theory of Bloch oscillations, we expect the width of each stripe to oscillate with a maximal half-width of $A = 4t_h/F$ and a period of $T = h/Fa_{\mathrm{latt}}$. Thus, by fitting a sinusoid to the evolution of the width of each stripe, we can extract the tilt strength at their respective positions. Fig. 23.6(a) shows an example of such oscillations.

For stronger tilts, directly measuring the Bloch oscillations becomes challenging due to their small amplitude. Instead we use a modulation technique analogous to what was done in [33]. We modulate the lattice potential at frequencies on the order of the tilt strength. This brings lattice sites that were decoupled due to the tilt into resonance which results in photon-assisted tunneling. We again measure the width of the thin stripes versus modulation frequency and observe a broadening of the stripes at resonance. Fig. 23.6(b) shows an example of such a measurement.

We corroborated that for the same potential strength at intermediate tilts, the gradient extracted using the two techniques agrees.

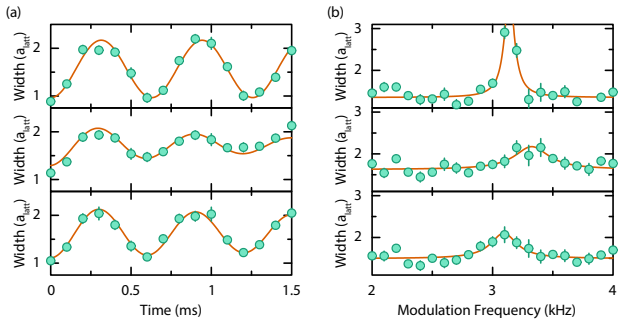

Figure 23.6: **Tilt potential calibration.** (a) Bloch oscillation method for characterization of tilt strengths. Each graph corresponds to a measurement of the local gradient at the position of one of the three stripes. The measured tilt strength is $Fa_{\mathrm{latt}} = h \times 1.64(3)\,\mathrm{kHz}$ with a maximal difference of 4.6% between stripes. (b) Lattice modulation method for characterization of tilt strengths. The measured tilt strength is $Fa_{\mathrm{latt}} = h \times 3.19(7)\,\mathrm{kHz}$ with a maximal difference of 7.5% between stripes.

23.1.2 Linear Response

Our hydrodynamic model assumes linearity in the amplitude of the initial inhomogeneities. In this experiment, we worked with relatively large amplitude density modulations. In a previous study ([18]), we worked with very small amplitude modulations and fit to a linear hydrodynamic model we developed. In the "tilted" system studied in this work, we are no longer working close to a ground state, and as such, the strength of the modulation is not expected to be as important.

Fig. 23.7 shows a comparison between the decay of strong and weak density modulations in a tilted potential. We observe that when we normalize the sinusoid amplitude and look at its decay, there is no measurable difference between the decays within the errorbars. This justifies working with strong modulations in this work to reduce the statistical error in the measurements for a fixed number of repetitions.

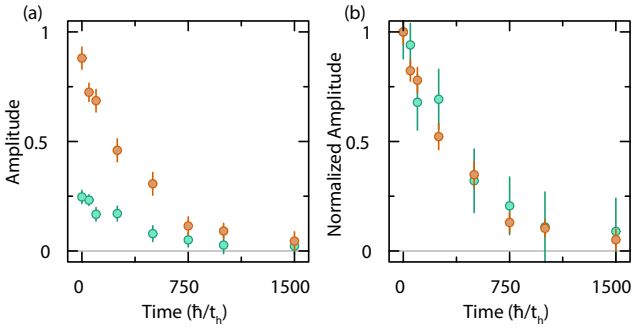

Figure 23.7: **Test of linear response.** Decay of the amplitude of the density modulation *vs.* time for two different initial amplitudes of the modulation. Here $\lambda = 11.46(3)a_{\mathrm{latt}}$, $Fa_{\mathrm{latt}}/t_h = 6.1(2)$ and $U/t_h = 3.9(1)$. (a) Shows the amplitudes. (b) Shows the amplitudes normalized to the baseline at $t = 0$.

23.1.3 Complete hydrodynamic model

We write our hydrodynamic theory in terms of the particle number density $n(x,t)$ and nontilt energy density $e(x,t)$, as well as their corresponding currents $j_n(x,t)$ and $j_e(x,t)$. Total particle number and total energy are conserved, and these conservation laws can be written as

$$\dot{n} + \nabla \cdot j_n = 0 \tag{23.6}$$

$$\dot{e} + \nabla \cdot j_e - F j_n = 0. \tag{23.7}$$

The entropic "force" laws that describe how currents are driven in this system are of the form $j_e = M_e\chi_e + M_{ne}\chi_n$ and $j_n = M_n\chi_n + M_{en}\chi_e$, where χ_e and χ_n are the entropic forces determined by the profiles of e and n, and we insist on writing the forces in a "canonical basis" for which Onsager's reciprocal relations take the simple form $M_{en} = M_{ne}$. The M coefficients are dynamical coefficients that are, in general, difficult to determine from the microscopic model. The off-diagonal coefficient M_{ne} is associated with thermopower-type effects in our system, thus this model is quite general aside from its assumption of linearity, which is well-supported by our experimental measurements. In this canonical basis, the force χ_e is determined by the local change of entropy when an infinitesimal current of nontilt energy flows but no particle current flows. The force χ_n is determined in a similar fashion, with an infinitesimal particle current and no nontilt energy current, but note that if an infinitesimal particle current flows, then due to energy conservation there must be a production (or depletion) of nontilt energy. Thus the forces in this system take the form

$$\chi_e = \nabla\left(\frac{\partial s}{\partial e}\right) \tag{23.8}$$

$$= -s_{ee}\nabla e + s_{ne}\nabla n \tag{23.9}$$

$$\chi_n = \nabla\left(\frac{\partial s}{\partial n}\right) + F\left(\frac{\partial s}{\partial e}\right) \tag{23.10}$$

$$= -s_{nn}\nabla n + s_{ne}\nabla e - s_{ee}F(e - \bar{e}(\bar{n})) + s_{ne}F(n - \bar{n}), \tag{23.11}$$

where s is the entropy density of the Fermi-Hubbard model, and we have expanded this entropy density near infinite-temperature equilibrium with $n = \bar{n}$ and $e = \bar{e}(\bar{n})$. The coefficients s_{ee}, s_{nn}, and s_{ne} come from this high-temperature expansion:

$$s \approx s(\bar{n}, \bar{e}(\bar{n})) + s_n(n-\bar{n}) - \frac{1}{2}s_{nn}(n-\bar{n})^2 + s_{ne}(n-\bar{n})(e-\bar{e}(\bar{n})) - \frac{1}{2}s_{ee}(e-\bar{e}(\bar{n}))^2 \tag{23.12}$$

and we emphasize that these coefficients are known functions of U, t_h and $\bar{n}$ for the Fermi-Hubbard model.

Now that we have specified our model, we proceed in determining its eigenmodes and respective relaxation rates, with a particular focus on the slowest mode, which is representative of the late-time behavior that we analyze in the main text. To do this, we first organize our model into a matrix eigenvalue problem. The eigenmodes are functions of definite wavelength λ, and they decay to equilibrium at a rate τ^{-1}, i.e. $e(x,t) - \bar{e}(\bar{n}) = \mathrm{e}^{-\Gamma t}(a\cos kx + b\sin kx)$ and $n(x,t) - \bar{n} = \mathrm{e}^{-\Gamma t}(c\cos kx + d\sin kx)$, where $k = 2\pi/\lambda$ and $\Gamma = 1/\tau$. We therefore write the above deviations of e and n from global equilibrium as $\boldsymbol{\rho} = (a\ b\ c\ d)^T$ in the basis $\{\mathrm{e}^{-\Gamma t}\cos kx, \mathrm{e}^{-\Gamma t}\sin kx, \mathrm{e}^{-\Gamma t}\cos kx, \mathrm{e}^{-\Gamma t}\sin kx\}$. In this language the currents are driven according to $\boldsymbol{j} = MU\boldsymbol{\rho}$ and the conservation laws are written as $-\Gamma\boldsymbol{\rho} = -\tilde{\nabla}\boldsymbol{j}$, where

$$U = \begin{pmatrix} 0 & -s_{ee}k & 0 & s_{ne}k \\ s_{ee}k & 0 & -s_{ne}k & 0 \\ -s_{ee}F & s_{ne}k & s_{ne}F & -s_{nn}k \\ -s_{ne}k & -s_{ee}F & s_{nn}k & s_{ne}F \end{pmatrix},\ M = \begin{pmatrix} M_e & 0 & M_{ne} & 0 \\ 0 & M_e & 0 & M_{ne} \\ M_{ne} & 0 & M_n & 0 \\ 0 & M_{ne} & 0 & M_n \end{pmatrix},\ \tilde{\nabla} = \begin{pmatrix} 0 & k & -F & 0 \\ -k & 0 & 0 & -F \\ 0 & 0 & 0 & k \\ 0 & 0 & -k & 0 \end{pmatrix} \tag{23.13}$$

Thus our model is solved via the eigenvalue problem $\Gamma\boldsymbol{\rho}_\Gamma = \tilde{\nabla}MU\boldsymbol{\rho}_\Gamma$. There are two solutions for Γ, each with a multiplicity of two corresponding to pure cos and sin waves for $n(x,t)-\bar{n}$. The only solution we need to consider at late times is the slow mode with $\Gamma = \Gamma_-$ and $n(x,t) - \bar{n} \propto \cos kx$. This eigenmode is representative of the dynamics of all monochromatic initial conditions at late times. In what follows we discuss some important features of the slowest eigenmode.

In the limit of small F (and/or large k) the slowest mode is diffusive, i.e. $\Gamma \propto k^2$. In the limit of large F (and/or small k) the slowest decay rate is

$$\Gamma_- \approx \frac{D_{\mathrm{th}}}{F^2}\left(\frac{s_{nn}}{s_{ee}} - \frac{s_{ne}^2}{s_{ee}^2}\right)k^4, \tag{23.14}$$

where $D_{\mathrm{th}} = (M_e - (M_{ne}^2/M_n))\, s_{ee}$ is the thermal diffusivity, and we will discuss why we identify it as such below. Thus we see that our model crosses over from diffusive to subdiffusive with $\tau \propto \lambda^4$ as $1/F\lambda$ becomes small.

If we assume a scaling of the form $\Gamma_- \propto k^\alpha$ we can estimate the exponent α by $\alpha = \left.\frac{d\log\Gamma_-}{d\log k}\right|_{k=k_e}$ evaluated at some k in the experimental range $k \in [2\pi/24, 2\pi/12]$ denoted k_e. The general expression for α evaluated this way depends on the dynamical coefficients M, but in the limit where $\frac{M_e}{M_n}, \frac{M_{ne}}{M_n} \ll \frac{s_{nn}}{s_{ee}}$ this dependence drops out and we get a parameter-free estimate of α as a function of F. In this limit

$$\alpha(F) = 2 + \frac{2}{1 + \frac{s_{nn}}{s_{ee}}\frac{k_e^2}{F^2}}, \tag{23.15}$$

and this is the theoretical estimate of $\alpha(F)$ that we use to compare to experimental results in the main text (Fig. 23.3).

Now we examine the structure of the slowest eigenmode itself and explain why we identify

D_{th} as mentioned above. At small k/F, to leading order, the slowest eigenmode has

$$\boldsymbol{\rho}_{\Gamma_-} = \begin{pmatrix} \frac{s_{ne}}{s_{ee}} \\ \left(\frac{s_{nn}}{s_{ee}} - \frac{s_{ne}^2}{s_{ee}^2}\right)\frac{k}{F} \\ 1 \\ 0 \end{pmatrix}, \quad \boldsymbol{j}_{\Gamma_-} = \begin{pmatrix} -\left(M_e - \frac{M_{ne}^2}{M_n}\right) s_{ee} \left(\frac{s_{nn}}{s_{ee}} - \frac{s_{ne}^2}{s_{ee}^2}\right)\frac{k^2}{F} \\ \left(M_e - \frac{M_{ne}^2}{M_n}\right) s_{ne} \left(\frac{s_{nn}}{s_{ee}} - \frac{s_{ne}^2}{s_{ee}^2}\right)\frac{k^3}{F^2} \\ 0 \\ -\left(M_e - \frac{M_{ne}^2}{M_n}\right) s_{ee} \left(\frac{s_{nn}}{s_{ee}} - \frac{s_{ne}^2}{s_{ee}^2}\right)\frac{k^3}{F^2} \end{pmatrix}. \tag{23.16}$$

We see that in this mode a modulation of number density with amplitude $\mathcal{O}(1)$ comes with a slow subdiffusive number density current $j_n \propto k^3$ that is "out of phase" by a quarter wavelength. This number current converts tilt energy to nontilt energy and this generates a small out of phase, nontilt energy profile with amplitude $\propto k/F$. That nontilt energy diffuses and we see that the ratio of amplitudes of the resulting "in phase" (with $n(x,t)$) energy current to the energy profile it is depleting is $|j_e|/|e| = D_{\text{th}}k$ with $D_{\text{th}} = (M_e - (M_{ne}^2/M_n))\, s_{ee}$ as mentioned earlier. This is why we identify D_{th} as such. The process of diffusing the nontilt energy that is generated by the particle current that is relaxing the density profile is the bottleneck process and obeys a diffusion equation with diffusivity D_{th}. That is why this diffusivity shows up as the one unknown coefficient in Γ_-, and thus we use our data to determine it in the regime where $\tau \propto \lambda^4$ where this mechanism is valid.

Now let's address the β profile in this mode. The "in phase" component of $e - \bar{e}(\bar{n})$ shown in Eqn. 23.16, which is larger than the out of phase component by a factor of F/k, is due to the difference between $\bar{e}(\bar{n})$ and $\bar{e}(n)$, and not due to a nonzero β component that is in phase. Since β is proportional to $e - \bar{e}(n)$ at high temperatures, to leading order in the high-temperature limit $\beta(x,t)$ is set by the out of phase component of $e - \bar{e}(n)$ which is the same as $e - \bar{e}(\bar{n})$ for that component because the out of phase component of $n - \bar{n}$ is zero by definition (since "in phase" and "out of phase" are defined relative to the $n(x,t)$ profile here). Thus this model predicts an out of phase local β modulation with amplitude

$$\text{amp}(\beta(x,t)) = -s_{ee}\left(\frac{s_{nn}}{s_{ee} - \frac{s_{ne}^2}{s_{ee}^2}}\right)\frac{k}{F} \tag{23.17}$$

$$= \frac{1}{\bar{n}\left(1 - \frac{\bar{n}}{2}\right)}\frac{k}{F}, \tag{23.18}$$

where we have used the high temperature expressions for s_{ee}, s_{ne}, and s_{nn}. Indeed in the main text we show measurements of the local β that are consistent with this prediction (Fig. 23.5). We call the nontilt energy current that results from this local β profile the "heat current" j_h. Thus D_{th} is the diffusivity corresponding to the heat current that is being driven by the nontilt energy that is generated by the relaxation of the particle number distribution.

23.1.4 High temperature expansion

We compute the grand partition function of the Fermi-Hubbard model in the high temperature expansion to second order in β and evaluate the second partial derivatives of the entropy density with respect to n, the particle number density, and e, the energy density due to t_h and U terms, in order to compute the coefficients s_{ee}, s_{nn}, and s_{ne}. The results are

$$s_{ee} = \frac{16}{\bar{n}(2-\bar{n})(32t_h^2 + \bar{n}(2-\bar{n})U^2)} \tag{23.19}$$

$$s_{nn} = \frac{64t_h^2 + 2\bar{n}(2+\bar{n})U^2}{\bar{n}(2-\bar{n})(32t_h^2 + \bar{n}(2-\bar{n})U^2)} \tag{23.20}$$

$$s_{ne} = \frac{8\bar{n}U}{\bar{n}(2-\bar{n})(32t_h^2 + \bar{n}(2-\bar{n})U^2)}. \tag{23.21}$$

For the experimental parameters $\bar{n} = 0.6$ and $U/t_h = 3.9$ these coefficients take the values $s_{nn} \approx 2.96$, $s_{ee} \approx 0.43$, $s_{ne} \approx 0.50$ in units where $t_h = 1$.

23.1.5 Simultaneous fitting of model

As explained in the previous sections, there is a fast and a slow exponential decay solution to our hydrodynamic model. In the strong tilt regime, Eqn. 23.14 shows that the slow decay depends only on the thermal diffusivity D_{th}.

We perform a simultaneous fit to all wavelengths at a given tilt strength as explained in the supplement of [18]. The fitting function is

$$A(t) = A_0 e^{-\Gamma_-(D_{\text{th}},F,k)t}, \tag{23.22}$$

and it is fitted only to the late-time decay. Here, A_0 is a fitting parameter that can vary for each wavelength while D_{th} is fitted globally to all wavelengths. The parameters F and k are fixed according to our experimentally measured values. The results of fitting this model to measurements in the strong tilt regime are shown in Fig. 23.8.

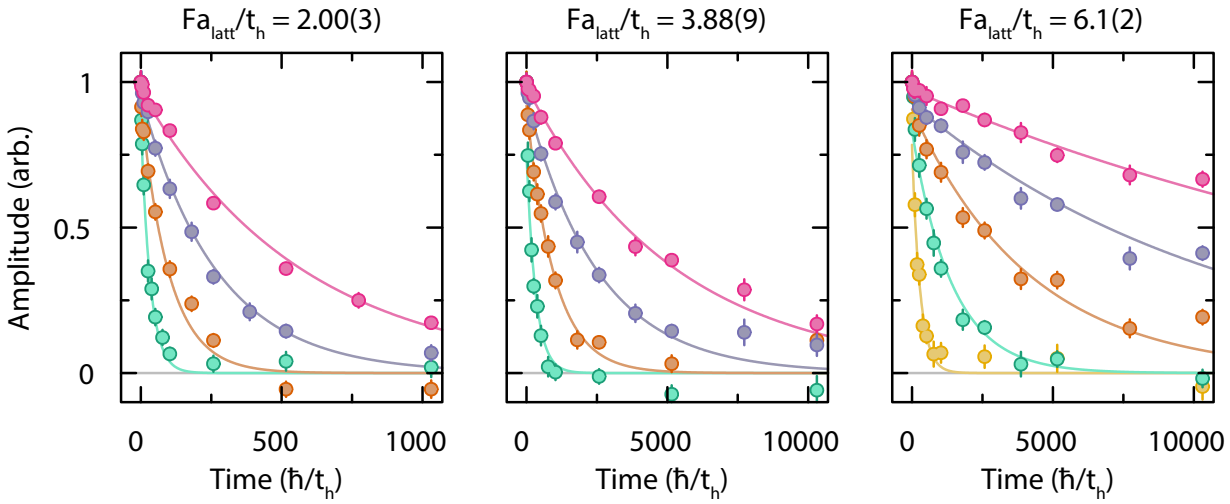

Figure 23.8: **Simultaneous fitting of hydrodynamic model.** Fitted normalized relative amplitudes of the periodic density modulation (circles) *vs.* time for wavelengths 7.69(3) a_{latt} (yellow), 11.46(3) a_{latt} (green), 15.16(5) a_{latt} (orange), 19.33(7) a_{latt} (purple), and 23.3(2) a_{latt} (pink) at different tilts. The lines are simultaneous fits of the hydrodynamic model to the long-time decay after the initial average heating (phase change). We are able to extract the thermal diffusivity through this fitting method.

24 Observing non-ergodicity due to kinetic constraints in tilted Fermi-Hubbard chains by Scherg, Kohlert, et al.

The thermalization of isolated quantum many-body systems is deeply related to fundamental questions of quantum information theory. While integrable or many-body localized systems display non-ergodic behavior due to extensively many conserved quantities, recent theoretical studies have identified a rich variety of more exotic phenomena in between these two extreme limits. The tilted one-dimensional Fermi-Hubbard model, which is readily accessible in experiments with ultracold

atoms, emerged as an intriguing playground to study non-ergodic behavior in a clean disorder-free system. While non-ergodic behavior was established theoretically in certain limiting cases, there is no complete understanding of the complex thermalization properties of this model. In this work, we experimentally study the relaxation of an initial charge-density wave and find a remarkably long-lived initial-state memory over a wide range of parameters. Our observations are well reproduced by numerical simulations of a clean system. Using analytical calculations we further provide a detailed microscopic understanding of this behavior, which can be attributed to emergent kinetic constraints.

Understanding the complex out-of-equilibrium dynamics of quantum many-body systems is central to a number of research areas ranging from statistical physics to quantum information theory [1, 2, 3]. State-of-the-art experimental platforms are now able to test novel theoretical concepts and approximate descriptions based on experimental observations. Important experimental results were obtained in particular with integrable [4] or many-body localized (MBL) [5, 6, 7] systems. Both phenomena emerge due to the existence of extensively many conserved quantities and have been of considerable interest, because they break the eigenstate thermalization hypothesis, which assumes that each individual eigenstate behaves locally like a thermal ensemble and is believed to hold for generic ergodic systems [8, 9, 10].

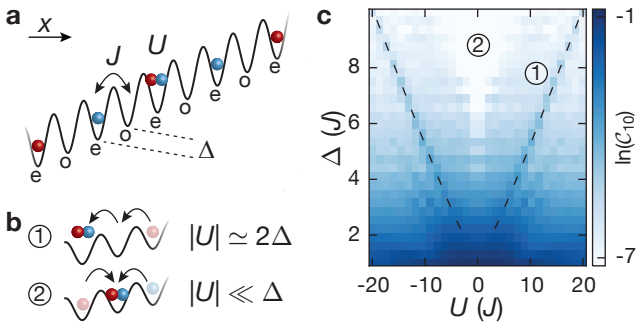

Figure 24.1: **Illustration of the experimental setup and the structure of the Hilbert space. a** Schematic of the tilted 1D Fermi-Hubbard model (with odd o and even e sites) with tunneling J, on-site interaction U and spin-dependent tilt $\Delta_\uparrow, \Delta_\downarrow$ (spin-up red, spin-down blue). **b** Dominant resonant tunneling processes for different regimes. **c** Finite-time connectivity $\mathcal{C}_\epsilon$ (for a cut-off $\epsilon = 10\%$) defined as the fraction of states that participate in the dynamics up to an evolution time $T_\mathcal{N} = 1000\tau$ (main text, Methods). The calculation was performed for a Néel-ordered singlon CDW initial state, using exact diagonalization (ED) with system size $L = 13$ and $\Delta_\uparrow = \Delta_\downarrow \equiv \Delta$. In the large-tilt limit, $\Delta/J \to \infty$, we find emergent strongly-fragmented effective Hamiltonians for regime ① and ② [11].

In between the two extreme limits of ergodic and localizing dynamics there exists a rich variety of more complex thermalizing behavior. Models with many-body scar states, e.g., host a vanishing fraction of non-thermal eigenstates embedded within an otherwise thermal spectrum [12, 13, 14, 15, 16, 17]. They exhibit a weak form of ergodicity-breaking, that strongly depends on the initial state, as has been observed with Rydberg atoms [18, 15, 19]. More recently, a whole new class of models has been suggested, where the presence of only few conserved quantities, in particular dipole conservation, results in non-ergodic dynamics due to an emergent fragmentation of the Hilbert space into exponentially many disconnected subspaces [20, 21, 22, 23]. Fragmented models offer an alternative view on a central open question, namely if many-body localization can occur in translationally-invariant models without disorder [24, 25, 26, 27, 28, 29, 30].

In this work we study non-ergodic behavior in the disorder-free tilted one-dimensional (1D)

Fermi-Hubbard model (Fig. 24.1a), which lies at the interface of MBL and Hilbert-space fragmentation. In the presence of additional weak disorder or harmonic confinement, theoretical studies have found characteristic MBL phenomenology, known as Stark MBL [31, 32, 33, 34, 35]. This, however, does not hold for a clean system with pure linear potential [31, 34]. While conventional MBL predicts localization for any typical initial state, we do not expect this to hold for our system, where resonances can occur between interaction and tilt energies (regime ① in Fig. 24.1b). Intriguingly, it has been predicted, that in the limit of large tilts, $\Delta \gg J, |U|$, non-ergodicity may still occur despite the absence of disorder. In this regime, the large tilt energy imposes kinetic constraints, which result in an emergent dipole conservation [32, 20, 21, 34, 23]. This emergent behavior is in fact governed by a fragmented Hamiltonian resulting in non-ergodic dynamics.

Starting from an initial charge-density wave (CDW) of singlons (singly-occupied site), we study relaxation dynamics in the tilted 1D Fermi-Hubbard model for a large range of interaction strengths and moderate values of the tilt ($\Delta < 4J$), where none of the two mechanisms described above should apply and where naively one may expect the system to thermalize [36, 37]. At short times we observe coherent dynamics due to Bloch oscillations, whose amplitude strongly depends on the Hubbard interactions. Surprisingly we find that after intermediate times and even close to resonance (regime ①), the evolution converges to a steady-state, that persists for long evolution times up to 700 tunneling times, signaling a robust memory of the initial CDW throughout.

Using numerical calculations we show that the observed non-ergodicity cannot be explained by the phenomenon of Stark-MBL, i.e., the robust memory is not due to experimental imperfections, such as residual harmonic confinement or disorder, and the bipartite entanglement entropy does not exhibit the characteristic behavior of MBL systems [38, 31] (Fig. 24.9). Hence, non-ergodicity appears to have a different origin, despite similar experimental signatures. This raises the question about the origin of the observed non-ergodicity. We construct effective Hamiltonians in two distinct regimes (① and ②, Fig. 24.1b) by taking the large tilt limit and find strongly-fragmented Hamiltonians in both cases (Sect. 24.5). While these models are only expected to describe the dynamics at large tilt values and for intermediate times (on the order of a few tens of tunneling times), they allow us to identify the microscopic processes that initiate dynamics at short times (Fig. 24.1b). In both regimes these are correlated tunneling processes, which result in the formation of doublons (doubly-occupied sites), either resonantly (regime ①) or detuned by the Hubbard interaction energy U (regime ②). Higher-order terms are expected to eventually drive the system towards thermalization [20]. However, we are able to show that energy penalties for the second- or higher-order tunneling processes, which occur naturally in the model, render these dynamics inefficient. This results in extremely slow relaxation (Sect. 24.5), which appears stable for $> 10^4$ tunneling times in our exact diagonalization studies of small systems, in agreement with our experimental observations (Fig. 24.7).

In order to characterize the dynamics across the whole parameter regime studied experimentally, we compute the finite-time connectivity of our initial CDW state $\mathcal{C}_\epsilon = \dim(\mathcal{N}_\epsilon)/\dim(\mathcal{H})$, which is defined by the fraction of states that participate in the time evolution up to a finite time $T_\mathcal{N}$; here $\mathcal{N}_\epsilon$ denotes the subspace in the complete Hilbert-space $\mathcal{H}$, which is defined, such that the residual overlap of the time-evolved state $|\psi(t)\rangle$ outside of $\mathcal{N}_\epsilon$ is at most ϵ at any time $t \leq T_\mathcal{N}$ (Methods). The value of ϵ is typically chosen between 1%-10%. The finite-time connectivity can be understood as a measure of non-ergodicity, similar to the more conventional return probability or other multifractality measures [39]. While effective Hamiltonians can only be derived explicitly in certain limits, the numerical construction is applicable in the whole parameter regime probed in this work (Fig. 24.1c). We find that the finite-time connectivity vanishes in the thermodynamic limit for all parameters, suggesting that only a small fraction of the states participates in the dynamics, signaling non-ergodic behavior. Our results

suggest that the emergent kinetic constraints result in transient non-ergodic behavior across the whole parameter range studied in this work. We further show analytically that the relevant microscopic constraints in the resonant ① regime give rise to Hilbert-space fragmentation in the large tilt limit (Sect.24.6 in [11]).

The experimental setup consists of a degenerate Fermi gas of $50(5) \times 10^3$ ^{40}K atoms that is prepared in an equal mixture of two spin components $|\uparrow\rangle = |m_F = -7/2\rangle$ and $|\downarrow\rangle = |m_F = -9/2\rangle$ in the $F = 9/2$ ground-state hyperfine manifold. The atoms are loaded into a 3D optical lattice with lattice constant $d_s = 266\,\mathrm{nm}$ along the x direction and deep transverse lattices, with constant $d_\perp = 369\,\mathrm{nm}$, to isolate the 1D chains along x (Methods). The central 1D chains have a length of about 290 lattice sites. The residual coupling along the transverse directions is less than $3 \times 10^{-4} J$. The dynamics along x is described by the tilted 1D Fermi-Hubbard model

$$\hat{H} = \sum_{i,\sigma=\uparrow,\downarrow} \left(-J \hat{c}^\dagger_{i,\sigma} \hat{c}_{i+1,\sigma} + \mathrm{h.c.} + \Delta_\sigma i \hat{n}_{i,\sigma} \right) + U \sum_i \hat{n}_{i,\uparrow} \hat{n}_{i,\downarrow} \,, \tag{24.1}$$

where $\hat{c}^\dagger_{i\sigma}$ ($\hat{c}_{i\sigma}$) is the fermionic creation (annihilation) operator and $\hat{n}_{i,\sigma} = \hat{c}^\dagger_{i\sigma} \hat{c}_{i\sigma}$. The on-site interaction strength U is controlled by a Feshbach resonance centered at 202.1 G and a magnetic field gradient is used to create the tilt Δ_σ, with $\Delta_\uparrow \simeq 0.9 \Delta_\downarrow$. The weak spin-dependence arises due to the different m_F quantum numbers [11]. The initial state for all subsequent measurements is a CDW of singlons on even sites, which is prepared using a bichromatic optical superlattice (Sect. 24.9 in [11]). The initial state can be described as an incoherent mixture of site-localized particles with random spin configuration (Methods). The subsequent evolution is monitored by extracting the spin-resolved imbalance $\mathcal{I}^\sigma = (N^\sigma_e - N^\sigma_o)/N^\sigma$ [40]; here $N^\sigma_{e(o)}$ denotes the total number of spin-σ atoms on even (odd) sites and $N^\sigma = N^\sigma_e + N^\sigma_o$. A non-zero steady-state imbalance signals a memory of the initial state [41], where $\mathcal{I}^\sigma(t = 0) = 1$.

In a first set of measurements we study the effect of interactions on the coherent short-time dynamics. In a tilted lattice an initially localized particle exhibits Bloch oscillations [42], with a characteristic period $T_\sigma = h/\Delta_\sigma$, set by the spin-dependent tilt. In the presence of interactions, Bloch oscillations persist, showing a rich variety of dynamics, such as interaction-induced dephasing and amplitude modulation [43, 44, 45, 46, 47, 48]. Here, we use the spin-resolved imbalance to probe real-space Bloch oscillations in a parity-projected manner. In the non-interacting limit the time-dependence can be computed analytically:

$$\mathcal{I}^\sigma(t) = \mathcal{J}_0 \left(\frac{8J}{\Delta_\sigma} \sin\left(\frac{\pi \Delta_\sigma t}{h} \right) \right), \tag{24.2}$$

which enables a precise calibration of the model parameters Δ_σ and J (Fig. 24.2a) at short times. Here, $\mathcal{J}_0$ denotes the 0th-order Bessel function of the first kind. The dephasing of the oscillations is caused by a residual harmonic confinement that results in a weak local variation δT_σ of the Bloch oscillation period T_σ between adjacent sites. An upper bound for the trap frequency $\omega_h/(2\pi) = 39\,\mathrm{Hz}$ was extracted from independent measurements [11] and corresponds to $\delta T_\sigma / T_\sigma \ll 10^{-3}$. Since the imbalance dynamics for both spin components is very similar (see Fig. 24.14), we focus on one component $\mathcal{I}^\downarrow$.

For weak tilt values, $\Delta_\downarrow = 1.2J$, we find that the dynamics of the interacting spin-mixture ($U = 3J$) exhibits the same dominant frequency components as the non-interacting Bloch oscillations, while the dephasing is strongly enhanced. This can be seen more directly by calculating the power spectral density (PSD) of the imbalance $|\tilde{\mathcal{I}}^\sigma(\nu)|^2$ (inset of Fig. 24.2a). We find three distinct peaks in the spectrum, the Bloch frequency $\Delta_\downarrow$ and an admixture of two

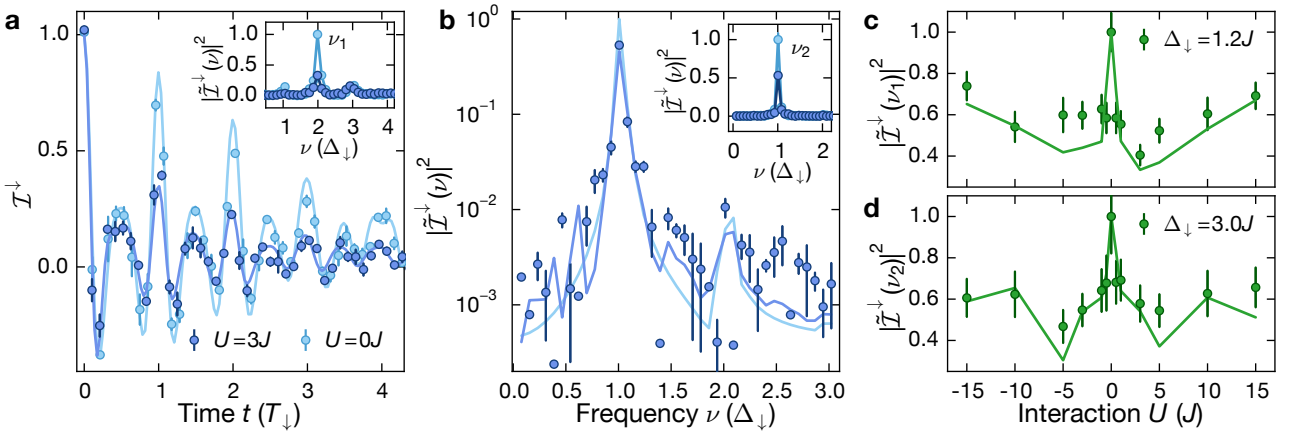

Figure 24.2: **Short-time interacting Bloch oscillations. a** Imbalance $\mathcal{I}^{\downarrow}$ for $U = 0J$ (spin-polarized gas, light blue) and $U = 3J$ (spin-resolved measurement, dark blue) with $J/h = 0.88(2)\,\mathrm{kHz}$ and $\Delta_{\downarrow} = 1.22(1)J$. Inset: Power spectral density (PSD) $|\tilde{\mathcal{I}}(\nu)|^2$ of the time traces shown in the main panel, normalized to the maximum of the non-interacting spectrum; $\nu_1 = 2\Delta_{\downarrow}/h$ indicates the dominant frequency component. **b** PSD $|\tilde{\mathcal{I}}(\nu)|^2$ for $U = 3J$ (spin-resolved measurement, dark blue), normalized to the maximum of the non-interacting spectrum; $J/h = 0.54(1)\,\mathrm{kHz}$ and $\Delta_{\downarrow} = 2.96(3)J$. The data was obtained from time-traces as in (a). Inset: PSD as in the main panel and for $U = 0J$ (spin-polarized gas, light blue). $\nu_2 = \Delta_{\downarrow}/h$ indicates the dominant frequency. **c,d** Interaction scan of the peak power spectral density $|\tilde{\mathcal{I}}(\nu_j)|^2$ evaluated by summing the PSD in a window of ± 3 data points around the dominant frequency ν_j, $j = \{1, 2\}$ at (c)$\Delta_{\downarrow} = 1.22(1)J$ and (d) $\Delta_{\downarrow} = 2.96(3)J$ obtained from traces as in (a). Each data point in (a),(b) consists of four independent measurements and the error bars denote the standard error of the mean (SEM). Solid lines in all panels are numerical simulations using TEBD (Methods).

higher harmonics with the largest spectral weight in the second harmonic at $\nu_1 = 2\Delta_{\downarrow}/h$. For $U = 3J$ its weight is decreased by 70% compared to the non-interacting case. The higher-order harmonics originate from the real-space evolution within one Bloch cycle and are determined by the Bloch oscillation amplitude $A_\sigma/d_s = 4J/\Delta_\sigma$. We anticipate frequency components at integer multiples of Δ_σ, with an upper bound determined by A_σ/d_s, in agreement with our data.

Interaction effects are expected to be less relevant once the Bloch oscillation amplitude is smaller than one site, resulting in negligible overlap between neighboring particles for our CDW initial state. In Fig. 24.2b we show the PSD of the coherent short-time dynamics for $\Delta_{\downarrow} = 3.0J$. While the largest spectral weight of the PSD is now contained in the Bloch frequency $\nu_2 = \Delta_{\downarrow}/h$, the reduction is still about 50% compared to the non-interacting case. Indeed, the spectral weight is a sensitive measure of the interaction-induced dephasing. Moreover, the on-site interactions lift the degeneracy of the energy levels in the Wannier-Stark spectrum, which results in additional frequency components in the PSD. For our parameters (Fig. 24.2b) they occur at $\approx \nu_2 \pm 0.5\Delta_{\downarrow}/h$ in the time-evolving block decimation (TEBD) simulations [49, 50, 51], which is consistent with our data.

The sensitivity of the coherent short-time dynamics on the interaction strength is further highlighted by the strong interaction-dependence of the peak power spectral density (PPSD) $|\tilde{\mathcal{I}}(\nu_j)|^2$ of the respective dominant frequency components ν_j, $j = \{1, 2\}$ (Fig. 24.2c,d). We find a sharp decrease of the PPSD by about 40% already for small interaction strength $U = \pm 0.5J$ for $\Delta_\sigma = 1.2J$. After reaching a global minimum at intermediate interaction strength, it slowly recovers to the non-interacting value in the limit of large interactions.

For long enough evolution times, the coherent Bloch oscillations are dephased and a finite

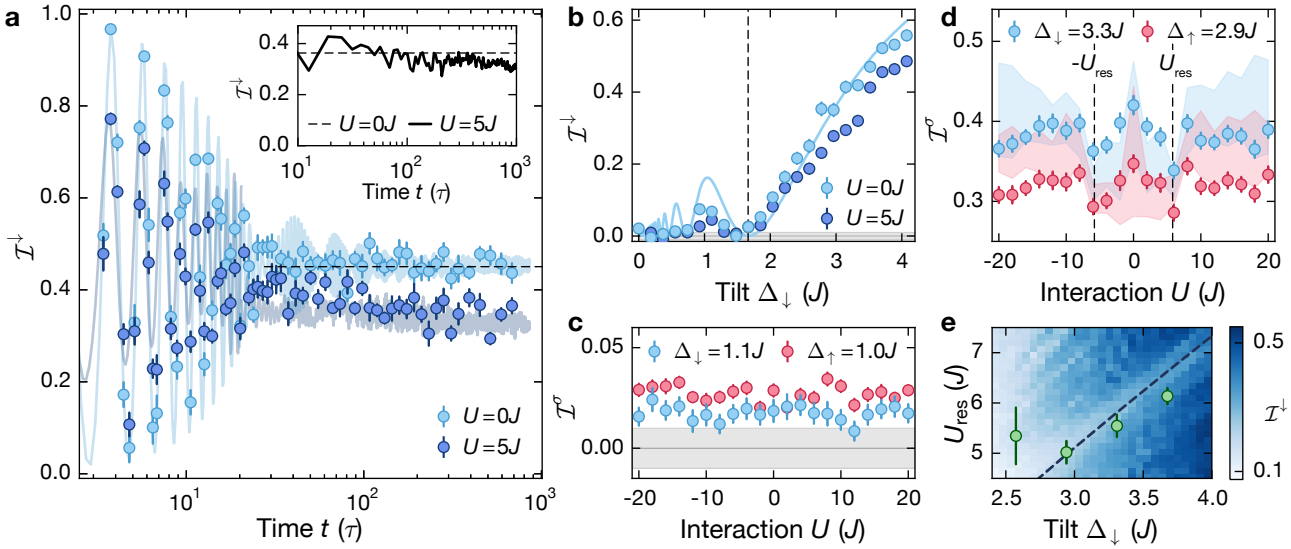

Figure 24.3: **Long-time dynamics.** **a** Imbalance time traces at $\Delta_\downarrow = 3.30(3)J$ and $J/h = 0.54(1)\,\mathrm{kHz}$ for $U = 0J$ (spin-polarized, light blue) and $U = 5J$ (spin-resolved measurement, dark blue). The shaded trace is an ED calculation for $L = 16$ (Methods). Each data point is averaged over 12 individual experimental realizations. Inset: ED calculation for $L = 16$ in a clean system with $\Delta_\downarrow = \Delta_\uparrow = 3J$, $\omega_h = 0$ and $U = 5J$ using a Néel-ordered initial CDW. The dashed lines show the analytic prediction for the non-interacting steady-state imbalance [Eq. (24.3)]. **b** Steady-state imbalance versus $\Delta_\downarrow$ measured at $U = 0J$ (spin-polarized, light blue) and $U = 5J$ (spin-resolved measurement, dark blue). Each data point is averaged over ten equally spaced times in a time window between 70τ and 100τ ($U = 0J$) and 340τ and 370τ ($U = 5J$). The solid line shows the analytic prediction for $\mathcal{I}^\downarrow$ [Eq. (24.3)] and the dashed line indicates the first root of the Bessel function at $\Delta_\downarrow \approx 1.5J$. **c** Spin-resolved steady-state imbalance versus interaction strength at $\Delta_\downarrow = 1.10(1)J$. Each point is averaged over ten time steps equally spaced between 170τ and 200τ. **d** Spin-resolved steady-state imbalance versus interaction strength as in (c) for $\Delta_\downarrow = 3.30(3)J$. The shaded trace is an ED simulation, which is averaged over the same time steps as in (c) and where the width indicates the 1σ standard deviation. **e** Resonances extracted from interaction scans for $U > 0$ as in (d) for different tilt values [11]. The color plot shows ED calculations for the same parameters as in the experiment, but with $\omega_h = 0$, for $L = 13$ sites. The dashed line indicates the analytic prediction for the resonance $U_\mathrm{res} \simeq 2\Delta_\downarrow - 8J^2/(3\Delta_\downarrow)$. The grey shaded area in (b),(c) indicates our calibrated detection resolution. In all panels error bars denote the SEM.

steady-state imbalance develops in the non-interacting limit (Fig. 24.3a). Note that, if the dephasing was solely due to residual harmonic confinement, we would expect a coherent revival of the oscillations, which is suppressed in our experiment by additional dephasing mechanisms and ensemble averaging. The observed finite steady-state imbalance is caused by Wannier-Stark localization and can be computed analytically by time averaging the short-time dynamics:

$$\mathcal{I}^\sigma = \lim_{T\to\infty} \frac{1}{T} \int_0^T \mathcal{I}^\sigma(t)\, dt = \mathcal{J}_0^2\left(\frac{4J}{\Delta_\sigma}\right). \tag{24.3}$$

Excellent agreement between our data and the analytical result provides strong evidence that the effect of the harmonic confinement is negligible for the late-time steady-state imbalance, in contrast to previous fermionic transport experiments [36, 37]. This is further supported by the data in Fig. 24.3b, where the steady-state value is probed for a larger range of tilt values, even reproducing the non-monotonous behavior that is found for small values of the tilt. Note, that the vanishing imbalance, as observed for $\Delta_\downarrow \approx 1.5J$ (dashed line in Fig. 24.3b), does not

indicate delocalization. It results from localized Wannier-Stark orbitals with equal weight on even and odd sites.

In the presence of weak interactions localization was predicted to survive in the limit of small additional disorder or harmonic confinement, signaled by a finite steady-state imbalance [31, 32]. Here, we find that after a small decay at intermediate times a plateau of the imbalance develops, which persists for long evolution times up to 700τ (Fig. 24.3a) in the strongly-interacting regime. A comparison with ED simulations (inset Fig. 24.3a) in a clean system without spin-dependent tilt and without harmonic confinement for a Néel-ordered initial CDW (as opposed to the random-spin initial state realized in the experiment) further highlights that this non-ergodic behavior is not due to experimental imperfections at least for the experimentally relevant observation times (see Fig. 24.9 for a systematic finite-size scaling analysis). Moreover, this robust steady-state value survives over a wide range of parameters (Fig. 24.3b). As a function of the tilt it qualitatively follows the behavior of the non-interacting system, but shows consistently lower steady-state values.

The persistence of non-ergodicity down to very small values of the tilt is surprising at first sight. One may expect that for large Bloch-oscillation amplitudes the interactions between particles result in a dephasing of the coherent dynamics that give rise to Wannier-Stark localization in the non-interacting limit and hence cause ergodic behavior [43, 44, 45, 46, 36, 37]. We study the plateau value for $\Delta_\downarrow = 1.1J$ and find that it is largely independent of interactions (Fig. 24.3c). In a numerical analysis of this regime for a Néel-ordered singlon CDW we indeed find that the imbalance decays to zero for evolution times on the order of $10^4\,\tau$ (Fig. 24.9), which further agrees with the finite imbalance measured at $\sim 200\,\tau$. The observed inversion of the spin-resolved imbalance $\mathcal{I}^\downarrow < \mathcal{I}^\uparrow$ after long evolution times (although $\Delta_\downarrow > \Delta_\uparrow$) is explained by the non-monotonic dependence of the stationary imbalance on the tilt for $\Delta_\sigma < 2J$ as shown in Fig. 24.3b.

For intermediate values of the tilt $\Delta/J \simeq 3$ on the other hand, we find a surprisingly robust steady-state imbalance, in agreement with numerical calculations, with a clear interaction dependence (Fig. 24.3d). The behavior is similar for both spin components and well reproduced by numerical simulations. The deviation between experiment and numerical simulations at larger interaction strengths is most likely due to the finite coupling between 1D chains, which plays a larger role for increased interactions [52]. The steady-state imbalance is symmetric around $U = 0$ due to a dynamical symmetry [for $(\Delta_\downarrow - \Delta_\uparrow) \ll J$] between attractive and repulsive interactions (Sect. 24.4), similar to the homogeneous Fermi-Hubbard model [53, 54]. The curve displays a global minimum for intermediate interactions, which we identify with resonant processes at $|U| \simeq 2\Delta$, where two singlons separated by two lattice sites form a doublon. This coincides with regime ① in Fig. 24.1c, where the largest connectivities were found. The precise value of the resonance is slightly shifted, $U_{\mathrm{res}} \simeq 2\Delta - 8J^2/(3\Delta)$, due to perturbative corrections for finite J/Δ, in agreement with our data (dashed line in Fig. 24.3e). For large interactions and weak spin-dependence $(\Delta_\downarrow - \Delta_\uparrow) \ll J$, we expect the system to recover the non-interacting regime [11].

In order to gain additional insights into the observed non-ergodic behavior, we study the properties of our model perturbatively in the large tilt limit for the two distinct regimes ① and ② (Fig. 24.1c). In regime ②, $\Delta \gg J, |U|$, an effective Hamiltonian can be derived in powers of $\lambda = J/\Delta$. As predicted [32, 23, 20, 21, 34], we find an emergent dipole-conserving Hamiltonian $\hat{H}_{\mathrm{eff}}^{\mathrm{dip}}$ [Eq. (24.12)] up to third order in λ (Sect. 24.5), where the dipole-moment operator is defined as $\sum_{i,\sigma} i\hat{n}_{i,\sigma}$. The dominant off-diagonal terms of $\hat{H}_{\mathrm{eff}}^{\mathrm{dip}}$ are of similar nature as those in the fragmented Hamiltonians studied previously [20, 21], seemingly consistent with the observed non-ergodic behavior. Yet, higher-order processes $\mathcal{O}(\lambda^4)$, relevant for $\Delta \simeq 3J$, are expected to melt the CDW within the experimentally studied timescales [20]. These higher-order processes as well as the dominant off-diagonal contribution, however, require the production of doublons,

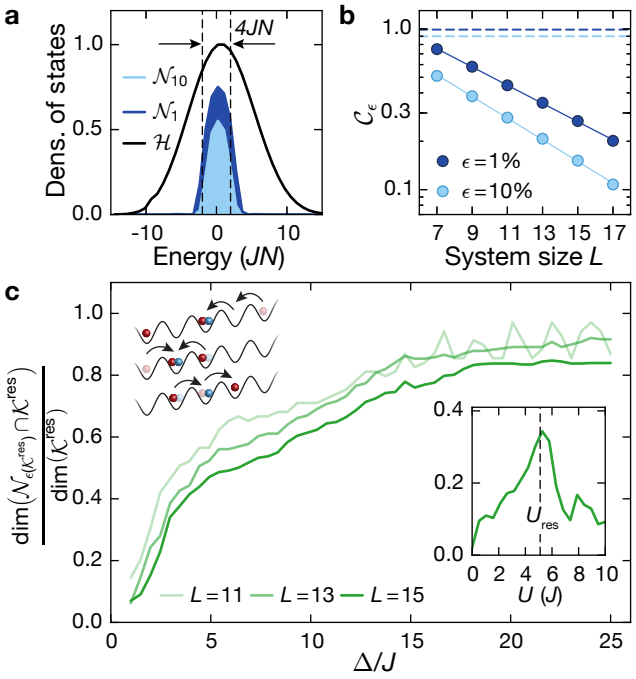

Figure 24.4: **Theoretical analysis of the relevant many-body states for $\omega_h = 0$, $\Delta_\uparrow = \Delta_\downarrow \equiv \Delta$ and a Néel-ordered initial state. a** Density of states in the full Hilbert space $\mathcal{H}$ restricted to quarter filling and zero magnetization for the numerical fragments $\mathcal{N}_1$ ($\epsilon = 1\%$), $\mathcal{N}_{10}$ ($\epsilon = 10\%$), $U = 5J$, $\Delta = 3J$ and $T_\mathcal{N} = 1000\tau$, normalized to the maximum in $\mathcal{H}$; $L = 15$. **b** Scaling of the finite-time connectivity $\mathcal{C}_\epsilon$ with system size for a time window $T_\mathcal{N} = 1000\tau$, $U = 5J$ and $\Delta = 3J$. Solid lines are exponential fits to the data. Dashed lines are the prediction for the finite-time connectivity of a thermal state, showing a constant scaling at $1 - \epsilon$. **c** Normalized intersection for $U = U_{\text{res}}$ between the Krylov subspace $\mathcal{K}^{\text{res}}$ and the numerical fragment $\mathcal{N}_{\epsilon(\mathcal{K}^{\text{res}})}$ (Methods), where $\dim(\mathcal{N}_{\epsilon(\mathcal{K}^{\text{res}})}) = \dim(\mathcal{K}^{\text{res}})$ (main text). The schematic shows the most important processes, connecting the states within the Krylov subspace $\mathcal{K}^{\text{res}}$ [11]. Inset: Normalized intersection as in the main plot for $\Delta = 3J$. The dashed line illustrates the resonance condition found in regime ①.

which is penalized by the on-site interaction U. We numerically show that this leads to a significant slowdown of the dynamics (Sect. 24.5), which explains the robustness of the steady-state value observed in the experiment. Thus, for large values of the tilt, the doublon number is effectively conserved as well, as suggested in Ref. [32].

On resonance, $|U| \simeq 2\Delta$ (regime ① in Fig. 24.1c), doublons can be formed without energy penalties, possibly leading to faster dynamics. Indeed, after an initial faster dynamics, we find a lower steady-state imbalance, which cannot be solely explained by the second-order resonant tunneling process shown in Fig. 24.1c, because it leaves the imbalance invariant. In this regime, we derive an effective Hamiltonian $\hat{H}^{\text{res}}_{\text{eff}}$ [Eq. (24.22)] up to second order in λ (the third order vanishes), conserving the dipole moment, the doublon number or the sum of the two ($\sum_{i,\sigma} i\hat{n}_{i,\sigma} + 2\sum_i \hat{n}_{i,\uparrow}\hat{n}_{i,\downarrow}$). The corresponding symmetry sector exhibits strong fragmentation and results in a finite steady-state imbalance [11]. In Fig. 24.4c we show the dominant second-order tunneling terms for our initial state, illustrating the importance of doublon-assisted tunneling processes for the reduction of the steady-state imbalance. For finite λ or longer evolution times, higher-order hopping processes $\mathcal{O}(\lambda^4)$ enable additional dynamics. These processes are expected to eventually melt the CDW completely, although the required timescales may be very large. In the experiment, we find robust steady-state values even for rather low values of the tilt ($\Delta \simeq 3J$) up to evolution times of about 700τ (Fig. 24.3a).

In order to connect the large-tilt limit described by $\hat{H}^{\text{res}}_{\text{eff}}$ to the experimental parameter

regime, we investigate the states within the explored subspace $\mathcal{N}_\epsilon$, which we denote numerical fragment in analogy to the phenomenon of Hilbert-space fragmentation. For simplicity, we study a clean system ($\omega_h = 0$, $\Delta_\uparrow = \Delta_\downarrow \equiv \Delta$) and a Néel-ordered CDW initial state. In Fig. 24.4a, we show the density of states in the Hilbert space $\mathcal{H}$ and compare it to the density of states in the numerical fragment $\mathcal{N}_\epsilon$ for different values of the cut-off ϵ. Centered around the energy of the initial state, the density of states acquires a finite width within the numerical fragments, that is approximately set by the many-body bandwidth $\pm 2JN$ (dashed line in Fig. 24.4a), where $N = N^\uparrow + N^\downarrow$ denotes the total number of atoms. In stark contrast to thermal systems, the low finite-time connectivity indicates that only a small number of states is relevant for the dynamics. Moreover, it vanishes exponentially in the thermodynamic limit for finite evolution times up to $1000\,\tau$ (Fig. 24.4b). Since the perturbative Hamiltonian $\hat{H}_{\text{eff}}^{\text{res}}$ is only valid in the limit of large tilts, the intersection between the numerically constructed fragment and the analytical one $\mathcal{K}^{\text{res}}$ (Methods), which was derived using the perturbative Hamiltonian $\hat{H}_{\text{eff}}^{\text{res}}$ up to third order in $\lambda = J/\Delta$, is small for our experimental parameters $\Delta = 3J$ and $U = 5J$ (Fig. 24.4c). We expect, however, that the two subsectors coincide for $\lambda \to 0$. Indeed the normalized intersection saturates to one, although only for $\Delta/J \gg 20$. For this comparison the cut-off value $\epsilon(\mathcal{K}^{\text{res}})$ is chosen such that $\dim(\mathcal{N}_{\epsilon(\mathcal{K}^{\text{res}})}) = \dim(\mathcal{K}^{\text{res}})$, since generally, $\mathcal{N}_\epsilon$ contains a much larger number of states. Despite the large value of λ realized in the experiment, we find strong evidence that the slow dynamics is due to kinetic constraints and that the energetically allowed microscopic processes give rise to the phenomenon of Hilbert-space fragmentation in the large tilt limit, as demonstrated for the two regimes (① and ②). This is further supported by the resonance feature that is shown in the inset of Fig. 24.4c for the resonant regime ①.

In conclusion, we have demonstrated both experimentally and numerically non-ergodic behavior in the tilted 1D Fermi-Hubbard model over a wide range of parameters and have provided a microscopic understanding based on perturbative analytical calculations. For future studies it would be interesting to study the limit of large tilts, where strongly-fragmented effective Hamiltonians were identified and to investigate the initial-state dependence of the transient dynamics. This is a characteristic feature of Hilbert-space fragmentation, where distinct thermalization properties are expected for different fragments [23, 21, 20]. Although experimentally challenging due to finite evolution times, it would be interesting to reconcile the phenomenon of Stark MBL and Hilbert-space fragmentation, by studying the impact of weak disorder or residual harmonic confinement on the long-time dynamics [34]. Adding periodic modulation as an additional ingredient, other strongly-fragmented models, scarred models and time crystals could be engineered [55, 56, 57] or drive-induced localization could be investigated [58, 59]. By tuning the direction of the tilt in a 2D lattice, dipole- and higher-moment conserving models could be realized [21, 60] enabling studies beyond the hydrodynamic regime [61]. Moreover, it will be interesting to explore the connection between lattice gauge theories and the phenomenon of Hilbert-space fragmentation [28, 30, 62, 63, 22, 64], which could be addressed experimentally in a similar model [65].

Acknowledgements

We thank D. Abanin, G. De Tomasi, M. Filippone, M. Knap, N. Lindner, R. Moessner, T. Rakovszky and N. Yao for inspiring discussions. We thank C. Schweizer for very useful discussion about the experimental results and their interpretation. We thank M. Buser for illuminating discussions regarding the ED calculations. This work was supported by the Deutsche Forschungsgemeinschaft (DFG, German Research Foundation) under Germany's Excellence Strategy – EXC-2111 – 39081486. The work at LMU was additionally supported by DIP and B. H. M. acknowledges support from the European Union (Marie Curie, Pasquans). The work at TU was additionally supported by the European Research Council (ERC) under the European Union's Horizon 2020 research and innovation program (grant agreement No.

771537).

Author contributions

S.S., T.K. and B.H.M. conceived and performed the experiments and analyzed the data. B.H.M. and P.S. carried out the numerical simulations. P.S. carried out the analytic derivations. M.A., F.P. and I.B. supervised the work. All authors contributed critically to the writing of the manuscript and the interpretation of experimental and numerical results.

Data availability

The data that support the plots within this paper and other findings of this study are available from the corresponding author upon reasonable request.

Code availability

The code that supports the plots within this paper are available from the corresponding author upon reasonable request.

Competing interests

The authors declare no competing interests.

24.1 Methods

Experimental sequence.

Our sequence begins with loading a degenerate Fermi gas with temperature $T/T_F = 0.15(1)$, where T_F is the Fermi temperature, into a three-dimensional (3D) optical lattice. The wavelength is $\lambda_l = 1064\,\mathrm{nm}$ along the x direction and $\lambda_\perp = 738\,\mathrm{nm}$ in the transverse directions. Repulsive interactions during loading in combination with a short, off-resonant light pulse after loading ensure an initial state free of double occupancies [11]. By adding a short lattice with wavelength $\lambda_s = \lambda_l/2$ along the x direction, we generate a CDW initial state consisting of singlons [11]. Holding the gas in this deep 3D lattice with a tilted, bichromatic superlattice along the x direction, dephases remaining correlations between neighboring sites and suppresses any residual dynamics, while ramping up a magnetic field gradient and adjusting the interaction strength. The lattice depths are $18\,E_{rs}$ for the short lattice, $20\,E_{rl}$ for the long lattice and $55\,E_{r\perp}$ for the transverse lattices. The depths are given in the respective recoil energies, $E_{rj} = \hbar^2 k_j^2/(2m)$, with $j \in \{l, s, \perp\}$, $k_j = 2\pi/\lambda_j$ the corresponding wave vector, m the mass of ^{40}K and and $\hbar = h/(2\pi)$ the reduced Planck constant. The deep transverse lattices decouple the 1D chains aligned along x and generate a 2D array of nearly independent 1D systems. The residual coupling along the transverse directions is typically less then 0.03 % of the coupling J along x. The dynamics to probe the tilted 1D Fermi-Hubbard model described by the Hamiltonian in Eq. (24.1) is initiated by suddenly switching off the long lattice and quenching the short lattice to depths between $6\,E_{rs}$ and $8\,E_{rs}$. Simultaneously, the strength of the dipole trap is adjusted in order to compensate the anti-confining harmonic potential introduced by the lattice [11]. After a variable evolution time t the on-site population is frozen by suddenly ramping up the longitudinal lattices to $18\,E_{rs}$ and $20\,E_{rl}$ respectively. Subsequently, we extract the spin-resolved imbalance $\mathcal{I}^\sigma$, by using a bandmapping technique [66, 67] in conjunction with Stern-Gerlach resolved absorption imaging.

Initial state.

The initial state in all experiments consists of a CDW of singlons, where $|\uparrow\rangle$ and $|\downarrow\rangle$ states are randomly distributed on even lattice sites and odd lattice sites are empty. We work with an equal mixture of both states ($N_\uparrow = N_\downarrow$) such that the total magnetization is zero. The fraction of residual holes on even lattice sites, due to imperfections in the loading sequence and due to removed doublons is expected to be about 10% [68]. Excellent agreement between the data and numerical simulations, which do not consider residual holes on even sites, indicates, that the hole fraction has a negligible effect on our dynamics. The initial state can be modelled as incoherent mixture within the zero magnetization sector with density matrix $\hat{\rho} = \frac{1}{\mathcal{N}} \sum_{\{\sigma\}|\sum_i \sigma_i = 0} |\psi_0(\{\sigma\})\rangle\langle\psi_0(\{\sigma\})|$, where each product state $|\psi_0(\{\sigma\})\rangle$, is given by a CDW of singlons and where the sum runs over all $\mathcal{N}$ possible permutations of spin configurations $\{\sigma\}$. The product state $|\psi_0(\{\sigma\})\rangle$ is defined as $|\psi_0(\{\sigma\})\rangle = \prod_{i=\text{even}\in\text{trap}} \left(\hat{c}^\dagger_{i\uparrow}\right)^{n_{i\uparrow}} \left(\hat{c}^\dagger_{i\downarrow}\right)^{n_{i\downarrow}} |0\rangle$, where $\hat{c}^\dagger_{i\sigma}$ is the fermionic creation operator, $n_{i\sigma} \in \{0,1\}$, $\sigma \in \{\uparrow,\downarrow\}$, $n_i = n_{i\uparrow} + n_{i\downarrow} \leq 1$ and i is the lattice-site index along x.

Details of numerical calculations

The numerical computations that are compared with the experiment in Fig. 24.2 and Fig. 24.3 of the main text were performed using ED or TEBD. The parameters J, $\Delta_\uparrow$ and $\Delta_\downarrow$ used in the computations were obtained as fit parameters from the corresponding non-interacting data. Additionally, the effect of harmonic confinement present in the experiment was simulated by scaling the trap frequency by a factor $\sqrt{\frac{L_{\text{exp}}}{L}}$ where $L_{\text{exp}} = 290$ is the system size in the experiment and L is the system size used in the numerical calculation. This is done so as to appropriately simulate the collapse and revival dynamics in the Bloch oscillations induced by the harmonic confinement [11].

We use TEBD for short-time dynamics (Fig. 24.2 of the main text) and ED for long-time dynamics (Fig. 24.3 of the main text). In ED, we consider the Hilbert space as a tensor product $\mathcal{H}_\uparrow \otimes \mathcal{H}_\downarrow$ where $\mathcal{H}_\sigma$ is the Hilbert space of spin-σ atoms. In order to efficiently compute the time dynamics, we decompose each time step in the dynamics into three unitary propagators. One each corresponding to the hopping of the two spin components and the third one corresponding to the on-site potential and interactions. We use a Trotter-Suzuki approximation in this decomposition (see Supplementary Information [11] for details and error analysis). In Fig. 24.3a,d, we use $L = 16, N_\uparrow = N_\downarrow = 4$. In order to effectively model a mixed CDW initial state, in Fig. 24.3a, this computation is averaged over 20 randomly chosen pure CDW states. In Fig. 24.3d we use a superposition of pure CDW product states as we are concerned only with time-averaged steady-state value. The parameters J, Δ_σ and the harmonic confinement are fixed by fitting to the corresponding non-interacting data.

In Fig. 24.2, we use TEBD calculations with $L = 100$ and bond-dimension $\chi = 120$. The truncation error was less than 10^{-2}. In Fig. 24.2b,c, we compare the experimental and numerical data in Fourier space. If the two data sets have different number of samplings in the time domain, we scale the numerical data appropriately after the fast Fourier transform.

Construction of the Krylov subspace

The Krylov subspace (corresponding to the fragment $\mathcal{K}^{\text{res}}$) is constructed by using the effective Hamiltonian on resonance $\hat{H}^{\text{res}}_{\text{eff}}$ in Eq. (24.22). This Hamiltonian is then interpreted as an adjacency matrix in the Wannier basis and the Krylov subspace consists of all states, which are connected to the Néel-ordered CDW initial state. The Krylov subspace $\mathcal{K}^{\text{res}}$ is closed under time-evolution generated by the effective Hamiltonian $\hat{H}^{\text{res}}_{\text{eff}}$. Starting from initial states within the Krylov subspace $\mathcal{K}^{\text{res}}$ and including higher-order terms $\mathcal{O}(\lambda^4)$, the dynamics is captured

only approximately [11]. An improvement is obtained by further rotating the diagonal basis in which the effective Hamiltonian becomes fragmented with the unitary transformation obtained in powers of λ (as given by the Schrieffer-Wolff perturbative expansion [11]). This results in a rotated Krylov subspace.

Construction of the numerical fragment

We define the numerical fragment $\mathcal{N}_\epsilon$ as the span of a subset $\mathcal{B}_\epsilon$ of the number basis $\mathcal{B}$ of $\mathcal{H}$, where $\mathcal{H}$ is restricted to quarter filling and zero magnetization. We define the set $\mathcal{B}_\epsilon$ via its complement, $\mathcal{B}_\epsilon = \mathcal{B}\backslash\mathcal{B}_\epsilon^c$, where $\mathcal{B}_\epsilon^c$ would be ideally defined as the largest subset of $\mathcal{B}$ satisfying $\max_{t<T_\mathcal{N}} \sum_{n^c\in\mathcal{B}_\epsilon^c} |\langle n^c|\psi(t)\rangle|^2 < \epsilon$. Here $T_\mathcal{N}$ defines a time window for the evolution of the initial state $|\psi(t=0)\rangle$. Equivalently, one could define the subset $\mathcal{B}_\epsilon$ as the smallest one, satisfying $\min_{t<T_\mathcal{N}} \sum_{n\in\mathcal{B}_\epsilon} |\langle n|\psi(t)\rangle|^2 \geq 1-\epsilon$. We work with the complement, because it is easier to implement numerically. This inequality condition for the complement would ensure that the residual overlap of $|\psi(t)\rangle$ outside of $\mathcal{N}_\epsilon$ at any time $t \leq T_\mathcal{N}$ is bounded by ϵ. Constructing this $\mathcal{B}_\epsilon^c$, however, involves a search in the powerset of $\mathcal{B}$, which is exponential in the dimension of $\mathcal{H}$. This is intractable even for relatively small system sizes such as $L = 7$. It follows from the inequality $\max_{t<T_\mathcal{N}} \sum_{n^c} |\langle n^c|\psi(t)\rangle|^2 \leq \sum_{n^c} \max_{t<T_\mathcal{N}} |\langle n^c|\psi(t)\rangle|^2$ that keeping the latter sum smaller than ϵ will ensure that the former sum is also bounded by ϵ. Moreover, the latter sum is computationally easier to handle and therefore, we use it to define the fragment. We construct the numerical fragment $\mathcal{N}_\epsilon$ using a $\mathcal{B}_\epsilon^c$, defined such that $\sum_{n^c} \max_{t<T_\mathcal{N}} |\langle n^c|\psi(t)\rangle|^2 < \epsilon$. The gap in the inequality $\max_{t<T_\mathcal{N}} \sum_{n^c} |\langle n^c|\psi(t)\rangle|^2 \leq \sum_{n^c} \max_{t<T_\mathcal{N}} |\langle n^c|\psi(t)\rangle|^2$ loosely depends on the sum $\sum_{n\in\mathcal{B}} \max_{t<T_\mathcal{N}} |\langle n|\psi(t)\rangle|^2$, which is in general, not normalized. Although this sum can be as large as the dimension of $\mathcal{H}$, in the examples that we study, it remains small, i.e., < 10 for $L < 20$, and grows logarithmically in the dimension of $\mathcal{H}$.

24.2 Supplementary information

In this supporting material we give a detailed overview of the analytical derivations, the experimental setup, the measurement techniques, the data acquisition and numerical techniques, employed in this work.

24.3 Interaction picture

The Hamiltonian (24.1) does not commute with spatial translations because of the tilted field. However, due to the gauge covariance of the Schrödinger equation, we can transform from the Schrödinger picture to the interaction picture, where the Hamiltonian becomes translational invariant and time-periodic [69, 70]. We apply a unitary transformation $\hat{T}(t) \equiv e^{it\hat{H}_0}$ with $\hat{H}_0 = \sum_\sigma \Delta_\sigma \sum_i i\hat{n}_{i,\sigma}$ according to (we set $\hbar = 1$ in the following)

$$\hat{H}_I(t) = \hat{T}(t)\hat{H}\hat{T}^\dagger(t) - i\hat{T}(t)\partial_t\hat{T}^\dagger(t), \tag{24.4}$$

with

$$\begin{aligned}\hat{H}_I(t) = &- J\sum_{i,\sigma}\left(e^{-i\Delta_\sigma t}\hat{c}_{i,\sigma}^\dagger\hat{c}_{i+1,\sigma} + \text{h.c.}\right) \\ &+ U\sum_i \hat{n}_{i,\uparrow}\hat{n}_{i,\downarrow},\end{aligned} \tag{24.5}$$

which for incommensurate $\Delta_\uparrow \neq \Delta_\downarrow$ gives rise to a quasi-periodic Hamiltonian [71]. Since density operators are gauge invariant $\hat{n}_{i,I}(t) = \hat{T}(t)\hat{n}_i\hat{T}^\dagger(t) = \hat{n}_i$, we can study the evolution and long-time value of the imbalance in the interaction picture, starting from the experimentally

prepared charge-density wave (CDW) configuration without requiring an additional change of frame. We emphasize that the Hamiltonian in the interaction picture [Eq. (24.5)] explicitly commutes with lattice translations, is well-defined in the thermodynamic limit [70, 32] and avoids the superextensive-scaling contribution of the potential energy to the total energy of the system.

For $\Delta_\uparrow = \Delta_\downarrow \equiv \Delta$, the interacting Hamiltonian [Eq. (24.5)] can be understood as a periodically-driven system [72, 73, 74]. For generic ergodic Hamiltonians, we expect the system to heat up to infinite temperature in the intermediate driving-frequency regime, which we probe in the experiment as a consequence of the energy absorption from the external drive [75, 76]. Therefore, we anticipate the density distribution to become homogeneous and the imbalance to decay to zero at infinite times. In order to give a lower bound on this heating timescale, we can make use of the rigorous theory of prethermalization for periodic [75, 77, 78, 79, 80] or quasi-periodic Hamiltonians (for $\Delta_\uparrow \neq \Delta_\downarrow$) [71] in the large tilt $\Delta \gg J$ regime [47]. This predicts a heating timescale $\tau_* \sim \tau e^{c\Delta/\mu}$ for the former, where c is a numerical constant of order one and $\mu \sim (J+U)$. However, for the tilts employed in the experiment $\Delta \sim 3J$, this lower bound is far from the experimentally observed non-ergodicity until times $t \sim 1000\tau$.

24.4 Dynamical symmetry: $U \to -U$

According to the theorem proven in Ref. [53] (Supplementary material section SD), the Fermi-Hubbard model exhibits a dynamical symmetry between repulsive and attractive interactions for any observable, which is invariant under both time-reversal and π-boost $\hat{B}_Q = e^{i\pi \sum_{i,\sigma} i\hat{n}_{i,\sigma}}$, when considering initial states, that are time reversal invariant and only acquire a global phase under the π-boost transformation. While our interaction scans in the main text are consistent with this symmetry, the assumptions are not valid in the presence of a tilt. We can, however, generalize these assumptions and show that the dynamical symmetry holds for our system as well. Under a spatial inversion $\hat{\mathcal{P}}$, i.e. sending $i \to -i$ with respect to the center of a finite chain with length L, the tilted potential of the Hamiltonian changes sign

$$\hat{H}(U, \Delta_\uparrow, \Delta_\downarrow) \xrightarrow{\hat{\mathcal{P}}} \hat{H}(U, -\Delta_\uparrow, -\Delta_\downarrow)\,. \tag{24.6}$$

Using the π-boost $\hat{B}_Q$ together with the inversion $\hat{\mathcal{P}}$

$$\hat{\mathcal{P}}\hat{B}_Q\hat{H}(U, \Delta_\uparrow, \Delta_\downarrow)\hat{B}_Q^\dagger\hat{\mathcal{P}}^\dagger = -\hat{H}(-U, \Delta_\uparrow, \Delta_\downarrow) \tag{24.7}$$

an equation similar to Eq. (S11) in [53] can be obtained. The experimental observable is the spin-resolved imbalance $\hat{\mathcal{I}}^\sigma = \sum_{i=-\frac{L}{2}}^{\frac{L}{2}} (-1)^i \hat{n}_{i,\sigma}$, which is invariant under inversion $\hat{\mathcal{I}}^\sigma \xrightarrow{\hat{\mathcal{P}}} \hat{\mathcal{I}}^\sigma$ and π-boost $\hat{\mathcal{I}}^\sigma \xrightarrow{\hat{B}_Q} \hat{\mathcal{I}}^\sigma$, but breaks time-reversal symmetry $\hat{\mathcal{T}}$. This symmetry is violated, because the spin degrees of freedom of the density operator $\hat{n}_{i,\sigma}$ are exchanged.

Assuming that $\Delta_\uparrow = \Delta_\downarrow$, the Hamiltonian has an additional SU(2) spin symmetry and is invariant under spin-rotations around $\hat{S}^x = \sum_{\beta,\gamma=\uparrow,\downarrow} 1/2 \hat{c}_\beta^\dagger \sigma^x_{\beta\gamma} \hat{c}_\gamma$, where $\sigma^x_{\beta\gamma}$ are the matrix elements of the Pauli matrix. The local observable $\hat{n}_{i,\sigma}$ is invariant under the product of time reversal $\hat{\mathcal{T}}$ and π-rotations around x, and thus we obtain for the time-evolved imbalance operator $\hat{\mathcal{I}}^\sigma_{(U,\Delta_\uparrow,\Delta_\downarrow)}$

$$\begin{aligned}\hat{\mathcal{P}}\hat{B}_Q e^{-i\pi\hat{S}^x}\hat{\mathcal{T}}\hat{\mathcal{I}}^\sigma_{(U,\Delta_\uparrow,\Delta_\downarrow)}(t)\hat{\mathcal{T}}^{-1}e^{i\pi\hat{S}^x}\hat{B}_Q^\dagger\hat{\mathcal{P}}^\dagger = \\ \hat{\mathcal{I}}^\sigma_{(-U,\Delta_\uparrow,\Delta_\downarrow)}(t).\end{aligned} \tag{24.8}$$

[47] This discussion would also apply in the limit of incommensurate Δ_σ and U when going to the frame with respect to the interacting term.

As long as $\Delta_\downarrow - \Delta_\uparrow$ is sufficiently small, an approximate dynamical symmetry is present for our observable.

We next focus on the required symmetries of the initial state. For all experiments, we consider initial states that are an incoherent sum within the zero magnetization sector (thus $N_\uparrow = N_\downarrow$) with density matrix $\hat{\rho} = \frac{1}{\mathcal{N}} \sum_{\{\sigma\}|\sum_i \sigma_i = 0} |\psi_0(\{\sigma\})\rangle\langle\psi_0(\{\sigma\})|$, where each product state $|\psi_0(\{\sigma\})\rangle$, is given by a CDW of singlons. The sum runs over all possible permutations $\{\sigma\}$ of the spins within the zero magnetization sector. Under the combined action of time reversal and π-rotation around x, this state is left invariant up to a global phase. This is also the case for the π-boost $\hat{B}_Q$. Moreover under spatial inversion $\hat{\mathcal{P}}$ a configuration $\{\sigma_i\}$ is mapped onto another one $\{\sigma_i'\}$ appearing in the mixed state $\hat{\rho}$ with equal weight. Thus, the mixed state is also invariant under $\hat{\mathcal{P}}$. In conclusion, we find for our initial states

$$\mathcal{I}^{\sigma}_{(U,\Delta_\uparrow,\Delta_\downarrow)}(t) = \mathcal{I}^{\sigma}_{(-U,\Delta_\uparrow,\Delta_\downarrow)}(t). \tag{24.9}$$

Note that this dynamical symmetry is weakly broken by experimental imperfections such as the harmonic confinement (see Sec. 24.10) and varying onsite-interaction strength (see Sec. 24.12).

24.5 Effective Hamiltonians

In this section we analytically derive several effective Hamiltonians, starting from the clean tilted Fermi-Hubbard model without harmonic confinement and without spin-dependent tilt, described by the Hamiltonian

$$\begin{aligned}\hat{H}_{\mathrm{tFH}} = &- J \sum_{i,\sigma} \left(\hat{c}^\dagger_{i,\sigma} \hat{c}_{i+1,\sigma} + \mathrm{h.c.} \right) + U \sum_i \hat{n}_{i,\uparrow} \hat{n}_{i,\downarrow} \\ &+ \Delta \sum_{i,\sigma} i \hat{n}_{i,\sigma} \,.\end{aligned} \tag{24.10}$$

In particular we will derive effective Hamiltonians corresponding to: (1) large tilt $\Delta \gg J, |U|$, (2) large interaction $|U| \gg J, \Delta$ and (3) the resonant regime $|U| \simeq 2\Delta$.

24.5.1 Large tilt limit: dipole conservation

Here, we focus on the parameter regime $\Delta \gg |U|, J$ and derive an effective Hamiltonian using the high-frequency expansion (HFE) in the interaction picture. The Hamiltonian in the interaction picture is time-periodic $\hat{H}_I(t + \frac{2\pi}{\Delta}) = \hat{H}_I(t)$. According to Floquet theory [73, 74] the unitary evolution generated by $\hat{H}_I(t)$ can be written as

$$\hat{U}_I(t, t_0) = e^{-i\hat{K}_{\mathrm{eff}}(t)} e^{-i(t-t_0)\hat{H}_{\mathrm{eff}}} e^{i\hat{K}_{\mathrm{eff}}(t_0)}, \tag{24.11}$$

with a time-independent Floquet-gauge invariant Hamiltonian $\hat{H}_{\mathrm{eff}}$ and a gauge-dependent and time-periodic kick operator $\hat{K}_{\mathrm{eff}}(t)$. It has been noticed that the first orders in the perturbative Schrieffer-Wolff (SW) transformation approach for static Hamiltonians (see e.g., [82]), coincide with those in the HFE in the interaction picture (which provides the gauge-invariant effective Hamiltonian) [83, 74], with the SW generator given by the kick operators. Following this approach, we obtain the effective Hamiltonian as a Floquet expansion in powers of $1/\Delta$ with $\hat{H}_{\mathrm{eff}} = \sum_n \hat{H}^{(n)}_{\mathrm{eff}}$ and $\hat{K}_{\mathrm{eff}}(t) = \sum_n \hat{K}^{(n)}_{\mathrm{eff}}(t)$. Up to third order the effective Hamiltonian is [72, 73, 74, 84]:

$$\begin{aligned}\hat{H}^{\mathrm{dip}}_{\mathrm{eff}} = &J^{(3)} \hat{T}_3 + 2J^{(3)} \hat{T}_{XY} + U \left(1 - \frac{4J^2}{\Delta^2}\right) \sum_i \hat{n}_{i,\uparrow} \hat{n}_{i,\downarrow} \\ &+ 2J^{(3)} \sum_{i,\sigma} \hat{n}_{i,\sigma} \hat{n}_{i+1,\bar{\sigma}},\end{aligned} \tag{24.12}$$

up to constant terms, where $\bar{\sigma} = \{\downarrow, \uparrow\}$ indicates the respective opposite spin of $\sigma = \{\uparrow, \downarrow\}$, $J^{(3)} = \frac{J^2 U}{\Delta^2}$ and

$$\hat{T}_3 = \sum_{i,\sigma} \hat{c}_{i,\sigma} \hat{c}^\dagger_{i+1,\sigma} \hat{c}^\dagger_{i+1,\bar{\sigma}} \hat{c}_{i+2,\bar{\sigma}} + \text{h.c.}, \tag{24.13}$$

$$\hat{T}_{XY} = \sum_{i,\sigma} \hat{c}^\dagger_{i,\bar{\sigma}} \hat{c}_{i+1,\bar{\sigma}} \hat{c}^\dagger_{i+1,\sigma} \hat{c}_{i,\sigma}. \tag{24.14}$$

The kick-operator to third order is expressed as

$$\begin{aligned} \hat{K}_{\text{eff}}(t) = &- i\frac{J}{\Delta} \sum_{i,\sigma} \left(\hat{c}^\dagger_{i,\sigma} e^{-it\Delta} \hat{c}_{i+1,\sigma} - \text{h.c.} \right) \\ &- i\frac{JU}{\Delta^2} \sum_{i,\sigma} \left(\hat{n}_{i+1,\bar{\sigma}} - \hat{n}_{i,\bar{\sigma}} \right) \times \\ &\left(\hat{c}^\dagger_{i,\sigma} e^{-it\Delta} \hat{c}_{i+1,\sigma} - \text{h.c.} \right) \end{aligned} \tag{24.15}$$

and the time-evolution operator is approximated as

$$\hat{U}_I(t, t_0) \approx e^{-i\hat{K}_{\text{eff}}(t)} e^{-i(t-t_0)\hat{H}_{\text{eff}}} e^{i\hat{K}_{\text{eff}}(t_0)}. \tag{24.16}$$

Rotating back to the Schrödinger picture, we find

$$\begin{aligned} \hat{U}(t, t_0) =& e^{-it\hat{H}_0} \hat{U}_I(t, t_0) e^{it_0 \hat{H}_0} \\ \approx& e^{-\hat{S}} e^{-i(t-t_0)\left(\hat{H}_{\text{eff}} + \hat{H}_0\right)} e^{\hat{S}}, \end{aligned} \tag{24.17}$$

where we have used the fact that $[\hat{H}_{\text{eff}}, \hat{H}_0] = 0$ and that $e^{-it\hat{H}_0} \hat{K}_{\text{eff}}(t) e^{it\hat{H}_0} = \hat{K}_{\text{eff}}(0)$ [83], namely the product on the left hand side does not depend on time. Therefore, the Hamiltonian in the large-tilt limit can be approximated (up to higher-order terms) via

$$\hat{H} \approx e^{-\hat{S}} \left(\hat{H}_{\text{eff}} + \hat{H}_0 \right) e^{\hat{S}}, \tag{24.18}$$

taking the form of a perturbative SW transformation at third order in J/Δ, with the SW generator given by $\hat{S} = i\hat{K}_{\text{eff}}(0)$. We have thus obtained an effective Hamiltonian which conserves the dipole moment (or center of mass $\sum_{i,\sigma} i\hat{n}_{i,\sigma}$), with $\hat{T}_3$ in Eq. (24.13) the strongly-fragmented dipole-conserving Hamiltonian studied in [20, 21], up to additional spin degrees of freedom. The fact that the hopping rate $J^{(3)}$ is proportional to the interaction strength highlights that interactions are necessary to generate dipole-conserving processes [34] (pure off-diagonal non-interacting contributions destructively interfere at any order). $J^{(3)}$ agrees with the two particle picture [34] yielding $J_{\text{eff}} \propto \frac{UJ^2}{\Delta^2 - U^2}$ with $|U| \ll \Delta$. For CDW initial states of singlons, the connected dynamical sector $\mathcal{K}$ only represents a vanishing fraction of the whole (effective) symmetry sector $\mathcal{S}$, thus severely restricting the dynamics of the system. The dipole-conserving processes in general involve the generation of doublons. This is, however, penalized by the Fermi-Hubbard on-site interaction in Eq. (24.12) and therefore, we expect a slowing down of the dipole-conserving dynamics (see Sec. 24.7). The additional spin-exchange $\hat{T}_{XY}$ increases the connectivity, but cannot fully connect the whole dipole symmetry sector and the system remains fragmented.

24.5.2 Large interaction limit

We study the limit $|U| \gg J, \Delta$ with $||U| - n\Delta| \neq 0$ for any $n \in \mathbb{N}$ to avoid possible resonances [78]. In this limit, the number of doublons N_{doub} is effectively conserved up to times

that scale exponentially in the interaction strength U [85, 86]. Dealing with initial singlon configurations, we have $N_{\mathrm{doub}} = 0$ and assume a negligible fraction of dynamically-generated doublons after the quench. In this limit, the effective Hamiltonian provides non-trivial dynamics at first order in perturbation theory

$$\begin{aligned}\hat{H}^{U}_{\mathrm{eff}} = &- J \sum_{i,\sigma} \left[(1-\hat{n}_{i,\bar{\sigma}})\hat{c}^{\dagger}_{i,\sigma}\hat{c}_{i+1,\sigma}(1-\hat{n}_{i+1,\bar{\sigma}}) + \mathrm{h.c.}\right] \\ &+ \Delta \sum_{i,\sigma} i\hat{n}_{i,\sigma}. \end{aligned} \tag{24.19}$$

Note that the dynamics generated by this Hamiltonian conserves the configuration of spins $|\{\sigma_1, \ldots, \sigma_N\}\rangle$, with $\sigma_i = \{\uparrow, \downarrow\}$ and the total particle number N. The last term in Eq. (24.19) equally couples to both spin degrees of freedom and the many-body states expressed in the particle-number basis factorize in terms of N free Wannier-Stark localized spinless fermions with many-body wave function $|\{i_1, \ldots, i_N\}\rangle$, with $i_i \in \{-\frac{L}{2}, \ldots, 0, \ldots, \frac{L}{2}\}$ and fixed spin configuration $|\{\sigma_1, \ldots, \sigma_N\}\rangle$ [87]. As a result the effective Hamiltonian [Eq. (24.19)] takes the form

$$\hat{H}^{U}_{\mathrm{eff}} = -J \sum_{i} \left(\hat{c}^{\dagger}_{i}\hat{c}_{i+1} + \mathrm{h.c.}\right) + \Delta \sum_{i} i\hat{n}_{i}. \tag{24.20}$$

This has to be compared with the non-interacting Hamiltonian in Eq. (24.1) for $N = N_{\uparrow} + N_{\downarrow}$ spinful fermions, which for a one-body observable like the imbalance gives exactly the same result. Higher-order terms at finite U do not conserve the spin configuration $|\{\sigma_1, \ldots, \sigma_N\}\rangle$. The leading terms in second-order perturbation are spin-exchange and longer-range hopping terms, as well as nearest-neighbors interactions $-2J^2/U \sum_{i,\sigma} \hat{n}_{i,\sigma}\hat{n}_{i+1,\bar{\sigma}}$, which lead to an interaction-induced decay of the imbalance to lower values compared to the non-interacting case at sufficiently long times ($t \sim U/J^2$).

The experimental setup has a weak spin-dependent tilt ($\Delta_{\downarrow} - \Delta_{\uparrow} \approx 0.3J < J$), hence, the previous discussion provides a good approximation for sufficiently strong U. Only in the limit $\Delta_{\downarrow} - \Delta_{\uparrow} > J$, the effective Hamiltonian in Eq. (24.19) does not map onto spinless fermions, because it depends on the spin configuration. This implies that the non-quadratic interaction terms, appearing in the hopping, have to be taken into account. This corresponds to two Stark ladders with different slopes constraining the mobility within each other.

24.5.3 Resonant regime $|U| \simeq 2\Delta$

The singlon CDW structure of the initial states makes the resonance $|U| \simeq 2\Delta$ more prominent in the dynamics than the one at $|U| = \Delta$, where any hopping process from the initial state would require an energy Δ. Consider the family of states for which $\hat{H}_0 = \Delta \sum_{i,\sigma} i\hat{n}_{i,\sigma} + 2\Delta \sum_i \hat{n}_{i,\uparrow}\hat{n}_{i,\downarrow}$ takes the same value. This defines a subspace, within which an effective Hamiltonian $\hat{H}_{\mathrm{eff}}$ with $[\hat{H}_0, \hat{H}_{\mathrm{eff}}] = 0$ can be obtained as an expansion in $\lambda = J/\Delta$. Such Hamiltonian can either independently conserve the dipole moment and the number of doublons or the sum of the two. Using a Schrieffer-Wolf unitary transformation $e^{\lambda \hat{S}}$ [82, 88, 85] with $\hat{S} = \sum_{n=0} \lambda^n \hat{S}_n$ up to an optimal order n^*, we can generate order-by-order an effective local Hamiltonian that is "close" to a block diagonal form with respect to $\hat{H}_0$

$$e^{\lambda \hat{S}_{n\le n^*}} \hat{H} e^{-\lambda \hat{S}_{n\le n^*}} = \hat{H}^{(n^*)}_{\mathrm{eff}} + \hat{V}_{n\ge n^*}, \tag{24.21}$$

where $[\hat{H}_0, \hat{V}_{n\geq n^*}] \neq 0$ with $\hat{V}_{n\geq n^*}$ exponentially small in $1/\lambda$ [85, 79, 80]. In particular, we obtain the explicit form of the effective Hamiltonian to second order in λ:

$$\begin{aligned}\hat{H}_{\text{eff}}^{\text{res}} =& \hat{H}_0 + \frac{8J^2}{3\Delta}\sum_i \hat{n}_{i,\uparrow}\hat{n}_{i,\downarrow} - \frac{4J^2}{3\Delta}\hat{T}_{XY} + \frac{4J^2}{3\Delta}\hat{H}_D \\ &+ \frac{J^2}{\Delta}\hat{T}_1 - \frac{2J^2}{\Delta}\hat{T}_2 + \frac{2J^2}{3\Delta}\hat{T}_3^D\,,\end{aligned} \tag{24.22}$$

with

$$\begin{aligned}\hat{T}_1 &= \sum_{i,\sigma}(1-\hat{n}_{i+2,\bar{\sigma}})(1-2\hat{n}_{i+1,\bar{\sigma}})\hat{n}_{i,\bar{\sigma}}\hat{c}^\dagger_{i,\sigma}\hat{c}_{i+2,\sigma} + \text{h.c.},\\ \hat{T}_2 &= \sum_{i,\sigma}(1-\hat{n}_{i+2,\bar{\sigma}})\hat{n}_{i,\sigma}c^\dagger_{i,\bar{\sigma}}\hat{c}_{i+1,\bar{\sigma}}\hat{c}^\dagger_{i+1,\sigma}\hat{c}_{i+2,\sigma} + \text{h.c.},\\ \hat{T}_3^D &= \sum_{i,\sigma}(\hat{n}_{i,\sigma}-\hat{n}_{i+2,\bar{\sigma}})^2(1-2(\hat{n}_{i+2,\bar{\sigma}}-\hat{n}_{i,\sigma}))\\ &\times \hat{c}_{i,\bar{\sigma}}\hat{c}^\dagger_{i+1,\bar{\sigma}}\hat{c}^\dagger_{i+1,\sigma}\hat{c}_{i+2,\sigma} + \text{h.c.}\\ \hat{H}_D &= -2\sum_i \hat{n}_{i,\uparrow}\hat{n}_{i,\downarrow}(\hat{n}_{i+1}-\hat{n}_{i-1}) - \sum_{i,\sigma}\hat{n}_{i,\sigma}\hat{n}_{i+1,\bar{\sigma}}.\end{aligned} \tag{24.23}$$

The first term in the expansion of the SW generator $\hat{S} = \sum \lambda^n \hat{S}_n$ takes the form

$$\hat{S}_0 = \sum_{i,\sigma}\big(1 - 2\hat{n}_{i,\bar{\sigma}} - \frac{2}{3}\hat{n}_{i+1,\bar{\sigma}} + \frac{8}{3}\hat{n}_{i,\bar{\sigma}}\hat{n}_{i+1,\bar{\sigma}}\big)\hat{c}^\dagger_{i+1,\sigma}\hat{c}_{i,\sigma} - \text{h.c.}. \tag{24.24}$$

Similar to the Hamiltonian $\hat{H}_{\text{eff}}^{\text{dip}}$ [Eq. (24.12)], $\hat{H}_{\text{eff}}^{\text{res}}$ involves a "dressed" $\hat{T}_3^D$ term conserving both the dipole moment and the number of doublons independently, giving rise to doublon-assisted dipole conserving processes. This is the diagonal part of $\hat{T}_3$ commuting with $\hat{N}_{\text{doub}}$.

24.6 Fragmentation in the resonant regime $|U| \simeq 2\Delta$

Here, we study the effective Hamiltonian $\hat{H}_{\text{eff}}^{\text{res}}$ in the resonant regime [Eq. (24.22)] regarding both its diagonal and off-diagonal terms in the number basis. While the diagonal terms cause a renormalized Fermi-Hubbard interaction and a shifted resonance, the off-diagonal terms result in a connectivity of the initial product states with other number basis states, causing strong fragmentation and a finite steady-state imbalance.

24.6.1 Renormalized Fermi-Hubbard interaction

The diagonal terms of the effective Hamiltonian in Eq. (24.22) add long-range interactions and renormalize the Fermi-Hubbard interaction such that the resonant point is shifted for finite λ according to $U + \frac{8J^2}{3\Delta} + \mathcal{O}(\frac{J^2}{\Delta}) = 2\Delta$ and the overall resonance is broadened. We numerically identify the resonance for large tilt $\Delta = 10J$ (Fig. 24.5a) and intermediate tilt $\Delta = 3J$ (Fig. 24.5b) using different system sizes $L = 9, 11, 13, 15$ probing the time-averaged imbalance $\bar{\mathcal{I}}(T) \equiv \frac{1}{T}\int_0^T dt\,\mathcal{I}(t)$. Fig. 24.5 depicts a sharp resonance at strong tilt, while a rather broad feature is present at intermediate tilt. Away from $|U| \simeq 2\Delta$ in the large U regime, we find that the system is Wannier-Stark localized. For both regimes, the numerical results are consistent with the analytic prediction for the shifted resonance to second order even after 1000τ, as shown in Fig. 24.3e in the main text.

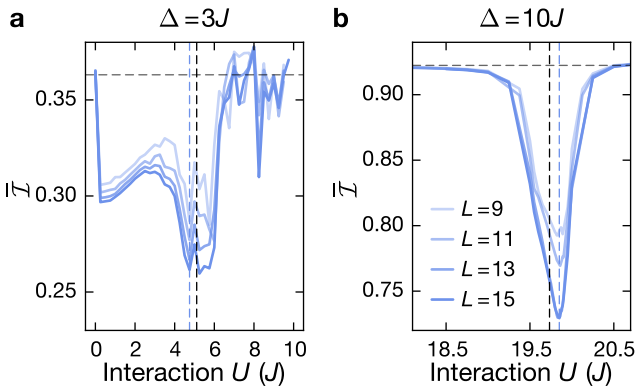

Figure 24.5: **Identification of the resonance $|U| \simeq 2\Delta$.** ED calculation of the time-averaged imbalance $\overline{\mathcal{I}} = 1/T \int_0^T \mathcal{I} dt$ for system sizes $L = 9, 11, 13, 15$ with increasing opacity and $T = 1000\tau$. We use $\Delta_\uparrow = \Delta_\downarrow$. The horizontal dashed line shows the analytical value $\mathcal{J}_0(4J/\Delta)^2$ in the non-interacting case ($U = 0$) in the limit $T \to \infty$. The vertical black dashed line indicates the resonant point, including the second order correction $U_{\text{res}} = 2\Delta - 8J^2/(3\Delta)$. **a** Time-averaged imbalance for $\Delta = 3J$. Close to the minimum, we use a uniform grid with spacing $\delta U = 0.25J$ and identify the lowest imbalance at $U = 4.75J$ (blue dashed line). **b** Time-averaged imbalance for $\Delta = 10J$. Close to the minimum we use a grid with steps $\delta U = 0.01J$, allowing us to locate the minimum at $U = 19.85J$ (blue dashed line).

24.6.2 Strong Fragmentation

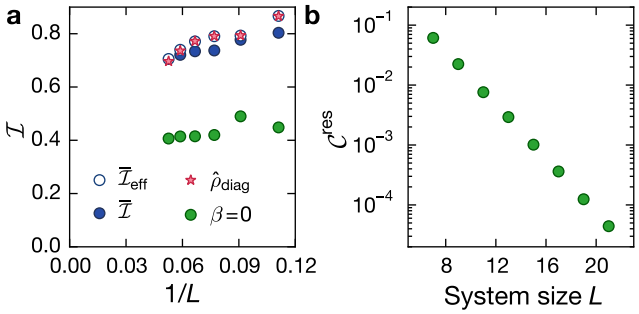

Figure 24.6: **Imbalance in the large tilt limit $\Delta = 10J$.** **a** Finite size scaling of the long-time value of the imbalance calculated with the effective Hamiltonian in Eq.(24.22) using a time-averaged imbalance with $T = 3000\tau$ ($\overline{\mathcal{I}}_{\text{eff}}$), a diagonal ensemble ansatz ($\hat{\rho}_{\text{diag}}$) and an infinite temperature prediction ($\beta = 0$). Additionally, the original Hamiltonian in Eq. (24.10) is used to compare to the time-averaged imbalance calculated with $T = 1000\tau$ ($\overline{\mathcal{I}}$). All ED calculations were done with a Néel-ordered CDW initial state. **b** System size scaling of the connectivity $\mathcal{C}^{\text{res}}$ of the fragment $\mathcal{K}^{\text{res}}$, capturing the Néel-ordered CDW initial state within the full Hilbert space $\mathcal{H}$, restricted to quarter filling and zero magnetization.

The off-diagonal terms of the effective Hamiltonian in Eq. (24.22) consist of three different kinds of correlated hoppings $\hat{T}_1, \hat{T}_2, \hat{T}_3^D$ (see Fig. 24.4d in the main text) and all hopping rates scale as J^2/Δ. Since $[\hat{H}_{\text{eff}}^{\text{res}}, \hat{H}_0] = 0$, $\hat{H}_0$ becomes a new global quantum number fixed by the initial configuration, i.e. the linear combination of the dipole moment and the number of doublons is perturbatively conserved. Generically, after fixing this new global quantum number, the corresponding symmetry sector $\mathcal{S}$ is fully connected by the action of the effective Hamiltonian and the Krylov subspace, hosting the initial state, agrees with the global symmetry sector $\mathcal{S}$. In contrast, we realize that this is not the case for the effective Hamiltonian in Eq. (24.22). Here, the symmetry sector decomposes into exponentially many disconnected

fragments $\mathcal{K}^{\text{res}}$ and the initial state remains trapped within such a fragment without exploring the whole symmetry sector.

For the subsequent analysis, we use a Néel-ordered CDW initial state, expected to show the strongest interaction effects and fastest dynamics. The correlated hoppings $\hat{T}_1, \hat{T}_2, \hat{T}_3^D$ of the effective Hamiltonian connect the initial state with a set of states defining the fragment $\mathcal{K}^{\text{res}}$. Similarly to the finite-time connectivity $\mathcal{C}_\epsilon$ of the numerical fragment (Fig. 24.1, Fig. 24.4 in the main text), we define the connectivity $\mathcal{C}^{\text{res}} = \dim(\mathcal{K}^{\text{res}})/\dim(\mathcal{H})$ as the ratio between the dimension of the fragment $\dim(\mathcal{K}^{\text{res}})$ and the Hilbert space $\dim(\mathcal{H})$, which is restricted to quarter filling and zero magnetization. Experimentally, we do not realize Néel-ordered CDW states, but the connectivity of our initial state with random CDW spin-sector is the same as for the Néel-ordered CDW state. In Fig.24.6b, we show the system size scaling of the connectivity and find that it vanishes exponentially in the thermodynamics limit as expected in the regime of strong fragmentation (The same scaling holds for the connectivity of the fragment within the symmetry sector $\mathcal{S}$.) [20, 23, 21, 22].

In Fig. 24.6a we analyze the system size scaling of both the infinite temperature (within the fragment containing the initial state) and diagonal ensemble predictions for the imbalance, obtaining a positive result in both cases for system sizes $L = 9, 11, 13, 15, 17, 19$ with no clear convergence towards zero imbalance in the thermodynamic limit. The scaling of the infinite temperature prediction suggests a finite value even in this limit. This apparent finite imbalance for $\hat{H}_{\text{eff}}^{\text{res}}$ could be interpreted as follows: Given an initial state that breaks even-odd sublattice symmetry, most dynamical processes in Eq.(24.22), except those generated by $\hat{T}_3^D$, do only transport particles in one of the sublattices. Thus, most states within the fragment have positive imbalance in agreement with the positive infinite temperature value. This explanation is in line with the observed ergodicity-breaking in dipole-conserving systems, where a finite value of the autocorrelation was observed even at infinite temperatures [20].

In Fig. 24.6a, simulations with the exact Hamiltonian $\hat{H}_{\text{tFH}}$ [Eq. (24.10)] for $\Delta = 10J$, $U = 19.85J$ agree well with the results of the effective Hamiltonian [Eq. (24.22)] even up to remarkably long times $T \sim 10^3\tau$. Consistent with a perturbative expansion in λ, which neglects higher order terms in the effective Hamiltonian, it yields a systematically larger imbalance compared to the original Hamiltonian. Since the conservation law, i.e. the linear combination of the dipole moment and the number of doublons, only holds perturbatively, one would expect that it is valid only up to a certain timescale.

24.6.3 Numerical fragment $\mathcal{N}_\epsilon$ versus fragment $\mathcal{K}^{\text{res}}$

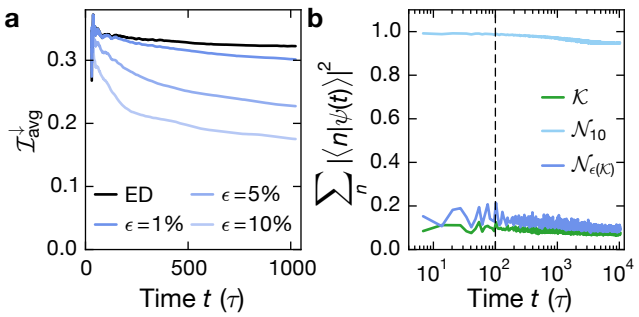

Figure 24.7: **Numerical fragment $\mathcal{N}_\epsilon$.** Both figures use $U = 5J$ and $\Delta_\downarrow = \Delta_\uparrow = 3J$. **a** Imbalance time traces calculated with different sets of states $\mathcal{N}_\epsilon$ and ED for $U = 5J$ and $\Delta = 3J$. $I_{\text{avg}}^{\downarrow}$ is calculated using a cumulative sum to reduce fluctuations; $L = 11$. **b** Contribution of the set of states $|n\rangle$ in the numerical fragments $\mathcal{N}_{\epsilon(\mathcal{K}^{\text{res}})}$ and $\mathcal{N}_{10}$ and the fragment $\mathcal{K}^{\text{res}}$ to the time-evolved initial state $|\psi(t)\rangle$. $T_{\mathcal{N}} = 100\tau$ (dashed line).

In Fig. 24.7a, we investigate how well the imbalance can be captured, when using only the states within the numerical fragment. These states correspond to a small fraction compared to the states within the full Hilbert space and this fraction was found to vanish in the thermodynamic limit (Fig 24.4b). We show imbalance time traces, calculated with a cumulative sum to reduce fluctuations and compare traces with different cut-off values ϵ to the exact numerical result, which we obtained with ED. We find that for $U = 5J$ and $\Delta = 3J$, already with a cut-off $\epsilon = 1\%$ we can reproduce the exact result well, larger cut-off values result in a deviation, which becomes more pronounced at later times. In Fig. 24.7b the overlap of the states $|n\rangle$ in different numerical fragments and in the Krylov subspace $\mathcal{K}^{\text{res}}$ with the time evolved initial state $|\psi(t)\rangle$ is analyzed by calculating $\sum_n |\langle n|\psi(t)\rangle|^2$. While the overlap in our parameter regime is poorly captured by the states in the Krylov subspace $\mathcal{K}^{\text{res}}$ (as expected because these states best describe the time evolution only in the limit $|U| = 2\Delta \gg J$), we can find the proper states by choosing a small enough ϵ. For $\mathcal{N}_1$ we get $\sum_n |\langle n|\psi(t)\rangle|^2 \approx 1$, which shows a very weak decay even up to $t = 10^4\tau$. Note that it is crucial to choose enough states for the numerical fragment. If we choose the same number of states as used in the Krylov subspace $\mathcal{K}^{\text{res}}$ for the numerical fragment $\mathcal{N}_{\epsilon(\mathcal{K}^{\text{res}})}$, we cannot capture the time evolved initial state $|\psi(t)\rangle$ well.

24.7 Constrained dynamics in the presence of higher order terms and on-site interactions

Dynamics caused by fragmentation is captured by effective Hamiltonians and is therefore a transient phenomenon. The perturbative derivation of the effective Hamiltonian neglects higher-order terms which are known to eventually couple different fragments and symmetry sectors, such that the dynamics no longer solely occur within a certain fragment. Estimating the time scales, which capture the dynamics caused due to fragmentation, requires a detailed analysis of both the diagonal and off-diagonal terms of the effective Hamiltonian. Note that the off-diagonal term $\hat{T}_3$, occurring at a rate $J^{(3)} = \frac{J^2U}{\Delta^2}$ in the dipole conserving limit ($\Delta/J \to \infty$, Eq. (24.12)), requires the production of doublons. Creating a doublon is, however, penalized by the diagonal Fermi-Hubbard interaction with strength $\sim U$. Therefore, an initial state consisting of a CDW of singlons without doublons remains frozen for exponentially long times $t \geq e^{c(\Delta/J)^2}$, analogously to the stability of doublons in the repulsive Fermi-Hubbard model in the $U \gg J$ regime [86, 75]. This effectively gives rise to a fragmentation not only due to the conservation law of the respective effective Hamiltonian, but additionally due to the conservation of the doublon number [22]. A similar argument can be made for the time scale on which higher-order off-diagonal terms, coupling different fragments, become effective and eventually destroy fragmentation. We will give a brief outline here for the dipole conserving limit, where higher order terms are easier to capture. These terms add longer-range processes to the effective Hamiltonian and in general order-n terms generate longer range-n processes whose effective hopping rate scales as $J^{(n)} \sim J^{2k}U^{n-2k}/\Delta^{n-1}$ for some k. Any even order vanishes due to destructive interference: For every process started by a particle hopping to the left, there exists another process with a particle hopping to the right, thus contributing with opposite signs. The hopping rate of the next non-vanishing fifth-order scales as $J^{(5)} \sim J^4U/\Delta^4$.

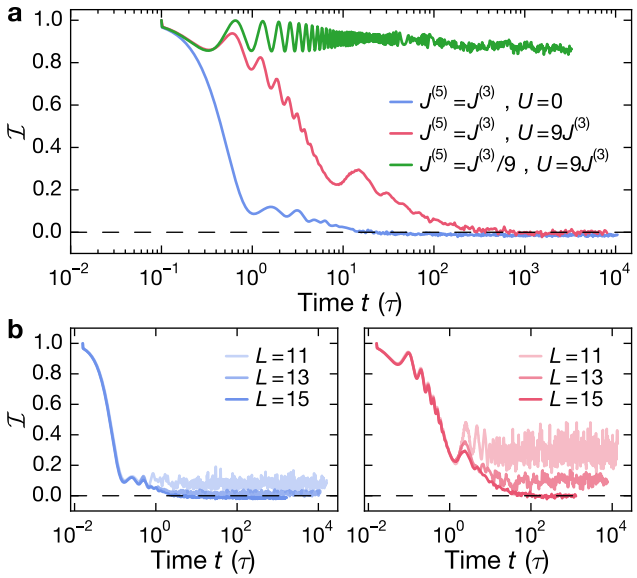

Figure 24.8: **Role of higher-order diagonal and off-diagonal terms.** ED calculation of the imbalance for the Hamiltonian $\hat{H} = J^{(3)}\left(\hat{T}_3 + \hat{T}_{XY}\right) + J^{(5)}\left(\hat{T}_4 + \hat{T}_5\right) + U\hat{N}_{\text{doub}}$. **a** Imbalance for $J^{(5)} = J^{(3)}$, $U = 0$ (blue), $J^{(5)} = J^{(3)}$, $U = 9J^{(3)}$ (red), and $J^{(5)} = J^{(3)}/9$, $U = 9J^{(3)}$ (green) for system size $L = 15$. **b** Finite size scaling of the imbalance for $J^{(5)} = J^{(3)}$, $U = 0$ (left) and for $J^{(5)} = J^{(3)}$, $U = 9J^{(3)}$ (right). In both cases, we use $L = 11, 13, 15$ and increasing opacity corresponds to increasing system size.

Using a qualitative Kato-Bloch perturbative approach [89, 90], which is easier to handle than a Schrieffer-Wolf transformation or a Floquet expansion [91] for higher-order terms, two terms emerge at fifth order in the dipole conserving limit: a 5-local Hamiltonian $\hat{T}_5 = \sum_{i,\sigma}\left(\hat{c}_{i,\sigma}\hat{c}^\dagger_{i+2,\sigma}\hat{c}^\dagger_{i+2,\bar{\sigma}}\hat{c}_{i+4,\bar{\sigma}} + \text{h.c.}\right)$, with two opposite spins hopping to an intermediate site, requiring the creation of a doublon in the central site. A 4-local term $\hat{T}_4$ similar to the $\hat{H}_4$ Hamiltonian studied in [20] $\hat{T}_4 = \sum_{i,\sigma}\left(\hat{c}_{i,\sigma}\hat{c}^\dagger_{i+1,\sigma}\hat{c}^\dagger_{i+2,\bar{\sigma}}\hat{c}_{i+3,\bar{\sigma}} + \text{h.c.}\right)$, which populates nearby sites with opposite spin, thus interacting via the nearest-neighbor interaction appearing at third order. We now consider the time-evolution of an Néel-ordered CDW initial state for system size $L = 15$ with the toy model Hamiltonian $\hat{H} = J^{(3)}\left(\hat{T}_3 + \hat{T}_{XY}\right) + J^{(5)}\left(\hat{T}_4 + \hat{T}_5\right) + U\hat{N}_{\text{doub}}$ using $J^{(3)} = 1$ as unit of energy. Here, $\hat{N}_{\text{doub}}$ measures the number of doublons. In Fig. 24.8a we clearly observe an exponential decay of the imbalance for $J^{(3)}, J^{(5)} \sim O(1)$ and $U = 0$ in agreement with the results in Refs. [20, 21]. The decay time scale increases strikingly, when adding on-site interactions such that $J^{(3)} = J^{(5)} = 1$, $U = 9$ corresponding to a ratio $U/J^{(3)} = 9$ in the perturbative expansion, which is consistent with $\Delta = 3J$ although the higher-order term is still unrealistically large ($J^{(5)} = J^{(3)}$).

A more realistic regime is captured with $J^{(5)} = J^{(3)}/9$ and $U = 9$ due to the perturbative scalings. Here, the imbalance clearly stays finite on our time scales. Thus, the energy penalty given by the on-site interaction has a drastic effect on the decay of the imbalance caused by higher order terms, slowing down the dynamics tremendously. Fig. 24.8b and Fig. 24.8c show a finite-size scaling in the regimes $J^{(5)} = J^{(3)}$ with $U = 0$ and $J^{(3)} = J^{(5)}$ with $U = 9$, clearly indicating that large system sizes are necessary to capture the correct steady-state imbalance.

Unlike the previous regime, at perfect resonance $U_{\text{res}} = 2\Delta \gg J$, neither the lowest-order dynamical processes generated by $\hat{H}^{\text{res}}_{\text{eff}}$ in Eq. (24.22) nor in general higher-order terms, are energetically suppressed. Thus, at a time scale given by the fourth-order term $t \propto \Delta^3/J^4$, fragmentation phenomena are expected to breakdown with the result that imbalance decays. Note that the third-order and in general any odd-order term vanishes due to the CDW initial

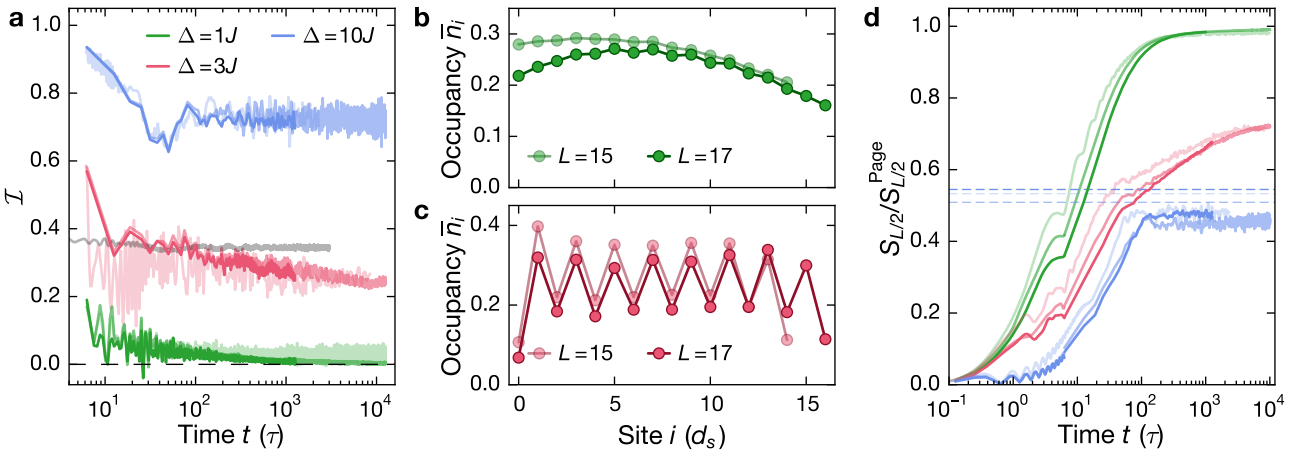

Figure 24.9: **Finite-size scaling analysis of imbalance, entanglement entropy and occupancy.** **a** Long-time behavior of imbalance $\mathcal{I}$ for system sizes $L = 13, 15, 17$ and $(\Delta = 10J, U = 19.85J)$ (blue), $(\Delta = 3J, U = 4.75J)$ (red) and system sizes $L = 12, 14, 16$ for $(\Delta = 1J, U = 4.75J)$ (green). The grey line corresponds to a simulation of the imbalance according to the effective Hamiltonian $\hat{H}^{\text{res}}_{\text{eff}}$ [Eq.(24.22), Eq. (24.17)] for $L = 15$ and $\Delta = 3J$ up to 3000τ. Fluctuations in the data are reduced by using a running average with a time-window of 10τ. **b** ,**c** Time-averaged on-site occupancy $\overline{n}_i = 10/T \int_{0.9T}^{T} n_i dt$ for system sizes $L = 15, 17$ and **b** $(\Delta = 1J, U = 4.75J)$ and **c** $(\Delta = 3J, U = 4.75J)$. The time average was performed with $T = 12600\tau$ for $L = 15$ and $T = 1260\tau$ for $L = 17$. **d** Long-time behavior of the half-chain entanglement entropy $S_{L/2}$ normalized to the Page value $S^{\text{Page}}_{L/2}$ within the $(N_\uparrow, N_\downarrow)$ symmetry sector for the same parameters as in (a) and system sizes $L = 13, 15, 17$. The dashed horizontal lines shows the entanglement entropy of a random state within the fragment $\mathcal{K}^{\text{res}}$ containing the Néel-ordered CDW initial state. Increasing opacity corresponds to increasing system size. All calculations were done using ED.

state, requiring an even number of hoppings for a resonant exchange between tilt and interaction energy. Locating such a resonant point (at finite Δ) requires fine-tuning: every order in perturbation theory gives a diagonal contribution renormalizing the Fermi-Hubbard interaction. As numerically shown in Fig. 24.5a, this is even more subtle at lower values of the tilt. In general, we expect a finite detuning from the resonance, which can be comparable to higher-order contributions, thus 'shielding' the fragmentation of the lowest order Hamiltonian and slowing down the dynamics.

24.8 Scaling analysis of the steady-state imbalance and the entanglement entropy

Here, we study the system-size scaling of the long-time dynamics in a clean system without spin-dependent tilt and harmonic confinement for a large range of tilts: We choose a weak tilt $\Delta = 1J$, an intermediate tilt $\Delta = 3J$ and a large tilt $\Delta = 10J$. We focus on the dynamics close to the resonant point $|U| \approx 2\Delta$, and consider an initial Néel-ordered CDW state. This state has a symmetric charge distribution with respect to the center site and thus its dipole moment coincides with that of a homogeneous charge distribution. In Fig. 24.9a we show numerical simulations of the imbalance $\mathcal{I}$ up to late times for different system sizes. In the large tilt regime, we find a stable imbalance for all system sizes, whereas the intermediate and weak tilt regime show an imbalance decay. This decay is very weak in the intermediate tilt regime and a conclusive answer on whether and at what timescale the imbalance decays to zero cannot be given. In contrast, the imbalance calculated with the effective Hamiltonian $\hat{H}^{\text{res}}_{\text{eff}}$ [Eq.(24.22),

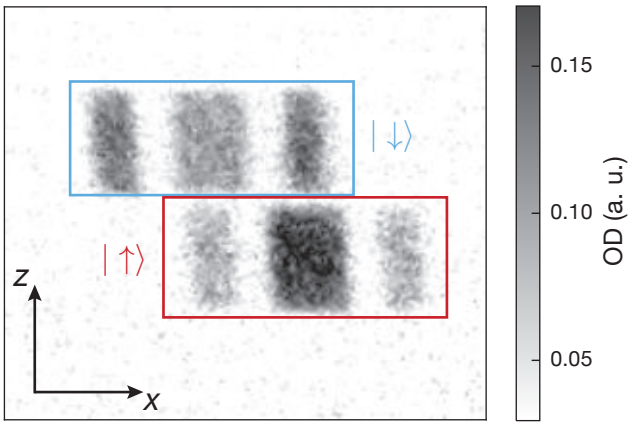

Figure 24.10: **Exemplary raw image.** The two spin states $|\uparrow\rangle$, $|\downarrow\rangle$ are spatially separated using Stern-Gerlach resolved time-of-flight imaging to extract the imbalances of each component $\mathcal{I}^\sigma$ independently. The populations of first and third band are extracted via a pixel sum of the optical density (OD).

Eq. (24.17)] is stable (grey shaded trace in Fig. 24.9a), as expected due to the absence of higher-order terms in the perturbative construction. Additionally, we find that the imbalance weakly scales down with system size. For small tilts, we clearly observe a decay of the imbalance to zero for large enough system sizes.

Note that, while we used $L = 13, 15, 17$ for the intermediate and large tilt regime to minimize edge effects with an unoccupied odd site at the left and the right end of the system, we choose $L = 12, 14, 16$ for the weak tilt regime. In this regime, the initial CDW relaxes to a potentially thermal density distribution and such a distribution only has zero imbalance for an equal number of even and odd sites. Additionally, the breathing amplitude of the dynamics for $\Delta = 1J$ is four sites and boundary effects cannot be easily prevented by including an empty site at the edges. We confirm in Fig. 24.9b that the on-site occupancy shows no more memory of the initial CDW order in the regime of weak tilt, consistent with a zero imbalance. For the intermediate tilt in Fig. 24.9c, we clearly find a remaining CDW order.

In Fig. 24.9d we show numerical simulations of the half-chain entanglement entropy $S_{L/2}$, normalized to the Page value $S^{\text{Page}}_{L/2}$ [92, 93, 94]. The Page value $S^{\text{Page}}_{L/2}$ is the half-chain entanglement entropy of a pure random state within the symmetry sector fixed by particle number $N_\uparrow, N_\downarrow$. The half-chain entanglement entropy of an ergodic system at infinite temperature is in general expected to reach $S_{L/2} = S^{\text{Page}}_{L/2}$. In the weak tilt regime, the half-chain entanglement entropy converges towards the thermal Page value for large enough system sizes, which is consistent with a lack of memory of the initial state as observed with the imbalance and the on-site occupancy. For an intermediate tilt, we observe a sub-thermal entanglement entropy, growing only very slowly at late times, which is consistent with the finite imbalance up to the latest times accessible in the simulations. For large tilt, the entanglement entropy reaches a plateau, which slightly depends on the system size. This saturation value of the entanglement entropy is slightly smaller then the entanglement entropy of a random state within the fragment $\mathcal{K}^{\text{res}}$ (blue dashed lines for the different system sizes) in which the initial state is contained.

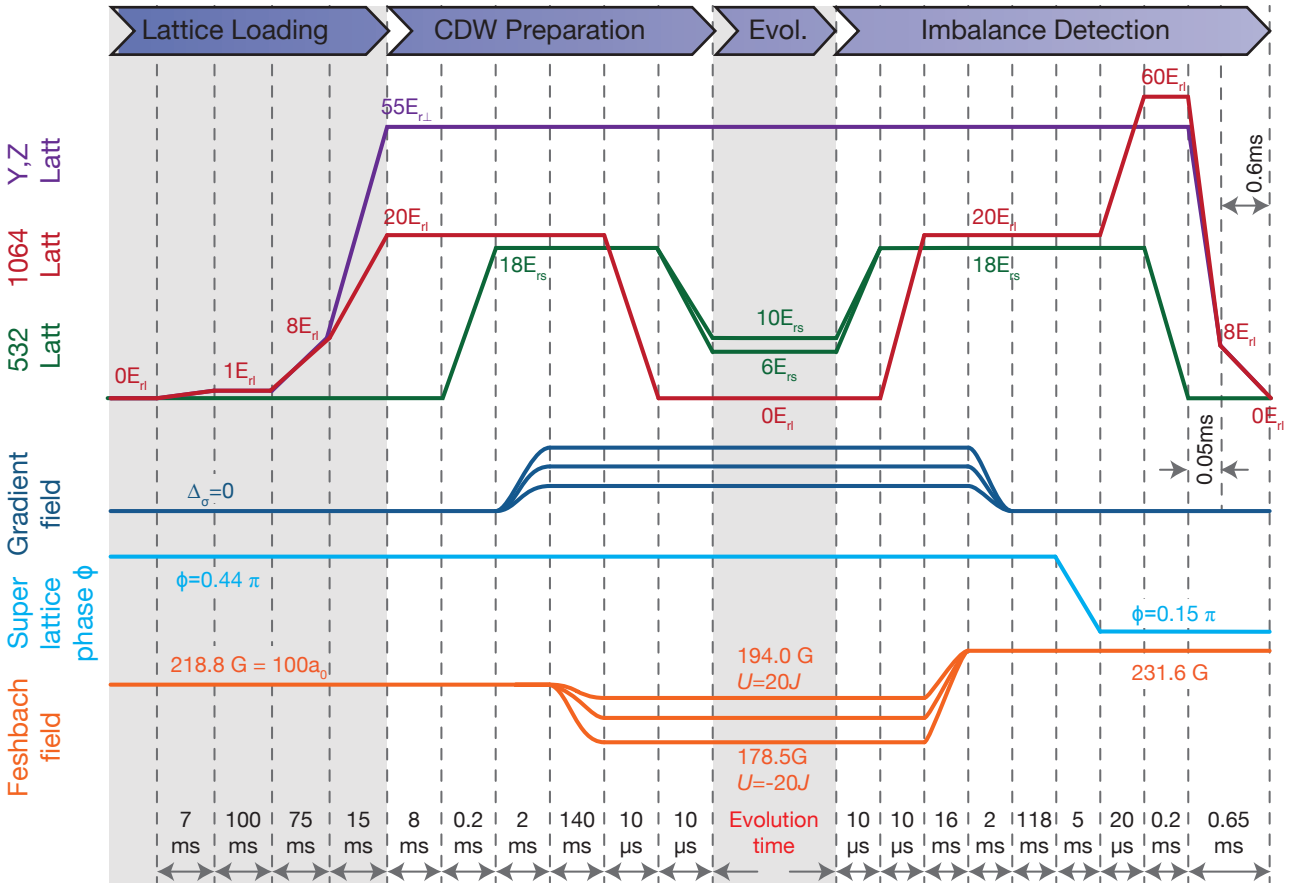

Figure 24.11: **Timing protocol of the experimental sequence.** Schematic showing the lattice depths, the superlattice phase, Feshbach field ramps and the gradient field ramps for loading, CDW preparation, time evolution and detection of the imbalance.

24.9 Experimental sequence

24.9.1 General description

We create a degenerate Fermi gas of ^{40}K atoms in a crossed beam dipole trap. While the non-interacting traces are measured with a spin-polarized gas with all atoms in the state $|\downarrow\rangle = |F = 9/2, m_F = -9/2\rangle$, we work with an equal mixture of the states $|\uparrow\rangle = |F = 9/2, m_F = -7/2\rangle$ and $|\downarrow\rangle$ when studying interacting dynamics. Details of both the cooling sequence and the preparation of the spin-polarized gas can be found in a previous publication [54]. The initial state preparation starts with repulsively loading the atoms at a scattering length of $a = 100a_0$ into a three-dimensional (3D) optical lattice by a series of linear ramps (see Fig. 24.11). The scattering length can be tuned with a Feshbach resonance between the two states of the spin mixture centered at 202.1 G. While the repulsive scattering length suppresses the formation of doubly-occupied sites (doublons) during the loading, we extinguish any residual doublons by applying a 100 µs off-resonant light pulse right after loading the deep lattice [68]. The off-resonant light pulse results in light assisted collisions, which remove doublons without harming atoms on singly-occupied sites (singlons). Afterwards, we end up with singlons in an array of 1D tubes to which the dynamics is restricted on the observed timescales due to the deep orthogonal lattices. Using Gaussian fits to the atom cloud in the lattice, we characterize the 4σ width of the central tubes to $L_{\mathrm{exp}} = 290$ sites. Along the y direction and the z direction, we populate about 150 sites and 22 sites, respectively.

We create the tilted lattice by applying a magnetic field gradient with a single coil. This

coil, however, not only creates a field gradient, but additionally a strong homogeneous magnetic field component up to 110 G is present, which adds to the homogeneous Feshbach field created by a pair of Helmholtz coils. Independent control of both the tilt and the interaction strength requires a tilt-dependent reduction of the Feshbach field and leads to extended wait times to reach stable currents through the coils. We use a wait time of 140 ms before time evolution and another 136 ms after time evolution before the band transfer to ensure a stable Feshbach field (see Fig. 24.11). Residual dynamics within a 1D tube during the wait time are suppressed by holding the atoms in strongly tilted double wells. All experiments throughout this work employ Stern-Gerlach resolved absorption imaging after 6.4 ms time-of-flight (Fig. 24.10).

24.9.2 CDW preparation and spin-resolved imbalance readout

After creating an array of 1D tubes in a deep 3D optical lattice, we ramp up the short lattice $\lambda_s = 532\,\text{nm}$ in addition to the long lattice $\lambda_l = 1064\,\text{nm}$ along the x direction at a superlattice phase of $\phi = 0.44\pi$ within 200 µs. Here, we use the convention that a symmetric double-well potential is realized for $\phi = k \cdot \pi$, with $k = \mathbb{Z}$. This creates strongly tilted double wells with one atom located on the low-energy site of each double well (even site), while the high energy site (odd site) is empty. This charge-density wave (CDW) state is time evolved in all experiments throughout this work. After time evolution, we apply a band transfer technique in the superlattice [66, 67], which maps atoms on odd sites (high-energy site of each double well) into the third band of the long lattice, while atoms on even sites remain in the first band. Here, we require a different superlattice phase of $\phi = 0.15\pi$. Afterwards we perform bandmapping and Stern-Gerlach resolved absorption imaging to evaluate the spin-resolved imbalance. The Stern-Gerlach gradient and the magnetic field gradient during time evolution are created by the same coil.

A large enough spatial separation of the two spin states $|\uparrow\rangle$ and $|\downarrow\rangle$ during Stern-Gerlach resolved bandmapping is achieved by applying a Landau-Zener sweep before the band transfer to convert atoms from $|\uparrow\rangle = |F = 9/2, m_F = -7/2\rangle$ to $|\rightarrow\rangle = |F = 9/2, m_F = -5/2\rangle$. This sweep is performed at a set magnetic field of 231.6 G, corresponding to the zero crossing of the Feshbach resonance between the two states $|\downarrow\rangle$ and $|\rightarrow\rangle$, centered around 224.2 G. We perform a linear frequency ramp with a duration of 10 ms centered at 51.87 MHz with a deviation of 1 MHz. Switching off interactions between these two states ensures the absence of interband oscillations after the transfer to the third band. Additionally, non-interacting bandmapping results in sharper edges of the absorption images and improves the accuracy of the imbalance measurement. A sample raw image used for data acquisition is shown in Fig. 24.10.

Measuring a perfect imbalance equal to one can be compromised by many artifacts such as an imperfect initial state preparation and a finite transfer efficiency of the population on odd sites into the third band. In order to calibrate these imperfections, we take two different sets of images. The first set measures the highest possible initial imbalance (around 0.92(2)) with no evolution time. The second set measures the imbalance after 25 ms evolution time without tilt, which is supposed to yield zero. We then calculate a matrix that maps the measured imbalances for these two sets to 1 (first set) and 0 (second set). In particular, we have to determine a 2×2-matrix A^σ, for each state $\sigma = \uparrow, \downarrow$, which satisfies

$$\begin{pmatrix} n^\sigma_{e,1} & n^\sigma_{e,2} \\ n^\sigma_{o,1} & n^\sigma_{o,2} \end{pmatrix} A^\sigma = \begin{pmatrix} 1 & 0.5 \\ 0 & 0.5 \end{pmatrix}. \tag{24.25}$$

Here, $n^\sigma_{e,i}$ ($n^\sigma_{o,i}$) denote the relative atom number on even (odd) sites for the respective spin state and $i = 1, 2$ refers to the imbalance in the respective set (first or second set). This matrix is then used to rescale the measured imbalance for each spin component.

24.10 Creating a homogeneous potential

Before loading into the lattice the atoms are confined by three dipole trap beams. The horizontal beams along x (dynamics) and y are elliptical ($30 \times 300\,\mu m$) and the vertical beam along the z-direction is circular with a Gaussian beam waist of $150\,\mu m$. All optical lattice beams have the same size as the z-dipole trap and are blue-detuned, thus providing an anti-trapping potential. A flat potential during the Bloch oscillations can be achieved by compensating the confinement of the vertical dipole trap with the anti-confinement of the optical lattices. The horizontal traps should only marginally contribute to the total confinement and we find the optimal configuration if the x-dipole trap is switched off and the y-dipole trap provides a very weak confinement during the time evolution. The confinement is optimized by fixing the time to four Bloch cycles ($t = 4T_\downarrow$) and scanning the dipole trap strength on maximal imbalance. This method works because the confinement does not lead to a frequency change of the oscillations.

24.11 Creating a linear potential

The tilt is created by applying a magnetic field gradient. The energy E^σ of each state $|\sigma\rangle$ in the $F = 9/2$ hyperfine ground-state manifold in the presence of a magnetic field can be analytically calculated using the Breit-Rabi formula and a magnetic field gradient results in a linear potential $\Delta_\sigma i$ according to $\Delta_\sigma = \frac{dE^\sigma}{dB}\partial_x B$. The first factor $\frac{dE^\sigma}{dB}$ causes the tilt to be spin-dependent and in the Zeeman limit of weak field $B \to 0$, we get $\Delta_\uparrow/\Delta_\downarrow = 7/9 = 78\%$. With increasing field, the spin-dependence reduces (in the Paschen-Back limit $B \to \infty$ we have $\Delta_\uparrow/\Delta_\downarrow = 1$) and for the magnetic field used in this work ($B \approx 210\,G$), we have $\Delta_\uparrow/\Delta_\downarrow = 90.6\%$. The second factor $\partial_x B$ is spin-independent and describes the magnetic field gradient, which we create with a single coil close to the atom cloud. The magnetic field along the 1D tubes is given by $B(x) = B_0 + a(x - x_0) + b(x - x_0)^2$ plus higher orders which are negligible for our parameters. Here, x_0 is the center of the coil, x is the relative distance of the atomic cloud, a is the field gradient and b is the field curvature. The coil has a diameter of 25 mm, 20 windings and a mean distance to the atoms of 26.5 mm. Currents up to 55 A are applied. We note that the magnetic field generated by this configuration mainly possesses a large homogeneous contribution and a gradient part producing the linear potential. The weak field curvature part adds to the harmonic confinement of the lattice and dipole beams.

24.12 Interaction averaging

The magnetic field gradient used for generating the tilt causes a local variation of the total magnetic field. Since we use the total magnetic field to set the interaction strength with a Feshbach resonance, the variation of the total magnetic field also induces a variation of the interaction strength over the length of a tube. From the typical center tube length of 290 lattice sites (4σ width of the cloud) and the width of the Feshbach resonance we can calculate the impact of this averaging effect for a certain tilt and lattice configuration. Due to the Gaussian density distribution of the cloud, assuming 290 sites as tube length overestimates the averaging effect and gives a crude upper bound. Fig. 24.12 shows the strength of the averaging effect $U_{\text{var}} = U \pm dU$ as a function of the central interaction strength for a 1D system with $8E_r$ primary lattice depth. For shallower lattices this effect diminishes. Note that while the Stark model exhibits a dynamical U vs. $-U$ symmetry the interaction averaging slightly breaks this symmetry. It also underlines why the non-interacting data we show in this work is mostly taken with a spin-polarized sample. Even if the scattering length is set to zero via the Feshbach resonance, small residual interactions remain due to the averaging.

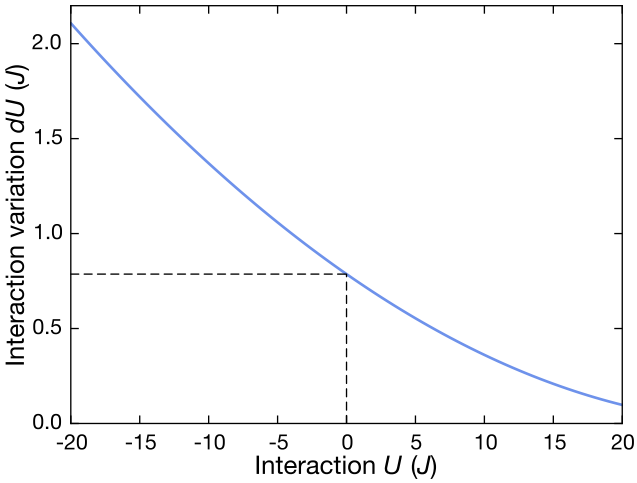

Figure 24.12: **Impact of interaction averaging.** Variation of the interaction strength across one tube with 290 lattice sites, a tilt of $\Delta_\downarrow/h = 1.8\,\mathrm{kHz}$ and tunneling rate $J/h = 540\,\mathrm{Hz}$. For the orthogonal lattices we use $55E_r$.

24.13 Calibration of parameters

24.13.1 Curvature α and trap frequency ω_h

Any non-linear correction to the linear on-site potential leads to a spectrum of Bloch oscillation frequencies in the system that are averaged over in the measurement. The non-linearity in our system is caused by the residual harmonic confinement, modelled as a quadratic correction term to the linear potential, $\Delta_\downarrow i + \alpha(i - i_0)^2$, where i_0 is the center of the lattice. The observed Bloch oscillation is then a sum of Bloch oscillations with frequencies ranging between $\Delta_\downarrow - 2\alpha L/2$ and $\Delta_\downarrow + 2\alpha L/2$ with a step of 2α and a system size of L sites. In order to understand the result of such a sum, consider, for instance, a sum of sinusoidal oscillations,

$$\begin{aligned} f(t) &= \sum_{i=-L/2}^{L/2} \cos(2\pi(\Delta_\downarrow + \alpha i)t) \\ &= \cos(2\pi\Delta_\downarrow t)\frac{\sin(2\pi(L+1)\alpha t)}{\sin(2\pi\alpha t)}. \end{aligned} \tag{24.26}$$

This is an oscillation at frequency $\Delta_\downarrow$ together with a beat note envelope at a frequency $(L+1)\alpha \approx L\alpha$ and nodes at $1/(2L\alpha)$. The Bessel-type Bloch oscillations, which can be expressed as sum of few sinusoidal oscillations, would behave in a qualitatively similar manner. Therefore, we expect a collapse at time $T_c \approx 1/(2L\alpha)$, before the imbalance revives. We use numerical calculations of the imbalance time trace for a non-interacting system in a lattice of size $L = 290(20)d$ to determine the value of α, as a fit parameter. Corresponding to an experimentally measured imbalance time trace $\mathcal{I}^\downarrow(t_j) : j = 1, 2, \cdots, n$, where n is the number of data points in time, we compute, numerically, the trace $\mathcal{I}^\downarrow_{\mathrm{num}}(t_j; J, \Delta_\downarrow, \alpha)$ and then minimize $\sum_j |\mathcal{I}^\downarrow(t_j) - \mathcal{I}^\downarrow_{\mathrm{num}}(t_j; J, \Delta_\downarrow, \alpha)|^2$ over alpha to determine the fit value. The harmonic confinement is extracted in Fig. 24.13. We find a collapse time of $T_c = 8\,\mathrm{ms}$, corresponding to $\alpha = h \cdot 0.216\,\mathrm{Hz}$ and $\omega_h/2\pi = \sqrt{\frac{\alpha\hbar}{md^2\pi}} = 39\,\mathrm{Hz}$. Due to the local nature of the dynamics in the Stark Hamiltonian, α is the important energy scale for the dynamics, characterizing the amount of curvature, experienced by every single atom. In our system, the tilt is on the order of $\Delta_\downarrow \approx h \cdot 1000\,\mathrm{Hz}$ and the curvature is very weak ($\alpha/\Delta_\downarrow \approx 10^{-4}$). Theoretically, the imbalance oscillations should revive partially, but due to anharmonic confinement, residual onsite disorder and other dephasing mechanisms we cannot see such revivals. All these artifacts can affect the

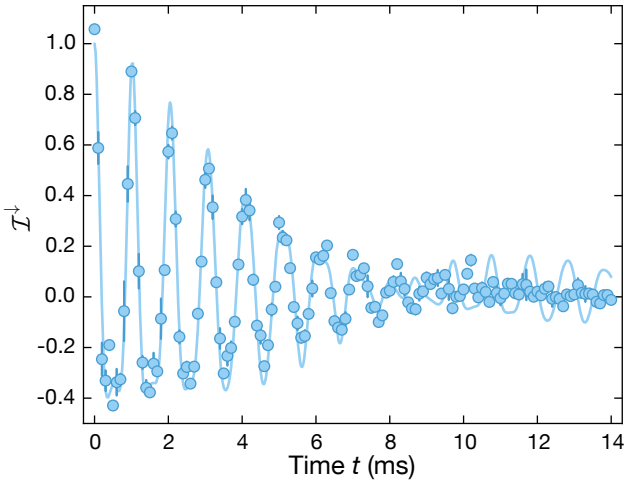

Figure 24.13: **Calibration of the harmonic confinement.** Imbalance $\mathcal{I}^{\downarrow}$ for a spin-polarized gas at $\Delta_{\downarrow} = 1.8J$ and $J = h \cdot 540\,\mathrm{Hz}$. Each data point is averaged twice and error bars denote the SEM. The solid line is a fit to the data using an ED calculation, which includes the harmonic confinement. The resulting collapse time is $T_c = 8\,\mathrm{ms}$.

envelope of the Bloch oscillations in addition to the dephasing of the harmonic confinement and are also included in the extracted collapse time. Hence, extracting the harmonic confinement from the collapse time yields an upper bound for the true harmonic confinement.

24.13.2 Spin-dependent tilt Δ_σ

The setup consists of one pair of coils in Helmholtz configuration to generate a homogeneous magnetic field B_z along the vertical z direction for controlling the interactions between the two spin states by a Feshbach resonance. Additionally, a gradient coil is used to create a magnetic field B_x consisting of a homogeneous field B_{x0} and the field gradient $\frac{\mathrm{d}B_x}{\mathrm{d}x}$ along the x direction. Therefore, the total field is $B_0 = \sqrt{B_x^2 + B_z^2}$. Expanding the above expression up to first order, we get for the total field

$$\begin{aligned} B_0(x) = \sqrt{B_z^2 + B_x^2} &= \sqrt{B_z^2 + \left(B_{x0} + x\frac{\mathrm{d}B_x}{\mathrm{d}x}\right)^2} \\ &\simeq B_z + \frac{B_{x0}^2}{2B_z} + \frac{B_{x0}}{B_z} \cdot x\frac{\mathrm{d}B_x}{\mathrm{d}x}. \end{aligned} \tag{24.27}$$

In the last step we used that B_z is the strongest contribution such that the square root can be expanded up to first order and we neglected the term of the squared gradient. We note that the strength of the gradient is reduced by the vertical field component and amplified by the homogeneous horizontal field. It follows that the calibration of tilt and interactions has to be an iterative process, since these quantities strongly depend on each other. We determine the required vertical magnetic field B_z in the presence of a current I_G in the gradient coil in order to generate a fixed total homogeneous magnetic field B_0. For this sake we employ an RF sweep from $|{\downarrow}\rangle$ to $|{\uparrow}\rangle$, whose frequency is set to the value corresponding to B_0. We find the relation

$$B_z(I_G) = B_0 - \frac{(aI_G)^2}{B_0} + bI_G\,, \tag{24.28}$$

with fit parameters a and b. From Eq. (24.27) it follows that $\Delta_\sigma \propto I_G^2$ where the proportionality constant depends on B_z. The current required to generate a certain tilt Δ_σ can thus be expressed as

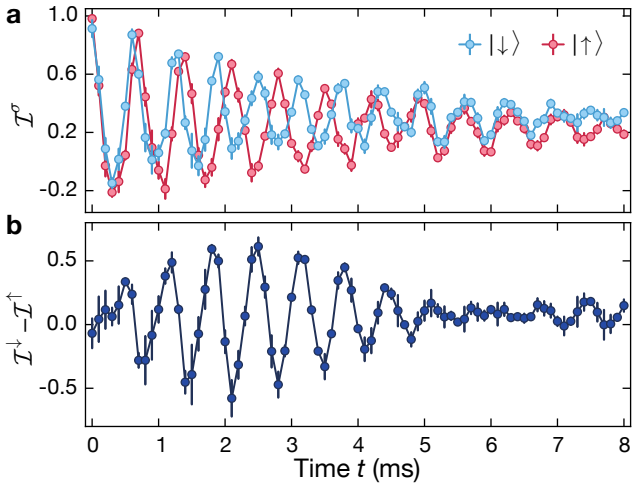

Figure 24.14: **Spin-resolved Bloch oscillations.** **a** Typical calibration measurement of the tilt Δ_σ for both spin-components using the spin-resolved imbalance $\mathcal{I}^\sigma$. Here, $\Delta_\downarrow/h = 1.60(1)\,\mathrm{kHz}$ and we extract a frequency difference of $(\Delta_\downarrow - \Delta_\uparrow)/h = 170(2)\,\mathrm{Hz}$, which is in reasonable agreement with the calculated difference. Each data point is averaged four times and error bars denote the SEM. **b** Imbalance difference between $|\downarrow\rangle$ and $|\uparrow\rangle$. The resulting pattern exhibits a beat note similar to the trigonometric identity $\cos(\omega_1 t) - \cos(\omega_2 t) = -2\sin((\omega_1 + \omega_2)t/2)\sin((\omega_1 - \omega_2)t/2)$.

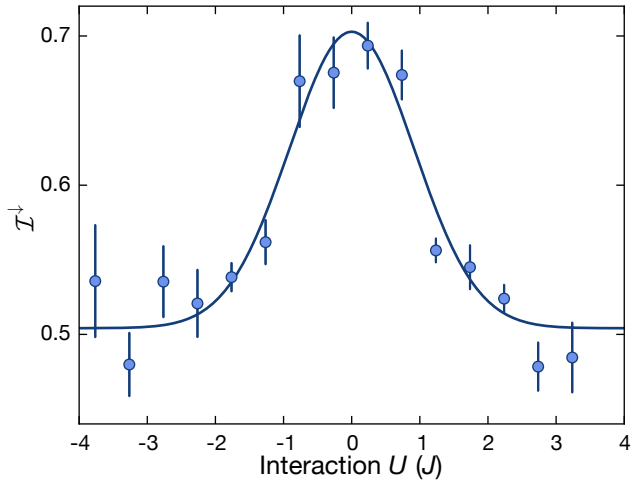

Figure 24.15: **Calibration of the zero-crossing.** Imbalance of one spin-component $\mathcal{I}^\downarrow$ versus interaction strength. We use a tilt $\Delta_\downarrow/h = 1.2\,\mathrm{kHz}$ and measure the imbalance after $t = h/\Delta_\downarrow$. The tunneling rate is $J/h = 540\,\mathrm{Hz}$. The solid line is a Gaussian fit to capture the peak of the imbalance, corresponding to the zero-crossing of the Feshbach resonance. Each data point consists of four independent measurements and error bars denote the SEM.

$$I_G = c\sqrt{\Delta_\sigma \cdot B_z} \tag{24.29}$$

with constant c. We calibrate this fit parameter using single-particle Bloch oscillations and extract the oscillation frequency, set by the tilt Δ_σ, with the analytical model using the first four oscillations to minimize effects of the damping. A typical calibration measurement is illustrated in Fig. 24.14 for a spin-mixture at $\Delta_\downarrow = h \cdot 1.60(1)\,\mathrm{kHz}$. We clearly see the different tilts in the oscillation frequency of the respective spin component. Finally, from Eq. (24.27) and Eq. (24.29) we see that it requires an iterative adaption of the current and the vertical field, since they are strongly correlated. In the experiment we do two full iteration steps until the values sufficiently converge.

24.13.3 Lattice depth

All optical lattices are calibrated using Kapitza-Dirac scattering with a Bose-Einstein condensate of ^{87}Rb and the lattice depth calibration is then converted to ^{40}K. While this technique in principle also calibrates the tunneling J in Eq. (24.1), we determine the tunneling J for the data in Fig. 24.2 and Fig. 24.3 directly by using a fit of Eq. (24.2) to the short-time dynamics ($U = 0J$, spin-polarized). We only use times $t \leq 1.5\,\mathrm{ms}$ such that the damping of the oscillations is negligible (the collapse time is $T_c = 8\,\mathrm{ms}$). For a set lattice depth of $8E_{rs}$ ($6E_{rs}$) the fit yields $J = h \cdot 0.54(1)\,\mathrm{kHz}$ ($J = h \cdot 0.88(2)\,\mathrm{kHz}$) and agrees in both cases well with the calculated tunnelling rate $J_{8E_{rs}} = h \cdot 0.543\,\mathrm{kHz}$ and $J_{6E_{rs}} = h \cdot 0.896\,\mathrm{kHz}$. Note that the solid line in Fig. 24.3b in the main text is a plot of Eq. (24.3), where we use $J = h \cdot 0.54(1)\,\mathrm{kHz}$, obtained from the short time dynamics, without any additional free parameter. The excellent agreement of analytic prediction and data at late times emphasizes the accuracy of calibrating J with the short time dynamics.

24.13.4 Onsite interaction U

The non-interacting point of the Feshbach resonance between the states $|\uparrow\rangle$ and $|\downarrow\rangle$ is calibrated with Bloch oscillations by taking advantage of the interaction-induced damping and the dynamical symmetry between repulsive and attractive interactions. For every tilt $\Delta_\downarrow$ we fix the time t at $t = T_\downarrow = h/\Delta_\downarrow$, while scanning the Feshbach field. In Fig. 24.15 we show a typical calibration measurement, where the zero-crossing of the Feshbach resonance is well detectable as the interaction strength, which has the largest imbalance. A finite interaction U causes a strong damping, which decreases the imbalance. Since the magnetic field $B_0 = 202.1\,\mathrm{G}$ of the center of the Feshbach resonance is well known [95], the zero crossing is set by the width w_{202} plus the magnetic field of the center B_0. We use the calibration of the zero crossing to determine a precise value for the width of the Feshbach resonance: $w_{202} = 7.1(1)\,\mathrm{G}$, in agreement with the literature [53]. The same measurement was performed for the Feshbach resonance between $|\downarrow\rangle$ and $|\rightarrow\rangle$ centered at $B = 224.2\,\mathrm{G}$ [96], where we extract a width $w_{224} = 7.4(1)\,\mathrm{G}$ in agreement with the literature [97]. The characterization of the Feshbach resonance together with the calibration of the lattice depth yields a calibration for the onsite interaction U.

24.14 Extraction of the interaction energy U_{res}

In Fig. 24.3e in the main text we discuss the resonant process connecting two singlons on even sites with a doublon via a second-order hopping process, with $U \simeq 2\Delta_\downarrow$. In Fig. 24.16, we show how the interaction energy U_{res} of the resonance for different tilts $\Delta_\downarrow$ was extracted using a Gaussian fit $f(x) = Ae^{-(x-x_c)^2/(2\sigma^2)} + C$ to locate the minimum of the imbalance $\mathcal{I}^\downarrow$. Note that the naive expectation for the interaction energy $U_{\mathrm{res}} = 2\Delta_\downarrow$ does not apply here, because the resonance is of second order and therefore the interaction energy is renormalized such that we expect $U_{\mathrm{res}} + 8J^2/(3\Delta_\downarrow) = 2\Delta_\downarrow$ up to second-order perturbation theory.

24.15 Details on numerical methods

We use an exact diagonalization technique to simulate the long-time dynamics. The dimension of the subspace of N_σ spin σ atoms on L lattice sites is $d_\sigma = \binom{L}{N_\sigma}$. The state ψ is a $d_\uparrow d_\downarrow$ dimensional vector. The total dimension of the Hilbert space is $d_\uparrow d_\downarrow$ — H is a $d_\uparrow d_\downarrow \times d_\uparrow d_\downarrow$ matrix. For $L = 12, N_\sigma = 3$, this dimension is $220^2 = 48400$; for $L = 16, N_\sigma = 4$, it is $1820^2 = 3312400$ and for $L = 20, N_\sigma = 5$, it is $15504^2 = 240374016$. At $L = 12$, the Hamiltonian already consists of 48400^2 floating point numbers, occupying up to 75 GB of RAM. We therefore use the following method for the computation, which enables us to go up to $L = 20$ before using

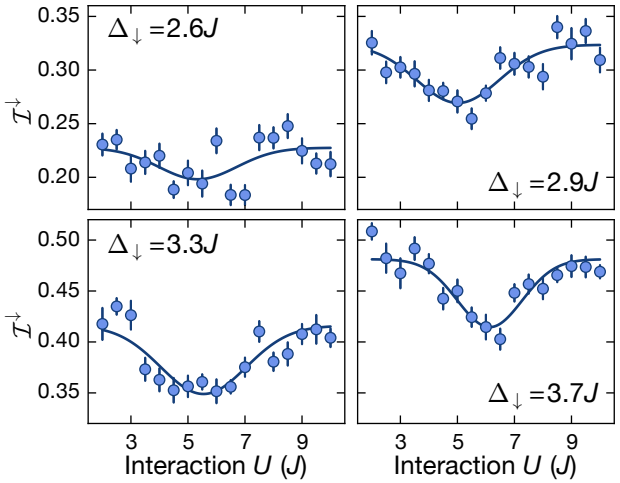

Figure 24.16: **Probing the interaction energy $U_{\rm res}$.** Interaction scan of the imbalance $\mathcal{I}^\downarrow$ of one spin component for different tilts $\Delta_\downarrow$. The solid line is a Gaussian fit $\mathcal{I}^\downarrow(U) = Ae^{-(U-U_{\rm res})^2/(2\sigma^2)}+C$ to the data extracting the interaction energy $U_{\rm res}$ for which the imbalance is minimal. The fit yields $U_{\rm res} = 5.3(6)J$ ($\Delta_\downarrow = 2.6J$), $U_{\rm res} = 5.0(2)J$ ($\Delta_\downarrow = 2.9J$), $U_{\rm res} = 5.5(2)J$ ($\Delta_\downarrow = 3.3J$) and $U_{\rm res} = 6.1(2)J$ ($\Delta_\downarrow = 3.7J$). Each data point is averaged three times over ten equally spaced times in a window between 170τ and 200τ. Error bars denote the SEM.

sparse matrices or a Lanczos algorithm. Below, we describe the construction of the basis, the Hamiltonian and time evolution.

24.15.1 Basis construction

Accounting for atom number conservation in both the spins, as mentioned before, we are working in a subspace of dimension $d_\uparrow \times d_\downarrow$. This is a system of $N_\uparrow + N_\downarrow$ fermions with a total of $2L$ fermionic modes represented by the creation operators $\hat{c}^\dagger_{1,\uparrow}, \hat{c}^\dagger_{2,\uparrow}, \cdots, \hat{c}^\dagger_{L,\uparrow}, \hat{c}^\dagger_{1,\downarrow}, \hat{c}^\dagger_{2,\downarrow}, \cdots, \hat{c}^\dagger_{L,\downarrow}$. A typical number state can be written as $\hat{c}^\dagger_{i_1,\uparrow}\hat{c}^\dagger_{i_2,\uparrow}\cdots\hat{c}^\dagger_{i_{N_\uparrow},\uparrow}\hat{c}^\dagger_{j_1,\downarrow}\hat{c}^\dagger_{j_2,\downarrow}\cdots\hat{c}^\dagger_{j_{N_\downarrow},\downarrow}|0\rangle$, where $\{i_1, \cdots, i_{N_\uparrow}\}$ and $\{j_1, \cdots, j_{N_\downarrow}\}$ are subsets (not necessarily disjoint) of $\{1, 2, \cdots, L\}$. We construct a canonical representation of this state by ordering the operators such that $i_1 < i_2 < \cdots < i_{N_\uparrow}$ and $j_1 < j_2 < \cdots < j_{N_\downarrow}$. This state can be represented by the pair of tuples $((i_1, i_2, \cdots, i_{N_\uparrow}), (j_1, j_2, \cdots, j_{N_\downarrow}))$. Next we order the tuples $\{(i_1, i_2, \cdots, i_{N_\uparrow})\}$ lexicographically to construct a list of tuples $\mathcal{V}_\uparrow$ and $\mathcal{V}_\downarrow$. The full basis would then be $\mathcal{V}_\uparrow \times \mathcal{V}_\downarrow$. In this basis, the non-interacting part of the Hamiltonian remains separable and we make use of this property to optimize the time and memory consumption.

Off-diagonal elements of the Hamiltonian:

Note that a typical hopping term in the Hamiltonian corresponding to spin $\uparrow$ atoms not only leaves the spin $\downarrow$ part of a basis element unchanged, but also maintains the sign of the state with the trivial exception of the boundary hopping (e.g., $\hat{c}^\dagger_{1,\uparrow}\hat{c}_{L,\uparrow}$). The hopping matrix can, therefore, be written as $\hat{H}^{\rm hop}_\uparrow \otimes 1 + 1 \otimes \hat{H}^{\rm hop}_\downarrow$ where $\hat{H}^{\rm hop}_\sigma = \sum_i \hat{c}^\dagger_{i,\sigma}\hat{c}_{i+1,\sigma} + {\rm h.c.}$ is the $d_\sigma \times d_\sigma$ matrix corresponding to the hopping of spin σ atoms, acting on ${\rm span}(\mathcal{V}_\sigma)$. We construct $\hat{H}^{\rm hop}_\uparrow$ and $\hat{H}^{\rm hop}_\downarrow$ separately. These two matrices are *small*, in the sense that their dimensions are $d_\uparrow$ and $d_\downarrow$, much smaller than the full Hilbert space $d_\uparrow \times d_\downarrow$. These matrices can be stored in as dense matrices even when $L = 20$ and $N_\sigma = 5$.

Diagonal elements:

We represent the potential of a spin σ atom at site i by $V_{i,\sigma}$. We store *only* the diagonal entries of the Hamiltonian in a matrix V of size $d_\uparrow \times d_\downarrow$. The matrix element $V_{\alpha\beta}$ is the energy of the basis element corresponding to α-th tuple in $\mathcal{V}_\uparrow$ and β-th tuple in $\mathcal{V}_\downarrow$. If this basis element is $((i_1, i_2, \cdots, i_{N_\uparrow}), (j_1, j_2, \cdots, j_{N_\downarrow}))$, the energy is

$$V_{\alpha\beta} = \sum_{k=1}^{N_\uparrow} V_{i_k,\uparrow} + \sum_{k=1}^{N_\downarrow} V_{j_k,\downarrow} + U|\{i_1, \cdots, i_{N_\uparrow}\} \cap \{j_1, \cdots, j_{N_\downarrow}\}|$$

Here, $|\{i_1, \cdots, i_{N_\uparrow}\} \cap \{j_1, \cdots, j_{N_\downarrow}\}|$ is the number of elements in the intersection of $\{i_1, \cdots, i_{N_\uparrow}\}$ and $\{j_1, \cdots, j_{N_\downarrow}\}$. This is the number of doublons in the state and the last term in the above equation corresponds to the Hubbard interaction.

24.15.2 Intermediate time evolution

We define a $d_\uparrow \times d_\downarrow$ matrix $M^{(\psi)}$, storing the state ψ, whose $\alpha\beta$-th element is $M^{(\psi)}_{\alpha\beta} = \langle \alpha, \beta | \psi \rangle$. Here, $|\alpha\beta\rangle$ is the basis element with indices (α, β) in $\mathcal{V}_\uparrow \times \mathcal{V}_\downarrow$. The rows of $M^{(\psi)}$ correspond to spin $\uparrow$ and columns correspond to spin $\downarrow$. With this setting, the state is $M^{(\psi)}$ and the Hamiltonian, represented by the triplet $\{\hat{H}^{\text{hop}}_\uparrow, \hat{H}^{\text{hop}}_\downarrow, \hat{V}\}$, all of which are $d_\uparrow \times d_\downarrow$, $d_\downarrow \times d_\downarrow$ or $d_\uparrow \times d_\uparrow$ matrices. Therefore it is convenient to work in this picture rather than use the full Hamiltonian which is much bigger. The Schrödinger equation in this representation is given by

$$\dot{M^{(\psi)}} = -i\hat{H}^{\text{hop}}_\uparrow M^{(\psi)} - iM^{(\psi)}\hat{H}^{\text{hop}}_\downarrow - i\hat{V} \circ M^{(\psi)} \tag{24.30}$$

Here, $\circ$ represents element-by-element multiplication, known as Hadamard product. To see that this is the correct equation of time evolution, consider the Schrödinger equation in the standard representation

$$\dot{\psi} = -i\hat{H}^{\text{hop}}_\uparrow \otimes 1\psi - i1 \otimes \hat{H}^{\text{hop}}_\downarrow \psi - i\hat{H}^{diag}\psi \tag{24.31}$$

Here, $\hat{H}^{\text{diag}}$ is a $d_\uparrow d_\downarrow \times d_\uparrow d_\downarrow$ diagonal matrix consisting of the elements in $\hat{V}$. The first term in the above equation reads $\hat{H}^{\text{hop}}_\uparrow \otimes 1\psi = \sum_{\alpha,\beta}\sum_\gamma \hat{H}^{\text{hop}}_{\uparrow\alpha\gamma} M^{(\psi)}_{\gamma\beta}|\alpha\beta\rangle = \sum_{\alpha,\beta}(\hat{H}^{\text{hop}}_\uparrow M^{(\psi)})_{\alpha\beta}|\alpha\beta\rangle$. The second terms reads $1 \otimes \hat{H}^{\text{hop}}_\downarrow \psi = \sum_{\alpha,\beta}\sum_\gamma \hat{H}^{\text{hop}}_{\downarrow\beta\gamma} M^{(\psi)}_{\alpha\gamma}|\alpha\beta\rangle = \sum_{\alpha,\beta}(M^{(\psi)}\hat{H}^{\text{hop}}_\downarrow)_{\alpha\beta}|\alpha\beta\rangle$. Thus the first term corresponds to a *left* multiplication of $M^{(\psi)}$ by $\hat{H}^{\text{hop}}_\uparrow$ and the second term corresponds to a *right* multiplication by $\hat{H}^{\text{hop}}_\downarrow$. The third term reads $\hat{H}^{\text{diag}}\psi = \sum_{\alpha,\beta}\hat{V}_{\alpha\beta}M^{(\psi)}_{\alpha\beta}|\alpha\beta\rangle$; this corresponds to a *term-by-term* multiplication of $M^{(\psi)}$ by $\hat{V}$. Using Trotter-Suzuki decomposition to solve Eq. (24.30) yields

$$M^{(\psi)}(t+\delta t) \approx e^{-i\delta t \circ \hat{V}} \circ e^{-i\delta t\hat{H}^{\text{hop}}_\uparrow} M^{(\psi)}(t) e^{-i\delta t\hat{H}^{\text{hop}}_\downarrow} \tag{24.32}$$

Here, $e^{-i\delta t \circ \hat{V}}$ is an element-by-element exponentiation.

24.15.3 Error estimates

The key problem here is to estimate the error accumulated due to the Trotter-Suzuki decomposition. We consider n trotter steps per Bloch period, that is, $\delta t = \frac{1}{n\Delta}$. We consider time evolutions up to time T. If $\mathcal{I}_n(t)$ is the imbalance computed using n trotter steps per Bloch period, our objective is to estimate $||\mathcal{I} - \mathcal{I}_n||$ where $\mathcal{I}(t)$ is the imbalance at $n = \infty$, which we can calculate for small system sizes using Eq. (24.31), by exponentiating the full Hamiltonian.

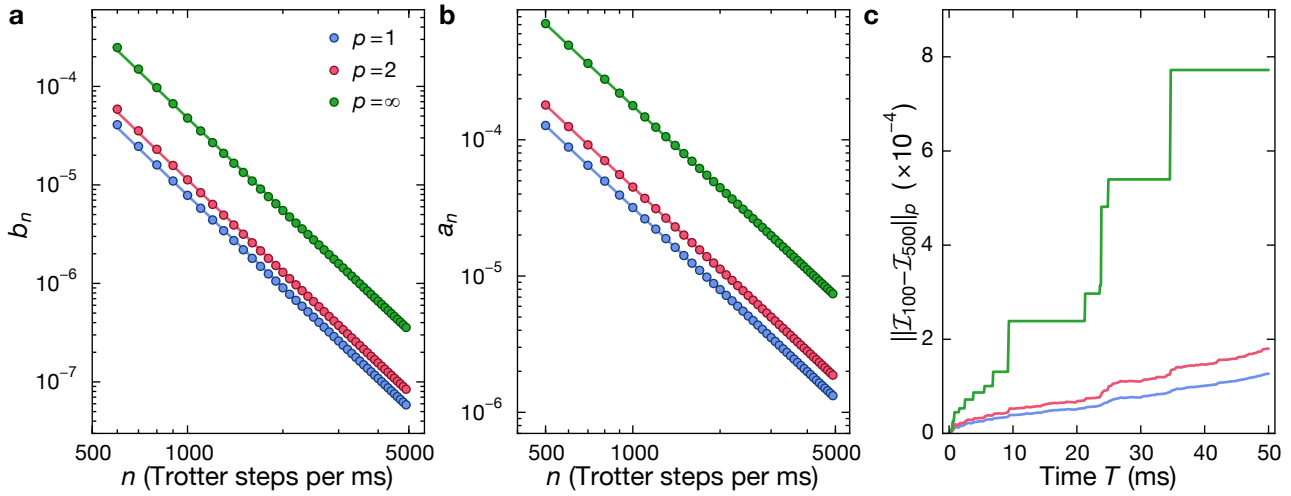

Figure 24.17: **Error estimates in Eq. (24.32).** In panels **a** and **b**, the $p-$norms are calculated for $T = 100\,\text{ms}$ **a** Computation of $b_n = ||\mathcal{I}_n - \mathcal{I}_{n+r}||_p$ with $r = 100$ for $L = 8, N_\sigma = 2$. We show b_n for $p = 1, 2$ and ∞. The solid lines are power law fits, and the corresponding exponent is about -3.09. **b** Computation of $a_n = ||\mathcal{I} - \mathcal{I}_n||_p$ for a system with $L = 8, N_\sigma = 2$. The solid lines correspond to the respective estimates of $\mathcal{I}(t)$ given by Eq. (24.33). The three colors represent $p = 1, 2$ and ∞. **c** The growth of the errors $||\mathcal{I}_{100} - \mathcal{I}_{500}||_p$ in time for $p = 1, 2$ and ∞, for $L = 8$ and $N_\sigma = 2$.

We use the standard $\mathcal{L}^p$-norm, i.e., $||\mathcal{I}_n - \mathcal{I}||_p = \left(\int_0^T |\mathcal{I}_n(t) - \mathcal{I}(t)|^p dt\right)^{\frac{1}{p}}$ for $p = 1, 2$ and ∞. In the latter case, $||\mathcal{I}_n - \mathcal{I}||_\infty = \max(|\mathcal{I}(t) - \mathcal{I}_n(t)|)$. Intuitively, $p = 1$ corresponds to the "average case" distance between $\mathcal{I}$ and $\mathcal{I}_\infty$ and $p = \infty$ represents the "worst case" distance.

We numerically show that $a_n = ||\mathcal{I} - \mathcal{I}_n|| = O\left(\frac{1}{n^2}\right)$. In other words, $||\mathcal{I} - \mathcal{I}_n|| \to 0$ as $1/n^2$. To see this, let us consider the sequence $b_n = ||\mathcal{I}_{n+r} - \mathcal{I}_n||$, for a fixed k. Fig. 24.17a shows that $b_n = O\left(\frac{1}{n^3}\right)$. Moreover, from triangle inequality, $|a_{n+r} - a_n| \leq b_n$ and therefore, $a_n = O\left(\text{cusum}\left(\frac{1}{n^3}\right)\right) = O\left(\frac{1}{n^2}\right)$. Here, cusum$(x)$ is the cumulative sum. Thus, for large n and some k, we can assume that $a_n \sim k^2 a_{kn}$ and it follows from the triangle inequality, $a_n - a_{kn} \leq ||\mathcal{I}_{kn} - \mathcal{I}_n||$ that $a_n \approx \frac{k^2}{k^2-1}||\mathcal{I}_{kn} - \mathcal{I}_n||$. The RHS of last inequality can be computed numerically. Thus, we obtain

$$||\mathcal{I}_m - \mathcal{I}|| \approx \frac{k^2 n^2}{(k^2-1)m^2}||\mathcal{I}_{kn} - \mathcal{I}_n|| \tag{24.33}$$

We use $n = 100$ and $k = 5$ in Fig. 24.17b. We use the above expression to estimate $a_n = ||\mathcal{I} - \mathcal{I}_n||$, for $L = 12$ and higher, and choose n such that $a_n \leq 10^{-3}$.

General error analysis In the previous section, the error accumulated due to the Trotter-Suzuki approximation was analysed using the deviations in the imbalance as the figure of merit. While this approach is relevant for our purpose, the deviations in the state vector itself would be relevant in a more general context. Indeed, if $\psi(t)$ is the many body state vector at time t and $\psi_n(t)$ is the state vector computed using a Trotter-Suzuki approximation using n Trotter steps per Bloch period, the deviation $||||\psi_n(t) - \psi(t)||_2||_p$ can be related to the deviation in any arbitrary observable $\hat{O}$ (Note that we use the standard 2-norm to quantify the distance between $\psi(t)$ and $\psi_n(t)$ at a given time t and then use a $p-$norm to quantify the overall deviation). For instance, consider $\langle\psi|\hat{O}|\psi\rangle - \langle\psi_n|\hat{O}|\psi_n\rangle = \langle\psi|\hat{O}|\psi\rangle - \langle\psi|\hat{O}|\psi_n\rangle + \langle\psi|\hat{O}|\psi_n\rangle - \langle\psi_n|\hat{O}|\psi_n\rangle = \langle\psi - \psi_n|\hat{O}|\psi\rangle + \langle\psi_n|\hat{O}|\psi - \psi_n\rangle \leq 2||\hat{O}||||\psi - \psi_n||_2$. Here, $||\hat{O}||$ is the operator norm, i.e., the largest singular value of $\hat{O}$, assuming $\hat{O}$ is finite-dimensional. Thus, the deviation $||\langle\psi_n(t)|\hat{O}|\psi_n(t)\rangle - \langle\psi(t)|\hat{O}|\psi(t)\rangle||_p$ can be estimated, loosely, using $||||\psi_n(t) - \psi(t)||_2||_p$. In

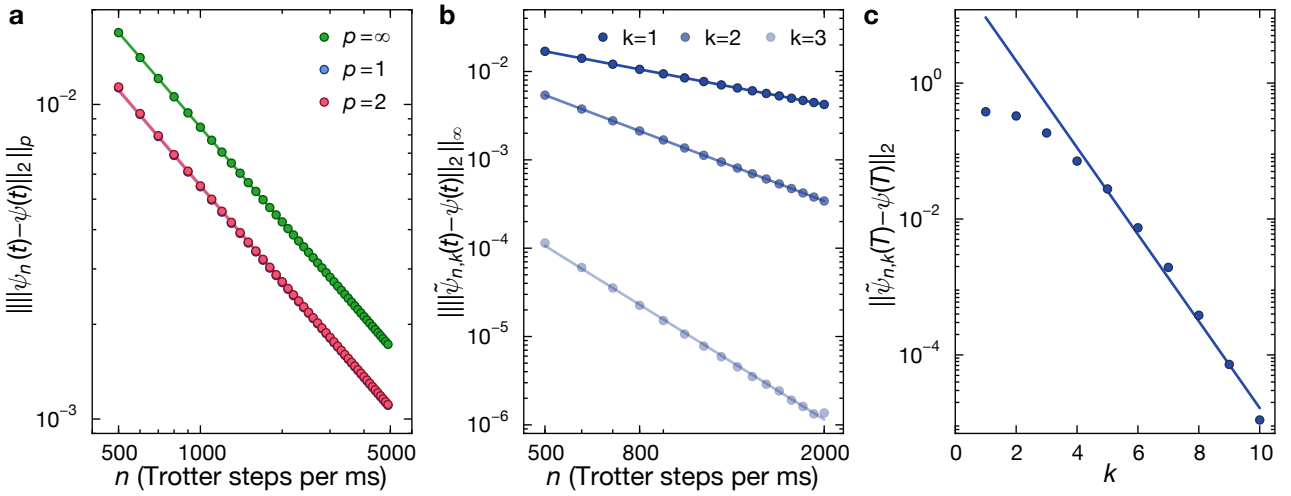

Figure 24.18: **General error analysis. a** $||||\psi_n(t)-\psi(t)||_2||_p$ for a system with $L=8, N_\sigma=2$, indicating a convergence rate of $\frac{1}{n}$. **b** $||||\tilde{\psi}_{n,k}(t)-\psi(t)||_2||_\infty$ for different $k=1,2,3$, system size $L=8$ and $N_\sigma=2$ with $T=100\,\text{ms}$. $k=2$ corresponds to the elimination of the first order error following Eq. (24.34). The $k=3$ curve corresponds to an elimination of the first two orders in error. The straight lines are power law fits with exponents -0.99, -1.99 and -3.26 respectively for $k=1,2$ and 3, indicating a convergence rate of $\frac{1}{n^k}$. **c** $||\tilde{\psi}_{n,k}(T)-\psi(T)||_2$ at $T=100\,\text{ms}$ for a system with $L=8, N_\sigma=2$ and $n_1=40$ for various k, indicating a convergence rate of $\frac{1}{n_1^k}$.

Fig. 24.18a we show that $||||\psi_n(t)-\psi(t)||_2||_p \sim \frac{1}{n}$ for a system with $L=8$ sites and $N_\sigma=2$. It is interesting to note that the imbalance converges much faster $\sim \frac{1}{n^2}$.

24.15.4 Long-time evolution

At the outset it appears that by making a Trotter-Suzuki decomposition, we lose the logarithmic scaling of complexity in time of the scaling-and-squaring procedure of matrix exponentiation. That is, for a long time T, the unitary $e^{-i\hat{H}T}$ can be computed by scaling T to $T/2^n$ for some integer n, computing $e^{-i\hat{H}T/2^n} \approx 1-i\hat{H}T/2^n-\hat{H}^2/2T^2/4^n$ and squaring it repeatedly, n times. The complexity of this procedure is linear in n. For a fixed tolerance, it is logarithmic in T, enabling a computation of very long-time dynamics. Although it appears that we lose this advantage while using the Trotter-Suzuki decomposition, we show below that the scaling can be improved, asymptotically.

In Fig. 24.17c we show how the error of the computation increases with time for a fixed trotter step, suggesting at least a linear growth in T. Moreover, for fixed trotter step, the computational time also grows linearly in T. Thus, for a fixed tolerance, the computational time grows at least quadratically in T. We show below that this can be improved to a linear scaling in T. The idea is to reduce the error in the computation using an elimination technique so that it scales down faster. Let $T \gg 1/\Delta$ be a long time up to which we intend to compute the evolution the system. That is, we want to compute $\psi(T)$. Let us suppose that we computed $\psi(T)$ twice, using the above described procedure, once using $\delta t = 1/(n\Delta)$ and the second time using $\delta t = 1/((n+1)\Delta)$ and obtained two state vectors $\psi_n(T)$ and $\psi_{n+1}(T)$. From the above considerations, we know that $||\psi(T)-\psi_n(T)|| = \kappa/n + O(1/n^2)$ for some κ. We consider a linear combination of $\psi_n(T)$ and $\psi_{n+1}(T)$:

$$\tilde{\psi}_{n,2}(T) = (n+1)\psi_{n+1}(T) - n\psi_n(T) \tag{24.34}$$

$\tilde{\psi}_{n,2}$ is an attempt to eliminate the first order term in the error and therefore, we expect the error scaling to be lower for this state. Indeed, as shown in Fig. 24.18b, $||\tilde{\psi}_{n,2}-\psi(T)|| \sim 1/n^2$. We

may consider a general procedure to eliminate the higher order error terms. We pick k integers $n_1, \cdots, n_k$ and compute $\psi_{n_1}(T), \cdots, \psi_{n_k}(T)$ independently and eliminate the first $k-1$ orders of error. This is done using the Vandermonde matrix

$$W_k = \begin{pmatrix} 1 & 1/n_1 & \cdots & 1/n_1^{k-1} \\ 1 & 1/n_2 & \cdots & 1/n_2^{k-1} \\ \vdots & \vdots & \ddots & \vdots \\ 1 & 1/n_k & \cdots & 1/n_k^{k-1} \end{pmatrix}$$

We can eliminate the errors using the expression $\tilde{\psi}_{n_1,k} = \sum_j (W_k^{-1})_{1j} \psi_{n_j}(T)$. Fig. 24.18c shows that the error in $\tilde{\psi}_{n_1,k}$ scales down as $\sim 1/n_1^k$.

Bibliography

References

24.16 Bibliography from Most Useful Articles

From Generalized Gibbs ensemble in integrable lattice models by Vidmar

References

[1] E. Lieb, T. Schultz, and D. Mattis, Two soluble models of an antiferromagnetic chain, Annals of Physics **16**, 407 (1961).

[2] B. Sutherland, Beautiful Models (World Scientific, Singapore, 2004).

[3] T. Niemeijer, Some exact calculations on a chain of spins 1/2, Physica **36**, 377 (1967).

[4] P. Mazur, Non-ergodicity of phase functions in certain systems, Physica **43**, 533 (1969).

[5] E. Barouch and M. Dresden, Exact time-dependent analysis for the one-dimensional XY model, Phys. Rev. Lett. **23**, 114 (1969).

[6] E. Barouch, B. M. McCoy, and M. Dresden, Statistical mechanics of the XY model. I, Phys. Rev. A **2**, 1075 (1970).

[7] E. Barouch and B. M. McCoy, Statistical mechanics of the XY model. III, Phys. Rev. A **3**, 2137 (1971).

[8] H. Castella, X. Zotos, and P. Prelovšek, Integrability and ideal conductance at finite temperatures, Phys. Rev. Lett. **74**, 972 (1995).

[9] X. Zotos, F. Naef, and P. Prelovšek, Transport and conservation laws, Phys. Rev. B **55**, 11029 (1997).

[10] T. Prosen, Open XXZ spin chain: Nonequilibrium steady state and a strict bound on ballistic transport, Phys. Rev. Lett. **106**, 217206 (2011).

[11] X. Zotos and P. Prelovšek, Transport in one dimensional quantum systems, Strong interactions in low dimensions, edited by D. Baeriswyl and L. Degiorgi (Springer Netherlands, 2004).

[12] F. Heidrich-Meisner, A. Honecker, and W. Brenig, Transport in quasi one-dimensional spin-1/2 systems, Eur. Phys. J. Special Topics **151**, 135 (2007).

[13] R. Vasseur and J. E. Moore, Nonequilibrium quantum dynamics and transport: from integrability to many-body localization, J. Stat. Mech. 064010 (2016).

[14] I. Bloch, J. Dalibard, and W. Zwerger, Many-body physics with ultracold gases, Rev. Mod. Phys. **80**, 885 (2008).

[15] M. A. Cazalilla, R. Citro, T. Giamarchi, E. Orignac, and M. Rigol, One dimensional bosons: From condensed matter systems to ultracold gases, Rev. Mod. Phys. **83**, 1405 (2011).

[16] H. Moritz, T. Stöferle, M. Köhl, and T. Esslinger, Exciting collective oscillations in a trapped 1D gas, Phys. Rev. Lett. **91**, 250402 (2003).

[17] T. Kinoshita, T. Wenger, and D. S. Weiss, Observation of a one-dimensional Tonks-Girardeau gas, Science **305**, 1125 (2004).

[18] B. Paredes, A. Widera, V. Murg, O. Mandel, S. Fölling, I. Cirac, G. Shlyapnikov, T. H. Hänsch, and I. Bloch, Tonks-Girardeau gas of ultracold atoms in an optical lattice, Nature (London) **429**, 277 (2004).

[19] R. Folman, P. Krüger, D. Cassettari, B. Hessmo, T. Maier, and J. Schmiedmayer, Controlling cold atoms using nanofabricated surfaces: Atom chips, Phys. Rev. Lett. **84**, 4749 (2000).

[20] M. Greiner, O. Mandel, T. Hänsch, and I. Bloch, Collapse and revival of the matter wave field of a Bose-Einstein condensate, Nature (London) **419**, 51 (2002).

[21] S. Will, T. Best, U. Schneider, L. Hackermüller, D.-S. Lühmann, and I. Bloch, Time-resolved observation of coherent multi-body interactions in quantum phase revivals, Nature (London) **465**, 197 (2010).

[22] S. Will, D. Iyer, and M. Rigol, Observation of coherent quench dynamics in a metallic many-body state of fermionic atoms, Nature Communications **6**, 6009 (2015).

[23] T. Kinoshita, T. Wenger, and D. S. Weiss, A quantum Newton's cradle, Nature (London) **440**, 900 (2006).

[24] S. Hofferberth, I. Lesanovsky, B. Fisher, T. Schumm, and J. Schmiedmayer, Non-equilibrium coherence dynamics in one-dimensional Bose gases, Nature (London) **449**, 324 (2007).

[25] M. Gring, M. Kuhnert, T. Langen, T. Kitagawa, B. Rauer, M. Schreitl, I. Mazets, D. A. Smith, E. Demler, and J. Schmiedmayer, Relaxation and prethermalization in an isolated quantum system, Science **337**, 1318 (2012).

[26] T. Langen, S. Erne, R. Geiger, B. Rauer, T. Schweigler, M. Kuhnert, W. Rohringer, I. E. Mazets, T. Gasenzer, and J. Schmiedmayer, Experimental observation of a generalized Gibbs ensemble, Science **348**, 207 (2015).

[27] T. Langen, T. Gasenzer, and J. Schmiedmayer, Prethermalization and universal dynamics in near-integrable quantum systems, J. Stat. Mech. 064009 (2016).

[28] J. P. Ronzheimer, M. Schreiber, S. Braun, S. S. Hodgman, S. Langer, I. P. McCulloch, F. Heidrich-Meisner, I. Bloch, and U. Schneider, Expansion dynamics of interacting bosons in homogeneous lattices in one and two dimensions, Phys. Rev. Lett. **110**, 205301 (2013).

[29] L. Vidmar, J. P. Ronzheimer, M. Schreiber, S. Braun, S. S. Hodgman, S. Langer, F. Heidrich-Meisner, I. Bloch, and U. Schneider, Dynamical quasicondensation of hard-core bosons at finite momenta, Phys. Rev. Lett. **115**, 175301 (2015).

[30] J. Simon, W. S. Bakr, R. Ma, M. E. Tai, P. M. Preiss, and M. Greiner, Quantum simulation of antiferromagnetic spin chains in an optical lattice, Nature (London) **472**, 307 (2011).

[31] F. Meinert, M. J. Mark, E. Kirilov, K. Lauber, P. Weinmann, A. J. Daley, and H.-C. Nägerl, Quantum quench in an atomic one-dimensional Ising chain, Phys. Rev. Lett. **111**, 053003 (2013).

[32] T. Fukuhara, A. Kantian, M. Endres, M. Cheneau, P. Schauß, S. Hild, D. Bellem, U. Schollwöck, T. Giamarchi, C. Gross, I. Bloch, and S. Kuhr, Quantum dynamics of a mobile spin impurity, Nature Physics **9**, 235 (2013).

[33] T. Fukuhara, P. Schauß, M. Endres, S. Hild, M. Cheneau, I. Bloch, and C. Gross, Microscopic observation of magnon bound states and their dynamics, Nature (London) **502**, 76 (2013).

[34] S. Hild, T. Fukuhara, P. Schauß, J. Zeiher, M. Knap, E. Demler, I. Bloch, and C. Gross, Far-from-equilibrium spin transport in Heisenberg quantum magnets, Phys. Rev. Lett. **113**, 147205 (2014).

[35] M. Rigol, V. Dunjko, V. Yurovsky, and M. Olshanii, Relaxation in a completely integrable many-body quantum system: An ab initio study of the dynamics of the highly excited states of 1D lattice hard-core bosons, Phys. Rev. Lett. **98**, 050405 (2007).

[36] M. Rigol, A. Muramatsu, and M. Olshanii, Hard-core bosons on optical superlattices: Dynamics and relaxation in the superfluid and insulating regimes, Phys. Rev. A **74**, 053616 (2006).

[37] E. T. Jaynes, Information theory and statistical mechanics, Phys. Rev. **106**, 620 (1957).

[38] E. T. Jaynes, Information theory and statistical mechanics. II, Phys. Rev. **108**, 171 (1957).

[39] M. A. Cazalilla, Effect of suddenly turning on interactions in the Luttinger model, Phys. Rev. Lett. **97**, 156403 (2006).

[40] A. Iucci and M. A. Cazalilla, Quantum quench dynamics of the Luttinger model, Phys. Rev. A **80**, 063619 (2009).

[41] M. A. Cazalilla, A. Iucci, and M.-C. Chung, Thermalization and quantum correlations in exactly solvable models, Phys. Rev. E **85**, 011133 (2012).

[42] M. Kollar and M. Eckstein, Relaxation of a one-dimensional Mott insulator after an interaction quench, Phys. Rev. A **78**, 013626 (2008).

[43] A. Iucci and M. A. Cazalilla, Quantum quench dynamics of the sine-Gordon model in some solvable limits, New J. Phys. **12**, 055019 (2010).

[44] P. Calabrese, F. H. L. Essler, and M. Fagotti, Quantum quench in the transverse-field Ising chain, Phys. Rev. Lett. **106**, 227203 (2011).

[45] P. Calabrese, F. H. L. Essler, and M. Fagotti, Quantum quench in the transverse field Ising chain: I. time evolution of order parameter correlators, J. Stat. Mech. P07016 (2012).

[46] P. Calabrese, F. H. L. Essler, and M. Fagotti, Quantum quenches in the transverse field Ising chain: II. stationary state properties, J. Stat. Mech. P07022 (2012).

[47] F. H. L. Essler, S. Evangelisti, and M. Fagotti, Dynamical correlations after a quantum quench, Phys. Rev. Lett. **109**, 247206 (2012).

[48] M. Fagotti, Finite-size corrections versus relaxation after a sudden quench, Phys. Rev. B **87**, 165106 (2013).

[49] M. Fagotti and F. H. L. Essler, Reduced density matrix after a quantum quench, Phys. Rev. B **87**, 245107 (2013).

[50] L. Bucciantini, M. Kormos, and P. Calabrese, Quantum quenches from excited states in the Ising chain, J. Phys. A: Math. Theor. **47**, 175002 (2014).

[51] C. Gramsch and M. Rigol, Quenches in a quasidisordered integrable lattice system: Dynamics and statistical description of observables after relaxation, Phys. Rev. A **86**, 053615 (2012).

[52] T. M. Wright, M. Rigol, M. J. Davis, and K. V. Kheruntsyan, Nonequilibrium dynamics of one-dimensional hard-core anyons following a quench: Complete relaxation of one-body observables, Phys. Rev. Lett. **113**, 050601 (2014).

[53] J.-S. Caux and R. M. Konik, Constructing the generalized Gibbs ensemble after a quantum quench, Phys. Rev. Lett. **109**, 175301 (2012).

[54] J. Mossel and J.-S. Caux, Exact time evolution of space- and time-dependent correlation functions after an interaction quench in the one-dimensional Bose gas, New J. Phys. **14**, 075006 (2012).

[55] M. Collura, S. Sotiriadis, and P. Calabrese, Equilibration of a Tonks-Girardeau gas following a trap release, Phys. Rev. Lett. **110**, 245301 (2013).

[56] M. Collura, S. Sotiriadis, and P. Calabrese, Quench dynamics of a Tonks-Girardeau gas released from a harmonic trap, J. Stat. Mech. P09025 (2013).

[57] B. Pozsgay, Quantum quenches and generalized Gibbs ensemble in a Bethe Ansatz solvable lattice model of interacting bosons, J. Stat. Mech. P10045 (2014).

[58] S. Sotiriadis and P. Calabrese, Validity of the GGE for quantum quenches from interacting to noninteracting models, J. Stat. Mech. P07024 (2014).

[59] G. Goldstein and N. Andrei, Equilibration and generalized Gibbs ensemble for hard wall boundary conditions, Phys. Rev. B **92**, 155103 (2015).

[60] P. Calabrese and J. Cardy, Quantum quenches in extended systems, J. Stat. Mech. P06008 (2007).

[61] D. Fioretto and G. Mussardo, Quantum quenches in integrable field theories, New J. Phys. **12**, 055015 (2010).

[62] G. Mussardo, Infinite-time average of local fields in an integrable quantum field theory after a quantum quench, Phys. Rev. Lett. **111**, 100401 (2013).

[63] J. Cardy, Quantum quenches to a critical point in one dimension: some further results, J. Stat. Mech. 023103 (2016).

[64] B. Pozsgay, The generalized Gibbs ensemble for Heisenberg spin chains, J. Stat. Mech. P07003 (2013).

[65] M. Fagotti, M. Collura, F. H. L. Essler, and P. Calabrese, Relaxation after quantum quenches in the spin-$\frac{1}{2}$ Heisenberg XXZ chain, Phys. Rev. B **89**, 125101 (2014).

[66] M. Mierzejewski, P. Prelovšek, and T. Prosen, Breakdown of the generalized Gibbs ensemble for current-generating quenches, Phys. Rev. Lett. **113**, 020602 (2014).

[67] B. Wouters, J. De Nardis, M. Brockmann, D. Fioretto, M. Rigol, and J.-S. Caux, Quenching the anisotropic Heisenberg chain: Exact solution and generalized Gibbs ensemble predictions, Phys. Rev. Lett. **113**, 117202 (2014).

[68] B. Pozsgay, M. Mestyán, M. A. Werner, M. Kormos, G. Zaránd, and G. Takács, Correlations after quantum quenches in the XXZ spin chain: Failure of the generalized Gibbs ensemble, Phys. Rev. Lett. **113**, 117203 (2014).

[69] E. Ilievski, J. De Nardis, B. Wouters, J.-S. Caux, F. H. L. Essler, and T. Prosen, Complete generalized Gibbs ensembles in an interacting theory, Phys. Rev. Lett. **115**, 157201 (2015).

[70] F. H. L. Essler and M. Fagotti, Quench dynamics and relaxation in isolated integrable quantum spin chains, J. Stat. Mech. 064002 (2016).

[71] A. C. Cassidy, C. W. Clark, and M. Rigol, Generalized thermalization in an integrable lattice system, Phys. Rev. Lett. **106**, 140405 (2011).

[72] J. M. Deutsch, Quantum statistical mechanics in a closed system, Phys. Rev. A **43**, 2046 (1991).

[73] M. Srednicki, Chaos and quantum thermalization, Phys. Rev. E **50**, 888 (1994).

[74] M. Rigol, V. Dunjko, and M. Olshanii, Thermalization and its mechanism for generic isolated quantum systems, Nature (London) **452**, 854 (2008).

[75] T. Holstein and H. Primakoff, Field dependence of the intrinsic domain magnetization of a ferromagnet, Phys. Rev. **58**, 1098 (1940).

[76] M. Rigol, Finite-temperature properties of hard-core bosons confined on one-dimensional optical lattices, Phys. Rev. A **72**, 063607 (2005).

[77] P. Jordan and E. Wigner, Über das Paulische Aquivalenzverbot, Z. Phys. **47**, 631 (1928).

[78] M. Rigol and A. Muramatsu, Universal properties of hard-core bosons confined on one-dimensional lattices, Phys. Rev. A **70**, 031603 (2004).

[79] M. Rigol and A. Muramatsu, Ground-state properties of hard-core bosons confined on one-dimensional optical lattices, Phys. Rev. A **72**, 013604 (2005).

[80] M. Rigol and A. Muramatsu, Free expansion of impenetrable bosons on one-dimensional optical lattices, Mod. Phys. Lett. B **19**, 861 (2005).

[81] S. Katsura, Statistical mechanics of the anisotropic linear Heisenberg model, Phys. Rev. **127**, 1508 (1962).

[82] S. Sachdev, Quantum Phase Transitions (Cambridge University Press, New York, 2011).

[83] M. Mierzejewski, P. Prelovšek, and T. Prosen, Identifying local and quasilocal conserved quantities in integrable systems, Phys. Rev. Lett. **114**, 140601 (2015).

[84] E. Ilievski, M. Medenjak, and T. Prosen, Quasilocal conserved operators in the isotropic Heisenberg spin-1/2 chain, Phys. Rev. Lett. **115**, 120601 (2015).

[85] E. Ilievski, M. Medenjak, T. Prosen, and L. Zadnik, Quasilocal charges in integrable lattice systems, J. Stat. Mech. 064008 (2016).

[86] M. Rigol, Breakdown of thermalization in finite one-dimensional systems, Phys. Rev. Lett. **103**, 100403 (2009).

[87] M. Rigol, Quantum quenches and thermalization in one-dimensional fermionic systems, Phys. Rev. A **80**, 053607 (2009).

[88] S. Sorg, L. Vidmar, L. Pollet, and F. Heidrich-Meisner, Relaxation and thermalization in the one-dimensional Bose-Hubbard model: A case study for the interaction quantum quench from the atomic limit, Phys. Rev. A **90**, 033606 (2014).

[89] M. Rigol and M. Fitzpatrick, Initial-state dependence of the quench dynamics in integrable quantum systems, Phys. Rev. A **84**, 033640 (2011).

[90] L. C. Venuti and P. Zanardi, Gaussian equilibration, Phys. Rev. E **87**, 012106 (2013).

[91] S. Ziraldo, A. Silva, and G. E. Santoro, Relaxation dynamics of disordered spin chains: Localization and the existence of a stationary state, Phys. Rev. Lett. **109**, 247205 (2012).

[92] S. Ziraldo and G. E. Santoro, Relaxation and thermalization after a quantum quench: Why localization is important, Phys. Rev. B **87**, 064201 (2013).

[93] K. He, L. F. Santos, T. M. Wright, and M. Rigol, Single-particle and many-body analyses of a quasiperiodic integrable system after a quench, Phys. Rev. A **87**, 063637 (2013).

[94] J. Mossel, G. Palacios, and J.-S. Caux, Geometric quenches in quantum integrable systems, J. Stat. Mech. L09001 (2010).

[95] V. Alba and F. Heidrich-Meisner, Entanglement spreading after a geometric quench in quantum spin chains, Phys. Rev. B **90**, 075144 (2014).

[96] M. Fagotti, On conservation laws, relaxation and pre-relaxation after a quantum quench, J. Stat. Mech. P03016 (2014).

[97] S. Sachdev and A. P. Young, Low temperature relaxational dynamics of the Ising chain in a transverse field, Phys. Rev. Lett. **78**, 2220 (1997).

[98] F. Iglói and H. Rieger, Long-range correlations in the nonequilibrium quantum relaxation of a spin chain, Phys. Rev. Lett. **85**, 3233 (2000).

[99] K. Sengupta, S. Powell, and S. Sachdev, Quench dynamics across quantum critical points, Phys. Rev. A **69**, 053616 (2004).

[100] D. Rossini, A. Silva, G. Mussardo, and G. E. Santoro, Effective thermal dynamics following a quantum quench in a spin chain, Phys. Rev. Lett. **102**, 127204 (2009).

[101] D. Rossini, S. Suzuki, G. Mussardo, G. E. Santoro, and A. Silva, Long time dynamics following a quench in an integrable quantum spin chain: Local versus nonlocal operators and effective thermal behavior, Phys. Rev. B **82**, 144302 (2010).

[102] F. Iglói and H. Rieger, Quantum relaxation after a quench in systems with boundaries, Phys. Rev. Lett. **106**, 035701 (2011).

[103] H. Rieger and F. Iglói, Semiclassical theory for quantum quenches in finite transverse Ising chains, Phys. Rev. B **84**, 165117 (2011).

[104] A. Polkovnikov, Microscopic diagonal entropy and its connection to basic thermodynamic relations, Ann. Phys. **326**, 486 (2011).

[105] L. F. Santos, A. Polkovnikov, and M. Rigol, Entropy of isolated quantum systems after a quench, Phys. Rev. Lett. **107**, 040601 (2011).

[106] V. Gurarie, Global large time dynamics and the generalized Gibbs ensemble, J. Stat. Mech. P02014 (2013).

[107] M. Kormos, L. Bucciantini, and P. Calabrese, Stationary entropies after a quench from excited states in the Ising chain, EPL (Europhysics Letters) **107**, 40002 (2014).

[108] M. Collura, M. Kormos, and P. Calabrese, Stationary entanglement entropies following an interaction quench in 1D Bose gas, J. Stat. Mech. P01009 (2014).

[109] M. Rigol, Quantum quenches in the thermodynamic limit, Phys. Rev. Lett. **112**, 170601 (2014).

[110] M. Rigol, Fundamental asymmetry in quenches between integrable and nonintegrable systems, Phys. Rev. Lett. **116**, 100601 (2016).

[111] K. He and M. Rigol, Initial-state dependence of the quench dynamics in integrable quantum systems. II. Thermal states, Phys. Rev. A **85**, 063609 (2012).

[112] L. D'Alessio, Y. Kafri, A. Polkovnikov, and M. Rigol, From quantum chaos and eigenstate thermalization to statistical mechanics and thermodynamics, arXiv:1509.06411.

[113] J.-S. Caux and F. H. L. Essler, Time evolution of local observables after quenching to an integrable model, Phys. Rev. Lett. **110**, 257203 (2013).

[114] J. De Nardis, B. Wouters, M. Brockmann, and J.-S. Caux, Solution for an interaction quench in the Lieb-Liniger Bose gas, Phys. Rev. A **89**, 033601 (2014).

[115] J.-S. Caux, The quench action, J. Stat. Mech. 064006 (2016).

[116] E. A. Yuzbashyan, Generalized microcanonical and Gibbs ensembles in classical and quantum integrable dynamics, Annals of Physics **367**, 288 (2016).

[117] T. N. Ikeda, Y. Watanabe, and M. Ueda, Finite-size scaling analysis of the eigenstate thermalization hypothesis in a one-dimensional interacting Bose gas, Phys. Rev. E **87**, 012125 (2013).

[118] V. Alba, Eigenstate thermalization hypothesis and integrability in quantum spin chains, Phys. Rev. B **91**, 155123 (2015).

[119] R. Nandkishore and D. A. Huse, Many-body localization and thermalization in quantum statistical mechanics, Annual Review of Condensed Matter Physics **6**, 15 (2015).

[120] E. Altman and R. Vosk, Universal dynamics and renormalization in many-body-localized systems, Annual Review of Condensed Matter Physics **6**, 383 (2015).

From Stable Quantum-Correlated Many Body States through Engineered Dissipation

References

[1] I. Bloch, J. Dalibard, W. Zwerger, *Rev. Mod. Phys.* **80**, 885 (2008).

[2] R. Blatt, C. F. Roos, *Nat. Phys.* **8**, 277 (2012).

[3] E. Altman, *et al.*, *PRX Quantum* **2**, 017003 (2021).

[4] M. Cerezo, *et al.*, *Nat. Rev. Phys.* **3**, 625 (2021).

[5] J. R. McClean, S. Boixo, V. N. Smelyanskiy, R. Babbush, H. Neven, *Nat. Commun.* **9**, 4812 (2018).

[6] J. Q. You, Z. D. Wang, W. Zhang, F. Nori, *Sci. Rep.* **4**, 5535 (2014).

[7] A. Kitaev, *Ann. Phys.* **303**, 2 (2003).

[8] M. B. Plenio, S. F. Huelga, A. Beige, P. L. Knight, *Phys. Rev. A* **59**, 2468 (1999).

[9] B. Kraus, *et al.*, *Phys. Rev. A* **78**, 042307 (2008).

[10] S. Diehl, *et al.*, *Nat. Phys.* **4**, 878 (2008).

[11] F. Verstraete, M. M. Wolf, J. Ignacio Cirac, *Nat. Phys.* **5**, 633 (2009).

[12] C. Aron, M. Kulkarni, H. E. Türeci, *Phys. Rev. X* **6**, 011032 (2016).

[13] P. M. Harrington, E. J. Mueller, K. W. Murch, *Nat. Rev. Phys.* **4**, 660 (2022).

[14] M. Raghunandan, F. Wolf, C. Ospelkaus, P. O. Schmidt, H. Weimer, *Sci. Adv.* **6**, eaaw9268 (2020).

[15] S. Polla, Y. Herasymenko, T. E. O'Brien, *Phys. Rev. A* **104**, 012414 (2021).

[16] J. T. Barreiro, *et al.*, *Nature* **470**, 486 (2011).

[17] Y. Lin, *et al.*, *Nature* **504**, 415 (2013).

[18] S. Shankar, *et al.*, *Nature* **504**, 419 (2013).

[19] R. Ma, *et al.*, *Nature* **566**, 51 (2019).

[20] R. Acharya, *et al.*, *Nature* **614**, 676 (2023).

[21] M. McEwen, *et al.*, *Nat. Commun.* **12**, 1761 (2021).

[22] K. C. Miao, *et al.*, *Nat. Phys.* (2023).

[23] M. Ziman, P. Štelmachovič, V. Bužek, *Open Syst. Inf. Dyn.* **12**, 81 (2005).

[24] S. Boixo, *et al.*, *Nat. Phys.* **14**, 595 (2018).

[25] W. K. Wootters, *Phys. Rev. Lett.* **80**, 2245 (1998).

[26] F. Arute, *et al.*, *Science* **369**, 1084 (2020).

[27] D. J. Yates, F. H. L. Essler, A. Mitra, *Phys. Rev. B* **99**, 205419 (2019).

[28] X. Mi, *et al.*, *Science* **378**, 785 (2022).

[29] R. McWeeny, *Rev. Mod. Phys.* **32**, 335 (1960).

[30] R. Islam, *et al.*, *Nature* **528**, 77 (2015).

[31] A. Mazurenko, *et al.*, *Nature* **545**, 462 (2017).

[32] S. Ebadi, *et al.*, *Nature* **595**, 227 (2021).

[33] T. Brydges, *et al.*, *Science* **364**, 260 (2019).

[34] E. Lieb, T. Schultz, D. Mattis, *Ann. Phys.* **16**, 407 (1961).

[35] B. Bertini, *et al.*, *Rev. Mod. Phys.* **93**, 025003 (2021).

[36] A. Scheie, *et al.*, *Nat. Phys.* **17**, 726 (2021).

[37] D. Wei, *et al.*, *Science* **376**, 716 (2022).

[38] N. Keenan, N. F. Robertson, T. Murphy, S. Zhuk, J. Goold, *Npj Quantum Inf.* **9**, 72 (2023).

[39] V. Gritsev, A. Polkovnikov, *SciPost Phys.* **2**, 021 (2017).

[40] A. Morvan, *et al.*, *Nature* **612**, 240 (2022).

[41] X. Zotos, P. Prelovšek, *Phys. Rev. B* **53**, 983 (1996).

[42] M. Žnidarič, *Phys. Rev. Lett.* **106**, 220601 (2011).

[43] The current from Q_{26} to $Q_{\mathrm{a},2}$ should in principle be subtracted from $J(Q_1)$ to account for the particle loss into the drain. Since we are focusing on early time ($d < 15$) dynamics, this current is near or exactly 0 and does not affect the transport exponent. See SM for an explicit verification.

[44] B. Buča, C. Booker, M. Medenjak, D. Jaksch, *New J. Phys.* **22**, 123040 (2020).

[45] T. c. v. Prosen, *Phys. Rev. Lett.* **107**, 137201 (2011).

[46] E. Kapit, P. Roushan, C. Neill, S. Boixo, V. Smelyanskiy, *Phys. Rev. Res.* **2**, 043042 (2020).

[47] N. C. Harris, *et al.*, *Nat. Photonics* **11**, 447 (2017).

[48] S. Diehl, E. Rico, M. A. Baranov, P. Zoller, *Nat. Phys.* **7**, 971 (2011).

[49] C.-E. Bardyn, *et al.*, *New J. Phys.* **15**, 085001 (2013).

[50] E. Kapit, M. Hafezi, S. H. Simon, *Phys. Rev. X* **4**, 031039 (2014).

[51] X. Mi, *et al.*, *Nature* **601**, 531 (2022).

[52] X. Mi, *et al.*, *Science* **374**, 1479 (2021).

[53] P. V. Klimov, *et al.*, *Phys. Rev. Lett.* **121**, 090502 (2018).

[54] P. V. Klimov, J. Kelly, J. M. Martinis, H. Neven, *Preprint at https://arxiv.org/abs/2006.04594* (2020).

[55] F. Arute, *et al.*, *Nature* **574**, 505 (2019).

[56] C. Neill, *et al.*, *Nature* **594**, 508 (2021).

[57] K. W. Murch, *et al.*, *Phys. Rev. Lett.* **109**, 183602 (2012).

[58] Y. Lu, *et al.*, *Phys. Rev. Lett.* **119**, 150502 (2017).

[59] A. M. Kaufman, *et al.*, *Science* **353**, 794 (2016).

[60] J. C. Hoke, *et al.*, *Nature* **622**, 481 (2023).

[61] I. Peschel, *Journal of Physics A: Mathematical and General* **36**, L205 (2003).

[62] Z. Jiang, K. J. Sung, K. Kechedzhi, V. N. Smelyanskiy, S. Boixo, *Phys. Rev. Appl.* **9**, 044036 (2018).

[63] F. Verstraete, J. J. García-Ripoll, J. I. Cirac, *Phys. Rev. Lett.* **93**, 207204 (2004).

[64] G. Vidal, *Phys. Rev. Lett.* **93**, 040502 (2004).

[65] M. Fishman, S. R. White, E. M. Stoudenmire, *SciPost Phys. Codebases* p. 4 (2022).

[66] B. Li, J. Wang, *Phys. Rev. Lett.* **91**, 044301 (2003).

From Stark many-body localization

References

[350] P. W. Anderson, Phys. Rev. **109**, 1492 (1958).

[2] E. Abrahams, P. W. Anderson, D. C. Licciardello, and T. V. Ramakrishnan, Phys. Rev. Lett. **42**, 673 (1979).

[3] D. M. Basko, I. L. Aleiner, and B. L. Altshuler, Ann. Phys. (N. Y). **321**, 1126 (2006).

[359] I. V. Gornyi, A. D. Mirlin, and D. G. Polyakov, Phys. Rev. Lett. **95**, 206603 (2005).

[5] J. Z. Imbrie, J. Stat. Phys. **163**, 998 (2016).

[6] R. Nandkishore and D. A. Huse, Annu. Rev. Condens. Matter Phys. **6**, 15 (2014).

[7] D. A. Huse, R. Nandkishore, and V. Oganesyan, Phys. Rev. B **90**, 174202 (2014).

[8] M. Žnidarič, T. Prosen, and P. Prelovšek, Physical Review B **77**, 064426 (2008).

[9] J. H. Bardarson, F. Pollmann, and J. E. Moore, Phys. Rev. Lett. **109**, 017202 (2012).

[10] M. Serbyn, Z. Papić, and D. A. Abanin, Phys. Rev. Lett. **110**, 260601 (2013).

[11] R. Vosk, D. A. Huse, and E. Altman, Phys. Rev. X **5**, 031032 (2015).

[12] K. Agarwal, S. Gopalakrishnan, M. Knap, M. Müller, and E. Demler, Phys. Rev. Lett. **114**, 160401 (2015).

[13] M. Žnidarič, A. Scardicchio, and V. K. Varma, Phys. Rev. Lett. **117**, 040601 (2016).

[14] Y. Bar Lev, G. Cohen, and D. R. Reichman, Phys. Rev. Lett. **114**, 100601 (2015).

[15] M. Schreiber, S. S. Hodgman, P. Bordia, H. P. Lüschen, M. H. Fischer, R. Vosk, E. Altman, U. Schneider, and I. Bloch, Science **349**, 842 (2015).

[16] P. Bordia, H. Lüschen, S. Scherg, S. Gopalakrishnan, M. Knap, U. Schneider, and I. Bloch, Phys. Rev. X **7**, 041047 (2017).

[13] J.-Y. Choi, S. Hild, J. Zeiher, P. Schauß, A. Rubio-Abadal, T. Yefsah, V. Khemani, D. A. Huse, I. Bloch, and C. Gross, Science **352**, 1547 (2016).

[18] M. Rigol, V. Dunjko, V. Yurovsky, and M. Olshanii, Phys. Rev. Lett. **98**, 050405 (2007).

[13] T. Kinoshita, T. Wenger, and D. S. Weiss, Nature **440**, 900 (2006).

[37] M. Van Horssen, E. Levi, and J. P. Garrahan, Phys. Rev. B **92**, 100305(R) (2015).

[21] J. M. Hickey, S. Genway, and J. P. Garrahan, J. Stat. Mech. Theory Exp. **5**, 054047 (2016).

[22] W. De Roeck and F. Huveneers, Commun. Math. Phys. **332**, 1017 (2014).

[23] A. Smith, J. Knolle, R. Moessner, and D. L. Kovrizhin, Phys. Rev. Lett. **119**, 176601 (2017).

[24] N. Y. Yao, C. R. Laumann, J. I. Cirac, M. D. Lukin, and J. E. Moore, Phys. Rev. Lett. **117**, 240601 (2016).

[25] A. Bols and W. De Roeck, J. Math. Phys. **59**, 021901 (2018).

[2] G. Wannier, Rev. Mod. Phys. **34**, 645 (1962).

[27] For a treatment of a metal-insulator transition in a uniform electric field, see [34].

[28] C. Hooley and J. Quintanilla, Phys. Rev. Lett. **93**, 080404 (2004).

[29] See Supplemental Material below for further details.

[30] A. Polkovnikov, Ann. Phys. (N. Y). **326**, 486 (2011).

[9] V. Oganesyan and D. A. Huse, Phys. Rev. B **75**, 155111 (2007).

[32] D. J. Luitz, N. Laflorencie, and F. Alet, Phys. Rev. B **91**, 081103(R) (2015).

[33] E. P. L. van Nieuwenburg, Y. Baum, and G. Refael, arXiv:1808.00471 (2018).

[34] V. Prigodin and B. Altshuler, Phys. Lett. A **137**, 301 (1989).

From Transport in Stark MB Loca Syst

References

[357] D. Basko, I. L. Aleiner, and B. L. Altshuler, Metal-insulator transition in a weakly interacting many-electron system with localized single-particle states, Ann. Phys. **321**, 1126 (2006).

[359] I. V. Gornyi, A. Mirlin, and D. Polyakov, Interacting Electrons in Disordered Wires: Anderson Localization and Low-T Transport, Phys. Rev. Lett. **95**, 206603 (2005).

[3] E. Altman and R. Vosk, Universal Dynamics and Renormalization in Many-Body-Localized Systems, Annu. Rev. Condens. Matter Phys. **6**, 383 (2015).

[356] R. Nandkishore and D. A. Huse, Many-Body Localization and Thermalization in Quantum Statistical Mechanics, Annu. Rev. Condens. Matter Phys. **6**, 15 (2015).

[5] R. Vasseur and J. E. Moore, Nonequilibrium quantum dynamics and transport: From integrability to many-body localization, J. Stat. Mech. Theory Exp. **2016**, 064010 (2016).

[6] D. A. Abanin and Z. Papić, Recent progress in many-body localization, Ann. Phys. **529**, 1700169 (2017).

[7] D. A. Abanin, E. Altman, I. Bloch, and M. Serbyn, Colloquium: Many-body localization, thermalization, and entanglement, Rev. Mod. Phys. **91**, 021001 (2019).

[8] D. M. Basko, I. L. Aleiner, and B. L. Altshuler, Possible experimental manifestations of the many-body localization, Phys. Rev. B **76**, 052203 (2007).

[9] M. Ovadia, D. Kalok, I. Tamir, S. Mitra, B. Sacépé, and D. Shahar, Evidence for a Finite-Temperature Insulator, Sci. Rep. **5**, 13503 (2015).

[10] M. Schreiber, S. S. Hodgman, P. Bordia, H. P. Luschen, M. H. Fischer, R. Vosk, E. Altman, U. Schneider, and I. Bloch, Observation of many-body localization of interacting fermions in a quasirandom optical lattice, Science **349**, 842 (2015).

[11] P. Bordia, H. P. Lüschen, S. S. Hodgman, M. Schreiber, I. Bloch, and U. Schneider, Coupling Identical one-dimensional Many-Body Localized Systems, Phys. Rev. Lett. **116**, 140401 (2016).

[12] J. Smith, A. Lee, P. Richerme, B. Neyenhuis, P. W. Hess, P. Hauke, M. Heyl, D. A. Huse, and C. Monroe, Many-body localization in a quantum simulator with programmable random disorder, Nat. Phys. **12**, 907 (2016).

[13] J.-Y. Choi, S. Hild, J. Zeiher, P. Schauss, A. Rubio-Abadal, T. Yefsah, V. Khemani, D. A. Huse, I. Bloch, and C. Gross, Exploring the many-body localization transition in two dimensions, Science **352**, 1547 (2016).

[14] M. Žnidarič, Dephasing-induced diffusive transport in the anisotropic Heisenberg model, New J. Phys. **12**, 043001 (2010).

[15] S. Gopalakrishnan, K. R. Islam, and M. Knap, Noise-Induced Subdiffusion in Strongly Localized Quantum Systems, Phys. Rev. Lett. **119**, 046601 (2017).

[16] A. Lazarides, A. Das, and R. Moessner, Fate of Many-Body Localization Under Periodic Driving, Phys. Rev. Lett. **115**, 030402 (2015).

[17] P. Ponte, Z. Papić, F. Huveneers, and D. A. Abanin, Many-Body Localization in Periodically Driven Systems, Phys. Rev. Lett. **114**, 140401 (2015).

[18] D. A. Abanin, W. De Roeck, and F. Huveneers, Theory of many-body localization in periodically driven systems, Ann. Phys. **372**, 1 (2016).

[19] E. Bairey, G. Refael, and N. H. Lindner, Driving induced many-body localization, Phys. Rev. B **96**, 020201 (2017).

[367] J. Z. Imbrie, On Many-Body Localization for Quantum Spin Chains, J. Stat. Phys. **163**, 998 (2016).

[21] P. W. Anderson, Absence of Diffusion in Certain Random Lattices, Phys. Rev. **109**, 1492 (1958).

[22] R. Nandkishore and A. C. Potter, Marginal Anderson localization and many-body delocalization, Phys. Rev. B **90**, 195115 (2014).

[23] X. Li, S. Ganeshan, J. H. Pixley, and S. Das Sarma, Many-Body Localization and Quantum Nonergodicity in a Model with a Single-Particle Mobility Edge, Phys. Rev. Lett. **115**, 186601 (2015).

[24] X. Li, J. H. Pixley, D.-L. Deng, S. Ganeshan, and S. Das Sarma, Quantum nonergodicity and fermion localization in a system with a single-particle mobility edge, Phys. Rev. B **93**, 184204 (2016).

[25] R. Modak, S. Ghosh, and S. Mukerjee, Criterion for the occurrence of many-body localization in the presence of a single-particle mobility edge, Phys. Rev. B **97**, 104204 (2018).

[26] R. Modak and S. Mukerjee, Many-Body Localization in the Presence of a Single-Particle Mobility Edge, Phys. Rev. Lett. **115**, 230401 (2015).

[27] K. Hyatt, J. R. Garrison, A. C. Potter, and B. Bauer, Many-body localization in the presence of a small bath, Phys. Rev. B **95**, 035132 (2017).

[28] Y. Bar Lev, D. R. Reichman, and Y. Sagi, Many-body localization in system with a completely delocalized single-particle spectrum, Phys. Rev. B **94**, 201116 (2016).

[29] R. Vasseur, A. J. Friedman, S. A. Parameswaran, and A. C. Potter, Particle-hole symmetry, many-body localization, and topological edge modes, Phys. Rev. B **93**, 134207 (2016).

[376] G. Carleo, F. Becca, M. Schiró, and M. Fabrizio, Localization and glassy dynamics of many-body quantum systems, Sci. Rep. **2**, 243 (2012).

[31] M. Schiulaz and M. Müller, Ideal quantum glass transitions: Many-body localization without quenched disorder, in AIP Conf. Proc., Vol. 1610 (American Institute of Physics, 2014) p. 11.

[32] T. Grover and M. P. A. Fisher, Quantum Disentangled Liquids, J. Stat. Mech. Theory Exp. **2014**, P10010 (2013).

[33] M. Schiulaz, A. Silva, and M. Müller, Dynamics in many-body localized quantum systems without disorder, Phys. Rev. B **91**, 184202 (2015).

[375] N. Y. Yao, C. R. Laumann, J. I. Cirac, M. D. Lukin, and J. E. Moore, Quasi-Many-Body Localization in Translation-Invariant Systems, Phys. Rev. Lett. **117**, 240601 (2016).

[35] J. M. Hickey, S. Genway, and J. P. Garrahan, Signatures of many-body localisation in a system without disorder and the relation to a glass transition, J. Stat. Mech. Theory Exp. **2016**, 054047 (2016).

[36] Z. Papić, E. M. Stoudenmire, and D. A. Abanin, Many-body localization in disorder-free systems: The importance of finite-size constraints, Ann. Phys. **362**, 714 (2015).

[37] M. Van Horssen, E. Levi, and J. P. Garrahan, Dynamics of many-body localization in a translation-invariant quantum glass model, Phys. Rev. B **92**, 100305 (2015).

[38] M. Pino, L. B. Ioffe, and B. L. Altshuler, Nonergodic metallic and insulating phases of Josephson junction chains, Proc. Natl. Acad. Sci. **113**, 536 (2016).

[39] D. H. Dunlap and V. M. Kenkre, Dynamic localization of a charged particle moving under the influence of an electric field, Phys. Rev. B **34**, 3625 (1986).

[40] D. Dunlap and V. Kenkre, Dynamic localization of a particle in an electric field viewed in momentum space: Connection with Bloch oscillations, Phys. Lett. A **127**, 438 (1988).

[41] G. H. Wannier, Wave Functions and Effective Hamiltonian for Bloch Electrons in an Electric Field, Phys. Rev. **117**, 432 (1960).

[42] Y. Bar Lev, D. J. Luitz, A. Lazarides, Y. B. Lev, and A. Lazarides, Absence of dynamical localization in interacting driven systems, SciPost Phys. **3**, 029 (2017).

[43] M. Schulz, C. A. Hooley, R. Moessner, and F. Pollmann, Stark Many-Body Localization, Phys. Rev. Lett. **122**, 040606 (2019).

[44] E. van Nieuwenburg, Y. Baum, and G. Refael, From Bloch oscillations to many-body localization in clean interacting systems, Proc. Natl. Acad. Sci. **116**, 9269 (2019).

[45] A. A. Michailidis, M. Žnidarič, M. Medvedyeva, D. A. Abanin, T. Prosen, and Z. Papić, Slow dynamics in translation-invariant quantum lattice models, Phys. Rev. B **97**, 104307 (2018).

[46] S. Pai, M. Pretko, and R. M. Nandkishore, Localization in Fractonic Random Circuits, Phys. Rev. X **9**, 021003 (2019).

[47] V. Khemani, M. Hermele, and R. Nandkishore, Localization from Hilbert space shattering: From theory to physical realizations, Phys. Rev. B **101**, 174204 (2020).

[48] See supplemental material at [URL] for analysis of the spectral statistics, and additional analysis of the magnus expansion.

[49] P. Zhang, Subdiffusion in strongly tilted lattice systems, Phys. Rev. Res. **2**, 033129 (2020).

[50] E. V. H. Doggen, I. V. Gornyi, and D. G. Polyakov, Stark many-body localization: Evidence for Hilbert-space shattering, Phys. Rev. B **103**, L100202 (2021).

[51] E. Guardado-Sanchez, A. Morningstar, B. M. Spar, P. T. Brown, D. A. Huse, and W. S. Bakr, Subdiffusion and Heat Transport in a Tilted Two-Dimensional Fermi-Hubbard System, Phys. Rev. X **10**, 011042 (2020).

[52] W. Morong, F. Liu, P. Becker, K. S. Collins, L. Feng, A. Kyprianidis, G. Pagano, T. You, A. V. Gorshkov, and C. Monroe, Observation of Stark Many-Body Localization without Disorder, Tech. Rep. (2021).

[53] S. Scherg, T. Kohlert, P. Sala, F. Pollmann, B. Hebbe Madhusudhana, I. Bloch, and M. Aidelsburger, Observing non-ergodicity due to kinetic constraints in tilted Fermi-Hubbard chains, Nat. Commun. **12**, 4490 (2021).

[54] R. Yao, T. Chanda, and J. Zakrzewski, Nonergodic dynamics in disorder-free potentials, Ann. Phys. , 168540 (2021).

[55] P. Jordan and E. Wigner, über das Paulische Äuivalenzverbot, Z. Für Phys. **47**, 631 (1928).

[56] R. Steinigeweg, H. Wichterich, and J. Gemmer, Density dynamics from current auto-correlations at finite time- and length-scales, EPL Europhys. Lett. **88**, 10004 (2009).

[57] Y. Yan, F. Jiang, and H. Zhao, Energy spread and current-current correlation in quantum systems, Eur. Phys. J. B **88**, 11 (2015).

[58] D. J. Luitz and Y. Bar Lev, The ergodic side of the many-body localization transition, Ann. Phys. **529**, 1600350 (2017).

[59] R. Steinigeweg, F. Jin, D. Schmidtke, H. De Raedt, K. Michielsen, and J. Gemmer, Real-time broadening of nonequilibrium density profiles and the role of the specific initial-state realization, Phys. Rev. B **95**, 035155 (2017).

[60] S. Popescu, A. J. Short, and A. Winter, Entanglement and the foundations of statistical mechanics, Nat. Phys. **2**, 754 (2006).

[61] C. Moler and C. Van Loan, Nineteen dubious ways to compute the exponential of a matrix, twenty-five years later, SIAM Rev. **45**, 3 (2003).

[62] U. Schollwöck, The density-matrix renormalization group in the age of matrix product states, Ann. Phys. **326**, 96 (2011).

[63] D. Kennes and C. Karrasch, Extending the range of real time density matrix renormalization group simulations, Computer Physics Communications **200**, 37 (2016).

[64] P. Zhang, Subdiffusion in strongly tilted lattice systems, Phys. Rev. Res. **2**, 33129 (2020).

[65] A. Gromov, A. Lucas, and R. M. Nandkishore, Fracton hydrodynamics, Phys. Rev. Res. **2**, 033124 (2020).

[66] J. Feldmeier, P. Sala, G. De Tomasi, F. Pollmann, and M. Knap, Anomalous Diffusion in Dipole- and Higher-Moment-Conserving Systems, Phys. Rev. Lett. **125**, 245303 (2020).

[38] The entanglement entropy here would be an entanglement of an MPO, which is also not a measurable physical quantity.

[68] D. A. Abanin, W. De Roeck, and F. F. Huveneers, Exponentially Slow Heating in Periodically Driven Many-Body Systems, Phys. Rev. Lett. **115**, 256803 (2015).

[69] D. A. Abanin, W. De Roeck, W. W. Ho, and F. Huveneers, Effective Hamiltonians, prethermalization, and slow energy absorption in periodically driven many-body systems, Phys. Rev. B **95**, 014112 (2017).

[70] D. A. Abanin, W. De Roeck, W. W. Ho, F. Huveneers, W. D. Roeck, W. W. Ho, and F. Huveneers, A Rigorous Theory of Many-Body Prethermalization for Periodically Driven and Closed Quantum Systems, Commun Math Phys **354**, 809 (2017).

[71] S. Blanes, F. Casas, J. A. Oteo, and J. Ros, The Magnus expansion and some of its applications, Phys. Rep. **470**, 151 (2009).

[72] T. Mori, T. Kuwahara, and K. Saito, Rigorous Bound on Energy Absorption and Generic Relaxation in Periodically Driven Quantum Systems, Phys. Rev. Lett. **116**, 120401 (2016).

[73] T. Kuwahara, T. Mori, and K. Saito, Floquet-Magnus theory and generic transient dynamics in periodically driven many-body quantum systems, Ann. Phys. **367**, 96 (2016).

From An Open-System Quantum Simulator with Trapped Ions

References

[1] Ladd, T. D., Jelezko, F., Laflamme, R., Nakamura, Y., Monroe, C. et al. Quantum computers. Nature **464**, 45–53 (2010)

[2] Kimble, H. J. The quantum internet. Nature **453**, 1023–1030 (2008)

[3] Schoelkopf, R. J. & Girvin, S. M. Wiring up quantum systems. Nature **451**, 664–669 (2008)

[4] Neeley, M., Bialczak, R. C., Lenander, M., Lucero, E., Mariantoni, M. et al. Generation of three-qubit entangled states using superconducting phase qubits. Nature **467**, 570–573 (2010)

[5] Saffman, M., Walker, T. G. & Mølmer, K. Quantum information with Rydberg atoms. Rev. Mod. Phys. **82**, 2313–2363 (2010)

[6] Bloch, I., Dalibard, J. & Zwerger, W. Many-body physics with ultracold gases. Rev. Mod. Phys. **80**, 885–964 (2008)

[7] O'Brien, J. L. Optical quantum computing. Science **318**, 1567–1570 (2007)

[8] Clarke, J. & Wilhelm, F. K. Superconducting quantum bits. Nature **453**, 1031–1042 (2008)

[9] Hanson, R., Kouwenhoven, L. P., Petta, J. R., Tarucha, S. & Vandersypen, L. M. K. Spins in few-electron quantum dots. Rev. Mod. Phys. **79**, 1217–1265 (2007)

[10] Wrachtrup, J. & Jelezko, F. Processing quantum information in diamond. J. Phys.: Condens. Matter **18**, S807–S824 (2006)

[11] Feynman, R. Simulating physics with computers. Int. J. Theor. Phys. **21**, 467–488 (1982)

[12] Lloyd, S. Universal quantum simulators. Science **273**, 1073–1078 (1996)

[13] Buluta, I. & Nori, F. Quantum simulators. Science **326**, 108–111 (2009)

[14] Myatt, C. J. et al. Decoherence of quantum superpositions through coupling to engineered reservoirs. Nature **403**, 269–273 (2000)

[15] Deleglise, S., Dotsenko, I., Sayrin, C., Bernu, J., Brune, M. et al. Reconstruction of non-classical cavity field states with snapshots of their decoherence. Nature **455**, 510–514 (2008)

[16] Barreiro, J. T., Schindler, P., Gühne, O., Monz, T., Chwalla, M. et al. Experimental multiparticle entanglement dynamics induced by decoherence. Nature Phys. (2010). Advance Online Publication, doi:10.1038/nphys1781

[17] Krauter, H., Muschik, C. A., Jensen, K., Wasilewski, W., Petersen, J. M. et al. Entanglement generated by dissipation. arXiv:1006.4344 (2010)

[18] Diehl, S. et al. Quantum states and phases in driven open quantum systems with cold atoms. Nature Phys. **4**, 878–883 (2008)

[19] Cho, J., Bose, S. & Kim, M. S. Optical pumping into many-body entanglement. arXiv:1008.4088 (2010)

[20] Goldstein, G., Cappellaro, P., Maze, J. R., Hodges, J. S., Jiang, L. et al. Environment-assisted precision measurement. arXiv:1001.0089 (2010)

[21] Diehl, S., Yi, W., Daley, A. & Zoller, P. Driven dissipative d-wave pairing of atomic fermions. arXiv:1007.3420 (2010)

[22] Verstraete, F., Wolf, M. M. & Cirac, J. I. Quantum computation and quantum-state engineering driven by dissipation. Nature Phys. **5**, 633–636 (2009)

[23] Häffner, H., Roos, C. F. & Blatt, R. Quantum computing with trapped ions. Phys. Rep. **469**, 155–203 (2008)

[24] Home, J. P., Hanneke, D., Jost, J. D., Amini, J. M., Leibfried, D. et al. Complete methods set for scalable ion trap quantum information processing. Science **325**, 1227–1230 (2009)

[25] Kitaev, A. Y. Fault-tolerant quantum computation by anyons. Ann. Phys. **303**, 2 – 30 (2003)

[26] Nielsen, M. A. & Chuang, I. L. Quantum Computation and Quantum Information. Cambridge University Press (2000)

[27] Steane, A. M. Efficient fault-tolerant quantum computing. Nature **399**, 124–126 (1999)

[28] Lloyd, S. & Viola, L. Engineering quantum dynamics. Phys. Rev. A **65**, 010101 (2001)

[29] Dür, W., Bremner, M. J. & Briegel, H. J. Quantum simulation of interacting high-dimensional systems: The influence of noise. Phys. Rev. A **78**, 052325 (2008)

[30] Wiseman, H. M. & Milburn, G. J. Quantum Measurement and Control. Cambridge University Press (2009)

[31] Schmidt-Kaler, F. et al. How to realize a universal quantum gate with trapped ions. App. Phys. B **77**, 789–796 (2003)

[32] Mølmer, K. & Sørensen, A. Multiparticle entanglement of hot trapped ions. Phys. Rev. Lett. **82**, 1835–1838 (1999)

[33] Roos, C. F. Ion trap quantum gates with amplitude-modulated laser beams. New J. Phys. **10**, 013002 (2008)

[34] Monz, T. et al. Coherence of large-scale entanglement. arXiv:1009.6126 (2010)

[35] Schindler, P. et al. Experimental repetitive quantum error correction. In preparation (2010)

[36] Roos, C. F. et al. Control and measurement of three-qubit entangled states. Science **304**, 1478–1480 (2004)

[37] Gilchrist, A., Langford, N. K. & Nielsen, M. A. Distance measures to compare real and ideal quantum processes. Phys. Rev. A **71**, 062310 (2005)

[38] Jozsa, R. Fidelity for mixed quantum states. J. Mod. Opt. **41**, 2315–2353 (1994)

[39] Sackett, C. A. et al. Experimental entanglement of four particles. Nature **404**, 256–259 (2000)

[40] Gühne, O. & Seevinck, M. Separability criteria for genuine multiparticle entanglement. New J. Phys. **12**, 053002 (2010)

[41] Friedenauer, A., Schmitz, H., Glueckert, J., Porras, D. & Schaetz, T. Simulating a quantum magnet with trapped ions. Nature Phys. **4**, 757–761 (2008)

[42] Kim, K., Chang, M.-S., Korenblit, S., Islam, R., Edwards, E. E. et al. Quantum simulation of frustrated ising spins with trapped ions. Nature **465**, 590–593 (2010)

[43] Porras, D. & Cirac, J. I. Effective quantum spin systems with trapped ions. Phys. Rev. Lett. **92**, 207901 (2004)

[44] Müller, M., Hammerer, K., Zhou, Y., Roos, C. F. & Zoller, P. Open-system quantum simulation with trapped ions. In preparation (2010)

[45] Nayak, C., Simon, S. H., Stern, A., Freedman, M. & Das Sarma, S. Non-abelian anyons and topological quantum computation. Rev. Mod. Phys. **80**, 1083–1159 (2008)

[46] Moessner, R. & Sondhi, S. L. Resonating valence bond phase in the triangular lattice quantum dimer model. Phys. Rev. Lett. **86**, 1881–1884 (2001)

[47] Ralph, T. C., Bartlett, S. D., OBrien, J. L., Pryde, G. J. & Wiseman, H. M. Quantum nondemolition measurements for quantum information. Phys. Rev. A **73**, 012113 (2006)

[48] Fleming, G. R., Huelga, S. & Plenio, M., editors. Focus on Quantum Effects and Noise in Biomolecules, New J. Phys., volume 12. Institute of Physics (2010)

[49] R. Schmied, J. H. W. & Leibfried, D. Optimal surface-electrode trap lattices for quantum simulation with trapped ions. Phys. Rev. Lett. **102**, 233002 (2009)

[50] Weimer, H., Müller, M., Lesanovsky, I., Zoller, P. & Büchler, H. P. A Rydberg quantum simulator. Nature Phys. **6**, 382–388 (2010)

From Suppl-An Open-System Quantum Simulator with Trapped Ions

References

[1] Barrett, M. D., J. Chiaverini, T. Schaetz, J. Britton, W. M. Itano, J. D. Jost, E. Knill, C. Langer, D. Leibfried, R. Ozeri, and D. J. Wineland, 2004, Nature **429** (6993), 737

[2] Bouwmeester, D., et al., 1997, Nature **390**, 575

[3] Gilchrist, A., N. K. Langford, and M. A. Nielsen, 2005, Phys. Rev. A **71**, 062310

[4] Jezek, M., J. Fiurasek, and Z. Hradil, 2003, Phys. Rev. A **68** (1), 012305

[5] Jozsa, R., 1994, J. Mod. Opt. **41** (12), 2315

[6] Kitaev, A. Y., 2003, Ann. Phys. **303** (1), 2

[7] Lu, C.-Y., W.-B. Gao, O. Gühne, X.-Q. Zhou, Z.-B. Chen, and J.-W. Pan, 2009, Phys. Rev. Lett. **102** (3), 030502

[8] Monz, T., et al., 2010, arXiv:1009.6126

[9] Müller, M., K. Hammerer, Y. Zhou, C. F. Roos, and P. Zoller, 2010, In preparation

[10] Nebendahl, V., H. Häffner, and C. F. Roos, 2009, Phys. Rev. A **79** (1), 012312

[11] Pachos, J. K., W. Wieczorek, C. Schmid, N. Kiesel, R. Pohlner, and H. Weinfurter, 2009, New J. Phys. **11** (8), 083010

[12] Ralph, T. C., S. D. Bartlett, J. L. OBrien, G. J. Pryde, and H. M. Wiseman, 2006, Phys. Rev. A **73** (1), 012113

[13] Riebe, M., H. Häffner, C. F. Roos, W. Hänsel, J. Benhelm, G. P. T. Lancaster, T. W. Körber, C. Becher, F. Schmidt-Kaler, D. F. V. James, and R. Blatt, 2004, Nature **429** (6993), 734

From Collective Excitations and Nonequilibrium Phase Transition in Dissipative Fermionic Superfluids

References

[1] P. W. Anderson, "Random-Phase Approximation in the Theory of Superconductivity," Phys. Rev. **112**, 1900 (1958).

[2] A. Leggett, "Number-phase fluctuations in two-band superconductors," Prog. Theor. Phys. **36**, 901 (1966).

[3] A. Volkov and S. M. Kogan, "Collisionless relaxation of the energy gap in superconductors," Sov. Phys. JETP **38**, 1018 (1974).

[4] P. B. Littlewood and C. M. Varma, "Gauge-Invariant Theory of the Dynamical Interaction of Charge Density Waves and Superconductivity," Phys. Rev. Lett. **47**, 811 (1981).

[5] P. B. Littlewood and C. M. Varma, "Amplitude collective modes in superconductors and their coupling to charge-density waves," Phys. Rev. B **26**, 4883 (1982).

[6] C. M. Varma, "Higgs boson in superconductors," J. Low Temp. Phys. **126**, 901 (2002).

[7] A. V. Andreev, V. Gurarie, and L. Radzihovsky, "Nonequilibrium Dynamics and Thermodynamics of a Degenerate Fermi Gas Across a Feshbach Resonance," Phys. Rev. Lett. **93**, 130402 (2004).

[8] R. A. Barankov, L. S. Levitov, and B. Z. Spivak, "Collective Rabi Oscillations and Solitons in a Time-Dependent BCS Pairing Problem," Phys. Rev. Lett. **93**, 160401 (2004).

[9] R. A. Barankov and L. S. Levitov, "Dynamical selection in developing fermionic pairing," Phys. Rev. A **73**, 033614 (2006).

[10] E. A. Yuzbashyan and M. Dzero, "Dynamical Vanishing of the Order Parameter in a Fermionic Condensate," Phys. Rev. Lett. **96**, 230404 (2006).

[11] R. A. Barankov and L. S. Levitov, "Synchronization in the BCS Pairing Dynamics as a Critical Phenomenon," Phys. Rev. Lett. **96**, 230403 (2006).

[12] E. A. Yuzbashyan, O. Tsyplyatyev, and B. L. Altshuler, "Relaxation and Persistent Oscillations of the Order Parameter in Fermionic Condensates," Phys. Rev. Lett. **96**, 097005 (2006).

[13] V. Gurarie, "Nonequilibrium Dynamics of Weakly and Strongly Paired Superconductors," Phys. Rev. Lett. **103**, 075301 (2009).

[14] E. A. Yuzbashyan, M. Dzero, V. Gurarie, and M. S. Foster, "Quantum quench phase diagrams of an s-wave BCS-BEC condensate," Phys. Rev. A **91**, 033628 (2015).

[15] S. Hannibal, P. Kettmann, M. D. Croitoru, A. Vagov, V. M. Axt, and T. Kuhn, "Quench dynamics of an ultracold Fermi gas in the BCS regime: Spectral properties and confinement-induced breakdown of the Higgs mode," Phys. Rev. A **91**, 043630 (2015).

[16] P. Kettmann, S. Hannibal, M. D. Croitoru, V. M. Axt, and T. Kuhn, "Pure Goldstone mode in the quench dynamics of a confined ultracold Fermi gas in the BCS-BEC crossover regime," Phys. Rev. A **96**, 033618 (2017).

[17] S. Hannibal, P. Kettmann, M. D. Croitoru, V. M. Axt, and T. Kuhn, "Dynamical vanishing of the order parameter in a confined Bardeen-Cooper-Schrieffer Fermi gas after an interaction quench," Phys. Rev. A **97**, 013619 (2018).

[18] S. Hannibal, P. Kettmann, M. D. Croitoru, V. M. Axt, and T. Kuhn, "Persistent oscillations of the order parameter and interaction quench phase diagram for a confined Bardeen-Cooper-Schrieffer Fermi gas," Phys. Rev. A **98**, 053605 (2018).

[19] D. Pekker and C. Varma, "Amplitude/Higgs modes in condensed matter physics," Annu. Rev. Condens. Matter Phys. **6**, 269 (2015).

[20] R. Shimano and N. Tsuji, "Higgs Mode in Superconductors," Annu. Rev. Condens. Matter Phys. **11**, 103 (2020).

[21] U. Bissbort, S. Götze, Y. Li, J. Heinze, J. S. Krauser, M. Weinberg, C. Becker, K. Sengstock, and W. Hofstetter, "Detecting the Amplitude Mode of Strongly Interacting Lattice Bosons by Bragg Scattering," Phys. Rev. Lett. **106**, 205303 (2011).

[22] M. Endres, T. Fukuhara, D. Pekker, M. Cheneau, P. Schauβ, C. Gross, E. Demler, S. Kuhr, and I. Bloch, "The 'Higgs' amplitude mode at the two-dimensional superfluid/Mott insulator transition," Nature (London) **487**, 454 (2012).

[23] A. Behrle, T. Harrison, J. Kombe, K. Gao, M. Link, J.-S. Bernier, C. Kollath, and M. Köhl, "Higgs mode in a strongly interacting fermionic superfluid," Nat. Phys. **14**, 781 (2018).

[24] T. Harrison, M. Link, A. Behrle, K. Gao, A. Kell, J. Kombe, J.-S. Bernier, C. Kollath, and M. Köhl, "Decay and revival of a transient trapped Fermi condensate," arXiv:2007.11466 .

[25] R. Matsunaga, Y. I. Hamada, K. Makise, Y. Uzawa, H. Terai, Z. Wang, and R. Shimano, "Higgs Amplitude Mode in the BCS Superconductors $Nb_{1-x}Ti_xN$ Induced by Terahertz Pulse Excitation," Phys. Rev. Lett. **111**, 057002 (2013).

[26] R. Matsunaga, N. Tsuji, H. Fujita, A. Sugioka, K. Makise, Y. Uzawa, H. Terai, Z. Wang, H. Aoki, and R. Shimano, "Light-induced collective pseudospin precession resonating with Higgs mode in a superconductor," Science **345**, 1145 (2014).

[27] T. Papenkort, V. M. Axt, and T. Kuhn, "Coherent dynamics and pump-probe spectra of BCS superconductors," Phys. Rev. B **76**, 224522 (2007).

[28] T. Papenkort, T. Kuhn, and V. M. Axt, "Coherent control of the gap dynamics of BCS superconductors in the nonadiabatic regime," Phys. Rev. B **78**, 132505 (2008).

[29] A. P. Schnyder, D. Manske, and A. Avella, "Resonant generation of coherent phonons in a superconductor by ultrafast optical pump pulses," Phys. Rev. B **84**, 214513 (2011).

[30] M. Zachmann, M. D. Croitoru, A. Vagov, V. M. Axt, T. Papenkort, and T. Kuhn, "Ultrafast terahertz-field-induced dynamics of superconducting bulk and quasi-1D samples," New J. Phys. **15**, 055016 (2013).

[31] H. Krull, D. Manske, G. S. Uhrig, and A. P. Schnyder, "Signatures of nonadiabatic BCS state dynamics in pump-probe conductivity," Phys. Rev. B **90**, 014515 (2014).

[32] N. Tsuji and H. Aoki, "Theory of Anderson pseudospin resonance with Higgs mode in superconductors," Phys. Rev. B **92**, 064508 (2015).

[33] H. Krull, N. Bittner, G. Uhrig, D. Manske, and A. Schnyder, "Coupling of Higgs and Leggett modes in non-equilibrium superconductors," Nat. Commun. **7**, 11921 (2016).

[34] S. Sharapov, V. Gusynin, and H. Beck, "Effective action approach to the Leggett's mode in two-band superconductors," Eur. Phys. J. B **30**, 45 (2002).

[35] F. J. Burnell, J. Hu, M. M. Parish, and B. A. Bernevig, "Leggett mode in a strong-coupling model of iron arsenide superconductors," Phys. Rev. B **82**, 144506 (2010).

[36] N. Bittner, D. Einzel, L. Klam, and D. Manske, "Leggett Modes and the Anderson-Higgs Mechanism in Superconductors without Inversion Symmetry," Phys. Rev. Lett. **115**, 227002 (2015).

[37] T. Cea and L. Benfatto, "Signature of the Leggett mode in the A_{1g} Raman response: From MgB_2 to iron-based superconductors," Phys. Rev. B **94**, 064512 (2016).

[38] Y. Murotani, N. Tsuji, and H. Aoki, "Theory of light-induced resonances with collective Higgs and Leggett modes in multiband superconductors," Phys. Rev. B **95**, 104503 (2017).

[39] G. Lindblad, "On the generators of quantum dynamical semigroups," Commun. Math. Phys. **48**, 119 (1976).

[40] A. J. Daley, "Quantum trajectories and open many-body quantum systems," Adv. Phys. **63**, 77 (2014).

[41] Y. Ashida, S. Furukawa, and M. Ueda, "Parity-time-symmetric quantum critical phenomena," Nat. Commun. **8**, 15791 (2017).

[42] M. Nakagawa, N. Kawakami, and M. Ueda, "Non-Hermitian Kondo Effect in Ultracold Alkaline-Earth Atoms," Phys. Rev. Lett. **121**, 203001 (2018).

[43] S. Diehl, A. Tomadin, A. Micheli, R. Fazio, and P. Zoller, "Dynamical Phase Transitions and Instabilities in Open Atomic Many-Body Systems," Phys. Rev. Lett. **105**, 015702 (2010).

[44] M. Höning, M. Moos, and M. Fleischhauer, "Critical exponents of steady-state phase transitions in fermionic lattice models," Phys. Rev. A **86**, 013606 (2012).

[45] L. M. Sieberer, S. D. Huber, E. Altman, and S. Diehl, "Dynamical Critical Phenomena in Driven-Dissipative Systems," Phys. Rev. Lett. **110**, 195301 (2013).

[46] F. Damanet, E. Mascarenhas, D. Pekker, and A. J. Daley, "Controlling Quantum Transport via Dissipation Engineering," Phys. Rev. Lett. **123**, 180402 (2019).

[47] K. Yamamoto, Y. Ashida, and N. Kawakami, "Rectification in nonequilibrium steady states of open many-body systems," Phys. Rev. Research **2**, 043343 (2020).

[48] Y.-J. Han, Y.-H. Chan, W. Yi, A. J. Daley, S. Diehl, P. Zoller, and L.-M. Duan, "Stabilization of the p-wave superfluid state in an optical lattice," Phys. Rev. Lett. **103**, 070404 (2009).

[49] K. Yamamoto, M. Nakagawa, K. Adachi, K. Takasan, M. Ueda, and N. Kawakami, "Theory of Non-Hermitian Fermionic Superfluidity with a Complex-Valued Interaction," Phys. Rev. Lett. **123**, 123601 (2019).

[50] T. Tomita, S. Nakajima, I. Danshita, Y. Takasu, and Y. Takahashi, "Observation of the Mott insulator to superfluid crossover of a driven-dissipative Bose-Hubbard system," Sci. Adv. **3**, e1701513 (2017).

[51] G. Barontini, R. Labouvie, F. Stubenrauch, A. Vogler, V. Guarrera, and H. Ott, "Controlling the Dynamics of an Open Many-Body Quantum System with Localized Dissipation," Phys. Rev. Lett. **110**, 035302 (2013).

[52] R. Labouvie, B. Santra, S. Heun, S. Wimberger, and H. Ott, "Negative Differential Conductivity in an Interacting Quantum Gas," Phys. Rev. Lett. **115**, 050601 (2015).

[53] R. Labouvie, B. Santra, S. Heun, and H. Ott, "Bistability in a Driven-Dissipative Superfluid," Phys. Rev. Lett. **116**, 235302 (2016).

[54] H. P. Lüschen, P. Bordia, S. S. Hodgman, M. Schreiber, S. Sarkar, A. J. Daley, M. H. Fischer, E. Altman, I. Bloch, and U. Schneider, "Signatures of Many-Body Localization in a Controlled Open Quantum System," Phys. Rev. X **7**, 011034 (2017).

[55] M. J. Mark, E. Haller, K. Lauber, J. G. Danzl, A. Janisch, H. P. Büchler, A. J. Daley, and H.-C. Nägerl, "Preparation and Spectroscopy of a Metastable Mott-Insulator State with Attractive Interactions," Phys. Rev. Lett. **108**, 215302 (2012).

[56] K. Sponselee, L. Freystatzky, B. Abeln, M. Diem, B. Hundt, A. Kochanke, T. Ponath, B. Santra, L. Mathey, K. Sengstock, and C. Becker, "Dynamics of ultracold quantum gases in the dissipative Fermi–Hubbard model," Quantum Sci. Technol. **4**, 014002 (2018).

[57] R. Bouganne, M. B. Aguilera, A. Ghermaoui, J. Beugnon, and F. Gerbier, "Anomalous decay of coherence in a dissipative many-body system," Nat. Phys. **16**, 21 (2020).

[58] T. Tomita, S. Nakajima, Y. Takasu, and Y. Takahashi, "Dissipative Bose-Hubbard system with intrinsic two-body loss," Phys. Rev. A **99**, 031601(R) (2019).

[59] Y. Takasu, T. Yagami, Y. Ashida, R. Hamazaki, Y. Kuno, and Y. Takahashi, "PT-symmetric non-Hermitian quantum many-body system using ultracold atoms in an optical lattice with controlled dissipation," Prog. Theor. Exp. Phys. **2020**, 12A110 (2020).

[60] D. Witthaut, F. Trimborn, and S. Wimberger, "Dissipation Induced Coherence of a Two-Mode Bose-Einstein Condensate," Phys. Rev. Lett. **101**, 200402 (2008).

[61] I. Vidanović, D. Cocks, and W. Hofstetter, "Dissipation through localized loss in bosonic systems with long-range interactions," Phys. Rev. A **89**, 053614 (2014).

[62] M. Nakagawa, N. Tsuji, N. Kawakami, and M. Ueda, "Dynamical Sign Reversal of Magnetic Correlations in Dissipative Hubbard Models," Phys. Rev. Lett. **124**, 147203 (2020).

[63] M. Nakagawa, N. Kawakami, and M. Ueda, "Exact Liouvillian Spectrum of a One-Dimensional Dissipative Hubbard Model," Phys. Rev. Lett. **126**, 110404 (2021).

[64] R. Zhang, Y. Cheng, H. Zhai, and P. Zhang, "Orbital Feshbach Resonance in Alkali-Earth Atoms," Phys. Rev. Lett. **115**, 135301 (2015).

[65] M. Iskin, "Two-band superfluidity and intrinsic Josephson effect in alkaline-earth-metal Fermi gases across an orbital Feshbach resonance," Phys. Rev. A **94**, 011604(R) (2016).

[66] J. Xu, R. Zhang, Y. Cheng, P. Zhang, R. Qi, and H. Zhai, "Reaching a Fermi-superfluid state near an orbital Feshbach resonance," Phys. Rev. A **94**, 033609 (2016).

[67] L. He, J. Wang, S.-G. Peng, X.-J. Liu, and H. Hu, "Strongly correlated Fermi superfluid near an orbital Feshbach resonance: Stability, equation of state, and Leggett mode," Phys. Rev. A **94**, 043624 (2016).

[68] M. Höfer, L. Riegger, F. Scazza, C. Hofrichter, D. R. Fernandes, M. M. Parish, J. Levinsen, I. Bloch, and S. Fölling, "Observation of an Orbital Interaction-Induced Feshbach Resonance in ^{173}Yb," Phys. Rev. Lett. **115**, 265302 (2015).

[69] G. Pagano, M. Mancini, G. Cappellini, L. Livi, C. Sias, J. Catani, M. Inguscio, and L. Fallani, "Strongly Interacting Gas of Two-Electron Fermions at an Orbital Feshbach Resonance," Phys. Rev. Lett. **115**, 265301 (2015).

[70] G. Cappellini, L. F. Livi, L. Franchi, D. Tusi, D. Benedicto Orenes, M. Inguscio, J. Catani, and L. Fallani, "Coherent Manipulation of Orbital Feshbach Molecules of Two-Electron Atoms," Phys. Rev. X **9**, 011028 (2019).

[71] N. Darkwah Oppong, L. Riegger, O. Bettermann, M. Höfer, J. Levinsen, M. M. Parish, I. Bloch, and S. Fölling, "Observation of Coherent Multiorbital Polarons in a Two-Dimensional Fermi Gas," Phys. Rev. Lett. **122**, 193604 (2019).

[72] S. Smale, P. He, B. A. Olsen, K. G. Jackson, H. Sharum, S. Trotzky, J. Marino, A. M. Rey, and J. H. Thywissen, "Observation of a transition between dynamical phases in a quantum degenerate Fermi gas," Sci. Adv. **5**, eaax1568 (2019).

[73] J. A. Muniz, D. Barberena, R. J. Lewis-Swan, D. J. Young, J. R. Cline, A. M. Rey, and J. K. Thompson, "Exploring dynamical phase transitions with cold atoms in an optical cavity," Nature (London) **580**, 602 (2020).

[74] N. Syassen, D. M. Bauer, M. Lettner, T. Volz, D. Dietze, J. J. Garcia-Ripoll, J. I. Cirac, G. Rempe, and S. Dürr, "Strong dissipation inhibits losses and induces correlations in cold molecular gases," Science **320**, 1329 (2008).

[75] J. J. García-Ripoll, S. Dürr, N. Syassen, D. M. Bauer, M. Lettner, G. Rempe, and J. I. Cirac, "Dissipation-induced hard-core boson gas in an optical lattice," New J. Phys. **11**, 013053 (2009).

[76] S. Dürr, J. J. García-Ripoll, N. Syassen, D. M. Bauer, M. Lettner, J. I. Cirac, and G. Rempe, "Lieb-Liniger model of a dissipation-induced Tonks-Girardeau gas," Phys. Rev. A **79**, 023614 (2009).

[77] L. M. Sieberer, M. Buchhold, and S. Diehl, "Keldysh field theory for driven open quantum systems," Rep. Prog. Phys. **79**, 096001 (2016).

[78] A. Kamenev, Field theory of non-equilibrium systems (Cambridge University Press, Cambridge, England, 2011).

[79] B. Buča and T. Prosen, "A note on symmetry reductions of the Lindblad equation: transport in constrained open spin chains," New J. Phys. **14**, 073007 (2012).

[80] V. V. Albert and L. Jiang, "Symmetries and conserved quantities in Lindblad master equations," Phys. Rev. A **89**, 022118 (2014).

[81] See Supplemental Material, which includes Refs. [95, 96, 97], for detailed calculations of the time-dependent dissipative BCS theory, the operator formalism of the BCS theory for a dissipative superfluid, a generalization of the Bogoliubov-de Gennes analysis with a time-dependent BCS state, the dynamics of pseudospins after switch-on of dissipation, the dynamics after sudden change of both the interaction and the dissipation, and a simplified model for understanding the nonequilibrium phase transition. I am not sure, if it is true, since the articles look like they are on another topic.

[82] A. Spuntarelli, P. Pieri, and G. C. Strinati, "Josephson Effect throughout the BCS-BEC Crossover," Phys. Rev. Lett. **99**, 040401 (2007).

[83] G. Valtolina, A. Burchianti, A. Amico, E. Neri, K. Xhani, J. A. Seman, A. Trombettoni, A. Smerzi, M. Zaccanti, M. Inguscio, and G. Roati, "Josephson effect in fermionic superfluids across the BEC-BCS crossover," Science **350**, 1505 (2015).

[84] A. Burchianti, F. Scazza, A. Amico, G. Valtolina, J. A. Seman, C. Fort, M. Zaccanti, M. Inguscio, and G. Roati, "Connecting Dissipation and Phase Slips in a Josephson Junction between Fermionic Superfluids," Phys. Rev. Lett. **120**, 025302 (2018).

[85] N. Luick, L. Sobirey, M. Bohlen, V. P. Singh, L. Mathey, T. Lompe, and H. Moritz, "An ideal Josephson junction in an ultracold two-dimensional Fermi gas," Science **369**, 89 (2020).

[86] W. Kwon, G. Del Pace, R. Panza, M. Inguscio, W. Zwerger, M. Zaccanti, F. Scazza, and G. Roati, "Strongly correlated superfluid order parameters from dc Josephson supercurrents," Science **369**, 84 (2020).

[87] M. Tinkham, Introduction to superconductivity (Courier Corporation, 2004).

[88] B. Zhu, B. Gadway, M. Foss-Feig, J. Schachenmayer, M. L. Wall, K. R. A. Hazzard, B. Yan, S. A. Moses, J. P. Covey, D. S. Jin, J. Ye, M. Holland, and A. M. Rey, "Suppressing the Loss of Ultracold Molecules Via the Continuous Quantum Zeno Effect," Phys. Rev. Lett. **112**, 070404 (2014).

[89] A. J. Daley, J. M. Taylor, S. Diehl, M. Baranov, and P. Zoller, "Atomic Three-Body Loss as a Dynamical Three-Body Interaction," Phys. Rev. Lett. **102**, 040402 (2009).

[90] B. Yan, S. A. Moses, B. Gadway, J. P. Covey, K. R. Hazzard, A. M. Rey, D. S. Jin, and J. Ye, "Observation of dipolar spin-exchange interactions with lattice-confined polar molecules," Nature (London) **501**, 521 (2013).

[91] In Ref. [63], it is shown that exceptional points of a non-Hermitian Hamiltonian and a Liouvillian are the same when the system has either gain or loss. Thus, the Liouvillian under consideration exhibits the spectral singularity originating from the same exceptional points as those of the non-Hermitian BCS Hamiltonian [49].

[92] A. O. Caldeira and A. J. Leggett, "Influence of Dissipation on Quantum Tunneling in Macroscopic Systems," Phys. Rev. Lett. **46**, 211 (1981).

[93] A. Schmid, "Diffusion and Localization in a Dissipative Quantum System," Phys. Rev. Lett. **51**, 1506 (1983).

[94] F. Guinea, V. Hakim, and A. Muramatsu, "Diffusion and Localization of a Particle in a Periodic Potential Coupled to a Dissipative Environment," Phys. Rev. Lett. **54**, 263 (1985).

[95] N. Shibata and H. Katsura, "Dissipative spin chain as a non-Hermitian Kitaev ladder," Phys. Rev. B **99**, 174303 (2019).

[96] N. Shibata and H. Katsura, "Dissipative quantum Ising chain as a non-Hermitian Ashkin-Teller model," Phys. Rev. B **99**, 224432 (2019).

[97] H. T. C. Stoof, "Time-dependent Ginzburg-Landau theory for a weak-coupling superconductor," Phys. Rev. B **47**, 7979 (1993).

From Thermalization at Low Temperatures via Weakly-Damped Multi-Site Baths by Zanoci, Yoo, Swingle

References

[1] G. T. Landi, D. Poletti, and G. Schaller, Rev. Mod. Phys. **94**, 045006 (2022).

[2] B. Bertini, F. Heidrich-Meisner, C. Karrasch, T. Prosen, R. Steinigeweg, and M. Žnidarič, Rev. Mod. Phys. **93**, 025003 (2021).

[46] S. Diehl, A. Micheli, A. Kantian, B. Kraus, H. P. Büchler, and P. Zoller, Nat. Phys. **4**, 878 (2008).

[4] S. Diehl, A. Tomadin, A. Micheli, R. Fazio, and P. Zoller, Phys. Rev. Lett. **105**, 015702 (2010).

[5] M. Müller, S. Diehl, G. Pupillo, and P. Zoller, Engineered open systems and quantum simulations with atoms and ions, in Adv. At. Mol. Opt. Phys., Vol. 61 (Academic Press, 2012) pp. 1–80.

[6] H. Weimer, A. Kshetrimayum, and R. Orús, Rev. Mod. Phys. **93**, 015008 (2021).

[7] F. Verstraete, V. Murg, and J. Cirac, Adv. Phys. **57**, 143 (2008).

[8] U. Schollwöck, Ann. Phys. **326**, 96 (2011).

[9] R. Orús, Ann. Phys. **349**, 117 (2014).

[10] J. C. Bridgeman and C. T. Chubb, J. Phys. A: Math. Theor. **50**, 223001 (2017).

[11] J. I. Cirac, D. Pérez-García, N. Schuch, and F. Verstraete, Rev. Mod. Phys. **93**, 045003 (2021).

[12] A. J. Daley, Adv. Phys. **63**, 77 (2014).

[13] M. J. Hartmann and G. Carleo, Phys. Rev. Lett. **122**, 250502 (2019).

[14] N. Yoshioka and R. Hamazaki, Phys. Rev. B **99**, 214306 (2019).

[15] A. Nagy and V. Savona, Phys. Rev. Lett. **122**, 250501 (2019).

[16] F. Vicentini, A. Biella, N. Regnault, and C. Ciuti, Phys. Rev. Lett. **122**, 250503 (2019).

[17] M. Reh, M. Schmitt, and M. Gärttner, Phys. Rev. Lett. **127**, 230501 (2021).

[18] D. Luo, Z. Chen, J. Carrasquilla, and B. K. Clark, Phys. Rev. Lett. **128**, 090501 (2022).

[19] F. Verstraete, J. J. García-Ripoll, and J. I. Cirac, Phys. Rev. Lett. **93**, 207204 (2004).

[20] M. Zwolak and G. Vidal, Phys. Rev. Lett. **93**, 207205 (2004).

[21] H. Weimer, Phys. Rev. Lett. **114**, 040402 (2015).

[22] J. Cui, J. I. Cirac, and M. C. Bañuls, Phys. Rev. Lett. **114**, 220601 (2015).

[23] E. Mascarenhas, H. Flayac, and V. Savona, Phys. Rev. A **92**, 022116 (2015).

[24] A. H. Werner, D. Jaschke, P. Silvi, M. Kliesch, T. Calarco, J. Eisert, and S. Montangero, Phys. Rev. Lett. **116**, 237201 (2016).

[25] M. Brenes, J. J. Mendoza-Arenas, A. Purkayastha, M. T. Mitchison, S. R. Clark, and J. Goold, Phys. Rev. X **10**, 031040 (2020).

[26] S. Nakajima, Prog. Theor. Phys. **20**, 948 (1958).

[27] R. Zwanzig, J. Chem. Phys. **33**, 1338 (1960).

[28] A. G. Redfield, The theory of relaxation processes, in Advances in Magnetic and Optical Resonance, Vol. 1 (Academic Press, 1965) pp. 1–32.

[29] G. Lindblad, Comm. Math. Phys. **48**, 119 (1976).

[43] V. Gorini, A. Kossakowski, and E. C. G. Sudarshan, J. Math. Phys. **17**, 821 (1976).

[31] T. Prosen and M. Žnidarič, J. Stat. Mech.: Theory Exp. **2009** (02), P02035.

[32] M. Žnidarič, T. Prosen, G. Benenti, G. Casati, and D. Rossini, Phys. Rev. E **81**, 051135 (2010).

[33] M. Žnidarič, J. Stat. Mech.: Theory Exp. **2011** (12), P12008.

[34] M. Žnidarič, Phys. Rev. Lett. **106**, 220601 (2011).

[35] T. Prosen and M. Žnidarič, Phys. Rev. B **86**, 125118 (2012).

[36] M. Žnidarič, Phys. Rev. Lett. **110**, 070602 (2013).

[37] M. Žnidarič, Phys. Rev. B **88**, 205135 (2013).

[38] J. J. Mendoza-Arenas, S. Al-Assam, S. R. Clark, and D. Jaksch, J. Stat. Mech.: Theory Exp. **2013** (07), P07007.

[39] J. J. Mendoza-Arenas, S. R. Clark, and D. Jaksch, Phys. Rev. E **91**, 042129 (2015).

[40] J. J. Mendoza-Arenas, M. Žnidarič, V. K. Varma, J. Goold, S. R. Clark, and A. Scardicchio, Phys. Rev. B **99**, 094435 (2019).

[41] C. Zanoci and B. Swingle, Phys. Rev. B **103**, 115148 (2021).

[42] H. Wichterich, M. J. Henrich, H.-P. Breuer, J. Gemmer, and M. Michel, Phys. Rev. E **76**, 031115 (2007).

[43] A. Levy and R. Kosloff, EPL **107**, 20004 (2014).

[44] X. Xu, J. Thingna, and J.-S. Wang, Phys. Rev. B **95**, 035428 (2017).

[45] D. Tupkary, A. Dhar, M. Kulkarni, and A. Purkayastha, Phys. Rev. A **105**, 032208 (2022).

[46] D. Tupkary, A. Dhar, M. Kulkarni, and A. Purkayastha, Searching for lindbladians obeying local conservation laws and showing thermalization (2023), arXiv:2301.02146 .

[47] Ángel Rivas, A. D. K. Plato, S. F. Huelga, and M. B. Plenio, New J. Phys. **12**, 113032 (2010).

[48] A. Purkayastha, A. Dhar, and M. Kulkarni, Phys. Rev. A **93**, 062114 (2016).

[49] I. Reichental, A. Klempner, Y. Kafri, and D. Podolsky, Phys. Rev. B **97**, 134301 (2018).

[50] S. Sachdev and J. Ye, Phys. Rev. Lett. **70**, 3339 (1993).

[51] O. Parcollet and A. Georges, Phys. Rev. B **59**, 5341 (1999).

[52] A. Georges, O. Parcollet, and S. Sachdev, Phys. Rev. Lett. **85**, 840 (2000).

[53] A. Georges, O. Parcollet, and S. Sachdev, Phys. Rev. B **63**, 134406 (2001).

[54] S. Sachdev, Phys. Rev. X **5**, 041025 (2015).

[55] W. Fu and S. Sachdev, Phys. Rev. B **94**, 035135 (2016).

[56] R. A. Davison, W. Fu, A. Georges, Y. Gu, K. Jensen, and S. Sachdev, Phys. Rev. B **95**, 155131 (2017).

[57] K. Bulycheva, J. High Energy Phys. **2017** (12), 69.

[58] Y. Gu, A. Kitaev, S. Sachdev, and G. Tarnopolsky, J. High Energy Phys. **2020** (2), 157.

[59] M. Tikhanovskaya, H. Guo, S. Sachdev, and G. Tarnopolsky, Phys. Rev. B **103**, 075141 (2021).

[60] M. Tikhanovskaya, H. Guo, S. Sachdev, and G. Tarnopolsky, Phys. Rev. B **103**, 075142 (2021).

[61] D. Chowdhury, A. Georges, O. Parcollet, and S. Sachdev, Rev. Mod. Phys. **94**, 035004 (2022).

[11] T. Prosen, New J. Phys. **10**, 043026 (2008).

[63] T. Prosen, J. Stat. Mech. Theory Exp. **2010**, P07020 (2010).

[64] B. Ye, F. Machado, C. D. White, R. S. K. Mong, and N. Y. Yao, Phys. Rev. Lett. **125**, 030601 (2020).

[65] D. A. Huse, Phys. Rev. B **24**, 5180 (1981).

[66] S. Ostlund, Phys. Rev. B **24**, 398 (1981).

[67] D. A. Huse and M. E. Fisher, Phys. Rev. Lett. **49**, 793 (1982).

[68] D. A. Huse, A. M. Szpilka, and M. E. Fisher, Phys. A: Stat. Mech. Appl. **121**, 363 (1983).

[69] F. D. M. Haldane, P. Bak, and T. Bohr, Phys. Rev. B **28**, 2743 (1983).

[70] S. Howes, L. P. Kadanoff, and M. Den Nijs, Nucl. Phys. B **215**, 169 (1983).

[71] H. Au-Yang, B. M. McCoy, J. H. Perk, S. Tang, and M.-L. Yan, Phys. Lett. A **123**, 219 (1987).

[72] P. Fendley, J. Stat. Mech.: Theory Exp. **2012** (11), P11020.

[73] G. Ortiz, E. Cobanera, and Z. Nussinov, Nuclear Physics B **854**, 780 (2012).

[74] Y. Zhuang, H. J. Changlani, N. M. Tubman, and T. L. Hughes, Phys. Rev. B **92**, 035154 (2015).

[75] Y.-W. Dai, S. Y. Cho, M. T. Batchelor, and H.-Q. Zhou, Phys. Rev. B **95**, 014419 (2017).

[76] R. Samajdar, S. Choi, H. Pichler, M. D. Lukin, and S. Sachdev, Phys. Rev. A **98**, 023614 (2018).

[77] S. Whitsitt, R. Samajdar, and S. Sachdev, Phys. Rev. B **98**, 205118 (2018).

[68] G. Vidal, Phys. Rev. Lett. **91**, 147902 (2003).

[69] G. Vidal, Phys. Rev. Lett. **93**, 040502 (2004).

[80] S. Paeckel, T. Köhler, A. Swoboda, S. R. Manmana, U. Schollwöck, and C. Hubig, Ann. Phys. **411**, 167998 (2019).

[81] C. Zanoci and B. G. Swingle, Entanglement and thermalization in open fermion systems (2016), arXiv:1612.04840 .

[82] K. Damle and S. Sachdev, Phys. Rev. B **57**, 8307 (1998).

[83] K. Damle and S. Sachdev, Phys. Rev. Lett. **95**, 187201 (2005).

[84] M. Žnidarič, Phys. Rev. E **92**, 042143 (2015).

[85] S. R. Clark, J. Prior, M. J. Hartmann, D. Jaksch, and M. B. Plenio, New J. Phys. **12**, 025005 (2010).

[86] D. Karevski, V. Popkov, and G. M. Schütz, Phys. Rev. Lett. **110**, 047201 (2013).

[87] T. Prosen, Phys. Rev. Lett. **107**, 137201 (2011).

[88] T. Prosen, Phys. Rev. Lett. **106**, 217206 (2011).

[89] T. Prosen, Phys. Rev. Lett. **112**, 030603 (2014).

[90] V. Popkov and T. Prosen, Phys. Rev. Lett. **114**, 127201 (2015).

[91] V. Popkov and C. Presilla, Phys. Rev. A **93**, 022111 (2016).

[92] V. Popkov, T. Prosen, and L. Zadnik, Phys. Rev. Lett. **124**, 160403 (2020).

[93] V. Popkov, T. Prosen, and L. Zadnik, Phys. Rev. E **101**, 042122 (2020).

[94] M. Suzuki, Phys. Lett. A **146**, 319 (1990).

[95] Z. Cai and T. Barthel, Phys. Rev. Lett. **111**, 150403 (2013).

[96] M. V. Medvedyeva, T. Prosen, and M. Žnidarič, Phys. Rev. B **93**, 094205 (2016).

[97] M. Hartmann, G. Mahler, and O. Hess, Phys. Rev. Lett. **93**, 080402 (2004).

[98] M. Hartmann and G. Mahler, EPL **70**, 579 (2005).

[99] M. Hartmann, Contemp. Phys. **47**, 89 (2006).

[100] A. García-Saez, A. Ferraro, and A. Acín, Phys. Rev. A **79**, 052340 (2009).

[101] A. Ferraro, A. García-Saez, and A. Acín, EPL **98**, 10009 (2012).

[102] M. Kliesch, C. Gogolin, M. J. Kastoryano, A. Riera, and J. Eisert, Phys. Rev. X **4**, 031019 (2014).

[103] A. Almheiri, A. Milekhin, and B. Swingle, Universal constraints on energy flow and syk thermalization (2019), arXiv:1912.04912 .

[104] C. Zanoci and B. Swingle, Phys. Rev. Research **4**, 023001 (2022).

[105] C. Zanoci and B. Swingle, Phys. Rev. B **105**, 235131 (2022).

[106] T. Giamarchi, Quantum Physics in One Dimension, International Series of Monographs on Physics (Clarendon Press, 2003).

[107] A. M. Lacerda, A. Purkayastha, M. Kewming, G. T. Landi, and J. Goold, Phys. Rev. B **107**, 195117 (2023).

[108] M. M. Rams and M. Zwolak, Phys. Rev. Lett. **124**, 137701 (2020).

[109] G. Wójtowicz, J. E. Elenewski, M. M. Rams, and M. Zwolak, Phys. Rev. A **101**, 050301 (2020).

[110] X. Xu, J. Thingna, C. Guo, and D. Poletti, Phys. Rev. A **99**, 012106 (2019).

[111] M. Palmero, X. Xu, C. Guo, and D. Poletti, Phys. Rev. E **100**, 022111 (2019).

[112] J. Martyn and B. Swingle, Phys. Rev. A **100**, 032107 (2019).

[113] T. J. Sewell, C. D. White, and B. Swingle, Thermal multi-scale entanglement renormalization ansatz for variational gibbs state preparation (2022), arXiv:2210.16419 .

[114] R. Mahajan, C. D. Freeman, S. Mumford, N. Tubman, and B. Swingle, Entanglement structure of non-equilibrium steady states (2016), arXiv:1608.05074 .

From Correlations after Quantum Quenches in the *XXZ* Spin Chain: Failure of the Generalized Gibbs Ensemble by Pozsgay et al.

References

[1] T. Kinoshita, T. Wenger, and D. S. Weiss, Nature (London) **440**, 900 (2006).

[2] M. Cheneau, P. Barmettler, D. Poletti, M. Endres, P. Schauss, T. Fukuhara, C. Gross, I. Bloch, C. Kollath, and S. Kuhr, Nature (London) **481**, 484 (2012).

[3] S. Trotzky, Y.-A. Chen, A. Flesch, I. P. McCulloch, U. Schollwöck, J. Eisert, and I. Bloch, Nat. Phys. **8**, 325 (2012).

[4] T. Fukuhara, P. Schauß, M. Endres, S. Hild, M. Cheneau, I. Bloch, and C. Gross, Nature (London) **502**, 76 (2013).

[5] A. Polkovnikov, K. Sengupta, A. Silva, and M. Vengalattore, Rev. Mod. Phys. **83**, 863 (2011).

[6] C. Kollath, A. M. Läuchli, and E. Altman, Phys. Rev. Lett. **98**, 180601 (2007).

[7] M. Rigol, V. Dunjko, and M. Olshanii, Nature (London) **452**, 854 (2008).

[8] T. Barthel and U. Schollwöck, Phys. Rev. Lett. **100**, 100601 (2008).

[9] M. Rigol, Phys. Rev. Lett. **103**, 100403 (2009).

[10] M. Cramer and J. Eisert, New J. Phys. **12**, 055020 (2010).

[11] L. F. Santos and M. Rigol, Phys. Rev. E **81**, 036206 (2010).

[12] P. Barmettler, M. Punk, V. Gritsev, E. Demler, and E. Altman, New J. Phys. **12**, 055017 (2010).

[13] M. C. Bañuls, J. I. Cirac, and M. B. Hastings, Phys. Rev. Lett. **106**, 050405 (2011).

[14] P. Calabrese, F. H. L. Essler, and M. Fagotti, Phys. Rev. Lett. **106**, 227203 (2011).

[15] P. Calabrese, F. H. L. Essler, and M. Fagotti, J. Stat. Mech. (2012) P07016.

[16] N. Sedlmayr, J. Ren, F. Gebhard, and J. Sirker, Phys. Rev. Lett. **110**, 100406 (2013).

[17] M. Marcuzzi, J. Marino, A. Gambassi, and A. Silva, Phys. Rev. Lett. **111**, 197203 (2013).

[18] D. Iyer, H. Guan, and N. Andrei, Phys. Rev. A **87**, 053628 (2013).

[19] M. Rigol, V. Dunjko, V. Yurovsky, and M. Olshanii, Phys. Rev. Lett. **98**, 050405 (2007).

[20] M. A. Cazalilla, Phys. Rev. Lett. **97**, 156403 (2006).

[21] D. Rossini, A. Silva, G. Mussardo, and G. E. Santoro, Phys. Rev. Lett. **102**, 127204 (2009).

[22] P. Calabrese, F. H. L. Essler, and M. Fagotti, J. Stat. Mech. (2012) P07022.

[23] M. A. Cazalilla, A. Iucci, and M.-C. Chung, Phys. Rev. E **85**, 011133 (2012).

[24] V. Gurarie, J. Stat. Mech. P02014 (2013).

[25] M. Fagotti and F. H. L. Essler, Phys. Rev. B **87**, 245107 (2013).

[26] M. Collura, S. Sotiriadis, and P. Calabrese, Phys. Rev. Lett. **110**, 245301 (2013).

[27] M. Fagotti, J. Stat. Mech. P03016 (2014).

[28] M. Kormos, M. Collura, and P. Calabrese, Phys. Rev. A **89**, 013609 (2014).

[29] S. Sotiriadis and P. Calabrese, J. Stat. Mech. (2014) P07024.

[30] A. C. Cassidy, C. W. Clark, and M. Rigol, Phys. Rev. Lett. **106**, 140405 (2011).

[31] T. M. Wright, M. Rigol, M. J. Davis, and K. V. Kheruntsyan, Phys. Rev. Lett. **113**, 050601 (2014).

[32] J.-S. Caux and R. M. Konik, Phys. Rev. Lett. **109**, 175301 (2012).

[33] M. Kormos, A. Shashi, Y.-Z. Chou, J.-S. Caux, and A. Imambekov, Phys. Rev. B **88**, 205131 (2013).

[34] J. De Nardis, B. Wouters, M. Brockmann, and J.-S. Caux, Phys. Rev. A **89**, 033601 (2014).

[35] B. Pozsgay, J. Stat. Mech. (2013) P07003.

[36] M. Fagotti and F. H. L. Essler, J. Stat. Mech. (2013) P07012.

[37] M. Fagotti, M. Collura, F. H. L. Essler, and P. Calabrese, Phys. Rev. B **89**, 125101 (2014).

[38] D. Fioretto and G. Mussardo, New J. Phys. **12**, 055015 (2010).

[39] G. Mussardo, Phys. Rev. Lett. **111**, 100401 (2013).

[40] S. Sotiriadis, G. Takács, and G. Mussardo, Phys. Lett. B **734**, 52 (2014).

[41] J.-S. Caux and F. H. L. Essler, Phys. Rev. Lett. **110**, 257203 (2013).

[42] J.-S Caux, in *Proceedings of the Workshop on Emergent Phenomena in the Dynamics of Quantum Matter, New York, 2014* (unpublished).

[43] B. Wouters, M. Brockmann, J. De Nardis, D. Fioretto, M. Rigol, and J.-S. Caux, Phys. Rev. Lett. **113**, 117202 (2014)

[44] A. Auerbach, Interacting Electrons and Quantum Magnetism (Springer, New York, 1994).

[45] F. H. L. Essler and R. M. Konik, in *From Fields to Strings: Circumnavigating Theoretical Physics*, edited by Misha Shifman, Arkady Vainshtein, and John Wheater, Ian Kogan Memorial Collection Vol. 3 (World Scientific, Singapore, 2004), p. 684.

[46] P. Calabrese and J. Cardy, J. Stat. Mech. (2005) P04010.

[47] P. Calabrese and J. Cardy, Phys. Rev. Lett. **96**, 136801 (2006).

[48] A. B. Kuklov and B. V. Svistunov, Phys. Rev. Lett. **90**, 100401 (2003).

[49] L.-M. Duan, E. Demler, and M. D. Lukin, Phys. Rev. Lett. **91**, 090402 (2003).

[50] T. Barthel, C. Kasztelan, I. P. McCulloch, and U. Schollwöck, Phys. Rev. A **79**, 053627 (2009).

[51] J. Simon, W. S. Bakr, R. Ma, M. E. Tai, P. M. Preiss, and M. Greiner, Nature (London) **472**, 307 (2011).

[52] Y.-A. Chen, S. Nascimbène, M. Aidelsburger, M. Atala, S. Trotzky, and I. Bloch, Phys. Rev. Lett. **107**, 210405 (2011).

[53] C. K. Majumdar and D. K. Ghosh, J. Math. Phys. **10**, 1388 (1969).

[54] G. Vidal, Phys. Rev. Lett. **93**, 040502 (2004).

[55] G. Vidal, Phys. Rev. Lett. **98**, 070201 (2007).

[56] This approach is justified in the TDL, where off-diagonal contributions vanish.

[57] The region of validity of the ITEBD simulations was determined by comparing results using different bond dimensions and the observed saturation of the entanglement. Our real-time simulation results are consistent with those obtained in Ref. [1].

[58] See the Supplemental Material below for details of the ITEBD simulation and numerical data.

[59] B. Pozsgay, M. Mestyán, M. A. Werner, M. Kormos, and G. Takács (to be published).

[60] H. Bethe, Zeitschrift fur Physik **71**, 205 (1931).

[61] M. Takahashi, Thermodynamics of One-Dimensional Solvable Models (Cambridge University Press, Cambridge, England, 1999).

[62] K. K. Kozlowski and B. Pozsgay, J. Stat. Mech. (2012) P05021.

[63] B. Pozsgay, J. Stat. Mech. (2014) P06011.

[64] M. Brockmann, J. De Nardis, B. Wouters, and J.-S. Caux, J. Phys. A **47**, 145003 (2014).

[65] M. Brockmann, J. De Nardis, B. Wouters, and J.-S. Caux, arXiv:1403.7469.

[66] C. N. Yang and C. P. Yang, J. Math. Phys. **10**, 1115 (1969).

[67] M. Lüscher, Nucl. Phys. B **117**, 475 (1976).

[68] M. Mestyán and B. Pozsgay, J. Stat. Mech. (2014) P09020.

References

[1] M. Fagotti, M. Collura, F. H. L. Essler, and P. Calabrese, Phys. Rev. B **89**, 125101 (2014).

[2] B. Pozsgay, J. Stat. Mech. P07003 (2013).

From "A note on symmetry reductions of the Lindblad equation: transport in constrained open spin chains" by Buč, Prosen

References

[1] I. Bloch, J. Dalibard, and W. Zwerger, Many-Body Physics with Ultracold Gases, Rev. Mod. Phys. 80, 885 (2008).

[2] A. Polkovnikov, K. Sengupta, A. Silva, and M. Vengalattore, Nonequilibrium dynamics of closed interacting quantum systems, Rev. Mod. Phys. **83**, 863 (2011) .

[3] C. W. Gardiner and P. Zoller, Quantum Noise, A Handbook of Markovian and Non-Markovian Quantum Stochastic Methods with Applications to Quantum Optics Springer, Berlin (2004).

[4] H.-P. Breuer and F. Petruccione, The Theory of Open Quantum Systems (Oxford University Press, Oxford 2002).

[5] R. Alicki and K. Lendi, Quantum Dynamical Semigroups and Applications, (Springer, Berlin Heidelberg 2007).

[6] G. Lindblad, On the generators of quantum dynamical semigroups, Comm. Math. Phys. **48**, 119 (1976).

[7] V. Gorini, A. Kossakowski and E. C. G. Sudarshan, Completely positive semigroups of N-level systems, J. Math. Phys. **17**, 821 (1976).

[8] K. Saito, Strong evidence of normal heat conduction in a one-dimensional quantum system, Europhys. Lett. **61**, 34 (2003).

[9] M. Michel, M. Hartmann, J. Gemmer and G. Mahler, Fourier's Law confirmed for a class of small quantum systems, Eur. Phys. J. B **34**, 325 (2003).

[10] C. Mejia-Monasterio, T. Prosen and G. Casati, Fourier's law in a quantum spin chain and the onset of quantum chaos, Europhys. Lett. **72**, 520 (2005).

[11] R. Steinigeweg, J. Gemmer and M. Michel, Normal-transport behavior in finite one-dimensional chaotic quantum systems, Europhys. Lett. **75**, 406 (2006).

[12] H. Wichterich, M. J. Henrich, H.-P. Breuer, J. Gemmer, and M. Michel, Modeling heat transport through completely positive maps, Phys. Rev. E **76**, 031115 (2007).

[13] T. Prosen, Third quantization: a general method to solve master equations for quadratic open Fermi systems, New J. Phys **10**, 043026 (2008).

[14] M. Michel, O. Hess, H. Wichterich and J. Gemmer, Transport in open spin chains: A Monte Carlo wave-function approach, Phys. Rev. B **77**, 104303 (2008).

[15] Y. Yan, C.-Q. Wu, G. Casati, T. Prosen, and B. Li, Nonballistic heat conduction in an integrable random-exchange Ising chain studied with quantum master equations, Phys. Rev. B **77**, 172411 (2008).

[16] X. Zotos and P. Prelovšek, Transport in one dimensional quantum systems, `http://arxiv.org/abs/cond-mat/0304630`.

[17] J. Sirker, R. G. Pereira, and I. Affleck, Conservation laws, integrability, and transport in one-dimensional quantum systems, Phys. Rev. B **83**, 035115 (2011).

[18] F. Heidrich-Meisner, A. Honecker, W. Brenig, Transport in quasi one-dimensional spin-1/2 systems, Eur. Phys. J. Special Topics **151**, 135 (2007).

[19] B. Kraus, H. P. Bchler, S. Diehl, A. Kantian, A. Micheli, P. Zoller, Preparation of Entangled States by Quantum Markov Processes, Phys. Rev. A **78**, 042307 (2008); S. Diehl, A. Micheli, A. Kantian, B. Kraus, H.P. Bchler, P. Zoller, Quantum States and Phases in Driven Open Quantum Systems with Cold Atoms, Nature Physics **4**, 878 (2008).

[20] D. A. Lidar and K. B. Whaley, Decoherence-Free Subspaces and Subsystems, in "Irreversible Quantum Dynamics", F. Benatti and R. Floreanini (Eds.), pp. 83-120 (Springer Lecture Notes in Physics vol. 622, Berlin, 2003); R. Blume-Kohout, Hui Khoon Ng, D. Poulin and L. Viola, The structure of preserved information in quantum processes, Phys. Rev. Lett. 100 030501 (2008).

[21] C. Simon et al., Quantum memories, Eur. Phys. J. D **58**, 1 (2010).

[22] D. E. Evans, Irreducible Quantum Dynamical Semigroups, Comm. Math. Phys. **54**, 293 (1977).

[23] H. Spohn, An algebraic condition for the approach to equilibrium of an open N-Level system, Lett. Math. Phys. **2**, 33 (1977).

[24] J. Eisert and T. Prosen, Noise-driven quantum criticality, `arXiv:1012.5013`; M. Hoening, M. Moos and M. Fleischhauer, Critical exponents of flux-equilibrium phase transitions in fermionic lattice models, `arXiv:1108.2263` .

[25] T. Prosen and M. Žnidarič, Matrix product simulations of non-equilibrium steady states of quantum spin chains, J. Stat. Mech, P02035 (2009).

[26] R. Steinigeweg, Decay of currents for strong interactions, Phys. Rev. E **84**, 011136 (2011).

[27] Mierzejewski, Bonca, Prelovsek, Integrable Mott Insulators Driven by a Finite Electric Field, Phys. Rev. Lett. **107**, 126601 (2011); R. Steinigeweg, J. Herbrych, P. Prelovšek and M. Mierzejewski, Coexistence of Anomalous and Normal Diffusion in Integrable Mott Insulators, `http://arxiv.org/abs/1201.2844`.

[28] V. Eisler, Crossover between ballistic and diffusive transport: the quantum exclusion process, J. Stat. Mech. (2011) P06007.

[29] K. Temme, M. M. Wolf and F. Verstraete, Stochastic exclusion processes versus coherent transport, `http://arxiv.org/abs/0912.0858`.

[30] M. Žnidarič, Solvable quantum nonequilibrium model exhibiting a phase transition and a matrix product representation, Phys. Rev. E 83, 011108 (2011); M. Žnidarič, Dephasing-induced diffusive transport in the anisotropic Heisenberg model, New J. Phys. **12**, 043001 (2010).

[31] G. Benenti, G. Casati, T. Prosen and D. Rossini, Negative differential conductivity in far-from-equilibrium quantum spin chains, Europhys. Lett. **85**, 37001 (2009)

[32] G. Benenti, G. Casati, T. Prosen, D. Rossini and M. Žnidarič, Charge and spin transport in strongly correlated one-dimensional quantum systems driven far from equilibrium, Phys. Rev. B **80**, 035110 (2009).

[33] T. Prosen and M. Žnidarič, Long-Range Order in Nonequilibrium Interacting Quantum Spin Chains, Phys. Rev. Lett. 105, 060603 (2010).

[34] T. Prosen, Open XXZ Spin Chain: Nonequilibrium Steady State and a Strict Bound on Ballistic Transport, Phys. Rev. Lett. **106**, 217206 (2011); T. Prosen, Exact Nonequilibrium Steady State of a Strongly Driven Open XXZ Chain, Phys. Rev. Lett. **107**, 137201 (2011).

[35] M. Žnidarič, Spin transport in a one-dimensional anisotropic Heisenberg model, Phys. Rev. Lett. **106**, 220601 (2011); M. Žnidarič, Transport in a one-dimensional isotropic Heisenberg model at high temperature, J. Stat. Mech. 2011, P12008 (2011).

[36] T. Prosen and I. Pižorn, High order non-unitary split-step decomposition of unitary operators, J. Phys. A: Math. Gen. 39, 5957 (2006).

[37] P. Prelovšek, S. El Shawish, X. Zotos, and M. Long, Anomalous scaling of conductivity in integrable fermion systems, Phys. Rev. B **70**, 205129 (2004).

[38] R. Steinigeweg and W. Brenig, Spin transport in the XXZ chain at finite temperature and momentum, Phys. Rev. Lett. **107**, 250602 (2011).

From Engineering GGE with trapped ions

References

[7] A. Polkovnikov, K. Sengupta, A. Silva, and M. Vengalattore, Rev. Mod. Phys. **83**, 863 (2011).

[2] C. Gogolin and J. Eisert, Rep. Prog. Phys. **79**, 056001 (2016).

[1] M. Rigol, V. Dunjko, V. Yurovsky, and M. Olshanii, Phys. Rev. Lett. **98**, 050405 (2007).

[4] F. H. L. Essler and M. Fagotti, J. Stat. Mech.: Theory Exp. P064002 (2016).

[3] L. Vidmar and M. Rigol, J. Stat. Mech.: Theory Exp. P064007 (2016).

[11] M. A. Cazalilla and M.-C. Chung, J. Stat. Mech.: Theory Exp. **2016**, 064004 (2016).

[5] J.-S. Caux, J. Stat. Mech.: Theory Exp. P064006 (2016).

[47] P. Calabrese and J. Cardy, J. Stat. Mech.: Theory Exp. **2007**, P06008 (2007).

[48] M. Cramer, C. M. Dawson, J. Eisert, and T. J. Osborne, Phys. Rev. Lett. **100**, 030602 (2008).

[49] T. Barthel and U. Schollwöck, Phys. Rev. Lett. **100**, 100601 (2008).

[50] F. H. L. Essler, S. Evangelisti, and M. Fagotti, Phys. Rev. Lett. **109**, 247206 (2012).

[36] B. Pozsgay, J. Stat. Mech.: Theory Exp. P07003 (2013).

[37] M. Fagotti and F. H. L. Essler, Phys. Rev. B **87**, 245107 (2013).

[25] M. Fagotti and F. H. Essler, J. Stat. Mech.: Theory Exp. P07012 (2013).

[15] B. Wouters, J. De Nardis, M. Brockmann, D. Fioretto, M. Rigol, and J.-S. Caux, Phys. Rev. Lett. **113**, 117202 (2014).

[16] B. Pozsgay, J. Stat. Mech.: Theory Exp. **2014**, P10045 (2014).

[58] S. Sotiriadis and P. Calabrese, J. Stat. Mech.: Theory Exp. **2014**, P07024 (2014).

[59] G. Goldstein and N. Andrei, Phys. Rev. A **90**, 043625 (2014).

[60] M. Brockmann, B. Wouters, D. Fioretto, J. De Nardis, R. Vlijm, and J.-S. Caux, J. Stat. Mech.: Theory Exp. **2014**, P12009 (2014).

[62] M. Rigol, Phys. Rev. E **90**, 031301(R) (2014).

[63] M. Mestyán, B. Pozsgay, G. Takács, and M. A. Werner, J. Stat. Mech.: Theory Exp. **2015**, P04001 (2015).

[2] E. Ilievski, J. De Nardis, B. Wouters, J.-S. Caux, F. H. L. Essler, and T. Prosen, Phys. Rev. Lett. **115**, 157201 (2015).

[64] J. Eisert, M. Friesdorf, and C. Gogolin, Nat. Phys. **11**, 124 (2015).

[65] E. Ilievski, E. Quinn, J. De Nardis, and M. Brockmann, J. Stat. Mech.: Theory Exp. **2016**, 063101 (2016).

[66] L. Piroli, E. Vernier, and P. Calabrese, Phys. Rev. B **94**, 054313 (2016).

[19] T. Langen, S. Erne, R. Geiger, B. Rauer, T. Schweigler, M. Kuhnert, W. Rohringer, I. E. Mazets, T. Gasenzer, and J. Schmiedmayer, Science **348**, 207 (2015).

[41] B. Bertini, F. H. L. Essler, S. Groha, and N. J. Robinson, Phys. Rev. Lett. **115**, 180601 (2015).

[11] B. Bertini, F. H. L. Essler, S. Groha, and N. J. Robinson, Phys. Rev. B **94**, 245117 (2016).

[29] K. Mallayya and M. Rigol, Phys. Rev. Lett. **120**, 070603 (2018).

[30] K. Mallayya, M. Rigol, and W. De Roeck, Phys. Rev. X **9**, 021027 (2019).

[31] J. Durnin, M. Bhaseen, and B. Doyon, arXiv preprint arXiv:2004.11030 (2020).

[32] Y. Tang, W. Kao, K.-Y. Li, S. Seo, K. Mallayya, M. Rigol, S. Gopalakrishnan, and B. L. Lev, Phys. Rev. X **8**, 021030 (2018).

[33] C. Li, T. Zhou, I. Mazets, H.-P. Stimming, Z. Zhu, Y. Zhai, W. Xiong, X. Zhou, X. Chen, and J. Schmiedmayer, arXiv preprint arXiv:1804.01969 (2018).

[34] J.-S. Caux, B. Doyon, J. Dubail, R. Konik, and T. Yoshimura, SciPost Phys. **6**, 70 (2019).

[13] M. Schemmer, I. Bouchoule, B. Doyon, and J. Dubail, Phys. Rev. Lett. **122**, 090601 (2019).

[36] F. Møller, C. Li, I. Mazets, H.-P. Stimming, T. Zhou, Z. Zhu, X. Chen, and J. Schmiedmayer, arXiv preprint arXiv:2006.08577 (2020).

[40] M. Moeckel and S. Kehrein, Phys. Rev. Lett. **100**, 175702 (2008).

[95] M. Kollar, F. A. Wolf, and M. Eckstein, Physical Review B **84**, 054304 (2011).

[103] R. Barnett, A. Polkovnikov, and M. Vengalattore, Phys. Rev. A **84**, 023606 (2011).

[29] M. Gring, M. Kuhnert, T. Langen, T. Kitagawa, B. Rauer, M. Schreitl, I. Mazets, D. A. Smith, E. Demler, and J. Schmiedmayer, Science **337**, 1318 (2012).

[97] A. Mitra, Phys. Rev. B **87**, 205109 (2013).

[98] M. Marcuzzi, J. Marino, A. Gambassi, and A. Silva, Phys. Rev. Lett. **111**, 197203 (2013).

[52] F. H. L. Essler, S. Kehrein, S. R. Manmana, and N. J. Robinson, Phys. Rev. B **89**, 165104 (2014).

[104] N. Nessi, A. Iucci, and M. A. Cazalilla, Phys. Rev. Lett. **113**, 210402 (2014).

[100] M. Babadi, E. Demler, and M. Knap, Phys. Rev. X **5**, 041005 (2015).

[106] E. Canovi, M. Kollar, and M. Eckstein, Phys. Rev. E **93**, 012130 (2016).

[26] F. Lange, Z. Lenarčič, and A. Rosch, Nat. Commun. **8**, 15767 (2017).

[25] F. Lange, Z. Lenarčič, and A. Rosch, Phys. Rev. B **97**, 165138 (2018).

[18] Z. Lenarčič, F. Lange, and A. Rosch, Phys. Rev. B **97**, 024302 (2018).

[25] J. T. Barreiro, M. Müller, P. Schindler, D. Nigg, T. Monz, M. Chwalla, M. Hennrich, C. F. Roos, P. Zoller, and R. Blatt, Nature **470**, 486 (2011).

[51] Y. Lin, J. Gaebler, F. Reiter, T. Tan, R. Bowler, A. Sørensen, D. Leibfried, and D. Wineland, Nature **504** (2013), 10.1038/nature12801.

[52] D. Leibfried, R. Blatt, C. Monroe, and D. Wineland, Rev. Mod. Phys. **75**, 281 (2003).

[17] D. Porras and J. I. Cirac, Phys. Rev. Lett. **92**, 207901 (2004).

[54] X.-L. Deng, D. Porras, and J. I. Cirac, Phys. Rev. A **72**, 063407 (2005).

[18] A. Friedenauer, H. Schmitz, J. T. Glueckert, D. Porras, and T. Schaetz, Nat. Phys. **4**, 757 (2008).

[56] K. Kim, M.-S. Chang, S. Korenblit, R. Islam, E. E. Edwards, J. K. Freericks, G.-D. Lin, L.-M. Duan, and C. Monroe, Nature **465**, 590 (2010).

[25] J. W. Britton, B. C. Sawyer, A. C. Keith, C.-C. J. Wang, J. K. Freericks, H. Uys, M. J. Biercuk, and J. J. Bollinger, Nature **484**, 489 (2012).

[6] R. Islam, C. Senko, W. C. Campbell, S. Korenblit, J. Smith, A. Lee, E. E. Edwards, C.-C. J. Wang, J. K. Freericks, and C. Monroe, Science **340**, 583 (2013).

[21] P. Jurcevic, B. P. Lanyon, P. Hauke, C. Hempel, P. Zoller, R. Blatt, and C. F. Roos, Nature **511**, 202 (2014).

[60] P. Richerme, Z.-X. Gong, A. Lee, C. Senko, J. Smith, M. Foss-Feig, S. Michalakis, A. V. Gorshkov, and C. Monroe, Nature **511**, 198 (2014).

[61] J. G. Bohnet, B. C. Sawyer, J. W. Britton, M. L. Wall, A. M. Rey, M. Foss-Feig, and J. J. Bollinger, Science **352**, 1297 (2016).

[47] J. Zhang, G. Pagano, P. W. Hess, A. Kyprianidis, P. Becker, H. Kaplan, A. V. Gorshkov, Z.-X. Gong, and C. Monroe, Nature **551**, 601 (2017).

[63] C. Kokail, C. Maier, R. van Bijnen, T. Brydges, M. K. Joshi, P. Jurcevic, C. A. Muschik, P. Silvi, R. Blatt, C. F. Roos, and P. Zoller, Nature **569**, 355 (2019).

[64] A. Safavi-Naini, R. J. Lewis-Swan, J. G. Bohnet, M. Gärttner, K. A. Gilmore, J. E. Jordan, J. Cohn, J. K. Freericks, A. M. Rey, and J. J. Bollinger, Phys. Rev. Lett. **121**, 040503 (2018).

[65] E. Jordan, K. A. Gilmore, A. Shankar, A. Safavi-Naini, J. G. Bohnet, M. J. Holland, and J. J. Bollinger, Phys. Rev. Lett. **122**, 053603 (2019).

[66] J. I. Cirac and P. Zoller, Nature **404**, 579 (2000).

[67] A. C. Wilson, Y. Colombe, K. R. Brown, E. Knill, D. Leibfried, and D. J. Wineland, Nature **512**, 57 (2014).

[68] D. Yang, G. S. Giri, M. Johanning, C. Wunderlich, P. Zoller, and P. Hauke, Phys. Rev. A **94**, 052321 (2016).

[69] M. Mielenz, H. Kalis, M. Wittemer, F. Hakelberg, U. Warring, R. Schmied, M. Blain, P. Maunz, D. L. Moehring, D. Leibfried, and T. Schaetz, Nat. Commun. **7**, 11839 (2016).

[70] S. Jain, J. Alonso, M. Grau, and J. P. Home, Phys. Rev. X **10**, 031027 (2020).

[71] M. D. Barrett, B. DeMarco, T. Schaetz, V. Meyer, D. Leibfried, J. Britton, J. Chiaverini, W. M. Itano, B. Jelenković, J. D. Jost, C. Langer, T. Rosenband, and D. J. Wineland, Phys. Rev. A **68**, 042302 (2003).

[72] M. Guggemos, D. Heinrich, O. A. Herrera-Sancho, R. Blatt, and C. F. Roos, New Journal of Physics **17**, 103001 (2015).

[73] V. Negnevitsky, M. Marinelli, K. K. Mehta, H.-Y. Lo, C. Flühmann, and J. P. Home, Nature **563**, 527 (2018).

[24] A. Bastianello, J. De Nardis, and A. De Luca, arXiv preprint arXiv:2003.01702 (2020).

[75] K. Yamamoto, Y. Ashida, and N. Kawakami, arXiv preprint arXiv:2009.00838 (2020).

[8] F. Reiter and A. S. Sørensen, Phys. Rev. A **85**, 032111 (2012).

[77] F. Reiter, D. Reeb, and A. S. Sørensen, Phys. Rev. Lett. **117**, 040501 (2016).

[78] F. Reiter, A. S. Sørensen, P. Zoller, and C. Muschik, Nat. Commun. **8**, 1822 (2017).

[79] D. V. F. James, Applied Physics B **66**, 181 (1998).

[80] P. Schindler, D. Nigg, T. Monz, J. T. Barreiro, E. Martinez, S. X. Wang, S. Quint, M. F. Brandl, V. Nebendahl, C. F. Roos, M. Chwalla, M. Hennrich, and R. Blatt, New Journal of Physics **15**, 123012 (2013).

[81] U. Warring, C. Ospelkaus, Y. Colombe, R. Jördens, D. Leibfried, and D. J. Wineland, Phys. Rev. Lett. **110**, 173002 (2013).

[82] S. Debnath, N. M. Linke, C. Figgatt, K. A. Landsman, K. Wright, and C. Monroe, Nature **536**, 63 (2016).

[83] K. A. Landsman, Y. Wu, P. H. Leung, D. Zhu, N. M. Linke, K. R. Brown, L. Duan, and C. Monroe, Phys. Rev. A **100**, 022332 (2019).

[84] A. Johnson, S. S. Szigeti, M. Schemmer, and I. Bouchoule, Phys. Rev. A **96**, 013623 (2017).

[30] I. Bouchoule, B. Doyon, and J. Dubail, arXiv preprint arXiv:2006.03583 (2020).

[35] Z. Lenarčič, O. Alberton, A. Rosch, and E. Altman, arXiv preprint arXiv:1910.01548 (2019).

[87] T. Shirai and T. Mori, Phys. Rev. E **101**, 042116 (2020).

[8] T. Prosen, Phys. Rev. Lett. **106**, 217206 (2011).

From Quasiparticle cooling algorithms for quantum many-body state preparation

References

[1] B. P. Lanyon, J. D. Whitfield, G. G. Gillett, M. E. Goggin, M. P. Almeida, I. Kassal, J. D. Biamonte, M. Mohseni, B. J. Powell, M. Barbieri, et al., Towards quantum chemistry on a quantum computer, Nature chemistry **2**, 106 (2010).

[2] A. Kandala, A. Mezzacapo, K. Temme, M. Takita, M. Brink, J. M. Chow, and J. M. Gambetta, Hardware-efficient variational quantum eigensolver for small molecules and quantum magnets, nature **549**, 242 (2017).

[3] B. Bauer, S. Bravyi, M. Motta, and G. K.-L. Chan, Quantum algorithms for quantum chemistry and quantum materials science, Chemical Reviews **120**, 12685 (2020).

[4] G. A. Quantum, Collaborators*†, F. Arute, K. Arya, R. Babbush, D. Bacon, J. C. Bardin, R. Barends, S. Boixo, M. Broughton, B. B. Buckley, et al., Hartree-fock on a superconducting qubit quantum computer, Science **369**, 1084 (2020).

[5] A. B. Finnila, M. A. Gomez, C. Sebenik, C. Stenson, and J. D. Doll, Quantum annealing: A new method for minimizing multidimensional functions, Chemical physics letters **219**, 343 (1994).

[6] E. Farhi, J. Goldstone, S. Gutmann, J. Lapan, A. Lundgren, and D. Preda, A quantum adiabatic evolution algorithm applied to random instances of an np-complete problem, Science **292**, 472 (2001).

[7] A. Y. Kitaev, Quantum measurements and the abelian stabilizer problem (1995), arXiv:quant-ph/9511026 [quant-ph] .

[8] D. S. Abrams and S. Lloyd, Quantum algorithm providing exponential speed increase for finding eigenvalues and eigenvectors, Phys. Rev. Lett. **83**, 5162 (1999).

[9] E. Farhi, J. Goldstone, S. Gutmann, and M. Sipser, Quantum computation by adiabatic evolution, arXiv preprint quant-ph/0001106 (2000).

[10] D. Poulin and P. Wocjan, Preparing ground states of quantum many-body systems on a quantum computer, Phys. Rev. Lett. **102**, 130503 (2009).

[11] S. Boixo, E. Knill, and R. D. Somma, Eigenpath traversal by phase randomization, Quantum Inf. Comput. **9**, 833 (2009).

[12] Y. Ge, J. Tura, and J. I. Cirac, Faster ground state preparation and high-precision ground energy estimation with fewer qubits, Journal of Mathematical Physics **60**, 022202 (2019).

[13] J. Preskill, Quantum computing in the nisq era and beyond, Quantum **2**, 79 (2018).

[14] T. Albash and D. A. Lidar, Adiabatic quantum computation, Reviews of Modern Physics **90**, 015002 (2018).

[15] M. Greiner, O. Mandel, T. Esslinger, T. W. Hänsch, and I. Bloch, Quantum phase transition from a superfluid to a mott insulator in a gas of ultracold atoms, Nature **415**, 39 (2002).

[16] J. Simon, W. S. Bakr, R. Ma, M. E. Tai, P. M. Preiss, and M. Greiner, Quantum simulation of antiferromagnetic spin chains in an optical lattice, Nature **472**, 307 (2011).

[17] G. Semeghini, H. Levine, A. Keesling, S. Ebadi, T. T. Wang, D. Bluvstein, R. Verresen, H. Pichler, M. Kalinowski, R. Samajdar, A. Omran, S. Sachdev, A. Vishwanath, M. Greiner, V. Vuletić, and M. D. Lukin, Probing topological spin liquids on a programmable quantum simulator, Science **374**, 1242 (2021), https://www.science.org/doi/pdf/10.1126/science.abi8794 .

[18] P. Scholl, M. Schuler, H. J. Williams, A. A. Eberharter, D. Barredo, K.-N. Schymik, V. Lienhard, L.-P. Henry, T. C. Lang, T. Lahaye, A. M. Läuchli, and A. Browaeys, Quantum simulation of 2d antiferromagnets with hundreds of rydberg atoms, Nature **595**, 233 (2021).

[19] M. Cerezo, A. Arrasmith, R. Babbush, S. C. Benjamin, S. Endo, K. Fujii, J. R. McClean, K. Mitarai, X. Yuan, L. Cincio, et al., Variational quantum algorithms, Nature Reviews Physics **3**, 625 (2021).

[20] J. Tilly, H. Chen, S. Cao, D. Picozzi, K. Setia, Y. Li, E. Grant, L. Wossnig, I. Rungger, G. H. Booth, and J. Tennyson, The variational quantum eigensolver: A review of methods and best practices, Physics Reports **986**, 1 (2022).

[21] D. A. Fedorov, B. Peng, N. Govind, and Y. Alexeev, Vqe method: a short survey and recent developments, Materials Theory **6**, 1 (2022).

[22] K. Bharti, A. Cervera-Lierta, T. H. Kyaw, T. Haug, S. Alperin-Lea, A. Anand, M. Degroote, H. Heimonen, J. S. Kottmann, T. Menke, W.-K. Mok, S. Sim, L.-C. Kwek, and A. Aspuru-Guzik, Noisy intermediate-scale quantum algorithms, Rev. Mod. Phys. **94**, 015004 (2022).

[23] T. Louvet, T. Ayral, and X. Waintal, Go-no go criteria for performing quantum chemistry calculations on quantum computers (2023), arXiv:2306.02620 [quant-ph] .

[24] J. R. McClean, S. Boixo, V. N. Smelyanskiy, R. Babbush, and H. Neven, Barren plateaus in quantum neural network training landscapes, Nature communications **9**, 4812 (2018).

[25] S. Wang, E. Fontana, M. Cerezo, K. Sharma, A. Sone, L. Cincio, and P. J. Coles, Noise-induced barren plateaus in variational quantum algorithms, Nature Communications **12**, 6961 (2021).

[26] S. H. Sack, R. A. Medina, A. A. Michailidis, R. Kueng, and M. Serbyn, Avoiding barren plateaus using classical shadows, PRX Quantum **3**, 020365 (2022).

[27] B. M. Terhal and D. P. DiVincenzo, Problem of equilibration and the computation of correlation functions on a quantum computer, Phys. Rev. A **61**, 022301 (2000).

[28] E. B. Davies, Markovian master equations, Communications in mathematical Physics **39**, 91 (1974).

[6] B. Kraus, H. P. Büchler, S. Diehl, A. Kantian, A. Micheli, and P. Zoller, Preparation of entangled states by quantum markov processes, Phys. Rev. A **78**, 042307 (2008).

[1] S. Diehl, A. Micheli, A. Kantian, B. Kraus, H. P. Büchler, and P. Zoller, Quantum states and phases in driven open quantum systems with cold atoms, Nat. Phys. **4**, 878 (2008).

[31] F. Verstraete, M. M. Wolf, and J. Ignacio Cirac, Quantum computation and quantum-state engineering driven by dissipation, Nat. Phys. **5**, 633 (2009).

[32] S. Roy, J. Chalker, I. Gornyi, and Y. Gefen, Measurement-induced steering of quantum systems, Physical Review Research **2**, 033347 (2020).

[33] M. J. Kastoryano and F. G. Brandao, Quantum gibbs samplers: The commuting case, Communications in Mathematical Physics **344**, 915 (2016).

[34] C.-F. Chen, M. J. Kastoryano, F. G. S. L. Brandão, and A. Gilyén, Quantum thermal state preparation (2023), arXiv:2303.18224 [quant-ph] .

[25] J. T. Barreiro, M. Müller, P. Schindler, D. Nigg, T. Monz, M. Chwalla, M. Hennrich, C. F. Roos, P. Zoller, and R. Blatt, An open-system quantum simulator with trapped ions, Nature **470**, 486 (2011).

[36] Y. Lin, J. P. Gaebler, F. Reiter, T. R. Tan, R. Bowler, A. S. Sørensen, D. Leibfried, and D. J. Wineland, Dissipative production of a maximally entangled steady state of two quantum bits, Nature **504**, 415 (2013).

[37] S. Shankar, M. Hatridge, Z. Leghtas, K. M. Sliwa, A. Narla, U. Vool, S. M. Girvin, L. Frunzio, M. Mirrahimi, and M. H. Devoret, Autonomously stabilized entanglement between two superconducting quantum bits, Nature **504**, 419 (2013).

[38] X. Mi, A. Michailidis, S. Shabani, K. Miao, P. Klimov, J. Lloyd, E. Rosenberg, R. Acharya, I. Aleiner, T. Andersen, et al., Stable quantum-correlated many-body states through engineered dissipation, Science **383**, 1332 (2024).

[39] D. A. Abanin, W. De Roeck, W. W. Ho, and F. Huveneers, Effective Hamiltonians, prethermalization, and slow energy absorption in periodically driven many-body systems, Physical Review B **95**, 014112 (2017).

[40] M. Metcalf, J. E. Moussa, W. A. de Jong, and M. Sarovar, Engineered thermalization and cooling of quantum many-body systems, Physical Review Research **2**, 023214 (2020).

[41] M. Raghunandan, F. Wolf, C. Ospelkaus, P. O. Schmidt, and H. Weimer, Initialization of quantum simulators by sympathetic cooling, Sci. Adv. **6**, eaaw9268 (2020).

[42] S. Polla, Y. Herasymenko, and T. E. O'Brien, Quantum digital cooling, Phys. Rev. A **104**, 012414 (2021).

[43] A. Matthies, M. Rudner, A. Rosch, and E. Berg, Programmable adiabatic demagnetization for systems with trivial and topological excitations (2023), arXiv:2210.17256 [quant-ph] .

[44] D. A. Puente, F. Motzoi, T. Calarco, G. Morigi, and M. Rizzi, Quantum state preparation via engineered ancilla resetting, arXiv preprint arXiv:2305.08641 (2023).

[45] L. Marti, R. Mansuroglu, and M. J. Hartmann, Efficient quantum cooling algorithm for fermionic systems (2024), arXiv:2403.14506 [quant-ph] .

[46] P. Coleman, Introduction to Many-Body Physics (Cambridge University Press, 2015).

[47] E. Lieb, T. Schultz, and D. Mattis, Two soluble models of an antiferromagnetic chain, Annals of Physics **16**, 407 (1961).

[48] S. Sachdev, Quantum phase transitions, Physics world **12**, 33 (1999).

[49] A. A. Ovchinnikov, D. V. Dmitriev, V. Y. Krivnov, and V. O. Cheranovskii, Antiferromagnetic ising chain in a mixed transverse and longitudinal magnetic field, Phys. Rev. B **68**, 214406 (2003).

[50] E. Dagotto and T. Rice, Surprises on the way from one-to two-dimensional quantum magnets: The ladder materials, Science **271**, 618 (1996).

[38] For protocols considered below, f_τ can be positive or negative, but for this choice the sum $\sum_{\tau=1}^{T} |f_\tau| \gtrsim 1$.

[52] H.-P. Breuer and F. Petruccione, The theory of open quantum systems (Oxford University Press, USA, 2002).

[53] D. A. Lidar, Lecture notes on the theory of open quantum systems (2020), arXiv:1902.00967 [quant-ph] .

[54] M. Rigol, V. Dunjko, V. Yurovsky, and M. Olshanii, Relaxation in a completely integrable many-body quantum system: An ab initio study of the dynamics of the highly excited states of 1d lattice hard-core bosons, Phys. Rev. Lett. **98**, 050405 (2007).

[55] F. Lange, Z. Lenarčič, and A. Rosch, Time-dependent generalized gibbs ensembles in open quantum systems, Physical Review B **97**, 165138 (2018).

[56] F. Gerbino, I. Lesanovsky, and G. Perfetto, Large-scale universality in quantum reaction-diffusion from keldysh field theory, Physical Review B **109**, L220304 (2024).

[57] M. B. Hastings and X.-G. Wen, Quasiadiabatic continuation of quantum states: The stability of topological ground-state degeneracy and emergent gauge invariance, Physical Review B—Condensed Matter and Materials Physics **72**, 045141 (2005).

[40] In practice it is the spectral function that is measured in experiment and the validity of the quasiparticle description requires the existence of a sharp pole.

[59] We note that the normalization factor is chosen according to the condition $\sum_{\tau=1}^{T} f_\tau = 1$. The modulated coupling in Eq. (**??**) is sign-changing, however, $\sum_{\tau=1}^{T} |f_\tau|$ is of order 1 for all cases considered below.

[60] M. Thakurathi, A. A. Patel, D. Sen, and A. Dutta, Floquet generation of majorana end modes and topological invariants, Phys. Rev. B **88**, 155133 (2013).

[61] B. Bauer, T. Pereg-Barnea, T. Karzig, M.-T. Rieder, G. Refael, E. Berg, and Y. Oreg, Topologically protected braiding in a single wire using floquet majorana modes, Phys. Rev. B **100**, 041102 (2019).

[62] A. Lerose, M. Sonner, and D. A. Abanin, Scaling of temporal entanglement in proximity to integrability, Phys. Rev. B **104**, 035137 (2021).

[63] M. Žnidarič, Relaxation times of dissipative many-body quantum systems, Physical Review E **92**, 042143 (2015).

[64] Heating processes, in particular due to noise, may in principle involve a large number of particles; however, we will find that few-quasiparticle processes are dominant, and considering them gives an accurate approximation of heating rates.

[65] G. B. Mbeng, A. Russomanno, and G. E. Santoro, The quantum ising chain for beginners (2020), arXiv:2009.09208 [quant-ph] .

[66] F. Verstraete, J. J. García-Ripoll, and J. I. Cirac, Matrix product density operators: Simulation of finite-temperature and dissipative systems, Phys. Rev. Lett. **93**, 207204 (2004).

[67] M. Zwolak and G. Vidal, Mixed-state dynamics in one-dimensional quantum lattice systems: A time-dependent superoperator renormalization algorithm, Phys. Rev. Lett. **93**, 207205 (2004).

[68] G. Vidal, Efficient classical simulation of slightly entangled quantum computations, Physical review letters **91**, 147902 (2003).

[69] G. Vidal, Efficient simulation of one-dimensional quantum many-body systems, Physical review letters **93**, 040502 (2004).

[70] M. Fishman, S. R. White, and E. M. Stoudenmire, The ITensor Software Library for Tensor Network Calculations, SciPost Phys. Codebases , 4 (2022).

[71] T. Barnes, E. Dagotto, J. Riera, and E. Swanson, Excitation spectrum of heisenberg spin ladders, Physical Review B **47**, 3196 (1993).

[72] M. Azuma, Z. Hiroi, M. Takano, K. Ishida, and Y. Kitaoka, Observation of a spin gap in sr cu 2 o 3 comprising spin-1/2 quasi-1d two-leg ladders, Physical review letters **73**, 3463 (1994).

[73] S. Notbohm, P. Ribeiro, B. Lake, D. Tennant, K. Schmidt, G. Uhrig, C. Hess, R. Klingeler, G. Behr, B. Büchner, et al., One-and two-triplon spectra of a cuprate ladder, Physical review letters **98**, 027403 (2007).

[74] L. Vanderstraeten, F. Verstraete, and J. Haegeman, Scattering particles in quantum spin chains, Physical Review B **92**, 125136 (2015).

[75] S. V. Isakov, D. Kafri, O. Martin, C. V. Heidweiller, W. Mruczkiewicz, M. P. Harrigan, N. C. Rubin, R. Thomson, M. Broughton, K. Kissell, et al., Simulations of quantum circuits with approximate noise using qsim and cirq, arXiv preprint arXiv:2111.02396 (2021).

[76] X. Mi, M. Sonner, M. Y. Niu, K. W. Lee, B. Foxen, R. Acharya, I. Aleiner, T. I. Andersen, F. Arute, K. Arya, et al., Noise-resilient edge modes on a chain of superconducting qubits, Science **378**, 785 (2022).

[77] The steady state can be efficiently found by root-finding algorithms, after the cooling and noise-induced rates have been calculated via Wick's theorem. In practice, the system reaches its steady state quickly and we evolve the rate equation in time until the quasiparticle occupations have effectively converged.

[78] G. Modugno, G. Ferrari, G. Roati, R. J. Brecha, A. Simoni, and M. Inguscio, Bose-einstein condensation of potassium atoms by sympathetic cooling, Science **294**, 1320 (2001), https://www.science.org/doi/pdf/10.1126/science.1066687 .

[79] C.-F. Chen, H.-Y. Huang, J. Preskill, and L. Zhou, Local minima in quantum systems, in Proceedings of the 56th Annual ACM Symposium on Theory of Computing (2024) pp. 1323–1330.

[80] S. Bravyi, M. B. Hastings, and F. Verstraete, Lieb-robinson bounds and the generation of correlations and topological quantum order, Physical review letters **97**, 050401 (2006).

[81] M. B. Hastings, Topological order at nonzero temperature, Physical review letters **107**, 210501 (2011).

[82] G. Kishony, M. S. Rudner, A. Rosch, and E. Berg, Gauged cooling of topological excitations and emergent fermions on quantum simulators, arXiv preprint arXiv:2310.16082 (2023).

[83] C.-F. Chen and F. G. Brandao, Fast thermalization from the eigenstate thermalization hypothesis, arXiv preprint arXiv:2112.07646 (2021).

[84] J. Kempe, A. Kitaev, and O. Regev, The complexity of the local hamiltonian problem, Siam journal on computing **35**, 1070 (2006).

[85] O. Shtanko and R. Movassagh, Preparing thermal states on noiseless and noisy programmable quantum processors (2023), arXiv:2112.14688 [quant-ph] .

[86] I. Ulčakar and Z. Lenarčič, Generalized gibbs ensembles in weakly interacting dissipative systems and digital quantum computers, arXiv preprint arXiv:2406.17033 (2024).

[87] P. Rall, C. Wang, and P. Wocjan, Thermal State Preparation via Rounding Promises, Quantum **7**, 1132 (2023).

[88] A. Lerose, M. Sonner, and D. A. Abanin, Scaling of temporal entanglement in proximity to integrability, Physical Review B **104**, 035137 (2021).

[89] N. Iorgov, V. Shadura, and Y. Tykhyy, Spin operator matrix elements in the quantum ising chain: fermion approach, Journal of Statistical Mechanics: Theory and Experiment **2011**, P02028 (2011).

[90] E. Barouch and B. M. McCoy, Statistical mechanics of the x y model. ii. spin-correlation functions, Physical Review A **3**, 786 (1971).

[91] T. Barthel and Y. Zhang, Solving quasi-free and quadratic lindblad master equations for open fermionic and bosonic systems, Journal of Statistical Mechanics: Theory and Experiment **2022**, 113101 (2022).

[92] R. Orús, A practical introduction to tensor networks: Matrix product states and projected entangled pair states, Annals of physics **349**, 117 (2014).

[93] J. C. Bridgeman and C. T. Chubb, Hand-waving and interpretive dance: an introductory course on tensor networks, Journal of physics A: Mathematical and theoretical **50**, 223001 (2017).

From Equilibration, thermalisation, and the emergence of statistical mechanics in closed quantum systems

References

[1] Gibbs J W 1902 Elementary principles in statistical mechanics (New York: C. Scribner)

[2] Uffink J 2006 Compendium of the foundations of classical statistical physics URL http://philsci-archive.pitt.edu/id/eprint/2691

[3] Neumann J 1929 Z. Phys. **57** 30

[4] Landau L D and Lifshitz E M 1980 Statistical physics 3rd ed (Course of Theoretical Physics vol 5) (Butterworth-Heinemann)

[5] Greiner M, Mandel O, Hänsch T W and Bloch I 2002 Nature **419** 51 doi: 10.1038/nature00968

[6] Greiner M, Mandel O, Esslinger T, Hänsch T W and Bloch I 2002 Nature **415** 39 doi: 10.1038/415039a

[7] Tuchman A, Orzel C, Polkovnikov A and Kasevich M 2006 Phys. Rev. A **74** 051601 doi: 10.1103/PhysRevA.74.051601

[8] Aidelsburger M, Atala M, Nascimbène S, Trotzky S, Chen Y A and Bloch I 2011 Phys. Rev. Lett. **107** 255301 doi: 10.1103/PhysRevLett.107.255301

[9] Bloch I 2005 Nature Phys. **1** 23 doi: 10.1038/nphys138

[10] Langen T, Geiger R and Schmiedmayer J 2015 Ann. Rev. Condens. Matter Phys. **6** 201 doi: 10.1146/annurev-conmatphys-031214-014548

[11] Sadler L E, Higbie J M, Leslie S R, Vengalattore M and Stamper-Kurn D M 2006 Nature **443** 312 doi: 10.1038/nature05094

[12] Regal C and Jin D S 2005 Experimental realization of BCS-BEC crossover physics with a Fermi gas Phd thesis University of Colorado preprint `arXiv:0601054`

[13] Kinoshita T, Wenger T and Weiss D S 2006 Nature **440** 900 doi: 10.1038/nature04693

[14] Hofferberth S, Lesanovsky I, Fischer B, Schumm T and Schmiedmayer J 2007 Nature **449** 324 doi: 10.1038/nature06149

[15] Weller A, Ronzheimer J P, Gross C, Esteve J, Oberthaler M K, Theocharis G and Kevrekidis P G 2008 Phys. Rev. Lett. **101** 130401 doi: 10.1103/PhysRevLett.101.130401

[16] Strohmaier N, Takasu Y, Günter K, Jördens R, Köhl M, Moritz H and Esslinger T 2007 Phys. Rev. Lett. **99** 220601 doi: 10.1103/PhysRevLett.99.220601

[17] Porras D and Cirac J I 2004 Phys. Rev. Lett. **92** 207901 doi: 10.1103/PhysRevLett.92.207901

[18] Friedenauer A, Schmitz H, Glückert J T, Porras D and Schätz T 2008 Nature Phys. **4** 757 doi: 10.1038/nphys1032

[19] Bissbort U, Cocks D, Negretti a, Idziaszek Z, Calarco T, Schmidt-Kaler F, Hofstetter W and Gerritsma R 2013 Phys. Rev. Lett. **111** 080501 doi: 10.1103/PhysRevLett.111.080501

[20] Häffner H, Hänsel W, Roos C F, Benhelm J, Chek-al Kar D, Chwalla M, Körber T, Rapol U D, Riebe M, Schmidt P O, Becher C, Gühne O, Dür W and Blatt R 2005 Nature **438** 643 doi: 10.1038/nature04279

[21] Jurcevic P, Lanyon B P, Hauke P, Hempel C, Zoller P, Blatt R and Roos C F 2014 Nature **511** 202 doi: 10.1038/nature13461

[22] Lanyon B P, Hempel C, Nigg D, Müller M, Gerritsma R, Zähringer F, Schindler P, Barreiro J T, Rambach M, Kirchmair G, Hennrich M, Zoller P, Blatt R and Roos C F 2011 Science **334** 57 doi: 10.1126/science.1208001

[23] Schindler P, Müller M, Nigg D, Barreiro J T, Martinez E A, Hennrich M, Monz T, Diehl S, Zoller P and Blatt R 2013 Nature Phys. **9** 361 doi: 10.1038/nphys2630

[24] Blatt R and Roos C F 2012 Nature Phys. **8** 277 doi: 10.1038/nphys2252

[25] Britton J W, Sawyer B C, Keith A C, Wang C C J, Freericks J K, Uys H, Biercuk M J and Bollinger J J 2012 Nature **484** 489 doi: 10.1038/nature10981

[26] Trotzky S, Chen Y A, Flesch A, McCulloch I P, Schollwöck U, Eisert J and Bloch I 2012 Nature Phys. **8** 325 doi: 10.1038/nphys2232

[27] Cheneau M, Barmettler P, Poletti D, Endres M, Schauss P, Fukuhara T, Gross C, Bloch I, Kollath C and Kuhr S 2012 Nature **481** 484 doi: 10.1038/nature10748

[28] Langen T, Geiger R, Kuhnert M, Rauer B and Schmiedmayer J 2013 Nature Phys. **9** 640 doi: 10.1038/nphys2739

[29] Gring M, Kuhnert M, Langen T, Kitagawa T, Rauer B, Schreitl M, Mazets I, Smith D A, Demler E and Schmiedmayer J 2012 Science **337** 1318 doi: 10.1126/science.1224953

[30] Ronzheimer J P, Schreiber M, Braun S, Hodgman S S, Langer S, McCulloch I P, Heidrich-Meisner F, Bloch I and Schneider U 2013 Phys. Rev. Lett. **110** 205301 doi: 10.1103/PhysRevLett.110.205301

[31] Orus R 2014 Ann. Phys. **349** 117 doi: 10.1016/j.aop.2014.06.013

[32] Schollwöck U 2011 Ann. Phys. **326** 96 doi: 10.1016/j.aop.2010.09.012

[33] Rigol M, Dunjko V and Olshanii M 2008 Nature **452** 854 doi: 10.1038/nature06838

[34] Rigol M 2009 Phys. Rev. Lett. **103** 100403 doi: 10.1103/PhysRevLett.103.100403

[35] Luitz D J, Laflorencie N and Alet F 2015 Phys. Rev. B **91** 081103(R) doi: 10.1103/PhysRevB.91.081103

[36] Troyer M, Alet F, Trebst S and Wessel S 2003 AIP Conf. Proc. **690** 156 doi: 10.1063/1.1632126

[37] Foulkes W, Mitas L, Needs R and Rajagopal G 2001 Rev. Mod. Phys. **73** 33 doi: 10.1103/RevModPhys.73.33

[38] Aoki H, Tsuji N, Eckstein M, Kollar M, Oka T and Werner P 2014 Rev. Mod. Phys. **86** 779 doi: 10.1103/RevModPhys.86.779

[39] Engel E, Dreizler R M, Rankings I, Algorithms S, Introduction A, Preferences M, Algorithms R S and Algorithms C S 2011 Density functional theory Theoretical and Mathematical Physics (Springer)

[40] Kohn W 1999 Rev. Mod. Phys. **71** 1253 doi: 10.1103/RevModPhys.71.1253

[41] Braun S, Friesdorf M, Hodgman S S, Schreiber M, Ronzheimer J P, Riera A, del Rey M, Bloch I, Eisert J and Schneider U 2015 Proc. Natl. Acad. Sc. **112** 3641 doi: 10.1073/pnas.1408861112

[42] Rigol M, Dunjko V, Yurovsky V and Olshanii M 2007 Phys. Rev. Lett. **98** 50405 doi: 10.1103/PhysRevLett.98.050405

[43] Lesanovsky I, Olmos B and Garrahan J P 2010 Phys. Rev. Lett. **105** 100603 doi: 10.1103/PhysRevLett.105.100603

[44] Dubey S, Silvestri L, Finn J, Vinjanampathy S and Jacobs K 2012 Phys. Rev. E **85** 011141 doi: 10.1103/PhysRevE.85.011141

[45] Beugeling W, Moessner R and Haque M 2014 Phys. Rev. E **89** 042112 doi: 10.1103/PhysRevE.89.042112

[46] Yukalov V 2011 Laser Phys. Lett. **8** 485 doi: 10.1002/lapl.201110002

[47] Ikeda T N, Watanabe Y and Ueda M 2013 Phys. Rev. E **87** 012125 doi: 10.1103/PhysRevE.87.012125

[48] Fine B V, Elsayed T A, Kropf C M and de Wijn A S 2014 Phys. Rev. E **89** 012923 doi: 10.1103/PhysRevE.89.012923

[49] Jensen R and Shankar R 1985 Phys. Rev. Lett. **54** 1879 doi: 10.1103/PhysRevLett.54.1879

[50] Moeckel M and Kehrein S 2008 Phys. Rev. Lett. **100** 175702 doi: 10.1103/PhysRevLett.100.175702

[51] Kollath C, Läuchli A and Altman E 2007 Phys. Rev. Lett. **98** 180601 doi: 10.1103/PhysRevLett.98.180601

[52] Deng S, Ortiz G and Viola L 2011 Phys. Rev. B **83** 094304 doi: 10.1103/PhysRevB.83.094304

[53] Campos Venuti L and Zanardi P 2010 Phys. Rev. A **81** 032113 doi: 10.1103/PhysRevA.81.032113

[54] Goth F and Assaad F F 2012 Phys. Rev. B **85** 085129 doi: 10.1103/PhysRevB.85.085129

[55] Rigol M and Fitzpatrick M 2011 Phys. Rev. A **84** 033640 doi: 10.1103/PhysRevA.84.033640

[56] Torres-Herrera E J and Santos L F 2014 Phys. Rev. A **89** 043620 doi: 10.1103/PhysRevA.89.043620

[57] Sengupta K, Powell S and Sachdev S 2004 Phys. Rev. A **69** 053616 doi: 10.1103/PhysRevA.69.053616

[58] Flesch A, Cramer M, McCulloch I, Schollwöck U and Eisert J 2008 Phys. Rev. A **78** 33608 doi: 10.1103/PhysRevA.78.033608

[59] Ates C, Garrahan J P and Lesanovsky I 2012 Phys. Rev. Lett. **108** 110603 doi: 10.1103/PhysRevLett.108.110603

[60] Fagotti M 2013 Phys. Rev. B **87** 165106 doi: 10.1103/PhysRevB.87.165106

[61] Calabrese P and Cardy J 2007 J. Stat. Mech. **2007** P06008 doi: 10.1088/1742-5468/2007/06/P06008

[62] Cazalilla M 2006 Phys. Rev. Lett. **97** 156403 doi: 10.1103/PhysRevLett.97.156403

[63] Fioretto D and Mussardo G 2010 New J. Phys. **12** 055015 doi: 10.1088/1367-2630/12/5/055015

[64] Calabrese P, Essler F H L and Fagotti M 2011 Phys. Rev. Lett. **106** 227203 doi: 10.1103/PhysRevLett.106.227203

[65] Eckstein M and Kollar M 2008 Phys. Rev. Lett. **100** 120404 doi: 10.1103/PhysRevLett.100.120404

[66] Campos Venuti L and Zanardi P 2010 Phys. Rev. A **81** 22113 doi: 10.1103/PhysRevA.81.022113

[67] Lloyd S 1988 Black holes, demons and the loss of coherence: How complex systems get information, Phd thesis Rockefeller University

[68] Popescu S, Short A J and Winter A 2005 preprint arXiv:quant-ph/0511225

[69] Gemmer J, Michel M and Mahler G 2009 Quantum thermodynamics (Lecture Notes in Physics vol 784) (Berlin, Heidelberg: Springer)

[70] Garnerone S 2013 Phys. Rev. B **88** 165140 doi: 10.1103/PhysRevB.88.165140

[71] Garnerone S and de Oliveira T R 2013 Phys. Rev. B **87** 214426 doi: 10.1103/PhysRevB.87.214426

[72] Hastings M B and Koma T 2006 Commun. Math. Phys. **265** 781 doi: 10.1007/s00220-006-0030-4

[73] Nachtergaele B and Sims R 2009 Locality estimates for quantum spin systems New trends in mathematical physics ed Sidoravičius V (Springer Netherlands) p 591

[74] Bravyi S, Hastings M and Verstraete F 2006 Phys. Rev. Lett. **97** 50401 doi: 10.1103/PhysRevLett.97.050401

[75] Kliesch M, Gogolin C and Eisert J 2014 Lieb-Robinson bounds and the simulation of time evolution of local observables in lattice systems Many-electron approaches in physics, chemistry and mathematics Mathematical Physics Studies ed Bach V and Delle Site L (Springer) p 301 preprint arXiv:1306.0716

[76] Calabrese P and Cardy J 2007 J. Stat. Mech. P10004 doi: 10.1088/1742-5468/2007/10/P10004

[77] Chiara G D, Montangero S, Calabrese P and Fazio R 2006 J. Stat. Mech. **2006** P03001 doi: 10.1088/1742-5468/2006/03/P03001

[78] Eisert J and Osborne T 2006 Phys. Rev. Lett. **97** 150404 doi: 10.1103/PhysRevLett.97.150404

[79] Läuchli A and Kollath C 2008 J. Stat. Mech. P05018 doi: 10.1088/1742-5468/2008/05/P05018

[80] Van Acoleyen K, Mariën M and Verstraete F 2013 Phys. Rev. Lett. **111** 5 doi: 10.1103/PhysRevLett.111.170501

[81] Lloyd S 2013 preprint arXiv:1307.0378

[82] Eisert J, Friesdorf M and Gogolin C 2015 Nature Phys. **11** 124 doi: 10.1038/nphys3215

[83] Cazalilla M A and Rigol M 2010 New J. Phys. **12** 55006 doi: 10.1088/1367-2630/12/5/055006

[84] Polkovnikov A, Sengupta K, Silva A and Vengalattore M 2011 Rev. Mod. Phys. **83** 863 doi: 10.1103/RevModPhys.83.863

[85] Seifert U 2012 Rep. Prog. Phys. **75** 126001 doi: 10.1088/0034-4885/75/12/126001

[86] Goold J, Huber M, Riera A, del Rio L and Skrzypzyk P 2016 J. Phys. A **49** 143001 doi: 10.1088/1751-8113/49/14/143001

[87] Nielsen M A and Chuang I L 2007 Quantum computation and quantum information (Cambridge University Press)

[88] Bhatia R 1997 Matrix analysis (New York: Springer)

[89] Short A J 2011 New J. Phys. **13** 053009 doi: 10.1088/1367-2630/13/5/053009

[90] Aubrun G and Lancien C 2013 Positivity preprint arXiv:1309.6003v1

[91] Short A J and Farrelly T C 2012 New J. Phys. **14** 013063 doi: 10.1088/1367-2630/14/1/013063

[92] Besicovitch A S 1926 Proc. Lond. Math. Soc. **s2-25** 495 doi: 10.1112/plms/s2-25.1.495

[93] Bañuls M C, Cirac J I and Wolf M M 2009 J. Phys. **171** 012032 doi: 10.1088/1742-6596/171/1/012032

[94] Friis N, Lee A and Bruschi D 2013 Phys. Rev. A **87** 022338 doi: 10.1103/PhysRevA.87.022338

[95] Kastoryano M J 2011 Quantum Markov chain mixing and dissipative engineering Phd thesis University of Copenhagen

[96] Kastoryano M J and Eisert J 2013 J. Math. Phys. **54** 102201 doi: 10.1063/1.4822481

[97] Plenio M B and Virmani S 2005 Quant. Inf. Comput. **7** 1 doi: 10.1007/978-3-319-04063-9-8

[98] Thirring W 2002 Quantum mathematical physics 2nd ed (Berlin Heidelberg: Springer)

[99] Bhattacharyya K and Mukherjee D 1986 J. Chem. Phys. **84** 3212 doi: 10.1063/1.450251

[100] Schulman L 1978 Phys. Rev. A **18** 2379 doi: 10.1103/PhysRevA.18.2379

[101] Peres A 1982 Phys. Rev. Lett. **49** 1118 doi: 10.1103/PhysRevLett.49.1118

[102] Bocchieri P and Loinger A 1957 Phys. Rev. **107** 337 doi: 10.1103/PhysRev.107.337

[103] Wallace D 2013 J. Math. Phys. **56** 022105 doi: 10.1063/1.4907384

[104] Haar D 1955 Rev. Mod. Phys. **27** 289 doi: 10.1103/RevModPhys.27.289

[105] Tasaki H 1998 Phys. Rev. Lett. **80** 1373 doi: 10.1103/PhysRevLett.80.1373

[106] Reimann P 2008 Phys. Rev. Lett. **101** 190403 doi: 10.1103/PhysRevLett.101.190403

[107] Linden N, Popescu S, Short A and Winter A 2009 Phys. Rev. E **79** 61103 doi: 10.1103/PhysRevE.79.061103

[108] Reimann P 2012 Phys. Scr. **86** 058512 doi: 10.1088/0031-8949/86/05/058512

[109] Reimann P and Kastner M 2012 New J. Phys. **14** 043020 doi: 10.1088/1367-2630/14/4/043020

[110] Hübener R, Sekino Y and Eisert J 2015 JHEP 166 doi: 10.1007/JHEP04(2015)166

[111] Cramer M and Eisert J 2009 New J. Phys. **12** 27 doi: 10.1088/1367-2630/12/5/055020

[112] Cramer M, Dawson C M, Eisert J and Osborne T J 2008 Phys. Rev. Lett. **100** 30602 doi: 10.1103/PhysRevLett.100.030602

[113] Neuenhahn C and Marquardt F 2012 Phys. Rev. E **85** 060101 doi: 10.1103/PhysRevE.85.060101

[114] Levstein P R, Usaj G and Pastawski H M 1998 J. Chem. Phys. **108** 2718 doi: 10.1063/1.475664

[115] Ledoux M 2001 The concentration of measure phenomenon (Mathematical Surveys and Monographs vol 89) (Americal Mathematical Society)

[116] Chatterjee S 2007 J. Func. Ana. **245** 379 doi: 10.1016/j.jfa.2007.01.003

[117] Popescu S, Short A J and Winter A 2006 Nature Phys. **2** 754 doi: 10.1038/nphys444

[118] Gogolin C 2010 Pure state quantum statistical mechanics Master's thesis Universität Würzburg preprint arXiv:1003.5058

[119] Bocchieri P and Loinger A 1959 Phys. Rev. **114** 948 doi: 10.1103/PhysRev.114.948

[120] Gogolin C 2014 Equilibration and thermalization in quantum systems Phd thesis Freie Universität Berlin URL http://www.cgogolin.de/downloads/Dissertation_Christian_Gogolin_Published.pdf

[121] Gong Z X and Duan L M 2011 preprint arXiv:1109.4696

[122] Cui S, Cao J P, Jing H, Fan H and Liu W M 2011 preprint arXiv:1110.4690

[123] Rigol M, Muramatsu A and Olshanii M 2006 Phys. Rev. A **74** 053616 doi: 10.1103/PhysRevA.74.053616

[124] Zhuang Q and Wu B 2013 Phys. Rev. E **88** 062147 doi: 10.1103/PhysRevE.88.062147

[125] Hutter A 2011 Understanding equipartition and thermalization from decoupling Master's thesis Institute for Theoretical Physics ETH Zürich

[126] Dupuis F, Berta M, Wullschleger J and Renner R 2014 Commun. Math. Phys. **328** 251 doi: 10.1007/s00220-014-1990-4

[127] Szehr O, Dupuis F, Tomamichel M and Renner R 2013 New J. Phys. **15** 053022 doi: 10.1088/1367-2630/15/5/053022

[128] Szehr O 2012 Decoupling theorems Master's thesis ETH Zurich preprint arXiv:1207.3927

[129] Konig R, Renner R and Schaffner C 2009 IEEE Trans. Inf. Th. **55** 4337 doi: 10.1109/TIT.2009.2025545

[130] Ciganović N, Beaudry N J and Renner R 2014 IEEE Trans. Inf. Th. **60** 1573 doi: 10.1109/TIT.2013.2295314

[131] Neumann J 2010 Europ. Phys. J. H **35** 201 doi: 10.1140/epjh/e2010-00008-5

[132] Goldstein S, Lebowitz J L, Mastrodonato C, Tumulka R and Zanghi N 2010 Proc. Roy. Soc. A **466** 3203 doi: 10.1098/rspa.2009.0635

[133] Brandão F G S L, Ćwikliński P, Horodecki M, Horodecki P, Korbicz J K and Mozrzymas M 2012 Phys. Rev. E **86** 031101 doi: 10.1103/PhysRevE.86.031101

[134] Masanes L, Roncaglia A J and Acín A 2013 Phys. Rev. E **87** 032137 doi: 10.1103/PhysRevE.87.032137

[135] Cramer M 2011 New J. Phys. **14** 053051 doi: 10.1088/1367-2630/14/5/053051

[136] Žnidarič M 2012 J. Phys. A **45** 125204 doi: 10.1088/1751-8113/45/12/125204

[137] Eisert J and Plenio M B 2003 Int. J. Quant. Inf. **1** 479 doi: 10.1142/S0219749903000371

[138] Braunstein S L 2005 Rev. Mod. Phys. **77** 513 doi: 10.1103/RevModPhys.77.513

[139] Adesso G and Illuminati F 2007 J. Phys. A **40** 7821 doi: 10.1088/1751-8113/40/28/S01

[140] Weedbrook C, Pirandola S, Garcia-Patron R, Cerf N J, Ralph T C, Shapiro J H and Lloyd S 2012 Rev. Mod. Phys. **84** 621 doi: 10.1103/RevModPhys.84.621

[141] Dudnikova T V, Komech a I and Spohn H 2003 J. Math. Phys. **44** 2596 doi: 10.1063/1.1571658

[142] Lanford O E and Robinson D W 1972 Commun. Math. Phys. **24** 193 doi: 10.1007/BF01877712

[143] Tegmark M and Yeh L 1994 Physica A **202** 342 doi: 10.1016/0378-4371(94)90181-3

[144] Barthel T and Schollwöck U 2008 Phys. Rev. Lett. **100** 100601 doi: 10.1103/PhysRevLett.100.100601

[145] Reed M and Simon B 1980 Methods of modern mathematical physics I: Functional Analysis (San Diego: Academic Press)

[146] Reed M and Simon B 1975 Methods of modern mathematical physics II: Fourier analysis, self-adjoint (San Diego: Academic Press)

[147] Goldstein S, Hara T and Tasaki H 2015 New J. Phys. **17** 045002 doi: 10.1088/1367-2630/17/4/045002

[148] Batu T, Fischer E, Fortnow L, Kumar R, Rubinfeld R and White P 2001 Testing random variables for independence and identity Proc. 2001 IEEE Int. Conf. Cluster Comp. (IEEE Comput. Soc) p 442 doi: 10.1109/SFCS.2001.959920

[149] Batu T, Fortnow L, Rubinfeld R, Smith W D and White P 2000 Testing that distributions are close Proceedings 41st Annual Symposium on Foundations of Computer Science (IEEE Comput. Soc) p 259 doi: 10.1109/SFCS.2000.892113

[150] Canonne C, Ron D and Servedio R A 2012 preprint arXiv:1211.2664

[151] Audenaert K M R, Mosonyi M and Verstraete F 2012 J. Math. Phys. **53** 122205 doi: 10.1063/1.4768252

[152] Audenaert K M R 2014 Quant. Inf. Comput. **14** 31

[153] Ududec C, Wiebe N and Emerson J 2013 Phys. Rev. Lett. **111** 080403 doi: 10.1103/PhysRevLett.111.080403

[154] Lieb E H and Robinson D W 1972 Commun. Math. Phys. **28** 251 doi: 10.1007/BF01645779

[155] Nachtergaele B and Sims R 2010 Contemp. Math. **529** 141

[156] Calabrese P and Cardy J 2006 Phys. Rev. Lett. **96** 136801 doi: 10.1103/PhysRevLett.96.136801

[157] Calabrese P and Cardy J 2005 J. Stat. Mech. P04010 doi: 10.1088/1742-5468/2005/04/P04010

[158] Geiger R, Langen T, Mazets I E and Schmiedmayer J 2014 New J. Phys. **16** 22 doi: 10.1088/1367-2630/16/5/053034

[159] Hauke P and Tagliacozzo L 2013 Phys. Rev. Lett. **111** 207202 doi: 10.1103/PhysRevLett.111.207202

[160] Mazza L, Rossini D, Endres M and Fazio R 2014 Phys. Rev. B **90** 020301(R) doi: 10.1103/PhysRevB.90.020301

[161] Richerme P, Gong Z X, Lee A, Senko C, Smith J, Foss-Feig M, Michalakis S, Gorshkov A V and Monroe C 2014 Nature **511** 198 doi: 10.1038/nature13450

[162] Nachtergaele B, Vershynina A and Zagrebnov V A 2011 AMS Contemp. Math. **552** 161

[163] Poulin D 2010 Phys. Rev. Lett. **104** 190401 doi: 10.1103/PhysRevLett.104.190401

[164] Eisert J, van den Worm M, Manmana S R and Kastner M 2013 Phys. Rev. Lett. **111** 260401 doi: 10.1103/PhysRevLett.111.260401

[165] Schuch N, Harrison S K, Osborne T J and Eisert J 2011 Phys. Rev. A **84** 032309 doi: 10.1103/PhysRevA.84.032309

[166] Nachtergaele B, Raz H, Schlein B and Sims R 2009 Commun. Math. Phys. **286** 1073 doi: 10.1007/s00220-008-0630-2

[167] Cramer M, Serafini A and Eisert J 2007 Locality of dynamics in general harmonic quantum systems Quantum information and many-body quantum systems preprint arXiv:0803.0890

[168] Burrell C K and Osborne T J 2007 Phys. Rev. Lett. **99** 167201 doi: 10.1103/PhysRevLett.99.167201

[169] Kim I H, Chandran A and Abanin D A 2014 preprint arXiv:1412.3073

[170] Hamza E and Sims Rand Stolz G 2012 Commun. Math. Phys. **315** 215 doi: 10.1007/s00220-012-1544-6

[171] Friesdorf M, Werner A H, Brown W, Scholz V B and Eisert J 2015 Phys. Rev. Lett. **14** 170505 doi: 10.1103/PhysRevLett.114.170505

[172] Malabarba A S L, García-Pintos L P, Linden N, Farrelly T C and Short A J 2014 Phys. Rev. E **90** 012121 doi: 10.1103/PhysRevE.90.012121

[173] Schiulaz M, Silva A and Markus M 2015 Phys. Rev. B **91** 184202 doi: 10.1103/PhysRevB.91.184202

[174] Sirker J, Konstantinidis N P, Andraschko F and Sedlmayr N 2014 Phys. Rev. A **89** 042104 doi: 10.1103/PhysRevA.89.042104

[175] Campos Venuti L, Jacobson N T, Santra S and Zanardi P 2011 Phys. Rev. Lett. **107** 010403 doi: 10.1103/PhysRevLett.107.010403

[176] Sorg S, Vidmar L, Pollet L and Heidrich-Meisner F 2014 Phys. Rev. A **90** 033606 doi: 10.1103/PhysRevA.90.033606

[177] Kim H, Bañuls M C, Cirac J I, Hastings M B and Huse D A 2015 Phys. Rev. E **92** 012128 doi: 10.1103/PhysRevE.92.012128

[178] Khatami E, Rigol M, Relaño A and García-García A M 2012 Phys. Rev. E **85** 050102 doi: 10.1103/PhysRevE.85.050102

[179] Brandino G P, De Luca A, Konik R M and Mussardo G 2012 Phys. Rev. B **85** 214435 doi: 10.1103/PhysRevB.85.214435

[180] Brandao F G S L, Harrow A W and Horodecki M 2012 preprint arXiv:1208.0692

[181] Kota V K B, Relaño A, Retamosa J and Vyas M 2011 J. Stat. Mech. **2011** P10028 doi: 10.1088/1742-5468/2011/10/P10028

[182] Fyodorov Y V 2005 Recent perspectives in random matrix theory and number theory, 31–78, London Math. Soc. Lecture Note Ser., 322

[183] Guhr T, Müller, Groeling A and Weidenmüller H A 1998 Phys. Rep. **299** 189 doi: 10.1016/S0370-1573(97)00088-4

[184] Canovi E, Rossini D, Fazio R, Santoro G E and Silva A 2011 Phys. Rev. B **83** 094431 doi: 10.1103/PhysRevB.83.094431

[185] Tabor M 1989 Chaos and integrability in nonlinear dynamics: An introduction (New York: Wiley)

[186] Bohigas O, Giannoni M and Schmit C 1984 Phys. Rev. Lett. **52** 1 doi: 10.1103/PhysRevLett.52.1

[187] Tao T 2012 Topics in random matrix theory (Graduate studies in mathematics vol 132) (Americal Mathematical Society)

[188] Mehta M L 1991 Random matrices Pure and Applied Mathematics (Academic Press)

[189] Srednicki M 1994 Phys. Rev. E **50** 888 doi: 10.1103/PhysRevE.50.888

[190] Hutter A and Wehner S 2013 Phys. Rev. A **87** 012121 doi: 10.1103/PhysRevA.87.012121

[191] Kastner M 2011 Phys. Rev. Lett. **106** 130601 doi: 10.1103/PhysRevLett.106.130601

[192] Bochner S and Chandrasekharan K 1949 Fourier transforms (Princeton University Press)

[193] Flambaum V V and Izrailev F M 2001 Phys. Rev. E **64** 026124 doi: 10.1103/PhysRevE.64.026124

[194] Torres-Herrera E J and Santos L F 2014 Phys. Rev. A **90** 033623 doi: 10.1103/PhysRevA.90.033623

[195] Torres-Herrera E J, Vyas M and Santos L F 2014 New J. Phys. **16** 063010 doi: 10.1088/1367-2630/16/6/063010

[196] Barouch E, McCoy B and Dresden M 1970 Phys. Rev. A **2** 1075 doi: 10.1103/PhysRevA.2.1075

[197] Krutitsky K V, Navez P, Queisser F and Schützhold R 2014 EPJ Quant. Tech. **1** doi: 10.1140/epjqt12

[198] Barmettler P, Punk M, Gritsev V, Demler E and Altman E 2009 Phys. Rev. Lett. **102** 130603 doi: 10.1103/PhysRevLett.102.130603

[199] Bañuls M C, Hastings M B, Verstraete F and Cirac J I 2009 Phys. Rev. Lett. **102** 240603 doi: 10.1103/PhysRevLett.102.240603

[200] Müller-Hermes A, Cirac J I and Bañuls M C 2012 New J. Phys. **14** 075003 doi: 10.1088/1367-2630/14/7/075003

[201] Hallberg K A 2006 Adv. Phys. **55** 477 doi: 10.1080/00018730600766432

[202] Cramer M, Flesch A, McCulloch I, Schollwöck U and Eisert J 2008 Phys. Rev. Lett. **101** 063001 doi: 10.1103/PhysRevLett.101.063001

[203] Karrasch C, Rentrop J, Schuricht D and Meden V 2012 Phys. Rev. Lett. **109** 126406 doi: 10.1103/PhysRevLett.109.126406

[204] Queisser F, Krutitsky K V, Navez P and Schützhold R 2014 Phys. Rev. A **89** 033616 doi: 10.1103/PhysRevA.89.033616

[205] Manmana S R, Wessel S, Noack R M and Muramatsu A 2009 Phys. Rev. B **79** 155104 doi: 10.1103/PhysRevB.79.155104

[206] del Campo A and Zurek W H 2014 Int. J. Mod. Phys. A **29** 1430018 doi: 10.1142/S0217751X1430018X

[207] Chandran A, Erez A, Gubser S S and Sondhi S L 2012 Phys. Rev. B **86** 064304 doi: 10.1103/PhysRevB.86.064304

[208] Stephan J M and Dubail J 2011 J. Stat. Mech. P08019 doi: 10.1088/1742-5468/2011/08/P08019

[209] Zangara P R, Dente A D, Torres-Herrera E J, Pastawski H M, Iucci A and Santos L F 2013 Phys. Rev. E **88** 032913 doi: 10.1103/PhysRevE.88.032913

[210] Ponomarev A V, Denisov S and Hänggi P 2011 Phys. Rev. Lett. **106** 010405 doi: 10.1103/PhysRevLett.106.010405

[211] Mossel J, Palacios G and Caux J S 2010 J. Stat. Mech. **2010** L09001 doi: 10.1088/1742-5468/2010/09/L09001

[212] Alba V and Heidrich-Meisner F 2014 Phys. Rev. B **90** 075144 doi: 10.1103/PhysRevB.90.075144

[213] Ponomarev A V, Denisov S, Gemmer J and Hänggi P 2012 Europhys. Lett. **98** 40011 doi: 10.1209/0295-5075/98/40011

[214] Bernard D and Doyon B 2015 Ann. Henri Poincaré **16** 113 doi: 10.1007/s00023-014-0314-8

[215] Bernard D and Doyon B 2012 J. Phys. A **45** 362001 doi: 10.1088/1751-8113/45/36/362001

[216] Bhaseen M J, Doyon B, Lucas A and Schalm K 2015 Nature Phys. **11** 509 doi: 10.1038/nphys3220

[217] Doyon B, Lucas A, Schalm K and Bhaseen M J 2015 J. Phys. A **48** 095002 doi: 10.1088/1751-8113/48/9/095002

[218] De Luca A, Viti J, Bernard D and Doyon B 2013 Phys. Rev. B **88** 134301 doi: 10.1103/PhysRevB.88.134301

[219] Bernard D, Doyon B and Viti J 2015 J. Phys. A **48** 05FT01 doi: 10.1088/1751-8113/48/5/05FT01

[220] Castro-Alvaredo O, Chen Y, Doyon B and Hoogeveen M 2014 J. Stat. Mech. P03011 doi: 10.1088/1742-5468/2014/03/P03011

[221] Gritsev V, Rostunov T and Demler E 2010 J. Stat. Mech. P05012 doi: 10.1088/1742-5468/2010/05/P05012

[222] Cramer M, Eisert J, Plenio M and Dreißig J 2006 Phys. Rev. A **73** 012309 doi: 10.1103/PhysRevA.73.012309

[223] Schuch N, Wolf M M, Verstraete F and Cirac J I 2008 Phys. Rev. Lett. **100** 030504 doi: 10.1103/PhysRevLett.100.030504

[224] Ge Y and Eisert J 2014 preprint `arXiv:1411.2995`

[225] Schuch N, Wolf M M, Vollbrecht K G H and Cirac J I 2008 New J. Phys. **10** 33032 doi: 10.1088/1367-2630/10/3/033032

[226] Eisert J, Cramer M and Plenio M B 2010 Rev. Mod. Phys. **82** 277 doi: 10.1103/RevModPhys.82.277

[227] Horodecki R, Horodecki P, Horodecki M and Horodecki K 2009 Rev. Mod. Phys. **81** 865 doi: 10.1103/RevModPhys.81.865

[228] Bennett C H, Bernstein H J, Popescu S and Schumacher B 1996 Phys. Rev. A **53** 2046

[229] Wootters W K 1998 Phys. Rev. Lett. **80** 2245 doi: 10.1103/PhysRevLett.80.2245

[230] Vidal G and Werner R F 2002 Phys. Rev. A **65** 032314 doi: 10.1103/PhysRevA.65.032314

[231] Eisert J 2001 Entanglement in quantum information theory Phd thesis University of Potsdam preprint `quant-ph/0610253`

[232] Eisert J and Plenio M B 1999 J. Mod. Opt. **46** 145 doi: 10.1080/09500349908231260

[233] Seevinck M P 2010 Quant. Inf. Proc. **9** 273 doi: 10.1007/s11128-009-0161-6

[234] Eisert J, Plenio M B, Bose S and Hartley J 2004 Phys. Rev. Lett. **93** 190402 doi: 10.1103/PhysRevLett.93.190402

[235] Sengupta K and Sen D 2009 Phys. Rev. A **80** 032304 doi: 10.1103/PhysRevA.80.032304

[236] Mazza L, Rossini D, Fazio R and Endres M 2015 New J. Phys. **17** 013015 doi: 10.1088/1367-2630/17/1/013015

[237] Ruutu V M H, Eltsov V B, Gill A J, Kibble T W B, Krusius M, Makhlin Y G, Placais B, Volovik G E and Xu W 1996 Nature **382** 334 doi: 10.1038/382334a0

[238] Ulm S, Roßnagel J, Jacob G, Degünther C, Dawkins S T, Poschinger U G, Nigmatullin R, Retzker A, Plenio M B, Schmidt-Kaler F and Singer K 2013 Nature communications **4** 2290 doi: 10.1038/ncomms3290

[239] Pyka K, Keller J, Partner H L, Nigmatullin R, Burgermeister T, Meier D M, Kuhlmann K, Retzker A, Plenio M B, Zurek W H, del Campo A and Mehlstдubler T E 2013 Nat. Comm. **4** 2291 doi: 10.1038/ncomms3291

[240] Polkovnikov A and Gritsev V 2008 Nature Phys. **4** 477 doi: 10.1038/nphys963

[241] Polkovnikov A 2005 Phys. Rev. B **72** 161201(R) doi: 10.1103/PhysRevB.72.161201

[242] Sen D, Sengupta K and Mondal S 2008 Phys. Rev. Lett. **101** 016806 doi: 10.1103/PhysRevLett.101.016806

[243] Barankov R and Polkovnikov A 2008 Phys. Rev. Lett. **101** 076801 doi: 10.1103/PhysRevLett.101.076801

[244] Schützhold R, Uhlmann M, Xu Y and Fischer U R 2006 Phys. Rev. Lett. **97** 200601 doi: 10.1103/PhysRevLett.97.200601

[245] Fischer U R, Schützhold R and Uhlmann M 2008 Phys. Rev. A **77** 043615 doi: 10.1103/PhysRevA.77.043615

[246] Chen D, White M, Borries C and DeMarco B 2011 Phys. Rev. Lett. **106** 235304 doi: 10.1103/PhysRevLett.106.235304

[247] Bernier J S, Poletti D, Barmettler P, Roux G and Kollath C 2012 Phys. Rev. A **85** 033641 doi: 10.1103/PhysRevA.85.033641

[248] Bernier J S, Roux G and Kollath C 2011 Phys. Rev. Lett. **106** 200601 doi: 10.1103/PhysRevLett.106.200601

[249] Dóra B, Haque M and Zaránd G 2011 Phys. Rev. Lett. **106** 156406 doi: 10.1103/PhysRevLett.106.156406

[250] Uhlmann M, Schützhold R and Fischer U R 2007 Phys. Rev. Lett. **99** 120407 doi: 10.1103/PhysRevLett.99.120407

[251] Uhlmann M, Schützhold R and Fischer U R 2010 New J. Phys. **12** 095020 doi: 10.1088/1367-2630/12/9/095020

[252] Uhlmann M, Schützhold R and Fischer U R 2010 Phys. Rev. D **81** 025017 doi: 10.1103/PhysRevD.81.025017

[253] Campo A and Sengupta K 2015 Eur. Phys. J. Special Topics **224** 189 doi: 10.1140/epjst/e2015-02350-4

[254] Gogolin C, Müller M P and Eisert J 2011 Phys. Rev. Lett. **106** 040401 doi: 10.1103/PhysRevLett.106.040401

[255] Boyd S and Vandenberghe L 2004 Convex optimization (Cambridge: Cambridge University Press)

[256] Brody D C, Hook D W and Hughston L P 2007 J. Phys. A **40** F503 doi: 10.1088/1751-8113/40/26/F01

[257] Perk J, Capel H and Siskens T 1977 Physica A **89** 304 doi: 10.1016/0378-4371(77)90106-6

[258] Girardeau M 1969 Phys. Lett. A **30** 442 doi: 10.1016/0375-9601(69)90232-1

[259] Caux J S and Essler F H L 2013 Phys. Rev. Lett. **110** 257203 doi: 10.1103/PhysRevLett.110.257203

[260] Brockmann M, Wouters B, Fioretto D, Nardis J D, Vlijm R and Caux J S 2014 J. Stat. Mech. **2014** P12009 doi: 10.1088/1742-5468/2014/12/P12009

[261] Cassidy A C, Clark C W and Rigol M 2011 Phys. Rev. Lett. **106** 140405 doi: 10.1103/PhysRevLett.106.140405

[262] Mussardo G 2013 Phys. Rev. Lett. **111** 100401 doi: 10.1103/PhysRevLett.111.100401

[263] Prosen T 2014 Nuclear Physics B **886** 1177 doi: 10.1016/j.nuclphysb.2014.07.024

[264] Wouters B, De Nardis J, Brockmann M, Fioretto D, Rigol M and Caux J S 2014 Phys. Rev. Lett. **113** 117202 doi: 10.1103/PhysRevLett.113.117202

[265] Mestyan M, Pozsgay B, Takacs G and Werner M A 2015 J. Stat. Mech. **2015** P04001 doi: 10.1088/1742-5468/2015/04/P04001

[266] Pozsgay B, Mestyán M, Werner M A, Kormos M, Zaránd G and Takács G 2014 Phys. Rev. Lett. **113** 117203 doi: 10.1103/PhysRevLett.113.117203

[267] Sels D and Wouters M 2015 Phys. Rev. E **92** 022123 doi: 10.1103/PhysRevE.92.022123

[268] Iucci A and Cazalilla M A 2009 Phys. Rev. A **80** 063619 doi: 10.1103/PhysRevA.80.063619

[269] Iucci A and Cazalilla M A 2010 New J. Phys. **12** 055019 doi: 10.1088/1367-2630/12/5/055019

[270] Fagotti M, Collura M, Essler F H L and Calabrese P 2014 Phys. Rev. B **89** 125101 doi: 10.1103/PhysRevB.89.125101

[271] Cazalilla M A, Iucci A and Chung M C 2012 Phys. Rev. E **85** 011133 doi: 10.1103/PhysRevE.85.011133

[272] Sotiriadis S and Calabrese P 2014 J. Stat. Mech. P07024 doi: 10.1088/1742-5468/2014/07/P07024

[273] Kormos M, Collura M and Calabrese P 2014 Phys. Rev. A **89** 013609 doi: 10.1103/PhysRevA.89.013609

[274] Mazza P P, Collura M, Kormos M and Calabrese P 2014 J. of Stat. Mech. **2014** P11016 doi: 10.1088/1742-5468/2014/01/P01009

[275] Kormos M, Shashi A, Chou Y Z, Caux J S and Imambekov A 2013 Phys. Rev. B **88** 205131 doi: 10.1103/PhysRevB.88.205131

[276] Nardis J D, Wouters B, Brockmann M and Caux J S 2014 Phys. Rev. A **89** 033601 doi: 10.1103/PhysRevA.89.033601

[277] Goldstein G and Andrei N 2012 preprint arXiv:1405.4224

[278] Prosen T and Ilievski E 2013 Phys. Rev. Lett. **111** 057203 doi: 10.1103/PhysRevLett.111.057203

[279] Zhang J M, Cui F C and Hu J 2012 Phys. Rev. E **85** 041138 doi: 10.1103/PhysRevE.85.041138

[280] Chen Y and Doyon B 2014 J. Stat. Mech. P09021 doi: 10.1088/1742-5468/2014/09/P09021

[281] Schrödinger E 1927 Ann. Phys. **388** 956 doi: 10.1002/andp.19273881504

[282] Kinchin A I 1949 Mathematical foundations for statistical mechanics (Mineola: Dover Publications, Inc.)

[283] Goldstein S, Lebowitz J, Tumulka R and Zanghì N 2006 Phys. Rev. Lett. **96** 50403 doi: 10.1103/PhysRevLett.96.050403

[284] Schrödinger E 1952 Statistical thermodynamics (Cambridge: Cambridge University Press)

[285] Halmos P R 1974 Measure theory Graduate Texts in Mathematics (New York: Springer)

[286] Haar A 1933 Ann. Math. **34** 147

[287] Zyczkowski K and Sommers H J 2001 J. Phys. A **34** 7111 doi: 10.1088/0305-4470/34/35/335

[288] Brody D C and Hughston L P 1998 J. Math. Phys. **39** 6502 doi: 10.1063/1.532661

[289] Bender C M, Brody D C and Hook D W 2005 J. Phys. A **38** L607 doi: 10.1088/0305-4470/38/38/L01

[290] Brody D C, Hook D W and Hughston L P 2007 Proc. Roy. Soc. A **463** 2021 doi: 10.1098/rspa.2007.1865

[291] Müller M P, Gross D and Eisert J 2011 Commun. Math. Phys. **303** 785 doi: 10.1007/s00220-011-1205-1

[292] Fresch B and Moro G J 2013 Eur. Phys. J. B **86** 233 doi: 10.1140/epjb/e2013-40023-6

[293] Ji K and Fine B V 2011 Phys. Rev. Lett. **107** 050401 doi: 10.1103/PhysRevLett.107.050401

[294] Reimann P 2007 Phys. Rev. Lett. **99** 160404 doi: 10.1103/PhysRevLett.99.160404

[295] Bartsch C and Gemmer J 2009 Phys. Rev. Lett. **102** 110403 doi: 10.1103/PhysRevLett.102.110403

[296] Sugiura S and Shimizu A 2012 Phys. Rev. Lett. **108** 240401 doi: 10.1103/PhysRevLett.108.240401

[297] White S 2009 Phys. Rev. Lett. **102** 190601 doi: 10.1103/PhysRevLett.102.190601

[298] Garnerone S, de Oliveira T R and Zanardi P 2010 Phys. Rev. A **81** 032336 doi: 10.1103/PhysRevA.81.032336

[299] Garnerone S, de Oliveira T R, Haas S and Zanardi P 2010 Phys. Rev. A **82** 052312 doi: 10.1103/PhysRevA.82.052312

[300] Steinigeweg R, Khodja A, Niemeyer H, Gogolin C and Gemmer J 2014 Phys. Rev. Lett. **112** 130403 doi: 10.1103/PhysRevLett.112.130403

[301] Bocchieri P and Loinger A 1958 Phys. Rev. **111** 668 doi: 10.1103/PhysRev.111.668

[302] Farquhar I E and Landsberg P T 1957 Proc. Roy. Soc. A **239** 134 doi: 10.1098/rspa.1957.0027

[303] Jaynes E T 1957 Phys. Rev. **106** 620 doi: 10.1103/PhysRev.106.620

[304] Jaynes E T 1957 Phys. Rev. **108** 171 doi: 10.1103/PhysRev.108.171

[305] Deutsch J 1991 Phys. Rev. A **43** 2046 doi: 10.1103/PhysRevA.43.2046

[306] Reimann P and Evstigneev M 2013 Phys. Rev. E **88** 052114 doi: 10.1103/PhysRevE.88.052114

[307] Berry M V 1977 J. Phys. A **10** 2083 doi: 10.1088/0305-4470/10/12/016

[308] Tasaki H 1997 preprint arXiv:9707255

[309] Mueller M P, Adlam E, Masanes L and Wiebe N 2015 Comm. Math. Phys. **340** 499 doi: 10.1007/s00220-015-2473-y

[310] Bañuls M C, Cirac J I and Hastings M B 2011 Phys. Rev. Lett. **106** 050405 doi: 10.1103/PhysRevLett.106.050405

[311] Riera A, Gogolin C and Eisert J 2012 Phys. Rev. Lett. **108** 080402 doi: 10.1103/PhysRevLett.108.080402

[312] Singh N 2011 preprint arXiv:1103.4003

[313] Larson J 2013 J. Phys. B **46** 224016 doi: 10.1088/0953-4075/46/22/224016

[314] Caux J S and Mossel J 2011 J. Stat. Mech. **2011** P02023 doi: 10.1088/1742-5468/2011/02/P02023

[315] Benet L, Leyvraz F and Seligman T 2003 Phys. Rev. E **68** 045201 doi: 10.1103/PhysRevE.68.045201

[316] Sakurai J J 1994 Modern quantum mechanics, revised edition (Reading: Addison Wesley Publishing Company)

[317] Hartmann M, Mahler G and Hess O 2005 J. Stat. Phys. **119** 1139 doi: 10.1007/s10955-004-4298-5

[318] Keating J P, Linden N and Wells H J 2015 Commun. Math. Phys. **338** 81 doi: 10.1007/s00220-015-2366-0

[319] Davis C and Kahan W M 1970 SIAM J. Num. Ana. **7** 1 doi: 10.1137/0707001

[320] Bhatia R, Davis C and McIntosh A 1983 Lin. Alg. App. **52-53** 45 doi: 10.1016/0024-3795(83)80007-X

[321] Kulkarni M, Tiwari K L and Segal D 2012 Phys. Rev. B **86** 155424 doi: 10.1103/PhysRevB.86.155424

[322] Brandao F G S L and Cramer M 2015 preprint arXiv:1502.03263

[323] Ikeda T N, Watanabe Y and Ueda M 2011 Phys. Rev. E **84** 021130 doi: 10.1103/PhysRevE.84.021130

[324] Foini L, Cugliandolo L F and Gambassi A 2011 Phys. Rev. B **84** 212404 doi: 10.1103/PhysRevB.84.212404

[325] Foini L, Cugliandolo L F and Gambassi A 2012 J. Stat. Mech. P09011 doi: 10.1088/1742-5468/2012/09/P09011

[326] del Rio L, Hutter A, Renner R and Wehner S 2014 preprint arXiv:1401.7997

[327] Santos L F and Rigol M 2010 Phys. Rev. E **82** 031130 doi: 10.1103/PhysRevE.82.031130

[328] Steinigeweg R, Herbrych J and Prelovšek P 2013 Phys. Rev. E **87** 012118 doi: 10.1103/PhysRevE.87.012118

[329] Rigol M and Srednicki M 2012 Phys. Rev. Lett. **108** 110601 doi: 10.1103/PhysRevLett.108.110601

[330] Rutkevich S B 2012 preprint arXiv:1201.0578

[331] Berges J, Borsányi S and Wetterich C 2004 Phys. Rev. Lett. **93** 142002 doi: 10.1103/PhysRevLett.93.142002

[332] Essler F H L, Kehrein S, Manmana S R and Robinson N J 2014 Phys. Rev. B **89** 165104 doi: 10.1103/PhysRevB.89.165104

[333] Marcuzzi M, Marino J, Gambassi A and Silva A 2013 Phys. Rev. Lett. **111** 197203 doi: 10.1103/PhysRevLett.111.197203

[334] Marino J and Silva A 2012 Phys. Rev. B **86** 060408 doi: 10.1103/PhysRevB.86.060408

[335] Marino J and Silva A 2014 Phys. Rev. B **89** 024303 doi: 10.1103/PhysRevB.89.024303

[336] Karzig T, Glazman L I and von Oppen F 2010 Phys. Rev. Lett. **105** 226407 doi: 10.1103/PhysRevLett.105.226407

[337] Pagel D, Alvermann A and Fehske H 2013 Phys. Rev. E **87** 012127 doi: 10.1103/PhysRevE.87.012127

[338] Santos L F, Borgonovi F and Izrailev F M 2012 Phys. Rev. E **85** 036209 doi: 10.1103/PhysRevE.85.036209

[339] Biroli G, Kollath C and Läuchli A M 2010 Phys. Rev. Lett. **105** 250401 doi: 10.1103/PhysRevLett.105.250401

[340] Žnidarič M, Prosen T, Benenti G, Casati G and Rossini D 2010 Phys. Rev. E **81** 051135 doi: 10.1103/PhysRevE.81.051135

[341] Yuzbashyan E A and Shastry B S 2013 J. Stat. Phys. **150** 704 doi: 10.1007/s10955-013-0689-9

[342] Braak D 2011 Phys. Rev. Lett. **107** 100401 doi: 10.1103/PhysRevLett.107.100401

[343] Pal A and Huse D A 2010 Phys. Rev. B **82** 174411 doi: 10.1103/PhysRevB.82.174411

[344] Oganesyan V and Huse D 2007 Phys. Rev. B **75** 155111 doi: 10.1103/PhysRevB.75.155111

[345] Huse D A, Nandkishore R and Oganesyan V 2014 Phys. Rev. B **90** 174202 doi: 10.1103/PhysRevB.90.174202

[346] Shimony A 1995 Annals of the New York Academy of Sciences **755** 675 doi: 10.1111/j.1749-6632.1995.tb39008.x

[347] Barnum H and Linden N 2001 J. Phys. A **34** 6787 doi: 10.1088/0305-4470/34/35/305

[348] Wei T C and Goldbart P 2003 Phys. Rev. A **68** 042307 doi: 10.1103/PhysRevA.68.042307

[349] Lychkovskiy O 2010 Phys. Rev. E **82** 11123 doi: 10.1103/PhysRevE.82.011123

[350] Anderson P W 1958 Phys. Rev. **109** 1492 doi: 10.1103/PhysRev.109.1492

[351] Sims R and Ueltschi D (eds) 2010 An introduction to the mathematics of Anderson localisation preprint arXiv:1104.2317

[352] Abrahams E (ed) 2010 50 years of Anderson localisation (World Scientific Publishing)

[353] 2008 A short introduction to Anderson localization (Bath: Oxford University Press)

[354] Lagendijk A, Van Tiggelen B and Wiersma D S 2009 Physics Today **62** 24 doi: 10.1063/1.3206091

[355] Fleishman L and Anderson P W 1980 Phys. Rev. B **21** 2366 doi: 10.1103/PhysRevB.21.2366

[356] Nandkishore R and Huse D A 2015 Ann. Rev. Condens. Matter Phys. **6** 15 doi: 10.1146/annurev-conmatphys-031214-014726

[357] Basko D M, Aleiner I L and Altshuler B L 2006 Ann. Phys. **321** 1126 doi: 10.1016/j.aop.2005.11.014

[358] Altshuler B, Gefen Y, Kamenev A and Levitov L 1997 Phys. Rev. Lett. **78** 2803 doi: 10.1103/PhysRevLett.78.2803

[359] Gornyi I V, Mirlin A D and Polyakov D G 2005 Phys. Rev. Lett. **95** 206603 doi: 10.1103/PhysRevLett.95.206603

[360] Bauer B and Nayak C 2013 J. Stat. Mech. **2013** P09005 doi: 10.1088/1742-5468/2013/09/P09005

[361] Abdul-Rahman H and Stolz G 2015 preprint 1505.02117v1

[362] Žnidarič M, Prosen T and Prelovšek P 2008 Phys. Rev. B **77** 064426 doi: 10.1103/PhysRevB.77.064426

[363] Bardarson H, Pollmann F and Moore J E 2012 Phys. Rev. Lett. **109** 017202 doi: 10.1103/PhysRevLett.109.017202

[364] Friesdorf M, Werner A H, Goihl M, Eisert J and Brown W 2015 New J. Phys. **17** 113054 doi: 10.1088/1367-2630/17/11/113054

[365] Chandran A, Kim I H, Vidal G and Abanin D a 2014 Phys. Rev. B **91** 085425 doi: 10.1103/PhysRevB.91.085425

[366] Chandran A, Carrasquilla J, Kim I H, Abanin D A and Vidal G 2015 Phys. Rev. B **92** 024201 doi: 10.1103/PhysRevB.92.024201

[367] Vosk R and Altman E 2013 Phys. Rev. Lett. **110** 067204 doi: 10.1103/PhysRevLett.110.067204

[368] Vosk R, Huse D A and Altman E 2015 Phys. Rev. X **5** 031032 doi: 10.1103/PhysRevX.5.031032

[369] Jacquod P and Shepelyansky D L 1997 Phys. Rev. Lett. **70** 1837 doi: 10.1103/PhysRevLett.79.1837

[370] Georgeot B and Shepelyansky D L 1998 Phys. Rev. Lett. **81** 5129 doi: 10.1103/PhysRevLett.81.5129

[371] Haake F 2010 Quantum signatures of chaos Springer Series in Synergetics (Berlin, Heidelberg: Springer)

[372] Serbyn M, Papić Z and Abanin D 2014 Phys. Rev. B **90** 174302 doi: 10.1103/PhysRevB.90.174302

[373] Torres-Herrera E J and Santos L F 2015 Phys. Rev. B **92** 014208 doi: 10.1103/PhysRevB.92.014208

[374] Hickey J M, Genway S and Garrahan J P 2014 preprint arXiv:1405.5780

[375] Yao N Y, Laumann C R, Cirac J I, Lukin M D and Moore J E 2014 7 preprint arXiv:1410.7407

[376] Carleo G, Becca F, Schiró M and Fabrizio M 2012 Sc. Rep. **2** 243 doi: 10.1038/srep00243

[377] Billy J, Josse V, Zuo Z, Bernard A, Hambrecht B, Lugan P, Clément D, Sanchez-Palencia L, Bouyer P and Aspect A 2008 Nature **453** 891 doi: 10.1038/nature07000

[378] Schreiber M, Hodgman S S, Bordia P, Lüschen H P, Fischer M H, Vosk R, Altman E, Schneider U and Bloch I 2015 Science **349** 842 doi: 10.1126/science.aaa7432

[379] Weigert S 1992 Physica D **56** 107 doi: 10.1016/0167-2789(92)90053-P

[380] Arnold V I 1989 Mathematical methods of classical mechanics (Springer)

[381] Moradi G, Napoli F and Ercolessi E 2001 Statistical mechanics: An intermediate course 2nd ed (Singapore: World Scientific)

[382] Pöschel J 2003 Proc. Symp. Pure Math. **69** 707

[383] Sutherland B 2004 Beautiful models (World Scientific)

[384] Hawkins M S 2008 Local conservation laws in quantum integrable systems Phd thesis University of Birmingham

[385] Castagnino M and Lombardi O 2006 Ch. Sol. Fract. **28** 879 doi: 10.1016/j.chaos.2005.08.149

[386] Casati G, Chirikov B and Guarneri I 1985 Phys. Rev. Lett. **54** 1350 doi: 10.1103/PhysRevLett.54.1350

[387] Prosen T and Žnidarič M 2013 Phys. Rev. Lett. **111** 124101 doi: 10.1103/PhysRevLett.111.124101

[388] Atas Y Y, Bogomolny E, Giraud O and Roux G 2013 Phys. Rev. Lett. **110** 084101 doi: 10.1103/PhysRevLett.110.084101

[389] Stepanov V V, Müller G and Stolze J 2008 Phys. Rev. E **77** 066202 doi: 10.1103/PhysRevE.77.066202

[390] Berry M V and Tabor M 1977 Proc. Roy. Soc. A **356** 375 doi: 10.1098/rspa.1977.0140

[391] Fendley P, Ludwig A and Saleur H 1995 Phys. Rev. Lett. **74** 3005 doi: 10.1103/PhysRevLett.74.3005

[392] Hartmann M, Mahler G and Hess O 2004 Lett. Math. Phys. **68** 103 doi: 10.1023/B:MATH.0000043321.00896.86

[393] Hartmann M, Mahler G and Hess O 2004 Phys. Rev. E **70** 066148 doi: 10.1103/PhysRevE.70.066148

[394] Hartmann M and Mahler G 2005 Europhys. Lett. **70** 579 doi: 10.1209/epl/i2004-10518-5

[395] Ferraro A, Aolita L, Cavalcanti D, Cucchietti F M and Acín A 2010 Phys. Rev. A **81** 052318 doi: 10.1103/PhysRevA.81.052318

[396] Kliesch M, Gogolin C, Kastoryano M J, Riera A and Eisert J 2014 Phys. Rev. X **4** 031019 doi: 10.1103/PhysRevX.4.031019

[397] Ruelle D 1999 Statistical mechanics: Rigorous results (World Scientific Publishing)

[398] Ruelle D 1964 Rev. Mod. Phys. **36** 580 doi: 10.1103/RevModPhys.36.580

[399] Ginibre J 1965 J. Math. Phys. **6** 252 doi: 10.1063/1.1704276

[400] Bratteli O and Robinson D W 1987 Operator algebras and quantum statisticaI mechanics 1 2nd ed (Springer Berlin Heidelberg)

[401] Greenberg W 1969 Commun. Math. Phys. **13** 335 doi: 10.1007/BF01645417

[402] Park Y M and Yoo H J 1995 J. Stat. Phys. **80** 223 doi: 10.1007/BF02178359

[403] Cardy J 1996 Scaling and renormalization in statistical physics Cambridge Lecture Notes in Physics (Cambridge University Press)

[404] Mejia Miranda Y and Slade G 2011 Elec. Comm. Prob. **16** 129 doi: 10.1214/ECP.v16-1612

[405] Penrose M D 1994 J. Stat. Phys. **77** 3 doi: 10.1007/BF02186829

[406] Bhattacharjee S M and Khare A 1995 Curr. Sc. **69** 816

[407] Hastings M 2006 Phys. Rev. B **73** 085115 doi: 10.1103/PhysRevB.73.085115

[408] Sklar L 1995 Physics and chance: Philosophical issues in the foundations of statistical mechanics (Cambridge University Press)

[409] Ehrenfest P and Ehrenfest T 2002 The conceptual foundations of the statistical approach in mechani Dover Phoenix editions (Cornell University Press)

[410] Penrose O 1979 Rep. Prog. Phys. **42** 1937 doi: 10.1088/0034-4885/42/12/002

[411] Clausius R 1857 Ann. Phys. Chem. **176** 353 doi: 10.1002/andp.18571760302

[412] Maxwell J 1860 Phil. Mag. **19** 19

[413] Maxwell J 1860 Phil. Mag. **20** 21

[414] Boltzmann L 1872 Wiener Ber. **66** 275 doi: 10.1017/CBO9781139381420.023

[415] Boltzmann L 1896 Vorlesungen über Gastheorie. Bd. 1. (Leipzig: Barth)

[416] Loschmidt J 1877 Wiener Ber. **76** 209

[417] Thomson W 1874 Nature **9** 441 doi: 10.1038/009441c0

[418] Zermelo E 1896 Ann. Phys. Chem. **293** 485 doi: 10.1002/andp.18962930314

[419] Boltzmann L 1896 Ann. Phys. Chem. **293** 773 doi: 10.1002/andp.18962930414

[420] Boltzmann L and Hasenöhrl F 1868 Wiener Ber. **58** 517 doi: 10.1017/CBO9781139381420.006

[421] Boltzmann L 1871 Wiener Ber. **63** 679 doi: 10.1017/CBO9781139381420.020

[422] Shannon C E and Weaver W 1949 The mathematical theory of communication (Univ of Illinois Press)

[423] Fuchs C A 2010 preprint arXiv:1003.5209

[424] Timpson C G 2008 Stud. Hist. Phil. Sc. B **39** 579 doi: 10.1016/j.shpsb.2008.03.006

[425] Ballentine L, Yang Y and Zibin J 1994 Phys. Rev. A **50** 2854 doi: 10.1103/PhysRevA.50.2854

[426] Bohr N 1972 The Doctor's Dissertation (Text and Translation) Niels Bohr collected works (Niels Bohr Collected Works vol 1) ed Rosenfeld L and Nielsen J R (Elsevier) chap Early Work, p 163

[427] Aharoni A 2000 Introduction to the theory of ferromagnetism International series of monographs on physics (Oxford University Press)

[428] Nolting W and Ramakanth A 2009 Quantum theory of magnetism (Springer)

[429] Greiner Neise S 1995 Thermodynamics and statistical mechanics (Springer)

From observ to complex of q states via unsupervised learning

References

[1] G. Vidal, J. I. Latorre, E. Rico, and A. Kitaev, Phys. Rev. Lett. **90**, 227902 (2003).

[2] P. Calabrese and J. Cardy, J. Stat. Mech.: Theory Exp. **2004**, P06002 (2004).

[3] A. Kitaev and J. Preskill, Phys. Rev. Lett. **96**, 110404 (2006).

[4] E. Fradkin and J. E. Moore, Phys. Rev. Lett. **97**, 050404 (2006).

[5] F. Pollmann, A. M. Turner, E. Berg, and M. Oshikawa, Phys. Rev. B **81**, 064439 (2010).

[6] A. Szasz, J. Motruk, M. P. Zaletel, and J. E. Moore, Phys. Rev. X **10**, 021042 (2020).

[7] P. Calabrese and J. Cardy, J. Stat. Mech.: Theory Exp. **2005**, P04010 (2005).

[8] J. H. Bardarson, F. Pollmann, and J. E. Moore, Phys. Rev. Lett. **109**, 017202 (2012).

[9] U. Schollwöck, Ann. Phys. **326**, 96 (2011), january 2011 Special Issue.

[10] R. Orús, Ann. Phys. **349**, 117 (2014).

[11] S. Paeckel, T. Köhler, A. Swoboda, S. R. Manmana, U. Schollwöck, and C. Hubig, Ann. Phys. **411**, 167998 (2019).

[12] R. Islam, R. Ma, P. M. Preiss, M. Eric Tai, A. Lukin, M. Rispoli, and M. Greiner, Nature **528**, 77 (2015).

[13] C. Kokail, R. van Bijnen, A. Elben, B. Vermersch, and P. Zoller, arXiv:2009.09000 (2020).

[14] M. B. Plbnio and S. Virmani, Quantum Info. Comput. **7**, 1–51 (2007).

[15] B. M. Terhal, Theor. Comput. Sci. **287**, 313 (2002), natural Computing.

[16] A. C.-C. Yao, in Proceedings of 1993 IEEE 34th Annual Foundations of Computer Science (IEEE, 1993) pp. 352–361.

[17] M. R. Dowling and M. A. Nielsen, Quantum Information & Computation **8**, 861 (2008).

[18] J. Haferkamp, P. Faist, N. B. Kothakonda, J. Eisert, and N. Y. Halpern, arXiv:2106.05305 (2021).

[19] J. Lux, J. Müller, A. Mitra, and A. Rosch, Phys. Rev. A **89**, 053608 (2014).

[20] A. Bohrdt, C. B. Mendl, M. Endres, and M. Knap, New J. Phys. **19**, 063001 (2017).

[112] E. Leviatan, F. Pollmann, J. H. Bardarson, D. A. Huse, and E. Altman, arXiv:1702.08894 (2017).

[22] J. Dubail, J. Phys. A: Math. Theor. **50**, 234001 (2017).

[23] H. Wang and T. Zhou, J. High Energy Phys. **2019**, 20 (2019).

[24] K. Noh, L. Jiang, and B. Fefferman, Quantum **4**, 318 (2020).

[25] T. Rakovszky, C. W. von Keyserlingk, and F. Pollmann, arXiv:2004.05177 (2020).

[26] I. Reid and B. Bertini, Phys. Rev. B **104**, 014301 (2021).

[27] G. E. Hinton and R. R. Salakhutdinov, Science **313**, 504 (2006).

[28] M. Rigol, V. Dunjko, V. Yurovsky, and M. Olshanii, Phys. Rev. Lett. **98**, 050405 (2007).

[3] L. Vidmar and M. Rigol, J. Stat. Mech.: Theory Exp. P064007 (2016).

[4] F. H. L. Essler and M. Fagotti, J. Stat. Mech.: Theory Exp. P064002 (2016).

[26] F. Lange, Z. Lenarčič, and A. Rosch, Nat. Comm. **8**, 1 (2017).

[25] F. Lange, Z. Lenarčič, and A. Rosch, Phys. Rev. B **97**, 165138 (2018).

[33] F. Reiter, F. Lange, S. Jain, M. Grau, J. P. Home, and Z. Lenarčič, arXiv:1910.01593 (2019).

[18] Z. Lenarčič, E. Altman, and A. Rosch, Phys. Rev. Lett. **121**, 267603 (2018).

[35] Z. Lenarčič, O. Alberton, A. Rosch, and E. Altman, Phys. Rev. Lett. **125**, 116601 (2020).

[36] W. G. Brown and L. Viola, Phys. Rev. Lett. **104**, 250501 (2010).

[4] A. Nahum, J. Ruhman, S. Vijay, and J. Haah, Phys. Rev. X **7**, 031016 (2017).

[5] A. Nahum, S. Vijay, and J. Haah, Phys. Rev. X **8**, 021014 (2018).

[6] C. W. von Keyserlingk, T. Rakovszky, F. Pollmann, and S. L. Sondhi, Phys. Rev. X **8**, 021013 (2018).

[7] T. Rakovszky, F. Pollmann, and C. W. von Keyserlingk, Phys. Rev. X **8**, 031058 (2018).

[41] V. Khemani, A. Vishwanath, and D. A. Huse, Phys. Rev. X **8**, 031057 (2018).

[42] A. Chan, A. De Luca, and J. T. Chalker, Phys. Rev. X **8**, 041019 (2018).

[43] C. Sünderhauf, D. Pérez-García, D. A. Huse, N. Schuch, and J. I. Cirac, Phys. Rev. B **98**, 134204 (2018).

[44] A. J. Friedman, A. Chan, A. De Luca, and J. T. Chalker, Phys. Rev. Lett. **123**, 210603 (2019).

[45] A. Chan, A. De Luca, and J. T. Chalker, Phys. Rev. Lett. **121**, 060601 (2018).

[46] B. Bertini and L. Piroli, Phys. Rev. B **102**, 064305 (2020).

[47] D. Leibfried, R. Blatt, C. Monroe, and D. Wineland, Reviews of Modern Physics **75**, 281 (2003).

[48] I. Bloch, J. Dalibard, and W. Zwerger, Rev. Mod. Phys. **80**, 885 (2008).

[49] C. Gross and I. Bloch, Science **357**, 995 (2017).

[50] J. Preskill, Quantum **2**, 79 (2018).

[47] S. Ebadi, T. T. Wang, H. Levine, A. Keesling, G. Semeghini, A. Omran, D. Bluvstein, R. Samajdar, H. Pichler, W. W. Ho, S. Choi, S. Sachdev, M. Greiner, V. Vuletic, and M. D. Lukin, arXiv:2012.12281 (2020).

[48] P. Scholl, M. Schuler, H. J. Williams, A. A. Eberharter, D. Barredo, K.-N. Schymik, V. Lienhard, L.-P. Henry, T. C. Lang, T. Lahaye, A. M. Läuchli, and A. Browaeys, arXiv:2012.12268 (2020).

[53] A. Blais, A. L. Grimsmo, S. Girvin, and A. Wallraff, arXiv:2005.12667 (2020).

[54] R. Iten, T. Metger, H. Wilming, L. del Rio, and R. Renner, Phys. Rev. Lett. **124**, 010508 (2020).

[55] K. Kottmann, P. Huembeli, M. Lewenstein, and A. Acín, Phys. Rev. Lett. **125**, 170603 (2020).

[56] N. Sá and I. Roditi, "Beta-variational autoencoder as an entanglement classifier," (2020), arXiv:2004.14420 [quant-ph] .

[57] I. A. Luchnikov, A. Ryzhov, P.-J. Stas, S. N. Filippov, and H. Ouerdane, Entropy **21** (2019), 10.3390/e21111091.

[58] W. Zhong, J. M. Gold, S. Marzen, J. L. England, and N. Y. Halpern, "Learning about learning by many-body systems," (2020), arXiv:2004.03604 [cond-mat.stat-mech] .

[39] "Supplemental material includes (i) expression for conservation laws of transverse field ising model and lindblad operators, (ii) relation between lagrange parameter and latent representation, (iii) possibility of noise type detection in case of coupling to structured baths, more information on the (iii) random unitary model, (iv) training procedure, (v) intrinsic dimension and (vi) hamiltonian reconstruction," .

[60] H.-Y. Huang, R. Kueng, and J. Preskill, Nat. Phys. **16**, 1050 (2020).

[61] A. Elben, R. Kueng, H.-Y. R. Huang, R. van Bijnen, C. Kokail, M. Dalmonte, P. Calabrese, B. Kraus, J. Preskill, P. Zoller, et al., Phys. Rev. Lett. **125**, 200501 (2020).

[43] K. Kim, S. Korenblit, R. Islam, E. Edwards, M. Chang, C. Noh, H. Carmichael, G. Lin, L. Duan, C. J. Wang, et al., New J. Phys. **13**, 105003 (2011).

[44] R. Islam, E. Edwards, K. Kim, S. Korenblit, C. Noh, H. Carmichael, G.-D. Lin, L.-M. Duan, C.-C. J. Wang, J. Freericks, et al., Nat. Comm. **2**, 1 (2011).

[45] H. Labuhn, D. Barredo, S. Ravets, S. De Léséleuc, T. Macrì, T. Lahaye, and A. Browaeys, Nature **534**, 667 (2016).

[46] J. Zhang, G. Pagano, P. W. Hess, A. Kyprianidis, P. Becker, H. Kaplan, A. V. Gorshkov, Z.-X. Gong, and C. Monroe, Nature **551**, 601 (2017).

[43] M. Grady, Phys. Rev.D **25**, 1103 (1982).

[67] V. Alba and P. Calabrese, SciPost Phys. **4**, 017 (2018).

[12] L. Van der Maaten and G. Hinton, J. Mach. Learn. Res. **9** (2008).

[46] M. Zwolak and G. Vidal, Phys. Rev. Lett. **93**, 207205 (2004).

[45] F. Verstraete, J. J. García-Ripoll, and J. I. Cirac, Phys. Rev. Lett. **93**, 207204 (2004).

[71] L. Che, C. Wei, Y. Huang, D. Zhao, S. Xue, X. Nie, J. Li, D. Lu, and T. Xin, arXiv:2012.12520 (2020).

[72] A. Valenti, E. van Nieuwenburg, S. Huber, and E. Greplova, Phys. Rev. Res. **1**, 033092 (2019).

[73] X. Ma, Z. Tu, and S.-J. Ran, arXiv:2012.03019 (2020).

[74] T. Xin, S. Lu, N. Cao, G. Anikeeva, D. Lu, J. Li, G. Long, and B. Zeng, npj Quantum Info. **5**, 1 (2019).

[9] S. Wold, K. Esbensen, and P. Geladi, Chemometr. Intell. Lab. Syst. **2**, 37 (1987).

[10] I. Borg and P. J. Groenen, Modern multidimensional scaling: Theory and applications (Springer Science & Business Media, 2005).

[11] M. Balasubramanian, E. L. Schwartz, J. B. Tenenbaum, V. de Silva, and J. C. Langford, Science **295**, 7 (2002).

[13] L. McInnes, J. Healy, and J. Melville, arXiv:1802.03426 (2018).

[14] E. Levina and P. Bickel, Advances in neural information processing systems **17**, 777 (2004).

[15] P. Campadelli, E. Casiraghi, C. Ceruti, and A. Rozza, Math. Probl. Eng. **2015** (2015).

[16] E. Facco, M. d'Errico, A. Rodriguez, and A. Laio, Sci. Rep. **7**, 1 (2017).

[17] T. Mendes-Santos, X. Turkeshi, M. Dalmonte, and A. Rodriguez, arXiv:2006.12953 (2020).

[18] E. Lopez Tomas, A. Scheuer, E. Abisset-Chavanne, and F. Chinesta, Mathematics and Mechanics of Complex Systems **6**, 251 (2018).

[84] X. Turkeshi, arXiv:2101.06245 (2021).

[85] A. Khan, D. Quigley, M. Marcus, E. Thyrhaug, and A. Datta, Phys. Rev. Lett. **126**, 150402 (2021).

[86] A. Bohrdt, S. Kim, A. Lukin, M. Rispoli, R. Schittko, M. Knap, M. Greiner, and J. Léonard, arXiv:2012.11586 (2020).

[87] D. P. Kingma and M. Welling, Found. Trends Mach. Learn. **12**, 307 (2019).

[55] J. Bezanson, A. Edelman, S. Karpinski, and V. B. Shah, SIAM review **59**, 65 (2017).

[89] P. Weinberg and M. Bukov, SciPost Phys. **2**, 003 (2017).

[90] P. Weinberg and M. Bukov, SciPost Phys. **7**, 20 (2019).

[91] Repository containing training data and code: `https://github.com/markusschmitt/learning_quantum_complexity`.

References

[43] M. Grady, Phys. Rev.D **25**, 1103 (1982).

[4] F. H. L. Essler and M. Fagotti, J. Stat. Mech.: Theory Exp. P064002 (2016).

[25] F. Lange, Z. Lenarčič, and A. Rosch, Phys. Rev. B **97**, 165138 (2018).

[4] A. Nahum, J. Ruhman, S. Vijay, and J. Haah, Phys. Rev. X **7**, 031016 (2017).

[5] A. Nahum, S. Vijay, and J. Haah, Phys. Rev. X **8**, 021014 (2018).

[6] C. W. von Keyserlingk, T. Rakovszky, F. Pollmann, and S. L. Sondhi, Phys. Rev. X **8**, 021013 (2018).

[7] T. Rakovszky, F. Pollmann, and C. W. von Keyserlingk, Phys. Rev. X **8**, 031058 (2018).

[8] D. P. Kingma and J. Ba, arXiv:1412.6980 (2014).

[9] S. Wold, K. Esbensen, and P. Geladi, Chemometr. Intell. Lab. Syst. **2**, 37 (1987).

[10] I. Borg and P. J. Groenen, Modern multidimensional scaling: Theory and applications (Springer Science & Business Media, 2005).

[11] M. Balasubramanian, E. L. Schwartz, J. B. Tenenbaum, V. de Silva, and J. C. Langford, Science **295**, 7 (2002).

[12] L. Van der Maaten and G. Hinton, J. Mach. Learn. Res. **9** (2008).

[13] L. McInnes, J. Healy, and J. Melville, arXiv:1802.03426 (2018).

[14] E. Levina and P. Bickel, Advances in neural information processing systems **17**, 777 (2004).

[15] P. Campadelli, E. Casiraghi, C. Ceruti, and A. Rozza, Math. Probl. Eng. **2015** (2015).

[16] E. Facco, M. d'Errico, A. Rodriguez, and A. Laio, Sci. Rep. **7**, 1 (2017).

[17] T. Mendes-Santos, X. Turkeshi, M. Dalmonte, and A. Rodriguez, arXiv:2006.12953 (2020).

[18] E. Lopez Tomas, A. Scheuer, E. Abisset-Chavanne, and F. Chinesta, Mathematics and Mechanics of Complex Systems **6**, 251 (2018).

[19] E. Bairey, I. Arad, and N. H. Lindner, Phys. Rev. Lett. **122**, 020504 (2019).

From quantum chaos and eigenstate thermalization to statistical mechanics and thermodynamics

References

[1] S.K. Ma, Statistical mechanics, World Scientific, Singapore, Philadelphia, 1985.

[2] R.P. Feynman, Statistical Mechanics: A Set of Lectures, Westview Press; 2 edition, 1998.

[3] L. Boltzmann, Ann. Phys. (Leipzig) 57 (1896), p. 773.

[4] L. Boltzmann, Ann. Phys. (Leipzig) 60 (1897), p. 392.

[5] J.W. Gibbs, Elementary Principles in Statistical Mechanics, Dover, New York, 1960.

[6] O. Penrose, Foundations of Statistical Mechanics, Pergamon, Oxford, 1970.

[7] J.L. Lebowitz and O. Penrose, Physics Today 2 (1973), p. 23.

[8] Y.G. Sinai, Sov. Math Dokl. 4 (1963), pp. 1818–1822.

[9] Y.G. Sinai, Russian Mathematical Surveys 25 (1970), pp. 137–191.

[10] L.A. Bunimovich, Commun. Math. Phys. 65 (1979), p. 295.

[11] N. Simanyi, Ann. Henri Poincaré 5 (2004), p. 203.

[12] H. Poincaré, Acta Math. 13 (1890), p. 1.

[13] L.D. Faddeev and L.A. Takhtajan, Hamiltonian Methods in the Theory of Solitons (Classics in Mathematics), Springer, 2007.

[14] E. Fermi, J. Pasta, and S. Ulam, Studies of nonlinear problems, Tech. Rep., 1955.

[15] T. Dauxois, Physics Today 61 (2008), pp. 55–57.

[16] G.P. Berman and F.M. Izrailev, Chaos 15 (2005), p. 015104.

[17] E. Kozik and B. Svistunov, J. of Low Temp. Phys. 156 (2009), p. 215.

[18] J.P. Bouchaud, J. Phys. I France 2 (1992), p. 1705.

[19] D. Levesque and L. Verlet, Journal of Statistical Physics 72, pp. 519–537.

[20] C. Jarzynski, Phys. Rev. Lett. 78 (1997), p. 2690.

[21] G.E. Crooks, Phys. Rev. E 60 (1999), p. 2721.

[22] D. Collin, F. Ritort, C. Jarzynski, S.B. Smith, I. Tinoco Jr, and C. Bustamante, Nature 437 (2005), p. 231.

[23] J. Kurchan, arXiv:cond-mat/0007360 (2000).

[24] H. Tasaki, arXiv:cond-mat/0009244 (2000).

[25] M. Campisi, P. Hänggi, and P. Talkner, Rev. Mod. Phys. 83 (2011), p. 771.

[26] J.M. Deutsch, Phys. Rev. A 43 (1991), pp. 2046–2049.

[27] M. Srednicki, Phys. Rev. E 50 (1994), pp. 888–901.

[28] M. Rigol, V. Dunjko, and M. Olshanii, Nature 452 (2008), p. 854.

[29] M. Srednicki, J. Phys. A 32 (1999), p. 1163.

[30] J. von Neumann, Zeitschrift für Physik 57 (1929), pp. 30–70, translated to English in European Phys. J. H **35**, 201 (2010).

[31] E. Wigner, Ann. of Math. 62 (1955), pp. 548–564.

[32] I. Bloch, J. Dalibard, and W. Zwerger, Rev. Mod. Phys. 80 (2008), pp. 885–964.

[33] M.A. Cazalilla, R. Citro, T. Giamarchi, E. Orignac, and M. Rigol, Rev. Mod. Phys. 83 (2011), pp. 1405–1466.

[34] M. Greiner, O. Mandel, T.W. Hänsch, and I. Bloch, Nature 419 (2002), pp. 51–54.

[35] S. Will, T. Best, U. Schneider, L. Hackermüller, D.S. Lühmann, and I. Bloch, Nature 465 (2010), pp. 197–201.

[36] S. Will, T. Best, S. Braun, U. Schneider, and I. Bloch, Phys. Rev. Lett. 106 (2011), p. 115305.

[37] S. Will, D. Iyer, and M. Rigol, Nat. Commun. 6 (2015), p. 6009.

[38] T. Kinoshita, T. Wenger, and D.S. Weiss, Nature 440 (2006), p. 900.

[39] M. Gring, M. Kuhnert, T. Langen, T. Kitagawa, B. Rauer, M. Schreitl, I. Mazets, D.A. Smith, E. Demler, and J. Schmiedmayer, Science 337 (2012), pp. 1318–1322.

[40] T. Langen, S. Erne, R. Geiger, B. Rauer, T. Schweigler, M. Kuhnert, W. Rohringer, I.E. Mazets, T. Gasenzer, and J. Schmiedmayer, Science 348 (2015), p. 207.

[41] S. Trotzky, Y.A. Chen, A. Flesch, I.P. McCulloch, U. Schollwöck, J. Eisert, and I. Bloch, Nature Phys. 8 (2012), p. 325.

[42] K. Winkler, G. Thalhammer, F. Lang, R. Grimm, J.H. Denschlag, A.J. Daley, A. Kantian, H.P. Büchler, and P. Zoller, Nature 441 (2006), p. 853.

[43] L. Xia, L. Zundel, J. Carrasquilla, J.M. Wilson, M. Rigol, and D.S. Weiss, Nature Phys. 11 (2015), p. 316.

[44] L. Childress, M.V.G. Dutt, J.M. Taylor, A.S. Zibrov, F. Jelezko, J. Wrachtrup, P.R. Hemmer, and M.D. Lukin, Science 314 (2006), p. 281.

[45] S. Wall, D. Brida, S.R. Clark, H.P. Ehrke, D. Jaksch, A. Ardavan, S. Bonora, H. Uemura, Y. Takahashi, T. Hasegawa, H. Okamoto, G. Cerullo, and A. Cavalleri, Nature Physics 7 (2011), p. 114.

[46] D.N. Basov, R.D. Averitt, D. van der Marel, M. Dressel, and K. Haule, Rev. Mod. Phys. 83 (2011), p. 471.

[47] J. Berges, K. Boguslavski, S. Schlichting, and R. Venugopalan, Phys. Rev. D 89 (2014), p. 074011.

[48] J. Dziarmaga, Adv. Phys. 59 (2010), pp. 1063–1189.

[49] A. Polkovnikov, K. Sengupta, A. Silva, and M. Vengalattore, Rev. Mod. Phys. 83 (2011), pp. 863–883.

[50] V.I. Yukalov, Laser Phys. Lett. 8 (2011), pp. 485–507.

[51] R. Nandkishore and D.A. Huse, Annual Review of Condensed Matter Physics 6 (2015), pp. 15–38.

[52] J. Eisert, M. Friesdorf, and C. Gogolin, Nature Physics 11 (2015), p. 124.

[53] C. Gogolin and J. Eisert, Reports on Progress in Physics 79 (2016), p. 056001.

[54] M.A. Cazalilla and M. Rigol, New J. Phys. 12 (2010), p. 055006.

[55] A.J. Daley, M. Rigol, and D.S. Weiss, New J. Phys. 16 (2014), p. 095006.

[56] A.J. Lichtenberg and M.A. Liebermann, Regular and chaotic dynamics (2nd ed), Springer, Berlin, New York, 1992.

[57] P. Cvitanovic, R. Artuso, R. Mainieri, G. Tanner, and G. Vattay, Chaos: Classical and Quantum, ChaosBook.org, Niels Bohr Institute, Copenhagen, 2012.

[58] V.I. Arnold, Mathematical Methods of Classical Mechanics, Springer-Verlag, New York, 1989.

[59] J.V. José and E.J. Saletan, Classical Dynamics: A Contemporary Approach, Cambridge Univ. Press, Cambridge, 1998.

[60] H.J. Stöckmann, Scholarpedia 5 (2010), p. 10243.

[61] L.D. Landau and E.M. Lifshitz, Mechanics, Third Edition (Volume 1), Butterworth-Heinemann, 1976.

[62] A.N. Kolmogorov, Dokl. Akad. Nauk. SSR 98 (1954), pp. 527–530.

[63] V.I. Arnold, Russian Math. Survey 18 (1963), pp. 13–40.

[64] J.K. Moser, Nach. Akad. Wiss. Göttingen, Math. Phys. Kl. II 1 (1962), pp. 1–20.

[65] A.J. Lichtenberg and M.A. Lieberman, Regular and Chaotic Dynamics, Applied Mathematical Sciences, Vol. 38, Springer-Verlag, New York, 1992.

[66] H.W. Broer, I. Hoveijn, M. van Noort, C. Simo, and G. Vegter, Journal of Dynamics and Differential Equations 16 (2004), p. 897.

[67] B.V. Chirikov, Physics Reports 52 (1979), pp. 263–379.

[68] G.Casati, B.V. Chirikov, F.M. Izrailev, and J. Ford, Stochastic behavior of a quantum pendulum under a periodic perturbation, in Stochastic Behavior in Classical and Quantum Hamiltonian Systems, G. Casati and J. Ford, eds., Lecture Notes in Physics, Vol. 93, Springer Berlin Heidelberg, 1979, pp. 334–352.

[69] L.F. Santos and M. Rigol, Phys. Rev. E 81 (2010), p. 036206.

[70] L.F. Santos and M. Rigol, Phys. Rev. E 82 (2010), p. 031130.

[71] T. Guhr, A. Müller, Groeling, and H.A. Weidenmüller, Physics Reports 299 (1998), pp. 189–425.

[72] Y. Alhassid, Rev. Mod. Phys. 72 (2000), p. 895.

[73] M.L. Mehta, Random Matrices, Amsterdam: Elsevier/Academic Press, 2004.

[74] V.E. Kravtsov, Random matrix theory: Wigner-Dyson statistics and beyond, arXiv:0911.0639.

[75] M. Hillery, R.F. O'Connell, M.O. Scully, and E.P. Wigner, Physics Reports 106 (1984), pp. 121–167.

[76] A. Polkovnikov, Annals of Phys. 325 (2010), p. 1790.

[77] L.D. Landau and E.M. Lifshitz, Quantum Mechanics, Third Edition: Non-Relativistic Theory (Volume 3), Butterworth-Heinemann, 1981.

[78] D. Stone, Physics Today 58 (2005), p. 37.

[79] M.C. Gutzwiller, J. Math. Phys. 12 (1971), p. 343.

[80] Z. Rudnick, Notices of the AMS 55 (2008), p. 32.

[81] E. Wigner, Ann. of Math. 65 (1957), pp. 203–207.

[82] E. Wigner, Ann. of Math. 67 (1958), pp. 325–326.

[83] F.J. Dyson, J. Math. Phys. 3 (1962), p. 140.

[84] L.E. Reichl, The transition to Chaos: Conservative Classical Sysstems and Quantum Manifestations, Springer, New York, 2004.

[85] O. Bohigas, M.J. Giannoni, and C. Schmit, Phys. Rev. Lett. 52 (1984), pp. 1–4.

[86] E.B. Bogomolny, B. Georgeot, M.J. Giannoni, and C. Schmit, Phys. Rev. Lett. 69 (1992), p. 1477.

[87] T.A. Brody, J. Flores, J.B. French, P.A. Mello, A. Pandey, and S.S.M. Wong, Rev. Mod. Phys. 53 (1981), p. 385.

[88] M.V. Berry and M. Tabor, Proc. Roy. Soc. A 356 (1977), pp. 375–394.

[89] A. Pandey and R. Ramaswamy, Phys. Rev. A 43 (1991), pp. 4237–4243.

[90] M.V. Berry, J. Phys. A 10 (1977), p. 2083.

[91] V.V. Flambaum and F.M. Izrailev, Phys. Rev. E 55 (1997), pp. R13–R16.

[92] V.V. Flambaum and F.M. Izrailev, Phys. Rev. E 56 (1997), pp. 5144–5159.

[93] V.K.B. Kota, Lecture Notes in Physics 884 (2014).

[94] K.H. Böchhoff, Nuclear Data for Science and Technology, Springer, Brussels and Luxemburg, 1983.

[95] D. Wintgen and H. Friedrich, Phys. Rev. A 35 (1987), pp. 1464–1466.

[96] O. Bohigas, R.U. Haq, and A. Pandey, Fluctuation Properties of Nuclear Energy Levels and Widths: Comparison of Theory with Experiment, in Nuclear Data for Science and Technology, Reidel, Dordrecht (1983), p. 809.

[97] M.V. Berry and M. Robnik, Journal of Physics A: Mathematical and General 17, p. 2413.

[98] M. Robnik, J. Phys. A: Math. Gen. 14, p. 3195.

[99] M. Rigol and L.F. Santos, Phys. Rev. A 82 (2010), p. 011604(R).

[100] C. Kollath, G. Roux, G. Biroli, and A. Laeuchli, J. Stat. Mech. (2010), p. P08011.

[101] L.F. Santos, F. Borgonovi, and F.M. Izrailev, Phys. Rev. Lett. 108 (2012), p. 094102.

[102] L.F. Santos, F. Borgonovi, and F.M. Izrailev, Phys. Rev. E 85 (2012), p. 036209.

[103] Y.Y. Atas, E. Bogomolny, O. Giraud, and G. Roux, Phys. Rev. Lett. 110 (2013), p. 084101.

[104] Y.Y. Atas, E. Bogomolny, O. Giraud, P. Vivo, and E. Vivo, Journal of Physics A: Mathematical and Theoretical 46 (2013), p. 355204.

[105] R. Modak, S. Mukerjee, and S. Ramaswamy, Phys. Rev. B 90 (2014), p. 075152.

[106] R. Modak and S. Mukerjee, New J. Phys. 16 (2014), p. 093016.

[107] V.K.B. Kota and R. Sahu, Physics Letters B 429 (1998), p. 1.

[108] L.D. Landau and E.M. Lifshitz, Statistical Physics, Third Edition, Part 1, Volume 5, Butterworth-Heinemann, 1980.

[109] L.F. Santos, A. Polkovnikov, and M. Rigol, Phys. Rev. E 86 (2012), p. 010102(R).

[110] J.M. Deutsch, H. Li, and A. Sharma, Phys. Rev. E 87 (2013), p. 042135.

[111] M. Mierzejewski, T. Prosen, D. Crivelli, and P. Prelovšek, Phys. Rev. Lett. 110 (2013), p. 200602.

[112] H. Kim and D.A. Huse, Phys. Rev. Lett. 111 (2013), p. 127205.

[113] S. Khlebnikov and M. Kruczenski, Phys. Rev. E 90 (2014), p. 050101.

[114] J.H. Bardarson, F. Pollmann, and J.E. Moore, Phys. Rev. Lett. 109 (2012), p. 017202.

[115] R. Vosk and E. Altman, Phys. Rev. Lett. 110 (2013), p. 067204.

[116] M. Serbyn, Z. Papić, and D.A. Abanin, Phys. Rev. Lett. 110 (2013), p. 260601.

[117] A. Nanduri, H. Kim, and D.A. Huse, Phys. Rev. B 90 (2013), p. 064201.

[118] P. Ponte, Z. Papić, F. Huveneers, and D.A. Abanin, Phys. Rev. Lett. 114 (2015), p. 140401.

[119] C. Neill, P. Roushan, M. Fang, Y. Chen, M. Kolodrubetz, Z. Chen, A. Megrant, R. Barends, B. Campbell, B. Chiaro, A. Dunsworth, E. Jeffrey, J. Kelly, J. Mutus, P.J.J. O'Malley, C. Quintana, D. Sank, A. Vainsencher, J. Wenner, T.C. White, A. Polkovnikov, and J.M. Martinis, arXiv:1601.00600 (2016).

[120] A.M. Kaufman, M.E. Tai, A. Lukin, M. Rispoli, R. Schittko, P.M. Preiss, and M. Greiner, arXiv:1603.04409 (2016).

[121] A.J. Daley, H. Pichler, J. Schachenmayer, and P. Zoller, Phys. Rev. Lett. 109 (2012), p. 020505.

[122] R. Islam, R. Ma, P.M. Preiss, M.E. Tai, A. Lukin, M. Rispoli, and M. Greiner, Nature 528.

[123] J.R. Garrison and T. Grover, arXiv:1503.00729 (2015).

[124] D.N. Page, Phys. Rev. Lett. 71 (1993), p. 1291.

[125] L.F. Santos, A. Polkovnikov, and M. Rigol, Phys. Rev. Lett. 107 (2011), p. 040601.

[126] C. Neuenhahn and F. Marquardt, Phys. Rev. E 85 (2012), p. 060101.

[127] G. Casati, B.V. Chirikov, I. Guarneri, and F.M. Izrailev, Phys. Rev. E 48 (1993), p. R1613(R).

[128] G. Casati, B. Chirikov, I. Guarneria, and F. Izrailev, Physics Letters A 223 (1996), p. 430.

[129] V.V. Flambaum and F.M. Izrailev, Phys. Rev. E 61 (2000), pp. 2539–2542.

[130] M. Rigol, Phys. Rev. Lett. 116 (2016), p. 100601.

[131] A.C. Cassidy, C.W. Clark, and M. Rigol, Phys. Rev. Lett. 106 (2011), p. 140405.

[132] K. He, L.F. Santos, T.M. Wright, and M. Rigol, Phys. Rev. A 87 (2013), p. 063637.

[133] L. Vidmar and M. Rigol, J. Stat. Phys. (2016), p. 064007.

[134] A. Polkovnikov, Annals of Phys. 326 (2011), p. 486.

[135] M. Rigol, Phys. Rev. Lett. 112 (2014), p. 170601.

[136] M. Rigol and M. Fitzpatrick, Phys. Rev. A 84 (2011), p. 033640.

[137] K. He and M. Rigol, Phys. Rev. A 85 (2012), p. 063609.

[138] V. Gurarie, J. Stat. Mech. (2013), p. P02014.

[139] M. Kormos, L. Bucciantini, and P. Calabrese, EPL (Europhysics Letters) 107 (2014), p. 40002.

[140] M. Collura, M. Kormos, and P. Calabrese, J. Stat. Mech. (2014), p. P01009.

[141] S. Goldstein, J.L. Lebowitz, R. Tumulka, and N. Zanghi, European Phys. J. H 35 (2010), pp. 173–200.

[142] H. Tasaki, Phys. Rev. Lett. 80 (1998), pp. 1373–1376.

[143] S. Goldstein, J.L. Lebowitz, R. Tumulka, and N. Zanghì, Phys. Rev. Lett. 96 (2006), p. 050403.

[144] S. Popescu, A.J. Short, and A. Winter, Nature Phys. 2 (2006), p. 754.

[145] M. Rigol and M. Srednicki, Phys. Rev. Lett. 108 (2012), p. 110601.

[146] M. Srednicki, J. Phys. A 29 (1996), p. L75.

[147] R.V. Jensen and R. Shankar, Phys. Rev. Lett. 54 (1985), pp. 1879–1882.

[148] M. Feingold and A. Peres, Phys. Rev. A 34 (1986), pp. 591–595.

[149] M. Wilkinson, Journal of Physics A: Mathematical and General 20 (1987), p. 2415.

[150] T. Prosen, Annals of Phys. 235 (1994), pp. 115–164.

[151] B. Eckhardt, S. Fishman, J. Keating, O. Agam, J. Main, and K. Müller, Phys. Rev. E 52 (1995), pp. 5893–5903.

[152] S. Hortikar and M. Srednicki, Phys. Rev. E 57 (1998), pp. 7313–7316.

[153] E. Akkermans and G. Montambaux, Mesoscopic Physics of Electrons and Photons, Cambridge University Press, 2007.

[154] E. Khatami, G. Pupillo, M. Srednicki, and M. Rigol, Phys. Rev. Lett. 111 (2013), p. 050403.

[155] J. Lux, J. Müller, A. Mitra, and A. Rosch, Phys. Rev. A 89 (2014), p. 053608.

[156] P. Reimann, Phys. Rev. Lett. 115 (2015), p. 010403.

[157] M. Rigol, Phys. Rev. Lett. 103 (2009), p. 100403.

[158] M. Rigol, Phys. Rev. A 80 (2009), p. 053607.

[159] R. Steinigeweg, J. Herbrych, and P. Prelovšek, Phys. Rev. E 87 (2013), p. 012118.

[160] W. Beugeling, R. Moessner, and M. Haque, Phys. Rev. E 89 (2014), p. 042112.

[161] H. Kim, T.N. Ikeda, and D.A. Huse, Phys. Rev. E 90 (2014), p. 052105.

[162] R. Steinigeweg, A. Khodja, H. Niemeyer, C. Gogolin, and J. Gemmer, Phys. Rev. Lett. 112 (2014), p. 130403.

[163] A. Khodja, R. Steinigeweg, and J. Gemmer, Phys. Rev. E 91 (2015), p. 012120.

[164] W. Beugeling, R. Moessner, and M. Haque, Phys. Rev. E 91 (2015), p. 012144.

[165] E. Khatami, M. Rigol, A. Relaño, and A.M. Garcia-Garcia, Phys. Rev. E 85 (2012), p. 050102(R).

[166] S. Genway, A.F. Ho, and D.K.K. Lee, Phys. Rev. A 86 (2012), p. 023609.

[167] G. Biroli, C. Kollath, and A.M. Läuchli, Phys. Rev. Lett. 105 (2010), p. 250401.

[168] G. Roux, Phys. Rev. A 81 (2010), p. 053604.

[169] S. Sorg, L. Vidmar, L. Pollet, and F. Heidrich-Meisner, Phys. Rev. A 90 (2014), p. 033606.

[170] R. Mondaini, K.R. Fratus, M. Srednicki, and M. Rigol, Phys. Rev. E 93 (2016), p. 032104.

[171] T.N. Ikeda, Y. Watanabe, and M. Ueda, Phys. Rev. E 87 (2013), p. 012125.

[172] V. Alba, Phys. Rev. B 91 (2015), p. 155123.

[173] S. Mukerjee, V. Oganesyan, and D. Huse, Phys. Rev. B 73 (2006), p. 035113.

[174] H. Ott, E. de Mirandes, F. Ferlaino, G. Roati, G. Modugno, and M. Inguscio, Phys. Rev. Lett. 92 (2004), p. 160601.

[175] C.D. Fertig, K.M. O'Hara, J.H. Huckans, S.L. Rolston, W.D. Phillips, and J.V. Porto, Phys. Rev. Lett. 94 (2005), p. 120403.

[176] N. Strohmaier, Y. Takasu, K. Günter, R. Jördens, M. Köhl, H. Moritz, and T. Esslinger, Phys. Rev. Lett. 99 (2007), p. 220601.

[177] U. Schneider, L. Hackermüller, J.P. Ronzheimer, S. Will, S. Braun, T. Best, I. Bloch, E. Demler, S. Mandt, D. Rasch, and A. Rosch, Nature Phys 8 (2012), pp. 213–218.

[178] J.P. Ronzheimer, M. Schreiber, S. Braun, S.S. Hodgman, S. Langer, I.P. McCulloch, F. Heidrich-Meisner, I. Bloch, and U. Schneider, Phys. Rev. Lett. 110 (2013), p. 205301.

[179] C. Kollath, A.M. Läuchli, and E. Altman, Phys. Rev. Lett. 98 (2007), p. 180601.

[180] S.R. Manmana, S. Wessel, R.M. Noack, and A. Muramatsu, Phys. Rev. Lett. 98 (2007), p. 210405.

[181] M. Cramer, A. Flesch, I.P. McCulloch, U. Schollwöck, and J. Eisert, Phys. Rev. Lett. 101 (2008), p. 063001.

[182] A. Flesch, M. Cramer, I.P. McCulloch, U. Schollwöck, and J. Eisert, Phys. Rev. A 78 (2008), p. 033608.

[183] M. Eckstein, M. Kollar, and P. Werner, Phys. Rev. Lett. 103 (2009), p. 056403.

[184] M.C. Bañuls, J.I. Cirac, and M.B. Hastings, Phys. Rev. Lett. 106 (2011), p. 050405.

[185] P.R. Zangara, A.D. Dente, E.J. Torres-Herrera, H.M. Pastawski, A. Iucci, and L.F. Santos, Phys. Rev. E 88 (2013), p. 032913.

[186] G.E. Crooks, Journal of Statistical Physics 90 (1998), pp. 1481–1487.

[187] U. Seifert, Rep. Prog. Phys. 75 (2012), p. 126001.

[188] W. Thirring, Quantum Mathematical Physics. Second Ed., Springer-Verlag. Berlin, Heidelberg, 2002.

[189] E.M. Lifshitz and L.P. Pitaevskii, Physical Kinetics, Landau Lifshitz Course of Theoretical Physics, Vol. 10, Elsevier, 2006.

[190] N.G.V. Kampen, Stochastic Processes in Physics and Chemistry, Elsevier. Amsterdam, The Netherlands, 2003.

[191] A.W. Marshall and I. Olkin, Inequalities: Theory of Majorization, AcademicPress, NewYork, 1979.

[192] A. Polkovnikov, Phys. Rev. Lett. 101 (2008), p. 220402.

[193] G. Bunin, L. D'Alessio, Y. Kafri, and A. Polkovnikov, Nature Phys. 7 (2011), p. 913.

[194] A.E. Allahverdyan and K.V. Hovhannisyan, EPL (Europhysics Letters) 95 (2011), p. 60004.

[195] T.N. Ikeda, N. Sakumichi, A. Polkovnikov, and M. Ueda, Annals of Physics 354 (2015), p. 338.

[196] K. Ji and B.V. Fine, Phys. Rev. Lett. 107 (2011), p. 050401.

[197] M. Bukov, L. D'Alessio, and A. Polkovnikov, Advances in Physics 64 (2015), pp. 139–226.

[198] S. Kullback and R.A. Leibler, Annals of Mathematical Statistics 22 (1951), p. 79.

[199] A. Lenard, Journal of Statistical Physics 19 (1978), pp. 575–586.

[200] R. Balian, From microphysics to macrophysics. 2nd Ed., Springer, 2006.

[201] L. D'Alessio and A. Polkovnikov, Annals of Physics 345 (2014), p. 141.

[202] M. Kolodrubetz, B.K. Clark, and D.A. Huse, Phys. Rev. Lett. 109 (2012), p. 015701.

[203] L. Bonnes, F.H. Essler, and A.M. Läuchli, Phys. Rev. Lett. 113 (2014), p. 187203.

[204] A.E. Allahverdyan and T.M. Nieuwenhuizen, Phys. Rev. E 71 (2005), p. 046107.

[205] G.N. Bochkov and Y.E. Kuzovlev, JETP 45 (1977), p. 125.

[206] G.N. Bochkov and Y.E. Kuzovlev, Physica A 106 (1981), p. 443.

[207] C. Jarzynski, Annual Review Condensed Matter Physics 2 (2011), pp. 329–351.

[208] D. Andrieux and P. Gaspard, J. Stat. Mech. (2007), p. P02006.

[209] D.J. Evans and D.J. Searles, Phys. Rev. E 50 (1994), p. 1645.

[210] P. Pradhan, Y. Kafri, and D. Levine, Phys. Rev. E 77 (2008), p. 041129.

[211] P.L. Krapivsky, S. Redner, and E. Ben-Naim, A Kinetic View of Statistical Physics, Cambridge University Press, 2010.

[212] C. Jarzynski, Phys. Rev. A 46 (1992), p. 7498.

[213] C. Jarzynski, Phys. Rev. E 48 (1993), p. 4340.

[214] G. Bunin and Y. Kafri, Journal of Physics A: Mathematical and Theoretical 46 (2013), p. 095002.

[215] E. Ott, Phys. Rev. Lett. 42 (1979), p. 1628.

[216] D. Cohen, Ann. Phys. (NY) 283 (2000), p. 175.

[217] B. Cleuren, C.V. den Broeck, and R. Kawai, Phys. Rev. E 74 (2006), p. 021117.

[218] P. Gaspard and D. Andrieux, J. Stat. Mech. (2011), p. P03024.

[219] G.D. Mahan, Many-Particle Physics (Physics of Solids and Liquids), Third edition, Springer, 2000.

[220] C. Jarzynski and W.J. Świątecki, Nucl. Phys. A 552 (1993), p. 1.

[221] J. Blocki, F. Brut, and W.J. Swiatecki, Nuclear Physics A 554 (1993), pp. 107 – 117.

[222] J. Blocki, J. Skalski, and W.J. Swiatecki, Nuclear Physics A 594 (1995), pp. 137 – 155.

[223] A.V. Kargovsky, E.I. Anashkina, O.A. Chichigina, and A.K. Krasnova, Phys. Rev. E 87 (2013), p. 042133.

[224] J. Demers and C. Jarzynski, Phys. Rev. E 92 (2015), p. 042911.

[225] P. Mehta and A. Polkovnikov, Annals of Phys. 332 (2013), p. 110.

[226] L. D'Alessio and P.L. Krapivsky, Phys. Rev. E 83 (2011), p. 011107.

[227] M.P. Allen and D.J. Tildesley, Computer simulation of liquids, Oxford University Press, 1989.

[228] B. Sutherland, Beautiful Models, World Scientific, Singapore, 2004.

[229] J.S. Caux and J. Mossel, J. Stat. Mech. (2011), p. P02023.

[230] E.A. Yuzbashyan and B.S. Shastry, J. Stat. Phys. 150 (2013), p. 704.

[231] E.A. Yuzbashyan, Annals of Physics 367 (2016), pp. 288 – 296.

[232] M. Rigol, V. Dunjko, V. Yurovsky, and M. Olshanii, Phys. Rev. Lett. 98 (2007), p. 050405.

[233] E.T. Jaynes, Phys. Rev. 106 (1957), pp. 620–630.

[234] E.T. Jaynes, Phys. Rev. 108 (1957), pp. 171–190.

[235] M.A. Cazalilla, Phys. Rev. Lett. 97 (2006), p. 156403.

[236] M. Rigol, A. Muramatsu, and M. Olshanii, Phys. Rev. A 74 (2006), p. 053616.

[237] M. Kollar and M. Eckstein, Phys. Rev. A 78 (2008), p. 013626.

[238] T. Barthel and U. Schollwöck, Phys. Rev. Lett. 100 (2008), p. 100601.

[239] A. Iucci and M.A. Cazalilla, Phys. Rev. A 80 (2009), p. 063619.

[240] A. Iucci and M.A. Cazalilla, New J. Phys. 12 (2010), p. 055019.

[241] P. Calabrese, F.H.L. Essler, and M. Fagotti, Phys. Rev. Lett. 106 (2011), p. 227203.

[242] P. Calabrese, F.H.L. Essler, and M. Fagotti, J. Stat. Mech. (2012), p. P07022.

[243] M.A. Cazalilla, A. Iucci, and M.C. Chung, Phys. Rev. E 85 (2012), p. 011133.

[244] J.S. Caux and R.M. Konik, Phys. Rev. Lett. 109 (2012), p. 175301.

[245] C. Gramsch and M. Rigol, Phys. Rev. A 86 (2012), p. 053615.

[246] F.H.L. Essler, S. Evangelisti, and M. Fagotti, Phys. Rev. Lett. 109 (2012), p. 247206.

[247] M. Collura, S. Sotiriadis, and P. Calabrese, Phys. Rev. Lett. 110 (2013), p. 245301.

[248] M. Collura, S. Sotiriadis, and P. Calabrese, J. Stat. Mech. (2013), p. P09025.

[249] J.S. Caux and F.H.L. Essler, Phys. Rev. Lett. 110 (2013), p. 257203.

[250] G. Mussardo, Phys. Rev. Lett. 111 (2013), p. 100401.

[251] M. Fagotti, Phys. Rev. B 87 (2013), p. 165106.

[252] M. Fagotti and F.H.L. Essler, Phys. Rev. B 87 (2013), p. 245107.

[253] M. Fagotti, M. Collura, F.H.L. Essler, and P. Calabrese, Phys. Rev. B 89 (2014), p. 125101.

[254] B. Pozsgay, J. Stat. Mech. (2014), p. P10045.

[255] T.M. Wright, M. Rigol, M.J. Davis, and K.V. Kheruntsyan, Phys. Rev. Lett. 113 (2014), p. 050601.

[256] M. Cramer, C.M. Dawson, J. Eisert, and T.J. Osborne, Phys. Rev. Lett. 100 (2008), p. 030602.

[257] K. He and M. Rigol, Phys. Rev. A 87 (2013), p. 043615.

[258] M.C. Chung, A. Iucci, and M.A. Cazalilla, New J. Phys. 14 (2012), p. 075013.

[259] E.J. Torres-Herrera and L.F. Santos, Phys. Rev. E 88 (2013), p. 042121.

[260] S. Ziraldo and G.E. Santoro, Phys. Rev. B 87 (2013), p. 064201.

[261] T. Holstein and H. Primakoff, Phys. Rev. 58 (1940), pp. 1098–1113.

[262] P. Jordan and E. Wigner, Z. Phys. 47 (1928), p. 631.

[263] M. Rigol and A. Muramatsu, Phys. Rev. A 72 (2005), p. 013604.

[264] M. Rigol and A. Muramatsu, Mod. Phys. Lett. 19 (2005), p. 861.

[265] M. Rigol, Phys. Rev. A 72 (2005), p. 063607.

[266] S. Ziraldo, A. Silva, and G.E. Santoro, Phys. Rev. Lett. 109 (2012), p. 247205.

[267] L. Campos Venuti and P. Zanardi, Phys. Rev. E 87 (2013), p. 012106.

[268] S. Sachdev, Quantum Phase Transitions. 2nd Ed., Cambridge University Press, 2011.

[269] M. Kormos, A. Shashi, Y.Z. Chou, J.S. Caux, and A. Imambekov, Phys. Rev. B 88 (2013), p. 205131.

[270] J. De Nardis, B. Wouters, M. Brockmann, and J.S. Caux, Phys. Rev. A 89 (2014), p. 033601.

[271] F.H.L. Essler, G. Mussardo, and M. Panfil, Phys. Rev. A 91 (2015), p. 051602.

[272] B. Wouters, J. De Nardis, M. Brockmann, D. Fioretto, M. Rigol, and J.S. Caux, Phys. Rev. Lett. 113 (2014), p. 117202.

[273] B. Pozsgay, M. Mestyán, M.A. Werner, M. Kormos, G. Zaránd, and G. Takács, Phys. Rev. Lett. 113 (2014), p. 117203.

[274] M. Mierzejewski, P. Prelovšek, and T. Prosen, Phys. Rev. Lett. 113 (2014), p. 020602.

[275] G. Goldstein and N. Andrei, Phys. Rev. A 90 (2014), p. 043625.

[276] M. Rigol, Phys. Rev. E 90 (2014), p. 031301(R).

[277] B. Pozsgay, J. Stat. Mech. (2014), p. P09026.

[278] E. Ilievski, M. Medenjak, and T. Prosen, Phys. Rev. Lett. 115 (2015), p. 120601.

[279] E. Ilievski, J. De Nardis, B. Wouters, J.S. Caux, F.H.L. Essler, and T. Prosen, Phys. Rev. Lett. 115 (2015), p. 157201.

[280] J.S. Russel, Rep. Br. Assoc. Adv. Sci. (1844), pp. 311–390.

[281] D. Korteweg and G. de Vries, Philos. Mag. 39 (1895), pp. 422–443.

[282] I. Mazets, Eur. Phys. J. D 65 (2011), p. 43.

[283] J. Berges, S. Borsányi, and C. Wetterich, Phys. Rev. Lett. 93 (2004), p. 142002.

[284] M. Moeckel and S. Kehrein, Phys. Rev. Lett. 100 (2008), p. 175702.

[285] M. Moeckel and S. Kehrein, Ann. Phys. 324 (2009), p. 2146.

[286] M. Eckstein, A. Hackl, S. Kehrein, M. Kollar, M. Moeckel, P. Werner, and F.A. Wolf, Eur. Phys. J. Special Topics 180 (2010), p. 217.

[287] M. Kollar, F.A. Wolf, and M. Eckstein, Phys. Rev. B 84 (2011), p. 054304.

[288] T. Kitagawa, A. Imambekov, J. Schmiedmayer, and E. Demler, New J. Phys. 13 (2011), p. 073018.

[289] A. Mitra, Phys. Rev. B 87 (2013), p. 205109.

[290] E. Kaminishi, T. Mori, T.N. Ikeda, and M. Ueda, Nat. Phys. 11.

[291] M. Tavora, A. Rosch, and A. Mitra, Phys. Rev. Lett. 113 (2014), p. 010601.

[292] F.H.L. Essler, S. Kehrein, S.R. Manmana, and N.J. Robinson, Phys. Rev. B 89 (2014), p. 165104.

[293] M. Fagotti and M. Collura, arXiv:1507.02678 (2015).

[294] M. Babadi, E. Demler, and M. Knap, Phys. Rev. X 5 (2015), p. 041005.

[295] L. Mathey and A. Polkovnikov, Phys. Rev. A 81 (2010), p. 033605.

[296] R. Barnett, A. Polkovnikov, and M. Vengalattore, Phys. Rev. A 84 (2011), p. 023606.

[297] D.M. Stamper-Kurn and M. Ueda, Rev. Mod. Phys. 85 (2013), p. 1191.

[298] N. Nessi, A. Iucci, and M.A. Cazalilla, Phys. Rev. Lett. 113 (2014), p. 210402.

[299] V. Gurarie, Nucl.Phys. B 441 (1995), p. 569.

[300] C. Scheppach, J. Berges, and T. Gasenzer, Phys.Rev.A 81 (2010), p. 033611.

[301] B. Nowak, J. Schole, D. Sexty, and T. Gasenzer, Phys. Rev. A 85 (2012), p. 043627.

[302] E. Shimshoni, N. Andrei, and A. Rosch, Phys. Rev. B 68 (2003), p. 104401.

[303] E. Boulat, P. Mehta, N. Andrei, E. Shimshoni, and A. Rosch, Phys. Rev. B 76 (2007), p. 214411.

[304] M. Serbyn, Z. Papić, and D.A. Abanin, Phys. Rev. Lett. 111 (2013), p. 127201.

[305] D. Huse and V. Oganesyan, Phys. Rev. B 90 (2014), p. 174202.

[306] M. Stark and M. Kollar, arXiv:1308.1610 (2013).

[307] P.L. Kapitza, Soviet Phys. JETP 21 (1951), p. 588.

[308] B. Chirikov and D. Shepelyansky, Scholarpedia 3 (2008), p. 3550.

[309] J.M. Greene, J. Math. Phys. 20 (1979), p. 1183.

[310] R.S. MacKay, Physica D 7 (1983), p. 283.

[311] R.S. MacKay and I. Percival, Comm. Math. Phys. 94 (1985), p. 469.

[312] M.E. Fisher, The Nature of Critical Points, in Boulder Lectures in Theoretical Physics, Vol. 7, University of Colorado, Boulder (1965).

[313] C.N. Yang and T.D. Lee, Phys. Rev. 87 (1952), p. 404.

[314] M. Heyl and M. Vojta, Phys. Rev. B 92 (2015), p. 104401.

[315] M. Heyl, A. Polkovnikov, and S. Kehrein, Phys. Rev. Lett. 110 (2013), p. 135704.

[316] A.M. Odlyzko, The 10^{22}-nd zero of the Riemann zeta function, in Dynamical, spectral, and arithmetic zeta functions (San Antonio, TX, 1999), Contemp. Math., Vol. 290, Amer. Math. Soc., Providence, RI, 2001, pp. 139–144.

[317] D.A. Sivak and G.E. Crooks, Phys. Rev. Lett. 108 (2012), p. 190602.

From "Quench dynamics and relaxation in isolated integrable quantum spin chains" by Essler, Fagotti

References

[1] J. M. Deutsch, Quantum statistical mechanics in a closed system, Phys. Rev. A **43**, 2046 (1991); M. Srednicki, Chaos and quantum thermalization, Phys. Rev. E **50**, 888 (1994).

[2] M. Greiner, O. Mandel, T.W. Hänsch, and I. Bloch, Collapse and revival of the matter wave field of a Bose?Einstein condensate, Nature **419**, 51-54 (2002).

[3] T. Kinoshita, T. Wenger, D. S. Weiss, A quantum Newton's cradle, Nature **440**, 900 (2006).

[4] S. Hofferberth, I. Lesanovsky, B. Fischer, T. Schumm, and J. Schmiedmayer, Non-equilibrium coherence dynamics in one-dimensional Bose gases, Nature **449**, 324-327 (2007).

[5] L. Hackermuller, U. Schneider, M. Moreno-Cardoner, T. Kitagawa, S. Will, T. Best, E. Demler, E. Altman, I. Bloch and B. Paredes, Anomalous Expansion of Attractively Interacting Fermionic Atoms in an Optical Lattice, Science **327**, 1621 (2010).

[6] S. Trotzky Y.-A. Chen, A. Flesch, I. P. McCulloch, U. Schollwöck, J. Eisert, and I. Bloch, Probing the relaxation towards equilibrium in an isolated strongly correlated 1D Bose gas, Nature Phys. **8**, 325 (2012).

[7] M. Gring, M. Kuhnert, T. Langen, T. Kitagawa, B. Rauer, M. Schreitl, I. Mazets, D. A. Smith, E. Demler, and J. Schmiedmayer, Relaxation Dynamics and Pre-thermalization in an Isolated Quantum System, Science **337**, 1318 (2012).

[8] U. Schneider, L. Hackermüller, J. P. Ronzheimer, S. Will, S. Braun, T. Best, I. Bloch, E. Demler, S. Mandt, D. Rasch, and A. Rosch, Fermionic transport and out-of-equilibrium dynamics in a homogeneous Hubbard model with ultracold atoms, Nature Phys. **8**, 213 (2012).

[9] M. Cheneau, P. Barmettler, D. Poletti, M. Endres, P. Schauss, T. Fukuhara, C. Gross, I. Bloch, C. Kollath, and S. Kuhr, Light-cone-like spreading of correlations in a quantum many-body system, Nature **481**, 484 (2012).

[10] T. Langen, R. Geiger, M. Kuhnert, B. Rauer, and J. Schmiedmayer, Local emergence of thermal correlations in an isolated quantum many-body system, Nature Physics **9**, 640 (2013).

[11] F. Meinert, M.J. Mark, E. Kirilov, K. Lauber, P. Weinmann, A.J. Daley, and H.-C. Nägerl, Quantum Quench in an Atomic One-Dimensional Ising Chain, Phys. Rev. Lett. **111**, 053003 (2013).

[12] T. Fukuhara, A. Kantian, M. Endres, M. Cheneau, P. Schauß, S. Hild, D. Bellem, U. Schollwöck, T. Giamarchi, C. Gross, I. Bloch, and S. Kuhr, Quantum dynamics of a mobile spin impurity, Nature Physics **9**, 235 (2013).

[13] T. Fukuhara, P. Schauß, M. Endres, S. Hild, M. Cheneau, I. Bloch, and C. Gross, Microscopic observation of magnon bound states and their dynamics, Nature **502**, 76 (2013).

[14] J.P. Ronzheimer, M. Schreiber, S. Braun, S.S. Hodgman, S. Langer, I.P. McCulloch, F. Heidrich-Meisner, I. Bloch and U. Schneider, Expansion dynamics of interacting bosons in homogeneous lattices in one and two dimensions, Phys. Rev. Lett. **110**, 205301 (2013).

[15] N. Navon, A.L. Gaunt, R.P. Smith and Z. Hadzibabic, Critical Dynamics of Spontaneous Symmetry Breaking in a Homogeneous Bose gas, Science **347**, 167 (2015).

[16] P. Jurcevic, B. P. Lanyon, P. Hauke, C. Hempel, P. Zoller, R. Blatt, and C. F. Roos, Quasiparticle engineering and entanglement propagation in a quantum many-body system, Nature **511**, 202 (2014).

[17] P. Richerme, Z.-X. Gong, A. Lee, C. Senko, J. Smith, M. Moss-Feig, S. Michalakis, A. V. Gorshkov, and C. Monroe, Non-local propagation of correlations in quantum systems with long-range interactions, Nature **511**, 198 (2014).

[18] T. Langen, T. Gasenzer and J. Schmiedmayer, Prethermalization and universal dynamics in near-integrable quantum systems, arXiv:1603.09385 (2016).

[19] E. H. Lieb and W. Liniger, Exact Analysis of an Interacting Bose Gas. I. The General Solution and the Ground State Phys. Rev. **130**, 1605 (1963); E. H. Lieb, Exact Analysis of an Interacting Bose Gas. II. The Excitation Spectrum, Phys. Rev. **130**, 1616 (1963).

[20] V.E. Korepin, A.G. Izergin, and N.M. Bogoliubov, Quantum Inverse Scattering Method, Correlation Functions and Algebraic Bethe Ansatz (Cambridge University Press, 1993).

[21] B. Davies and V.E. Korepin, Higher conservation laws for the quantum non-linear Schroedinger equation, arXiv:1109.6604 (2011).

[22] A. C. Cassidy, C. W. Clark, and M. Rigol, Generalized Thermalization in an Integrable Lattice System, Phys. Rev. Lett. **106**, 140405 (2011).

[23] C. Gramsch and M. Rigol, Quenches in a quasidisordered integrable lattice system: Dynamics and statistical description of observables after relaxation, Phys. Rev. A **86**, 053615 (2012).

[24] T.M. Wright, M. Rigol, M.J. Davis, and K.V. Kheruntsyan, Nonequilibrium Dynamics of One-Dimensional Hard-Core Anyons Following a Quench: Complete Relaxation of One-Body Observables, Phys. Rev. Lett. **113**, 050601 (2014).

[25] P. Calabrese, F.H.L. Essler, and M. Fagotti, Quantum Quench in the Transverse-Field Ising Chain, Phys. Rev. Lett. **106**, 227203 (2011).

[26] P. Calabrese, F.H.L. Essler, and M. Fagotti, Quantum quench in the transverse field Ising chain: I. Time evolution of order parameter correlators. J. Stat. Mech. (2012) P07016.

[27] P. Calabrese, F.H.L. Essler, and M. Fagotti, Quantum Quench in the Transverse Field Ising Chain II: Stationary State Properties, J. Stat. Mech. (2012) P07022.

[28] M. Fagotti and F.H.L. Essler, Reduced density matrix after a quantum quench, Phys. Rev. B **87**, 245107 (2013).

[29] F.H.L. Essler, S. Evangelisti and M. Fagotti, Dynamical Correlations After a Quantum Quench, Phys. Rev. Lett. **109**, 247206 (2012).

[30] M. Fagotti, Finite-size corrections versus relaxation after a sudden quench, Phys. Rev. B **87**, 165106 (2013).

[31] M. Kormos, L. Bucciantini, and P. Calabrese, Stationary entropies after a quench from excited states in the Ising chain, EPL **107** 40002 (2014).

[32] L. Bucciantini, M. Kormos, P. Calabrese, Quantum quenches from excited states in the Ising chain, J. Phys. A: Math. Theor. **47** 175002 (2014).

[33] D. Rossini, A. Silva, G. Mussardo, and G.E. Santoro, Effective Thermal Dynamics Following a Quantum Quench in a Spin Chain, Phys. Rev. Lett. **102**, 127204 (2009); D. Rossini, S. Suzuki, G. Mussardo, G.E. Santoro, and A. Silva, Long time dynamics following a quench in an integrable quantum spin chain: Local versus nonlocal operators and effective thermal behavior, Phys. Rev. B **82**, 144302 (2010).

[34] F. Igói and H. Rieger, Long-Range Correlations in the Nonequilibrium Quantum Relaxation of a Spin Chain, Phys. Rev. Lett. **85**, 3233 (2000).

[35] K. Sengupta, S. Powell, and S. Sachdev, Quench dynamics across quantum critical points, Phys. Rev. A **69**, 053616 (2004).

[36] A. Silva, Statistics of the Work Done on a Quantum Critical System by Quenching a Control Parameter, Phys. Rev. Lett. **101**, 120603 (2008).

[37] F. Iglói and H. Rieger, Quantum Relaxation after a Quench in Systems with Boundaries, Phys. Rev. Lett. **106**, 035701 (2011).

[38] L. Foini, L.F. Cugliandolo, and A. Gambassi, Fluctuation-dissipation relations and critical quenches in the transverse field Ising chain, Phys. Rev. B **84**, 212404 (2011).

[39] H. Rieger and F. Iglói, Semiclassical theory for quantum quenches in finite transverse Ising chains, Phys. Rev. B **84**, 165117 (2011).

[40] D. Schuricht and F.H.L. Essler, Dynamics in the Ising field theory after a quantum quench, J. Stat. Mech. (2012) P04017.

[41] L. Foini, L.F. Cugliandolo, and A. Gambassi, Dynamic correlations, fluctuation-dissipation relations, and effective temperatures after a quantum quench of the transverse field Ising chain, J. Stat. Mech. (2012) P09011.

[42] M. Heyl, A. Polkovnikov, and S. Kehrein, Dynamical Quantum Phase Transitions in the Transverse-Field Ising Model, Phys. Rev. Lett. **110**, 135704 (2013).

[43] T. Caneva, E. Canovi, D. Rossini, G.E. Santoro, and A. Silva, Applicability of the generalized Gibbs ensemble after a quench in the quantum Ising chain, J. Stat. Mech. (2011) P07015.

[44] T. Antal, Z. Racz, A. Rakos, and G. M. Schutz, Transport in the XX chain at zero temperature: Emergence of flat magnetization profiles, Phys. Rev. E **59**, 4912 (1999).

[45] E. Barouch, B. McCoy, and M. Dresden, Statistical Mechanics of the XY Model. I, Phys. Rev. A **2**, 1075 (1970).

[46] E. Barouch and B. McCoy, Statistical Mechanics of the XY Model. II, Phys. Rev. A **3**, 786 (1971).

[47] E. Barouch and B. McCoy, Statistical Mechanics of the XY Model. III, Phys. Rev. A **3**, 2137 (1971).

[48] M. Fagotti and P. Calabrese, Evolution of entanglement entropy following a quantum quench: Analytic results for the XY chain in a transverse magnetic field, Phys. Rev. A **78**, 010306(R) (2008).

[49] M. A. Cazalilla, A. Iucci, and M.-C. Chung, Thermalization and quantum correlations in exactly solvable models, Phys. Rev. E **85**, 011133 (2012).

[50] B. Blass, H. Rieger, and F. Iglói, Quantum relaxation and finite-size effects in the XY chain in a transverse field after global quenches, EPL **99** 30004 (2012).

[51] M. Fagotti, On conservation laws, relaxation and pre-relaxation after a quantum quench, J. Stat. Mech. (2014) P03016.

[52] M. Fagotti, Local conservation laws in spin-1/2 XY chains with open boundary conditions, J. Stat. Mech. (2016) 063105 (doi:10.1088/1742-5468/2016/06/063105).

[53] M. Collura, P. Calabrese, and F.H.L. Essler, Quantum quench within the gapless phase of the spin-1/2 Heisenberg XXZ spin chain, Phys. Rev. B **92**, 125131 (2015).

[54] J. Lancaster and A. Mitra, Quantum quenches in an XXZ spin chain from a spatially inhomogeneous initial state, Phys. Rev. E **81**, 061134 (2010).

[55] T. Sabetta and G. Misguich, Nonequilibrium steady states in the quantum XXZ spin chain, Phys. Rev. B **88**, 245114 (2013).

[56] L. Bonnes, F.H.L. Essler and A. Läuchli, "Light-Cone" Dynamics After Quantum Quenches in Spin Chains, Phys. Rev. Lett. **113**, 187203 (2014).

[57] E. Canovi, D. Rossini, R. Fazio, G. Santoro, and A. Silva, Many-body localization and thermalization in the full probability distribution function of observables, New J. Phys. **14**, 095020 (2012).

[58] M. Fagotti and F.H.L. Essler, Stationary behaviour of observables after a quantum quench in the spin-1/2 Heisenberg XXZ chain, J. Stat. Mech. (2013) P07012.

[59] B. Pozsgay, The generalized Gibbs ensemble for Heisenberg spin chains, J. Stat. Mech. (2013) P07003.

[60] M. Fagotti, Dynamical Phase Transitions as Properties of the Stationary State: Analytic Results after Quantum Quenches in the Spin-1/2 XXZ Chain, arXiv:1308.0277; B. Pozsgay, Dynamical free energy and the Loschmidt-echo for a class of quantum quenches in the Heisenberg spin chain, Stat. Mech. (2013) P10028.

[61] W. Liu and N. Andrei, Quench Dynamics of the Anisotropic Heisenberg Model, Phys. Rev. Lett. **112**, 257204 (2014).

[62] P. Barmettler, M. Punk, V. Gritsev, E. Demler, and E. Altman, Relaxation of antiferromagnetic order in spin-1/2 chains following a quantum quench, Phys. Rev. Lett. **102**, 130603 (2009); P. Barmettler, M. Punk, V. Gritsev, E. Demler, and E. Altman, Quantum quenches in the anisotropic spin-1/2 Heisenberg chain: different approaches to many-body dynamics far from equilibrium, New J. Phys. **12**, 055017 (2010).

[63] M, Fagotti, M, Collura, F.H.L. Essler, and P. Calabrese, Relaxation after quantum quenches in the spin-1/2 Heisenberg XXZ chain, Phys. Rev. B **89**, 125101 (2014).

[64] E. Ilievski, J. De Nardis, B. Wouters, J.-S. Caux, F.H.L. Essler, T. Prosen, Complete Generalized Gibbs Ensemble in an interacting Theory, Phys. Rev. Lett. **115**, 157201 (2015).

[65] M. Brockmann, B. Wouters, D. Fioretto, J. De Nardis, R. Vlijm and J.-S. Caux, Quench action approach for releasing the Néel state into the spin-1/2 XXZ chain, Stat. Mech. (2014) P12009.

[66] B. Wouters, J. De Nardis, M. Brockmann, D. Fioretto, M. Rigol, and J.-S. Caux, Quenching the Anisotropic Heisenberg Chain: Exact Solution and Generalized Gibbs Ensemble Predictions, Phys. Rev. Lett. **113**, 117202 (2014).

[67] B. Pozsgay, Overlaps between eigenstates of the XXZ spin-1/2 chain and a class of simple product states, J. Stat. Mech. (2014) P06011.

[68] B. Pozsgay, M. Mestyán, M.A. Werner, M. Kormos, G. Zaránd, and G. Takács, Correlations after Quantum Quenches in the XXZ Spin Chain: Failure of the Generalized Gibbs Ensemble, Phys. Rev. Lett. **113**, 117203 (2014).

[69] M. Mestyán, B. Pozsgay, G. Takács, and M.A. Werner, Quenching the XXZ spin chain: quench action approach versus generalized Gibbs ensemble, J. Stat. Mech. (2015) P04001.

[70] M. Rigol, Quantum quenches in the thermodynamic limit. II. Initial ground states, Phys. Rev. E **90**, 031301(R) (2014).

[71] J. Mossel and J.-S. Caux, Relaxation dynamics in the gapped XXZ spin-1/2 chain, New J. Phys. **12** 055028 (2010).

[72] V. Alba and P. Calabrese, The quench action approach in finite integrable spin chains, arXiv:1512.02213 (2015).

[73] M. Kollar and M. Eckstein, Relaxation of a one-dimensional Mott insulator after an interaction quench, Phys. Rev. A **78**, 013626 (2008).

[74] T. Enss and J. Sirker, Lightcone renormalization and quantum quenches in one-dimensional Hubbard models, New J. Phys. **14**, 023008 (2012).

[75] D. Iyer, R. Mondaini, S. Will, and M. Rigol, Coherent quench dynamics in the one-dimensional Fermi-Hubbard model, Phys. Rev. A **90**, 031602(R) (2014).

[76] L. Riegger, G. Orso and F. Heidrich-Meisner, Interaction quantum quenches in the one-dimensional Fermi-Hubbard model with spin imbalance Phys. Rev. A **91**, 043623 (2015).

[77] A. Bauer, F. Dorfner and F. Heidrich-Meisner, Temporal decay of Néel order in the one-dimensional Fermi-Hubbard model, Phys. Rev. A **91**, 053628 (2015).

[78] S. Sotiriadis, P. Calabrese, and J. Cardy, Quantum quench from a thermal initial state, EPL **87** 20002 (2009).

[79] S. Sotiriadis, G. Martelloni, Equilibration and GGE in interacting-to-free Quantum Quenches in dimensions $d > 1$, J. Phys. A: Math. Theor. **49** 095002 (2016).

[80] P. Calabrese and J. Cardy, Quantum quenches in extended systems, J. Stat. Mech. (2007) P06008.

[81] M.A. Cazalilla, Effect of Suddenly Turning on Interactions in the Luttinger Model, Phys. Rev. Lett. **97**, 156403 (2006).

[82] A. Iucci and M. A. Cazalilla, Quantum quench dynamics of the Luttinger model, Phys. Rev. A **80**, 063619 (2009).

[83] J. Rentrop, D. Schuricht and V. Meden, Quench dynamics of the Tomonaga-Luttinger model with momentum-dependent interaction, New J. Phys. **14** 075001 (2012).

[84] C. Karrasch, J. Rentrop, D. Schuricht, and V. Meden, Luttinger-liquid universality in the time evolution after an interaction quench, Phys. Rev. Lett. **109**, 126406 (2012).

[85] B. Dóra, Á. Bácsi, and G. Zaránd, Generalized Gibbs ensemble and work statistics of a quenched Luttinger liquid, Phys. Rev. B **86**, 161109(R) (2012).

[86] N. Nessi and A. Iucci, Quantum quench dynamics of the Coulomb Luttinger model, Phys. Rev. B **87**, 085137 (2013).

[87] M. A. Cazalilla, M.-C. Chung, Quantum Quenches in the Luttinger model and its close relatives, arXiv:1603.04252 (2016).

[88] P. Calabrese and J. Cardy, Quantum quenches in 1+1 dimensional conformal field theories, arXiv:1603.02889 (2016)

[89] P. Calabrese and J. Cardy, Evolution of entanglement entropy in one-dimensional systems, J. Stat. Mech. (2005) P04010.

[90] P. Calabrese and J. Cardy, Time Dependence of Correlation Functions Following a Quantum Quench, Phys. Rev. Lett. **96**, 136801 (2006).

[91] J. Cardy, Thermalization and Revivals after a Quantum Quench in Conformal Field Theory, Phys. Rev. Lett. **112**, 220401 (2014).

[92] S. Sotiriadis, Memory-preserving equilibration after a quantum quench in a 1d critical model, arXiv:1507.07915 (2015).

[93] J. Cardy, Quantum quenches to a critical point in one dimension: some further results, J. Stat. Mech. (2016) 023103.

[94] V. Gritsev, E. Demler, M. Lukin, and A. Polkovnikov, Spectroscopy of Collective Excitations in Interacting Low-Dimensional Many-Body Systems Using Quench Dynamics, Phys. Rev. Lett. **99**, 200404 (2007).

[95] B. Bertini, D. Schuricht, and F.H.L. Essler, Quantum quench in the sine-Gordon model, J. Stat. Mech. (2014) P10035.

[96] M. Kormos and G. Zaránd, Quantum quenches in the sine-Gordon model: a semiclassical approach, arXiv:1507.02708 (2015).

[97] D. Fioretto and G. Mussardo, Quantum quenches in integrable field theories, New J. Phys. **12**, 055015 (2010).

[98] B. Bertini, L. Piroli, P. Calabrese, Quantum quenches in the sinh-Gordon model: steady state and one point correlation functions, arXiv:1602.08269 (2016).

[99] B. Pozsgay, Mean values of local operators in highly excited Bethe states, J. Stat. Mech. (2011) P01011.

[100] G. Mussardo, Infinite-Time Average of Local Fields in an Integrable Quantum Field Theory After a Quantum Quench, Phys. Rev. Lett. **111**, 100401 (2013).

[101] S. Evangelisti, Semi-classical theory for quantum quenches in the O(3) non-linear sigma model, J. Stat. Mech. (2013) P04003.

[102] A. Lamacraft, Noise correlations in the expansion of an interacting one-dimensional Bose gas from a regular array, Phys. Rev. A **84**, 043632 (2011).

[103] J. Mossel and J.-S. Caux, Exact time evolution of space- and time-dependent correlation functions after an interaction quench in the one-dimensional Bose gas, New J. Phys. **14**, 075006 (2012).

[104] M. Collura, S. Sotiriadis and P. Calabrese, Equilibration of a Tonks-Girardeau Gas Following a Trap Release, Phys. Rev. Lett. **110**, 245301 (2013); Quench dynamics of a Tonks-Girardeau gas released from a harmonic trap, J. Stat. Mech. (2013) P09025.

[105] M. Kormos, A. Shashi, Y.-Z. Chou, J.-S. Caux and A. Imambekov, Interaction quenches in the one-dimensional Bose gas, Phys. Rev. B **88**, 205131(2013)

[106] M. Collura, S. Sotiriadis, and P. Calabrese, Quench dynamics of a Tonks-Girardeau gas released from a harmonic trap, J. Stat. Mech. (2013) P09025.

[107] J. De Nardis, B. Wouters, M. Brockmann, and J.-S. Caux, Solution for an interaction quench in the Lieb-Liniger Bose gas, Phys. Rev. A **89**, 033601 (2014).

[108] P.P. Mazza, M. Collura, M. Kormos, and P. Calabrese, Interaction quench in a trapped 1D Bose gas, J. Stat. Mech. (2014) P11016.

[109] M. Collura, M. Kormos, and P. Calabrese, Stationary entanglement entropies following an interaction quench in 1D Bose gas, J. Stat. Mech. (2014) P01009.

[110] M. Kormos, M. Collura and P. Calabrese, Analytic results for a quantum quench from free to hard-core one-dimensional bosons, Phys. Rev. A **89**, 013609 (2014).

[111] J. De Nardis and J.-S. Caux, Analytical expression for a post-quench time evolution of the one-body density matrix of one-dimensional hard-core bosons, J. Stat. Mech. (2014) P12012.

[112] F.H.L. Essler, G. Mussardo, and M. Panfil, Generalized Gibbs ensembles for quantum field theories, Phys. Rev. A **91**, 051602(R) (2015).

[113] J. De Nardis, L. Piroli and J.-S. Caux, Relaxation dynamics of local observables in integrable systems, Phys. A: Math. Theor. **48** 43FT01 (2015).

[114] L. Piroli, P. Calabrese, and F.H.L. Essler, Multiparticle Bound-State Formation following a Quantum Quench to the One-Dimensional Bose Gas with Attractive Interactions, Phys. Rev. Lett. **116**, 070408 (2016).

[115] M. Collura and D. Karevski, Critical Quench Dynamics in Confined Systems, Phys. Rev. Lett. **104**, 200601 (2010).

[116] J. Dziarmaga, Dynamics of a Quantum Phase Transition and Relaxation to a Steady State, Adv. Phys. **59**, 1063 (2010); C. De Grandi, V. Gritsev and A. Polkovnikov, Quench dynamics near a quantum critical point: application to the sine-Gordon model, Phys. Rev. B **81**, 224301 (2010); A. Dutta, G. Aeppli, B.K. Chakrabarti, U. Divakaran, T.F. Rosenbaum and D. Sen, Quantum phase transitions in transverse field spin models: from statistical physics to quantum information, Cambridge University Press, Cambridge 2015.

[117] W.H. Zurek, Cosmological experiments in condensed matter systems, Phys. Rep. **276**, 177 (1996).

[118] A. Polkovnikov, K. Sengupta, A. Silva, and M. Vengalattore, Colloquium: Nonequilibrium dynamics of closed interacting quantum systems, Rev. Mod. Phys. **83**, 863 (2011).

[119] C. Gogolin and J. Eisert, Equilibration, thermalisation, and the emergence of statistical mechanics in closed quantum systems - a review, arXiv:1503.07538 (2015).

[120] A. Lamacraft and J.E. Moore, Potential insights into non-equilibrium behavior from atomic physics, in Ultracold Bosonic and Fermionic Gases, eds A. Fetter, K. Levin and D. Stamper-Kurn, Elseview 2012; arXiv:1106.3567 (2011).

[121] L. D'Alessio, Y. Kafri, A. Polkovnikov and M. Rigol, From Quantum Chaos and Eigenstate Thermalization to Statistical Mechanics and Thermodynamics, arXiv:1509.06411 (2015).

[122] R. A. Barankov, L. S. Levitov, Synchronization in the BCS Pairing Dynamics as a Critical Phenomenon, Phys. Rev. Lett. **96**, 230403 (2006); E.A. Yuzbashyan and M. Dzero, Dynamical vanishing of the order parameter in a fermionic condensate, Phys. Rev. Lett. **96**, 230404 (2006).

[123] G. Vidal, J.I. Latorre, E. Rico, and A. Kitaev, Entanglement in Quantum Critical Phenomena, Phys. Rev. Lett. **90**, 227902 (2003).

[124] I. Peschel and V. Eisler, Reduced density matrices and entanglement entropy in free lattice models, J. Phys. A: Math. Theor. **42** 504003 (2009).

[125] F. Verstraete, M.M. Wolf, D. Perez-Garcia, and J.I. Cirac, Criticality, the Area Law, and the Computational Power of Projected Entangled Pair States, Phys. Rev. Lett. **96** 220601 (2006); M. B. Hastings, Entropy and entanglement in quantum ground states, Phys. Rev.

B **76**, 035114 (2007); N. de Beaudrap, T.J. Osborne, and J. Eisert, Ground states of unfrustrated spin Hamiltonians satisfy an area law, New J. Phys. **12** 095007 (2010).

[126] T. Barthel and U. Schollwöck, Dephasing and the Steady State in Quantum Many-Particle Systems, Phys. Rev. Lett. **100**, 100601 (2008).

[127] M. Fagotti and M. Collura, Universal prethermalization dynamics of entanglement entropies after a global quench, arXiv:1507.02678 (2015).

[128] S. Sotiriadis and P. Calabrese, Validity of the GGE for quantum quenches from interacting to noninteracting models, J. Stat. Mech. (2014) P07024.

[129] E. Bettelheim, A.G. Abanov and P. Wiegmann, Quantum Shock Waves - the case for non-linear effects in dynamics of electronic liquids, Phys. Rev. Lett. **97**, 246401 (2006).

[130] E. Bettelheim, A.G. Abanov and P. Wiegmann, Orthogonality catastrophe and shock waves in a non-equilibrium Fermi gas, Phys.Rev.Lett. **97**, 246402 (2006).

[131] S. Sotiriadis and J. Cardy, Inhomogeneous Quantum Quenches, J. Stat. Mech. P11003 (2008).

[132] P. Calabrese, C. Hagendorf, and P. Le Doussal, Time evolution of 1D gapless models from a domain-wall initial state: SLE continued?, J. Stat. Mech. P07013 (2008).

[133] E. Bettelheim and P. Wiegmann, Fermi distribution of semicalssical non-eqilibrium Fermi states, Phys. Rev. B **84**, 085102 (2011).

[134] L. Vidmar, S. Langer, I.P. McCulloch, U. Schneider, U. Schollwoeck and F. Heidrich-Meisner, Sudden expansion of Mott insulators in one dimension Phys. Rev. B **88**, 235117 (2013).

[135] V. Eisler and Z. Racz, Full Counting Statistics in a Propagating Quantum Front and Random Matrix Spectra, Phys. Rev. Lett. **110**, 060602 (2013).

[136] M.A. Rajabpour and S. Sotiriadis, Quantum quench of the trap frequency in the harmonic Calogero model, Phys. Rev. A **89**, 033620 (2014).

[137] Z. Mei, L. Vidmar, F. Heidrich-Meisner and C. J. Bolech, Unveiling hidden structure of many-body wavefunctions of integrable systems via sudden expansion experiments, Phys. Rev. A **93**, 021607 (2016).

[138] W.H. Aschbacher and C.-A. Pillet, Non-Equilibrium Steady States of the XY Chain, J. Stat. Phys. **112**, 1153 (2003).

[139] W.H. Aschbacher and J.-M. Barbaroux, Out of Equilibrium Correlations in the XY Chain, Lett. Math. Phys. **77**, 11 (2006).

[140] D. Bernard and B. Doyon, Energy flow in non-equilibrium conformal field theory, J. Phys. A: Math. Theor. **45**, 362001 (2012).

[141] J.-S. Caux and R. M. Konik, Constructing the Generalized Gibbs Ensemble after a Quantum Quench, Phys. Rev. Lett. **109**, 175301 (2012).

[142] D. Bernard and B. Doyon, Non-Equilibrium Steady States in Conformal Field Theory, Ann. H. Poincaré **16**, 113 (2015).

[143] M. Mintchev and P. Sorba, Luttinger liquid in a non-equilibrium steady state, J. Phys. A: Math. Theor. **49**, 095006 (2013).

[144] A. De Luca, J. Viti, D. Bernard, and B. Doyon, Nonequilibrium thermal transport in the quantum Ising chain, Phys. Rev. B **88**, 134301 (2013).

[145] T. Sabetta and G. Misguich, Nonequilibrium steady states in the quantum XXZ spin chain, Phys. Rev. B **88**, 245114 (2013).

[146] B. Doyon, M. Hoogeveen, and D. Bernard, Energy flow and fluctuations in non-equilibrium conformal field theory on star graphs, Stat. Mech. (2014) P03002.

[147] O. Castro-Alvaredo, Y. Chen, B. Doyon, and M. Hoogeveen, Thermodynamic Bethe ansatz for non-equilibrium steady states: exact energy current and fluctuations in integrable QFT, J. Stat. Mech. (2014) P03011.

[148] A. De Luca, G. Martelloni, and J. Viti, Stationary states in a free fermionic chain from the quench action method, Phys. Rev. A **91**, 021603(R) (2014).

[149] B. Doyon, A. Lucas, K. Schalm, and M.J Bhaseen, Non-equilibrium steady states in the Klein-Gordon theory, J. Phys. A: Math. Theor. 48 095002 (2015).

[150] B. Doyon, Lower bounds for ballistic current and noise in non-equilibrium quantum steady states, Nucl. Phys. B **892**, 190 (2015).

[151] J. Viti; J.-M. Stéphan; J. Dubail; M. Haque, Inhomogeneous quenches in a fermionic chain: exact results, arXiv:1507.08132 (2015).

[152] T. Platini and D. Karevski, Relaxation in the XX quantum chain, J. Phys. A: Math. Theor. **40** 1711 (2007).

[153] V. Eisler, D. Karevski, T. Platini, and I. Peschel, Entanglement evolution after connecting finite to infinite quantum chains, J. Stat. Mech. (2008) **P01023**.

[154] D. Bernard and B. Doyon, Conformal field theory out of equilibrium: a review, arXiv:1603.07765 (2016).

[155] R. Vasseur and J.E. Moore, Nonequilibrium quantum dynamics and transport: from integrability to many-body localization, arXiv:1603.06618 (2016).

[156] M. Cramer, C.M. Dawson, J. Eisert, and T.J. Osborne, Exact Relaxation in a Class of Nonequilibrium Quantum Lattice Systems, Phys. Rev. Lett. **100**, 030602 (2008).

[157] M. Cramer and J. Eisert, A quantum central limit theorem for non-equilibrium systems: exact local relaxation of correlated states, New J. Phys. **12**, 055020 (2010).

[158] J. Sirker, N.P. Konstantinidis, F. Andraschko, and N. Sedlmayr, Locality and thermalization in closed quantum systems, Phys. Rev. A **89**, 042104 (2014).

[159] J.R. Garrison and T. Grover, Does a single eigenstate encode the full Hamiltonian?, arXiv:1503.00729.

[160] M. Rigol and M. Srednicki, Alternatives to Eigenstate Thermalization, Phys. Rev. Lett. **108**, 110601 (2012).

[161] M. Rigol, V. Dunjko, and M. Olshanii, Thermalization and its mechanism for generic isolated quantum systems, Nature **452**, 854 (2008).

[162] S. Braun, J.P. Ronzheimer, M. Schreiber, S.S. Hodgman, T. Rom, I. Bloch, U. Schneider, Negative Absolute Temperature for Motional Degrees of Freedom, Science **339**, 52 (2013).

[163] T. Prosen, A new class of completely integrable quantum spin chains, J. Phys. A: Math. Gen. **31** L397 (1998); M. Grady, Infinite set of conserved charges in the Ising model, Phys. Rev. D **25**, 1103 (1981).

[164] E.T. Jaynes, Information Theory and Statistical Mechanics, Phys. Rev. **106**, 620 (1957).

[165] M. Rigol, V. Dunjko, V. Yurovsky, and M. Olshanii, Relaxation in a Completely Integrable Many-Body Quantum System: An Ab Initio Study of the Dynamics of the Highly Excited States of 1D Lattice Hard-Core Bosons, Phys. Rev. Lett. **98**, 50405 (2007).

[166] B. Doyon, Thermalization and pseudolocality in extended quantum systems, arXiv:1512.03713 (2015).

[167] M. Rigol, Breakdown of thermalization in finite one-dimensional systems, Phys. Rev. Lett. **103**, 100403 (2009).

[168] M. Rigol, Quantum quenches and thermalization in one-dimensional fermionic systems, Phys. Rev. A **80**, 053607 (2009).

[169] G. Biroli, C. Kollath, and A.M. Läuchli, Effect of Rare Fluctuations on the Thermalization of Isolated Quantum Systems, Phys. Rev. Lett. **105**, 250401 (2010).

[170] L.F. Santos and M. Rigol, Localization and the effects of symmetries in the thermalization properties of one-dimensional quantum systems, Phys. Rev. E **82**, 031130 (2010).

[171] M. Rigol and L.F. Santos, Quantum chaos and thermalization in gapped systems, Phys. Rev. A **82**, 011604(R) (2010).

[172] C. Neuenhahn and F. Marquardt, Thermalization of interacting fermions and delocalization in Fock space, Phys. Rev. E **85** 060101 (2012).

[173] R. Steinigeweg, J. Herbrych, and P. Prelovsek, Eigenstate thermalization within isolated spin-chain systems, Phys. Rev. E **87**, 012118 (2013).

[174] W. Beugeling, R. Moessner, and M. Haque, Finite-size scaling of eigenstate thermalization, Phys. Rev. E **89** 042112 (2014).

[175] H. Kim, T.N. Ikeda, and D.A. Huse, Testing whether all eigenstates obey the Eigenstate Thermalization Hypothesis, Phys. Rev. E **90**, 052105 (2014).

[176] W. Beugeling, R. Moessner, and M. Haque, Off-diagonal matrix elements of local operators in many-body quantum systems, Phys. Rev. E **91**, 012144 (2015).

[177] J.-S. Caux and F.H.L. Essler, Time Evolution of Local Observables After Quenching to an Integrable Model, Phys. Rev. Lett. **110**, 257203 (2013).

[178] E. Lieb, T. Schultz, D. Mattis, Two soluble models of an antiferromagnetic chain, Ann. Phys. **16**, 407 (1961).

[179] V. Alba, Simulating the Generalized Gibbs Ensemble (GGE): a Hilbert space Monte Carlo approach, arXiv:1507.06994 (2015).

[180] B. Fröhlich, M. Feld, E. Vogt, M. Koschorreck, W. Zwerger, and M. Köhl Radio-Frequency Spectroscopy of a Strongly Interacting Two-Dimensional Fermi Gas, Phys. Rev. Lett. **106**, 105301 (2011).

[181] S. Bravyi, M. B. Hastings, and F. Verstraete, Lieb-Robinson Bounds and the Generation of Correlations and Topological Quantum Order, Phys. Rev. Lett. **97**, 050401 (2006).

[182] E. Khatami, G. Pupillo, M. Srednicki, and M. Rigol, Fluctuation-Dissipation Theorem in an Isolated System of Quantum Dipolar Bosons after a Quench, Phys. Rev. Lett. **111**, 050403 (2013).

[183] G. De Chiara, S. Montangero, P. Calabrese, and R. Fazio, Entanglement entropy dynamics of Heisenberg chains, J. Stat. Mech. (2006) P03001.

[184] A. Läuchli and C. Kollath, Spreading of correlations and entanglement after a quench in the one-dimensional Bose-Hubbard model, J. Stat. Mech. (2008) P05018.

[185] S. R. Manmana, S. Wessel, R. M. Noack, and A. Muramatsu, Time evolution of correlations in strongly interacting fermions after a quantum quench, Phys. Rev. B **79**, 155104 (2009).

[186] G. Carleo, F. Becca, L. Sanchez-Palencia, S. Sorella, and M. Fabrizio, Light-cone effect and supersonic correlations in one- and two-dimensional bosonic superfluids. Phys. Rev. A **89**, 031602 (2014).

[187] P. Hauke and L. Tagliacozzo, Spread of Correlations in Long-Range Interacting Quantum Systems, Phys. Rev. Lett. **111**, 207202 (2013).

[188] J. Schachenmayer, B. P. Lanyon, C. F. Roos, and A. J. Daley, Entanglement Growth in Quench Dynamics with Variable Range Interactions, Phys. Rev. X **3**, 031015 (2013).

[189] J. Eisert, M. van den Worm, S. R. Manmana, and M. Kastner, Breakdown of Quasilocality in Long-Range Quantum Lattice Models, Phys. Rev. Lett. **111**, 260401 (2013).

[190] D. Vodola, L. Lepori, E. Ercolessi, and G. Pupillo, Long-range Ising and Kitaev models: phases, correlations and edge modes, 2016 New J. Phys. **18** 015001.

[191] M. V. Regemortel, D. Sels, and M. Wouters, Information propagation and equilibration in long-range Kitaev chains, arXiv:1511.05459 (2015).

[192] A.S. Buyskikh, M. Fagotti, J. Schachenmayer, F.H.L. Essler, A. J. Daley, Entanglement growth and correlation spreading with variable-range interactions in spin and fermionic tunnelling models, Phys. Rev. A 93, 053620 (2016) [http://dx.doi.org/10.1103/PhysRevA.93.053620].

[193] D.B. Abraham, E. Barouch, G. Gallavotti and A. Martin-Löf, Thermalization of a Magnetic Impurity in the Isotropic XY Model, Phys. Rev. Lett. **25**, 1449 (1970); D.B. Abraham, E. Barouch, G. Gallavotti and A. Martin-Löf, Dynamics of a Local Perturbation in the XY Model. I-Approach to Equilibrium, Stud. Appl. Math. **50**, 121 (1971); C. Kollath, U. Schollwöck and W. Zwerger, Spin-charge separation in cold Fermi-gases: a real time analysis Phys. Rev. Lett. **95**, 176401 (2005); P. Calabrese and J. Cardy, Entanglement and correlation functions following a local quench: a conformal field theory approach, J. Stat. Mech. (2007) P10004; J.-M. Stéphan and Jérôme Dubail, Local quantum quenches in critical one-dimensional systems: entanglement, the

Loschmidt echo, and light-cone effects, J. Stat. Mech. (2011) P08019; M. Ganahl, E. Rabel, F.H.L. Essler and H.-G. Evertz, Observation of Complex Bound States in the Spin-1/2 Heisenberg XXZ Chain Using Local Quantum Quenches, Phys. Rev. Lett. **108**, 077206 (2012).

[194] E. H. Lieb and D. W. Robinson, The finite group velocity of quantum spin systems, Commun. Math. Phys. **28**, 251 (1972).

[195] R. Sims and B. Nachtergaele, Lieb-Robinson bounds in quantum many-body physics, edited by R. Sims and D. Ueltschi, Entropy and the Quantum, Vol. 529 (American Mathematical Society, 2010).

[196] J. Jünemann, A. Cadarso, D. Perez-Garcia, A. Bermudez, and J. J. García-Ripoll, Lieb-Robinson Bounds for Spin-Boson Lattice Models and Trapped Ions, Phys. Rev. Lett. **111**, 230404 (2013).

[197] M. Kliesch, C. Gogolin, and J. Eisert, Lieb-Robinson bounds and the simulation of time evolution of local observables in lattice systems, edited by L. D. Site and Bach, Many-Electron Approaches in Physics, Chemistry and Mathematics: A Multidisciplinary View (Springer, 2013).

[198] D. Poulin, Lieb-Robinson Bound and Locality for General Markovian Quantum Dynamics, Phys. Rev. Lett. **104**, 190401 (2010).

[199] P. Bocchieri and A. Loinger, Quantum Recurrence Theorem, Phys. Rev. **107**, 337 (1957).

[200] S. Sachdev, Quantum Phase Transitions, Cambridge University Press, 2001.

[201] O. Viehmann, J. von Delft, and F. Marquardt, Observing the Nonequilibrium Dynamics of the Quantum Transverse-Field Ising Chain in Circuit QED, Phys. Rev. Lett. **110**, 030601 (2013); O. Viehmann, J. von Delft, and F. Marquardt, The quantum transverse-field Ising chain in circuit quantum electrodynamics: effects of disorder on the nonequilibrium dynamics, New J. Phys. **15** 035013 (2013).

[202] E. Lieb, T. Schultz and D. Mattis, Two soluble models of an antiferromagnetic chain, **16**, 407 (1961).

[203] B.M. McCoy, E. Barouch and D.B. Abraham, Statistical Mechanics of the XY Model. IV. Time-Dependent Spin-Correlation Functions, **4**, 2331 (1971); O. Derzhko and T. Krokhmalskii, Dynamic structure factor of the spin-1/2 transverse Ising chain, **56**, 11659 (1997); O. Derzhko and T. Krokhmalskii, Numerical approach for the study of the spin-1/2 xy chains dynamic properties, Physica **B 208**, 221 (1999).

[204] A. Bugrij, Correlation function of the two-dimensional Ising model on the finite lattice. I, Theor. Math. Phys. **127**, 528 (2001); A. Bugrij and O. Lisovyy, Spin matrix elements in 2D Ising model on the finite lattice, Phys. Lett. **A 319**, 390 (2003); G. von Gehlen, N. Iorgov, S. Pakuliak, V. Shadura and Y. Tykhyy, Form-factors in the Baxter-Bazhanov-Stroganov model II: Ising model on the finite lattice, J. Phys. **A 41**, 095003 (2008); N. Iorgov, V. Shadura and Yu. Tykhyy, Spin operator matrix elements in the quantum Ising chain: fermion approach, J. Stat. Mech. (2011) P02028.

[205] I. Peschel, Calculation of reduced density matrices from correlation functions, J. Phys. A **36**, L205 (2003).

[206] M. C. Bañuls, J. I. Cirac, and M. B. Hastings, Strong and Weak Thermalization of Infinite Nonintegrable Quantum Systems, Phys. Rev. Lett. **106**, 050405 (2011).

[207] F. Iglói, Z. Szatmári, and Y.-C. Lin, Entanglement entropy dynamics of disordered quantum spin chains, Phys. Rev. B **85**, 094417 (2012).

[208] G. Torlai, L. Tagliacozzo, and G. De Chiara, Dynamics of the entanglement spectrum in spin chains, J. Stat. Mech. (2014) P06001.

[209] A. Coser, E. Tonni and P. Calabrese, Entanglement negativity after a global quantum quench, J. Stat. Mech. (2014) P12017.

[210] M.G. Nezhadhaghighi and M.A. Rajabpour, Entanglement dynamics in short- and long-range harmonic oscillators, Phys. Rev. B **90**, 205438 (2014).

[211] S. R. White and A. E. Feiguin, Real-Time Evolution Using the Density Matrix Renormalization Group, Phys. Rev. Lett. **93**, 076401 (2004); A. J. Daley, C. Kollath, U. Schollwöck, and G. Vidal, Time-dependent density-matrix renormalization-group using adaptive effective Hilbert spaces, J. Stat. Mech. (2004) P04005.

[212] G. Vidal, Classical Simulation of Infinite-Size Quantum Lattice Systems in One Spatial Dimension, Phys. Rev. Lett. **98**, 070201 (2007).

[213] V. Gurarie, Global large time dynamics and the generalized Gibbs ensemble, J. Stat. Mech. (2013) P02014.

[214] F. H. L. Essler, H. Frahm, F. Göhmann, A. Klümper, and V. E. Korepin, *The One-Dimensional Hubbard Model*, Cambridge University Press, Cambridge (2005).

[215] M. Gaudin, La fonction d'onde de Bethe, Masson, Paris 1983, English translation by J.-S. Caux, Cambridge University Press, Cambridge 2014.

[216] S. Sotiriadis, D. Fioretto, and G. Mussardo, Zamolodchikov-Faddeev algebra and quantum quenches in integrable field theories, J. Stat. Mech. (2012) P02017.

[217] D.X. Horváth, b, , S. Sotiriadis, and G. Takács, Initial states in integrable quantum field theory quenches from an integral equation hierarchy, Nucl. Phys. B **902**, 508 (2016).

[218] J.-S. Caux, The Quench Action, arXiv:1603.04689 (2016).

[219] B. Pozsgay, Quantum quenches and generalized Gibbs ensemble in a Bethe Ansatz solvable lattice model of interacting bosons, J. Stat. Mech. (2014) P10045.

[220] G. Goldstein and N. Andrei, Failure of the GGE hypothesis for integrable models with bound states, arXiv:1405.4224 (2014).

[221] A.B. Zamolodchikov and Al.B. Zamolodchikov, Factorized S-matrices in Two Dimensions as the Exact Solutions of Certain Relativistic Quantum Field Theory Models, Ann. Phys. **120**, 253 (1979).

[222] L. D. Faddeev, Quantum completely integral models of field theory, Sov. Sci. Rev. Math. Phys. C **1**, 107 (1980).

[223] F.H.L. Essler and R.M. Konik, Finite Temperature Dynamical Correlations in Massive Integrable Quantum Field Theories, J. Stat. Mech. (2009) P09018.

[224] E.H. Lieb, Exact Solution of the Problem of the Entropy of Two-Dimensional Ice, Exact Solution of the Problem of the Entropy of Two-Dimensional Ice, Phys. Rev. Lett. **18**, 692 (1967); E.H. Lieb, Exact Solution of the Two-Dimensional Slater KDP Model of a Ferroelectric, Phys. Rev. Lett. 19, **108** (1967); B. Sutherland, Exact Solution of a Two-Dimensional Model for Hydrogen-Bonded Crystals, Phys. Rev. Lett. **19**, 103 (1967).

[225] L.D. Faddeev and L. Takhtadzhyan, Spectrum and scattering of excitations in the one-dimensional isotropic Heisenberg model, J. Sov. Math. **24**, 241 (1984).

[226] M. Takahashi and M. Suzuki, One-Dimensional Anisotropic Heisenberg Model at Finite Temperatures, Prog. Theor. Phys. **48**, 2187 (1972); M. Takahashi, Thermodynamics of one dimensional solvable models, Cambridge University Press, Cambridge 1999.

[227] A.M. Tsvelik, Incommensurate phases of quantum one-dimensional magnetics, Phys. Rev. B **42**, 779 (1990); H. Frahm, Integrable spin-1/2 XXZ Heisenberg chain with competing interactions, J. Phys. A: Math. Gen. **25**, 1417 (1992); A.A. Zvyagin and A. Klümper, Quantum phase transitions and thermodynamics of quantum antiferromagnets with next-nearest-neighbor couplings, Phys. Rev. B **68**, 144426 (2003).

[228] N. Muramoto and M. Takahashi, Integrable Magnetic Model of Two Chains Coupled by Four-Body Interactions, J. Phys. Soc. Jpn **68**, 2098 (1999).

[229] M.P. Grabowski, P. Mathieu, Structure of the Conservation Laws in Quantum Integrable Spin Chains with Short Range Interactions, Ann. Phys. **243**, 299 (1995).

[230] A. Klümper and K. Sakai, The thermal conductivity of the spin-1/2 XXZ chain at arbitrary temperature, J. Phys. A **35**, 2173 (2002); K. Sakai and A. Klümper, Non-dissipative thermal transport in the massive regimes of the XXZ chain, J. Phys. A: Math. Gen. **36** 11617 (2003).

[231] A. Klümper, Thermodynamics of the anisotropic spin-1/2 Heisenberg chain and related quantum chains, Z. Phys. B **91**, 507 (1993); C. Destri and H.J. de Vega, Unified approach to Thermodynamic Bethe Ansatz and finite size corrections for lattice models and field theories, Nucl. Phys. B **438**, 314 (1995).

[232] M. Bortz and F. Göhmann, Exact thermodynamic limit of short-range correlation functions of the antiferromagnetic XXZ-chain at finite temperatures, Eur. Phys. J. B **46**, 399 (2005); H. E. Boos, F. Göhmann, A. Klümper, and J. Suzuki, Factorization of the finite temperature correlation functions of the XXZ chain in a magnetic field, J. Phys. A: Math. Theor. **40**, 10699 (2007); H.E. Boos, J. Damerau, F. Göhmann, A. Klümper, J. Suzuki, and A. Weiße, Short-distance thermal correlations in the XXZ chain, J. Stat. Mech. (2008) P08010; C. Trippe, F. Göhmann, and A. Klümper, Short-distance thermal correlations in the massive XXZ chain, Eur. Phys. J. B **73**, 253 (2010).

[233] F. Göhmann, A. Klümper, and A. Seel, Integral representation of the density matrix of the XXZ chain at finite temperatures, J. Phys. A: Math Gen. **37**, 7625 (2004).

[234] H.E. Boos, M. Jimbo, T. Miwa, F. Smirnov, and Y. Takeyama, Algebraic Representation of Correlation Functions in Integrable Spin Chains, Annales Henri Poincare **7**, 1395 (2006); H.E. Boos, M. Jimbo, T. Miwa, F. Smirnov, and Y. Takeyama, Hidden Grassmann Structure in the XXZ Model, Commun. Math. Phys **272**, 263 (2007); H.E. Boos, M. Jimbo, T. Miwa, F. Smirnov, and Y. Takeyama,Hidden Grassmann Structure in the XXZ Model II: Creation Operators, Commun. Math. Phys **286**, 875 (2009); M. Jimbo, T.

Miwa, and F. Smirnov, Hidden Grassmann structure in the XXZ model III: introducing the Matsubara direction, J. Phys. A: Math. Theor. **42**, 304018.

[235] E. Ilievski, M. Medenjak, and T. Prosen, Quasilocal Conserved Operators in the Isotropic Heisenberg Spin-1/2 Chain, Phys. Rev. Lett. **115**, 120601 (2015).

[236] E. Ilievski, M. Medenjak, T. Prosen, and L. Zadnik, arXiv:1603.00440 (2016).

[237] T. Prosen, Open XXZ Spin Chain: Nonequilibrium Steady State and a Strict Bound on Ballistic Transport, Phys. Rev. Lett. **106**, 217206 (2011); T. Prosen and E. Ilievski, Families of Quasilocal Conservation Laws and Quantum Spin Transport, Phys. Rev. Lett. **111**, 057203 (2013); T. Prosen, Quasilocal conservation laws in XXZ spin-1/2 chains: Open, periodic and twisted boundary conditions, Nucl. Phys. B **886**, 1177 (2014); R.G. Pereira, V. Pasquier, J. Sirker, and I. Affleck, Exactly conserved quasilocal operators for the XXZ spin chain, J. Stat. Mech. (2014); P09037; L. Piroli and E. Vernier, Quasi-local conserved charges and spin transport in spin-1 integrable chains, arXiv:1601.07289 (2016).

[238] J. Sirker, R.G. Pereira, I. Affleck Conservation laws, integrability and transport in one-dimensional quantum systems Phys. Rev. B **83**, 035115 (2011).

[239] L.A. Takhtajan, The picture of low-lying excitations in the isotropic Heisenberg chain of arbitrary spins, Phys. Lett. A **87**, 479 (1982); H.M. Babujian, Exact solution of the isotropic Heisenberg chain with arbitrary spins: Thermodynamics of the model, Nucl. Phys. **B215**, 317 (1983); A.N. Kirillov and N.Yu. Reshetikhin, Exact solution of the integrable XXZ Heisenberg models with arbitrary spin. I. The ground state and the excitation spectrum J. Phys. **A20**, 1565 (1987); A.N Kirillov and N.Yu. Reshetikhin Exact solution of the integrable XXZ Heisenberg model with arbitrary spin. II. Thermodynamics of the system J. Phys. **A20**, 1587 (1987).

[240] E. Ilievski, E. Quinn, J. De Nardis and M. Brockmann, String-charge duality in integrable lattice models, arXiv:1512.04454 (2015).

[241] B. Sutherland, Model for a multicomponent quantum system, Phys. Rev. B **12**, 3795 (1975); P.P. Kulish, E.K. Sklyanin, Solutions of the Yang-Baxter equation, J. Sov. Math. **19**, 1596 (1982); N. Andrei and H. Johannesson, Higher dimensional representations of the SU(N) Heisenberg model, Phys. Lett. A**104**, 370 (1984); P.P.Kulish, Integrable graded magnets, J. Soviet Math. **35**, 2648 (1985); F.H.L. Essler and V.E. Korepin, Algebraic Bethe Ansatz and Higher Conservation Laws for the Supersymmetric t-J Model, Phys. Rev. B **46**, 9147 (1992); A. Foerster and M. Karowski, Algebraic properties of the Bethe ansatz for an $spl(2,1)$ supersymmetric t-J model, Nucl.Phys. B **396**, 611 (1993); F.H.L. Essler, V.E. Korepin and K. Schoutens, Exact Solution of an Electronic Model of Superconductivity I, Int. J. Mod. Phys. B **8**, 3205 (1994); F. Göhmann, Algebraic Bethe ansatz for the gl(1|2) generalized model and Lieb-Wu equations, Nucl. Phys. B **620**, 5-1, (2002). S. Belliard and E. Ragoucy, Nested Bethe ansatz for 'all' closed spin chains, J. Phys. **A41**, 295202 (2008).

[242] B. Pozsgay and V. Eisler, Real-time dynamics in a strongly interacting bosonic hopping model: Global quenches and mapping to the XX chain, arXiv:1602.03065 (2016).

[243] P.P. Mazza, J.-M. Stéphan, E. Canovi, V. Alba, M. Brockmann, and M. Haque, Overlap distributions for quantum quenches in the anisotropic Heisenberg chain, J. Stat. Mech. (2016) 013104.

[244] C. Kollath, A. M. Läuchli, and E. Altman, Quench Dynamics and Nonequilibrium Phase Diagram of the Bose-Hubbard Model, Phys. Rev. Lett. **98**, 180601 (2007).

[245] M. Moeckel and S. Kehrein, Interaction Quench in the Hubbard Model, Phys. Rev. Lett. **100**, 175702 (2008).

[246] M. Moeckel and S. Kehrein, Real-time evolution for weak interaction quenches in quantum systems, Ann. of Phys. **324**, 2146 (2009).

[247] S. Sotiriadis and J. Cardy, Quantum quench in interacting field theory: A self-consistent approximation, Phys. Rev. B **81**, 134305 (2010).

[248] M. Kollar, F.A. Wolf, and M. Eckstein, Generalized Gibbs ensemble prediction of prethermalization plateaus and their relation to nonthermal steady states in integrable systems, Phys. Rev. B **84**, 054304 (2011).

[249] A. Mitra and T. Giamarchi, Mode-Coupling-Induced Dissipative and Thermal Effects at Long Times after a Quantum Quench, Phys. Rev. Lett. **107**, 150602 (2011).

[250] G. Carleo, F. Becca, M. Schiró, and M. Fabrizio, Localization and Glassy Dynamics Of Many-Body Quantum Systems, Scientific Reports **2** (2012).

[251] J. Marino and A. Silva, Relaxation, prethermalization, and diffusion in a noisy quantum Ising chain, Phys. Rev. B **86**, 060408(R) (2012).

[252] M. Stark and M. Kollar, Kinetic description of thermalization dynamics in weakly interacting quantum systems, arXiv:1308.1610 (2013).

[253] M. Marcuzzi, J. Marino, A. Gambassi, and A. Silva, Prethermalization in a Nonintegrable Quantum Spin Chain after a Quench, Phys. Rev. Lett. **111**, 197203 (2013).

[254] A. Mitra, Correlation functions in the prethermalized regime after a quantum quench of a spin-chain, Phys. Rev. B **87**, 205109 (2013)

[255] F.H.L. Essler, S. Kehrein, S.R. Manmana, and N.J. Robinson, Quench Dynamics in a Model with Tuneable Integrability Breaking, Phys. Rev. B **89**, 165104 (2014).

[256] B. Nowak, J. Schole, T. Gasenzer, Universal dynamics on the way to thermalisation, New J. Phys. **16**, 093052 (2014).

[257] G. Delfino, Quantum quenches with integrable pre-quench dynamics, J. Phys. A: Math. Theor. **47** 402001 (2014).

[258] B. Bertini and M. Fagotti, Pre-relaxation in weakly interacting models, J. Stat. Mech. (2015) P07012.

[259] B. Bertini, F.H.L. Essler, S. Groha, N.J. Robinson, Prethermalization and thermalization in models with weak integrability breaking, Phys. Rev. Lett. **115**, 180601 (2015).

[260] G.P. Brandino, J.-S. Caux, and R.M. Konik, Glimmers of a Quantum KAM Theorem: Insights from Quantum Quenches in One-Dimensional Bose Gases, Phys. Rev. X **5**, 041043 (2015).

[261] M. Babadi, E. Demler, and M. Knap, Far-from-Equilibrium Field Theory of Many-Body Quantum Spin Systems: Prethermalization and Relaxation of Spin Spiral States in Three Dimensions, Phys. Rev. X **5**, 041005 (2015).

[262] M. Olshanii, Geometry of Quantum Observables and Thermodynamics of Small Systems, Phys. Rev. Lett. **114**, 060401 (2015).

[263] M. Fagotti, Control of global properties in a closed many-body quantum system by means of a local switch, arXiv:1508.04401 (2015).

[264] N. Nessi and A. Iucci, Glass-like Behavior in a System of One Dimensional Fermions after a Quantum Quench, arXiv:1503.02507 (2015).

[265] T. Kitagawa, A. Imambekov, J. Schmiedmayer and E. Demler, The dynamics and prethermalization of one-dimensional quantum systems probed through the full distributions of quantum noise, New J. Phys. **13** 073018 (2011).

[266] T. Langen, S. Erne, R. Geiger, B. Rauer, T. Schweigler, M. Kuhnert, W. Rohringer, I.E. Mazets, T. Gasenzer and J. Schmiedmayer, Experimental Observation of a Generalized Gibbs Ensemble, Science **348**, 207 (2015).

[267] G. Goldstein and N. Andrei, Equilibration and Generalized GGE in the Lieb Liniger gas, arXiv:1309.3471 (2013).

[268] M. Kliesch, C. Gogolin, M.J. Kastoryano, A. Riera, and J. Eisert, Locality of Temperature, Phys. Rev. X **4**, 031019 (2014).

[269] A.M. Tsvelick and P.B. Wiegmann, Exact results in the theory of magnetic alloys, Adv. Phys. **32**, 453 (1983).

24.17 Bibliography from Old, Fundamental Articles

From Time-dependent generalized Gibbs ensembles in open quantum systems by Lange, Lenarčič, Rosch

References

[7] A. Polkovnikov, K. Sengupta, A. Silva, and M. Vengalattore, Rev. Mod. Phys. **83**, 863 (2011).

[2] C. Gogolin and J. Eisert, Reports on Progress in Physics **79**, 056001 (2016).

[19] L. D'Alessio, Y. Kafri, A. Polkovnikov, and M. Rigol, Advances in Physics **65**, 239 (2016).

[6] M. Rigol, V. Dunjko, and M. Olshanii, Nature **452**, 854 (2008).

[110] J. Lux, J. Müller, A. Mitra, and A. Rosch, Phys. Rev. A **89**, 053608 (2014).

[111] A. Bohrdt, C. Mendl, M. Endres, and M. Knap, New Journal of Physics (2017).

[112] E. Leviatan, F. Pollmann, J. H. Bardarson, and E. Altman, arXiv:1702.08894 (2017).

[4] F. H. L. Essler and M. Fagotti, Journal of Statistical Mechanics: Theory and Experiment P064002 (2016).

[3] L. Vidmar and M. Rigol, Journal of Statistical Mechanics: Theory and Experiment P064007 (2016).

[10] P. Calabrese and J. Cardy, Journal of Statistical Mechanics: Theory and Experiment **2016**, 064003 (2016).

[11] M. A. Cazalilla and M.-C. Chung, Journal of Statistical Mechanics: Theory and Experiment **2016**, 064004 (2016).

[1] M. Rigol, V. Dunjko, V. Yurovsky, and M. Olshanii, Phys. Rev. Lett. **98**, 050405 (2007).

[37] M. Fagotti and F. H. L. Essler, Phys. Rev. B **87**, 245107 (2013).

[36] B. Pozsgay, Journal of Statistical Mechanics: Theory and Experiment P07003 (2013).

[25] M. Fagotti and F. H. Essler, Journal of Statistical Mechanics: Theory and Experiment P07012 (2013).

[2] E. Ilievski, J. De Nardis, B. Wouters, J.-S. Caux, F. H. L. Essler, and T. Prosen, Phys. Rev. Lett. **115**, 157201 (2015).

[47] E. Ilievski, M. Medenjak, and T. Prosen, Phys. Rev. Lett. **115**, 120601 (2015).

[22] M. Mierzejewski, P. Prelovšek, and T. Prosen, Phys. Rev. Lett. **114**, 140601 (2015).

[48] E. Ilievski, M. Medenjak, T. Prosen, and L. Zadnik, Journal of Statistical Mechanics: Theory and Experiment P064008 (2016).

[5] J.-S. Caux, Journal of Statistical Mechanics: Theory and Experiment P064006 (2016).

[54] J.-S. Caux and F. H. L. Essler, Phys. Rev. Lett. **110**, 257203 (2013).

[60] M. Brockmann, B. Wouters, D. Fioretto, J. De Nardis, R. Vlijm, and J.-S. Caux, Journal of Statistical Mechanics: Theory and Experiment **2014**, P12009 (2014).

[15] B. Wouters, J. De Nardis, M. Brockmann, D. Fioretto, M. Rigol, and J.-S. Caux, Phys. Rev. Lett. **113**, 117202 (2014).

[16] B. Pozsgay, M. Mestyán, M. A. Werner, M. Kormos, G. Zaránd, and G. Takács, Phys. Rev. Lett. **113**, 117203 (2014).

[63] M. Mestyán, B. Pozsgay, G. Takács, and M. A. Werner, Journal of Statistical Mechanics: Theory and Experiment **2015**, P04001 (2015).

[66] L. Piroli, E. Vernier, and P. Calabrese, Phys. Rev. B **94**, 054313 (2016).

[38] B. Pozsgay, E. Vernier, and M. Werner, arXiv preprint arXiv:1703.09516 (2017).

[17] T. Kinoshita, T. Wenger, and D. S. Weiss, Nature **440**, 900 (2006).

[29] M. Gring, M. Kuhnert, T. Langen, T. Kitagawa, B. Rauer, M. Schreitl, I. Mazets, D. A. Smith, E. Demler, and J. Schmiedmayer, Science **337**, 1318 (2012).

[30] D. A. Smith, M. Gring, T. Langen, M. Kuhnert, B. Rauer, R. Geiger, T. Kitagawa, I. Mazets, E. Demler, and J. Schmiedmayer, New Journal of Physics **15**, 075011 (2013).

[92] T. Langen, T. Gasenzer, and J. Schmiedmayer, J. Stat. Mech. **2016**, 064009 (2016).

[19] T. Langen, S. Erne, R. Geiger, B. Rauer, T. Schweigler, M. Kuhnert, W. Rohringer, I. E. Mazets, T. Gasenzer, and J. Schmiedmayer, Science **348**, 207 (2015).

[23] Y. Tang, W. Kao, K.-Y. Li, S. Seo, K. Mallayya, M. Rigol, S. Gopalakrishnan, and B. L. Lev, arXiv preprint arXiv:1707.07031 (2017).

[19] P. Jung, R. W. Helmes, and A. Rosch, Phys. Rev. Lett. **96**, 067202 (2006).

[20] P. Jung and A. Rosch, Phys. Rev. B **76**, 245108 (2007).

[41] B. Bertini, F. H. L. Essler, S. Groha, and N. J. Robinson, Phys. Rev. Lett. **115**, 180601 (2015).

[37] M. Eckstein, M. Kollar, and P. Werner, Phys. Rev. Lett. **103**, 056403 (2009).

[38] M. Stark and M. Kollar, arXiv:1308.1610 (2013).

[96] J. Marino and A. Silva, Phys. Rev. B **86**, 060408 (2012).

[98] M. Marcuzzi, J. Marino, A. Gambassi, and A. Silva, Phys. Rev. Lett. **111**, 197203 (2013).

[11] B. Bertini, F. H. L. Essler, S. Groha, and N. J. Robinson, Phys. Rev. B **94**, 245117 (2016).

[42] M. Buchhold, M. Heyl, and S. Diehl, Phys. Rev. A **94**, 013601 (2016).

[43] F. R. A. Biebl and S. Kehrein, Phys. Rev. B **95**, 104304 (2017).

[40] M. Moeckel and S. Kehrein, Phys. Rev. Lett. **100**, 175702 (2008).

[95] M. Kollar, F. A. Wolf, and M. Eckstein, Physical Review B **84**, 054304 (2011).

[52] F. H. L. Essler, S. Kehrein, S. R. Manmana, and N. J. Robinson, Phys. Rev. B **89**, 165104 (2014).

[26] F. Lange, Z. Lenarčič, and A. Rosch, Nature communications **8**, 15767 (2017).

[48] M. Fagotti, Journal of Statistical Mechanics: Theory and Experiment **2014**, P03016 (2014).

[49] B. Bertini and M. Fagotti, Journal of Statistical Mechanics: Theory and Experiment **2015**, P07012 (2015).

[33] M. Genske and A. Rosch, Phys. Rev. A **92**, 062108 (2015).

[18] Z. Lenarčič, F. Lange, and A. Rosch, Phys. Rev. B **97**, 024302 (2018).

[52] M. P. Grabowski and P. Mathieu, Journal of Physics A: Mathematical and General **29**, 7635 (1996).

[36] B. Robertson, Phys. Rev. **144**, 151 (1966).

[37] B. Robertson, Phys. Rev. **160**, 206 (1968).

[38] K. Kawasaki and J. D. Gunton, Phys. Rev. A **8**, 2048 (1973).

[42] T. Koide, Prog. Theor. Phys. **107**, 525 (2002).

[43] H. P. Breuer and F. Petruccione, The theory of open quantum systems (Oxford University Press, New York, 2002).

[44] J. T. Barreiro, M. Müller, P. Schindler, D. Nigg, T. Monz, M. Chwalla, M. Hennrich, C. F. Roos, P. Zoller, and R. Blatt, Nature **470**, 486 (2011).

[8] F. Reiter and A. S. Sørensen, Phys. Rev. A **85**, 032111 (2012).

[60] N. Friis, O. Marty, C. Maier, C. Hempel, P. Jurcevic, M. Plenio, M. Huber, C. Roos, R. Blatt, B. Lanyon, et al., arXiv preprint arXiv:1711.11092 (2017).

[10] B. Bertini, M. Collura, J. De Nardis, and M. Fagotti, Phys. Rev. Lett. **117**, 207201 (2016).

[9] O. A. Castro-Alvaredo, B. Doyon, and T. Yoshimura, Phys. Rev. X **6**, 041065 (2016).

[63] V. B. Bulchandani, R. Vasseur, C. Karrasch, and J. E. Moore, Phys. Rev. Lett. **119**, 220604 (2017).

From Complete Generalized Gibbs Ensemble in an interacting Theory

References

[1] M. Rigol, V. Dunjko, V. Yurovsky, and M. Olshanii, Phys. Rev. Lett. **98**, 050405 (2007).

[2] M. Rigol, A. Muramatsu, and M. Olshanii, Phys. Rev. A **74**, 053616 (2006).

[3] M. A. Cazalilla, Phys. Rev. Lett. **97**, 156403 (2006).

[4] P. Calabrese and J. Cardy, J. Stat. Mech.: Th. Exp. **2007**, P06008 (2007).

[5] M. Cramer, C. M. Dawson, J. Eisert, and T. J. Osborne, Phys. Rev. Lett. **100**, 030602 (2008).

[6] T. Barthel and U. Schollwöck, Phys. Rev. Lett. **100**, 100601 (2008).

[7] D. Fioretto and G. Mussardo, New J. Phys. **12**, 055015 (2010).

[8] P. Calabrese, F. H. L. Essler, and M. Fagotti, Phys. Rev. Lett. **106**, 227203 (2011).

[9] P. Calabrese, F. H. L. Essler, and M. Fagotti, J. Stat. Mech.: Th. Exp. **2012**, P07016 (2012).

[10] M. Fagotti and F. H. L. Essler, Phys. Rev. B **87**, 245107 (2013).

[11] J.-S. Caux and R. M. Konik, Phys. Rev. Lett. **109**, 175301 (2012).

[12] F. H. L. Essler, S. Evangelisti, and M. Fagotti, Phys. Rev. Lett. **109**, 247206 (2012).

[13] A. C. Cassidy, C. W. Clark, and M. Rigol, Phys. Rev. Lett. **106**, 140405 (2011).

[14] J.-S. Caux and F. H. L. Essler, Phys. Rev. Lett. **110**, 257203 (2013).

[15] M. Collura, S. Sotiriadis, and P. Calabrese, Phys. Rev. Lett. **110**, 245301 (2013).

[16] G. Mussardo, Phys. Rev. Lett. **111**, 100401 (2013).

[17] B. Pozsgay, J. Stat. Mech.: Th. Exp. **2013**, P07003 (2013).

[18] M. Fagotti and F. H. L. Essler, J. Stat. Mech.: Th. Exp. **2013**, P07012 (2013).

[19] M. Kormos, A. Shashi, Y.-Z. Chou, J.-S. Caux, and A. Imambekov, Phys. Rev. B **88**, 205131 (2013).

[20] M. Fagotti, M. Collura, F. H. L. Essler, and P. Calabrese, Phys. Rev. B **89**, 125101 (2014).

[21] B. Wouters, J. De Nardis, M. Brockmann, D. Fioretto, M. Rigol, and J.-S. Caux, Phys. Rev. Lett. **113**, 117202 (2014).

[22] B. Pozsgay, M. Mestyán, M. A. Werner, M. Kormos, G. Zaránd, and G. Takács, Phys. Rev. Lett. **113**, 117203 (2014).

[23] M. Kormos, M. Collura, and P. Calabrese, Phys. Rev. A **89**, 013609 (2014).

[24] J. De Nardis, B. Wouters, M. Brockmann, and J.-S. Caux, Phys. Rev. A **89**, 033601 (2014).

[25] S. Sotiriadis and P. Calabrese, J. Stat. Mech.: Th. Exp. **2014**, P07024 (2014).

[26] F. H. L. Essler, G. Mussardo, and M. Panfil, Phys. Rev. A **91**, 051602 (2015).

[27] M. Mestyán, B. Pozsgay, G. Takács, and M. A. Werner, J. Stat. Mech.: Th. Exp. **2015**, P04001 (2015).

[28] V. E. Korepin, N. M. Bogoliubov, and A. G. Izergin, Quantum Inverse Scattering Method and Correlation Functions (Cambridge Univsity Press, Cambridge, 1993).

[29] B. Pozsgay, J. Stat. Mech.: Th. Exp. **2014**, P09026 (2014).

[30] G. Goldstein and N. Andrei, arXiv:1405.4224 .

[31] E. Ilievski, M. Medenjak, and T. Prosen, arXiv:1506.05049 .

[32] M. Brockmann, B. Wouters, D. Fioretto, J. D. Nardis, R. Vlijm, and J.-S. Caux, J. Stat. Mech.: Th. Exp. **2014**, P12009 (2014).

[33] H. Bethe, Zeit. für Physik **71**, 205 (1931).

[34] R. Orbach, Phys. Rev. **112**, 309 (1958).

[35] M. Gaudin, La fonction d'onde de Bethe (Masson, Paris, 1983) (English translation by J-S Caux, Cambridge University Press 2014).

[36] M. Takahashi, Thermodynamics of one-dimensional solvable models (Cambridge University Press, Cambridge, 1999).

[37] J. Mossel and J.-S. Caux, J. Phys. A: Math. Theor. **45**, 255001 (2012).

[38] M. Brockmann, J. D. Nardis, B. Wouters, and J.-S. Caux, J. Phys. A: Math. Theor. **47**, 145003 (2014).

[39] T. Prosen, Phys. Rev. Lett. **106**, 217206 (2011).

[40] T. Prosen and E. Ilievski, Phys. Rev. Lett. **111**, 057203 (2013).

[41] E. Ilievski and T. Prosen, Commun. Math. Phys. **318**, 809 (2013).

[42] T. Prosen, Nucl. Phys. B **886**, 1177 (2014).

[43] R. G. Pereira, V. Pasquier, J. Sirker, and I. Affleck, J. Stat. Mech.: Th. Exp. **2014**, P09037 (2014).

[44] M. Mierzejewski, P. Prelovšek, and T. Prosen, Phys. Rev. Lett. **114**, 140601 (2015).

[38] M. Medenjak, E. Ilievski and T. Prosen, to be published.

[46] V. V. Bazhanov, T. Łukowski, C. Meneghelli, and M. Staudacher, J. Stat. Mech.: Th. Exp. **2010**, P11002 (2010).

[47] V. V. Bazhanov and V. V. Mangazeev, Nucl. Phys. B **775**, 225 (2007).

[48] J. Suzuki, J. Phys. A: Math. Gen. **32**, 2341 (1999).

[49] A. Klümper and P. A. Pearce, Physica A **183**, 304 (1992).

[50] M. Mestyán and B. Pozsgay, J. Stat. Mech.: Th. Exp. **2014**, P09020 (2014).

From Pumping approximately integrable systems by Lange, Lenarčič, Rosch

References

[1] Kikkawa, J. M. & Awschalom, D. D. Resonant spin amplification in n-type GaAs. Phys. Rev. Lett. **80**, 4313–4316 (1998).

[2] Klaers, J., Schmitt, J., Vewinger, F. & Weitz, M. Bose-Einstein condensation of photons in an optical microcavity. Nature **468**, 545–548 (2010).

[3] Demokritov, S. et al. Bose–Einstein condensation of quasi-equilibrium magnons at room temperature under pumping. Nature **443**, 430–433 (2006).

[4] Kasprzak, J. et al. Bose–Einstein condensation of exciton polaritons. Nature **443**, 409–414 (2006).

[5] Allen, P. B. Theory of thermal relaxation of electrons in metals. Phys. Rev. Lett. **59**, 1460–1463 (1987).

[6] Faddeev, L. Algebraic aspects of the Bethe ansatz. International Journal of Modern Physics A **10**, 1845–1878 (1995).

[7] Grabowski, M. P. & Mathieu, P. Structure of the conservation laws in integrable spin chains with short range interactions. Ann. Phys. **243**, 299–371 (1995).

[8] Prosen, T. & Ilievski, E. Families of quasilocal conservation laws and quantum spin transport. Phys. Rev. Lett. **111**, 057203 (2013).

[9] Mierzejewski, M., Prelovšek, P. & Prosen, T. Identifying local and quasilocal conserved quantities in integrable systems. Phys. Rev. Lett. **114**, 140601 (2015).

[10] Ilievski, E., Medenjak, M. & Prosen, T. Quasilocal conserved operators in the isotropic Heisenberg spin-1/2 chain. Phys. Rev. Lett. **115**, 120601 (2015).

[11] Ilievski, E., Medenjak, M., Prosen, T. & Zadnik, L. Quasilocal charges in integrable lattice systems. Journal of Statistical Mechanics: Theory and Experiment **2016**, 064008.

[12] Rigol, M., Dunjko, V., Yurovsky, V. & Olshanii, M. Relaxation in a completely integrable many-body quantum system: An *Ab Initio* study of the dynamics of the highly excited states of 1d lattice hard-core bosons. Phys. Rev. Lett. **98**, 050405 (2007).

[13] Pozsgay, B. The generalized Gibbs ensemble for Heisenberg spin chains. Journal of Statistical Mechanics: Theory and Experiment **2013**, P07003.

[14] Fagotti, M. & Essler, F. H. Stationary behaviour of observables after a quantum quench in the spin-1/2 Heisenberg XXZ chain. Journal of Statistical Mechanics: Theory and Experiment **2013**, P07012.

[15] Wouters, B. et al. Quenching the anisotropic Heisenberg chain: Exact solution and generalized Gibbs ensemble predictions. Phys. Rev. Lett. **113**, 117202 (2014).

[16] Pozsgay, B. et al. Correlations after quantum quenches in the XXZ spin chain: Failure of the generalized Gibbs ensemble. Phys. Rev. Lett. **113**, 117203 (2014).

[17] Ilievski, E. et al. Complete generalized Gibbs ensembles in an interacting theory. Phys. Rev. Lett. **115**, 157201 (2015).

[18] Vidmar, L. & Rigol, M. Generalized Gibbs ensemble in integrable lattice models. Journal of Statistical Mechanics: Theory and Experiment **2016**, 064007.

[19] Essler, F. H. L. & Fagotti, M. Quench dynamics and relaxation in isolated integrable quantum spin chains. Journal of Statistical Mechanics: Theory and Experiment **2016**, 064002.

[20] Ilievski, E., Quinn, E. & Caux, J.-S. From interacting particles to equilibrium statistical ensembles. Phys. Rev. B **95**, 115128 (2017).

[21] De Luca, A., Collura, M. & De Nardis, J. Non-equilibrium spin transport in the XXZ chain: steady spin currents and emergence of magnetic domains. https://arxiv.org/abs/1612.07265 (2016).

[22] Langen, T. et al. Experimental observation of a generalized Gibbs ensemble. Science **348**, 207–211 (2015).

[23] Mourigal, M. et al. Fractional spinon excitations in the quantum Heisenberg antiferromagnetic chain. Nature Physics **9**, 435–441 (2013).

[24] Jung, P., Helmes, R. W. & Rosch, A. Transport in almost integrable models: Perturbed Heisenberg chains. Phys. Rev. Lett. **96**, 067202 (2006).

[25] Jung, P. & Rosch, A. Spin conductivity in almost integrable spin chains. Phys. Rev. B **76**, 245108 (2007).

[26] Jung, P. & Rosch, A. Lower bounds for the conductivities of correlated quantum systems. Phys. Rev. B **75**, 245104 (2007).

[27] Bertini, B., Essler, F. H. L., Groha, S. & Robinson, N. J. Prethermalization and thermalization in models with weak integrability breaking. Phys. Rev. Lett. **115**, 180601 (2015).

[28] De Luca, A. & Rosso, A. Dynamic nuclear polarization and the paradox of quantum thermalization. Phys. Rev. Lett. **115**, 080401 (2015).

[29] De Luca, A., Rodríguez-Arias, I., Müller, M. & Rosso, A. Thermalization and many-body localization in systems under dynamic nuclear polarization. Phys. Rev. B **94**, 014203 (2016).

[30] Cirac, J. I., Blatt, R., Zoller, P. & Phillips, W. D. Laser cooling of trapped ions in a standing wave. Phys. Rev. A **46**, 2668–2681 (1992).

[31] Benatti, F., Nagy, A. & Narnhofer, H. Asymptotic entanglement and Lindblad dynamics: a perturbative approach. Journal of Physics A: Mathematical and Theoretical **44**, 155303 (2011).

[32] Li, A. C. Y., Petruccione, F. & Koch, J. Perturbative approach to Markovian open quantum systems. Scientific Reports **4**, 4887 (2014).

[33] Petruccione, F. & Breuer, H.-P. The theory of open quantum systems (Oxford Univ. Press, 2002).

[34] Affleck, I. & Oshikawa, M. Field-induced gap in Cu benzoate and other $s = \frac{1}{2}$ antiferromagnetic chains. Phys. Rev. B **60**, 1038–1056 (1999).

[35] Nojiri, H., Ajiro, Y., Asano, T. & Boucher, J. Magnetic excitation of $s = 1/2$ antiferromagnetic spin chain Cu benzoate in high magnetic fields. New Journal of Physics **8**, 218 (2006).

[36] Kimura, S. et al. Collapse of magnetic order of the quasi one-dimensional ising-like antiferromagnet $BaCo_2V_2O_8$ in transverse fields. Journal of the Physical Society of Japan **82**, 033706 (2013).

[37] Niesen, S. K. et al. Substitution effects on the temperature versus magnetic field phase diagrams of the quasi-one-dimensional effective Ising spin-$\frac{1}{2}$ chain system $baco_2v_2o_8$. Phys. Rev. B **90**, 104419 (2014).

[38] Shindou, R. Quantum spin pump in $s = 1/2$ antiferromagnetic chains–holonomy of phase operators in sine-Gordon theory–. Journal of the Physical Society of Japan **74**, 1214–1223 (2005).

[39] Genske, M. & Rosch, A. Floquet-Boltzmann equation for periodically driven Fermi systems. Phys. Rev. A **92**, 062108 (2015).

[40] D'Alessio, L. & Rigol, M. Long-time behavior of isolated periodically driven interacting lattice systems. Phys. Rev. X **4**, 041048 (2014).

[41] Lazarides, A., Das, A. & Moessner, R. Equilibrium states of generic quantum systems subject to periodic driving. Phys. Rev. E **90**, 012110 (2014).

[42] Ponte, P., Chandran, A., Papić, Z. & Abanin, D. A. Periodically driven ergodic and many-body localized quantum systems. Annals of Physics **353**, 196–204 (2015).

[43] Lazarides, A., Das, A. & Moessner, R. Periodic Thermodynamics of Isolated Quantum Systems. Phys. Rev. Lett. **112**, 150401 (2014).

[44] Canovi, E., Kollar, M. & Eckstein, M. Stroboscopic prethermalization in weakly interacting periodically driven systems. Phys. Rev. E **93**, 012130 (2016).

[45] Zotos, X., Naef, F. & Prelovšek, P. Transport and conservation laws. Phys. Rev. B **55**, 11029–11032 (1997).

[46] Prosen, T. Open XXZ spin chain: Nonequilibrium steady state and a strict bound on ballistic transport. Phys. Rev. Lett. **106**, 217206 (2011).

[47] Mierzejewski, M., Prelovšek, P. & Prosen, T. Breakdown of the generalized Gibbs ensemble for current-generating quenches. Phys. Rev. Lett. **113**, 020602 (2014).

[48] Sinova, J., Valenzuela, S. O., Wunderlich, J., Back, C. H. & Jungwirth, T. Spin hall effects. Rev. Mod. Phys. **87**, 1213–1260 (2015).

[49] Berges, J., Borsányi, S. & Wetterich, C. Prethermalization. Phys. Rev. Lett. **93**, 142002 (2004).

[50] Moeckel, M. & Kehrein, S. Interaction quench in the hubbard model. Phys. Rev. Lett. **100**, 175702 (2008).

[51] Kollar, M., Wolf, F. A. & Eckstein, M. Generalized Gibbs ensemble prediction of prethermalization plateaus and their relation to nonthermal steady states in integrable systems. Physical Review B **84**, 054304 (2011).

[52] Essler, F. H. L., Kehrein, S., Manmana, S. R. & Robinson, N. J. Quench dynamics in a model with tuneable integrability breaking. Phys. Rev. B **89**, 165104 (2014).

[53] Mierzejewski, M., Prosen, T. & Prelovšek, P. Approximate conservation laws in perturbed integrable lattice models. Phys. Rev. B **92**, 195121 (2015).

[54] Caux, J.-S. & Essler, F. H. L. Time evolution of local observables after quenching to an integrable model. Phys. Rev. Lett. **110**, 257203 (2013).

[55] Caux, J.-S. The quench action. Journal of Statistical Mechanics: Theory and Experiment **2016**, 064006.

[56] Zotos, X. Finite temperature Drude weight of the one-dimensional spin- 1/2 Heisenberg model. Phys. Rev. Lett. **82**, 1764–1767 (1999).

[57] Forster, D. Hydrodynamic fluctuations, broken symmetry, and correlation functions, (Benjamin, Massachusetts, 1975).

From Generalized Gibbs ensembles in weakly interacting dissipative systems and digital quantum computers by Ulčakar, Lenarčič

References

[45] X. Mi, A. A. Michailidis, S. Shabani, K. C. Miao, P. V. Klimov, J. Lloyd, E. Rosenberg, R. Acharya, I. Aleiner, T. I. Andersen, et al., Stable quantum-correlated many-body states through engineered dissipation, Science **383**, 1332 (2024).

[44] J. T. Barreiro, M. Müller, P. Schindler, D. Nigg, T. Monz, M. Chwalla, M. Hennrich, C. F. Roos, P. Zoller, and R. Blatt, An open-system quantum simulator with trapped ions, Nature **470**, 486 (2011).

[3] F. Verstraete, M. M. Wolf, and J. Ignacio Cirac, Quantum computation and quantum-state engineering driven by dissipation, Nature physics **5**, 633 (2009).

[4] P. M. Harrington, E. J. Mueller, and K. W. Murch, Engineered dissipation for quantum information science, Nature Reviews Physics **4**, 660 (2022).

[5] B. Kraus, H. P. Büchler, S. Diehl, A. Kantian, A. Micheli, and P. Zoller, Preparation of entangled states by quantum Markov processes, Phys. Rev. A **78**, 042307 (2008).

[6] C.-F. Chen, H.-Y. Huang, J. Preskill, and L. Zhao, Local minima in quantum systems, arXiv:2309.16596 (2023).

[7] F. e. a. Fang, Probing critical phenomena in open quantum systems using atom arrays, arXiv:2402.15376 (2024).

[8] A. Matthies, M. Rudner, A. Rosch, and E. Berg, Programmable adiabatic demagnetization for systems with trivial and topological excitations, arXiv:2210.17256 .

[9] D. B. Kaplan, N. Klco, and A. Roggero, Ground states via spectral combing on a quantum computer, arXiv:1709.08250 (2017).

[10] H. Wang, Quantum algorithm for preparing the ground state of a system via resonance transition, Scientific Reports **7**, 16342 (2017).

[11] J.-J. Feng, B. Wu, F. Wilczek, et al., Quantum computing by coherent cooling, Physical Review A **105**, 052601 (2022).

[12] S. Polla, Y. Herasymenko, and T. E. O'Brien, Quantum digital cooling, Phys. Rev. A **104**, 012414 (2021).

[13] M. P. Zaletel, A. Kaufman, D. M. Stamper-Kurn, and N. Y. Yao, Preparation of low entropy correlated many-body states via conformal cooling quenches, Phys. Rev. Lett. **126**, 103401 (2021).

[14] M. Metcalf, J. E. Moussa, W. A. de Jong, and M. Sarovar, Engineered thermalization and cooling of quantum many-body systems, Phys. Rev. Res. **2**, 023214 (2020).

[15] G. Kishony, M. S. Rudner, A. Rosch, and E. Berg, Gauged cooling of topological excitations and emergent fermions on quantum simulators, arXiv:2310.16082 (2023).

[16] J. Lloyd, A. Michailidis, X. Mi, V. Smelyanskiy, and D. A. Abanin, Quasiparticle cooling algorithms for quantum many-body state preparation, arXiv:2404.12175 (2024).

[4] F. H. L. Essler and M. Fagotti, Quench dynamics and relaxation in isolated integrable quantum spin chains, J. Stat. Mech. Theory Exp. **2016**, 064002 (2016).

[3] L. Vidmar and M. Rigol, Generalized Gibbs ensemble in integrable lattice models, J. Stat. Mech. Theory Exp. **2016**, 064007 (2016).

[19] L. D'Alessio, Y. Kafri, A. Polkovnikov, and M. Rigol, From quantum chaos and eigenstate thermalization to statistical mechanics and thermodynamics, Advances in Physics **65**, 239 (2016).

[1] M. Rigol, V. Dunjko, V. Yurovsky, and M. Olshanii, Relaxation in a Completely Integrable Many-Body Quantum System: An Ab Initio Study of the Dynamics of the Highly Excited States of 1D Lattice Hard-Core Bosons, Phys. Rev. Lett. **98**, 050405 (2007).

[67] P. Calabrese, F. H. L. Essler, and M. Fagotti, Quantum quench in the transverse-field ising chain, Phys. Rev. Lett. **106**, 227203 (2011).

[69] P. Calabrese, F. H. L. Essler, and M. Fagotti, Quantum quenches in the transverse field ising chain: Ii. stationary state properties, Journal of Statistical Mechanics: Theory and Experiment **2012**, P07022 (2012).

[68] P. Calabrese, F. H. L. Essler, and M. Fagotti, Quantum quench in the transverse field ising chain: I. time evolution of order parameter correlators, Journal of Statistical Mechanics: Theory and Experiment **2012**, P07016 (2012).

[24] F. H. L. Essler, S. Evangelisti, and M. Fagotti, Dynamical correlations after a quantum quench, Phys. Rev. Lett. **109**, 247206 (2012).

[25] M. Fagotti, Finite-size corrections versus relaxation after a sudden quench, Phys. Rev. B **87**, 165106 (2013).

[37] M. Fagotti and F. H. L. Essler, Reduced density matrix after a quantum quench, Phys. Rev. B **87**, 245107 (2013).

[27] L. Bucciantini, M. Kormos, and P. Calabrese, Quantum quenches from excited states in the ising chain, Journal of Physics A: Mathematical and Theoretical **47**, 175002 (2014).

[26] F. Lange, Z. Lenarčič, and A. Rosch, Pumping approximately integrable systems, Nat. Commun. **8**, 1 (2017).

[18] Z. Lenarčič, F. Lange, and A. Rosch, Perturbative approach to weakly driven many-particle systems in the presence of approximate conservation laws, Phys. Rev. B **97**, 024302 (2018).

[25] F. Lange, Z. Lenarčič, and A. Rosch, Time-dependent generalized Gibbs ensembles in open quantum systems, Phys. Rev. B **97**, 165138 (2018).

[28] F. Reiter, F. Lange, S. Jain, M. Grau, J. P. Home, and Z. Lenarčič, Engineering generalized Gibbs ensembles with trapped ions, Phys. Rev. Res. **3**, 033142 (2021).

[29] M. Schmitt and Z. Lenarčič, From observations to complexity of quantum states via unsupervised learning, Phys. Rev. B **106**, L041110 (2022).

[33] I. Ulčakar and Z. Lenarčič, Iterative construction of conserved quantities in dissipative nearly integrable systems, Phys. Rev. Lett. **132**, 230402 (2024).

[30] I. Bouchoule, B. Doyon, and J. Dubail, The effect of atom losses on the distribution of rapidities in the one-dimensional Bose gas, SciPost Phys. **9**, 044 (2020).

[32] D. Rossini, A. Ghermaoui, M. B. Aguilera, R. Vatré, R. Bouganne, J. Beugnon, F. Gerbier, and L. Mazza, Strong correlations in lossy one-dimensional quantum gases: From the quantum Zeno effect to the generalized Gibbs ensemble, Phys. Rev. A **103**, L060201 (2021).

[33] F. Gerbino, I. Lesanovsky, and G. Perfetto, Large-scale universality in Quantum Reaction-Diffusion from Keldysh field theory, arXiv:2307.14945 (2023).

[34] G. Perfetto, F. Carollo, J. P. Garrahan, and I. Lesanovsky, Reaction-Limited Quantum Reaction-Diffusion Dynamics, Phys. Rev. Lett. **130**, 210402 (2023).

[35] S. Rowlands, I. Lesanovsky, and G. Perfetto, Quantum reaction-limited reaction–diffusion dynamics of noninteracting bose gases, New Journal of Physics **26**, 043010 (2024).

[39] F. Riggio, L. Rosso, D. Karevski, and J. Dubail, Effects of atom losses on a one-dimensional lattice gas of hard-core bosons, Phys. Rev. A **109**, 023311 (2024).

[40] M. Ringbauer, M. Meth, L. Postler, R. Stricker, R. Blatt, P. Schindler, and T. Monz, A universal qudit quantum processor with trapped ions, Nature Physics **18**, 1053 (2022).

[22] A. Scheie, N. E. Sherman, M. Dupont, S. E. Nagler, M. B. Stone, G. E. Granroth, J. E. Moore, and D. A. Tennant, Detection of Kardar–Parisi–Zhang hydrodynamics in a quantum Heisenberg spin-1/2 chain, Nat. Phys. **17**, 726 (2021).

[42] A. Scheie, P. Laurell, B. Lake, S. E. Nagler, M. B. Stone, J.-S. Caux, and D. A. Tennant, Quantum wake dynamics in Heisenberg antiferromagnetic chains, Nature Communications **13**, 5796 (2022).

[43] K. Kim, S. Korenblit, R. Islam, E. Edwards, M. Chang, C. Noh, H. Carmichael, G. Lin, L. Duan, C. J. Wang, et al., Quantum simulation of the transverse ising model with trapped ions, New J. Phys. **13**, 105003 (2011).

[44] R. Islam, E. Edwards, K. Kim, S. Korenblit, C. Noh, H. Carmichael, G.-D. Lin, L.-M. Duan, C.-C. J. Wang, J. Freericks, et al., Onset of a quantum phase transition with a trapped ion quantum simulator, Nat. Comm. **2**, 1 (2011).

[45] H. Labuhn, D. Barredo, S. Ravets, S. De Léséleuc, T. Macrì, T. Lahaye, and A. Browaeys, Tunable two-dimensional arrays of single rydberg atoms for realizing quantum ising models, Nature **534**, 667 (2016).

[46] J. Zhang, G. Pagano, P. W. Hess, A. Kyprianidis, P. Becker, H. Kaplan, A. V. Gorshkov, Z.-X. Gong, and C. Monroe, Observation of a many-body dynamical phase transition with a 53-qubit quantum simulator, Nature **551**, 601 (2017).

[47] S. Ebadi, T. T. Wang, H. Levine, A. Keesling, G. Semeghini, A. Omran, D. Bluvstein, R. Samajdar, H. Pichler, W. W. Ho, et al., Quantum phases of matter on a 256-atom programmable quantum simulator, Nature **595**, 227 (2021).

[48] P. Scholl, M. Schuler, H. J. Williams, A. A. Eberharter, D. Barredo, K.-N. Schymik, V. Lienhard, L.-P. Henry, T. C. Lang, T. Lahaye, A. M. Läuchli, and A. Browaeys, Programmable quantum simulation of 2D antiferromagnets with hundreds of Rydberg atoms, arXiv:2012.12268 (2020).

[49] K. J. Satzinger et al., Realizing topologically ordered states on a quantum processor, Science **374**, 1237 (2021).

[50] D. A. Lidar, Lecture notes on the theory of open quantum systems, arXiv:1902.00967 (2019).

[43] M. Grady, Infinite set of conserved charges in the ising model, Phys. Rev. D **25**, 1103 (1982).

[55] W. H. Press, Numerical recipes 3rd edition: The art of scientific computing (Cambridge university press, 2007).

[36] B. Pozsgay, The generalized gibbs ensemble for heisenberg spin chains, J. Stat. Mech. Theory Exp. **2013**, P07003 (2013).

[38] B. Pozsgay, E. Vernier, and M. A. Werner, On generalized gibbs ensembles with an infinite set of conserved charges, J. Stat. Mech. Theory Exp. **2017**, 093103 (2017).

From "From Bloch Oscillations to Many Body Localization in Clean Interacting Systems" by van Nieuwenburg, Baum, Refael

References

[1] P. W. Anderson, "Absence of diffusion in certain random lattices," Phys. Rev. **109**, 1492–1505 (1958).

[2] D.M. Basko, I.L. Aleiner, and B.L. Altshuler, "Metal–insulator transition in a weakly interacting many-electron system with localized single-particle states," Annals of Physics **321**, 1126 – 1205 (2006).

[3] I. V. Gornyi, A. D. Mirlin, and D. G. Polyakov, "Interacting electrons in disordered wires: Anderson localization and low-t transport," Phys. Rev. Lett. **95**, 206603 (2005).

[4] Rahul Nandkishore and David A. Huse, "Many-body localization and thermalization in quantum statistical mechanics," Annual Review of Condensed Matter Physics **6**, 15–38 (2015).

[5] Dmitry A. Abanin and Zlatko Papić, "Recent progress in many-body localization," Annalen der Physik **529**, 1700169–n/a (2017), 1700169.

[6] John Z. Imbrie, "Diagonalization and many-body localization for a disordered quantum spin chain," Phys. Rev. Lett. **117**, 027201 (2016).

[7] David A. Huse, Rahul Nandkishore, and Vadim Oganesyan, "Phenomenology of fully many-body-localized systems," Phys. Rev. B **90**, 174202 (2014).

[8] Vadim Oganesyan and David A. Huse, "Localization of interacting fermions at high temperature," Phys. Rev. B **75**, 155111 (2007).

[9] Arijeet Pal and David A. Huse, "Many-body localization phase transition," Phys. Rev. B **82**, 174411 (2010).

[10] Ronen Vosk, David A. Huse, and Ehud Altman, "Theory of the many-body localization transition in one-dimensional systems," Phys. Rev. X **5**, 031032 (2015).

[11] Yevgeny Bar Lev and David R. Reichman, "Dynamics of many-body localization," Phys. Rev. B **89**, 220201 (2014).

[12] Christopher David White, Michael Zaletel, Roger S. K. Mong, and Gil Refael, "Quantum dynamics of thermalizing systems," Phys. Rev. B **97**, 035127 (2018).

[13] E. van Nieuwenburg, E. Bairey, and G. Refael, "Learning phase transitions from dynamics," ArXiv e-prints (2017), arXiv:1712.00450 [cond-mat.dis-nn] .

[14] Bela Bauer and Chetan Nayak, "Area laws in a many-body localized state and its implications for topological order," Journal of Statistical Mechanics: Theory and Experiment **2013**, P09005 (2013).

[15] Marko Žnidarič, Tomaž Prosen, and Peter Prelovšek, "Many-body localization in the heisenberg XXZ magnet in a random field," Phys. Rev. B **77**, 064426 (2008).

[16] Jens H. Bardarson, Frank Pollmann, and Joel E. Moore, "Unbounded growth of entanglement in models of many-body localization," Phys. Rev. Lett. **109**, 017202 (2012).

[17] Vedika Khemani, S. P. Lim, D. N. Sheng, and David A. Huse, "Critical properties of the many-body localization transition," Phys. Rev. X **7**, 021013 (2017).

[18] Sarang Gopalakrishnan, Markus Müller, Vedika Khemani, Michael Knap, Eugene Demler, and David A. Huse, "Low-frequency conductivity in many-body localized systems," Phys. Rev. B **92**, 104202 (2015).

[19] Timothy C. Berkelbach and David R. Reichman, "Conductivity of disordered quantum lattice models at infinite temperature: Many-body localization," Phys. Rev. B **81**, 224429 (2010).

[20] Achilleas Lazarides, Arnab Das, and Roderich Moessner, "Fate of many-body localization under periodic driving," Phys. Rev. Lett. **115**, 030402 (2015).

[21] Luca D'Alessio and Anatoli Polkovnikov, "Many-body energy localization transition in periodically driven systems," Annals of Physics **333**, 19 – 33 (2013).

[22] Vedika Khemani, Achilleas Lazarides, Roderich Moessner, and S. L. Sondhi, "Phase structure of driven quantum systems," Phys. Rev. Lett. **116**, 250401 (2016).

[23] J. Smith, A. Lee, P. Richerme, B. Neyenhuis, P. W. Hess, P. Hauke, M. Heyl, D. A. Huse, and C. Monroe, "Many-body localization in a quantum simulator with programmable random disorder," Nature Phys. **12** (2016), 10.1038/nphys3783.

[24] Jae-yoon Choi, Sebastian Hild, Johannes Zeiher, Peter Schauß, Antonio Rubio-Abadal, Tarik Yefsah, Vedika Khemani, David A. Huse, Immanuel Bloch, and Christian Gross, "Exploring the many-body localization transition in two dimensions," Science **352**, 1547–1552 (2016).

[25] Michael Schreiber, Sean S. Hodgman, Pranjal Bordia, Henrik P. Lüschen, Mark H. Fischer, Ronen Vosk, Ehud Altman, Ulrich Schneider, and Immanuel Bloch, "Observation of many-body localization of interacting fermions in a quasirandom optical lattice," Science **349**, 842–845 (2015).

[26] S. S. Kondov, W. R. McGehee, W. Xu, and B. DeMarco, "Disorder-induced localization in a strongly correlated atomic hubbard gas," Phys. Rev. Lett. **114**, 083002 (2015).

[27] Pranjal Bordia, Henrik Lüschen, Sebastian Scherg, Sarang Gopalakrishnan, Michael Knap, Ulrich Schneider, and Immanuel Bloch, "Probing slow relaxation and many-body localization in two-dimensional quasiperiodic systems," Phys. Rev. X **7**, 041047 (2017).

[28] Wojciech De Roeck, Francois Huveneers, Markus Müller, and Mauro Schiulaz, "Absence of many-body mobility edges," Phys. Rev. B **93**, 014203 (2016).

[29] A. Smith, J. Knolle, D. L. Kovrizhin, and R. Moessner, "Disorder-free localization," Phys. Rev. Lett. **118**, 266601 (2017).

[30] A. Smith, J. Knolle, R. Moessner, and D. L. Kovrizhin, "Absence of ergodicity without quenched disorder: From quantum disentangled liquids to many-body localization," Phys. Rev. Lett. **119**, 176601 (2017).

[31] Adam Smith, Johannes Knolle, Roderich Moessner, and Dmitry L. Kovrizhin, "Dynamical localization in F_2 lattice gauge theories," Phys. Rev. B **97**, 245137 (2018).

[32] Tarun Grover and Matthew P A Fisher, "Quantum disentangled liquids," Journal of Statistical Mechanics: Theory and Experiment **2014**, P10010 (2014).

[33] Yu. Kagan and L.A. Maksimov, "Localization in a system of interacting particles diffusing in a regular crystal," JETP **60**, 201 (1984).

[34] Wojciech De Roeck and Francois Huveneers, "Scenario for delocalization in translation-invariant systems," Phys. Rev. B **90**, 165137 (2014).

[35] Mauro Schiulaz, Alessandro Silva, and Markus Müller, "Dynamics in many-body localized quantum systems without disorder," Phys. Rev. B **91**, 184202 (2015).

[36] N. Y. Yao, C. R. Laumann, J. I. Cirac, M. D. Lukin, and J. E. Moore, "Quasi-many-body localization in translation-invariant systems," Phys. Rev. Lett. **117**, 240601 (2016).

[37] Shankar Iyer, Vadim Oganesyan, Gil Refael, and David A. Huse, "Many-body localization in a quasiperiodic system," Phys. Rev. B **87**, 134202 (2013).

[38] Henrik P. Lüschen, Pranjal Bordia, Sebastian Scherg, Fabien Alet, Ehud Altman, Ulrich Schneider, and Immanuel Bloch, "Observation of slow dynamics near the many-body localization transition in one-dimensional quasiperiodic systems," Phys. Rev. Lett. **119**, 260401 (2017).

[39] Vedika Khemani, D. N. Sheng, and David A. Huse, "Two universality classes for the many-body localization transition," Phys. Rev. Lett. **119**, 075702 (2017).

[40] Isaac H. Kim and Jeongwan Haah, "Localization from superselection rules in translationally invariant systems," Phys. Rev. Lett. **116**, 027202 (2016).

[41] Gregory H. Wannier, "Wave functions and effective hamiltonian for bloch electrons in an electric field," Phys. Rev. **117**, 432–439 (1960).

[42] Casati G., Chirikov B.V., Izraelev, and F.M. Ford J., "Stochastic behavior of a quantum pendulum under a periodic perturbation," Casati G., Ford J. (eds) Stochastic Behavior in Classical and Quantum Hamiltonian Systems. Lecture Notes in Physics, vol 93. Springer, Berlin, Heidelberg **93** (1979).

[43] Yuval Baum, Evert P. L. van Nieuwenburg, and Gil Refael, "From dynamical localization to bunching in interacting floquet systems," SciPost Phys. **5**, 17 (2018).

[44] David J. Luitz, Yevgeny Bar Lev, and Achilleas Lazarides, "Absence of dynamical localization in interacting driven systems," SciPost Phys. **3**, 029 (2017).

[45] Martin Eckstein and Philipp Werner, "Damping of bloch oscillations in the hubbard model," Phys. Rev. Lett. **107**, 186406 (2011).

[46] Dmitry O. Krimer, Ramaz Khomeriki, and Sergej Flach, "Delocalization and spreading in a nonlinear stark ladder," Phys. Rev. E **80**, 036201 (2009).

[47] P. Pieri and G. C. Strinati, "Derivation of the gross-pitaevskii equation for condensed bosons from the bogoliubov–de gennes equations for superfluid fermions," Phys. Rev. Lett. **91**, 030401 (2003).

[48] Jean-Claude Garreau, "Quantum simulation of disordered systems with cold atoms," Comptes Rendus Physique **18**, 31 – 46 (2017), prizes of the French Academy of Sciences 2015 / Prix de l'Académie des sciences 2015.

[49] L. Sanchez-Palencia, D. Clément, P. Lugan, P. Bouyer, G. V. Shlyapnikov, and A. Aspect, "Anderson localization of expanding bose-einstein condensates in random potentials," Phys. Rev. Lett. **98**, 210401 (2007).

[50] Thomas Guhr, Axel Müller–Groeling, and Hans A. Weidenmüller, "Random-matrix theories in quantum physics: common concepts," Physics Reports **299**, 189 – 425 (1998).

[51] Maxim Olshanii, Kurt Jacobs, Marcos Rigol, Vanja Dunjko, Harry Kennard, and Vladimir A. Yurovsky, "An exactly solvable model for the integrability and chaos transition in rough quantum billiards," Nature Communications **3** (2012), 10.1038/ncomms1653.

[52] David J. Luitz, Nicolas Laflorencie, and Fabien Alet, "Many-body localization edge in the random-field heisenberg chain," Phys. Rev. B **91**, 081103 (2015).

[53] Corentin L. Bertrand and Antonio M. García-García, "Anomalous thouless energy and critical statistics on the metallic side of the many-body localization transition," Phys. Rev. B **94**, 144201 (2016).

[54] Kazue Kudo and Tetsuo Deguchi, "Finite-size scaling with respect to interaction and disorder strength at the many-body localization transition," Phys. Rev. B **97**, 220201 (2018).

[55] A. Chandran, A. Pal, C. R. Laumann, and A. Scardicchio, "Many-body localization beyond eigenstates in all dimensions," Phys. Rev. B **94**, 144203 (2016).

[56] Wojciech De Roeck and Francois Huveneers, "Stability and instability towards delocalization in many-body localization systems," Phys. Rev. B **95**, 155129 (2017).

[57] Wojciech De Roeck and John Z. Imbrie, "Many-body localization: stability and instability," Philosophical Transactions of the Royal Society of London A: Mathematical, Physical and Engineering Sciences **375** (2017), 10.1098/rsta.2016.0422.

[58] Shriya Pai, Michael Pretko, and Rahul M. Nandkishore, "Localization in fractonic random circuits," arXiv e-prints , arXiv:1807.09776 (2018), arXiv:1807.09776 [cond-mat.stat-mech] .

[59] M. Schulz, C. A. Hooley, R. Moessner, and F. Pollmann, "Stark many-body localization," ArXiv e-prints (2018), arXiv:1808.01250 [cond-mat.dis-nn] .

[60] D.P. Kingma and J. Ba, "Adam: A Method for Stochastic Optimization," ArXiv e-prints (2014), arXiv:1412.6980 .

[61] C. Moler and C. Van Loan, "Nineteen dubious ways to compute the exponential of a matrix, twenty-five years later," SIAM Review **45**, 3–49 (2003), https://doi.org/10.1137/S00361445024180 .

[62] Luc Giraud, Julien Langou, Miroslav Rozložník, and Jasper van den Eshof, "Rounding error analysis of the classical gram-schmidt orthogonalization process," Numerische Mathematik **101**, 87–100 (2005).

From "A quantum Newton's cradle" by Kinoshita, Wenger, Weiss

1. Coleman, S. Quantum sine-Gordon equation as the massiveThipring model. Phys. Rev. D 11, 2088-2097(1975).
2. Tabor, M. Chaos and Integrability in Nonlinear Dynamics(Wiley, New York, 1989).
3. Bemman, G. P. & Izrailev, F. M. The Fermi-Pastalam problem: fifty years of progress. Chaos 15 , 015104 (2005).
4. Benman, G. P. , Borgonoxi, F. , Izrailev, F. M. & Smenzi, A. Irregular dynamics in a one-dimensional Bose system. Phys. Rev. Lett. 92, 030404 (2004). I
5. Minguzzi, A. & Gangardt, D. M. Exact coherent states of a harmonically confined Tonks-Ginardeau gas. Phys. Rev. Lett. 94, 240404 (2005). I
6. Proukakis, N. P., Schmiedmayer, J. & && Stopf, H. T. C. Quasi-condensate growth on an atom chip. Preprint at http://anxix. org/ cond-mat/0509154 (2005). II 7. Hercmann, F. & Schmalzle, P. Simple explanation of a well-known collision experiment. Am. J. Phys. 49, 761-764(1981).
8. Ginardeau, M. Relationship between systems of impenetrable bosons and fermions in one dimension. J. Math. Phys. 1, 516-523(1960). II
9. Girardeau, M. D. & Wright, E. M. Measurement of one-particle correlations and momentum distributions for trapped 1D gases. Phys. Rev. Lett. 87, 050403 (2001). II
10 ParedesBet alTonksGirardeau gas of ultracold atoms in an optical lattice Nature 4292772812004
11 KinoshitaTWengerT & WeissDSObservation of a onedimensional TonksGirardeau gasScience 305112511282004
12 RigolM & MuramatsuAFermionization in an expanding 1D gas of hardcore bosonsPhysRevLett94 240403 2005
13 PedriPSantosLhbergP & StringariSViolation of selfsimilarity in the expansion of a onedimensional Bose gasPhysRevA 68 043601 2003
14 DunjkoVLorentV & OlshaniiMBosons in cigarshaped trapsThomas Fermi regimeTonksGirardeau regimeand in betweenPhysRevLett86 541354162001
15 KinoshitaTWengerT & WeissDSLocal pair correlations in one dimensional Bose gasesPhysRevLett95 190406 2005
16 GangardtDM & ShlyapnikovGVStability and phase coherence of trapped 1D Bose gasesPhysRevLett90 010401 2003
17 TolraBLet alObservation of reduced threebody recombination in a correlated 1D degenerate Bose gasPhysRevLett92 190401 2004
18 LiebEH & LinigerWExact analysis of an interacting Bose gasThe general solution and the ground statePhysRev130160516161963
19 WuSWangYJDiotQ & PrentissMSplitting matter waves using an optimized standingwave lightpulse sequencePhysRevA 71 043602 2005
20 WangYJet alAtom Michelson interferometer on a chip using a Bose Einstein condensatePhysRevLett94 090405 2005
21 MooreMGBergemanT & OlshaniiMScattering in tight atom waveguidesJPhysIV 11669862004
22 OlshaniiMAtomic scattering in the presence of an external confinement and a gas of impenetrable bosonsPhysRevLett819389411998
23 WuH & FootCJDirect simulation of evaporative coolingJPhysB 29 L321L3281996
24 RamanCet alEvidence for a critical velocity in a BoseEinstein condensed gasPhysRevLett83250225051999
25 CarusottoIet alSensitive measurement of forces at the micron scale using Bloch oscillations of ultracold atomsPhysRevLett95 093202 2005
26 FallaniLet alObservation of dynamical instability for a BoseEinstein condensate in a

moving 1D optical latticePhysRevLett93 140406 2004
27 GustavsonTLLandraginA & KasevichMARotation sensing with a dual atominterferometer Sagnac gyroscopeClassQuantum Grav1723852398 2000
28 OlshaniiM & DunjkoVInterferometry in dense nonlinear media and interactioninduced loss of contrast in microfabricated atom interferometers Preprint at httparxivorgcondmat05053582005
29 MiesnerHJet alBosonic stimulation in the formation of a BoseEinstein condensateScience 279100510071998
30 KinoshitaTWengerT & WeissDSAlloptical BoseEinstein condensation using a compressible crossed dipole trapPhysRevA 7111602R2005

From Chaos and Quantum Thermalization by Srednicki

[1] Ya. G. Sinai, Ups. Mat. Nauk 25, 137 (1970) [Russ. Math. Surv. 25, 137 (1970)].
[2] M. V. Berry, in Topics in Nonlinear Dynamics, S. Jorna, ed. (AIP, New York, 1978).
[3] G. M. Zaslavsky, Chaos in Dynamic Systems (Harwood, Chur, 1985).
[4] M. C. Gutzwiller, Chaos in Classical and Quantum Mechanics (Springer-Verlag, New York, 1990).
[5] L. E. Reichl, A Modern Course in Statistical Physics (Univ. of Texas, Austin, 1980).
[6] A. N. Kolmogorov, Dokl. Acad. Nauk SSSR 98, 527 (1954); V. I. Arnol'd, Usp. Mat. Nauk 18, 13 (1963) [Russ. Math. Surv. 18, 9 (1963)]; J. Moser, Nachr. Akad. Wiss. Göttingen 1 (1962).
[7] N. S. Krylov, Works on the Foundations of Statistical Mechanics (Princeton Univ., Princeton, 1979).
[8] M. V. Berry, J. Phys. A 10, 2083 (1977).
[9] M. V. Berry, in Les Houches XXXVI, Chaotic Behavior of Deterministic Systems, G. Iooss, R. H. G. Helleman, and R. Stora, eds. (North-Holland, Amsterdam, 1983).
[10] M. V. Berry, in Les Houches LII, Chaos and Quantum Physics, M.-J. Giannoni, A. Voros, and J. Zinn-Justin, eds. (North-Holland, Amsterdam, 1991).
[11] A. Voros, Ann. Inst. H. Poincaré A 24, 31 (1976); 26, 343 (1977); in Stochastic Behavior in Classical and Quantum Hamiltonian Systems, G. Casati and J. Ford, eds. (SpringerVerlag, Berlin, 1979).
[12] A. I. Shnirelman, Ups. Mat. Nauk 29, 181 (1974); Y. Colin de Verdière, Comm. Math. Phys. 102, 497 (1985); S. Zelditch, Duke Math J. 55, 919 (1987).
[13] M. V. Berry, Phil. Trans. R. Soc. Lond. A 287, 237 (1977).
[14] S. W. McDonald and A. N. Kaufman, Phys. Rev. Lett. 42, 1189 (1979).
[15] E. J. Heller, Phys. Rev. Lett. 53, 1515 (1984).
[16] S. W. McDonald and A. N. Kaufman, Phys. Rev. A 37, 3067 (1988).
[17] M. Shapiro, J. Ronkin, and P. Brumer, Chem. Phys. Lett. 148, 177 (1988).
[18] E. J. Heller, in Les Houches LII, Chaos and Quantum Physics, M.-J. Giannoni, A. Voros, and J. Zinn-Justin, eds. (North-Holland, Amsterdam, 1991).
[19] R. Aurich and F. Steiner, Physica D 48, 445 (1991).
[20] R. Aurich and F. Steiner, Physica D 64, 185 (1993).
[21] F. Steiner, in Festschrift Universität Hamburg 1994: Schlaglichter der Forschung zum 75. Jahrestag, R. Ansorge, ed. (Dietrich Reimer Verlag, Hamburg, 1994).
[22] L. D. Landau and E. M. Lifshitz, Statistical Physics (Permagon, Oxford, 1980).
[23] R. Jancel, Foundations of Classical and Quantum Statistical Mechanics (Permagon, Oxford, 1969).
[24] E. B. Bogomolny, Physica D 31, 169 (1988).
[25] M. V. Berry, Proc. R. Soc. Lond. A 423, 219 (1989).
[26] P. Gaspard, in Quantum Chaos - Quantum Measurement, P. Cvitanović, I. Percival, and

A. Wirzba, eds. (Kluwer, Dordrecht, 1992).
[27] M. V. Berry and J. P. Keating, Proc. R. Soc. Lond. A 437, 151 (1992); O. Agam and S. Fishman, J. Phys. A 26, 2113 (1993).
[28] S. Tomsovic and E. J. Heller, Phys. Rev. Lett. 67, 664 (1991); Phys. Rev. E 47, 282 (1993); M. A. Sepúlveda, S. Tomsovic and E. J. Heller, Phys. Rev. Lett. 69, 402 (1992).
[29] G. H. Wannier, Statistical Physics (Wiley, New York, 1966).
[30] A. L. Fetter and J. D. Walecka, Quantum Theory of Many-Particle Systems (McGrawHill, San Francisco, 1971).
[31] J. S. Langer, private communication.
[32] N. G. van Kampen, in Chaotic Behavior in Quantum Systems, G. Casati, ed. (Plenum, New York, 1985).
[33] O. Bohigas, in Les Houches LII, Chaos and Quantum Physics, M.-J. Giannoni, A. Voros, and J. Zinn-Justin, eds. (North-Holland, Amsterdam, 1991).

From Subdiffusion and heat transport in a tilted 2D Fermi-Hubbard system by Guardado-Sanchez, Morningstar et al.

References

[1] F. Bloch, Z. Phys. **52**, 555 (1929).

[2] G. H. Wannier, Rev. Mod. Phys. **34**, 645 (1962).

[3] E. E. Mendez, F. Agulló-Rueda, and J. M. Hong, Phys. Rev. Lett. **60**, 2426 (1988).

[4] P. Voisin, J. Bleuse, C. Bouche, S. Gaillard, C. Alibert, and A. Regreny, Phys. Rev. Lett. **61**, 1639 (1988).

[5] A. Nahum, J. Ruhman, S. Vijay, and J. Haah, Phys. Rev. X **7**, 031016 (2017).

[6] A. Nahum, S. Vijay, and J. Haah, Phys. Rev. X **8**, 021014 (2018).

[7] C. W. von Keyserlingk, T. Rakovszky, F. Pollmann, and S. L. Sondhi, Phys. Rev. X **8**, 021013 (2018).

[8] V. Khemani, A. Vishwanath, and D. A. Huse, Phys. Rev. X **8**, 031057 (2018).

[9] T. Rakovszky, F. Pollmann, and C. W. von Keyserlingk, Phys. Rev. X **8**, 031058 (2018).

[10] S. Gopalakrishnan, D. A. Huse, V. Khemani, and R. Vasseur, Phys. Rev. B **98**, 220303 (2018).

[11] T. Banks and A. Lucas, Phys. Rev. E **99**, 022105 (2019).

[12] F. Meinert, M. J. Mark, E. Kirilov, K. Lauber, P. Weinmann, M. Gröbner, and H.-C. Nägerl, Phys. Rev. Lett. **112**, 193003 (2014).

[13] J.-y. Choi, S. Hild, J. Zeiher, P. Schauß, A. Rubio-Abadal, T. Yefsah, V. Khemani, D. A. Huse, I. Bloch, and C. Gross, Science **352**, 1547 (2016).

[14] H. Bernien, S. Schwartz, A. Keesling, H. Levine, A. Omran, H. Pichler, S. Choi, A. S. Zibrov, M. Endres, M. Greiner, V. Vuletić, and M. D. Lukin, Nature **551**, 579 (2017).

[15] S. Scherg, T. Kohlert, J. Herbrych, J. Stolpp, P. Bordia, U. Schneider, F. Heidrich-Meisner, I. Bloch, and M. Aidelsburger, Phys. Rev. Lett. **121**, 130402 (2018).

[16] M. Rispoli, A. Lukin, R. Schittko, S. Kim, M. E. Tai, J. Léonard, and M. Greiner, Nature , 579 (2019).

[17] E. Guardado-Sanchez, P. T. Brown, D. Mitra, T. Devakul, D. A. Huse, P. Schauß, and W. S. Bakr, Phys. Rev. X **8**, 021069 (2018).

[18] P. T. Brown, D. Mitra, E. Guardado-Sanchez, R. Nourafkan, A. Reymbaut, C.-D. Hébert, S. Bergeron, A.-M. S. Tremblay, J. Kokalj, D. A. Huse, P. Schauß, and W. S. Bakr, Science **363**, 379 (2019).

[19] S. Mandt, A. Rapp, and A. Rosch, Phys. Rev. Lett. **106**, 250602 (2011).

[20] A. Rapp, S. Mandt, and A. Rosch, Phys. Rev. Lett. **105**, 220405 (2010).

[21] S. Braun, J. P. Ronzheimer, M. Schreiber, S. S. Hodgman, T. Rom, I. Bloch, and U. Schneider, Science **339**, 52 (2013).

[22] E. van Nieuwenburg, Y. Baum, and G. Refael, Proc. Natl. Acad. Sci. U.S.A. **116**, 9269 (2019).

[23] M. Schulz, C. A. Hooley, R. Moessner, and F. Pollmann, Phys. Rev. Lett. **122**, 040606 (2019).

[24] P. Sala, T. Rakovszky, R. Verresen, M. Knap, and F. Pollmann, arXiv:1904.04266 (2019).

[25] V. Khemani and R. Nandkishore, arXiv:1904.04815 (2019).

[26] P. T. Brown, D. Mitra, E. Guardado-Sanchez, P. Schauß, S. S. Kondov, E. Khatami, T. Paiva, N. Trivedi, D. A. Huse, and W. S. Bakr, Science **357**, 1385 (2017).

[27] See the Supplemental Material.

[28] S. Pai, M. Pretko, and R. M. Nandkishore, Phys. Rev. X **9**, 021003 (2019).

[29] S. Pai and M. Pretko, arXiv:1903.06173 (2019).

[30] R. M. Nandkishore and M. Hermele, Annu. Rev. Condens. Matter Phys. **10**, 295 (2019).

[31] P. T. Brown, E. Guardado-Sanchez, B. M. Spar, E. W. Huang, T. P. Devereaux, and W. S. Bakr, arXiv:1903.05678 (2019).

[32] P. M. Preiss, R. Ma, M. E. Tai, A. Lukin, M. Rispoli, P. Zupancic, Y. Lahini, R. Islam, and M. Greiner, Science **347**, 1229 (2015).

[33] R. Ma, M. E. Tai, P. M. Preiss, W. S. Bakr, J. Simon, and M. Greiner, Phys. Rev. Lett. **107**, 095301 (2011).

From Perturbative approach to weakly driven many-particle systems in the presence of approximate conservation laws by Lenarčič, Lange, Rosch

References

[1] F. Benatti, A. Nagy and H. Narnhofer, Journal of Physics A: Mathematical and Theoretical **44**, 155303 (2011).

[2] A. C. Y. Li, F. Petruccione and J. Koch, Scientific Reports **4**, 4887 (2014).

[3] A. C. Y. Li, F. Petruccione and J. Koch, Phys. Rev. X **6**, 021037 (2016).

[4] Z. Maizelis, M. Rudner and M. I. Dykman, Phys. Rev. B **89**, 155439 (2014).

[5] J. J. García-Ripoll, S. Dürr, N. Syassen, D. M. Bauer, M. Lettner, G. Rempe, and J. I. Cirac, New Journal of Physics **11**, 013053 (2009).

[6] E. M. Kessler, Phys. Rev. A **86**, 012126 (2012).

[7] M. Žnidarič, Phys. Rev. E **92**, 042143 (2015).

[8] F. Reiter and A. S. Sørensen, Phys. Rev. A **85**, 032111 (2012).

[9] H. C. F. Lemos and T. Prosen, Phys. Rev. E **95**, 042137 (2017).

[10] L. V. Butov, A. L. Ivanov, A. Imamoglu, P. B. Littlewood, A. A. Shashkin, V. T. Dolgopolov, K. L. Campman, A. C. Gossard, Phys. Rev. Lett. **86**, 5608 (2001).

[11] J. Kasprzak, M. Richard, S. Kundermann, A. Baas, P. Jeambrun, J. M. J. Keeling, F. M. Marchetti, M. H. Szymańska, R. Andre, J. L. Staehli, V. Savona, P. B. Littlewood, B. Deveaud, Le Si Dang, Nature **443**, 409 (2006).

[12] R. Balili, V. Hartwell, D. Snoke, L. Pfeiffer and K. West, Science **316**, 1007 (2007).

[13] J. Klaers, J. Schmitt, F. Vewinger and M. Weitz, Nature **468**, 545 (2010).

[14] J. Klaers, J. Schmitt, T. Damm, F. Vewinger and M. Weitz, Phys. Rev. Lett. **108**, 160403 (2012).

[15] J. Schmitt, T. Damm, D. Dung, F. Vewinger, J. Klaers, M. Weitz, Phys. Rev. Lett. **112**, 030401 (2014).

[16] S. O. Demokritov, V. E. Demidov, O. Dzyapko, G. A. Melkov, A. A. Serga, B. Hillebrands, A. N. Slavin, Nature **443**, 430 (2006).

[17] A. V. Chumak, G. A. Melkov, V. E. Demidov, O. Dzyapko, V. L. Safonov, S. O. Demokritov, Phys. Rev. Lett. **102**, 187205 (2009).

[18] T. G. Walker and W. Happer, Reviews of Modern Physics **69**, 629 (1997).

[19] S. Anisimov, B. Kapeliovich and T. Perelman, Zh. Eksp. Teor. Fiz **66**, 375 (1974).

[20] B. H. Armstrong, Phys. Rev. B **23**, 883 (1981).

[21] G. L. Eesley, Phys. Rev. B **33**, 2144 (1986).

[22] P. B. Allen, Phys. Rev. Lett. **59**, 1460 (1987).

[23] N. Singh, International Journal of Modern Physics B **24**, 1141 (2010).

[24] F. Lange, Z. Lenarčič and A. Rosch, Nature communications **8**, 15767 (2017).

[25] H. Dehghani, T. Oka and A. Mitra, Phys. Rev. B **90**, 195429 (2014).

[26] T. Shirai, T. Mori and S. Miyashita, Phys. Rev. E **91**, 030101 (2015).

[27] T. Iadecola, T. Neupert and C. Chamon, Phys. Rev. B **91**, 235133 (2015).

[28] D. E. Liu, Phys. Rev. B **91**, 144301 (2015).

[29] K. Iwahori and N. Kawakami, Phys. Rev. B **94**, 184304 (2016).

[30] T. Shirai, J. Thingna, T. Mori, S. Denisov, P. Hänggi and S. Miyashita, New Journal of Physics **18**, 053008 (2016).

[31] K. I. Seetharam, C.-E. Bardyn, N. H. Lindner, M. S. Rudner and G. Refael, Phys. Rev. X **5**, 041050 (2015).

[32] K. Iwahori and N. Kawakami, arXiv:1702.03506 (2017).

[33] M. Genske and A. Rosch, Phys. Rev. A **92**, 062108 (2015).

[34] G. Jotzu, M. Messer, R. Desbuquois, M. Lebrat, T. Uehlinger, D. Greif, T. Esslinger, Nature **515**, 237 (2014).

[35] M. Sentef, A. F. Kemper, B. Moritz, J. K. Freericks, Z. X. Shen, T. P. Devereaux, Phys. Rev. X **3**, 041033 (2013).

[36] B. Robertson, Phys. Rev. **144**, 151 (1966).

[37] B. Robertson, Phys. Rev. **160**, 206 (1968).

[38] K. Kawasaki and J. D. Gunton, Phys. Rev. A **8**, 063604 (1973).

[39] M. Ochiai, Phys. Rev. A **44**, 145 (1973).

[40] C. R. Willis and R. H. Picard, Phys. Rev. A **9**, 1343 (1974).

[41] H. Grabert and W. Weidlich, Z. Phys. **268**, 139 (1974).

[42] T. Koide, Prog. Theor. Phys. **107**, 525 (2002).

[43] H. P. Breuer and F. Petruccione, The theory of open quantum systems (Oxford University Press, New York, 2002).

[44] A. Polkovnikov, K. Sengupta, A. Silva and M. Vengalattore, Rev. Mod. Phys. **83**, 863 (2011).

[45] R. Nandkishore and D. A. Huse, Annu. Rev. Condens. Matter Phys. **6**, 15 (2015).

[46] M. Rigol, V. Dunjko, V. Yurovsky and M. Olshanii, Phys. Rev. Lett. **98**, 050405 (2007).

[47] P. Calabrese and J. Cardy, Journal of Statistical Mechanics: Theory and Experiment **2007**, P06008 (2007).

[48] M. Cramer, C. M. Dawson, J. Eisert and T. J. Osborne, Phys. Rev. Lett. **100**, 030602 (2008).

[49] T. Barthel and U. Schollwöck, Phys. Rev. Lett. **100**, 100601 (2008).

[50] F. H. L. Essler, S. Evangelisti and M. Fagotti, Phys. Rev. Lett. **109**, 247206 (2012).

[51] B. Pozsgay, Journal of Statistical Mechanics: Theory and Experiment **2013**, P07003 (2013).

[52] M. Fagotti and F. H. L. Essler, Journal of Statistical Mechanics: Theory and Experiment **2013**, P07012 (2013).

[53] M. Fagotti and F. H. L. Essler, Phys. Rev. B **87**, 245107 (2013).

[54] M. Fagotti, Journal of Statistical Mechanics: Theory and Experiment **2014**, P03016 (2014).

[55] M. Fagotti, M. Collura, F. H. L. Essler and P. Calabrese, Phys. Rev. B **89**, 125101 (2014).

[56] B. Wouters, J. DeNardis, M. Brockmann, D. Fioretto, M. Rigol, J.-S. Caux, Phys. Rev. Lett. **113**, 117202 (2014).

[57] B. Pozsgay, M. Mestyan, M. A. Werner, M. Kormos, G. Zarand, G. Takács, Phys. Rev. Lett. **113**, 117203 (2014).

[58] S. Sotiriadis and P. Calabrese, Journal of Statistical Mechanics: Theory and Experiment **2014**, P07024 (2014).

[59] G. Goldstein and N. Andrei, Phys. Rev. A **90**, 043625 (2014).

[60] M. Brockmann, B. Wouters, D. Fioretto, J. De Nardis, R. Vlijm and J.-S. Caux, Journal of Statistical Mechanics: Theory and Experiment **2014**, P12009 (2014).

[61] B. Pozsgay, Journal of Statistical Mechanics: Theory and Experiment **2014**, P10045 (2014).

[62] M. Rigol, Phys. Rev. E **90**, 031301 (2014).

[63] M. Mestyán, B. Pozsgay, G. Takács and M. A. Werner, Journal of Statistical Mechanics: Theory and Experiment **2015**, P04001 (2015).

[64] J. Eisert, M. Friesdorf and C. Gogolin, Nature Physics **11**, 124 (2015).

[65] E. Ilievski, E. Quinn, J. De Nardis and M. Brockmann, Journal of Statistical Mechanics: Theory and Experiment **2016**, 063101 (2016).

[66] L. Piroli, E. Vernier and P. Calabrese, Phys. Rev. B **94**, 054313 (2016).

[67] P. Calabrese, F. H. L. Essler and M. Fagotti, Phys. Rev. Lett. **106**, 227203 (2011).

[68] P. Calabrese, F. H. L. Essler and M. Fagotti, Journal of Statistical Mechanics: Theory and Experiment **2012**, P07016 (2012).

[69] P. Calabrese, F. H. L. Essler and M. Fagotti, Journal of Statistical Mechanics: Theory and Experiment **2012**, P07022 (2012).

[70] J.-S. Caux and F. H. L. Essler, Phys. Rev. Lett. **110**, 257203 (2013).

[71] F. H. L. Essler and M. Fagotti, Journal of Statistical Mechanics: Theory and Experiment **2016**, 064002 (2016).

[72] F. H. L. Essler, G. Mussardo and M. Panfil, Journal of Statistical Mechanics: Theory and Experiment **2017**, 013103 (2017).

[73] E. Ilievski, M. Medenjak, T. Prosen and L. Zadnik, Journal of Statistical Mechanics: Theory and Experiment P064008 (2016).

[74] E. Ilievski, J. DeNardis, B. Wouters, J. S. Caux, F. H. L. Essler, T. Prosen, Phys. Rev. Lett. **115**, 157201 (2015).

[75] B. Pozsgay, E. Vernier and M. Werner, arXiv preprint arXiv:1703.09516 (2017).

[76] P. Jung, R. W. Helmes and A. Rosch, Phys. Rev. Lett. **96**, 067202 (2006).

[77] Z. Lenarčič and T. Prosen, Phys. Rev. E **91**, 030103 (2015).

[78] G. Benenti, G. Casati, T. c. v. Prosen, D. Rossini and M. Žnidarič, Phys. Rev. B **80**, 035110 (2009).

[79] D. ForsterHydrodynamic fluctuations, broken symmetry, and correlation functions Vol. 47 (Reading, Mass., WA Benjamin, Inc.(Frontiers in Physics), 1975).

[80] H. Mori, Progress of theoretical physics **33**, 423 (1965).

[81] R. Zwanzig and R. Balescu, J. Chem. Phys **33**, 1338 (1960).

[82] P. Jung and A. Rosch, Phys. Rev. B **75**, 245104 (2007).

[83] P. Mazur, Physica **43**, 533 (1969).

[84] M. Suzuki, Physica **51**, 277 (1971).

[85] X. Zotos, F. Naef and P. Prelovsek, Phys. Rev. B **55**, 11029 (1997).

[86] A. Rosch, J. Paaske, J. Kroha and P. Wölfle, Phys. Rev. Lett. **90**, 076804 (2003).

[87] Article in preparation.

[88] J. Berges, S. Borsányi and C. Wetterich, Phys. Rev. Lett. **93**, 142002 (2004).

[89] G. Aarts, G. F. Bonini and C. Wetterich, Phys. Rev. D **63**, 025012 (2000).

[90] M. Gring, M. Kuhnert, T. Langen, T. Kitagawa, B. Rauer, M. Schreitl, I. Mazets, D. Adu Smith, E. Demler and J. Schmiedmayer, Science **337**, 1318 (2012).

[91] T. Langen, S. Erne, R. Geiger, B. Rauer, T. Schweigler, M. Kuhnert, W. Rohringer, I. Mazets, T. Gasenzer, J. Schmiedmayer, Science **348** (2015).

[92] T. Langen, T. Gasenzer and J. Schmiedmayer, J. Stat. Mech. **2016**, 064009 (2016).

[93] M. Moeckel and S. Kehrein, Phys. Rev. Lett. **100**, 175702 (2008).

[94] C. Kollath, A. M. Läuchli and E. Altman, Phys. Rev. Lett. **98**, 180601 (2007).

[95] M. Kollar, F. A. Wolf and M. Eckstein, Physical Review B **84**, 054304 (2011).

[96] J. Marino and A. Silva, Phys. Rev. B **86**, 060408 (2012).

[97] A. Mitra, Phys. Rev. B **87**, 205109 (2013).

[98] M. Marcuzzi, J. Marino, A. Gambassi and A. Silva, Phys. Rev. Lett. **111**, 197203 (2013).

[99] B. Bertini, F. H. L. Essler, S. Groha and N. J. Robinson, Phys. Rev. Lett. **115**, 180601 (2015).

[100] M. Babadi, E. Demler and M. Knap, Phys. Rev. X **5**, 041005 (2015).

[101] M. Buchhold and S. Diehl, Phys. Rev. A **92**, 013603 (2015).

[102] M. Marcuzzi, J. Marino, A. Gambassi and A. Silva, Phys. Rev. B **94**, 214304 (2016).

[103] R. Barnett, A. Polkovnikov and M. Vengalattore, Phys. Rev. A **84**, 023606 (2011).

[104] N. Nessi, A. Iucci and M. A. Cazalilla, Phys. Rev. Lett. **113**, 210402 (2014).

[105] B. Nowak, J. Schole and T. Gasenzer, New J. Phys. **16**, 093052 (2014).

[106] E. Canovi, M. Kollar and M. Eckstein, Phys. Rev. E **93**, 012130 (2016).

[107] D. Golež, P. Werner and M. Eckstein, Phys. Rev. B **94**, 035121 (2016).

[108] A. Chiocchetta, A. Gambassi, S. Diehl and J. Marino, Phys. Rev. Lett. **118**, 135701 (2017).

[109] V. Gurarie, Nuclear Physics B **441**, 569 (1995).

[110] J. Lux, J. Müller, A. Mitra and A. Rosch, Phys. Rev. A **89**, 053608 (2014).

[111] A. Bohrdt, C. Mendl, M. Endres and M. Knap, New Journal of Physics (2017).

[112] E. Leviatan, F. Pollmann, J. H. Bardarson, D. A. Huse, and E. Altman, arXiv:1702.08894 (2017).

From "Observing non-ergodicity due to kinetic constraints in tilted Fermi-Hubbard chains" by Scherg, Kohlert, et al.

References

[1] C. Gogolin and J. Eisert, Equilibration, thermalisation, and the emergence of statistical mechanics in closed quantum systems, Rep. Prog. Phys. **79**, 056001 (2016).

[2] L. D'Alessio, Y. Kafri, A. Polkovnikov, and M. Rigol, From quantum chaos and eigenstate thermalization to statistical mechanics and thermodynamics, Advances in Physics **65**, 239 (2016).

[3] T. Mori, T. N. Ikeda, E. Kaminishi, and M. Ueda, Thermalization and prethermalization in isolated quantum systems: a theoretical overview, Journal of Physics B: Atomic, Molecular and Optical Physics **51**, 112001 (2018).

[4] P. Calabrese, F. H. L. Essler, and M. Fagotti, Quantum Quench in the Transverse-Field Ising Chain, Phys. Rev. Lett. **106**, 227203 (2011).

[5] R. Nandkishore and D. A. Huse, Many-Body Localization and Thermalization in Quantum Statistical Mechanics, Annu. Rev. Condens. Matter Phys. **6**, 15 (2015).

[6] E. Altman and R. Vosk, Universal Dynamics and Renormalization in Many-Body-Localized Systems, Annu. Rev. Condens. Matter Phys. **6**, 383 (2015).

[7] D. A. Abanin, E. Altman, I. Bloch, and M. Serbyn, Colloquium: Many-body localization, thermalization, and entanglement, Rev. Mod. Phys. **91**, 021001 (2019).

[8] J. M. Deutsch, Quantum statistical mechanics in a closed system, Phys. Rev. A **43**, 2046 (1991).

[9] M. Srednicki, Chaos and quantum thermalization, Phys. Rev. E **50**, 888 (1994).

[10] M. Rigol, V. Dunjko, and M. Olshanii, Thermalization and its mechanism for generic isolated quantum systems, Nature **452**, 854 (2008).

[11] See Supplemental Material, which includes Refs. [69, 70, 71, 72, 73, 74, 75, 77, 78, 79, 76, 80, 82, 83, 84, 85, 86, 87, 88, 89, 90, 91, 92, 93, 94, 95, 96, 97], not cited in the main text, for details on: the interaction picture, the dynamical symmetry between attractive and repulsive interactions, the effective Hamiltonians for different regimes, fragmentation in the resonant regime, constrained dynamics in the presence of higher order terms and on-site interactions, the scaling analysis of the steady-state imbalance and the entanglement entropy, details on the experimental sequence, creating a homogeneous potential, creating a linear potential, interaction averaging, calibration of parameters, extraction of the interaction energy U_{res} and the numerical implementation of the exact diagonalization technique.

[12] N. Shiraishi and T. Mori, Systematic Construction of Counterexamples to the Eigenstate Thermalization Hypothesis, Phys. Rev. Lett. **119**, 030601 (2017).

[13] R. Mondaini, K. Mallayya, L. F. Santos, and M. Rigol, Comment on "Systematic Construction of Counterexamples to the Eigenstate Thermalization Hypothesis", Phys. Rev. Lett. **121**, 038901 (2018).

[14] S. Moudgalya, S. Rachel, B. A. Bernevig, and N. Regnault, Exact excited states of nonintegrable models, Phys. Rev. B **98**, 235155 (2018).

[15] C. J. Turner, A. A. Michailidis, D. A. Abanin, M. Serbyn, and Z. Papić, Weak ergodicity breaking from quantum many-body scars, Nature Physics **14**, 745 (2018).

[16] T. Iadecola and M. Schecter, Quantum many-body scar states with emergent kinetic constraints and finite-entanglement revivals, Phys. Rev. B **101**, 024306 (2020).

[17] S. Chattopadhyay, H. Pichler, M. D. Lukin, and W. W. Ho, Quantum many-body scars from virtual entangled pairs, Phys. Rev. B **101**, 174308 (2020).

[18] H. Bernien, S. Schwartz, A. Keesling, H. Levine, A. Omran, H. Pichler, S. Choi, A. S. Zibrov, M. Endres, M. Greiner, V. Vuletić, and M. D. Lukin, Probing many-body dynamics on a 51-atom quantum simulator, Nature **551**, 579 (2017).

[19] C. J. Turner, A. A. Michailidis, D. A. Abanin, M. Serbyn, and Z. Papić, Quantum scarred eigenstates in a Rydberg atom chain: Entanglement, breakdown of thermalization, and stability to perturbations, Phys. Rev. B **98**, 155134 (2018).

[20] P. Sala, T. Rakovszky, R. Verresen, M. Knap, and F. Pollmann, Ergodicity Breaking Arising from Hilbert Space Fragmentation in Dipole-Conserving Hamiltonians, Phys. Rev. X **10**, 011047 (2020).

[21] V. Khemani, M. Hermele, and R. Nandkishore, Localization from Hilbert space shattering: From theory to physical realizations, Phys. Rev. B **101**, 174204 (2020).

[22] T. Rakovszky, P. Sala, R. Verresen, M. Knap, and F. Pollmann, Statistical localization: From strong fragmentation to strong edge modes, Phys. Rev. B **101**, 125126 (2020).

[23] S. Moudgalya, A. Prem, R. Nandkishore, N. Regnault, and B. A. Bernevig, Thermalization and its absence within Krylov subspaces of a constrained Hamiltonian, arXiv:1910.14048 (2019).

[24] M. van Horssen, E. Levi, and J. P. Garrahan, Dynamics of many-body localization in a translation-invariant quantum glass model, Phys. Rev. B **92**, 100305 (2015).

[25] M. Schiulaz, A. Silva, and M. Müller, Dynamics in many-body localized quantum systems without disorder, Phys. Rev. B **91**, 184202 (2015).

[26] N. Y. Yao, C. R. Laumann, J. I. Cirac, M. D. Lukin, and J. E. Moore, Quasi-Many-Body Localization in Translation-Invariant Systems, Phys. Rev. Lett. **117**, 240601 (2016).

[27] Z. Papić, E. M. Stoudenmire, and D. A. Abanin, Many-body localization in disorder-free systems: The importance of finite-size constraints, Annals of Physics **362**, 714 (2015).

[28] A. Smith, J. Knolle, D. L. Kovrizhin, and R. Moessner, Disorder-Free Localization, Phys. Rev. Lett. **118**, 266601 (2017).

[29] A. Smith, J. Knolle, R. Moessner, and D. L. Kovrizhin, Absence of Ergodicity without Quenched Disorder: From Quantum Disentangled Liquids to Many-Body Localization, Phys. Rev. Lett. **119**, 176601 (2017).

[30] M. Brenes, M. Dalmonte, M. Heyl, and A. Scardicchio, Many-Body Localization Dynamics from Gauge Invariance, Phys. Rev. Lett. **120**, 030601 (2018).

[31] M. Schulz, C. A. Hooley, R. Moessner, and F. Pollmann, Stark Many-Body Localization, Phys. Rev. Lett. **122**, 040606 (2019).

[32] E. v. Nieuwenburg, Y. Baum, and G. Refael, From Bloch oscillations to many-body localization in clean interacting systems, PNAS **116**, 9269 (2019).

[33] L.-N. Wu and A. Eckardt, Bath-Induced Decay of Stark Many-Body Localization, Phys. Rev. Lett. **123**, 030602 (2019).

[34] S. R. Taylor, M. Schulz, F. Pollmann, and R. Moessner, Experimental probes of Stark many-body localization, Phys. Rev. B **102**, 054206 (2020).

[35] R. Yao and J. Zakrzewski, Many-body localization of bosons in an optical lattice: Dynamics in disorder-free potentials, Phys. Rev. B **102**, 104203 (2020).

[36] H. Ott, E. de Mirandes, F. Ferlaino, G. Roati, G. Modugno, and M. Inguscio, Collisionally Induced Transport in Periodic Potentials, Phys. Rev. Lett. **92**, 160601 (2004).

[37] N. Strohmaier, Y. Takasu, K. Günter, R. Jördens, M. Köhl, H. Moritz, and T. Esslinger, Interaction-Controlled Transport of an Ultracold Fermi Gas, Phys. Rev. Lett. **99**, 220601 (2007).

[38] J. H. Bardarson, F. Pollmann, and J. E. Moore, Unbounded Growth of Entanglement in Models of Many-Body Localization, Phys. Rev. Lett. **109**, 017202 (2012).

[39] A. D. Luca and A. Scardicchio, Ergodicity breaking in a model showing many-body localization, EPL **101**, 37003 (2013).

[40] Note, imbalance is defined as a charge imbalance between even and odd lattice sites in our system and does not probe spin imbalances. The magnetization of systems is conserved during the evolution and it is equal to zero at all times.

[41] Note, that in the clean translationally-invariant Fermi-Hubbard model the initial CDW corresponds to an infinite temperature state and a finite imbalance value is a hallmark signature of localization. In the tilted model, the spectrum is superextensive complicating a meaningful definition of temperature. This is overcome by transforming into the interaction picture with respect to the tilt potential, which leaves all density observables invariant and allows us to establish the imbalance as a good probe for ergodicity breaking [11].

[42] M. Ben Dahan, E. Peik, J. Reichel, Y. Castin, and C. Salomon, Bloch Oscillations of Atoms in an Optical Potential, Phys. Rev. Lett. **76**, 4508 (1996).

[43] A. Buchleitner and A. R. Kolovsky, Interaction-Induced Decoherence of Atomic Bloch Oscillations, Phys. Rev. Lett. **91**, 253002 (2003).

[44] A. R. Kolovsky and A. Buchleitner, Floquet-Bloch operator for the Bose-Hubbard model with static field, Phys. Rev. E **68**, 056213 (2003).

[45] A. Tomadin, R. Mannella, and S. Wimberger, Many-Body Interband Tunneling as a Witness of Complex Dynamics in the Bose-Hubbard Model, Phys. Rev. Lett. **98**, 130402 (2007).

[46] A. Tomadin, R. Mannella, and S. Wimberger, Many-body Landau-Zener tunneling in the Bose-Hubbard model, Phys. Rev. A **77**, 013606 (2008).

[47] M. Gustavsson, E. Haller, M. J. Mark, J. G. Danzl, G. Rojas-Kopeinig, and H.-C. Nägerl, Control of Interaction-Induced Dephasing of Bloch Oscillations, Phys. Rev. Lett. **100**, 080404 (2008).

[48] P. M. Preiss, R. Ma, M. E. Tai, A. Lukin, M. Rispoli, P. Zupancic, Y. Lahini, R. Islam, and M. Greiner, Strongly correlated quantum walks in optical lattices, Science **347**, 1229 (2015).

[49] U. Schollwöck, The density-matrix renormalization group in the age of matrix product states, Annals of Physics **326**, 96 (2011).

[50] S. Paeckel, T. Köhler, A. Swoboda, S. R. Manmana, U. Schollwöck, and C. Hubig, Time-evolution methods for matrix-product states, Annals of Physics **411**, 167998 (2019).

[51] J. Hauschild and F. Pollmann, Efficient numerical simulations with Tensor Networks: Tensor Network Python (TeNPy), SciPost Phys. Lect. Notes , 5 (2018).

[52] P. Bordia, H. P. Lüschen, S. S. Hodgman, M. Schreiber, I. Bloch, and U. Schneider, Coupling Identical one-dimensional Many-Body Localized Systems, Phys. Rev. Lett. **116**, 140401 (2016).

[53] U. Schneider, L. Hackermüller, J. P. Ronzheimer, S. Will, S. Braun, T. Best, I. Bloch, E. Demler, S. Mandt, D. Rasch, and A. Rosch, Fermionic transport and out-of-equilibrium dynamics in a homogeneous Hubbard model with ultracold atoms, Nature Physics **8**, 213–218 (2012).

[54] M. Schreiber, S. S. Hodgman, P. Bordia, H. P. Lüschen, M. H. Fischer, R. Vosk, E. Altman, U. Schneider, and I. Bloch, Observation of many-body localization of interacting fermions in a quasirandom optical lattice, Science **349**, 842 (2015).

[55] S. Pai and M. Pretko, Dynamical Scar States in Driven Fracton Systems, Phys. Rev. Lett. **123**, 136401 (2019).

[56] H. Zhao, J. Vovrosh, F. Mintert, and J. Knolle, Quantum Many-Body Scars in Optical Lattices, Phys. Rev. Lett. **124**, 160604 (2020).

[57] A. Kshetrimayum, J. Eisert, and D. M. Kennes, Stark time crystals: Symmetry breaking in space and time, arXiv:2007.13820 (2020).

[58] E. Bairey, G. Refael, and N. H. Lindner, Driving induced many-body localization, Phys. Rev. B **96**, 020201 (2017).

[59] D. S. Bhakuni, R. Nehra, and A. Sharma, Drive-induced many-body localization and coherent destruction of Stark many-body localization, Phys. Rev. B **102**, 024201 (2020).

[60] J. Feldmeier, P. Sala, G. de Tomasi, F. Pollmann, and M. Knap, Anomalous Diffusion in Dipole- and Higher-Moment Conserving Systems, arXiv:2004.00635 (2020).

[61] E. Guardado-Sanchez, A. Morningstar, B. M. Spar, P. T. Brown, D. A. Huse, and W. S. Bakr, Subdiffusion and Heat Transport in a Tilted Two-Dimensional Fermi-Hubbard System, Phys. Rev. X **10**, 011042 (2020).

[62] S. Pai and M. Pretko, Fractons from confinement in one dimension, Phys. Rev. Research **2**, 013094 (2020).

[63] R. Verdel, F. Liu, S. Whitsitt, A. V. Gorshkov, and M. Heyl, Real-time dynamics of string breaking in quantum spin chains, Phys. Rev. B **102**, 014308 (2020).

[64] Z.-C. Yang, F. Liu, A. V. Gorshkov, and T. Iadecola, Hilbert-Space Fragmentation from Strict Confinement, Phys. Rev. Lett. **124**, 207602 (2020).

[65] B. Yang, H. Sun, R. Ott, H.-Y. Wang, T. V. Zache, J. C. Halimeh, Z.-S. Yuan, P. Hauke, and J.-W. Pan, Observation of gauge invariance in a 71-site Bose-Hubbard quantum simulator, arXiv:2003.08945 (2020).

[66] J. Sebby-Strabley, M. Anderlini, P. S. Jessen, and J. V. Porto, Lattice of double wells for manipulating pairs of cold atoms, Phys. Rev. A **73**, 033605 (2006).

[67] S. Fölling, S. Trotzky, P. Cheinet, M. Feld, R. Saers, A. Widera, T. Müller, and I. Bloch, Direct observation of second-order atom tunnelling, Nature **448** (2007).

[68] S. Scherg, T. Kohlert, J. Herbrych, J. Stolpp, P. Bordia, U. Schneider, F. Heidrich-Meisner, I. Bloch, and M. Aidelsburger, Nonequilibrium Mass Transport in the 1D Fermi-Hubbard Model, Phys. Rev. Lett. **121**, 130402 (2018).

[69] C. Parra-Murillo and S. Wimberger, Manifold Approach for a Many-Body Wannier-Stark System: Localization and Chaos in Energy Space, Acta Physica Polonica A **124** (2014).

[70] C. A. Parra-Murillo, J. Madroñero, and S. Wimberger, Two-band Bose-Hubbard model for many-body resonant tunneling in the Wannier-Stark system, Phys. Rev. A **88**, 032119 (2013).

[71] D. V. Else, W. W. Ho, and P. T. Dumitrescu, Long-Lived Interacting Phases of Matter Protected by Multiple Time-Translation Symmetries in Quasiperiodically Driven Systems, Phys. Rev. X **10**, 021032 (2020).

[72] N. Goldman and J. Dalibard, Periodically Driven Quantum Systems: Effective Hamiltonians and Engineered Gauge Fields, Phys. Rev. X **4**, 031027 (2014).

[73] A. Eckardt and E. Anisimovas, High-frequency approximation for periodically driven quantum systems from a Floquet-space perspective, New Journal of Physics **17**, 093039 (2015).

[74] M. Bukov, L. D'Alessio, and A. Polkovnikov, Universal high-frequency behavior of periodically driven systems: from dynamical stabilization to Floquet engineering, Adv. Phys. **64**, 139 (2015).

[75] D. A. Abanin, W. De Roeck, and F. Huveneers, Exponentially Slow Heating in Periodically Driven Many-Body Systems, Phys. Rev. Lett. **115**, 256803 (2015).

[76] L. D'Alessio and M. Rigol, Long-time Behavior of Isolated Periodically Driven Interacting Lattice Systems, Physical Review X **4** (2014).

[77] D. A. Abanin, W. De Roeck, W. W. Ho, and F. Huveneers, Effective Hamiltonians, prethermalization, and slow energy absorption in periodically driven many-body systems, Phys. Rev. B **95**, 014112 (2017).

[78] W. De Roeck and V. Verreet, Very slow heating for weakly driven quantum many-body systems, arXiv:1911.01998 (2019).

[79] D. V. Else, B. Bauer, and C. Nayak, Prethermal Phases of Matter Protected by Time-Translation Symmetry, Phys. Rev. X **7**, 011026 (2017).

[80] T. Kuwahara, T. Mori, and K. Saito, Floquet–Magnus theory and generic transient dynamics in periodically driven many-body quantum systems, Annals of Physics **367**, 96–124 (2016).

[38] This discussion would also apply in the limit of incommensurate Δ_σ and U when going to the frame with respect to the interacting term.

[82] S. Bravyi, D. P. DiVincenzo, and D. Loss, Schrieffer–Wolff transformation for quantum many-body systems, Annals of Physics **326**, 2793–2826 (2011).

[83] E. S. Mananga and T. Charpentier, Introduction of the Floquet-Magnus expansion in solid-state nuclear magnetic resonance spectroscopy, The Journal of Chemical Physics **135**, 044109 (2011).

[84] T. Mikami, S. Kitamura, K. Yasuda, N. Tsuji, T. Oka, and H. Aoki, Brillouin-Wigner theory for high-frequency expansion in periodically driven systems: Application to Floquet topological insulators, Phys. Rev. B **93**, 144307 (2016).

[85] D. Abanin, W. De Roeck, W. W. Ho, and F. Huveneers, A Rigorous Theory of Many-Body Prethermalization for Periodically Driven and Closed Quantum Systems, Commun. Math. Phys. **354**, 809 (2017).

[86] R. Sensarma, D. Pekker, E. Altman, E. Demler, N. Strohmaier, D. Greif, R. Jördens, L. Tarruell, H. Moritz, and T. Esslinger, Lifetime of double occupancies in the Fermi-Hubbard model, Phys. Rev. B **82**, 224302 (2010).

[87] N. M. R. Peres, R. G. Dias, P. D. Sacramento, and J. M. P. Carmelo, Finite-temperature transport in finite-size Hubbard rings in the strong-coupling limit, Phys. Rev. B **61**, 5169 (2000).

[88] C.-J. Lin and O. I. Motrunich, Explicit construction of quasiconserved local operator of translationally invariant nonintegrable quantum spin chain in prethermalization, Phys. Rev. B **96**, 214301 (2017).

[89] C. E. Soliverez, An effective Hamiltonian and time-independent perturbation theory, Journal of Physics C: Solid State Physics **2**, 2161 (1969).

[90] T. Kato, On the Convergence of the Perturbation Method. I, Progress of Theoretical Physics **4**, 514 (1949).

[91] D. Prato and P. W. Lamberti, A note on Magnus formula, The Journal of Chemical Physics **106**, 4640 (1997).

[92] D. N. Page, Average entropy of a subsystem, Phys. Rev. Lett. **71**, 1291 (1993).

[93] L. Vidmar and M. Rigol, Entanglement Entropy of Eigenstates of Quantum Chaotic Hamiltonians, Phys. Rev. Lett. **119** (2017).

[94] G. De Tomasi and I. M. Khaymovich, Multifractality meets entanglement: Relation for nonergodic extended states, Phys. Rev. Lett. **124** (2020).

[95] C. A. Regal, M. Greiner, and D. S. Jin, Observation of Resonance Condensation of Fermionic Atom Pairs, Phys. Rev. Lett. **92**, 040403 (2004).

[96] C. A. Regal and D. S. Jin, Measurement of Positive and Negative Scattering Lengths in a Fermi Gas of Atoms, Phys. Rev. Lett. **90**, 230404 (2003).

[97] R. Jördens, Metallic and Mott-Insulating Phases in Fermionic Quantum Gases, Ph.D. thesis, ETH Zurich, Zürich (2010).

24.18 Bibliography from Other Articles

From "A new class of completely integrable quantum spin chains" by Prosen

References

[1] see e.g. V.E.Korepin, N.M.Bogoliubov, and A.G.Izergin, Quantum Inverse scattering Method and Correlation Functions, Cambridge University Press (Cambridge, 1993); also [5] and references therein.

[2] X.Zotos and P.Prelovšek, Phys.Rev.B **53**, 983 (1996); H.Castella, X.Zotos and P.Prelovšek, Phys.Rev.Lett. **74**, 972 (1995); X.Zotos, F.Naef and P.Prelovšek, Phys. Rev. B **55**, 11029 (1997).

[3] In the forthcoming publication we discuss an 'exponentially large' invariant dynamical Lie subalgebra of $\mathfrak{U}$, corresponding to non-integrable kicked Heisenberg XXZ chain, whose power grows as $\sim 1.7^p$ and in which we find a unique nontrivial conservation law that explains deviations from quantum ergodicity and normal transport as observed numerically in (T. Prosen, cond-mat/9707180).

[4] M.Grady, Phys.Rev.D **25**, 1103 (1982).

[5] M.P.Grabowski and P.Mathieu, Ann.Phys.(NY) **243**, 299 (1995).

From Understanding many-body physics in one dimension from the Lieb-Liniger model by Jiang, Chen, Guan

References

[1] Bethe H 1931 *Z. Physik* **71** 205

[2] Lieb E H and Liniger W 1963 *Phys. Rev.* **130** 1605

[3] Yang C N and Yang C P 1969 *J. Math. Phys.* **10** 1115

[4] Yang C N 1967 *Phys. Rev. Lett.* **19** 1312

[5] Baxter R J 1972 *Ann. Phys.* **70** 193

[6] Baxter R J 1972 *Ann. Phys.* **70** 323

[7] Gaudin M 1967 *Phys. Lett. A* **24** 55

[8] Baxter R J 1982 Exactly Solved Models in Statistical Mechanics (London: Academic Press)

[9] Yang C N 1983 Selected Papers 1945–1980 W. H. Freeman and Company

[10] Yang C N 2013 Selected Papers II World Scientific

[11] Korepin V E, Izergin A G and Bogoliubov N M 1993 Quantum Inverse Scattering Method and Correlation Functions (Cambridge: Cambridge University Press)

[12] Takahashi M 1999 Thermodynamics of One-Dimensional Solvable Models (Cambridge: Cambridge University Press)

[13] Essler F H L, Frahm H, Ghmann F, Klmper A and Korepin V E 2005 The One-Dimensional Hubbard Model (Cambridge: Cambridge University Press)

[14] Sutherland B 2004 Beautiful Models (Singapore: World Scientific)

[15] Gaudin M 2014 The Bethe Wavefunction (Cambridge: Cambridge University Press)

[16] Olshanii M 1998 Phys. Rev. Lett. **81** 938

[17] Olshanii M and Dunjko V 2003 Phys. Rev. Lett. **91** 090401

[18] Dunjko V, Lorent V and Olshanii M 2001 *Phys. Rev. Lett.* **86** 5413

[19] Girardeau M, Nguyen H and Olshanii M 2004 *Opt. Commun.* **243** 3

[20] Gaudin M 1971 *Phys. Rev. A* **4** 386

[21] Iida T and Wadati M 2005 *J. Phys. Soc. Jpn.* **74** 1724

[22] Batchelor M T, Guan X W and Mcguire J B 2004 *J. Phys. A* **37** L497

[23] Bortz M private communications

[24] Paredes P 2004 *Nature* **429** 277

[25] Kinoshita T, Wenger T and Weiss D S 2004 *Science* **305** 1125

[26] Guan X W and Batchelor M T 2011 *J. Phys. A: Math. Theor.* **44** 102001

[27] Guan L M private communications

[28] Panfil M and Caux J S 2014 *Phys. Rev. A* **89** 033605

[29] Ristivojevic Z 2014 *Phys. Rev. Lett.* **113** 015301

[30] Astrakharchik G E, Boronat J, Casulleras and Giorgini S 2005 *Phys. Rev. Lett.* **95** 190407

[31] Batchelor M T, Bortz M, Guan X W and Oelkers N 2005 *J. Stat. Mech.: Theory Exp.* L10001

[32] Chen S, Guan L, Yin X, Hao Y and Guan X W 2010 *Phys. Rev. A* **81** 031609

[33] Panfil M, Nardis J D and Caux J S 2013 *Phys. Rev. Lett.* **110** 125302

[34] Kormos M, Mussardo G and Trombettoni A 2011 *Phys. Rev. A* **83** 013617

[35] Girardeau M D and Astrakharchik G E 2009 *Phys. Rev. A* **81** 061601(R)

[36] Giamarchi T 2004 Quantum Physics in One Dimension (Cambridge: Cambridge University Press)

[37] Cazalilla M A, Citro R, Giamarchi T, Orignac E and Rigol M 2011 *Rev. Mod. Phys.* **83** 1405

[38] Caux J S and Calabrese P 2006 *Phys. Rev. A* **74** 031605

[39] Panfil M and Caux J S 2014 *Phys. Rev. A* **89** 033605

[40] Belavin A A, Polyakov A M and Zamolodchikov A B 1984 *Nucl. Phys. B* **241** 333

[41] Guan X W, Batchelor M T and Lee C 2013 *Rev. Mod. Phys.* **85** 1633

[42] Gangardt D M and Shlyapnikov G V 2003 *Phys. Rev. Lett.* **90** 010401

[43] Kheruntsyan K V, Gangardt D M, Drummond P D and Shlyapnikov G V 2003 *Phys. Rev. Lett.* **91** 040403

[44] Batchelor M T and Guan X W 2007 *Laser Phys. Lett.* **4** 77

[45] Klumper A and Patu O I 2014 *Phys. Rev. A* **90** 053626

[46] Gangardt D M and Shlyapnikov G V 2003 *Phys. Rev. Lett.* **90** 010401

[47] Kheruntsyan K V, Gangardt D M, Drummond P D and Shlyapnikov G V 2003 *Phys. Rev. Lett.* **91** 040403

[48] Kheruntsyan K V, Gangardt D M, Drummond P D and Shlyapnikov G V 2005 *Phys. Rev. A* **71** 053615

[49] Tan S 2008 *Ann. Phys.* **323** 2952

[50] Tan S 2008 *Ann. Phys.* **323** 2971

[51] Tan S 2008 *Ann. Phys.* **323** 2987

[52] Chen Y Y, Jiang Y Z, Guan X W and Zhou Q 2014 *Nat. Commun.* **5** 51040

[53] Cazalilla M A 2003 *Phys. Rev. A* **67** 053606

[54] Guan X W, Batchelor M T and Takahashi M 2007 *Phys. Rev. A* **76** 043617

[55] Batchelor M T 2014 *Int. J. Mod. Phys. B* **28** 1430010

[56] Kinoshita T, Wenger T and Weiss D S 2005 *Phys. Rev. Lett.* **95** 190406

[57] Guarrera V, Muth D, Labouvle R, Vogler A, Barontlnl G, Flelschhauer M and Ott H 2012 *Phys. Rev. A* **86** 021601

[58] Armijo J, Jacqmin T, Kheruntsyan and Bouchoule 2010 *Phys. Rev. Lett.* **105** 230402

[59] Tolra B L, O'Hara K M, Huckans J H, Phillips W D, Rolston S L and Porto J V 2004 *Phys. Rev. Lett.* **92** 190401

[60] Haller E, Rabie M, Mark M J, Danzl J G, Hart R, Lauber K, Pupillo G and Ngerl H C 2011 *Phys. Rev. Lett.* **107** 230404

[61] Kuhnert M, Geiger R, Langen T, Gring M, Rauer B, Kitagawa T, Demler E, Smith D A and Schmiedmayer J 2013 *Phys. Rev. Lett.* **110** 090405

[62] van Amerongen A H, van Es J J P, Wicke P, Kheruntsyan K V and van Druten N J 2008 *Phys. Rev. Lett.* **100** 090402

[63] Vogler A, Labouvie R, Stubenrauch F, Barontini G, Guarrera V and Ott H 2013 *Phys. Rev. A* **88** 031603

[64] Haller E, Gustavss M, Mark M J, Danzl J G, Hart R, Pupillo G and Ngerl H C 2009 *Science* **325** 1224

[65] Jacqmin T, Armijo J, Berrada T, Kheruntsyan K V and Bouchoule I 2011 *Phys. Rev. Lett.* **106** 230405

[66] Esteve J, Trebbia J B, Schumm T, Aspect A, Westbrook C I and Bouchoule I 2006 *Phys. Rev. Lett.* **96** 130403

[67] Armijo J 2012 *Phys. Rev. Lett.* **108** 225306

[68] Karpiuk T, Deuar P, Bienias P, Witkowska E, Pawlowski K, Gajda M, Rzazewski K and Brewczyk M 2012 *Phys. Rev. Lett.* **109** 205302

[69] Fabbri N, Panfil M, Clment D, Fallani L, Inguscio M, Fort C and Caux J S 2014 arXiv:1406.2176v2 [cond-mat.quant-gas]

[70] Kinoshita T, Wenger T and Weiss D S 2006 *Nature* **440** 900

[71] Hofferberth S, Lesanovsky I, Fischer B, Schumm T and Schmiedmayer J 2007 *Nature* **449** 324

[72] Ronzheimer J P 2013 *Phys. Rev. Lett.* **110** 205301

[73] The experiments are chosen for the most relative to the Lieb–Liniger model, and by no means exhaustive.

[74] Langen T, Geiger R, Kuhnert M, Rauer B and Schmiedmayer J 2013 *Nat. Phys.* **9** 640

[75] Stimming H P, Mauser N J, Schmiedmayer J and Mazets I E 2010 *Phys. Rev. Lett.* **105** 015301

[76] Langen T, Erne S, Geiger R, Rauer B, Schweigler T, Kuhnert M, Rohringer W, Mazets I E, Gasenzer T and Schmiedmayer J 2014 arXiv:1411.7185v1 [cond-mat.quant-gas])

[77] Witkowska E, Deuar P, Gajda M and Rzaewski K 2011 *Phys. Rev. Lett.* **106** 135301

[78] Jacqmin T, Fang B, Berrada T, Rosclde T and Bouchoule I 2012 *Phys. Rev. A* **86** 043626

[79] Haller E, Hart R, Mark M J, Danzl J G, Reichsllner L, Gustavsson M, Dalmonte M, Pupillo G and Ngerl H C 2010 *Nature* **466** 597

[80] Guan X W 2014 *Int. J. Mod. Phys. B* **28** 1430015

[81] Guan X W, Batchelor M T and Takahashi M 2007 *Phys. Rev. A* **76** 043617

[82] Rigol M, Dunjko V, Yurovsky V and Olshanii M 2007 *Phys. Rev. Lett.* **98** 050405

[83] Rigol M, Dunjko V and Olshanii M 2008 *Nature* **452** 854

[84] Kormos M, Chou Y Z and Imambekov A 2011 *Phys. Rev. Lett.* **107** 230405

[85] Cheianov V V, Smith H and Zvonarev M B 2006 J. Stat. Mech.: Theory Exp. P08015

[86] Kormos M, Mussardo G and Trombettoni A 2009 *Phys. Rev. Lett.* **103** 210404

[87] Kormos M, Mussardo G and Trombettoni A 2010 *Phys. Rev. A* **81** 043606

[88] Kormos M, Mussardo G and Pozsgay B 2010 *J. Stat. Mech.: Theory Exp.* P05014

[89] Caux J S and Essler F H L 2013 *Phys. Rev. Lett.* **110** 257203

[90] Nardis J, Wouters B, Brockmann M and Caux J S 2014 *Phys. Rev. A.* **89** 033601

[91] Goldstein G and Andrei N 2014 arXiv:1405.6365v1 [cond-mat.quant-gas]

[92] Goldstein G and Andrei N 2013 arXiv:1309.3471v1 [cond-mat.quant-gas]

[93] Lyer D and Andrei N 2012 *Phys. Rev. Lett.* **109** 115304

[94] Pozsgay B 2014 arXiv:1406.4613v2 [cond-mat.stat-mech]

[95] Wouters B, Nardis J D, Brockmann M, Fioretto D, Rigol M and Caux J S 2014 *Phys. Rev. Lett.* **113** 117202

[96] Brockmann M, Wouters B, Fioretto D, Nardis J D, Vlijm R and C J S 2014 *J. Stat. Mech.* P12009

[97] Pozsgay B, Mestyn M, Werner M A, Kormos M, Zarnd G and Takcs G 2014 *Phys. Rev. Lett.* **113** 117203

[98] Goldstein G and Andrei N 2014 arXiv:1405.4224v2 [cond-mat.quant-gas]

From "From dissip-less to norm diffus in easy-axis Heisen sp ch"

References

[1] B. Bertini, F. Heidrich-Meisner, C. Karrasch, T. Prosen, R. Steinigeweg, and M. Žnidarič, "Finite-temperature transport in one-dimensional quantum lattice models," Rev. Mod. Phys. **93**, 025003 (2021).

[2] A. Bastianello, A. De Luca, and R. Vasseur, "Hydrodynamics of weak integrability breaking," J. Stat. Mech. **2021**, 114003 (2021).

[3] K. Mallayya, M. Rigol, and W. De Roeck, "Prethermalization and thermalization in isolated quantum systems," Phys. Rev. X **9**, 021027 (2019).

[25] F. Lange, Z. Lenarčič, and A. Rosch, "Time-dependent generalized gibbs ensembles in open quantum systems," Phys. Rev. B **97**, 165138 (2018).

[5] H. Castella, X. Zotos, and P. Prelovšek, "Integrability and ideal conductance at finite temperatures," Phys. Rev. Lett. **74**, 972 (1995).

[6] X Zotos and P Prelovšek, "Evidence for ideal insulating or conducting state in a one-dimensional integrable system." Phys. Rev. B **53**, 983 (1996).

[7] X. Zotos, F. Naef, and P. Prelovšek, "Transport and conservation laws," Phys. Rev. B **55**, 11029 (1997).

[8] T. Prosen, "Open XXZ spin chain: Nonequilibrium steady state and a strict bound on ballistic transport," Phys. Rev. Lett. **106**, 217206 (2011).

[9] T. Prosen and E. Ilievski, "Families of quasilocal conservation laws and quantum spin transport," Phys. Rev. Lett. **111**, 057203 (2013).

[48] E. Ilievski, M. Medenjak, T. Prosen, and L. Zadnik, "Quasilocal charges in integrable lattice systems," J. Stat. Mech. **2016**, 064008.

[11] B. Bertini, M. Collura, J. De Nardis, and M. Fagotti, "Transport in out-of-equilibrium xxz chains: Exact profiles of charges and currents," Phys. Rev. Lett. **117**, 207201 (2016).

[9] O. A. Castro-Alvaredo, B. Doyon, and T. Yoshimura, "Emergent hydrodynamics in integrable quantum systems out of equilibrium," Phys. Rev. X **6**, 041065 (2016).

[13] E. Ilievski and J. De Nardis, "Microscopic Origin of Ideal Conductivity in Integrable Quantum Models," Phys. Rev. Lett. **119**, 020602 (2017).

[14] V. B. Bulchandani, R. Vasseur, C. Karrasch, and J. E. Moore, "Bethe-Boltzmann hydrodynamics and spin transport in the XXZ chain," Phys. Rev. B **97**, 045407 (2018).

[15] J. De Nardis, D. Bernard, and B. Doyon, "Hydrodynamic diffusion in integrable systems," Phys. Rev. Lett. **121**, 160603 (2018).

[16] J. de Nardis, D. Bernard, and B. Doyon, "Diffusion in generalized hydrodynamics and quasiparticle scattering," SciPost Phys. **6**, 049 (2019).

[17] S. Gopalakrishnan and R. Vasseur, "Kinetic Theory of Spin Diffusion and Superdiffusion in XXZ Spin Chains," Physical Review Letters **122**, 127202 (2019).

[18] H. Castella and X. Zotos, "Finite-temperature mobility of a particle coupled to a fermionic environment," Phys. Rev. B **54**, 4375 (1996).

[19] P. Jung, R. W. Helmes, and A. Rosch, "Transport in almost integrable models: Perturbed Heisenberg chains," Phys. Rev. Lett. **96**, 067202 (2006).

[20] P. Jung and A. Rosch, "Spin conductivity in almost integrable spin chains," Phys. Rev. B **76**, 245108 (2007).

[21] M. Žnidarič, "Weak integrability breaking: Chaos with integrability signature in coherent diffusion," Phys. Rev. Lett. **125**, 180605 (2020).

[22] M. Mierzejewski, T. Prosen, and P. Prelovšek, "Approximate conservation laws in perturbed integrable lattice models," Phys. Rev. B **92**, 195121 (2015).

[23] S. Hild, T. Fukuhara, P. Schauß, J. Zeiher, M. Knap, E. Demler, I. Bloch, and C. Gross, "Far-from-equilibrium spin transport in heisenberg quantum magnets," Phys. Rev. Lett. **113**, 147205 (2014).

[24] P. N. Jepsen, J. Amato-Grill, I. Dimitrova, W. W. Ho, E. Demler, and W. Ketterle, "Spin transport in a tunable Heisenberg model realized with ultracold atoms," Nature **588**, 403 (2020).

[25] D. Wei, A. Rubio-Abadal, B. Ye, F. Machado, J. Kemp, K. Srakaew, S. Hollerith, J. Rui, S. Gopalakrishnan, N. Y. Yao, I. Bloch, and J. Zeiher, "Quantum gas microscopy of Kardar-Parisi-Zhang superdiffusion," Science **376**, 716 (2022).

[26] M. Žnidarič, "Spin transport in a one-dimensional anisotropic Heisenberg model," Phys. Rev. Lett. **106**, 220601 (2011).

[27] R. Steinigeweg and J. Gemmer, "Density dynamics in translationally invariant spin-$\frac{1}{2}$ chains at high temperatures: A current-autocorrelation approach to finite time and length scales," Phys. Rev. B **80**, 184402 (2009).

[28] R. Steinigeweg, J. Herbrych, P. Prelovšek, and M. Mierzejewski, "Coexistence of anomalous and normal diffusion in integrable mott insulators," Phys. Rev. B **85**, 214409 (2012).

[29] C. Karrasch, J. E. Moore, and F. Heidrich-Meisner, "Real-time and real-space spin and energy dynamics in one-dimensional spin- 1 2 systems induced by local quantum quenches at finite temperatures," Phys. Rev. B **89**, 075139 (2014).

[30] R. Steinigeweg, J. Gemmer, and W. Brenig, "Spin and energy currents in integrable and nonintegrable spin-$\frac{1}{2}$ chains: A typicality approach to real-time autocorrelations," Phys. Rev. B **91**, 104404 (2015).

[31] P. Prelovšek, S. El Shawish, X. Zotos, and M. Long, "Anomalous scaling of conductivity in integrable fermion systems," Phys. Rev. B **70**, 205129 (2004).

[32] M. Medenjak, C. Karrasch, and T. Prosen, "Lower bounding diffusion constant by the curvature of drude weight," Phys. Rev. Lett. **119**, 080602 (2017).

[33] E. Ilievski, J. De Nardis, M. Medenjak, and T. Prosen, "Superdiffusion in one-dimensional quantum lattice models," Phys. Rev. Lett. **121**, 230602 (2018).

[34] M. Mierzejewski, J. Bonča, and P. Prelovšek, "Integrable mott insulators driven by a finite electric field," Phys. Rev. Lett. **107**, 126601 (2011).

[35] J. De Nardis, S. Gopalakrishnan, R. Vasseur, and B. Ware, "Subdiffusive hydrodynamics of nearly-integrable anisotropic spin chains," arXiv:2109.13251 .

[36] J. De Nardis, S. Gopalakrishnan, R. Vasseur, and B. Ware, "Stability of superdiffusion in nearly integrable spin chains," Phys. Rev. Lett. **127**, 057201 (2021).

[37] M. W. Long, P. Prelovšek, S. El Shawish, J. Karadamoglou, and X. Zotos, "Finite-temperature dynamical correlations using the microcanonical ensemble and the lanczos algorithm," Phys. Rev. B **68**, 235106 (2003).

[38] P. Prelovšek and J. Bonča, "Ground state and finite temperature lanczos methods," Strongly Correlated Systems - Numerical Methods, (2013), 10.1007/978-3-642-35106-8.

[39] P. Prelovšek, M. Mierzejewski, and J. Herbrych, "Coexistence of diffusive and ballistic transport in integrable quantum lattice models," Phys. Rev. B **104**, 115163 (2021).

[40] R. Steinigeweg and W. Brenig, "Spin Transport in the XXZ Chain at Finite Temperature and Momentum," Phys. Rev. Lett. **107**, 250602 (2011).

[41] M. Mierzejewski, J. Pawłowski, P. Prelovšek, and J. Herbrych, "Multiple relaxation times in perturbed XXZ chain," arXiv:2112.08158 .

[46] M. Zwolak and G. Vidal, "Mixed-state dynamics in one-dimensional quantum lattice systems: A time-dependent superoperator renormalization algorithm," Phys. Rev. Lett. **93**, 207205 (2004).

[45] F. Verstraete, J. J. García-Ripoll, and J. I. Cirac, "Matrix product density operators: Simulation of finite-temperature and dissipative systems," Phys. Rev. Lett. **93**, 207204 (2004).

[55] J. Bezanson, A. Edelman, S. Karpinski, and V. B. Shah, "Julia: A fresh approach to numerical computing," SIAM Review **59**, 65 (2017).

From bbl-Dissip Q Ising ch as a non-Herm Ashkin-Teller model

References

[1] S. Diehl, A. Micheli, A. Kantian, B. Kraus, H. P. Büchler, and P. Zoller, Nat. Phys. **4**, 878 (2008).

[11] T. Prosen and I. Pižorn, Phys. Rev. Lett. **101**, 105701 (2008).

[3] S. Diehl, A. Tomadin, A. Micheli, R. Fazio, and P. Zoller, Phys. Rev. Lett. **105**, 015702 (2010).

[4] S. Diehl, E. Rico, M. A. Baranov, and P. Zoller, Nat. Phys. **7**, 971 (2011).

[5] C.-E. Bardyn, M. A. Baranov, C. V. Kraus, E. Rico, A. İmamoğlu, P. Zoller, and S. Diehl, New J. Phys. **15**, 085001 (2013).

[6] B. Kraus, H. P. Büchler, S. Diehl, A. Kantian, A. Micheli, and P. Zoller, Phys. Rev. A **78**, 042307 (2008).

[7] M. J. Kastoryano, F. Reiter, and A. S. Sørensen, Phys. Rev. Lett. **106**, 090502 (2011).

[8] F. Verstraete, M. M. Wolf, and J. Ignacio Cirac, Nat. Phys. **5**, 633 (2009).

[9] T. Prosen, E. Ilievski, and V. Popkov, New J. Phys. **15**, 073051 (2013).

[1] H.-P. Breuer and F. Petruccione, The Theory of Open Quantum Systems (Oxford University Press, Oxford, UK, 2002).

[7] A. C. Y. Li, F. Petruccione, and J. Koch, Sci. Rep. **4**, 4887 (2014).

[4] M. Žnidarič, Phys. Rev. E **92**, 042143 (2015).

[2] T. Prosen and M. Žnidarič, J. Stat. Mech. , P02035 (2009).

[14] M. Žnidarič, Phys. Rev. Lett. **106**, 220601 (2011).

[15] M. J. Hartmann and G. Carleo, (2019), arXiv:1902.05131 .

[16] A. Nagy and V. Savona, (2019), arXiv:1902.09483 .

[17] F. Vicentini, A. Biella, N. Regnault, and C. Ciuti, (2019), arXiv:1902.10104 .

[18] N. Yoshioka and R. Hamazaki, (2019), arXiv:1902.07006 .

[12] T. Prosen, Phys. Rev. Lett. **107**, 137201 (2011).

[20] D. Karevski, V. Popkov, and G. M. Schütz, Phys. Rev. Lett. **110**, 047201 (2013).

[21] T. Prosen, Phys. Rev. Lett. **112**, 030603 (2014).

[5] M. V. Medvedyeva, F. H. L. Essler, and T. Prosen, Phys. Rev. Lett. **117**, 137202 (2016).

[23] N. Shibata and H. Katsura, Phys. Rev. B **99**, 174303 (2019).

[24] S. Sachdev, Quantum Phase transitions (Cambridge University Press, Cambridge, UK, 1999).

[25] A. Dutta, G. Aeppli, B. K. Chakrabarti, U. Divakaran, T. F. Rosenbaum, and D. Sen, Quantum phase transitions in transverse field spin models: from statistical physics to quantum infor (Cambridge University Press, Cambridge, UK, 2015).

[26] C. Ates, B. Olmos, J. P. Garrahan, and I. Lesanovsky, Phys. Rev. A **85**, 043620 (2012).

[27] A. De Luca, J. Viti, D. Bernard, and B. Doyon, Phys. Rev. B **88**, 134301 (2013).

[28] B. Horstmann, J. I. Cirac, and G. Giedke, Phys. Rev. A **87**, 012108 (2013).

[28] L. M. Vasiloiu, F. Carollo, and J. P. Garrahan, Phys. Rev. B **98**, 094308 (2018).

[30] T. Prosen, New J. Phys. **10**, 043026 (2008).

[31] M. Kohmoto, M. den Nijs, and L. P. Kadanoff, Phys. Rev. B **24**, 5229 (1981).

[32] F. C. Alcaraz, M. N. Barber, and M. T. Batchelor, Annals of Phys. **182**, 280 (1988).

[33] M. Yamanaka, Y. Hatsugai, and M. Kohmoto, Phys. Rev. B **48**, 9555 (1993).

[34] F. C. Alcaraz and J. D. de Felício, J. Phys. A: Math. Gen. **17**, L651 (1984).

[35] M. Yamanaka, Y. Hatsugai, and M. Kohmoto, Phys. Rev. B **50**, 559 (1994).

[36] Y. Qiao, Z. Xin, K. Hao, J. Cao, W.-L. Yang, K. Shi, and Y. Wang, New J. Phys. **20**, 073046 (2018).

[3] M. Žnidarič, Phys. Rev. E **89**, 042140 (2014).

[38] F. Minganti, A. Biella, N. Bartolo, and C. Ciuti, Phys. Rev. A **98**, 042118 (2018).

[38] In the case where N is odd, our model and the quantum Ashkin-Teller model has difference in the boundary terms.

[40] The same model can be constructed from the one-dimensional quantum compass model

$$H = -\sum_{i=1}^{N/2} J_x \sigma_{2i-1}^x \sigma_{2i}^x - \sum_{i=1}^{N/2-1} J_y \sigma_{2i}^y \sigma_{2i+1}^y \tag{24.35}$$

with the Lindblad operators

$$L_{2i-1} = \sqrt{\Delta_1}\sigma_{2i-1}^x \sigma_{2i}^x, \; L_{2i} = \sqrt{\Delta_2}\sigma_{2i}^y \sigma_{2i+1}^y, \tag{24.36}$$

although there exist many conserved charges in this case, and hence degenerate NESSs.

[41] M. T. Batchelor, R. J. Baxter, M. J. O'Rourke, and C. M. Yung, J. Phys. A: Math. Gen. **28**, 2759 (1995).

[42] S. Niekamp, T. Wirth, and H. Frahm, J. Phys. A: Math. Theor. **42**, 195008 (2009).

[43] J. Cao, W.-L. Yang, K. Shi, and Y. Wang, Phys. Rev. Lett. **111**, 137201 (2013).

[44] Y. Wang, W.-L. Yang, J. Cao, and K. Shi, Off-diagonal Bethe ansatz for exactly solvable models (Springer, Berlin-Heidelberg, DE, 2015).

[27] Ángel Rivas and S. F. Huelga, Open Quantum Systems: An Introduction (Springer, Heidelberg, DE, 2011).

[46] P. Di Francesco, P. Mathieu, and D. Sénéchal, Conformal field theory (Springer-Verlag, NewYork, US, 1997).

[47] L. V. Avdeev and A. A. Vladimirov, Theor. Math. Phys. **69**, 1071 (1986).

[48] F. H. L. Essler, V. E. Korepin, and K. Schoutens, J. Phys. A: Math. Gen. **25**, 4115 (1992).

[49] J. D. Noh, D.-S. Lee, and D. Kim, Physica A **287**, 167 (2000).

[50] R. I. Nepomechie and C. Wang, J. Phys. A: Math. Theor. **46**, 325002 (2013).

[51] F. C. Alcaraz, M. Baake, U. Grimmn, and V. Rittenberg, J. Phys. A: Math. Gen. **21**, L117 (1988).

[52] P. Fendley, J. Stat. Mech. , P11020 (2012).

[53] N. Moran, D. Pellegrino, J. K. Slingerland, and G. Kells, Phys. Rev. B **95**, 235127 (2017).

[54] A. Calzona, T. Meng, M. Sassetti, and T. L. Schmidt, Phys. Rev. B **98**, 201110(R) (2018).

[55] A. Chew, D. F. Mross, and J. Alicea, Phys. Rev. B **98**, 085143 (2018).

References

[1] H.-P. Breuer and F. Petruccione, The Theory of Open Quantum Systems (Oxford University Press, Oxford, UK, 2002).

[2] T. Prosen and M. Žnidarič, J. Stat. Mech. (2009) P02035.

[3] M. Žnidarič, Phys. Rev. E **89**, 042140 (2014).

[4] M. Žnidarič, Phys. Rev. E **92**, 042143 (2015).

[5] M. V. Medvedyeva, F. H. L. Essler, and T. Prosen, Phys. Rev. Lett. **117**, 137202 (2016).

[6] M. R. Gallis, Phys. Rev. A **53**, 655 (1996).

[7] A. C. Y. Li, F. Petruccione, and J. Koch, Sci. Rep. **4**, 4887 (2014).

[8] J. Cui, J. I. Cirac, and M. C. Bañuls, Phys. Rev. Lett. **114**, 220601 (2015).

[9] A. Kshetrimayum, H. Weimer, and R. Orús, Nat. Comm. **8**, 1291 (2017).

[10] M. Raghunandan, J. Wrachtrup, and H. Weimer, Phys. Rev. Lett. **120**, 150501 (2018).

[11] T. Prosen, New J. Phys. **10**, 043026 (2008).

[12] T. Prosen, Phys. Rev. Lett. **107**, 137201 (2011).

[13] W. DeGottardi, D. Sen, and S. Vishveshwara, New J. Phys. **13**, 065028 (2011).

[14] N. Wu, Phys. Lett. A **376**, 3530 (2012).

[15] A. Kitaev, Ann. Phys. **321**, 2 (2006).

[16] W. Brzezicki, J. Dziarmaga, and A. M. Oleś, Phys. Rev. B **75**, 134415 (2007).

[17] X.-Y. Feng, G.-M. Zhang, and T. Xiang, Phys. Rev. Lett. **98**, 087204 (2007).

[18] W.-L. You and G.-S. Tian, Phys. Rev. B **78**, 184406 (2008).

[19] E. Eriksson and H. Johannesson, Phys. Rev. B **79**, 224424 (2009).

[20] R. Jafari, Phys. Rev. B **84**, 035112 (2011).

[21] G.-H. Liu, W. Li, W.-L. You, G.-S. Tian, and G. Su, Phys. Rev. B **85**, 184422 (2012).

[22] Z. Cai and T. Barthel, Phys. Rev. Lett. **111**, 150403 (2013).

[23] M. van Caspel and V. Gritsev, Phys. Rev. A **97**, 052106 (2018).

[24] W. P. Su, J. R. Schrieffer, and A. J. Heeger, Phys. Rev. Lett. **42**, 1698 (1979).

[25] M. Klett, H. Cartarius, D. Dast, J. Main, and G. Wunner, Phys. Rev. A **95**, 053626 (2017).

[26] S. Lieu, Phys. Rev. B **97**, 045106 (2018).

[27] Ángel Rivas and S. F. Huelga, Open Quantum Systems: An Introduction (Springer, Heidelberg, DE, 2011).

[28] L. M. Vasiloiu, F. Carollo, and J. P. Garrahan, Phys. Rev. B **98**, 094308 (2018).

[29] J. Kemp, N. Y. Yao, C. R. Laumann, and P. Fendley, J. Stat. Mech. (2017) 063105.

[30] U. Brandt and K. Jacoby, Z. Physik B **25**, 181 (1976).

[31] M. Foss-Feig, J. T. Young, V. V. Albert, A. V. Gorshkov, and M. F. Maghrebi, Phys. Rev. Lett. **119**, 190402 (2017).

[32] W. Y. Chen, E. Y. Deng, and L. L. Yang, Discrete Math. **308**, 2222 (2008).

[33] E. Cohen, T. Hansen, and N. Itzhaki, Sci. Rep. **6**, 30232 (2016).

[34] R. P. Stanley, Enumerative Combinatorics vol. 2 (Cambridge University Press, Cambridge, UK, 1999).

[35] H. Prodinger, Sém. Lothar. Combin. **50**, Art. B50f, 19 pp. (electronic) (2003/04).

[36] D. C. Brody, J. Phys. A: Math. Theor. **47**, 035305 (2014).

[37] M. M. Sternheim and J. F. Walker, Phys. Rev. C **6**, 114 (1972).

[38] We can easily generalize the following discussion to the case where A is degenerate but diagonalizable. However, some degenerate matrices cannot be diagonalized, and such situations are sometimes called "coalescence" instead of "degeneracy". We do not consider "coalescence" here. See, e.g., Ref. [40] for more details about coalescence.

[39] U. Bilstein and B. Wehefritz, J. Phys. A: Math. Gen. **32**, 191 (1998).

[40] W. D. Heiss, J. Phys. A: Math. Theor. **45**, 444016 (2012).

From Effects of atom losses on a one-dimensional lattice gas of hardcore bosons

References

[1] I. Bloch, J. Dalibard, and W. Zwerger, "Many-body physics with ultracold gases," Rev. Mod. Phys., vol. 80, pp. 885–964, Jul 2008. http://dx.doi.org/10.1103/RevModPhys.80.885.

[2] S. Knoop, J. S. Borbely, R. van Rooij, and W. Vassen, "Nonexponential one-body loss in a bose-einstein condensate," Phys. Rev. A, vol. 85, p. 025602, Feb 2012. http://dx.doi.org/10.1103/PhysRevA.85.025602.

[3] Browaeys, A., Poupard, J., Robert, A., Nowak, S., Rooijakkers, W., Arimondo, E., Marcassa, L., Boiron, D., Westbrook, C. I., and Aspect, A., "Two body loss rate in a magneto-optical trap of metastable he," Eur. Phys. J. D, vol. **8**, no. 2, pp. 199–203, (2000). http://dx.doi.org/10.1007/s100530050027.

[4] L. Franchi, L. F. Livi, G. Cappellini, G. Binella, M. Inguscio, J. Catani, and L. Fallani, "State-dependent interactions in ultracold 174yb probed by optical clock spectroscopy," New Journal of Physics, vol. 19, p. 103037, nov 2017. http://dx.doi.org/10.1088/1367-2630/aa8fb4.

[5] T. Tomita, S. Nakajima, I. Danshita, Y. Takasu, and Y. Takahashi, "Observation of the mott insulator to superfluid crossover of a driven-dissipative bose-hubbard system," Science Advances, vol. 3, no. 12, p. e1701513, 2017. http://dx.doi.org/10.1126/sciadv.1701513.

[6] N. Syassen, D. M. Bauer, M. Lettner, T. Volz, D. Dietze, J. J. García-Ripoll, J. I. Cirac, G. Rempe, and S. Dürr, "Strong dissipation inhibits losses and induces correlations in cold molecular gases," Science, vol. 320, no. 5881, pp. 1329–1331, 2008. http://dx.doi.org/10.1126/science.1155309.

[7] T. Tomita, S. Nakajima, Y. Takasu, and Y. Takahashi, "Dissipative bose-hubbard system with intrinsic two-body loss," Phys. Rev. A, vol. 99, p. 031601, Mar 2019. http://dx.doi.org/10.1103/PhysRevA.99.031601.

[8] B. Yan, S. A. Moses, B. Gadway, J. P. Covey, K. R. A. Hazzard, A. M. Rey, D. S. Jin, and J. Ye, "Observation of dipolar spin-exchange interactions with lattice-confined polar molecules," Nature, vol. 501, pp. 521–525, Sep 2013. http://dx.doi.org/10.1038/nature12483.

[9] K. Sponselee, L. Freystatzky, B. Abeln, M. Diem, B. Hundt, A. Kochanke, T. Ponath, B. Santra, L. Mathey, K. Sengstock, and C. Becker, "Dynamics of ultracold quantum gases in the dissipative fermi–hubbard model," Quantum Science and Technology, vol. 4, p. 014002, sep 2018. http://dx.doi.org/10.1088/2058-9565/aadccd.

[10] K. Honda, S. Taie, Y. Takasu, N. Nishizawa, M. Nakagawa, and Y. Takahashi, "Observation of the sign reversal of the magnetic correlation in a driven-dissipative fermi gas in double wells," Phys. Rev. Lett., vol. 130, p. 063001, Feb 2023. http://dx.doi.org/10.1103/PhysRevLett.130.063001.

[11] J. Söding, D. Guéry-Odelin, P. Desbiolles, F. Chevy, H. Inamori, and J. Dalibard, "Three-body decay of a rubidium bose–einstein condensate," Applied Physics B, vol. 69, pp. 257–261, Oct 1999. http://dx.doi.org/10.1007/s003400050805.

[12] T. Weber, J. Herbig, M. Mark, H.-C. Nägerl, and R. Grimm, "Three-body recombination at large scattering lengths in an ultracold atomic gas," Phys. Rev. Lett., vol. 91, p. 123201, Sep 2003. http://dx.doi.org/10.1103/PhysRevLett.91.123201.

[13] B. L. Tolra, K. M. O'Hara, J. H. Huckans, W. D. Phillips, S. L. Rolston, and J. V. Porto, "Observation of reduced three-body recombination in a correlated 1d degenerate bose gas," Phys. Rev. Lett., vol. 92, p. 190401, May 2004. http://dx.doi.org/10.1103/PhysRevLett.92.190401.

[14] F. Ferlaino, S. Knoop, M. Berninger, W. Harm, J. P. D'Incao, H.-C. Nägerl, and R. Grimm, "Evidence for universal four-body states tied to an efimov trimer," Phys. Rev. Lett., vol. 102, p. 140401, Apr 2009. http://dx.doi.org/10.1103/PhysRevLett.102.140401.

[15] J. H. Gurian, P. Cheinet, P. Huillery, A. Fioretti, J. Zhao, P. L. Gould, D. Comparat, and P. Pillet, "Observation of a resonant four-body interaction in cold cesium rydberg atoms," Phys. Rev. Lett., vol. 108, p. 023005, Jan 2012. http://dx.doi.org/10.1103/PhysRevLett.108.023005.

[16] D. M. Harber, J. M. McGuirk, J. M. Obrecht, and E. A. Cornell, "Thermally Induced Losses in Ultra-Cold Atoms Magnetically Trapped Near Room-Temperature Surfaces," Journal of Low Temperature Physics, vol. **133**, pp. 229–238, Nov. (2003). http://dx.doi.org/10.1023/A:1026084606385.

[17] A. Johnson, S. S. Szigeti, M. Schemmer, and I. Bouchoule, "Long-lived nonthermal states realized by atom losses in one-dimensional quasicondensates," Physical Review A, vol. **96**, p. 013623, July (2017). http://dx.doi.org/10.1103/PhysRevA.96.013623.

[18] I. Bouchoule, M. Schemmer, and C. Henkel, "Cooling phonon modes of a Bose condensate with uniform few body losses," SciPost Phys., vol. 5, p. 043, 2018. http://dx.doi.org/10.21468/SciPostPhys.5.5.043.

[19] L. H. Dogra, J. A. P. Glidden, T. A. Hilker, C. Eigen, E. A. Cornell, R. P. Smith, and Z. Hadzibabic, "Can three-body recombination purify a quantum gas?," Phys. Rev. Lett., vol. 123, p. 020405, Jul 2019. http://dx.doi.org/10.1103/PhysRevLett.123.020405.

[20] P. Grišins, B. Rauer, T. Langen, J. Schmiedmayer, and I. E. Mazets, "Degenerate bose gases with uniform loss," Phys. Rev. A, vol. 93, p. 033634, Mar 2016. http://dx.doi.org/10.1103/PhysRevA.93.033634.

[21] B. Rauer, P. Grišins, I. E. Mazets, T. Schweigler, W. Rohringer, R. Geiger, T. Langen, and J. Schmiedmayer, "Cooling of a one-dimensional bose gas," Phys. Rev. Lett., vol. 116, p. 030402, Jan 2016. http://dx.doi.org/10.1103/PhysRevLett.116.030402.

[22] M. Schemmer, A. Johnson, R. Photopoulos, and I. Bouchoule, "Monte carlo wavefunction description of losses in a one-dimensional bose gas and cooling to the ground state by quantum feedback," Phys. Rev. A, vol. 95, p. 043641, Apr 2017. http://dx.doi.org/10.1103/PhysRevA.95.043641.

[23] M. Schemmer and I. Bouchoule, "Cooling a bose gas by three-body losses," Phys. Rev. Lett., vol. 121, p. 200401, Nov 2018. http://dx.doi.org/10.1103/PhysRevLett.121.200401.

[24] I. Bouchoule and M. Schemmer, "Asymptotic temperature of a lossy condensate," SciPost Phys., vol. 8, p. 060, 2020. http://dx.doi.org/10.21468/SciPostPhys.8.4.060.

[25] D. Rossini, A. Ghermaoui, M. B. Aguilera, R. Vatré, R. Bouganne, J. Beugnon, F. Gerbier, and L. Mazza, "Strong correlations in lossy one-dimensional quantum gases: from the quantum Zeno effect to the generalized Gibbs ensemble," Physical Review A, vol. 103, p. L060201, June (2021). http://dx.doi.org/10.1103/PhysRevA.103.L060201.

[26] J. J. García-Ripoll, S. Dürr, N. Syassen, D. M. Bauer, M. Lettner, G. Rempe, and J. I. Cirac, "Dissipation-induced hard-core boson gas in an optical lattice," New Journal of Physics, vol. **11**, p. 013053, Jan. (2009). http://dx.doi.org/10.1088/1367-2630/11/1/013053.

[27] E. Misra and C. Sudarshan, "The zeno's paradox in quantum theory," J. Math. Phys., vol. 18, p. 756, 1977.

[28] W. M. Itano, D. J. Heinzen, J. J. Bollinger, and D. J. Wineland, "Quantum zeno effect," Phys. Rev. A, vol. 41, pp. 2295–2300, 1990. http://dx.doi.org/10.1103/PhysRevA.41.2295.

[29] A. Beige, D. Braun, and P. L. Knight, "Driving atoms into decoherence-free states," New J. Phys., vol. 2, pp. 22–22, sep 2000. http://dx.doi.org/10.1088/1367-2630/2/1/322.

[30] A. Beige, D. Braun, B. Tregenna, and P. L. Knight, "Quantum computing using dissipation to remain in a decoherence-free subspace," Phys. Rev. Lett., vol. 85, pp. 1762–1765, Aug 2000. http://dx.doi.org/10.1103/PhysRevLett.85.1762.

[31] J. Kempe, D. Bacon, D. A. Lidar, and K. B. Whaley, "Theory of decoherence-free fault-tolerant universal quantum computation," Phys. Rev. A, vol. 63, p. 042307, Mar 2001. http://dx.doi.org/10.1103/PhysRevA.63.042307.

[32] P. Facchi, H. Nakazato, and S. Pascazio, "From the quantum zeno to the inverse quantum zeno effect," Phys. Rev. Lett., vol. 86, pp. 2699–2703, Mar 2001. http://dx.doi.org/10.1103/PhysRevLett.86.2699.

[33] P. Facchi and S. Pascazio, "Quantum zeno subspaces," Phys. Rev. Lett., vol. 89, p. 080401, Aug 2002. http://dx.doi.org/10.1103/PhysRevLett.89.080401.

[34] R. Schützhold and G. Gnanapragasam, "Quantum zeno suppression of three-body losses in bose-einstein condensates," Phys. Rev. A, vol. 82, p. 022120, Aug 2010. http://dx.doi.org/10.1103/PhysRevA.82.022120.

[35] K. Stannigel, P. Hauke, D. Marcos, M. Hafezi, S. Diehl, M. Dalmonte, and P. Zoller, "Constrained dynamics via the zeno effect in quantum simulation: Implementing non-abelian lattice gauge theories with cold atoms," Phys. Rev. Lett., vol. 112, p. 120406, Mar 2014. http://dx.doi.org/10.1103/PhysRevLett.112.120406.

[36] Z. Gong, S. Higashikawa, and M. Ueda, "Zeno hall effect," Phys. Rev. Lett., vol. 118, p. 200401, May 2017. http://dx.doi.org/10.1103/PhysRevLett.118.200401.

[37] H. Fröml, C. Muckel, C. Kollath, A. Chiocchetta, and S. Diehl, "Ultracold quantum wires with localized losses: Many-body quantum zeno effect," Phys. Rev. B, vol. 101, p. 144301, Apr 2020. http://dx.doi.org/10.1103/PhysRevB.101.144301.

[38] K. Snizhko, P. Kumar, and A. Romito, "Quantum zeno effect appears in stages," Phys. Rev. Research, vol. 2, p. 033512, Sep 2020. http://dx.doi.org/10.1103/PhysRevResearch.2.033512.

[39] A. Biella and M. Schiró, "Many-Body Quantum Zeno Effect and Measurement-Induced Subradiance Transition," Quantum, vol. 5, p. 528, Aug. 2021. http://dx.doi.org/10.22331/q-2021-08-19-528.

[40] I. Bouchoule, B. Doyon, and J. Dubail, "The effect of atom losses on the distribution of rapidities in the one-dimensional Bose gas," SciPost Phys. 9, 044, June (2020). http://dx.doi.org/10.21468/SciPostPhys.9.4.044.

[41] I. Bouchoule, L. Dubois, and L.-P. Barbier, "Losses in interacting quantum gases: Ultraviolet divergence and its regularization," Phys. Rev. A, vol. 104, p. L031304, Sep 2021. http://dx.doi.org/10.1103/PhysRevA.104.L031304.

[42] F. Minganti, V. Savona, and A. Biella, "Dissipative phase transitions in n-photon driven quantum nonlinear resonators," 2023. http://dx.doi.org/10.48550/arXiv.2303.03355.

[43] L. Rosso, A. Biella, and L. Mazza, "The one-dimensional Bose gas with strong two-body losses: the effect of the harmonic confinement," SciPost Physics, vol. **12**, p. 044, Jan. (2022). http://dx.doi.org/10.21468/SciPostPhys.12.1.044.

[44] C.-H. Huang, T. Giamarchi, and M. A. Cazalilla, "Modeling particle loss in open systems using keldysh path integral and second order cumulant expansion," 2023. http://dx.doi.org/10.48550/arXiv.2305.13090.

[45] B. Zhu, B. Gadway, M. Foss-Feig, J. Schachenmayer, M. L. Wall, K. R. A. Hazzard, B. Yan, S. A. Moses, J. P. Covey, D. S. Jin, J. Ye, M. Holland, and A. M. Rey, "Suppressing the loss of ultracold molecules via the continuous quantum zeno effect," Phys. Rev. Lett., vol. 112, p. 070404, Feb 2014. http://dx.doi.org/10.1103/PhysRevLett.112.070404.

[46] L. Rosso, D. Rossini, A. Biella, and L. Mazza, "One-dimensional spin-1/2 fermionic gases with two-body losses: Weak dissipation and spin conservation," Phys. Rev. A, vol. 104, p. 053305, Nov 2021. http://dx.doi.org/10.1103/PhysRevA.104.053305.

[47] L. Rosso, L. Mazza, and A. Biella, "Eightfold way to dark states in su(3) cold gases with two-body losses," Phys. Rev. A, vol. 105, p. L051302, May 2022. http://dx.doi.org/10.1103/PhysRevA.105.L051302.

[48] L. Rosso, A. Biella, J. De Nardis, and L. Mazza, "Dynamical theory for one-dimensional fermions with strong two-body losses: Universal non-hermitian zeno physics and spin-charge separation," Phys. Rev. A, vol. 107, p. 013303, Jan 2023. http://dx.doi.org/10.1103/PhysRevA.107.013303.

[49] M. Nakagawa, N. Tsuji, N. Kawakami, and M. Ueda, "Dynamical sign reversal of magnetic correlations in dissipative hubbard models," Phys. Rev. Lett., vol. 124, p. 147203, Apr 2020. http://dx.doi.org/10.1103/PhysRevLett.124.147203.

[50] M. Nakagawa, N. Kawakami, and M. Ueda, "Exact liouvillian spectrum of a one-dimensional dissipative hubbard model," Phys. Rev. Lett., vol. 126, p. 110404, Mar 2021. http://dx.doi.org/10.1103/PhysRevLett.126.110404.

[51] G. Perfetto, F. Carollo, J. P. Garrahan, and I. Lesanovsky, "Reaction-limited quantum reaction-diffusion dynamics," Phys. Rev. Lett., vol. 130, p. 210402, May 2023. http://dx.doi.org/10.1103/PhysRevLett.130.210402.

[52] B. Paredes, A. Widera, V. Murg, O. Mandel, S. Fölling, I. Cirac, G. V. Shlyapnikov, T. W. Hänsch, and I. Bloch, "Tonks–girardeau gas of ultracold atoms in an optical lattice," Nature, vol. 429, no. 6989, pp. 277–281, 2004.

[53] T. Kinoshita, T. Wenger, and D. S. Weiss, "Observation of a one-dimensional tonks-girardeau gas," Science, vol. 305, no. 5687, pp. 1125–1128, 2004.

[54] E. Haller, M. Gustavsson, M. J. Mark, J. G. Danzl, R. Hart, G. Pupillo, and H.-C. Nägerl, "Realization of an excited, strongly correlated quantum gas phase," Science, vol. 325, no. 5945, pp. 1224–1227, 2009.

[55] A. Van Amerongen, J. Van Es, P. Wicke, K. Kheruntsyan, and N. Van Druten, "Yang-yang thermodynamics on an atom chip," Physical review letters, vol. 100, no. 9, p. 090402, 2008.

[56] T. Jacqmin, J. Armijo, T. Berrada, K. V. Kheruntsyan, and I. Bouchoule, "Sub-poissonian fluctuations in a 1d bose gas: from the quantum quasicondensate to the strongly interacting regime," Physical review letters, vol. 106, no. 23, p. 230405, 2011.

[57] H. Moritz, T. Stöferle, K. Günter, M. Köhl, and T. Esslinger, "Confinement induced molecules in a 1d fermi gas," Physical review letters, vol. 94, no. 21, p. 210401, 2005.

[58] Y.-a. Liao, A. S. C. Rittner, T. Paprotta, W. Li, G. B. Partridge, R. G. Hulet, S. K. Baur, and E. J. Mueller, "Spin-imbalance in a one-dimensional fermi gas," Nature, vol. 467, no. 7315, pp. 567–569, 2010.

[59] G. Pagano, M. Mancini, G. Cappellini, P. Lombardi, F. Schäfer, H. Hu, X.-J. Liu, J. Catani, C. Sias, M. Inguscio, et al., "A one-dimensional liquid of fermions with tunable spin," Nature Physics, vol. 10, no. 3, pp. 198–201, 2014.

[60] P. Wicke, S. Whitlock, and N. Van Druten, "Controlling spin motion and interactions in a one-dimensional bose gas," arXiv preprint arXiv:1010.4545, 2010.

[61] J. P. Ronzheimer, M. Schreiber, S. Braun, S. S. Hodgman, S. Langer, I. P. McCulloch, F. Heidrich-Meisner, I. Bloch, and U. Schneider, "Expansion dynamics of interacting bosons in homogeneous lattices in one and two dimensions," Physical review letters, vol. 110, no. 20, p. 205301, 2013.

[62] L. Vidmar, J. P. Ronzheimer, M. Schreiber, S. Braun, S. S. Hodgman, S. Langer, F. Heidrich-Meisner, I. Bloch, and U. Schneider, "Dynamical quasicondensation of hard-core bosons at finite momenta," Physical review letters, vol. 115, no. 17, p. 175301, 2015.

[63] F. H. Essler, H. Frahm, F. Göhmann, A. Klümper, and V. E. Korepin, The one-dimensional Hubbard model. Cambridge University Press, 2005.

[64] B. Doyon, "Lecture notes on Generalised Hydrodynamics," SciPost Physics Lecture Notes, p. 18, Aug. (2020). http://dx.doi.org/10.21468/SciPostPhysLectNotes.18.

[65] A. Hutsalyuk and B. Pozsgay, "Integrability breaking in the one dimensional Bose gas: Atomic losses and energy loss," Physical Review E, vol. **103**, p. 042121, Apr. (2021). http://dx.doi.org/10.1103/PhysRevE.103.042121.

[66] B. Bertini, F. H. Essler, S. Groha, and N. J. Robinson, "Prethermalization and Thermalization in Models with Weak Integrability Breaking," Physical Review Letters, vol. **115**, p. 180601, Oct. (2015). http://dx.doi.org/10.1103/PhysRevLett.115.180601.

[67] M. Rigol and A. Muramatsu, "Fermionization in an expanding 1d gas of hard-core bosons," Physical review letters, vol. 94, no. 24, p. 240403, 2005.

[68] M. Rigol, A. Muramatsu, and M. Olshanii, "Hard-core bosons on optical superlattices: Dynamics and relaxation in the superfluid and insulating regimes," Physical Review A, vol. 74, no. 5, p. 053616, 2006.

[69] M. Rigol, V. Dunjko, V. Yurovsky, and M. Olshanii, "Relaxation in a completely integrable many-body quantum system: an ab initio study of the dynamics of the highly excited states of 1d lattice hard-core bosons," Physical review letters, vol. 98, no. 5, p. 050405, 2007.

[70] L. Vidmar, S. Langer, I. McCulloch, U. Schneider, U. Schollwöck, and F. Heidrich-Meisner, "Sudden expansion of mott insulators in one dimension," Physical Review B, vol. 88, no. 23, p. 235117, 2013.

[71] L. Vidmar, W. Xu, and M. Rigol, "Emergent eigenstate solution and emergent gibbs ensemble for expansion dynamics in optical lattices," Physical Review A, vol. 96, no. 1, p. 013608, 2017.

[72] W. Xu and M. Rigol, "Expansion of one-dimensional lattice hard-core bosons at finite temperature," Physical Review A, vol. 95, no. 3, p. 033617, 2017.

[73] O. A. Castro-Alvaredo, B. Doyon, and T. Yoshimura, "Emergent Hydrodynamics in Integrable Quantum Systems Out of Equilibrium," Physical Review X, vol. **6**, p. 041065, Dec. (2016). http://dx.doi.org/10.1103/PhysRevX.6.041065.

[74] B. Bertini, M. Collura, J. De Nardis, and M. Fagotti, "Transport in Out-of-Equilibrium X X Z Chains: Exact Profiles of Charges and Currents," Physical Review Letters, vol. **117**, p. 207201, Nov. (2016). http://dx.doi.org/10.1103/PhysRevLett.117.207201.

[75] I. Bouchoule and J. Dubail, "Generalized hydrodynamics in the one-dimensional bose gas: theory and experiments," Journal of Statistical Mechanics: Theory and Experiment, vol. 2022, p. 014003, jan 2022. http://dx.doi.org/10.1088/1742-5468/ac3659.

[76] F. Lange, Z. Lenarčič, and A. Rosch, "Time-dependent generalized Gibbs ensembles in open quantum systems," Physical Review B, vol. **97**, p. 165138, Apr. (2018). http://dx.doi.org/10.1103/PhysRevB.97.165138.

[77] F. Lange, Z. Lenarčič, and A. Rosch, "Pumping approximately integrable systems," Nature Communications, vol. 8, p. 15767, Jun 2017. http://dx.doi.org/10.1038/ncomms15767.

[78] Z. Lenarčič, F. Lange, and A. Rosch, "Perturbative approach to weakly driven many-particle systems in the presence of approximate conservation laws," Phys. Rev. B, vol. 97, p. 024302, Jan 2018. http://dx.doi.org/10.1103/PhysRevB.97.024302.

[79] P. L. Butzer and R. J. Nessel, Fourier analysis and approximation. Lehrbücher und Monographien aus dem Gebiete der exakten Wissenschaften. Mathematische Reihe, Bd. 40, Basel, Stuttgart: Birkhäuser, 1971.

[80] M. Schemmer, I. Bouchoule, B. Doyon, and J. Dubail, "Generalized hydrodynamics on an atom chip," Phys. Rev. Lett., vol. 122, p. 090601, Mar 2019. http://dx.doi.org/10.1103/PhysRevLett.122.090601.

[81] N. Malvania, Y. Zhang, Y. Le, J. Dubail, M. Rigol, and D. S. Weiss, "Generalized hydrodynamics in strongly interacting 1d bose gases," Science, vol. 373, no. 6559, pp. 1129–1133, 2021. http://dx.doi.org/10.1126/science.abf0147.

[82] M. Coppola and D. Karevski, "Some speculations about local thermalization of nonequilibrium extended quantum systems," Condensed Matter Physics, vol. **26**, no. 1, p. 13502, (2023). http://dx.doi.org/10.5488/CMP.26.13502.

[83] G. Perfetto, F. Carollo, J. P. Garrahan, and I. Lesanovsky, "Quantum reaction-limited reaction-diffusion dynamics of annihilation processes," arXiv preprint arXiv:2305.06944, 2023. http://dx.doi.org/10.48550/arXiv.2305.06944.

From Quantum reaction-limited reaction-diffusion dynamics of noninteracting Bose gases

References

[1] V. Privman, Nonequilibrium statistical mechanics in one dimension (Cambridge University Press, 1997).

[2] M. Henkel, H. Hinrichsen, S. Lübeck, and M. Pleimling, Non-equilibrium phase transitions, Vol. 1 (Springer, 2008).

[3] H. Hinrichsen, Non-equilibrium critical phenomena and phase transitions into absorbing states, Adv. Phys. **49**, 815 (2000).

[4] P. L. Krapivsky, S. Redner, and E. Ben-Naim, A kinetic view of statistical physics (Cambridge University Press, 2010).

[5] U. C. Täuber, Critical dynamics: a field theory approach to equilibrium and non-equilibrium scaling (Cambridge University Press, 2014).

[6] M. Henkel and H. Hinrichsen, The non-equilibrium phase transition of the pair-contact process with diffusion, J. Phys. A: Math. Gen. **37**, R117 (2004).

[7] K. Kang and S. Redner, Fluctuation-dominated kinetics in diffusion-controlled reactions, Phys. Rev. A **32**, 435 (1985).

[8] V. Privman and M. D. Grynberg, Fast-diffusion mean-field theory for k-body reactions in one dimension, J. Phys. A. Math. Gen. **25**, 6567 (1992).

[9] S. J. V. Urbano, D. L. González, and G. Téllez, Steady state of a two-species annihilation process with separated reactants, Phys. Rev. E **108**, 024118 (2023).

[10] D. Toussaint and F. Wilczek, Particle–antiparticle annihilation in diffusive motion, J. Chem. Phys. **78**, 2642 (1983).

[11] J. L. Spouge, Exact solutions for a diffusion-reaction process in one dimension, Phys. Rev. Lett. **60**, 871 (1988).

[12] V. Privman, Exact results for diffusion-limited reactions with synchronous dynamics, Phys. Rev. E **50**, 50 (1994).

[13] D. C. Torney and H. M. McConnell, Diffusion-limited reactions in one dimension, J. Phys. Chem. **87**, 1941 (1983).

[14] K. Kang and S. Redner, Fluctuation effects in Smoluchowski reaction kinetics, Phys. Rev. A **30**, 2833 (1984).

[15] K. Kang and S. Redner, Scaling approach for the kinetics of recombination processes, Phys. Rev. Lett. **52**, 955 (1984).

[16] K. Kang, P. Meakin, J. Oh, and S. Redner, Universal behaviour of n-body decay processes, J. Phys. A: Math. Gen. **17**, L665 (1984).

[17] Z. Rácz, Diffusion-controlled annihilation in the presence of particle sources: Exact results in one dimension, Phys. Rev. Lett. **55**, 1707 (1985).

[18] U. C. Tauber, Dynamic phase transitions in diffusion-limited reactions, arXiv:cond-mat/0205327 (2002) .

[19] U. C. Täuber, M. Howard, and B. P. Vollmayr-Lee, Applications of field-theoretic renormalization group methods to reaction–diffusion problems, J. Phys. A: Math. Gen. **38**, R79 (2005).

[20] M. Doi, Stochastic theory of diffusion-controlled reaction, J. Phys. A: Math. Gen. **9**, 1479 (1976).

[21] M. Doi, Second quantization representation for classical many-particle system, J. Phys. A: Math. Gen. **9**, 1465 (1976).

[22] L. Peliti, Path integral approach to birth-death processes on a lattice, J. Phys. France **46**, 1469 (1985).

[23] L. Peliti, Renormalisation of fluctuation effects in the a+ a to a reaction, J. Phys. A: Math. Gen. **19**, L365 (1986).

[24] D. C. Mattis and M. L. Glasser, The uses of quantum field theory in diffusion-limited reactions, Rev. Mod. Phys. **70**, 979 (1998).

[25] M. Paessens and G. M. Schütz, Phase transitions and correlations in the bosonic pair contact process with diffusion: exact results, J. Phys. A. Math. Gen. **37**, 4709 (2004).

[26] M. van Horssen and J. P. Garrahan, Open quantum reaction-diffusion dynamics: Absorbing states and relaxation, Phys. Rev. E **91**, 032132 (2015).

[27] I. Bouchoule and J. Dubail, Breakdown of tan's relation in lossy one-dimensional bose gases, Phys. Rev. Lett. **126**, 160603 (2021).

[28] I. Bouchoule and J. Dubail, Generalized hydrodynamics in the one-dimensional bose gas: theory and experiments, J. Stat. Mech.: Theory Exp. **2022** (1), 014003.

[29] J. J. García-Ripoll, S. Dürr, N. Syassen, D. M. Bauer, M. Lettner, G. Rempe, and J. I. Cirac, Dissipation-induced hard-core boson gas in an optical lattice, New J. Phys. **11**, 013053 (2009).

[30] C. Ates, B. Olmos, W. Li, and I. Lesanovsky, Dissipative binding of lattice bosons through distance-selective pair loss, Phys. Rev. Lett. **109**, 233003 (2012).

[31] B. Everest, M. R. Hush, and I. Lesanovsky, Many-body out-of-equilibrium dynamics of hard-core lattice bosons with nonlocal loss, Phys. Rev. B **90**, 134306 (2014).

[32] I. Bouchoule, L. Dubois, and L.-P. Barbier, Losses in interacting quantum gases: Ultraviolet divergence and its regularization, Phys. Rev. A **104**, L031304 (2021).

[33] G. Mazza and M. Schirò, Dissipative dynamics of a fermionic superfluid with two-body losses, Phys. Rev. A **107**, L051301 (2023).

[34] D. Rossini, A. Ghermaoui, M. B. Aguilera, R. Vatré, R. Bouganne, J. Beugnon, F. Gerbier, and L. Mazza, Strong correlations in lossy one-dimensional quantum gases: From the quantum zeno effect to the generalized gibbs ensemble, Phys. Rev. A **103**, L060201 (2021).

[35] L. Rosso, A. Biella, and L. Mazza, The one-dimensional Bose gas with strong two-body losses: the effect of the harmonic confinement, SciPost Phys. **12**, 44 (2022).

[36] L. Rosso, A. Biella, J. De Nardis, and L. Mazza, Dynamical theory for one-dimensional fermions with strong two-body losses: Universal non-hermitian zeno physics and spin-charge separation, Phys. Rev. A **107**, 013303 (2023).

[37] I. Bouchoule, B. Doyon, and J. Dubail, The effect of atom losses on the distribution of rapidities in the one-dimensional Bose gas, SciPost Phys. **9**, 44 (2020).

[38] G. Perfetto, F. Carollo, J. P. Garrahan, and I. Lesanovsky, Reaction-limited quantum reaction-diffusion dynamics, Phys. Rev. Lett. **130**, 210402 (2023).

[39] G. Perfetto, F. Carollo, J. P. Garrahan, and I. Lesanovsky, Quantum reaction-limited reaction-diffusion dynamics of annihilation processes, arXiv:2305.06944 (2023) .

[40] F. Riggio, L. Rosso, D. Karevski, and J. Dubail, Effects of atom losses on a one-dimensional lattice gas of hardcore bosons, arXiv:2307.02298 (2023) .

[41] F. Gerbino, I. Lesanovsky, and G. Perfetto, Large-scale universality in quantum reaction-diffusion from keldysh field theory, arXiv:2307.14945 (2023) .

[42] G. Lindblad, On the generators of quantum dynamical semigroups, Comm. Math. Phys. **48**, 119 (1976).

[43] V. Gorini, A. Kossakowski, and E. C. G. Sudarshan, Completely positive dynamical semigroups of n-level systems, J. Math. Phys. **17**, 821 (1976).

[44] H.-P. Breuer and F. Petruccione, The theory of open quantum systems (Oxford University Press on Demand, 2002).

[45] A. Griessner, A. J. Daley, S. R. Clark, D. Jaksch, and P. Zoller, Dark-state cooling of atoms by superfluid immersion, Phys. Rev. Lett. **97**, 220403 (2006).

[46] S. Diehl, A. Micheli, A. Kantian, B. Kraus, H. P. Büchler, and P. Zoller, Quantum states and phases in driven open quantum systems with cold atoms, Nat. Phys. **4**, 878 (2008).

[47] B. Kraus, H. P. Büchler, S. Diehl, A. Kantian, A. Micheli, and P. Zoller, Preparation of entangled states by quantum markov processes, Phys. Rev. A **78**, 042307 (2008).

[48] S. Diehl, E. Rico, M. A. Baranov, and P. Zoller, Topology by dissipation in atomic quantum wires, Nat. Phys. **7**, 971 (2011).

[49] A. Tomadin, S. Diehl, and P. Zoller, Nonequilibrium phase diagram of a driven and dissipative many-body system, Phys. Rev. A **83**, 013611 (2011).

[50] C.-E. Bardyn, M. A. Baranov, C. V. Kraus, E. Rico, A. İmamoğlu, P. Zoller, and S. Diehl, Topology by dissipation, New J. Phys. **15**, 085001 (2013).

[51] C. Pérez-Espigares, M. Marcuzzi, R. Gutiérrez, and I. Lesanovsky, Epidemic dynamics in open quantum spin systems, Phys. Rev. Lett. **119**, 140401 (2017).

[52] B. Buča, C. Booker, M. Medenjak, and D. Jaksch, Bethe ansatz approach for dissipation: exact solutions of quantum many-body dynamics under loss, New J. Phys. **22**, 123040 (2020).

[53] F. Carollo and I. Lesanovsky, Nonequilibrium dark space phase transition, Phys. Rev. Lett. **128**, 040603 (2022).

[54] I. Lesanovsky and J. P. Garrahan, Kinetic Constraints, Hierarchical Relaxation, and Onset of Glassiness in Strongly Interacting and Dissipative Rydberg Gases, Phys. Rev. Lett. **111**, 215305 (2013).

[55] B. Olmos, I. Lesanovsky, and J. P. Garrahan, Out-of-equilibrium evolution of kinetically constrained many-body quantum systems under purely dissipative dynamics, Phys. Rev. E **90**, 042147 (2014).

[56] B. Everest, M. Marcuzzi, J. P. Garrahan, and I. Lesanovsky, Emergent kinetic constraints, ergodicity breaking, and cooperative dynamics in noisy quantum systems, Phys. Rev. E **94**, 052108 (2016).

[57] M. Marcuzzi, M. Buchhold, S. Diehl, and I. Lesanovsky, Absorbing state phase transition with competing quantum and classical fluctuations, Phys. Rev. Lett. **116**, 245701 (2016).

[58] M. Buchhold, B. Everest, M. Marcuzzi, I. Lesanovsky, and S. Diehl, Nonequilibrium effective field theory for absorbing state phase transitions in driven open quantum spin systems, Phys. Rev. B **95**, 014308 (2017).

[59] R. Gutiérrez, C. Simonelli, M. Archimi, F. Castellucci, E. Arimondo, D. Ciampini, M. Marcuzzi, I. Lesanovsky, and O. Morsch, Experimental signatures of an absorbing-state phase transition in an open driven many-body quantum system, Phys. Rev. A **96**, 041602 (2017).

[60] D. Roscher, S. Diehl, and M. Buchhold, Phenomenology of first-order dark-state phase transitions, Phys. Rev. A **98**, 062117 (2018).

[61] F. Carollo, E. Gillman, H. Weimer, and I. Lesanovsky, Critical behavior of the quantum contact process in one dimension, Phys. Rev. Lett. **123**, 100604 (2019).

[62] E. Gillman, F. Carollo, and I. Lesanovsky, Numerical simulation of critical dissipative non-equilibrium quantum systems with an absorbing state, New J. Phys. **21**, 093064 (2019).

[63] E. Gillman, F. Carollo, and I. Lesanovsky, Nonequilibrium phase transitions in $(1+1)$-dimensional quantum cellular automata with controllable quantum correlations, Phys. Rev. Lett. **125**, 100403 (2020).

[64] T. M. Wintermantel, Y. Wang, G. Lochead, S. Shevate, G. K. Brennen, and S. Whitlock, Unitary and nonunitary quantum cellular automata with Rydberg arrays, Phys. Rev. Lett. **124**, 070503 (2020).

[65] S. Helmrich, A. Arias, G. Lochead, T. M. Wintermantel, M. Buchhold, S. Diehl, and S. Whitlock, Signatures of self-organized criticality in an ultracold atomic gas, Nature **577**, 481 (2020).

[66] R. Nigmatullin, E. Wagner, and G. K. Brennen, Directed percolation in nonunitary quantum cellular automata, Phys. Rev. Research **3**, 043167 (2021).

[67] J. Kazemi and H. Weimer, Genuine bistability in open quantum many-body systems, arXiv:211.05352 (2021).

[68] F. Carollo, M. Gnann, G. Perfetto, and I. Lesanovsky, Signatures of a quantum stabilized fluctuating phase and critical dynamics in a kinetically constrained open many-body system with two absorbing states, Phys. Rev. B **106**, 094315 (2022).

[69] N. Syassen, D. M. Bauer, M. Lettner, T. Volz, D. Dietze, J. J. García-Ripoll, J. I. Cirac, G. Rempe, and S. Dürr, Strong dissipation inhibits losses and induces correlations in cold molecular gases, Science **320**, 1329 (2008).

[70] A. Traverso, R. Chakraborty, Y. N. Martinez de Escobar, P. G. Mickelson, S. B. Nagel, M. Yan, and T. C. Killian, Inelastic and elastic collision rates for triplet states of ultracold strontium, Phys. Rev. A **79**, 060702 (2009).

[71] A. Yamaguchi, S. Uetake, D. Hashimoto, J. M. Doyle, and Y. Takahashi, Inelastic collisions in optically trapped ultracold metastable ytterbium, Phys. Rev. Lett. **101**, 233002 (2008).

[72] B. Yan, S. A. Moses, B. Gadway, J. P. Covey, K. R. Hazzard, A. M. Rey, D. S. Jin, and J. Ye, Observation of dipolar spin-exchange interactions with lattice-confined polar molecules, Nature **501**, 521 (2013).

[73] B. Zhu, B. Gadway, M. Foss-Feig, J. Schachenmayer, M. L. Wall, K. R. A. Hazzard, B. Yan, S. A. Moses, J. P. Covey, D. S. Jin, J. Ye, M. Holland, and A. M. Rey, Suppressing the loss of ultracold molecules via the continuous quantum zeno effect, Phys. Rev. Lett. **112**, 070404 (2014).

[74] K. Sponselee, L. Freystatzky, B. Abeln, M. Diem, B. Hundt, A. Kochanke, T. Ponath, B. Santra, L. Mathey, K. Sengstock, et al., Dynamics of ultracold quantum gases in the dissipative fermi–hubbard model, Quantum Sci. Technol. **4**, 014002 (2018).

[75] T. Kinoshita, T. Wenger, and D. S. Weiss, Local pair correlations in one-dimensional bose gases, Phys. Rev. Lett. **95**, 190406 (2005).

[76] T. Tomita, S. Nakajima, I. Danshita, Y. Takasu, and Y. Takahashi, Observation of the mott insulator to superfluid crossover of a driven-dissipative bose-hubbard system, Sci. Adv. **3**, e1701513 (2017).

[77] J. Zeiher, R. Van Bijnen, P. Schauß, S. Hild, J.-y. Choi, T. Pohl, I. Bloch, and C. Gross, Many-body interferometry of a Rydberg-dressed spin lattice, Nat. Phys. **12**, 1095 (2016).

[78] H. Kim, Y. Park, K. Kim, H.-S. Sim, and J. Ahn, Detailed balance of thermalization dynamics in Rydberg-atom quantum simulators, Phys. Rev. Lett. **120**, 180502 (2018).

[79] S. Ebadi, T. T. Wang, H. Levine, A. Keesling, G. Semeghini, A. Omran, D. Bluvstein, R. Samajdar, H. Pichler, W. W. Ho, et al., Quantum phases of matter on a 256-atom programmable quantum simulator, Nature **595**, 227 (2021).

[80] M. Jo and M. Kim, Simulating open quantum many-body systems using optimised circuits in digital quantum simulation, arXiv:2203.14295 (2022).

[81] M. Jo, J. Lee, K. Choi, and B. Kahng, Absorbing phase transition with a continuously varying exponent in a quantum contact process: A neural network approach, Phys. Rev. Research **3**, 013238 (2021).

[82] F. Lange, Z. Lenarčič, and A. Rosch, Time-dependent generalized gibbs ensembles in open quantum systems, Phys. Rev. B **97**, 165138 (2018).

[83] K. Mallayya, M. Rigol, and W. De Roeck, Prethermalization and thermalization in isolated quantum systems, Phys. Rev. X **9**, 021027 (2019).

[84] F. Lange, Z. Lenarčič, and A. Rosch, Pumping approximately integrable systems, Nat. Commun. **8**, 1 (2017).

[85] Z. Lenarčič, F. Lange, and A. Rosch, Perturbative approach to weakly driven many-particle systems in the presence of approximate conservation laws, Phys. Rev. B **97**, 024302 (2018).

[86] I. Ulčakar and Z. Lenarčič, Iterative construction of conserved quantities in dissipative nearly integrable systems, arXiv:2310.03809 (2023) .

[87] P. Grassberger, On phase transitions in schlögl's second model, Z. Phys. B **47**, 365 (1982).

[88] S. Lübeck, Tricritical directed percolation, J. Stat. Phys. **123**, 193 (2006).

[89] P. Grassberger, Tricritical directed percolation in 2+ 1 dimensions, J. Stat. Mech.: Theory Exp. **2006** (01), P01004.

[90] M. Henkel, E. Orlandini, and G. Schutz, Equivalences between stochastic systems, J. Phys. A: Math. Gen. **28**, 6335 (1995).

[91] M. Henkel, E. Orlandini, and J. Santos, Reaction–diffusion processes from equivalent integrable quantum chains, Ann. Phys. **259**, 163 (1997).

[92] K. Krebs, M. P. Pfannmüller, B. Wehefritz, and H. Hinrichsen, Finite-size scaling studies of one-dimensional reaction-diffusion systems. part i. analytical results, J. Stat. Phys. **78**, 1429 (1995).

[93] H. Simon, Concentration for one and two-species one-dimensional reaction-diffusion systems, J. Phys. A: Math. Gen. **28**, 6585 (1995).

[94] D. Ben-Avraham and É. Brunet, On the relation between one-species diffusion-limited coalescence and annihilation in one dimension, J. Phys. A: Math. Gen. **38**, 3247 (2005).

[95] F. H. Essler and M. Fagotti, Quench dynamics and relaxation in isolated integrable quantum spin chains, J. Stat. Mech.: Theory Exp. **2016** (6), 064002.

[96] L. Vidmar and M. Rigol, Generalized gibbs ensemble in integrable lattice models, J. Stat. Mech.: Theory Exp. **2016** (6), 064007.

[97] M. Kiefer-Emmanouilidis and J. Sirker, Current reversals and metastable states in the infinite bose-hubbard chain with local particle loss, Phys. Rev. A **96**, 063625 (2017).

[98] C. J. Pethick and H. Smith, Bose–Einstein condensation in dilute gases (Cambridge university press, 2008).

[99] M. A. Cazalilla, R. Citro, T. Giamarchi, E. Orignac, and M. Rigol, One dimensional bosons: From condensed matter systems to ultracold gases, Rev. Mod. Phys. **83**, 1405 (2011).

[100] R. Landig, L. Hruby, N. Dogra, M. Landini, R. Mottl, T. Donner, and T. Esslinger, Quantum phases from competing short-and long-range interactions in an optical lattice, Nature **532**, 476 (2016).

[101] T. Wu, S. Ray, and J. Kroha, Temporal bistability in the dissipative dicke-bose-hubbard system, arXiv:2311.13301 (2023) .

[102] A. Kamenev, Field theory of non-equilibrium systems (Cambridge University Press, 2023).

[103] L. M. Sieberer, M. Buchhold, and S. Diehl, Keldysh field theory for driven open quantum systems, Rep. Prog. Phys. **79**, 096001 (2016).

From "Reconstructing effective Hamiltonians from nonequilibrium (pre-)thermal steady states" by Nandy, Schmitt et al

References

[1] M. Lewenstein, A. Sanpera, V. Ahufinger, B. Damski, A. Sen(De), and U. Sen, Ultracold atomic gases in optical lattices: mimicking condensed matter physics and beyond, Advances in Physics **56**, 243 (2007), https://doi.org/10.1080/00018730701223200 .

[2] D. Jaksch and P. Zoller, The cold atom hubbard toolbox, Annals of Physics **315**, 52 (2005), special Issue.

[3] R. Blatt and C. F. Roos, Quantum simulations with trapped ions, Nature Physics **8**, 277 (2012).

[4] C. Schneider, D. Porras, and T. Schaetz, Experimental quantum simulations of many-body physics with trapped ions, Reports on Progress in Physics **75**, 10.1088/0034-4885/75/2/024401 (2012).

[5] S. Korenblit, D. Kafri, W. C. Campbell, R. Islam, E. E. Edwards, Z. X. Gong, G. D. Lin, L. M. Duan, J. Kim, K. Kim, and C. Monroe, Quantum simulation of spin models on an arbitrary lattice with trapped ions, New Journal of Physics **14**, 10.1088/1367-2630/14/9/095024 (2012), arXiv:1201.0776 .

[6] R. Islam, C. Senko, W. C. Campbell, S. Korenblit, J. Smith, A. Lee, E. E. Edwards, C. C. Wang, J. K. Freericks, and C. Monroe, Emergence and frustration of magnetism with variable-range interactions in a quantum simulator, Science **340**, 583 (2013).

[7] J. Simon, W. S. Bakr, R. Ma, M. E. Tai, P. M. Preiss, and M. Greiner, Quantum simulation of antiferromagnetic spin chains in an optical lattice, Nature **472**, 307 (2011), arXiv:1103.1372 .

[8] J. M. Gambetta, J. M. Chow, and M. Steffen, Building logical qubits in a superconducting quantum computing system, npj Quantum Information **3**, 0 (2017), arXiv:1510.04375 .

[9] I. Bloch, J. Dalibard, and W. Zwerger, Many-body physics with ultracold gases, Rev. Mod. Phys. **80**, 885 (2008).

[10] R. Jördens, N. Strohmaier, K. Günter, H. Moritz, and T. Esslinger, A Mott insulator of fermionic atoms in an optical lattice, Nature **455**, 204 (2008), arXiv:0804.4009 .

[11] C. Gross and I. Bloch, Quantum simulations with ultracold atoms in optical lattices, Science **357**, 995 (2017).

[12] A. Mazurenko, C. S. Chiu, G. Ji, M. F. Parsons, M. Kanász-Nagy, R. Schmidt, F. Grusdt, E. Demler, D. Greif, and M. Greiner, A cold-atom Fermi-Hubbard antiferromagnet, Nature **545**, 462 (2017).

[13] E. Zohar, J. I. Cirac, and B. Reznik, Quantum simulations of lattice gauge theories using ultracold atoms in optical lattices, Reports on Progress in Physics **79**, 014401 (2015).

[14] I. Bloch, J. Dalibard, and S. Nascimbène, Quantum simulations with ultracold quantum gases, Nature Physics **8**, 267 (2012).

[15] M. Aidelsburger, M. Atala, M. Lohse, J. T. Barreiro, B. Paredes, and I. Bloch, Realization of the hofstadter hamiltonian with ultracold atoms in optical lattices, Phys. Rev. Lett. **111**, 185301 (2013).

[16] I. Bloch and M. Greiner, Exploring quantum matter with ultracold atoms in optical lattices (Academic Press, 2005) pp. 1–47.

[17] R. P. Feynman, Simulating physics with computers, International Journal of Theoretical Physics **21**, 467 (1982).

[18] S. Lloyd, Universal quantum simulators, Science **273**, 1073 (1996), https://www.science.org/doi/pdf/10.1126/science.273.5278.1073 .

[19] U. L. Heras, A. Mezzacapo, L. Lamata, S. Filipp, A. Wallraff, and E. Solano, Digital quantum simulation of spin systems in superconducting circuits, Phys. Rev. Lett. **112**, 200501 (2014).

[20] R. Barends, L. Lamata, J. Kelly, L. García-Álvarez, A. G. Fowler, A. Megrant, E. Jeffrey, T. C. White, D. Sank, J. Y. Mutus, B. Campbell, Y. Chen, Z. Chen, B. Chiaro, A. Dunsworth, I. C. Hoi, C. Neill, P. J. O'Malley, C. Quintana, P. Roushan, A. Vainsencher, J. Wenner, E. Solano, and J. M. Martinis, Digital quantum simulation of fermionic models with a superconducting circuit, Nature Communications **6**, 1 (2015), arXiv:1501.07703 .

[21] L. Lamata, A. Parra-Rodriguez, M. Sanz, and E. Solano, Digital-analog quantum simulations with superconducting circuits, Advances in Physics: X **3**, 519 (2018), arXiv:1711.09810 .

[22] H. Weimer, M. Müller, H. P. Büchler, and I. Lesanovsky, Digital quantum simulation with Rydberg atoms, Quantum Information Processing **10**, 885 (2011), arXiv:1104.3081 .

[23] M. Müller, S. Diehl, G. Pupillo, and P. Zoller, Engineered Open Systems and Quantum Simulations with Atoms and Ions, Advances in Atomic, Molecular and Optical Physics **61**, 1 (2012), arXiv:1203.6595 .

[24] B. P. Lanyon, C. Hempel, D. Nigg, M. Müller, R. Gerritsma, F. Zähringer, P. Schindler, J. T. Barreiro, M. Rambach, G. Kirchmair, M. Hennrich, P. Zoller, R. Blatt, and C. F. Roos, Universal digital quantum simulation with trapped ions, Science **334**, 57 (2011), https://www.science.org/doi/pdf/10.1126/science.1208001 .

[25] J. T. Barreiro, M. Müller, P. Schindler, D. Nigg, T. Monz, M. Chwalla, M. Hennrich, C. F. Roos, P. Zoller, and R. Blatt, An open-system quantum simulator with trapped ions, Nature **470**, 486 (2011), arXiv:1104.1146 .

[26] N. Goldman and J. Dalibard, Periodically driven quantum systems: Effective hamiltonians and engineered gauge fields, Phys. Rev. X **4**, 031027 (2014).

[27] M. Bukov, L. D'Alessio, and A. Polkovnikov, Universal high-frequency behavior of periodically driven systems: from dynamical stabilization to floquet engineering, Advances in Physics **64**, 139 (2015).

[28] A. Eckardt, Colloquium: Atomic quantum gases in periodically driven optical lattices, Rev. Mod. Phys. **89**, 011004 (2017).

[29] L. Viola and S. Lloyd, Dynamical suppression of decoherence in two-state quantum systems, Phys. Rev. A **58**, 2733 (1998).

[30] L. Viola, E. Knill, and S. Lloyd, Dynamical decoupling of open quantum systems, Phys. Rev. Lett. **82**, 2417 (1999).

[31] J. Bylander, S. Gustavsson, F. Yan, F. Yoshihara, K. Harrabi, G. Fitch, D. G. Cory, Y. Nakamura, J.-S. Tsai, and W. D. Oliver, Noise spectroscopy through dynamical decoupling with a superconducting flux qubit, Nature Physics **7**, 565 (2011).

[32] J. Choi, H. Zhou, H. S. Knowles, R. Landig, S. Choi, and M. D. Lukin, Robust dynamic hamiltonian engineering of many-body spin systems, Phys. Rev. X **10**, 031002 (2020).

[33] A. Eckardt, C. Weiss, and M. Holthaus, Superfluid-insulator transition in a periodically driven optical lattice, Phys. Rev. Lett. **95**, 260404 (2005).

[34] A. Zenesini, H. Lignier, D. Ciampini, O. Morsch, and E. Arimondo, Coherent control of dressed matter waves, Phys. Rev. Lett. **102**, 100403 (2009).

[35] T. Oka and H. Aoki, Photovoltaic hall effect in graphene, Phys. Rev. B **79**, 081406 (2009).

[36] T. Kitagawa, E. Berg, M. Rudner, and E. Demler, Topological characterization of periodically driven quantum systems, Phys. Rev. B **82**, 235114 (2010).

[37] G. Jotzu, M. Messer, R. Desbuquois, M. Lebrat, T. Uehlinger, D. Greif, and T. Esslinger, Experimental realization of the topological Haldane model with ultracold fermions, Nature **515**, 237 (2014).

[38] N. H. Lindner, G. Refael, and V. Galitski, Floquet topological insulator in semiconductor quantum wells, Nature Physics **7**, 490 (2011), arXiv:1008.1792 .

[39] B.-Y. Sun, N. Goldman, M. Aidelsburger, and M. Bukov, Engineering and probing non-abelian chiral spin liquids using periodically driven ultracold atoms, PRX Quantum **4**, 020329 (2023).

[40] M. Aidelsburger, M. Atala, S. Nascimbène, S. Trotzky, Y.-A. Chen, and I. Bloch, Experimental realization of strong effective magnetic fields in an optical lattice, Phys. Rev. Lett. **107**, 255301 (2011).

[41] J. Struck, C. Ölschläger, M. Weinberg, P. Hauke, J. Simonet, A. Eckardt, M. Lewenstein, K. Sengstock, and P. Windpassinger, Tunable gauge potential for neutral and spinless particles in driven optical lattices, Phys. Rev. Lett. **108**, 225304 (2012).

[42] A. Bermudez, T. Schaetz, and D. Porras, Synthetic gauge fields for vibrational excitations of trapped ions, Phys. Rev. Lett. **107**, 150501 (2011).

[43] D. V. Else, C. Monroe, C. Nayak, and N. Y. Yao, Discrete time crystals, Annual Review of Condensed Matter Physics **11**, 467 (2020), https://doi.org/10.1146/annurev-conmatphys-031119-050658 .

[44] V. Khemani, R. Moessner, and S. L. Sondhi, A Brief History of Time Crystals, (2019), arXiv:1910.10745 .

[45] K. Sacha and J. Zakrzewski, Time crystals: a review, Reports on Progress in Physics **81**, 016401 (2017).

[46] X. Mi, M. Ippoliti, C. Quintana, A. Greene, Z. Chen, J. Gross, F. Arute, K. Arya, J. Atalaya, R. Babbush, J. C. Bardin, J. Basso, A. Bengtsson, A. Bilmes, A. Bourassa, L. Brill, M. Broughton, B. B. Buckley, D. A. Buell, B. Burkett, N. Bushnell, B. Chiaro, R. Collins, W. Courtney, D. Debroy, S. Demura, A. R. Derk, A. Dunsworth, D. Eppens, C. Erickson, E. Farhi, A. G. Fowler, B. Foxen, C. Gidney, M. Giustina, M. P. Harrigan, S. D. Harrington, J. Hilton, A. Ho, S. Hong, T. Huang, A. Huff, W. J. Huggins, L. B. Ioffe, S. V. Isakov, J. Iveland, E. Jeffrey, Z. Jiang, C. Jones, D. Kafri, T. Khattar, S. Kim, A. Kitaev, P. V. Klimov, A. N. Korotkov, F. Kostritsa, D. Landhuis, P. Laptev, J. Lee, K. Lee, A. Locharla, E. Lucero, O. Martin, J. R. McClean, T. McCourt, M. McEwen, K. C. Miao, M. Mohseni, S. Montazeri, W. Mruczkiewicz, O. Naaman, M. Neeley, C. Neill, M. Newman, M. Y. Niu, T. E. O'Brien, A. Opremcak, E. Ostby, B. Pato, A. Petukhov, N. C. Rubin, D. Sank, K. J. Satzinger, V. Shvarts, Y. Su, D. Strain, M. Szalay, M. D. Trevithick, B. Villalonga, T. White, Z. J. Yao, P. Yeh, J. Yoo, A. Zalcman, H. Neven, S. Boixo, V. Smelyanskiy, A. Megrant, J. Kelly, Y. Chen, S. L. Sondhi, R. Moessner, K. Kechedzhi, V. Khemani, and P. Roushan, Time-crystalline eigenstate order on a quantum processor, Nature **601**, 531 (2022).

[47] J. Zhang, P. W. Hess, A. Kyprianidis, P. Becker, A. Lee, J. Smith, G. Pagano, I. D. Potirniche, A. C. Potter, A. Vishwanath, N. Y. Yao, and C. Monroe, Observation of a discrete time crystal, Nature **543**, 217 (2017), arXiv:1609.08684 .

[48] S. Choi, J. Choi, R. Landig, G. Kucsko, H. Zhou, J. Isoya, F. Jelezko, S. Onoda, H. Sumiya, V. Khemani, C. Von Keyserlingk, N. Y. Yao, E. Demler, and M. D. Lukin, Observation of discrete time-crystalline order in a disordered dipolar many-body system, Nature **543**, 221 (2017), arXiv:1610.08057 .

[49] F. M. Gambetta, F. Carollo, M. Marcuzzi, J. P. Garrahan, and I. Lesanovsky, Discrete time crystals in the absence of manifest symmetries or disorder in open quantum systems, Phys. Rev. Lett. **122**, 015701 (2019).

[50] W. Beatrez, C. Fleckenstein, A. Pillai, E. de Leon Sanchez, A. Akkiraju, J. Diaz Alcala, S. Conti, P. Reshetikhin, E. Druga, M. Bukov, et al., Critical prethermal discrete time crystal created by two-frequency driving, Nature Physics **19**, 407 (2023).

[51] C. H. Johansen, J. Lang, A. Morales, A. Baumgärtner, T. Donner, and F. Piazza, Multimode-polariton superradiance via floquet engineering, SciPost Physics **12**, 094 (2022).

[52] T. Mori, T. Kuwahara, and K. Saito, Rigorous bound on energy absorption and generic relaxation in periodically driven quantum systems, Phys. Rev. Lett. **116**, 120401 (2016).

[53] T. Kuwahara, T. Mori, and K. Saito, Floquet–magnus theory and generic transient dynamics in periodically driven many-body quantum systems, Annals of Physics **367**, 96 (2016).

[54] D. A. Abanin, W. De Roeck, W. W. Ho, and F. m. c. Huveneers, Effective hamiltonians, prethermalization, and slow energy absorption in periodically driven many-body systems, Phys. Rev. B **95**, 014112 (2017).

[55] M. Bukov, S. Gopalakrishnan, M. Knap, and E. Demler, Prethermal floquet steady states and instabilities in the periodically driven, weakly interacting bose-hubbard model, Phys. Rev. Lett. **115**, 205301 (2015).

[56] A. Morningstar, D. A. Huse, and V. Khemani, Universality classes of thermalization for mesoscopic floquet systems, arXiv preprint arXiv:2210.13444 (2022).

[57] E. Altman, K. R. Brown, G. Carleo, L. D. Carr, E. Demler, C. Chin, B. DeMarco, S. E. Economou, M. A. Eriksson, K.-M. C. Fu, M. Greiner, K. R. Hazzard, R. G. Hulet, A. J. Kollár, B. L. Lev, M. D. Lukin, R. Ma, X. Mi, S. Misra, C. Monroe, K. Murch, Z. Nazario, K.-K. Ni, A. C. Potter, P. Roushan, M. Saffman, M. Schleier-Smith, I. Siddiqi, R. Simmonds, M. Singh, I. Spielman, K. Temme, D. S. Weiss, J. Vučković, V. Vuletić, J. Ye, and M. Zwierlein, Quantum simulators: Architectures and opportunities, PRX Quantum **2**, 017003 (2021).

[58] A. J. Daley, I. Bloch, C. Kokail, S. Flannigan, N. Pearson, M. Troyer, and P. Zoller, Practical quantum advantage in quantum simulation, Nature **607**, 667 (2022).

[59] W. Dür, M. J. Bremner, and H. J. Briegel, Quantum simulation of interacting high-dimensional systems: The influence of noise, Phys. Rev. A **78**, 052325 (2008).

[60] G. G. Guerreschi, J. Hogaboam, F. Baruffa, and N. P. D. Sawaya, Intel quantum simulator: a cloud-ready high-performance simulator of quantum circuits, Quantum Science and Technology **5**, 034007 (2020).

[61] X. L. Qi and D. Ranard, Determining a local Hamiltonian from a single eigenstate, Quantum **3**, 1 (2019), arXiv:1712.01850 .

[62] E. Chertkov and B. K. Clark, Computational inverse method for constructing spaces of quantum models from wave functions, Phys. Rev. X **8**, 031029 (2018).

[63] M. Greiter, V. Schnells, and R. Thomale, Method to identify parent hamiltonians for trial states, Phys. Rev. B **98**, 081113 (2018).

[64] E. Bairey, I. Arad, and N. H. Lindner, Learning a local hamiltonian from local measurements, Phys. Rev. Lett. **122**, 020504 (2019).

[65] C. E. Granade, C. Ferrie, N. Wiebe, and D. G. Cory, Robust online hamiltonian learning, New Journal of Physics **14**, 103013 (2012).

[66] N. Wiebe, C. Granade, C. Ferrie, and D. G. Cory, Hamiltonian learning and certification using quantum resources, Phys. Rev. Lett. **112**, 190501 (2014).

[67] J. Wang, S. Paesani, R. Santagati, S. Knauer, A. A. Gentile, N. Wiebe, M. Petruzzella, J. L. O'brien, J. G. Rarity, A. Laing, and M. G. Thompson, Experimental quantum Hamiltonian learning, Nature Physics **13**, 551 (2017), arXiv:1703.05402 .

[68] D. Burgarth, K. Maruyama, and F. Nori, Coupling strength estimation for spin chains despite restricted access, Phys. Rev. A **79**, 020305 (2009).

[69] C. Di Franco, M. Paternostro, and M. S. Kim, Hamiltonian tomography in an access-limited setting without state initialization, Phys. Rev. Lett. **102**, 187203 (2009).

[70] J. Zhang and M. Sarovar, Quantum hamiltonian identification from measurement time traces, Phys. Rev. Lett. **113**, 080401 (2014).

[71] J. Kim, J. Kwon, M. Kim, J. Do, D. Lee, and H. Han, Low-dielectric-constant polyimide aerogel composite films with low water uptake, Polymer Journal **48**, 829 (2016).

[72] A. Sone and P. Cappellaro, Hamiltonian identifiability assisted by a single-probe measurement, Phys. Rev. A **95**, 022335 (2017).

[73] Y. Wang, D. Dong, B. Qi, J. Zhang, I. R. Petersen, and H. Yonezawa, A quantum hamiltonian identification algorithm: Computational complexity and error analysis, IEEE Transactions on Automatic Control **63**, 1388 (2018).

[74] Z. Li, L. Zou, and T. H. Hsieh, Hamiltonian Tomography via Quantum Quench, Physical Review Letters **124**, 160502 (2020), arXiv:1912.09492 .

[75] K. Rudinger and R. Joynt, Compressed sensing for hamiltonian reconstruction, Phys. Rev. A **92**, 052322 (2015).

[76] M. Kieferová and N. Wiebe, Tomography and generative training with quantum boltzmann machines, Phys. Rev. A **96**, 062327 (2017).

[77] A. Valenti, E. Van Nieuwenburg, S. Huber, and E. Greplova, Hamiltonian learning for quantum error correction, Physical Review Research **1**, 1 (2019), arXiv:1907.02540 .

[78] L. Pastori, T. Olsacher, C. Kokail, and P. Zoller, Characterization and verification of trotterized digital quantum simulation via hamiltonian and liouvillian learning, PRX Quantum **3**, 030324 (2022).

[79] T. Olsacher, L. Pastori, C. Kokail, L. M. Sieberer, and P. Zoller, Digital quantum simulation, learning of the floquet hamiltonian, and quantum chaos of the kicked top, Journal of Physics A: Mathematical and Theoretical **55**, 334003 (2022).

[80] M. Bukov, M. Heyl, D. A. Huse, and A. Polkovnikov, Heating and many-body resonances in a periodically driven two-band system, Phys. Rev. B **93**, 155132 (2016).

[81] H. Bourlard and Y. Kamp, Auto-association by multilayer perceptrons and singular value decomposjournaition, Biological Cybernetics **59**, 291 (2004).

[82] M. Tschannen, O. Bachem, and M. Lucic, Recent Advances in Autoencoder-Based Representation Learning, , 1 (2018), arXiv:1812.05069 .

[83] M. Schmitt and Z. Lenarčič, From observations to complexity of quantum states via unsupervised learning, Phys. Rev. B **106**, L041110 (2022) .

[84] A. Lazarides, A. Das, and R. Moessner, Equilibrium states of generic quantum systems subject to periodic driving, Phys. Rev. E **90**, 012110 (2014).

[85] A. Lazarides, A. Das, and R. Moessner, Equilibrium states of generic quantum systems subject to periodic driving, Phys. Rev. E **90**, 012110 (2014).

[86] L. D'Alessio and M. Rigol, Long-time behavior of isolated periodically driven interacting lattice systems, Phys. Rev. X **4**, 041048 (2014).

[87] S. A. Weidinger and M. Knap, Floquet prethermalization and regimes of heating in a periodically driven, interacting quantum system, Scientific Reports **7**, 1 (2017), arXiv:1609.09089 .

[88] W. W. Ho, T. Mori, D. A. Abanin, and E. G. Dalla Torre, Quantum and classical floquet prethermalization, Annals of Physics , 169297 (2023).

[89] M. Bukov, L. D'Alessio, and A. Polkovnikov, Universal high-frequency behavior of periodically driven systems: from dynamical stabilization to floquet engineering, Advances in Physics **64**, 139 (2015), https://doi.org/10.1080/00018732.2015.1055918 .

[90] C. Fleckenstein and M. Bukov, Thermalization and prethermalization in periodically kicked quantum spin chains, Phys. Rev. B **103**, 144307 (2021).

[91] T. N. Ikeda and A. Polkovnikov, Fermi's golden rule for heating in strongly driven floquet systems, Phys. Rev. B **104**, 134308 (2021).

[92] D. E. Parker, X. Cao, A. Avdoshkin, T. Scaffidi, and E. Altman, A universal operator growth hypothesis, Phys. Rev. X **9**, 041017 (2019).

[93] H. Zhao, F. Mintert, R. Moessner, and J. Knolle, Random multipolar driving: Tunably slow heating through spectral engineering, Phys. Rev. Lett. **126**, 040601 (2021).

[94] T. Mori, H. Zhao, F. Mintert, J. Knolle, and R. Moessner, Rigorous bounds on the heating rate in thue-morse quasiperiodically and randomly driven quantum many-body systems, Phys. Rev. Lett. **127**, 050602 (2021).

[95] M. Heyl, P. Hauke, and P. Zoller, Quantum localization bounds trotter errors in digital quantum simulation, Science advances **5**, eaau8342 (2019).

[96] H. Zhao, M. Bukov, M. Heyl, and R. Moessner, Making trotterization adaptive for nisq devices and beyond, arXiv preprint arXiv:2209.12653 (2022).

[97] H. Zhao, M. Bukov, M. Heyl, and R. Moessner, Adaptive trotterization for time-dependent hamiltonian quantum dynamics using instantaneous conservation laws, arXiv preprint arXiv:2307.10327 (2023).

[98] M. Dalmonte, V. Eisler, M. Falconi, and B. Vermersch, Entanglement Hamiltonians: From Field Theory to Lattice Models and Experiments, Annalen der Physik **534**, 1 (2022), arXiv:2202.05045 .

[99] C. Bartsch and J. Gemmer, Dynamical typicality of quantum expectation values, Phys. Rev. Lett. **102**, 110403 (2009).

[100] P. Reimann, Dynamical typicality of isolated many-body quantum systems, Phys. Rev. E **97**, 062129 (2018).

[101] P. Reimann and L. Dabelow, Typicality of prethermalization, Phys. Rev. Lett. **122**, 080603 (2019).

[102] J. Richter and R. Steinigeweg, Combining dynamical quantum typicality and numerical linked cluster expansions, Phys. Rev. B **99**, 094419 (2019).

From Iterative construction of conserved quantities in dissipative nearly integrable systems

References

[1] M. Rigol, V. Dunjko, V. Yurovsky, and M. Olshanii, Relaxation in a Completely Integrable Many-Body Quantum System: An Ab Initio Study of the Dynamics of the Highly Excited States of 1D Lattice Hard-Core Bosons, Phys. Rev. Lett. **98**, 050405 (2007).

[2] E. Ilievski, J. De Nardis, B. Wouters, J.-S. Caux, F. H. L. Essler, and T. Prosen, Complete Generalized Gibbs Ensembles in an Interacting Theory, Phys. Rev. Lett. **115**, 157201 (2015).

[3] L. Vidmar and M. Rigol, Generalized Gibbs ensemble in integrable lattice models, J. Stat. Mech. Theory Exp. **2016**, 064007 (2016).

[4] F. H. L. Essler and M. Fagotti, Quench dynamics and relaxation in isolated integrable quantum spin chains, J. Stat. Mech. Theory Exp. **2016**, 064002 (2016).

[5] J.-S. Caux, The Quench Action, J. Stat. Mech. Theory Exp. **2016**, 064006 (2016).

[6] M. Rigol, V. Dunjko, and M. Olshanii, Thermalization and its mechanism for generic isolated quantum systems, Nature **452**, 854 (2008).

[7] A. Polkovnikov, K. Sengupta, A. Silva, and M. Vengalattore, Colloquium: Nonequilibrium dynamics of closed interacting quantum systems, Rev. Mod. Phys. **83**, 863 (2011).

[8] T. Langen, S. Erne, R. Geiger, B. Rauer, T. Schweigler, M. Kuhnert, W. Rohringer, I. E. Mazets, T. Gasenzer, and J. Schmiedmayer, Experimental observation of a generalized Gibbs ensemble, Science **348**, 207 (2015).

[9] O. A. Castro-Alvaredo, B. Doyon, and T. Yoshimura, Emergent Hydrodynamics in Integrable Quantum Systems Out of Equilibrium, Phys. Rev. X **6**, 041065 (2016).

[10] B. Bertini, M. Collura, J. De Nardis, and M. Fagotti, Transport in Out-of-Equilibrium XXZ Chains: Exact Profiles of Charges and Currents, Phys. Rev. Lett. **117**, 207201 (2016).

[11] B. Doyon, Lecture notes on Generalised Hydrodynamics, SciPost Phys. Lect. Notes , 18 (2020).

[12] N. Malvania, Y. Zhang, Y. Le, J. Dubail, M. Rigol, and D. S. Weiss, Generalized hydrodynamics in strongly interacting 1D Bose gases, Science **373**, 1129 (2021).

[13] M. Schemmer, I. Bouchoule, B. Doyon, and J. Dubail, Generalized Hydrodynamics on an Atom Chip, Phys. Rev. Lett. **122**, 090601 (2019).

[14] F. Cataldini, F. Møller, M. Tajik, J. a. Sabino, S.-C. Ji, I. Mazets, T. Schweigler, B. Rauer, and J. Schmiedmayer, Emergent Pauli Blocking in a Weakly Interacting Bose Gas, Phys. Rev. X **12**, 041032 (2022).

[15] F. Møller, C. Li, I. Mazets, H.-P. Stimming, T. Zhou, Z. Zhu, X. Chen, and J. Schmiedmayer, Extension of the Generalized Hydrodynamics to the Dimensional Crossover Regime, Phys. Rev. Lett. **126**, 090602 (2021).

[16] K. Yang, Y. Zhang, K.-Y. Li, K.-Y. Lin, S. Gopalakrishnan, M. Rigol, and B. L. Lev, Phantom energy in the nonlinear response of a quantum many-body scar state, arXiv:2308.11615 (2023).

[17] T. Kinoshita, T. Wenger, and D. S. Weiss, A quantum Newton's cradle, Nature **440**, 900 (2006).

[18] F. Meinert, M. Panfil, M. J. Mark, K. Lauber, J.-S. Caux, and H.-C. Nägerl, Probing the Excitations of a Lieb-Liniger Gas from Weak to Strong Coupling, Phys. Rev. Lett. **115**, 085301 (2015).

[19] T. Langen, S. Erne, R. Geiger, B. Rauer, T. Schweigler, M. Kuhnert, W. Rohringer, I. E. Mazets, T. Gasenzer, and J. Schmiedmayer, Experimental observation of a generalized Gibbs ensemble, Science **348**, 207 (2015).

[20] C. Hess, Heat conduction in low-dimensional quantum magnets, Eur. Phys. J. Spec. Top. **151**, 73 (2007).

[21] S. K. Niesen, O. Breunig, S. Salm, M. Seher, M. Valldor, P. Warzanowski, and T. Lorenz, Substitution effects on the temperature versus magnetic field phase diagrams of the quasi-one-dimensional effective Ising spin-$\frac{1}{2}$ chain system $BaCo_2V_2O_8$, Phys. Rev. B **90**, 104419 (2014).

[22] A. Scheie, N. E. Sherman, M. Dupont, S. E. Nagler, M. B. Stone, G. E. Granroth, J. E. Moore, and D. A. Tennant, Detection of Kardar–Parisi–Zhang hydrodynamics in a quantum Heisenberg spin-1/2 chain, Nat. Phys. **17**, 726 (2021).

[23] Y. Tang, W. Kao, K.-Y. Li, S. Seo, K. Mallayya, M. Rigol, S. Gopalakrishnan, and B. L. Lev, Thermalization near Integrability in a Dipolar Quantum Newton's Cradle, Phys. Rev. X **8**, 021030 (2018).

[24] A. Bastianello, A. De Luca, B. Doyon, and J. De Nardis, Thermalization of a Trapped One-Dimensional Bose Gas via Diffusion, Phys. Rev. Lett. **125**, 240604 (2020).

[25] F. Lange, Z. Lenarčič, and A. Rosch, Time-dependent generalized Gibbs ensembles in open quantum systems, Phys. Rev. B **97**, 165138 (2018).

[26] F. Lange, Z. Lenarčič, and A. Rosch, Pumping approximately integrable systems, Nat. Commun. **8**, 1 (2017).

[18] Z. Lenarčič, F. Lange, and A. Rosch, Perturbative approach to weakly driven many-particle systems in the presence of approximate conservation laws, Phys. Rev. B **97**, 024302 (2018).

[28] F. Reiter, F. Lange, S. Jain, M. Grau, J. P. Home, and Z. Lenarčič, Engineering generalized Gibbs ensembles with trapped ions, Phys. Rev. Res. **3**, 033142 (2021).

[29] M. Schmitt and Z. Lenarčič, From observations to complexity of quantum states via unsupervised learning, Phys. Rev. B **106**, L041110 (2022).

[30] I. Bouchoule, B. Doyon, and J. Dubail, The effect of atom losses on the distribution of rapidities in the one-dimensional Bose gas, SciPost Phys. **9**, 044 (2020).

[31] A. Hutsalyuk and B. Pozsgay, Integrability breaking in the one-dimensional Bose gas: Atomic losses and energy loss, Phys. Rev. E **103**, 042121 (2021).

[32] D. Rossini, A. Ghermaoui, M. B. Aguilera, R. Vatré, R. Bouganne, J. Beugnon, F. Gerbier, and L. Mazza, Strong correlations in lossy one-dimensional quantum gases: From the quantum Zeno effect to the generalized Gibbs ensemble, Phys. Rev. A **103**, L060201 (2021).

[33] F. Gerbino, I. Lesanovsky, and G. Perfetto, Large-scale universality in Quantum Reaction-Diffusion from Keldysh field theory, arXiv:2307.14945 (2023).

[34] G. Perfetto, F. Carollo, J. P. Garrahan, and I. Lesanovsky, Reaction-Limited Quantum Reaction-Diffusion Dynamics, Phys. Rev. Lett. **130**, 210402 (2023).

[35] S. Rowlands, I. Lesanovsky, and G. Perfetto, Quantum reaction-limited reaction–diffusion dynamics of noninteracting bose gases, New Journal of Physics **26**, 043010 (2024).

[36] B. Pozsgay, The generalized gibbs ensemble for heisenberg spin chains, J. Stat. Mech. Theory Exp. **2013**, P07003 (2013).

[37] M. Fagotti and F. H. L. Essler, Reduced density matrix after a quantum quench, Phys. Rev. B **87**, 245107 (2013).

[38] B. Pozsgay, E. Vernier, and M. A. Werner, On generalized gibbs ensembles with an infinite set of conserved charges, J. Stat. Mech. Theory Exp. **2017**, 093103 (2017).

[39] In the case of degeneracies of H_0, Eq. (**??**) should be extended to a block-diagonal form; however, we expect that thermodynamically, both descriptions are equivalent, and we will work with diagonal ensemble here.

[40] M. Moeckel and S. Kehrein, Interaction Quench in the Hubbard Model, Phys. Rev. Lett. **100**, 175702 (2008).

[41] B. Bertini, F. H. L. Essler, S. Groha, and N. J. Robinson, Prethermalization and Thermalization in Models with Weak Integrability Breaking, Phys. Rev. Lett. **115**, 180601 (2015).

[42] See Supplemental Material for information on (i) regularization of χ^{-1} in the case of non-local basis of projectors $Q_m = |m\rangle\langle m|$, (ii) explicit form for the local conserved quantities of the transverse field Ising model, (iii) analysis of different tGGE descriptions in the case of the Heisenberg model, and (iv) additional unitary perturbation. All citation are included in the main text.

[43] M. Grady, Infinite set of conserved charges in the ising model, Phys. Rev. D **25**, 1103 (1982).

[44] J. T. Barreiro, M. Müller, P. Schindler, D. Nigg, T. Monz, M. Chwalla, M. Hennrich, C. F. Roos, P. Zoller, and R. Blatt, An open-system quantum simulator with trapped ions, Nature **470**, 486 (2011).

[45] X. Mi, A. A. Michailidis, S. Shabani, K. C. Miao, P. V. Klimov, J. Lloyd, E. Rosenberg, R. Acharya, I. Aleiner, T. I. Andersen, et al., Stable quantum-correlated many-body states through engineered dissipation, Science **383**, 1332 (2024).

[46] Here, we used the natural normalization $||\tilde{C}_k||^2 = L$ with $||A||^2 = \frac{\mathrm{tr}[AA^\dagger]}{N_H} - \frac{\mathrm{tr}[A]\mathrm{tr}[A^\dagger]}{N_H^2}$ and N_H the Hamiltonian Hilbert space dimension. The Hamiltonian has it's own Lagrange multiplier, so $\Lambda_0^{(k)} = |\tilde{\lambda}_0^{(k)}|$.

[47] E. Ilievski, M. Medenjak, and T. Prosen, Quasilocal Conserved Operators in the Isotropic Heisenberg Spin-1/2 Chain, Phys. Rev. Lett. **115**, 120601 (2015).

[48] E. Ilievski, M. Medenjak, T. Prosen, and L. Zadnik, Quasilocal charges in integrable lattice systems, J. Stat. Mech. Theory Exp. **2016**, 064008 (2016).

[49] Here, we use the normalization $\mathcal{N}_k = \sqrt{\frac{1}{LN_H}\sum_m |w_m^{(k)}|^2}$, where N_H is the Hamiltonian Hilbert space dimension. Therefore $\tilde{C}_k$ are scaling extensively, $||\tilde{C}_k||^2 \sim L$, where $||A||^2 = \frac{\mathrm{tr}[AA^\dagger]}{N_H} - \frac{\mathrm{tr}[A]\mathrm{tr}[A^\dagger]}{N_H^2}$.

[50] M. Grabowski and P. Mathieu, Structure of the Conservation Laws in Quantum Integrable Spin Chains with Short Range Interactions, Annals of Physics **243**, 299 (1995).

[51] G. Bentsen, I.-D. Potirniche, V. B. Bulchandani, T. Scaffidi, X. Cao, X.-L. Qi, M. Schleier-Smith, and E. Altman, Integrable and chaotic dynamics of spins coupled to an optical cavity, Phys. Rev. X **9**, 041011 (2019).

[52] Our current study used exact diagonalization on Hilbert space of dimension N_H with its own complexity $\mathcal{O}(N_H^3)$. Then the reduction of complexity from $\mathcal{O}(L^2\,N_H)$ to $\mathcal{O}(k^3\,N_H)$ for solving equations (**??**) does not remove the bottleneck. Here, we used that k is the number of necessary iterative steps and that finding roots for n variables scales as $\mathcal{O}(n^a)$, with $a = 2$ for the Powell method employed [55]. Scaling $\mathcal{O}(k^3 N_H)$ is obtained by taking into account that in each (intermediate) iterative step $k' \leq k$, $\mathcal{O}(k'^2)$ root findings are performed, summing up to $\mathcal{O}(k^3)$ in total. However, at least for non-interacting many-body integrable systems, one can evaluate Eq. (**??**) and construct iterative conserved quantities (**??**) in the basis of mode occupation operators in $\mathcal{O}(L^b)$ steps. Then our iterative method diminishes the complexity from $O(L^{b+2})$ for finding Lagrange multipliers of all conserved quantities to $O(k^3\,L^b)$ for k iterative conserved quantities.

[53] E. Ilievski, E. Quinn, J. D. Nardis, and M. Brockmann, String-charge duality in integrable lattice models, J. Stat. Mech. Theory Exp. **2016**, 063101 (2016).

[54] E. Ilievski and E. Quinn, The equilibrium landscape of the Heisenberg spin chain, SciPost Phys. **7**, 033 (2019).

[55] W. H. Press, Numerical recipes 3rd edition: The art of scientific computing (Cambridge university press, 2007).

From Quasilocal conserved operators in isotropic Heisenberg spin 1/2 chain by Ilievski et al.

References

[1] H. Bethe, Z. Phys. **71**, 205 (1931).

[2] L. D. Faddeev, How Algebraic Bethe Ansatz works for integrable model, Les-Houches lectures, `arXiv:hep-th/9605187`.

[3] V. E. Korepin, N. M. Bogoliubov and A. G. Izergin, Quantum Inverse Scattering Method and Correlation Functions, (Cambridge University Press, Cambridge, 1993).

[4] W. Heisenberg, Z. Phys. **49**, 619 (1928).

[5] A. V. Sologubenko et al., J. Low Temp. Phys. **147**, 387 (2007); F. Heidrich-Meisner et al., Eur. Phys. J. Special Topics **151**, 135 (2007).

[6] A. Polkovnikov et al., Rev.Mod.Phys. **83**, 863 (2011).

[7] E. T. Jaynes, Phys. Rev. **108**, 171 (1957); J. M. Deutsch, Phys. Rev. A **43**, 2046 (1991); M. Srednicki, Phys. Rev. E **50**, 888 (1994).

[8] M. Rigol et al., Phys. Rev. Lett., **98**, 050405 (2007); M. A. Cazalilla, Phys. Rev. Lett. **97**, 156403 (2006); P. Calabrese and J. Cardy, Phys. Rev. Lett., **96**, 136801 (2006); T. Barthel and U. Schollwöck, Phys. Rev. Lett. **100**, 100601 (2008); D. Fioretto and G. Mussardo, New J. of Phys. **12**, 055015 (2010); J.-S. Caux and F. H. L. Essler, Phys. Rev. Lett. **110**, 257203 (2013).

[9] B. Wouters et al., Phys. Rev. Lett. **113**, 117202 (2014); M. Brockmann et al., J. Stat. Mech. P12009 **(2014)**.

[10] M. Mierzejewski, P. Prelovšek, and T. Prosen, Phys. Rev. Lett. **113**, 020602 (2014).

[11] B. Pozsgay et al., Phys. Rev. Lett. **113**, 117203 (2014); M. Mestyan et al., J. Stat. Mech. P04001 **(2015)**.

[12] G. Goldstein and N. Andrei, `arXiv:1405.4224`.

[13] M. Mierzejewski, P. Prelovšek, and T. Prosen, Phys. Rev. Lett. **114**, 140601 (2015).

[14] T. Prosen, Open XXZ Spin Chain: Nonequilibrium Steady State and a Strict Bound on Ballistic Transport Phys. Rev. Lett. **106**, 217206 (2011).

[15] T. Prosen and E. Ilievski, Phys. Rev. Lett. **111**, 057203 (2013).

[16] T. Prosen, Nucl. Phys. B **886**, 1177 (2014).

[17] R. G. Pereira, V. Pasquier, J. Sirker, I. Affleck, J. Stat. Mech. P09037 (**2014**).

[18] T. Prosen, `arXiv:1504.0078` to appear as a Topical Review in J. Phys. A.

[19] M. Fagotti and F. H. L. Essler, J. Stat. Mech. P07012 **(2013)**.

[20] Similarly as has been discussed for the $s = 1/2$ case in: H. Katsura, J. Stat. Mech. P01006 **(2015)**.

[21] Supplemental material associated with this manuscript.

[22] M. P. Grabowski and P. Mathieu, Ann. Phys. **243** 299 (1995).

[23] Similar inversion relations in fundamental representations, corresponding $s = 1/2$ in our case, are discussed in: J. M. Maillard, J. Physique **46**, 329 (1985); P. A. Pearce, Phys. Rev. Lett. **58**, 1502 (1987); A. Klümper, A. Schadschneider, and J. Zittartz, Z. Phys. B **76**, 247 (1989).

[24] X. Zotos, F. Naef, and P. Prelovšek. Phys. Rev. B **55**, 11029 (1997).

[25] R. Steinigeweg, J. Herbrych, and P. Prelovšek, Phys. Rev. E **87**, 012118 (2013).

[26] E. Ilievski and T. Prosen, Commun. Math. Phys. **318**, 809 (2013).

From Critical behavior near the many-body localization transition in driven open systems by Zala Lenarčič, Alberton, Rosch, Altman

References

[1] D. Basko, I. Aleiner and B. Altshuler, Annals of Physics **321**, 1126 (2006).

[2] I. V. Gornyi, A. D. Mirlin and D. G. Polyakov, Phys. Rev. Lett. **95**, 206603 (2005).

[3] D. A. Abanin, E. Altman, I. Bloch and M. Serbyn, Rev. Mod. Phys. **91**, 021001 (2019).

[4] M. Schreiber et al., Science **349**, 842 (2015).

[5] H. P. Lüschen, P. Bordia, S. Scherg, F. Alet, E. Altman, U. Schneider, and I. Bloch, Phys. Rev. Lett. **119**, 260401 (2017).

[6] A. Lukin et al., Science **364**, 256 (2019).

[7] J. Smith et al., Nat. Phys. **12**, 907 (2016).

[8] D. J. Luitz, N. Laflorencie and F. Alet, Phys. Rev. B **91**, 081103(R) (2015).

[9] V. Oganesyan and D. A. Huse, Phys. Rev. B **75**, 155111 (2007).

[10] A. Pal and D. A. Huse, Phys. Rev. B **82**, 174411 (2010).

[11] J. A. Kjäll, J. H. Bardarson and F. Pollmann, Phys. Rev. Lett. **113**, 107204 (2014).

[12] V. Khemani, S. P. Lim, D. N. Sheng and D. A. Huse, Phys. Rev. X **7**, 021013 (2017).

[13] M. Serbyn and J. E. Moore, Phys. Rev. B **93**, 041424(R) (2016).

[14] R. Vasseur, S. A. Parameswaran and J. E. Moore, Phys. Rev. B **91**, 140202(R) (2015).

[15] J. Šuntajs, J. Bonča, T. Prosen and L. Vidmar, arXiv:1905.06345 (2019).

[16] D. A. Abanin et al, arXiv:1911.04501 (2019).

[17] R. .K. Panda, A. Scardicchio, M. Schulz, S. R. Taylor, and M. Žnidarič, EPL 128 (2019) 67003.

[18] Z. Lenarčič, E. Altman and A. Rosch, Phys. Rev. Lett. **121**, 267603 (2018).

[19] M. Žnidarič, New Journal of Physics **12**, 043001 (2010).

[20] R. Nandkishore, S. Gopalakrishnan and D. A. Huse, Phys. Rev. B **90**, 064203 (2014).

[21] K. Agarwal, S. Gopalakrishnan, M. Knap, M. Müller and E. Demler, Phys. Rev. Lett. **114**, 160401 (2015).

[22] S. Johri, R. Nandkishore and R. N. Bhatt, Phys. Rev. Lett. **114**, 117401 (2015).

[23] M. H. Fischer, M. Maksymenko and E. Altman, Phys. Rev. Lett. **116**, 160401 (2016).

[24] M. Žnidarič, A. Scardicchio and V. K. Varma, Phys. Rev. Lett. **117**, 040601 (2016).

[25] M. V. Medvedyeva, T. Prosen and M. Žnidarič, Phys. Rev. B **93**, 094205 (2016).

[26] P. Bordia, H. P. Luschen, S. S. Hodgman, M. Schreiber, I. Bloch,U. Schneider, Phys. Rev. Lett. **116**, 140401 (2016).

[27] P. Prelovšek, Phys. Rev. B **94**, 144204 (2016).

[28] E. Levi, M. Heyl, I. Lesanovsky and J. P. Garrahan, Phys. Rev. Lett. **116**, 237203 (2016).

[29] H. P. Lüschen et al., Phys. Rev. X **7**, 011034 (2017).

[30] D. J. Luitz, F. Huveneers and W. De Roeck, Phys. Rev. Lett. **119**, 150602 (2017).

[31] R. Nandkishore and S. Gopalakrishnan, Annalen der Physik **529** (2017).

[32] B. Everest, I. Lesanovsky, J. P. Garrahan and E. Levi, Phys. Rev. B **95**, 024310 (2017).

[33] J. Marino and R. M. Nandkishore, Phys. Rev. B **97**, 054201 (2018).

[34] A. Rubio-Abadal et al., Phys. Rev. X 9, 041014 (2019).

[35] M. Schulz, S. R. Taylor, C. A. Hooley and A. Scardicchio, Phys. Rev. B **98**, 180201(R) (2018).

[36] F. Weiner, F. Evers and S. Bera, Phys. Rev. B **100**, 104204 (2019).

[37] M. Schulz, S. Taylor, A. Scardicchio and M. Žnidarič, J. Stat. Mech. (2020) 023107.

[38] J. J. Mendoza-Arenas, M. Žnidaric, V. K. Varma, J. Goold, S. R. Clark, A. Scardicchio, Phys. Rev. B **99**, 094435 (2019).

[39] See Supplementary Material for (i) a derivation of relation between temperature fluctuations and transport properties of disordered systems, (ii) a comparison to a more standard measure of subdiffusivity, (iii) resistor network results in two dimensions, (iv) the discussion on an alternative experimental realization involving current measurement, (v) numerical aspects of our TEBD calculation, (vi) a derivation on how the phenomenological terms in hydrodynamic description can emerge from the microscopic Liouville equation. Supplementary Material includes Refs. [56, 57, 43, 18].

[40] J. Hulin, J. Bouchaud and A. Georges, Journal of Physics A: Mathematical and General **23**, 1085 (1990).

[41] R. Vosk, D. A. Huse and E. Altman, Phys. Rev. X **5**, 031032 (2015).

[42] A. C. Potter, R. Vasseur and S. A. Parameswaran, Phys. Rev. X **5**, 031033 (2015).

[43] S. Gopalakrishnan, K. Agarwal, E. A. Demler, D. A. Huse and M. Knap, Phys. Rev. B **93**, 134206 (2016).

[44] S. D. Geraedts, N. Regnault and R. M. Nandkishore, New Journal of Physics **19**, 113021 (2017).

[45] F. Verstraete, J. J. García-Ripoll and J. I. Cirac, Phys. Rev. Lett. **93**, 207204 (2004).

[46] M. Zwolak and G. Vidal, Phys. Rev. Lett. **93** 207205, (2004).

[47] M. C. Bañuls, J. I. Cirac and M. B. Hastings, Phys. Rev. Lett. **106**, 050405 (2011).

[48] A. B. Harris, Journal of Physics C: Solid State Physics **7**, 3082 (1974).

[49] J. T. Chayes, L. Chayes, D. S. Fisher and T. Spencer, Phys. Rev. Lett. **57**, 2999 (1986).

[50] A. Goremykina, R. Vasseur and M. Serbyn, Phys. Rev. Lett. **122**, 040601 (2019).

[51] P. T. Dumitrescu, A. Goremykina, S. A. Parameswaran, M. Serbyn and R. Vasseur, Phys. Rev. B **99**, 094205 (2019).

[52] K. X. Wei, C. Ramanathan and P. Cappellaro, Phys. Rev. Lett. **120**, 070501 (2018).

[53] M. S. Anderson, Applied Physics Letters **76**, 3130 (2000).

[54] A. Sternbach et al., arXiv:1706.08478 (2017).

[55] J. Bezanson, A. Edelman, S. Karpinski and V. B. Shah, SIAM review **59**, 65 (2017).

[56] S. Ş. Bayın, Journal of Mathematical Physics **57**, 123501 (2016).

[57] A. A. A. Kilbas, H. M. Srivastava and J. J. Trujillo, Theory and applications of fractional differential equations Vol. 204 (Elsevier Science Limited, 2006).